DIOLEFIN COMPLEXES OF TRANSITION METALS AS 'VENUS FLY-TRAP' TEMPLATES

A thesis submitted to meet the requirements for the degree of

PHILOSOPHIAE DOCTOR

in the
DEPARTMENT OF CHEMISTRY
FACULTY OF NATURAL AND AGRICULTURAL SCIENCES

at the
UNIVERSITY OF THE FREE STATE
BLOEMFONTEIN

by
Tania Nicola Hill

Promotor
Prof. A. Roodt

Co-promotor
Assoc. Prof. G. Steyl

June 2011

Prologue

I hereby express my gratitude to the following:

Dr. Regine Herbst-Irmer, from the Department of Structural Chemistry at the University of Goettingen, for the determination of the single crystal structure of [Pt(cod)(dbm)]BF_4 and the guidance on solving twinned and disordered crystals. Prof. Andreas Roodt for his patience, perseverance and continued enthusiasm though this long study. Assoc. Prof. Gideon Steyl for his enthusiasm in theoretical chemistry and the discussions thereof. A special thanks to Mr. Charles Smith for his patience, help and understanding with the ordering of equipment and chemicals. To the inorganic chemistry group for the motivation to complete this study. To my close friends for the understanding that life is a journey not a sprint. To Juan-Marie Bower, a special thanks for the assistance with the translations and the numerous survival kits. The NRF (National Research Foundation) for funding.

My family who have loved, raised, guided and helped in both the happy and troubled times of this journey.

Table of Contents

Abbreviations & Glossary …ix

Chapter 1 - Introduction
1.1 Introduction …1
1.2 Bonding in Diolefins …2
1.3 Aims of Study …4

Chapter 2 - Theoretical & Literature Overview
2.1 Introduction …6
2.2 Ligand Effects of β-Diketones, β-Enaminones and Dienes …13
2.3 Transition Metal Properties on Middle to Late Transition Metals …15
2.4 General Homogeneous Catalytic Processes …17
2.5 General Medical Characteristics of O,O-Bidentate and Olefin Transition Metal Complexes …24

Chapter 3 - Synthesis and Characterization of Complexes
3.1 Introduction …27
3.2 Instruments and Chemicals …29
3.3 Preparation of Ligands
3.3.1 Synthesis of β-Enaminones
3.3.1.1 4-aminopent-3-en-2-one (HNH-acac) …31
3.3.1.2 4-(methylamino)pent-3-en-2-one (HNMe-acac) …31
3.3.1.3 4-anilinopent-3-en-2one (HNPh-acac) …31
3.4 Preparation of Palladium(II) Complexes
3.4.1 Synthesis of $[Pd(L_1)Cl_2]$ (L_1 = cod, nbd) …32
3.4.2 Synthesis of [Pd(cod)(LL')]A (LL' = acac, hfacac, tfacac, dbm, nh-acac, nMe-acac, nPh-acac, trop, 3Br-trop; A = BF_4^-, PF_6^-)
3.4.2.1 (1,5-cyclo-octadine)(2,4-pentanedionato)palladium(II) tetrafluoroborate $[Pd(cod)(acac)]BF_4$ …33
3.4.2.2 (1,5-cyclo-octadiene)(2,4-pentanedionato)palladium(II) hexafluorophosphate $[Pd(cod)(acac)]PF_6$ …33
3.4.2.3 (1,5-cyclo-octadiene)(1,1,1-trifluoropentane-2,4-dionato)palladium(II) tetrafluoroborate $[Pd(cod)(tfacac)]BF_4$ …34
3.4.2.4 (1,5-cyclo-octadiene)(1,1,1-trifluoropentane-2,4-dionato)palladium(II) hexafluorophosphate $[Pd(cod)(tfacac)]PF_6$ …34
3.4.2.5 (1,5-cyclo-octadiene)(1,1,1,5,5,5-hexafluoropentane-2,4-dionato)palladium(II) tetrafluoroborate $[Pd(cod)(hfacac)]BF_4$ …34
3.4.2.6 (1,5-cyclo-octadiene)(1,1,1,5,5,5-hexafluoropentane-2,4-dionato)palladium(II) hexafluorophosphate $[Pd(cod)(hfacac)]PF_6$ …34
3.4.2.7 (1,5-cyclo-octadiene)(2-hydroxy-cyclohepta-2,4,6-trieneonato)palladium(II) tetrafluoroborate $[Pd(cod)(trop)]BF_4$ …35

3.4.2.8 (1,5-cyclo-octadiene)(2-hydroxy-cyclohepta-2,4,6-trieneonato)palladium(II) hexafluorophosphate
[Pd(cod)(trop)]PF_6 …35
3.4.2.9 (1,5-cyclo-octadiene)(3,5,7-tribromo-2-hydroxy-cyclohepta-2,4,6-trieneonato)palladium(II) tetrafluoroborate
[Pd(cod)(3Br-trop)]BF_4 …35
3.4.2.10 (1,5-cyclo-octadiene)(3,5,7-tribromo-2-hydroxy-cyclohepta-2,4,6-trieneonato)palladium(II) hexafluorophosphate
[Pd(cod)(3Br-trop)]PF_6 …35
3.4.2.11 (1,5-cyclo-octadiene)(4-aminopent-3-en-2-onato)palladium(II) tetrafluoroborate
[Pd(cod)(NH-acac)]BF_4 …36
3.4.2.12 (1,5-cyclo-octadiene)(4-aminopent-3-en-2-onato)palladium(II) hexafluorophosphate
[Pd(cod)(NH-acac)]PF_6 …36
3.4.2.13 (1,5-cyclo-octadiene)(4-(methylamino)pent-3-en-2-onato)palladium(II) tetrafluoroborate
[Pd(cod)(NMe-acac)]BF_4 …36
3.4.2.14 (1,5-cyclo-octadiene)(4-(methylamino)pent-3-en-2-onato)palladium(II) hexafluorophosphate
[Pd(cod)(NMe-acac)]PF_6 …36
3.4.2.15 (1,5-cyclo-octadiene)(4-anilinopent-3-en-2-onato)palladium(II) tetrafluoroborate
[Pd(cod)(NPh-acac)]BF_4 …37
3.4.2.16 (1,5-cyclo-octadiene)(4-anilinopent-3-en-2-onato)palladium(II) hexafluorophosphate
[Pd(cod)(NPh-acac)]PF_6 …37
3.4.2.17 (1,5-cyclo-octadiene)(4,4,4-trifluoro-1-(2-thienyl)-1,3-butenedionato)palladium(II) tetrafluoroborate
[Pd(cod)(thtfac)]BF_4 …37
3.4.2.18 (1,5-cyclo-octadiene)(4,4,4-trifluoro-1-(2-thienyl)-1,3-butenedionato)palladium(II) hexafluorophosphate
[Pd(cod)(thtfac)]PF_6 …38
3.4.2.19 (1,5-cyclo-octadiene)(1,3-diphenylpropane-1,3-dionato)palladium(II) tetrafluoroborate
[Pd(cod)(dbm)]BF_4 …38
3.4.2.20 (1,5-cyclo-octadiene)(1,3-diphenylpropane-1,3-dionato)palladium(II) hexafluorophosphate
[Pd(cod)(dbm)]PF_6 …38
3.5 Preparation of Platinum(II) Complexes
3.5.1 Synthesis of [Pt(L_1)Cl_2] (L_1 = cod, nbd) …39
3.5.2 Synthesis of [Pt(cod)(LL')]A (LL' = acac, hfacac, tfacac, dbm, nh-acac, nMe-acac, nPh-acac, trop, 3Br-trop; A = BF_4^-, PF_6^-)
3.5.2.1 (1,5-cyclo-octadiene)(2,4-pentanedionato)platinum(II) tetrafluoroborate
[Pt(cod)(acac)]BF_4 …40
3.5.2.2 (1,5-cyclo-octadiene)(2,4-pentanedionato)platinum(II) hexafluorophosphate
[Pt(cod)(acac)]PF_6 …40
3.5.2.3 (1,5-cyclo-octadiene)(1,1,1-trifluoropentane-2,4-dionato)platinum(II) tetrafluoroborate
[Pt(cod)(tfacac)]BF_4 …41
3.5.2.4 (1,5-cyclo-octadiene)(1,1,1-trifluoropentane-2,4-dionato)platinum(II) hexafluorophosphate
[Pt(cod)(tfacac)]PF_6 …41

Table of Contents

3.5.2.5 (1,5-cyclo-octadiene)(1,1,1,5,5,5-hexafluoropentane-2,4-dionato)platinum(II) tetrafluoroborate
[Pt(cod)(hfacac)]BF_4 …41
3.5.2.6 (1,5-cyclo-octadiene)(1,1,1,5,5,5-hexafluoropentane-2,4-dionato)platinum(II) hexafluorophosphate
[Pt(cod)(hfacac)]PF_6 …41
3.5.2.7 (1,5-cyclo-octadiene)(2-hydroxy-cyclohepta-2,4,6-trieneonato)platinum(II) tetrafluoroborate
[Pt(cod)(trop)]BF_4 …42
3.5.2.8 (1,5-cyclo-octadiene)(2-hydroxy-cyclohepta-2,4,6-trieneonato)platinum(II) hexafluorophosphate
[Pt(cod)(trop)]PF_6 …42
3.5.2.9 (1,5-cyclo-octadiene)(3,5,7-tribromo-2-hydroxy-cyclohepta-2,4,6-trieneonato)platinum(II) tetrafluoroborate
[Pt(cod)(3Br-trop)]BF_4 …42
3.5.2.10 (1,5-cyclo-octadiene)(3,5,6-tribromo-2-hydroxy-cyclohepta-2,4,6-trieneonato)platinum(II) hexafluorophosphate
[Pt(cod)(3Br-trop)]PF_6 …42
3.5.2.11 (1,5-cyclo-octadiene)(4-aminopent-3-en-2-onato)platinum(II) tetrafluoroborate
[Pt(cod)(NH-acac)]BF_4 …43
3.5.2.12 (1,5-cyclo-octadiene)(4-aminopent-3-en-2-onato)platinum(II) hexafluorophosphate
[Pt(cod)(NH-acac)]PF_6 …43
3.5.2.13 (1,5-cyclo-octadiene)(4-(methylamino)pent-3-en-2-onato)platinum(II) tetrafluoroborate
[Pt(cod)(NMe-acac)]BF_4 …43
3.5.2.14 (1,5-cyclo-octadiene)(4-(methylamino)pent-3-en-2-onato)platinum(II) hecafluorophosphate
[Pt(cod)(NMe-acac)]PF_6 …44
3.5.2.15 (1,5-cyclo-octadiene)(4-anilinopent-3-en-2-onato)platinum(II) tetrafluoroborate
[Pt(cod)(NPh-acac)]BF_4 …44
3.5.2.16 (1,5-cyclo-octadiene)(4-anilinopent-3-en-2-onato)platinum(II) hexafluorophosphate
[Pt(cod)(NPh-acac)]PF_6 …44
3.5.2.17 (1,5-cyclo-octadiene)(4,4,4-trifluoro-1-(2-thienyl)-1,3-butenedionato)platinum(II) tetrafluoroborate
[Pt(cod)(thtfac)]BF_4 …45
3.5.2.18 (1,5-cyclo-octadiene)(4,4,4-trifluoro-1-(2-thienyl)-1,3-butenedionato)platinum(II) hexafluorophosphate
[Pt(cod)(thtfac)]PF_6 …45
3.5.2.19 (1,5-cyclo-octadiene)(1,3-diphenylpropane-1,3-dionato)platinum(II) tetrafluoroborate
[Pt(cod)(dbm)]BF_4 …45
3.5.2.20 (1,5-cyclo-octadiene)(1,3-diphenylpropane-1,3-dionato)platinum(II) hexafluorophosphate
[Pt(cod)(dbm)]PF_6 …46

3.6 Preparation of Rhodium(I) Complexes
3.6.1 Synthesis of $[Rh(L_1)Cl]_2$ (L_1 = cod, nbd) …47
3.6.2 Synthesis of [Pt(cod)(LL')] (LL' = acac, hfacac, tfacac, dbm, nh-acac, nMe-acac, nPh-acac, trop, 3Br-trop, thtfac)

Table of Contents

3.6.2.1 (1,5-cyclo-octadiene)(2,4-pentanedionato)rhodium(I) [Rh(cod)(acac)] …47
3.6.2.2 (1,5-cyclo-octadiene)(1,1,1,5,5,5-hexafluoropentane-2,4-dionato)rhodium(I) [Rh(cod)(hfacac)] …48
3.6.2.3 (1,5-cyclo-octadiene)(1,1,1-trifluoropentane-2,4-dionato)rhodium(I) [Rh(cod)(tfacac)] …48
3.6.2.4 (1,5-cyclo-octadiene)(4-aminopent-3-en-2-onato)rhodium(I) [Rh(cod)(NH-acac)] …48
3.6.2.5 (1,5-cyclo-octadiene)(4-(methylamino)pent-3-en-2-onato)rhodium(I) [Rh(cod)(NMe-acac)] …48
3.6.2.6 (1,5-cyclo-octadine)(4-anilinopent-3-en-2-onato)rhodium(I) [Rh(cod)(NPh-acac)] …49
3.6.2.7 (1,5-cyclo-octadiene)(1,3-diphenylpropane-1,3-dioato)rhodium(I) [Rh(cod)(dbm)] …49
3.6.2.8 (1,5-cyclo-octadiene)(2-hydroxy-cyclohepta-2,4,6-trieneonato)rhodium(I) [Rh(cod)(trop)] …49
3.6.2.9 (1,5-cyclo-octadiene)(3,5,7-tribromo-2-hydroxy-cyclohepta-2,4,6-trieneonato)rhodium(I) [Rh(cod)(3Br-trop)] …50
3.6.2.10 (1,5-cyclo-octadiene)(4,4,4-trifluoro-1-(2-thienyl)-1,3-butenedionato)rhodium(I) [Rh(cod)(thtfac)] …50
3.7 Discussion
3.7.1 Palladium(II) Complexes …54
3.7.2 Platinum(II) Complexes …60
3.7.3 Rhodium(I) Complexes …67

Chapter 4 - Crystallographic Study of β-Diketonato Type Complexes of Palladium(II)
4.1 Introduction …72
4.2 Experimental …73
4.3 X-Ray Structures of Palladium Complexes
4.3.1 Crystal Structure of $[Pd(cod)(acac)]PF_6$ and $[Pd(cod)(acac)]BF_4$ …76
4.3.2 Crystal Structure of $[Pd(cod)(thtfac)]PF_6$ and $[Pd(cod)(thtfac)]BF_4$ …86
4.3.3 Crystal Structure of $[Pd(cod)(tfacac)]PF_6$ …95
4.3.4 Crystal Structure of $[Pd(cod)(hfacac)]PF_6$ …101
4.4 Discussion …108

Chapter 5 - Cystallographic Study of β-Diketonato Type Complexes of Platinum(II)
5.1 Introduction …112
5.2 Experimental …113
5.3 X-Ray Structures of Platinum(II) Complexes
5.3.1 Crystal Structure of $[Pt(cod)(acac)]BF_4$ and $[Pt(cod)(acac)]PF_6$ …115
5.3.2 Crystal Structure of $[Pt(cod)(dbm)]BF_4$ …122
5.3.3 Crystal Structure of $[Pt(cod)(thtfac)]BF_4$ …125
5.4 Discussion …132

Chapter 6 - Solid State *vs.* Optimized Structure Correlation of β-Diketonato Complexes
6.1 Introduction …136
6.2 Experimental …139
6.3 Crystal Structure Correlation of Palladium(II) *vs.* Platinum(II) Complexes …136
6.4 Theoretical Correlation of Palladium(II) *vs.* Platinum(II) Complexes

Table of Contents

6.4.1 Visual Associations …147
6.4.2 Crystal Structure *vs.* Computed Structure Bond Relationships …150
6.4.3 Energies …153
6.4.4 Infra-red Spectroscopic Correlations …155
6.4.5 Molecular Orbital Comparisons …158
6.4.6 Venus fly-trap (χ and ψ) Angle Evaluation …162

Chapter 7 - Crystallographic Study of Tropolonato Type Complexes of Palladium(II) and Platinum(II)
7.1 Introduction …164
7.2 Experimental …164
7.3 X-Ray Structures of Palladium(II) Complexes
7.3.1 Crystal Structures of $[Pd(cod)(3Br\text{-}trop)]PF_6$ and $[Pd(cod)(3Br\text{-}trop)]BF_4$ …167
7.3.2 Crystal Structure of $[Pd(cod)(trop)]PF_6$ …178
7.4 X-Ray Structures of Platinum(II) Complexes
7.4.1 Crystal Structures of $[Pt(cod)(trop)]PF_6$ and $[Pt(cod)(trop)]BF_4$ …183
7.4.2 Crystal Structures of $[Pt(cod)(3Br\text{-}trop)]PF_6$ and $[Pt(cod)(3Br\text{-}trop)]BF_4$ …190
7.5 Discussion …199

Chapter 8 - Solid State *vs.* Optimized Structure Correlation of Tropolonato Complexes
8.1 Introduction …204
8.2 Experimental …205
8.3 Crystal Structure Correlation of Palladium(II) *vs.* Platinum(II) Complexes …205
8.4 Theoretical Correlation of Palladium(II) *vs.* Platinum(II) Complexes
8.4.1 Visual Associations …215
8.4.2 Crystal Structure *vs.* Computed Structure Bond Relationships …219
8.4.3 Energies …223
8.4.4 Infra-red Spectroscopic Correlations …224
8.4.5 Molecular Orbital Comparisons …226
8.4.6 Venus fly-trap (χ and ψ) Angle Evaluation …229

Chapter 9 - Crystallographic Study of β-Enaminonato Type Complexes of Palladium(II) and Platinum(II)
9.1 Introduction …231
9.2 Experimental …232
9.3 X-Ray Structures of Palladium(II) Complexes
9.3.1 Crystal Structure of $[Pd(cod)(NH\text{-}acac)]BF_4$ …235
9.4 X-Ray Structures of Platinum(II) Complexes
9.4.1 Crystal Structures of $[Pt(cod)(NH\text{-}acac)]BF_4$ and $[Pt(cod)(NH\text{-}acac)]PF_6$ …239
9.4.2 Crystal Structures of $[Pt(cod)(NMe\text{-}acac)]BF_4$ and $[Pt(cod)(NMe\text{-}acac)]PF_6$ …246
9.4.3 Crystal Structures of $[Pt(cod)(NPh\text{-}acac)]BF_4$ and $[Pt(cod)(NPh\text{-}acac)]PF_6$ …253
9.5 Discussion …262

Chapter 10 - Solid State *vs.* Optimized Structure Correlation of β-Enaminonato Complexes
10.1 Introduction …267
10.2 Experimental …268
10.3 Crystal Structure Correlation of Palladium(II) *vs.* Platinum(II) Complexes …269
10.4 Theoretical Correlation of Palladium(II) *vs.* Platinum(II) Complexes
10.4.1 Visual Associations …278

10.4.2 Crystal Structure *vs.* Computed Structure Bond Relationships …283
10.4.3 Energies …287
10.4.4 Infra-red Spectroscopic Correlations …288
10.4.5 Molecular Orbital Comparisons …292
10.4.6 Venus fly-trap (χ and ψ) Angle Evaluation …296

Chapter 11 - Crystallographic and Theoretical Study of Rhodium(I) Complexes
11.1 Introduction …298
11.2 Experimental …300
11.3 X-Ray Structures of Palladium Complexes
11.3.1 Crystal Structure of $[Rh(cod)Cl]_2$ …303
11.3.2 Crystal Structure of [Rh(cod)(acac)] …307
11.3.3 Crystal Structure of [Rh(cod)(dbm)] …311
11.3.4 Crystal Structure of [Rh(cod)(thtfac)] …314
11.3.5 Crystal Structure of [Rh(cod)(trop)] …317
11.4 Discussion …320
11.5 Theoretical Correlation of Rhodium(I) Complexes
11.5.1 Visual Associations …326
11.5.2 Crystal Structure *vs.* Computed Structure Bond Relationships …327
11.5.3 Energies …329
11.5.4 Infra-red Spectroscopic Correlations …331
11.5.5 Molecular Orbital Comparisons …332
11.5.6 Venus fly-trap (χ and ψ) Angle Evaluation …335

Chapter 12 - Correlation of Computational Structures
12.1 Introduction …337
12.2 Experimental …339
12.3 Correlation of Group 7-11 Transition Metal Zero-Point Corrected Energies …340
12.4 Correlation of Group 7-11 Transition Metal Relative Energies (E_{rel}^{M}) …342
12.5 Correlation of Group 7-11 Transition Metal Ligand Relative Energies (E_{rel}^{L}) …345
12.6 Visual Correlation of Group 7-11 Transition Metal Molecular Orbitals
12.6.1 Symmetrical O,O-Bidentate Ligands …348
12.6.2 Unsymmetrical β-Enaminonato Ligands …352
12.7 Correlation of Group 7-11 Transition Metal Molecular Orbital Energies
12.7.1 Orbital Energies …356
12.7.2 Relative Band Gap Energies …362
12.8 Correlation of Group 7-11 Transition Metal Infra-red Spectroscopic Data …364
12.9 Correlation of Group 7-11 Transition Metal Geometrical Parameters – Total Core Area …369
12.10 Correlation of Group 7-11 Lateral in-plane Metal Displacement …371
12.11 Correlation of Group 7-11 Transition Metal Geometrical Parameters - "*trans* Ligand" Bite Angles …374
12.12 Correlation of Group 7-11 Transition Metal Geometrical Parameters - Venus fly-trap Bite and Jaw (χ and ψ) Angles …376
12.13 Discussion …380

Chapter 13 - Evaluation of Study
13.1 Introduction …384
13.2 Evaluation …384
13.3 Future Studies …389

Table of Contents

Appendix

A Supplementary Infra-red Spectroscopic Data …391

B Supplementary Crystal Data

B.1 Crystal Data of $[Pd(cod)(acac)]PF_6$ …408

B.2 Crystal Data of $[Pd(cod)(3Br\text{-}trop)]BF_4$ …411

B.3 Crystal Data of $[Pd(cod)(3Br\text{-}trop)]PF_6$ …413

B.4 Crystal Data of $[Pd(cod)(thtfac)]PF_6$ …416

B.5 Crystal Data of $[Pd(cod)(tfacac)]PF_6$ …419

B.6 Crystal Data of $[Pd(cod)(hfacac)]PF_6$ …423

B.7 Crystal Data of $[Pd(cod)(acac)]BF_4$ …426

B.8 Crystal Data of $[Pd(cod)(thtfac)]BF_4$ …428

B.9 Crystal Data of $[Pd(cod)(trop)]PF_6$ …431

B.10 Crystal Data of $[Pd(cod)(NH\text{-}acac)]BF_4$ …434

B.11 Crystal Data of $[Pt(cod)(acac)]BF_4$ …436

B.12 Crystal Data of $[Pt(cod)(acac)]PF_6$ …439

B.13 Crystal Data of $[Pt(cod)(thtfac)]BF_4$ …441

B.14 Crystal Data of $[Pt(cod)(3Br\text{-}trop)]PF_6$ …446

B.15 Crystal Data of $[Pt(cod)(3Br\text{-}trop)]BF_4$ …449

B.16 Crystal Data of $[Pt(cod)(trop)]PF_6$ …451

B.17 Crystal Data of $[Pt(cod)(trop)]BF_4$ …453

B.18 Crystal Data of $[Pt(cod)(NH\text{-}acac)]BF_4$ …455

B.19 Crystal Data of $[Pt(cod)(NH\text{-}acac)]PF_6$ …457

B.20 Crystal Data of $[Pt(cod)(NMe\text{-}acac)]BF_4$ …460

B.21 Crystal Data of $[Pt(cod)(NMe\text{-}acac)]PF_6$ …462

B.22 Crystal Data of $[Pt(cod)(NPh\text{-}acac)]BF_4$ …465

B.23 Crystal Data of $[Pt(cod)(NPh\text{-}acac)]PF_6$ …467

B.24 Crystal Data of $[Rh(cod)(Cl)]_2$ (293 K) …473

B.25 Crystal Data of $[Rh(cod)(Cl)]_2$ (100 K) …475

B.26 Crystal Data of [Rh(cod)(acac)] …478

B.27 Crystal Data of [Rh(cod)(dbm)] …480

B.28 Crystal Data of [Rh(cod)(thtfac)] …482

B.29 Crystal Data of [Rh(cod)(trop)] …484

C Supplementary Theoretical / Computational Data

C.1 Theoretical / Calculation Data of the Molecular Energy Orbitals

C.1.1 Group 7-11 Transition Metal Acetylacetonato Complexes Molecular Orbitals …487

C.1.2 Group 7-11 Transition Metal Trifluoroacetylacetonato Complexes Molecular Orbitals …492

C.1.3 Group 7-11 Transition Metal Hexafluoroacetylacetonato Complexes Molecular Orbitals …497

C.1.4 Group 7-11 Transition Metal 4-Aminopent-3-en-2-onato Complexes Molecular Orbitals …502

C.1.5 Group 7-11 Transition Metal 4-(Methylamino)pent-3-en-2-onato Complexes Molecular Orbitals …507

C.1.6 Group 7-11 Transition Metal 4-Anilinopent-3-en-2-onato Complexes Molecular Orbitals …512

C.1.7 Group 7-11 Transition Metal Tropolonato Complexes Molecular Orbitals …517

Table of Contents

C.1.8 Group 7-11 Transition Metal Tribromotropolonato Complexes Molecular Orbitals …522

C.2 Theoretical / Calculation Data of the Calculated Infra-red Spectra

C.2.1 Group 7-11 Transition Metal Acetylacetonato Complexes Infra-red Spectra …528

C.2.2 Group 7-11 Transition Metal Trifluoroacetylacetonato Complexes Infra-red Spectra …530

C.2.3 Group 7-11 Transition Metal Hexafluoroacetylacetonato Complexes Infra-red Spectra …531

C.2.4 Group 7-11 Transition Metal 4-Aminopent-3-en-2-onato Complexes Infra-red Spectra …533

C.2.5 Group 7-11 Transition Metal 4-(Methylamino)pent-3-en-2-onato Complexes Infra-red Spectra …535

C.2.6 Group 7-11 Transition Metal 4-Anilinopent-3-en-2-onato Complexes Infra-red Spectra …536

C.2.7 Group 7-11 Transition Metal Tropolonato Complexes Infra-red Spectra …538

C.2.8 Group 7-11 Transition Metal Tribromotropolonato Complexes Infra-red Spectra …540

C.3 Theoretical / Calculation Data of the Calculated Bond Distances and Angles …541

C.4 Theoretical / Calculation Data of the Molecular Orbital Energies

C.4.1 Group 7-11 Transition Metal Acetylacetonato Complexes Molecular Orbital Energies …543

C.4.2 Group 7-11 Transition Metal Trifluoroacetylacetonato Complexes Molecular Orbital Energies …548

C.4.3 Group 7-11 Transition Metal Hexafluoroacetylacetonato Complexes Molecular Orbital Energies …553

C.4.4 Group 7-11 Transition Metal 4-Aminopent-3-en-2-onato Complexes Molecular Orbital Energies …558

C.4.5 Group 7-11 Transition Metal 4-(Methylamino)pent-3-en-2-onato Complexes Molecular Orbital Energies …563

C.4.6 Group 7-11 Transition Metal 4-Anilinopent-3-en-2-onato Complexes Molecular Orbital Energies …658

C.4.7 Group 7-11 Transition Metal Tropolonato Complexes Molecular Orbital Energies …573

C.4.8 Group 7-11 Transition Metal Tribromotropolonato Complexes Molecular Orbital Energies …578

C.5 Theoretical / Calculation Data of the Calculated Zero-point Corrected Energies …582

C.6 Theoretical / Calculation Data of the Calculated Metal Relative Energies (E_{rel}^{M}) …583

C.7 Theoretical / Calculation Data of the Calculated Ligand Relative Energies (E_{rel}^{L}) …584

C.8 Theoretical / Calculation Data of the Co-ordination Geometry …585

C.9 Theoretical / Calculation Output Data …586

Summary …587

Opsomming …590

Abbreviations & Glossary

LL’	Bidentate Ligand
A	Anion
δ	Chemical Shift
v	Stretching frequency for Infra-red Spectroscopy
γ	Out of plane wag for Infra-Red Spectroscopy
ppm	parts per million
DFT	Density Functional Theory
DMF	N,N-dimethylformamide
nbd	norbornadiene
cod	1,5-cyclooctadiene
atms	allyl trimethylsilane
Hacac	Acetylacetone *Alt. Name:* pentane-2,4-dione
Hhfacac	Hexafluoroacetylacetone *Alt. Name:* 1,1,1,5,5,5-hexafluoropentane-2,4-dione
Htfacac	Trifluoroacectylacetone *Alt. Name:* 1,1,1-trifluoropentane-2,4-dione
Hdbm	Dibenzoylmethane *Alt. Name:* 1,3-diphenylpropane-1,3-dione
Hthtfac	2-Thenoyltrifluoroacetone *Alt. Name:* 4,4,4-trifluoro-1-(2-thienyl)-1,3-butenedione
HNH-acac	4-aminopent-3-en-2-one
HNMe-acac	4-(methylamino)pent-3-en-2-one

Table of Contents

HNPh-acac	4-anilinopent-3-en-2-one	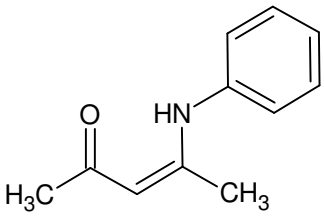
Htrop	Tropolone *Alt. Name:* 2-hydroxycyclohepta-2,4,6-trieneone	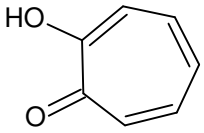
H3Br-trop	Tribromotropolone *Alt. Name:* 3,5,7-tribromo-2-hydroxycyclohepta-2,4,6-trieneone	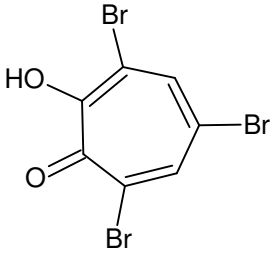

Chapter 1
Introduction and Aim

1.1 Introduction

To understand the importance of catalysis in present day society, a step back needs to be taken. Firstly, what is a catalyst? Simply stated it is a substance that changes the rate of a chemical reaction. This area of science is known as catalysis and can be divided into three major categories, namely heterogeneous, homogenous and biocatalysis. Why is it so important? It is estimated that approximately 90 % of commercially produced chemical products use catalysis in their production[1]. A few examples are synthetic fuels by the Fischer-Tropsch synthesis[2], acetic acid from the Monsanto process[3], vehicle catalytic converters and the hydrogenation of fats to produce margarines. Hot topic of the day: Environmental Issues / Green Chemistry[4]. Catalysis weighs in, with its ability to "fine-tune" the production of chemicals and reduce waste products.

A brief background into catalysis: for heterogeneous catalysis the catalyst is in a different phase generally supported by a secondary material (*e.g.* SiO_2, TiO_2, $CaCO_3$) than the reactants, while homogenous catalysis, the catalyst is in the same phase as the reactants. Each of these methods have their pro's and con's. The largest pro for homogenous catalysis is in the ability to determine the mechanism of the catalytic cycle and to tailor a catalyst for the process. Olefins and diolefins have been used in catalysis for many years. Their uses range from olefin polymerization with the use of the Ziegler-Natta catalysts[5] employing titanium, aluminum, zirconium and hafnium. Olefin metathesis utilizing nickel, tungsten, rhenium, ruthenium and molybdenum. The most famous of these are the Grubb's catalyst[6,7], the Heck reaction[8] and the

[1] "Recognizing the Best in Innovation: Breakthrough Catalyst", *R&D Magazine*, 20, (2005)
[2] Leckel D., *Energy Fuels*, **23**, 2342, (2009)
[3] Haynes A., Mann B.E., Gullivier D.J., Morris G.E, Maitlis P.M., *J. Am. Chem. Soc.*, **113**, 8567, (1991)
[4] Anastas P.T., Warner J.C, *Green Chemisry: Theory and Practice*, Oxford Univeristy Press, New York, (1998)
[5] Kissin Y.V., *Alkene Polymerization Reactions with Transition Metal Catalysts*, Elsevier, Amsterdam, (2008)
[6] Grubbs R.H, *Handbook of Metathesis*, Wiley-VCH, Germany, (2003)

Friedel-Crafts reactions[9,10,11]. Hydroformylation of alkenes to aldehydes using the oxo process[12], to the use of cyclo-octadiene to produce bicyclic phosphines[13,14] . Olefins and diolefins have also been known to act as catalyst poisons or catalyst sinks, thus a detailed understanding of their bonding behavior is significant.

1.2 Bonding in Diolefins

Diolefins usually bond in a twofold di-hapto mode, and readily co-ordinate to the middle to late transition metals. A wide variety of diene transition metal complexes are known, this study thus limited its scope to only the cyclic diene *cis,cis*-1,5-cyclo-octadiene.

Cyclo-octadiene (cod) is an organic compound used mainly as a precursor in organic type reactions, it serves as a weak co-ordinating ligand in organometallic chemistry and as an important substrate in catalytic reactions. It is simply prepared by the dimerization of butadiene in the presence of a nickel catalyst. The reasons for the selection of the diene were in that it is known to only have two conformers that of the boat and chair, reducing the formation of isomers. Another reason is the well known ability to of cod to co-ordinate with middle to late transition metals, generally forming complexes with halogens. The O,O- and N,O-bidentate co-ordination to cod transition metal complexes is known, but there are few complexes that have been synthesized and characterized. Cyclo-octadiene however has one more interesting aspect. That of its ability to "mimic" the Venus Fly Trap (*Dionaea muscipula*), what is meant by this statement.

---

[7] Grubbs R.H., Trnka T.M, *Ruthenium-Catalyzed Olefin Metathesis*, *Ruthenium in Organic Synthesis*, Murahashi S.-I. Ed., Wiley-VCH, Germany, (2004)
[8] Heck R.F., Nolley Jr. J.P., *J. Org. Chem.*, **37**, 2320, (1972)
[9] Friedel C., Crafts J.M. *Compt. Rend.*, 84, (1877)
[10] Groves J.K., *Chem. Soc. Rev.*, 73, (1972)
[11] Heaney H., *Comp. Org. Syn.*, **2**, 733, (1991)
[12] Ojima I., Tsai C.-Y., Tzamarioudaki M., Bonafoux D., *Org. React.*, **56**, 1, (2000)
[13] Bungu P.N., Otto S., *Dalton Trans.*, 2876, (2007)
[14] Bungu P.N., Otto S., *J. Organomet. Chem.*, **692**, 3370, (2007)

Figure 1.1 Left, an example of a *Dionaea muscipula* (Venus Fly Trap). Right, an overlay of a single Venus Fly Trap leaf with the cyclo-octadiene moiety (depicted in grey) and the rhodium metal centre (depicted in cyan).

If one looks at a three dimensional diagram of the *cis,cis*-1,5-cyclo-octadiene ring when co-ordinated to a metal centre, in Figure 1.1 the metal in question is rhodium, one finds that the plane passing though the alkene carbons and the metal centre maybe viewed as the throat of the fly-trap and the planes passing though the alkane carbons conversely may be seen as the jaws of the fly-trap.

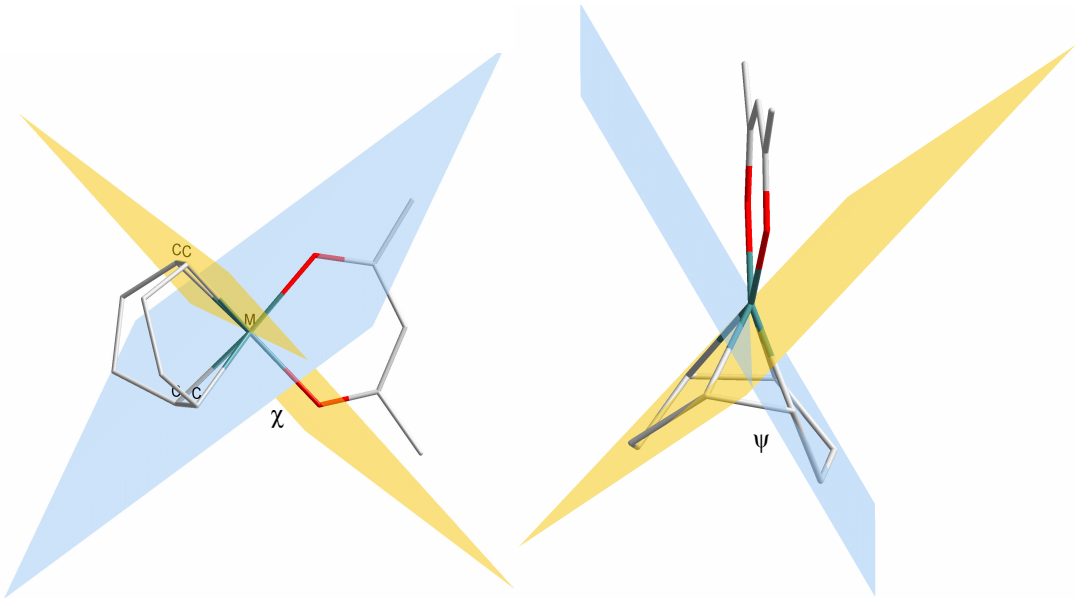

Figure 1.2 Left, the interplanar bond angle χ (bite angle) formed by the olefinic moieties through the metal centre. Right, the extent of the opening of the Venus fly-trap angle ψ (jaw angle) as defined by the planes through the alkane carbons of the cyclo-octadiene moiety.

To make matters more scientific we will define two new parameters that of the chi (χ) and psi (ψ) angles. The chi (χ) angle is defined by the intersection of the planes,

defined by adjacent alkene carbons and the metal centre and will be known as the bite angle. The psi (ψ) angle is again an intersection between planes defined by the alkane carbons of the cyclo-ocatadiene moiety and will be identified as the jaw angle, this can be seen in Figure 1.2.

1.3 Aims of Study

With the above in mind, this study commenced and the following step-wise aims were set

- A literature study for the known range of solid state data of cyclo-octadiene complexes.

- An evaluation of synthetic processes of various cyclo-octadiene complexes.

- To synthesize a range of cyclo-octadiene complexes with middle to late transition metals, focusing on platinum group metals as used in catalysis to evaluate *inter* metal bonding.
    - Varying the mono anionic *trans* ligand LL'
        - For these, three distinct ligand sets were selected
            - β-Diketone, wherein the six membered chelate ring with O,O donor atoms was left constant, varying the CF_3 substituents
            - β-Enaminone wherein the six membered chelate ring was retained, but different donor atoms were exchanged (*i.e.* N and O)
            - Tropolone, in which the O,O donor atoms were retained in a five membered chelate ring.
    - Three d^8 metal complexes were selected for studying. Rhodium(I), palladium(II) and platinum(II), which enabled comparison across groups 9 and 10, as well as down the nickel triad (4*d* and 5*d* metals)
        - By choosing the above mono anionic bidentate ligands, neutral rhodium(I) complexes would be obtained, as opposed to

palladium(II) and platinum(II) which would yield charged complexes with different counter ions.

- Allowing for the evaluation of the effect of hydrogen bonding on the solid state packing and the influence of the counter ion within the charged and neutral complexes.
- Investigation of the influence of the various metals and ligands on the complexes co-ordination geometry.

- XRD studies on the range of complexes synthesized

- To optimize the selected range of complexes by DFT, including the above solid state isolated examples and compare.

- Expanding the DFT calculations to the middle to late transition metals (groups 7-11) to obtain the energies, orbitals and other geometrical parameters.

- Evaluate effects on the geometry of cyclo-octadiene, utilizing the Venus fly-trap model.

Chapter 2
Theoretical & Literature Overview

2.1 Introduction

In this chapter a brief overview of the current and historical literature will be presented with special attention given to both the catalytic and medical aspects of the 1,5-cyclo-octadiene complexes. General background on diolefins, and specifically that of 1,5-cyclo-octadiene was presented in Chapter 1. The ligands and metals used in the study will also briefly be introduced, with regards to their binding, electronic and steric properties and effects.

As previously stated in Chapter 1 the study investigates molecules that mimic the Venus fly-trap and focused on 1,5-cyclo-octadiene when co-ordinated. Other molecules that show a similar ability as 1,5-cyclo-octadiene to "mimic" which were also considered for this study are 1,3-cyclobutadiene, cyclopentadiene, cyclohexa-1,4-diene, bicyclo[2.2.1]hepta-2,5-diene (2,5-norbornadiene) and bicyclo[3.2.2]nona-6,8-diene.

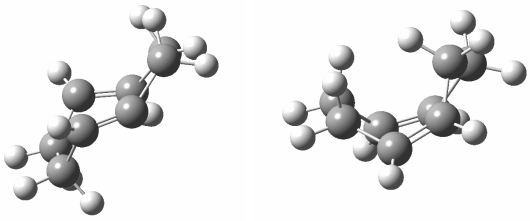

(a) **(b)**

Figure 2.1 The conformations of 1,5-cyclo-octadiene (a) the chair, and (b) the boat.

1,5-Cyclo-octadiene was selected due to its simple non-rigidity. It is known to have only two conformations with little to no possibility of full twisting. A slightly twisted boat conformation for cyclo-octadiene is well known when it is co-ordinated to middle to late transition metal centers.

In the selection of a counter ligand to the cyclo-octadiene the idea was to keep the complex as simple as possible, with the chance of multiple isomers / conformers

reduced as far as possible. The bidentate LL' ligand *trans* to the cyclo-octadiene had to be versatile and should be easy to functionalize. Of the ligand systems investigated, halogens, carbenes, phosphines and shiff bases, a β-diketonoate six membered ring system was selected. The reasons for the selection were that the β-diketonoate systems are well known for their ability to co-ordinate to middle to late transition metals[1,2], there are several commercially available, the functionlization and syntheses are straightforward and well documented[3,4,5,6,7], the ring system is generally planar with only slight puckering and both symmetrical and non-symmetrical ligands maybe studied.

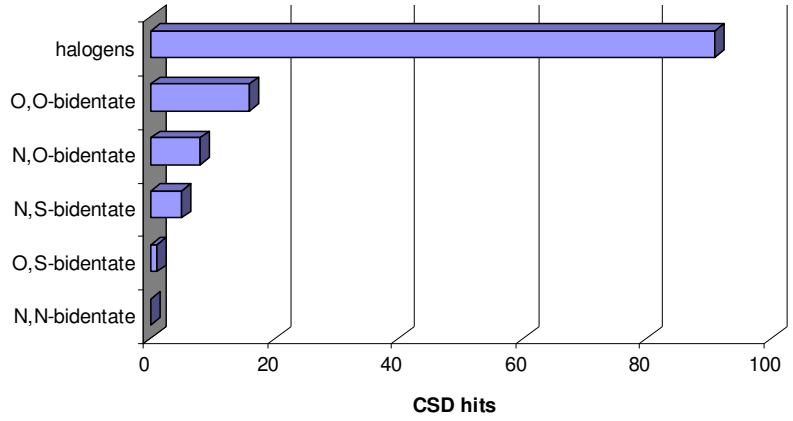

Figure 2.2 A graph showing search results from the Cambridge Structural Database[8,9] (CSD) with 1,5-cyclo-octadiene complexes of group 7- 11 transition metals with six membered bidentate ligands.

A search of the Cambridge Structural Database[8,9] (CSD) for 1,5-cyclo-octadiene (cod), group 7-11 transition metals with a series of ligands, six membered bidentate ring systems with a combination of oxygen, nitrogen and sulfur as donor atoms, yielded interesting results in that although cod is a well known ligand it is predominantly paired with halogens (Figure 2.2).

---

[1] Mehrotra R.C., Bohra R., Gaur D.P., *Metal β-Diketonates and Allied Derivatives*, Academic Press, Burlington USA, 1-3, (1978)
[2] Cotton F.A., Wilkinson G., Murillo C.A., Bochmann M., *Advanced Inorganic Chemistry 6th edition*, John Wiley & Sons, 47-480, (1999)
[3] Combs A., *Ann. Chim.*, **12**, 199, (1887)
[4] Claisen L., Stylos N., *Ber.*, **21**, 1144, (1888)
[5] Hauser C.R., Levine R., Kibler R.F., *J. Am. Chem. Soc.*, **68**, 26, (1946)
[6] March J., *Advanced Organic Chemistry 3rd Edition,* John Wiley & Sons, New York, 437, (1985)
[7] Park K., Cox L.J., *Tetrahedron Letters*, **44**, 1067, (2003)
[8] Allen F.H., *Acta. Cryst.*, **B58**, 380, (2002)
[9] Bruno I.J., Cole J.C., Edginton P.R., Kessler M., Macrae C.F., McCabe P., Pearson J., Taylor R., *Acta. Cryst.*, **B58**, 389, (2002)

The most predominant of the bidentate six membered ligand systems is that of oxygen-oxygen, this is partly due to their availability and their uses in chemical and photochemical deposition[10], metal-organic frameworks (MOFs), heterogeneous and homogenous[11] catalysis, enantioselective separation[12] and light-emitting diodes[13] (LEDs). The second highest in the sequence was that of the nitrogen-oxygen bidentate ring systems.

Relevant information from the CSD pertaining to the O,O-bidentate transition metal complexes bond distances and angles that are of interest to this study were obtained and are given in Table 2.1 and Figure 2.3.

[10] Kunkely H., Vogler A., *Z. Naturforsch*, **58b**, 704, (2003)
[11] Åkermark B., Martin J., Nyström J-E., Strömberg S., Svensson M., Zetterberg K., Zuber M., *Organometallics*, **17**, 5367, (1998)
[12] Ye Q., Wang X-S., Zhao H., Xiong R-G., *Chem. Soc. Rev.*, **34**, 208, (2005)
[13] Zhao Q., Jiang C-Y., Shi M., Li F-Y., Yi T., Cao Y., Huang C-H., *Organometallics*, **25**, 3631, (2006)

Table 2.1 CSD Search results of O,O-bidentate transition metal systems.

Complex	CSD Ref	M-O_1	M-O_2	O-M-O	C=C	C=C	Ce-M-Ce
[Rh(cod)(bta)][a]	BFACRH[14]	2.063	2.048	90.27	1.41	1.394	89.66
[Pt(cod)(acac)]BF_4	BIWHUK10[15]	2.121	1.995	96.04	1.316	1.336	90.70
[Ir(cod)(acac)$(Cl)_2$]	CESPEV[16]	2.021	2.021	94.83	1.377	1.377	86.30
[Rh(cod)(acac)]	COCACR[17]	2.066	2.054	90.09	1.401	1.412	87.90
[Cu(cod)(hfacac)]	KUDFIY[18]	1.999	2.001	93.30	1.366	1.332	86.22
[Rh(cod)(fca)][b]	LABLIJ[19]	2.063	2.038	91.29	1.401	1.396	88.78
[Rh(cod)(tfacac)]	LEVCEU[20]	2.055	2.068	90.84	1.417	1.397	89.12
[Ir(cod)(hfacac)]	QOZZAG[21]	2.064	2.067	90.57	1.398	1.42	88.50
[Ir(cod)(acac)]	QQQCXV01[22]	2.044	2.038	91.57	1.407	1.395	88.80
[Rh(cod)(hfacac)]	RAFNER[23]	2.067	2.069	90.10	1.377	1.393	87.91
[Ir(cod)(acac)(I)(CH_3)]	VAZBED[24]	2.05	2.048	95.84	1.409	1.373	88.47
[Rh(cod)(acPh)][c]	VOTCUC[25]	2.019	2.055	89.62	1.409	1.405	88.68
[Rh(cod)(bncmp)][d]	WUQHUL[26]	2.074	2.047	90.30	1.408	1.372	89.37
[Rh(cod)(MePhthpyr)][e]	XUDGIM[27]	2.067	2.077	91.24	1.415	1.411	89.07
[Rh(cod)(heptacac)][f]	ZIQXEC[28]	2.049	2.055	90.31	1.364	1.383	88.74
[Ag(cod)(hfacac)]$_2$	HEDLAD[29]	2.559	2.541	67.10	1.311	1.24	74.97

a bta – benzoyl-1,1,1-trifluoracetonato
complex name: (Benzoyl-1,1,1-trifluoroacetonato)-(cyclo-octa-1,5-diene)-rhodium(I)
b fca – 1-ferrocenyl-1,3-butanedionato
complex name: (η^4-1,5-Cyclo-octadiene)-(1-ferrocenyl-1,3-butanedionato)-rhodium(I)
c acPh – 2'-acetylphenoxy-O,O'
complex name: (η^4-1,5-Cyclo-octadiene)-(2'-acetylphenoxy-O,O')-rhodium(I)
d bncmp – (1R)-(+)-3-benzoylcampforyl
complex name: (η^4-1,5-Cyclo-octadiene)-((1R)-(+)-3-benzoylcampforyl)-rhodium(I)
e MePhthpyr – 1-penyl-3-methyl-4-(2-thienoyl)pyrazole-5-one
complex name: (η^4-1,5-Cyclo-octadiene)-(1-penyl-3-methyl-4-(2-thienoyl)pyrazole-5-one)-rhodium(I)
f heptacac – 2,2-Dimethyl-7-(6,6-dimethylbicyclo(3.1.1)hept-2-en-2-yl)hept-6-ene-3,5-dionato
complex name: μ^2-η^4-2,2-Dimethyl-7-(6,6-dimethylbicyclo(3.1.1)hept-2-en-2-yl)hept-6-ene-3,5-dionato-O,O')-(η^4-1,5-cyclo-octadiene)-rhodium-tricarbonyl-iron

[14] Leipoldt J.G., Basson S.S., Lamprecht G.J., Bok L.D.C., Schlebusch J.J.J., *Inorg. Chim. Acta.*, **40**, 43, (1980)
[15] Venkatasubramanian K., *Proc. Indian Acad. Chem. Sci.*, **93**, 1237, (1984)
[16] Tucker P.A., *Acta Cryst.*, **C40**, 620, (1984)
[17] Tucker P.A., Scutcher W., Russell D.R., *Acta. Cryst.*, **B31**, 592, (1975)
[18] Chi K.M., Shin H.-K., Hampden-Smith M.J., Duesler E.N., Kodas T.T., *Polyhedron*, **10**, 2293, (1991)
[19] Swarts J.C., Vosloo T.G., Leipoldt J.G., Lamprecht G.J., *Acta Cryst.*, **C49**, 760, (1993)
[20] Duan Z., Hamden-Smith M.J., Duesler E.N., Rheingold A.L., *Polyhedron*, **13**, 609, (1994)
[21] Xu C., Baum T.H., Rheingold A.L., *Chem. Mater.*, **10**, 2329, (1998)
[22] Tucker P.A., *Acta. Cryst.*, **B37**, 1113, (1981)
[23] Angermund K., Baumann W., Dinius E., Fornika R., Gorls H., Kessler M., Kruger C., Leitner W., Lutz F., *Chem. Eur. J.*, **3**, 755, (1997)
[24] Basson S.S., Leipoldt J.G., Purcell W., Schoeman J.B., *Acta. Cryst.*, **C45**, 2000, (1989)
[25] Cullen W.R., Rettig S.J., Wickenheiser E.B., *J. Mol. Catal.*, **66**, 251, (1991)
[26] Spannenberg A., Fdil N., Firdoussi L.B., Karim A., *Z. Kristallogr. – New Cryst. Struct.*, **217**, 549, (2002)
[27] Pettinari C., Marchetti F., Cingolani A., Bianchini G., Drozdov A., Vertlib V., Troyanov S., *J. Organomet. Chem.*, **651**, 5, (2002)
[28] Englert U., Kaser M., Salzer A., *Inorg. Chem.*, **34**, 6231, (1995)
[29] Bailey A., Corbitt T.S., Hampden-Smith, Duesler E.N. Kodas T.T., *Polyhedron*, **12**, 1785, (1993)

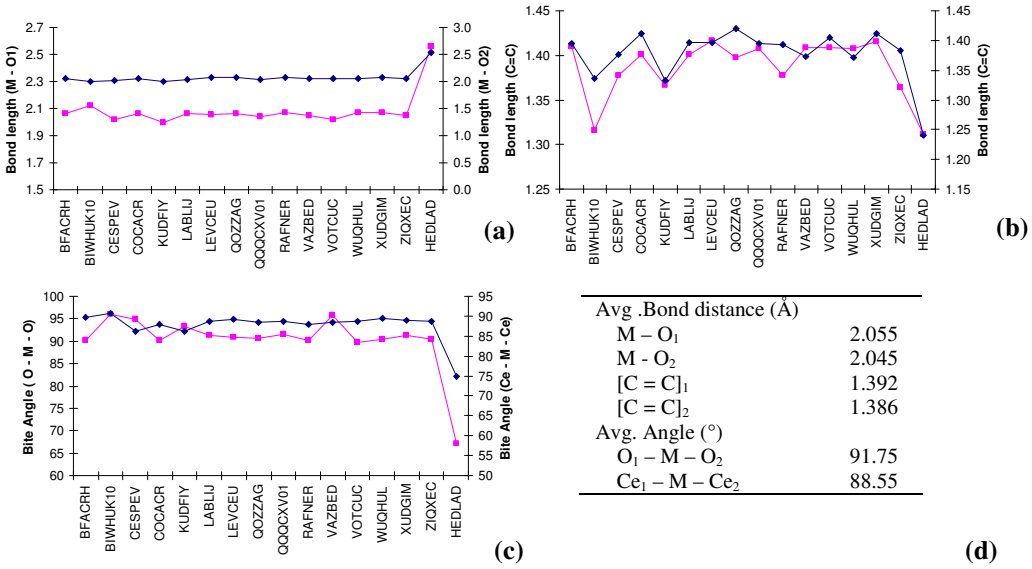

Avg .Bond distance (Å)	
$M - O_1$	2.055
$M - O_2$	2.045
$[C = C]_1$	1.392
$[C = C]_2$	1.386
Avg. Angle (°)	
$O_1 - M - O_2$	91.75
$Ce_1 - M - Ce_2$	88.55

Figure 2.3 Graphs showing (a) O,O-bidentate ligands (M-O) selected bond distances (Å) where M-O_1 (pink squares), M-O_2 (blue diamonds) , (b) cyclo-octadine (C=C) selected bond distances (Å) and (c) O-M-O bite angle (°, pink square) and centriod metal centriod angle (°, blue diamond) *vs.* CSD codes of compounds. (d) Table of average bond distances (Å) and angles (°) as from the above search.

Figure 2.3 it is observed that HEDLAD (Figure 2.4a) is an exception to the general trend, this is as a result of the O,O-bidentate ligand bridging between two silver atoms altering the binding mode of the metal centre. It can be seen in Figure 2.3c that the VAZBED (Figure 2.4b) oxygen metal oxygen bite angle is also an outlier due to the compound not having a square planar geometry but rather octahedral geometry, the oxidation state of the metal centre (iridium) changes from +1 to +3.

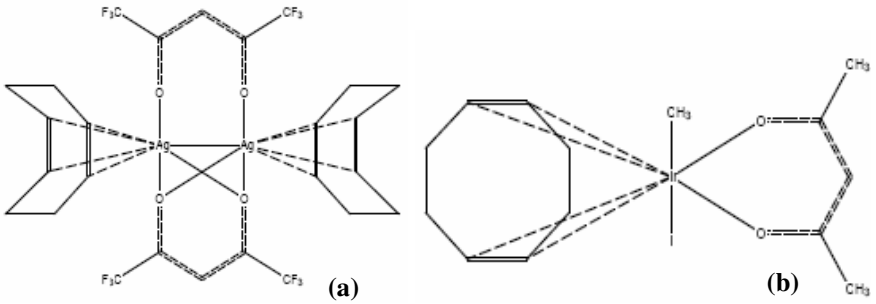

Figure 2.4 Structures of (a) HEDLAD and (b) VAZBED.

A table listing the average bond distances and angles found for the N,O-bidentate transition metal complexes is portrayed in Figure 2.3.. The metal oxygen (M-O_1 and M-O_2) and olefinic carbon (C=C) bond distances are given as two separate values, the reason being the unsymmetrical nature of several bidentate ligands resulting in non-

symmetrical distances. A complete listing of the bond distances and angles can be found in Table 2.1.

Relevant information from the CSD pertaining to the N,O-bidentate transition metal complexes bond distances and angles that are of interest to this study were obtained and are given in Table 2.2 and Figure 2.5.

Table 2.2 CSD Search results of N,O-bidentate transition metal systems.

Complex	CSD Ref	M-O	M-N	O-M-N	C=C	C=C	Ce-M-Ce
[Rh(cod)(PhEt-Salen)][a]	EDOSAS[30]	2.027	2.084	90.93	1.396	1.378	87.41
[Rh(cod)(N26iPrPh-acac)][b]	HIHRUM[31]	2.040	2.098	90.43	1.398	1.402	87.10
[Ir(cod)(PhMe-Salen)][c]	MIJPIF[32]	2.020	2.066	90.66	1.418	1.399	87.62
[Ir(cod)(Ph-Salen)][d]	MIJPOL[32]	2.029	2.073	90.38	1.410	1.407	87.23
[Ir(cod)(NMe-tfmp)][e]	ODIXEE[33]	2.039	2.112	88.05	1.403	1.391	87.74
[Rh(cod)(NpTol-acac-EtOidenyl)][f]	QENXUC[34]	2.012	2.072	88.72	1.377	1.378	86.89
[Ir(cod)(oTol-Salen)][g]	SCLIRA10[35]	2.004	2.098	90.16	1.414	1.429	88.02
$[Rh_2(cod)_2(Phen\text{-}Salen)]$[h]	SCLIRB10[36]	2.032	2.085	89.34	1.362	1.416	86.80

a PhEt-Salen – (R)-N-phenylethylsalicylaldiminato-N,O
complex name: (η^2,η^2-Cycloocta-1,5-diene)-((R)-N-phenylethylsalicylaldiminato-N,O)-rhodium
b N26iPrPh-acac – 4-(2,6-diisopropylphenylamino)pent-3-en-2-onato
complex name: (η^2,η^2-Cycloocta-1,5-diene)-(4-(2,6-diisopropylphenylamino)pent-3-en-2-onato-N,O)-rhodium
c PhMe-Salen – ((salicylideneamino)methyl)benzene-N,O
complex name: (η^2,η^2-Cycloocta-1,5-diene)-(((salicylideneamino)methyl)benzene-N,O)-iridium
d Ph-Salen – salicylideneaniline-N,O
complex name: (η^2,η^2-Cycloocta-1,5-diene)-(salicylideneaniline-N,O)-iridium
e NMe-tfmp – N-methyl-5,5,5-trifluoro-4-(trifluoromethyl)-4-oxy-2-iminopentane-N,O
complex name: (η^2,η^2-Cycloocta-1,5-diene)-(N-methyl-5,5,5-trifluoro-4-(trifluoromethyl)-4-oxy-2-iminopentane-N,O)-iridium
f NpTol-acac-EtOidenyl – (3aR)-3-(3-ethoxy-4,5,6,7-tetrahydro-3aH-iden-1-yl)-4-(4-tolylamino)-pent-3-en-2-onate
complex name: (η^2,η^2-Cycloocta-1,5-diene)-rhodium(I) (3aR)-3-(3-ethoxy-4,5,6,7-tetrahydro-3aH-iden-1-yl)-4-(4-tolylamino)-pent-3-en-2-onate
g oTol-Salen – o-tolylsalicylaldiminato
complex name: (η^4-cyclo-ocata-1,5-diene)-N-o-tolylslicylaldiminato-iridium(I)
h Phen-Salen – μ^2-N,N'-o-Phenylene-bis(salicylaldiminato)
complex name: (μ^2-N,N'-o-Phenylene-bis(salicylaldiminato))-bis(η^4-cyclo-ocata-1,5-diene)-dirhodium(I)

[30] Enamullah M., Uddin A.K.M.R., Chamayou A.-C., Janiak C., *Z. Naturforsch.*, **B62**, 807, (2007)
[31] Sasamori T., Matsumoto T., Takeda N., Tokitoh N., *Organometallics*, **26**, 3621, (2007)
[32] Yinghuai Z., Yan K.C., Jizhong L., Hwei C.S., Hon Y.C., Emi A., Zhenshun S., Winata M., Hosmane N.S., Maguire J.A., *J. Organomet. Chem.*, **692**, 4244, (2007)
[33] Chen Y.-L., Liu C.-S., Chi Y., Carty A.J., Peng S.-M., Lee G.-H, *Chem. Vap. Deposition*, **8**, 17, (2002)
[34] Aumann R., Gottker-Schnetmann I., Frohlich R., Saarenketo P., Holst C., *Chem –Eur. J.*, **7**, 711, (2001)
[35] Bonnaire R., Manoli J.M., Potyin C., Platzer N., Goasdoue N., *Inorg. Chem.*, **20**, 2691, (1981)
[36] Bonnaire R., Manoli J.M., Platzer N., Goasdoue N., Davoust D., *Inorg. Chem.*, **21**, 2032, (1982)

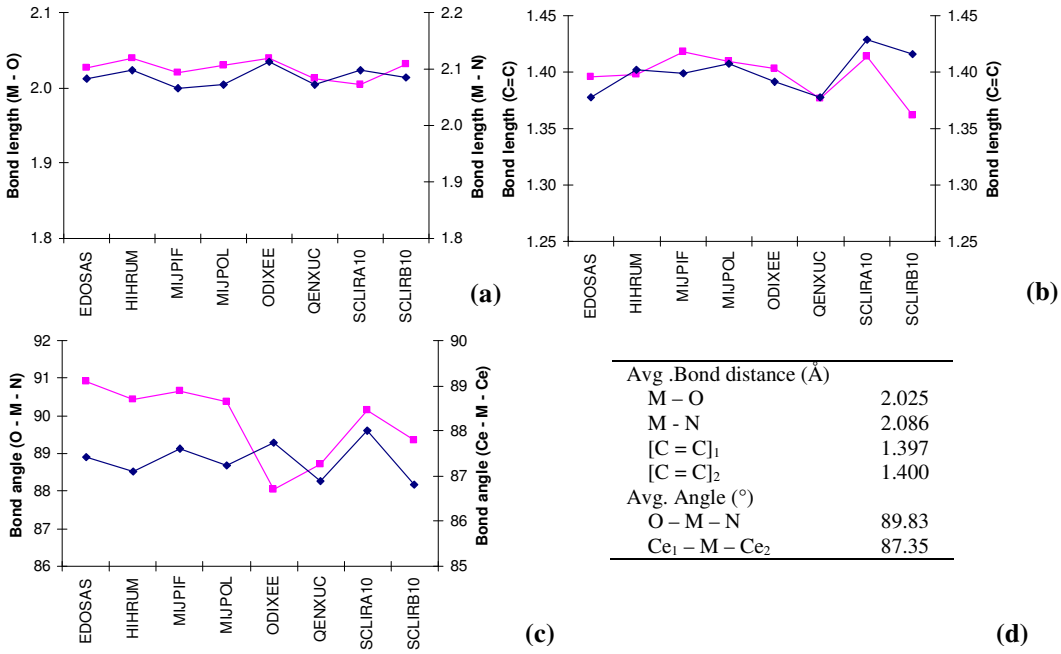

Avg .Bond distance (Å)	
M – O	2.025
M - N	2.086
$[C = C]_1$	1.397
$[C = C]_2$	1.400
Avg. Angle (°)	
O – M – N	89.83
$Ce_1 – M – Ce_2$	87.35

Figure 2.5 Graphs showing (a) N,O-bidentate ligands selected bond distances (Å) where M-O (pink squares), M-N (blue diamonds), (b) cyclo-octadine (C=C) selected bond distances (Å) and (c) O-M-N bite angle (°, pink squares) and centriod metal centriod angle (°, blue diamonds) *vs.* CSD codes of compounds. (d) Table of average bond distances (Å) and angles (°) as from the above search.

A similar set of graphs can be setup for the N,O-bidentate ligands. It is interesting to note that most of the hits that were obtained from the CSD are based on functionalized shiff base N,O chelating ligands. Due to the similar nature for oxygen and nitrogen it is found that the bond lengths given in Figure 2.5a are not significantly different with the metal oxygen bonds being generally shorter than their nitrogen counterparts. A marginally smaller oxygen metal nitrogen bite angle is observed as a result of the conjugation of the phenyl ring in the shiff base. The average centriod metal centriod angle is also found to be smaller for the N,O-chelating bidentate ligands (87.53°) than that found for the O,O-chelating bidentate ligands (88.55°).

A pattern starts developing in that the olefinic bond distances do not significantly change when altering the counter ligand. The centriod metal centriod angle is affected, implying that there is a closing of the ring when moving from the O,O-chelating bidentate ligands to the N,O-chelating bidentate ligands.

2.2 Ligand Effects of β-Diketones, β-Enaminones and Dienes

In looking at ligand effects two major effects are known that of the steric and electronic properties. As previously discussed we have two types of co-ordinating ligands cyclo-octadiene, Venus fly-trap mimicker, and the O,O- and N,O- chelating bidentate ligands. As a sub category the ketimines are also capable of forming stable metal chelates with most transition metals, although they have not been as exhaustively investigated as the O,O-chelates.

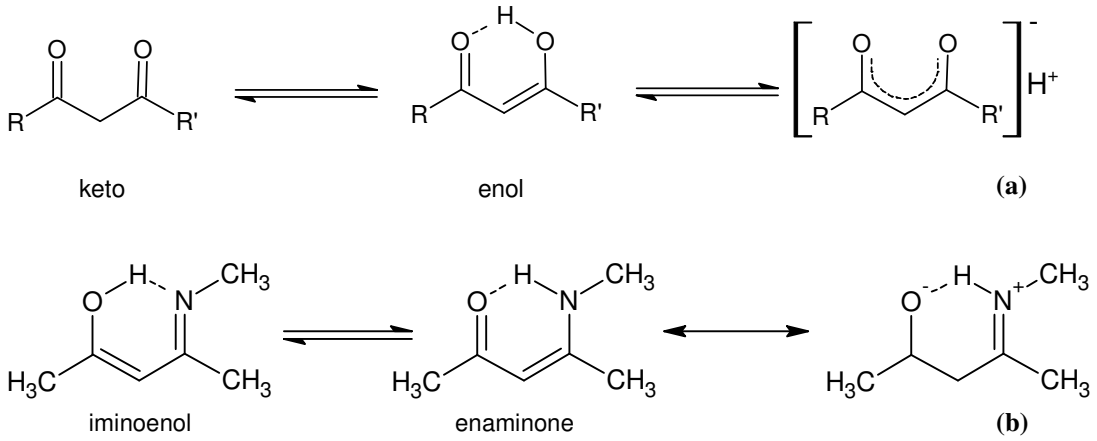

Figure 2.6 The enolization and ionization of (a) β-diketones, α-diketones and (b) β-enaminones.

It should be noted that although β-diketones (six memembered) and α-diketones (five memberd chelate ring) are mostly represented in the ketonic form, many of them exist mainly in the enolic form, which is stabilized by a hydrogen bridge[37]. Figure 2.6a shows the enolization and ionization of β-diketones, as a result of the ability of the ligand to form an anion, very stable metal chelates are formed with most transition metals. Acid base characteristics of these ligands may be tuned by subtle variation of electron withdrawing and donating (R, R') substituents[38].

β-Enaminones are well known for their tautomerism which is stabilized by intramolecular hydrogen bonds (Figure 2.6b) and are generally found in the enaminone conformation. Their co-ordinating characteristics can be varied by the substitution of various alkyl or aryl groups on the nitrogen atom.

[37] Hauser C.R., Swamer F.W, Adams J.T., *Organic Reactions*, John Wiley & Sons, New York, Vol. 8, 61-64, (1954)
[38] Gschneidner K.A., Bünzli J-C.G., Pecharsky V.K., *Handbook on the Physics and Chemistry of Rare Earths, Volume 35*, Elsevier B.V., The Netherlands, 244, (2005)

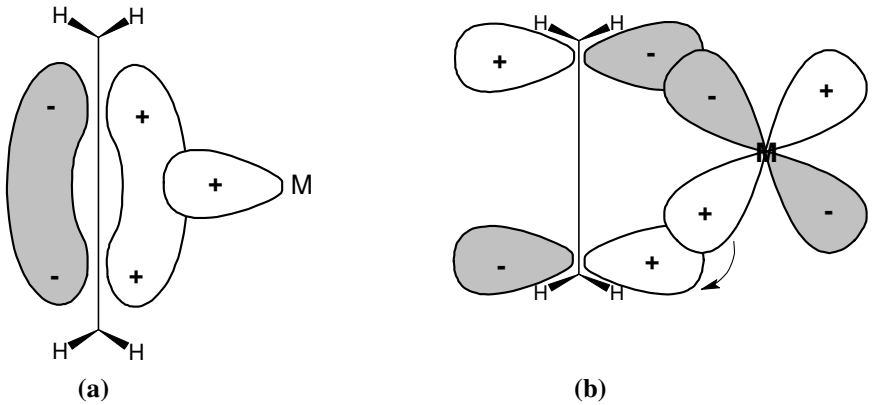

Figure 2.7 Molecular orbital diagrams (Dewar-Chatt-Duncanson bonding model, 1953) showing the synergystic (a) donation of π-electron density from the alkene to the metal (b) and back-bonding from the metal to the π^*-orbital of the alkene.[39]

A depiction of an alkene bond to a transition metal is shown in Figure 2.7, it consists of two interdependent components firstly (Figure 2.7a), that of the overlap of the π-electron density of the alkene with the σ-orbital on the metal centre and secondly (Figure 2.7b), the flow of electron density from the filled d_{xz} (or $d\pi$-$p\pi$ hybrid) metal orbital to the π^*-anti-bonding orbital of the alkene.

With this methodology of bonding significant "double bond" character in the olefinic bon is retained. However, again due to this bonding we find that there is a lengthening of the C-C bond as a result of the donation of π-electrons to the metal σ-orbital as well as electrons into the π^*-anti-bonding orbitals.

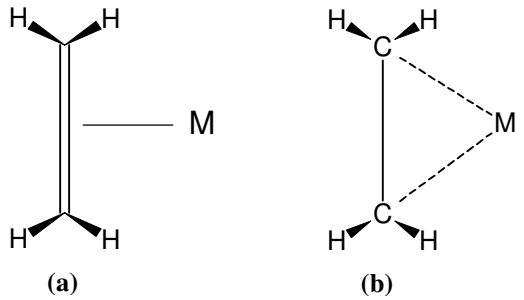

Figure 2.8 Structures of mono –alkene type bonding.

In the case where the C-C bond distance is significantly affected (*i.e.* an electron rich metal centre and / or electron withdrawing groups on the alkene) one may view the bonding type more as a metallocyclopropane ring (Figure 2.8b). There exists the possibility of a formal oxidation of the metal via the transfer of two electrons to the

[39] Cotton F.A, Wilkinson G., Gaus P.L., *Basic Inorganic Chemistry*, 3rd Edition, John Wiley and Sons Inc., 682, (1995)

alkene thus generating a dianionic ligand rather than the neutral two electron donor (Figure 2.8a).

The electronic effects of alkenes can be readily monitored using infra-red (IR) spectroscopy, *i.e.* the larger the back-bonding, the weaker the C-C double bond and the lower the stretching frequency.

Table 2.3 Metal-alkene *ν*(C=C) stretching frequencies.

Alkene Complex	***ν*(C=C) (cm^{-1})**
Free Ethylene	1623
$[Ag(H_2C=CH_2)]^+$	1584
$[(cp)Rh(H_2C=CH_2)]$	1493
$[PtCl_3(H_2C=CH_2)]^-$	1516
$[Pt(H_2C=CH_2)Cl_2]_2$	1506
$[Pd(H_2C=CH_2)Cl_2]_2$	1525
Free cod	
$[Rh(cod)Cl]_2$	1466
$[Pd(cod)Cl_2]$	1523

Table 2.3 lists selected alkene complexes with varying back donation capabilities, it is currently believed that the silver ethylene complex have no back-bonding and thus the lowering in stretching frequency is purely due to the σ-donation from the ethylene to the silver. In the $[PtCl_3(H_2C=CH_2)]^-$ the platinum is found in the +4 oxidation state thus there is less back-bonding between the platinum and the ethylene as opposed to the $[PtCl_2(H_2C=CH_2)]_2$.

Upon investigation of the steric effects of ligands, a few laws hold true. Firstly when *cis-trans* isomerization is possible the *cis* isomer is generally the more stable. Secondly third-row metals form the strongest bonds and most stable complexes. Thirdly metal complexes of ring-strained cycloalkenes (e.g. cyclopropene) display elevated stability. For dienes the stabilization is found in its chelating ability, with the benefit of being relatively labile (*i.e.* readily substituted with a stronger co-ordinating ligand).

2.3 Transition Metal Properties of Middle to Late Transition Metal Complexes

For insight into the middle to late transition metals one starts with their basic properties, *e.g.* oxidation states, co-ordination geometries and radii (Table 2.4).

Table 2.4 Selected properties including atomic, covalent, vd Waals radii, electron configuration of the middle to late transition element.

7	8	9	10	11
^{25}**Mn**	^{26}**Fe**	^{27}**Co**	^{28}**Ni**	^{29}**Cu**
OS 0 d^7	*OS* 0 d^8	*OS* 0 d^9	*OS* **0** d^{10}	*OS*
1 d^6		**1** d^8	1 d^9	**1** d^{10} — Tet or SQ
2 d^5	**2** d^6	**2** d^7 Tet / d^6 Oct	**2** d^8 — Mix	**2** d^9 — *dis*-Oct
3 d^4 } Oct	**3** d^5 } Oct	**3** d^6	3 d^7	3 d^8
4 d^3	**4** d^4	4 d^5	4 d^6	
5 d^2		5 d^4		
6 d^1 } Tet	6 d^2			
7 d^0				
radii[a]	*radii*	*radii*	*radii*	*radii*
Atomic(e) 1.40	Atomic (e) 1.40	Atomic (e) 1.35	Atomic (e) 1.35	Atomic (e) 1.35
(c) 1.61	(c) 1.56	(c) 1.52	(c) 1.49	(c) 1.45
covalent 1.39	covalent 1.25	covalent 1.26	covalent 1.21	covalent 1.38
2008[b] (LS) 1.39	2008 (LS) 1.32	2008 (LS) 1.26	2008 1.24	2008 1.32
2008 (HS) 1.61	2008 (HS) 1.52	2008 (HS) 1.50		
vdWaal na	vdWaal na	vdWaal na	vdWaal 1.63	vdWaal 1.40
^{43}**Tc**	^{44}**Ru**	^{45}**Rh**	^{46}**Pd**	^{47}**Ag**
OS 0 d^7	*OS* **0** d^8	*OS* 0 d^9	*OS* **0** d^{10}	*OS* 0 d^{11}
1 d^6	1 d^7	**1** d^8 — SQ or 5-Co		**1** d^{10}
2 d^5	**2** d^6 — Oct or 5-Co	2 d^7	**2** d^8 — SQ or 5-Co	**2** d^9
3 d^4	**3** d^5 } Oct	**3** d^6 } Oct		**3** d^8 — Oct
4 d^3	**4** d^4 } Oct	**4** d^5 } Oct	4 d^6 — Oct	
5 d^2	5 d^3	5 d^4	5 d^5	
6 d^1	6 d^2	6 d^3	6 d^4	
7 d^0	7 d^1			
	8 d^0			
radii	*radii*	*radii*	*radii*	*radii*
Atomic (e) 1.35	Atomic (e) 1.30	Atomic (e) 1.35	Atomic (e) 1.40	Atomic (e) 1.60
(c) 1.83	(c) 1.78	(c) 1.73	(c) 1.69	(c) 1.65
covalent 1.56	covalent 1.26	covalent 1.35	covalent 1.31	covalent 1.53
2008 1.47	2008 1.46	2008 1.42	2008 1.39	2008 1.45
vdWaal na	vdWaal na	vdWaal na	vdWaal 1.63	vdWaal 1.72
^{75}**Re**	^{76}**Os**	^{77}**Ir**	^{78}**Pt**	^{79}**Au**
OS 0 d^7	*OS* **0** d^8	*OS* 0 d^9	*OS* 0 d^{10}	*OS* 0 d^{11}
1 d^6		**1** d^8 — SQ or 5-Co		**1** d^{10}
2 d^5	2 d^6 — Oct or 5-Co	2 d^7	**2** d^8 — SQ or 5-Co	**2** d^9
3 d^4	**3** d^5	**3** d^6	3 d^7	**3** d^8
4 d^3	**4** d^4	**4** d^5	**4** d^6	
5 d^2	5 d^3	5 d^4	5 d^5	
6 d^1	6 d^2	6 d^3	6 d^4	
7 d^0	7 d^1			
	8 d^0			
radii	*radii*	*radii*	*radii*	*radii*
Atomic (e) 1.35	Atomic (e) 1.30	Atomic (e) 1.35	Atomic (e) 1.35	Atomic (e) 1.35
(c) 1.88	(c) 1.85	(c) 1.80	(c) 1.77	(c) 1.74
covalent 1.59	covalent 1.28	covalent 1.37	covalent 1.28	covalent 1.44
2008 1.51	2008 1.44	2008 1.41	2008 1.36	2008 1.36
vdWaal na	vdWaal na	vdWaal na	vdWaal 1.75	vdWaal 1.66

OS – Oxidation States, most common in bold type.
Common stereochemistries - Oct – octahedral, Tet – tetrahedral, SQ – square planar, Mix (Ni) – octahedral, trigonal bipyramidal, square pyramidal, tetrahedral & square planar, 5-Co – trigonal bipyramidal & square pyamidal.
Radii – Atomic (e) – empirical, Atomic (c) – calculated, na – not available, LS – low spin, HS – high spin.
a http://www.webelements.com
b Cordero B., Gómez V., Platero-Prats A.E., Revés M., Echeverría J., Cremades E., Barragán F., Alvarez S., *Dalton Trans.*, (2008)

In Table 2.4 the periodic group's seven to eleven are listed, below the element name the oxidation states in which the element can be found, the most common oxidation states are denoted in bold type. Both silver and gold have an *s* electron outside a completed *d* shell limiting the similarities with the last element in group eleven that of copper.

Both the empirical and calculated atomic radii are presented, the covalent radii are listed, the updated values (2008, high spin and low spin where available) obtained by Cordero *et al.* are shown as well. For the first row, it is interesting to note that the atomic and covalent radii are not significantly different, this trend continues to the second and third rows as well. The only exception to this trend is that of silver. A similar trend can be found for the individual groups.

For the purpose of this study we will be looking at the square planar stereochemistry of the transition metals. This places group seven in the d^6 configuration state whereas group's eight to ten are in the d^8 configuration state and group eleven is found in the d^{10} configuration. Square planar geometry is associated with four co-ordinating ligands to a metal centre, there are only two possible geometric isomers, namely that of *cis* and *trans*. The plane of the molecule is the internal mirror plane, and these compounds are rarely chiral though exceptions are known to exist. Due to the planar nature of these compounds they are often found stacked in crystal structures, thus leading to possible weak metal to metal interactions. Even though the distances for true metal to metal bonding maybe to long, interactions can occur between *d* orbitals on adjacent metal atoms.

2.4 General Homogeneous Catalytic Processes

There are two categories of catalytic behavior namely that of homogeneous and heterogeneous. The primary difference between heterogeneous and homogeneous is that the homogenous catalyst and substrates are found in one phase. The other advantages of homogenous catalysis is in the ability to determine and understand the mechanism of the catalytic cycle and to tailor and optimize the catalyst.

A historical time line of homogeneous catalytic processes mostly for olefins is as follows.

- 1950's
  - Wacker[40] process uses ethylene for an oxidative conversion to acetaldehyde.
  - Oligomerization of ethene using cobalt complexes[41]
- 1960's
  - Nickel hydrocyanation (DuPont)[42]
  - Cobalt carbonylation of methanol (BASF)[43]
  - Cobalt hydroformylation (Shell - 1938 Ruhrchemie)[44,45]
  - Molybdenum epoxidation of propene[46] (Halcon Corporation)
- 1970's
  - Rhodium carbonylation of methanol[47] (Monsanto)
  - Rhodium hydroformylation[48] (Union Carbide Corporation[49])
  - Shell's higher olefin process[50,51]
  - Asymmetric hydrogenation to L-DOPA[52] (Monsanto)
  - Ring-opening polymerization of cyclo-octene (Huels)[53]
- 1980's
  - Aqueous biphasic two-phase oxo process[54] (Rhône Poulenc / Rhurchemie)

[40] Reinhard J., *Angew. Chem. Int. Ed.*, **48**, 9034, (2009)
[41] Burnham D.R., *Oligomerization of Ethylene*, Imperial Chemical Industries Limited, US Patent 4032590, (1977)
[42] Arthur Jr. P., Pratt B.C., E.I. DuPont de Nemours & Co., US Patent 2.571.099, (1951)
[43] Kummer R., Schwirten K., BASF AG, DE Patent 3.301.591, (1983)
[44] Roelen O., *ChED Chem. Exp. Didakt.*, **3**, 119, (1977)
[45] Kohlpaintner C., *Hydroformylation – Industrial. Encyclopedia of Catalysis*, John Wiley and Sons Inc., (2002)
[46] Sheldon R.A., *Recueil des Travaux Chimiques des Pays-Bas*, **92**, 367, (1973)
[47] Haynes A., Mann B.E., Gullivier D.J., Morris G.E., Maitlis P.M., *J. Am. Chem. Soc.*, **113**, 8567, (1991)
[48] Buisman G.J.H., Vos E.J., Kamer P.C.J., van Leeuwen P.W.N.M., *J. Chem. Soc., Dalton Trans.*, 409, (1995)
[49] Babin J.E., Whitecker G.T, Union Carbide, PCT Int. Appl. WO 93/03839, (1993)
[50] Reuben B., Wittcoff H., *J. Chem. Educ.*, **65**, 605, (1988)
[51] Kuhn P., Sémeril D., Matt D., Chetcuti M.J. Lutz P., *J. Chem. Soc., Dalton Trans.*, 515, (2007)
[52] Knowles W.S., *J. Chem. Ed.*, **63**, 222, (1986)
[53] Jadamus H., Ribbing W., Feinauer R., Schafer W., Chemische Werke Huls Aktiengesellschaft, US Patent 4656220, (1987)
[54] Kohlpaintner C., Fischer R.W., Cornils B., *Appl. Cat.*, **A221**, 219, (2001)

- 1990's
    - Improved the LP oxo process[55] (Union Carbide Corporation and Davy Process Technology Limited)
- 2000's
    - Oxo alcohols process[55], formerly ICI high pressure oxo process (Davy Process Technology Limited and Johnson Matthey)
    - Hydration of ethylene[56] for production of ethanol

As has already been mentioned 1,5-cyclo-octadiene (cod) is produced from butadiene in the presence of a nickel catalyst, cod is mainly converted to cyclo-octene.

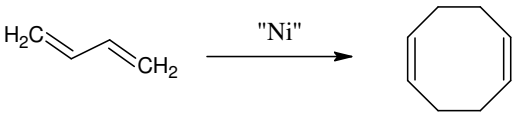

When looking at a catalyst there are several aspects that need to be kept in mind

- Ligand Effects
- Anion Effects
- Creation of a "vacant" site
- Co-ordination of the substrate
- Activation of the substrate

Ligand effects mainly comprise of both steric and electronic properties, which have been previously discussed in § 2.2. Anion effects have been overlooked but recent interest into weakly co-ordinating anions has allowed for greater control over the species that are formed in the reactor. The anion effect also has the additional benefit of helping with the creation of the "vacant" site on the catalyst precursor which was originally achieved by Lewis acids. Lastly there are instances of the anion being a reactant as well an example of this is the palladium cross-coupling reactions.

There are several methods of activation of the substrate the most common for alkenes being that of nucleophilic attack.

[55] Tudor R., Ashley A., *Platinum Metals Review*, **51**, 116, (2007)
[56] Fougret C.M., Holderich W.F., *Appl. Catal. A. General*, **207**, 295, (2001)

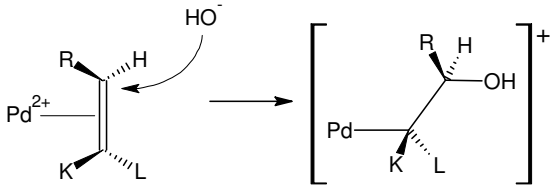

Scheme 2.1 Nucleophilic attack of a co-ordinated alkene.

Co-ordination of an alkene to a cationic metal complex activates the alkene for a nucleophilic attack. After the nucleophilic attack the metal alkene complex has been converted into a σ-bonded alkyl complex with the nucleophile at the β-position (Scheme 2.1) giving rise to the *anti*-addition product. The Wacker-type processes catalyzed by palladium utilize this directionality as their key step.

As the field of homogeneous catalysis is so extensive only a few select examples of alkene interacting catalysis will be discussed.

The first being hydrogenation of alkenes the most well-known being that of Wilkinson's[57] catalyst [$Rh(Cl)(PPh_3)_3$].

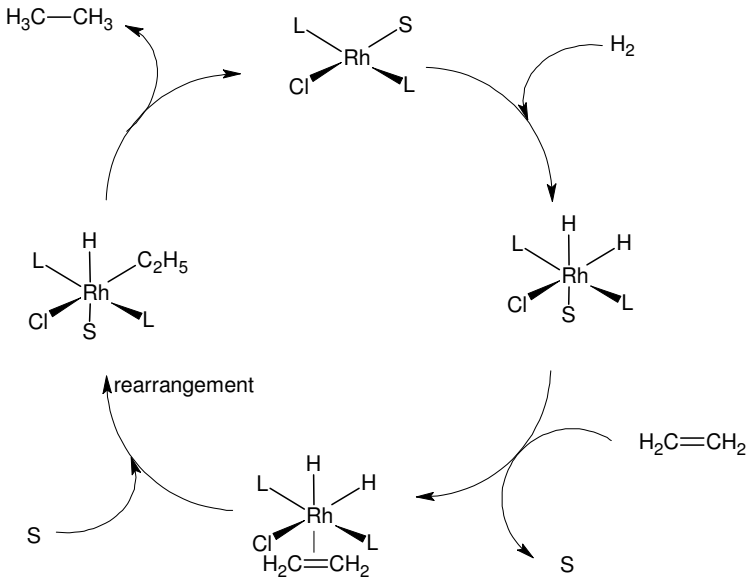

Scheme 2.2 Wilkinson's hydrogenation cycle

From Scheme 2.2 a metal dihydride intermediate is formed prior to the binding of the unsaturated molecule. This is then followed by a four-centered rearrangement which leads to a σ-bonded metal alkyl; the cycle is completed by the loss of an alkane from the metal in a reductive elimination step. An alternative to the aforementioned cycle

[57] Jardine F.H., Osborn J.A., Wilkinson G., *J. Chem. Soc.*, **A**, 1574, (1967)

is that the two hydrogens attached to the metal centre can transfer simultaneously to the co-ordinated alkene, which could result in a concerted reaction.

There are three groups of hydrogenation catalysts that are of interest namely that of Crabtree's[58], Pfaltz's[59] phosphine-oxazoline and Burgess'[60] carbine-oxazoline catalysts seen in Figure 2.9.

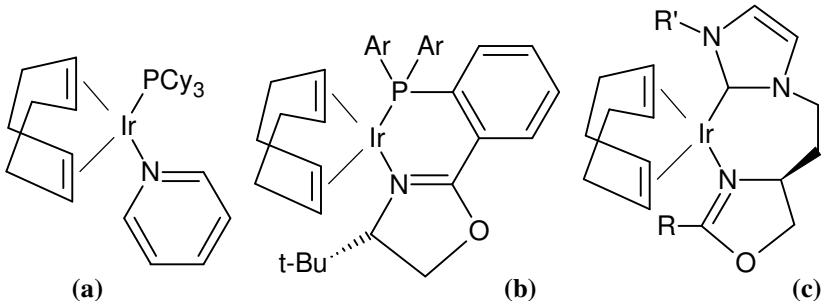

Figure 2.9 Structures of hydrogenation catalysts (a) Crabtree's catalyst[58] where Cy = cyclohexyl, (b) Pfaltz's phosphine-oxazoline[59] where Ar = aryl, *t*-Bu = *tert*-butyl and (c) Burgess' carbene-oxazoline[60] where R = 1-adamantyl, R' = 2,6-diisopropylbenzene.

The next type of catalytic cycle that will be discussed is that of hydrogen-transfer isomerizations.

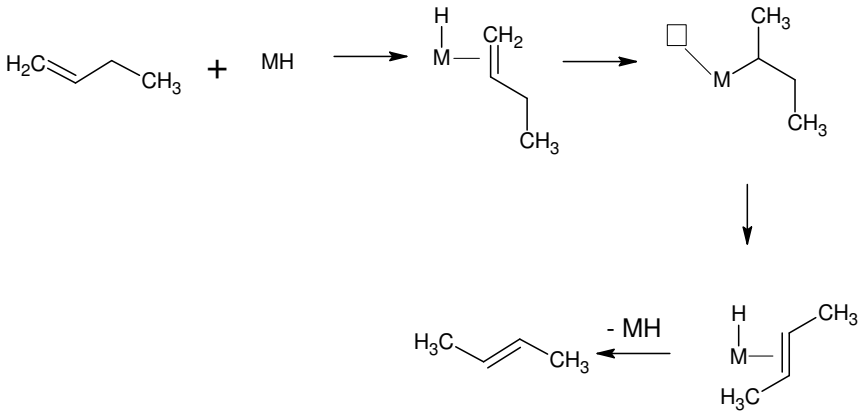

Scheme 2.3 Simplified isomerization scheme involving β-elimination

Shaw and Tucker[61] proposed three mechanisms for hydrogen transfer isomerization.

[58] Crabtree R., *Acc. Chem. Res.,* **12**, 331, (1979)
[59] Pfaltz A., Blankenstein J., Hilgraf R., Hörmann E., McIntyre S., Henges F., Schönleber M., Smidt S.P., Wüstenberg B., Zimmerman N., *Adv. Synth. Catal.*, **345**, 33, (2003)
[60] Cui X., Ogle J.W., Burgess K., *Chem. Commun.*, 672, (2005)
[61] Shaw B.L., Tucker N.I., *Comprehensive Inorganic Chemistry*, ed. J.C. Bailar, Pergamon, Oxford, chapter 53, (1973): *Pergamon Texts in Inorganic Chemistry*, vol 23

Firstly the binding of the metal hydride to the unsaturated molecule a migratory insertion process occurs thereafter a β-elimination with the cycle being completed with the loss of the metal hydride (Scheme 2.3).

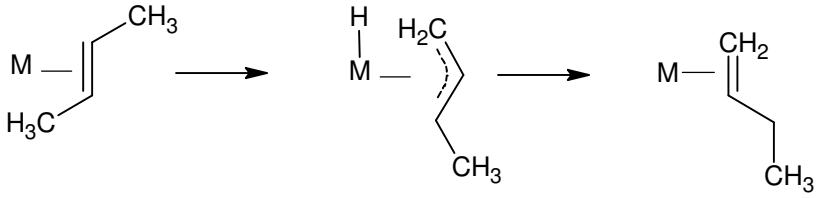

Scheme 2.4 Simplified isomerization scheme involving π-allylic hydride intermediate

The second mechanism that has been proposed is that of one with the formation of allylic intermediates (1,3 shift of hydrogen), thus making the presence of the hydride non-critical (Scheme 2.4). The last mechanism proposed is a 1,2-hydrogen shift involving a carbene intermediate.

An example of isomerization catalysis is the DuPont process for making adiponitrile[62] in which internal pentenenitriles need to be converted to terminal alkenes.

The last type of catalytic process to be discussed is that of hydroformylation. This covers two important examples namely that of the cobalt catalyzed hydroformylation which covers the well-known Fischer-Tropsch reaction and the rhodium catalyzed hydroformylation which covers the Union Carbide process.

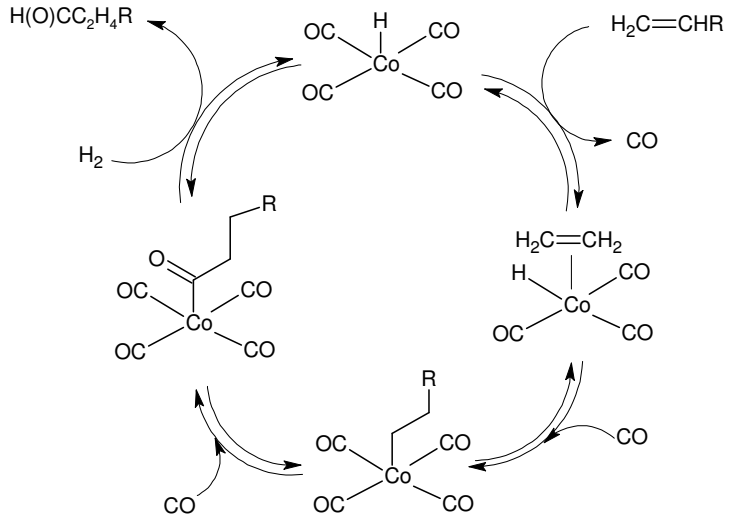

Scheme 2.5 Simplified mechanism of the cobalt catalyzed hydroformylation

[62] McKinney R.J., Roe D.C., *J. Am. Chem. Soc.*, **108**, 5167, (1986)

The catalytic cycle for the cobalt catalyzed hydroformylation is shown in Scheme 2.5. The first step is the replacement of a carbon monoxide ligand by an alkene. There after the migration of the hydride ion give an alkyl cobalt complex, which may be either linear or branched. An incoming carbon monoxide occupies the vacant site. The migration of the alkyl to a co-ordinated carbon monoxide to give an acyl complex. Lastly dihydrogen reacts with the acyl complex to form the aldehyde product and regenerates the starting complex.

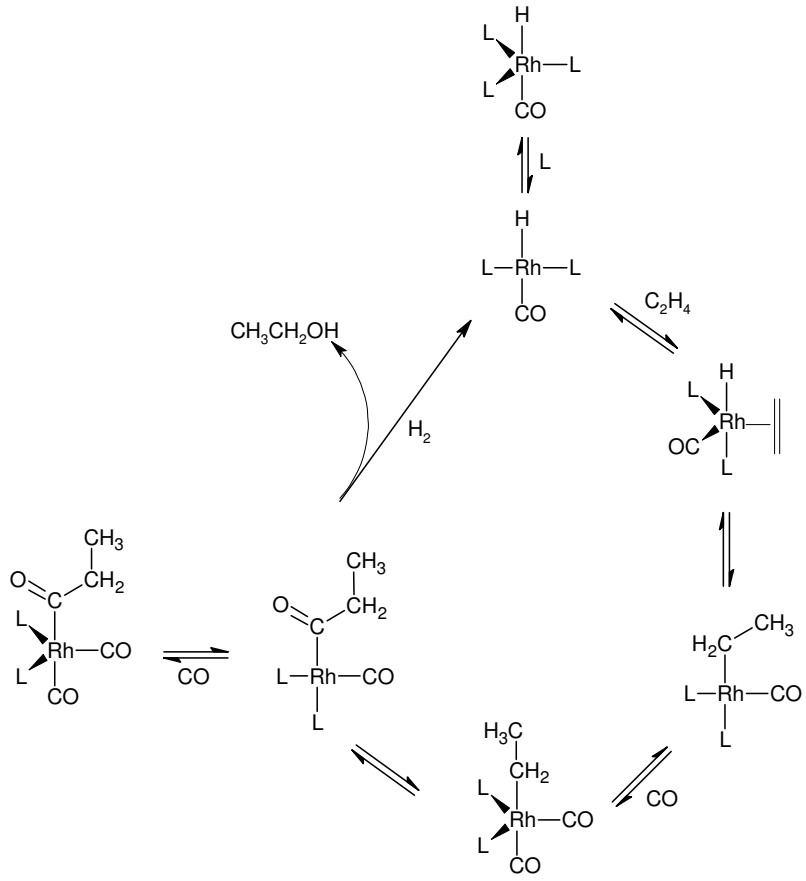

Scheme 2.6 Simplified mechanism of the rhodium catalyzed hydroformylation

The catalytic cycle for the rhodium catalyzed hydroformylation is shown in Scheme 2.6. The first step is the addition of the alkene followed by insertion of the alkene into the Rh-H bond to give the alkyl complex. The latter complex undergoes addition of carbon monoxide followed by migratory insertion of carbon monoxide into the Rh-C bond to yield the acyl derivative. Oxidative addition of H_2 then gives the dihydido acyl complex which is followed by reductive elimination of the aldehyde to reform the original complex in the catalytic cycle.

2.5 General Medical Characteristics of O,O-Bidentate and Olefin Transition Metal Complexes

As early as the sixteenth century metal or metal-containing compounds have been used in the treatment of illnesses. With the current pandemic of cancers in modern society[63,64] the study of possible treatments has become of prime importance. With the discovery of *cis*-diamminedichloroplatinum(II) otherwise known as cisplatin[65] (Figure 2.10a) anti-tumor activity the hunt was full swing. However, even with this necessity cisplatin and *cis*-diammine-1,1'-cyclobutane dicarboxylate platinum(II) (carboplatin Figure 2.10b) are still the only treatments that are widely used, even with their well documented and potential severe side effects[66,67]. Over 3000 platinum analogues of cisplatin have been synthesized but few have made it to clinical trails[68].

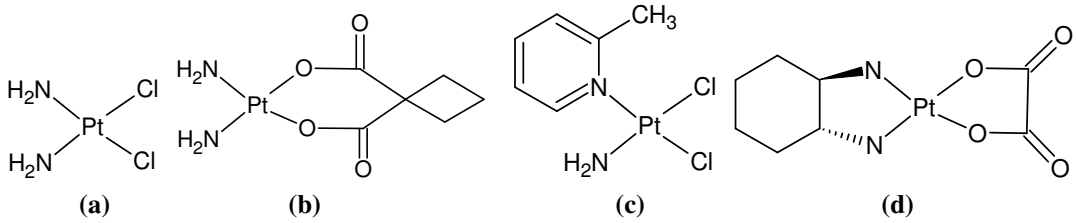

Figure 2.10 Structures of complexes of possible and current anti-tumor drugs (a) cisplatin (b) carboplatin (c) AMD-473 (d) oxaliplatin.

The most prominent of these aside the previously mentioned cisplatin and carboplatin are AMD-473 (Figure 2.10c), which shows promising *in vitro* activity against cisplatin-resistant A2780cisR cells[66,69] and oxaliplatin (Figure 2.10d) which has been approved for clinical use in Europe, China and the United States.

[63] Shibuya K., Mathers C.D., Boschi-Pinto C., Lopez A.D., Murray C.J.L., *BMC Cancer*, **2**, 37, (2002)
[64] Schwartsmann G. Ratain M.J., Cragg G.M., Wong J.E. Saijo N., Parkinson D.R., Fujiwara Y., Pazdur R., Newman D.J., Dagher R., Di Leone L., *J. Clin. Oncol.*, **20**, 47, (2002)
[65] Rosenberg B., Van Camp L., Krigas T., *Nature*, **205**, 698, (1965)
[66] Kelland L.R., Sharp S.Y., O'Neill C.F., Raynaud F.I., Beale P.J., Judson I.R., *Inorg. Biochem.*, **77**, 111, (1999)
[67] Cadron I., Leunen K., Amant F., van Grop T., Neven P., Vergote I., *Gynecol. Oncol.*, **106**, 354, (2007)
[68] Marzano C., Trevisan A., Giovagnini L., Fregona D., *Toxicology in Vitro*, **16**, 413, (2002)
[69] Holford J., Sharp S.Y., Murrer B.A., Abrams M., Kelland L.R., *Br. J. Cancer*, **77**, 366, (1998)

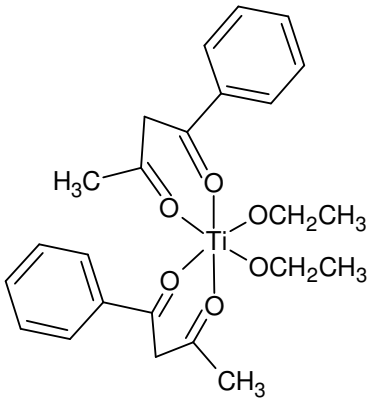

Figure 2.11 Structure of budotitane (*cis*-dietoxybis(1-penylbutane-1,3-dionato)titanium(IV))[70].

Budotitane (*cis*-dietoxybis(1-penylbutane-1,3-dionato)titanium(IV) Figure 2.11) is one the first non-platinum metal drugs to reach phase I clinical trials[70] many analogs of the β-diktonato complexes that have been prepared have been screened for anti-cancer activity[71].

Palladium(II) is known to be both isoelectronic and isostructural to platinum(II) as a result recent interest in the development of anti-cancer drugs of palladium(II) which are analogous to that of the platinum dugs have been investigated[72]. Most notable is that of palladium with the presence of biologically active fragments (O,O chelating ligands) which have shown promising anti-cancer activity *in vitro*[73] against prostatic cancer cell lines. Due to their multifunctional nature they are an interesting and innovative new development in possible anti-cancer treatments in the foreseeable future.

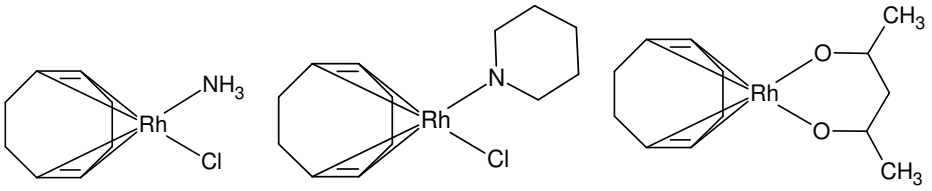

Figure 2.12 Structures of complexes of possible anti-tumor drugs (a) [RhCl(cod)(NH_3)] (b) [RhCl(cod)(piperidine)] (c) [Rh(cod)(acac)]

[70] Keppler B.K., Friesen C., Vongerichten H., Vogel E., *Met. Complexes Cancer Chemother.*, 297, (1993)
[71] Huang R., Wallqvist A., Covell D.G., *Biochem. Pharmacol.*, **69**, 1009, (2005)
[72] Szűčová L., Trávniček Z., Zatloukal M., Popa I., *Bioorg. Med. Chem.*, **14**, 479, (2006)
[73] Crispini A., Ghedini M., Pucci D., *Beilstein J. Org. Chem.*, **5**, (2009)

Rhodium(I), rhodium(II) and rhodium(III) have d^8, d^7 and d^6 electron configurations respectively and are isoelectronic to platinum(II), platinum(III) and platinum(IV). Consequently, they make an interesting alternative to the platinum complexes, however even with activity comparable to cisplatin they are not widely studied. A review has been recently published on rhodium and its potential in cancer treatment[74].

In this review the square-planar [Rh(cod)(acac)] (Figure 2.12c) complex demonstrated activity against leukemia L1210, sarcoma 180, Ehrlich ascites carcinoma and has shown antimetastatic activity in the metastasizing Lewis lung carcinoma. This activity is comparable with cisplatin whilst being only marginally nephrotoxic. Other cyclo-octadiene complexes of rhodium (Figure 2.12a and b) have also displayed antitumor activity against Ehrlich ascities tumors.

Even with the demonstrated activity of other metal based therapeutic drugs the perculation of these complexes into clinical use is still very slow. This is partly due to the limited understanding of the mechanisms and actions of these complexes.

Next, a series of Chapters follow which in a systematic way addresses the aims set out in Chapter 1 § 1.3.

[74] Katsaros N., Anagnostopoulou A., *Critical Reviews in Oncology / Hematology*, **42**, 297, (2002)

Chapter 3
Synthesis and Characterization of Complexes

3.1 Introduction

In this chapter the synthesis and spectroscopic characterization of the functionalized ligands and the co-ordinated compounds prepared during the study are reported. Several of the complexes described in this chapter were also further characterized by means of X-ray crystallography and will be discussed in more detail in later chapters.

The original "Venus fly-trap" mimic is the 1,5-cyclo-octadiene, however it is not the only mimic and for the purposes of this study bicyclo[2.2.1]hepta-2,5-diene (2,5-norbornadiene) was also considered.

The counter ligands were selected for several properties (Table 3.1), the first being O,O-bidentate co-ordination with a chelate ring size of six and five. Examples of these are acetylacetone (Hacac) the six membered chelate O,O-bidentate and tropolone (Htrop) which is a five membered chelate O,O-bidentate. The second being N,O-bidentate six membered chelates, which were synthesized for this study. Lastly, the acid dissociation constant (pK_a) of the ligands which ranged from 4.27 – 9.35, the steric and packing effects of dibenzoylmethane (Hdbm), Htrop and tribromotropolone (H3Br-trop) which are well known for their ability to π-stack in solid state. This phenomenon will be further discussed in the crystallographic chapters.

Table 3.1 Ligands selected for this study.

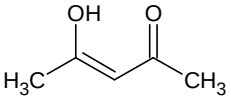 Hacac acetylacetone $pK_a = 8.80$[1,2]	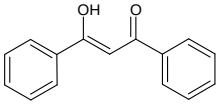 Hdbm dibenzoylmethane $pK_a = 9.35$[2]	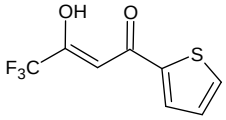 Hthtfac thenoyltrifluoroacetone $pK_a = 6.23$[3]	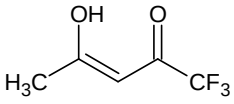 Htfacac trifluoroacetylacetone $pK_a = 6.30$[2]	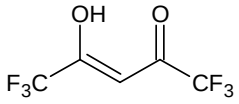 Hhfacac hexafluoroacetylacetone $pK_a = 4.35$[2]
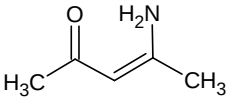 HNH-acac 4-aminopent-3-en-2-one $pK_a = 4.151$	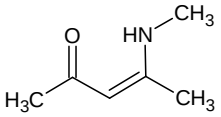 HNMe-acac 4-(methylamino)pent-3-en-2-one $pK_a = 2.569$	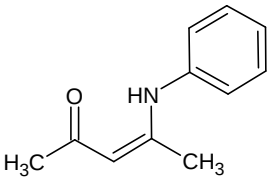 HNPh-acac 4-anilinopent-3-en-2-one $pK_a = 1.579$		
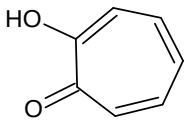 Htrop tropolone $pK_a = 6.70$[4]	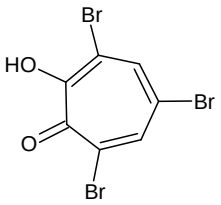 H3Br-trop tribromotropolone $pK_a = 4.27$[5]			

The Pd(II) and Pt(II) complexes involved in this line of investigation are of the general type [M(cod)(LL')]A where M= Pt, Pd and LL' = O,O-, N,O- bidentate ligands as seen in Table 3.1 and A = BF_4, PF_6. Whereas the Rh(I) complexes are of the general type [Rh(cod)(LL')] where LL' = O,O-, N,O- bidentate ligands as seen in Table 3.1. A general reaction scheme for the preparations may be seen in Figure 3.1a-3.1c.

[1] Ōki S., *Bull. Soc. Jp.*, **38**, 522, (1965)
[2] Leipoldt J.G., Grobler E.C., *Transition Met. Chem.*, **11**, 110, (1986)
[3] Gschneidner K.A., Bünzli J-C.G., Pecharsky V.K., *Handbook on the Physics and Chemistry of Rare Earths, Volume 35*, Elsevier B.V., The Netherlands, 244, (2005)
[4] Von E. Doering W., Knox L.H., *J. Am. Chem. Soc.*, **73**, 828, (1951)
[5] Pauson P.L., *J. Chem. Soc.*, 1, (1954)

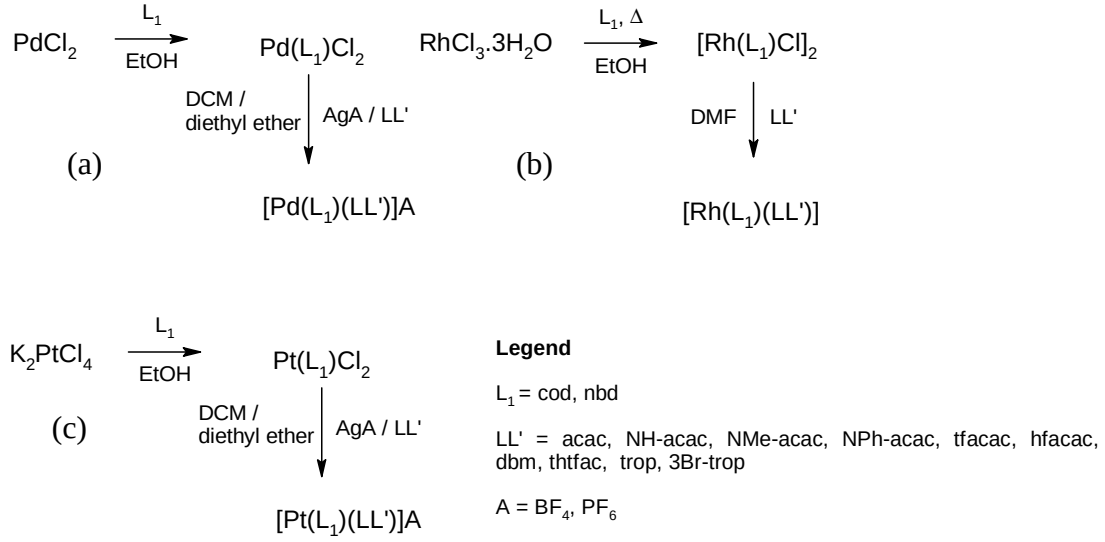

Figure 3.1 General reaction schemes of (a) Palladium(II), (b) Rhodium(I) and (c) Platinum(II) Complexes

Upon further inspection of the number of compounds generated by the selection of metal centres and bidentate ligand systems with 1,5-cyclo-octadiene, the bicyclo[2.2.1]hepta-2,5-diene (2,5-norbornadiene) "Venus fly-trap" mimic mentioned above, it was concluded to leave these compounds for a future study.

3.2 Instruments and Chemicals

All chemicals used for the preparation of the complexes were of reagent grade. All preparations were carried out in air, except when indicated otherwise. In the case of moisture and oxygen sensitive chemicals all reactions were performed under a nitrogen atmosphere using standard anaerobic techniques and all solvents were dried by standard procedures[6].

The following metal complexes and ligands were available commercially : [$PdCl_2$] (Next Chimica, South Africa), $RhCl_3.xH_2O$ (Next Chimica, South Africa), [K_4PtCl_4] (Next Chimica, South Africa), 1,5-cyclo-octadiene (Sigma-Aldrich), acetylacetone (Sigma-Aldrich), dibenzoylacetone (Sigma-Aldrich), trifluoroacetone (Sigma-Aldrich), hexafluoroacetone (Sigma-Aldrich), thenoyltrifluoroacetone (Sigma-Aldrich), tropolone (Sigma-Aldrich) and were used without further purification.

[6] Perrin D.D., Armarego W.L.F., *Purification of Laboratory Chemicals*, 3rd Edition, Pergamon Press, (1988)

NMR spectra were recorded on a Bruker Advance II 600 (^{1}H: 600.28 MHz; ^{13}C: 150.96 MHz), ^{1}H NMR spectra were referenced internally using residual protons in the deuterated solvent ($CDCl_3$: d 7.28; CD_2Cl_2: s 5.32; CD_3CN: m 1.94). ^{13}C NMR spectra were similarly referenced internally to the solvent resonance ($CDCl_3$: t 77.36; CD_2Cl_2 m 53.8; CD_3CN: s 1.32 and s 118.26) with values reported relative to tetramethylsilane (d 0.0).

Infrared spectra were recorded on a Bruker Tensor 27, with ATR attachment (goldstone), with solid samples prepared as potassium bromide disks and solution samples in a solution cell with sodium chloride windows.

3.3 Preparation of Ligands

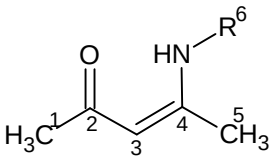

Figure 3.2 Line drawing representing general numbering of the uncoordinated ligands prepared where R = H, CH_3, Ph. Additional carbons are numbered in increasing order.

Figure 3.2 represents a line drawing of the β-enaminone ligands prepared as well as the numbering of the atoms. In the section to follow a general synthetic route will be presented followed by tables for the different functionalizations containing the masses of reagents, yields, infra-red (IR) and nuclear magnetic resonance (NMR) characterization. For the NMR characterization it should be noted that the superscripts given, represents the number of the atom given in the line drawing (Figure 3.2)

3.3.1 Synthesis of β-enaminones (HNH-acac, HNMe-acac, HNPh-acac)

A solution of acetylacetone (11 g, 0.11 mol), a primary amine (L_1 = NH_4OH, H_2NCH_3, H_2NPh 0.1 mol) and 2 drops H_2SO_4 (conc) in benzene (100 ml) was refluxed for 24 hrs in a Dean-Stark trap. The solvent was removed on a rotary evaporator where upon the oil was allowed to stand overnight.

An alternative synthesis for NH-acac is as follows[7]

To acetylacetone (5.0 g, 50 mmol) in a beaker, NH_4OH (3.5 g, 100 mmol) was added and the solution slightly heated (40 °C) for 1 hour while stirring. The solution was allowed to stand overnight to allow evaporation of the excess NH_4OH. The mixtrure changed color from a light yellow to a dark yellow.

3.3.1.1 4-aminopent-3-en-2-one (HNH-acac)

L_1	Mass (g)	Yield	$IR_{KBr\ or\ ATR}$ (cm^{-1})
NH_4OH (28 % in H_2O)	12.5 g	9.7 g 89 %	$\nu_{C=O}$ 1700, ν_{N-H} 3338 § Appendix A.1
^1H NMR (600.28 MHz, $CDCl_3$) δ 1.911 (s, 3H, C^1H_3), 2.033 (s, 3H, C^5H_3), 5.032 (s, 1H, C^3H), 9.701 (s, 1H, NH) ^{13}C NMR (150.96 MHz, $CDCl_3$) δ 22.56 (C^1), 29.53 (C^5), 96.08 (C^3), 161.27 (C^4), 197.07 (C_2)			

3.3.1.2 4-(methylamino)pent-3-en-2-one (HNMe-acac)

L_1	Mass (g)	Yield
H_2NCH_3 (40 % sol)	7.76 g	8.9 g 72 %
^1H NMR (600.28 MHz, $CDCl_3$) δ 1.918 (s, 3H, C^1H_3), 1.970 (s, 3H, C^5H_3), 2.932 (d, 3H, C^6H_3, J = 4.8 Hz), 4.981 (s, 1H, C^3H), 10.699 (s, 1H, NH) ^{13}C NMR (150.96 MHz, $CDCl_3$) δ18.97 (C^1), 28.95 (C^6), 29.77 (C^5), 95.43 (C^3), 164.55 (C^4), 195.01 (C^2)		

3.3.1.3 4-anilinopent-3-en-2-one (HNPh-acac)

L_1	Mass (g)	Yield	$IR_{KBr\ or\ ATR}$ (cm^{-1})
H_2NPh	9.31	15.4 g 80 %	$\nu_{C=O}$ 1606, ν_{N-H} 3050 § Appendix A.2
^1H NMR (600.28 MHz, $CDCl_3$) δ 2.005 (s, 3H, C^1H_3), 2.113 (s, 3H, C^5H_3), 5.201 (s, 1H, C^3H), 7.12 (d, 2H, $C^{7,11}H$, J = 7.2 Hz), 7.203 (t, 1H, C^9H, J = 7.2 Hz), 7.35 (t, 2H, $C^{8,10}H$, J = 7.2 Hz), 12.486 (s, 1H, NH) ^{13}C NMR (150.96 MHz, $CDCl_3$) δ 20.15 (C^1), 29.49 (C^5), 97.91 (C^3), 125.07 ($C^{7,11}$), 125.87 (C^9), 129.4 ($C^{8,10}$), 139.06 (C^6), 160.56 (C^4), 196.45 (C^2)			

[7] L.J. Damoense, *Fundamental Aspects of Selected Rhodium Complexes in Homogeneous Catalytic Acetic Acid Production*, PhD Thesis, Free State University, Bloemfontein, South Africa, (2000)

3.4 Preparation of Palladium(II) Complexes

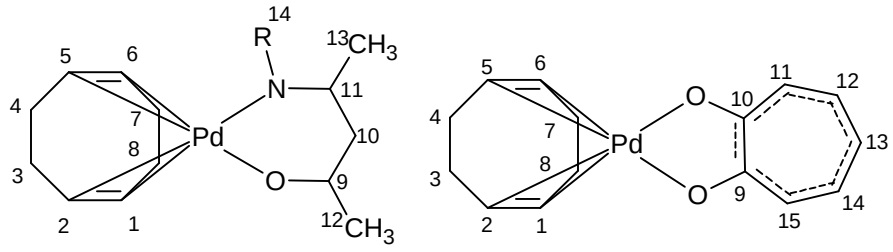

Figure 3.3 Line drawings representing general numbering of the palladium complexes where R = H, CH_3, Ph. Additional carbons are numbered in increasing order. Anions have been omitted for simplicity.

Figure 3.3 represents line drawings of the 1,5-cyclo-octadiene O,O- and N,O-bidentate palladium(II) complexes prepared as well as the numbering of the carbon atoms. In the sections to follow a general synthetic route will be presented followed by tables for the different complexes containing the masses of reagents, yields, infra-red (IR) and nuclear magnetic resonance (NMR) characterization. For the NMR characterization it should be noted that the superscripts given, represents the number of the atom given in the line drawings (Figure 3.3)

3.4.1 Synthesis of $[Pd(L_1)Cl_2]$ (L_1 = cod[8], nbd)

Palladium dichloride, $PdCl_2$ (2 g, 1.13 x 10^{-2} mol) was dissolved in hydrochloric acid (5 cm^3, conc., hot) and allowed to cool to room temperature (25 ^{0}C) then further diluted with ethanol (150 cm^3, absolute) and filtered. To the filtrate, with rapid stirring, was added bis-allyl (L_1 = cod / nbd, 3 cm^3), the yellow product precipitated immediately. After allowing the reaction mixture to stand for 10 minutes the solution was filtered and washed with diethyl ether (100 cm^3).

L_1	Yield	IR_{KBr} (cm^{-1})	NMR
cod	3.1g 96%	$\nu_{C=C}$ 1523 $\nu_{Pd-[C=C]}$ 560 § Appendix A.3	^{1}H NMR (600.28 MHz, $CDCl_3$) δ 2.588 (dd, 4H, CH_2, J = 7.8 Hz), 2.944 (m, 4H, CH_2), 6.334 (s, CH) ^{13}C NMR (150.96 MHz, $CDCl_3$) δ31 32 (s, CH_2), 117.01 (s, CH)
nbd	3.1 g 94 %		

[8] A.M.M. Meij, PhD Thesis, Rand Afrikaans University, Johannesburg, South Africa, (2004)

3.4.2 Synthesis of [Pd(cod)LL']A (LL' = acac, hfacac, tfacac, dbm, NH-acac, NMe-acac, NPh-acac, trop, 3Br-trop, thtfac; A = BF_4, PF_6)

Using a modified synthetic procedure[9]

[Pd(cod)Cl_2] (100 mg, 3.5 x 10^{-4} mol) was dissolved in dicholormethane (5 ml). To this AgA (A = BF_4, PF_6, 7.01 x 10^{-4} mol) was added, the resulting solution was stirred for ± 15 minutes. An equivalent of a bidentate ligand (LL' = Hacac, Hhfacac, Htfacac, Hdbm, HNH-acac, HNMe-acac, HNPh-acac, Htrop, H3Br-trop, Hthtfac, 3.5 x 10^{-4} mol) was added and the mixture stirred for a few minutes to allow the reaction to complete. The solution was then centrifuged and the precipitate discarded. Diethyl ether (30 ml) was added to the filtrate to precipitate the product. The solution was filtered and the precipitate washed with diethyl ether (3 x 3 ml portions).

The different complexes synthesized are summarized below. The complexes were prepared using the procedure described above.

3.4.2.1 (1,5-cyclo-octadiene)(2,4-pentanedionato)palladium(II) tetrafluoroborate [Pd(cod)(acac)]BF_4

LL'	Mass (mg)	A	Mass (mg)	Yield	IR_{KBr} (cm^{-1})
acac	112.2	BF_4	272.8	108 mg 75 %	$\nu_{C=C}$ 1558, $\nu_{C=O}$ 1694, ν_{Pd-O} 690 and 463, $\nu_{Pd-[C=C]}$ 521 § Appendix A.4
^{1}H NMR (600.28 MHz, CD_2Cl_2) δ 2.161 (s, 6H, $C^{12,13}H_3$), 2.715 (q, 4H, CH_2, J = 7.8 Hz), 3.029 (t, 4H, CH_2, J = 11.4 Hz), 5.653 (s, 1H, $C^{10}H$), 6.223 (s, 4H, $C^{1,2,5,6}H$) ^{13}C NMR (150.96 MHz, CD_2Cl_3) δ 26.13 (2 x $C^{12,13}H_3$), 30.27 (4 x CH_2), 100.7 ($C^{10}H$), 117.4 (4 x CH), 187.16 (2 x CO)					

3.4.2.2 (1,5-cyclo-octadiene)(2,4-pentanedionato)palladium(II) hexafluorophosphate [Pd(cod)(acac)]PF_6

LL'	Mass (mg)	A	Mass (mg)	Yield	IR_{KBr} (cm^{-1})
acac	112.2	PF_6	354	100 mg 62 %	$\nu_{C=C}$ 1556, $\nu_{C=O}$ 1694,ν_{Pd-O} 690 and 461, $\nu_{Pd-[C=C]}$ 557 § Appendix A.5
^{1}H NMR (600.28 MHz, $CDCl_3$) δ 2.167 (s, 6H, $C^{12,13}H_3$), 2.738 (q, 4H, CH_2, J = 7.2 Hz), 3.093 (m, 4H, CH_2), 5.625 (s, 1H, $C^{10}H$), 6.267 (d, 4H, CH, J = 10.8 Hz) ^{13}C NMR (150.96 MHz, $CDCl_3$) δ 26.25 (2 x CH_3), 30.18 (4 x CH_2), 100.87 ($C^{10}H$), 117.30 (4 x CH), 186.96 (2 x CO)					

[9] White D.A., *Inorganic Synthesis*, **13**, 55, (1972)

3.4.2.3 (1,5-cyclo-octadiene)(1,1,1-trifluoropentane-2,4-dionato)palladium(II) tetrafluoroborate [Pd(cod)(tfacac)]BF_4

LL'	Volume (µl)	A	Mass (mg)	Yield	IR_{KBr} (cm^{-1})
tfacac	42.4	BF_4	136	28 mg 17 %	$\nu_{C=C}$ 1523, $\nu_{C=O}$ 1610, ν_{Pd-O} 689 and 454, $\nu_{Pd-[C=C]}$ 521 § Appendix A.6
^1H NMR (600.28 MHz, $CDCl_3$) δ 2.397 (s, 3H, CH_3), 2.725 (d, 4H, CH_2, J = 8.4 Hz), 3.192 (s, 4H, CH_2), 6.072 (s, 1H, $C^{10}H$), 6.368 (s, 2H, CH), 6.523 (s, 2H, CH)					

3.4.2.4 (1,5-cyclo-octadiene)(1,1,1-trifluoropentane-2,4-dionato)palladium(II) hexafluorophosphate [Pd(cod)(tfacac)]PF_6

LL'	Volume (µl)	A	Mass (mg)	Yield	IR_{KBr} (cm^{-1})
tfacac	42.4	PF_6	177	88 mg 46 %	$\nu_{C=C}$ 1524, $\nu_{C=O}$ 1600, ν_{Pd-O} 649 and 448, $\nu_{Pd-[C=C]}$ 557 § Appendix A.7
^1H NMR (600.28 MHz, CD_2Cl_2) δ 2.383 (s, 3H, CH_3), 2.728 (q, 4H, CH_2, J = 8.4 Hz), 3.112 (m, 4H, CH_2), 6.121 (s, 1H, $C^{10}H$), 6.361 (s, 2H, CH), 6.442 (s, 2H, CH) ^{13}C NMR (150.96 MHz, CD_2Cl_2) δ 28.28 (CH_3), 30.53 (4 x CH_2), 97.68 ($C^{10}H$), 116.95 (CH), 118.91 (CH), 166.87 (CF_3), 197.21 (2 x CO)					

3.4.2.5 (1,5-cyclo-octadiene)(1,1,1,5,5,5-hexafluoropentane-2,4-dionato)palladium(II) tetrafluoroborate [Pd(cod)(hfacac)]BF_4

LL'	Volume (µl)	A	Mass (mg)	Yield	IR_{KBr} (cm^{-1})	NMR
hfacac	48.9	BF_4	136	Reaction failed		

3.4.2.6 (1,5-cyclo-octadiene)(1,1,1,5,5,5-hexafluoropentane-2,4-dionato)palladium(II) hexafluorophosphate [Pd(cod)(hfacac)]PF_6

LL'	Volume (µl)	A	Mass (mg)	Yield	IR_{KBr} (cm^{-1})
hfacac	48.9	PF_6	177	14 mg 7 %	$\nu_{C=C}$ 1571, $\nu_{C=O}$ 1618, ν_{Pd-O} 687 and 451, $\nu_{Pd-[C=C]}$ 558 § Appendix A.8
^1H NMR (600.28 MHz, CD_2Cl_2) δ 2.717 (q, 4H, CH_2, J = 7.2 Hz), 3.200 (d, 4H, CH_2, J = 10.8 Hz), 6.474 (s, 1H, $C^{10}H$), 6.575 (s, 4H, CH) ^{13}C NMR (150.96 MHz, CD_2Cl_2) δ 30.78 (4 x CH_2), 97.19 ($C^{10}H$), 120.13 (4 x CH), 176.0 (2 x CO)					

3.4.2.7 (1,5-cyclo-octadiene)(2-hydroxy-cyclohepta-2,4,6-trieneonato)palladium(II) tetrafluoroborate [Pd(cod)(trop)]BF_4

LL'	Mass (mg)	A	Mass (mg)	Yield	IR_{KBr} (cm^{-1})
trop	42.8	BF_4	136	27 mg 17 %	$\nu_{C=C}$ 1588, $\nu_{C=O}$ 1513, ν_{Pd-O} 589 and 456, $\nu_{Pd-[C=C]}$ 522 § Appendix A.9
^{1}H NMR (600.28 MHz, CD_2Cl_2) δ 2.732 (d, 4H, CH_2, *J* = 9 Hz), 3.023 (d, 4H, CH_2, *J* = 12.0 Hz), 6.324 (s, 4H, CH), 7.527 (t, 3H, CH-trop, *J* = 10.8 Hz), 7.808 (t, 2H, CH-trop, *J* = 10.8 Hz) ^{13}C NMR (150.96 MHz, CD_2Cl_2) δ 30.48 (4 x CH_2), 114.32 (4 x CH), 129.94 (2 x CH), 133.06 (CH), 140.09 (2 x CH), 185.51 (2 x CO)					

3.4.2.8 (1,5-cyclo-octadiene)(2-hydroxy-cyclohepta-2,4,6-trieneonato)palladium(II) hexafluorophosphate [Pd(cod)(trop)]PF_6

LL'	Mass (mg)	A	Mass (mg)	Yield	IR_{KBr} (cm^{-1})
trop	42.8	PF_6	177	104 mg 58 %	$\nu_{C=C}$ 1588, ν_{Pd-O} 650 and 455, $\nu_{Pd-[C=C]}$ 533 § Appendix A.10
^{1}H NMR (600.28 MHz, CD_2Cl_2) δ 2.726 (q, 4H, CH_2, *J* = 8.4 Hz), 3.021 (m, 4H, CH_2), 6.318 (t, 4H, CH, *J* = 1.2 Hz), 7.532 (t, 3H, CH-trop, *J* = 10.8 Hz), 7.809 (t, 2H, CH-trop, *J* = 10.8 Hz) ^{13}C NMR (150.96 MHz, CD_2Cl_2) δ 30.45 (4 x CH_2), 114.28 (4 x CH), 129.99 (2 x CH), 133.74 (CH), 140.1 (2 x CH), 185.5 (2 x CO)					

3.4.2.9 (1,5-cyclo-octadiene)(3,5,7-tribromo-2-hydroxy-cyclohepta-2,4,6-trieneonato)palladium(II) tetrafluoroborate [Pd(cod)(3Br-trop)]BF_4

LL'	Mass (mg)	A	Mass (mg)	Yield	IR_{KBr} (cm^{-1})
3Br-trop	251	BF_4	136	160 mg 67 %	$\nu_{C=C}$ 1574, ν_{Pd-O} 610 and 452, $\nu_{Pd-[C=C]}$ 520 § Appendix A.11
^{1}H NMR (600.28 MHz, $CDCl_3$) δ 2.782 (q, 4H, CH_2, *J* = 7.8 Hz), 3.159 (m, 4H, CH_2), 6.549 (s, 4H, CH), 8.688 (s, 2H, CH-trop) ^{13}C NMR (150.96 MHz, $CDCl_3$) δ 30.61 (4 x CH_2), 115.52 (4 x CH), 130.5 (CH), 145.5 (3 x CBr), 176.5 (2 x CO)					

3.4.2.10 (1,5-cyclo-octadiene)(3,5,7-tribromo-2-hydroxy-cyclohepta-2,4,6-trieneonato)palladium(II) hexafluorophosphate [Pd(cod)(3Br-trop)]PF_6

LL'	Mass (mg)	A	Mass (mg)	Yield	IR_{KBr} (cm^{-1})
trop	251	PF_6	177	134 mg 47 %	$\nu_{C=C}$ 1468, ν_{Pd-O} 666 and 454, $\nu_{Pd-[C=C]}$ 558 § Appendix A.12
^{1}H NMR (600.28 MHz, CD_2Cl_2) δ 2.761 (q, 4H, CH_2, *J* = 7.8 Hz), 3.076 (m, 4H, CH_2), 6.495 (s, 4H, CH), 8.774 (s, 2H, CH-trop) ^{13}C NMR (150.96 MHz, CD_2Cl_2) δ 30.63 (4 x CH_2), 115.82 (4 x CH), 130.64 (CH-trop), 145.99 (3 x CBr), 176.21 (2 x CO)					

3.4.2.11 (1,5-cyclo-octadiene)(4-aminopent-3-en-2-onato)palladium(II) tetrafluoroborate [Pd(cod)(NH-acac)]BF_4

LL'	Volume (µl)	A	Mass (mg)	Yield	IR_{KBr} (cm^{-1})
NH-acac	31.6	BF_4	136	36 mg 24 %	ν_{N-H} 3314, $\nu_{C=C}$ 1589, $\nu_{C=O}$ 1708, ν_{Pd-O} 717 and 476, $\nu_{Pd-[C=C]}$ 522 § Appendix A.13
^1H NMR (600.28 MHz, CD_2Cl_2) δ 2.086 (s, 3H, CH_3), 2.231 (s, 3H, CH_3), 2.681 (m, 4H, CH_2), 2.884 (m, 4H, CH_2), 5.216 (d, 1H, $C^{10}H$, *J* = 2.4 Hz), 6.111 (m, 2H, CH), 6.222 (m, 2H, CH) ^{13}C NMR (150.96 MHz, CD_2Cl_2) δ 24.91 (CH_3), 24.84 (CH_3), 28.93 (2 x CH_2), 31.08 (2 x CH_2), 97.25 ($C^{10}H$), 110.76 (2 x CH), 118.82 (2 x CH), 166.24 (CN), 177.4 (CO)					

3.4.2.12 (1,5-cyclo-octadiene)(4-aminopent-3-en-2-onato)palladium(II) hexafluorophosphate [Pd(cod)(NH-acac)]PF_6

LL'	Volume (µl)	A	Mass (mg)	Yield	IR_{KBr} (cm^{-1})
NH-acac	31.6	PF_6	177	32 mg 21 %	ν_{N-H} 3368, $\nu_{C=C}$ 1582, $\nu_{C=O}$ 1699, ν_{Pd-O} 692 and 474, $\nu_{Pd-[C=C]}$ 557 § Appendix A.14
^1H NMR (600.28 MHz, CD_2Cl_2) δ 2.097 (s, 3H, CH_3), 2.220 (s, 3H, CH_3), 2.698 (m, 4H, CH_2), 2.891 (m, 4H, CH_2), 5.239 (d, 1H, $C^{10}H$, *J* = 2.4 Hz), 6.127 (m, 4H, CH) ^{13}C NMR (150.96 MHz, CD_2Cl_2) δ 24.93 (CH_3), 25.15 (CH_3), 28.97 (2 x CH_2), 31.05 (2 x CH_2), 97.31 ($C^{10}H$), 110.76 (2 x CH), 119.08 (2 x CH), 166.36 (CN), 178.01 (CO)					

3.4.2.13 (1,5-cyclo-octadiene)(4-(methylamino)pent-3-en-2-onato)palladium(II) tetrafluoroborate [Pd(cod)(NMe-acac)]BF_4

LL'	Mass (mg)	A	Mass (mg)	Yield	IR_{KBr} (cm^{-1})
NMe-acac	43	BF_4	136	Reaction failed	

3.4.2.14 (1,5-cyclo-octadiene)(4-(methylamino)pent-3-en-2-onato)palladium(II) hexafluorophosphate [Pd(cod)(NMe-acac)]PF_6

LL'	Mass (mg)	A	Mass (mg)	Yield	IR_{KBr} (cm^{-1})
NMe-acac	43	PF_6	177	3 mg 1 %	$\nu_{C=C}$ 1725, $\nu_{C=O}$ 1676, $\nu_{Pd-[C=C]}$ 558 § Appendix A.15
Yield too low to characterize via NMR					

3.4.2.15 (1,5-cyclo-octadiene)(4-anilinopent-3-en-2-onato)palladium(II) tetrafluoroborate [Pd(cod)(NPh-acac)]BF_4

LL'	Mass (mg)	A	Mass (mg)	Yield	IR_{KBr} (cm^{-1})
NPh-acac	61.4	BF_4	136	72 mg 43 %	decomposed
^1H NMR (600.28 MHz, CD_3CN) δ 5.524 (m, 4H, CH), 6.005 (m, 1H, $C^{10}H$) ^{13}C NMR (150.96 MHz, CD_3CN) δ 102.13 (4 x CH), 106.16 ($C^{10}H$)					

Attempts to purify the compound lead to decomposition. A mixture of reactants in equilibrium was obtained with the desired product.

3.4.2.16 (1,5-cyclo-octadiene)(4-anilinopent-3-en-2-onato)palladium(II) hexafluorophosphate [Pd(cod)(NPh-acac)]PF_6

LL'	Mass (mg)	A	Mass (mg)	Yield	IR_{KBr} (cm^{-1})
NPh-acac	61.4	PF_6	177	45 mg 23 %	$\nu_{C=O}$ 1694, ν_{Pd-O} 696 and 499, $\nu_{Pd-[C=C]}$ 558 § Appendix A.16
^1H NMR (600.28 MHz, $CDCl_3$) δ 5.523 (m, 4H, CH), 6.007 (m, 1H, $C^{10}H$) ^{13}C NMR (150.96 MHz, $CDCl_3$) δ 103.12 (4 x CH), 107.09 ($C^{10}H$)					

Attempts to purify the compound lead to decomposition. A mixture of reactants in equilibrium was obtained with the desired product.

3.4.2.17 (1,5-cyclo-octadiene)(4,4,4-trifluoro-1-(2-thienyl)-1,3-butenedionato)palladium(II) tetrafluoroborate [Pd(cod)(thtfac)]BF_4

LL'	Mass (mg)	A	Mass (mg)	Yield	IR_{KBr} (cm^{-1})
thtfac	77.6	BF_4	136	140 mg 72 %	$\nu_{C=C}$ 1526, $\nu_{C=O}$ 1574, ν_{Pd-O} 678 and 451, $\nu_{Pd-[C=C]}$ 521 § Appendix A.17
^1H NMR (600.28 MHz, CD_2Cl_2) δ 2.771 (d, 4H, CH_2, J = 6.6 Hz), 3.146 (s, 4H, CH_2), 6.399 (s, 2H, CH), 6.493 (s, 2H, CH), 6.601 (s, 1H, $C^{10}H$), 7.257 (t, 1H, $C^{15}H$, J = 4.8 Hz), 7.915 (d, 1H, $C^{14}H$, J = 4.8 Hz), 7.961 (d, 1H, $C^{16}H$, J = 3.6 Hz) ^{13}C NMR (150.96 MHz, CD_2Cl_2) δ 30.68 (4 x CH_2), 93.71 ($C^{10}H$), 118.82 (2 x CH), 119.3 (2 x CH), 130.08 ($C^{16}H$), 135.49 ($C^{15}H$), 138.69 ($C^{14}H$), 139.68 (C^{13}), 167.14 (d, $C^{12}F_3$, J = 34.72 Hz), 179.23 (2 x CO)					

3.4.2.18 (1,5-cyclo-octadiene)(4,4,4-trifluoro-1-(2-thienyl)-1,3-butenedionato)palladium(II) hexafluorophosphate [Pd(cod)(thtfac)]PF_6

LL'	Mass (mg)	A	Mass (mg)	Yield	IR_{KBr} (cm^{-1})
thtfac	77.6	PF_6	177	24 mg 12 %	$\nu_{C=C}$ 1524, $\nu_{C=O}$ 1575, ν_{Pd-O} 679 and 451, $\nu_{Pd-[C=C]}$ 558 § Appendix A.18

^{1}H NMR (600.28 MHz, CD_2Cl_2) δ 2.777 (q, 4H, CH_2, *J* = 8.4 Hz), 3.151 (d, 4H, CH_2, *J* = 12.0 Hz), 6.446 (s, 4H, CH), 6.614 (s, 1H, $C^{10}H$), 7.263 (t, 1H, $C^{15}H$, *J* = 4.2 Hz), 7.925 (dd, 1H, $C^{14}H$, *J* = 0.6 Hz, 4.2 Hz), 7.964 (dd, 1H, $C^{16}H$, *J* = 0.6Hz, 4.2 Hz)

^{13}C NMR (150.96 MHz, CD_2Cl_2) δ 30.69 (4 x CH_2), 93.76 ($C^{10}H$), 119.08 (4 x CH), 130.15 ($C^{16}H$), 135.6 ($C^{15}H$), 138.9 ($C^{14}H$), 139.6 (C^{13}), 179.23 (2 x CO)

3.4.2.19 (1,5-cyclo-octadiene)(1,3-diphenylpropane-1,3-dionato)palladium(II) tetrafluoroborate [Pd(cod)(dbm)]BF_4

LL'	Mass (mg)	A	Mass (mg)	Yield	IR_{KBr} (cm^{-1})
dbm	78.6	BF_4	136	6 mg 6 %	$\nu_{C=C}$ 1523, $\nu_{C=O}$ 1588, ν_{Pd-O} 686 and 457, $\nu_{Pd-[C=C]}$ 521 § Appendix A.19

^{1}H NMR (600.28 MHz, CD_2Cl_2) δ 2.825 (sex, 4H, CH_2, *J* = 9.0 Hz, 7.2 Hz), 3.141 (d, 4H, CH_2, *J* = 10.8 Hz), 6.439 (s, 4H, CH), 6.919 (s, 1H, $C^{10}H$), 7.508 (t, 4H, CH, *J* = 7.8 Hz), 7.624 (t, 2H, CH, *J* = 7.2 Hz), 7.896 (d, 4H, CH, *J* = 7.2 Hz)

^{13}C NMR (150.96 MHz, CD_2Cl_2) δ 30.51 (4 x CH_2), 95.45 ($C^{10}H$), 118.02 (4 x CH-cod), 128.47 (4 x CH), 129.34 (4 x CH), 133.64 (2 x CH), 135.95 (2 x C), 181.33 (2 x CO)

3.4.2.20 (1,5-cyclo-octadiene)(1,3-diphenylpropane-1,3-dionato)palladium(II) hexafluorophosphate [Pd(cod)(dbm)]PF_6

LL'	Mass (mg)	A	Mass (mg)	Yield	IR_{KBr} (cm^{-1})
dbm	78.6	PF_6	177	24 mg 11 %	$\nu_{C=C}$ 1521, $\nu_{C=O}$ 1588, ν_{Pd-O} 685 and 455, $\nu_{Pd-[C=C]}$ 558 § Appendix A.20

^{1}H NMR (600.28 MHz, CD_2Cl_2) δ 2.815 (sex, 4H, CH_2, *J* = 8.4 Hz), 3.135 (d, 4H, CH_2, *J* = 12.0 Hz), 6.431 (s, 4H, CH), 6.922 (s, 1H, $C^{10}H$), 7.508 (t, 4H, CH, *J* = 7.8 Hz), 7.625 (t, 2H, CH, *J* = 7.2 Hz), 7.894 (d, 4H, CH, *J* = 7.2 Hz)

^{13}C NMR (150.96 MHz, CD_2Cl_2) δ 30.48 (4 x CH_2), 95.47 ($C^{10}H$), 118.0 (4 x CH-cod), 128.48 (4 x CH), 129.35 (4 x CH), 133.67 (2 x CH), 135.92 (2 x C), 181.35 (2 x CO)

3.5 Preparation of Platinum(II) Complexes

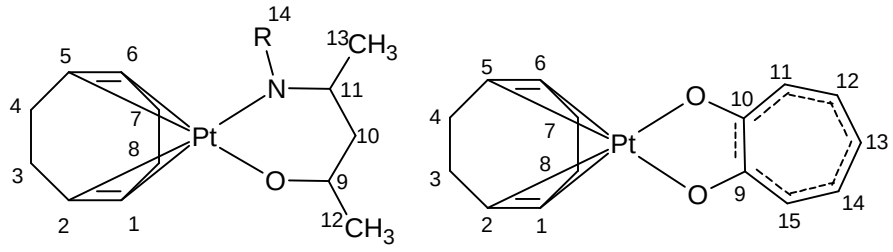

Figure 3.4 Line drawings representing general numbering of the palladium complexes where R = H, CH_3, Ph. Additional carbons are numbered in increasing order. Anions have been omitted for simplicity.

Figure 3.4 represents line drawings of the 1,5-cyclo-octadiene O,O- and N,O-bidentate platinum(II) complexes prepared as well as the numbering of the carbon atoms. In the sections to follow a general synthetic route will be presented followed by tables for the different complexes containing the masses of reagents, yields, infra-red (IR) and nuclear magnetic resonance (NMR) characterization. For the NMR characterization it should be noted that the superscripts given, represents the number of the atom given in the line drawings (Figure 3.4)

3.5.1 Preparation of dichlorido-1,5-cyclo-octadieneplatinum(II) [Pt(cod)Cl$_2$][10]

A solution of K_2PtCl_4 (1 g, 2.4 x 10^{-3} mol) in distilled water (16 cm^3) and n-propanol (11 cm^3) was added L_1 and a catalytic amount of $SnCl_2$ (15 mg). The mixture was stirred for two days until nearly colorless after which it was evaporated to dryness and later extracted with boiling dicholormethane (DCM). Slow evaporation of the solvent yielded a pure crystalline product.

L_1		**Yield**	**IR_{KBr} (cm^{-1})**	**NMR**
cod	2 cm^3	90 mg 92 %	$\nu_{C=C}$ 1728 § Appendix A.21	^{1}H NMR (600.28 MHz, $CDCl_3$) δ 2.284 (sex, 4H, CH_2, J = 14.4 Hz, 7.8 Hz, 9 Hz), 2.733 (m, 4H, CH_2), 5.631 (t, 4H, CH, $J_{Pt\text{-}H}$ = 32.4 Hz) ^{13}C NMR (150.96 MHz, $CDCl_3$) δ 31.28 (4 x CH_2), 100.43 (4 x CH, $J_{Pt\text{-}C}$ = 75.5 Hz)

[10] Otto S., *Structural and Reactivity Relationships in Platinum(II) and Rhodium(I) complexes*, PhD Thesis, University of the Free State, Bloemfontein, South Africa, (1999)

3.5.2 Preparation of [Pt(cod)LL']A (LL' = acac, hfacac, tfacac, dbm, NH-acac, NMe-acac, NPh-acac, trop, 3Br-trop; A = BF_4, PF_6)

[Pt(cod)Cl_2] (100 mg, 2.67 x 10^{-4} mol) dissolved in dichlormethane (5 ml). To this is added AgA (A = BF_4, PF_6, 5.35 x 10^{-4} mol), stir the resulting solution for ± 15 minutes. An equivalent of a bidentate ligand (LL' = Hacac, Hhfacac, Htfacac, Hdbm, HNH-acac, HNMe-acac, HNPh-acac, Htrop, H3Br-trop, Hthtfac, 6.73 x 10^{-4} mol) was added and the mixture stirred for a few minutes to allow reaction to complete. The solution was then centrifuged and the precipitate discarded. Diethyl ether (30 ml) was added to the filtrate to precipitate the product. The solution was filtered and the precipitate was washed with diethyl ether (3 x 3 ml) portions.

The different complexes synthesized are summarized below. The complexes were prepared using the procedure described above.

3.5.2.1 (1,5-cyclo-octadiene)(2,4-pentanedionato)platinum(II) tetrafluoroborate [Pt(cod)(acac)]BF_4

LL'	Volume (µl)	A	Mass (mg)	Yield	IR_{KBr} (cm^{-1})
acac	27.4	BF_4	104.1	100 mg 74 %	$\nu_{C=C}$ 1529, $\nu_{C=O}$ 1555, ν_{Pt-O} 645 and 474, $\nu_{Pt-[C=C]}$ 521 § Appendix A.22

^{1}H NMR (600.28 MHz, CD_2Cl_2) δ 2.209 (s, 6H, CH_3), 2.499 (q, 4H, CH_2, *J* = 8.4 Hz, isomer 1), 2.254 (q, 4H, CH_2, *J* = 8.4 Hz, isomer 2), 2.683 (dd, 4H, CH_2, *J* = 2.4 Hz, 6Hz, isomer 2), 2.841 (d, 4H, CH_2, *J* = 10.8 Hz, isomer 1), 5.556 (t, 4H, CH, *J* = 33, isomer 2), 5.75 (t, 4H, CH, *J* = 33.6 Hz, isomer 1), 5.862 (s, 1H, $C^{10}H$)

^{13}C NMR (150.96 MHz, CD_2Cl_2) δ 26.81 (2 x CH_3), 29.97 (4 x CH_2, isomer 1), 31.23 (4 x CH_2, isomer 2), 99.53 (t, 4 x CH, *J* = 83.6 Hz, isomer 1), 100.94 (4 x CH, isomer 2), 103.02 ($C^{10}H$), 187.81 (2 x CO)

3.5.2.2 (1,5-cyclo-octadiene)(2,4-pentanedionato)platinum(II) hexafluorophosphate [Pt(cod)(acac)]PF_6

LL'	Volume (µl)	A	Mass (mg)	Yield	IR_{KBr} (cm^{-1})
acac	27.4	PF_6	135.1	42 mg 53 %	$\nu_{C=C}$ 1526, $\nu_{C=O}$ 1556, ν_{Pt-O} 647 and 473, $\nu_{Pt-[C=C]}$ 558 § Appendix A.23

^{1}H NMR (600.28 MHz, CD_2Cl_2) δ 2.008 (s, 6H, CH_3), 2.492 (q, 4H, CH_2, *J* = 8.4 Hz), 2.836 (d, 4H, CH_2, *J* = 10.8 Hz), 5.744 (t, 4H, CH, *J* = 32.4 Hz), 5861 (s, 1H, $C^{10}H$)

^{13}C NMR (150.96 MHz, CD_2Cl_2) δ 26.79 (2 x CH_3), 29.95 (4 x CH_2), 99.51 (4 x CH), 103.02 ($C^{10}H$), 187.84 (2 x CO)

3.5.2.3 (1,5-cyclo-octadiene)(1,1,1-trifluoropentane-2,4-dionato)platinum(II) tetrafluoroborate [Pt(cod)(tfacac)]BF_4

LL'	Volume (µl)	A	Mass (mg)	Yield	IR_{KBr} (cm^{-1})
tfacac	32.3	BF_4	104.1	65 mg 43 %	$\nu_{C=C}$ 1530, $\nu_{C=O}$ 1596, ν_{Pt-O} 658 and 470, $\nu_{Pt-[C=C]}$ 520 § Appendix A.24

^{1}H NMR (600.28 MHz, CD_2Cl_2) δ 2.253 (q, 4H, CH_2, *J* = 8.4 Hz, isomer 2), 2.442 (s, 3H, CH_3), (2.509 (q, 4H, CH_2, *J* = 8.4 Hz, isomer 1), 2.683 (d, 4H, CH_2, *J* = 10.8 Hz, isomer 2), 2.905 (s, 4H, CH_2, isomer 1), 5.554 (t, 4H, CH, *J* = 33 Hz, isomer 2), 5.942 (q, 4H, CH, *J* = 28.2 Hz, 52.2 Hz, 34.2 Hz, isomer 1), 6.310 (s, 1H, $C^{10}H$)

^{13}C NMR (150.96 MHz, CD_2Cl_2) δ 28.9 (CH_3), 30.97 (2 x CH_2), 31.22 (2 x CH_2), 99.85 ($C^{10}H$), 100.97 (t, 4 x CH, *J* = 75.48 Hz), 166.39 (d, CF_3, *J* = 34.7 Hz) 198.15 (2 x CO)

3.5.2.4 (1,5-cyclo-octadiene)(1,1,1-trifluoropentane-2,4-dionato)platinum(II) hexafluorophosphate [Pt(cod)(tfacac)]PF_6

LL'	Mass (mg)	A	Mass (mg)	Yield	IR_{KBr} (cm^{-1})
tfacac	32.3	PF_6	135.1	85 mg 52 %	$\nu_{C=C}$ 1529, $\nu_{C=O}$ 1599, ν_{Pt-O} 659 and 470, $\nu_{Pt-[C=C]}$ 559 § Appendix A.25

^{1}H NMR (600.28 MHz, CD_2Cl_2) δ 2.444 (s, 3H, CH_3), 2.515 (q, 4H, CH_2, *J* = 9 Hz), 2.902 (d, 4H, CH_2, *J* = 8.4 Hz), 5.949 (d, 4H, CH, *J* = 9.6 Hz), 6.321 (s, 1H, $C^{10}H$)

^{13}C NMR (150.96 MHz, CD_2Cl_2) δ 28.89 (CH_3), 30.07 (4 x CH_2), 99.9 ($C^{10}H$), 101.8 (4 x CH), 166.54 (CF_3), 198.23 (2 x CO)

3.5.2.5 (1,5-cyclo-octadiene)(1,1,1,5,5,5-hexafluoropentane-2,4-dionato)platinum(II) tetrafluoroborate [Pt(cod)(hfacac)]BF_4

LL'	Volume (µl)	A	Mass (mg)	Yield	IR_{KBr} (cm^{-1})
hfacac	37.3	BF_4	104.1	5 mg 3 %	$\nu_{C=C}$ 1424, $\nu_{C=O}$ 1474, ν_{Pt-O} 694 and 474, $\nu_{Pt-[C=C]}$ 582 § Appendix A.26

^{1}H NMR (600.28 MHz, CD_2Cl_2) δ 2.246 (dq, 4H, CH_2, *J* = 8.4 Hz), 2.685 (q, 4H, CH_2, *J* = 6 Hz, 2.4 Hz), 5.56 (t, 4H, CH, *J* = 33.6 Hz)

^{13}C NMR (150.96 MHz, CD_2Cl_2) δ 30.08 (2 x CH_2), 31.27 (2 x CH_2), 97.38 ($C^{10}H$), 100.9 (t, CH, *J* = 76.7 Hz), 143.73 (d, CF_3, *J* = 29.7 Hz), 184.88 (2 x CO)

3.5.2.6 (1,5-cyclo-octadiene)(1,1,1,5,5,5-hexafluoropentane-2,4-dionato)platinum(II) hexafluorophosphate [Pt(cod)(hfacac)]PF_6

LL'	Volume (µl)	A	Mass (mg)	Yield	IR_{KBr} (cm^{-1})
hfacac	37.3	PF_6	135.1	23 mg 13 %	$\nu_{C=C}$ 1533, $\nu_{C=O}$ 1613, ν_{Pt-O} 695 and 472, $\nu_{Pt-[C=C]}$ 559 § Appendix A.27

^{1}H NMR (600.28 MHz, CD_2Cl_2) δ 2.251 (d, 4H, CH_2, *J* = 8.4 Hz, isomer 1), 2.512 (d, 4H, CH_2, *J* = 8.4 Hz, isomer 2), 2.787 (s, 4H, CH_2, isomer 1), 2.971 (s, 4H, CH_2, isomer 2), 5.668 (s, 4H, CH, isomer 1), 6.128 (t, 4H, CH, *J* = 31.2 Hz, isomer 2), 6.426 (s, 1H, $C^{10}H$, isomer 2), 6.697 (s, 1H, $C^{10}H$, isomer 1)

3.5.2.7 (1,5-cyclo-octadiene)(2-hydroxy-cyclohepta-2,4,6-trieneonato)platinum(II) tetrafluoroborate [Pt(cod)(trop)]BF_4

LL'	Mass (mg)	A	Mass (mg)	Yield	IR_{KBr} (cm^{-1})
trop	32.6	BF_4	104.1	101 mg 71 %	$\nu_{C=C}$ 1520, $\nu_{C=O}$ 1589, ν_{Pt-O} 666 and 475, $\nu_{Pt-[C=C]}$ 522 § Appendix A.28

^{1}H NMR (600.28 MHz, $CDCl_3$) δ 2.287 (oct, 4H, CH_2, *J* = 10.2 Hz, 6 Hz, 7.8 Hz, isomer 1), 2.548 (q, 4H, CH_2, *J* = 8.4 Hz, isomer 2), 2.731 (m, 4H, CH_2, isomer 1), 2.886 (d, 4H, CH_2, *J* = 11.4 Hz, isomer 2), 5.627 (t, 4H, CH, *J* = 33 Hz, isomer 1), 5.901 (t, 4H, CH, *J* = 30.6 Hz, isomer 2), 7.498 (q, 2H, CH, *J* = 2.4 Hz, 9.6 Hz, isomer 1), 7.588 (d, 2H, CH, *J* = 10.8 Hz, isomer 1), 7.718 (t, 1H, CH, *J* = 9.6 Hz, isomer 1), 8.021 – 7.825 (m, 5H, isomer 2)

^{13}C NMR (150.96 MHz, $CDCl_3$) δ 30.25 (4 x CH_2, isomer 2), 31.26 (4 x CH_2, isomer 1), 96.21 (4 x CH_2, isomer 2), 100.38 (4 x CH_2, isomer 1), 126.46 (CH, isomer 2), 126.96 (CH, isomer 1), 129.06 (CH, isomer 2), 130.87 (CH, isomer 2), 131.7 (CH, isomer 1) 140.53 (CH, isomer 2), 142.66 (CH, isomer 2), 142.98 (CH, isomer 1), 175.94 (2 x CO)

3.5.2.8 (1,5-cyclo-octadiene)(2-hydroxy-cyclohepta-2,4,6-trieneonato)platinum(II) hexafluorophosphate [Pt(cod)(trop)]PF_6

LL'	Mass (mg)	A	Mass (mg)	Yield	IR_{KBr} (cm^{-1})
trop	32.6	PF_6	135.1	33 mg 21 %	$\nu_{C=C}$ 1517, $\nu_{C=O}$ 1589, ν_{Pt-O} 662 and 472, $\nu_{Pt-[C=C]}$ 559 § Appendix A.29

^{1}H NMR (600.28 MHz, CD_2Cl_2) δ 2.509 (d, 4H, CH_2, *J* = 9 Hz), 2.807 (d, 4H, CH_2, *J* = 8.4 Hz), 5.832 (t, 4H, CH, *J* = 33.6 Hz), 7.755 (t, 1H, CH, *J* = 9.6 Hz), 7.884 (d, 2H, CH, *J* = 11.4 Hz), 8.026 (t, 2H, CH, *J* = 10.2 Hz)

^{13}C NMR (150.96 MHz, CD_2Cl_2) δ 30.2 (4 x CH_2), 96.2 (4 x CH), 130.86 (2 x CH), 135.9 (CH), 140.86 (2 x CH), 184.23 (2 x CO)

3.5.2.9 (1,5-cyclo-octadiene)(3,5,7-tribromo-2-hydroxy-cyclohepta-2,4,6-trieneonato)platinum(II) tetrafluoroborate [Pt(cod)(3Br-trop)]BF_4

LL'	Mass (mg)	A	Mass (mg)	Yield	IR_{KBr} (cm^{-1})
3Br-trop	95.8	BF_4	104.1	132 mg 61 %	$\nu_{C=C}$ 1432, $\nu_{C=O}$ 1509, ν_{Pt-O} 612 and 474, $\nu_{Pt-[C=C]}$ 519 § Appendix A.30

^{1}H NMR (600.28 MHz, $CDCl_3$) δ 2.291 (q, 4H, CH_2, *J* = 7.8 Hz, 8.4 Hz, isomer 2), 2.56 (q, 4H, CH_2, *J* = 7.8 Hz, 8.4 Hz, isomer 1), 2.727 (d, 4H, CH_2, *J* = 10.8 Hz, isomer 2), 2.927 (d, 4H, CH_2, *J* = 11.4 Hz, isomer 1), 5.523 (t, 4H, CH, *J* = 32.4 Hz, isomer 2), 6.067 (s, 4H, CH, isomer 1), 8.358 (s, 2H, CH, isomer 2), 8.835 (s, 2H, CH, isomer 1)

^{13}C NMR (150.96 MHz, $CDCl_3$) δ 30.26 (4 x CH_2, isomer 1), 31.24 (4 x CH_2, isomer 2), 97.6 (4 x CH, isomer 1), 100.49 (4 x CH, isomer 2), 124.78 (2 x CH, isomer 1), 131.91 (CBr, isomer 1), 146.34 (2 x CBr, isomer 1), 176.42 (2 x CO, isomer 1)

3.5.2.10 (1,5-cyclo-octadiene)(3,5,7-tribromo-2-hydroxy-cyclohepta-2,4,6-trieneonato)platinum(II) hexafluorophosphate [Pt(cod)(3Br-trop)]PF_6

LL'	Mass (mg)	A	Mass (mg)	Yield	IR_{KBr} (cm^{-1})
3Br-trop	95.8	PF_6	135.1	100 mg 38 %	$\nu_{C=C}$ 1472, $\nu_{C=O}$ 1508, ν_{Pt-O} 675 and 475, $\nu_{Pt-[C=C]}$ 557 § Appendix A.31

^{1}H NMR (600.28 MHz, CD_2Cl_2) δ 2.544 (q, 4H, CH_2, *J* = 7.8 Hz, 9 Hz), 2.851 (d, 4H, CH_2, *J* = 11.4 Hz), 6.016 (t, 4H, CH, *J* = 33 Hz), 8.927 (s, 2H, CH)

^{13}C NMR (150.96 MHz, CD_2Cl_2) δ 30.27 (4 x CH_2), 97.87 (4 x CH), 125.63 (2 x CH), 132.06 (CBr), 146.93 (2 x CBr), 176.15 (2 x CO)

3.5.2.11 (1,5-cyclo-octadiene)(4-aminopent-3-en-2-onato)platinum(II) tetrafluoroborate [Pt(cod)(NH-acac)]BF_4

LL'	Volume (µl)	A	Mass (mg)	Yield	IR_{KBr} (cm^{-1})
NH-acac	25.8	BF_4	104.1	55 mg 41 %	$\nu_{C=C}$ 1539, $\nu_{C=O}$ 1587, ν_{Pt-O} 664 and 470, $\nu_{Pt-[C=C]}$ 521 § Appendix A.32

^{1}H NMR (600.28 MHz, CD_2Cl_2) δ 2.136 (s, 3H, CH_3), 2.281 (s, 3H, CH_3), 2.508 (m, 4H, CH_2), 2.718 (m, 4H, CH_2), 5.428 (d, 1H, $C^{10}H$, *J* = 2.4 Hz), 5.658 (dt, 4H, CH, *J* = 3 Hz, 15.6 Hz), 9.212 (s, 1H, NH)

^{13}C NMR (150.96 MHz, CD_2Cl_2) δ 25.55 (d, CH_3, *J* = 7.5 Hz), 28.76 (CH_3), 30.06 (2 x CH_2), 31.09 (2 x CH_2), 92.28 ($C^{10}H$), 100.01 (2 x CH), 102.51 (2 x CH), 166.48 (CN), 177.57 (CO)

3.5.2.12 (1,5-cyclo-octadiene)(4-aminopent-3-en-2-onato)platinum(II) hexafluorophosphate [Pt(cod)(NH-acac)]PF_6

LL'	Volume (µl)	A	Mass (mg)	Yield	IR_{KBr} (cm^{-1})
NH-acac	25.8	PF_6	135.1	91 mg 60 %	$\nu_{C=C}$ 1539, $\nu_{C=O}$ 1587, ν_{Pt-O} 664 and 471, $\nu_{Pt-[C=C]}$ 557 § Appendix A.33

^{1}H NMR (600.28 MHz, CD_2Cl_2) δ 2.147 (2, 3H, CH_3), 2.269 (s, 3H, CH_3), 2.522 (m, 4H, CH_2), 2.725 (m, 4H, CH_2), 5.325 (d, 1H, $C^{10}H$, *J* = 6.6 Hz), 5.627 (dt, 4H, CH, *J* = 33 Hz, 57 Hz), 8.601 (s, 1H, NH)

^{13}C NMR (150.96 MHz, CD_2Cl_2) δ 25.66 (d, CH_3, *J* = 28.7 Hz), 28.76 (CH_3), 29.95 (2 x CH_2), 31.04 (2 x CH_2), 92.21 ($C^{10}H$), 99.78 (d, 2 x CH, *J* = 83 Hz), 102.79 (2 x CH), 166.51 (NH), 178.15 (CO)

3.5.2.13 (1,5-cyclo-octadiene)(4-(methylamino)pent-3-en-2-onato)platinum(II) tetrafluoroborate [Pt(cod)(NMe-acac)]BF_4

LL'	Volume (µl)	A	Mass (mg)	Yield	IR_{KBr} (cm^{-1})
NMe-acac	31.9	BF_4	104.1	96 mg 70 %	$\nu_{C=C}$ 1522, $\nu_{C=O}$ 1584, ν_{Pt-O} 635 and 416, $\nu_{Pt-[C=C]}$ 521, ν_{Pt-N} 472 § Appendix A.34

^{1}H NMR (600.28 MHz, CD_2Cl_2) δ 2.117 (s, 3H, CH_3), 2.228 (s, 3H, CH_3), 2.485 (m, 2H, CH_2), 2.607 (m, 2H, CH_2), 2.734 (m, 2H, CH_2), 2.890 (m, 2H, CH_2), 3.315 (t, 3H, $C^{14}H_3$, *J* = 12.6 Hz), 5.450 (s, 1H, $C^{10}H$), 5.486 (sep, 2H, CH, *J* = 19.8 Hz, 7.8 Hz, 3 Hz), 5.791 (sep, 2H, CH, *J* = 14.4 Hz, 9 Hz, 3 Hz)

^{13}C NMR (150.96 MHz, CD_2Cl_2) δ 24.62 (CH_3), 24.97 (CH_3), 28.22 (2 x CH_2), 31.84 (2 x CH_2), 42.69 ($C^{14}H$), 97.32 ($C^{10}H$), 102.17 (2 x CH), 104.83 (2 x CH), 167.45 (CN), 174.94 (CO)

3.5.2.14 (1,5-cyclo-octadiene)(4-(methylamino)pent-3-en-2-onato)platinum(II) hexafluorophosphate [Pd(cod)(NMe-acac)]PF_6

LL'	Volume (µl)	A	Mass (mg)	Yield	IR_{KBr} (cm^{-1})
NMe-acac	31.9	PF_6	135.1	125 mg 82 %	$\nu_{C=C}$ 1518, $\nu_{C=O}$ 1580, ν_{Pt-O} 636 and 419, $\nu_{Pt-[C=C]}$ 557, ν_{Pt-N} 467 § Appendix A.35

^{1}H NMR (600.28 MHz, CD_2Cl_2) δ 2.120 (s, 3H, CH_3), 2.224 (s, 3H, CH_3), 2.483 (m, 2H, CH_2), 2.602 (m, 2H, CH_2), 2.731 (m, 2H, CH_2), 2.881 (m, 2H, CH_2), 3.299 (t, 3H, $C^{14}H_3$, *J* = 12.6 Hz), 5.454 (s, 1H, $C^{10}H$), 5.448 (sep, 2H, CH, *J* = 22.2 Hz, 8.4 Hz, 3 Hz), 5.797 (sep, 2H, CH, *J* = 14.4 Hz, 8.4 Hz, 3 Hz)

^{13}C NMR (150.96 MHz, CD_2Cl_2) δ 24.61 (CH_3), 24.94 (CH_3), 28.2 (2 x CH_2), 31.21 (2 x CH_2), 42.59 ($C^{14}H_3$), 97.16 ($C^{10}H$), 102.17 (2 x CH), 104.89 (2 x CH), 167.46 (CN), 175.01 (CO)

3.5.2.15 (1,5-cyclo-octadiene)(4-anilinopent-3-en-2-onato)platinum(II) tetrafluoroborate [Pt(cod)(NPh-acac)]BF_4

LL'	Mass (mg)	A	Mass (mg)	Yield	IR_{KBr} (cm^{-1})
NPh-acac	46.8	BF_4	104.1	85 mg 55 %	$\nu_{C=C}$ 1518, $\nu_{C=O}$ 1566, ν_{Pt-O} 659 and 474, $\nu_{Pt-[C=C]}$ 522, ν_{Pt-N} 548 § Appendix A.36

^{1}H NMR (600.28 MHz, CD_2Cl_2) δ 1.806 (s, 3H, CH_3), 2.228 (s, 3H, CH_3), 2.392 (m, 4H, CH_2), 2.696 (m, 4H, CH_2), 4.712 (sep, 2H, CH, *J* = 18.6 Hz, 8.4 Hz, 3 Hz), 5.619 (s, $C^{10}H$), 5.869 (sep, 2H, CH, *J* = 15 Hz, 9 Hz, 2.4 Hz), 7.037 (d, 2H, CH, *J* = 7.2 Hz), 7.34 (t, 1H, CH, *J* = 7.8 Hz), 7.514 (t, 2 H, CH, *J* = 7.8 Hz)

^{13}C NMR (150.96 MHz, CD_2Cl_2) δ 24.9 (CH_3), 25.43 (CH_3), 28.03 (2 x CH_2), 30.77 (d, 2 x CH_2, *J* = 25.6 Hz), 98.33 (2 x CH), 101.45 ($C^{10}H$), 104.43 (2 x CH), 146.91 (CN), 166.23 (CN), 177.35 (CO)

3.5.2.16 (1,5-cyclo-octadiene)(4-anilinopent-3-en-2-onato)platinum(II) hexafluorophosphate [Pt(cod)(NPh-acac)]PF_6

LL'	Mass (mg)	A	Mass (mg)	Yield	IR_{KBr} (cm^{-1})
NPh-acac	46.8	PF_6	135.1	132 mg 78 %	$\nu_{C=C}$ 1519, $\nu_{C=O}$ 1563, ν_{Pt-O} 658 and 473, $\nu_{Pt-[C=C]}$ 557, ν_{Pt-N} 525 § Appendix A.37

^{1}H NMR (600.28 MHz, CD_2Cl_2) δ 1.804 (s, 2H, CH_3), 2.227 (s, 3H, CH_3), 2.387 (m, 4H, CH_2), 2.722 (m, 4H, CH_2), 4.705 (sep, 2H, CH, *J* = 20.4 Hz, 9 Hz, 2.4 Hz), 5.619 (s, 1H, $C^{10}H$), 5.866 (sep, 2H, CH, *J* = 14.4 Hz, 9 Hz, 2.4 Hz), 7.03 (s, 2H, CH, *J* = 7.8 Hz), 7.34 (t, 1H, CH, *J* = 7.2 Hz), 7.513 (t, 2H, CH, *J* = 7.8 Hz)

^{13}C NMR (150.96 MHz, CD_2Cl_2) δ 25. 27 (CH_3), 25.8 (CH_3), 28.4 (2 x CH_2), 31.05 (2 x CH_2) 98.68 (2 x CH), 101.83 ($C^{10}H$), 04.81 (2 x CH), 125.51 (2 x CH), 128.73 (CH), 130.25 (2 x CH), 147.29 (CN), 166.62 (CN), 177.76 (CO)

3.5.2.17 (1,5-cyclo-octadiene)(4,4,4-trifluoro-1-(2-thienyl)-1,3-butenedionato)platinum(II) tetrafluoroborate [Pt(cod)(thtfac)]BF_4

LL'	Mass (mg)	A	Mass (mg)	Yield	IR_{KBr} (cm^{-1})
thtfac	59.3	BF_4	104.1	90 mg 54 %	$\nu_{C=C}$ 1540, $\nu_{C=O}$ 1579, ν_{Pt-O} 613 and 473, $\nu_{Pt-[C=C]}$ 522 § Appendix A.38

^{1}H NMR (600.28 MHz, $CDCl_3$) δ 2.604 (m, 4H, CH_2), 2.727 (m, 4H, CH_2), 5.626 (t, 4H, CH, *J* = 31.8 Hz), 6.717 (s, 1H, $C^{10}H$), 7.969 (d, 1H, CH, *J* = 4.8 Hz), 8.085 (d, 2H, CH, *J* = 3.6 Hz)

^{13}C NMR (150.96 MHz, $CDCl_3$) δ 30.22 (2 x CH_2), 31.28 (2 x CH_2), 100.42 (t, 4 x CH, *J* = 76.8 Hz), 120.94 ($C^{10}H$), 130.59 (2 x CH), 136.72 (CH), 139.73 (CF_3), 198.87 (CO)

3.5.2.18 (1,5-cyclo-octadiene)(4,4,4-trifluoro-1-(2-thienyl)-1,3-butenedionato)platinum(II) hexafluorophosphate [Pt(cod)(thtfac)]PF_6

LL'	Mass (mg)	A	Mass (mg)	Yield	IR_{KBr} (cm^{-1})
thtfac	59.3	PF_6	135.1	14 mg 7 %	$\nu_{C=C}$ 1539, $\nu_{C=O}$ 1577, ν_{Pt-O} 613 and 470, $\nu_{Pt-[C=C]}$ 558 § Appendix A.39

^{1}H NMR (600.28 MHz, CD_2Cl_2) δ 2.218 (m, 4H, CH_2, isomer 2), 2.559 (q, 4H, CH_2, *J* = 7.8 Hz, isomer 1), 2.789 (m, 4H, CH_2, isomer 2), 2.933 (m, 4H, CH_2, isomer 1), 5.726 (s, 4H, CH, isomer 2), 5.953 (t, 4H, CH, *J* = 33 Hz, isomer 1), 6.505 (s, 1H, $C^{310}H$, isomer 2), 6.780 (s, 1H, $C^{10}H$, isomer 1), 7.235 (t, 1H, CH, *J* = 4.2 Hz, isomer 2), 7.330 (t, 1H, CH, *J* = 4.2 Hz, isomer 1), 7.818 (q, 1H, CH, *J* = 0.6 Hz, 4.2 Hz, isomer 2), 7.874 (q, 1H, CH, *J* = 1.2 Hz, 3 Hz, isomer 2), 8.057 (q, 1H, CH, *J* = 1.2 Hz, 3.6 Hz, isomer 1), 8.086 (q, 1H, CH, *J* = 0.6 Hz, 3.6 Hz, isomer 1)

^{13}C NMR (150.96 MHz, CD_2Cl_2) δ 29.83 (4 x CH_2), 100.8 (4 x CH), 130.41 (CH), 136.59 (CH), 140.36 (CH), 165.72 (CF_3)

Experimental time for the ^{13}C spectra not sufficant for all the peaks to be elucidated.

3.5.2.19 (1,5-cyclo-octadiene)(1,3-diphenylpropane-1,3-dionato)platinum(II) tetrafluoroborate [Pt(cod)(dbm)]BF_4

LL'	Mass (mg)	A	Mass (mg)	Yield	IR_{KBr} (cm^{-1})
dbm	59.9	BF_4	104.1	40 mg 24 %	$\nu_{C=C}$ 1522, $\nu_{C=O}$ 1587, ν_{Pt-O} 682 and 474, $\nu_{Pt-[C=C]}$ 521 § Appendix A.40

^{1}H NMR (600.28 MHz, CD_2Cl_2) δ 2.245 (sex, 4H, CH_2, *J* = 15.5 Hz, 7.2 Hz, 9 Hz, isomer 1), 2.594 (t, 4H, CH_2, *J* = 8.4 Hz, isomer 2), 2.679 (d, 4H, CH_2, *J* = 9 Hz, isomer 1), 2.941 (d, 4H, CH_2, *J* = 9.6 Hz, isomer 2), 5.554 (t, 4H, CH, *J* = 33 Hz, isomer 1), 5.947 (t, 4H, CH, *J* = 28.2 Hz, isomer 2), 7.126 (s, 1H, $C^{10}H$), 7.545 (t, 4H, CH, *J* = 7.8 Hz), 7.675 (t, 2H, CH, *J* = 7.2 Hz), 7.964 (d, 4H, CH, *J* =7.8 Hz)

^{13}C NMR (150.96 MHz, CD_2Cl_2) δ 31.22 (4 x CH_2), 96.98 ($C^{10}H$), 100.0 (4 x CH, isomer 2), 100.88 (t, 4 x CH, *J* = 76 Hz, isomer 1), 128.58 (CH), 129.51 (CH), 134.26 (CH), 135.6 (C), 181.04 (2 x CO)

3.5.2.20 (1,5-cyclo-octadiene)(1,3-diphenylpropane-1,3-dionato)platinum(II) hexafluorophosphate [Pt(cod)(dbm)]PF_6

LL'	Mass (mg)	A	Mass (mg)	Yield	IR_{KBr} (cm^{-1})
dbm	59.9	PF_6	135.1	30 mg 16 %	$\nu_{C=C}$ 1521, $\nu_{C=O}$ 1598, ν_{Pt-O} 682 and 474, $\nu_{Pt-[C=C]}$ 558 § Appendix A.41

^{1}H NMR (600.28 MHz, CD_2Cl_2) δ 2.196 (d, 4H, CH_2, *J* = 8.4 Hz, isomer 2), 2.602 (q, 4H, CH_2, *J* = 7.8 Hz, 8.4 Hz, isomer 1), 2.773 (d, 4H, CH_2, *J* = 7.8 Hz, isomer 2), 2.938 (d, 4H, CH_2, *J* = 11.4 Hz, isomer 1), 5.715 (s, 4H, CH, isomer 2), 5.945 (t, 4H, CH, *J* = 20.4 Hz, isomer 1), 6.909 (s, 1H, $C^{10}H$, isomer 2), 7.125 (s, 1H, $C^{10}H$, isomer 1), 7.516 (t, 4H, CH, *J* = 7.2 Hz, isomer 2), 7.545 (t, 4H, CH, *J* = 7.8 Hz, isomer 1), 7.585 (t, 2H, CH, *J* = 7.2 Hz, isomer 2), 7.675 (t, 2H, CH, *J* = 7.2 Hz, isomer 1), 7.963 (d, 4H, CH, *J* = 7.2 Hz, isomer 1), 8.006 (d, 4H, CH, *J* = 7.2 Hz, isomer 2)

^{13}C NMR (150.96 MHz, CD_2Cl_2) δ 30.15 (8 x CH_2, isomer 1 and 2), 93.1 ($C^{10}H$, isomer 2), 97.0 ($C^{10}H$, isomer 1), 100.03 (8 x CH, isomer 1 and 2), 127.49 (2 x CH, isomer 2), 128.59 (2 x CH, isomer 1), 129.07 (CH, isomer 2), 129.52 (CH, isomer 1), 132.9 (2 x CH, isomer 2), 134.26 (2 x CH, isomer 1), 135.67 (2 x C, isomer 1), 135.85 (2 x C, isomer 2), 181.07 (2 x CO, isomer 1), 186.15 (2 x CO, isomer 2)

3.6 Preparation of Rhodium Complexes

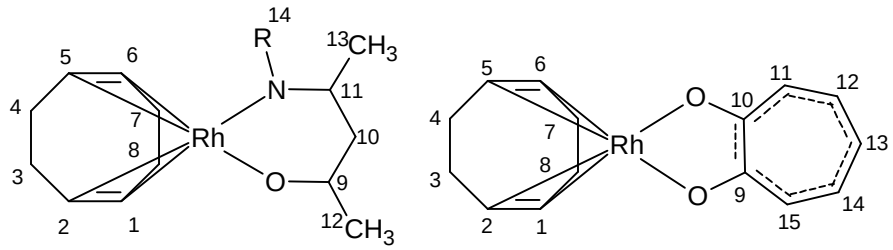

Figure 3.5 Line drawings representing general numbering of the rhodium complexes where R = H, CH_3, Ph additional carbons are numbered in increasing order.

Figure 3.5 represents a line drawings of the 1,5-cyclo-octadiene O,O- and N,O-bidentate rhodium(I) complexes prepared as well as the numbering of the carbon atoms. In the sections to follow a general synthetic route will be presented followed by tables for the different complexes containing the masses of reagents, yields, infra-red (IR) and nuclear magnetic resonance (NMR) characterization. For the NMR characterization it should be noted that the superscripts given, represents the number of the atom given in the line drawings (Figure 3.5)

3.6.1 Preparation of $[Rh(L_1)Cl]_2$[11] (L_1 = cod, nbd)

$RhCl_3.3H_2O$ (1 g, 3.84 x 10^{-3} mol) was dissolved in ethanol (absolute, 20 cm^3), an excess of the functionalized olefin (L_1 = cod, nbd) was added to the aforementioned solution. The resulting mixture was then refluxed (not exceeding 40 °C) until an orange-yellow precipitate formed (*c.a.* 3 hours). The precipitate was filtered and washed with (2 x 5 ml portions) cold methanol and air dried.

L_1		Yield	IR_{KBr} (cm^{-1})	NMR
cod	3 cm^3	79 mg 84 %	$\nu_{C=C}$ 1468 $\nu_{Rh-[C=C]}$ 486 § Appendix A.42	^{1}H NMR (600.28 MHz, $CDCl_3$) δ 1.770 (q, 8H, CH_2, *J* = 7.2 Hz, 8.4 Hz), 2.510 (d, 8H, CH_2, *J* = 10.8 Hz), 4.244 (t, 4H, CH, *J* = 79.2 Hz) ^{13}C NMR (150.96 MHz, $CDCl_3$) δ 31.23 (8 x CH_2), 79.04 (d, 8 x CH, *J* = 13.6 Hz)
nbd	3 cm^3	50 mg 45 %		

3.6.2 Preparation of [Rh(cod)(LL')] (LL' = acac, hfacac, tfacac, thtfac, dbm, NH-acac, NMe-acac, NPh-acac, trop, 3Br-trop)

$[Rh(cod)Cl]_2$ (50 mg, 1.01 x 10^{-4} mol) was dissolved in a minimum N,N-dimethylformamide (DMF) to which two equivalents of a bidentate ligand (LL' = Hacac, Htfacac, Hhfacac, Hthtfac, Hdbm, HNH-acac, HNMe-acac, HNPh-acac, Htrop, H3Br-trop, 2.03 x 10^{-4} mol) was added. The mixture was stirred at room temperature (25 °C) for approximately 5 minutes, precipitated with ice water and centrifuged. Alternatively the precipitate was filtered and dried *in vacuo*.

The different complexes synthesized are summarized below. The complexes were prepared using the procedure described above.

3.6.2.1 (1,5-cyclo-octadiene)(2,4-pentanedionato)rhodium(I) [Rh(cod)(acac)]

LL'	Mass (mg)	Yield	IR_{KBr} (cm^{-1})
acac	20.3	59 mg 95 %	$\nu_{C=C}$ 1563, $\nu_{C=O}$ 1665, ν_{Rh-O} 662 and 439, $\nu_{Rh-[C=C]}$ 487 § Appendix A.43
^{1}H NMR (600.28 MHz, $CDCl_3$) δ 1.771 (d, 4H, CH_2, *J* = 8.4 Hz), 1.951 (s, 6H, CH_3), 2.510 (s, 4H, CH_2), 4.246 (s, 4H, CH), 5.34 (s, 1H, $C^{10}H$) ^{13}C NMR (150.96 MHz, $CDCl_3$) δ 27.8 (2 x CH_3), 30.59 (CH_2), 31.23 (CH_2),79.05 (d, CH, *J* = 13.6 Hz), 100.09 ($C^{10}H$)			

[11] E.C. Steynberg, *Substitusiereaksies van ß-diketonatorodium(I)- en verwante Komplekse: Kinetiese en Kristallografiese Studie*, PhD Thesis, Free State University, Bloemfontein, South Africa, (1998)

3.6.2.2 (1,5-cyclo-octadiene)(1,1,1,5,5,5-hexafluoropentane-2,4-dionato)rhodium(I) [Rh(cod)(hfacac)]

LL'	Mass (mg)	Yield	IR_{KBr} (cm^{-1})
hfacac	42.2	50 mg 60 %	$\nu_{C=C}$ 1553, $\nu_{C=O}$ 1621, ν_{Rh-O} 592 and 382, $\nu_{Rh-[C=C]}$ 485 § Appendix A.44

^{1}H NMR (600.28 MHz, $CDCl_3$) δ 1.772 (d, 4H, CH_2, *J* = 7.8 Hz, isomer 1), 1.924 (d, 4H, CH_2, *J* = 7.8 Hz, isomer 2), 2.512 (s, 4H, CH_2, isomer 1), 3.128 (s, 4H, CH_2, isomer 2), 4.246 (s, 4H, CH, isomer 1), 4.318 (s, 4H, CH, isomer 2), 6.131 (s, 1H, $C^{10}H$, isomer 1), 6.224 (s, 1H, $C^{10}H$, isomer 2)

^{13}C NMR (150.96 MHz, $CDCl_3$) δ 30.4 (4 x CH_2, isomer 2), 31.23 (4 x CH_2, isomer 1), 78.67 (d, 4 x CH, *J* = 14.2 Hz, isomer 2), 79.05 (d, 4 x CH, *J* = 13.9 Hz, isomer 1), 117.06 (2 x CF_3, isomer 2), 118.94 (2 x CF_3, isomer 1), 174.97 (2 x CO, isomer 2), 175.2 (2 x CO, isomer 1)

3.6.2.3 (1,5-cyclo-octadiene)(1,1,1-trifluoropentane-2,4-dionato)rhodium(I) [Rh(cod)(tfacac)]

LL'	Volume (µl)	Yield	IR_{KBr} (cm^{-1})
tfacac	24.6	57 mg 73 %	$\nu_{C=C}$ 1520 ,$\nu_{C=O}$ 1607, ν_{Rh-O} 627 and 385, $\nu_{Rh-[C=C]}$ 486 § Appendix A.45

^{1}H NMR (600.28 MHz, $CDCl_3$) δ 1.771 (d, 4H, CH_2, *J* = 8.4 Hz, isomer 1), 1.868 (d, 4H, CH_2, *J* = 7.8 Hz, isomer 2), 2.100 (s, 3H, CH_3, isomer 1), 2.243 (s, 3H, CH_3, isomer 2), 4.246 (s, 4H, CH, isomer 1), 5.743 (s, 1H, $C^{10}H$, isomer 1), 5.947 (s, 1H, $C^{10}H$, isomer 2)

^{13}C NMR (150.96 MHz, $CDCl_3$) δ 28.97 (CH_3), 31.22 (4 x CH_2), 79.05 (d, 4 x CH, *J* = 13.6 Hz), 95.45 ($C^{10}H$)

3.6.2.4 (1,5-cyclo-octadiene)(4-aminopent-3-en-2-onato)rhodium(I) [Rh(cod)(NH-acac)]

LL'	Mass (mg)	Yield	IR_{KBr} (cm^{-1})
NH-acac	20.3	45 mg 72 %	ν_{N-H} 3290, $\nu_{C=C}$ 1566, $\nu_{C=O}$ 1677, ν_{Rh-O} 608 and 439, $\nu_{Rh-[C=C]}$ 487 § Appendix A.46

^{1}H NMR (600.28 MHz, $CDCl_3$) δ 1.837 (d, 4H, CH_2, *J* = 7.8 Hz), 2.008 (s, 3H, CH_3), 2.038 (s, 2H, CH_3), 2.459 (m, 4H, CH_2), 4.085 (s, 4H, CH), 4.395 (s, 4H, CH), 4.999 (s, 1H, $C^{10}H$)

^{13}C NMR (150.96 MHz, $CDCl_3$) δ 27.14 (CH_3), 27.93 (CH_3), 30.58 (2 x CH_2), 31.42 (2 x CH_2), 76.82 (d, 2 x CH, *J* = 14 Hz), 82.9 (d, 2 x CH, *J* = 10.5 Hz), 96.62 ($C^{10}H$), 166.03 (CN), 180.18 (CO)

The NMR sample was found to be a mixture, with [Rh(cod)(acac)] present due to the starting compound acetylacetone present in the ligand sample used.

3.6.2.5 (1,5-cyclo-octadiene)(4-(methylamino)pent-3-en-2-onato)rhodium(I) [Rh(cod)(NMe-acac)]

LL'	Volume (µl)	Yield
NMe-acac	24.2	40 mg 59 %

Product decomposed.

3.6.2.6 (1,5-cyclo-octadiene)(4-anilinopent-3-en-2-onato)rhodium(I) [Rh(cod)(NPh-acac)]

LL'	Mass (mg)	Yield	IR_{KBr} (cm^{-1})
NPh-acac	35.5	78 mg 98 %	$\nu_{C=C}$ 1563, γ_{C-H}[a] 765 and 716, $\nu_{Rh=O}$ 607 and 439, $\nu_{Rh-[C=C]}$ 487 § Appendix A.47
^1H NMR (600.28 MHz, $CDCl_3$) δ 1.836 (d, 4H, CH_2, *J* = 7.8 Hz), 2.479 (s, 4H, CH_2), 4.084 (s, 2H, CH), 4.399 (s, 2H, CH), 5.120 (s, 1H, $C^{10}H$), 6.868 (d, 2H, CH, *J* = 7.2 Hz), 7.095 (t, 1H, CH, *J* = 7.2 Hz), 7.298 (t, 2H, CH, *J* = 7.2 Hz) ^{13}C NMR (150.96 MHz, $CDCl_3$) δ 29.28 (2 x CH_2), 30.58 (2 x CH_2), 79.04 (d, 2 x CH, *J* = 13.9 Hz), 82.05 (d, 2 x CH, *J* = 12.1 Hz), 98.64 ($C^{10}H$), 124.89 (CH), 125.13 (2 x CH), 128.63 (2 x CH), 150.84 (CN-phenyl), 165.46 (CN), 178.76 (CO)			

[a] Aromatic C - H out of plane bend, monosubstitution (phenyl)

The NMR sample was found to be a mixture, with [Rh(cod)(acac)] present due to the starting compound acetylacetone present in the ligand sample used.

3.6.2.7 (1,5-cyclo-octadiene)(1,3-diphenylpropane-1,3-dionato)rhodium(I) [Rh(cod)(dbm)]

LL'	Mass (mg)	Yield	IR_{KBr} (cm^{-1})
dbm	45.5	90 mg 98 %	$\nu_{C=C}$ 1540, $\nu_{C=O}$ 1589, γ_{C-H}[a] 756 and 694, ν_{Rh-O} 539 and 445, $\nu_{Rh-[C=C]}$ 490 § Appendix A.48
^1H NMR (600.28 MHz, $CDCl_3$) δ 1.772 (d, 4H, CH_2, *J* = 8.4 Hz, isomer 2), 1.939 (d, 4H, CH_2, *J* = 7.8 Hz, isomer 1), 2.529 (s, 4H, CH_2, isomer 2), 2.552 (s, 4H, CH_2, isomer 1), 4.250 (s, 4H, CH, isomer 2), 4.301 (s, 4H, CH, isomer 1), 6.673 (s, 1H, $C^{10}H$, isomer 1), 6.886 (s, 1H, $C^{10}H$, isomer 2), 7.399 (t, 2H, CH, *J* = 7.8 Hz, isomer 1), 4.463 (t, 2H, CH, *J* = 7.2 Hz, isomer 1), 7.518 (t, 1H, CH, *J* = 7.2 Hz, isomer 1), 7.582 (t, 1H, CH, *J* = 7.2 Hz, isomer 1) 7.850 (d, 2H, CH, *J* = 7.8 Hz, isomer 1), 8.017 (d, 2H, CH, *J* = 7.2 Hz, isomer 1) ^{13}C NMR (150.96 MHz, $CDCl_3$) δ 30.69 (4 x CH_2), 31.22 (4 x CH_2), 79.05 (d, 2 x CH_2, *J* = 13.6 Hz), 93.51 ($C^{10}H$, isomer 2), 94.42 ($C^{10}H$, isomer 1), 127.53(CH), 127.67 (CH), 128.57 (CH), 129.04 (CH), 131.13 (CH), 132.80 (CH), 135.92 (C), 140.02 (C), 181.9 (CO), 186.12 (CO)			

3.6.2.8 (1,5-cyclo-octadiene)(2-hydroxy-cyclohepta-2,4,6-trieneonato)rhodium(I) [Rh(cod)(trop)]

LL'	Mass (mg)	Yield	IR_{KBr} (cm^{-1})
trop	28.8	64 mg 93 %	$\nu_{C=C}$ 1504, $\nu_{C=O}$ 1588, ν_{Rh-O} 628 and 492, $\nu_{Rh-[C=C]}$ 559 § Appendix A.49
^1H NMR (600.28 MHz, $CDCl_3$) δ 1.845 (d, 4H, CH_2, *J* = 7.8 Hz), 2.467 (s, 4H, CH_2), 4.29 (s, 1H, CH), 7.027 (t, 1H, CH, *J* = 9 Hz), 7.307 (d, 2H, CH, *J* = 10.8 Hz), 7.426 (t, 2H, CH, *J* = 9.6 Hz) ^{13}C NMR (150.96 MHz, $CDCl_3$) δ 30.75 (4 x CH_2), 75.02 (d, 4 x CH, *J* 15Hz), 127.33 (2 x CH), 127.68 (2 x CH), 137.23 (2 x CH), 186.14 (2 x CO)			

3.6.2.9 (1,5-cyclo-octadiene)(3,5,7-tribromo-2-hydroxy-cyclohepta-2,4,6-trieneonato)rhodium(I) [Rh(cod)(3Br-trop)]

LL'	Mass (mg)	Yield	IR_{KBr} (cm^{-1})
3Br-trop	72.7	118 mg 93 %	$\nu_{C=C}$ 1461, $\nu_{C=O}$ 1567, ν_{Rh-O} 603 and 384, $\nu_{Rh-[C=C]}$ 542 § Appendix A.50

^{1}H NMR (600.28 MHz, $CDCl_3$) δ 1.772 (d, 4H, CH_2, J = 8.4 Hz, isomer 2), 1.867 (d, 4H, CH_2, J = 7.8 Hz, isomer 1), 2.476 (s, 4H, CH_2, isomer 1), 4.423 (s, 4H, CH, isomer 1), 4.246 (s, 4H, CH, isomer 2), 8.359 (s, 2H, CH, isomer 2), 8.445 (s, 2H, CH, isomer 1)

^{13}C NMR (150.96 MHz, $CDCl_3$) δ 30.67 (4 x CH_2, isomer 1), 31.22 (4 x CH_2, isomer 2), 76.03 (d, 4 x CH, J = 15 Hz, isomer 1), 79.05 (d, 4 x CH, J = 13.5 Hz, isomer 2), 115.05 (CBr), 124.66 (CBr), 127.73 (CBr), 142.74 (2 x CH, isomer 1), 144.31 (2 x CH, isomer 2), 177.3 (2 x CO, isomer 1), 164.9 (2 x CO, isomer 2)

3.6.2.10 (1,5-cyclo-octadiene)(4,4,4-trifluoro-1-(2-thienyl)-1,3-butenedionato)rhodium(I) [Rh(cod)(thtfac)]

LL'	Mass (mg)	Yield	IR_{KBr} (cm^{-1})
thtfac	45.1	41 mg 47 %	$\nu_{C=C}$ 1589, ν_{Rh-O} 669 and 384, $\nu_{Rh-[C=C]}$ 470 § Appendix A.51

^{1}H NMR (600.28 MHz, $CDCl_3$) δ 1.904 (d, 4H, CH_2, J = 7.8 Hz), 2.521 (s, 4H, CH_2), 4.25 (d, 4H, CH, J = 9.6 Hz), 6.301 (s, 1H, $C^{10}H$), 7.096 (t, 1H, CH, J = 4.2 Hz), 7.582 (d, 1H, CH, J = 4.2 Hz), 7.656 (d, 1H, CH, J = 4.2 Hz)

^{13}C NMR (150.96 MHz, $CDCl_3$) δ 30.6 (4 x CH_2), 79.06 (d, 4 x CH, J = 14 Hz), 91.53 ($C^{10}H$), 128.68 (CH), 130.34 (CH), 133.25 (CH), 144.32 (C), 169.13 (CF_3), 179.21 (2 x CO)

3.7 Discussion

The synthesis of the enaminones was achieved by the condensation of a primary or secondary amine with a β-diketone. For the synthesis of NH-acac a deep yellow oil was obtained. Several attempts at recrystalization of the oil proved unsuccessful. Single crystals were obtained for 4-(methylamino)pent-3-en-2-one and will be further discussed in Chapter 11. The crystalline product of 4-anilinopent-3-en-2-one was used as obtained. The single crystal X-ray structure of this product has previously been reported[12]. The products were characterized by both NMR and IR spectroscopy.

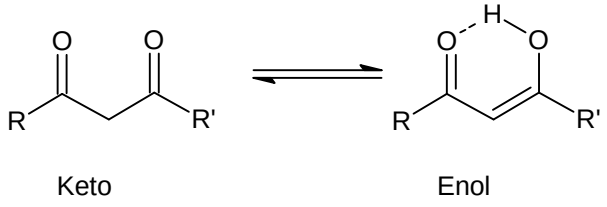

Scheme 3.1 The enolization process of β-diketones.

[12] Shaheen F., Marchio L., Badshah A., Khosa M.K., *Acta Cryst.*, **E62**, o873, (2006)

β-Diketones are known for their keto-enol tautomeric formations (Scheme 3.1). This is characteristically seen on the NMR spectra where the keto (CH_2) peak is present and used to determine the keto-enol ratio. This is achieved by taking the relative integrals of the keto (CH_2) peak and dividing it by the relative integral for the enol (CH) peak, which gives a percentage of keto configuration present for the compound. An example of this is shown for acetylactone with a ratio of 3.03 % as seen in Figure 3.6.

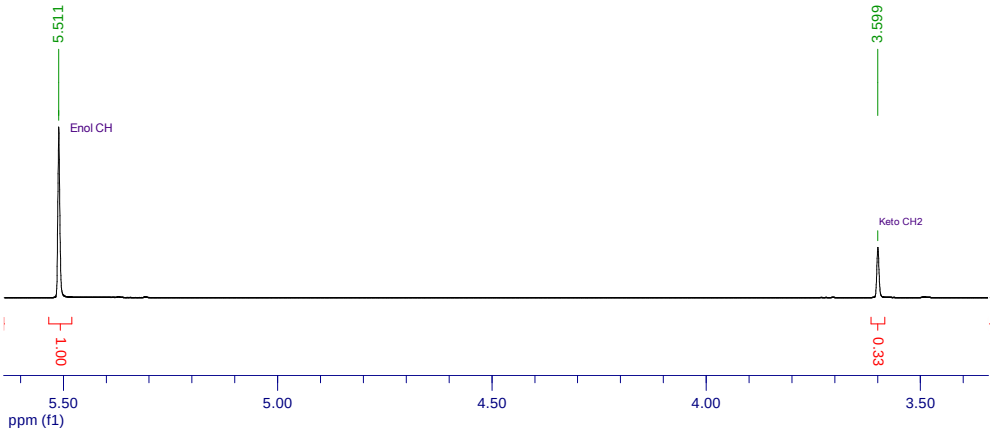

Figure 3.6 Excerpt of the ^{1}H spectra for acetylacetone at 25 °C in $CDCl_3$ depicting the keto-enol tautomerism.

It is interesting to note that the enaminones do not have the characteristic keto (CH_2) group to easily determine their keto-enol formations. Scheme 3.2 shows the keto-enol process for the enaminones the only method of determining the keto-enol ratio would be to look at δ(OH) *vs.* δ(NH), however the δ(OH) peak is not always easily determined.

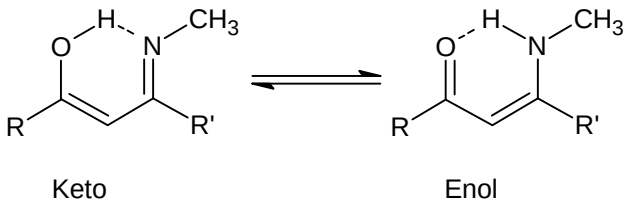

Scheme 3.2 The enolization process of enaminones.

Figure 3.7 shows an example of NH-acac keto-enol determination, where the ratio was found to be 10.6 % (0.32 / 0.03). No δ(OH) peak was observed for NMe-acac, for NPh-acac we observe a similar situation as with NH-acac, the keto-enol ratio was

found to be 100 % (1 / 0.01) leading us to the conclusion that the enol form is far preferred for the enaminones selected in this study.

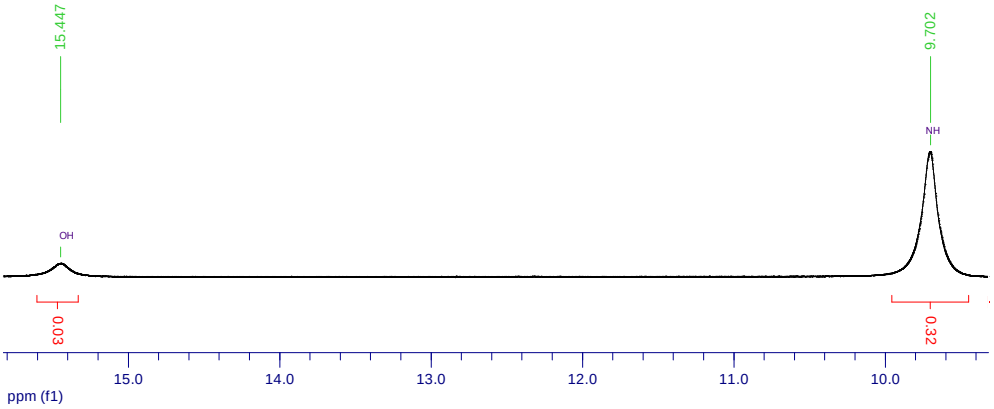

Figure 3.7 Excerpt of the ^{1}H spectra for NH-acac at 25 °C in $CDCl_3$ depicting the keto-enol tautomerism.

For the infra-red spectra a lowering of the expected wavenumber for ν(N-H) *ca.* 3500 cm^{-1} was observed due to the strong hydrogen interaction with the oxygen, this change is reflected in the NMR spectra where the δ(NH) for NH-, NMe- and NPh-acac are 9.701, 10.699 and 12.486 ppm, the δ(OH) for acac is 15.465 ppm. With an increase in the electron withdrawing nature of the groups attached to the nitrogen an upfield shift (increased shielding) in the NMR spectra was observed. This shielding can be further observed in the δ(CH_3), for NMe-acac where the methyl group attached to the nitrogen shows a shift of 2.932 ppm whilst the methyl groups attached to the acetylactone backbone show shifts of 1.970 and 1.918 ppm respectively. For NPh-acac the methyl groups attached to the backbone were found to be 2.113 and 2.005 ppm respectively with the higher shift values being the methyl closest to the nitrogen.

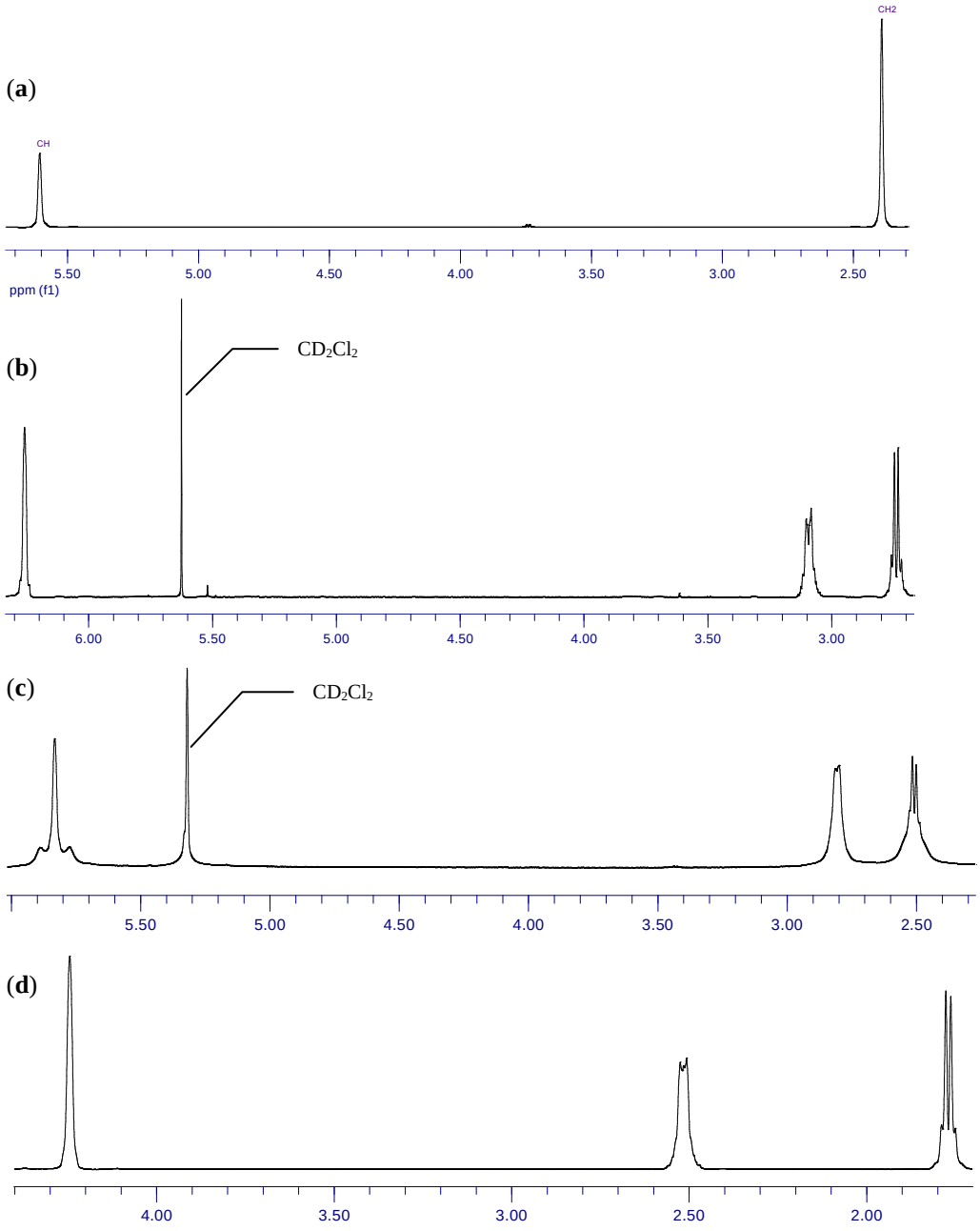

Figure 3.8 Excerpts of NMR Spectra for (a) Free cod in $CDCl_3$ (b) $[Pd(cod)(acac)]PF_6$ in CD_2Cl_2 (c) $[Pt(cod)(trop)]PF_6$ in CD_2Cl_2 (d) $[Rh(cod)Cl]_2$ in $CDCl_3$ at 25 °C.

In Figure 3.8 a series of ^1H NMR spectra of 1,5-cyclo-octadiene both unco-ordinated and co-ordinated to various metals (palladium(II) Figure 3.8b, platinum(II) Figure 3.8c and rhodium(I) Figure 3.8d) are listed. Upon co-ordination with a metal centre, the methylene protons of the cyclo-octadiene become non-equivalent and thus result in the peak being split into a doublet. The additional splitting which is observed is due to geminal coupling as well as vicinal coupling with the methine protons. The

methine protons show similar chemical environments upon co-ordination with the various metal centres as a result the singlet seen in the free cyclo-octadine spectra Figure 3.8a remains.

3.7.1 Palladium(II) Complexes

The palladium complexes were synthesized by reacting palladium chloride dissolved in ethanol and adding 1,5-cyclo-octadiene (cod). The products were isolated in good yield (96 %). The palladium cyclo-octadiene complex was further reacted with the range of bidentate ligands selected (Table 3.1) in dichloromethane in the presence of a silver salt, either tetrafluoroborate or hexafluorophosphate. Several other silver salts were attempted but it was found that the products either did not form as in the case of silver nitrate or the products decomposed within a few hours with very poor yields using silver triflate. It was found that the silver hexafluorophosphate was the most stable yielding higher than its counterpart tetrafluoroborate. The yields for the reactions varied between 1.6% - 76 %, with only a few of the bidentate ligands yielding higher than 50 % generally most of the compounds formed were of lower yields.

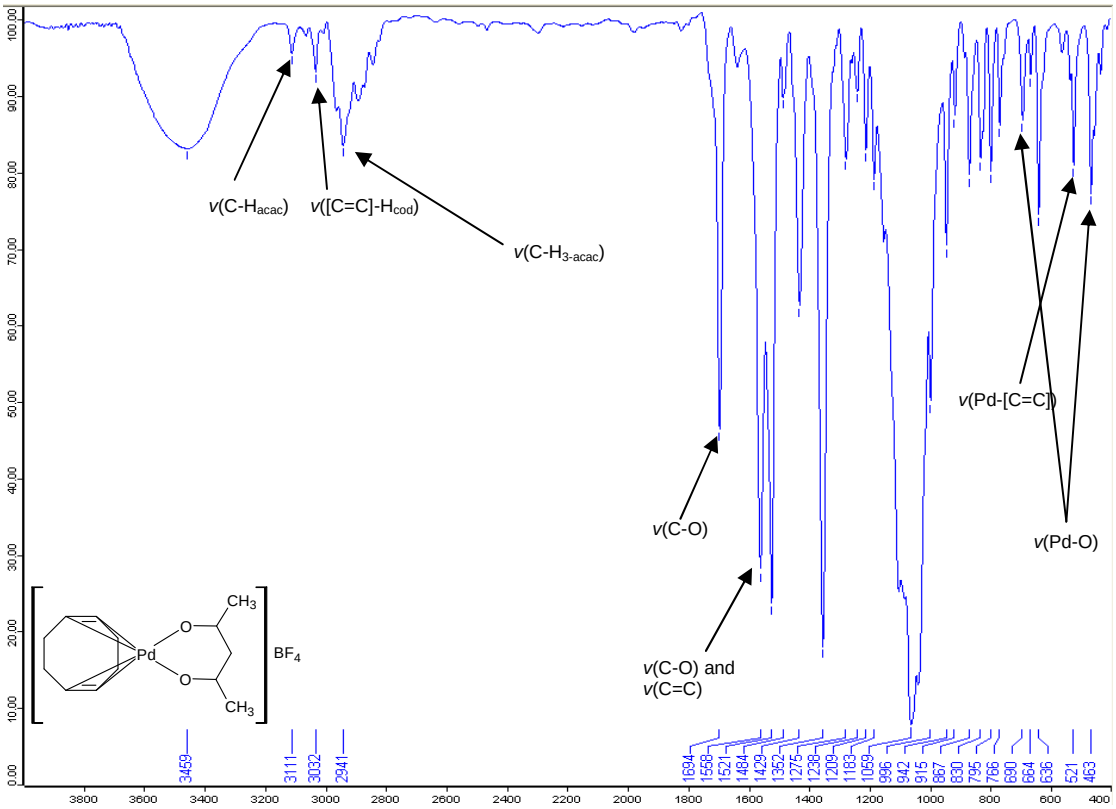

Figure 3.9 Infra-red spectrum of [Pd(cod)(acac)]BF_4 in KBr.

Figure 3.9 represents a typical infra-red (IR) spectrum obtained for the palladium complexes. In the spectra several distinctive stretching frequencies have been illustrated. Firstly, the CH stretching region, methyl (CH_3) stretching frequencies are usually found between 2970-2950 cm^{-1} / 2880-2860 cm^{-1} (asym. / sym.), the methine (CH) stretching frequency 3040-3010 cm^{-1}, in Figure 3.9 $\nu_{asym}(CH_3)$ = 2941 cm^{-1}, ν([C=C]-H) = 3032 cm^{-1} and ν(CH) = 3111 cm^{-1} the acetylacetonato methine proton is higher than expected as a result of the conjugation / co-ordination with the palladium metal centre the proton has a more aromatic nature due to being part of the chelate ring, the aromatic CH stretching region is 3130-3070 cm^{-1}. In examining the ketone (CO) and olefinic (C=C) regions, the ketone region of the compounds it is best to use the conjugated ketone range which is 1690-1675 / (1650-1600 cm^{-1}) the second set of values is from the frequency band of the conjugation. However the olefinic region is 1680-1620 cm^{-1} which overlaps with the conjugated ketone region, this has caused much controversy in the assignment of the respective stretching frequencies, with the help of computational chemistry the assignments for the complexes were found. For [Pd(cod)(acac)]BF_4, ν(CO) = 1694 cm^{-1} and ν_{asym}(CO) and ν(C=C) overlapping at 1558 cm^{-1}. The broad strong band at 1059 cm^{-1} is attributed to the BF_4^- counter ion.

Lastly the co-ordination to the palladium metal centre, thus usually occurs in the far infra-red region (400-20 cm^{-1}), however it was lucky that the palladium ligand stretching frequencies were observed in the mid infra-red region (400-4000 cm^{-1}). The ν(Pd-[C=C]) = 521 cm^{-1} and for ν(Pd-O) we observed two frequencies, the first being a combination of ν(Pd-O) + Δ ring (in-plane ring distortion), while the second ν(Pd-O) with values of 636 cm^{-1} and 463 cm^{-1} respectively. These bands were assigned based on the previous assignments of similar compounds by Mikami *et al.*[13] and Nakamoto *et al.*[14] which studied a range of bis-acetylacetonato transition metal complexes.

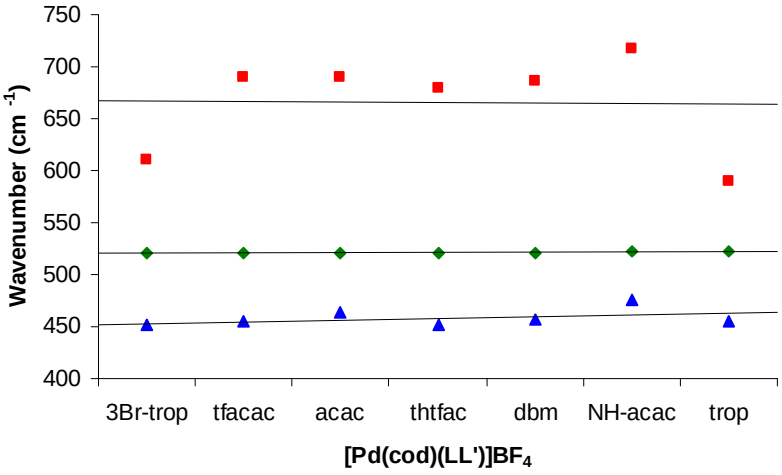

Figure 3.10 A graph of Wavenumber (cm^{-1}) *vs.* [Pd(cod)(LL')]BF_4 where LL' = acac, tfacac, thtfac, dbm, trop, 3Br-trop, NH-acac for ν(Pd-[C=C]) (green diamond), ν(Pd-O) first (red square) and ν(Pd-O) second (blue triangle) arranged in ascending ν(Pd-[C=C]) order.

The infra-red stretching frequencies for [Pd(cod)(LL')]BF_4 where LL' = acac, tfacac, thtfac, dbm, trop, 3Br-trop, NH-acac are represented in Figure 3.10, the ν(Pd-O) first (red square) is a combination of both the palladium oxygen stretching frequency and Δ (in plane ring distortion) ring as can be seen from the graph the general trend is linear with the tropolone (trop) and tribromotropolone (3Br-trop) being the out-liers, however it is of note that trop and 3Br-trop are the only five membered chelate rings and thus the contribution of the in-plane ring distortion will be reflected in the frequency values. The ν(Pd-[C=C]) frequency is generally not affected by the change of bidentate ligand (green diamond), there is only a slight increase found for the ν(Pd-O) second (blue triangles).

[13] Mikami M., Nakagawa I., Shimanouchi T., *Spectrochim. Acta*, **A23**, 1037, (1967)
[14] Nakamoto N., McCarthy P.J., Ruby A., Martell A.E., *J. Am. Chem. Soc.*, **83**, 1066, 1272, (1961)

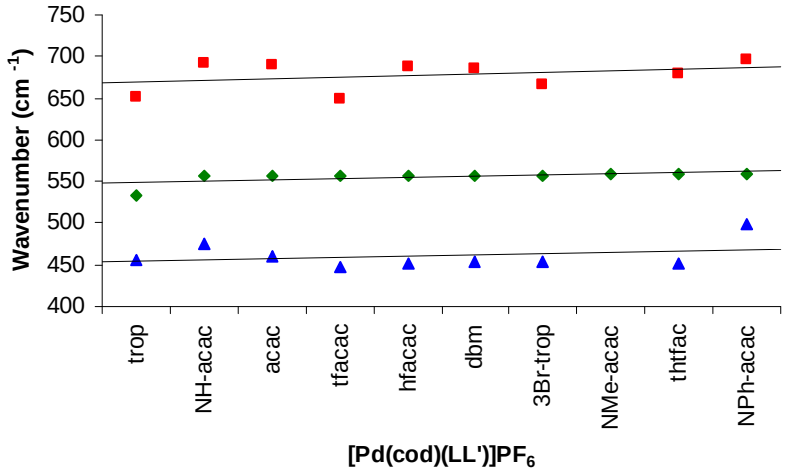

Figure 3.11 A graph of Wavenumber (cm^{-1}) *vs.* [Pd(cod)(LL')]PF_6 where LL' = acac, tfacac, hfacac, thtfac, dbm, NH-acac, NMe-acac, NPh-acac, trop, 3Br-trop for ν(Pd-[C=C]) (green diamond), ν(Pd-O) first (red square) and ν(Pd-O) second (blue triangle) arranged in ascending ν(Pd-[C=C]) order.

The infra-red stretching frequencies for [Pd(cod)(LL')]PF_6 where LL' = acac, tfacac, hfacac, thtfac, dbm, NH-acac, NMe-acac, NPh-acac, trop, 3Br-trop are presented in Figure 3.11, it is clear that the values are very similar to the [Pd(cod)(LL')]BF_4 complexes (Figure 3.10), in that the ν(Pd-[C=C]) frequency remains relatively constant. There is a shift in the stretching frequencies from the BF_4 complexes to the PF_6 complexes of *ca.* 34 cm^{-1}. The ν(Pd-O) (blue triangle) shows little to no difference in the stretching frequencies with and average 458 cm^{-1} leading to the conclusion that the anion does not influence the palladium oxygen bond. It is of note that the both the *ν*(Pd-O) frequencies were not observed for [Pd(cod)(NMe-acac)]PF_6.

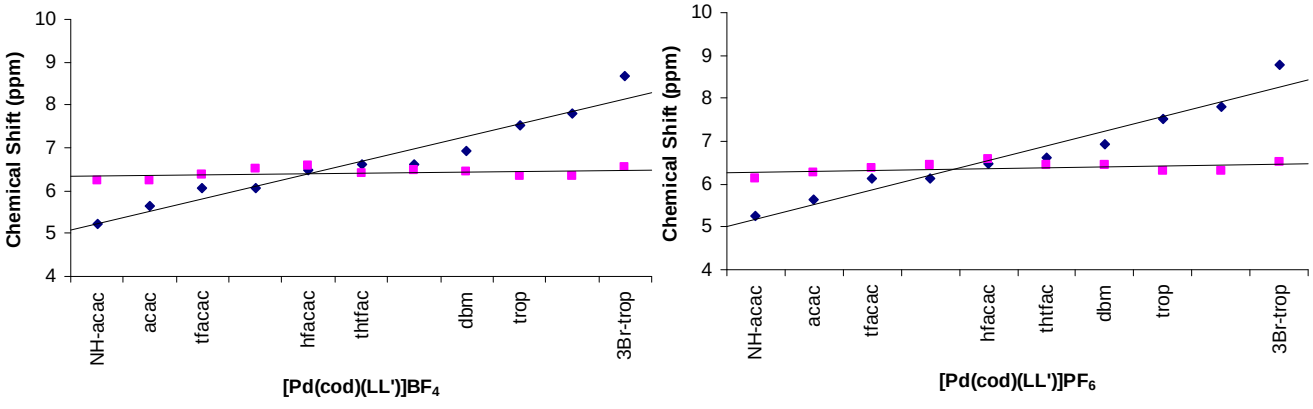

Figure 3.12 A graph of NMR chemical shift *vs.* [Pd(cod)(LL')]A where (a) BF_4 and (b) PF_6 where δ(CH-cod) is the pink squares and δ(CH-LL') are the blue diamonds. Arranged in ascending δ(CH-LL').

In Figure 3.12 the NMR chemical shifts for both the [Pd(cod)(LL')]BF_4 and [Pd(cod)(LL')]PF_6 where LL' = acac, hfacac, tfacac, thtfac, dbm, NH-acac, trop, 3Br-trop complexes are nearly identical with the gaps on the x-axis indicating multiple values for the preceding bidentate represented. These multiple values are generally the different isomers that were observed for the complexes involved. With the olefinic protons (pink squares) showing little change with an average value for the [Pd(cod)(LL')]BF_4 complexes of 6.404 ppm and for the [Pd(cod)(LL')]PF_6 complexes 6.378 ppm, a difference of *ca*. 0.03 ppm was found, the methine proton on the bidentate ligand is shown to be affected by the substituents on the acetylactone type backbone. In the case of the tropolone and tribromotropolone complexes the aromatic CH chemical shift values were used for the graph. The variation of anion did not significantly affect the chemical shifts of the complexes.

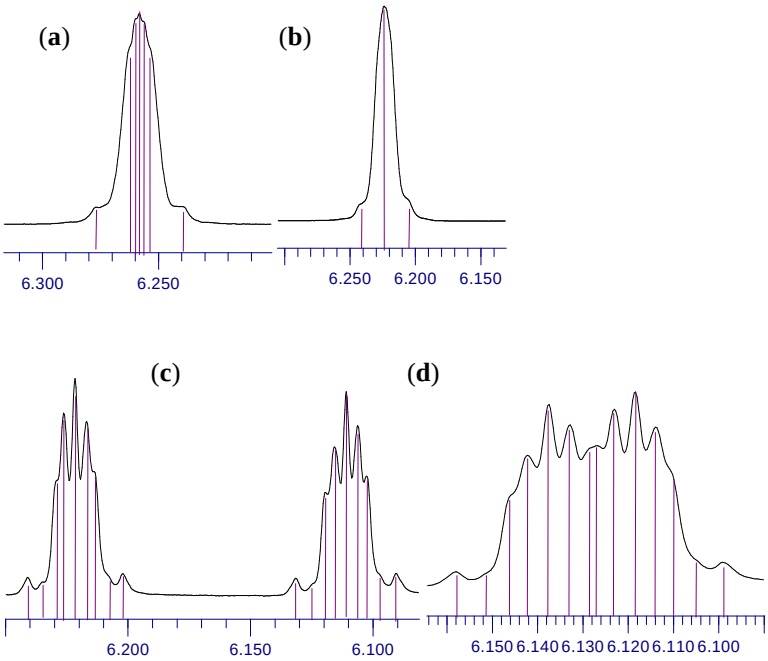

Figure 3.13 Excerpts of ^{1}H spectra of (a) [Pd(cod)(acac)]PF_6 (b) [Pd(cod)(acac)]BF_4 (c) [Pd(cod)(NH-acac)]PF_6 and (d) [Pd(cod)(NH-acac)] at 25 °C in CD_2Cl_2 with only (a) being in $CDCl_3$ showing the δ(CH) coupling.

Palladium (^{105}Pd) is known to be a spin active metal centre with a 5/2 spin and a 22.33(8) % natural abundance, this results in coupling between palladium and hydrogen which is reflected in the δ(CH) being split into a septet (7), which can be clearly seen in Figure 3.13a, however in Figure 3.13b we only observe a triplet this is due to the change in counter ion from PF_6 to BF_4. It was found that the PF_6 counter

ion complex shows the complete palladium hydrogen coupling, the coupling constant $^{3}J_{Pd\text{-}H}$ was found to be 2.4 Hz for all the palladium complexes synthesized. In Figure 3.13c and Figure 3.13d it was found that there is an additional coupling from the vicinal hydrogen on the olefinic carbons, this further splits the multiplets into a doublet of multiplets, again it is observed that the PF_6 counter ion complex expands the coupling. The $^{3}J_{HH}$ coupling for the [Pd(cod)(NH-acac)]BF_4 complex is 12 Hz and the overlap of the multiplets can be clearly seen whereas for the [Pd(cod)(NH-acac)]PF_6 is 66.6 Hz and the multiplets are clearly separated. This interaction has an additional effect on the long distance coupling of the $\delta(CH_2)$ shifts which results in hard to determine mulitplets.

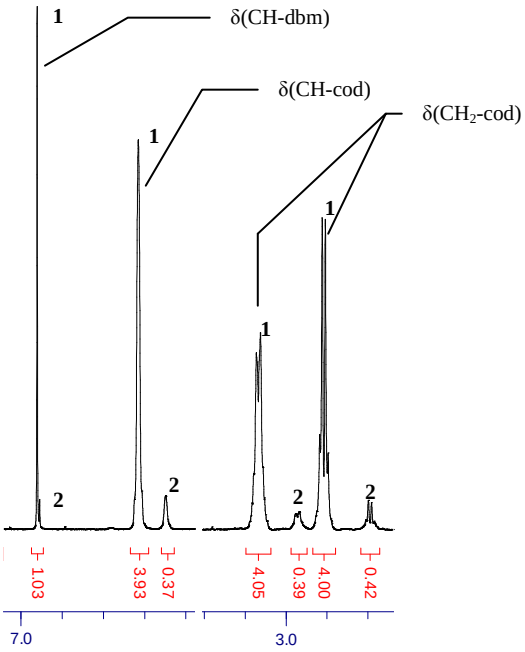

Figure 3.14 Excerpt of the ^{1}H NMR spectra of [Pd(cod)(dbm)]PF_6 at 25 °C in CD_2Cl_2 showing the formation of isomers.

Figure 3.14 shows the cyclo-octadiene chemical shifts and the methine chemical shift for the dibenzoylmethane ligand, the bold numbers indicate isomer, the ratio was found to be *ca.* 9.5 % with an average chemical shift of *ca.* 0.2 ppm, the shift decreases as we move to the dibenzoylmethane peaks.

3.7.2 Platinum(II) Complexes

The platinum complexes were synthesized by taking potassium tetrachloroplatinate and dissolving it in a mixture of water and propanol to this was added a catalytic amount of tin chloride and the 1,5-cyclo-octadiene (cod), the mixture was stirred for several days and allowed to evaporate to dryness where upon it was extracted with dichloromethane the yields obtained were excellent (92 %). This platinum cyclo-octadiene complex was then further reacted with an equivalent of the selected bidentate ligand (Table 3.1) in the presence of a silver salt, either tetrafluoroborate (BF_4) or hexafluorophosphate (PF_6). The yields for the reactions varied between 82.5 % - 3.5 %, most of the compounds formed were of higher yield (50+ %) the lower yield compounds were found to be the higher electron withdrawing bidentate ligands an example of this is the Hhfacac ligand which shows the poorest yields.

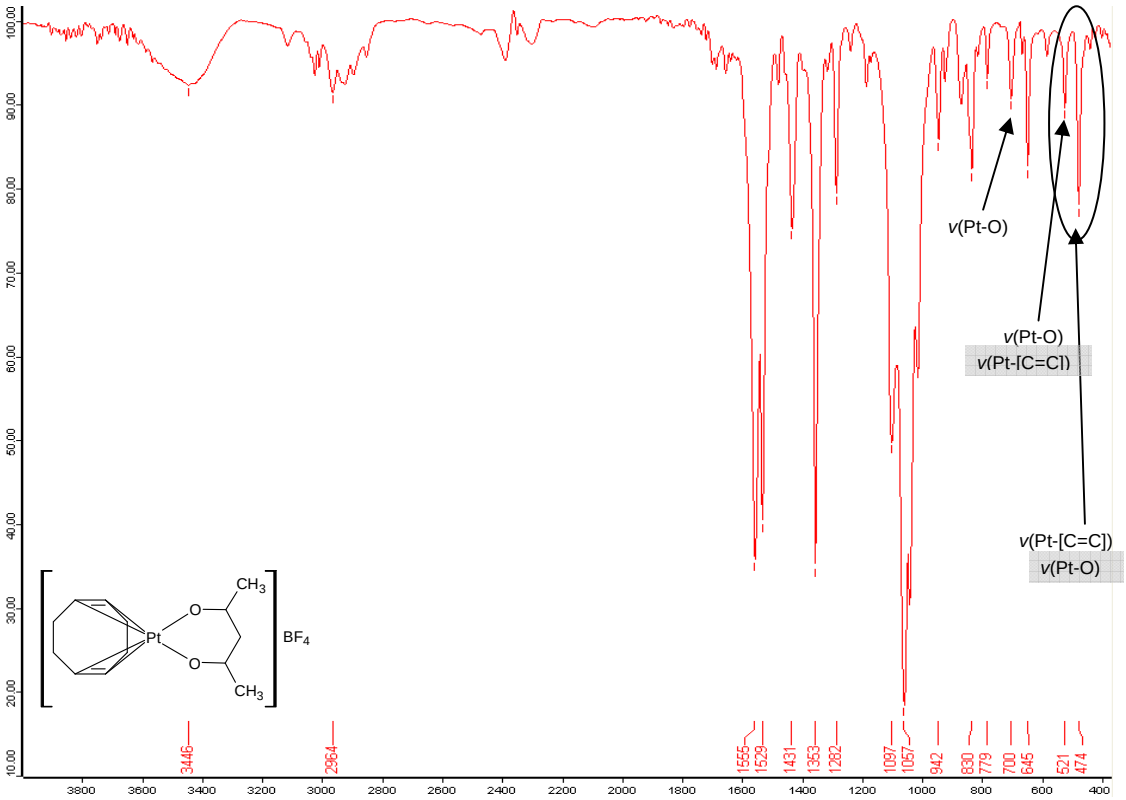

Figure 3.15 Infra-red spectra of [Pt(cod)(acac)]BF_4 in KBr.

Figure 3.15 represents a typical spectrum of the platinum complexes obtained in this study. The first peaks of interest are highlighted within the oval in Figure 3.15. For the peak seen at 521 cm^{-1}, the computed spectra suggests the assignment of the *ν*(Pt-O) frequency, however upon inspection of the infra-red tables and the comparison with the palladium complexes presented previously the assignment of the

peak to *ν*(Pt-[C=C]) frequency was selected. The reverse logic holds for the 474 cm^{-1} peak, being that the computed spectra suggests *ν*(Pt-[C=C]) whilst the tables suggest *ν*(Pt-O). Thus the final assignments are ν(Pt-O)+Δ ring (first) = 644.77 cm^{-1}, ν(Pt-O) = 473.46 cm^{-1} and ν(Pt-[C=C]) = 520.97 cm^{-1}. The other peaks within the spectra are as expected and have been listed in the synthetic section (§ 3.5.2). In comparing the ν(Pd-O) and ν(Pt-O) frequencies we find that there is not a dramatic difference between the two, this holds true for the ν(Pd-[C=C]) and ν(Pt-[C=C]) frequencies as well.

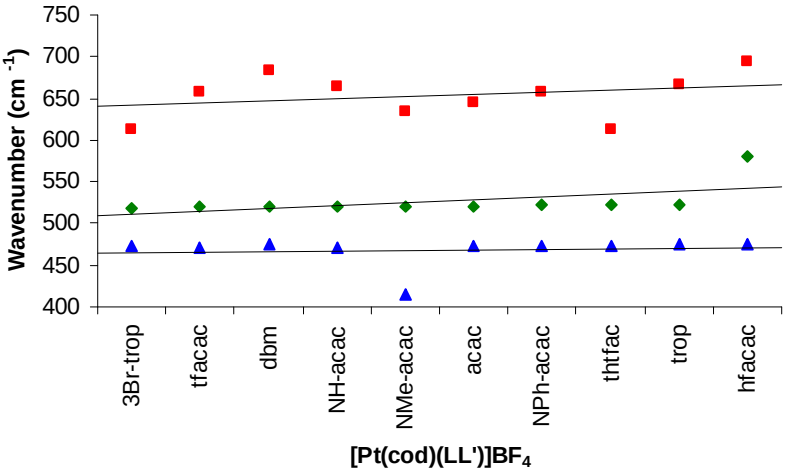

Figure 3.16 A graph of Wavenumber (cm^{-1}) *vs.* [Pt(cod)(LL')]BF_4 where LL' = acac, tfacac, hfacac, thtfac, dbm, NH-acac, NMe-acac, NPh-acac, trop, 3Br-trop for ν(Pt-[C=C]) (green diamond), ν(Pt-O) + Δ ring (red square) and ν(Pt-O) second (blue triangle) arranged in ascending ν(Pt-[C=C]) order.

Figure 3.16 is arranged in ascending order of ν(Pt-[C=C]), generally linear trends are observed for all the stretching frequencies listed. The ν(Pt-O) + Δ ring (first) frequencies (red squares) are the most varied from linear due to the nature and size of the metallocycle formed. The lowest of these values are found for the 5 membered metallocycles of tropolone and tribromotropolone. The order observed for the platinum complexes is as follows 3Br-trop > tfacac > dbm > NH-acac > NMe-acac > acac > NPh-acac > thtfac > trop > hfacac. On comparison with the [Pd(cod)(LL')]BF_4 complexes represented in Figure 3.10 we find that the general trends are similar with the greatest variance being the ν(Pd-O) + Δ ring frequencies. The order found for the palladium complexes is as follows 3Br-trop > tfacac > acac > thtfac > dbm > NH-acac > trop.

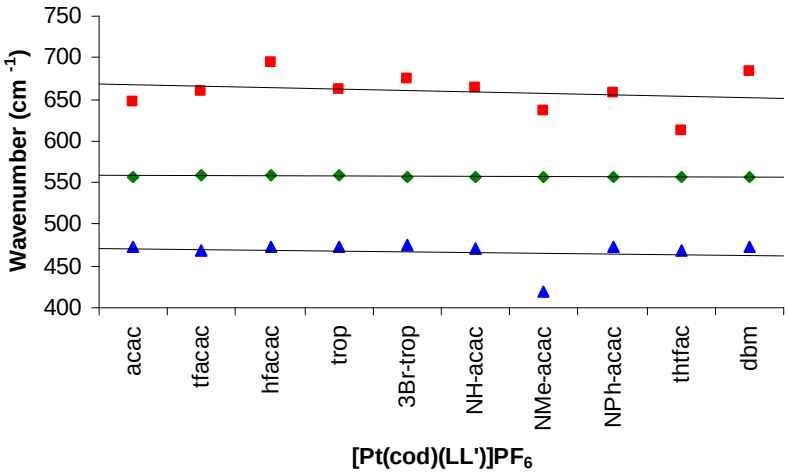

Figure 3.17 A graph of Wavenumber (cm^{-1}) *vs.* [Pt(cod)(LL')]PF_6 where LL' = acac, tfacac, hfacac, dbm, NH-acac, NMe-acac, NPh-acac, trop, 3Br-trop for ν(Pt-[C=C]) (green diamond), ν(Pt-O) + Δ ring (red square) and ν(Pt-O) second (blue triangle) arranged in ascending ν(Pt-[C=C]) order.

The IR values in Figure 3.17 represent [Pt(cod)(LL')]PF_6 complexes, their values are similar to those in Figure 3.16 for [Pt(cod)(LL')]BF_4. The average value for ν(Pt-[C=C]) (green diamonds) is 557.8 cm^{-1} which is a *ca.* 30 cm^{-1} difference from the average value for the BF_4 complexes (526.8 cm^{-1}). There is no difference found in the average values of ν(Pt-O) (blue triangles) with a value of 467 cm^{-1}. There is also a small shift in the ν(M-O) frequencies for platinum and palladium with a value found at 9 cm^{-1}. We are lead to conclude that the nature of the anion does not change the overall trends found in the platinum and palladium complexes.

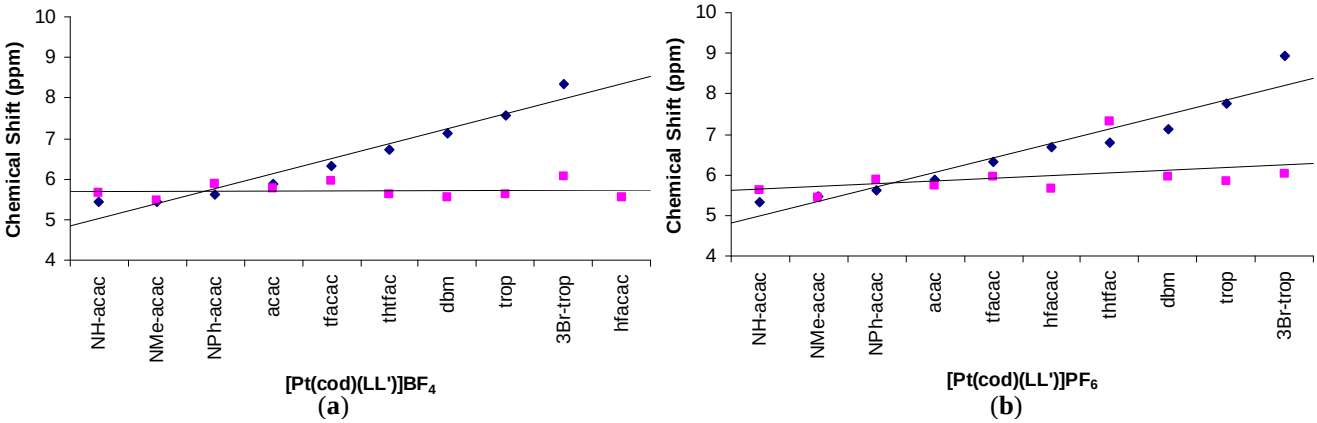

Figure 3.18 A graph of NMR chemical shift *vs.* [Pt(cod)(LL')]A where (a) BF_4 and (b) PF_6 where δ(CH-cod) is the pink squares and δ(CH-LL') are the blue diamonds. Arranged in ascending δ(CH-LL').

In Figure 3.18 the NMR chemical shifts for both the [Pt(cod)(LL')]BF_4 and [Pt(cod)(LL')]PF_6 complexes are presented. The graphs show nearly identical trends

where the olefinic protons (pink squares) show little change with an average value of 5.82 ppm. The methine proton is affected by the nature of the groups on the backbone of the ligand. The order found for the shifts is NH-acac > NMe-acac > NPh-acac > acac > tfacac > hfacac > thtfac > dbm > trop > 3Br-trop. Resulting in an order of the O,N- six membered bidentate ligands followed by the O,O- six membered bidentate ligands and lastly the O,O- five membered bidentate ligands, each of these sections is arranged in firstly increasing electron withdrawing groups then increasing the conjugation level leading to the conclusion that the level of conjugation is more influential than the electron withdrawing capabilities of the substituents. This pattern holds for the palladium compounds.

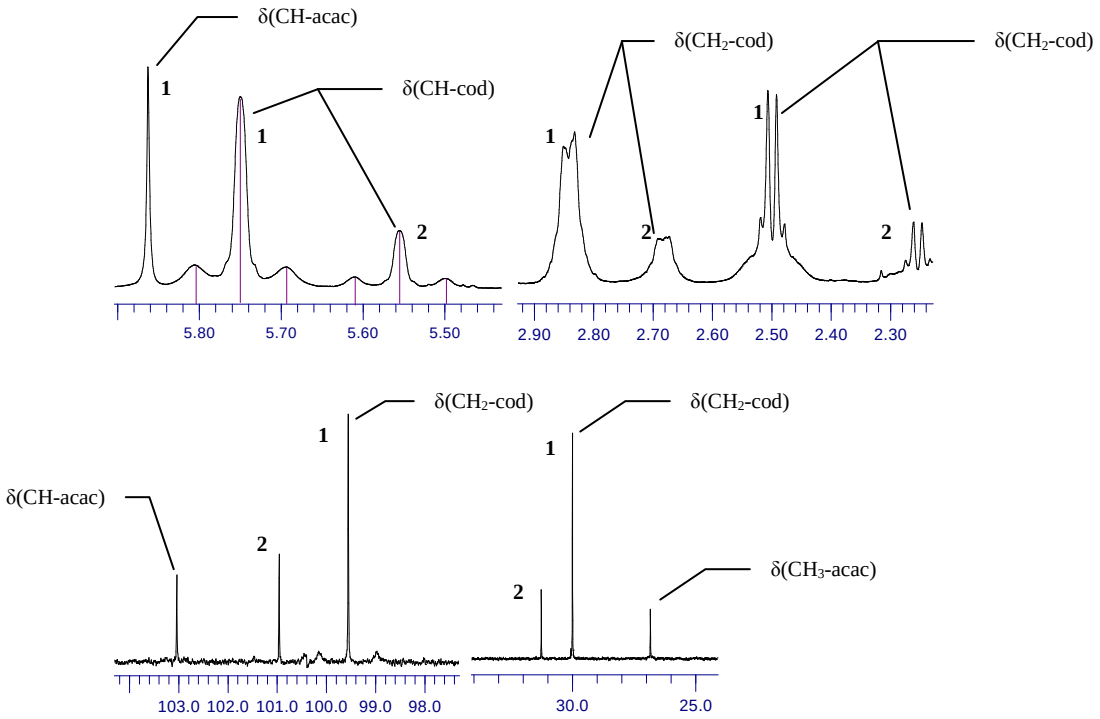

Figure 3.19 Excerpts of the ^{1}H and ^{13}C spectra of $[Pt(cod)(acac)]BF_4$ in CD_2Cl_2 at 25 °C.

Platinum (^{195}Pt) is a spin active metal centre with a spin ½ and a 33.83(1) % natural abundance resulting in coupling between the platinum and hydrogen seen as a triplet. This triplet is clearly observed in Figure 3.19, the triplet is also present in the ^{13}C spectra where the coupling is between platinum and carbon. For $[Pt(cod)(acac)]BF_4$ seen in Figure 3.19 a roto-isomer of 36 % was observed for the cyclo-octadiene (cod) moiety with a chemical shift of *ca.* 2 ppm. It is interesting to note that the $[Pt(cod)(acac)]PF_6$ spectra does not have the roto-isomer that was found for the $[Pt(cod)(acac)]BF_4$ complex.

The reactions of $[Pt(cod)Cl_2]$ with AgA (where A = BF_4 and PF_6) and Hhfacac were found to produce very low yields (Scheme 3.3). Green *et al.*[15] postulated the formation of **1** and proved the formation of isomers **3** and **4** though the use of ^{13}C NMR. He went on to use the analogous $[Pd(cod)Cl_2]$ compound and found an air-stable solid which he characterized as $[Pd(1\text{-}3\text{-}\eta\text{-}C_8H_{13})(cod)]BF_4$, which differs from the platinum which rather forms the 1-σ,4-5-η-enyl system.

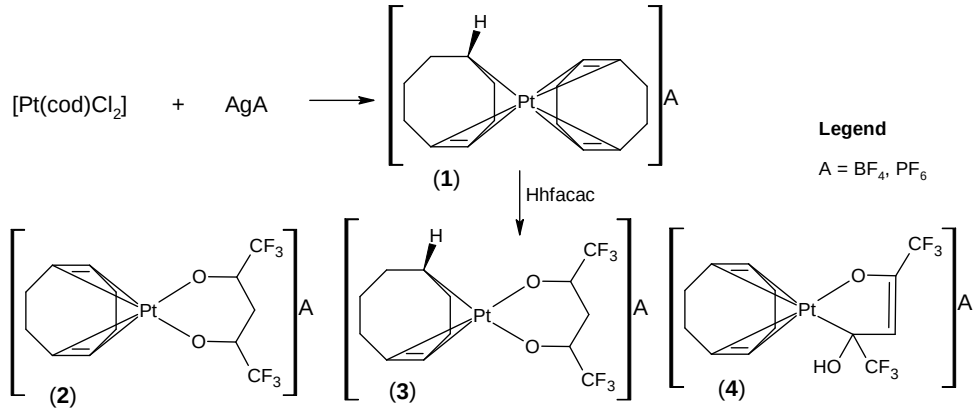

Scheme 3.3 Reaction scheme of platinum with possible isomer formation.

Using a different synthetic route than Green low yields still resulted. In the case of the $[Pt(cod)(hfacac)]BF_4$ complex the ^1H NMR showed only the peaks for the cyclo-octadiene indicting π-bonded of the olefinic carbons. Upon inspection of the ^{13}C spectra it was found that the carbons for the hexafluoroacetylacetonato ligand were infact present. For the $[Pt(cod)(hfacac)]PF_6$ complex isomerization was observed for both the cyclo-octadiene as well as the hexafluoroacetylacetonato moieties.

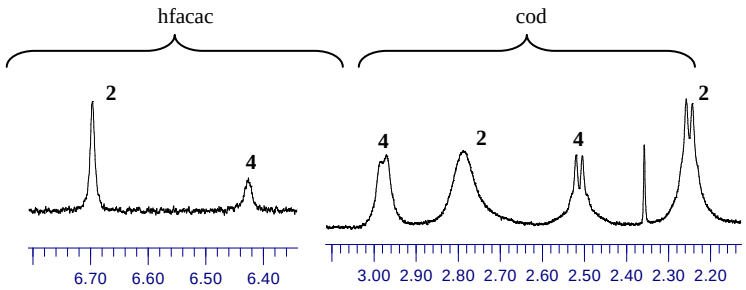

Figure 3.20 Excerpt of the ^1H spectra of $[Pt(cod)(hfacac)]PF_6$ in CD_2Cl_2 at 25 °C.

[15] Green M., Grove D.M., Spencer J.L., Stone F.G.A., *J.C.S. Dalton*, 2228, (1977)

Upon inspection of the ^{1}H spectra (Figure 3.20) we find that the cyclo-octadiene (cod) remains π-bonded to the platinum metal centre, there is a shift in the single proton found on the backbone of the hfacac moiety, as can be seen the values are reversed for the proton this is as a result of the aromatic and methine natures of the proton. For isomer **2** we find that the backbone proton has a more aromatic nature due to the formation of a metallocycle with a chemical shift of 6.697 ppm. For isomer **4** we find a straight forward methine proton with a chemical shift of 6.426 ppm. Due to the low solubility of the mixture of isomers and even with extended time the ^{13}C spectra could not be obtained. Other deuterated solvents were not attempted given the low yields obtained and the tendency of the complex to decompose in solution.

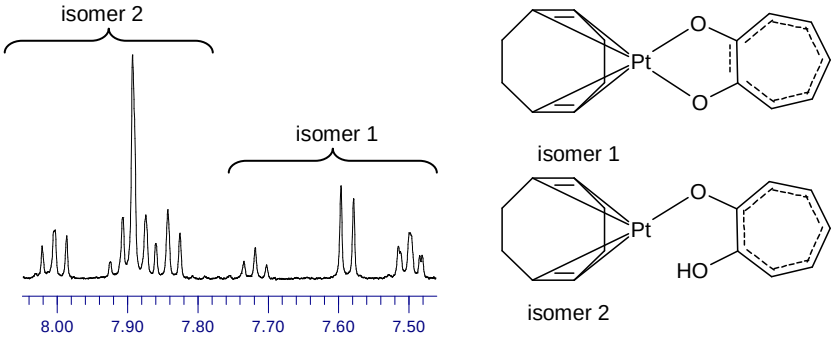

Figure 3.21 Excerpt of a ^{1}H of $[Pt(cod)(trop)]BF_4$ in $CDCl_3$ at 25 °C showing the peaks for the tropolone protons.

In Figure 3.21 an excerpt of the ^{1}H spectra of $[Pt(cod)(trop)]BF_4$ for the tropolone peaks shows a dynamic behavior in solution between the fully co-ordinated (isomer **1**) and the mono co-ordinated (isomer **2**) tropolone. This behavior partly explains the decomposition reactions encountered with the complex, after a few hours the tropolone peaks resemble that of free tropolone, after a few days there is plating on the inside of the NMR tube indicating the presence of Pt(0). The ratio in the above figure is 16 %, the decomposition is also reflected in the cyclo-octadiene peaks. Again we find that the $[Pt(cod)(trop)]PF_6$ complex does not form the isomers found in the $[Pt(cod)(trop)]BF_4$ complex.

In the search to find a parameter to quantify the "strength" of an anion, the acid dissociation constant of the resulting acid (pK_a) is a fair measure The following table (Table 3.2) shows a list of common anions which have been converted into their respective acids and the pK_a's which have been determined.

Table 3.2 pK_a values of common anion acids.

acid	pK_a[16]
CF_3COOH	0
HNO_3	- 1.4
$HClO_4$	- 5
HBF_4	- 5
CF_3SO_3H	- 13
HPF_6	- 20

The result of the increased strength of the PF_6 anion is that for the O,O-bidentate complexes isomerization is observed for the BF_4 counter ion complexes but not for the PF_6 counter ion complexes (Figure 3.23). For the N,O-bidentate complexes no isomerization is observed for either of the counter ion complexes (Figure 3.22).

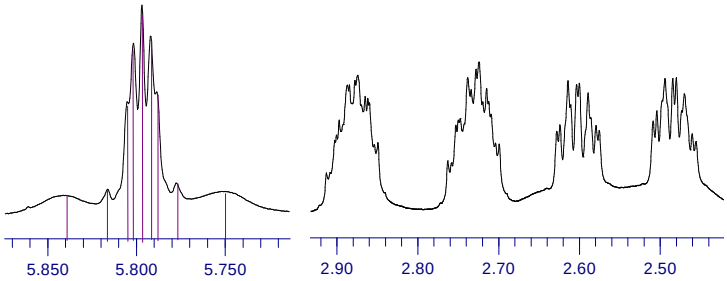

Figure 3.22 Excerpt of ^1H NMR of [Pt(cod)(NMe-acac)]PF_6 at 25 oC in CD_2Cl_2 showing the methine and methylene protons.

In Figure 3.22 [Pt(cod)(NMe-acac)]PF_6 is represented, the spectra on the left shows the methine splitting only one of the peaks was shown here but the second peak is an exact duplicate of the first. The methylene protons have also been found to be unequivalent therefore they each have there own separate peaks. The spectra for [Pt(cod)(NMe-acac)]BF_4 is identical to that shown in Figure 3.22.

In Figure 3.22 the δ(CH) shift was observed as a nonet (9) this is as a result of the coupling with platinum and two adjacent non-equivalent CH_2 moieties which are seen on the right hand side of the spectra. Previously as has been stated the second nonet is not shown in the above spectra. The complexity of the δ(CH_2) shifts is due to coupling with the vicinal methine protons and as well as geminal coupling from the CH_2 moiety this results in a complex multiplet that is not easily resolved.

[16] Shoichiro M., Makoto U., Kazuhiko I., *Electrolyte for aluminum electrolytic capacitor*, Mistubishi Petrochemical Co., Ltd., Patent 4774011, (1988)

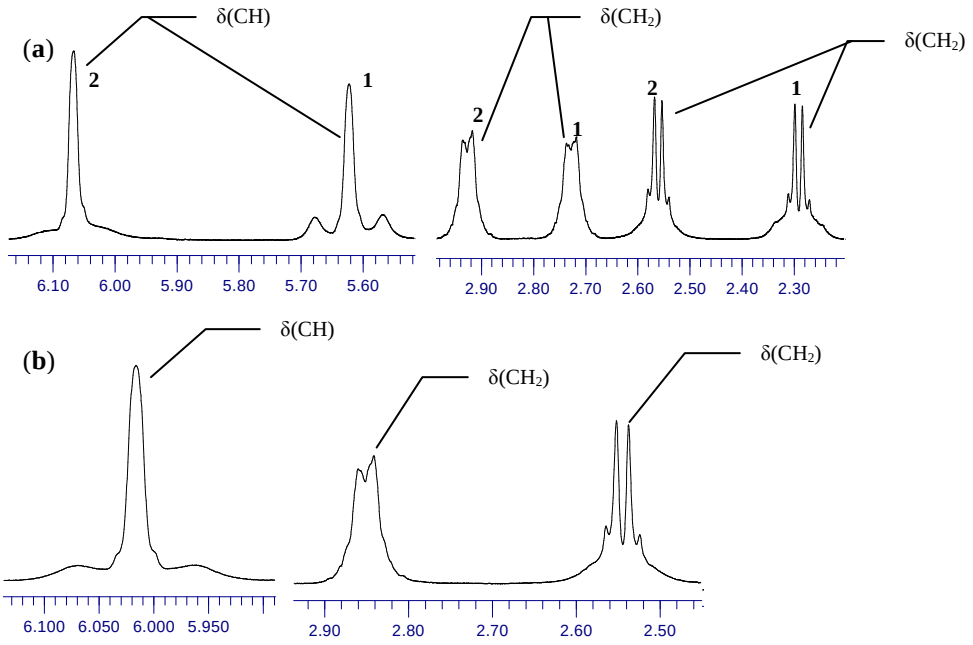

Figure 3.23 Excerpt of ^{1}H NMR Spectra of [Pt(cod)(3Br-trop)]A at 25 °C (a) BF_4 in $CDCl_3$ (b) PF_6 in CD_2Cl_2 showing the isomerization that occurs for the methine and methylene protons.

3.7.3 Rhodium(I) Complexes

The rhodium complexes were synthesized by taking rhodium trichloride in ethanol with the addition of 1,5-cyclo-octadine and refluxed, the product precipitated out in good yield (84 %). To this dimeric compound was added two equivalents of a bidentate ligand (Table 3.1) dissolved in N,N-dimethylformamide the solution was stirred and precipitated with ice, filtered and dried. The yields obtained were moderate to excellent (98 % - 47 %). Albeit the complexes were relatively simple and straightforward to prepare the crystallization of these complexes proved difficult, several methods were attempted but were met with limited success.

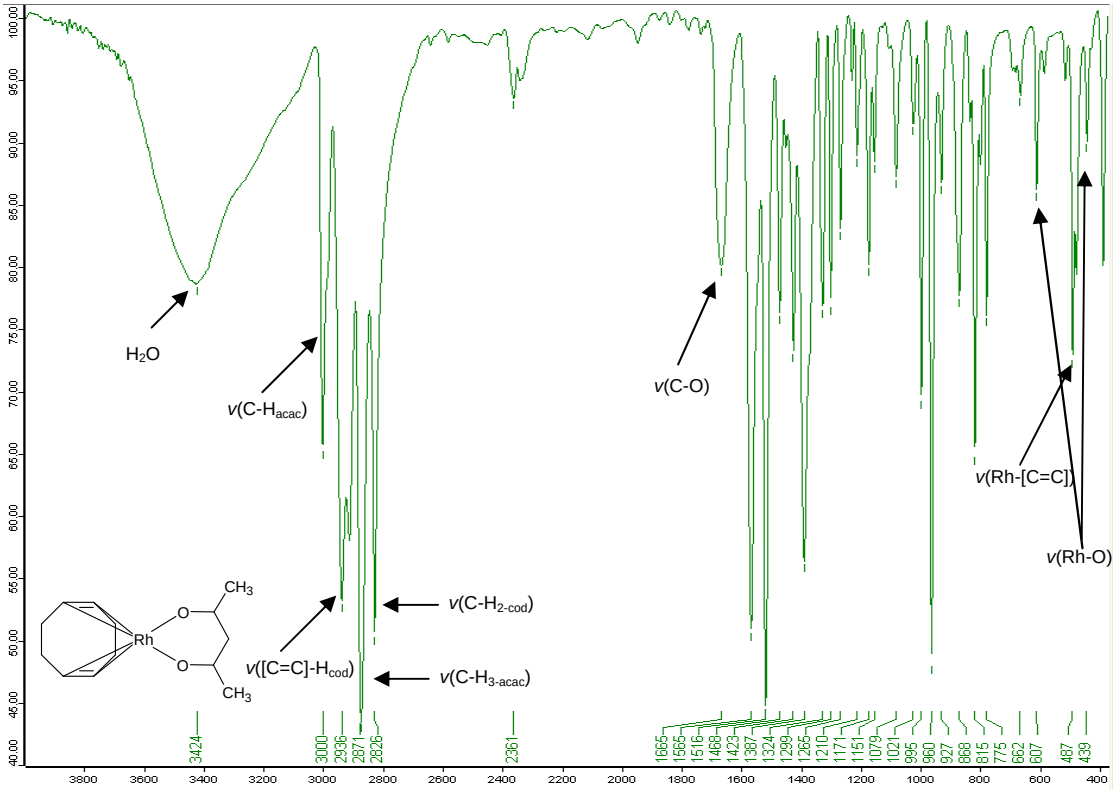

Figure 3.24 Infra-red spectra of [Rh(cod)(acac)] in KBr.

Figure 3.24 represents a typical rhodium complex spectra. From the spectra we observe that the ν(Rh-[C=C]), ν(Rh-O) and ν(Rh-O) + Δ ring are again present in the mid infra-red range with values of 486.68 cm^{-1}, 438.44 cm^{-1} and 661.5 cm^{-1} respectively.

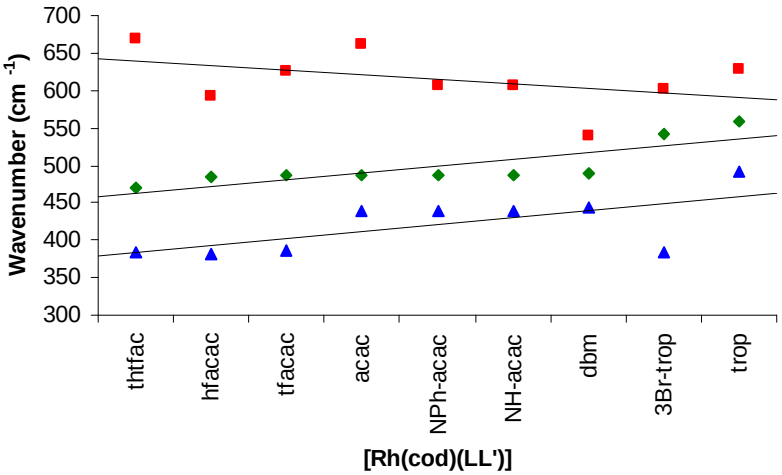

Figure 3.25 A graph of Wavenumber (cm^{-1}) *vs.* [Rh(cod)(LL')] where LL' = acac, tfacac, hfacac, thtfac, dbm, NH-acac, NPh-acac, trop, 3Br-trop for ν(Pt-[C=C]) (green diamond), ν(Pt-O) + Δ ring (red square) and ν(Pt-O) second (blue triangle) arranged in ascending ν(Pt-[C=C]) order.

Figure 3.25 is arranged in ascending order of ν(Rh-[C=C]), generally linear trends are observed for the frequencies listed. The ν(Rh-O) + Δ ring (first) frequencies (red squares) are the most varied from linear due to the nature and size of the metallocycle formed. It is also seen that the increased electron withdrawing groups result in a decrease in the wavenumber. Interestingly the trop and 3Br-trop complexes show an increase in the ν(Rh-[C=C]) shifts indicating that the there is infact an influence from the bidentate ligand, which was not found for the platinum and palladium complexes. The order observed for the rhodium complexes is as follows thtfac > hfacac > tfacac > acac > NPh-acac > NH-acac > dbm > 3Br-trop > trop. This order differs from the orders found for both the platinum and palladium complexes. When looking at the electronegativities of the groups attached to the bidentate ligands methyl (2.3), phenyl (3.0) and trifluoromethyl (3.35) values were found, this results in a well known order of reactivity for the β-diketones being acac < dbm « tfacac « hfacac. This order of reactivity is generally followed for the rhodium complexes

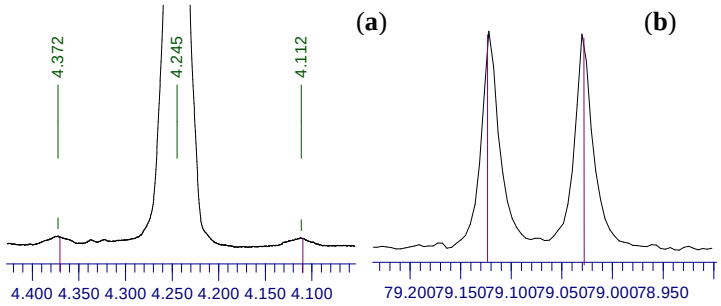

Figure 3.26 Excerpt of (a) ^{1}H NMR of [Rh(cod)Cl]$_2$ (b) ^{13}C NMR of [Rh(cod)(acac)] at 25 °C in CDCl$_3$ showing the methine protons and carbons.

Rhodium (^{103}Rh) is a spin active metal centre with a spin ½ and a natural abundance of 100 % resulting in coupling between the rhodium and hydrogen which should be seen as a doublet. However, this doublet is not always seen as the relative frequency to ^{1}H (100 MHz) is 3.172 with a receptivity of 3.17 x 10^{-5} relative to ^{1}H (1.0) an example of this coupling can be seen in Figure 3.26a. The coupling is more easily observed in the ^{13}C spectra which has a receptivity of 0.181 relative to ^{13}C (1.0) where the olefinic carbons are split into a clear doublet as a result of the coupling an example is seen in Figure 3.26b.

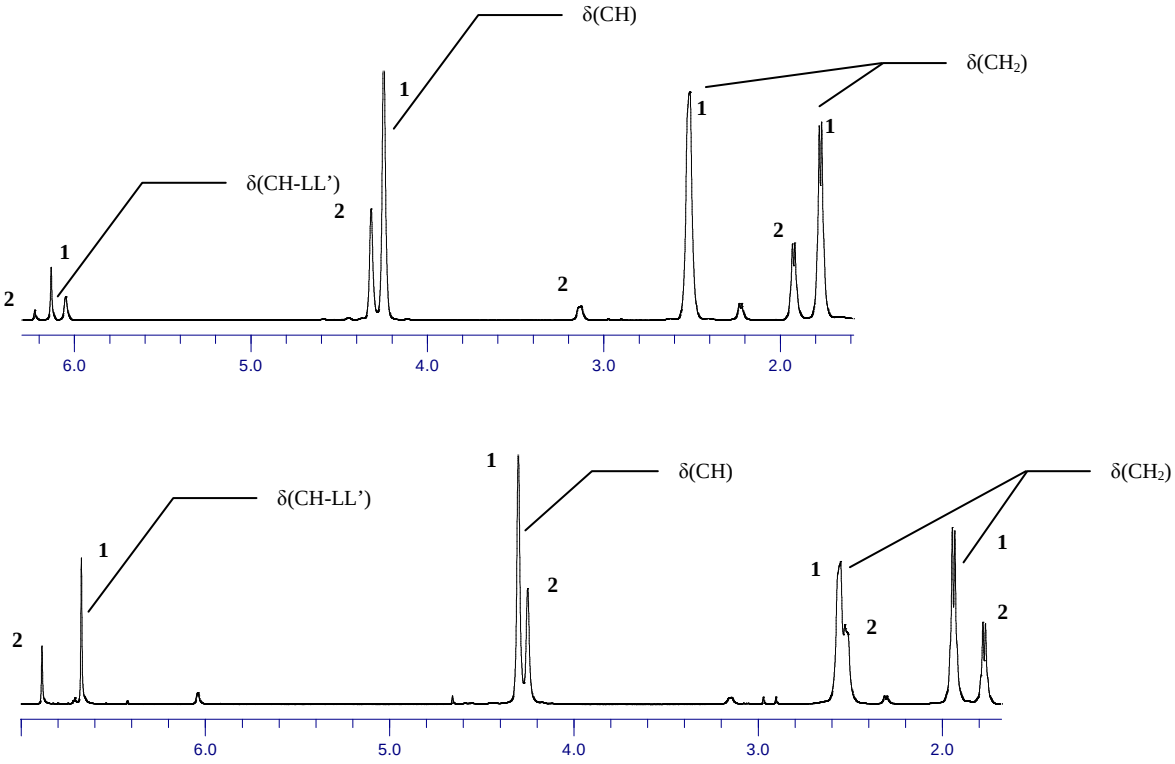

Figure 3.27 Excerpt of ^{1}H NMR Spectra of (a) [Rh(cod)(hfacac)] (b) [Rh(cod)(dbm)] in $CDCl_3$ at 25 °C showing isomerization.

It has been found as with the platinum and palladium complexes, rhodium also shows isomerization of selected complexes. Figure 3.27 shows two examples of such isomerization. This is not exclusive to the six membered metallocycles as [Rh(cod)(3Br-trop)] also displays similar isomerization. The differences in the isomers remains unclear at this point.

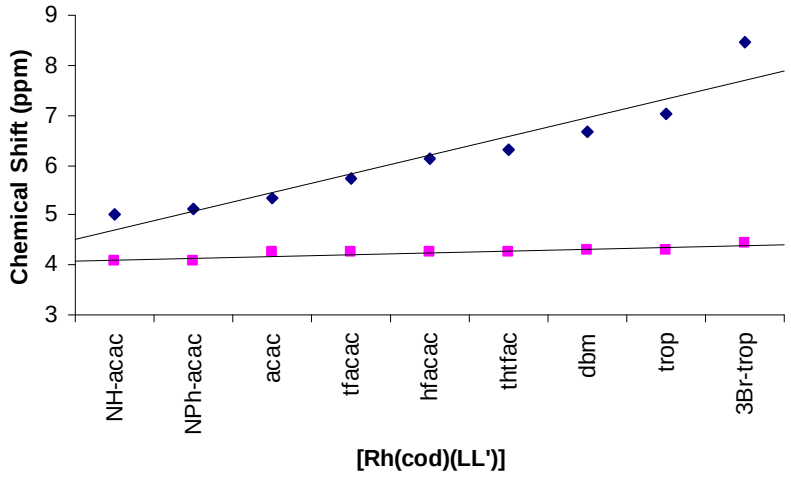

Figure 3.28 A graph of NMR chemical shift *vs.* [Rh(cod)(LL')] where δ(CH-cod) is the pink squares and δ(CH-LL') are the blue diamonds. Arranged in ascending δ(CH-LL').

In Figure 3.28 we see the NMR data for [Rh(cod)(LL')] complexes. The olefinic protons (pink squares) show little change with an average value of 4.24 ppm, which is lower than the average values found for the corresponding platinum and palladium complexes. This again shows that the cod ligand is not significantly affected by the *trans* ligand. The methine proton is affected by the nature of the groups on the backbone of the bidentate ligand. The order found is NH-acac < NPh-acac < acac < tfacac < hfacac < thtfac < dbm < trop < 3Br-trop which is identical to the order found for both platinum and palladium complexes.

Correlations between the IR and NMR data reported in this chapter will be presented in the following chapters and compared with the solid state X-ray crystallographic data of selected complexes.

Chapter 4
Crystallographic Study of β-Diketonato Type Complexes of Palladium(II)

4.1 Introduction

Within the current domain of crystal engineering and design hydrogen bonding plays an increasingly important role. These hydrogen bonding networks allow for the possibility of channeling and inclusion molecules, albeit counter ions or solvents. These crystals additionally hold the possibility of hydrogen or small molecule storage which is a hot topic within the current energy crisis. It is thus important to correctly define and understand the theory of hydrogen bonding[1,2].

A simple definition of hydrogen bonding is a non-covalent, attractive interaction between a proton donor, which forms a polar σ-bond with hydrogen, (D-H) and at least one or more proton acceptor(s) (A) in the same or in a different molecule(s).

Contained in the definition the hydrogen atom carries a partial positive charge and can thus be viewed as a Lewis acid, in Lewis acid-base type interactions. However in inorganic molecules the influence of a metal centre plays a fair role in influencing hydrogen bonding. The table below gives a summary of the types of hydrogen bonding that are currently defined.

[1] G.R. Desiraju, *Crystal Design: Structure and Function Perspectives in Supramolecular Chemistry*, John Wiley & Sons, Ltd., West Sussex, Vol. 7, ISBN 0-470-84333-0, (2003)

[2] J. Leszczynski, S.J. Grabowski, *Challenges and Advances in Computational Chemistry and Physics: Hydrogen Bonding – New Insights*, Springer, Dordrecht, Vol. 3, ISBN-10 1-4020-4853-X (e-book), (2006)

Table 4.1 Classification and properties of hydrogen bonds, D-H···A[3].

H-bond parameters	Strong	Moderate	Weak
Interaction type	Strongly covalent	Mostly electrostatic	Electrostatic / dispersed
Examples	$[F\cdots H\cdots F]^+$ $[N\cdots H\cdots N]^+$	N-H···O=C	C-H···O N-H···F-C O-H···π
Bond energy (kcal.mol^{-1})	15 – 40	4 – 15	< 4
D-H *vs.* H···A	D-H ≈ H···A	D-H < H···A	D-H << H···A
Lengthening of D-H (Å)	0.05 – 0.2	0.01 – 0.05	≤ 0.01
D···A range(Å)	2.2 – 2.5	2.5 – 3.0	3.0 – 4.5
H···A range (Å)	1.2 – 1.5	1.5 – 2.2	> 2.2
D-H···A angels range (°)	170 – 180	> 130	> 90
Effect on crystal packing	Strong	Distinctive	Variable
Covalency	Pronounced	Weak	Vanishing
Electrostatic contribution	Significant	Dominant	Moderate
IR *vs.* relative shift (cm^{-1})	> 25	5 – 25	< 5

The complexes that were prepared as described in § 3.4.2 were analyzed by single crystal X-ray crystallography and the results are summarized in Table 4.2. A diagram indicating the numbering scheme of each compound is presented, along with selected bond lengths and angles, hydrogen bonding interactions and additional interactions if applicable. A discussion highlighting some of the important aspects of each particular structure is presented thereafter.

Additional correlations with other structures and theoretical calculated structures are done in Chapter 6, whilst complete lists of the crystal structures presented in this chapter are given in the supplementary data.

4.2 Experimental

Data collections for $[Pd(cod)(acac)]PF_6$, $[Pd(cod)(acac)]BF_4$, $[Pd(cod)(thtfac)]BF_4$, $[Pd(cod)(tfacac)]PF_6$ and $[Pd(cod)(hfacac)]PF_6$ were obtained on a Bruker Apex II 4K CCD diffractometer. The data for $[Pd(cod)(thtfac)]PF_6$ was collected on an Oxford Diffraction Xcalibur 3 Crysalis CCD system[4]. Both systems were equipped with a graphite-monochromated Mo Kα radiation, for the Bruker system all the reflections were merged and integrated with SAINT-PLUS[5] and corrected for Lorentz,

[3] Grabowski S.J., *Hydrogen Bonding – New Insights*, Springer, Netherlands, ISBN 978-1-4020-4852-4, (2006)
[4] Crysalis CCD. Oxford Diffraction Ltd., Abingdon, Oxfordshire, U.K., (2005)
[5] Bruker SAINT-PLUS (including XPREP), Version 7.12, Bruker AXS Inc., Madison, WI., (2004)

polarization and absorption effects with SADABS[6], while Crysalis RED[7] was used for the Oxford system.

Structures were solved by direct and conventional Patterson methods using the SHELX-97[8] as part of the WinGX[9] package, and anisotropic refinement was performed on all non-hydrogen atoms by a full-matrix least-squares method. The positions of the hydrogen atoms were calculated using a riding model to the adjacent carbon, unless otherwise stipulated. Hydrogen interactions were calculated using the PLATON[10,11,12] and PARST[13] programs. Molecular graphics were obtained using DIAMOND[14], while overlay graphics were obtained using HyperChem 7.5[15].

[6] Bruker SADABS (Version 2004/1), Bruker AXS Inc., Madison, WI., (1998)
[7] Crysalis RED Oxford Diffraction Ltd., Abingdon, Oxfordshire, U.K., (2005)
[8] Sheldrick G.M., *Acta Cryst.*, **A64**, 112, (2008)
[9] Farrugia L.J., *Appl. Cryst.*, **32**, 837, (1999)
[10] Spek A.L., PLATON A multipurpose crystallographic tool, Utrecht University, Utrecht, Netherlands, (2005)
[11] Speck A.L., *J. Appl. Cryst.*, **36**, 7, (2003)
[12] Speck A.L., *Acta Cryst*, **D65**, 148, (2009)
[13] Nardelli M., *J. Appl. Cryst.*, **28**, 659, (1995)
[14] Brandenburg K., Brendt M., DIAMOND, Release 2.1e. Crystal Impact GbR, Potfach 1251, D53002 Bonn, Germany., (2001)
[15] HyperChem™ Release 7.52, Windows Molecular Modeling System, HyperCube Inc., (2002)

Table 4.2 Crystallographic data and refinement parameters where A = PF_6^- or BF_4^-

Crystal Data	[Pd(cod)(acac)]A		[Pd(cod)(thtfac)]A		[Pd(cod)(tfacac)]A	[Pd(cod)(hfacac)]A
	PF_6 (**1**)	BF_4 (**2**)	PF_6 (**3**)	BF_4 (**4**)	PF_6 (**5**)	PF_6 (**6**)
Empirical formula	$C_{13}H_{19}F_6O_2PPd$	$C_{13}H_{19}BF_4O_2Pd$	$C_{16}H_{16}F_9O_2PPdS$	$C_{12}H_{16}BF_7O_2PdS$	$C_{13}H_{16}F_9O_2PPd$	$C_{13}H_{13}F_{12}O_2PPd$
Formula weight	458.65	400.49	580.72	474.52	512.63	566.60
Temperature (K)	100(2)	100(2)	100(2)	100(2)	100(2)	100(2)
Wavelength (Å)	0.71073	0.71073	0.71073	0.71073	0.71073	0.71073
Crystal system	Monoclinic	Orthorhombic	Monoclinic	Monoclinic	Triclinic	Monoclinic
Space group	$P2_1/n$	$Pca2_1$	$P2_1/n$	$P2_1/n$	$P\bar{1}$	$P2_1/c$
Unit cell dimensions						
a (Å)	9.3166(6)	26.2908(11)	9.9691(2)	10.0528(3)	8.1027(8)	8.5885(2)
b (Å)	15.4676(8)	7.1684(3)	17.0294(3)	16.6333(6)	14.3018(14)	10.6304(2)
c (Å)	11.4844(7)	7.7782(3)	11.4750(2)	10.9501(4)	15.4557(14)	19.4093(4)
α (°)	90	90	90	90	75.286(5)	90
β (°)	106.171(2)	90	101.327(2)	102.534(1)	89.963(5)	93.4150(10)
γ (°)	90	90	90	90	73.556(5)	90
Volume ($Å^3$)	1589.48(16)	1465.90(10)	1910.14(6)	1787.34(11)	1656.6(3)	1768.91(6)
Z	4	4	4	4	4	4
Density (calculated) ($Mg.m^{-3}$)	1.917	1.815	2.019	1.763	2.055	2.128
Absorption coefficient (mm^{-1})	1.335	1.309	1.262	1.225	1.318	1.269
F(000)	912	800	1144	936	1008	1104
Crystal size (mm^3)	0.13 x 0.07 x 0.03	0.34 x 0.10 x 0.07	0.35 x 0.20 x 0.10	0.28 x 0.16 x 0.11	0.24 x 0.11 x 0.11	0.38 x 0.22 x 0.07
Theta range for data collection (°)	2.27 to 28.29	1.55 to 28.38	2.17 to 27.00	2.26 to 28.41	1.37 to 27.00	2.10 to 28.00
Index ranges	-12<=h<=12, -13<=k<=20, -15<=l<=15	-35<=h<=35, -9<=k<=9, -10<=l<=6	-12<=h<=11, -21<=k<=21, -11<=l<=14	-13<=h<=12, -22<=k<=22, -14<=l<=14	-10<=h<=10, -18<=k<=18, -19<=l<=19	-11<=h<=11, -14<=k<=13, -25<=l<=25
Reflections collected	10774	15664	14017	21931	24498	17008
Independent reflections	3958 [R(int) = 0.0413]	3119 [R(int) = 0.0254]	4177 [R(int) = 0.0235]	4469 [R(int) = 0.0327]	6985 [R(int) = 0.0671]	4251 [R(int) = 0.0294]
Completeness to θ (°; %)	28.29, 99.8	28.38, 99.9	27.00, 100.0	28.41, 99.4	27.00, 96.2	28.00, 99.9
Max. and min. transmission	0.9610 and 0.8456	0.9139 and 0.6644	0.8842 and 0.6665	0.8771 and 0.7255	0.8686 and 0.7427	0.9164 and 0.6442
Refinement method	Full-matrix least-squares on F^2	Full-matrix least-squares on F^2	Full-matrix least-squares on F^2	Full-matrix least-squares on F^2	Full-matrix least-squares on F^2	Full-matrix least-squares on F^2
Data / restraints / parameters	3958 / 0 / 210	3119 / 1 / 192	4177 / 0 / 271	4469 / 0 / 253	6985 / 0 / 461	4251 / 1 / 295
Goodness-of-fit on F^2	1.145	1.224	1.070	1.211	1.136	1.191
Final R indices [I>2σ(I)]	$R_1 = 0.0359$, $wR_2 = 0.0939$	$R_1 = 0.0224$, $wR_2 = 0.0613$	$R_1 = 0.0243$, $wR_2 = 0.0589$	$R_1 = 0.0283$, $wR_2 = 0.0832$	$R_1 = 0.1341$, $wR_2 = 0.3481$	$R_1 = 0.0260$, $wR_2 = 0.0785$
R indices (all data)	$R_1 = 0.0521$, $wR_2 = 0.1380$	$R_1 = 0.0254$, $wR_2 = 0.0814$	$R_1 = 0.0319$, $wR_2 = 0.0624$	$R_1 = 0.0361$, $wR_2 = 0.1132$	$R_1 = 0.1406$, $wR_2 = 0.3548$	$R_1 = 0.0319$, $wR_2 = 0.0996$
Largest diff. peak and hole ($e.Å^{-3}$)	1.006 and -1.124	1.142 and -0.783	1.052 and -0.679	0.668 and -0.911	9.473 and -2.275	0.840 and -1.056

4.3 X-Ray Structures of Palladium Complexes

4.3.1 Crystal structures of [Pd(cod)(acac)]PF_6 and [Pd(cod)(acac)]BF_4

The compounds, [Pd(cod)(acac)]PF_6 (**1**), crystallized in the monoclinic space group $P2_1/n$, with a cationic [Pd(cod)(acac)]$^+$ (**1a**) species and an anionic PF_6^- (**1b**) species in the asymmetric unit, whilst [Pd(cod)(acac)]BF_4 (**2**) crystallized in the orthorhombic space group $Pca2_1$, with a cationic [Pd(cod)(acac)]$^+$ (**2a**) species and an anionic BF_4^- (**2b**) species in the asymmetric unit. The numbering scheme is presented in Figure 4.1, while atomic co-ordinates, bond angles and distances, anisotropic displacement parameters and hydrogen co-ordinates are reported in Appendix B.1 and B.7. General crystallographic data and refinement parameters are reported in Table 4.2, while significant bond angles and distances are reported in Table 4.3.

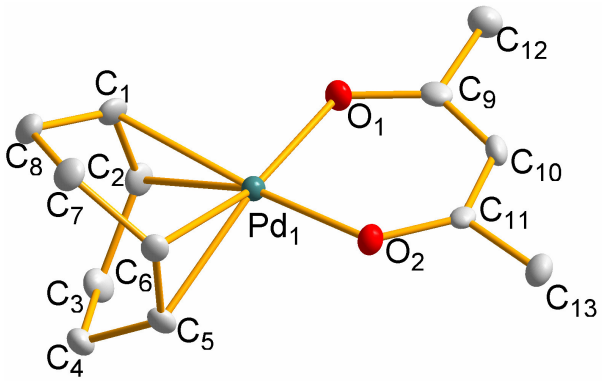

Figure 4.1 Diamond illustration of [Pd(cod)(acac)]A (A = PF_6. BF_4) at 100 K showing the numbering scheme and displacement ellipsoids (50 %) of the complex. Hydrogen atoms and counter ions omitted for clarity.

Table 4.3 Selected bond distances and angles for [Pd(cod)(acac)]A (A = PF_6, BF_4)

Bond Distance (Å)	Counter ion		Bond Angles (°)	Counter ion	
	PF_6 (**1**)	BF_4 (**2**)		PF_6 (**1**)	BF_4 (**2**)
Pd-O_1	2.003(3)	2.001(3)	O_1-Pd-O_2	94.4(1)	94.5(1)
Pd-O_2	2.001(3)	1.998(2)	C_1-Pd-C_2	36.8(2)	36.8(2)
Pd-C_1	2.195(5)	2.202(3)	C_5-Pd-C_6	36.7(2)	37.1(2)
Pd-C_2	2.181(4)	2.183(4)	C_1-Pd-C_6	81.6(2)	81.5(2)
Pd-C_5	2.197(4)	2.205(3)	C_2-Pd-C_5	81.7(2)	81.4(1)
Pd-C_6	2.189(4)	2.181(4)	χ^a	86.0(3)	85.9(1)
C_1-C_2	1.381(7)	1.386(7)	ψ^b	81.9(3)	80.2(2)
C_5-C_6	1.380(6)	1.394(7)			

a χ: $C_1MC_2 \cap C_5MC_6$ b ψ: $C_2C_3C_4C_5 \cap C_1C_8C_7C_6$ see Figure 1.2

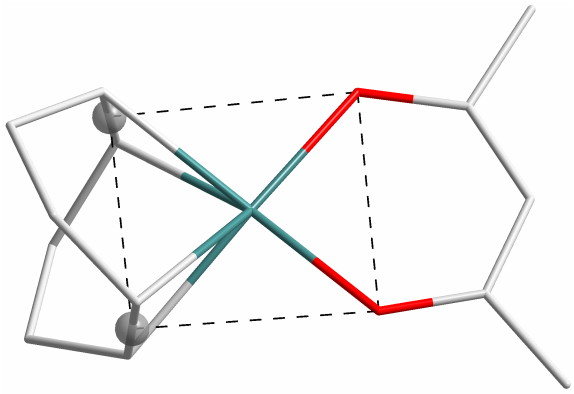

Figure 4.2 Diamond illustration of the square planar geometry around the metal centre, depicted by dashed lines.

The palladium metal centre is bonded to two oxygen atoms from the acetylacetonato (acac) ligand and π-bonded with the alkene carbons of the 1,5-cyclo-octadiene (cod) ligand giving rise to a square planar geometry around the metal centre. In Figure 4.2 the square plane is shown by dashed lines. The additional atoms shown are the centroid atoms defined as the mid-point distance of the alkene. Palladium is in the +2 oxidation state and thus has either a hexafluorophosphate (PF_6^-) or tetrafluoroborate (BF_4^-) counter ion within the asymmetric unit to balance the resulting charge. Even with the variation of the counter ion the bond distances of the complex are not significantly altered (Table 4.3). The counter ions display classical tetragonal (BF_4^-) or octahedral (PF_6^-) geometry with no disorder present.

The hydrogen bonding of complex **1** is graphically presented in Figure 4.3-4.6 with Table 4.4 listing the bond distances and angles.

Table 4.4 Hydrogen bond distances and angles for [Pd(cod)(acac)]PF_6 (1) (Å and °)

D-H...A	d(D-H)	d(H...A)	d(D...A)	<(DHA)
C_3-H_{3A}...F_1	0.99	2.65	3.487(6)	141.9
C_4-H_{4B}...F_2	0.99	2.82	3.399(6)	118.3
C_5-H_5...F_2	1.00	2.35	3.139(5)	135.2
C_{13}-H_{13C}...F_6	0.98	2.81	3.483(5)	126.5
C_1-H_1...$O_1^{\#1}$	1.00	2.99	3.623(5)	121.9
C_1-H_1...$F_3^{\#2}$	1.00	2.95	3.702(6)	132.5
C_7-H_{7A}...$F_5^{\#2}$	0.99	2.48	3.326(5)	143.4
C_1-H_1...$F_2^{\#2}$	1.00	2.98	3.636(5)	124.4
C_3-H_{3A}...$F_6^{\#3}$	0.99	2.74	3.295(6)	115.6
C_3-H_{3B}...$O_2^{\#3}$	0.99	3.00	3.687(5)	127.9
C_2-H_2...$F_2^{\#3}$	1.00	2.53	3.259(5)	129.4
C_2-H_2...$F_3^{\#3}$	1.00	2.53	3.374(6)	141.9
C_8-H_{8A}...$F_4^{\#4}$	0.99	2.52	3.463(6)	160.2
C_4-H_{4A}...$F_4^{\#4}$	0.99	2.70	3.623(6)	155.9
C_7-H_{7B}...$F_1^{\#5}$	0.99	2.57	3.347(5)	135.1
C_6-H_6...$F_4^{\#5}$	1.00	2.44	3.232(5)	135.9
C_7-H_{7A}...$F_5^{\#5}$	0.99	2.70	3.303(6)	120.0
C_{10}-H_{10}...$F_4^{\#6}$	0.95	2.87	3.679(5)	143.8
C_{12}-H_{12B}...$F_3^{\#6}$	0.98	2.56	3.449(6)	150.8
C_{13}-H_{13B}...$F_5^{\#6}$	0.98	2.64	3.602(6)	167.9
C_{10}-H_{10}...$F_3^{\#6}$	0.95	2.39	3.292(5)	158.4
C_{13}-H_{13A}...$O_2^{\#7}$	0.98	2.71	3.523(5)	140.5
C_{13}-H_{13C}...$F_1^{\#8}$	0.98	2.83	3.604(6)	136.3

Symmetry transformations used to generate equivalent atoms:

#1 -x,-y+2,-z	#2 -x+1/2,y+1/2,-z+1/2	#3 x-1/2,-y+3/2,z-1/2
#4 x-1,y,z	#5 x-1/2,-y+3/2,z+1/2	#6 -x+3/2,y+1/2,-z+1/2
#7 -x+1,-y+2,-z+1	#8 x+1/2,-y+3/2,z+1/2	

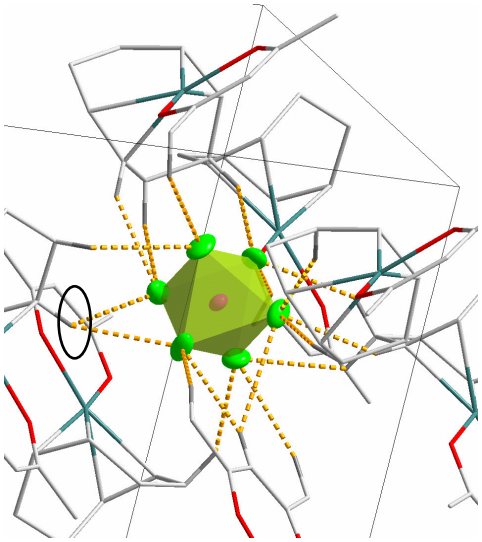

Figure 4.3 Partial unit cell of [Pd(cod)(acac)]PF_6 (1) illustrating weak intermolecular hydrogen interactions (dashed yellow bonds) with the PF_6 counter ion polyhedron (Fluorine at the corners indicated in green and phosphorus indicated in the centre of the polyhedron in pink). Only selected hydrogen atoms are included.

Two types of weak hydrogen bonding were observed for the [Pd(cod)(acac)]PF_6 (**1**) complex (Table 4.4), firstly between **1a**···**1b** and secondly that of **1a**···**1a**. In Figure

4.3 is the hydrogen bonding between the fluorido ligands of the PF_6^- anion (**1b**), shown as an octahedral polyhedron with the fluorine atoms at the corners (green) and the phosphorous atom at the centre (pink), and the hydrogens of the carbons of both the cyclo-octadiene rings and the acetylacetonato moieties are depicted. The result of these interactions shows how the counter-ion is cradled within several cationic complexes. The oval within Figure 4.3 highlights a bifurcated hydrogen (H_2) atom (a single hydrogen interacting with two distinct atoms), each fluorine interacts with a minimum of three different hydrogen atoms this branched type of bonding does not fall into the classical definition of a hydrogen bond, but none the less still hold the **1b** complex in place. A more detailed discussion on the hydrogen interactions follows in Figure 4.4, 4.5 and 4.6.

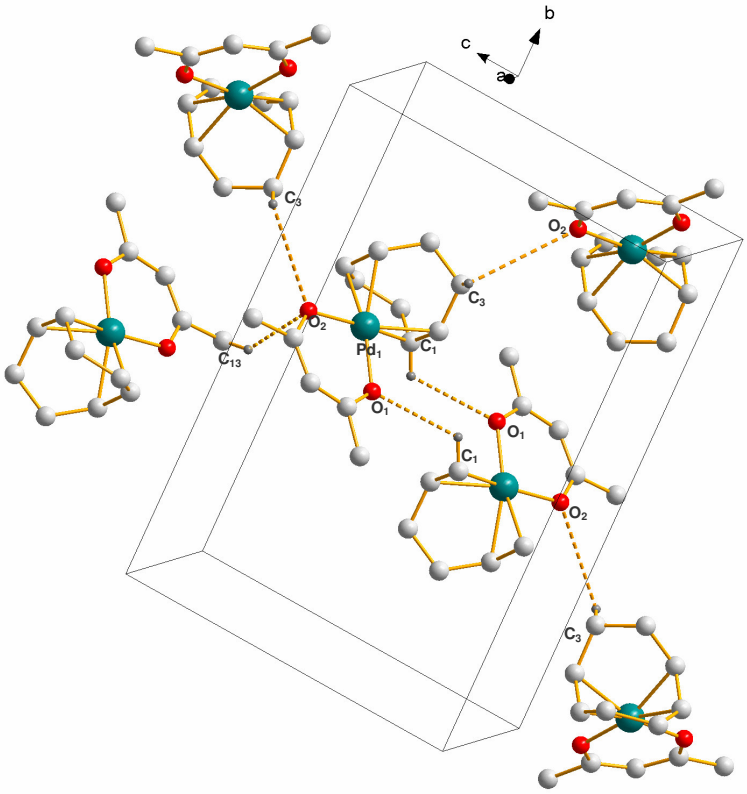

Figure 4.4 Partial unit cell of [Pd(cod)(acac)]PF_6 (1) illustrating weak intermolecular hydrogen bonding interactions with the acetylacetonato moiety indicated by dashed bonds. Only selected hydrogen atoms are included. Counter ions have been omitted for clarity. Palladium (cyan), carbon (grey), oxygen (red), phosphorus (pink) and fluorine (green).

In Figure 4.4 the second type of weak hydrogen bonding can be seen; that of the oxygen interaction from the acetylactonato ligand with the methylene carbon atoms of

the cyclo-octadiene ring. There are two distinct forms, the first being the interaction between $C_1 \cdots O_1$ and $C_{13} \cdots O_2$ which assist with tail to head packing of the **1a** complex. Secondly, that of the interaction between $O_2 \cdots C_3$ this gives rise to the second orientation in the unit cell extending the packing to a second ribbon and creating the overall clustered head-to-tail (Figure 4.11). These ribbons are more easily identified in Figure 4.7 where the **1a** complexes are depicted in lime and the **1b** complexes in olive.

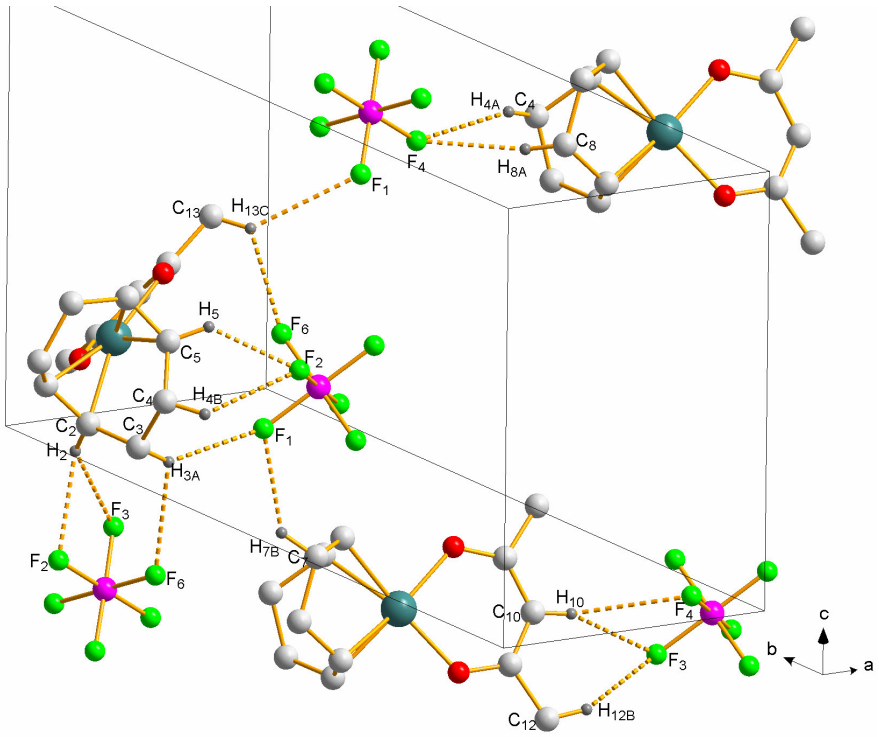

Figure 4.5 Partial unit cell of [Pd(cod)(acac)]PF_6 (1) illustrating weak intermolecular hydrogen bonding interactions indicated by dashed bonds. Only selected hydrogen atoms are included. Counter ions have been omitted for clarity. Palladium (cyan), carbon (grey), oxygen (red), phosphorus (pink) and fluorine (green).

The interactions observed in Figure 4.5 are divided into the hydrogen atoms of the acetylacetonato moieties and the hydrogen atoms of the cyclo-octadiene moieties. The methine hydrogen (H_{10}) of the acetylacetonato moiety interacts with the fluorido ligand (F_4 and F_3) of the **1b** complex, presenting a classic example of a bi-furcated hydrogen. While the methyl hydrogens (H_{12B} and H_{13C}) interact with the fluorido ligands (F_3, F_1 and F_6). The hydrogens of the alkene carbons (C_2 and C_5) of the cyclo-octadiene interact with the fluorido ligands (F_2, F_3 and F_2) of **1b**, with the hydrogen (H_2) being another example of a bi-furcated hydrogen. The last interaction seen in Figure 4.5 is that of the hydrogens of the alkane carbons (C_3, C_4, C_8, C_4, C_7 and C_3) of

the cyclo-octadiene with the fluorido ligands (F_1, F_2, F_4, F_4, F_1 and F_6) of the **1b** complex.

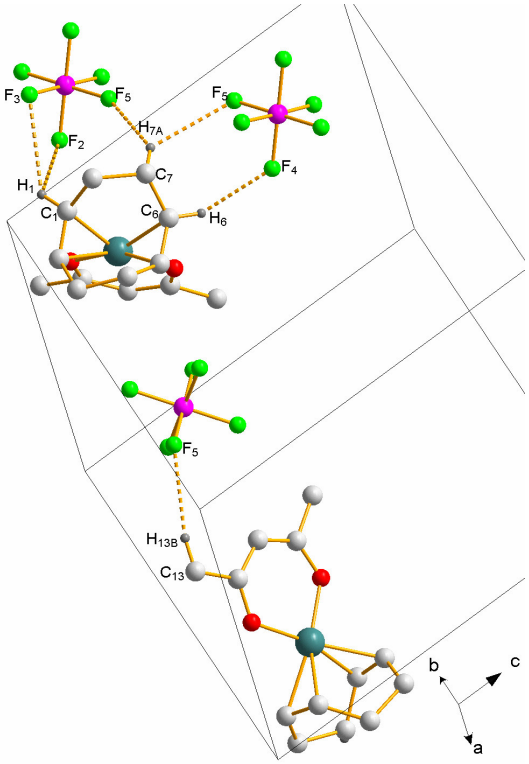

Figure 4.6 Partial unit cell of [Pd(cod)(acac)]PF_6 (1) illustrating weak intermolecular hydrogen bonding interactions indicated by dashed bonds. Only selected hydrogen atoms are included. Counter ions have been omitted for clarity. Palladium (cyan), carbon (grey), oxygen (red), phosphorus (pink) and fluorine (green).

One acetylacetonato hydrogen (H_{13B}) interaction with the fluorido ligand (F_5) is shown in Figure 4.6. Two bi-furcated hydrogens (H_1 and H_{7A}) interact with the fluorido ligands (F_2, F_3 and F_5, F_5). The last interaction observed was that of the hydrogen of the alkene carbon (C_6) of the cyclo-octadiene with the fluorido ligand (F_4) of the **1b** complex.

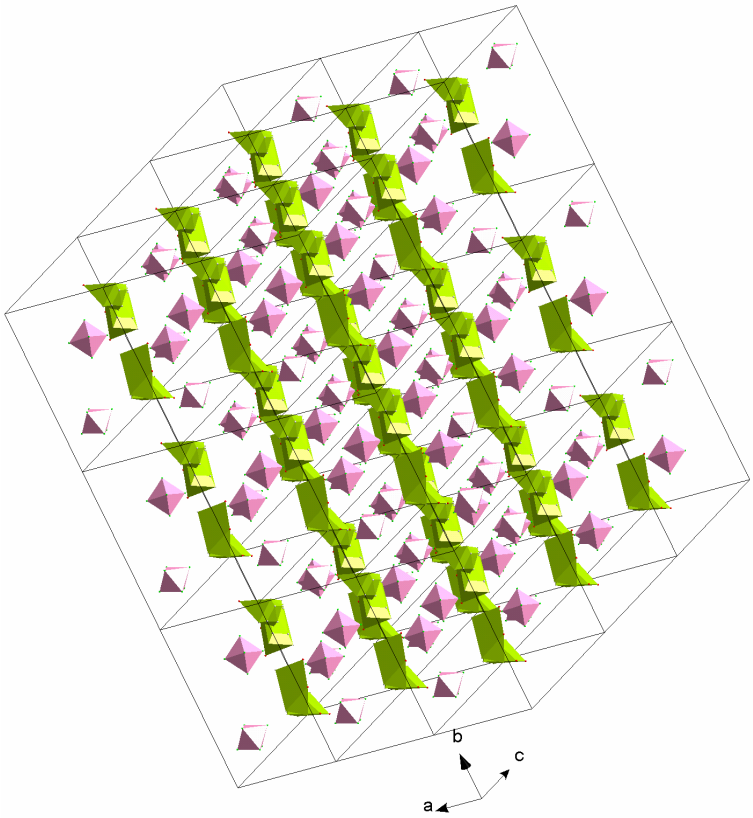

Figure 4.7 3x3x3 Super-cell of [Pd(cod)(acac)]PF_6 (1) illustrating the packing of the cell, the PF_6^- (1b) counter ion is depicted by the octahedral polyhedra (rose) and the $[Pd(cod)(acac)]^+$ (1a) polyhedra (olive).

The hydrogen bonding of complex **2** is graphically presented in Figure 4.8 and 4.9 with Table 4.5 listing the bond distances and angles.

Table 4.5 Hydrogen bond distances and angles for [Pd(cod)(acac)]BF_4 (2)[Å and °]

D-H...A	d(D-H)	d(H...A)	d(D...A)	<(DHA)
C_7-H_{7B}...F_{01}	0.99	2.37	3.200(6)	141.4
C_2-H_2...$F_{02}^{\#1}$	1.00	2.52	3.221(6)	126.7
C_6-H_6...$F_{04}^{\#2}$	1.00	2.26	3.140(6)	146.0
C_{12}-H_{12B}...$F_{04}^{\#3}$	0.98	2.53	3.500(4)	169.1
C_{10}-H_{10}...$F_{03}^{\#3}$	0.95	2.42	3.325(5)	159.0
C_{13}-H_{13B}...$F_{03}^{\#3}$	0.98	2.54	3.440(5)	152.7

Symmetry transformations used to generate equivalent atoms:
#1 -x+1,-y+1,z+1/2 #2 -x+1,-y+2,z-1/2 #3 x+1/2,-y+2,z

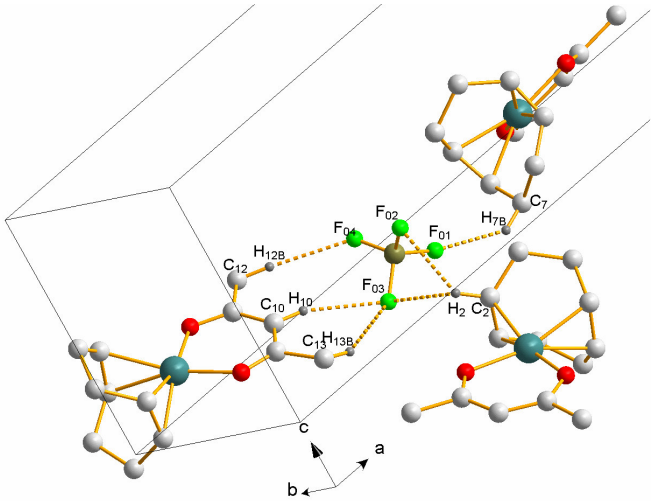

Figure 4.8 Partial unit cell of [Pd(cod)(acac)]BF_4 (2) illustrating weak intermolecular hydrogen bonding interactions indicated by dashed yellow bonds. Only selected hydrogen atoms are included. Palladium (cyan), carbon (grey), oxygen (red), boron (olive) and fluorine (green).

Figure 4.8 and Figure 4.9 show the hydrogen interactions listed in Table 4.5 for complex **2**. It is of note that there are no interactions of the type **2a···2a** which is not the case for complex **1** (Figure 4.4). A bifurcated hydrogen atom is again observed in the methine hydrogen of carbon (C_2) for the cyclo-octadiene ring with the fluorido ligands of **2b** (F_{02} and F_{03}). The hydrogens of the bonded to carbons C_{12}, C_{10} and C_{13} of the acetylacetonato ligand interacts with the **2b** (F_{04} and F_{03}) complex.

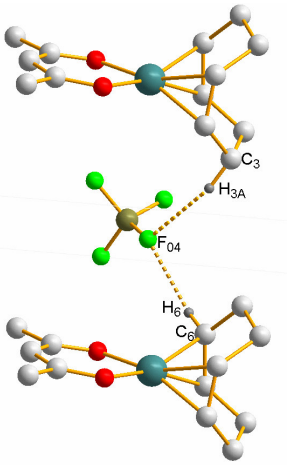

Figure 4.9 Reverse view of the [Pd(cod)(acac)]BF_4 (2) illustrating the remaining weak intermolecular hydrogen bonding interactions (dashed yellow bonds). Only selected hydrogen atoms are included. Palladium (cyan), carbon (grey), oxygen (red), boron (olive) and fluorine (green).

The methylene hydrogens of the carbons (C_3 and C_6) interact with the fluorido ligand (F_{04}) of **2b** (Figure 4.9). The average d(D…A) lengths of the methine hydrogens

linked to the carbons of the cyclo-octadiene in complex **1** and complex **2** are 3.221(6) Å and 3.390(5) Å, while the methylene hydrogens bonded to the carbons of the cyclo-octadiene are 3.170(6) Å and 3.460(6) Å. The acetylacetonato ligands were found to be 3.422(5) Å and 3.519(5) Å with the fluorido ligands respectively. There is a general weakening of the interactions for complex **1** as opposed to complex 2. The most significant include the methylene hydrogens of the carbons bonded to the cyclo-octadiene ligand with a difference of 0.29 Å which results in a larger distance between the counter ions. The differences observed for the hydrogen interactions affect the packing of these complexes even though the bond lengths and angles within the cationic species are similar.

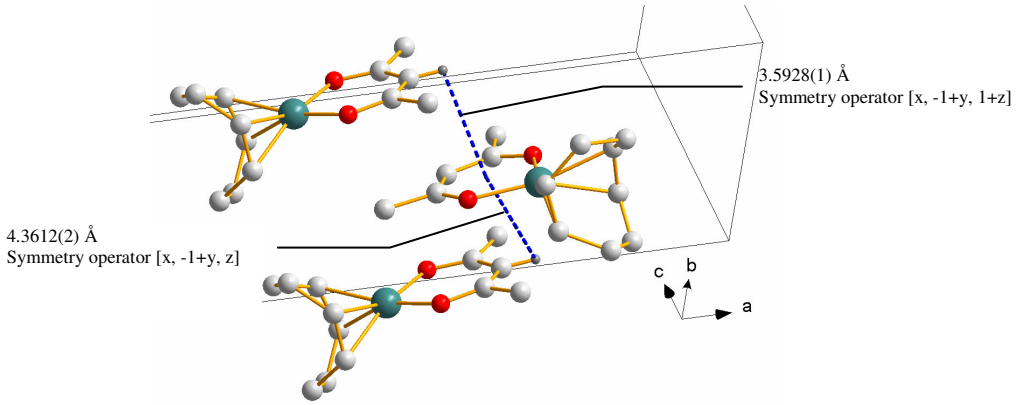

Figure 4.10 Partial unit cell of the [Pd(cod)(acac)]BF_4 (2) complex indicating the metal chelate ring interactions (dashed blue bonds) of the acetylacetonato ligands. Counter ions have been omitted for clarity and only selected hydrogens are shown. Palladium (cyan), carbon (grey) and oxygen (red).

In Figure 4.10 an additional factor in the packing of complex **2** is presented, that of metal chelate ring interactions of the palladium co-ordinated acetylacetonato metallocycle with the methine hydrogen of an adjacent acetylacetonato moiety, with distances of 3.5928(1) Å and 4.3612(2) Å, respectively. No metal chelate ring interactions were observed for complex **1**, Figure 4.11 shows the packing of complex **1** whilst Figure 4.12 illustrates the packing of complex **2**.

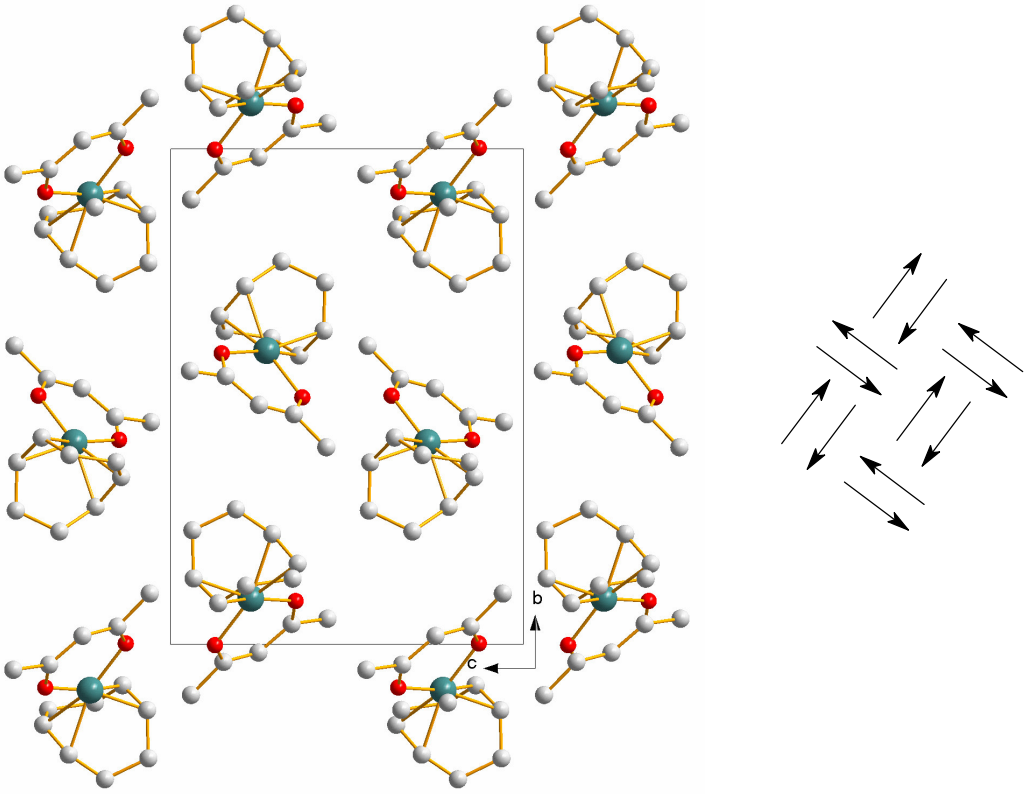

Figure 4.11 Packing of [Pd(cod)(acac)]PF_6 (1a) viewed along the *a*-axis with the packing motif incorporated to the right of the figure.

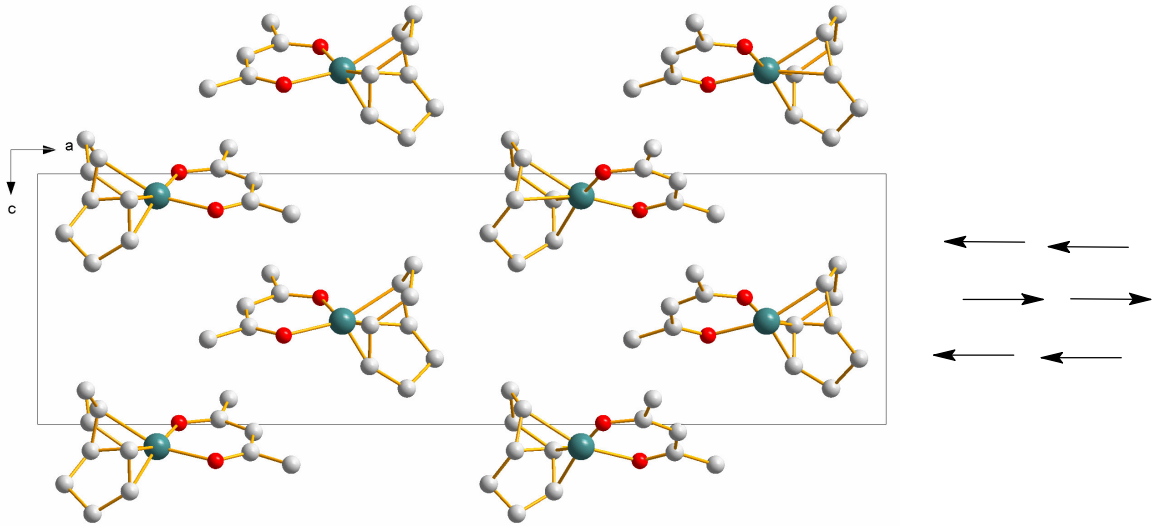

Figure 4.12 Packing of [Pd(cod)(acac)]BF_4 (2a) viewed along the *b*-axis with the packing motif incorporated to the right of the figure.

The packing motif is defined as the head of the arrow corresponding to the 1,5-cyclo-octadiene moiety and the tail of the arrow corresponding to the acetylacetonato moiety. The packing of the **2a** complex was found to be a classic head-to-tail (Figure

4.12) when viewed along the *b*-axis whereas the packing for the **1a** complex was found to be a clustered head-to-tail (Figure 4.11) when viewed along the *a*-axis as previously stated this is as a result of the multiple weak interactions observed between **1a** and **1b** (Figure 4.3) and **2a** and **2b** (Figure 4.8-4.8).

4.3.2 Crystal structures of [Pd(cod)(thtfac)]PF_6 and [Pd(cod)(thtfac)]BF_4

The compounds [Pd(cod)(thtfac)]PF_6 (**3**) crystallized in the monoclinic space group $P2_1/n$, with a cationic [Pd(cod)(thtfac)]$^+$ (**3a**) species and an anionic PF_6^- (**3b**) species in the asymmetric unit, whilst [Pd(cod)(thtfac)]BF_4 (**4**) also crystallized in the monoclinic space group $P2_1/n$, with a cationic [Pd(cod)(thtfac)]$^+$ (**4a**) species and an anionic BF_4^- (**4b**) species. The numbering scheme is presented in Figure 4.13, while atomic co-ordinates, bond angles and distances, anisotropic displacement parameters and hydrogen co-ordinates are reported in Appendix B.4 and B.8. General crystallographic data and refinement parameters are reported in Table 4.2, while significant bond angles and distances are reported in Table 4.6.

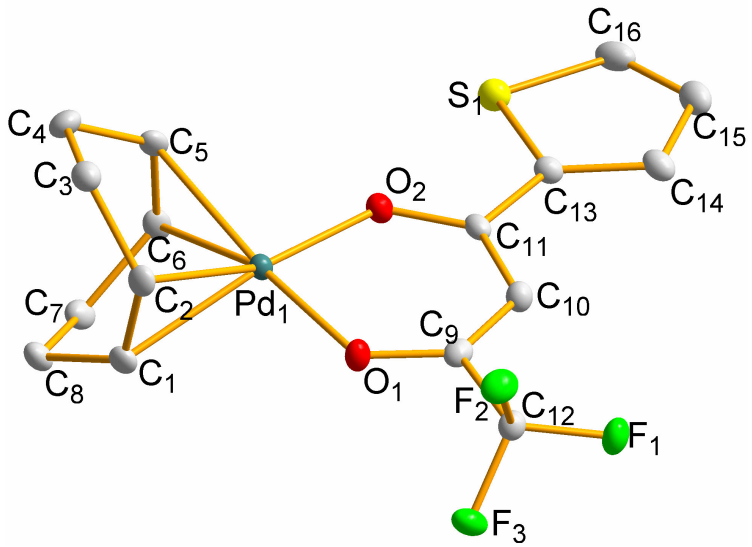

Figure 4.13 Diamond illustration of [Pd(cod)(thtfac)]PF_6 (3) at 100 K showing the numbering scheme and displacement ellipsoids (50 %) of the complex. Hydrogen atoms and counter ions omitted for clarity.

Table 4.6 Selected bond distances and angles for [Pd(cod)(thtfac)]A where A = PF_6 or BF_4

Bond Distance (Å)	Counter ion		Bond Angles (°)	Counter ion	
	PF_6 (**3**)	BF_4 (**4**)		PF_6 (**3**)	BF_4 (**4**)
Pd-O_1	2.007(2)	2.003(2)	O_1-Pd-O_2	93.34(6)	93.27(8)
Pd-O_2	2.012(2)	2.005(2)	C_1-Pd-C_2	36.88(9)	36.9(1)
Pd-C_1	2.193(2)	2.197(3)	C_5-Pd-C_6	36.99(8)	36.9(1)
Pd-C_2	2.181(2)	2.176(3)	C_1-Pd-C_6	82.20(9)	82.3(1)
Pd-C_5	2.184(2)	2.195(3)	C_2-Pd-C_5	81.98(9)	81.9(1)
Pd-C_6	2.174(2)	2.175(3)	χ^a	86.6(1)	86.6(1)
C_1-C_2	1.383(3)	1.382(4)	ψ^b	79.2(1)	82.0(2)
C_5-C_6	1.383(3)	1.385(4)			

a χ: $C_1MC_2 \cap C_5MC_6$ b ψ: $C_2C_3C_4C_5 \cap C_1C_8C_7C_6$ see Figure 1.2

The palladium metal centre is bonded to a 1,5-cyclo-octadine and a mono-anionic 2-thenoyltriflouroacetone ligand, which leaves a resulting cationic charge on the complex. This is accommodated by the hexafluorophosphate (PF_6^-) and tetrafluoroborate (BF_4^-) counter ions. Square planar geometry is observed around the palladium metal centre (Figure 4.2) for both complex **3** and **4** which is consistent for complexes of this type. The mean distances of Pd-O and C=C are 2.007(2) Å and 1.383(3) Å, respectively, again showing a similar behavior as was seen in complex **1a** and **2a** with little to no changes in the bond lengths and angles between the cationic species. The average palladium oxygen bite angle of 93.31(7)° is typical of a six membered ring. No disorder was found for either complex **3** or **4**. The intersection between the planes defined by the oxygen, carbon and palladium atoms of the thenoyltrifluoroacetonato ligand backbone and the thenoyl ring of the ligand were found to be 5.95(4)° for the **3a** species and 7.16(5)° for the **4a** species. The increase in the angle of intersection is as a result of short contacts of the sulfur of the thenoyl ring with adjacent ligands (Figure 4.16 and 4.20).

The hydrogen bonding of complex **3** is graphically presented in Figure 4.14 with Table 4.7 and 4.8 listing the bond distances and angles.

Table 4.7 Hydrogen bond distances and angles for [Pd(cod)(thtfac)]PF_6 (3) [Å and °]

D-H...A	d(D-H)	d(H...A)	d(D...A)	<(DHA)
C_{14}-H_{14}...F_{05}	0.95	2.32	3.193(3)	152.3
C_1-H_1...$F_{05}^{\#1}$	1.00	2.47	3.277(3)	136.9
C_2-H_2...$F_{04}^{\#2}$	1.00	2.48	3.175(3)	126.0
C_2-H_2...$F_{05}^{\#2}$	1.00	2.57	3.566(3)	177.4
C_3-H_{3A}...$F_2^{\#3}$	0.99	2.55	3.388(3)	141.7

Symmetry transformations used to generate equivalent atoms:
#1 x+1,y,z #2 -x,-y+2,-z+1 #3 x+1/2,-y+3/2,z+1/2

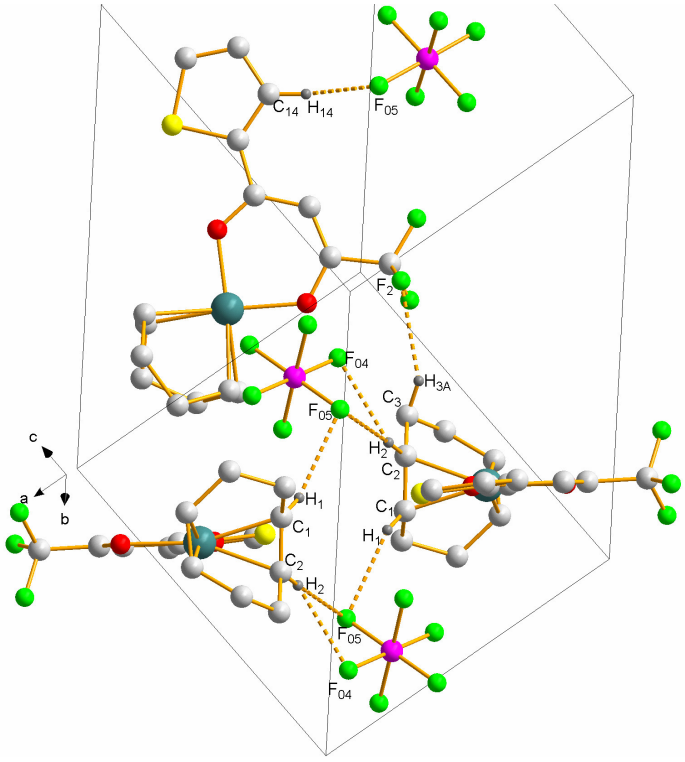

Figure 4.14 Partial unit cell of [Pd(cod)(thtfac)]PF_6 (3) showing intermolecular hydrogen bonding interactions indicated by a dashed bond. Only selected hydrogen atoms are included. Palladium (cyan), carbon (grey), oxygen (red), sulfur (yellow), phosphorus (pink) and fluorine (green).

Figure 4.14 shows the intermolecular hydrogen bonding of [Pd(cod)(thtfac)]PF_6 (**3**) with the listing in Table 4.7. The first type interaction is between the methylene hydrogens bonded to the carbon (C_3) of the cyclo-octadiene ring and an adjacent fluorido ligand (F_2) of the thenoyltriflouroactonato ligand. The second type interaction is that of the cyclo-octadiene (C_1 and C_2) ring from complex **3a**, with bifurcated H_2 hydrogen, with the fluorido ligands (F_{05} and F_{04}) of the **3b** complex. The last interaction is between the thenoyltriflouroacetonato (C_{14}) ligand of the **3a** complex and the fluorido ligand (F_{05}) of the **3b** complex. Additional weak hydrogen interactions which are not depicted in Figure 4.14 are shown in Table 4.8 below. These interactions albeit not classical hydrogen bonding still play a role in the packing of the complex.

Table 4.8 Additional weak hydrogen interactions for [Pd(cod)(thtfac)]PF_6 (3)

D-H...A	d(D-H)	d(D...A)	d(H...A)	<(DHA)
C_{10}-H_{10}...F_{01}	0.95	3.894(3)	2.97	164.2
C_{10}-H_{10}…F_{1}	0.95	2.712(2)	2.33	103.6
C_{10}-H_{10}…F_{05}	0.95	3.763(3)	2.91	150.4
C_{14}-H_{14}…F_{01}	0.95	3.711(3)	2.82	156.3
C_{14}-H_{14}…F_{04}	0.95	3.575(3)	2.84	135.0
C_{8}-H_{8B}…$F_{2}^{\#1}$	0.99	3.267(3)	2.83	107.7
C_{8}-H_{8B}…$F_{03}^{\#1}$	0.99	3.278(3)	2.90	103.7
C_{8}-H_{8B}…$F_{05}^{\#1}$	0.99	3.450(3)	2.76	127.4
C_{1}-H_{1}…$F_{02}^{\#1}$	1.00	3.570(3)	2.71	144.2
C_{1}-H_{1}…$F_{03}^{\#1}$	1.00	3.241(3)	2.82	105.9
C_{7}-H_{7A}…$F_{03}^{\#1}$	0.99	3.355(3)	2.64	129.0
C_{7}-H_{7B}…$F_{2}^{\#1}$	0.99	3.232(3)	2.65	117.9
C_{8}-H_{8B}…$F_{1}^{\#1}$	0.99	3.592(3)	2.82	135.4
C_{2}-H_{2}…$F_{02}^{\#2}$	1.00	3.411(3)	2.72	126.8
C_{3}-H_{3A}…$F_{04}^{\#2}$	0.99	3.152(3)	2.79	102.3
C_{4}-H_{4B}…$F_{3}^{\#3}$	0.99	3.484(3)	2.73	132.9
C_{5}-H_{5}…$F_{02}^{\#4}$	1.00	3.421(3)	2.63	136.6
C_{5}-H_{5}…$F_{06}^{\#4}$	1.00	3.325(3)	2.90	106.7
C_{3}-H_{3A}…$F_{06}^{\#4}$	0.99	3.452(3)	2.75	128.1
C_{4}-H_{4B}…$F_{06}^{\#4}$	0.99	3.352(3)	2.94	105.8
C_{4}-H_{4B}…$F_{02}^{\#4}$	0.99	3.554(3)	2.83	130.3
C_{7}-H_{7B}…$F_{06}^{\#5}$	0.99	3.751(3)	2.93	140.9
C_{7}-H_{7A}…$F_{1}^{\#5}$	0.99	3.439(3)	2.61	141.2
C_{7}-H_{7A}…$F_{03}^{\#5}$	0.99	3.551(3)	2.94	120.9
C_{6}-H_{6}…$F_{01}^{\#5}$	1.00	3.255(3)	2.61	122.3

Symmetry transformations used to generate equivalent atoms:
#1 x+1,y,z #2 -x,-y+2,-z+1 #3 x+½,y-½,-z+½ #4 –x-½,y-½,-z+½ #5 –x,-y+2,-z

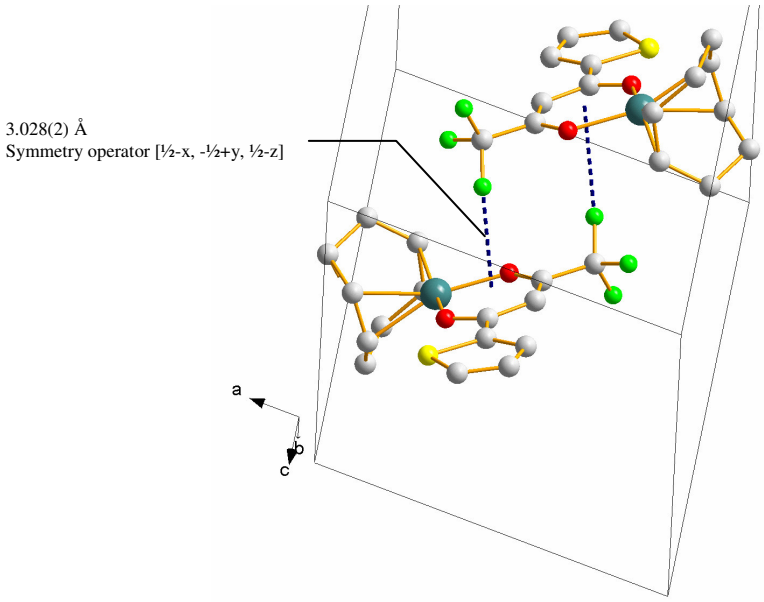

Figure 4.15 Partial unit cell of [Pd(cod)(thtfac)]PF_6 (3) showing F···metal chelate ring interactions indicated by dashed dark blue bonds. Hydrogens and hexafluorophosphate counter ions omitted for clarity. Palladium (cyan), carbon (grey), oxygen (red), sulfur (yellow) and fluorine (green).

The F···metal chelate ring interaction as shown in Figure 4.15, has a distance of 3.028(2) Å. There is an additional short contact between the sulfur (S_1) of the thenoyltrifluoroactonato ligand and the methylene hydrogen bonded to the carbon (C_8) of the cyclo-octadiene ring of 3.491(2) Å (Figure 4.16). The closest Pd-Pd contact is 7.4433(3) Å, indicating no metal interactions.

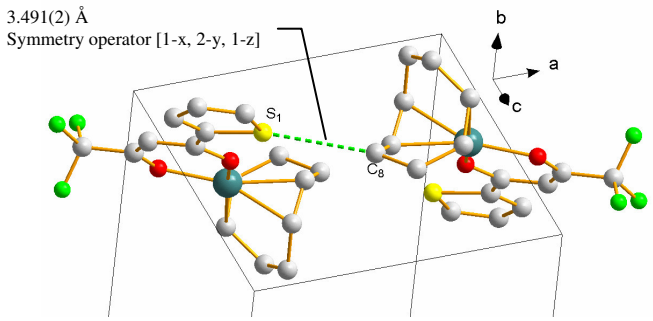

Figure 4.16 Partial unit cell of [Pd(cod)(thtfac)]PF_6 (3) showing a short contact between sulfur (S_1) and carbon (C_8) indicated by dashed green bonds. Hydrogens and hexafluorophosphate counter ions omitted for clarity. Palladium (cyan), carbon (grey), oxygen (red), sulfur (yellow) and fluorine (green).

The hydrogen bonding of complex **4** is graphically presented in Figure 4.17-4.18 with Table 4.9 listing the bond distances and angles.

Table 4.9 Hydrogen bond distances and angles for [Pd(cod)(thtfac)]BF_4 (4) [Å and °]

D-H...A	d(D-H)	d(H...A)	d(D...A)	<(DHA)
C_{10}-H_{10}...F_{01}	0.95	2.51	3.418(3)	161.2
C_{14}-H_{14}...F_{01}	0.95	2.49	3.348(4)	149.6
C_{14}-H_{14}...F_{02}	0.95	2.47	3.350(3)	154.8
C_8-H_{8B}...$F_{03}^{\#1}$	0.99	2.51	3.500(4)	177.0
C_1-H_1...$F_{01}^{\#1}$	1.00	2.49	3.277(4)	134.8
C_2-H_2...$F_{04}^{\#2}$	1.00	2.56	3.368(3)	137.7
C_3-H_{3A}...$F_{03}^{\#2}$	0.99	2.62	3.476(4)	144.9
C_4-H_{4B}...$F_{04}^{\#3}$	0.99	2.60	3.370(4)	134.2
C_5-H_5...$F_{02}^{\#3}$	1.00	2.29	3.289(4)	173.7
C_5-H_5...$F_{04}^{\#3}$	1.00	2.59	3.337(4)	131.3
C_6-H_6...$F_{02}^{\#4}$	1.00	2.39	3.105(4)	127.8
C_{16}-H_{16}...$F_{01}^{\#5}$	0.95	2.48	3.165(4)	128.6
C_{16}-H_{16}...$F_{04}^{\#5}$	0.95	2.56	3.266(4)	131.8

Symmetry transformations used to generate equivalent atoms:
#1 -x,-y,-z+1 #2 -x-1/2,y+1/2,-z+3/2 #3 -x,-y,-z+2
#4 x+1,y,z #5 x+1/2,-y-1/2,z+1/2

Previously as seen for [Pd(cod)(acac)]BF_4 (**2**) again only interactions of the type **4a**···**4b** for [Pd(cod)(thtfac)]BF_4 (**4**) (Table 4.9) were observed.

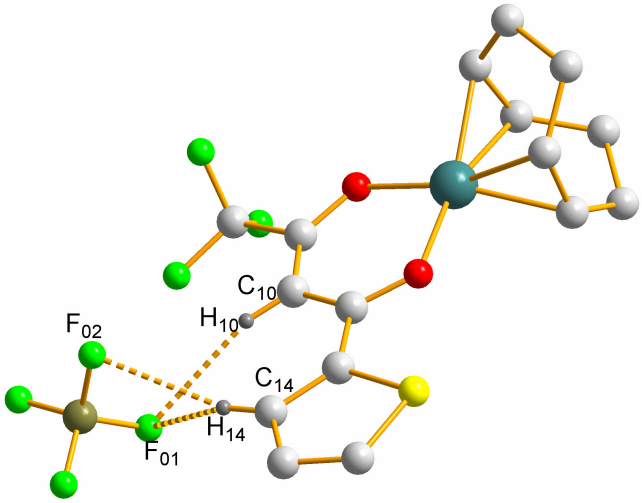

Figure 4.17 Intramolecular hydrogen bonding of [Pd(cod)(thtfac)]BF_4 (4) illustrated by dashed yellow bonds. Hydrogens have been omitted for clarity. Palladium (cyan), carbon (grey), oxygen (red), sulfur (yellow), boron (olive) and fluorine (green).

In Figure 4.17 intramolecular hydrogen bonding is depicted between a bifurcated hydrogen (H_{14}) of the thenoyltrifluoroacetonato ligand of the **4a** cationic species and the fluorido (F_{01} and F_{02}) ligand of the **4b** anionic species. The last intramolecular hydrogen interaction is that of the hydrogen of the enolic carbon (C_{10}) of the thenolytrifluoroacetonato ligand and the fluorido (F_{01}) ligand. A similar intramolecular hydrogen bonding occurs in the **3a** and **3b** complexes (Table 4.7 and 4.8) however it is significantly weaker than that of complex **4**.

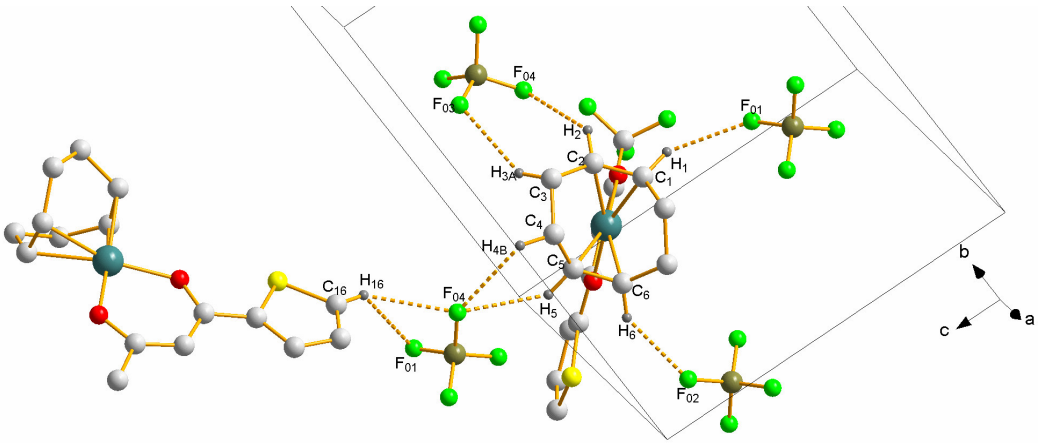

Figure 4.18 Partial unit cell of [Pd(cod)(thtfac)]BF_4 (4) showing intermolecular hydrogen bonding interactions indicated by a dashed bond. Only selected hydrogen atoms are included. Palladium (cyan), carbon (grey), oxygen (red), sulfur (yellow), boron (olive) and fluorine (green).

The remaining intramolecular hydrogen bonding interactions for [Pd(cod)(thtfac)]BF_4 are shown in Figure 4.18 and listed in Table 4.9. It is of interest to note that there are

interactions between all the methine hydrogens bonded to the carbons (C_1, C_2, C_5 and C_6) of the cyclo-octadiene ring of the cationic **4a** species with the fluorido (F_{01}, F_{04} and F_{02}) ligands of the anionic **4b** species this is not the case for the [Pd(cod)(ththac)]PF_6 (**3**) complex which only has the methine hydrogens bonded to the carbons (C_1 and C_2) showing fair interactions. The methylene hydrogens bonded to the C_3 and C_4 carbons of the cyclo-octadiene also interact with the fluorido (F_{03} and F_{04}) ligands. Thenoyltrifluoroacetonato (C_{16}) ligand has a bifurcated hydrogen with the fluorido (F_{04} and F_{01}) ligands of the anionic **4b** species. One of the differences in the interactions between the **4a**···**3a** species is that of the **3a**···**3a** interaction (C_3···F_2) which is absent in the **4a** species. Also no F···F interactions were found for either the **3a** or the **4a** species.

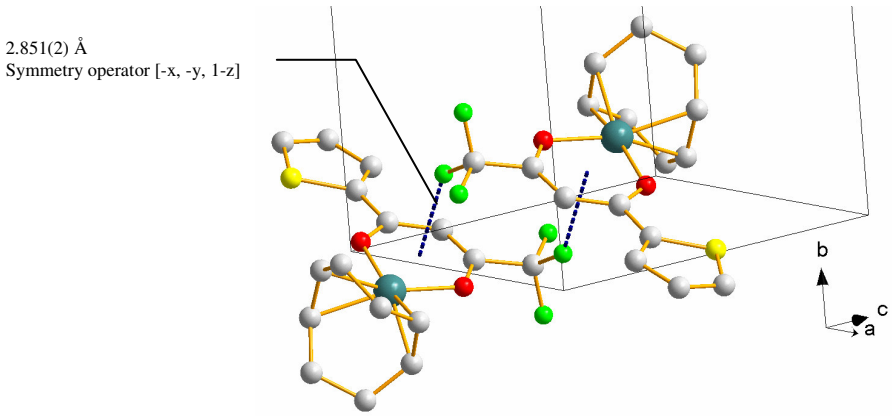

Figure 4.19 Partial unit cell of [Pd(cod)(thtfac)]BF_4 (4) showing F···metal chelate ring interactions indicated by dashed dark blue bonds. Hydrogens and tetrafluoroborate counter ions omitted for clarity. Palladium (cyan), carbon (grey), oxygen (red), sulfur (yellow) and fluorine (green).

In Figure 4.19, the F···metal chelate ring interactions between adjacent thenoyltrifluoroacetonato ligands of the **4a** complex were observed with a distance of 2.851(2) Å. An identical interaction was also observed (Figure 4.15) for the **3a** species with a distance of 3.028(2) Å which is 0.18 Å longer than that of the **4a** species. This indicates a tighter packing for the **4a** complex, which is not surprising as the expected volumes of the **3b** and **4b** species differ.

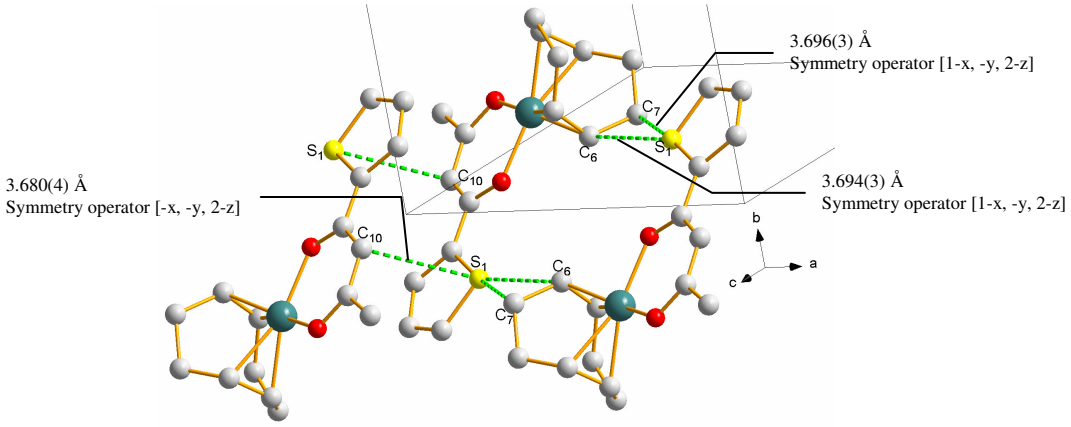

Figure 4.20 Partial unit cell of [Pd(cod)(thtfac)]BF_4 (4) showing a short contact between sulfur and carbon indicated by dashed green bonds. Hydrogens and tetrafluoroborate counter ions omitted for clarity. Palladium (cyan), carbon (grey), oxygen (red), sulfur (yellow) and fluorine (green).

The sulfur carbon short contact observed for the **3a** complex was to the methylene carbon (C_8) of the cyclo-octadiene ring (Figure 4.16). The short contacts for the **4a** complex can be seen in Figure 4.20. The contacts for the **4a** species are found between the thenoyltrifluroacetonato (C_{10}) ligand with a distance of 3.680(4) Å and the cyclo-octadiene (C_6 and C_7) ring with distances of 3.694(3) Å and 3.696(3) Å respectively. The difference in distance of the methylene carbons of the **3a** and **4a** species was found to be *c.a.* 0.2 Å.

Thus the weakening of the F···metal chelate ring interactions for the **3a** species and the strengthening of the sulfur carbon short contact leads to a shifting of the head-to-tail packing of the **3a** species. A similar shifting occurs for the **4a** species with the distances between the head-to-tail packing being shifted slightly apart.

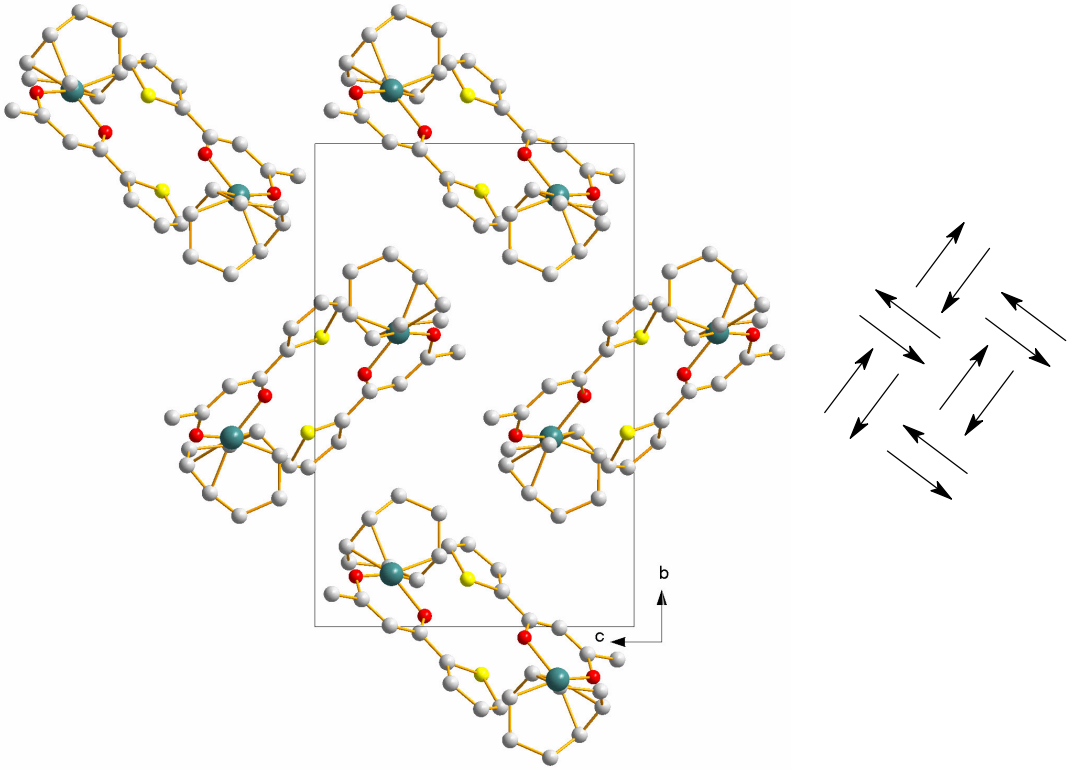

Figure 4.21 Packing of [Pd(cod)(thtfac)]PF_6 (3a) viewed along the *a*-axis with the packing motif incorporated to the right of the figure. Hydrogens and Fluorines and counter ions have been omitted for clarity.

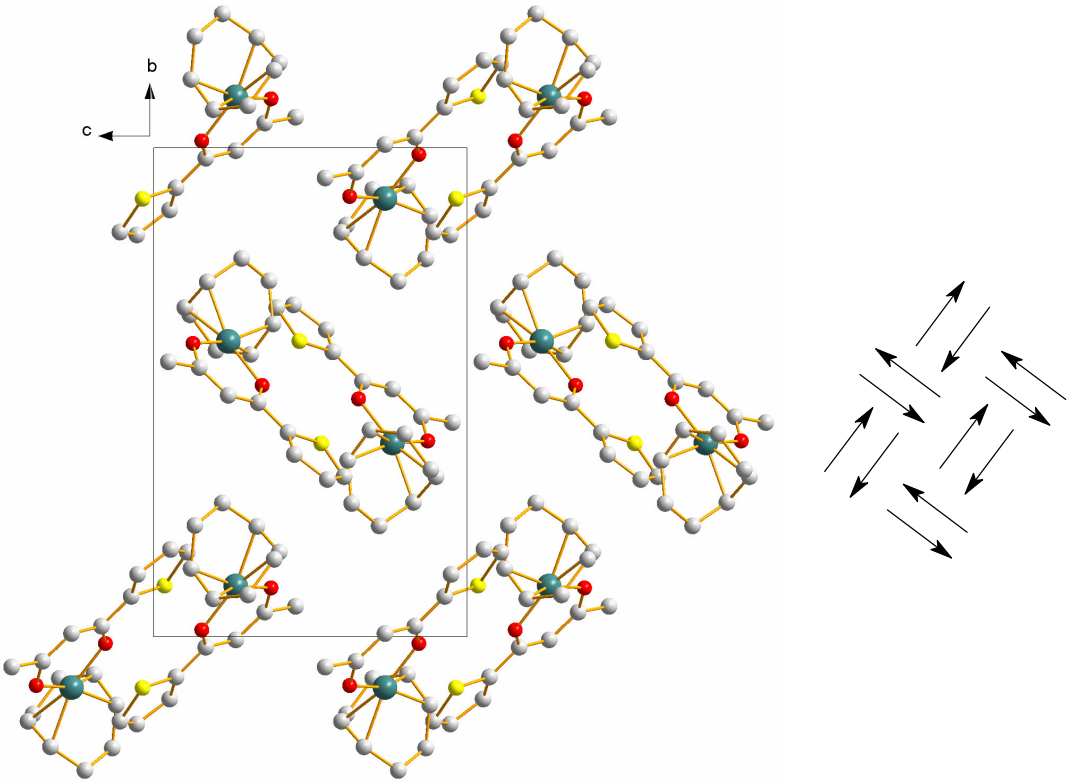

Figure 4.22 Packing of [Pd(cod)(thtfac)]BF_4 (4a) viewed along the *a*-axis with the packing motif incorporated to the right of the figure. Hydrogens and Fluorines and counter ions have been omitted for clarity.

The packing motif is defined as the head of the arrow corresponding to the 1,5-cyclo-octadiene moiety and the tail of the arrow corresponding to the thenoyltrifluoroacetylacetonato moiety. It can be seen from Figure 4.21 and Figure 4.22, that both complexes demonstrate a clustered head-to-tail packing conformation. The only differences between these figures is in the distances between the head-to-tail clusters with the **1a** species being more evenly distributed (Figure 4.11).

4.3.3 Crystal structure of [Pd(cod)(tfacac)]PF_6

The compound [Pd(cod)(tfacac)]PF_6 (**5**) is reported in the triclinic space group $P\bar{1}$, with two cationic [Pd(cod)(tfacac)]$^+$ (**5a1** and **5a2**) species and two anionic PF_6^- (**5b1** and **5b2**) species in the asymmetric unit. The compound however, may also be solved in *C*2/*c* and *Cc* space groups, the R-values for all space groups are poor indicating possible unresolved disorder or twinning present in the compound. Upon investigation it was found that disorder was not present in the compound and that only minor merohedral twinning was present the R-values still remained poor even with the merohedral twinning included. A systematic error was found in the original data this systematic error has not been omitted in the data presented below. The reason for this systematic error remains unresolved. Several crystals were attempted as well as crystals from when the compound was resynthesized, the systematic error occurred in all.

The numbering scheme is presented in Figure 4.23, while atomic co-ordinates, bond angles and distances, anisotropic displacement parameters and hydrogen co-ordinates are reported in Appendix B.5. General crystallographic data and refinement parameters are reported in Table 4.2, while significant bond angles and distances are reported in Table 4.10.

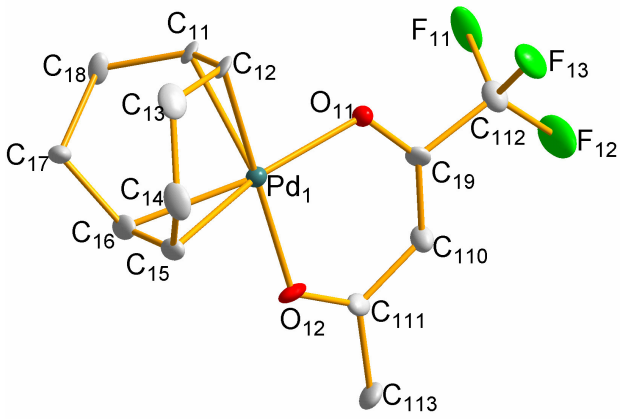

Figure 4.23 Diamond illustration of [Pd(cod)(tfacac)]PF_6 (5) at 100 K showing the numbering scheme and displacement ellipsoids (50 %) of the complex. Hydrogen atoms and counter ions omitted for clarity.

Figure 4.23 presents the numbering scheme of the first cationic species (**5a1**) in the unit cell the second cationic species (**5a2**) numbering prefixes with a 2 instead of a 1 e.g. O_{11} is then O_{21}. The anionic species have been omitted for clarity and are numbered in a similar fashion e.g. P_1 and P_2.

Table 4.10 Selected bond distances and angles for [Pd(cod)(tfacac)]PF_6

Bond Distance (Å)	Species		Bond Angles (°)	Species	
	5a1	**5a2**		**5a1**	**5a2**
Pd-O_1	2.007(11)	2.011(10)	O_1-Pd-O_2	93.2(5)	93.5(5)
Pd-O_2	2.018(11)	2.017(11)	C_1-Pd-C_2	36.4(6)	37.2(6)
Pd-C_1	2.171(14)	2.197(14)	C_5-Pd-C_6	36.6(7)	36.0(7)
Pd-C_2	2.208(15)	2.154(15)	C_1-Pd-C_6	82.3(6)	82.2(6)
Pd-C_5	2.180(16)	2.197(16)	C_2-Pd-C_5	82.6(6)	81.7(6)
Pd-C_6	2.191(17)	2.182(16)	χ^a	86.8(6)	86.1(2)
C_1-C_2	1.37(2)	1.39(2)	ψ^b	86.9(9)	86.9(9)
C_5-C_6	1.37(3)	1.35(3)			

a χ: $C_1MC_2 \cap C_5MC_6$ b ψ: $C_2C_3C_4C_5 \cap C_1C_8C_7C_6$ see Figure 1.2

The selected bond distances and angles for both the **5a1** and **5a2** cationic species are presented in Table 4.10, as can be seen the values do not differ significantly from each other. Therefore for future discussions and comparisons we will be working with the **5a1** species values.

The palladium metal centre is π-bonded to one 1,5-cyclo-octadiene ligand and to a single trifluoroacetylacetonato ligand. The resulting charge of the complex is balanced by a PF_6 anion. The co-ordination geometry remains square planar (Figure 4.2). The palladium oxygen bond is symmetrical with an average distance of

2.013(11) Å. The palladium carbon bonds are similar with an average distance of 2.185(15) Å. The average distance of the alkene carbons was found to be 1.37(5) Å.

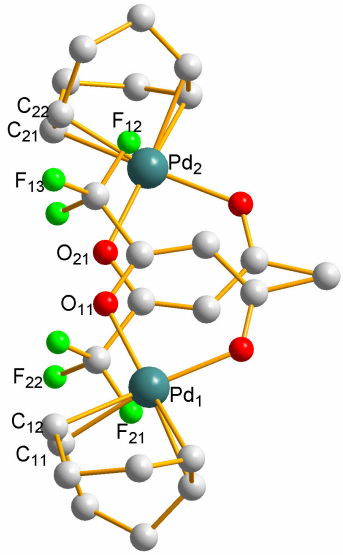

Figure 4.24 Diamond illustration of both cationic [Pd(cod)(tfacac)]$^+$ species showing the manifested disorder by the overlap of the cationic species. Hydrogen and counter ions have been omitted for clarity.

A systematic error was observed near C_{11} and C_{12} which is mirrored at C_{21} and C_{22} with three high value Q-peaks, the distances to these Q-peaks are as follows C_{11}-Q_1, C_{11}-Q_2, C_{11}-Q_3, C_{12}-Q_1, C_{12}-Q_2 and C_{12}-Q_3 are 0.98 Å, 1.30 Å, 1.897 Å, 1.839 Å, 1.279 Å and 1.079 Å respectively. The distances between Q_1-Q_2 and Q_2-Q_3 are 0.962 Å and 0.863 Å respectively. In Figure 4.24 both cationic species are viewed along the *c*-axis, it is of interest to note that the CF_3 group of the trifluoracetylactonato ligand is in a similar spatial position to the systematic error observed. This lead to the conclusion that the crystal might be twinned. Upon inspection it was found that only minor merohedral twinning (6 %) was present along the *c*-axis. Even with the twinning included the R-values did not improve and the systematic error was still present. This systematic error increases the anisotropic displacement parameters (ADP) of the atoms (C_{11}, C_{12}, C_{21}, C_{22}, F_{12}, F_{13}, F_{21} and F_{22}).

The hydrogen bonding of complex **5** is graphically presented in Figure 4.25-4.27 with Table 4.11 listing the bond distances and angles.

Table 4.11 Hydrogen bond distances and angles for [Pd(cod)(tfacac)]PF_6 (5) [Å and °].

D-H...A	d(D-H)	d(H...A)	d(D...A)	<(DHA)
C_{25}-H_{25}...F_{106}	1.00	2.38	3.36(2)	165.2
C_{110}-H_{110}...F_{12}	0.95	2.27	2.68(2)	105.1
C_{110}-H_{110}...F_{103}	0.95	2.54	3.38(2)	148.2
C_{210}-H_{210}...F_{21}	0.95	2.27	2.67(2)	104.5
C_{13}-H_{13A}...$F_{104}^{\#1}$	0.99	2.51	3.39(2)	148.9
C_{12}-H_{12}...$F_{105}^{\#1}$	1.00	2.48	3.33(2)	142.2
C_{210}-H_{210}...$F_{201}^{\#2}$	0.95	2.51	3.36(2)	148.7
C_{16}-H_{16}...$F_{205}^{\#2}$	1.00	2.36	3.34(2)	165.2
C_{21}-H_{21}...$F_{206}^{\#3}$	1.00	2.49	3.344(19)	142.9
C_{28}-H_{28A}...$F_{203}^{\#3}$	0.99	2.49	3.38(2)	149.3

Symmetry transformations used to generate equivalent atoms:
#1 -x+1,-y+1,-z+1 #2 x+1,y,z #3 -x,-y+1,-z

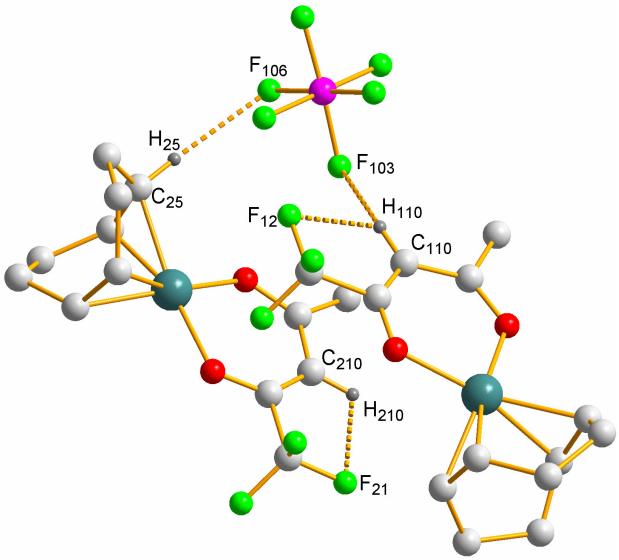

Figure 4.25 Intramolecular hydrogen bonding of [Pd(cod)(tfacac)]PF_6 (5) illustrated by dashed yellow bonds. Hydrogens have been omitted for clarity. Palladium (cyan), carbon (grey), oxygen (red), phosphorus (pink) and fluorine (green).

Figure 4.25 shows intramolecular hydrogen bonding of the [Pd(cod)(tfacac)]PF_6 (**5**) complex. Firstly, in **5a2** complex we see the methine hydrogen bonded to the carbon (C_{210}) of the trifluoroacetylacetonato ligand interacting with the fluorine atom (F_{21}) of the same ligand, in the **5a1** complex we find a similar interaction (C_{110}···F_{12}), however the hydrogen in both the **5a1** and **5a2** complexes are bifurcated with an additional interaction between the fluorido (F_{103}) ligand of the **5b1** complex and the **5a1** complex. The second half of the bifurcated hydrogen of the **5a2** complex can be seen in Figure 4.26 between the fluorido (F_{201}) ligands of the **5b2** complex. The last interaction can be observed between the **5a2** complexes alkene carbon (C_{25}) of the cyclo-octadiene and the **5b1** complex fluorido ligand (F_{106}).

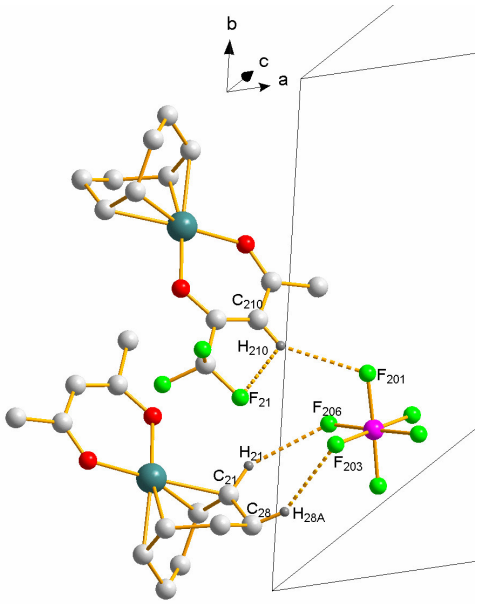

Figure 4.26 Partial unit cell of [Pd(cod)(tfacac)]PF_6 (5) showing intermolecular hydrogen bonding interactions indicated by a dashed bond. Only selected hydrogen atoms are included. Palladium (cyan), carbon (grey), oxygen (red), phosphorus (pink) and fluorine (green).

The two intermolecular hydrogen interactions between the cyclo-octadiene (C_{21} and C_{28}) ligand of **5a2** and fluorido (F_{206} and F_{203}) ligand of the **5b2** complex are illustrated in Figure 4.26. The last interactions are observed in Figure 4.27, between the cyclo-octadiene (C_{16}, C_{13} and C_{12}) moieties of the **5a1** complexes and the fluorido (F_{205}, F_{104} and F_{105}) ligands of the **5b1** and **5b2** complexes.

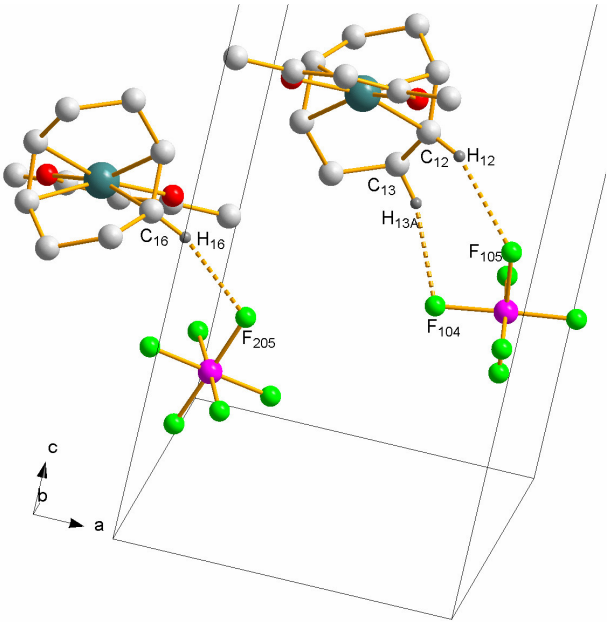

Figure 4.27 Partial unit cell of [Pd(cod)(tfacac)]PF_6 (5) showing intermolecular hydrogen bonding interactions indicated by a dashed bond. Only selected hydrogen atoms are included. Palladium (cyan), carbon (grey), oxygen (red), phosphorus (pink) and fluorine (green).

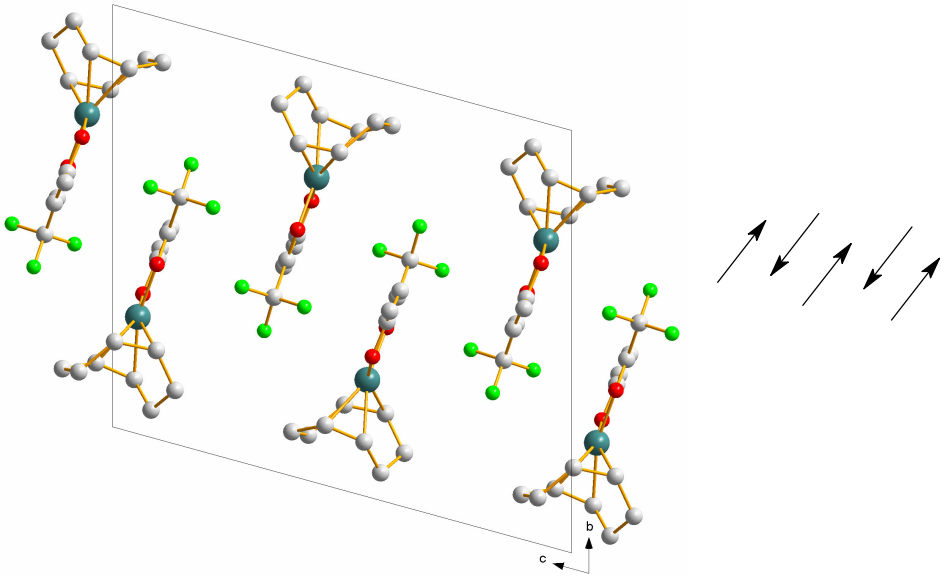

Figure 4.28 Packing of [Pd(cod)(tfacac)]PF_6 (5a1 and 5a2) viewed along the *a*-axis with the packing motif incorporated to the right of the figure. Hydrogens and counter ions have been omitted for clarity.

The packing motif in Figure 4.28 is defined as the head of the arrow corresponding to the 1,5-cyclo-octadiene moiety and the tail of the arrow corresponding to the trifluoroacetylacetonato moiety. The packing of [Pd(cod)(tfacac)]PF_6 (**5**) is depicted in Figure 4.28 when viewed along the *a*-axis we find the classic head-to-tail packing.

4.3.4 Crystal structure of [Pd(cod)(hfacac)]PF_6

The compound [Pd(cod)(hfacac)]PF_6 (**6**) crystallized in the monoclinic space group $P2_1/c$, with a cationic [Pd(cod)(hfacac)]$^+$ (**6a**) species and an anionic PF_6^- (**6b**) species in the asymmetric unit. The numbering scheme is presented in Figure 4.29, while atomic co-ordinates, bond angles and distances, anisotropic displacement parameters and hydrogen co-ordinates are reported in Appendix B.6. General crystallographic data and refinement parameters are reported in Table 4.2, while significant bond angles and distances are reported in Table 4.12.

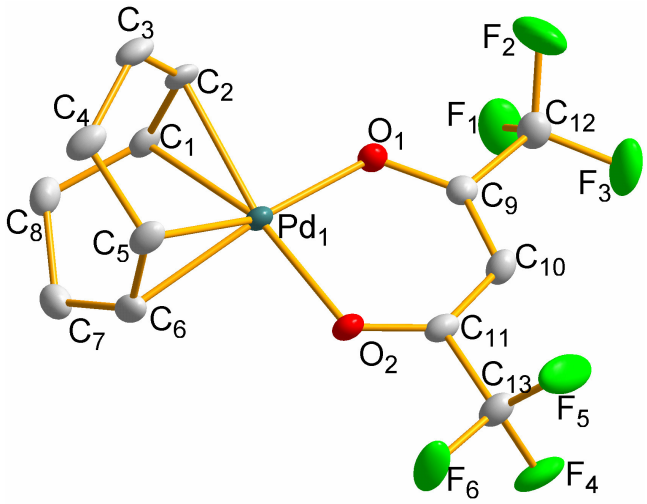

Figure 4.29 Diamond illustration of [Pd(cod)(hfacac)]PF_6 (6) at 100 K showing the numbering scheme and displacement ellipsoids (50 %) of the complex. Hydrogen atoms and PF_6 counter ion omitted for clarity.

Table 4.12 Selected bond distances and angles for [Pd(cod)(hfacac)]PF_6 (6)

Bond Distance (Å)		Bond Angles (°)	
Pd-O_1	2.027(2)	O_1-Pd-O_2	93.06(8)
Pd-O_2	2.026(2)	C_1-Pd-C_2	37.13(10)
Pd-C_1	2.191(3)	C_5-Pd-C_6	36.98(10)
Pd-C_2	2.166(3)	C_1-Pd-C_6	82.02(10)
Pd-C_5	2.190(3)	C_2-Pd-C_5	81.99(10)
Pd-C_6	2.171(3)	χ^a	86.5(1)
C_1-C_2	1.387(4)	ψ^b	83.2(1)
C_5-C_6	1.383(4)		

a χ: $C_1MC_2 \cap C_5MC_6$ b ψ: $C_2C_3C_4C_5 \cap C_1C_8C_7C_6$ see Figure 1.2

The palladium has a square planar geometry (Figure 4.2) with bonded hexafluoroacetylacetonato (hfacac) and cylo-octadinato (cod) moieties. The resulting charge is again balanced by a hexafluorophosphinato (PF_6) anion. The PF_6 counter ion shows typical bond angles and distances. The Pd-O and C=C bond distances are

equivalent at mean bond distance of 2.026(2) Å and 1.385(4) Å. With the Pd-C bond distances, Pd-C_1 being longer than Pd-C_2 by 0.025(3) Å, indicating that the olefinic bond is tilted away from the palladium metal centre by *c.a.* 2° with the angles confirming this trend Pd-C_1-C_2 (70.4(2)°) and Pd-C_2-C_1 (72.4(2)°) respectively. Both olefinic bonds display the same trend. The average Pd-C bond distance was found to be 2.180(3) Å.

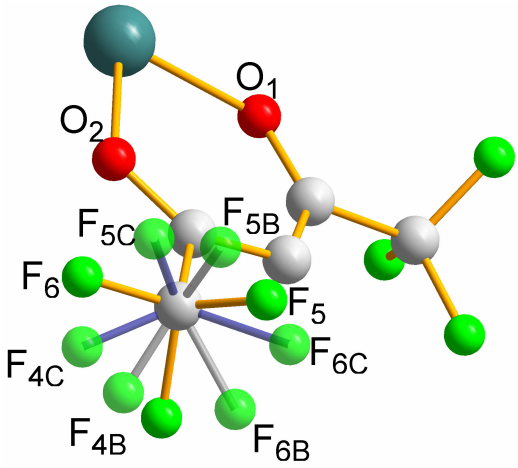

Figure 4.30 Diamond illustration of the multiple disordered CF_3 group indicated by dark grey, indigo and yellow bonds respectively. Palladium (cyan), oxygen (red), carbon (grey) and fluorine (green). Cyclo-octadiene moiety and the hydrogens have been omitted for clarity.

There is a three-way disorder observed on the hfacac moiety, which is depicted with dark grey and indigo bonds respectively (Figure 4.30). The other CF_3 group on hfacac was not found to be disordered.

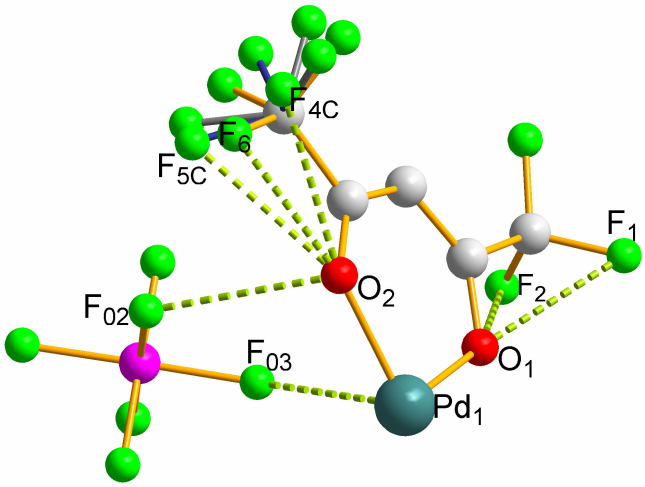

Figure 4.31 Diamond illustration of [Pd(cod)(hfacac)]PF_6 (6) showing the intramolecular bonding indicated by a dashed lime bond. Palladium (cyan), oxygen (red), carbon (grey) and fluorine (green). Cyclo-octadiene moiety as well as the hydrogens have been omitted for clarity.

There are seven intramolecular short contacts within [Pd(cod)(hfacac)]PF_6 (**6**) complex (Figure 4.31). The first set being between $O_1 \cdots F_1$ and $O_1 \cdots F_2$ with distances of 2.690(3) Å and 2.782(3) Å correspondingly. The second set is between O_2 and F_{4C}, F_6, F_{5C} and F_{02} with respective distances of 2.78(1) Å, 2.519(4) Å, 2.68(3) Å and 2.943(3) Å. A fairly long contact exists between C_{11} (adjacent carbon to O_2) and F_{02} with a distance of 3.156(4) Å and is not depicted in the figure above. Last but by no means least is a short contact between $Pd_1 \cdots F_{03}$ of the **6b** species with a distance of 2.983(2) Å.

The hydrogen bonding of complex **6** is graphically presented in Figure 4.32-4.33 with Table 4.13 listing the bond distances and angles.

Table 4.13 Hydrogen bond distances and angles for [Pd(cod)(hfacac)]PF_6 (6) [Å and °].

D-H...A	d(D-H)	d(H...A)	d(D...A)	<(DHA)
C_7-H_{7B}...$F_{06}^{\#1}$	0.99	2.74	3.449(4)	128.7
C_1-H_1...$F_{04}^{\#1}$	1.00	2.48	3.313(3)	140.1
C_2-H_2...$F_{4B}^{\#2}$	1.00	2.39	3.06(2)	123.8
C_2-H_2...$F_{4C}^{\#2}$	1.00	2.53	3.366(17)	141.4
C_3-H_{3A}...$F_{6B}^{\#2}$	0.99	2.34	3.053(16)	128.3
C_3-H_{3B}...$F_2^{\#3}$	0.99	2.55	3.305(3)	133.1
C_8-H_{8B}...$F_{04}^{\#3}$	0.99	2.52	3.489(3)	166.4
C_4-H_{4A}...$F_6^{\#4}$	0.99	2.44	3.209(4)	134.6
C_5-H_5...$F_{5C}^{\#4}$	1.00	2.17	2.806(18)	120.2
C_6-H_6...$F_{05}^{\#4}$	1.00	2.55	3.482(3)	156.0
C_7-H_{7A}...$F_3^{\#5}$	0.99	2.56	3.348(3)	136.2
C_{10}-H_{10}...$F_{01}^{\#6}$	0.95	2.35	3.288(4)	168.1
C_{10}-H_{10}...F3	0.95	2.33	2.709(3)	102.8

Symmetry transformations used to generate equivalent atoms:
#1 x+1,y,z #2 x,-y+1/2,z-1/2 #3 -x,y-1/2,-z+1/2
#4 -x,-y,-z+1 #5 x,y-1,z #6 -x,-y+1,-z+1

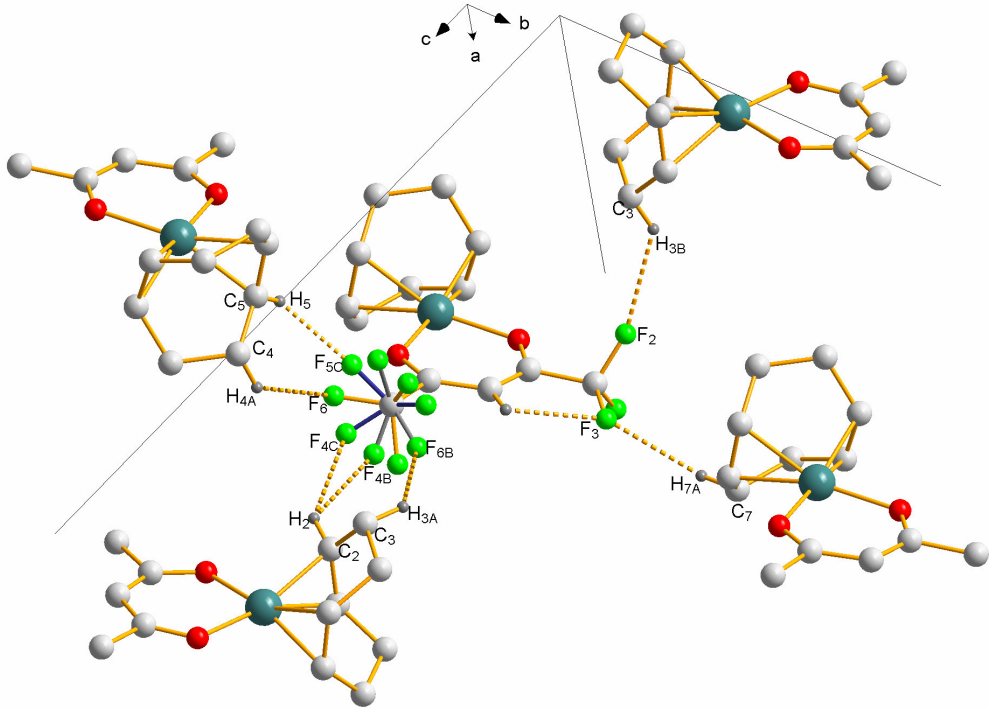

Figure 4.32 Partial unit cell of [Pd(cod)(hfacac)]PF_6 (6) showing hydrogen bonding interactions indicated with a dashed yellow bonds. Select hydrogens, fluorines, carbons and PF_6 have been omitted for clarity. Palladium (cyan), oxygen (red), carbon (grey) and fluorine (green).

Figure 4.32 shows the intramolecular hydrogen bonding interactions between **6a**···**6a** complexes. The interactions between the hfacac and the cod moieties can be clearly seen. The interactions between the fluorines (F_{4C}, F_{4B}, F_{6B} and F_6) of the hfacac moiety and carbons (C_5, C_4, C_2 and C_3) of the cyclo-octadiene ring stabilize the 3-part disorder observed. Lastly interactions between the non-disordered CF_3 (F_2 and F_3) group and the cod (C_3 and C_7) moiety are also observed.

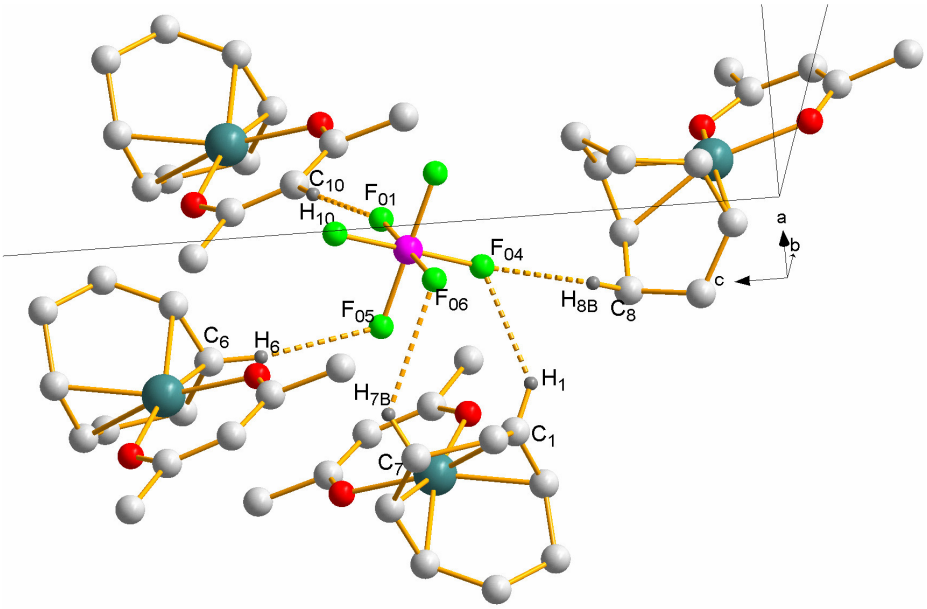

Figure 4.33 Partial unit cell of [Pd(cod)(hfacac)]PF_6 (6) showing hydrogen bonding interactions indicated with a dashed yellow bonds. Select hydrogens, fluorines and carbons have been omitted for clarity. Palladium (cyan), oxygen (red), carbon (grey), phosphorous (pink) and fluorine (green).

In Figure 4.33 the **6a**···**6b** interactions are depicted, the first type being that of the hfacac methine hydrogen bonded to the carbon (C_{10}) with the fluorido (F_{01}) ligand of the **6b** complex. The second type is between the hydrogens of the cod carbons (C_6, C_7, C_1 and C_8) again with the fluorido (F_{05}, F_{06} and F_{04}) ligands of the **6b** complex. Additional weak hydrogen interactions which are not depicted in Figure 4.32 and Figure 4.33 are show in Table 4.14 below.

Table 4.14 Addition weak hydrogen interactions for [Pd(cod)(hfacac)]PF_6 (6)

D-H...A	d(D-H)	d(D...A)	d(H...A)	<(DHA)
C_3-H_{3B}...F03	0.97	3.528(3)	2.89	124.2
C_3-H_{3B}…F06	0.97	3.560(4)	2.83	133.1
C_{10}-H_{10}…F_{6B}	0.93	2.81(2)	2.44	103.6
C_7-H_{7B}…$F_{05}^{\#1}$	0.97	3.367(3)	2.70	126.4
C_8-H_{8A}…$F_{06}^{\#1}$	0.97	3.272(4)	2.67	120.3
C_3-H_{3A}…$F_{6C}^{\#3}$	0.97	3.50(3)	2.77	131.74
C_2-H_2…$F_4^{\#3}$	0.98	3.043(4)	2.55	111.0
C_2-H_2…$F_{6B}^{\#3}$	0.98	3.20(2)	2.86	101.2
C_3-H_{3A}…$F_4^{\#3}$	0.97	3.347(4)	2.81	115.4
C_4-H_{4B}…$F_{04}^{\#4}$	0.97	3.376(4)	2.65	131.8
C_3-H_{3A}…$F_{04}^{\#4}$	0.97	3.401(4)	2.71	128.4
C_3-H_{3A}…$F_{03}^{\#4}$	0.97	3.752(3)	2.98	137.7
C_4-H_{4A}…$F_{5C}^{\#5}$	0.97	3.01(3)	2.46	115.8
C_4-H_{4A}…$F_{5B}^{\#5}$	0.97	3.32(3)	2.85	110.4
C_5-H_5…$F_{02}^{\#5}$	0.98	3.400(4)	2.69	130.0
C_5-H_5…$F_6^{\#5}$	0.98	3.228(5)	2.56	125.7
C_5-H_5…$F_{5B}^{\#5}$	0.98	3.12(3)	2.61	112.2
C_4-H_{4A}..$F_{4C}^{\#5}$	0.97	3.75(2)	2.87	151.1

C_6-H_6…$F_{02}^{\#5}$	0.98	3.441(4)	2.77	126.7
C_7-H_{7A}…$F_1^{\#6}$	0.97	3.836(3)	2.89	165.0
C_7-H_{7B}…$F_6^{\#7}$	0.97	3.405(6)	2.82	120.0
C_7-H_{7A}…$F_{4C}^{\#7}$	0.97	3.01(2)	2.60	105.1
C_7-H_{7A}…$F_4^{\#7}$	0.97	3.581(5)	2.84	134.0
C_7-H_{7A}…$F_{4B}^{\#7}$	0.97	3.23(3)	2.60	122.6
C_{10}-H_{10}…$F_5^{\#8}$	0.93	3.468(6)	2.98	114.2

Symmetry transformations used to generate equivalent atoms:
#1 x+1,y,z #2 –x+1,y-½,-z+½ #3 x,-y+½,z-½ #4 -x,y-½,-z+½ #5 -x,-y,-z+1
#6 x,y-1,z #7 –x+1,-y,-z+1 #8 –x,-y+1,-z+1

Figure 4.34 describes F···F bond interactions which are illustrated with dashed grey bonds. The following bond interactions are observed F_{5B}···F_{02} and F_{02}···F_{5C} with respective distances of 2.64(3) Å and 2.67(3) Å. The next three interactions are to an adjacent molecule (symmetry operation: -x, 1-y, 1-z), F_3-F_{5B}^{adj} with a distance of 2.76(2) Å, F_{6B}···F_{01}^{adj} with a distance of 2.63(2) Å) and F_{6C}···F_{01}^{adj} with a distance of 2.75(3) Å. There is an additional C-F bond interaction which is not depicted in the figure above that of the C_5···F_{5C} bond with a distance of 2.81 Å, the C_5 atom is located on the cyclo-octadienato moiety.

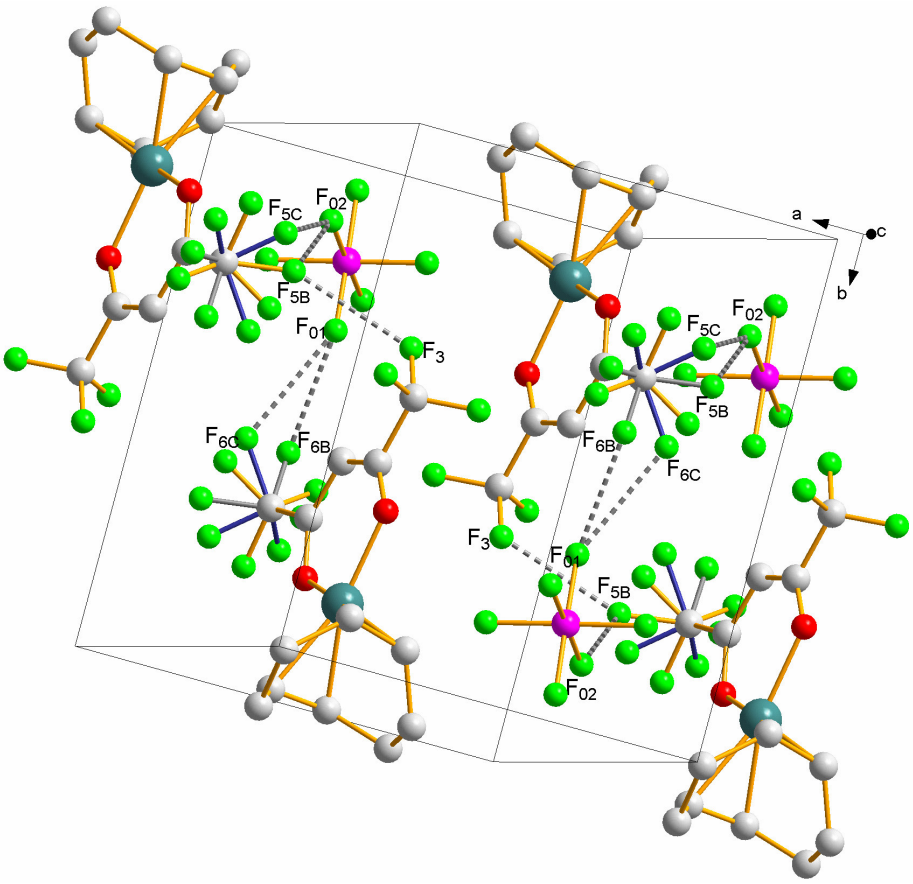

Figure 4.34 Partial unit cell of [Pd(cod)(hfacac)]PF_6 (6) showing the F···F intramolecular bonding indicated by a dashed grey bond. Palladium (cyan), oxygen (red), carbon (grey), fluorine (green) and phosphorus (pink). Hydrogens have been omitted for clarity.

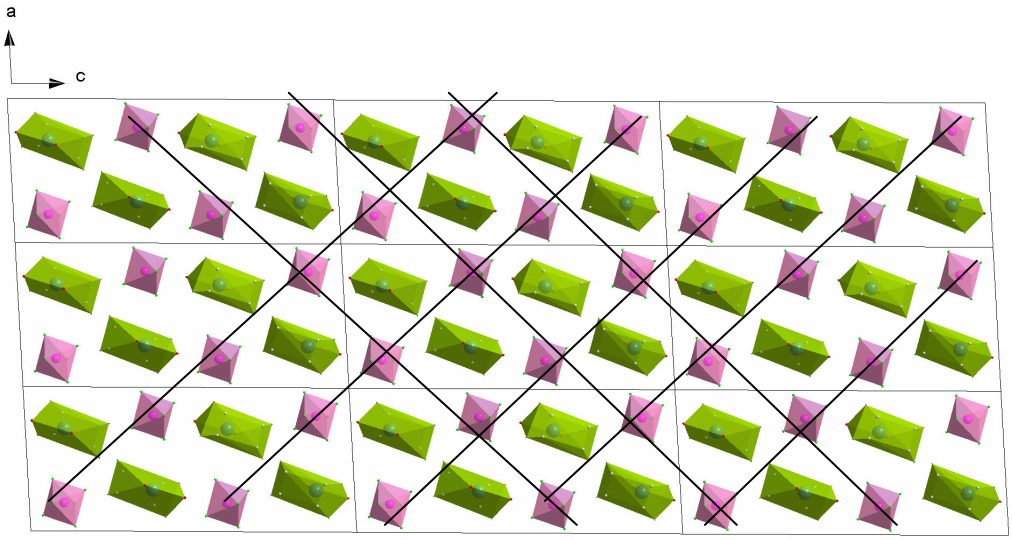

Figure 4.35 Diamond illustration of the packing of a 3x3 super cell viewed along the *b*-axis of [Pd(cod)(hfacac)]PF_6 (6) where the olive polyhedra is the $[Pd(cod)(hfacac)]^+$ (6a) complex and the rose polyhedra is the PF_6^- (6b) complex.

The **6b** complex is packed along diagonal parallel lines as indicated in Figure 4.35 by the black lines superimposed over the 3x3 super cell, which is depicted as rose polyhedra and the **6a** complex as olive polyhedra. The distance between the parallel lines sloping to the right is 9.724(1) Å and the distance between the lines sloping to the left is 9.121(1) Å. At the intersection points of these parallel lines one finds a **6b** complex, this encloses a single **6a** complex.

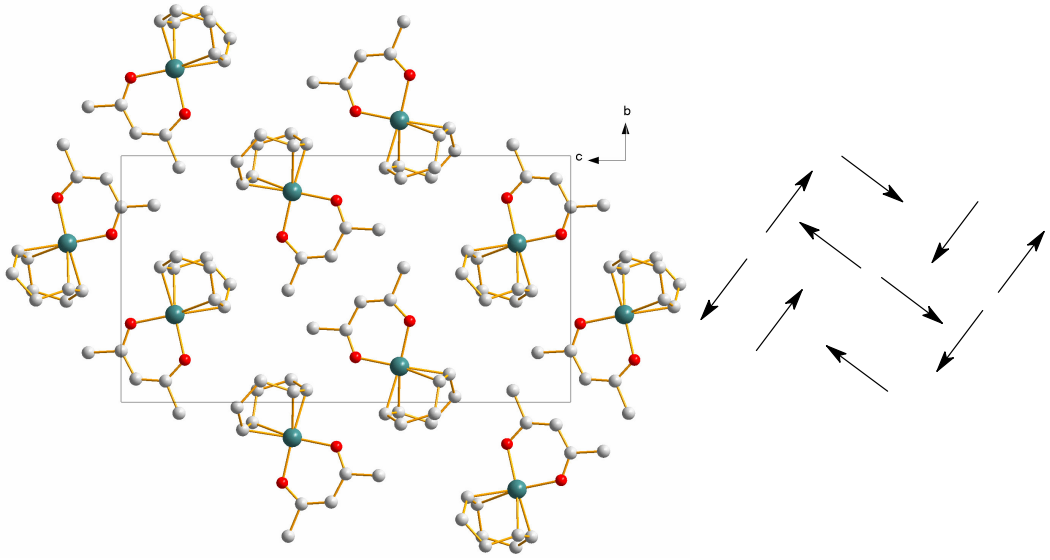

Figure 4.36 Packing of [Pd(cod)(hfacac)]PF_6 (6a) viewed along the *a*-axis with the packing motif incorporated to the right of the figure. Hydrogens, Fluorines and counter ions have been omitted for clarity.

The packing motif in Figure 4.36 is defined as the head of the arrow corresponding to the 1,5-cyclo-octadiene moiety and the tail of the arrow corresponding to the hexafluoroacetylacetonato moiety. In looking at Figure 4.36 we observe a tail-to-tail packing this unit is then intersected by another tail-to-tail unit in the mid-point of the **6a** complex. This packing motif has similarities to the clustered head-to-tail motif that we see for the **4a** complex; however it is not as tightly packed.

4.4 Discussion

In overview, the compounds have been varied by increasing the electron withdrawing nature of the β-diketonoate ligand (hfacac > tfacac > thtfac >> acac) whilst keeping the metal centre constant. Two types of counter ions were investigated namely the hexafluorophosphate (PF_6^-) and the tetrafluoroborate (BF_4^-) counter ions. The oxidation state of the metal centre remains constant at +2 and the co-ordination geometry square planar (Figure 4.2) with the coordination of a cyclo-octadienato moiety and a β-diketonato moiety. Table 4.15 gives a synopsis of the cell dimensions of the crystal structures described in this chapter.

Table 4.15 Cell dimension overview for palladium crystals obtained.

	[Pd(cod)(acac)]		[Pd(cod)(thtfac)]		[Pd(cod)(tfacac)]	[Pd(cod)(hfacac)]
	PF_6 (**1**)	BF_4 (**2**)	PF_6 (**3**)	BF_4 (**4**)	PF_6 (**5**)	PF_6 (**6**)
Crystal system	Monoclinic	Orthorhombic	Monoclinic	Monoclinic	Triclinic	Monoclinic
Space group	$P2_1/n$	$Pca2_1$	$P2_1/n$	$P2_1/n$	$P\bar{1}$	$P2_1/c$
Cell dimensions						
a (Å)	9.3166(6)	26.2908(11)	9.9691(2)	10.0528(3)	8.1027(8)	8.5885(2)
b (Å)	15.4676(8)	7.1684(3)	17.0294(3)	16.6333(6)	14.3018(14)	10.6304(2)
c (Å)	11.4844(7)	7.7782(3)	11.4750(2)	10.9501(4)	15.4557(14)	19.4093(4)
α (°)	90	90	90	90	75.286(5)	90
β (°)	106.171(2)	90	101.327(2)	102.534(1)	89.963(5)	93.415(1)
γ (°)	90	90	90	90	73.556(5)	90
Z	4	4	4	4	4	4

It is of interest to note that the general trend of the crystals is toward monoclinic space groups. The exceptions to this are the [Pd(cod)(acac)]BF_4 (**2**) complex being orthorhombic and the [Pd(cod)(tfacac)]PF_6 (**5**) complex being triclinic, however as previously discussed (§ 4.3.3) the crystal structure can be solved in monoclinc *C*2/*c* space group. All the cationic species (i.e. **1a**-**6a**) are isoelectronic though only compounds **1**, **3** and **4** were found to be isostructural. An isostructural crystal is one

where the crystals have the same structure but not the same cell dimensions or chemical composition.

The distortion from square planar as measured by the intersection of the planes defined by the mid-point of the alkene carbons of the cyclo-octadiene ring with the oxygens of the β-diketones and the palladium metal centre with the β-diketone back-bone is as follows : complex **5** >> **3** > **1** >> **6** being 5.6(3)°, 3.63(3)°, 3.42(5)° and 2.62(4)° respectively. In this series the counter ion (PF_6) of the compounds was kept constant. The increase in distortion found in complex **3** is as a result of the F···π interactions observed in Figure 4.15. The F···F interactions observed in complex **6** (Figure 4.34) results in a decrease in the distortion from the planar geometry. The largest distortion observed is that of complex **5** with both cationic **5a1** and **5a2** complexes showing similar distortion values (5.6(3)° and 5.7(3)°) this increase is believed to be a result of the systematic error observed. When analyzing the BF_4 counter ion complexes (**2** and **4**) we find that the distortion from planar, 3.48(5)° and 2.75(4)°, is not significantly affected for complexes **1** and **2**. When looking at complexes **3** and **4** it can be seen that the hydrogen interactions between the cationic and anionic species do infact influence the square planar distortion, complex **3** was found to have minimal interactions with the PF_6 counter ion (Figure 4.14) where as complex **4** had significantly more interactions (Figure 4.17 and 4.18) with the BF_4 counter ion. The overall series was found to be **5** >> **3** > **1** ≈ 2 > 4 > **6** which gives an indication as to the level of interaction of the β-diketonato ligand within the cationic species with the fluorido ligands of the anionic species within the compounds.

When reviewing (Table 4.16) the palladium oxygen bond distances a small increase in bond lengths (0.024 Å) was observed as the electron withdrawing groups are increased and a similar reduction in the O-Pd-O bite angle (1.34°) is seen. There is a linear relationship between the bite angle and the acid dissociation constants (pK_a).

Table 4.16 Selected Geometric parameters (Å,°) for palladium metal complexes

	[Pd(cod)(acac)]		[Pd(cod)(thtfac)]		[Pd(cod)(tfacac)]	[Pd(cod)(hfacac)]
	PF_6 (**1**)	BF_4 (**2**)	PF_6 (**3**)	BF_4 (**4**)	PF_6 (**5**)	PF_6 (**6**)
$Pd-O_1$	2.003(3)	2.001(3)	2.007(11)	2.003(2)	2.007(11)	2.027(2)
$Pd-O_2$	2.001(3)	1.998(2)	2.012(2)	2.005(2)	2.018(11)	2.026(2)
$Pd-C_1$	2.195(5)	2.202(3)	2.193(2)	2.197(3)	2.171(14)	2.191(3)
$Pd-C_2$	2.181(4)	2.183(4)	2.181(2)	2.176(3)	2.208(15)	2.166(3)
$Pd-C_5$	2.197(4)	2.205(3)	2.184(2)	2.195(3)	2.180(16)	2.190(3)
$Pd-C_6$	2.189(4)	2.181(4)	2.174(2)	2.175(3)	2.191(17)	2.171(3)
C_1-C_2	1.381(7)	1.386(7)	1.383(3)	1.382(4)	1.37(2)	1.387(4)
C_5-C_6	1.380(6)	1.394(7)	1.383(3)	1.385(4)	1.37(3)	1.383(4)
O_1-Pd-O_2	94.4(1)	94.5(1)	93.34(6)	93.27(8)	93.2(5)	93.06(8)
C_1-Pd-C_2	36.8(2)	36.8(2)	36.88(9)	36.9(1)	36.4(6)	37.13(10)
C_5-Pd-C_6	36.7(2)	37.1(2)	36.99(8)	36.9(1)	36.6(7)	36.98(10)
C_1-Pd-C_6	81.6(2)	81.5(2)	82.20(9)	82.3(1)	82.3(6)	82.02(10)
C_2-Pd-C_5	81.7(2)	81.4(1)	81.98(9)	81.9(1)	82.6(6)	81.99(10)
χ^a	86.0(3)	85.9(1)	86.6(1)	86.6(1)	86.8(6)	86.5(1)
ψ^b	81.9(3)	80.2(2)	79.2(1)	82.0(2)	86.9(9)	83.2(1)

a χ: $C_1MC_2 \cap C_5MC_6$ b ψ: $C_2C_3C_4C_5 \cap C_1C_8C_7C_6$ see Figure 1.2

In Figure 4.37 the pK_a values of the β-diketonato ligands were plotted against the O-Pd-O bite angle. It was observed that there was an increase in bite angle with an increasing electron withdrawing effect from the β-diketonato ligand. Additionally there is also a marginal effect when altering the counter ion from BF_4^- to PF_6^-.

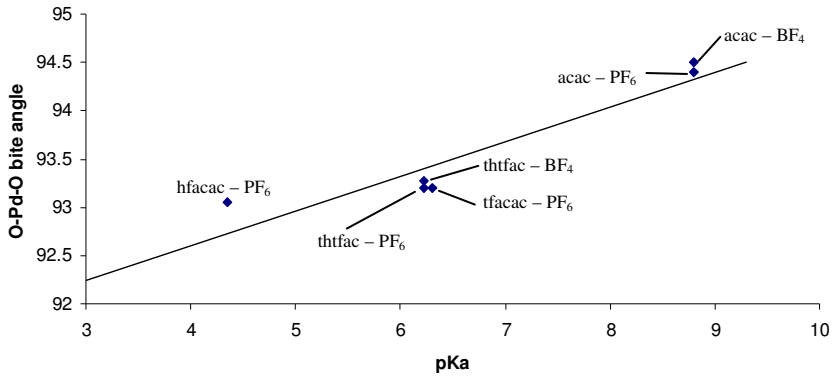

Figure 4.37 Graph of pK_a *vs.* O-Pd-O bite angle for the [Pd(cod)(LL')]A where LL' = acac, tfacac, hfacac, thtfac and A = BF_4^-, PF_6^- complexes.

The alkene (C=C) bond lengths in the 1,5-cyclo-octadiene (Table 4.16) were not affected by the increased electron withdrawing groups on the trans ligand and remain generally constant with a mean value of 1.38(1) Å. Upon looking at the χ and ψ angles in Figure 4.38, which is sorted by descending χ values, we find that as the χ angle decreases an opening and closing of 7.7° of the ψ was observed.

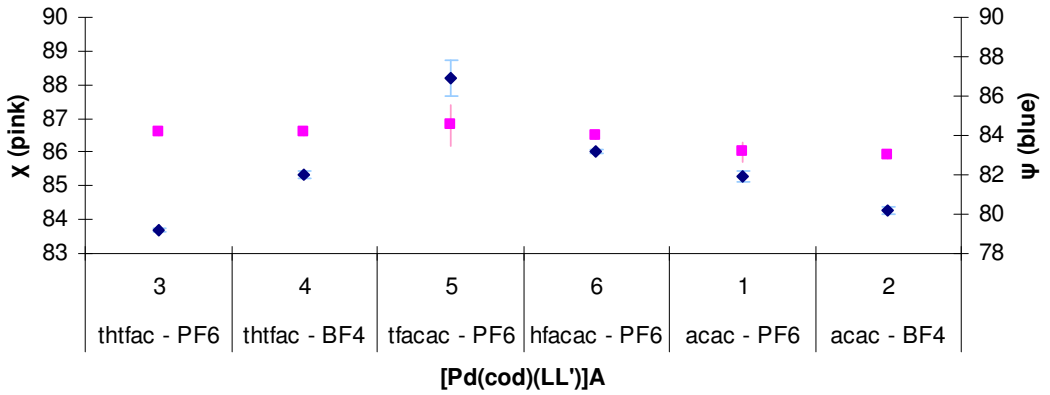

Figure 4.38 Graph of Palladium crystal complexes *vs.* χ (pink squares) and ψ (blue diamonds) angles arranged in descending order of χ angle (see Chapter 1 Figure 1.2 for definition of χ and ψ angles).

There are three packing modes that have been observed for the compounds that of the clustered head-to-tail structure observed for complexes **1a** (Figure 4.11), **3a** (Figure 4.21) and **4a** (Figure 4.22), head-to-tail complexes **2a** (Figure 4.12) and **5a1, 5a2** (Figure 4.28) and a tail-to-tail complex **6** (Figure 4.36). The differences in the packing modes are attributed to the level of interactions between the cationic and the anionic species within the compounds.

The next chapter describes the altering of the metal centre to platinum and comparing the results obtained in this chapter with the results obtained for the platinum compounds.

Chapter 5
Crystallographic Study of β-Diketonato Type Complexes of Platinum(II)

5.1 Introduction

Platinum has proven to be an important metal in both medicine and catalysis (as has previously been discussed in Chapter 2), it was therefore included in this study. Furthermore, being in the nickel triad, it provides an excellent model to further elaborate packing and co-ordination, and to be compared with its fourth row carry over palladium, as discussed in Chapter 4. A search of the Cambridge Structural Database (CSD) however only produced a single hit, that of $[Pt(cod)(acac)]BF_4$[1]. It was thus decided to focus our efforts in gaining a better understanding of the co-ordination of both 1,5-cyclo-octadiene and the β-diketonate ligands to the platinum(II) metal centre.

The complexes that were prepared as described in § 3.5.2 were analyzed by single crystal X-ray crystallography and are summarized in Table 5.1. A diagram indicating the numbering scheme of each compound is presented, along with selected bond lengths and angles, hydrogen bonding interactions and additional interactions if applicable. A discussion highlighting some of the important aspects of each particular structure is presented thereafter.

Additional correlations with other structures and theoretical calculated structures are done in Chapter 6 whilst complete list of the crystal structures presented in this chapter are given in the supplementary data.

[1] (a) Venkatasubramanian K., *Indian J. Phys.*., **A56**, 201, (1982)
(b) Venkatasubramanian K., *Proc. Indian Acad. Sci., Chem. Sci.*, **93**, 1237, (1984)

5.2 Experimental

Data collections for $[Pt(cod)(acac)]PF_6$ and $[Pt(cod)(dbm)]BF_4$ were obtained on a a Bruker Apex II 4K CCD diffractometer. The data for $[Pt(cod)(acac)]BF_4$ and $[Pt(cod)(thtfac)]BF_4$ were collected on an Oxford Diffraction Xcalibur 3 Crysalis CCD system[2]. Both systems were equipped with a graphite-monochromated Mo Kα radiation, for the Bruker system all the reflections were merged and integrated with SAINT-PLUS[3] and corrected for Lorentz, polarization and absorption effects with SADABS[4], while Crysalis RED[5] was used for the Oxford system.

Structures were solved by direct and conventional Patterson methods using the SHELX-97[6] as part of the WinGX[7] package, and anisotropic refinement was performed on all non-hydrogen atoms by a full-matrix least-squares method. The positions of the hydrogen atoms were calculated using a riding model to the adjacent carbon, unless otherwise stipulated. Hydrogen interactions were calculated using the PLATON[8,9,10] & PARST[11] programs. Molecular graphics were obtained using DIAMOND[12], while overlay graphics were obtained using HyperChem 7.5[13].

[2] Crysalis CCD. Oxford Diffraction Ltd., Abingdon, Oxfordshire, U.K., (2005)
[3] Bruker SAINT-PLUS (including XPREP), Version 7.12, Bruker AXS Inc., Madison, WI., (2004)
[4] Bruker SADABS (Version 2004/1), Bruker AXS Inc., Madison, WI., (1998)
[5] Crysalis RED Oxford Diffraction Ltd., Abingdon, Oxfordshire, U.K., (2005)
[6] Sheldrick G.M., *Acta Cryst.*, **A64**, 112, (2008)
[7] Farrugia L.J., *Appl. Cryst.*, **32**, 837, (1999)
[8] Spek A.L., PLATON A multipurpose crystallographic tool, Utrecht University, Utrecht, Netherlands, (2005)
[9] Speck A.L., *J. Appl. Cryst.*, **36**, 7, (2003)
[10] Speck A.L., *Acta Cryst*, **D65**, 148, (2009)
[11] Nardelli M., *J. Appl. Cryst.*, **28**, 659, (1995)
[12] Brandenburg K., Brendt M., DIAMOND, Release 2.1e. Crystal Impact GbR, Potfach 1251, D53002 Bonn, Germany., (2001)
[13] HyperChem™ Release 7.52, Windows Molecular Modeling System, HyperCube Inc., (2002)

Table 5.1 Crystallographic data and refinement parameters where A = PF_6^- or BF_4^-

Crystal Data	[Pt(cod)(acac)]A BF_4 (**7**)	 PF_6 (**8**)	[Pt(cod)(dbm)]A BF_4 (**9**)	[Pt(cod)(thtfac)]A BF_4 (**10**)
Empirical formula	C_{13} H_{19} B F_4 O_2 Pt	C_{13} H_{19} F_6 O_2 P Pt	C_{23} H_{23} O_2 P F_4 Pt	C_{16} H_{16} B F_7 O_2 Pt S
Formula weight	489.18	547.34		611.25
Temperature (K)	100(2)	100(2)		100(2)
Wavelength (Å)	0.71073	0.7103		0.7103
Crystal system	Orthorhombic	Monoclinic	Triclinic	Monoclinic
Space group	*Pca*2_1	*P*2_1/*n*	*P*1	*P*2_1/*n*
Unit cell dimensions				
a (Å)	26.3980(4)	9.3082(3)	10.4558(21)	14.4456(2)
b (Å)	7.19670(10)	15.4486(5)	10.6170(21)	15.1804(1)
c (Å)	7.71820(10)	11.4733(3)	10.894(22)	18.1656(2)
α (°)	90	90	89.28(3)	90
β (°)	90	105.944(1)	89.71(3)	107.281(1)
γ (°)	90	90	61.93(3)	90
Volume ($Å^3$)	1466.29(4)	1586.38(8)		3803.71(7)
Z	4	4	2	8
Density (calculated) ($Mg.m^{-3}$)	2.216	2.292		2.135
Absorption coefficient (mm^{-1})	9.613	9.013		7.563
F(000)	928	1040		2320
Crystal size (mm^3)	0.26 x 0.18 x 0.03	0.39 x 0.22 x 0.12		0.51 x 0.26 x 0.13
Theta range for data collection (°)	2.83 to 27.98	2.27 to 28.38		2.14 to 30.00
Index ranges	-34<=h<=34, -9<=k<=7, -10<=l<=8	-12<=h<=10, -20<=k<=18, -15<=l<=15		-20<=h<=20, -21<=k<=12, -25<=l<=25
Reflections collected	11111	15055		34343
Independent reflections	2884 [R(int) = 0.0233]	3968 [R(int) = 0.0479]		10963 [R(int) = 0.0354]
Completeness to θ (°; %)	27.98, 99.4	28.38, 99.5		30.00, 98.8
Max. and min. transmission	0.7613 and 0.1889	0.4110 and 0.1269		0.4397 and 0.1133
Refinement method	Full-matrix least-squares on F^2	Full-matrix least-squares on F^2		Full-matrix least-squares on F^2
Data / restraints / parameters	2884 / 1 / 186	3968 / 0 / 210		10963 / 0 / 505
Goodness-of-fit on F^2	1.054	1.149		0.977
Final R indices [I>2σ(I)]	R_1 = 0.0175, wR_2 = 0.0439	R_1 = 0.0302, wR_2 = 0.0719		R_1 = 0.0280, wR_2 = 0.0705
R indices (all data)	R_1 = 0.0195, wR_2 = 0.0445	R_1 = 0.0442, wR_2 = 0.1096		R_1 = 0.0446, wR_2 = 0.0749
Largest diff. peak and hole ($e.Å^{-3}$)	1.468 and -0.721	1.117 and -1.750		2.226 and -1.891

5.3 X-Ray Structures of Platinum Complexes

5.3.1 Crystal structures of [Pt(cod)(acac)]BF_4[1] and [Pt(cod)(acac)]PF_6

The compounds, [Pt(cod)(acac)]BF_4 (**7**), crystallized in the orthorhombic space group P*ca2*$_1$, with a cationic [Pt(cod)(acac)]$^+$ (**7a**) species and an anionic BF_4^- (**7b**) species in the asymmetric unit, whilst [Pt(cod)(acac)]PF_6 (**8**) crystallized in the monoclinic space group $P2_1/n$, with a cationic [Pt(cod)(acac)]$^+$ (**8a**) species and an anionic PF_6^- (**8b**) species in the asymmetric unit. The numbering scheme is presented in Figure 5.1, while atomic co-ordinates, bond angles and distances, anisotropic displacement parameters and hydrogen co-ordinates are reported in Appendix B.11 and B.12. General crystallographic data and refinement parameters are reported in Table 5.1, while significant bond angles and distances are reported in Table 5.2.

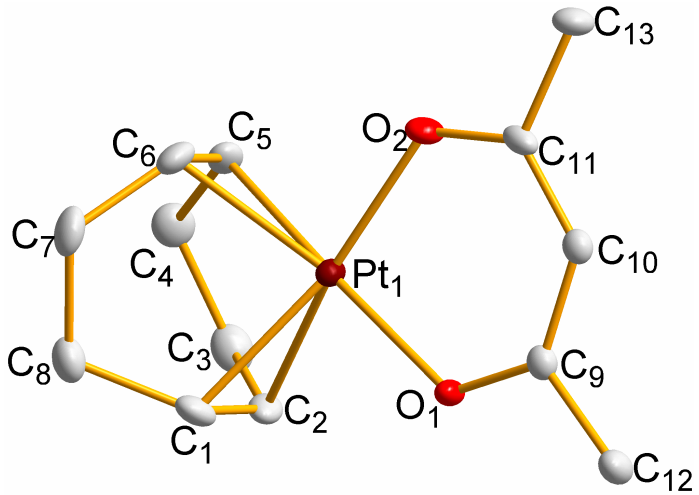

Figure 5.1 Diamond illustration of [Pt(cod)(acac)]BF_4 at 100 K showing the numbering scheme and displacement ellipsoids (50 %) of the complex. Hydrogen atoms and counter ion omitted for clarity.

Table 5.2 Selected bond distances and angles for [Pt(cod)(acac)]A (where A = BF_4, PF_6)

Bond Distance (Å)	Counter ion		Bond Angles (°)	Counter ion	
	BF_4 (**7**)	PF_6 (**8**)		BF_4 (**7**)	PF_6 (**8**)
Pt-O_1	2.015(3)	2.010(5)	O_1-Pt-O_2	93.5(1)	93.3(3)
Pt-O_2	2.013(3)	2.016(5)	C_1-Pt-C_2	37.6(2)	37.3(3)
Pt-C_1	2.160(3)	2.164(6)	C_5-Pt-C_6	38.2(2)	38.1(3)
Pt-C_2	2.153(4)	2.161(7)	C_1-Pt-C_6	82.2(2)	82.0(3)
Pt-C_5	2.164(3)	2.150(7)	C_2-Pt-C_5	82.0(2)	81.9(3)
Pt-C_6	2.147(4)	2.161(7)	χ^a	86.9(2)	86.8(4)
C_1-C_2	1.388(8)	1.382(10)	ψ^b	79.1(2)	78.9(5)
C_5-C_6	1.411(8)	1.406(11)			

a χ: $C_1MC_2 \cap C_5MC_6$ b ψ: $C_2C_3C_4C_5 \cap C_1C_8C_7C_6$ see Figure 1.2

Figure 5.1 depicts the cationic species (**7a**) and illustrates the atom numbering, this numbering holds for the **8a** cationic species also. The geometry around the metal centre is square planar (Chapter 4 Figure 4.2) with 1,5-cyclo-octadiene and acetylacetonato moieties bonded to the platinum. The oxidation state to the platinum metal centre is +2, thus resulting in a cationic charged species which is balanced by an anionic counter ion either hexafluorophosphate (PF_6^-) or tetrafluoroborate (BF_4^-). The average distances for the **7a** complex for Pt-O, Pt-C and C=C co-ordination were found to be 2.156(4) Å, 2.014(3) Å and 1.340(8) Å respectively. The **7b** and **8b** complexes were found to be well behaved. The shortest Pt-Pt distance found in the **7a** complex is 7.1967(2) Å indicating no metal interactions. Compound **7** was found to be isomorphous and isoelectronic to [Pd(cod)(acac)]BF_4 (**2**). Compound **8** is isomorphous and isoelectronic to [Pd(cod)(acac)]PF_6 (**1**), however **7** and **8** are not isomorphous.

The average distances for the **8a** complex for Pt-O, Pt-C and C=C are 2.013(5) Å, 2.159(7) Å and 1.394(11) Å respectively. There is a significant difference in the bond lengths *c.a.* 0.14 Å observed for the **7a** and **8a** species for Pt-O and Pt-C bond lengths which are inversely proportional to each other, as a result the cavity formed by the oxygens of the acetylacetonato ligand and the methine carbons of the cyclo-octadiene ring remains constant for both compounds. There is only a small difference *c.a.* 0.05 Å in the C=C bond distances, the bond angles remain similar.

The hydrogen bonding of complex **7** is graphically presented in Figure 5.2 and 5.3 with Table 5.3 listing the bond distances and angles.

Table 5.3 Hydrogen bond distances and angles for [Pt(cod)(acac)]BF_4 (7) [Å and °]

D-H...A	d(D-H)	d(H...A)	d(D...A)	<(DHA)
C_2-H_2...F_1	1.00	2.54	3.255(6)	128.1
C_2-H_2...F_3	1.00	2.47	3.145(6)	123.9
C_3-H_{3B}...$F_4^{\#1}$	0.99	2.39	3.320(7)	156.5
C_7-H_{7A}...$F_2^{\#2}$	0.99	2.40	3.266(7)	146.2
C_6-H_6...$F_4^{\#3}$	1.00	2.31	3.192(6)	146.7
C_{13}-H_{13C}...$F_1^{\#3}$	0.98	2.65	3.609(6)	166.0
C_7-H_{7B}...$F_1^{\#4}$	0.99	2.55	3.360(7)	138.7
C_{12}-H_{12B}...$F_4^{\#5}$	0.98	2.48	3.445(5)	166.9
C_{10}-H_{10}...$F_3^{\#5}$	0.95	2.44	3.328(5)	156.5
C_{13}-H_{13B}...$F_3^{\#5}$	0.98	2.48	3.368(6)	151.2

Symmetry transformations used to generate equivalent atoms:
#1 x,y-1,z #2 -x+1,-y+1,z-1/2 #3 x,y-1,z-1
#4 x,y,z-1 #5 -x+3/2,y-1,z-1/2

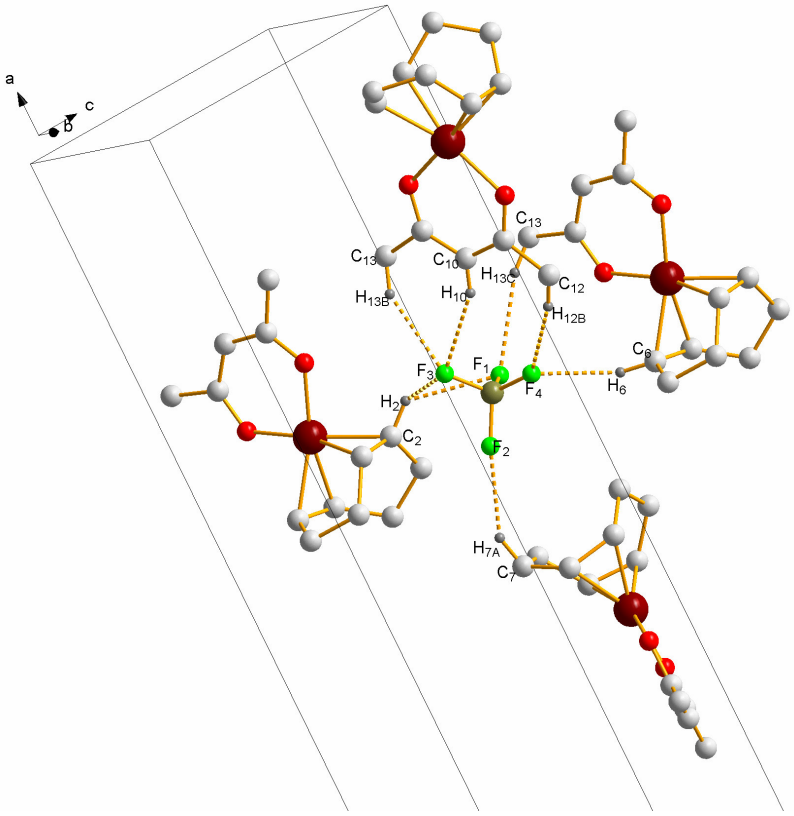

Figure 5.2 Partial unit cell of [Pt(cod)(acac)]BF_4 showing intermolecular hydrogen bonding interactions indicated by a dashed bond. Only selected hydrogen atoms are included. Platinum (dark red), carbon (grey), oxygen (red), boron (olive green) and fluorine (green).

No intramolecular interactions of the type **7a**···**7a** were observed for [Pt(cod)(acac)]BF_4 (**7**) which was expected due to the isomorphism. Several hydrogen interactions were observed (Figure 5.2) of the type **7a**···**7b** and are listed in Table 5.3. Again there are two types of interactions the first between the acetylacetonato hydrogens bonded to the carbons (C_{10}, C_{12} and C_{13}) and the fluorido (F_1, F_3 and F_4) ligands of the **7b** complex. The second type of interaction is between

cyclo-octadiene and the fluorido ligands of **7b**, this interaction type can be further sub-divided into two parts. Firstly the interaction between the methine hydrogens bonded to the carbons (C_2 and C_6) of the cyclo-octadine ring of the **7a** species and the fluorido (F_1, F_3 and F_4) ligands where H_2 is again a bifurcated hydrogen, and secondly between the methylene hydrogens bonded to the carbons (C_3 and C_7) and the fluorido (F_4 and F_1) ligands (Figure 5.3) of the **7b** species.

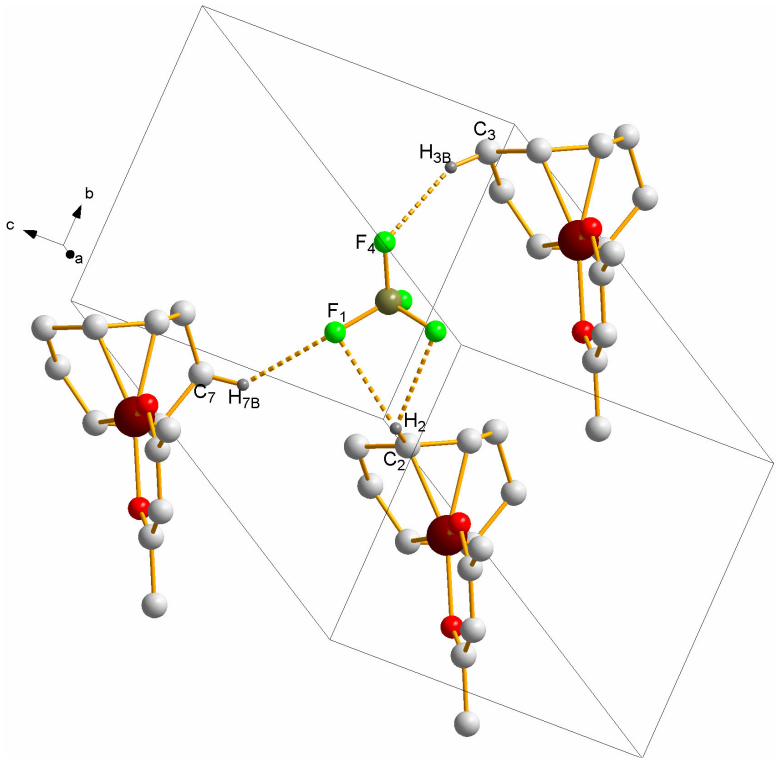

Figure 5.3 Partial unit cell of [Pt(cod)(acac)]BF_4 showing intermolecular hydrogen bonding interactions indicated by a dashed bond. Only selected hydrogen atoms are included. Platinum (dark red), carbon (grey), oxygen (red), boron (olive green) and fluorine (green).

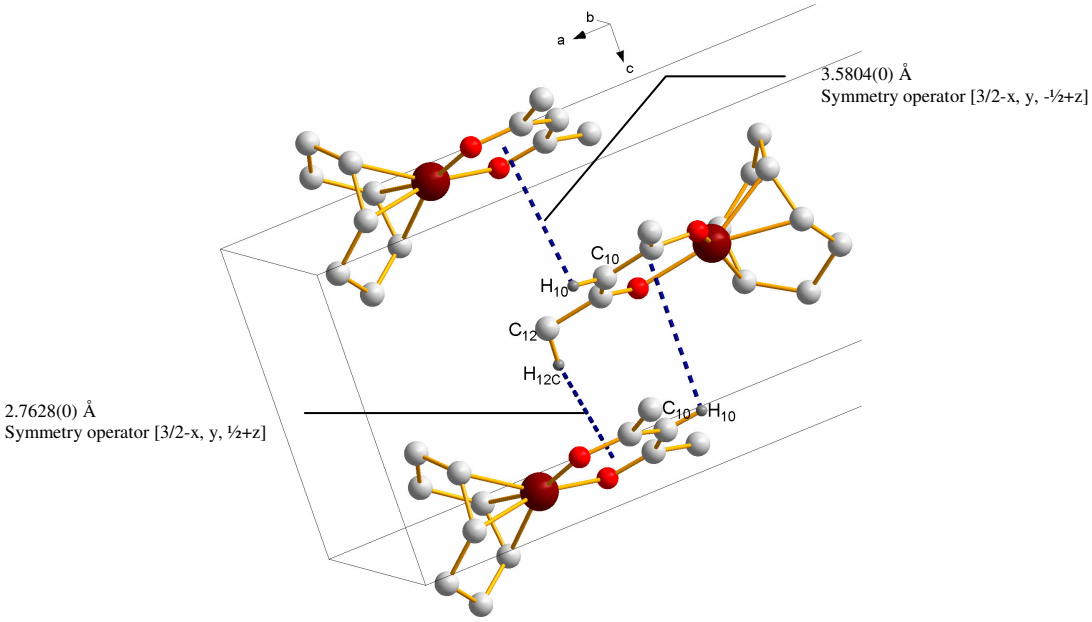

Figure 5.4 Partial unit cell of [Pt(cod)(acac)]BF_4 showing H···metal chelate ring intermolecular interactions indicated by a dashed dark blue bond. Only selected hydrogen atoms are included. Tetrafluoroborate counter ion omitted for clarity. Platinum (dark red), carbon (grey), oxygen (red).

In Figure 5.4 H···metal chelate ring interactions are observed between the acetylacetonato moieties with distances of 2.7628 Å and 3.5804 Å for C_{12} and C_{10} respectively. This interaction results in the observed staggered head-to-head packing (Figure 5.7) which can be clearly seen in the right hand side of the figure.

The hydrogen bonding of complex **8** is graphically presented in Figure 5.5 and 5.6 with Table 5.4 listing the bond distances and angles.

Table 5.4 Hydrogen bond distances and angles for [Pt(cod)(acac)]PF_6 (8) [Å and °]

D-H...A	d(D-H)	d(H...A)	d(D...A)	<(DHA)
C_2-H_2...F_1	1.00	2.35	3.138(9)	135.2
C_1-H_1...$F_3^{\#1}$	1.00	2.45	3.230(8)	134.6
C_7-H_{7A}...$F_3^{\#2}$	0.99	2.52	3.474(10)	160.8
C_5-H_5...$F_4^{\#3}$	1.00	2.53	3.375(9)	142.2
C_8-H_{8B}...$F_6^{\#4}$	0.99	2.54	3.364(10)	140.9
C_{10}-H_{10}...$F_4^{\#5}$	0.95	2.36	3.263(9)	158.3
C_{13}-H_{13B}...$F_4^{\#5}$	0.98	2.53	3.422(10)	151.8

Symmetry transformations used to generate equivalent atoms:
#1 x+1/2,-y+1/2,z-1/2 #2 x+1,y,z #3 x+1/2,-y+1/2,z+1/2
#4 -x+1/2,y-1/2,-z+3/2 #5 -x-1/2,y-1/2,-z+3/2

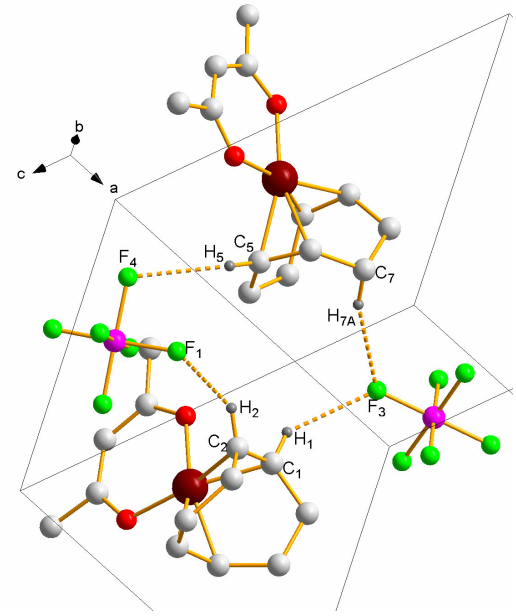

Figure 5.5 Partial unit cell of [Pt(cod)(acac)]PF_6 showing intermolecular hydrogen bonding interactions indicated by a dashed bond. Only selected hydrogen atoms are included. Platinum (dark red), carbon (grey), oxygen (red), phosphorus (pink) and fluorine (green).

With the **7a** complex one finds only interactions of the type **8a**···**8b**, which as we have previously established is subdivided into to parts namely that of the interactions with the acetylacetonato ligand of **8a** with the fluorido ligands of **8b** and the cyclo-octadiene ring of **8a** again with the fluorido ligands of **8b**. In Figure 5.5 we observe the second type of these interactions where the methine hydrogens bonded to the carbons (C_1 and C_2) and the methylene hydrogens bonded to the carbons (C_5 and C_7) of the cyclo-octadine ring interact with the fluorido (F_1, F_3 and F_4) ligands of adjacent counter ions.

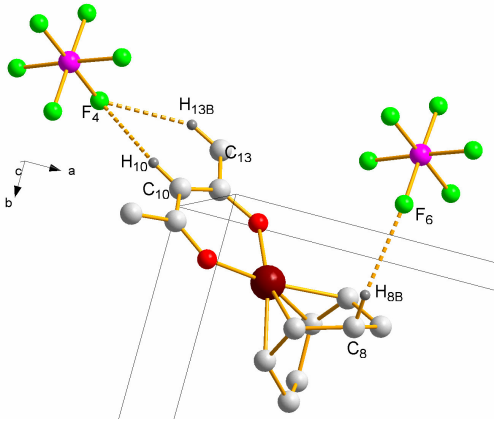

Figure 5.6 Partial unit cell of [Pt(cod)(acac)]PF_6 showing intermolecular hydrogen bonding interactions indicated by a dashed bond. Only selected hydrogen atoms are included. Platinum (dark red), carbon (grey), oxygen (red), phosphorus (pink) and fluorine (green).

The last of these interactions can be seen in Figure 5.6 where the methylene hydrogens bonded to the carbon (C_8) interacts with F_6 ligand. The first type, that of the acetylacetonato (C_{10} and C_{13}) ligand interacting with the fluorido (F_4) ligand of the **8b** complex is also found in Figure 5.6. The distances and angles for the hydrogen interactions shown in the above figures are listed in Table 5.4.

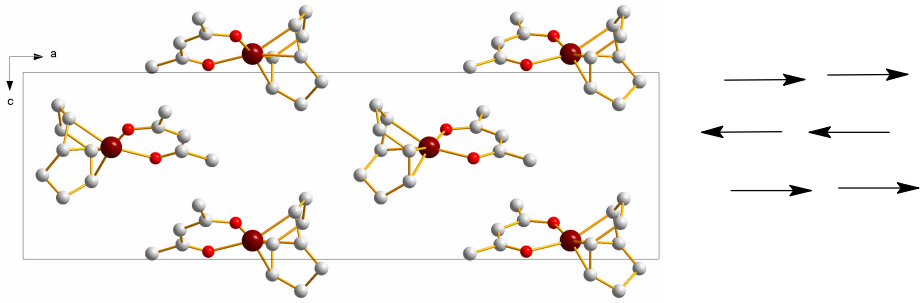

Figure 5.7 Packing of [Pt(cod)(acac)]BF_4 viewed along the *b*-axis with the packing motif incorporated to the right of the figure. Platinum (dark red), carbon (grey), oxygen (red). Hydrogens and BF_4 have been omitted for clarity.

The packing motif in Figure 5.7 is defined as the head of the arrow corresponding to the 1,5-cyclo-octadiene moiety and the tail of the arrow corresponding to the acetylacetonato moiety. The packing found for [Pt(cod)(acac)]BF_4 (**7a**) is head-to-tail (Figure 5.7). This is the same packing mode for [Pd(cod)(acac)]BF_4 (**2a**), which supports the claim of isomorphism.

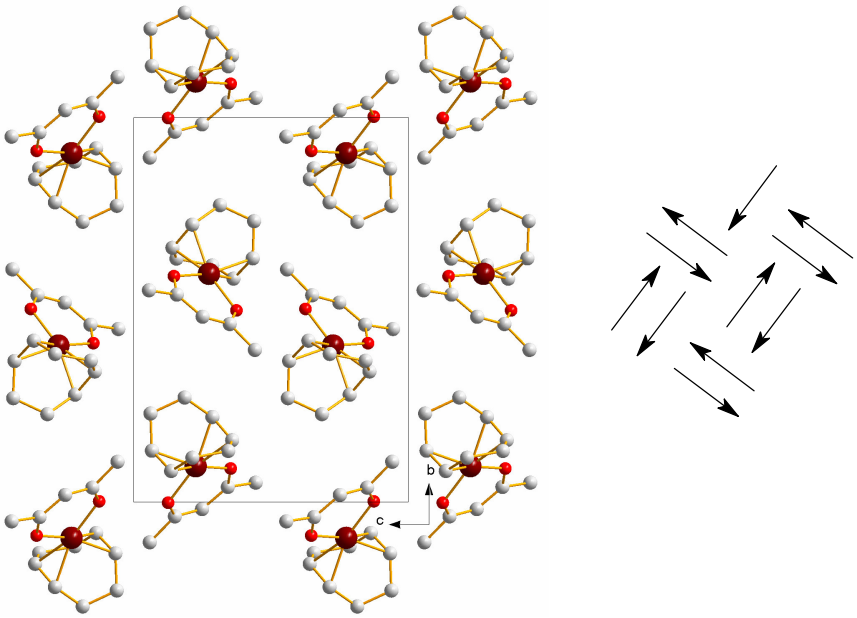

Figure 5.8 Packing of [Pt(cod)(acac)]PF_6 viewed along the *a*-axis with the packing motif incorporated to the right of the figure. Platinum (dark red), carbon (grey), oxygen (red). Hydrogens and PF_6 have been omitted for clarity.

The packing motif in Figure 5.8 is defined as the head of the arrow corresponding to the 1,5-cyclo-octadiene moiety and the tail of the arrow corresponding to the acetylacetonato moiety. With the isomorphism between complexes [Pd(cod)(acac)]PF_6 (**2a**) and [Pt(cod)(acac)]PF_6 (**8a**), identical packing modes are expected, this is found to be the case. In Figure 5.8 we see the now familiar clustered head-to-tail motif.

5.3.2 Crystal structure of [Pt(cod)(dbm)]BF_4

The compound, [Pt(cod)(dbm)]BF_4 (**9**), was severely disordered and twinned with eight merohedral and non-merohedral components. The structure was refined in the triclinic system with a space group of *P*1. General crystallographic data is reported in Table 5.1.

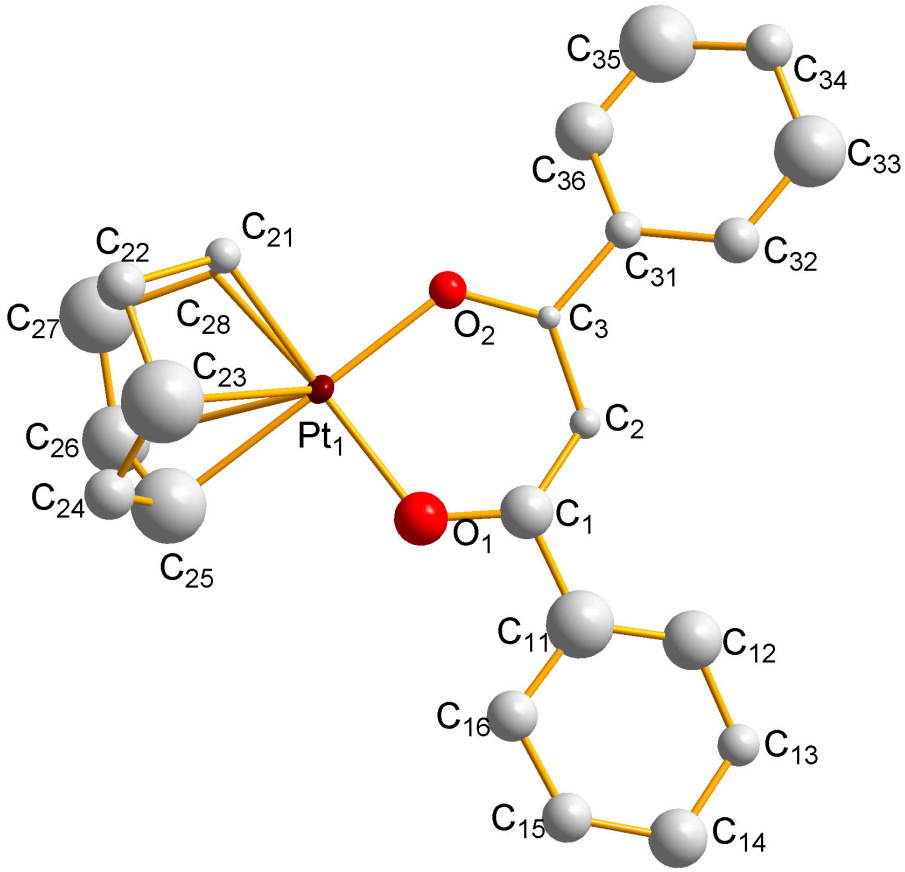

Figure 5.9 Diamond illustration of [Pt(cod)(dbm)]BF_4 showing displacement ellipsoids (50% probability). Disordered parts belonging together are colored with grey and yellow bonds. Hydrogen atoms omitted for clarity.

The above Figure 5.9 is a representation of the preliminary refined structure of [Pt(cod)(dbm)]BF_4. The tetraflouroborate counter ion is also disordered but is not shown in Figure 5.9. The *cis,cis*-1,5-cyclo-octadiene ring is abnormally co-ordinated to the platinum metal centre in that it is co-ordinated through two π bonds and a third σ type bond. The structure is still found to be in the square planar geometry with the platinum metal centre being in the +2 oxidation state.

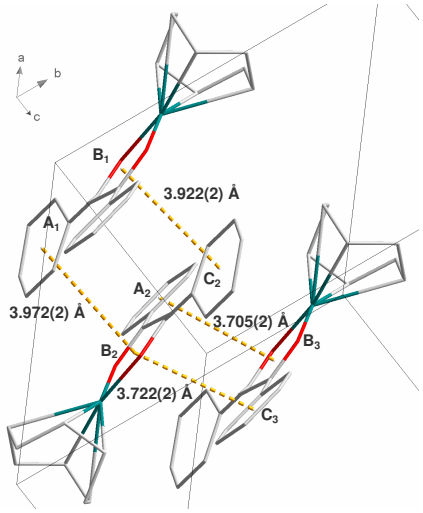

Figure 5.10 Diamond illustration indicating π – stacking for [Pt(cod)(dbm)]BF_4, hydrogen atoms and counter ions have been omitted for clarity.

A staggered head-to-tail stacking was observed with the shortest Pt-Pt distance of 7.968 Å. Two types of π-stacking (average distance = 3.83 Å) were discerned, firstly a ladder formed by the B1 ring and C2 ring and the A2 ring and C3 ring. Secondly, a pipe formed by the A1 ring to the B2 ring then to the C3 ring as can be seen in Figure 5.10.

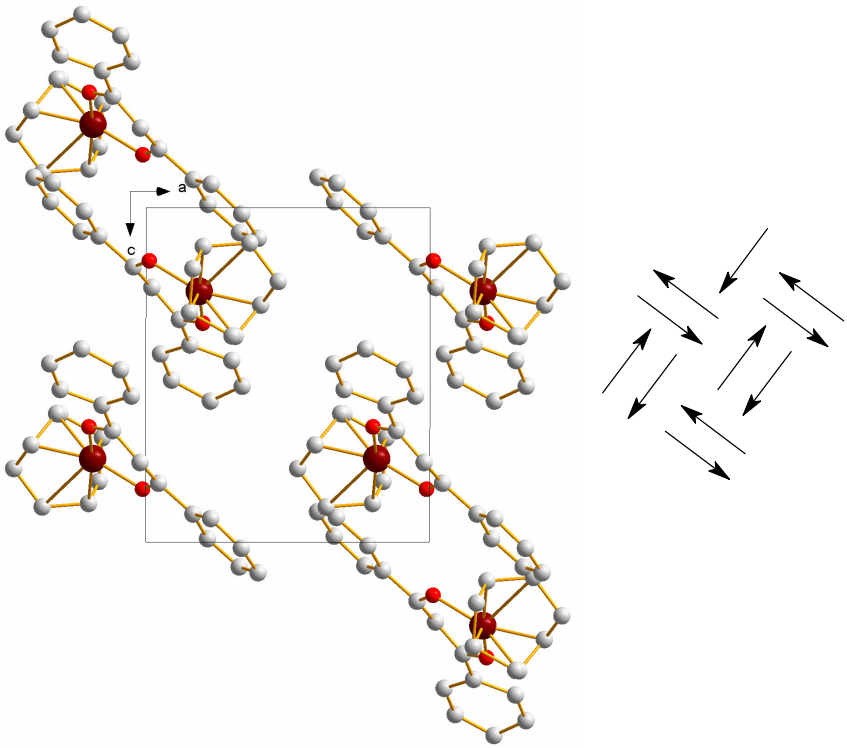

Figure 5.11 Packing of [Pt(cod)(dbm)]BF_4 viewed along the *b*-axis with the packing motif incorporated to the right of the figure. Platinum (dark red), carbon (grey) and oxygen (red). Hydrogens and BF_4 have been omitted for clarity.

The packing motif in Figure 5.11 is defined as the head of the arrow corresponding to the 1,5-cyclo-octadiene moiety and the tail of the arrow corresponding to the dibenzoylmethane moiety. This clustered head-to-tail type of packing is equivalent to that found for the [Pd(cod)(thtfac)]BF_4 (**4**) and the [Pd(cod)(thtfac)]PF_6 (**3**) complexes.

5.3.3 Crystal structure of [Pt(cod)(thtfac)]BF_4

The compound, [Pt(cod)(thtfac)]BF_4, crystallized in the monoclinic space group $P2_1/n$, with two cationic [Pt(cod)(thtfac)]$^+$ (**10a1** and **10a2**) species and two anionic BF_4^- (**10b1** and **10b2**) species in the asymmetric unit. The numbering scheme is presented in Figure 5.12, while atomic co-ordinates, bond angles and distances, anisotropic displacement parameters and hydrogen co-ordinates are reported in Appendix B.13. General crystallographic data and refinement parameters are reported in Table 5.1, while significant bond angles and distances are reported in Table 5.5.

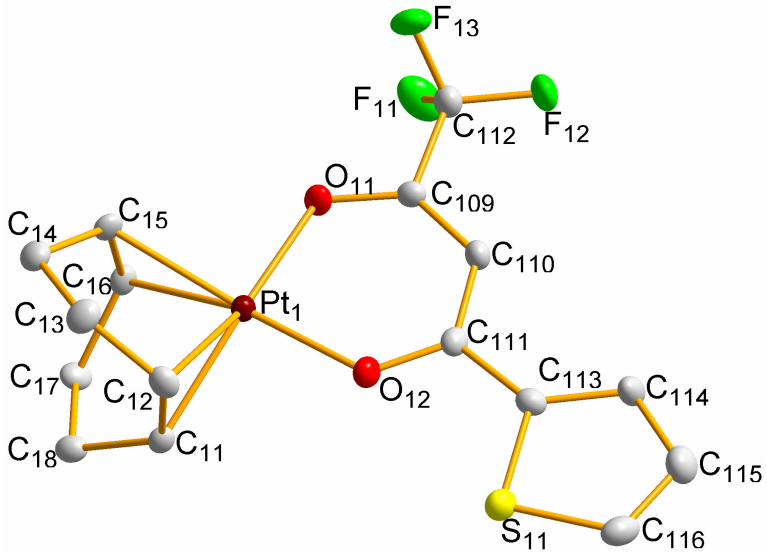

Figure 5.12 Diamond illustration of [Pt(cod)(thtfac)]BF_4 at 100 K showing the numbering scheme and displacement ellipsoids (50 %) of the complex. Hydrogen atoms and counter ion omitted for clarity.

Figure 5.12 presents the numbering scheme of the first cationic species (**10a1**) in the unit cell the second cationic species (**10a2**) numbering prefixes with a 2 instead of a 1 e.g. O_{11} is then O_{21}. The anionic species have been omitted for clarity and are numbered in a similar fashion e.g. B_1 and B_2.

In Table 5.5 the selected bond distances and angles for both the **10a1** and **10a2** cationic species are presented, as can be seen the values do not differ significantly from each other. Therefore for future discussions and comparisons we will be working with the **10a1** species values.

Table 5.5 Selected bond distances and angles for [Pd(cod)(thtfac)]BF_4

Bond Distance (Å)	Species		Bond Angles (°)	Species	
	10a1	**10a2**		**10a1**	**10a2**
Pt-O_1	2.012(3)	2.007(3)	O_1-Pt-O_2	92.3(1)	92.7(1)
Pt-O_2	2.017(3)	2.026(3)	C_1-Pt-C_2	37.8(2)	37.8(2)
Pt-C_1	2.159(4)	2.153(4)	C_5-Pt-C_6	37.8(2)	37.9(2)
Pt-C_2	2.153(4)	2.168(4)	C_1-Pt-C_6	82.3(2)	82.0(2)
Pt-C_5	2.169(4)	2.155(4)	C_2-Pt-C_5	82.2(2)	82.9(2)
Pt-C_6	2.155(4)	2.164(4)	χ^a	87.4(1)	87.4(2)
C_1-C_2	1.395(6)	1.401(6)	ψ^b	78.9(2)	80.5(2)
C_5-C_6	1.399(6)	1.401(6)			

a χ: $C_1MC_2 \cap C_5MC_6$ b ψ: $C_2C_3C_4C_5 \cap C_1C_8C_7C_6$ see Figure 1.2

The platinum metal centre is π-bonded to a cyclo-octadiene ligand and a thenoyltrifluoroacetonato ligand. The co-ordination geometry remains square planar, with the platinum metal centre remaining in the +2 oxidation state. The cationic species is balanced with a tetrafluoroborate (BF_4^-) counter ion. The co-ordination geometry is tetragonal for both the **10b1** and **10b2** species, no disorder is observed. The average bond distances for Pt-O, Pt-C and C=C are 2.016(3) Å, 2.160(4) Å and 1.399(6) Å respectively.

The hydrogen bonding of complex **10** is graphically presented in Figure 5.13-5.16 with Table 5.6 listing the bond distances and angles.

Table 5.6 Hydrogen bond distances and angles for [Pt(cod)(thtfac)]BF_4 (10) [Å and °]

D-H...A	d(D-H)	d(H...A)	d(D...A)	<(DHA)
C_{110}-H_{110}...F_{12}	0.95	2.31	2.706(5)	104.3
C_{210}-H_{210}...F_{23}	0.95	2.33	2.718(5)	103.6
C_{114}-H_{114}...$F_{08}^{\#1}$	0.95	2.48	3.370(6)	156.2
C_{16}-H_{16}...$F_{02}^{\#1}$	1.00	2.28	3.223(5)	156.4
C_{25}-H_{22}...$F_{08}^{\#1}$	1.00	2.36	3.191(5)	139.8
C_{216}-H_{216}...$F_{01}^{\#1}$	0.95	2.24	3.143(6)	157.5
C_{214}-H_{214}...$F_{06}^{\#2}$	0.95	2.46	3.351(6)	155.5
C_{214}-H_{214}...$F_{07}^{\#2}$	0.95	2.50	3.089(5)	120.4
C_{12}-H_{12}...$F_{05}^{\#3}$	1.00	2.32	3.312(5)	169.7
C_{15}-H_{15}...$F_{01}^{\#4}$	1.00	2.42	3.206(5)	134.6
C_{27}-H_{28B}...$F_{07}^{\#5}$	0.99	2.39	3.231(5)	141.8
C_{24}-H_{23B}...$F_{23}^{\#6}$	0.99	2.48	2.953(5)	109.1
C_{115}-H_{115}...$F_{03}^{\#7}$	0.95	2.44	3.345(6)	159.2
C_{22}-H_{25}...$F_{03}^{\#7}$	1.00	2.46	3.071(5)	118.8
C_{116}-H_{116}...$F_{04}^{\#7}$	0.95	2.41	3.033(6)	123.2
C_{21}-H_{26}...$F_{04}^{\#8}$	1.00	2.34	3.068(5)	128.9

Symmetry transformations used to generate equivalent atoms:
#1 -x+1/2,y+1/2,-z+3/2 #2 -x,-y+1,-z+1 #3 x-1/2,-y+3/2,z+1/2
#4 x,y+1,z #5 x,y,z+1 #6 x+1/2,-y+3/2,z+1/2
#7 -x,-y+1,-z+2 #8 x-1/2,-y+1/2,z+1/2

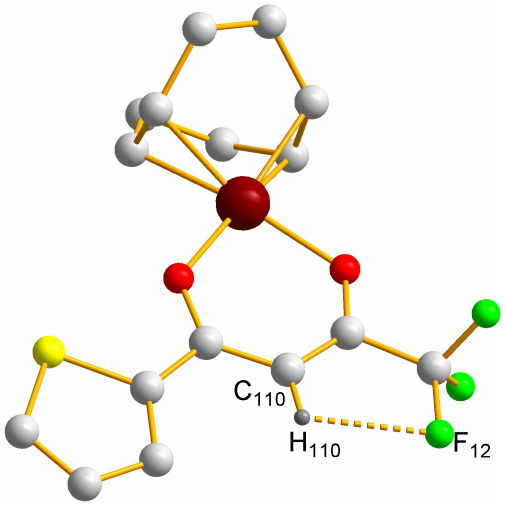

Figure 5.13 Intramolecular hydrogen bonding of [Pt(cod)(thtfac)]BF_4 illustrated by dashed yellow bonds. Hydrogens and counter ion have been omitted for clarity. Platinum (dark red), carbon (grey), oxygen (red), sulfur (yellow) and fluorine (green).

In Figure 5.13 the intramolecular hydrogen bonding for the cationic **10a1** species is presented, this is between the methine hydrogen bonded to the carbon (C_{110}) and the fluorine (F_{12}) of thenoyltrifluoroacetonato ligand. There is an identical interaction for the cationic **10a2** species the distances and angles are alike and can be seen in Table 5.6.

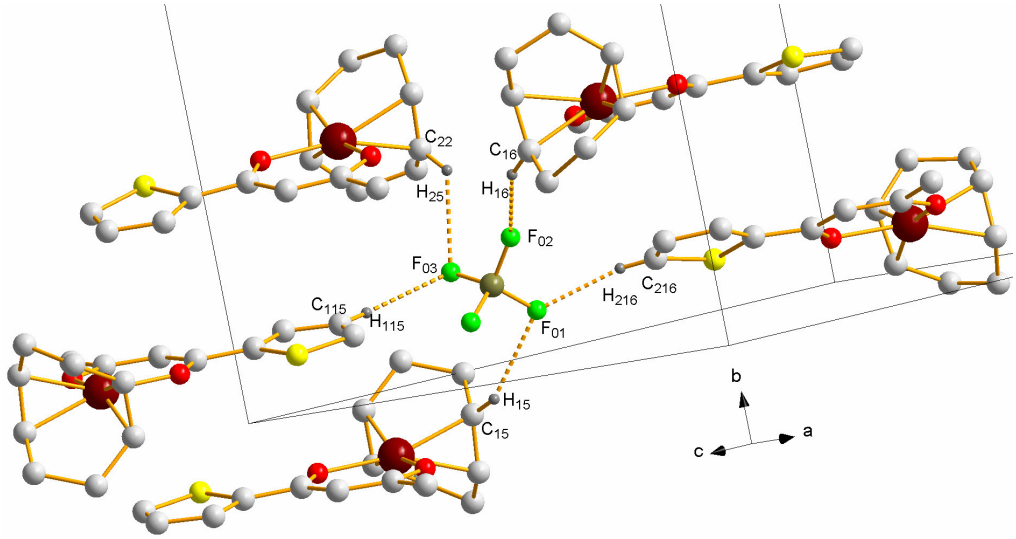

Figure 5.14 Partial unit cell of [Pt(cod)(thtfac)]BF_4 showing intermolecular hydrogen bonding interactions indicated by a dashed bond. Only selected hydrogen atoms are included. Fluorine atoms have been omitted for clarity. Platinum (dark red), carbon (grey), oxygen (red), boron (olive) and fluorine (green).

Figure 5.14 illustrates several intermolecular hydrogen interactions of the type **10a1**···**10b1** and **10a2**···**10b1**, these can be further sub-divided by the interacting ligand, namely that of thenoyltrifluoroacetone and cyclo-octadiene. The first of the interactions displayed are between the methine hydrogens bonded to the carbons (C_{22} and C_{15}) of the cyclo-octadine ligand and the fluorido (F_{03} and F_{01}) ligands and the methylene hydrogen bonded to carbon (C_{16}) with the fluorido (F_{02}) ligand of the **10b1** species. The second of the interactions displayed is that of the hydrogens of the ring carbons (C_{115} and C_{216}) of the thenoyltrifluoroacetonato ligand with the fluorido (F_{03} and F_{01}) ligands.

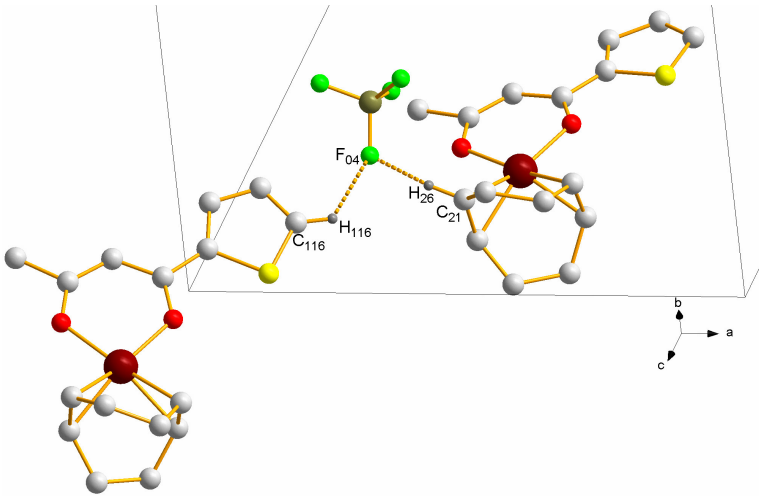

Figure 5.15 Partial unit cell of [Pt(cod)(thtfac)]BF_4 showing intermolecular hydrogen bonding interactions indicated by a dashed bond. Only selected hydrogen atoms are included. Fluorine atoms have been omitted for clarity. Platinum (dark red), carbon (grey), oxygen (red), boron (olive) and fluorine (green).

The last of the interactions can be seen in Figure 5.15, this is between the hydrogen of the ring carbon (C_{116}) of the thenoyltrifluoroacetonato ligand, methine hydrogen bonded to carbon (C_{21}) of the cyclo-octadine ring and the fluorido (F_{04}) ligand of the **10b1** species.

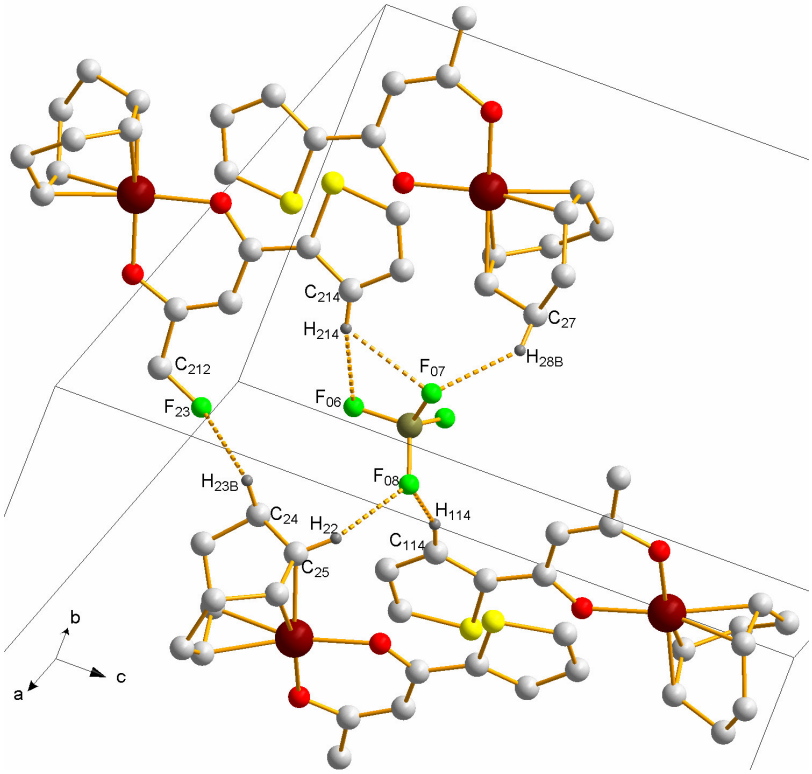

Figure 5.16 Partial unit cell of [Pt(cod)(thtfac)]BF_4 showing intermolecular hydrogen bonding interactions indicated by a dashed bond. Only selected hydrogen atoms are included. Fluorine atoms have been omitted for clarity. Platinum (dark red), carbon (grey), oxygen (red), boron (olive) and fluorine (green).

Figure 5.16 show intermolecular hydrogen interactions between **10a1**···**10b2** and **10a2**···**10b2**. The interactions for the **10b2** species is similar to that of the **10b1** species, the hydrogens of the ring carbons (C_{214} and C_{114}) of the thenoyltrifluoroacetonato ligand, the methine hydrogen bonded to carbon (C_{25}) and the methylene hydrogen bonded to carbon (C_{27}) of the cyclo-octadiene ligand with the fluorido (F_{06}, F_{07} and F_{08}) ligands of the **10b2** species. There is an additional interaction that is presented that of the methylene hydrogen bonded to carbon (C_{24}) of the cyclo-octadiene ring with the fluorine (F_{23}) of a thenoyltrifluoroacetonato ligand. The interactions are listed in Table 5.6.

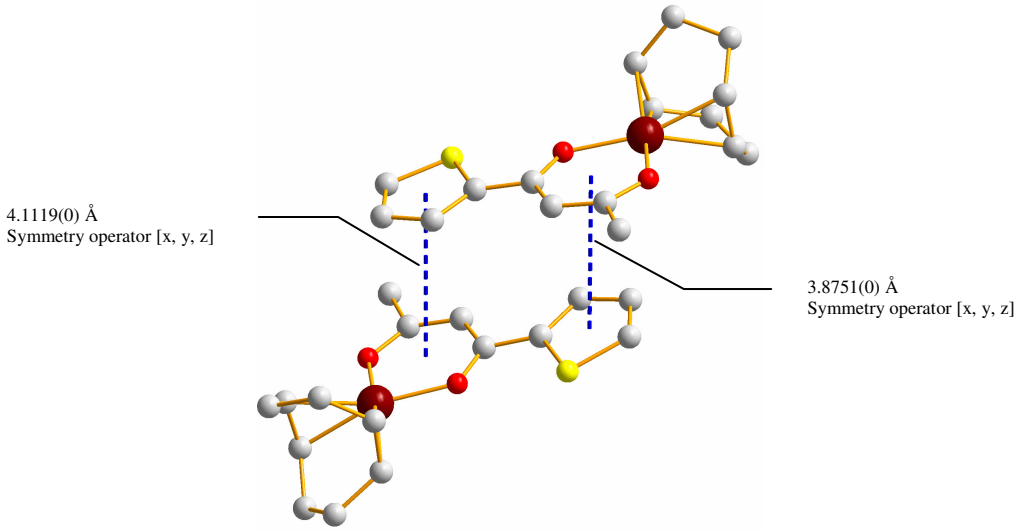

Figure 5.17 Partial unit cell of [Pt(cod)(thtfac)]BF_4 showing π···metal chelate ring intermolecular interactions indicated by a dashed blue bond. Hydrogens, Fluorines and tetrafluoroborate counter ion have been omitted for clarity. Platinum (dark red), carbon (grey), oxygen (red) and sulfur (yellow).

The last of the interactions that are observed for [Pt(cod)(thtfac)]BF_4 is that of the π···metal chelate ring interactions between the ring formed by the platinum, oxygens and the back-bone carbons of the thenoyltrifluoroacetonato ligand of the **10a1** species and the thenoyl ring of the thenoyltrifluoroacetonato ligand of the **10a2** species, the distances are 4.1119(0) Å and 3.8751(0) Å respectively.

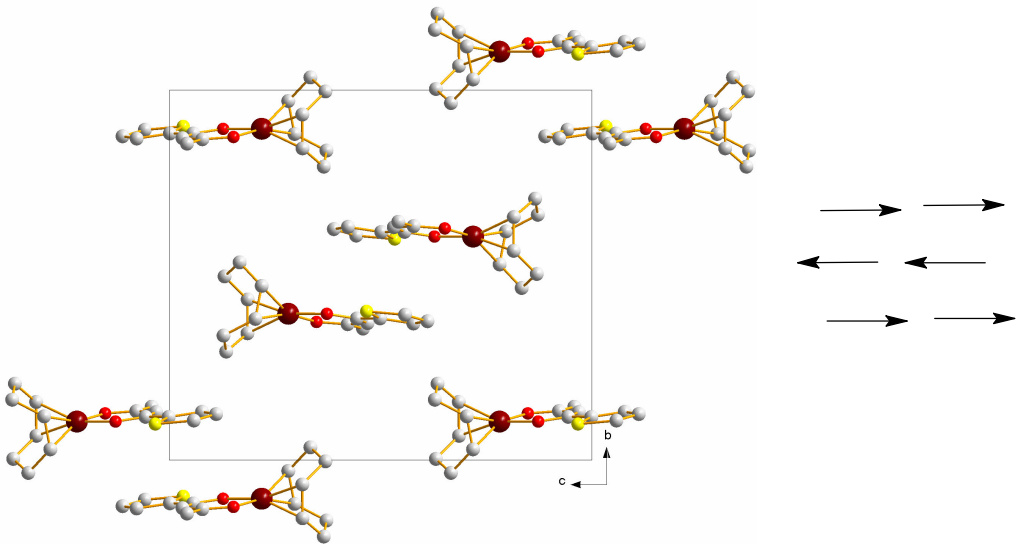

Figure 5.18 Packing of [Pt(cod)(thtfac)]$^+$ (10a1) species viewed along the *a*-axis with the packing motif incorporated to the right of the figure. Platinum (dark red), carbon (grey), oxygen (red) and sulfur (yellow). Hydrogen, Fluorine and BF_4 have been omitted for clarity.

The packing motif in Figure 5.18 is defined as the head of the arrow corresponding to the 1,5-cyclo-octadiene moiety and the tail of the arrow corresponding to the thenoyltrifluoroacetylacetonato moiety. In Figure 5.18 we see the packing for the **10a1** species viewed along the *a*-axis, the hydrogens, fluorines, **10a2** species, **10b1** species and **10b2** species have been omitted. When looking at the sketch we see the classic head-to-tail pattern that we have become accustomed to.

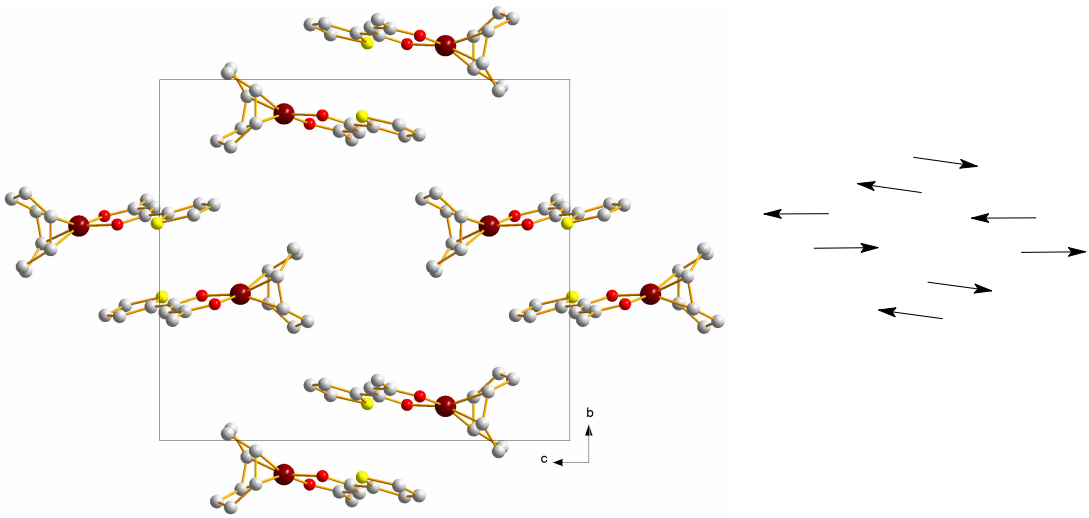

Figure 5.19 Packing of [Pt(cod)(thtfac)]$^+$ (10a2) species viewed along the *a*-axis with the packing motif incorporated to the right of the figure. Platinum (dark red), carbon (grey), oxygen (red) and sulfur (yellow). Hydrogen, Fluorine and BF_4 have been omitted for clarity.

The packing motif in Figure 5.19 is defined as the head of the arrow corresponding to the 1,5-cyclo-octadiene moiety and the tail of the arrow corresponding to the thenoyltrifluoroacetylacetonato moiety. Figure 5.19 shows the packing for the **10a2** species again viewed along the *a*-axis, the hydrogens, fluorines, **10a1** species, **10b1** species and **10b2** species have been omitted. When looking at the packing motif on the right one can see that the packing is a slightly deviated head-to-tail. This results in marginally different packing for the two cationic species found in the asymmetric unit cell.

5.4 Discussion

In an attempt to grow the crystals of the series hfacac < tfacac < thtfac << acac it was concluded that the platinum metal centre, seemingly co-ordinates more challenging with strongly electron withdrawing groups and could not be isolated with the same

ease as for palladium resulting in low yields and fiber-like crystals. All attempts at crystal growth modification did not improve the situation and no crystals of the stronger withdrawing groups were obtained. The crystals that were obtained are listed in Table 5.7.

The [Pt(cod)(dbm)BF_4 (**9**) compound is included in Table 5.7 only for its comparative value, due to the twinning encountered the crystal has not been completely solved and comparisons with the other crystals obtained have been omitted.

A square planar geometry is consistent throughout with distortions from planar, calculated as the intersection of the plane through the mid-points of the alkene carbons of the cyclo-octadiene ring and the oxygens of the β-diketone and a second plane through the platinum and the backbone of the β-diketone. The order observed was **10 < 7 < 8** with values of 5.36(6)°, 4.19(6)° and 2.57(9)° respectively. It is of note that the first two values are of the BF_4 counter ion whilst the last and lower value is that of the PF_6 counter ion complex. The platinum metal centre remains in the +2 oxidation state.

Table 5.7 Cell dimension overview for platinum crystals obtained where A = BF_4 or PF_6.

	[Pt(cod)(acac)]A		[Pt(cod)(thtfac)]A	[Pt(cod)(dbm)]A
	BF_4 (**7**)	PF_6 (**8**)	BF_4 (**10**)	BF_4 (**9**)
Crystal system	Orthorhombic	Monoclinic	Monoclinic	Triclinic
Space group	*Pca*2_1	*P*2_1/*n*	*P*2_1/*n*	*P*1
Unit Cell Dimensions				
a (Å)	26.395(8)	9.3082(3)	14.4456(2)	10.4558(21)
b (Å)	7.191(2)	15.4486(5)	15.1804(1)	10.6170(21)
c (Å)	7.710(2)	11.4733(3)	18.1656(2)	10.894(22)
α (°)	90	90	90	89.28(3)
β (°)	90	105.944(1)	107.281(1)	89.71(3)
γ (°)	90	90	90	61.93(3)
Z	4	4	8	2

When looking at the [Pt(cod)(acac)]PF_6 (**8**) compound we expected to find isomorphism with that of the [Pt(cod)(thtfac)]BF_4 (**10**) compound. However the *a*- and *c*- axis of **10** have been transformed and the *c*-axis is double that of the *a*-axis of compound **8**. This deviation is clearly shown in the packing of the respective structures, where complex **8a** shows a clustered head-to-tail packing (Figure 5.8) and complex **10a1** shows a classic head-to-tail (Figure 5.18), though in defense the **10a2**

complex was found to have a deviated head-to-tail that almost falls into the clustered head-to-tail packing (Figure 5.19).

Table 5.8 Selected geometric parameters (Å,°) for platinum metal complexes

	[Pt(cod)(acac)]		[Pt(cod)(thtfac)]
	BF_4	PF_6	BF_4
Pt-O_1	2.015(3)	2.010(5)	2.012(3)
Pt-O_2	2.013(3)	2.016(5)	2.017(3)
Pt-C_1	2.160(3)	2.164(6)	2.159(4)
Pt-C_2	2.153(4)	2.161(7)	2.153(4)
Pt-C_5	2.164(3)	2.150(7)	2.169(4)
Pt-C_6	2.147(4)	2.161(7)	2.155(4)
C_1-C_2	1.388(8)	1.382(10)	1.395(6)
C_5-C_6	1.411(8)	1.406(11)	1.399(6)
O_1-Pt-O_2	93.5(1)	93.3(3)	92.3(1)
C_1-Pt-C_2	37.6(2)	37.3(3)	37.8(2)
C_5-Pt-C_6	38.2(2)	38.1(3)	37.8(2)
C_1-Pt-C_5	82.2(2)	82.0(3)	82.3(2)
C_2-Pt-C_6	82.0(2)	81.9(3)	82.2(2)
χ^a	86.9(2)	86.8(4)	87.4(1)
ψ^b	79.1(2)	78.9(5)	78.9(2)

a χ: $C_1MC_2 \cap C_5MC_6$ b ψ: $C_2C_3C_4C_5 \cap C_1C_8C_7C_6$ see Figure 1.2

There are no significant differences in the bond distances of Pt-O, Pt-C and C=C for the different compounds, which would further corroborate the isomorphism prediction for complexes **8** and **10**. The values obtained for **7** and **8** are nearly identical suggesting that the counter ions (BF_4^- and PF_6^-) even with the hydrogen interactions which are observed do not play a major role in the structure of the cationic species.

There is only a minor increase in the χ value and the ψ value remains virtually constant this can be seen in Figure 5.20.

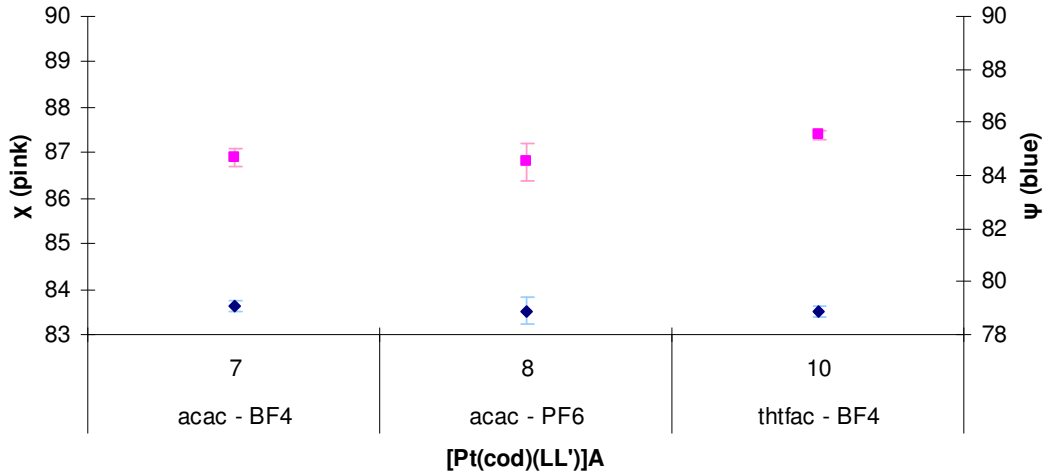

Figure 5.20 Graph of Platinum crystal complexes *vs.* χ (pink squares) and ψ (blue diamonds) angles arranged in ascending order of χ angle (see Chapter 1 Figure 1.2 for definition of χ and ψ angles).

In overview of the cationic species packing one finds that the **9a** complex shows a clustered head-to-tail structure with tight clusters (Figure 5.11), a looser clustered head-to-tail structure is observed for the **8a** complex (Figure 5.8), complexes **7a** (Figure 5.7) and **10a1** (Figure 5.18) show similar head-to-tail packing.

A detailed discussion of the relationships between the platinum and palladium β-diketonato complexes as obtained in Chapter 4 and 5 respectively, will be given in Chapter 6.

Chapter 6
Solid State *vs.* Optimized Structure Correlation of β-Diketonato Complexes

6.1 Introduction

In this chapter a comparison between the β-diketonato complexes of platinum(II) and palladium(II) with regards to their single crystal structures, including theoretical calculations thereof will be presented. Table 6.1 represents a list of the crystal structures that will be discussed in the sections to follow.

Table 6.1 β-diketonato complexes of platinum(II) and palladium(II)

Compound		Ref
$[Pd(cod)(acac)]PF_6$	**1**	§ 4.3.1
$[Pd(cod)(acac)]BF_4$	**2**	§ 4.3.1
$[Pd(cod)(thtfac)]PF_6$	**3**	§ 4.3.2
$[Pd(cod)(thtfac)]BF_4$	**4**	§ 4.3.2
$[Pd(cod)(tfacac)]PF_6$	**5**	§ 4.3.3
$[Pd(cod)(hfacac)]PF_6$	**6**	§ 4.3.4
$[Pt(cod)(acac)]PF_6$	**8**	§ 5.3.1
$[Pt(cod)(acac)]BF_4$	**7**	§ 5.3.1
$[Pt(cod)(dbm)]BF_4$	**9**	§ 5.3.2
$[Pt(cod)(thtfac)]BF_4$	**10**	§ 5.3.3

Computational chemistry is new to the range of techniques to which a chemist has access. However, it is a technique which should not be ignored though still in its infancy it can provide a wealth of information with regards to various chemical properties. Not a tool to be used on its own but in conjunction with existing techniques its position within the chemists toolbox is beyond question. With the worlds resources being taxed a technique allowing the chemist to sift though many possible compounds identifying the most likely candidates for further processing cannot be ignored.

It's history albeit brief, shows how this tool has been accepted with its humble beginnings in molecular mechanics to the present day *ab initio* methods[1,2,3]. With the

[1] Jensen F., *Introduction to Computational Chemistry, 2nd edition*, John Wiley & Sons Ltd., England, (2007)
[2] Ramachandran K.I., Deepa G., Namboori K., *Computational Chemistry and Molecular Modeling Principles and Applications*, Springer, Heidelberg, Germany, (2008)

advances in information technology and in particular personal computing, the technique has become more accessible to the chemist.

Computational chemistry in its beginning focused mainly on organic molecules and inorganic molecules were left by the way side. In recent times a growing interest in inorganic and organometallic molecules has come to light, as a result of recent advances in catalytic[4,5] systems, material sciences and bioinorganics. Transition metal compounds tend to be difficult to model due to the nature of the ligand metal bond, the fact that π-back bonding may be present for the ligand, along with low-lying excited states for the transition metal compounds. With both spin contamination and relativistic effects for the heavier transition metals having an increasing effect as one progresses along the periodic table

When investigating the different methods of calculations the most basic is of molecular mechanics. This is simply a parameterized force field to calculate the desired geometries and energies. Previously as has been said this type of calculation was mostly setup for organic compounds, with the use of these force fields for transition metal compounds very poor results were typically obtained. The result of this, force fields were created for specific classes of transition metal compounds with the resultant effect being good results for similar classes of transition metal compounds and extremely poor results for compounds far removed from the original description. Some of the major reasons for the failure of these force fields are the metal-organic bond which can have a large variance in value (*i.e.* soft bonding), the distorted or fluxional behavior of the bond angles and limited vibrational data for transition metal compounds. The best transition metal force field to date is the UFF force field.

The next method of calculation is that of semi-empirical methods. This method is well known for its ability to calculate symmetry properties of valence orbitals and

[3] Cramer C.J., *Essentials of Computational Chemistry Theories and Models, 2nd edition*, John Wiley & Sons Ltd., England, (2004)
[4] Maseras F., Lledós A., *Computational Modeling of Homogeneous Catalysis*, Kluwer Academic Publishers, Dordrecht, (2002)
[5] Cundari T.R., *Computational Organometallic Chemistry*, Marcel Dekker Inc., United States of America, (2001)

energies. It does not fair well with geometry optimization. The three top calculation methods used today are the Extended Hückel, ZINDO and PM3/TM.

The last method of calculation is that of *ab initio* methods. These methods are the closest to quantum chemistry that is presently achievable with the current state of technology. The methods associated with *ab initio* calculations those of Hartree-Fock (HF) both restricted open-shell (ROHF) and unrestricted (UHF). Mollar-Plessent perturbation theory (MP*n*), configuration interaction (CI), coupled cluster (CC), quadratic configuration interaction (QCI), multi-configurational self-consistent field (MSCF), multi-reference configuration interaction (MRCI) and n-electron valence state perturbation theory (NEVPT) the latter all fall under the group of correlated calculations and begin with a HF calculation and as a result suffer from the same weakness as the HF method.

To overcome this weakness the quantum Monte Carlo (QMC) method was developed, probably the most accurate method to date, but also the most time consuming. A midway between all of these options is that of the density functional theory (DFT). To ease the level of calculations core potentials for the heavier metals are generally used. The total energy is expressed in terms of one-electron density rather than a wave function. The convergence problems still remain with the open-shell systems and unfilled co-ordination spheres being the most difficult. Recently DFT calculations have become prominent with B3LYP being widely used. This hybrid functional is known for its reasonable results, fair accuracy and reasonable computational requirements.

For the theoretical calculations in this section of the study the following β-diketonato type donor ligands were chosen, acetylacetone (Hacac), trifluoroacetylacetone (Htfacac) and hexafluoroacetylacetone (Hhfacac) for their increasing electron withdrawing capability so as to study the effect that the additional electron withdrawal has on the geometry of cyclo-octadiene ring. For the sake of completeness the entire group 10 metal triad was computed.

6.2 Experimental

The DFT molecular orbital calculations were carried out using the Gaussian 03[6] software suite. Becke's three parameter hybrid (B3LYP)[7,8] exchange correlation functional was used. The basis set employed in this study was 6-311++G(d,p)[9,10,11] for the main group elements and LanL2DZ[12] for the middle to late transition metals. Vibrational frequencies were calculated at the 6-311++G(d,p)[9,10,11] level for the main group elements and at the LanL2DZ[12] level for the middle to late transition metals with minimum energies confirmed to have zero imaginary frequencies. The frequencies were unscaled and used to compute the zero-point vibrational energies. Molecular graphics were obtained using DIAMOND[13], while overlay graphics were obtained using HyperChem 7.5[14].

6.3 Crystal Structure Correlation of Palladium(II) *vs.* Platinum(II) complexes

By considering the various radii (atomic, covalent and van der Waal) for palladium and platinum it is observed that there are only marginal differences between the two metal centers (Table 2.4). The values obtained in 2008 by Cordero[15] *et al.* show a value of 1.39 Å for palladium and 1.36 Å for platinum. Both metals are known for

---

[6] Frisch M.J., Trucks G.W., Schlegel H.B., Scuseria G.E., Robb M.A., Cheeseman J.R., Montgomery J.A. Jr., Vreven T., Kudin K.N., Burant J.C., Millam J.M., Iyengar S.S., Tomasi J., Barone V., Mennucci B., Cossi M., Scalmani G., Rega N., Petersson G.A., Nakatsuji H., Hada M., Ehara M., Toyota K., Fukuda R., Hasegawa J., Ishida M., Nakajima T., Honda Y., Kitao O., Nakai H., Klene M., Li X., Knox J.E., Hratchian H.P., Cross J.B., Bakken V., Adamo C., Jaramillo J., Gomperts R., Stratmann R.E., Yazyev O., Austin A.J., Cammi R., Pomelli C., Ochterski J.W., Ayala P.Y., Morokuma K., Voth G.A., Salvador P., Dannenberg J.J., Zakrzewski V.G., Dapprich S., Daniels A.D., Strain M.C., Farkas O., Malick D.K., Rabuck A.D., Raghavachari K., Foresman J.B., Ortiz J.V., Cui Q., Baboul A.G., Clifford S., Cioslowski J., Stefanov B.B., Liu G., Liashenko A., Piskorz P., Komaromi I., Martin R.L., Fox D.J., Keith T., Al-Laham M.A., Peng C.Y., Nanayakkara A., Challacombe M., Gill P.M.W., Johnson B., Chen W., Wong M.W., Gonzalez C., Pople J.A., Gaussian 03, Revision E.01, Gaussian Inc., Wallingford CT, (2004)

[7] Becke A.D., *J. Chem. Phys.*, **98**, 5648, (1993)

[8] Lee C., Yang W., Parr R.G., *Phys. Rev.*, **B37**, 785, (1988)

[9] Ditchfield R., Hehre W.J., Pople J.A., *J. Chem. Phys.*, **54**, 724, (1971)

[10] Gordon M.S., *Chem. Phys. Lett.*, **76**, 163, (1980)

[11] Rassolov V.A., Ratner M.A., Pople J.A., Redfern P.C., Curiss L.A., *J. Comp. Chem.*, **22**, 976, (2001)

[12] Hay P.J., Wadt W.R., *J. Chem. Phys.*, **82**, 299, (1985)

[13] Brandenburg K., Brendt M., DIAMOND, Release 2.1e. Crystal Impact GbR, Potfach 1251, D53002 Bonn, Germany., (2001)

[14] HyperChem™ Release 7.52, Windows Molecular Modeling System, HyperCube Inc., (2002)

[15] Cordero B., Gómez V., Platero-Prats A.E., Revés M., Echeverría J., Cremades E., Barragán F., Alvarez S., *Dalton Trans.*, (2008)

their square planar co-ordination geometry, with the +2 oxidation state being the most common.

Table 6.2 Cell dimension overview for palladium(II) crystals obtained where A = BF_4 or PF_6.

	[Pd(cod)(acac)]A		[Pd(cod)(thtfac)]A		[Pd(cod)(tfacac)]A	[Pd(cod)(hfacac)]A
	PF_6 (**1**)	BF_4 (**2**)	PF_6 (**3**)	BF_4 (**4**)	PF_6 (**5**)	PF_6 (**6**)
Crystal system	Monoclinic	Orthorhombic	Monoclinic	Monoclinic	Triclinic	Monoclinic
Space group	$P2_1/n$	$Pca2_1$	$P2_1/n$	$P2_1/n$	$P\bar{1}$	$P2_1/c$
Unit Cell dimensions						
a (Å)	9.3166(6)	26.2908(11)	9.9691(2)	10.0528(3)	8.1027(8)	8.5885(2)
b (Å)	15.4676(8)	7.1684(3)	17.0294(3)	16.6333(6)	14.3018(14)	10.6304(2)
c (Å)	11.4844(7)	7.7782(3)	11.4750(2)	10.9501(4)	15.4557(14)	19.4093(4)
α (°)	90	90	90	90	75.286(5)	90
β (°)	106.171(2)	90	101.327(2)	102.534(1)	89.963(5)	93.415(1)
γ (°)	90	90	90	90	73.556(5)	90
Z	4	4	4	4	4	4

Table 6.3 Cell dimension overview for platinum(II) crystals obtained where A = BF_4 or PF_6.

	[Pt(cod)(acac)]A		[Pt(cod)(thtfac)]A	[Pt(cod)(dbm)]A
	BF_4 (**7**)	PF_6 (**8**)	BF_4 (**10**)	BF_4 (**9**)
Crystal system	Orthorhombic	Monoclinic	Monoclinic	Triclinic
Space group	$Pca2_1$	$P2_1/n$	$P2_1/n$	$P1$
Unit Cell Dimensions				
a (Å)	26.395(8)	9.3082(3)	14.4456(2)	10.4558(21)
b (Å)	7.191(2)	15.4486(5)	15.1804(1)	10.6170(21)
c (Å)	7.710(2)	11.4733(3)	18.1656(2)	10.894(22)
α (°)	90	90	90	89.28(3)
β (°)	90	105.944(1)	107.281(1)	89.71(3)
γ (°)	90	90	90	61.93(3)
Z	4	4	8	2

The crystal structures presented in Table 6.2 and 6.3, illustrate that the most common space group is monoclinic $P2_1/n$, with [Pd(cod)(tfacac)]PF_6 (**5**) being the exception in that it was solved in the triclinic $P\bar{1}$ space group. The complex can however be solved in monoclinic $C2/c$ space group but the *R*-values are weaker due to anomalies that were present in the crystal data. In comparing the platinum crystals with the palladium crystals it was found that both complexes **2** and **7** crystallize in the orthorhombic $Pca2_1$ space group, upon inspection of the unit cell dimensions the values are marginally different such that the complexes are isostructural and isoelectronic with each other. Complexes **1**, **3**, **4** and **8** are also isostructural. Complex **9** has been included here but due to the excessive twinning a complete elucidation of the structure could not be achieved, the compound will need to be re-collected at a later date.

The overlay of the isostructural X-ray crystal structures is a graphical representation of the pair-wise differences of the related structures. This mathematical value is represented by the root mean square (RMS) value, which is a measure of how far the average is from zero, providing information on the variations of bond lengths and angles and to a certain degree the orientation of the structures in relation to each other. These comparisons are presented in Figure 6.1-6.4.

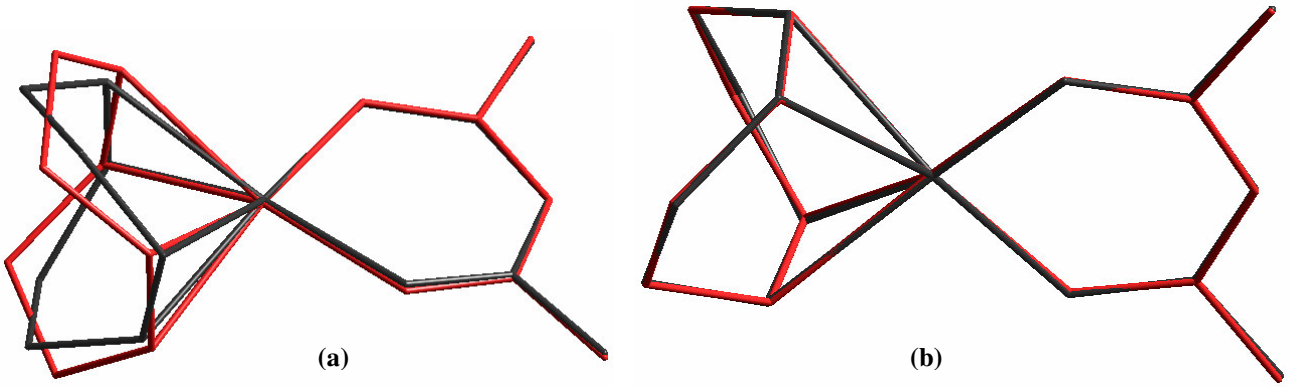

Figure 6.1 HyperChem superimposed image of (a) [Pd(cod)(acac)]PF_6 (1) (black) *vs.* [Pt(cod)(acac)]PF_6 (8) (red) with an RMS error of 0.56 Å (b) [Pd(cod)(acac)]PF_6 inverted crystal structure (1) (black) *vs.* [Pt(cod)(acac)]PF_6 (8) (red) with an RMS error of 0.03 Å. Counter ions have been omitted for clarity.

In the overlay of the complexes **1** and **8** (Figure 6.1a) an RMS error of 0.56 Å was observed for all the atoms excluding the methyl carbons of the acetylacetonato ligand. The inverse crystal structure of complex **1** was also overlaid (Figure 6.1b) and an RMS error of 0.029 Å was found for all the atoms excluding the methyl carbons of the acetylacetonato ligand, due to the fact that complex **1** has a centrosymmetric space group (monoclinic $P2_1/n$). The difference found in the twist angle (*i.e.* the intersection of the planes defined by the mid-points of the alkene carbons of the cyclo-octadine ring with the oxygens of the acetylacetonato ligand *vs.* the metal centre with the oxygens and the back-bone carbons of the acetylaceontato ligand) of 0.85° (**1** : 3.42(5)°; **8** : 2.57(9)°). The last difference observed is that of the cross-over of the positions alkane carbons of the cyclo-octadine ring, this cross-over does affect the difference in the ψ angle with a value of 3° (**1** : 81.9(3)°; **8** : 79.9(5)°) indicating that the opening of the ring is not as similar as originally thought for the one enantiomer (Figure 6.1a). For the second enatiomer however a good correlation between the two structures was observed (Figure 6.1b).

Figure 6.2 HyperChem superimposed image of (a) [Pd(cod)(acac)]BF_4 (2) (black) *vs.* [Pt(cod)(acac)]BF_4 (7) (red) with an RMS error of 1.72 Å (b) [Pd(cod)(acac)]BF_4 inverted crystal structure (2) (black) *vs.* [Pt(cod)(acac)]BF_4 (7) (red) with an RMS error of 0.02 Å. Counter ions have been omitted for clarity.

In the overlay of complexes **2** and **7** (Figure 6.2a) an RMS error of 1.72 Å was observed for all atoms except the methyl carbons of the acetylacetonato ligand. Complex **2** has a centrosymmetric space group (orthorhombic $Pca2_1$) and as such has a second enantiomer in the unit cell, this enantiomer was also overlaid (Figure 6.2b) with complex **7** and an RMS error of 0.02 Å was obtained. The differences resulted from the distortion of the square planar geometry around the metal centre. If one looks at the intersection of a plane through the mid-points of the alkene carbons of the cyclo-octadiene ring and the oxygen's of the acetylacetonato ligand and a second plane through the platinum and the back-bone carbons of the acetylacetonato ligand for complex **2** an angle of 3.48(5)° and for complex **7** an angle of 4.19(6)° were observed with a difference of 0.71(5)° contributing to the large RMS value that was encountered. A second contributing factor would be the cross-over of the alkane carbons of the cyclo-octadiene ring, this cross-over is also seen for the PF_6^- complexes (see Figure 6.1a). There is a smaller difference for the ψ angle than was found for the PF_6^- complexes of 1.1(2)° (**2** : 80.2(2)°; **7** : 79.1(2)°). For the second enantiomer (Figure 6.2b) a good correlation was found.

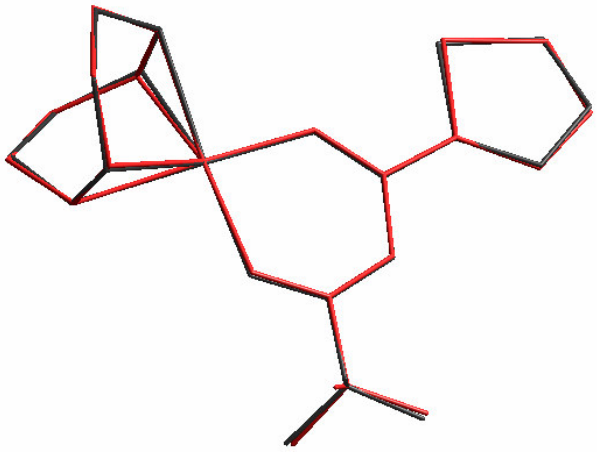

Figure 6.3 HyperChem superimposed image of [Pd(cod)(thtfac)]BF_4 (4) (black) *vs.* [Pt(cod)(thtfac)]BF_4 (10) (red) with an RMS error of 0.1 Å. Counter ions have been omitted for clarity.

In the overlay of complexes **4** and **10** (Figure 6.2) an RMS error of 0.1 Å was observed. There is an excellent correlation between the structures presented. The only variances, although very minor, which can be seen are in the flourines of the CF_3 group and the sulphur of the thenoyl group.

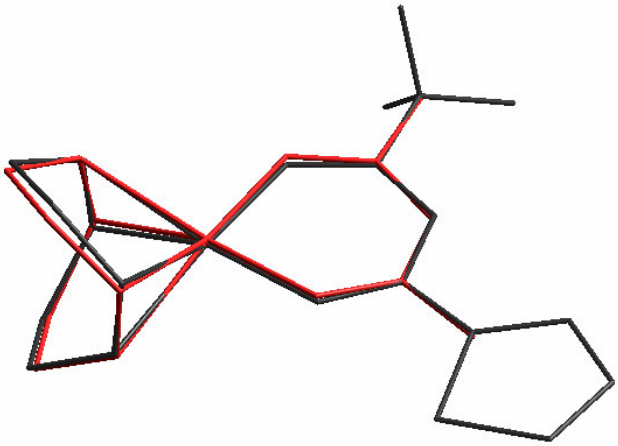

Figure 6.4 HyperChem superimposed image of [Pd(cod)(acac)]PF_6 (1) (red) *vs.* [Pd(cod)(thtfac)]PF_6 (3) (black) with an RMS error of 1.72 Å. Counter ions have been omitted for clarity.

In the overlay of complexes **1** and **3** (Figure 6.4) an RMS error of 1.72 Å was observed, the reason for the large error was again due to the intersection angles between the planes defined by the mid-points of the alkene carbons of the cyclo-octadiene ring and the oxygens of the β-diketonato ligands and the plane of the palladium metal centre with the backbone of the β-diketonato ligand. For complex **1** a value of 3.42(5)° was obtained and for complex **3** a value of 3.63(3)° was obtained

with a difference of *ca.* 0.21(4)°. However, if one only looks at the atoms connected with the metal centre and use this as the template for the overlay an RMS error of 0.87 Å is observed, with only marginal differences in the angles of the substituents on the β-diketonato ligands.

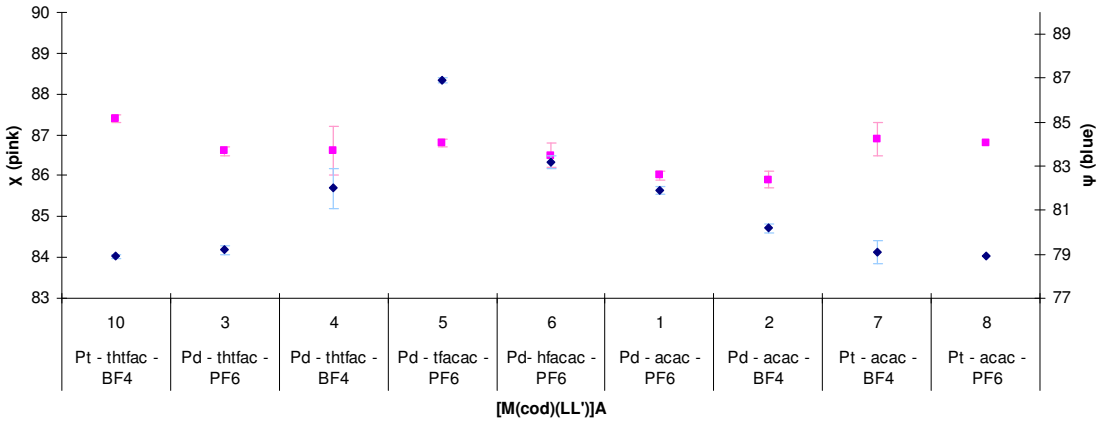

Figure 6.5 Graph of Palladium(II) and Platinum(II) crystal complexes *vs.* χ and ψ angles.

The combined graph of platinum and palladium crystal complexes *vs.* the χ and ψ angles continues to show the same trend as chapters 4 and 5, in that with an increase in the χ angle we find and opening and closing of the ψ angle. With the χ angle independent of the β-diketonato ligand however, a significant 8° change in ψ is observed.

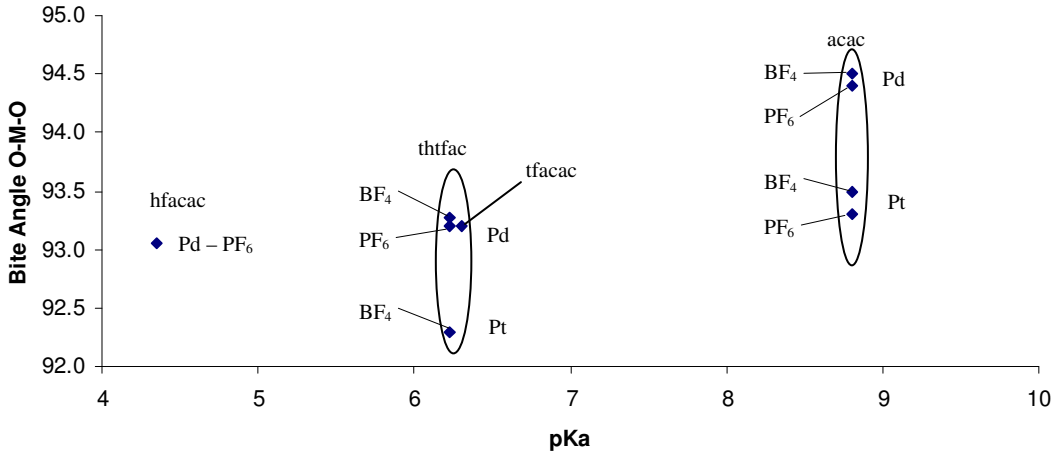

Figure 6.6 Graph of pKa *vs.* O-M-O bite angle for the [M(cod)(LL')]A where M = Pd(II), Pt(II), LL' = acac, tfacac, hfacac, thtfac and A = BF_4^-, PF_6^- complexes.

The graph of pKa *vs.* O-M-O bite angle (Figure 6.6) shows an increase in the bite angle with a decrease in the electron withdrawing capability of the ligand, hfacac >

thtfac > tfacac > acac, with an increase in the pKa value. This trend holds for both the palladium and platinum complexes. The clusters that are observed are as a result of the counter ions, tetrafluoroborate (BF_4^-) or hexafluorophosphate (PF_6^-), for the complexes, showing that the change of counter ion does not significantly affect the bite angle. The pKa values of thtfac and tfacac do not vary greatly and as a result the change in bite angle is also minor.

Table 6.4 Overview of the division of the complexes into packing categories.

Clustered head-to-tail	Ref	Head-to-tail	Ref
[Pd(cod)(acac)]PF_6 (**1**)	Figure 4.9	[Pd(cod)(acac)]BF_4 (**2**)	Figure 4.10
[Pd(cod)(thtfac)]PF_6 (**3**)	Figure 4.19	[Pt(cod)(acac)]BF_4 (**7**)	Figure 5.7
[Pd(cod)(thtfac)]BF_4 (**4**)	Figure 4.40	[Pt(cod)(thtfac)]BF_4 (**10**)	Figure5.18
[Pt(cod)(acac)]PF_6 (**8**)	Figure 5.8		
[Pt(cod)(dbm)]BF_4 (**9**)	Figure 5.11		

For the packing of the platinum and palladium complexes two major packing styles are observed that of a clustered head-to-tail (Figure 6.7) and a classic head-to-tail (Figure 6.8) packing. Table 6.4 shows a summary of the complexes and how they are divided into the two packing styles. The compounds which do not form part of these two major groups are [Pd(cod)(tfacac)]PF_6 (**5**) which has a distorted head-to-tail packing, this can be seen in Figure 4.26. The other complex [Pd(cod)(hfacac)]PF_6 (**6**) has a tail-to-tail packing which can be seen in Figure 4.36.

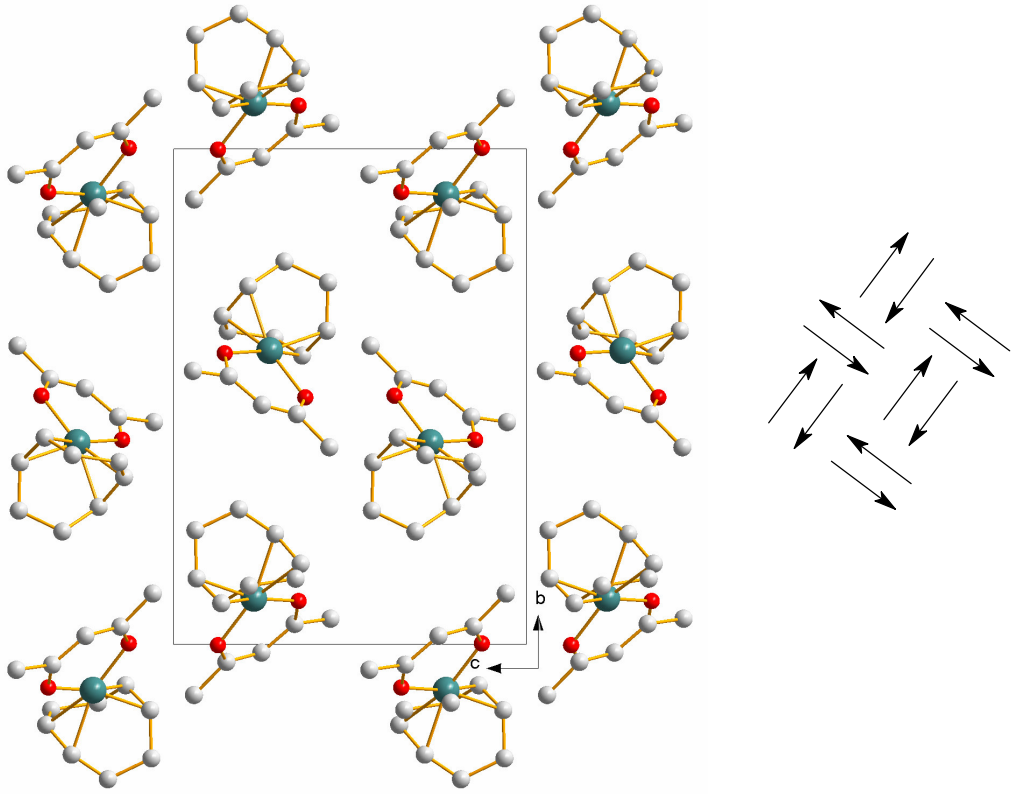

Figure 6.7 Clustered head-to-tail packing

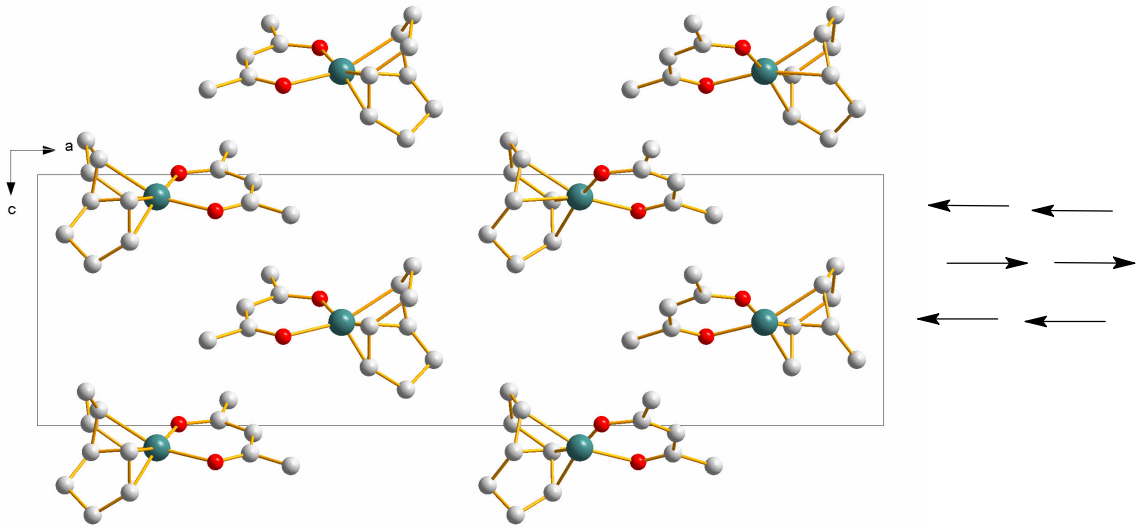

Figure 6.8 Head-to-tail packing.

6.4 Theoretical Correlation of Palladium(II) *vs.* Platinum(II) Complexes

In the periodic table, platinum and palladium fall into group 10, having a similar reaction properties one finds that both the metals prefer the square planar co-ordination with a d^8 electron configuration resulting in an oxidation state of +2. The atomic radii of platinum and palladium are 1.39 Å and 1.36 Å respectively (see Table 2.4). Nickel being the last of the group 10 metals also has a d^8 electron configuration though it does not have a preference for a specific co-ordination geometry with octahedral, trigonal bipyramidal, square pyramidal, tetrahedral and square planar all being observed. With this in mind we have limited the calculations for nickel to only the square planar geometry with a +2 oxidation state so as to compare it with the remainder of the metals in the group 10 triad. The atomic radius of nickel was found to be 1.24 Å (Table 2.4). With the similarity of the radii and configuration the relativistic effects are greatly reduced.

6.4.1 Visual Associations

The overlays of the X-ray crystal structures with the comparable calculated structures are a graphical representation of the pair-wise differences of the related structures. This mathematical value is represented by the root mean square (RMS) value, which is a measure of how far the average is from zero, providing information on the variations of bond lengths and angles and to a certain degree the orientation of the structures in relation to each other. These visual comparisons are presented in Figure 6.9-6.12.

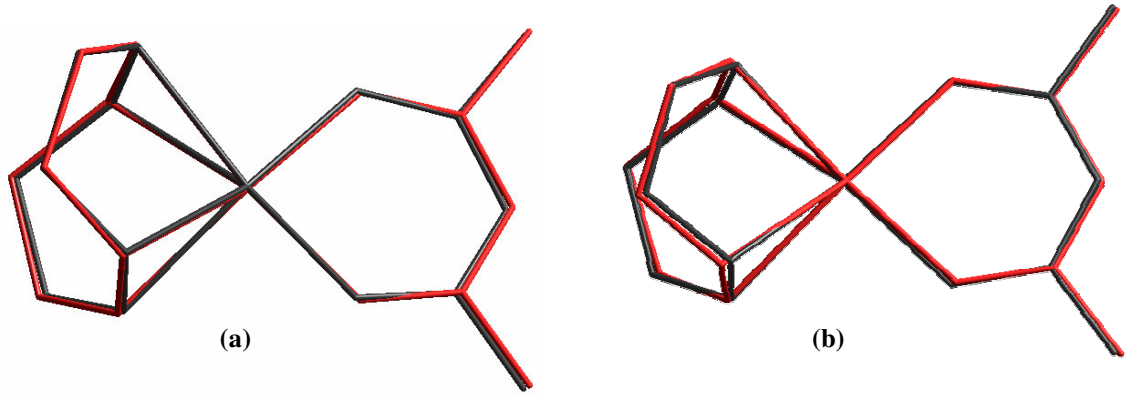

Figure 6.9 HyperChem superimposed image of (a) [Pd(cod)(acac)]BF_4 (2) (black) *vs.* [Pd(cod)(acac)]$^+$ (calculated) (red) with an RMS error of 0.07 Å (b) [Pd(cod)(acac)]PF_6 (1) (black) *vs.* [Pd(cod)(acac)]$^+$ (calculated) (red) with an RMS error of 0.087 Å. The counter ions of the X-ray crystal structures have been omitted for clarity.

An overlay of the X-ray crystal structures of [Pd(cod)(acac)]BF_4 (**2**) and [Pd(cod)(acac)]PF_6 (**1**) with the optimized computational structure is presented in Figure 6.9 with RMS error values of 0.07 Å and 0.09 Å respectively with all atoms except the methyl carbons of the acetylacetonato ligand.

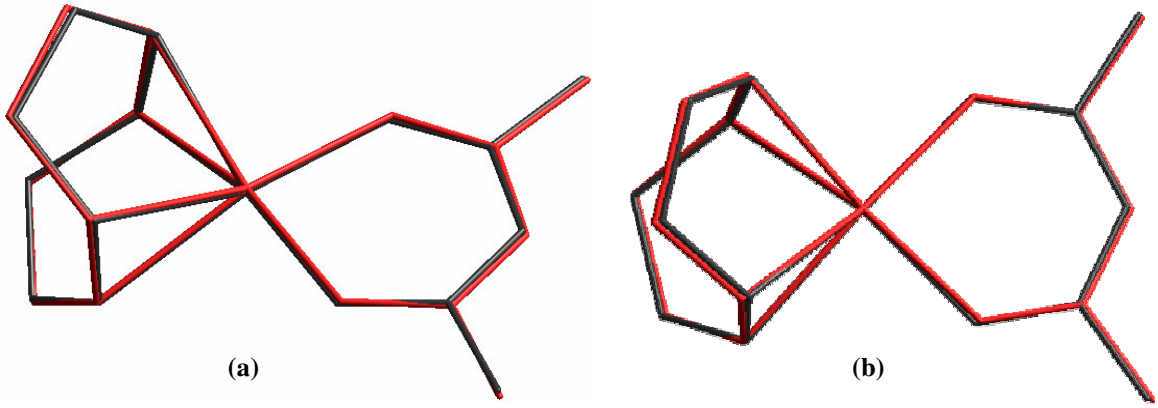

Figure 6.10 HyperChem superimposed image of (a) [Pt(cod)(acac)]BF_4 (7) (black) *vs.* [Pt(cod)(acac)]$^+$ (calculated) (red) with an RMS error of 0.067 Å (b) [Pt(cod)(acac)]PF_6 (8) (black) *vs.* [Pt(cod)(acac)]$^+$ (calculated) (red) with an RMS error of 0.076 Å. The counter ions of the X-ray crystal structures have been omitted for clarity.

An overlay of the X-ray crystal structures of [Pt(cod)(acac)]BF_4 (**7**) and [Pt(cod)(acac)]PF_6 (**8**) with the optimized computational structure is presented in Figure 6.10 with RMS error values of 0.07 Å and 0.08 Å respectively shows an excellent agreement with the optimized structure.

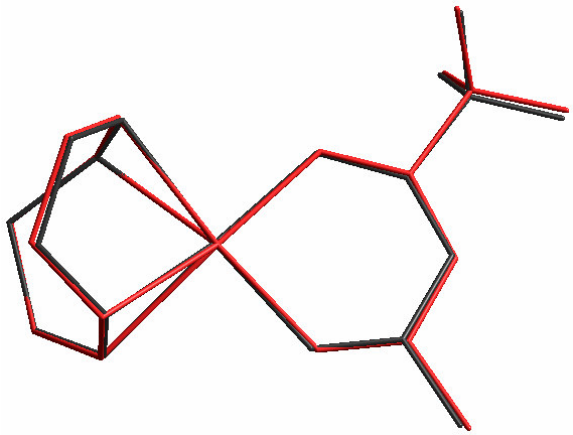

Figure 6.11 HyperChem superimposed image of [Pd(cod)(tfacac)]PF_6 (5) (black) *vs.* [Pd(cod)(tfacac)]$^+$ (calculated) (red) with an RMS error of 0.53 Å. The counter ions of the X-ray crystal structures have been omitted for clarity.

Although the RMS error for [Pd(cod)(tfacac)]PF_6 (**5**) and [Pd(cod)(tfacac)]$^+$ (Figure 6.11) was found to be 0.53 Å for all atoms except the methyl and CF_3 groups of the trifluoroacetylacetonato (tfacac) ligand, was higher than anticipated. The reason for the increased RMS error value is that the crystal data of the [Pd(cod)(tfacac)]PF_6 was taken from a less than ideal crystal (§ 4.3.3). Even with the errors known in the crystal system a good correlation was observed for the "core" bond angles and distances (§ 6.4.2 Figure 6.14).

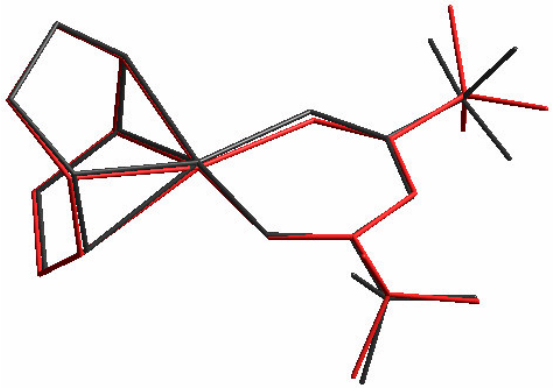

Figure 6.12 HyperChem superimposed image of [Pd(cod)(hfacac)]PF_6 (6) (black) *vs.* [Pd(cod)(hfacac)]$^+$ (calculated) (red) with an RMS error of 0.76 Å. The counter ions of the X-ray crystal structures have been omitted for clarity.

In the overlay of [Pd(cod)(hfacac)]PF_6 (**6**) with [Pd(cod)(hfacac)]$^+$ an RMS error value of 0.76 Å was obtained, although this is not as high as expected it is still above the accepted value. The reasons for this increase are the disorder found for the CF_3 moiety (§ 4.3.4 Figure 4.30)

6.4.2 Crystal Structure vs. Computed Structure Bond Relationships

In comparing the computed structures with their respective X-ray crystal structures only select bond distances and angles were chosen. The bond lengths and angles selected were those comprising of the "core" co-ordination geometry and the entire cyclo-octadiene ring so as to be able to compute the χ and ψ angles. The "core" co-ordination geometry is simply the bonds directly co-ordinated to the metal centre.

The *R*-values are given as a measure of the average accuracy of the computed (gas phase) bond lengths (Å) and angles (°) with the experimental crystal data (solid state) obtained. The following expression was used to calculate the *R*-values

$$R = n^{-1}\sum_{1\rightarrow n}^{i} x_{e_i} - \left| x_{c_i} - x_{e_i} \right| \Big/ x_{e_i}$$

with n = number of data points, x_e = experimental data and x_c = calculated data.

The following graphs (Figure 6.13-6.12) and tables (Table 6.5 and 6.6) represent the general degree of accuracy between calculated structures and experimental values with an average *R*-value of ≥ 98 %. Within the graphs the insert values are the actual calculated *R*-values for the complexes presented, the table that follows the graphs are the plotted values.

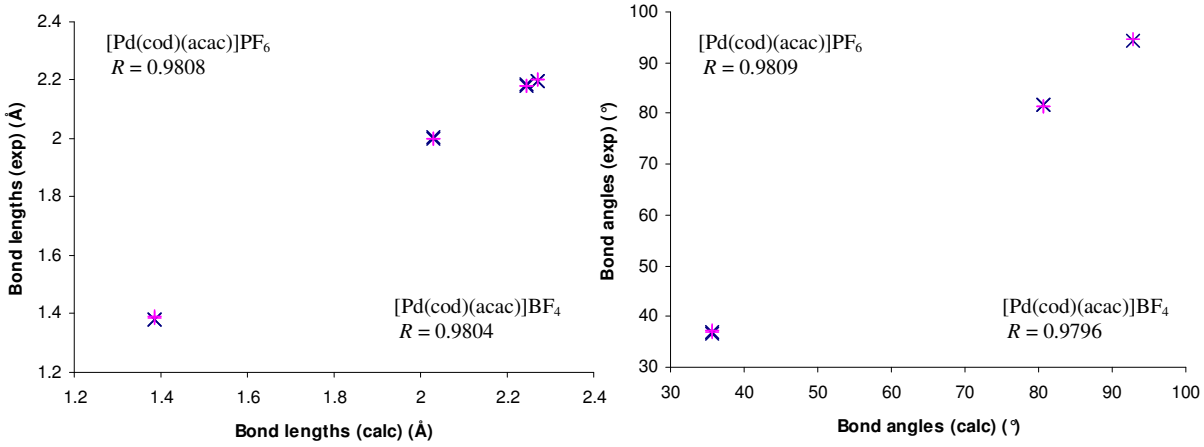

Figure 6.13 Graph of experimental *vs.* calculated bond lengths (Å) and angles (°) for [Pd(cod)(acac)]A where A = PF_6 (1) (pink plus sign) and BF_4 (2) (blue multiplication sign) with the calculated *R*-values shown, plotted values are given in Table 6.5 columns 1-3.

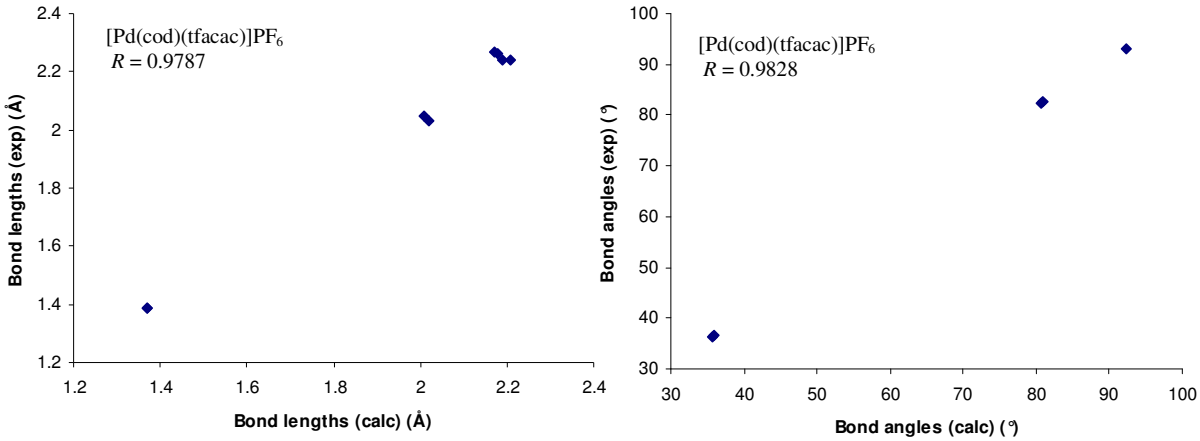

Figure 6.14 Graph of experimental *vs.* calculated bond lengths (Å) and angles (°) for [Pt(cod)(tfacac)]PF_6 (5) with the calculated *R*-value top left, plotted values are given in Table 6.5 columns 6 and 7.

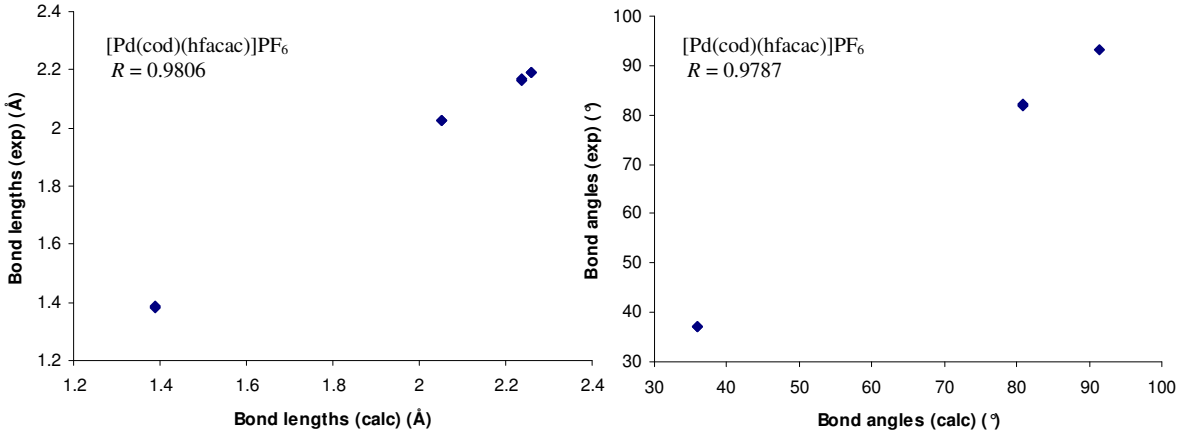

Figure 6.15 Graph of experimental *vs.* calculated bond lengths (Å) and angles (°) for [Pt(cod)(hfacac)]PF_6 (6) with the calculated *R*-value top left, plotted values are given in Table 6.5 columns 8 and 9.

Table 6.5 Selected geometric parameters (Å,°) for the palladium metal complexes

	[Pd(cod)(acac)]			[Pd(cod)(thtfac)]		[Pd(cod)(tfacac)]		[Pd(cod)(hfacac)]	
	PF_6 (**1**)	BF_4 (**2**)	calc	PF_6 (**5**)	BF_4 (**4**)	PF_6 (**5**)	calc	PF_6 (**6**)	calc
$Pd\text{-}O_1$	2.003(3)	2.001(3)	2.0299	2.007(11)	2.003(2)	2.007(11)	2.0460	2.027(2)	2.0503
$Pd\text{-}O_2$	2.001(3)	1.998(2)	2.0299	2.018(11)	2.005(2)	2.018(11)	2.0326	2.026(2)	2.0503
$Pd\text{-}C_1$	2.195(5)	2.202(3)	2.2696	2.171(14)	2.197(3)	2.171(14)	2.2677	2.191(3)	2.2606
$Pd\text{-}C_2$	2.181(4)	2.183(4)	2.2441	2.208(15)	2.176(3)	2.208(15)	2.2404	2.166(3)	2.2371
$Pd\text{-}C_5$	2.197(4)	2.205(3)	2.2696	2.180(16)	2.195(3)	2.180(16)	2.2629	2.190(3)	2.2606
$Pd\text{-}C_6$	2.189(4)	2.181(4)	2.2441	2.191(17)	2.175(3)	2.191(17)	2.2423	2.171(3)	2.2371
$C_1\text{-}C_2$	1.381(7)	1.386(7)	1.3837	1.37(2)	1.382(4)	1.37(2)	1.3852	1.387(4)	1.3878
$C_5\text{-}C_6$	1.380(6)	1.394(7)	1.3836	1.37(3)	1.385(4)	1.37(3)	1.3859	1.383(4)	1.3878
$O_1\text{-}Pd\text{-}O_2$	94.4(1)	94.5(1)	85.66	93.2(5)	93.27(8)	93.2(5)	92.349	93.06(8)	91.442
$C_1\text{-}Pd\text{-}C_2$	36.8(2)	36.8(2)	90.77	36.4(6)	36.9(1)	36.4(6)	35.784	37.13(10)	35.939
$C_5\text{-}Pd\text{-}C_6$	36.7(2)	37.1(2)	90.77	36.6(7)	36.9(1)	36.6(7)	35.827	36.98(10)	35.938
$C_1\text{-}Pd\text{-}C_6$	81.6(2)	81.5(2)	175.95	82.3(6)	82.3(1)	82.3(6)	80.784	82.02(10)	80.827
$C_2\text{-}Pd\text{-}C_5$	81.7(2)	81.4(1)	175.95	82.6(6)	81.9(1)	82.6(6)	80.899	81.99(10)	80.826
χ^a	86.0(3)	85.9(1)	84.784	86.8(6)	86.6(1)	86.8(6)	84.882	86.5(1)	84.904
ψ^b	81.9(3)	80.2(2)	84.929	86.9(9)	82.0(2)	86.9(9)	85.204	83.2(1)	84.972

a χ: $C_1MC_2 \cap C_5MC_6$ b ψ: $C_2C_3C_4C_5 \cap C_1C_8C_7C_6$ see Figure 1.2

For the platinum X-ray crystal structures the values for $[Pt(cod)(dbm)]BF_4$ (**9**) have been omitted as the crystal structure could not be solved satisfactorily due to the excessive twinning encountered for this crystal and have not been represented in Table 6.6.

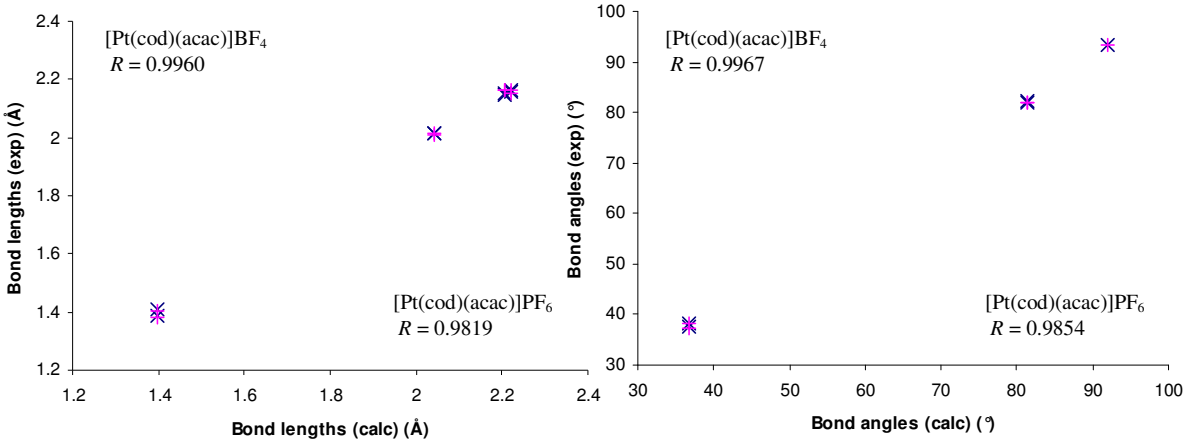

Figure 6.16 Graph of experimental *vs.* calculated bond lengths (Å) and angles (°) for [Pt(cod)(acac)]A where A = PF_6 (8) (pink plus sign) and BF_4 (7) (blue multiplication sign) with the calculated *R*-values shown, plotted values are given in Table 6.6 columns 1-3.

Table 6.6 Selected geometric parameters (Å,°) for the platinum metal complexes

	[Pt(cod)(acac)]			[Pt(cod)(thtfac)]
	BF_4 (**7**)	PF_6 (**8**)	calc	BF_4 (**10**)
Pt-O_1	2.015(3)	2.010(5)	2.0408	2.012(3)
Pt-O_2	2.013(3)	2.016(5)	2.0408	2.017(3)
Pt-C_1	2.160(3)	2.164(6)	2.2210	2.159(4)
Pt-C_2	2.153(4)	2.161(7)	2.2050	2.153(4)
Pt-C_5	2.164(3)	2.150(7)	2.2210	2.169(4)
Pt-C_6	2.147(4)	2.161(7)	2.2050	2.155(4)
C_1-C_2	1.388(8)	1.382(10)	1.3987	1.395(6)
C_5-C_6	1.411(8)	1.406(11)	1.3987	1.399(6)
O_1-Pt-O_2	93.5(1)	93.3(3)	91.95	92.3(1)
C_1-Pt-C_2	37.6(2)	37.3(3)	36.843	37.8(2)
C_5-Pt-C_6	38.2(2)	38.1(3)	36.843	37.8(2)
C_1-Pt-C_5	82.2(2)	82.0(3)	81.413	82.3(2)
C_2-Pt-C_6	82.0(2)	81.9(3)	81.413	82.2(2)
χ^a	86.9(2)	86.8(4)	85.927	87.4(1)
ψ^b	79.1(2)	78.9(5)	82.077	78.9(2)

a χ: $C_1MC_2 \cap C_5MC_6$ b ψ: $C_2C_3C_4C_5 \cap C_1C_8C_7C_6$ see Figure 1.2

Previously as was mentioned the counter ion do not play a significant role in the "core" bond distances and angles. It is clear from Table 6.5 and 6.6 that the calculated bond lengths are in excellent agreement with their experimental counterparts with the calculated values being slightly larger overall than the experimental values. This is assumed to be as a result of the calculations being in gas phase thus excluding intermolecular interactions which are present for the solid state.

Upon inspection of the *R*-values obtained and the overlays presented (§ 6.4.1) a good correlation between the computed structures and that of the experimental structures obtained was observed, leading to the conclusion that related structures computed data maybe extrapolated with a high degree of confidence.

6.4.3 Energies

In comparing the E_{corr} values of the computed complexes, found in Figure 6.17 with the data points given in Appendix C.5, these show a steady increase as the ligand becomes more electron withdrawing with only a slight change occurring as one moves down the triad.

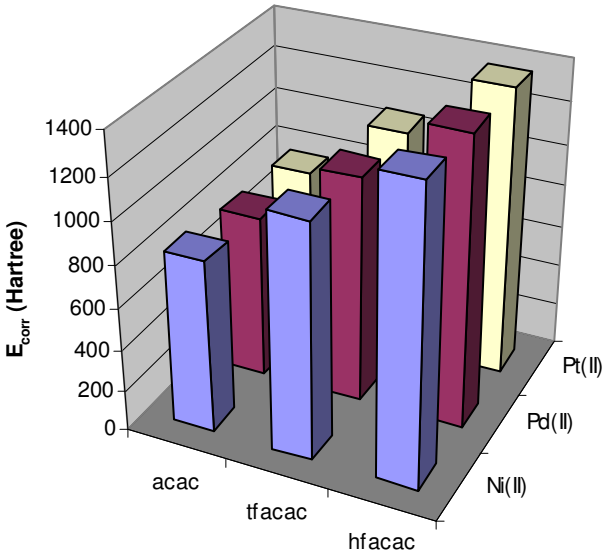

Figure 6.17 3D-graph of the total zero-point corrected energy (E_{corr}) for the computed complexes $[M(cod)(LL')]^+$ where M = group 10 transition metals and LL' = acac, tfacac, hfacac. Counter ions have not been calculated.

The E_{rel} values are calculated based on the relative energies of the complexes which are represented in Figure 6.18 with the data points given in Appendix C.6 and C.7 for the calculated structures, two general trends were observed. The first being where the energy values are corrected for the variation of metal centers, E_{rel}^{M} (Figure 6.18a).

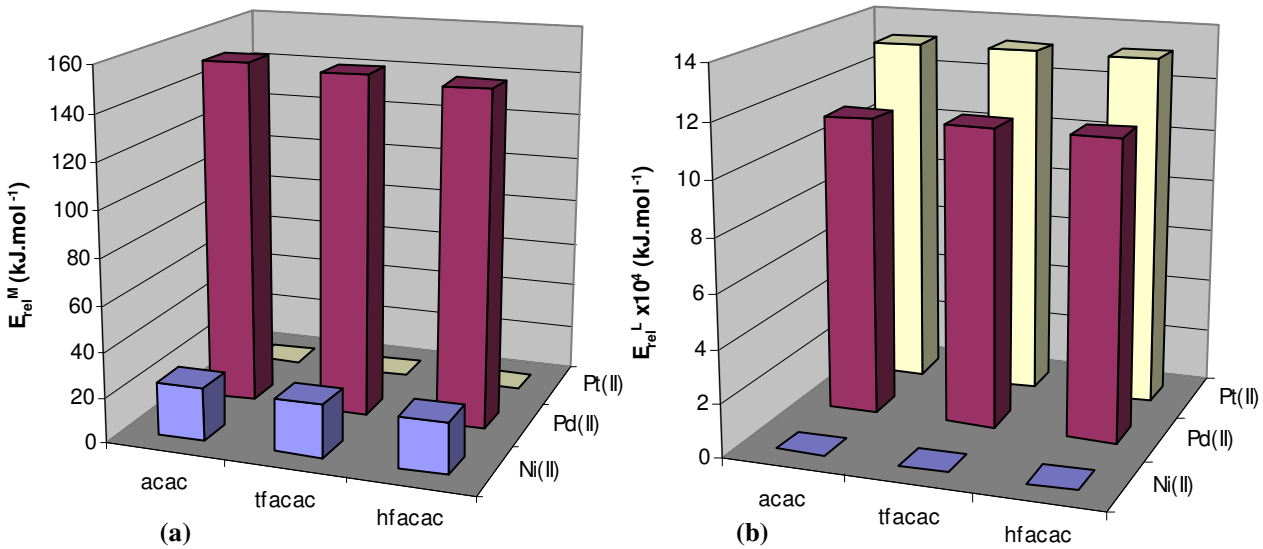

Figure 6.18 3D-graphs of the total energy relative to the appropriate metal centre (E_{rel}) for the calculated complexes (a) is corrected for metal centre (E_{rel}^{M}) and (b) is corrected for ligand (E_{rel}^{L}).

Here the series obtained where Ni(II) < Pd(II) >> Pt(II) the variance in these values are as a result of the increased reactivity of the palladium metal centre as opposed to that of platinum and nickel, with platinum having the lowest energy of the triad.

Yamamoto[16] proved this using neutral and cationic alkyl-, aryl-palladium and platinum complexes. For the graph in Figure 6.18b the energies are corrected by ligand, E_{rel}^{L}. A steady increase is observed Ni(II) < Pd(II) < Pt(II) as you proceed down the group 10 triad, with nickel having the lowest energy.

6.4.4 Infra-red Spectroscopic Correlations

The infra-red spectra of the calculated complexes are presented to gain a further insight into the bonding character of the complexes studied.

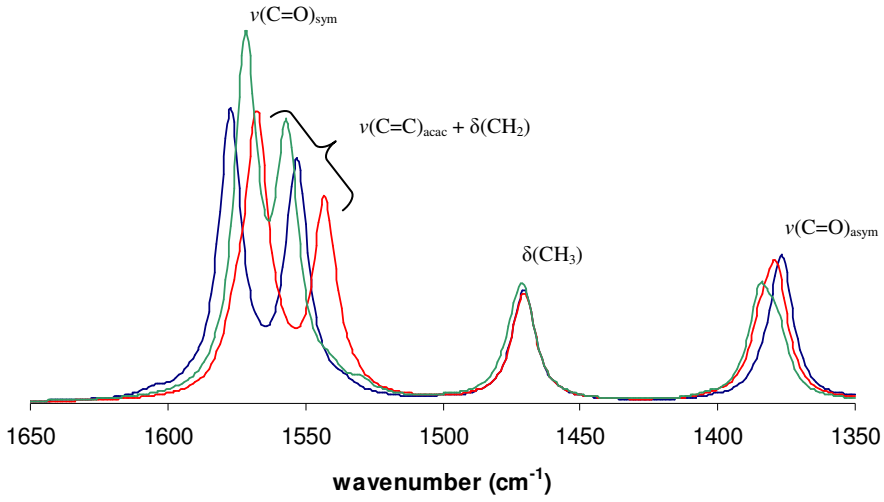

Figure 6.19 Calculated IR spectrum of [Ni(cod)(acac)]$^+$ (blue), [Pd(cod)(acac)]$^+$ (red) and [Pt(cod)(acac)]$^+$(green). *ν* – stretching, δ – in plane bending (rocking, scissoring).

In Figure 6.19 small changes to the symmetrical stretching frequencies (ν(C=O)$_{sym}$) of the co-ordinated conjugated ketone functionality of the acetylacetonato moiety with varying the group 10 metal centre is presented. A maximum difference of 8 cm^{-1} was found (1577 cm^{-1} – 1569 cm^{-1}). The other change that was observed is that of the stretching (ν(C=C)$_{acac}$) of the conjugated carbons of the acetylacetonato moiety.

[16] Yamamoto A., *J Organomet. Chem.*, **500**, 337, (1995)

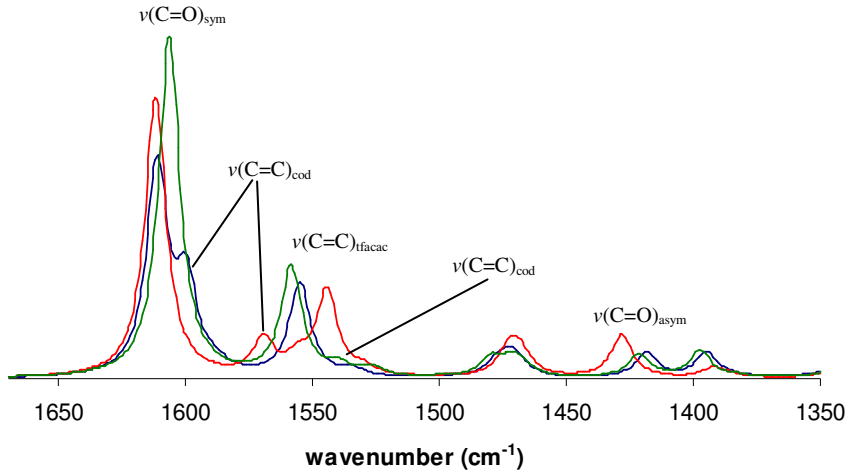

Figure 6.20 Calculated IR spectrum of $[Ni(cod)(tfacac)]^+$ (blue), $[Pd(cod)(tfacac)]^+$ (red) and $[Pt(cod)(tfacac)]^+$(green). *ν* – stretching.

For trifluoroacetylacetonato group 10 metal complexes there are only small changes observed for the symmetrical stretching frequencies ($\nu(C{=}O)_{sym}$) of the conjugated co-ordinated ketone functionality (1612 cm^{-1} – 1606 cm^{-1}) with a difference of 6 cm^{-1} which is smaller than that found for the acetylacetonato type complexes. Indicating that varying the metal centre only plays a marginal role in the shifting of the frequency. When comparing it to the acetylacetonato complexes we find that there is a shift up-field (35 cm^{-1}) as a result of the increasing electron withdrawing nature of the trifluoroacetonato ligand. The other difference found was that the symmetrical stretching frequencies ($\nu(C{=}C)_{cod}$) for the alkene carbons of the cyclo-octadiene ring have become slightly more prominent and are indicated in Figure 6.20.

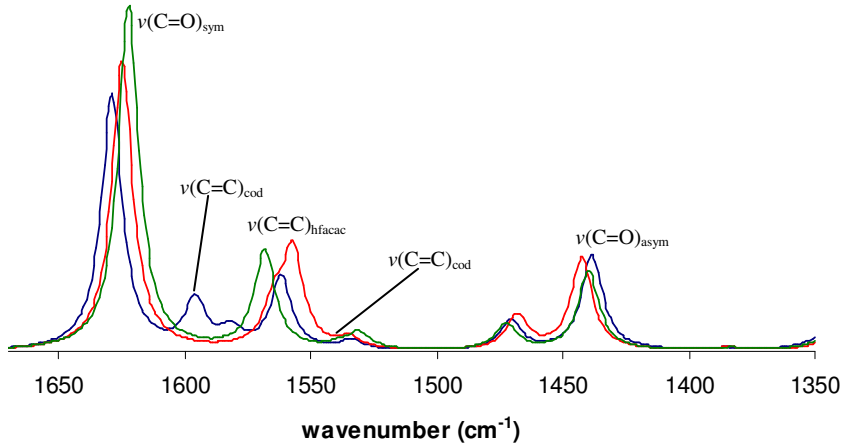

Figure 6.21 Calculated IR spectrum of $[Ni(cod)(hfacac)]^+$ (blue), $[Pd(cod)(hfacac)]^+$ (red) and $[Pt(cod)(hfacac)]^+$(green). *ν* – stretching.

For the hexafluoroacetylacetonato group 10 metal complexes there is an additional shift up-field (16 cm^{-1}) as a result of the increase in the electron withdrawing nature of the hexafluoroacetonato ligand. The changes observed for the symmetrical stretching frequencies ($\nu(C=O)_{sym}$) of the conjugated co-ordinated ketone are 1628 cm^{-1} – 1621 cm^{-1} with a difference of 7 cm^{-1}. For $[Pd(cod)(hfacac)]^+$ (red) the stretching frequency for the alkene carbons of the cyclo-octadiene are indicated as a shoulder to the $\nu(C=C)_{hfacac}$ peak.

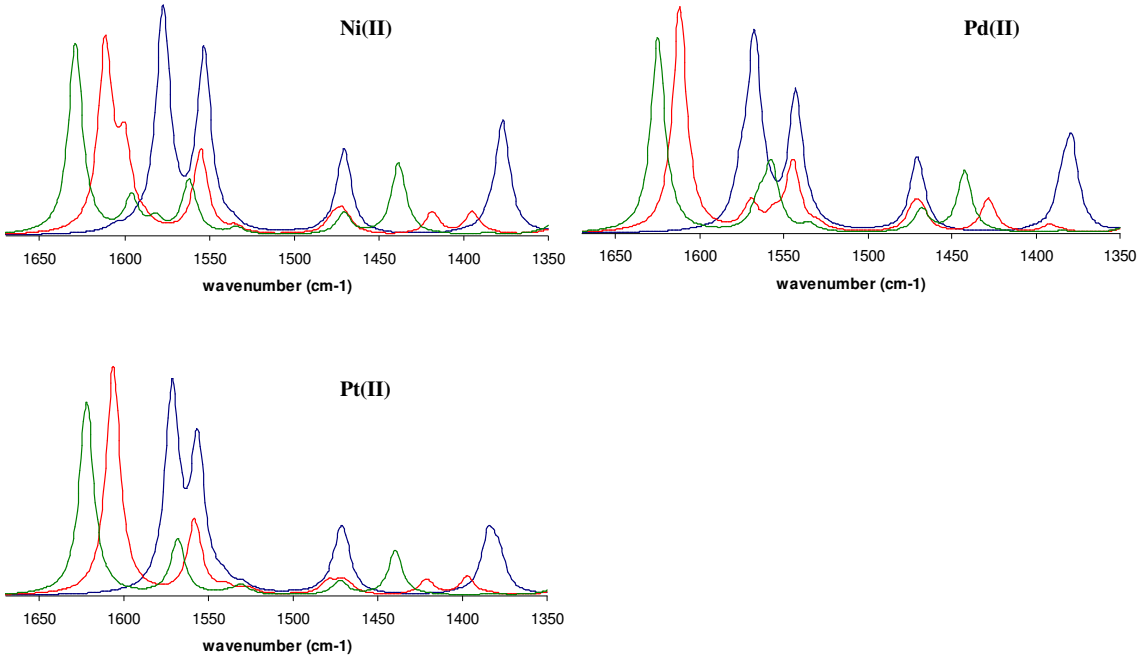

Figure 6.22 Calculated IR spectra of Ni(II), Pd(II) and Pt(II) with acac (blue), tfacac (red) and hfacac (green).

The trend observed in (Figure 6.19-6.20) is clearly shown in Figure 6.22 where as one increases the electron withdrawing nature of the ligand so the ketone stretching frequency is shifted up-field, Table 6.7 depicts the peak values of interest for the spectra presented.

Table 6.7 Selected IR values (cm^{-1}) for the group 10 metal complexes.

	$[Ni(cod)(A)]^+$			$[Pd(cod)(A)]^+$			$[Pt(cod)(A)]^+$		
	acac	tfacac	hfacac	acac	tfacac	hfacac	acac	tfacac	hfacac
$\nu(C=O)_{sym}$	1577.38	1611.46	1628.65	1568.76	1612.11	1624.75	1571.72	1606.14	1621.84
$\nu(C=C)_A$	1552.95	1554.93	1561.98	1543.29	1544.39	1557.44	1556.96	1558.04	1566.93
$\nu(C=C)_{cod}$		1599.74	1595.32		1569.79	1564.40		1539.38	1538.87
$\nu(C=O)_{asym}$	1376.62	1417.72	1438.46	1378.00	1428.71	1441.40	1384.23	1421.49	1440.04

6.4.5 Molecular Orbital Comparisons

The graphical representation of the molecular orbitals is another method whereby interactions of the cyclo-octadiene with the various metal centers and the trans ligands may be observed. The second-highest (HOMO-1) and highest (HOMO) occupied molecular orbitals and the lowest (LUMO) and second-lowest (LUMO+1) unoccupied molecular orbitals for the calculated complexes of $[M(cod)(LL')]^+$ where M = Ni, Pd, Pt and LL' = acac, tfacac, hfacac will be presented, along with the differences in the respective orbitals ($E_{g-1} \equiv \Delta|HOMO\text{-}1|\text{-}|HOMO|$; $E_g \equiv \Delta|HOMO|\text{-}|LUMO|$; $E_{g+1} \equiv \Delta|LUMO|\text{-}|LUMO+1|$). The contour plots shown with the molecular orbitals are viewed along the *z*-axis.

Table 6.8 Molecular Orbitals of calculated structures $[M(cod)(acac)]^+$.

	HOMO-1	HOMO	LUMO	LUMO+1
Ni(II)	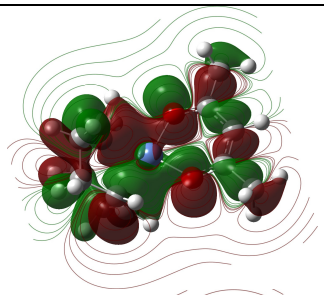	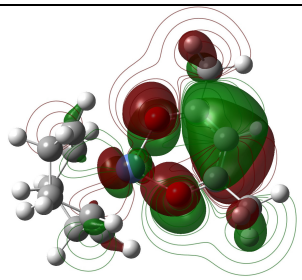	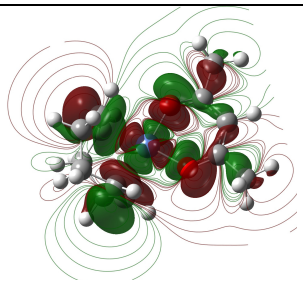	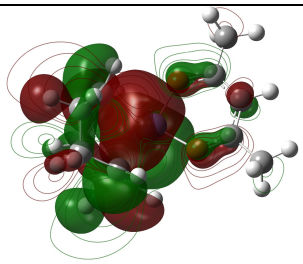
Pd(II)	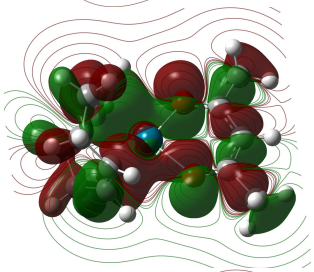	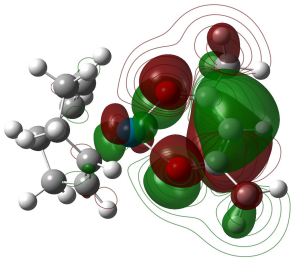	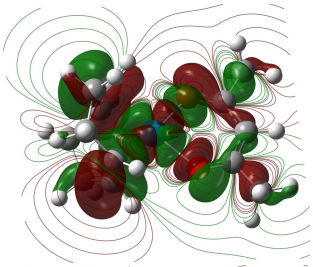	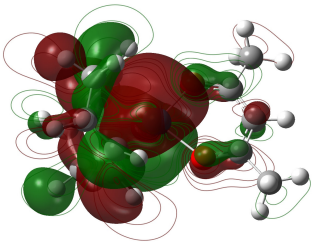
Pt(II)	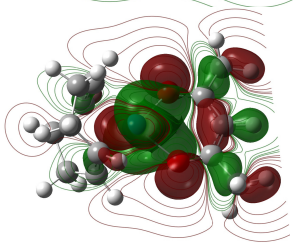	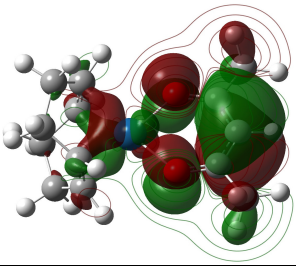	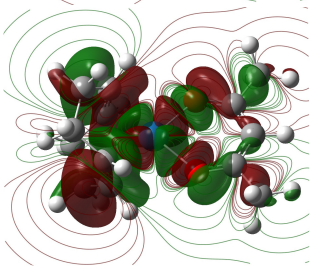	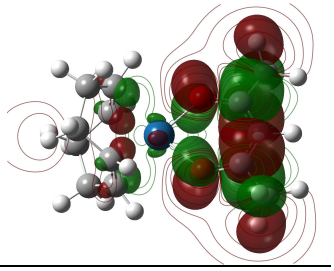

Table 6.9 Molecular Orbital Energies (Hartree) and energy gaps (eV) of the $[M(cod)(acac)]^+$ calculated structures.

	HOMO-1	HOMO	LUMO	LUMO+1	E_{g-1}	E_g	E_{g+1}
Ni(II)	-0.41512	-0.37704	-0.2485	-0.19038	1.036	3.498	1.582
Pd(II)	-0.41333	-0.37277	-0.24407	-0.18711	1.104	3.502	1.550
Pt(II)	-0.41536	-0.37796	-0.2089	-0.19198	1.018	4.600	0.460

In Table 6.8 the molecular orbitals for the group 10 metal acetylacetonato complexes are presented, their values are given in Table 6.9. The HOMO-1 molecular orbitals of nickel and palladium are comparable with π orbital delocalization occurring between both the cyclo-octadiene moiety and the acetylacetonato moiety. Platinum however only shows delocalization between the metal and the acetylacetonato moiety. For the HOMO molecular orbitals delocalization on the back-bone of the acetylacetonato moiety is seen for all three complexes, with the platinum complex showing some electron density around the cyclo-octadiene alkene carbons, with a d_{yz} orbital centered on the metals. A $d_{x^2-y^2}$ orbital is observed on the metal centers for the LUMO molecular orbitals.

The molecular orbitals of the HOMO level illustrate the orbitals that are used for back bonding in the cyclo-octadiene ligand. The additional orbitals around the oxygen are capable of shared hydrogen / fluorine interactions. The back bonding of the nickel complex was found to have minor back bonding capability whereas the palladium complex had almost none. This capability of back bonding is the reason why the platinum complexes are the most stable of the triad.

Table 6.10 Molecular Orbitals of calculated structures $[M(cod)(tfacac)]^+$.

	HOMO-1	HOMO	LUMO	LUMO+1
Ni(II)	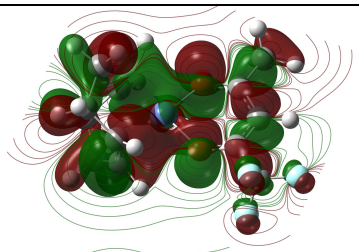	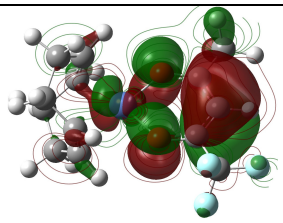	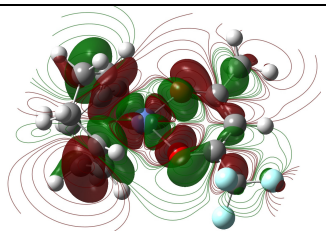	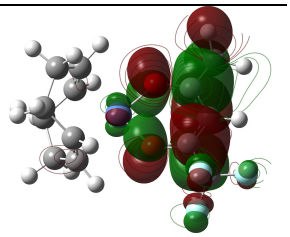
Pd(II)	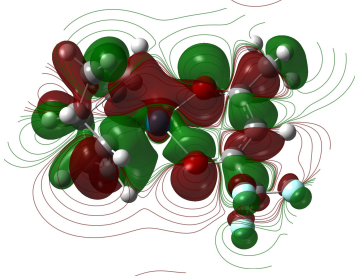	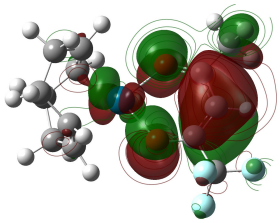	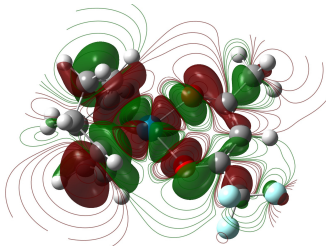	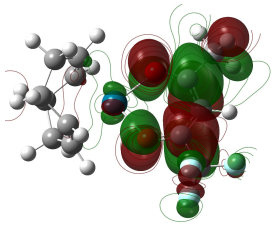
Pt(II)	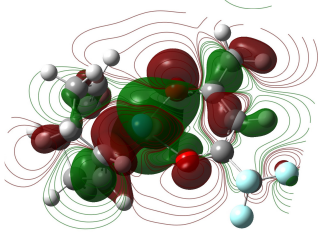	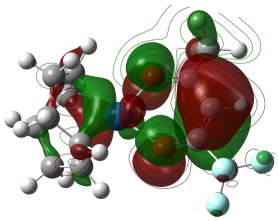	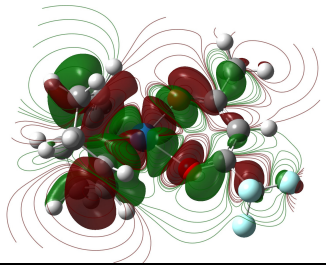	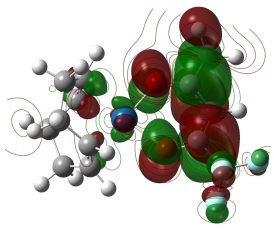

Table 6.11 Molecular Orbital Energies (Hartree) and energy gaps (eV) of the $[M(cod)(tfacac)]^+$ calculated structures.

	HOMO-1	HOMO	LUMO	LUMO+1	E_{g-1}	E_g	E_{g+1}
Ni(II)	-0.43120	-0.39845	-0.26550	-0.21647	0.891	3.618	1.334
Pd(II)	-0.42921	-0.39186	-0.26038	-0.20955	1.016	3.578	1.383
Pt(II)	-0.43061	-0.39882	-0.22539	-0.21889	0.865	4.719	0.177

In Table 6.10 the molecular orbitals for the group 10 metal trifluoroacetylacetonato complexes are presented, their values are given in Table 6.11. For the HOMO-1 molecular orbitals, for nickel and palladium π orbital delocalization can be seen between the cyclo-octadiene and trifluoroacetylacetonato (tfacac) ligands. The acetylacetonato (acac) group 10 metal complexes (Table 6.8) have a similar orbital pattern for the orbitals. The HOMO molecular orbitals have a d_{yz} orbital centered on the group metals, with an in-phase overlap of these with the *p* orbitals of the cyclo-octadiene, this overlap is most pronounced for platinum. A $d_{x^2-y^2}$ orbital is observed on the metal centers for the LUMO molecular orbitals. The only difference observed between the acetylacetonato complexes (Table 6.8) and that of the trifluoroacetylacetonato complexes (Table 6.10) are the *p* orbitals which are present

on the flourines of the ligand seen in the LUMO molecular orbitals. These orbitals however do not play any significant role in the bonding

Table 6.12 Molecular Orbitals of calculated structures [M(cod)(hfacac)]$^+$.

	HOMO-1	HOMO	LUMO	LUMO+1
Ni(II)	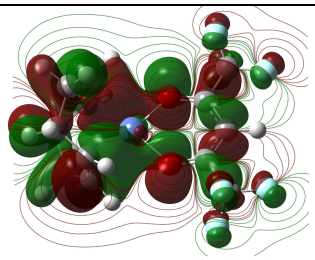	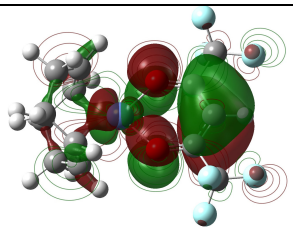	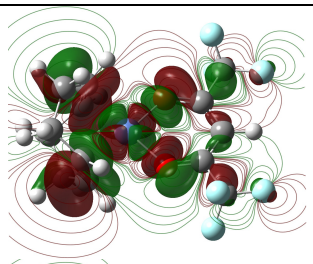	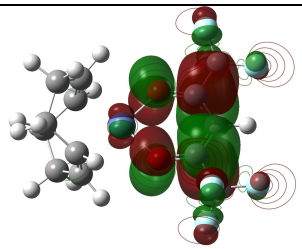
Pd(II)	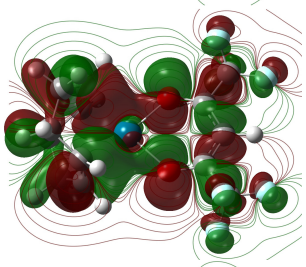	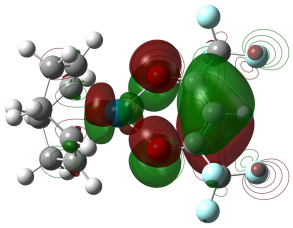	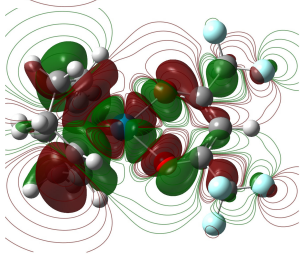	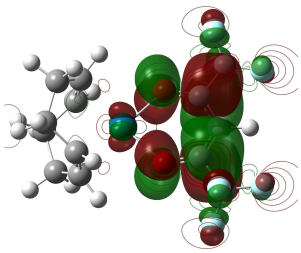
Pt(II)	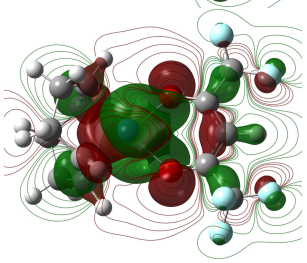	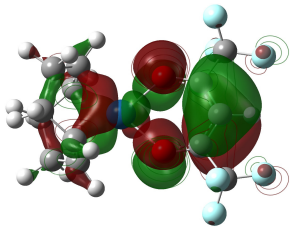	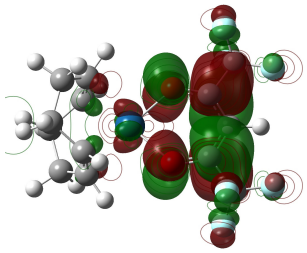	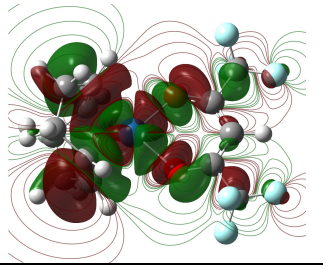

Table 6.13 Molecular Orbital Energies (Hartree) and energy gaps (eV) of the [M(cod)(hfacac)]$^+$ calculated structures.

	HOMO-1	HOMO	LUMO	LUMO+1	E_{g-1}	E_g	E_{g+1}
Ni(II)	-0.44688	-0.41904	-0.28213	-0.24358	0.758	3.726	1.049
Pd(II)	-0.44519	-0.41317	-0.27726	-0.23849	0.871	3.698	1.055
Pt(II)	-0.44604	-0.41874	-0.24547	-0.24215	0.743	4.715	0.090

In Table 6.12 the molecular orbitals for the group 10 metal hexafluoroacetylacetonato (hfacac) complexes are presented, their values are given in Table 6.13. For the HOMO-1 molecular orbitals, π orbital delocalization is seen for the nickel and palladium complexes with a d_{z^2} orbital for platinum. In the HOMO molecular orbitals, the d_{xy} orbital is centered on the metals whilst an in-phase overlap of the p_y obitals of the oxygens of the hfacac ligand is observed. This orbital pattern is also found for the acetylacetonato (acac) (Table 6.8) and trifluoroacetylaceonato (tfacac) (Table 6.10) complexes. In the LUMO molecular orbitals, a $d_{x^2-y^2}$ orbital is seen on the nickel and palladium metals, with an in-phase overlap of the d_{xy} orbitals of the

platinum metal and p_y orbitals of the hfacac ligand. For the LUMO+1 molecular orbitals, the *p* orbitals for the fluorine atoms of the hfacac ligand are seen whilst π-orbital delocalization is seen in the carbon back-bone of the ligand and the p_y orbitals of the oxygens overlap with the d_{xy} orbitals of the nickel and palladium metal. With platinum having a $d_{x^2-y^2}$ orbital.

6.4.6 Venus fly-trap (χ and ψ) Angle Evaluation

Figure 6.23 shows the correlation of the different nickel(II) triad complexes comparison of the χ and ψ angles.

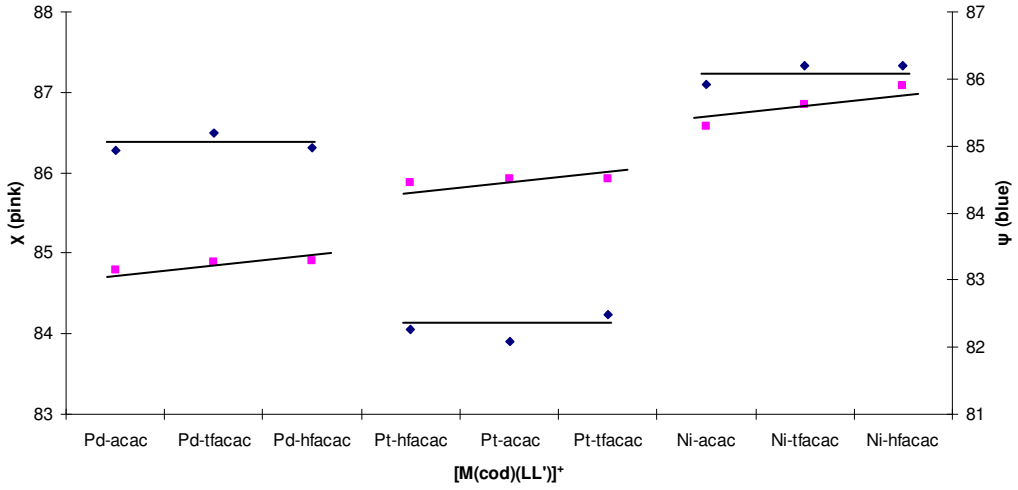

Figure 6.23 Graph of Nickel(II), Palladium(II) and Platinum(II) calculated complexes *vs.* χ (pink squares) and ψ (blue diamonds) angles (see Chapter 1 Figure 1.2 for definition of χ and ψ angles).

In Figure 6.23 it is found that there is a general increase in the χ angle as the ligand is varied from acetylacetonato (acac) to trifluoroacetylacetonato (tfacac) and lastly to hexafluoroacetylacetonato (hfacac) for a specific metal. In looking at the variation of the metal centers it is observed that there is still an increasing χ angle trend as one proceeds down the triad. A maximum difference in the ψ angle of 4.1° was found between the [Ni(cod)(hfacac)] and [Pt(cod)(acac)] complexes.

In overview a good correlation was found between the x-ray crystal structures and that of the computed compounds. The χ and ψ angles show a steady increase in the χ angle with and opening and closing of the ψ angle. The molecular orbital diagrams

show the influence of back bonding on the different metal centers as well as the various six membered conjugate co-ordination ligands.

The infra-red spectra showed that the change in the metal centre was not as great an influence on the *ν*(C=O) stretching frequency as that of the change in the co-ordinating ligands. This was to be expected as the series that was chosen had an increasing electron withdrawing capability.

This lead to the question of would five membered conjugated ligands follow the same trends as observed for the six membered conjugated ligands. In the following chapter the crystal structures of these five membered conjugated co-ordinated ligands are presented.

Chapter 7
Crystallographic Study of Tropolonato Type Complexes of Palladium(II) and Platinum(II)

7.1 Introduction

In this chapter crystals of the bidentate five membered ring class of complexes are reported. The ligands that have been chosen are tribromotropolone and tropolone with the palladium(II) and platinum(II) metal centers.

The complexes that were prepared as described in § 3.4.2 and 3.5.2 were analyzed by single crystal X-ray crystallography and the results were summarized in Table 7.1. A diagram indicating the numbering scheme of each compound is presented, along with selected bond lengths and angles, hydrogen bonding interactions and additional interactions if applicable. A discussion highlighting some of the important aspects of each particular structure is presented thereafter.

Additional correlations with other structures and theoretical calculated structures are done in Chapter 8 whilst complete lists of the crystal structures presented in this chapter are given in the supplementary data.

7.2 Experimental

Data collections for [Pt(cod)(3Br-trop)]PF_6, [Pt(cod)(trop)]PF_6, [Pd(cod)(3Br-trop)]BF_4, and [Pd(cod)(trop)]PF_6, and [Pd(cod)(3Br-trop)]BF_4 were obtained on a Bruker Apex II 4K CCD diffractometer. The data for [Pd(cod)(3Br-trop)]PF_6 and [Pt(cod)(trop)]BF_4 were collected on an Oxford Diffraction Xcalibur 3 Crysalis CCD system[1]. Both systems were equipped with a graphite-monochromated Mo Kα radiation, for the Bruker system all the reflections were merged and integrated with

[1] Crysalis CCD. Oxford Diffraction Ltd., Abingdon, Oxfordshire, U.K., (2005)

SAINT-PLUS[2] and corrected for Lorentz, polarization and absorption effects with SADABS[3], while Crysalis RED[4] was used for the Oxford system.

Structures were solved by direct and conventional Patterson methods using the SHELX-97[5] as part of the WinGX[6] package, and anisotropic refinement was performed on all non-hydrogen atoms by a full-matrix least-squares method. The positions of the hydrogen atoms were calculated using a riding model to the adjacent carbon, unless otherwise stipulated. Hydrogen interactions were calculated using the PLATON[7,8,9] and PARST[10] programs. Molecular graphics were obtained using DIAMOND[11], while overlay graphics were illustrated using HyperChem 7.5[12].

[2] Bruker SAINT-PLUS (including XPREP), Version 7.12, Bruker AXS Inc., Madison, WI., (2004)
[3] Bruker SADABS (Version 2004/1), Bruker AXS Inc., Madison, WI., (1998)
[4] Crysalis RED Oxford Diffraction Ltd., Abingdon, Oxfordshire, U.K., (2005)
[5] Sheldrick G.M., *Acta Cryst.*, **A64**, 112, (2008)
[6] Farrugia L.J., *Appl. Cryst.*, **32**, 837, (1999)
[7] Spek A.L., PLATON A multipurpose crystallographic tool, Utrecht University, Utrecht, Netherlands, (2005)
[8] Speck A.L., *J. Appl. Cryst.*, **36**, 7, (2003)
[9] Speck A.L., *Acta Cryst*, **D65**, 148, (2009)
[10] Nardelli M., *J. Appl. Cryst.*, **28**, 659, (1995)
[11] Brandenburg K., Brendt M., DIAMOND, Release 2.1e. Crystal Impact GbR, Potfach 1251, D53002 Bonn, Germany., (2001)
[12] HyperChem™ Release 7.52, Windows Molecular Modeling System, HyperCube Inc., (2002)

Table 7.1 Crystallographic data and refinement parameters where A = PF_6 or BF_4

Crystal Data	[Pd(cod)(3Br-trop)]A PF_6 (**11**)	BF_4 (**12**)	[Pd(cod)(trop)]A PF_6 (**13**)	[Pt(cod)(trop)]A PF_6 (**14**)	BF_4 (**15**)	[Pt(cod)(3Br-trop)]A PF_6 (**16**)	BF_4 (**17**)
Empirical formula	C_{15} H_{14} Br_3 F_6 O_2 P Pd	C_{15} H_{14} B Br_3 F_4 O_2 Pd	C_{15} H_{17} F_6 O_2 P Pd	C_{15} H_{17} F_6 O_2 P Pt	C_{15} H_{17} B F_4 O_2 Pt	C_{15} H_{14} Br_3 F_6 O_2 P Pt	C_{15} H_{14} B Br_3 F_4 O_2 Pt
Formula weight	717.36	659.20	480.66	569.35	511.19	806.05	747.89
Temperature (K)	100(2)	100(2)	100(2)	100(2)	293(2)	100(2)	100(2)
Wavelength (Å)	0.71073	0.71073	0.71073	0.71073	0.71073	0.71073	0.71073
Crystal system	Triclinic	Triclinic	Tetragonal	Tetragonal	Tetragonal	Monoclinic	Triclinic
Space group	$P\bar{1}$	$P\bar{1}$	$P4_2bc$	$P4_2/mbc$	$P4_2bc$	$C2/c$	$P\bar{1}$
Unit cell dimensions							
a (Å)	7.8517(10)	7.3729(7)	16.3117(15)	16.3729(3)	16.0818(1)	11.3615(18)	7.3583(6)
b (Å)	8.0071(12)	8.0026(7)	16.3117(15)	16.3729(3)	16.0818(1)	11.0127(16)	8.0058(6)
c (Å)	15.666(2)	15.9253(16)	11.9226(14)	12.0226(2)	11.9361(2)	31.056(5)	15.9652(10)
α (°)	79.000(12)	85.783(4)	90	90	90	90	86.181(6)
β (°)	88.357(10)	85.387(4)	90	90	90	93.456(3)	85.082(6)
γ (°)	87.737(11)	82.074(5)	90	90	90	90	81.724(7)
Volume ($Å^3$)	965.8(2)	925.78(15)	3172.3(6)	3222.92(10)	3086.96(6)	3878.6(10)	925.87(12)
Z	2	2	8	8	8	8	2
Density (calculated) ($Mg.m^{-3}$)	2.467	2.365	2.013	2.053	2.200	2.761	2.683
Absorption coefficient (mm^{-1})	7.315	7.522	1.343	7.768	9.138	13.565	14.097
F(000)	680	624	1904	1890	1936	2976	688
Crystal size (mm^3)	0.23 x 0.08 x 0.05	0.44 x 0.08 x 0.07	0.28 x 0.07 x 0.06	0.27 x 0.07 x 0.06	0.31 x 0.08 x 0.05	0.32 x 0.14 x 0.04	0.26 x 0.08 x 0.08
Theta range for data collection (°)	2.59 to 33.01	1.29 to 28.33	1.77 to 23.08	1.76 to 28.00	2.53 to 28.00	1.31 to 25.98	2.56 to 27.00
Index ranges	-11<=h<=11, -12<=k<=8, -24<=l<=21	-9<=h<=8, -8<=k<=10, -21<=l<=21	-17<=h<=17, -17<=k<=17, -13<=l<=13	-21<=h<=21, -21<=k<=21, -14<=l<=15	-21<=h<=21, -21<=k<=21, -7<=l<=15	-13<=h<=13, -13<=k<=13, -37<=l<=38	-9<=h<=8, -8<=k<=10, -19<=l<=20
Reflections collected	9396	16759	33777	42276	23083	17233	6850
Independent reflections	6209 [R(int) = 0.0481]	4489 [R(int) = 0.0500]	2205 [R(int) = 0.0921]	2044 [R(int) = 0.0453]	2449 [R(int) = 0.0426]	3790 [R(int) = 0.0594]	3912 [R(int) = 0.0285]
Completeness to θ (°; %)	33.01, 85.3	28.33, 97.2	23.08, 99.6	28.00, 100.0	28.00, 99.8	25.98, 99.5	27.00, 96.7
Max. and min. transmission	0.7112 and 0.2840	0.6287 and 0.1365	0.9237 and 0.7048	0.6529 and 0.2282		0.6130 and 0.0979	0.4103 and 0.1227
Refinement method	Full-matrix least-squares on F^2	Full-matrix least-squares on F^2	Full-matrix least-squares on F^2	Full-matrix least-squares on F^2	Full-matrix least-squares on F^2	Full-matrix least-squares on F^2	Full-matrix least-squares on F^2
Data / restraints / parameters	6209 / 0 / 253	4489 / 0 / 235	2205 / 1 / 222	2044 / 89 / 117	2449 / 192 / 202	3790 / 0 / 253	3912 / 0 / 235
Goodness-of-fit on F^2	1.025	1.060	1.155	1.113	1.001	1.207	0.968
Final R indices [I>2σ(I)]	R_1 = 0.0590, wR_2 = 0.1764	R_1 = 0.0340, wR_2 = 0.0728	R_1 = 0.0408, wR_2 = 0.0885	R_1 = 0.0345, wR_2 = 0.0925	R_1 = 0.0291, wR_2 = 0.0678	R_1 = 0.0438, wR_2 = 0.1205	R_1 = 0.0266, wR_2 = 0.0567
R indices (all data)	R_1 = 0.1057, wR_2 = 0.1889	R_1 = 0.0579, wR_2 = 0.0948	R_1 = 0.0431, wR_2 = 0.0926	R_1 = 0.0466, wR_2 = 0.1107	R_1 = 0.0498, wR_2 = 0.0776	R_1 = 0.0598, wR_2 = 0.1554	R_1 = 0.0371, wR_2 = 0.0596
Largest diff. peak and hole ($e.Å^{-3}$)	1.518 and -1.068	0.980 and -1.044	0.504 and -0.566	1.082 and -1.007	1.220 and -0.717	1.294 and -2.549	1.313 and -1.368

7.3 X-Ray Structures of Palladium(II) Complexes

7.3.1 Crystal structures of [Pd(cod)(3Br-trop)]PF_6 and [Pd(cod)(3Br-trop)]BF_4

The compounds, [Pd(cod)(3Br-trop)]BF_4 (**12**) and [Pd(cod)(3Br-trop)]PF_6 (**11**) both crystallize in the triclinic space group $P\bar{1}$, with a cationic [Pd(cod)(3Br-trop)]$^+$ species (**11a** or **12a**) and an anionic BF_4^- (**12b**) or PF_6^- (**11b**) species in the asymmetric unit. The numbering scheme is presented in Figure 7.1, while atomic co-ordinates, bond angles and distances, anisotropic displacement parameters and hydrogen co-ordinates are reported in Appendix B.2 and B.3. General crystallographic data and refinement parameters are reported in Table 7.1, while significant bond angles and distances are reported in Table 7.2.

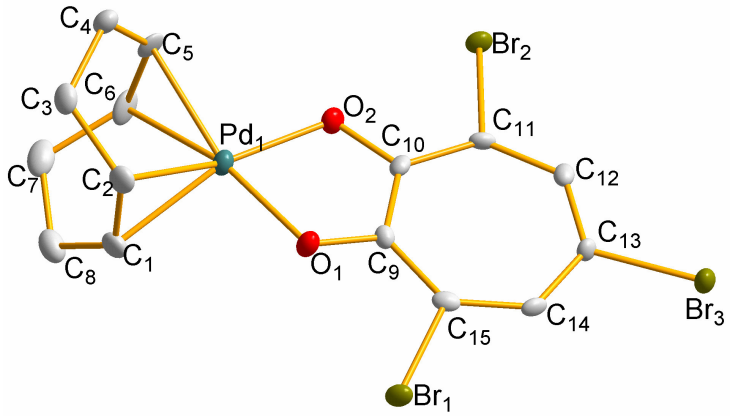

Figure 7.1 Diamond illustration of [Pd(cod)(3Br-trop)]BF_4 (12) at 100 K showing the numbering scheme and displacement ellipsoids (50 %) of the complex. Hydrogen atoms and anionic species omitted for clarity.

Table 7.2 Selected bond distances and angles for [Pd(cod)(3Br-trop)]A (where A = BF_4 and PF_6)

Bond Distance (Å)	Counter ion		Bond Angles (°)	Counter ion	
	BF_4 (**12**)	PF_6 (**11**)		BF_4 (**12**)	PF_6 (**11**)
Pd-O_1	2.003(3)	2.047(6)	O_1-Pd-O_2	80.6(1)	80.1(2)
Pd-O_2	2.023(3)	2.002(6)	C_1-Pd-C_2	37.1(2)	36.8(3)
Pd-C_1	2.180(5)	2.193(8)	C_5-Pd-C_6	36.8(2)	37.9(3)
Pd-C_2	2.177(5)	2.182(8)	C_1-Pd-C_6	81.4(2)	80.5(3)
Pd-C_5	2.176(5)	2.178(9)	C_2-Pd-C_5	82.3(2)	81.6(3)
Pd-C_6	2.201(5)	2.165(8)	χ^a	86.1(1)	85.6(3)
C_1-C_2	1.387(7)	1.382(12)	ψ^b	83.8(2)	79.7(4)
C_5-C_6	1.381(7)	1.410(11)			

a χ: $C_1MC_2 \cap C_5MC_6$ b ψ: $C_2C_3C_4C_5 \cap C_1C_8C_7C_6$ see Figure 1.2

Square planar geometry is observed around the metal centre for both the **11a** and **12a** species. The Pd-O bonds for **12a** are non-equivalent and vary 0.02 Å from each other

with an average value of 2.013(3) Å. This is as a result of transference from the alkene bond which has a bromine intermolecular hydrogen bond (Figure 7.2), which elongates the Pd-C_6 bond (2.201(5) Å) which in turn elongates the Pd-O_2 (2.023(3) Å) bond. The C=C bond distances are found to be equivalent with a mean distance of 1.384(7) Å. The oxygen palladium oxygen bite angle is 80.6(1)° which is consistent for a five membered ring. The angle between the planes defined by the tropolone ring and the palladium, oxygen and adjacent carbons is twisted by 6.7(1)° is a measure of the planarity of the complex.

For the **11a** complex the C=C bond distances remained equivalent with a mean distance of 1.39(1) Å. The Pd-O bond distances were found to be non-equivalent varying by 0.045 Å with an average of 2.025(6) Å this as a result of the increasing influence of the hexafluorophosphate counter ion. The O-Pd-O bite angle (80.1(2)°) however is not greatly affected. The average distance of Pd-C was found to be 2.180(8) Å. The angle between the planes defined by palladium, oxygens and the two carbons of the tropolone ring and the tropolone ring is 3.6(2)° showing an increase in the planarity of the complex in relation to the **12a** complex, this reduction is due to the size and influence of the counter ions present.

The hydrogen bonding of complex **12** is graphically presented in Figure 7.3 and 7.3 with Table 7.3 listing the bond distances and angles.

Table 7.3 Hydrogen bond distances and angles for [Pd(cod)(3Br-trop)]BF_4 (12) [Å and °]

D-H...A	d(D-H)	d(H...A)	d(D...A)	<(DHA)
C_2-H_2...F_2	1.00	2.42	3.192(6)	134.0
C_3-H_{3B}...$F_2^{\#1}$	0.99	2.52	3.427(6)	152.8
C_6-H_6...$Br_1^{\#2}$	1.00	2.90	3.765(5)	145.1
C_{12}-H_{14}...$F_1^{\#3}$	0.95	2.46	3.401(6)	168.3
C_8-H_{8B}...$F_3^{\#4}$	0.99	2.48	3.257(6)	135.6

Symmetry transformations used to generate equivalent atoms:
#1 -x,-y+1,-z #2 x+1,y,z #3 -x,-y+1,-z+1 #4 x+1,y-1,z

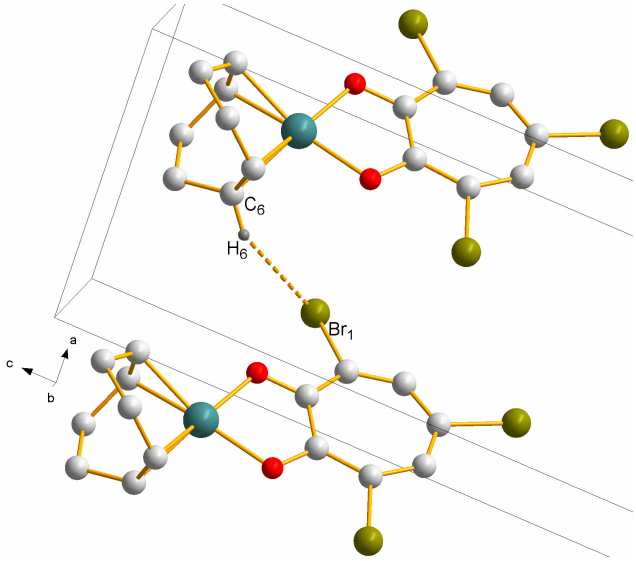

Figure 7.2 Partial unit cell of [Pd(cod)(3Br-trop)]BF_4 (12) showing intermolecular hydrogen bonding interactions indicated by a dashed bond. Only selected hydrogen atoms are included. Palladium (cyan), carbon (grey), oxygen (red) and bromine (dark yellow).

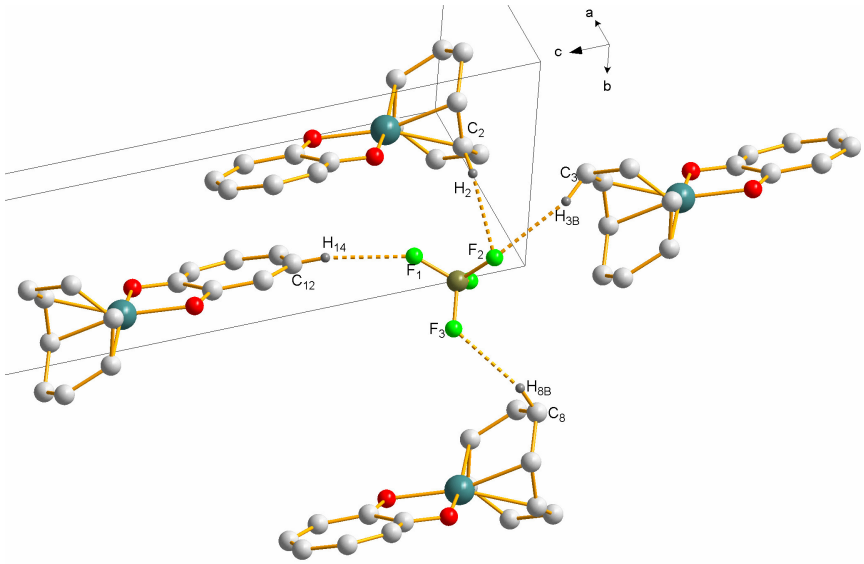

Figure 7.3 Partial unit cell of [Pd(cod)(3Br-trop)]BF_4 (12) showing intermolecular hydrogen bonding interactions indicated by a dashed bond. Only selected hydrogen atoms are included. Bromine atoms have been omitted for clarity Palladium (cyan), carbon (grey), oxygen (red), boron (olive green) and fluorine (green).

With these compounds two types of hydrogen interactions are observed namely that of **12a**···**12a** and **12a**···**12b** (Table 7.3). The first type of interaction is found between the hydrogen of the alkene carbon (C_6) of the cyclo-octadiene ring and a bromo substituent (Br_1) of a tribromotropolonato ligand as seen in Figure 7.2. The second type of interaction can be further subdivided into three categories namely, the hydrogen of the cyclo-octadiene alkene carbon (C_2) and the fluorido (F_2) ligand of the

12b anionic species. The hydrogens of the cyclo-octadiene alkane carbons (C_3 and C_8) and the fluorido (F_2 and F_3) ligands and lastly that of the hydrogen of the tribromotropolonato carbon (C_{12}) with the fluorido (F_3) ligand, these interactions are depicted in Figure 7.3.

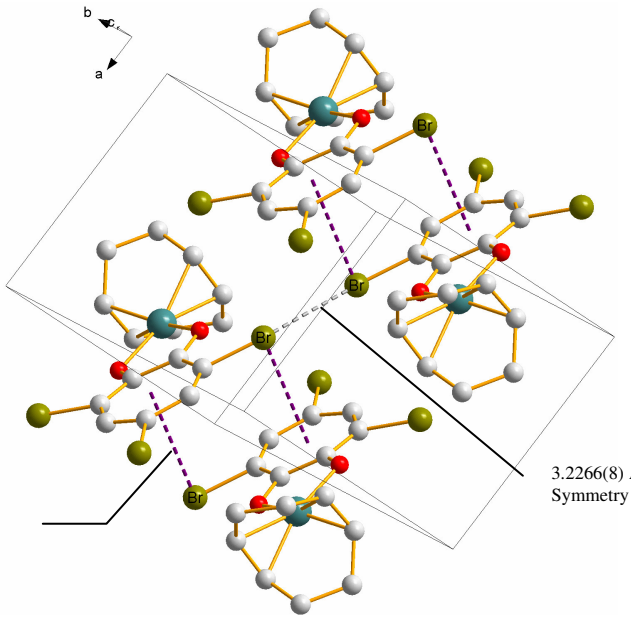

Figure 7.4 Partial Unit cell of [Pd(cod)(3Br-trop)]BF_4 (12) showing Br···Br and Br···π interactions indicated by a dashed grey and violet bonds respectively. Hydrogens and tetraflouroborate counter ions omitted for clarity. Palladium (cyan), carbon (grey), oxygen (red) and bromine (dark yellow).

Figure 7.4 illustrates the Br···Br interactions between the adjacent cationic complexes with a grey dashed line, a bond distance of 3.2266(8) Å was observed. A general range for Br···Br interactions was found to be between 3.6-4.6 Å with an interaction angle of 40°-180°[13]. Steyl *et. al.* also reported the formation of bromo triad units, even though the bromo triad unit is observed (centre of Figure 7.4) for complex **12a** the distances of 4.8927(8) Å and 4.2913(8) Å to the lower bromo subsituent of the tribromotropolonato ligand are elongated due to the Br···π interaction observed. These interactions are shown with a violet dashed line and have a distance of 3.4375(5) Å.

[13] Steyl G., Roodt A., *Models, mysteries and Magic of Molecules*, Boeyens J.C.A., Olgilvie J.F. (eds.), Springer, Netherlands, 325, (2008)

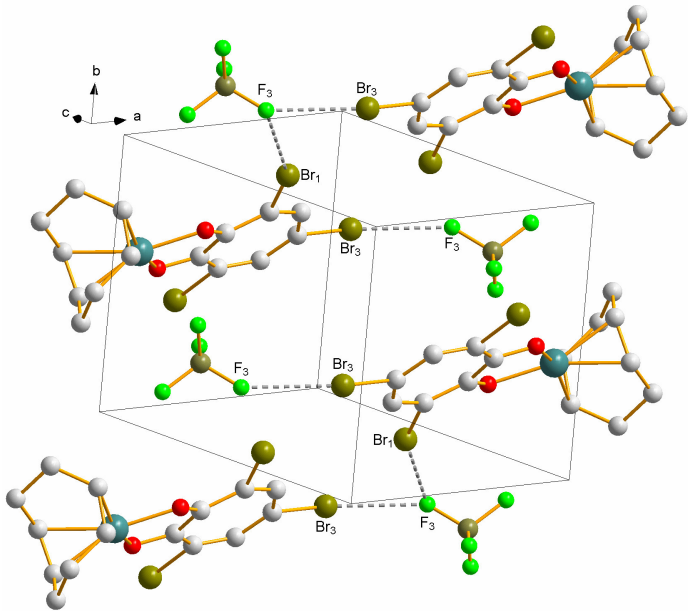

Figure 7.5 Partial Unit cell of [Pd(cod)(3Br-trop)]BF_4 (12) showing Br···F interactions indicated by a dashed grey bond. Hydrogens omitted for clarity. Palladium (cyan), carbon (grey), oxygen (red), boron (olive green), fluorine (green) and bromine (dark yellow).

Figure 7.5 depicts Br···F interactions between the cationic **12a** species and the fluorido ligands of the **12b** species their distances are as follows Br_1···F_3 3.121(3) Å and Br_3···F_3 2.950(3) Å. Figure 7.6 shows the packing of a filled 3x3x3 super cell along the *a*-axis.

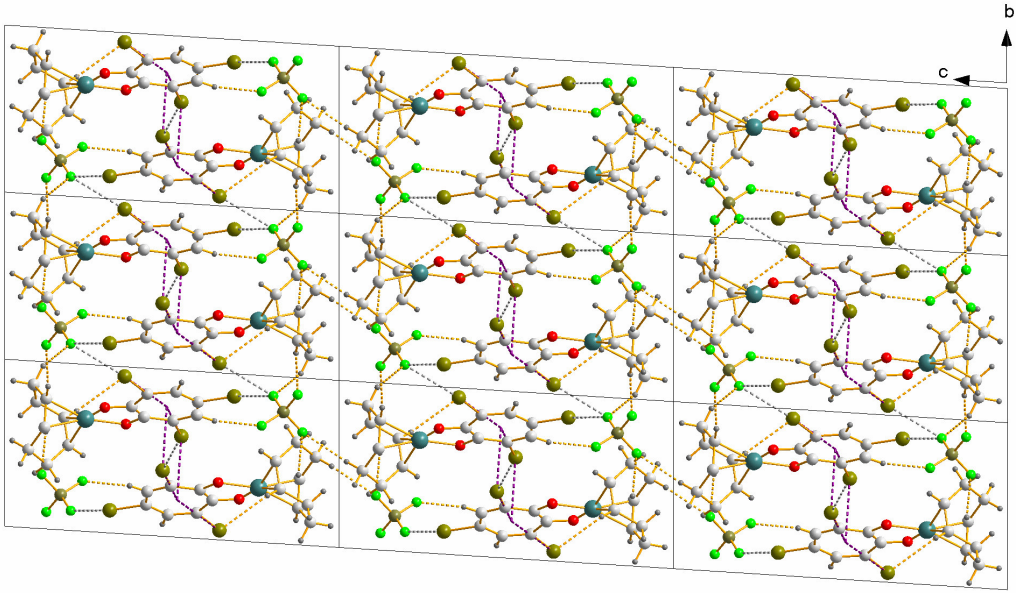

Figure 7.6 Packing of a filled 3x3x3 super cell of [Pd(cod)(3Br-trop)]BF_4 (12) viewed along the *a*-axis. Dashed bonds indicate interactions, Br···Br and Br···F indicated in grey, hydrogen bonding in yellow and Br···π indicated in violet. Palladium (cyan), carbon (grey), oxygen (red), boron (olive green), fluorine (green) and bromine (dark yellow).

The hydrogen bonding can be seen as yellow dashed lines, the Br···Br and Br···F interactions as grey dashed lines and Br···π interactions as violet dashed lines. The cell is tightly packed, with the tetraflouroborate counter ion kept in place by both hydrogen and Br···F bond interactions. A staggered head-to-tail packing is observed (Figure 7.7) as a result of the Br···π interactions. There are additional weak hydrogen interactions that have not been included in the above figure which are reflected in Table 7.4.

Table 7.4 Additional weak hydrogen interactions for [Pd(cod)(3Br-trop)]BF_4 (12)

D-H...A	d(D-H)	d(D...A)	d(H...A)	<(DHA)
C_2-H_2...F_1	1.00	3.309(6)	2.92	104.2
C_3-H_{3A}…F_2	0.99	3.354(6)	2.69	124.2
C_3-H_{3A}…F_4	0.99	3.505(6)	2.80	129.0
C_4-H_{4B}…F_1	0.99	3.482(6)	2.77	129.3
C_4-H_{4B}…F_4	0.99	3.524(6)	2.77	133.2
C_7-H_{7B}…$F_2^{\#1}$	0.99	3.574(6)	2.91	125.0
C_8-H_{8A}…$F_2^{\#1}$	0.99	3.355(6)	2.58	134.7
C_8-H_{8A}…$F_4^{\#1}$	0.99	3.715(7)	2.77	159.5
C_4-H_{4A}…$F_2^{\#2}$	0.99	3.312(6)	2.59	129.6
C_4-H_{4B}…$Br_3^{\#3}$	0.99	3.705(5)	3.00	129.3
C_7-H_{7A}…$F_4^{\#4}$	0.99	3.782(6)	2.83	161.0
C_7-H_{7A}…$F_3^{\#4}$	0.99	3.266(6)	2.75	113.4

Symmetry transformations used to generate equivalent atoms:
#1 -x,-y+1,-z #2 x+1,y,z #3 -x,-y+1,-z+1 #4 x+1,y-1,z

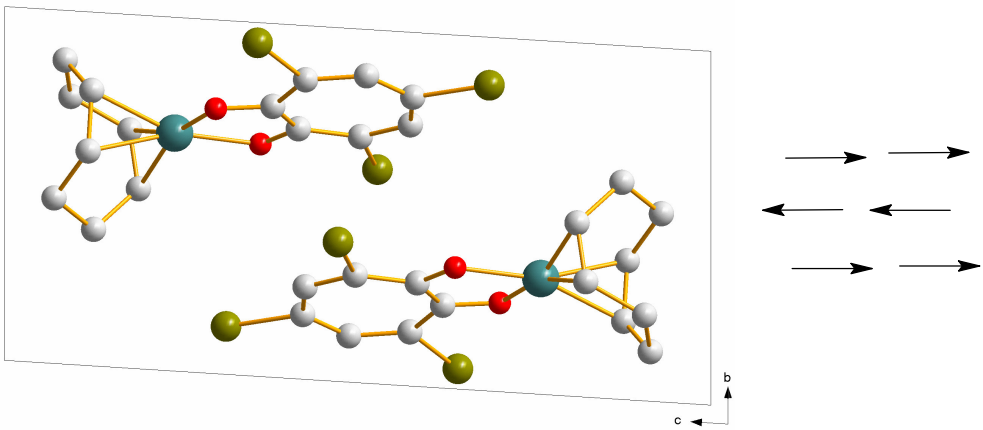

Figure 7.7 Packing of [Pd(cod)(3Br-trop)]BF_4 (12) viewed along the *a*-axis with the packing motif incorporated to the right of the figure. Palladium (cyan), carbon (grey), oxygen (red) and bromine (khaki). Hydrogens and BF_4 have been omitted for clarity.

The packing motif in Figure 7.7 is defined as the head of the arrow corresponding to the 1,5-cyclo-octadiene moiety and the tail of the arrow corresponding to the tribromotropolonato moiety. Previously as has been mentioned the packing found for the **12a** complex is a classic head-to-tail, Figure 7.7 shows the simplified unit cell viewed along the *a*-axis with the packing motif on the right hand side.

The hydrogen bonding of complex **11** is graphically presented in Figure 7.8 and 7.9 with Table 7.5 listing the bond distances and angles.

Table 7.5 Hydrogen bond distances and angles for [Pd(cod)(3Br-trop)]PF_6 (11) [Å and °]

D-H...A	d(D-H)	d(H...A)	d(D...A)	<(DHA)
C_7-H_{2A}...F_6	0.99	2.54	3.245(11)	127.9
C_2-H_5...$F_3^{\#1}$	1.00	2.37	3.340(10)	163.9
C_3-H_{6A}...$Br_3^{\#2}$	0.99	2.86	3.615(8)	133.7
C_6-H_1...$F_5^{\#3}$	1.00	2.39	3.142(10)	131.6
C_5-H_8...$Br_1^{\#3}$	1.00	2.87	3.698(8)	140.9
C_{12}-H_{13}...$F_1^{\#4}$	0.95	2.46	3.404(11)	169.9

Symmetry transformations used to generate equivalent atoms:
#1 x,y-1,z #2 -x,-y,-z #3 x+1,y,z #4 -x,-y+1,-z

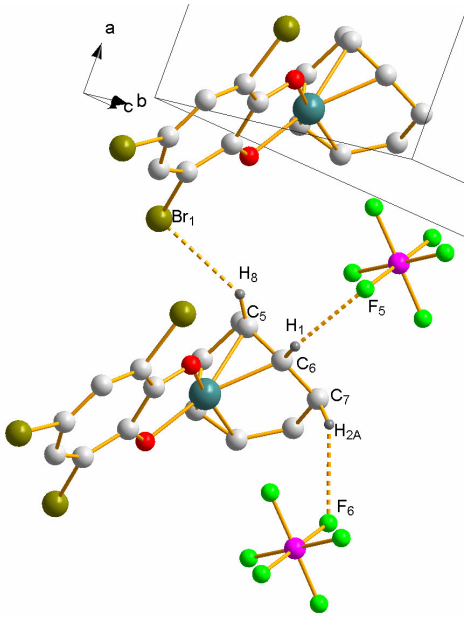

Figure 7.8 Partial unit cell of [Pd(cod)(3Br-trop)]PF_6 showing intermolecular hydrogen bonding interactions indicated by a dashed bond. Only selected hydrogen atoms are included. Palladium (cyan), carbon (grey), oxygen (red), phosphorus (pink), fluorine (green) and bromine (dark yellow).

In addition, as found with complex **12**, interactions of the type **11a···11b** were observed and are listed in Table 7.5. The Br···H interaction seen is the bromo substituent (Br_1 and Br_3) of the tribromotropolonato ligand with the hydrogens of both the alkane (C_3) and alkene (C_5) carbons of the cyclo-octadiene ring (Figure 7.8 and 7.9). The **11a···11b** interaction type can be further subdivided into three sub categories namely interaction with the tribromotropolonato ligand, with the hydrogens of the alkane carbons of the cyclo-octadiene ring system and with the hydrogens of the alkene carbons of the cyclo-octadiene ring system. The last two types of

interactions are shown in Figure 7.8 being between the fluorido (F_6) ligand of the hexafluorophosphate counter ion and the hydrogen of the alkane (C_7) carbon of the cyclo-octadiene. The hydrogen of the alkene carbon (C_6) is seen to interact with the fluorido (F_5) ligand of the **11b** complex.

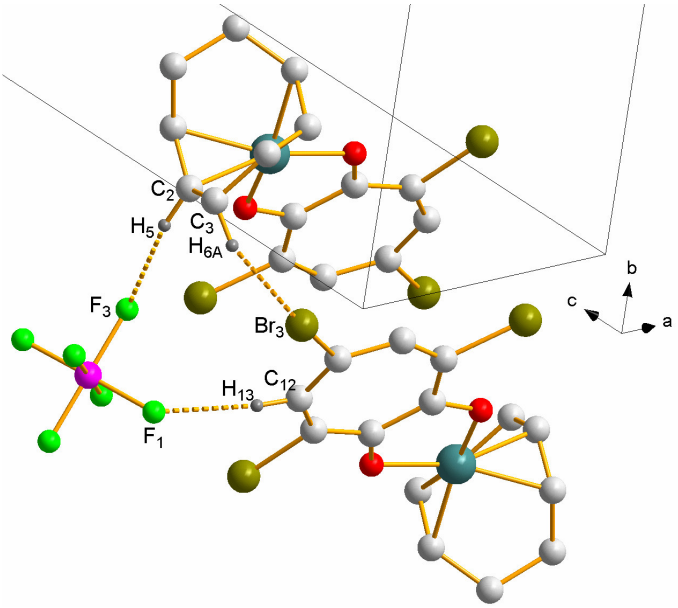

Figure 7.9 Partial unit cell of [Pd(cod)(3Br-trop)]PF_6 showing intermolecular hydrogen bonding interactions indicated by a dashed bond. Only selected hydrogen atoms are included. Palladium (cyan), carbon (grey), oxygen (red), phosphorus (pink), fluorine (green) and bromine (dark yellow).

An additional fluorido (F_3) hydrogen alkene (C_2) carbon interaction can be seen in Figure 7.9. The last sub-type of interaction is that of the hydrogen of the carbon (C_{12}) of the tribromotropolontao ligand with the fluorido (F_1) ligand of **11b** this is depicted in Figure 7.9.

Figure 7.10 illustrates a partial unit cell showing a Br···Br interaction as indicated by a dashed grey bond with a distance of 3.374(1) Å. The Br···π interaction is indicated by a dashed violet bond with a distance of 3.466(1) Å and π···π indicated by a dashed light blue bond with a distance of 3.578(5) Å. Again, the bromo "triad" is present to the lower right of the centre of Figure 7.10 consisting of the existing Br···Br interaction and the bromo substituent on the complex to the right.

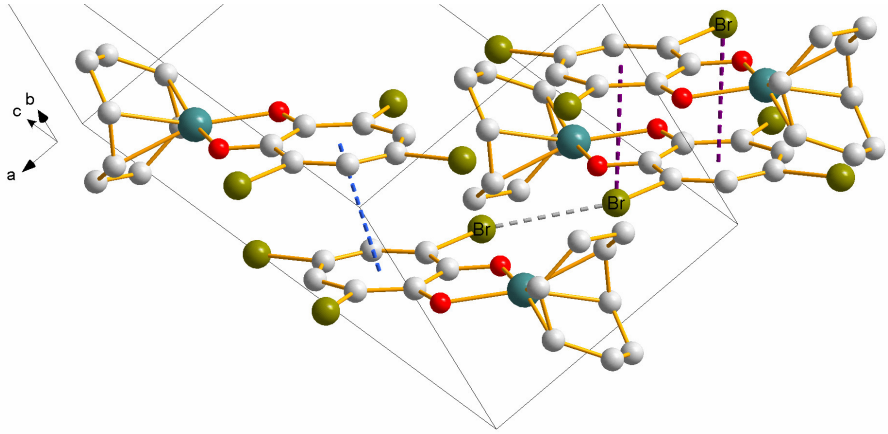

Figure 7.10 Partial Unit cell of [Pd(cod)(3Br-trop)]PF_6 showing Br···Br, Br···π and π···π interactions indicated by a dashed grey, violet and light blue bonds respectively. Hydrogens and hexafluorophosphate counter ions omitted for clarity. Palladium (cyan), carbon (grey), oxygen (red) and bromine (dark yellow).

The result of the Br···π and π···π interactions elongates the bromine distances to 4.970(1) Å and 4.896(1) Å respectively which is too long to be considered an interaction, though the pattern remains present.

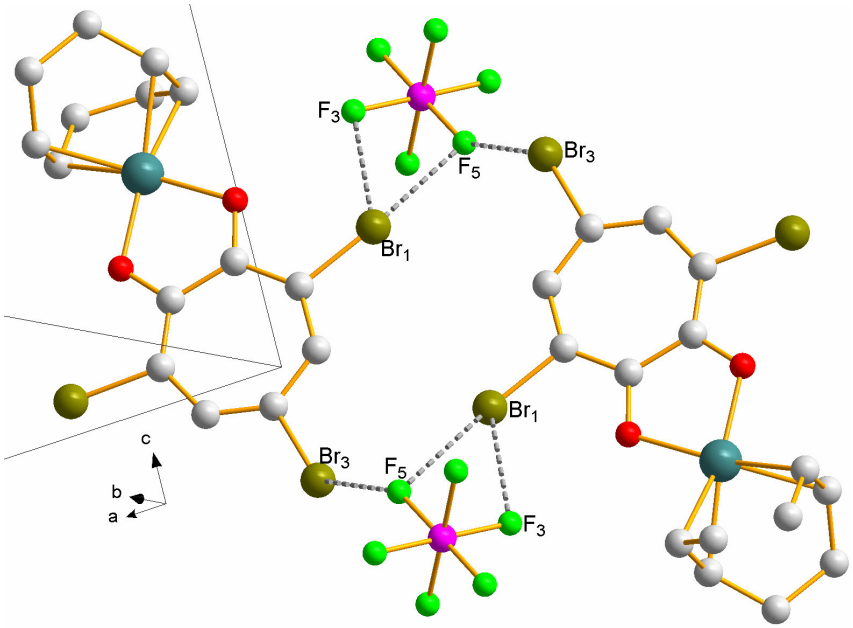

Figure 7.11 Partial Unit cell of [Pd(cod)(3Br-trop)]PF_6 showing bromine fluorine interactions indicated by a dashed bond. Hydrogens omitted for clarity. Palladium (cyan), carbon (grey), oxygen (red), phosphorous (pink), fluorine (green) and bromine (dark yellow).

Bromine fluorine interactions indicated by a grey dashed bond are seen in Figure 7.11. The respective distances are $Br_1 \cdots F_3$ 3.368(6) Å, $Br_1 \cdots F_5$ 3.326(5) Å and $Br_3 \cdots F_5$ 3.349(6) Å.

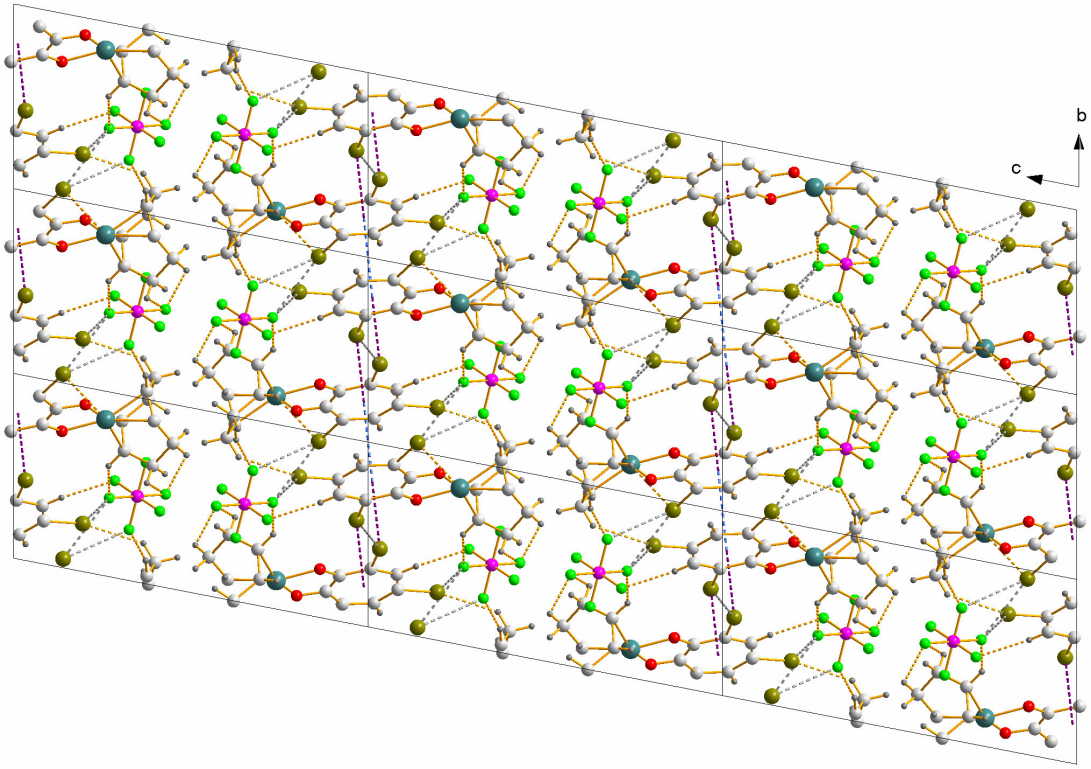

Figure 7.12 Packing of a filled 3x3x3 super cell of [Pd(cod)(3Br-trop)]PF_6 viewed along the *a*-axis. Dashed bonds indicate interactions, Br···Br and Br···F indicated in grey, hydrogen bonding in yellow, Br···π indicated in violet and π···π indicated in light blue. Palladium (cyan), carbon (grey), oxygen (red), phosphorus (pink), fluorine (green) and bromine (dark yellow).

The packing of a filled 3x3x3 super cell viewed along the *a*-axis shown in Figure 7.12, all interactions have been combined and are indicated by different colored dashed bonds. A staggered head-to-tail packing (Figure 7.13) is as a result of the Br···Br, Br···π and π···π interactions. Additional weak hydrogen interactions were found and are tabulated in Table 7.6, these interactions are not included in Figure 7.12.

Table 7.6 Additional weak hydrogen interactions for [Pd(cod)(3Br-trop)]PF_6

D-H...A	d(D-H)	d(D...A)	d(H...A)	<(DHA)
C_1-H_4...F_2	0.98	3.434(10)	2.62	140.4
C_7-H_{2A}…F_1	0.97	3.392(11)	2.71	128.0
C_8-H_{3A}…F_6	0.97	3.099(10)	2.47	122.5
C_3-H_{6A}…$F_2^{\#1}$	0.97	3.666(10)	2.70	173.6
C_3-H_{6B}…$F_4^{\#2}$	0.97	3.213(11)	2.68	114.8
C_4-H_{7B}…$F_3^{\#2}$	0.97	3.734(11)	2.77	171.8
C_4-H_{7B}…$F_4^{\#2}$	0.97	3.391(11)	2.73	126.0
C_7-H_{2B}…$F_4^{\#3}$	0.97	3.438(11)	2.63	141.6
C_4-H_{7A}…$F_2^{\#3}$	0.97	3.389(11)	2.99	105.5
C_7-H_{3B}…$F_2^{\#3}$	0.97	3.362(11)	2.77	119.8
C_6-H_1…$Br_3^{\#4}$	0.98	3.677(8)	2.93	134.3
C_8-H_{3A}…$F_6^{\#5}$	0.97	3.304(11)	2.62	127.8
C_7-H_{2B}…$F_4^{\#5}$	0.97	3.412(11)	2.63	138.0

Symmetry transformations used to generate equivalent atoms:
#1 -x,-y,-z+1 #2 x+1,y-1,z #3 x+1,y,z #4 -x,-y+1,-z #5 –x,-y+1,-z+1

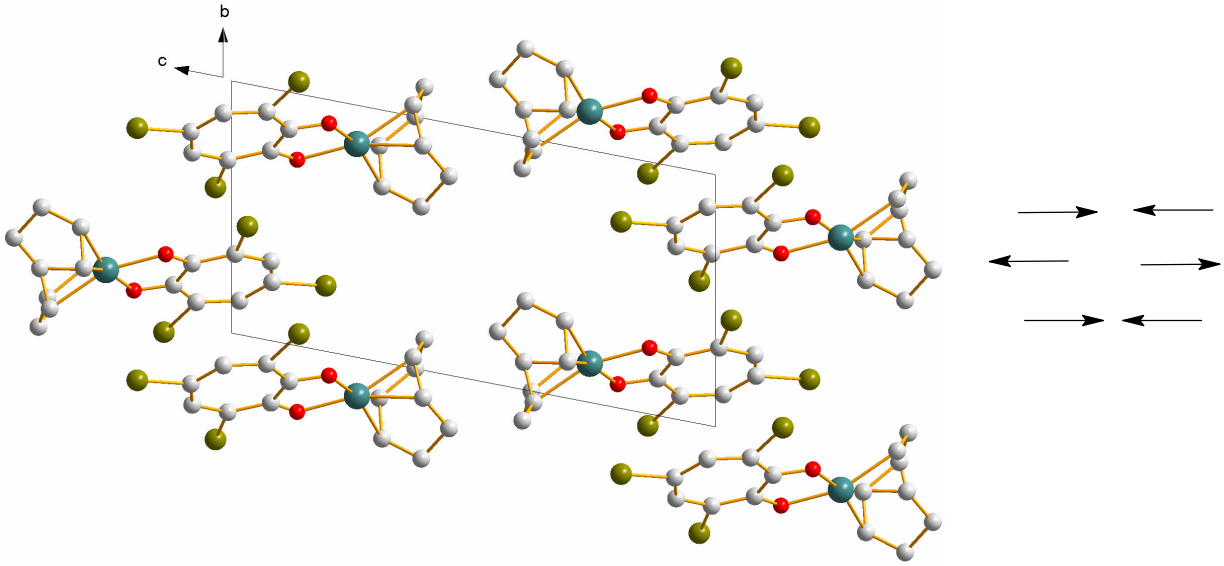

Figure 7.13 Packing of [Pd(cod)(3Br-trop)]PF_6 viewed along the *a*-axis with the packing motif incorporated to the right of the figure. Palladium (cyan), carbon (grey), oxygen (red) and bromine (khaki). Hydrogens and PF_6^- have been omitted for clarity.

The packing motif in Figure 7.13 is defined as the head of the arrow corresponding to the 1,5-cyclo-octadiene moiety and the tail of the arrow corresponding to the tribromotropolonato moiety. It is interesting to note that hexafluorophosphate counter ion is alternated with the cylo-octadiene ring (Figure 7.12). Also of note is the fact that the packing has distinct bands, i.e. there is no interaction found between the cyclo-octadiene - cyclo-octadiene and the hexafluorophosphate - hexafluorophosphate counter ions thus creating a "void" space, this can be clearly seen in the packing motif of Figure 7.13.

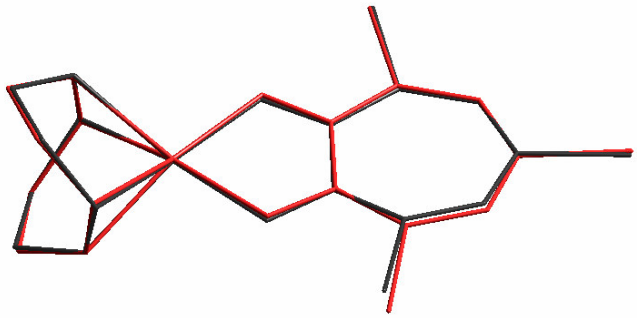

Figure 7.14 HyperChem superimposed image of [Pd(cod)(3Br-trop)]PF_6 (red) *vs.* [Pd(cod)(3Br-trop)]BF_4 (black) with an RMS error of 0.097 Å. Counter ions have been omitted for clarity.

An overlay of the two crystals shows that they have comparable bond distances, with an RMS error of 0.097 Å (Figure 7.14). The primary difference is found in the angle of the cyclo-octadiene ring, where there is an increase in the ψ angle of 4.1(3)°. The other difference is the bend of the planes of the tropolone ring with the ring formed by the palladium, oxygens and carbons of the tropolone ring the larger bend is that of the tetrafluoroborate counter ion with the difference being 3.1(1)°.

In looking at the super cells of the complexes we find that they have similar interactions (Figure 7.6 and 7.12). The two differences that catch one's eye are the lack of the π···π interactions in complex **12** and the "void" seen in complex **11** leading to a much tighter packing of the super cell for complex **12** than for complex **11**.

7.3.2 Crystal structure of [Pd(cod)(trop)]PF_6

The compound [Pd(cod)(trop)]PF_6 (**13**) crystallized in the tetragonal space group $P4_2bc$, with a cationic $[Pd(cod)(trop)]^+$ species (**13a**) and an anionic PF_6^- (**13b**) species in the asymmetric unit. The numbering scheme is presented in Figure 7.15, while atomic co-ordinates, bond angles and distances, anisotropic displacement parameters and hydrogen co-ordinates are reported in Appendix B.9. General crystallographic data and refinement parameters are reported in Table 7.1, while significant bond angles and distances are reported in Table 7.7.

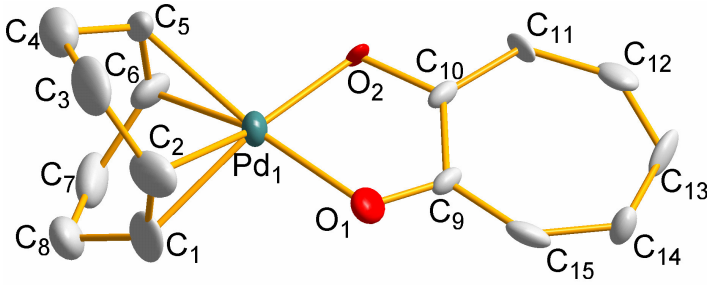

Figure 7.15 Diamond illustration of [Pd(cod)(trop)]PF_6 (13) at 100 K showing the numbering scheme and displacement ellipsoids (50 %) of the complex. Hydrogen atoms and anionic species omitted for clarity.

Table 7.7 Selected bond distances and angles for [Pd(cod)(trop)]PF_6 (13)

Bond Distance (Å)		Bond Angles (°)	
Pd-O_1	2.018(9)	O_1-Pd-O_2	82.1(2)
Pd-O_2	1.982(8)	C_1-Pd-C_2	37.0(5)
Pd-C_1	2.177(12)	C_5-Pd-C_6	36.1(4)
Pd-C_2	2.193(12)	C_1-Pd-C_6	81.5(4)
Pd-C_5	2.192(12)	C_2-Pd-C_5	83.0(4)
Pd-C_6	2.145(12)	χ^a	86.7(6)
C_1-C_2	1.387(18)	ψ^b	84.0(8)
C_5-C_6	1.343(16)		

a χ: $C_1MC_2 \cap C_5MC_6$ b ψ: $C_2C_3C_4C_5 \cap C_1C_8C_7C_6$ see Figure 1.2

The geometry around the metal centre is square planar (Figure 4.2) with 1,5-cyclo-octadiene and tropolonato moieties bonded to palladium. The oxidation state to the palladium metal centre is +2, thus resulting in a cationic charged species which is balanced by an anionic counter ion hexafluorophosphate (PF_6). The average distances for complex **13a** for Pd-O, Pd-C and C=C co-ordination were found to be 2.000(8) Å, 2.177(12) Å and 1.365(17) Å respectively. The angle between the planes defined by the tropolone ring and the palladium, oxygens and adjacent carbons was found to be 5.8(2)°.

The hydrogen bonding of complex **13** is graphically presented in Figure 7.16-7.18 with Table 7.8 listing the bond distances and angles.

Table 7.8 Hydrogen bond distances and angles for [Pd(cod)(trop)]PF_6 (13) [Å and °].

D-H...A	d(D-H)	d(H...A)	d(D...A)	<(DHA)
C_1-H_1...F_6	1.00	2.31	3.237(17)	153.1
C_2-H_2...$F_1^{\#1}$	1.00	2.45	3.139(17)	125.4
C_5-H_5...$F_4^{\#2}$	1.00	2.59	3.198(15)	118.8
C_7-H_{7B}...$F_2^{\#3}$	0.99	2.59	3.310(14)	129.6
C_6-H_6...$F_5^{\#3}$	1.00	2.28	3.091(17)	137.4
C_7-H_{7A}...$F_6^{\#4}$	0.99	2.48	3.412(12)	156.7
C_8-H_{8A}...$F_5^{\#5}$	0.99	2.39	3.220(13)	141.4
C_{11}-H_{11}...$O_1^{\#6}$	0.95	2.56	3.324(17)	138.1
C_{12}-H_{12}...$F_4^{\#6}$	0.95	2.54	3.384(15)	147.5
C_{12}-H_{12}...$F_6^{\#6}$	0.95	2.40	3.084(15)	128.5
C_{14}-H_{14}...$F_1^{\#7}$	0.95	2.49	3.219(14)	134.0

Symmetry transformations used to generate equivalent atoms:
#1 -x+3/2,y+1/2,z #2 y+1,-x+1,z-1/2 #3 -y+1/2,-x+1/2,z-1/2
#4 y+1/2,x-1/2,z-1/2 #5 -x+1,-y,z #6 -y+1,x-1,z-1/2
#7 x+1/2,-y-1/2,z

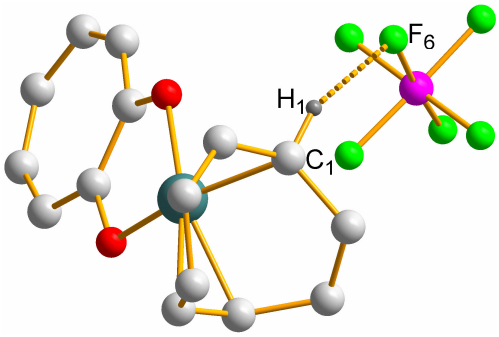

Figure 7.16 Intramolecular Hydrogen interactions of [Pd(cod)(trop)]PF_6 (13). Palladium (cyan), carbon (grey), oxygen (red), phosphorus (pink) and fluorine (green).

A single intramolecular hydrogen interaction is observed between the hydrogen of the olefinic carbon (C_1) and the fluorido (F_6) ligand of the **13b** complex (Figure 7.16).

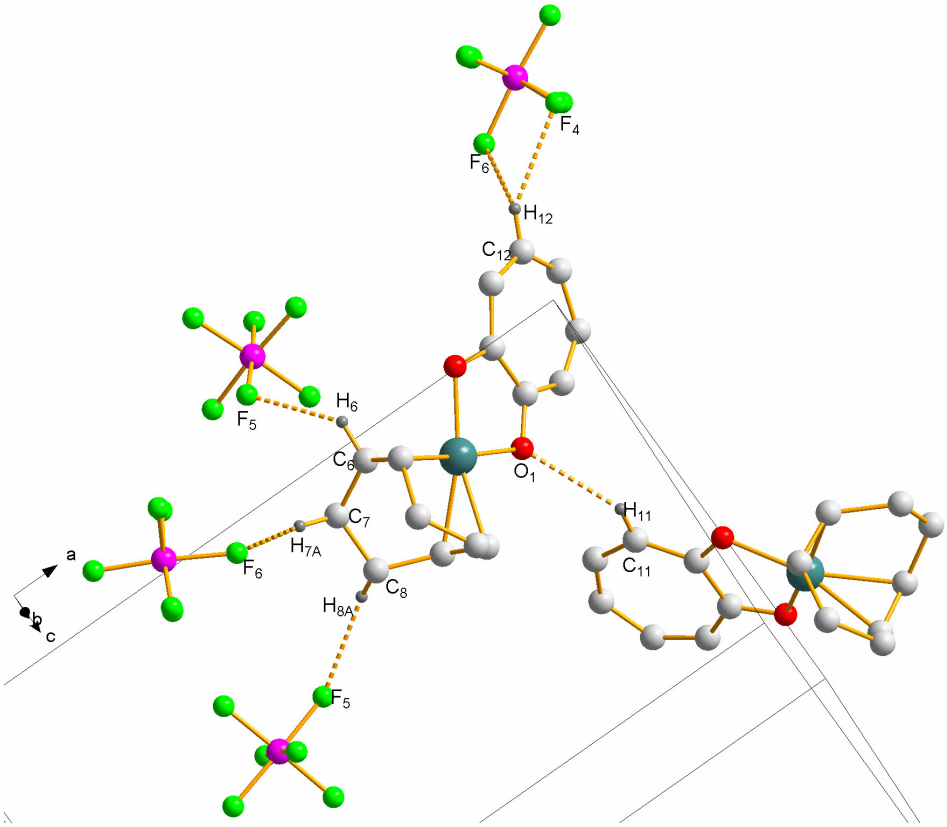

Figure 7.17 Partial unit cell of [Pd(cod)(trop)]PF_6 (13) showing intermolecular hydrogen bonding interactions indicated by a dashed bond. Only selected hydrogen atoms are included. Palladium (cyan), carbon (grey), oxygen (red), phosphorous (pink) and fluorine (green).

Several hydrogen interactions of the type **13a**···**13b** were observed (Figure 7.17 and 7.18) and are listed in Table 7.8, with only one interaction between **13a**···**13a** that being the hydrogen of the tropolonato carbon (C_{11}) with the oxygen (O_1) of an adjacent tropolonato moiety (Figure 7.17). Of the two types of **13a**···**13b** interactions, the first being the cyclo-octadiene interaction with the **13b** complex can be sub-divided into interactions from the hydrogens connected olefinic carbons (C_6 and C_2) with the fluorido (F_5 and F_1) ligands of the **13b** complex and secondly the hydrogens connected to the alkane carbons (C_7, C_8 and C_5) interacting with the fluorido (F_6, F_2, F_5 and F_4) ligands of the **13b** complex.

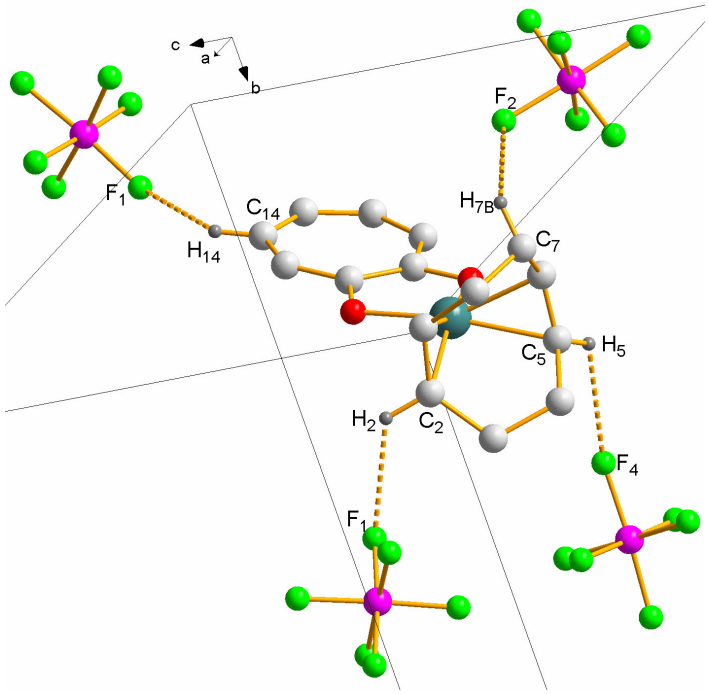

Figure 7.18 Partial unit cell of [Pd(cod)(trop)]PF_6 (13) showing intermolecular hydrogen bonding interactions indicated by a dashed bond. Only selected hydrogen atoms are included. Palladium (cyan), carbon (grey), oxygen (red), phosphorous (pink) and fluorine (green).

The second interaction is between the hydrogen connected tropolonato (C_{14} and C_{12}) ring and the fluorido (F_1, F_6 and F_4) ligand of the **13b** complex (Figure 7.18). Additionally a bifurcated hydrogen is observed with this interaction type for the hydrogen riding on the C_{12} carbon (Figure 7.17) of the tropolonato ring.

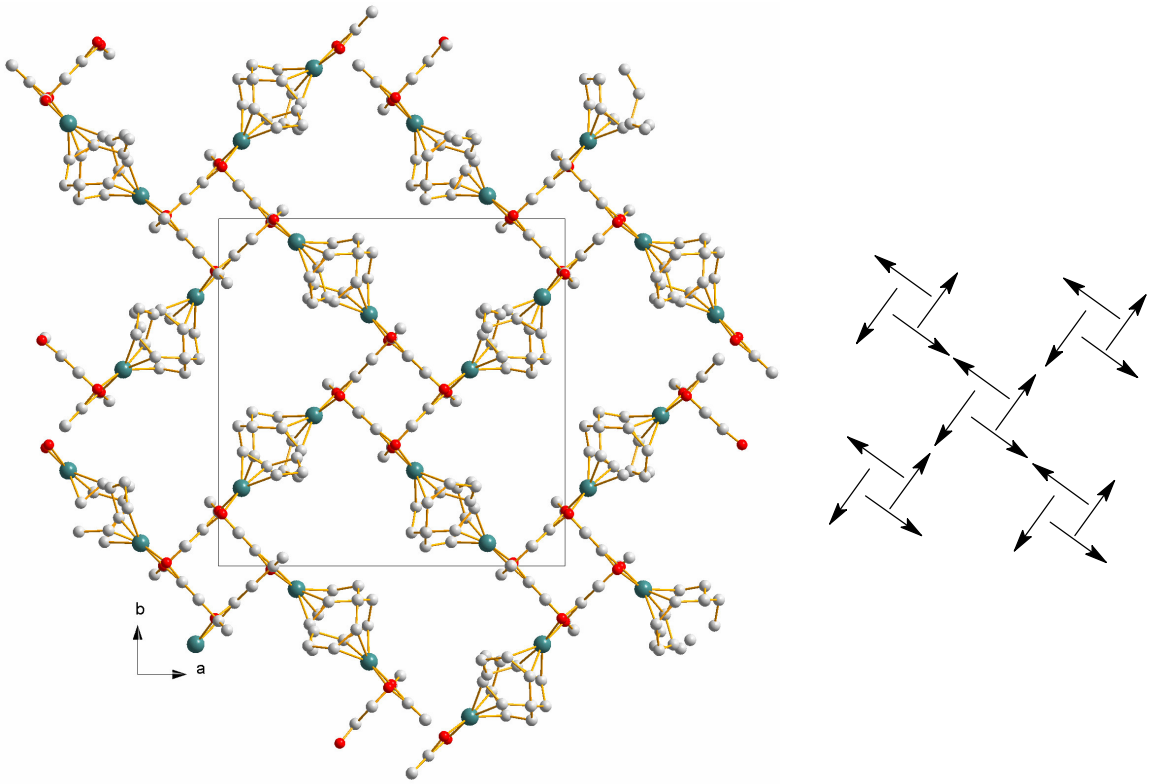

Figure 7.19 Packing of [Pd(cod)(trop)]PF_6 (13) viewed along the *a*-axis with the packing motif incorporated to the right of the figure. Palladium (cyan), carbon (grey) and oxygen (red). Hydrogens and PF_6^- have been omitted for clarity.

In the packing of the **13a** complex viewed along the *a*-axis seen in Figure 7.19 a four-fold rotation axis is clearly observed. It is interesting to note that there is also a pseudo-symmetry present in that there is an additional mirror plane perpendicular to the four-fold rotation axis. In looking at the packing motif to the right of the crystal structure we find that the arrows defined with the head of the arrow being that of the cyclo-octadiene moiety and the tail being the tropolonato moiety, illustrating the four-fold rotation axis clusters.

7.4 X-Ray Structures of Platinum(II) Complexes

7.4.1 Crystal structures of [Pt(cod)(trop)]PF_6 and [Pt(cod)(trop)]BF_4

The compound [Pt(cod)(trop)]PF_6 (**14**) crystallizes in the tetragonal space group $P4_2/mbc$, with a cationic $[Pt(cod)(trop)]^+$ species (**14a**) and an anionic PF_6^- (**14b**) species in the asymmetric unit. [Pt(cod)(trop)]BF_4 (**15**) crystallizes in the tetragonal

space group $P4_2bc$, with a cationic $[Pt(cod)(trop)]^+$ species (**15a**) and an anionic BF_4^- (**15b**) species in the asymmetric unit. The crystal was collected at room temperature. The numbering scheme is presented in Figure 7.20, while atomic co-ordinates, bond angles and distances, anisotropic displacement parameters and hydrogen co-ordinates are reported in Appendix B.16 and B.17. General crystallographic data and refinement parameters are reported in Table 7.1, while significant bond angles and distances are reported in Table 7.9.

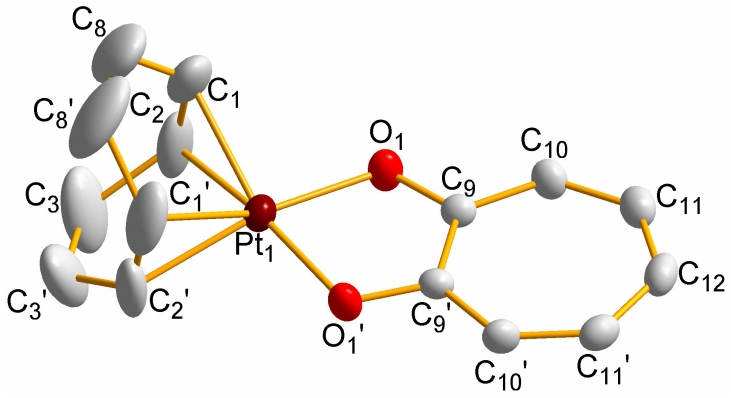

Figure 7.20 Diamond illustration of $[Pt(cod)(trop)]PF_6$ (14) at 100 K showing the numbering scheme and displacement ellipsoids (30 %) of the complex (primed labels indicate atoms generated by symmetry operations). Hydrogen atoms and anionic species omitted for clarity.

Table 7.9 Selected bond distances and angles for [Pt(cod)(trop)]A

Bond Distance (Å)	Counter ion		Bond Angles (°)	Counter ion	
	PF_6 (**14**)	BF_4 (**15**)		PF_6 (**14**)	BF_4 (**15**)
Pt-O_1	1.999(4)	1.974(15)	O_1-Pt-O_2	80.6(2)	80.2(2)
Pt-O_2[c]	1.999(4)	2.037(15)	C_1-Pt-C_2	39.9(5)	41.4(6)
Pt-C_1	2.155(10)	2.098(17)	C_5-Pt-C_6	39.9(5)	32.5(7)
Pt-C_2	2.123(9)	2.100(16)	C_1-Pt-C_6	78.7(8)	78.3(6)
Pt-C_5[c]	2.123(9)	2.09(2)	C_2-Pt-C_5	82.6(6)	85.5(5)
Pt-C_6[c]	2.155(10)	2.32(2)	χ[a]	87.2(5)	87.9(10)
C_1-C_2	1.460(19)	1.48(2)	ψ[b]	NA	85.6(15)
C_5-C_6	1.460(19)	1.25(3)			

a χ: $C_1MC_2 \cap C_5MC_6$ b ψ: $C_2C_3C_4C_5 \cap C_1C_8C_7C_6$ see Figure 1.2 c $O_2 \equiv O_1'$, $C_5 \equiv C_2'$, $C_6 \equiv C_1'$

The square planar geometry (Figure 4.2) around the platinum metal centre with co-ordinating moeties of 1,5-cyclo-octadine and tropolone . The oxidation state of the platinum(II) metal centre remains +2 resulting in the cationic nature of the complex. This resulting charge is balanced by a counter-ion either hexafluorophosphate (PF_6^-) or tetrafluoroborate (BF_4^-). The average distances for the **14a** complex for Pt-O, Pt-C and C=C co-ordination were found to be 1.999(4) Å, 2.139(9) Å and 1.46(2) Å respectively. The angle between the planes defined by the tropolone ring and the

platinum, oxygen and adjacent carbons is twisted by 10.8(1)°. The average distances found for the **15a** complex for Pt-O, Pt-C and C=C were found to be 2.006(15) Å, 2.152(18) Å and 1.37(3) Å respectively, with a twist angle of 9.7(2). There are no significant differences between the **14a** and **15a** complexes.

The hydrogen bonding of complex **14** is graphically presented in Figure 7.21 with Table 7.10 listing the bond distances and angles.

Table 7.10 Hydrogen bond distances and angles for [Pt(cod)(trop)]PF_6 (14) [Å and °].

D-H...A	d(D-H)	d(H...A)	d(D...A)	<(DHA)
C_8-H_{8A}...F_1	0.99	2.50	3.13(2)	121.7
C_1-H_1...$F_3^{\#2}$	1.00	2.29	3.16(2)	144.6
C_3-H_{3B}...$F_1^{\#3}$	0.99	2.54	3.51(2)	168.8
C_8-H_{8B}...$F_3^{\#4}$	0.99	2.47	3.258(17)	136.1
C_{11}-H_{11}...$F_2^{\#5}$	0.95	2.40	3.241(11)	146.8

Symmetry transformations used to generate equivalent atoms:
#1 x,y,-z #2 y-1/2,x+1/2,-z+1/2 #3 x+1/2,-y+1/2,z
#4 -x,-y+1,z #5 -y,x,-z+1/2

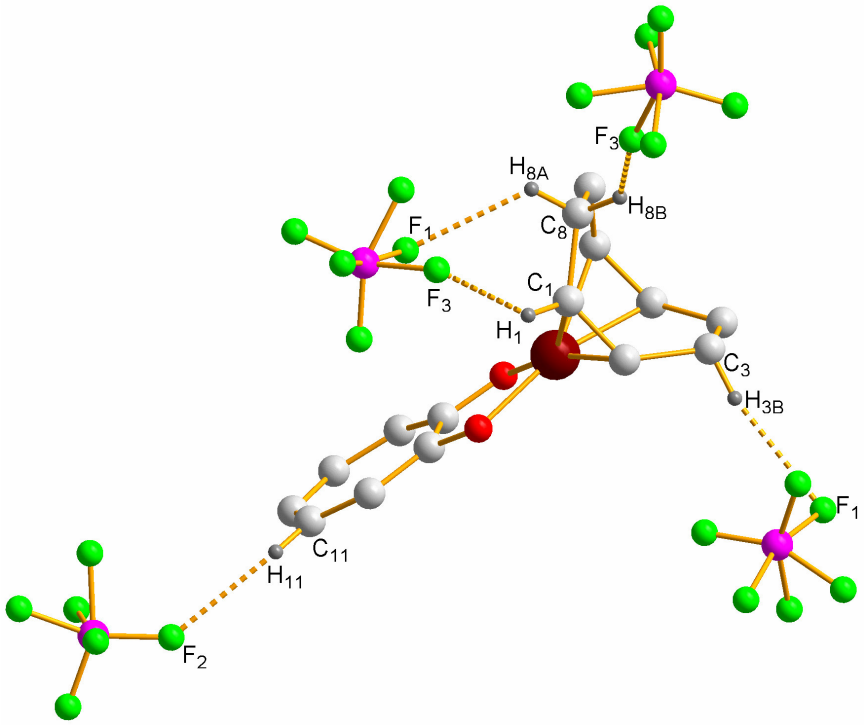

Figure 7.21 Intermolecular hydrogen bonding interactions of [Pt(cod)(trop)]PF_6 (14) indicated by a dashed bond. Only selected hydrogen atoms are included. Platinum (dark red), carbon (grey), oxygen (red), phosphorous (pink) and fluorine (green).

No intramolecular interactions between **14a**···**14a** were observed. Several hydrogen interactions of the type **14a**···**14b** were found and are listed in Table 7.10 and are seen in Figure 7.21. The first interaction is that of the hydrogens of the alkene carbons

(C_1) of the cyclo-octadiene ring with the fluorido (F_3) ligands of the **14b** complex. The second interaction is that of the hydrogens of the alkane carbons (C_8 and C_3) of the cyclo-octadiene ring with the fluorido (F_1 and F_3) ligands of the **14b** complex. The last interaction is that of the hydrogen of the tropolone carbon (C_{11}) with the fluorido (F_2) ligand of the **14b** complex.

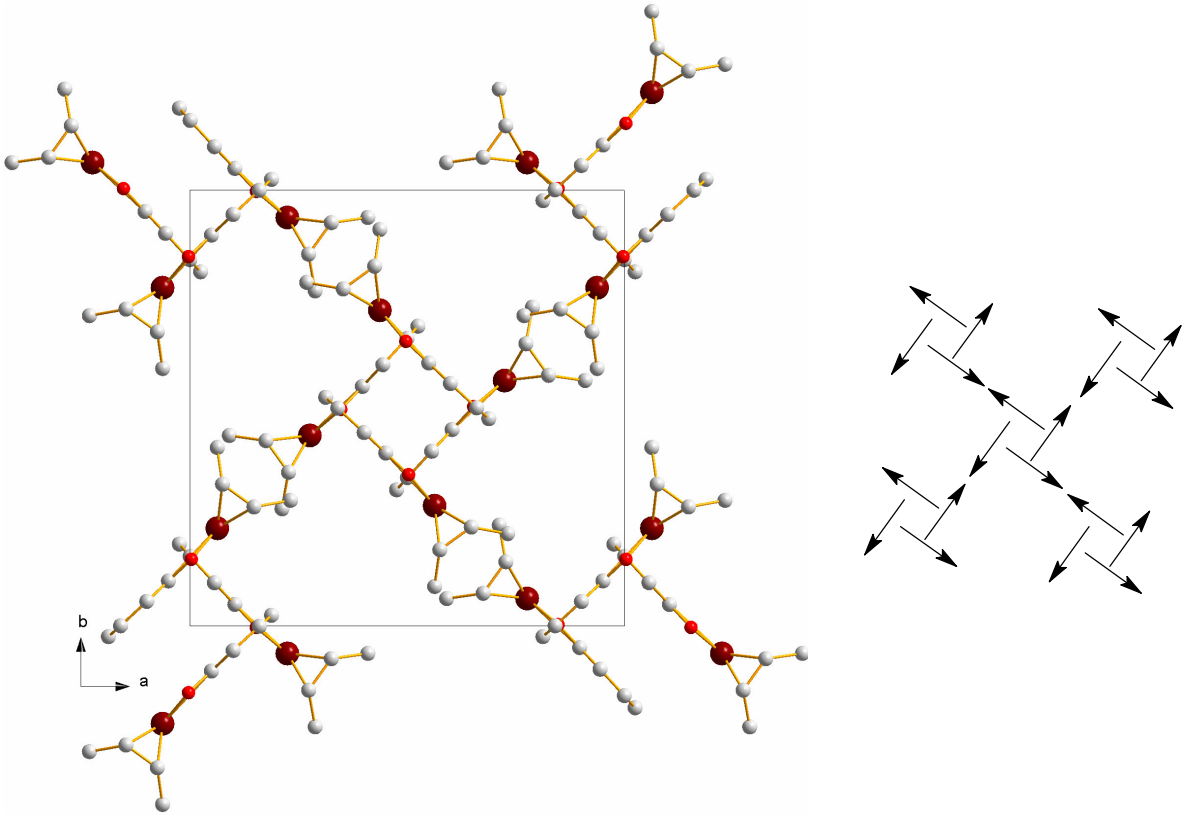

Figure 7.22 Packing of [Pt(cod)(trop)]PF_6 (14) viewed along the *c*-axis with the packing motif incorporated to the right of the figure. Platinum (dark red), carbon (grey) and oxygen (red). Hydrogens and PF_6^- have been omitted for clarity.

In the packing of the **14a** complex viewed along the *c*-axis seen in Figure 7.22 a four-fold rotation axis is clearly observed. It is interesting to note that there is also an additional mirror plane perpendicular to the four-fold rotation axis. In looking at the packing motif to the right of the crystal structure we find that the arrows defined with the head of the arrow being that of the cyclo-octadiene moiety and the tail being the tropolonato moiety.

The hydrogen bonding of complex **15** is graphically presented in Figure 7.23 and 7.24 with Figure 7.11 listing the bond distances and angles.

Table 7.11 Hydrogen bond distances and angles for [Pt(cod)(trop)]BF_4 (15) [Å and °].

D-H...A	d(D-H)	d(H...A)	d(D...A)	<(DHA)
C_4-H_{4A}...$F_3^{\#1}$	0.97	2.55	3.38(3)	143.1
C_4-H_{4A}...$F_1^{\#1}$	0.97	2.56	3.18(3)	121.6
C_6-H_6...$F_4^{\#2}$	0.98	2.31	3.22(4)	154.3
C_{14}-H_{14}...$F_1^{\#3}$	0.93	2.55	3.44(3)	161.5
C_{11}-H_{11}...$O_1^{\#4}$	0.93	2.53	3.28(2)	137.5
C_{12}-H_{12}...$F_3^{\#4}$	0.93	2.29	3.12(3)	148.0

Symmetry transformations used to generate equivalent atoms:
#1 -y+1,x-1,z+1/2 #2 -y+3/2,-x+3/2,z+1/2 #3 -x+5/2,y-1/2,z
#4 y+1,-x+1,z+1/2

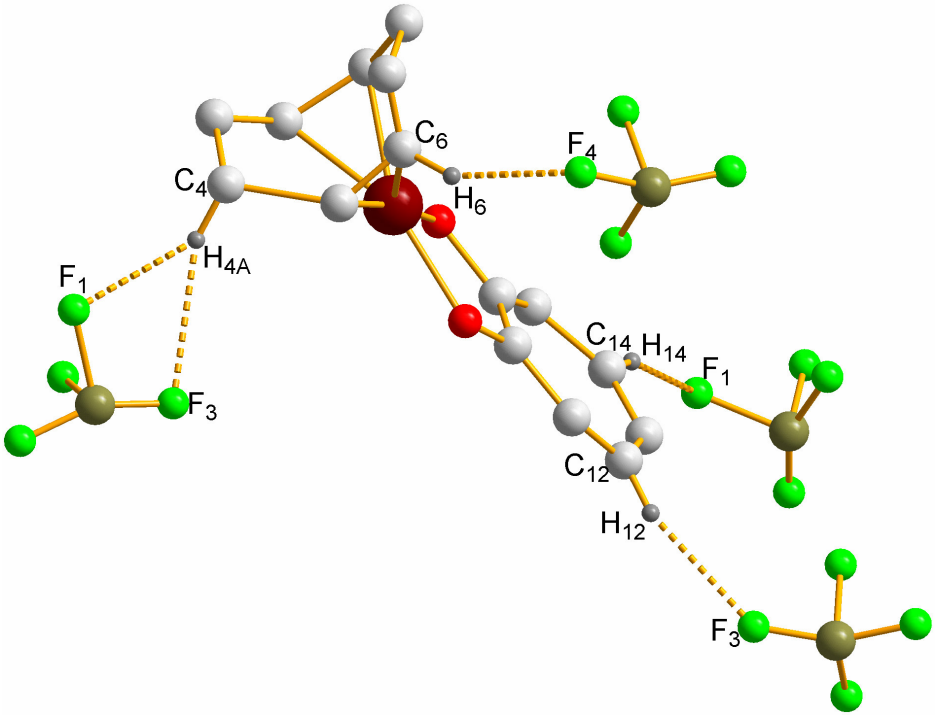

Figure 7.23 Intermolecular hydrogen bonding interactions of [Pt(cod)(trop)]BF_4 (15) at 293(2) K indicated by a dashed bond. Only selected hydrogen atoms are included. Platinum (dark red), carbon (grey), oxygen (red), phosphorous (pink) and fluorine (green).

Several intermolecular hydrogen interactions were found and are listed in Table 7.11 and are graphically presented in Figure 7.23 and 7.24. The first type of interactions that are presented are of the **15a**···**15b** type. Two interactions between the hydrogens of the carbons (C_{14} and C_{12}) of the tropolone ring with the fluorido (F_1 and F_3) ligands of the **15b** complex. The next two interactions are found between the hydrogens of both the alkene (C_6) and the alkane (C_4) carbons of the cyclo-octadine ring with the fluorido (F_4, F_1 and F_3) of the **15b** complex, it is of note that that the hydrogen (H_{4A}) is bifurcated.

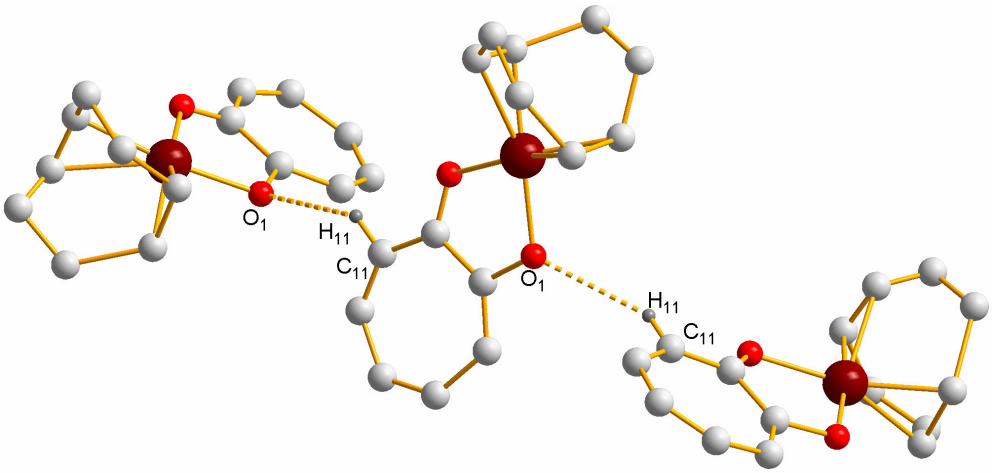

Figure 7.24 Intermolecular hydrogen bonding interactions of [Pt(cod)(trop)]BF_4 (15) at 293(2) K indicated by a dashed bond. Only selected hydrogen atoms are included. Platinum (dark red), carbon (grey), oxygen (red), phosphorous (pink) and fluorine (green).

An intramolecular hydrogen interaction (**15a**···**15a**) was observed between the hydrogen of the carbon (C_{11}) troplonato moiety and the oxygen (O_1) of an adjacent tropolonato moiety. The adjacent tropolonato moiety is at approx 90° to its neighbour. This chain like interaction contributes to the packing that is observed in Figure 7.25.

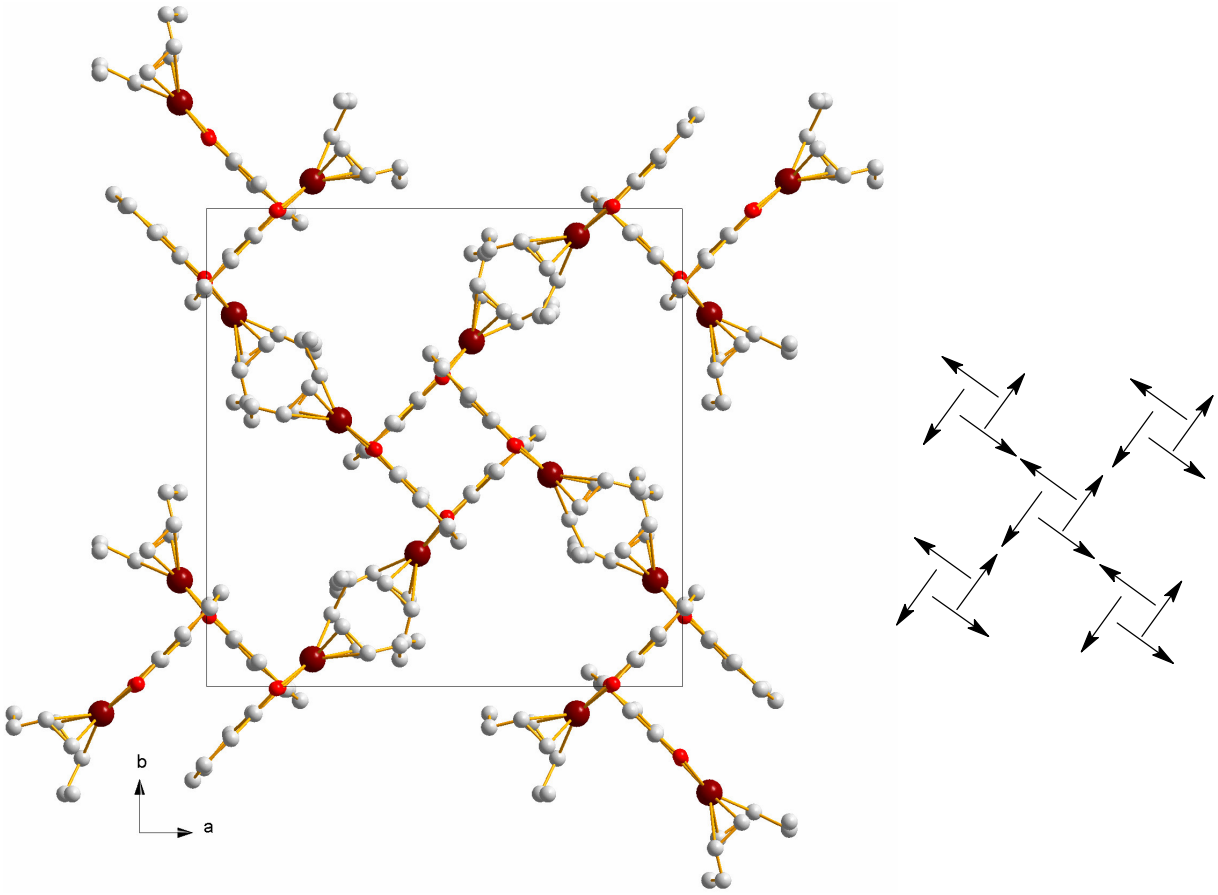

Figure 7.25 Packing of [Pt(cod)(trop)]BF_4 (15) viewed along the *c*-axis with the packing motif incorporated to the right of the figure. Platinum (dark red), carbon (grey) and oxygen (red). Hydrogens and BF_4^- have been omitted for clarity.

The packing of the **15a** complex viewed along the *c*-axis seen in Figure 7.25 where a four-fold rotation axis is clearly observed. It is interesting to note that there is also an additional pseudo-symmetry of a mirror plane perpendicular to the four-fold rotation axis. In looking at the packing motif to the right of the crystal structure we find that the arrows defined with the head of the arrow being that of the cyclo-octadiene moiety and the tail being the tropolonato moiety. In comparing the **14a** complex with the **15a** complex the packing of the complexes are identical, thus making the complexes isostructural to one another. However the **15a** complex was solved in the tetragonal $P4_2bc$ space group the additional mirror plane which is present in the **14a** complex is only a pseudo-symmetry for the **15a** complex.

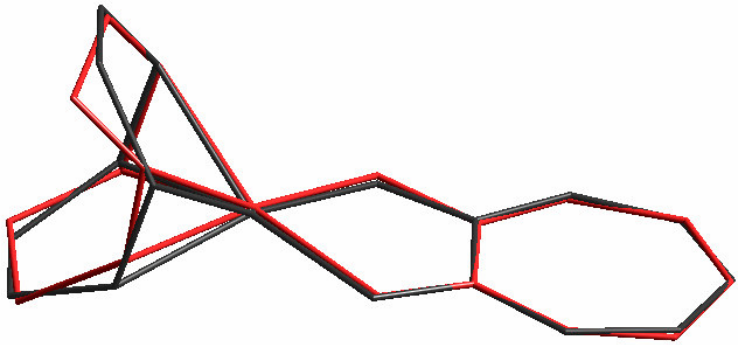

Figure 7.26 Overlay of [Pt(cod)(trop)]PF_6 (14) (black) and [Pt(cod)(trop)]BF_4 (15) (red) RMS error 0.19 Å.

The overlay of complexes **14a** and **15a** are presented in Figure 7.26 with an observed RMS error of 0.1952 Å. The variance in the overlay comes from the distortion of the square planar geometry. This is seen in the angle of intersection between the planes comprising of the mid points of the alkene carbons of the cyclo-octadiene ring and the oxygens of the troplonato moiety and the platinum metal centre with the full troplonato moiety a difference of *ca*. 1.1° was observed.

7.4.2 Crystal structures of [Pt(cod)(3Br-trop)]PF_6 and [Pt(cod)(3Br-trop)]BF_4

The compound, [Pt(cod)(3Br-trop)]BF_4 (**17**) crystallized in the triclinic space group $P\bar{1}$ with [Pt(cod)(3Br-trop)]PF_6 (**16**) crystallizing in the monoclinic space group *C*2/*c*. Both compounds have a cationic $[Pt(cod)(3Br\text{-}trop)]^+$ species (**16a** or **17a**) and an anionic BF_4^- (**17b**) or PF_6^- (**16b**) species in the asymmetric unit. The numbering scheme is presented in Figure 7.27, while atomic co-ordinates, bond angles and distances, anisotropic displacement parameters and hydrogen co-ordinates are reported in Appendix B.14 and B.15. General crystallographic data and refinement parameters are reported in Table 7.1, while significant bond angles and distances are reported in Table 7.12.

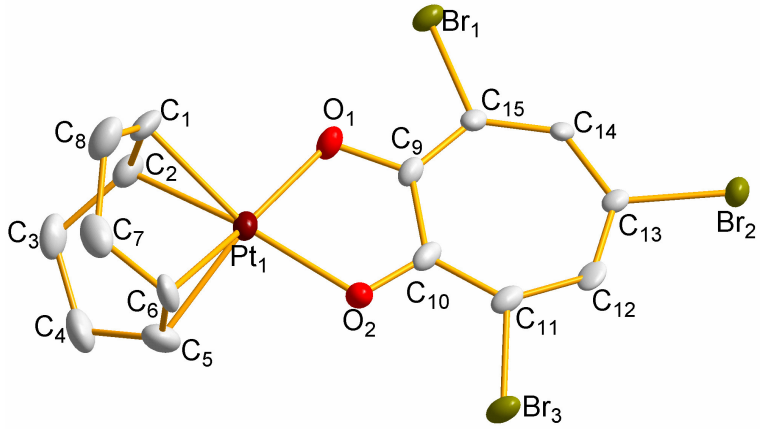

Figure 7.27 Diamond illustration of [Pt(cod)(3Br-trop)]PF_6 (16) at 100 K showing the numbering scheme and displacement ellipsoids (50 %) of the complex. Hydrogen atoms and anionic species omitted for clarity.

Table 7.12 Selected bond distances and angles for [Pt(cod)(3Br-trop)]A

Bond Distance (Å)	Counter ion		Bond Angles (°)	Counter ion	
	PF_6 (**16**)	BF_4 (**17**)		PF_6 (**16**)	BF_4 (**17**)
Pt-O_1	2.024(9)	2.008(3)	O_1-Pt-O_2	80.3(3)	79.8(1)
Pt-O_2	2.040(8)	2.030(4)	C_1-Pt-C_2	37.8(5)	38.0(2)
Pt-C_1	2.178(12)	2.156(5)	C_5-Pt-C_6	37.5(5)	37.6(2)
Pt-C_2	2.141(12)	2.154(5)	C_1-Pt-C_6	80.7(5)	82.9(2)
Pt-C_5	2.153(13)	2.171(5)	C_2-Pt-C_5	82.4(5)	81.0(2)
Pt-C_6	2.167(13)	2.151(5)	χ^a	86.7(6)	86.6(1)
C_1-C_2	1.400(17)	1.402(7)	ψ^b	78.8(7)	79.1(2)
C_5-C_6	1.387(19)	1.392(7)			

a χ: $C_1MC_2 \cap C_5MC_6$ b ψ: $C_2C_3C_4C_5 \cap C_1C_8C_7C_6$ see Figure 1.2

The cationic (**16a**) species of [Pt(cod)(3Br-trop)]PF_6 with its numbering scheme is depicted in Figure 7.27, this numbering scheme holds for the [Pt(cod)(3Br-trop)]BF_4 (**17**) complex. There is a square planar geometry (Figure 4.2) around the platinum metal centre with co-ordinating 1,5-cyclo-octadine and tribromotropolonato moieties . The oxidation state of the platinum(II) metal centre remains +2 resulting in the cationic nature of the complex. This resulting charge is balanced by a counter-ion either hexafluorophosphate (PF_6^-) or tetrafluoroborate (BF_4^-). The average distances for the **16a** complex for Pt-O, Pt-C and C=C co-ordination were found to be 2.032(8) Å, 2.160(13) Å and 1.394(18) Å respectively. The angle between the planes defined by the tropolone ring and the platinum, oxygen and adjacent carbons is twisted by 1.6(3)°. The average distances found for the **17a** complex for Pt-O, Pt-C and C=C were found to be 2.019(4) Å, 2.158(5) Å and 1.397(7) Å respectively, with a twist angle of 6.1(1)°. The Pt-O bond lengths are non-equivalent with a difference of *c.a.*

0.022 Å this as a result of the Br···Br and Br···F interactions that occur on the bromines (Br_1 and Br_3) of the tropolonato moiety.

The hydrogen bonding of complex **11** is graphically presented in Figure 7.28 and 7.29 with Table 7.13 listing the bond distances and angles.

Table 7.13 Hydrogen bond distances and angles for [Pt(cod)(3Br-trop)]PF_6 (16) [Å and °].

D-H...A	d(D-H)	d(H...A)	d(D...A)	<(DHA)
C_8-H_{8B}...F_{01}	0.99	2.40	3.171(16)	134.3
C_1-H_1...$F_{02}^{\#1}$	1.00	2.46	3.276(17)	138.0
C_2-H_2...$Br_3^{\#1}$	1.00	2.87	3.654(13)	136.2
C_{14}-H_{14}...$F_{03}^{\#2}$	0.95	2.43	3.359(14)	165.7
C_3-H_{3B}...$F_{01}^{\#3}$	0.99	2.49	3.411(16)	154.1
C_5-H_5...$F_{06}^{\#4}$	1.00	2.50	3.458(18)	160.2

Symmetry transformations used to generate equivalent atoms:
#1 x-1/2,y-1/2,z #2 -x+3/2,-y+1/2,-z+1 #3 -x+3/2,y-1/2,-z+3/2
#4 x+1/2,y-1/2,z

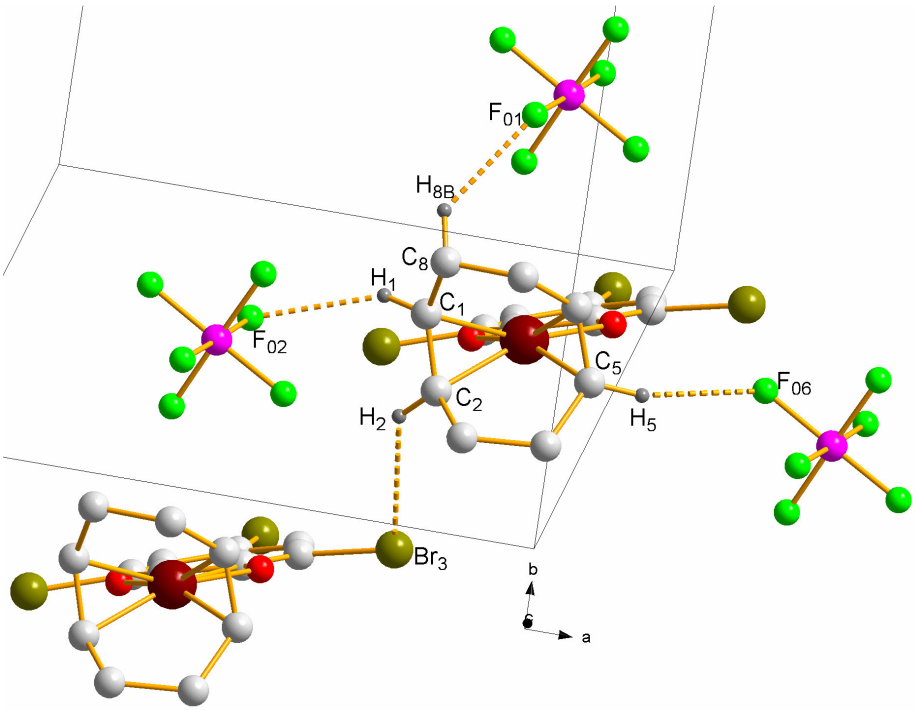

Figure 7.28 Partial unit cell of [Pt(cod)(3Br-trop)]PF_6 (16) showing intermolecular hydrogen bonding interactions indicated by a dashed bond. Only selected hydrogen atoms are included. Platinum (dark red), carbon (grey), oxygen (red), bromine (dark yellow), phosphorous (pink) and fluorine (green).

There is only a single interaction of the type **16a**···**16a** that of the hydrogen of the olefinic carbon (C_2) of the 1,5-cyclo-octadiene moiety with the bromine (Br_3) of the tribromotropolonato moiety (Figure 7.28). Several hydrogen interactions were observed (Figure 7.28 and Figure 7.29) of the type **16a**···**16b** and are listed in Table

7.13. The first being the interaction with the hydrogens of the olefinic carbons (C_1 and C_5) of the 1,5-cyclo-octadiene moiety with the florido (F_{02} and F_{06}) ligands of the **16b** species.

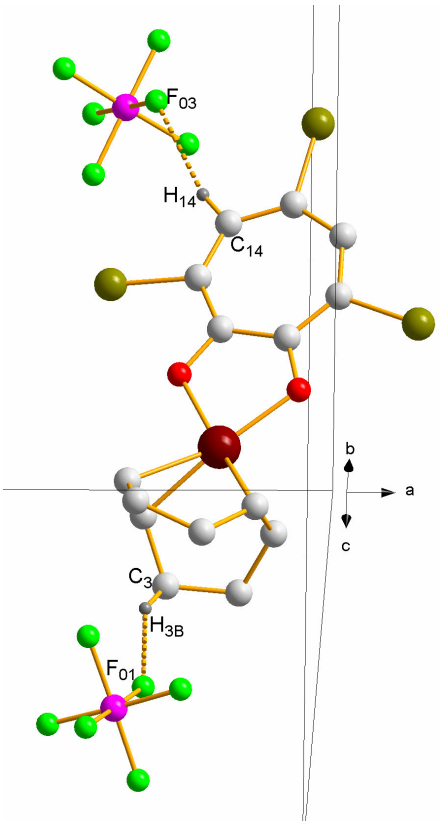

Figure 7.29 Partial unit cell of [Pt(cod)(3Br-trop)]PF_6 (16) showing intermolecular hydrogen bonding interactions indicated by a dashed bond. Only selected hydrogen atoms are included. Platinum (dark red), carbon (grey), oxygen (red), bromine (dark yellow), phosphorous (pink) and fluorine (green).

Secondly the hydrogen interactions between the hydrogens of the alkane carbons (C_8 and C_3) of the 1,5-cyclo-octadiene moiety with the fluorido (F_{01} and F_{06}) ligands of the **16b** species. The last hydrogen interaction is observed between the hydrogen of the carbon (C_{14}) of the tribromotropolonato moiety and the fluorido (F_{03}) ligand of the **16b** species.

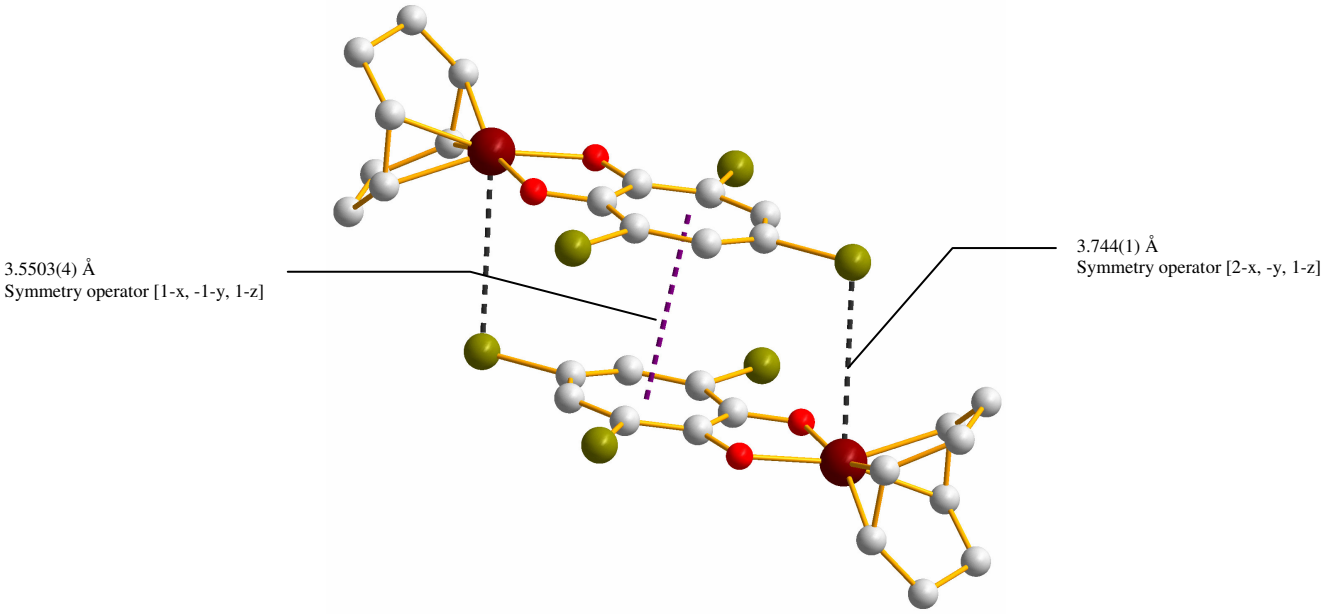

Figure 7.30 Pt···Br and π···π interactions for [Pt(cod)(3Br-trop)]PF_6 (16) indicated by dashed grey and violet bonds. Platinum (dark red), carbon (grey), oxygen (red) and bromine (dark yellow).

Both Pt···Br and π···π interactions were observed for [Pt(cod)(3Br-trop)]PF_6 (**16**) with distances of 3.744(1) Å and 3.5503(4) Å respectively (Figure 7.30). This results in dimeric clusters within the packing of the unit cell, an example of these clusters can be seen in Figure 7.31. Additional Br···π and Br···Br interactions are also observed in Figure 7.31.

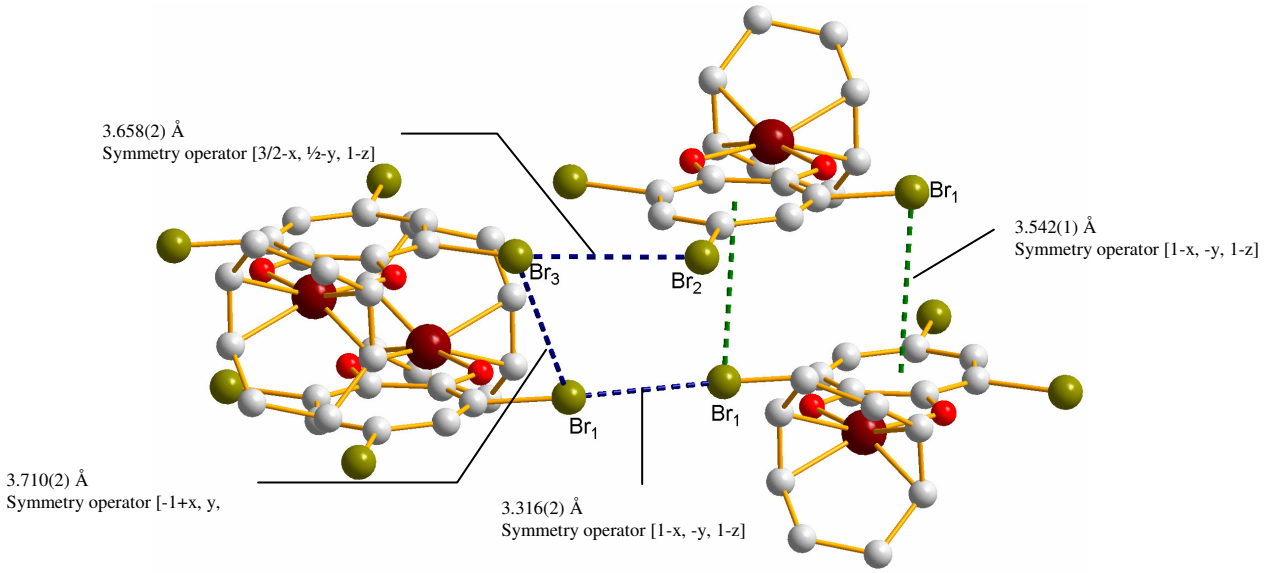

Figure 7.31 Br···π and Br···Br interactions for [Pt(cod)(3Br-trop)]PF_6 (16) indicated by dashed green and blue bonds. Platinum (dark red), carbon (grey), oxygen (red) and bromine (dark yellow).

With distances for the Br···Br interactions being 3.316(2) Å, 3.710(2) Å and 3.658(2) Å respectively. The bromo triad is seen for Br_1, Br_3 and Br_2 with a slightly long interaction between $Br_1 \cdots Br_2$ of 4.405(2) Å. The Br···π interaction has a distance of 3.542(1) Å.

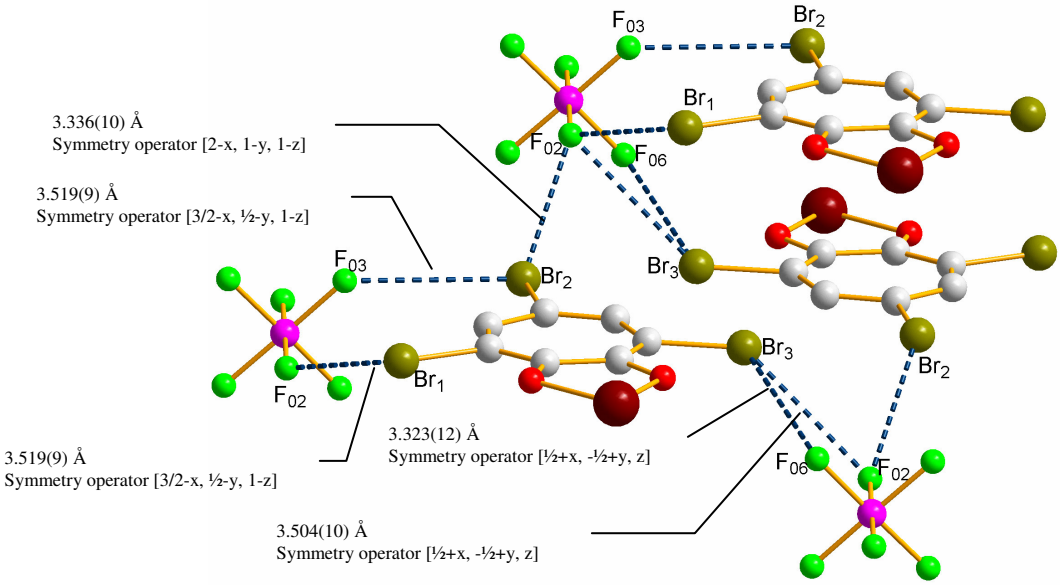

Figure 7.32 Br···F interactions for [Pt(cod)(3Br-trop)]PF_6 (16) indicated by dashed blue bonds. The hydrogens and the 1,5-cyclo-octadiene moieties have been omitted for clarity. Platinum (dark red), carbon (grey), oxygen (red), bromine (dark yellow), phosphorus (pink) and fluorine (green).

The last interaction observed was that of the Br···F interactions which can be seen in Figure 7.32. With both the Br···F and hydrogen interactions the counter ion is held tightly between the 1,5-cyclo-octadiene moiety and the adjacent tropolonato moiety.

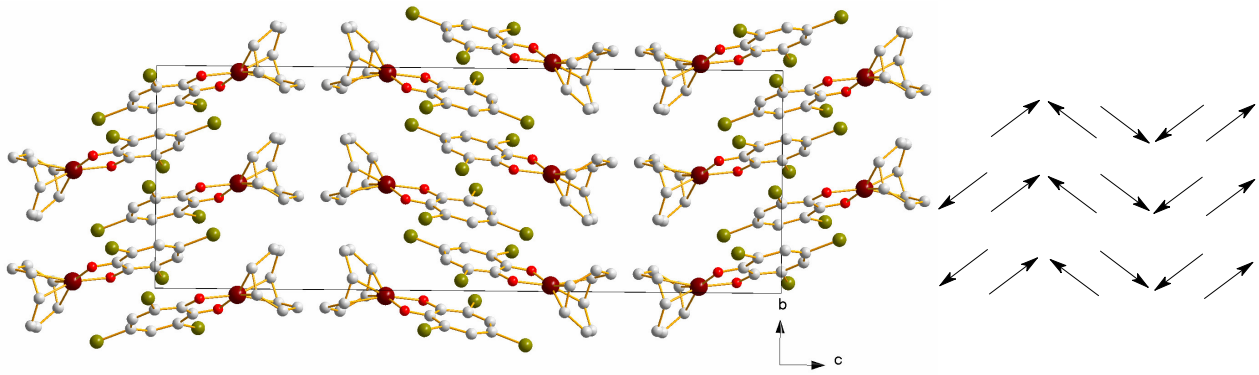

Figure 7.33 Packing of [Pt(cod)(3Br-trop)]PF_6 (16) viewed along the *a*-axis with the packing motif incorporated to the right of the figure. Platinum (dark red), carbon (grey), oxygen (red) and bromine (dark yellow). Hydrogens and PF_6^- have been omitted for clarity.

The packing motif in Figure 7.33 is defined as the head of the arrow corresponding to the 1,5-cyclo-octadiene moiety and the tail of the arrow corresponding to the tribromotropolonato moiety. When looking at the figure one observes a general zig-zag pattern as a result of the Br···π interactions when viewed along the *a*-axis. However when viewing the unit cell along the *c*-axis the clusters resulting from the π···π and Pt···Br interactions are clearly visible (Figure 7.34).

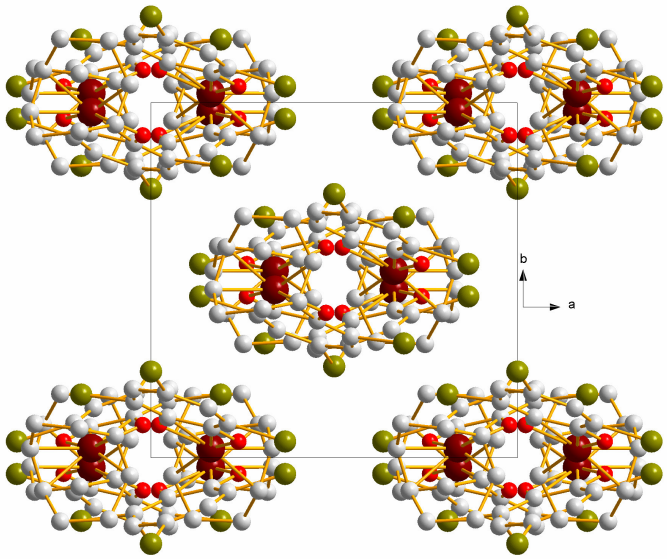

Figure 7.34 Packing of [Pt(cod)(3Br-trop)]PF_6 (16) viewed along the *c*-axis. Platinum (dark red), carbon (grey), oxygen (red) and bromine (dark yellow). Hydrogens and PF_6^- have been omitted for clarity.

The hydrogen bonding of complex **17** is graphically presented in Figure 7.35 with Table 7.14 listing the bond distances and angles.

Table 7.14 Hydrogen bond distances and angles for [Pt(cod)(3Br-trop)]BF_4 (17) [Å and °].

D-H...A	d(D-H)	d(H...A)	d(D...A)	<(DHA)
C_1-H_{01}...F_2	1.00	2.40	3.167(6)	132.7
C_2-H_{02}...$F_4^{\#1}$	1.00	2.51	3.477(7)	163.9
C_3-H_{03A}...$F_3^{\#2}$	0.99	2.51	3.281(6)	135.1
C_{12}-H_{12}...$F_1^{\#3}$	0.95	2.42	3.356(6)	168.8
C_5-H_{05}...$Br_1^{\#4}$	1.00	2.90	3.767(6)	145.7

Symmetry transformations used to generate equivalent atoms:
#1 x,y+1,z #2 x-1,y+1,z #3 -x+1,-y,-z #4 x-1,y,z

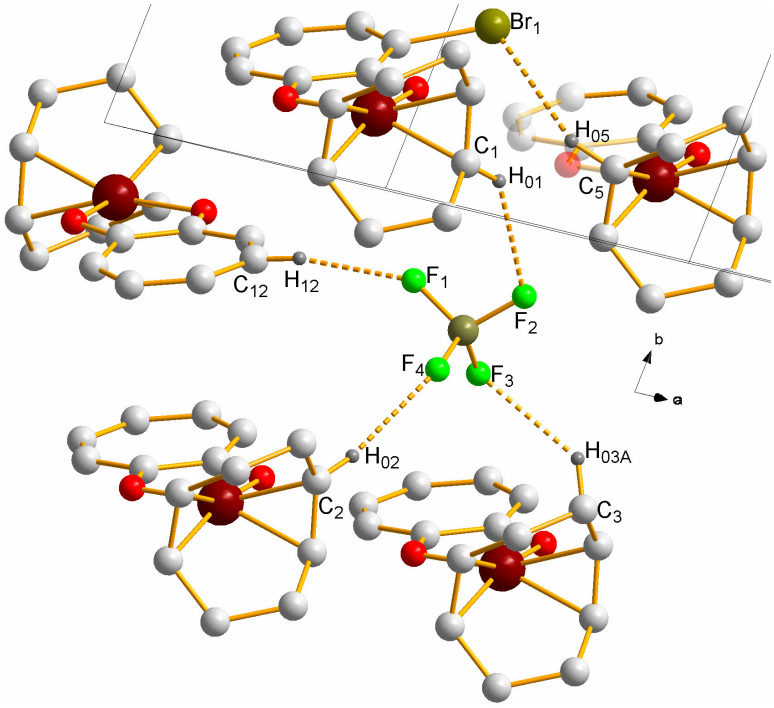

Figure 7.35 Partial unit cell of [Pt(cod)(3Br-trop)]BF_4 (17) showing intermolecular hydrogen bonding interactions indicated by a dashed bond. Only selected hydrogen and bromine atoms are included. Platinum (dark red), carbon (grey), oxygen (red), bromine (dark yellow), boron (olive green) and fluorine (green).

As with the **16a** complex one finds only one hydrogen interaction of the type **17a**···**17a** that of a bromine (Br_1) on the tropolonato moiety with the hydrogen of the olefinic carbon (C_5) of the cyclo-octadiene moiety. The second type being **17a**···**17b** makes up the remainder of the interactions. With the hydrogens of the olefinic carbons (C_1 and C_2) interacting with the fluorido ligands (F_2 and F_4) of the **17b** complex. The hydrogens of the alkane carbon (C_3) with the fluorido ligand (F_3) of the **17b** complex, and lastly the hydrogen bound to the tropolone carbon (C_{12}) with the fluorido ligand (F_1) of the **17b** complex. These interactions can be seen in Figure 7.35.

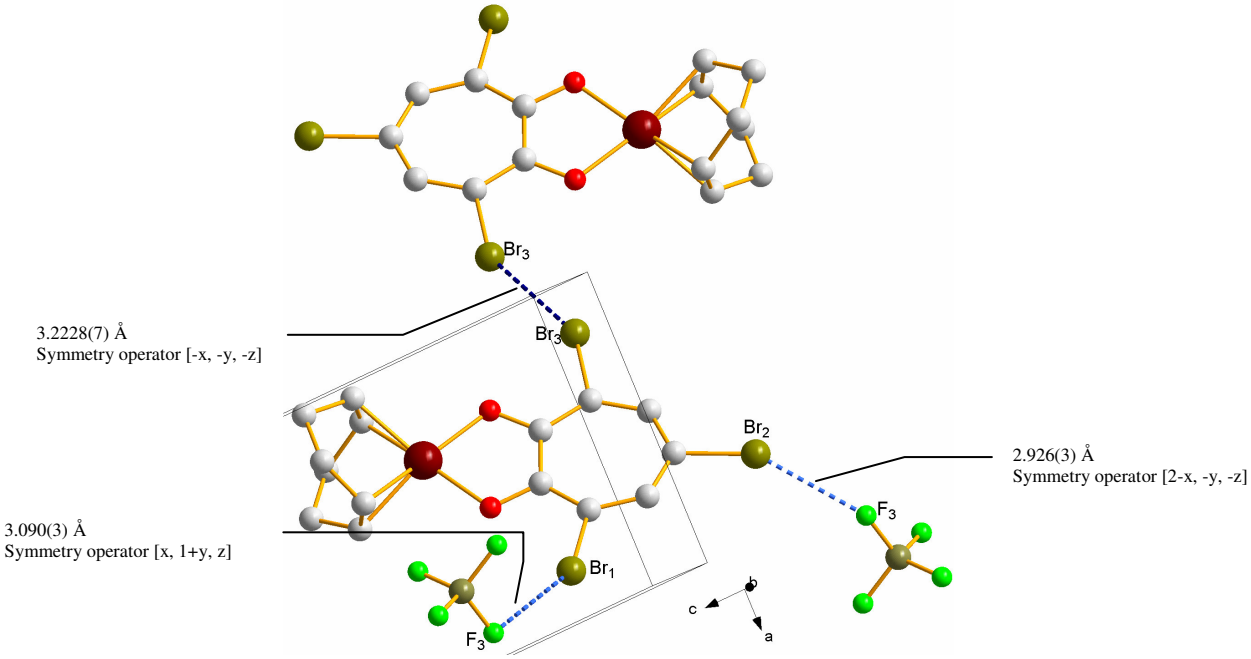

Figure 7.36 Br···F and Br···Br interactions for [Pt(cod)(3Br-trop)]BF_4 (17) indicated by dashed blue and dark blue bonds. The hydrogens have been omitted for clarity. Platinum (dark red), carbon (grey), oxygen (red), bromine (dark yellow), boron (olive green) and fluorine (green).

Additional interactions were observed namely that of the Br···Br and Br···F as are depicted in Figure 7.36. The Br···Br distance was found to be 3.2228(7) Å whereas the two Br···F distances were found to be 3.090(3) Å and 2,926(3) Å.

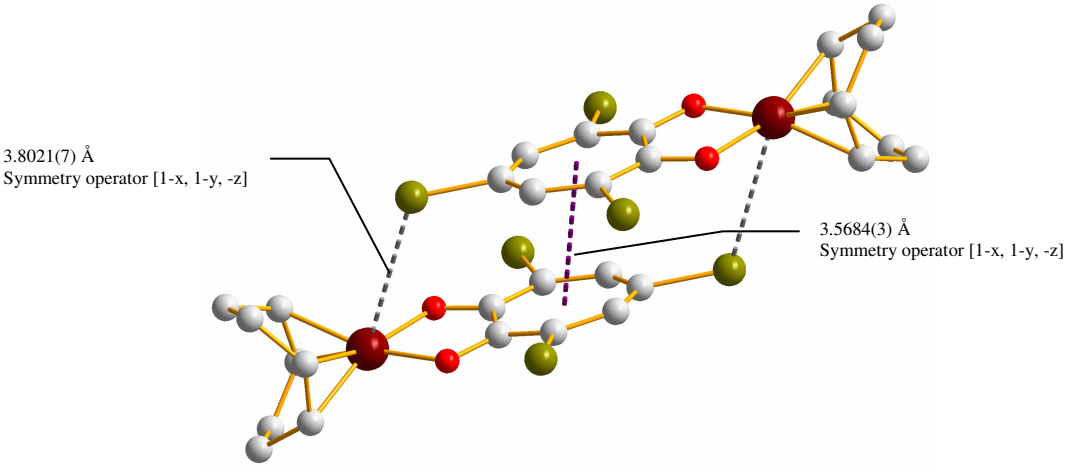

Figure 7.37 Pt···Br and π···π interactions for [Pt(cod)(3Br-trop)]BF_4 (17) indicated by dashed grey and violet bonds. Platinum (dark red), carbon (grey), oxygen (red) and bromine (dark yellow).

The last type of interactions observed were that of the Pt···Br and π···π as seen in Figure 7.37 with distances of 3.8021(7) Å and 3.5684(3) Å respectively. The π-stacking observed gives rise to the tail-to-tail packing seen in Figure 7.38. For

complex **16** identical Pt···Br and π···π interactions were observed with only differences found in the distances for the π···π a difference *c.a.* 0.02 Å and for Pt···Br a difference *c.a.* 0.06 Å the elongation of the distances is due to the **16b** complex interactions being stronger than the **17b** interactions.

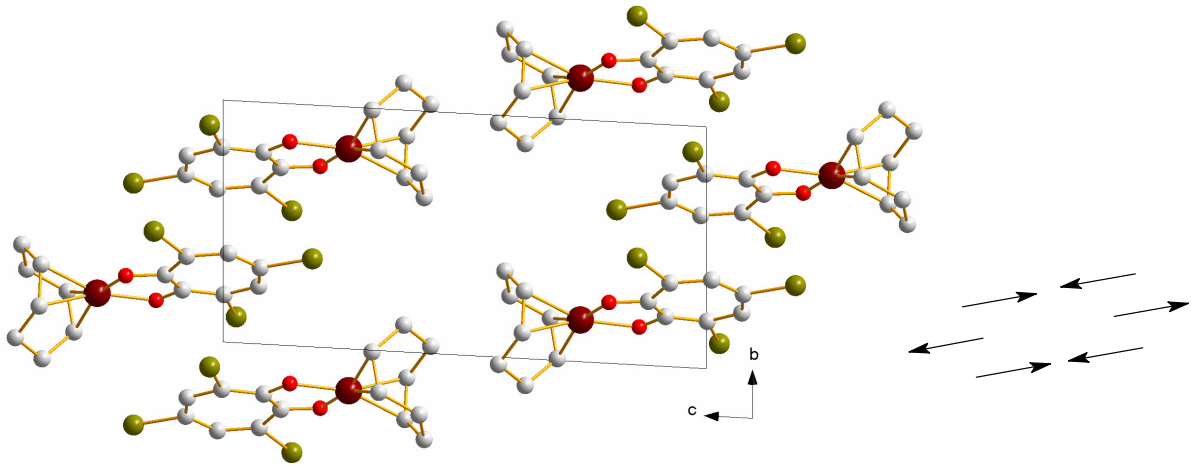

Figure 7.38 Packing of [Pt(cod)(3Br-trop)]BF_4 (17) viewed along the *a*-axis with the packing motif incorporated to the right of the figure. Platinum (dark red), carbon (grey), oxygen (red) and bromine (dark yellow). Hydrogens and BF_4^- have been omitted for clarity.

The packing motif in Figure 7.38 is defined as the head of the arrow corresponding to the 1,5-cyclo-octadiene moiety and the tail of the arrow corresponds to the tribromotropolonato moiety. When looking at the figure one observes a general tail-to-tail packing, clusters that were observed for complex **16** (Figure 7.34) were not found for complex **17**.

7.5 Discussion

The anionic five-membered tropolone and tribromotropolone ligand systems were chosen to determine the strain on the "trans" cyclo-octadiene ligand. The metal centers used for the investigation were platinum and palladium in the +2 oxidation state which resulted in a cationic charge for the four co-ordinated species. The counter ions investigated were hexafluorophosphate (PF_6^-) and tetrafluoroborate (BF_4^-). The cell dimensions of the crystals are summarized in Table 7.15 with selected bond distances and angles of the complexes in Table 7.16. All the compounds were found to have a slightly distorted square planar geometry see Figure 4.2 for an explanation / definition of the co-ordination geometry.

Table 7.15 Cell dimension overview for Palladium(II) and Platinum(II) crystals obtained.

	[Pd(cod)(3Br-trop)]		[Pd(cod)(trop)]	[Pt(cod)(trop)]		[Pt(cod)(3Br-trop)]	
	BF_4 (**12**)	PF_6 (**11**)	PF_6 (**13**)	BF_4 (**15**)	PF_6 (**14**)	BF_4 (**17**)	PF_6 (**16**)
Crystal system	Triclinic	Triclinic	Tetragonal	Tetragonal	Tetragonal	Triclinic	Monoclinic
Space group	$P\bar{1}$	$P\bar{1}$	$P4_2bc$	$P4_2bc$	$P4_2/mbc$	$P\bar{1}$	$C2/c$
a	7.3729(7)	7.8517(10)	16.3117(15)	16.0818(1)	16.3729(3)	7.3583(6)	11.3515(18)
b	8.0026(7)	8.0071(12)	16.3117(15)	16.0818(1)	16.3729(3)	8.0058(6)	11.0127(16)
c	15.9253(16)	15.666(2)	11.9226(14)	11.9361(2)	12.0226(2)	15.9652(10)	31.056(5)
α	85.783(4)	79.000(12)	90	90	90	86.181(6)	90
β	85.387(4)	88.357(10)	90	90	90	85.082(6)	93.456(3)
γ	82.074(5)	87.737(11)	90	90	90	81.742(7)	90
Z	2	2	8	8	7	2	8

The tribromotroplonato compounds **12**, **11** and **17** were found to be isostructural, with very small changes in their unit cells all solving in the triclinic $P\bar{1}$ space group. The troplonato compounds **13**, **14** and **15** were also found to be isostructural. An isostructural crystal is one where the crystals have the same structure but not the same cell dimensions or chemical composition. With the [Pt(cod)(trop)]BF_4 (**15**) having a pseudo-symmetry of a mirror plane perpendicular to the four-fold rotation axis. The result of the inclusion of this additional symmetry the [Pt(cod)(trop)]PF_6 (**14**) compound would then be isomorphous to its counterpart, however with the decrease in temperature to 100K and the recollection of the crystal of complex **15** it was found that there is a possible phase transition between space groups and the structure could not be elucidated satisfactory. Future work will need to be done to determine if a phase transition truly exists and at what temperature this might occur.

Table 7.16 Selected Geometric parameters (Å,°) for Palladium(II) and Platinum(II) metal complexes

	[Pd(cod)(3Br-trop)]		[Pd(cod)(trop)]	[Pt(cod)(trop)		[Pt(cod)(3Br-trop)]	
	BF_4 (**12**)	PF_6 (**11**)	PF_6 (**13**)	BF_4 (**15**)	PF_6 (**14**)	BF_4 (**17**)	PF_6 (**16**)
M-O_1	2.003(3)	2.047(6)	2.018(9)	1.974(15)	1.999(4)	2.008(3)	2.024(9)
M-O_2	2.023(3)	2.002(6)	1.982(8)	2.037(15)	1.999(4)	2.030(4)	2.040(8)
M-C_1	2.180(5)	2.193(8)	2.177(12)	2.098(17)	2.155(10)	2.156(5)	2.178(12)
M-C_2	2.177(5)	2.182(8)	2.193(12)	2.100(16)	2.123(9)	2.154(5)	2.141(12)
M-C_5	2.176(5)	2.178(9)	2.192(12)	2.09(2)	2.123(9)	2.171(5)	2.153(13)
M-C_6	2.201(5)	2.165(8)	2.145(12)	2.32(2)	2.155(10)	2.151(5)	2.167(13)
C_1-C_2	1.387(7)	1.382(12)	1.387(18)	1.48(2)	1.460(19)	1.402(7)	1.400(17)
C_5-C_6	1.381(7)	1.410(11)	1.343(16)	1.25(3)	1.460(19)	1.392(7)	1.387(19)
O_1-M-O_2	80.6(1)	80.1(2)	82.1(2)	80.2(2)	80.6(2)	79.8(1)	80.3(3)
C_1-M-C_2	37.1(2)	36.8(3)	37.0(5)	41.4(6)	39.9(5)	38.0(2)	37.8(5)
C_5-M-C_6	36.8(2)	37.9(3)	36.1(4)	32.5(7)	39.9(5)	37.6(2)	37.5(5)
C_1-M-C_6	81.4(2)	80.5(3)	81.5(4)	78.3(6)	78.7(8)	82.9(2)	80.7(5)
C_2-M-C_5	82.3(2)	81.6(3)	83.0(4)	85.5(5)	82.6(6)	81.0(2)	82.4(5)
χ^a	86.1(1)	85.6(3)	86.7(6)	87.9(10)	87.2(5)	86.6(1)	86.7(6)
ψ^b	83.8(2)	79.7(4)	84.0(8)	85.6(15)	NA	79.1(2)	78.8(7)

a χ: $C_1MC_2 \cap C_5MC_6$ b ψ: $C_2C_3C_4C_5 \cap C_1C_8C_7C_6$ see Figure 1.2

The distortion from square planar (as identified by the intersection of the planes defined by the mid-point of the alkene carbons of the cyclo-octadiene ring with the oxygens of the β-diketones and the metal centre with the β-diketone back-bone) is indicated as follows: **16 > 11 > 13 > 17 > 12 > 15 > 14** with values of 1.6(3)°, 3.6(2)°, 5.8(2)°, 6.1(1)°, 6.7(1)°, 9.7(2)° and 10.8(1)° respectively. From this series it is shown that the metal centers are grouped together and that the tribromotroplonato ligand shows less distortion to the square planar geometry than that of the tropolonato ligand. For the counter ions a similar grouping is observed with the PF_6^- showing again a smaller distortion than that of the BF_4^- counter ion. The values were obtained by the intersection of the planes defined by the mid-point of the alkene carbons of the cyclo-octadiene ring with the oxygens of the tropolonato type ligands and the metal centre with the full tropolone ring.

The bromo "triad" as first observed by Steyl *et. al.*[13] for [Pd(3Br-trop)Br(PCy_3)] is seen for [Pd(cod)(3Br-trop)]PF_6 (**11**) (Figure 7.10) and [Pd(cod)(3Br-trop)]BF_4 (**12**) (Figure 7.4) however the distances for Br···Br interactions are large, this is as a result of the additional Br···π interactions that were observed for complexes **11** and **12**. This pattern is continued for the [Pt(cod)(3Br-trop)]PF_6 (**16**) (Figure 7.31) where the interactions fall within the acceptable range for bromine interactions. The result of this contraction is the Pt···Br (Figure 7.30) interaction that was found, no comparable

interaction was found for either of the palladium complexes. It is interesting to note however that the [Pt(cod)(3Br-trop)]BF_4 (**17**) does not have this triad interaction.

In considering the packing of the compounds in this study it was observed that for compounds **13**, **14** and **15** an identical packing (Figure 7.19, 7.22 and 7.25) was found which was a classic four-fold rotation axis, the lack of π···π interactions results in a different packing for the remaining compounds. For [Pd(cod)(3Br-trop)]BF_4 (**12**) a classic head-to-tail packing was found (Figure 7.7) with a tail-to-tail (Figure 7.13) packing for the PF_6^- (**11**) counterpart, which is a result of the Br···π interactions. The [Pt(cod)(3Br-trop)]BF_4 (**17**) has a similar packing to complex **11** (Figure 7.38), with a zig-zag pattern found for [Pt(cod)(3Br-trop)]PF_6 (**16**) (Figure 7.33).

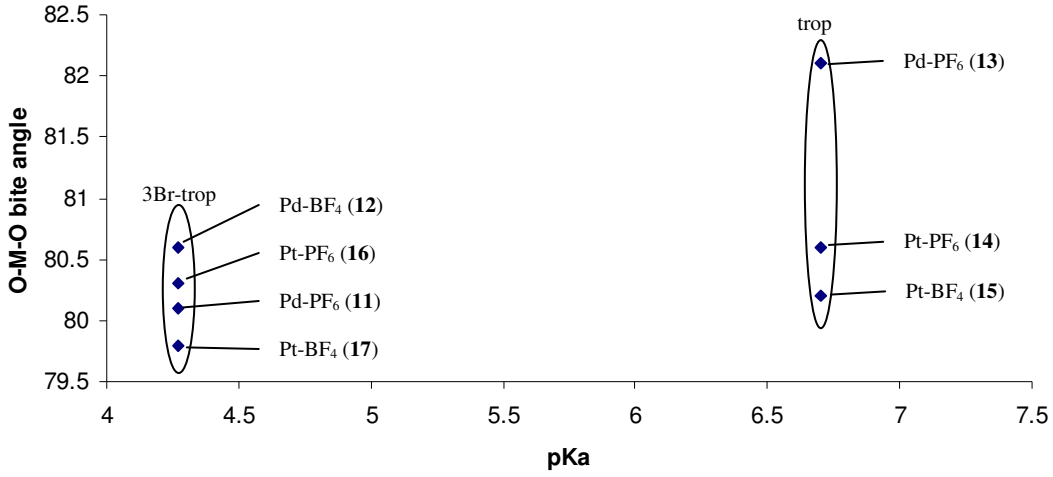

Figure 7.39 Graph of pK_a *vs.* O-M-O bite angle for the [M(cod)(LL')]A where M = Pt(II), Pd(II), LL' = trop, 3Br-trop and A = BF_4^-, PF_6^- complexes.

The graph of the acid dissociation constant (pK_a) *vs.* the O-M-O bite angle (Figure 7.39) indicates similar bite angles for most of the complexes with complex **13** being an outlier. There are several points of interest first it is noted that the 2008 covalent radii of platinum (1.36 Å) is smaller than for palladium (1.39 Å) (see Table 2.1) this contraction is seen in the table where the palladium bite angle is consistently larger than that of the platinum complexes. Also of interest is the variation of the counter ion in that the BF_4^- is known to have a smaller pK_a value as opposed to PF_6^- thus making it a "weaker" counter ion and resulting in a smaller bite angle than that seen for the PF_6^- ion.

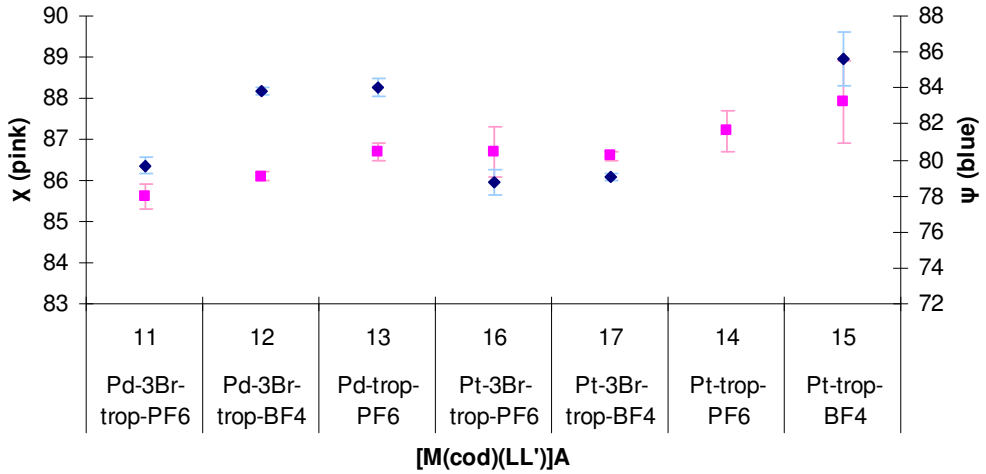

Figure 7.40 Graph of [M(cod)(LL')]A where LL' = trop, 3Br-trop and A = PF_6^-, BF_4^- crystal complexes *vs.* χ (pink squares) and ψ (blue diamonds) angles arranged in ascending order of χ angle (see Chapter 1 Figure 1.2 for definition of χ and ψ angles).

A general opening and closing of 6.8° for the ψ angle was observed in Figure 7.40 which was sorted in ascending value by the χ angle.

In the next chapter correlations between the crystal structures presented in this chapter and there respective computationally calculated / optimized structures will be compared and discussed.

Chapter 8
Solid State *vs.* Optimized Structure Correlation of Tropolonato Complexes

8.1 Introduction

This chapter will present the comparison between the tropolonato type complexes of platinum(II) and palladium(II) with regards to their respective crystal structures and theoretical calculations. Table 8.1 presents a list of the crystal structures that will be discussed the sections to follow.

Table 8.1 Tropolonato complexes of platinum(II) and palladium(II)

Compound		Ref
[Pd(cod)(trop)]PF_6	**13**	§ 7.3.2
[Pd(cod)(3Br-trop)]BF_4	**12**	§ 7.3.1
[Pd(cod)(3Br-trop)]PF_6	**11**	§ 7.3.1
[Pt(cod)(trop)]BF_4	**15**	§ 7.4.1
[Pt(cod)(trop)]PF_6	**14**	§ 7.4.1
[Pt(cod)(3Br-trop)]BF_4	**17**	§ 7.4.2
[Pt(cod)(3Br-trop)]PF_6	**16**	§ 7.4.2

For the theoretical calculations in this section, tropolone (Htrop) and tribromotropolone (H3Br-trop) were selected for their increasing electron donating capability. Together with studying the effect on the geometry of cyclo-octadiene ring. For the sake of completeness the entire group 10 metal triad was computed.

8.2 Experimental

The DFT molecular orbital calculations were carried out using the Gaussian 03[1] software suite. Becke's three parameter hybrid (B3LYP)[2,3] exchange correlation functional was used. The basis set employed in this study was 6-311++G(d,p)[4,5,6] for the main group elements and LanL2DZ[7] for the middle to late transition metals. Vibrational frequencies were calculated at the 6-311++G(d,p)[4,5,6] level for the main group elements and at the LanL2DZ[7] level for the middle to late transition metals with minimum energies confirmed to have zero imaginary frequencies. The frequencies are unscaled and were used to compute the zero-point vibrational energies. Molecular graphics were obtained using DIAMOND[8],while overlay graphics were obtained using HyperChem 7.5[9].

8.3 Crystal Structure Correlation of Palladium(II) *vs.* Platinum(II) Complexes

In looking at the various radii (atomic, covalent and van der Waal) for palladium and platinum it is observed that there are only marginal differences between the two metal centers (Table 2.4). The quantities obtained in 2008 by Cordero[10] *et al.* show a value

---

[1] Frisch M.J., Trucks G.W., Schlegel H.B., Scuseria G.E., Robb M.A., Cheeseman J.R., Montgomery J.A. Jr., Vreven T., Kudin K.N., Burant J.C., Millam J.M., Iyengar S.S., Tomasi J., Barone V., Mennucci B., Cossi M., Scalmani G., Rega N., Petersson G.A., Nakatsuji H., Hada M., Ehara M., Toyota K., Fukuda R., Hasegawa J., Ishida M., Nakajima T., Honda Y., Kitao O., Nakai H., Klene M., Li X., Knox J.E., Hratchian H.P., Cross J.B., Bakken V., Adamo C., Jaramillo J., Gomperts R., Stratmann R.E., Yazyev O., Austin A.J., Cammi R., Pomelli C., Ochterski J.W., Ayala P.Y., Morokuma K., Voth G.A., Salvador P., Dannenberg J.J., Zakrzewski V.G., Dapprich S., Daniels A.D., Strain M.C., Farkas O., Malick D.K., Rabuck A.D., Raghavachari K., Foresman J.B., Ortiz J.V., Cui Q., Baboul A.G., Clifford S., Cioslowski J., Stefanov B.B., Liu G., Liashenko A., Piskorz P., Komaromi I., Martin R.L., Fox D.J., Keith T., Al-Laham M.A., Peng C.Y., Nanayakkara A., Challacombe M., Gill P.M.W., Johnson B., Chen W., Wong M.W., Gonzalez C., Pople J.A., Gaussian 03, Revision E.01, Gaussian Inc., Wallingford CT, (2004)

[2] Becke A.D., *J. Chem. Phys.*, **98**, 5648, (1993)

[3] Lee C., Yang W., Parr R.G., *Phys. Rev.*, **B37**, 785, (1988)

[4] Ditchfield R., Hehre W.J., Pople J.A., *J. Chem. Phys.*, **54**, 724, (1971)

[5] Gordon M.S., *Chem. Phys. Lett.*, **76**, 163, (1980)

[6] Rassolov V.A., Ratner M.A., Pople J.A., Redfern P.C., Curiss L.A., *J. Comp. Chem.*, **22**, 976, (2001)

[7] Hay P.J., Wadt W.R., *J. Chem. Phys.*, **82**, 299, (1985)

[8] Brandenburg K., Brendt M., DIAMOND, Release 2.1e. Crystal Impact GbR, Potfach 1251, D53002 Bonn, Germany., (2001)

[9] HyperChem™ Release 7.52, Windows Molecular Modeling System, HyperCube Inc., (2002)

[10] Cordero B., Gómez V., Platero-Prats A.E., Revés M., Echeverría J., Cremades E., Barragán F., Alvarez S., *Dalton Trans.*, (2008)

of 1.39 Å for palladium and 1.36 Å for platinum. Both metals are known for their square planar co-ordination geometry, with the +2 oxidation state being the most widespread.

Table 8.2 Cell dimension overview for Palladium(II) and Platinum(II) crystal structures obtained.

	[Pd(cod)(3Br-trop)]		[Pd(cod)(trop)]	[Pt(cod)(trop)]		[Pt(cod)(3Br-trop)]	
	BF_4 (**12**)	PF_6 (**11**)	PF_6 (**13**)	BF_4 (**15**)	PF_6 (**14**)	BF_4 (**17**)	PF_6 (**16**)
Crystal system	Triclinic	Triclinic	Tetragonal	Tetragonal	Tetragonal	Triclinic	Monoclinic
Space group	$P\bar{1}$	$P\bar{1}$	$P4_2bc$	$P4_2bc$	$P4_2/mbc$	$P\bar{1}$	$C2/c$
a	7.3729(7)	7.8517(10)	16.3117(15)	16.0818(1)	16.3729(3)	7.3583(6)	11.3515(18)
b	8.0026(7)	8.0071(12)	16.3117(15)	16.0818(1)	16.3729(3)	8.0058(6)	11.0127(16)
c	15.9253(16)	15.666(2)	11.9226(14)	11.9361(2)	12.0226(2)	15.9652(10)	31.056(5)
α	85.783(4)	79.000(12)	90	90	90	86.181(6)	90
β	85.387(4)	88.357(10)	90	90	90	85.082(6)	93.456(3)
γ	82.074(5)	87.737(11)	90	90	90	81.742(7)	90
Z	2	2	8	8	7	2	8

Previously reported in Chapter 7, the tribromotroplonato compounds **12**, **11** and **17** were found to be isostructural, with very small changes in their unit cells all solving in the triclinic $P\bar{1}$ space group. The troplonato compounds **13**, **14** and **15** were also found to be isostructural. With the [Pt(cod)(trop)]BF_4 (**15**) having a pseudo-symmetry of a mirror plane perpendicular to the four-fold rotation axis, as a result inclusion of this additional symmetry the [Pt(cod)(trop)]PF_6 (**14**) compound would then be isomorphous.

The overlay of the isostructural X-ray crystal structures is a graphical representation of the pair-wise differences of the related structures. This mathematical value is represented by the root mean square (RMS) value, which is a measure of how far the average is from zero, providing information on the variations of bond lengths and angles and to a certain degree the orientation of the structures in relation to each other. These comparisons are presented in Figure 8.1-8.6.

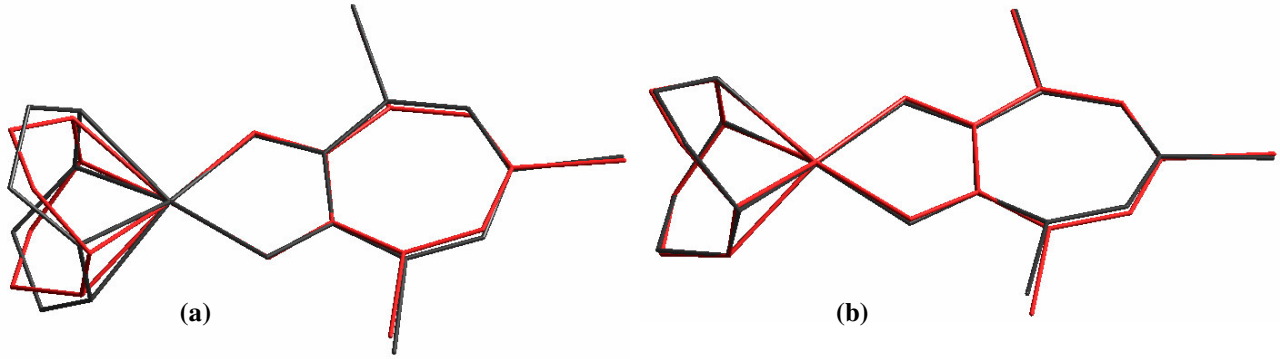

Figure 8.1 HyperChem superimposed image of (a) [Pd(cod)(3Br-trop)]BF_4 (12) (black) *vs.* [Pd(cod)(3Br-trop)]PF_6 (11) (red) with an RMS error of 0.3 Å (b) [Pd(cod)(3Br-trop)]BF_4 inverted crystal structure (12) (black) *vs.* [Pd(cod)(3Br-trop)]PF_6 (11) (red) with an RMS error of 0.1 Å. Counter ions have been omitted for clarity.

The overlay of complexes **11** and **12** depicted in Figure 8.1a has an RMS error of 0.3 Å. The difference observed is in the distortion from the square planar co-ordination geometry. The result of complex **12** having a centrosymmetric space group (triclinic $P\bar{1}$), a second enantiomer exists within the unit cell, this enantiomer has been overlaid with complex **12** (Figure 8.1b) and an RMS error of 0.097 Å was observed. Previously stated in Chapter 7 the difference in bend angle (*i.e.* the intersection of the planes defined by the metal centre with the oxygens and the two adjacent carbons of the tropolone ring *vs.* the plane defined by the tropolone ring) was found to be 3.1(1)°. Where the bend angle values for complex **11** and **12** are 3.6(2)° and 6.7(1)° respectively. The twist angle (*i.e.* the intersection of the planes defined by the mid-points of the alkene carbons of the cyclo-octadine ring with the oxygens of the tribromotropolonato ligand *vs.* the metal centre with the oxygens and the two adjacent carbons of the tropolone ring) for complex **11** and **12** are 1.2(1)° and 0.97(8)° which are similar leading to the lower RMS error value obtained.

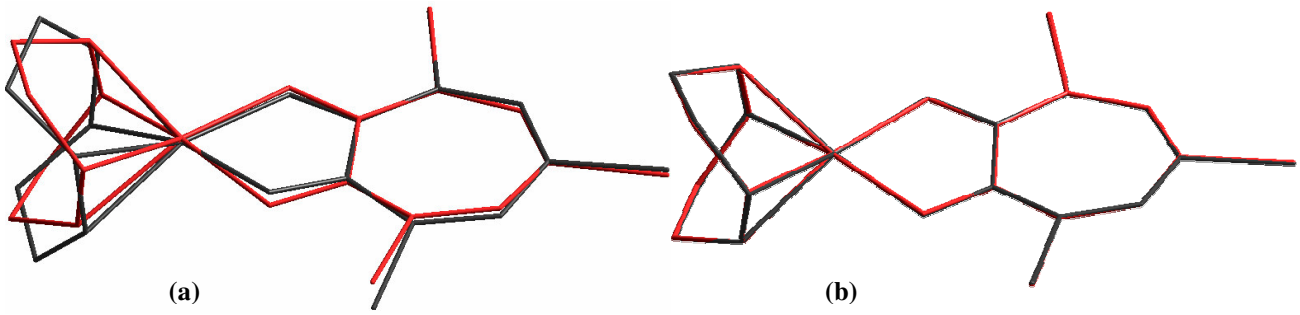

Figure 8.2 HyperChem superimposed image of (a) [Pd(cod)(3Br-trop)]BF_4 (12) (black) *vs.* [Pt(cod)(3Br-trop)]BF_4 (17) (red) with an RMS error of 0.1350 Å (b) [Pd(cod)(3Br-trop)]BF_4 inverted crystal structure (12) (black) *vs.* [Pt(cod)(3Br-trop)]BF_4 (17) (red) with an RMS error of 0.02 Å. Counter ions have been omitted for clarity.

The overlay of complexes **12** and **17** shown in Figure 8.2a has an RMS error of 0.135 Å based on the metal centre and the oxygens and two adjacent carbons of the tribromotroplonato ligand. Previously stated complex **12** has a centrosymmetric space group and as a result there are two enantiomers within the unit cell. The second enantiomer is overlaid with complex **17** (Figure 8.2b) and has an RMS error of 0.0219 Å based on all atoms excluding the bromines. The differences between these complexes is the bend angle (*i.e.* the intersection of the planes defined by the metal centre with the oxygens and the two adjacent carbons of the tropolone ring *vs.* the plane defined by the tropolone ring) with a difference of 0.6(1)° (**12** : 6.7(1)°; **17** : 6.1(1)°). The second difference is found in the twist angle (*i.e.* the intersection of the planes defined by the mid-points of the alkene carbons of the cyclo-octadine ring with the oxygens of the tribromotropolonato ligand *vs.* the metal centre with the oxygens and the two adjacent carbons of the tropolone ring) with a difference of 0.12(8)° (**12** : 0.97(8)°; **17** : 0.85(8)°). The last difference observed is that of the ψ angle with a difference of 4.7(1)° for the complexes (**12** : 83.8(2)°; **17** : 79.1(2)°). The bend and twist angle effects are cumulative on the orientation of the complexes to one another with the twist angle having the larger influence of the two and as a result if the RMS error value is re-calculated using all atoms excluding the bromine atoms an RMS error of 1.5868 Å is obtained.

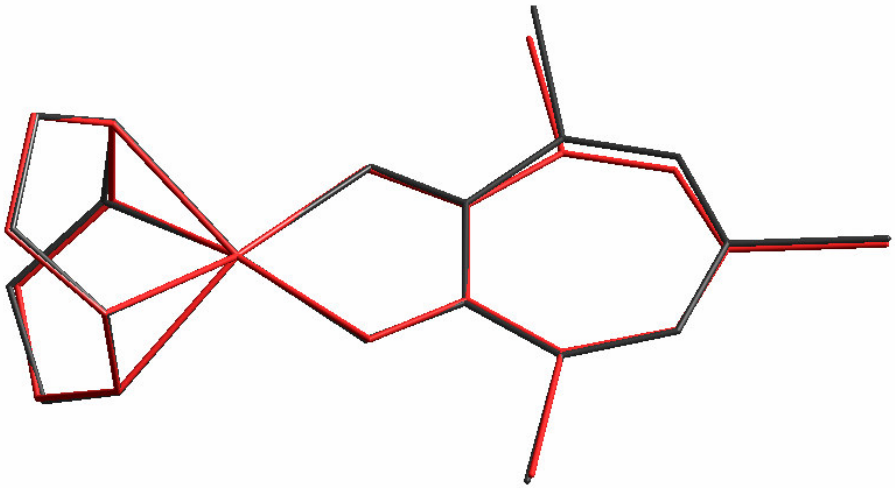

Figure 8.3 HyperChem superimposed image of [Pd(cod)(3Br-trop)]PF_6 (11) (black) *vs.* [Pt(cod)(3Br-trop)]PF_6 (16) (red) with an RMS error of 0.08 Å Counter ions have been omitted for clarity.

The overlay of complexes **11** and **16** shown in Figure 8.3 has an RMS error of 0.075 Å based on the metal centre and the oxygens and two adjacent carbons of the tribromotroplonato ligand. The differences between these complexes is the bend angle (*i.e.* the intersection of the planes defined by the metal centre with the oxygens and the two adjacent carbons of the tropolone ring *vs.* the plane defined by the tropolone ring) with a difference of 2.0(2)° (**11** : 3.6(2)°; **16** : 1.6(2)°). The second difference is found in the twist angle (*i.e.* the intersection of the planes defined by the mid-points of the alkene carbons of the cyclo-octadine ring with the oxygens of the tribromotropolonato ligand *vs.* the metal centre with the oxygens and the two adjacent carbons of the tropolone ring) with a difference of 1.5(2)° (**11** : 1.2(1)°; **16** : 2.7(2)°).

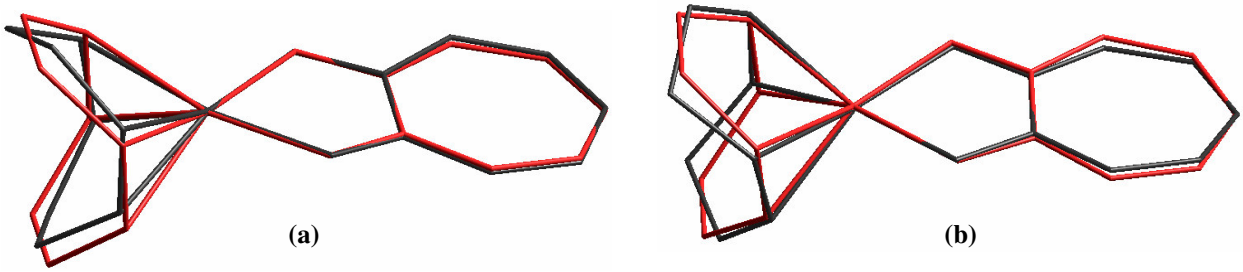

Figure 8.4 HyperChem superimposed image of (a) [Pd(cod)(trop)]PF_6 (13) (black) *vs.* [Pt(cod)(trop)]PF_6 (14) (red) with an RMS error of 0.04 Å (b) [Pd(cod)(trop)]PF_6 inverted crystal structure (13) (black) *vs.* [Pt(cod)(trop)]PF_6 (14) (red) with an RMS error of 0.19 Å. Counter ions have been omitted for clarity.

The overlay of complexes **13** and **14** shown in Figure 8.4a has an RMS error of 0.0385 Å based on the metal centre and the oxygens and two adjacent carbons of the troplonato ligand. A full RMS error based on all the atoms is computed, a value of 1.6908 Å is obtained. Due to complex **13** having a centrosymmetric space group (tetragonal $P4_2bc$) a secondary enantiomer exists, the overlay in Figure 8.4b has an RMS error of 0.19 Å based on all the atoms. The differences between these complexes is firstly the bend angle (*i.e.* the intersection of the planes defined by the metal centre with the oxygens and the two adjacent carbons of the tropolone ring *vs.* the plane defined by the tropolone ring) with a difference of 0.8(4)° (**13** : 5.8(2)°; **14** : 5.0(5)°), there is not a large variance in the bend angles when the errors on the values obtained are taken into account they are virtually similar to one another. The second difference is found in the twist angle (*i.e.* the intersection of the planes defined by the mid-points of the alkene carbons of the cyclo-octadine ring with the oxygens of

the tropolonato ligand *vs.* the metal centre with the oxygens and the two adjacent carbons of the tropolone ring) with a difference of 2.1(2)° (**13** : 8.7(2)°; **14** : 10.8(1)°). The last difference is in the positions of the alkane carbons of the cyclo-octadiene ring, there is a cross-over of the positions of the alkane carbons for the complexes.

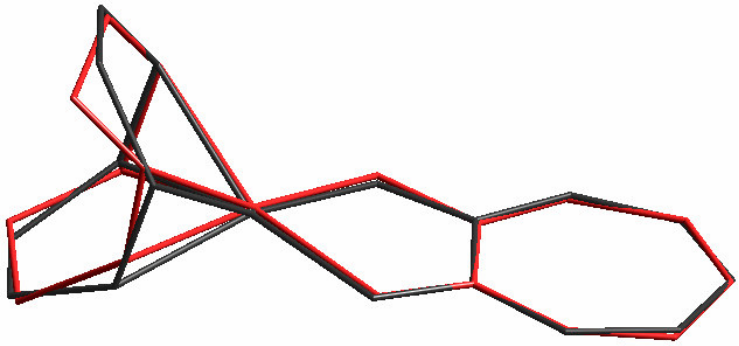

Figure 8.5 HyperChem superimposed image of [Pt(cod)(trop)]PF_6 (14) (black) *vs.* [Pt(cod)(trop)]BF_4 (15) (red) with an RMS error of 0.19 Å. Counter ions have been omitted for clarity.

The overlay of complexes **14** and **15** shown in Figure 8.5 has an RMS error of 0.1952 Å based on all atoms. The two differences that were observed are the differences in the bend and twist angles with values of 1.5(4)° (**14** : 5.0(5)°; **15** : 6.5(3)°) and 3.6(2)° (**14** : 10.8(1)°; **15** : 7.2(3)°) respectively. For the cyclo-octadiene ring a slight variance in a single alkane carbon is observed with the adjacent alkene carbons being only slightly distorted.

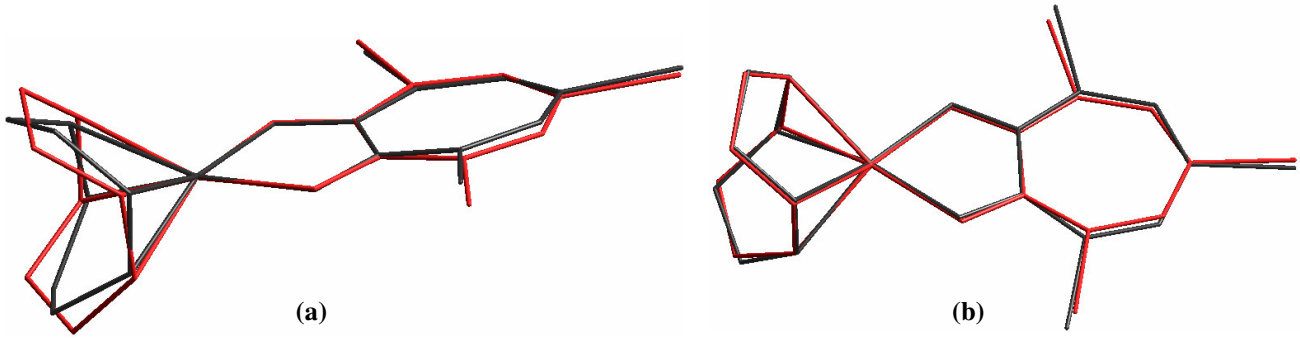

Figure 8.6 HyperChem superimposed image of (a) [Pt(cod)(3Br-trop)]BF_4 (16) (black) *vs.* [Pt(cod)(3Br-trop)]PF_6 (17) (red) with an RMS error of 0.02 Å (b) [Pt(cod)(3Br-trop)]BF_4 inverted crystal structure (16) (black) *vs.* [Pt(cod)(3Br-trop)]PF_6 (17) (red) with an RMS error of 0.14 Å. Counter ions have been omitted for clarity.

The overlay of complexes **16** and **17** shown in Figure 8.6a has an RMS error of 0.0216 Å based on the metal centre and the oxygens and two adjacent carbons of the

tribromotroplonato ligand. The full RMS error calculated on all atoms with the exception of the bromines has a value of 1.6038 Å. Complex **16** has a centrosymmetric space group (monoclinic *C*2/*c*) which results in an a second enantiomer. The overlay of the enantiomer is shown in Figure 8.6b with an RMS error of 0.142 Å based on all the metals excluding the bromines. The two differences that were observed are the differences in the bend and twist angles with values of 4.5(2)° (**16** : 1.6(2)°; **17** : 6.1(1)°) and 1.9(2)° (**16** : 2.7(2)°; **15** : 0.85(8)°) respectively. A cross-over for the alkane carbons of the cyclo-octadine is observed.

For the overlay's of the complexes presented it was found that they are well behaved. The only major differences that were observed are those of the bend and twist angles and shifting or cross-over of the positions of the alkane carbons of the cyclo-octadiene ring. The bond lengths and angles of the core remained similar across the board.

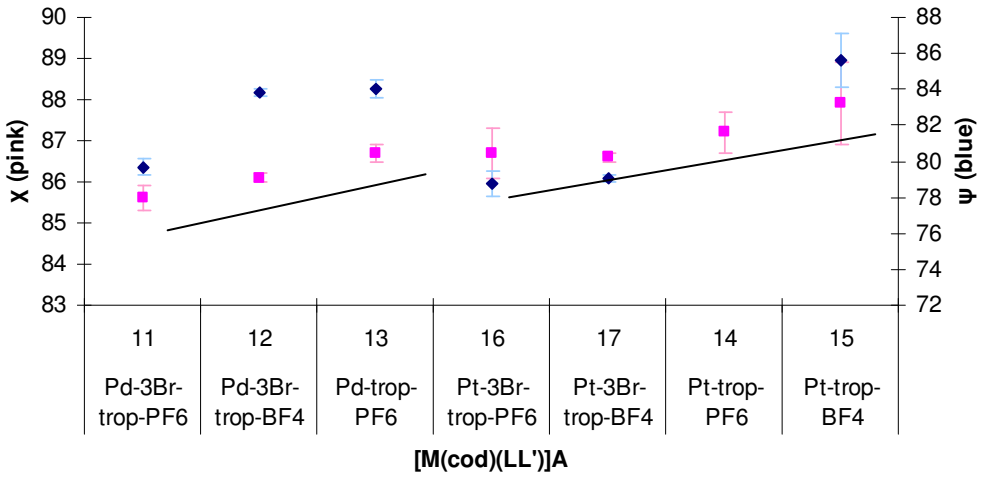

Figure 8.7 Graph of [M(cod)(LL')]A where M = Pd(II), Pt(II) and LL' = trop, 3Br-trop and A = PF_6^-, BF_4^- complexes *vs.* χ (pink squares) and ψ (blue diamonds) angles (see Chapter 1 Figure 1.2 for definition of χ and ψ angles).

The combined graph of platinum and palladium crystal complexes *vs.* the χ and ψ angles shows that with an increase in the χ angle we find and opening and closing of the ψ angle (Figure 8.7). A maximum difference in the ψ angle of 6.8° between [Pt(cod)(trop)]BF_4 (**15**) and [Pt(cod)(3Br-trop)]PF_6 (**16**) was found.

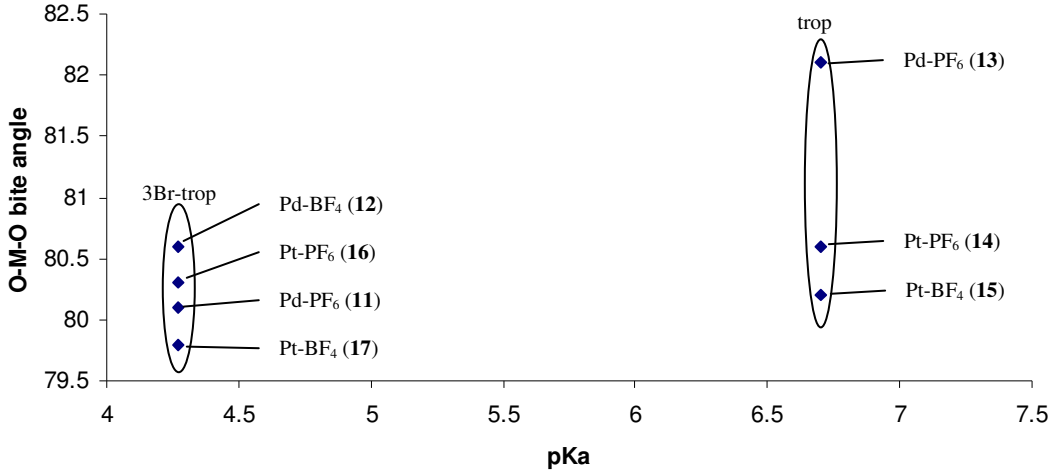

Figure 8.8 Graph of pKa *vs.* O-M-O bite angle for the [M(cod)(LL')]A where M = Pd(II), Pt(II), LL' = trop, 3Br-trop and A = BF_4^-, PF_6^- complexes.

The graph of the acid dissociation constant (pKa) *vs.* the O-M-O bite angle is shown in Figure 8.8. The 2008 covalent radii (given in Table 2.4) for palladium is larger than that of platinum, an increase in the bite angle is expected. An additional influence to the bite angle is the counter ion, with the PF_6^- ion being "stronger" than the BF_4^- counter ion (pKa(HPF_6) -20 *vs*. pKa(HBF_4) -5) placing more strain on the complex and therefore increasing the size of the bite angle. The difference observed between tribromotroplonato and troplonato ligands is in the withdrawing nature of the halogen groups on the tropolone ring resulting in a tighter grouping and smaller bite angle than is found for tropolonato complexes.

Table 8.3 Overview of the division of the complexes into packing categories.

Complex		Packing Type	Ref
[Pd(cod)(3Br-trop)]BF_4	(**12**)	head-to-tail	Figure 7.7
[Pd(cod)(3Br-trop)]PF_6	(**11**)	head-to-tail	Figure 7.13
[Pd(cod)(trop)]PF_6	(**11**)	four-fold rotation axis cluster	Figure 7.19
[Pt(cod)(trop)]PF_6	(**14**)	four-fold rotation axis cluster	Figure 7.22
[Pt(cod)(trop)]BF_4	(**15**)	four-fold rotation axis cluster	Figure 7.25
[Pt(cod)(3Br-trop)]PF_6	(**16**)	zig-zag	Figure 7.33
[Pt(cod)(3Br-trop)]BF_4	(**17**)	tail-to-tail	Figure 7.38

Four different forms of packing for the topolonato type complexes were observed, head-to-tail (Figure 8.9), four-fold rotation axis clusters (Figure 8.10), zig-zag (Figure 8.11) and tail-to-tail (Figure 8.12). The packing motif given in all the figures is defined as the head of the arrow being the cyclo-octadiene ring and the tail of the arrow the troplonato type ligand.

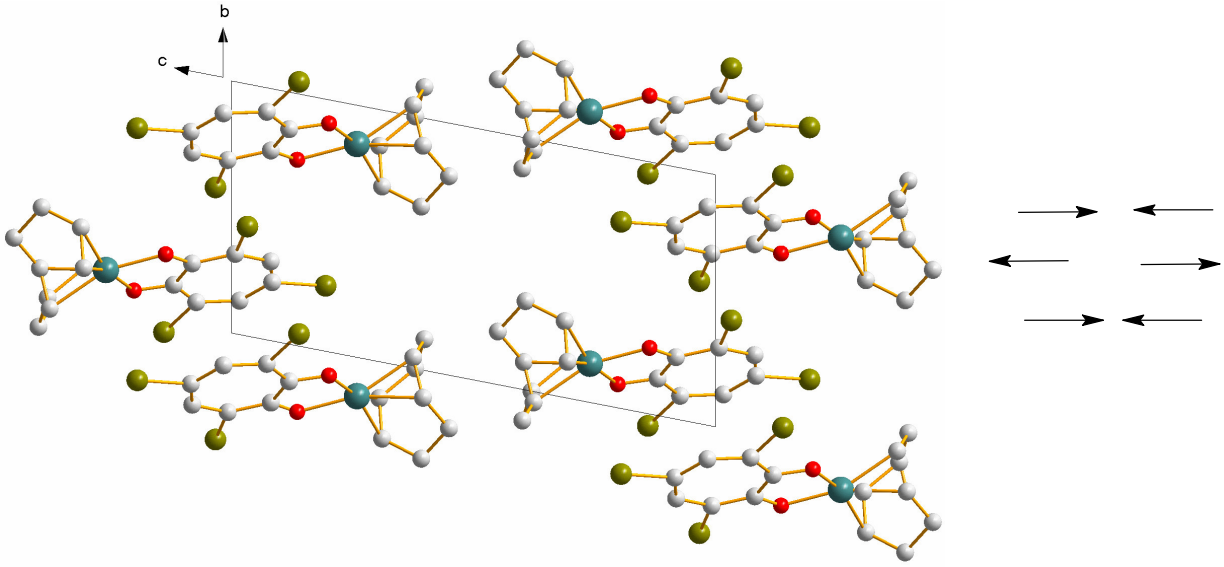

Figure 8.9 Packing of [Pd(cod)(3Br-trop)]PF_6 viewed along the *a*-axis to the right the packing motif. Palladium (cyan), carbon (grey), oxygen (red) and bromine (khaki). Hydrogens and PF_6^- have been omitted for clarity.

In Figure 8.9 an example of the head-to-tail packing is given, the figure represents the [Pd(cod)(3Br-trop)]PF_6 (**12**) complex and a similar packing motif was also observed for [Pd(cod)(3Br-trop)]BF_4 (**11**).

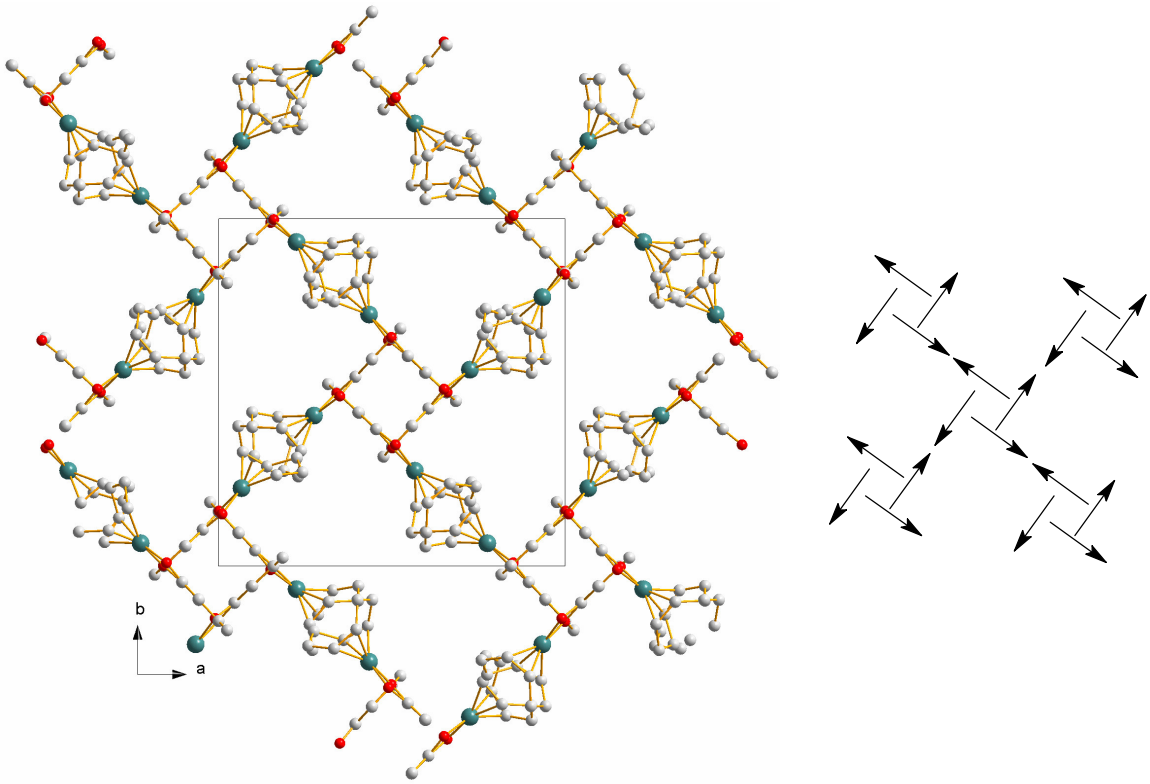

Figure 8.10 Packing of [Pd(cod)(trop)]PF_6 viewed along the *a*-axis to the right the packing motif. Palladium (cyan), carbon (grey) and oxygen (red). Hydrogens and PF_6^- have been omitted for clarity.

In Figure 8.10 an example of four-fold rotation axis cluster packing is given, the figure represents the [Pd(cod)(trop)]PF_6 (**11**) complex a similar packing motif was observed for [Pt(cod)(trop)]BF_4 (**15**) and [Pt(cod)(trop)]PF_6 (**14**).

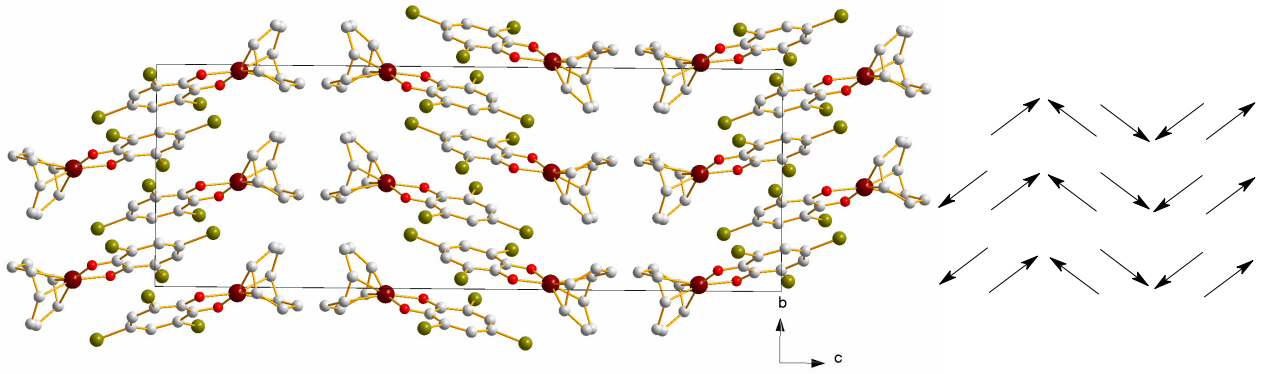

Figure 8.11 Packing of [Pt(cod)(3Br-trop)]PF_6 viewed along the *a*-axis to the right the packing motif. Platinum (dark red), carbon (grey), oxygen (red) and bromine (dark yellow). Hydrogens and PF_6^- have been omitted for clarity.

The only example of the zig-zag packing is given in Figure 8.11. While the only example of tail-to-tail packing is given in Figure 8.12.

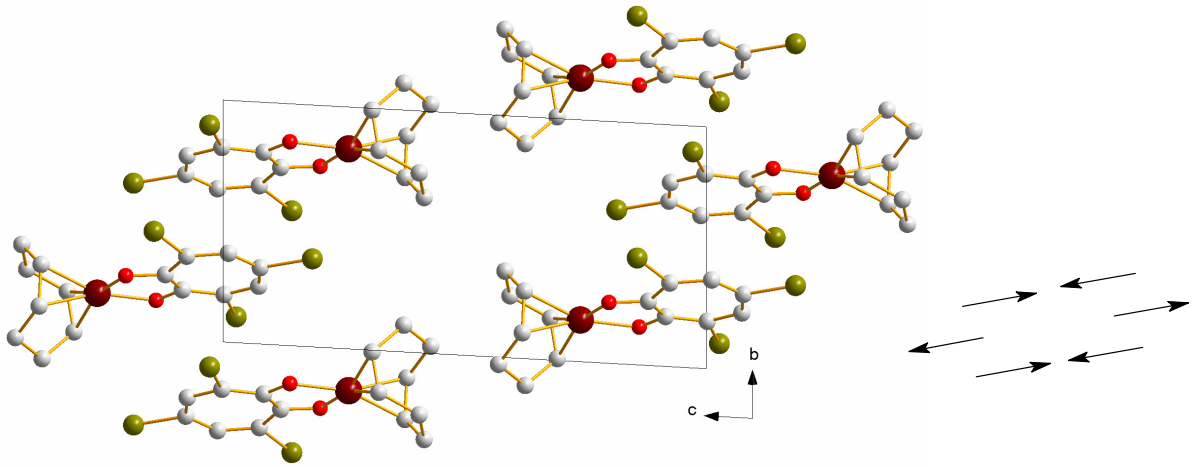

Figure 8.12 Packing of [Pt(cod)(3Br-trop)]BF_4 viewed along the *a*-axis to the right the packing motif. Platinum (dark red), carbon (grey), oxygen (red) and bromine (dark yellow). Hydrogens and BF_4^- have been omitted for clarity.

8.4 Theoretical Correlation of Palladium(II) *vs.* Platinum(II) Complexes

In the periodic table platinum and palladium fall into group 10, having a similar reaction properties one finds that both the metals prefer the square planar co-ordination with a d^8 electron configuration resulting in an oxidation state of +2. The 2008 covalent radii of platinum and palladium are 1.36 Å and 1.39 Å respectively (see Table 2.4). Nickel being the last of the group 10 metals also has a d^8 electron configuration though it does not have a preference for a specific co-ordination geometry with octahedral, trigonal bipyramidal, square pyramidal, tetrahedral and square planar all being observed. With this in mind the calculations for nickel were limited to only the square planar geometry with a +2 oxidation state so as to compare it with the remainder of the metals in the group 10 triad. The 2008 covalent radius of nickel was found to be 1.24 Å (see Table 2.4).

8.4.1 Visual Associations

Visual geometric comparisons of the computed structures *vs.* their X-ray crystal structures are presented. The overlay of the X-ray crystal structure and the calculated

structure is a graphical representation of the pair-wise differences of the related structures. This mathematical value is represented by the root mean square (RMS) value, which is a measure of how far the average is from zero, providing information on the variations of bond lengths and angles and to a certain degree the orientation of the structures in relation to each other. These comparisons are presented in Figure 8.13-8.16.

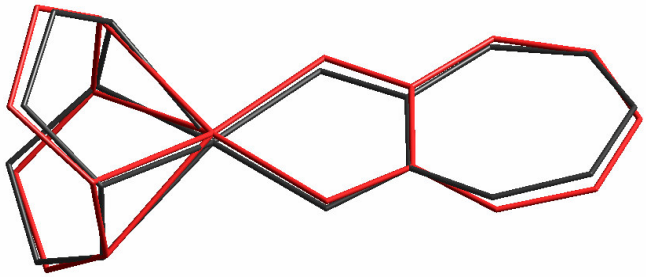

Figure 8.13 HyperChem superimposed image of [Pd(cod)(trop)]PF_6 (13) (black) *vs.* [Pd(cod)(trop)]$^+$ (computed) (red) with an RMS error of 0.18 Å. The counter ion of the X-ray crystal structure has been omitted for clarity.

The overlay of complexes **13** and [Pd(cod)(trop)]$^+$ (calculated) shown in Figure 8.13 has an RMS error of 0.18 Å based on all the atoms. The differences between complex **13** and the calculated complex is firstly the bend angle (*i.e.* the intersection of the planes defined by the metal centre with the oxygen atoms and the two adjacent carbons of the tropolone ring *vs.* the plane defined by the tropolone ring) with a difference of 5.8° (**13** : 5.8(2)°; calc : 0.035°). Secondly, the difference found in the twist angle (*i.e.* the intersection of the planes defined by the mid-points of the alkene carbons of the cyclo-octadine ring with the oxygen atoms of the tropolonato ligand *vs.* the metal centre with the oxygen atoms and the two adjacent carbons of the tropolone ring) of 7.7° (**13** : 8.7(2)°; calc : 0.995°). The last difference is in the positions of the alkane and alkene carbons of the cyclo-octadiene ring, with the large twist angle there is a shifting in the positions of the carbons. The large difference in both the bend and twist angles can be ascribed to the effect of the counter ion on the complex as well as the packing that results from these interactions. The bond lengths and angles of the central section of the complex are still well defined (see Table 8.4).

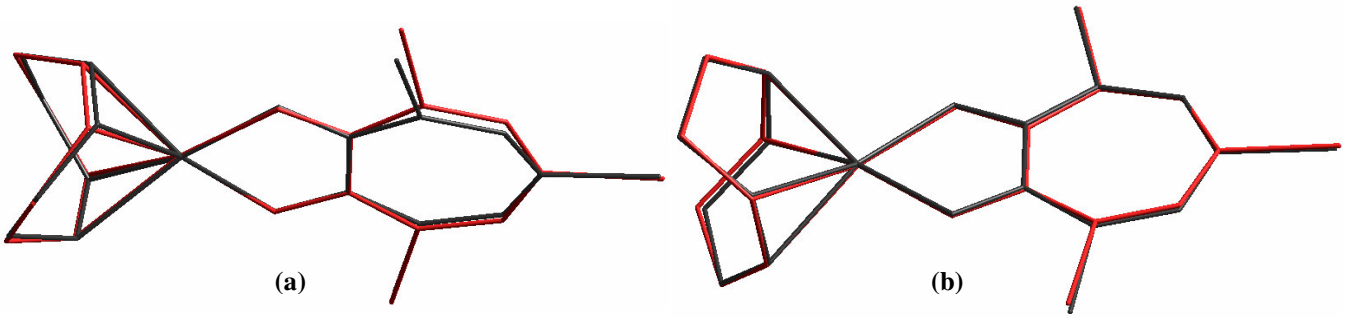

Figure 8.14 HyperChem superimposed image of (a) [Pd(cod)(3Br-trop)]BF_4 (12) (black) *vs.* [Pd(cod)(3Br-trop)]$^+$ (computed) (red) with an RMS error of 0.033 Å (b) [Pd(cod)(3Br-trop)]PF_6 (11) (black) *vs.* [Pd(cod)(3Br-trop)]$^+$ with an RMS error of 0.08 Å. The counter ions of the X-ray crystal structures have been omitted for clarity.

The overlay of complexes **11** and **12** with [Pd(cod)(3Br-trop)]$^+$ (calculated) are shown in Figure 8.14. The RMS error values are 0.03 Å for Figure 8.14a based on the metal centre and the oxygens and two adjacent carbons of the tribromotroplonato ligand, and 0.08 Å for Figure 8.14b for all atoms excluding the bromines. The major differences for complex **12** and the calculated structure were in the bend and twist angles with values of 6.43° (**12** : 6.7(1)°; calc : 0.268) and 0.03° (**12** : 0.97(8)°; calc : 0.943°) respectively. The large bend value results from the interactions with the counter ion as well as the Br···Br, Br···π (Figure 7.4) and Br···F (Figure 7.5) interactions observed. The differences observed for complex **11** and the calculated structure were in the bend and twist angles with values of 3.3° (**11** : 3.6(2)°; calc : 0.268°) and 0.3° (**11** : 1.2(1)°; calc : 0.943°) respectively. Again the larger bend value obtained was a result of the Br···Br, Br···π, π···π (Figure 7.10) and Br···F (Figure 7.11) interactions found. For both complexes the central co-ordination bond lengths and angles are generally well behaved (see Table 8.4).

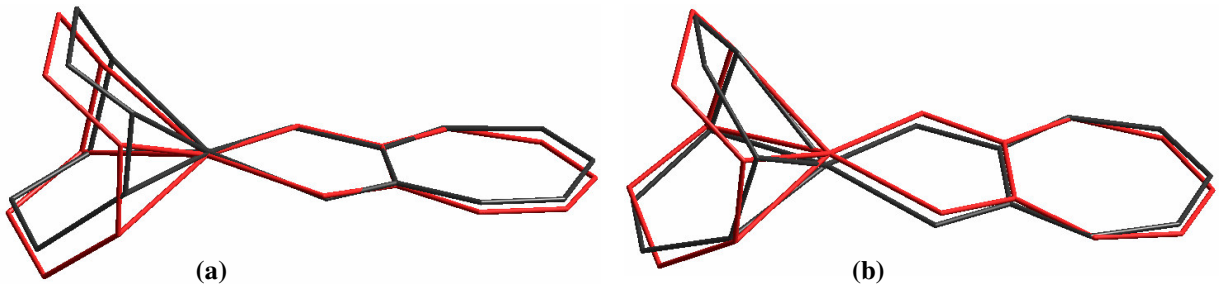

Figure 8.15 HyperChem superimposed image of (a) [Pt(cod)(trop)]BF_4 (15) (black) *vs.* [Pt(cod)(trop)]$^+$ (computed) (red) with an RMS error of 0.075 Å (b) [Pt(cod)(trop)]PF_6 (14) (black) *vs.* [Pt(cod)(trop)]$^+$ with an RMS error of 0.2246 Å. The counter ions of the X-ray crystal structures have been omitted for clarity.

The overlay of complexes **14** and **15** with $[Pt(cod)(trop)]^+$ (calculated) are shown in Figure 8.15. The RMS error values are 0.08 Å for Figure 8.15a based on the metal centre and the oxygens and two adjacent carbons of the troplonato ligand, and 0.22 Å for Figure 8.15b for all atoms. The major differences for complex **15** and the calculated structure were in the bend and twist angles with values of 6.4° (**15** : 6.5(3)°; calc : 0.065) and 6.3° (**15** : 7.2(3)°; calc : 0.894°) respectively. The large difference in value is due to the interactions with the counter ion. A full RMS error based on all atoms was found to be 1.6173 Å. The differences observed for complex **14** and the calculated structure were in the bend and twist angles with values of 4.9° (**14** : 5.0(5)°; calc : 0.065°) and 9.9° (**14** : 10.8(1)°; calc : 0.894°) respectively with the differences a result of the interactions with the counter ion. For both complexes the central co-ordination bond lengths and angles are generally well behaved (see Table 8.5).

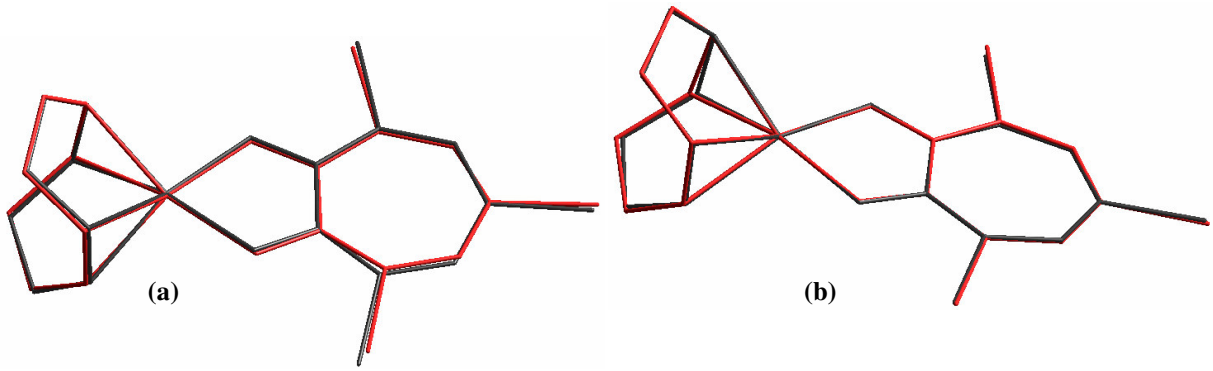

Figure 8.16 HyperChem superimposed image of (a) $[Pt(cod)(3Br\text{-}trop)]BF_4$ (17) (black) *vs.* $[Pt(cod)(3Br\text{-}trop)]^+$ (computed) (red) with an RMS error of 0.1071 Å (b) $[Pt(cod)(3Br\text{-}trop)]PF_6$ (16) (black) *vs.* $[Pt(cod)(3Br\text{-}trop)]^+$ with an RMS error of 0.02 Å. The counter ions of the X-ray crystal structures have been omitted for clarity.

The overlay of complexes **16** and **17** with $[Pt(cod)(3Br\text{-}trop)]^+$ (calculated) are shown in Figure 8.16. The RMS error values are 0.11 Å for Figure 8.16a based on all the atoms excluding the bromines, and 0.02 Å for Figure 8.16b for the metal centre and the oxygens and two adjacent carbons of the tribromotroplonato ligand. The major differences for complex **17** and the calculated structure were in the bend and twist angles with values of 1.37° (**17** : 1.6(2)°; calc : 0.229) and 1.88° (**15** : 2.7(2)°; calc : 0.816°) respectively. The differences in the values are due to the Pt···Br, π···π (Figure 7.37), Br···F and Br···Br (Figure 7.36) interactions. The differences observed for complex **16** and the calculated structure were in the bend and twist angles with values of 5.87° (**16** : 6.1(4)°; calc : 0.229°) and 0.03° (**16** : 0.85(8)°; calc : 0.816°)

respectively. The differences are a result of the Pt···Br, π····π (Figure 7.30), Br···π, Br···Br (Figure 7.31) and Br···F (Figure 7.32) interactions observed. For both complexes the central co-ordination bond lengths and angles are generally well behaved (see Table 8.5).

8.4.2 Crystal Structure vs. Computed Structure Bond Relationships

In comparing the computed structures with their respective X-ray crystal structures only selected bond distances and angles were used. The bond lengths and angles selected were those comprising of the "core" co-ordination geometry and the entire cyclo-octadiene ring so as to be able to compute the χ and ψ angles.

The *R*-values are given as a measure of the average accuracy of the computed (gas phase) bond lengths (Å) and angles (°) with the experimental crystal data (solid state) obtained. The following expression was used to calculate the *R*-values

$$R = n^{-1} \sum_{1 \to n}^{i} x_{e_i} - \left| x_{c_i} - x_{e_i} \right| \Big/ x_{e_i}$$

with n = number of data points, x_e = experimental data and x_c = calculated data.

The following graphs (Figure 8.17-8.16) and tables (Table 8.4 and 8.5) represent the general degree of accuracy between calculated structures and experimental values. Within the graphs the insert values are the actual calculated *R*-values for the complexes presented, the table that follows the graphs are the plotted values.

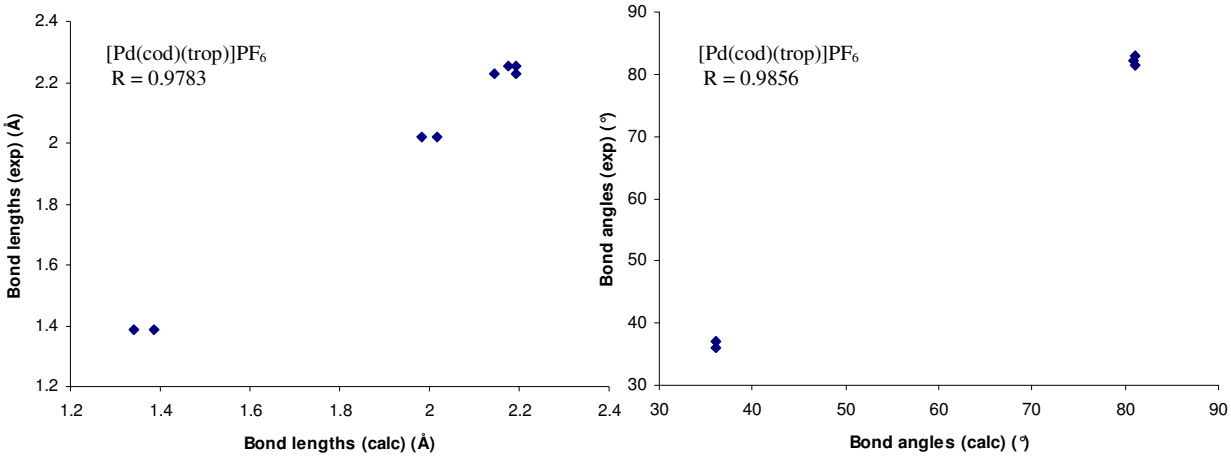

Figure 8.17 Graph of experimental *vs.* calculated bond lengths (Å) and angles (°) for [Pd(cod)(trop)]PF_6 (13) with calculated *R*-values top left, plotted values are given in Table 8.4 columns 1-3.

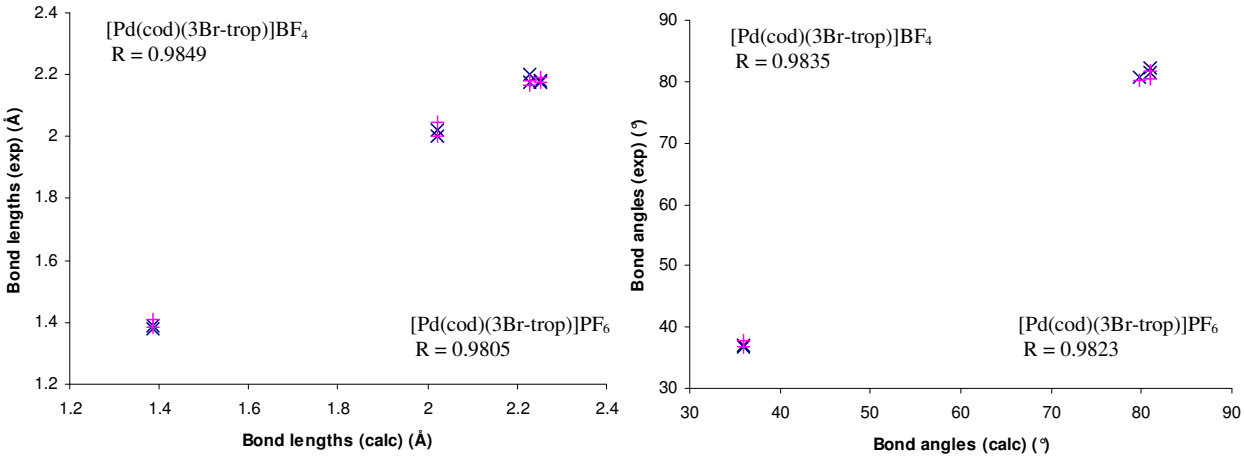

Figure 8.18 Graph of experimental *vs.* calculated bond lengths (Å) and angles (°) for [Pd(cod)(3Br-trop)]BF_4 (12) (blue multiplication sign) and [Pd(cod)(3Br-trop)]PF_6 (11) (pink plus sign) with calculated *R*-values shown, plotted values are given in Table 8.4 columns 4 and 5.

The graphs of [Pd(cod)(trop)]PF_6 (**13**), [Pd(cod)(3Br-trop)]PF_6 (**11**) and [Pd(cod)(3Br-trop)]BF_4 (**12**) *vs.* bond lengths (Å) and angles (°) (Figure 8.17 and 8.14) represent the general degree of accuracy between the calculated structures and the experimental values with an average *R*-value of ≥ 98 %. The values are listed in Table 8.4.

Table 8.4 Selected Geometric parameters (Å,°) for Palladium(II) metal complexes

	[Pd(cod)(3Br-trop)]			[Pd(cod)(trop)]	
	BF_4 (**12**)	PF_6 (**11**)	calc	PF_6 (**13**)	calc
Pd-O_1	2.003(3)	2.047(6)	2.0229	2.018(9)	2.0224
Pd-O_2	2.023(3)	2.002(6)	2.0229	1.982(8)	2.0223
Pd-C_1	2.180(5)	2.193(8)	2.2534	2.177(12)	2.2527
Pd-C_2	2.177(5)	2.182(8)	2.2293	2.193(12)	2.229
Pd-C_5	2.176(5)	2.178(9)	2.2534	2.192(12)	2.2526
Pd-C_6	2.201(5)	2.165(8)	2.2293	2.145(12)	2.229
C_1-C_2	1.387(7)	1.382(12)	1.3863	1.387(18)	1.3858
C_5-C_6	1.381(7)	1.410(11)	1.3863	1.343(16)	1.3858
O_1-Pd-O_2	80.6(1)	80.1(2)	79.739	82.1(2)	80.906
C_1-Pd-C_2	37.1(2)	36.8(3)	36.023	37.0(5)	36.019
C_5-Pd-C_6	36.8(2)	37.9(3)	36.023	36.1(4)	36.019
C_1-Pd-C_6	81.4(2)	80.5(3)	80.956	81.5(4)	81.063
C_2-Pd-C_5	82.3(2)	81.6(3)	80.955	83.0(4)	81.066
χ^a	86.1(1)	85.6(3)	85.068	86.7(6)	85.196
ψ^b	83.8(2)	79.7(4)	84.483	84.0(8)	84.45

a χ: $C_1MC_2 \cap C_5MC_6$ b ψ: $C_2C_3C_4C_5 \cap C_1C_8C_7C_6$ see Figure 1.2

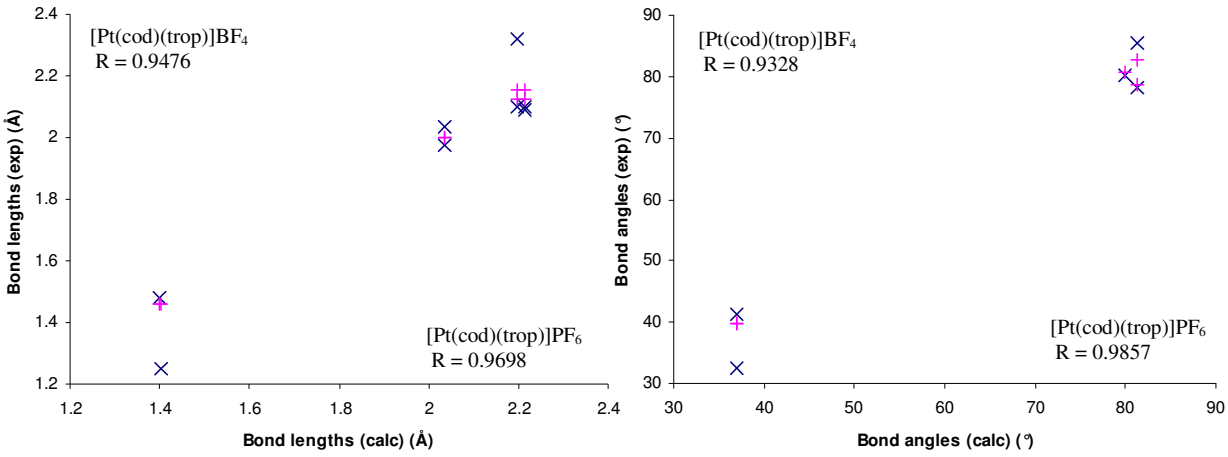

Figure 8.19 Graph of experimental *vs.* calculated bond lengths (Å) and angles (°) for [Pt(cod)(trop)]BF_4 (15) (blue multiplication sign) and [Pt(cod)(trop)]PF_6 (14) (pink plus sign) with calculated *R*-values shown, plotted values are given in Table 8.5 columns 1-3.

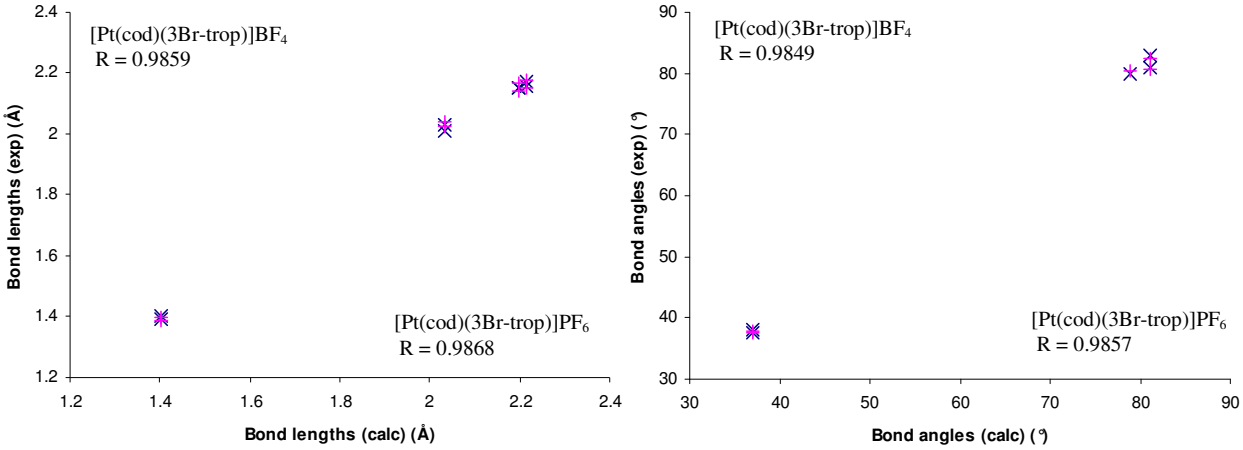

Figure 8.20 Graph of experimental *vs.* calculated bond lengths (Å) and angles (°) for [Pt(cod)(3Br-trop)]BF_4 (17) (blue multiplication sign) and [Pt(cod)(3Br-trop)]PF_6 (16) (pink plus sign) with calculated *R*-values shown, plotted values are given in Table 8.5 columns 4-6.

The graphs of [Pt(cod)(trop)]PF_6 (**14**), [Pt(cod)(trop)]BF_4 (**15**), [Pt(cod)(3Br-trop)]PF_6 (**16**) and [Pt(cod)(3Br-trop)]BF_4 (**17**) *vs.* bond lengths (Å) and angles (°) (Figure 8.19 and 8.16) represent the general degree of accuracy between the calculated structures and the experimental values with an average *R*-value of ≥ 97 %. The values are listed in Table 8.5.

Table 8.5 Selected Geometric parameters (Å,°) for Platinum(II) metal complexes

	[Pt(cod)(trop)			[Pt(cod)(3Br-trop)]		
	BF_4 (**15**)	PF_6 (**14**)	calc	BF_4 (**17**)	PF_6 (**16**)	calc
$Pt\text{-}O_1$	1.974(15)	1.999(4)	2.0357	2.008(3)	2.024(9)	2.0348
$Pt\text{-}O_2$	2.037(15)	1.999(4)	2.0357	2.030(4)	2.040(8)	2.0348
$Pt\text{-}C_1$	2.098(17)	2.155(10)	2.2131	2.156(5)	2.178(12)	2.2147
$Pt\text{-}C_2$	2.100(16)	2.123(9)	2.1971	2.154(5)	2.141(12)	2.1978
$Pt\text{-}C_5$	2.09(2)	2.123(9)	2.2131	2.171(5)	2.153(13)	2.2147
$Pt\text{-}C_6$	2.32(2)	2.155(10)	2.1972	2.151(5)	2.167(13)	2.1979
$C_1\text{-}C_2$	1.48(2)	1.460(19)	1.4011	1.402(7)	1.400(17)	1.4014
$C_5\text{-}C_6$	1.25(3)	1.460(19)	1.4012	1.392(7)	1.387(19)	1.4014
$O_1\text{-}Pt\text{-}O_2$	80.2(2)	80.6(2)	79.93	79.8(1)	80.3(3)	78.879
$C_1\text{-}Pt\text{-}C_2$	41.4(6)	39.9(5)	37.046	38.0(2)	37.8(5)	37.032
$C_5\text{-}Pt\text{-}C_6$	32.5(7)	39.9(5)	37.047	37.6(2)	37.5(5)	37.031
$C_1\text{-}Pt\text{-}C_6$	78.3(6)	78.7(8)	81.227	82.9(2)	80.7(5)	81.136
$C_2\text{-}Pt\text{-}C_5$	85.5(5)	82.6(6)	81.228	81.0(2)	82.4(5)	81.137
χ^a	87.9(10)	87.2(5)	85.759	86.6(1)	86.7(6)	85.648
ψ^b	85.6(15)	NA	81.717	79.1(2)	78.8(7)	81.636

a χ: $C_1MC_2 \cap C_5MC_6$ b ψ: $C_2C_3C_4C_5 \cap C_1C_8C_7C_6$ see Figure 1.2

The reason for the lower accuracy of the calculations for the platinum is that the [Pt(cod)(trop)]BF_4 only had an *R*-value of > 94 % it should be noted that the crystal data that is presented in the table is that of a room temperature collection with

additional pseudo-symmetry involved added to this the computations are done in gas phase and some variances are expected. Generally the calculated structures are slightly longer as a result of the level of theory chosen, also there is no intramolecular interactions from the counter ions in the calculated values. Even with these factors the values obtained are in fair agreement.

Upon inspection of the *R*-values obtained and the overlays presented (§ 8.4.1) a good correlation between the computed structures and that of the experimental structures obtained was observed, leading to the conclusion that related structures computed data maybe extrapolated with a high degree of confidence.

8.4.3 Energies

In looking at the E_{corr} values of the computed complexes found in Figure 8.21, with the values found in Appendix C.5, these show an increase as the ligand becomes more electron withdrawing and a decrease as one moves down the triad. This decrease is consistent with the 2008 covalent radii that have been obtained where there is a significant difference of 0.12 Å between nickel and platinum, with palladium and platinum being remarkably similar.

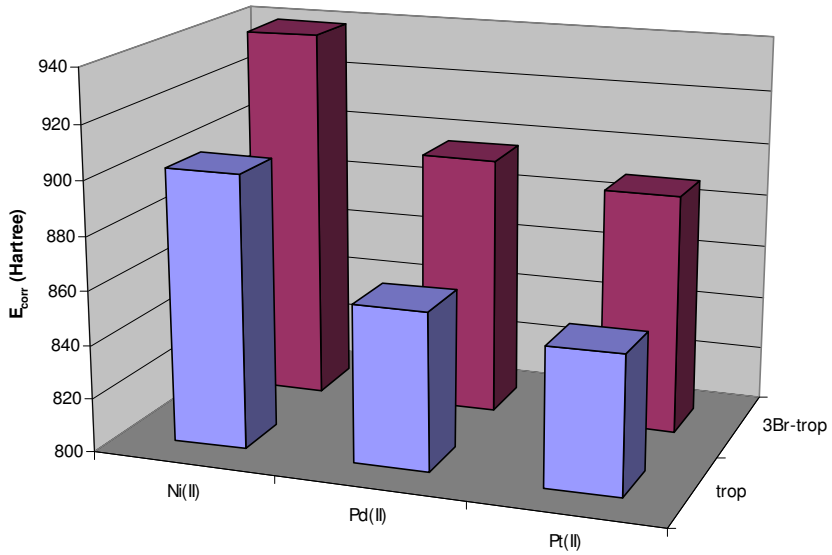

Figure 8.21 3D-graph of the total zero-point corrected energy (E_{corr}) for the computed complexes $[M(cod)(LL')]^+$ where M = group 10 transition metals and LL' = trop, 3Br-trop. Counter ions have not been calculated.

The E_{rel} values represented in Figure 8.22 are the corrected values for the metal effects (*i.e.* E_{rel}^{M}), which show a clear increasing trend as the ligand is interchanged. Surprisingly the E_{rel}^{L} (corrected for ligand effects) has an almost identical graph to that seen in Figure 8.22, the values of the relative energies can be obtained in Appendix C.6 and C.7.

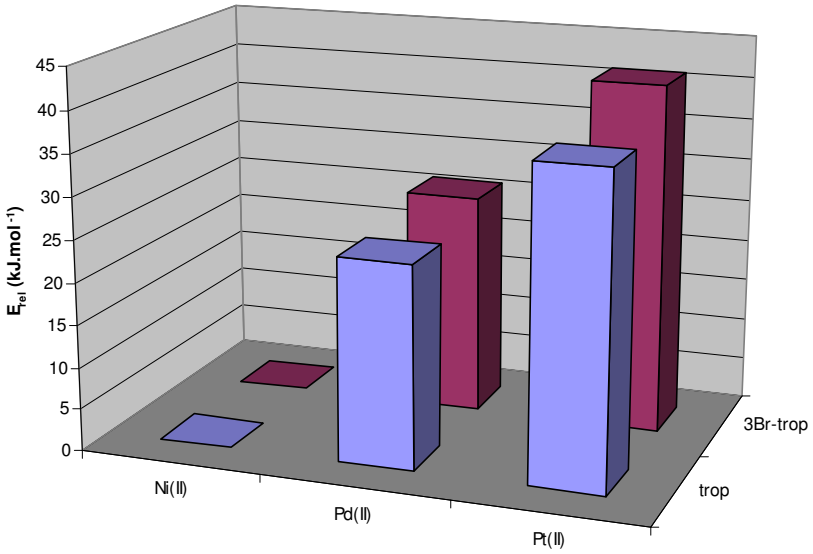

Figure 8.22 3D-graph of the total energy relative to the appropriate metal centre (E_{rel}) for the calculated complexes is corrected for metal centre (E_{rel}^{M}).

8.4.4 Infra-red Spectroscopic Correlations

The infra-red spectra of the calculated complexes are presented to gain a further insight into the bonding character of the complexes studied.

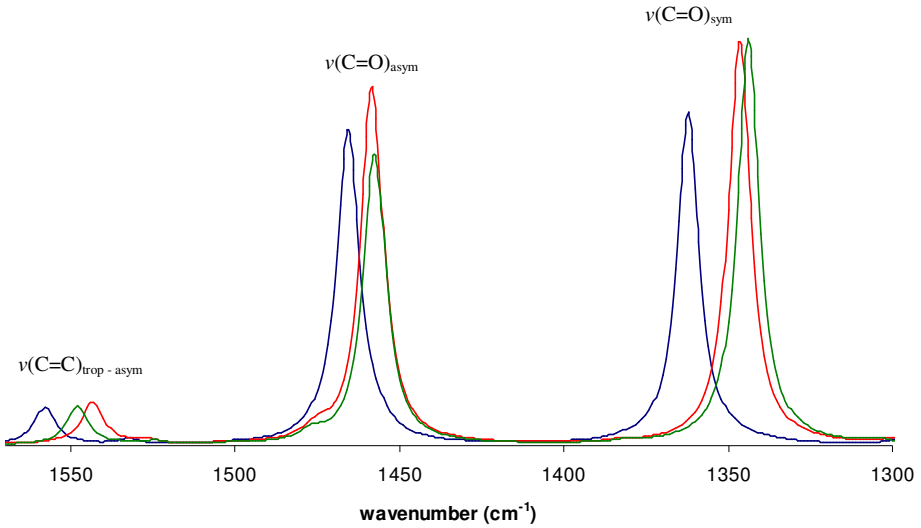

Figure 8.23 Calculated IR spectrum of [Ni(cod)(trop)]$^+$ (blue), [Pd(cod)(trop)]$^+$ (red) and [Pt(cod)(trop)]$^+$(green). *ν* – stretching, sym – symmetrical stretching, asym – asymmetrical stretching.

In Figure 8.23 small changes to both the symmetrical and unsymmetrical stretching frequencies (ν(C=O)$_{sym}$, ν(C=O)$_{asym}$) for the platinum (green) and palladium (red) were observed with nickel shifted up field, as a result of the covalent radii being smaller for nickel than for platinum and palladium. The maximum distances for the ν(C=O)$_{sym}$ and ν(C=O)$_{asym}$ frequencies were found to be 18 cm^{-1} and 11 cm^{-1} respectively, between nickel and platinum for the tropolonato complexes, while for the tribromotropolonato complexes the value was obtained between nickel and palladium.

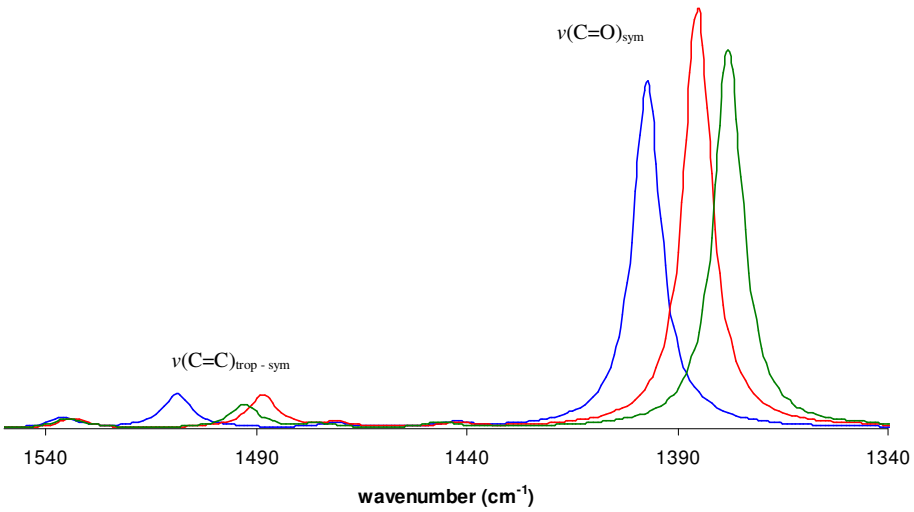

Figure 8.24 Calculated IR spectrum of [Ni(cod)(3Br-trop)]$^+$ (blue), [Pd(cod)(3Br-trop)]$^+$ (red) and [Pt(cod)(3Br-trop)]$^+$(green). *ν* – stretching, sym – symmetrical stretching.

In Figure 8.24 a similar trend for the $\nu(C{=}O)_{sym}$ is found in relation to the 2008 covalent radii of the metal centers, with a difference of 19 cm^{-1} between nickel and platinum.

Table 8.6 Selected IR values (cm^{-1}) for the group 10 metal complexes.

	[M(cod)(trop)]			[M(cod)(3Br-trop)]		
	Ni	Pd	Pt	Ni	Pd	Pt
$\nu(C{=}O)_{sym}$	1362	1347	1344	1397	1385	1378
$\nu(C{=}C)_{A}$	1630 / 1558[a]	1631 / 1543[a]	1631 / 1548[a]	1509	1488	1493
$\nu(C{=}C)_{cod}$	1600 / 1588[a]	1569 / 1555[a]	1537 / 1527[a]	1600 / 1587[a]	1568 / 1553[a]	1539 / 1526[a]
$\nu(C{=}O)_{asym}$	1466	1455	1457	-	-	-

A = trop or 3Br-trop a sym / asym

For both [M(cod)(LL')] where M = Ni, Pd, Pt and A = trop, 3Br-trop spectra it was observed that the symmetrical and asymmetrical frequencies of $\nu(C{=}C)_{cod}$ were not of sufficient intensity to be of note. They have however been included in Table 8.6 for comparative purposes.

8.4.5 Molecular Orbital Comparisons

The molecular orbitals give valuable information as to the nature and location of probable electron density within the complexes. This graphical representation of the molecular orbitals is another method whereby interactions of the cyclo-octadiene with the various metal centers and the *trans* ligands may be observed. The second-highest (HOMO-1) and highest (HOMO) occupied molecular orbitals and the lowest (LUMO) and second-lowest (LUMO+1) unoccupied molecular orbitals for the calculated complexes of $[M(cod)(trop)]^+$ and $[M(cod)(3Br\text{-}trop)]^+$ where M = Ni, Pd, Pt will be presented, along with the differences in the respective orbitals ($E_{g-1} \equiv \Delta|HOMO\text{-}1|\text{-}|HOMO|$; $E_g \equiv \Delta|HOMO|\text{-}|LUMO|$; $E_{g+1} \equiv \Delta|LUMO|\text{-}|LUMO+1|$). The contour plots shown with the molecular orbitals are viewed along the *z*-axis.

Table 8.7 Molecular Orbitals of calculated structures [M(cod)(trop)].

	HOMO-1	HOMO	LUMO	LUMO+1
Ni(II)	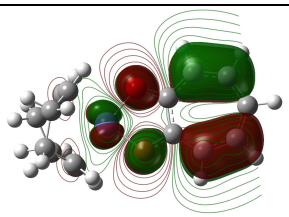	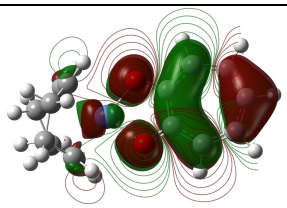	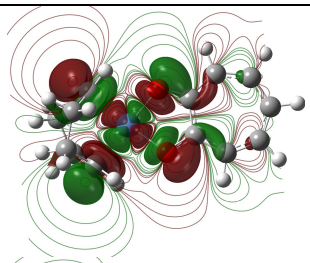	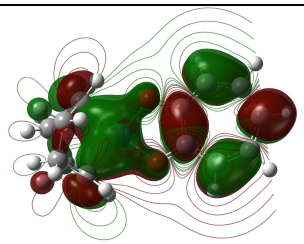
Pd(II)	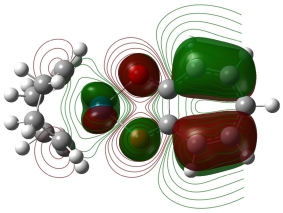	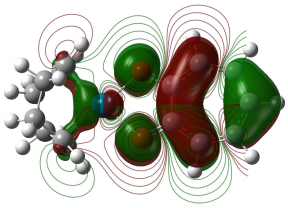	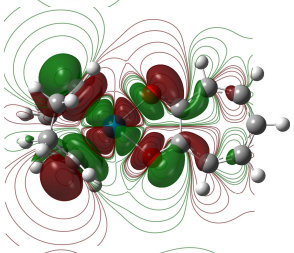	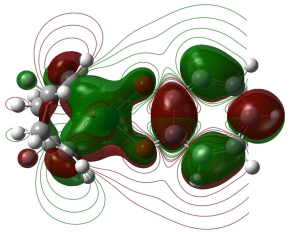
Pt(II)	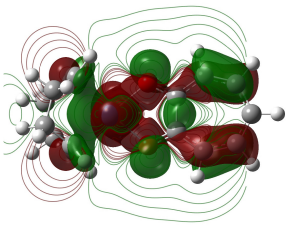	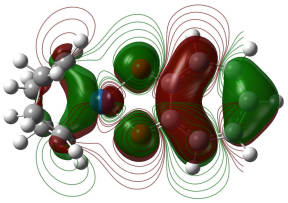	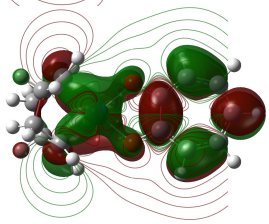	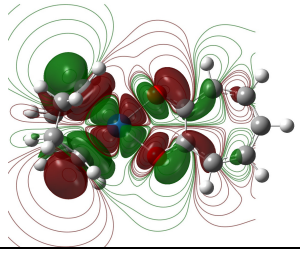

Table 8.8 Molecular Orbital Energies (Hartree) and energy gaps (eV) of the [M(cod)(trop)] calculated structures.

	HOMO-1	HOMO	LUMO	LUMO+1	E_{g-1}	E_g	E_{g+1}
Ni(II)	-0.40097	-0.35675	-0.24139	-0.20315	1.203	3.139	1.041
Pd(II)	-0.39855	-0.35141	-0.23860	-0.19929	1.283	3.070	1.070
Pt(II)	-0.40108	-0.35754	-0.20510	-0.20299	1.185	4.148	0.057

The molecular orbitals for [M(cod)(trop)] where the metal centers are nickel, palladium and platinum are given in Table 8.7 with their energies listed in Table 8.8. The HOMO-1 molecular orbitals, π orbital delocalization is seen in the tropolone ring, whilst platinum has additional orbitals seen for the overlap of the metal with the alkene π-bond. For the HOMO orbitals π orbital delocalization on the tropolonato ring is observed for all the computed structures with minor overlap for the metal and the alkene of the cyclo-octadiene being visible for palladium and platinum. For the LUMO orbitals, $d_{x^2-y^2}$ orbitals are observed around the metal centre for both nickel and palladium. The platinum's LUMO orbital tends to a d_{z^2} orbital centered on the metal whereas the $d_{x^2-y^2}$ orbital is observed in the second lowest unoccupied orbital.

This results in cross-over that is observed for the LUMO and LUMO+1 in relation to the other metal complexes.

Table 8.9 Molecular Orbitals of calculated structures [M(cod)(3Br-trop)].

	HOMO-1	HOMO	LUMO	LUMO+1
Ni(II)	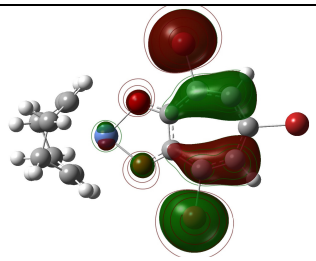	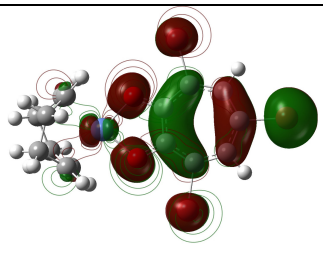	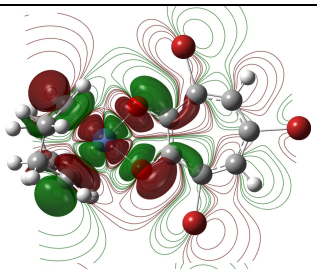	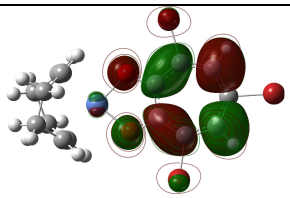
Pd(II)	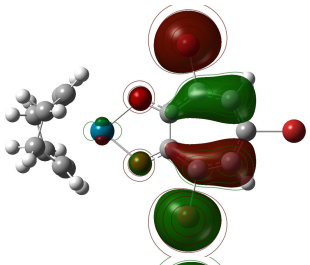	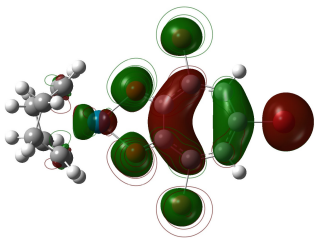	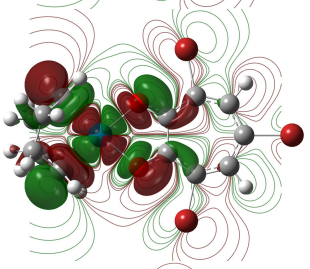	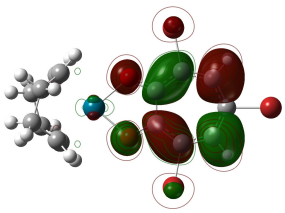
Pt(II)	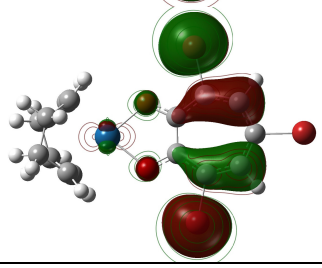	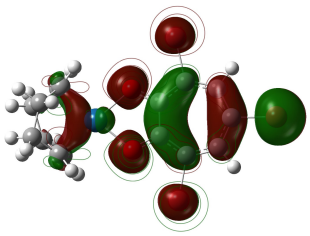	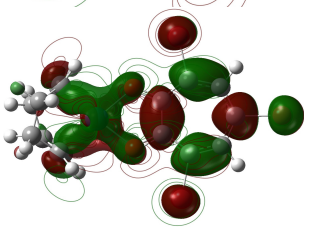	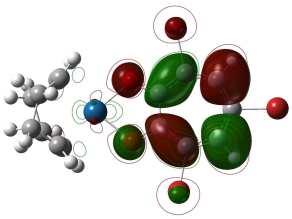

Table 8.10 Molecular Orbital Energies (Hartree) and energy gaps (eV) of the [M(cod)(3Br-trop)] calculated structures.

	HOMO-1	HOMO	LUMO	LUMO+1	E_{g-1}	E_g	E_{g+1}
Ni(II)	-0.38410	-0.35685	-0.24880	-0.21481	0.742	2.940	0.925
Pd(II)	-0.38007	-0.35190	-0.24708	-0.21047	0.767	2.852	0.996
Pt(II)	-0.38347	-0.35707	-0.21540	-0.21536	0.718	3.855	0.001

The molecular orbitals for [M(cod)(3Br-trop)] where the metal centers are nickel, palladium and platinum are given in Table 8.9 with their energies listed in Table 8.10. The HOMO-1 and HOMO molecular orbitals are dominated by the π orbital delocalization on the tropolone ring as well as the *p* orbitals of the bromines on the 3Br-trop ligand. The platinum's LUMO orbital tends to a d_{z^2} orbital centered on the metal whereas the $d_{x^2-y^2}$ orbital is observed in the second lowest unoccupied orbital. For the highest unoccupied orbital, the *p* orbitals are seen on the troplonato ring whereas the *s* orbitals are found for the bromine atoms. The back-bonding can be clearly seen between the metal centre and the cyclo-octadiene ring for the platinum

complex, another reason why the complexes formed are more stable than their palladium and nickel counterparts.

8.4.6 Venus fly-trap (χ and ψ) Angle Evaluation

Figure 8.25 shows the correlation of the different nickel(II) triad complexes comparison of the χ and ψ angles.

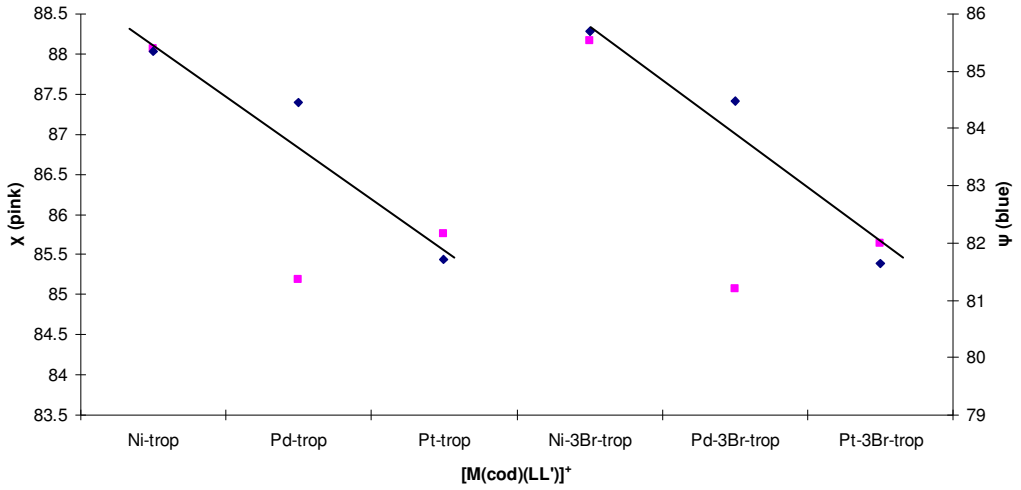

Figure 8.25 Graph of Nickel(II), Palladium(II) and Platinum(II) calculated complexes *vs.* χ (pink squares) and ψ (blue diamonds) angles (see Chapter 1 Figure 1.2 for definition of χ and ψ angles).

In Figure 8.25 it was found that there is a general decrease in the ψ angle as the metal is varied across the triad, with a maximum difference of 4.0° between the nickel tribromotropolonato complex and platinum tribromotropolonato complex. The χ angle follows a similar pattern to the 2008 covalent radii, with the higher bite angle corresponding to the smaller radii.

In overview a good correlation was found between the X-ray crystal structures and that of the computed compounds. The molecular orbital diagrams show the influence of both the *p* and *d* orbitals of the ligands as well as the metal centers. The infra-red spectra showed that the change in the metal centre was not as great an influence on the ν(C=O) stretching frequency as was expected. The $\nu(C=C)_{cod}$ stretching frequency showed a steady decrease in value but the calculated intensities were extremely low.

This concludes the section on the O,O-bidentate ligands for both platinum and palladium complexes, in continuing the study of the effect of the ligand opposite to the cyclo-octadiene, nitrogen known for its *trans* influence was selected. In keeping with the idea of the study a modified acetylacetonato type ligand was used. These ligands were synthesized and characterized in Chapter 3.

Chapter 9
Crystallographic Study of β-Enaminonato Type Complexes of Palladium(II) and Platinum(II)

9.1 Introduction

This chapter presents the use of nitrogen, oxygen bidentate donor atoms for platinum(II) and palladium(II) metal centers. The series is based on the acetylacetonato backbone having one of the oxygen atoms replaced with a secondary amine (§ 3.3) by a condensation reaction.

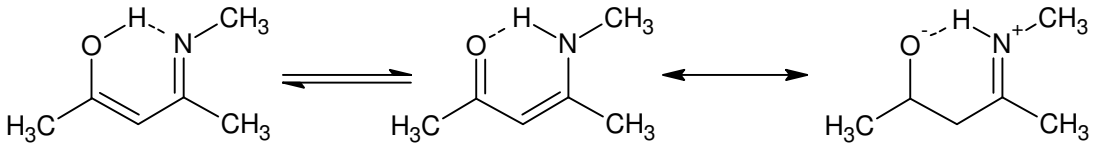

Figure 9.1 β-Enaminones tautomerism.

β-Enaminones are well known for their tautomerism which is stabilized by intramolecular hydrogen bonds (Figure 9.1) and are generally found in the enaminone conformation.

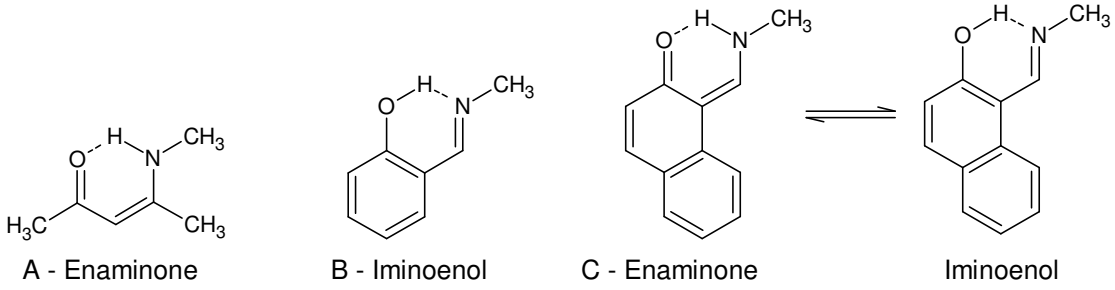

Figure 9.2 β-Enaminone classification categories.

Bertolasi *et al*[1] postulated that there are three different categories into which the β-enaminone maybe divided. The first category (A) simple, which can only form N-H···O hydrogen bonds, as a result of nitrogens proton affinity it is found that the

[1] Bertolasi V., Pretto L., Ferretti V., Gilli P., Gilli G., *Acta Cryst.*, **B62**, 1112, (2006)

resonance mixing N-H···O ↔ N···H-O is greatly hindered. The second category (B) fused phenyl ring, capable of forming both tautomeric forms however the O-H···N (iminoenol) is preferred as a result of ring stabilization. Lastly, the third category (C) fused naphthalene, where the two tautomers become isoenergetic. These categories are seen in Figure 9.2.

The complexes that were prepared as described in § 3.4.2 and 3.5.2 were analyzed by single crystal X-ray crystallography and the results are summarized in Table 9.1. A diagram indicating the numbering scheme of each compound is presented, along with selected bond lengths and angles, hydrogen bonding interactions and additional interactions if applicable. A discussion highlighting some of the important aspects of each particular structure is presented thereafter.

Additional correlations with other structures are done in Chapter 10, while complete lists of the crystal structures presented in this chapter are given in the supplementary data.

9.2 Experimental

Data collections for [Pd(cod)(NH-acac)]BF4, [Pt(cod)(NH-acac)]PF_6, [Pt(cod)(NMe-acac)]BF_4, [Pt(cod)(NMe-acac)]PF_6, and [Pt(cod)(NPh-acac)]PF_6 were obtained on a Bruker Apex II 4K CCD diffractometer. The data for [Pt(cod)(NH-acac)]BF_4 and [Pt(cod)(NPh-acac)]BF_4 were collected on an Oxford Diffraction Xcalibur 3 Crysalis CCD system[2]. Both systems were equipped with a graphite-monochromated Mo Kα radiation, for the Bruker system all the reflections were merged and integrated with SAINT-PLUS[3] and corrected for Lorentz, polarization and absorption effects with SADABS[4], while Crysalis RED[5] was used for the Oxford system.

Structures were solved by direct and conventional Patterson methods using the SHELX-97[6] as part of the WinGX[7] package, and anisotropic refinement was

[2] Crysalis CCD. Oxford Diffraction Ltd., Abingdon, Oxfordshire, U.K., (2005)
[3] Bruker SAINT-PLUS (including XPREP), Version 7.12, Bruker AXS Inc., Madison, WI., (2004)
[4] Bruker SADABS (Version 2004/1), Bruker AXS Inc., Madison, WI., (1998)
[5] Crysalis RED Oxford Diffraction Ltd., Abingdon, Oxfordshire, U.K., (2005)
[6] Sheldrick G.M., *Acta Cryst.*, **A64**, 112, (2008)
[7] Farrugia L.J., *Appl. Cryst.*, **32**, 837, (1999)

performed on all non-hydrogen atoms by a full-matrix least-squares method. The positions of the hydrogen atoms were calculated using a riding model to the adjacent carbon, unless otherwise stipulated. Hydrogen interactions were calculated using the PLATON[8] and PARST[9] programs. Molecular graphics were obtained using DIAMOND[10], while overlay graphics were obtained using HyperChem 7.5[11].

[8] Spek A.L., PLATON A multipurpose crystallographic tool, Utrecht University, Utrecht, The Netherlands (2005); Speck A.L., *J. Appl. Cryst.*, **36**, 7 (2003), Speck A.L., *Acta Cryst*, **D65**, 148 (2009)
[9] Nardelli M., *J. Appl. Cryst.*, **28**, 659, (1995)
[10] Brandenburg K., Brendt M., DIAMOND, Release 2.1e. Crystal Impact GbR, Potfach 1251, D53002 Bonn, Germany. (2001)
[11] HyperChem™ Release 7.52, Windows Molecular Modeling System, HyperCube Inc., (2002)

Table 9.1 Crystallographic data and refinement parameters where A = PF_6 or BF_4

Crystal Data	[Pd(cod)(NH-acac)]A BF_4 (**18**)	[Pt(cod)(NH-acac)]A BF_4 (**19**)	PF_6 (**20**)	[Pt(cod)(NMe-acac)]A BF_4 (**21**)	PF_6 (**22**)	[Pt(cod)(NPh-acac)]A BF_4 (**23**)	PF_6 (**24**)
Empirical formula	C_{13} H_{20} B F_4 N O Pd	C_{13} H_{20} B F_4 N O Pt	C_{13} H_{20} F_6 N O P Pt	C_{14} H_{22} B F_4 N O Pt	C_{14} H_{22} F_6 N O P Pt	C_{19} H_{24} B F_4 N O Pt	C_{19} H_{24} F_6 N O P Pt
Formula weight	399.51	488.20	546.36	502.23	560.39	564.29	622.45
Temperature (K)	100(2)	100(2)	100(2)	100(2)	100(2)	100(2)	100(2)
Wavelength (Å)	0.71073	0.71073	0.71073	0.71073	0.71073	0.71073	0.71073
Crystal system	Monoclinic	Monoclinic	Monoclinic	Orthorhombic	Monoclinic	Monoclinic	Triclinic
Space group	$P2_1/c$	$P2_1/c$	$C2/m$	$P2_12_12_1$	$C2$	$P2_1/n$	$P1$
Unit cell dimensions							
a (Å)	9.8665(3)	9.8588(2)	26.8871(12)	7.5277(2)	26.5792(6)	9.5952(7)	8.7064(2)
b (Å)	12.7836(3)	12.8652(2)	7.1009(3)	13.9653(4)	7.1903(1)	21.2609(16)	16.9618(3)
c (Å)	12.7126(3)	12.6969(3)	8.7130(4)	14.7872(4)	9.3146(2)	10.3335(8)	14.2377(3)
α (°)	90	90	90	90	90	90	90
β (°)	110.8510(10)	111.040(2)	105.305(3)	90	106.250(1)	117.66	105.7730(10)
γ (°)	90	90	90	90	90	90	90
Volume (Å^3)	1498.42(7)	1503.05(5)	1604.5(1)	1554.53(7)	1709.02(6)	1867.1(2)	2023.40(7)
Z	4	4	4	4	4	4	2
Density (calculated) (Mg.m^{-3})	1.771	2.157	2.262	2.146	2.178	2.007	1.022
Absorption coefficient (mm^{-1})	1.278	9.375	8.908	9.068	8.366	7.562	3.539
F(000)	800	928	1040	960	1072	1088	600
Crystal size (mm^3)	0.42 x 0.19 x 0.05	0.26 x 0.15 x 0.13	0.19 x 0.17 x 0.10	0.35 x 0.15 x 0.08	0.38 x 0.13 x 0.04	0.26 x 0.23 x 0.10	0.27 x 0.22 x 0.11
Theta range for data collection (°)	2.21 to 28.00	2.34 to 30.00	1.57 to 28.48	2.01 to 28.37	1.60 to 28.30	2.42 to 27.00	1.49 to 27.00
Index ranges	-13<=h<=12, -16<=k<=16, -16<=l<=16	-13<=h<=9, -17<=k<=18, -16<=l<=17	-35<=h<=35, -9<=k<=9, -11<=l<=11	-6<=h<=9, -18<=k<=18, -19<=l<=19	-35<=h<=35, -6<=k<=9, -12<=l<=12	-12<=h<=12, -26<=k<=27, -11<=l<=13	-10<=h<=11, -21<=k<=19, -18<=l<=18
Reflections collected	17362	13378	18484	28520	14829	13546	13615
Independent reflections	3615 [R(int) = 0.0267]	4374 [R(int) = 0.0226]	2170 [R(int) = 0.1076]	3855 [R(int) = 0.0403]	3442 [R(int) = 0.0387]	4000 [R(int) = 0.0641]	6700 [R(int) = 0.0307]
Completeness to θ (°; %)	28.00, 100.0	30.00, 100.0	28.48, 99.0	28.37, 99.5	28.30, 100.0	27.00, 98.0	27.00, 49.2
Max. and min. transmission	0.9389 and 0.6159	0.3754 and 0.1942	0.4695 and 0.2824	0.5307 and 0.1435	0.7308 and 0.1432	0.5185 and 0.2438	0.6969 and 0.4483
Refinement method	Full-matrix least-squares on F^2	Full-matrix least-squares on F^2	Full-matrix least-squares on F^2	Full-matrix least-squares on F^2	Full-matrix least-squares on F^2	Full-matrix least-squares on F^2	Full-matrix least-squares on F^2
Data / restraints / parameters	3615 / 0 / 215	4374 / 0 / 196	2170 / 0 / 124	3855 / 0 / 202	3442 / 1 / 200	4000 / 0 / 246	6700 / 3 / 499
Goodness-of-fit on F^2	1.293	1.003	1.322	1.249	1.218	0.995	1.248
Final R indices [I>2σ(I)]	R_1 = 0.0224, wR_2 = 0.0723	R_1 = 0.0209, wR_2 = 0.0490	R_1 = 0.0388, wR_2 = 0.1037	R_1 = 0.0150, wR_2 = 0.0385	R_1 = 0.0244, wR_2 = 0.0640	R_1 = 0.0325, wR_2 = 0.0792	R_1 = 0.0329, wR_2 = 0.0859
R indices (all data)	R_1 = 0.0286, wR_2 = 0.1015	R_1 = 0.0283, wR_2 = 0.0507	R_1 = 0.0439, wR_2 = 0.1300	R_1 = 0.0171, wR_2 = 0.0636	R_1 = 0.0285, wR_2 = 0.0887	R_1 = 0.0374, wR_2 = 0.0809	R_1 = 0.0421, wR_2 = 0.1309
Largest diff. peak and hole (e.Å^{-3})	0.937 and -0.855	2.427 and -0.952	1.491 and -2.363	0.819 and -1.101	0.779 and -1.252	3.119 and -2.480	0.695 and -1.132

9.3 X-Ray Structures of Palladium(II) Complexes

9.3.1 Crystal structure of [Pd(cod)(NH-acac)]BF_4

The compound [Pd(cod)(NH-acac)]BF_4 (**18**) crystallizes in the monoclinic space group $P2_1/c$, with a cationic [Pd(cod)(NH-acac)]$^+$ species (**18a**) and an anionic BF_4^- (**18b**) species in the asymmetric unit. The numbering scheme is presented in Figure 9.3, while atomic co-ordinates, bond angles and distances, anisotropic displacement parameters and hydrogen co-ordinates are reported in Appendix B.10. General crystallographic data and refinement parameters are reported in Table 9.1, while significant bond angles and distances are reported in Table 9.2.

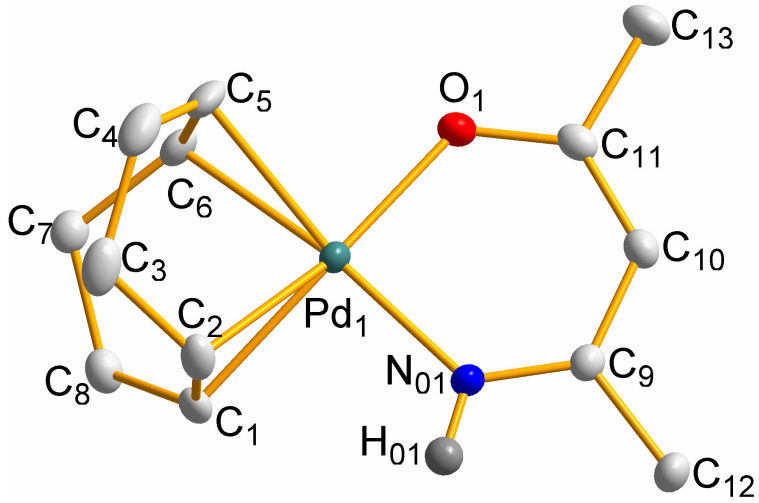

Figure 9.3 Diamond illustration of [Pd(cod)(NH-acac)]BF_4 (19) at 100 K showing the numbering scheme and displacement ellipsoids (50 %) of the complex. Hydrogen atoms and anionic species omitted for clarity, except for the H_{01} atom which was placed.

Table 9.2 Selected bond distances and angles for [Pd(cod)(NH-acac)]BF_4

Bond Distance (Å)		Bond Angles (°)	
Pd-O_1	1.999(2)	O_1-Pd-N_{01}	92.03(9)
Pd-N_{01}	1.972(2)	C_1-Pd-C_2	36.7(1)
Pd-C_1	2.185(3)	C_5-Pd-C_6	36.0(1)
Pd-C_2	2.208(3)	C_1-Pd-C_6	82.1(1)
Pd-C_5[c]	2.222(3)	C_2-Pd-C_5	81.8(1)
Pd-C_6[c]	2.228(3)	χ[a]	86.2(1)
C_1-C_2	1.384(4)	ψ[b]	81.9(2)
C_5-C_6	1.376(4)		

a χ: $C_1MC_2 \cap C_5MC_6$ b ψ: $C_2C_3C_4C_5 \cap C_1C_8C_7C_6$ see Figure 1.2

Square planar geometry is observed around the metal centre for the **18a** species (Figure 4.2) with 1,5-cyclo-octadiene and 4-aminopent-3-en-2-onato (NH-acac)

moieties bonded to the palladium. The oxidation state of the palladium metal centre was found to be +2 resulting in a cationic and an anionic species in the asymmetric unit. For the tetrafluoroborate counter ion (**18b**) a 5 % disorder was observed for fluorido ligands. Oxygen and nitrogen are electronically similar, only a slight change in bond distance was expected, a difference of 0.027 Å was observed. The C=C bond were minimally different with a mean distance of 1.380(4) Å. The *trans* influence of the nitrogen plays an effect on the Pd-C bond distances with the Pd-C_5 and Pd-C_6 distances being slightly longer than that of the Pd-C_1 and Pd-C_2 distances, with a mean value of 2.211(3) Å. The angle of distortion from square planar (twist angle) as calculated by the planes defined by the mid-points of the alkene carbons of the cyclo-octadiene ring and the oxygen and nitrogen of the 4-aminopent-3-en-2-onato moiety and the platinum with the oxygen, nitrogen and the back-bone carbons of the 4-aminopent-3-en-2-onato moiety was found to be 3.31(4) °.

The hydrogen bonding of complex **18** is graphically presented in Figure 9.4 and 9.5 with Table 9.3 listing the bond distances and angles.

Table 9.3 Hydrogen bond distances and angles for [Pd(cod)(NH-acac)]BF_4 (18) [Å and °].

D-H...A	d(D-H)	d(H...A)	d(D...A)	<(DHA)
C_7-H_{7A}...F_{01}	0.99	2.40	3.144(3)	131.0
C_{12}-H_{12A}...$F_{04B}^{\#1}$	0.98	2.30	3.23(5)	158.2
N_{01}-H_{01}...$F_{03}^{\#1}$	0.90(4)	2.22(5)	3.066(4)	157(4)
N_{01}-H_{01}...$F_{04}^{\#1}$	0.90(4)	2.36(4)	3.120(3)	143(4)
N_{01}-H_{01}...$F_{03B}^{\#1}$	0.90(4)	2.38(9)	3.20(8)	152(4)
C_3-H_{3B}...$F_{02}^{\#2}$	0.99	2.52	3.409(4)	148.8
C_5-H_5...$F_{02B}^{\#3}$	1.00	2.16	3.15(5)	176.2
C_5-H_5...$F_{02}^{\#3}$	1.00	2.53	3.487(4)	159.4
C_{12}-H_{12B}...$F_{03}^{\#4}$	0.98	2.55	3.370(4)	141.8
C_{13}-H_{13A}...$F_{03}^{\#5}$	0.98	2.42	3.365(4)	160.9
C_{13}-H_{13A}...$F_{03B}^{\#5}$	0.98	2.45	3.41(7)	166.0

Symmetry transformations used to generate equivalent atoms:
#1 -x,y+1/2,-z-1/2 #2 -x+1,y+1/2,-z-1/2 #3 -x+1,-y,-z
#4 -x,-y,-z #5 x,-y-1/2,z+1/2

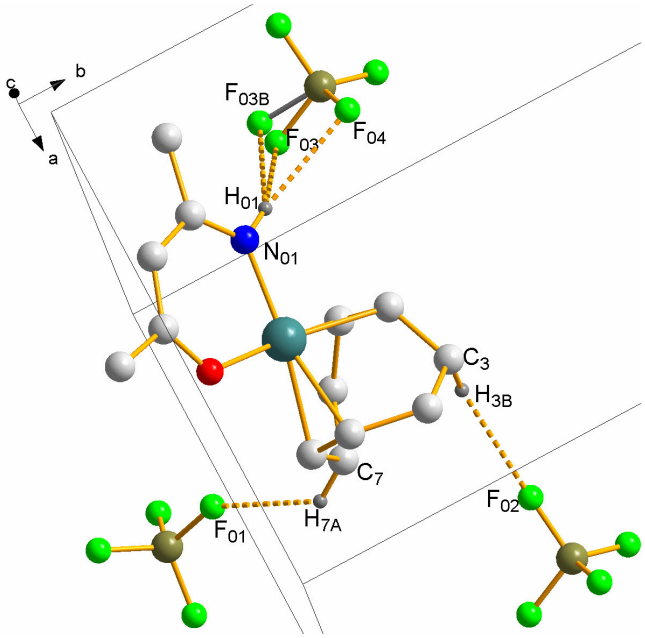

Figure 9.4 Partial unit cell of [Pd(cod)(NH-acac)]BF_4 showing intermolecular hydrogen bonding interactions indicated by a dashed bond. Only selected hydrogen atoms are included. Counter ion disorder is depicted by grey bonds. Palladium (cyan), carbon (grey), oxygen (red), nitrogen (blue), boron (olive) and fluorine (green).

No intramolecular interactions of the type **18a**···**18a** were observed for [Pd(cod)(NH-acac)]BF_4 (**18**). Several hydrogen interactions were observed (Figure 9.4 and 9.5) of the type **18a**···**18b** and are listed in Table 9.3. A bifurcated hydrogen is observed for the hydrogen (H_{01}) attached to the nitrogen (N_1) of the 4-aminopent-3-en-2-onato moiety which interacts with the fluorido (F_{04}, F_{03} and F_{03B}) ligands of **18b**. The grey bonds indicate the disorder present in the **18b** complex and are numbered with a subscript number and a letter indicating the part of the disorder. A second interaction is observed in Figure 9.4 which is that of the hydrogens of the alkane carbons (C_3 and C_7) of the cyclo-octadiene ring with the fluorido ligands (F_{02} and F_{01}) of the **18b** species.

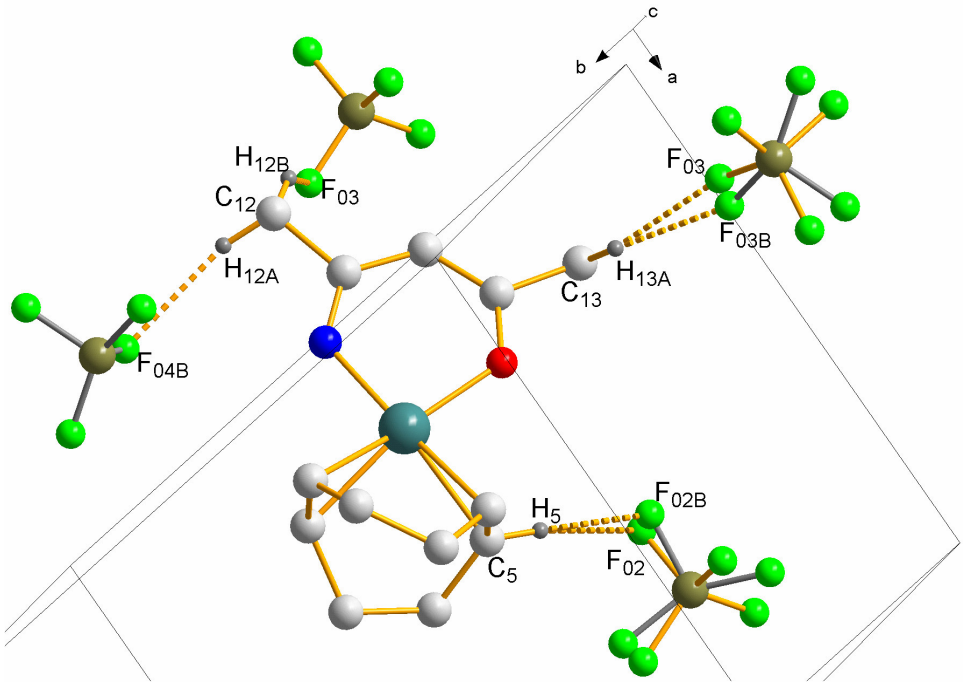

Figure 9.5 Partial unit cell of [Pd(cod)(NH-acac)]BF_4 showing intermolecular hydrogen bonding interactions indicated by a dashed bond. Only selected hydrogen atoms are included. Counter ion disorder is depicted by grey bonds. Palladium (cyan), carbon (grey), oxygen (red), nitrogen (blue), boron (olive) and fluorine (green).

There is an additional hydrogen interaction with the hydrogen of the alkene carbon (C_5) of the cyclo-octadiene ring with the fluorido ligands (F_{02} and F_{02B}) of the **18b** species. The methyl hydrogens (H_{12A}, H_{12B} and H_{13A}) interact with the fluorido ligands (F_{04B}, F_{03}, F_{03} and F_{03B}) of the **18b** species as seen in Figure 9.5. A metal chelate ring interaction is observed for [Pd(cod)(NH-acac)]BF_4 (**18**) with a distance of 3.5525(1) Å as seen in Figure 9.6.

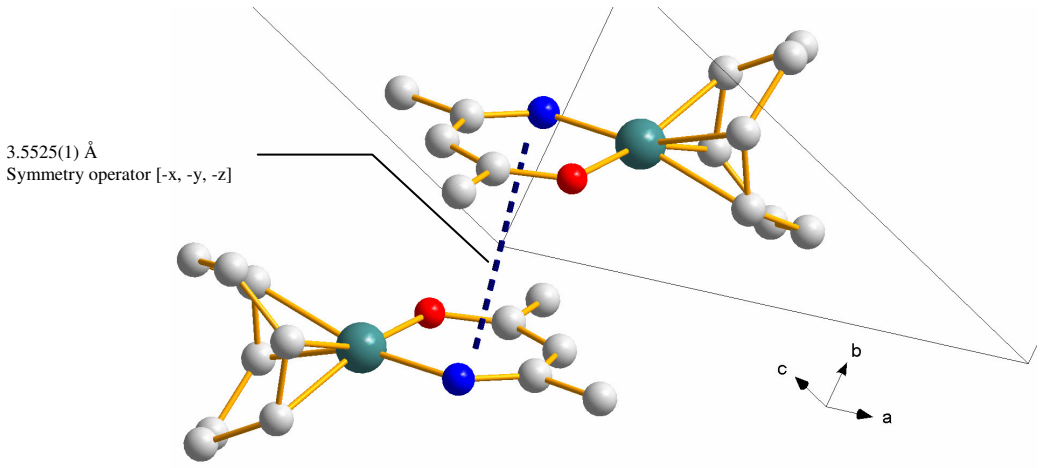

Figure 9.6 Partial unit cell of [Pd(cod)(NH-acac)]BF_4 showing metal chelate ring interactions indicated by a dashed dark blue bond. Hydrogens and tetrafluoroborate counter ion omitted for clarity. Palladium (cyan), carbon (grey), oxygen (red) and nitrogen (blue).

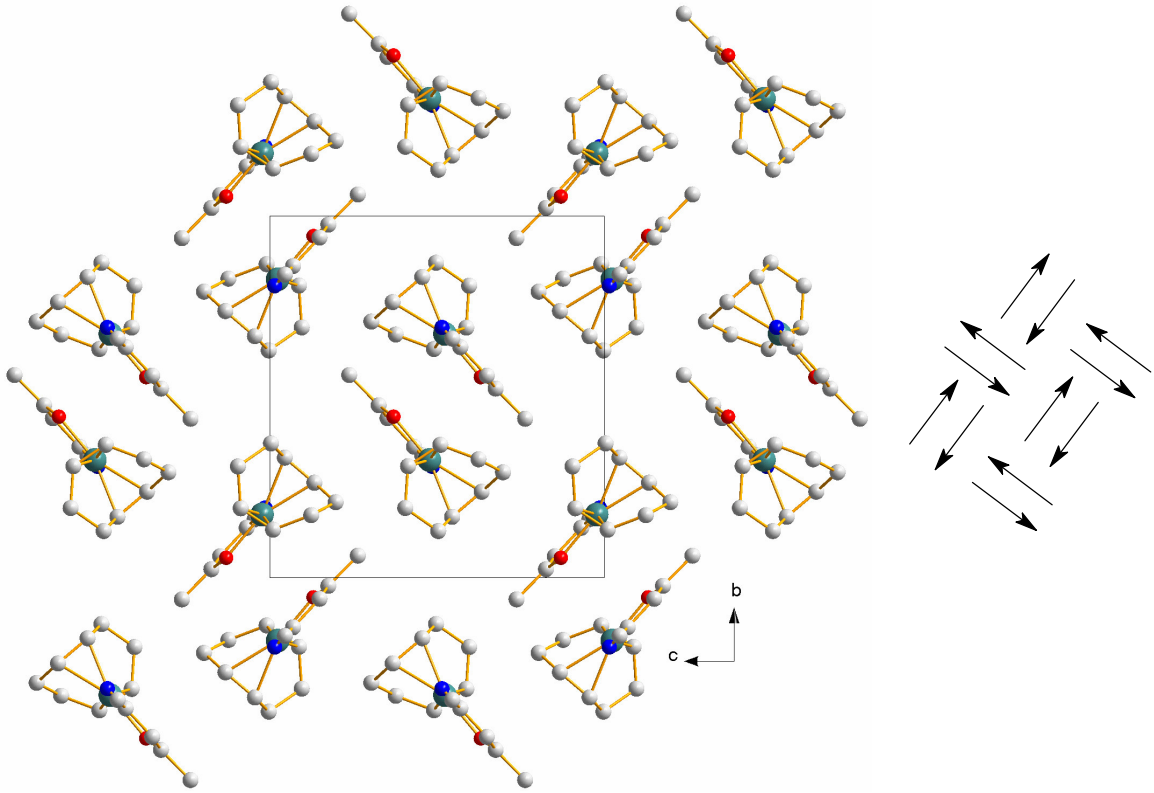

Figure 9.7 Packing of [Pd(cod)(NH-acac)]BF_4 viewed along the *a*-axis with the packing motif incorporated to the right of the figure. Palladium (cyan), carbon (grey), oxygen (red) and nitrogen (blue). Hydrogens and BF_4^- have been omitted for clarity.

In the packing motif shown in Figure 9.7 the head of the arrow is defined as the cyclo-octadiene moiety whilst the tail of the arrow is the 4-aminopent-3-en-2-onato moiety. The packing found for [Pd(cod)(NH-acac)]BF_4 (**18**) is a clustered head-to-tail as a result of the metal chelate interactions observed in Figure 9.6.

9.4 X-Ray Structures of Platinum(II) Complexes

9.4.1 Crystal structures of [Pt(cod)(NH-acac)]BF_4 and [Pt(cod)(NH-acac)]PF_6

The compound [Pt(cod)(NH-acac)]BF_4 (**19**) crystallizes in the monoclinic space group $P2_1/c$, with a cationic [Pt(cod)(NH-acac)]$^+$ species (**19a**) and an anionic BF_4^- (**19b**) species in the asymmetric unit. The compound [Pt(cod)(NH-acac)]PF_6 (**20**) crystallizes in the monoclinic space group $C2/m$, with a cationic [Pt(cod)(NH-acac)]$^+$ species (**20a**) and an anionic PF_6^- species (**20b**) in the asymmetric unit. The numbering scheme is presented in Figure 9.8, while atomic co-ordinates, bond angles

and distances, anisotropic displacement parameters and hydrogen co-ordinates are reported in Appendix B.18 and B.19. General crystallographic data and refinement parameters are reported in Table 9.1, while significant bond angles and distances are reported in Table 9.4.

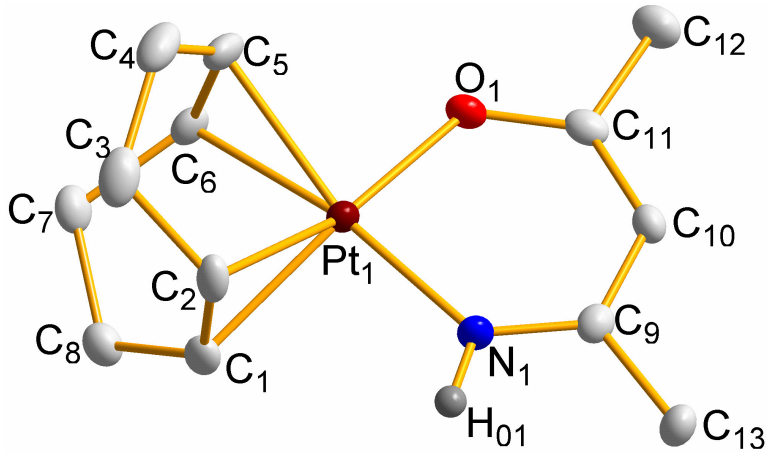

Figure 9.8 Diamond illustration of [Pt(cod)(NH-acac)]BF_4 (19) at 100 K showing the numbering scheme and displacement ellipsoids (50 %) of the complex. Hydrogen atoms and anionic species omitted for clarity, except H_{01} which was placed.

Table 9.4 Selected bond distances and angles for [Pt(cod)(NH-acac)]A

Bond Distance (Å)	Counter ion		Bond Angles (°)	Counter ion	
	PF_6 (**20**)	BF_4 (**19**)		PF_6 (**20**)	BF_4 (**19**)
Pt-O_1	2.006(9)	2.009(2)	O_1-Pt-N_1	92.0(4)	91.5(1)
Pt-N_1	1.999(9)	1.978(3)	C_1-Pt-C_2	36.6(5)	37.7(1)
Pt-C_1	2.195(8)	2.152(3)	C_5-Pt-C_6	37.9(6)	37.3(1)
Pt-C_2	2.195(8)	2.168(3)	C_1-Pt-C_6	82.5(3)	82.7(1)
Pt-C_5[c]	2.151(8)	2.183(3)	C_2-Pt-C_5	82.5(3)	82.1(1)
Pt-C_6[c]	2.151(8)	2.187(3)	χ[a]	88.1(2)	87.2(2)
C_1-C_2	1.38(2)	1.395(5)	ψ[b]	82.7(5)	78.6(2)
C_5-C_6	1.40(2)	1.396(5)			

a χ: $C_1MC_2 \cap C_5MC_6$ b ψ: $C_2C_3C_4C_5 \cap C_1C_8C_7C_6$ see Figure 1.2

Square planar geometry is observed around the metal centre for the **19a** species (Figure 4.2) with 1,5-cyclo-octadiene and 4-aminopent-3-en-2-onato (NH-acac) moieties bonded to the platinum. The oxidation state of the platinum metal centre was found to be +2 resulting in a cationic and an anionic species in the asymmetric unit. The Pt-O bonds for **19a** and **20a** are 2.009(2) Å and 2.006(9) Å respectively. The Pt-N bonds for **19a** and **20a** are 1.978(3) Å and 1.999(9) Å respectively. Oxygen and nitrogen have similar electron density only a marginal change in bond distance was expected resulting in a difference of 0.031 Å for **19a** and for **20a** a difference of 0.007 Å was observed. The C=C bond distances were found to be equivalent with a mean

distance of 1.395(5) Å for **19a**. The average distance for Pt-C was found to be 2.173(3) Å. A shorter bond for Pt-C_1 and Pt-C_2 was observed than for Pt-C_5 and Pt-C_6 this is as a result of the *trans* influence of the nitrogen. The angle of distortion from square planar (twist angle) as calculated by the planes defined by the mid-points of the alkene carbons of the cyclo-octadiene ring and the oxygen and nitrogen of the 4-aminopent-3-en-2-onato moiety and the platinum with the oxygen, nitrogen and the back-bone carbons of the 4-aminopent-3-en-2-onato moiety was found to be 3.77(5) °.

For [Pt(cod)(NH-acac)]PF_6 (**20**) the C=C bond distances were found to be equivalent with a mean distance of 1.39(2) Å. The average distance for Pt-C is 2.173(8) Å, again a shorter bond distance for Pt-C_1 than for Pt-C_5 was observed. In comparing the average distances with **19a** it is found that they are equivalent making the complexes isostructural. Due to the mirror plane for **20** no distortion of the square planar configuration was observed.

In the following paragraphs a detailed discussion of the hydrogen interactions and the packing of [Pt(cod)(NH-acac)]BF_4 (**19**) and [Pt(cod)(NH-acac)]PF_6 (**20**) are done.

The hydrogen bonding of complex **19** is graphically presented in Figure 9.9 and 9.10 with Table 9.5 listing the bond distances and angles.

Table 9.5 Hydrogen bond distances and angles for [Pt(cod)(NH-acac)]BF_4 (19) [Å and °].

D-H...A	d(D-H)	d(H...A)	d(D...A)	<(DHA)
C_5-H_5...F_1	1.00	2.54	3.499(4)	161.2
N_1-H_{01}...F_2 $^{\#1}$	0.93(4)	2.17(4)	3.051(3)	158(3)
N_1-H_{01}...F_4 $^{\#1}$	0.93(4)	2.36(4)	3.136(3)	141(3)
C_3-H_{3B}...F_1 $^{\#2}$	0.99	2.54	3.413(4)	146.8
C_7-H_{7A}...F_3 $^{\#3}$	0.99	2.43	3.175(4)	131.3
C_{12}-H_{12A}...F_2 $^{\#4}$	0.98	2.42	3.379(4)	164.6

Symmetry transformations used to generate equivalent atoms:
#1 x-1,-y+1/2,z-1/2 #2 x,-y+1/2,z-1/2 #3 -x+2,-y,-z+1
#4 -x+2,y-1/2,-z+3/2

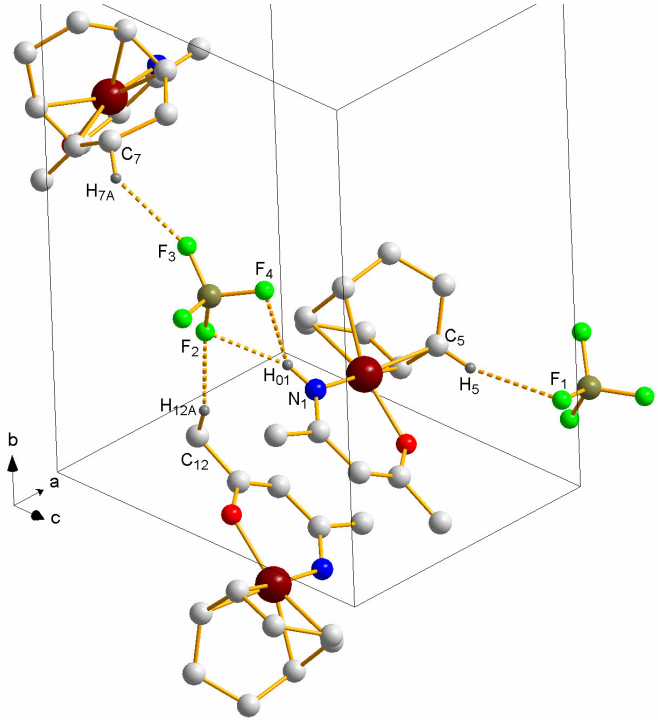

Figure 9.9 Partial unit cell of [Pt(cod)(NH-acac)]BF_4 showing intermolecular hydrogen bonding interactions indicated by a dashed bond. Only selected hydrogen atoms are included. Platinum (dark red), carbon (grey), oxygen (red), nitrogen (blue), boron (olive) and fluorine (green).

No intramolecular interactions of the type **19a**···**19a** were observed for [Pt(cod)(NH-acac)]BF_4 (**19**). Several hydrogen interactions were observed (Figure 9.9 and 9.10) of the type **19a**···**19b** and are listed in Table 9.5. The two types of hydrogen interactions observed for the cyclo-octadiene moiety are firstly between the hydrogens of the alkane carbons (C_7 and C_3) with the fluorido ligands (F_3 and F_1) of the **19b** complex and the hydrogens of the alkene carbon (C_5) with the fluorido ligand (F_1) of **19b**. A bifurcated hydrogen is observed for hydrogen (H_{01}) attached to the nitrogen (N_1) of the 4-aminopent-3-en-2-onato moiety which interacts with the fluorido (F_4 and F_2) ligands of **19b**. The methyl hydrogen of the 4-aminopent-3-en-2-onato moiety interacts with the fluorido ligand (F_2) of **19b**.

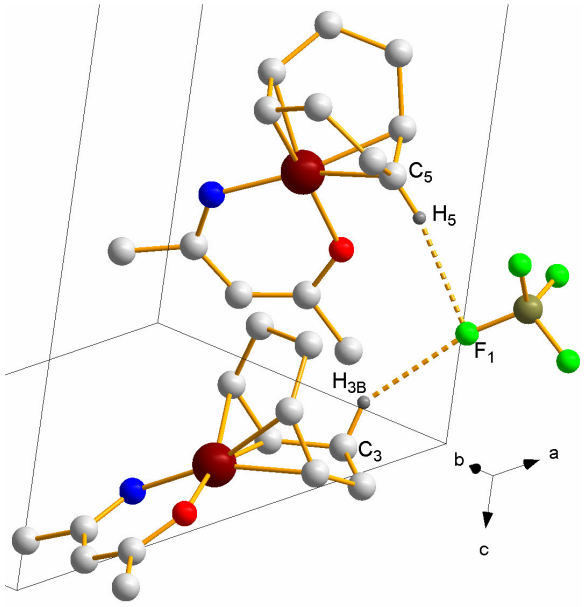

Figure 9.10 Partial unit cell of [Pt(cod)(NH-acac)]BF_4 showing intermolecular hydrogen bonding interactions indicated by a dashed bond. Only selected hydrogen atoms are included. Platinum (dark red), carbon (grey), oxygen (red), nitrogen (blue), boron (olive) and fluorine (green).

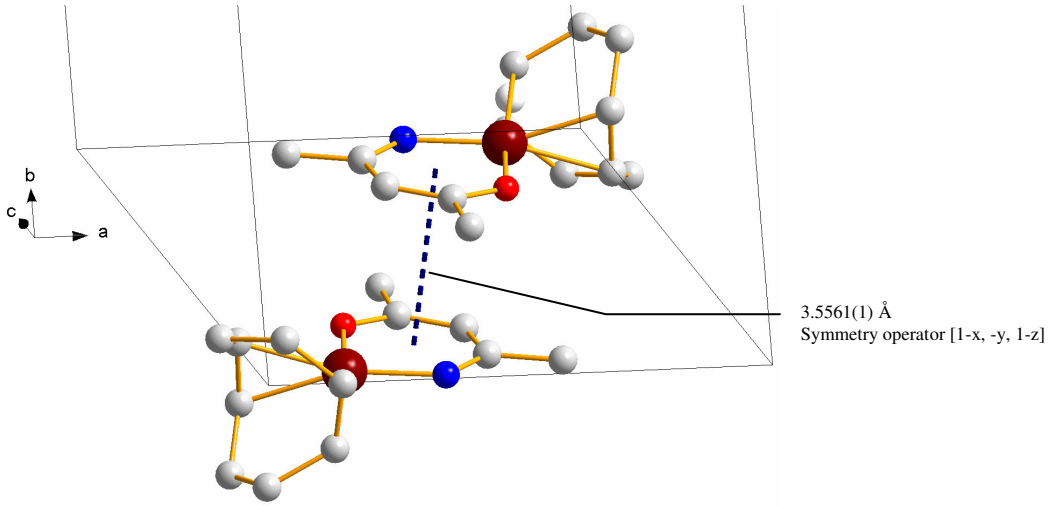

Figure 9.11 Partial unit cell of [Pt(cod)(NH-acac)]BF_4 showing metal chelate ring interactions indicated by a dashed dark blue bond. Hydrogens and Tetrafluoroborate counter ion omitted for clarity. Platinum (dark red), carbon (grey), oxygen (red) and nitrogen (blue).

A metal chelate ring interaction is observed for [Pt(cod)(NH-acac)]BF_4 (**19**) with a distance of 3.5561(1) Å as seen in Figure 9.11.

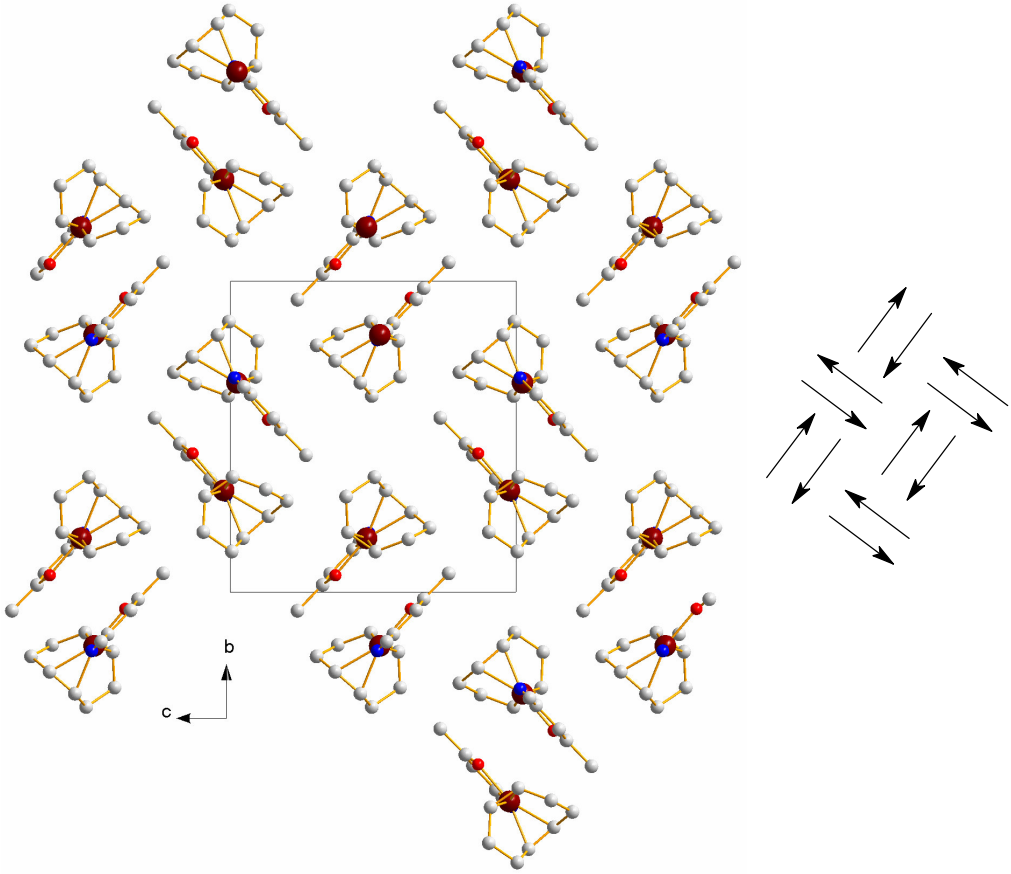

Figure 9.12 Packing of [Pt(cod)(NH-acac)]BF_4 viewed along the *a*-axis with the packing motif incorporated to the right of the figure. Platinum (dark red), carbon (grey), oxygen (red) and nitrogen (blue). Hydrogens and BF_4^- have been omitted for clarity.

In the packing motif shown in Figure 9.12 the head of the arrow is defined as the cyclo-octadiene moiety whilst the tail of the arrow is the 4-aminopent-3-en-2-onato moiety. The packing found for [Pt(cod)(NH-acac)]BF_4 (**19**) is a clustered head-to-tail.

The hydrogen bonding of complex **20** is graphically presented in Figure 9.13 with Table 9.6 listing the bond distances and angles.

Table 9.6 Hydrogen bond distances and angles for [Pt(cod)(NH-acac)]PF_6 (20) [Å and °]

D-H...A	d(D-H)	d(H...A)	d(D...A)	<(DHA)
C_{10}-H_{10}...F_3	0.95	2.40	3.354(14)	179.0
C_8-H_{8A}...$F_3^{\#2}$	0.99	2.48	3.265(15)	135.6
C_8-H_{8A}...$F_3^{\#3}$	0.99	2.48	3.265(15)	135.6
C_6-H_6...$F_1^{\#4}$	1.00	2.49	3.428(10)	157.0
C_{13}-H_{13A}...$F_4^{\#5}$	0.98	2.50	3.230(17)	130.8
C_{13}-H_{13A}...$F_4^{\#6}$	0.98	2.50	3.230(17)	130.8

Symmetry transformations used to generate equivalent atoms:
#1 x,-y,z #2 -x+1/2,-y+1/2,-z+1 #3 -x+1/2,y+1/2,-z+1
#4 -x+1/2,-y+1/2,-z #5 x,y,z+1 #6 x,-y,z+1

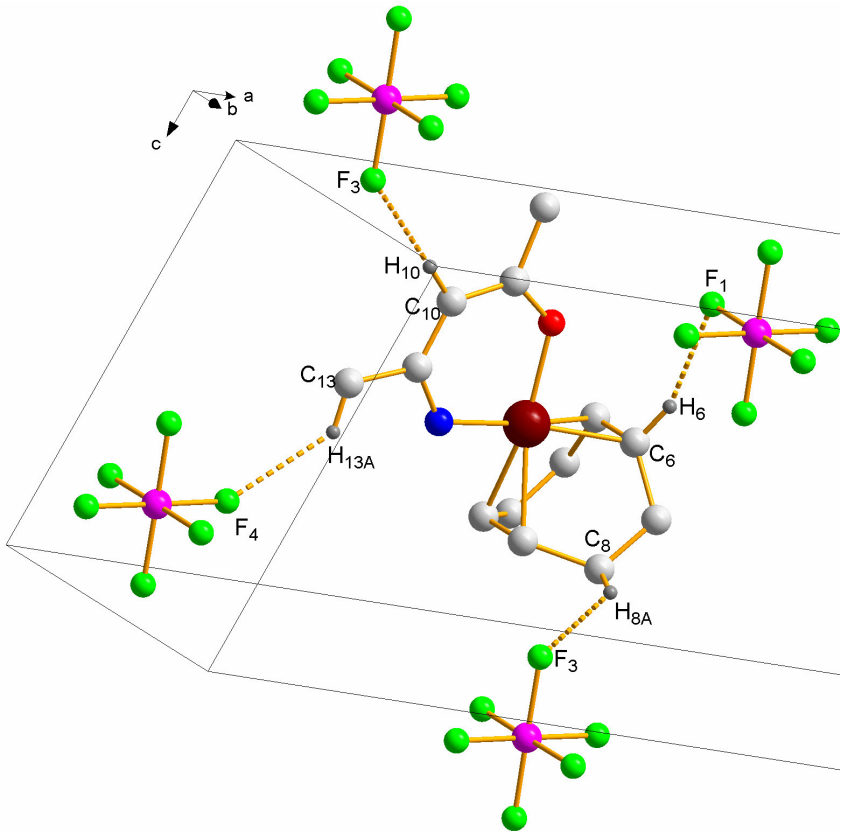

Figure 9.13 Partial unit cell of [Pt(cod)(NH-acac)]PF_6 showing intermolecular hydrogen bonding interactions indicated by a dashed bond. Only selected hydrogen atoms are included. Platinum (dark red), carbon (grey), oxygen (red), nitrogen (blue), phosphorous (pink) and fluorine (green).

No intramolecular interactions of the type **20a**···**20a** were observed for [Pt(cod)(NH-acac)]PF_6 (**20**). Several hydrogen interactions were observed (Figure 9.13) of the type **20a**···**20b** and are listed in Table 9.6. The hydrogen interactions observed for the cyclo-octadiene moiety are between the hydrogen of the alkane carbon (C_8) and the fluorido ligand (F_3) of the **20b** complex and between they hydrogen of the alkene carbon (C_6) and the fluorido ligand (F_1) of the **20b** complex. The methyl hydrogen (H_{13A}) of the 4-aminopent-3-en-2-onato moiety interacts with the fluorido ligand (F_3) of the **20b** complex. The methine hydrogen (H_{10}) also interacts with complex **20b**.

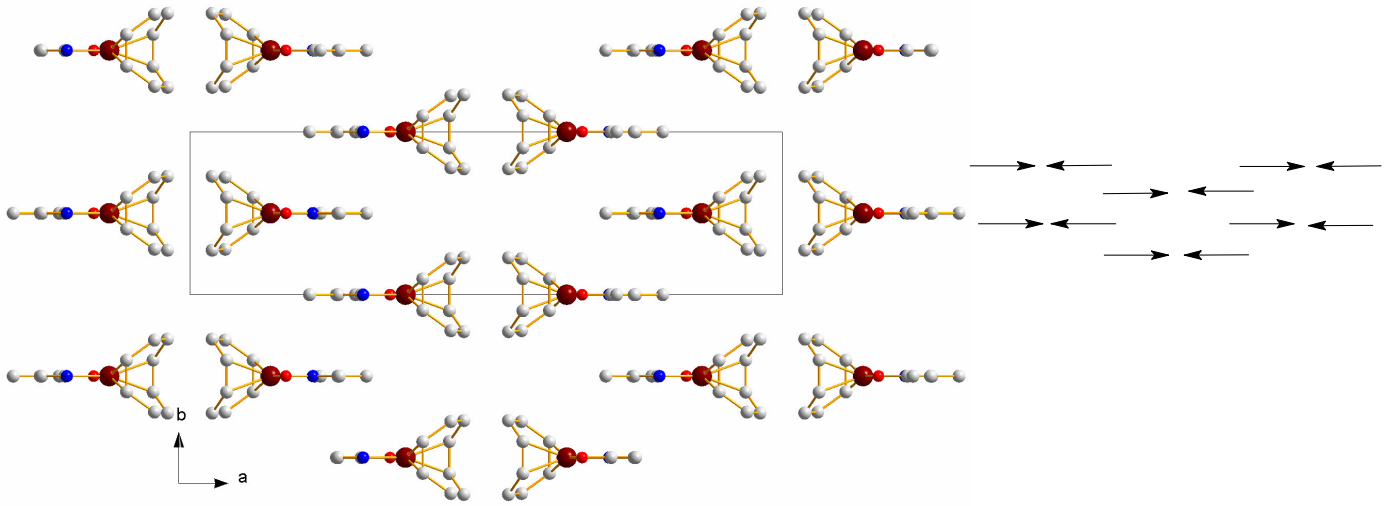

Figure 9.14 Packing of [Pt(cod)(NH-acac)]PF_6 viewed along the *c*-axis with the packing motif incorporated to the right of the figure. Platinum (dark red), carbon (grey), oxygen (red) and nitrogen (blue). Hydrogens and PF_6^- have been omitted for clarity.

In the packing motif shown in Figure 9.14 the head of the arrow is defined as the cyclo-octadine moiety whilst the tail of the arrow is the 4-aminopent-3-en-2-onato moiety. The packing found for [Pt(cod)(NH-acac)]PF_6 (**20**) is head-to-tail.

9.4.2 Crystal structures of [Pt(cod)(NMe-acac)]BF_4 and [Pt(cod)(NMe-acac)]PF_6

The compound [Pt(cod)(NMe-acac)]BF_4 (**21**) crystallizes in the orthorhombic space group $P2_12_12_1$, with a cationic [Pt(cod)(NMe-acac)]$^+$ species (**21a**) and an anionic BF_4^- (**21b**) species in the asymmetric unit. The compound [Pt(cod)(NMe-acac)]PF_6 (**22**) crystallizes in the monoclinic space group *C*2, with a cationic [Pt(cod)(NMe-acac)]$^+$ (**22a**) and an anionic PF_6^- (**22b**) species in the asymmetric unit. The crystal was found to be a racemic twin with a twin component 0.52(3):0.48(3). The numbering scheme is presented in Figure 9.15, while atomic co-ordinates, bond angles and distances, anisotropic displacement parameters and hydrogen co-ordinates are reported in Appendix B.20 and B.21. General crystallographic data and refinement parameters are reported in Table 9.1, while significant bond angles and distances are reported in Table 9.7.

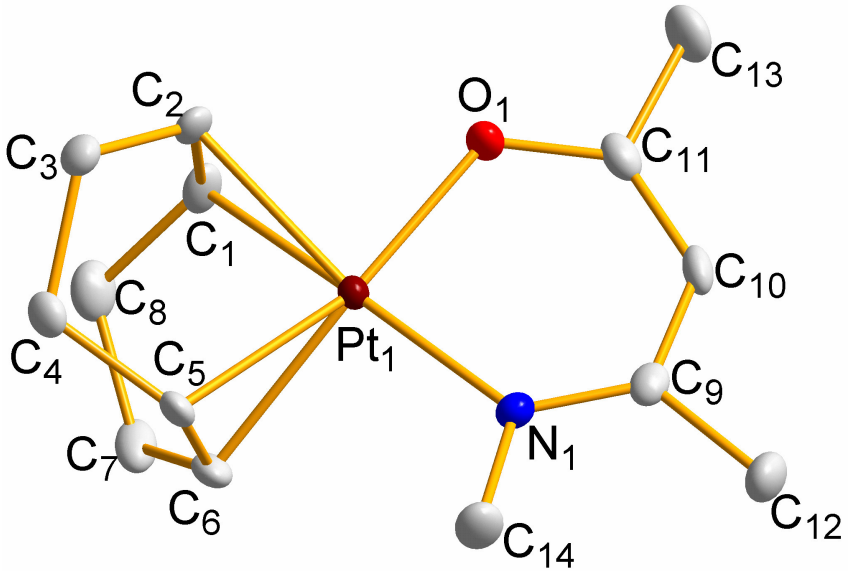

Figure 9.15 Diamond illustration of [Pt(cod)(NMe-acac)]BF_4 (21) at 100 K showing the numbering scheme and displacement ellipsoids (50 %) of the complex. Hydrogen atoms and anionic species omitted for clarity.

The numbering scheme for [Pt(cod)(NMe-acac)]PF_6 (**22**) has the following changes to Figure 9.15 *trans* to nitrogen is the Pt-C_5 and Pt-C_6 bonds and *trans* to oxygen is Pt-C_1 and Pt-C_2, resulting in a counter-clockwise numbering of the cyclo-octadiene moiety.

Table 9.7 Selected bond distances and angles for [Pt(cod)(NMe-acac)]A

Bond Distance (Å)	Counter ion		Bond Angles (°)	Counter ion	
	PF_6 (**22**)	BF_4 (**21**)		PF_6 (**22**)	BF_4 (**21**)
Pt-O_1	1.975(5)	1.985(3)	O_1-Pt-N_1	92.7(2)	92.3(1)
Pt-N_1	2.046(5)	2.036(4)	C_1-Pt-C_2	36.9(4)	37.1(2)
Pt-C_1	2.20(2)	2.192(5)	C_5-Pt-C_6	37.2(3)	37.5(2)
Pt-C_2	2.16(2)	2.182(5)	C_1-Pt-C_6	80.3(7)	81.5(2)
Pt-C_5	2.26(2)	2.184(4)	C_2-Pt-C_5	81.3(8)	81.6(2)
Pt-C_6	2.15(2)	2.168(4)	χ^a	86.1(5)	86.3(1)
C_1-C_2	1.38(1)	1.391(7)	ψ^b	79.9(9)	79.1(2)
C_5-C_6	1.41(1)	1.397(7)			

a χ: $C_1MC_2 \cap C_5MC_6$ b ψ: $C_2C_3C_4C_5 \cap C_1C_8C_7C_6$ see Figure 1.2

The co-ordination geometry is square planar with 1,5-cyclo-octadiene and 4-(methylamino)pent-3-en-2-onato (NMe-acac) ligands bonded to the platinum, with the metal centre remaining in the +2 oxidation state. This cationic species is balanced by a tetrafluoroborate counter ion (**21b**) or a hexafluorophosphate counter ion (**22b**). The Pt-O bonds for **21a** and **22a** are 1.985(3) Å and 1.975(5) Å respectively. The Pt-N bonds for **21a** and **22a** are 2.036(4) Å and 2.046(5) Å respectively. Oxygen and nitrogen have similar electron density only a marginal change in bond distance was observed resulting in a difference of 0.05 Å for **21a** and 0.071 Å for **22a** with the

nitrogen bond being longer in both complexes. The reason for the nitrogen bond being longer as opposed to shorter as is the case for [Pt(cod)(NH-acac)]A (A = BF_4^- and PF_6^-) is the electron donating ability of the methyl group (C_{14}) resulting in a weaker Pt-N bond. The C=C bond distances for **21a** were found to be equivalent with a mean distance of 1.394(7) Å. The average distance for Pt-C was found to be 2.182(5) Å with Pt-C_1 being the longest of the bonds as a result of the *trans* influence of the nitrogen. The reason Pt-C_2 is not affected by the *trans* influence is as a result of the 4-(methylamino)pent-3-en-2-onato ligand lying in line of the Pt-C_1 and Pt-C_5 bonds, resulting in the shortening of the Pt-C_6 bond. The C=C bond distances for **22a** were found to be equivalent with a mean distance of 1.40(1) Å. The average distance for Pt-C was found to be 2.19(2) Å the same situation with the Pt-C bond lengths occurs for **22a** as it did for **21a**. Both the C=C and Pt-C bond lengths are comparable for **21a** and **22a.** The two complexes were found to be isostructural. It is interesting to note that the methyl carbons on the 4-(methylamino)pent-3-en-2-onato moieties for the **21a** complex are not disordered however only one of the methyl carbons (C_{13}) has an idealized disorder for the **22a** complex.

The angle of distortion for the square planar co-ordination geometry (twist angle) as calculated by the planes defined by the mid-points of the alkene carbons of the cylo-octadiene ring and the oxygen and nitrogen of the 4-(methylamino)pent-3-en-2-onato moieties and the platinum with the oxygen, nitrogen and the back-bone carbons of the 4-(methylamino)pent-3-en-2-onato moiety was found to be 10.2(9)° for **21a** and 2.3(6)° for **22a**.

In the following paragraphs a detailed discussion of the hydrogen interactions and the packing of [Pt(cod)(NMe-acac)]BF_4 (**21**) and [Pt(cod)(NMe-acac)]PF_6 (**22**) will be undertaken. The hydrogen bonding of complex **21** is graphically presented in Figure 9.16 with Table 9.8 listing the bond distances and angles.

Table 9.8 Hydrogen bond distances and angles for [Pt(cod)(NMe-acac)]BF_4 (21) [Åand °].

D-H...A	d(D-H)	d(H...A)	d(D...A)	<(DHA)
C_1-H_1...$F_2^{\#1}$	1.00	2.46	3.246(6)	135.5
C_2-H_2...$F_1^{\#2}$	1.00	2.33	3.302(6)	164.0
C_5-H_5...$F_2^{\#3}$	1.00	2.49	3.279(6)	135.5
C_{13}-H_{13B}...$F_1^{\#4}$	0.98	2.54	3.514(7)	176.5
C_{10}-H_{10}...$F_4^{\#4}$	0.95	2.47	3.418(5)	173.9

Symmetry transformations used to generate equivalent atoms:
#1 -x+3/2,-y,z-1/2 #2 -x+1/2,-y,z-1/2 #3 x-1,y,z
#4 x-1/2,-y+1/2,-z+2

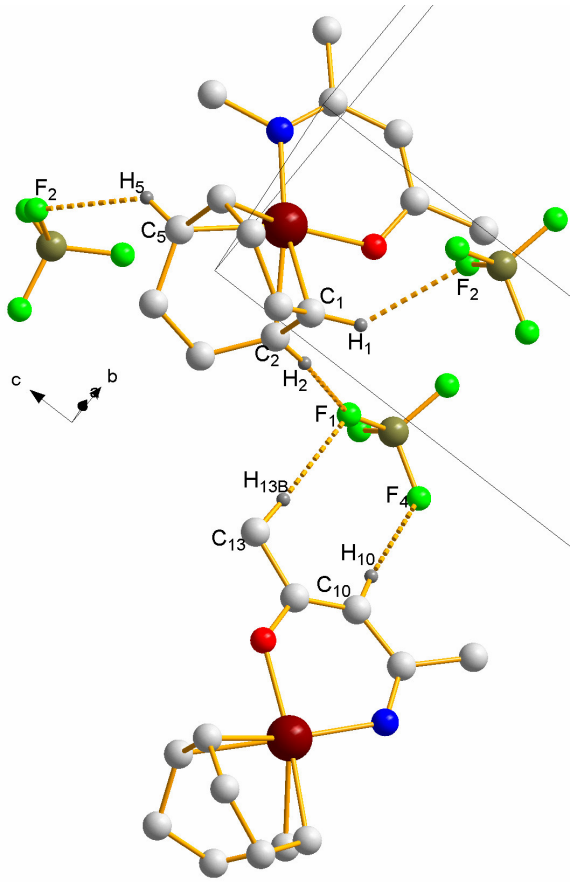

Figure 9.16 Partial unit cell of [Pt(cod)(NMe-acac)]BF_4 showing intermolecular hydrogen bonding interactions indicated by a dashed bond. Only selected hydrogen atoms are included. Platinum (dark red), carbon (grey), oxygen (red), nitrogen (blue), boron (olive) and fluorine (green).

No intramolecular interactions of the type **21a**···**21a** were observed for [Pt(cod)(NMe-acac)]BF_4 (**21**). Several hydrogen interactions were observed (Figure 9.16) of the type **21a**···**21b** and are listed in Table 9.8. The hydrogen interactions observed for cyclo-octadiene moiety are between the hydrogens of the alkene carbons (C_1, C_2 and C_5) with the fluorido ligands (F_2, F_1 and F_2) of the **21b** complex. The methyl hydrogen (H_{13B}) of the 4-(methylamino)pent-3-en-2-onato moiety interacts with the

fluorido ligand (F_1) of the **21b** complex. The methine hydrogen (H_{10}) interacts with the fluorido ligand (F_4).

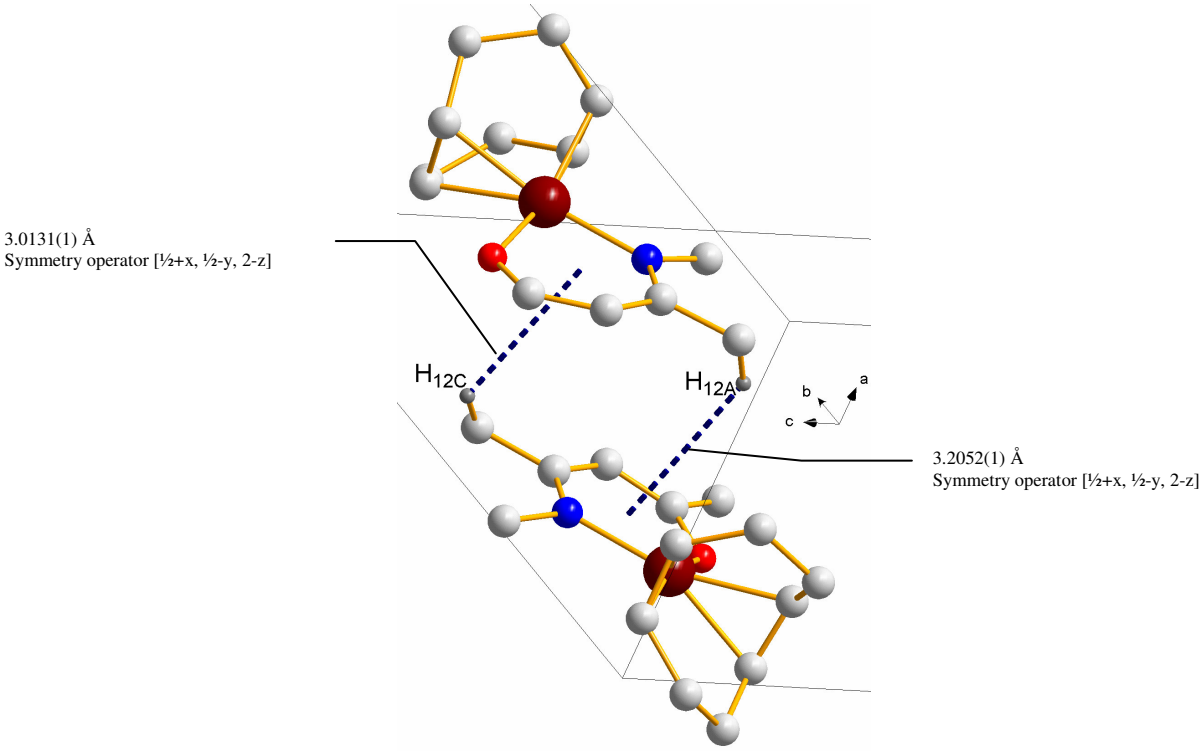

Figure 9.17 Partial unit cell of [Pt(cod)(NMe-acac)]BF_4 showing hydrogen metal chelate ring interactions indicated by a dashed dark blue bond. Tetrafluoroborate counter ion omitted for clarity. Only select hydrogens shown. Platinum (dark red), carbon (grey), oxygen (red) and nitrogen (blue).

The methyl hydrogens (H_{12C} and H_{12A}) of the 4-(methylamino)pent-3-en-2-onato moiety interact with the metal chelate ring formed by the platinum metal centre and the 4-(methylamino)pent-3-en-2-onato moiety with distances of 3.0131(1) Å and 3.2052(1) Å respectively. This leads to the packing illustrated in Figure 9.18.

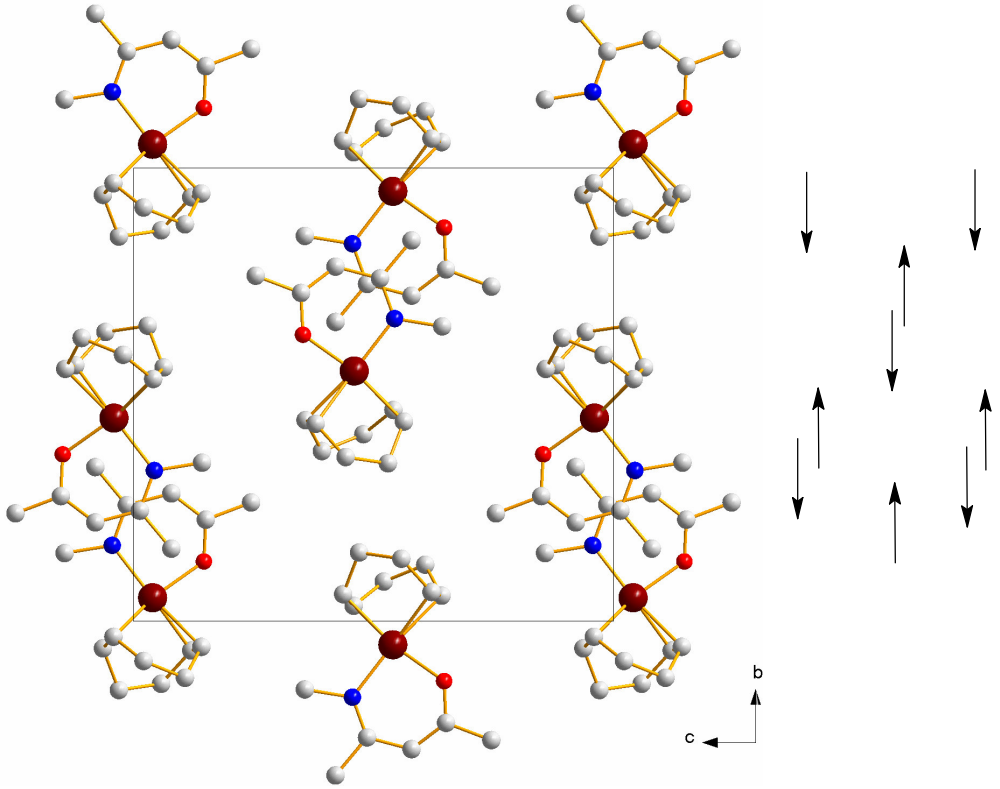

Figure 9.18 Packing of [Pt(cod)(NMe-acac)]BF_4 viewed along the *a*-axis with the packing motif incorporated to the right of the figure. Platinum (dark red), carbon (grey), oxygen (red) and nitrogen (blue). Hydrogens and BF_4^- have been omitted for clarity.

In the packing motif shown in Figure 9.18 the head of the arrow is defined as the cyclo-octadiene moiety whilst the tail of the arrow is the 4-(methylamino)pent-3-en-2-onato moiety. The packing is influenced by the hydrogen metal chelate ring interaction as previously mentioned resulting in a partial clustered head-to-head packing.

The hydrogen bonding of complex **18** is graphically presented in Figure 9.19 with Table 9.9 listing the bond distances and angles.

Table 9.9 Hydrogen bond distances and angles for [Pt(cod)(NMe-acac)]PF_6 [Å and °].

D-H...A	d(D-H)	d(H...A)	d(D...A)	<(DHA)
C_{10}-H_{10}...F_2	0.95	2.58	3.470(9)	156.9
C_{13}-H_{13D}...F_5	0.98	2.47	3.377(13)	153.3
C_2-H_2...$F_1^{\#1}$	1.00	2.53	3.29(2)	132.3
C_{12}-H_{12A}...$F_5^{\#2}$	0.98	2.37	3.236(12)	146.5

Symmetry transformations used to generate equivalent atoms:
#1 -x+1/2,y-1/2,-z+2 #2 x,y,z+1

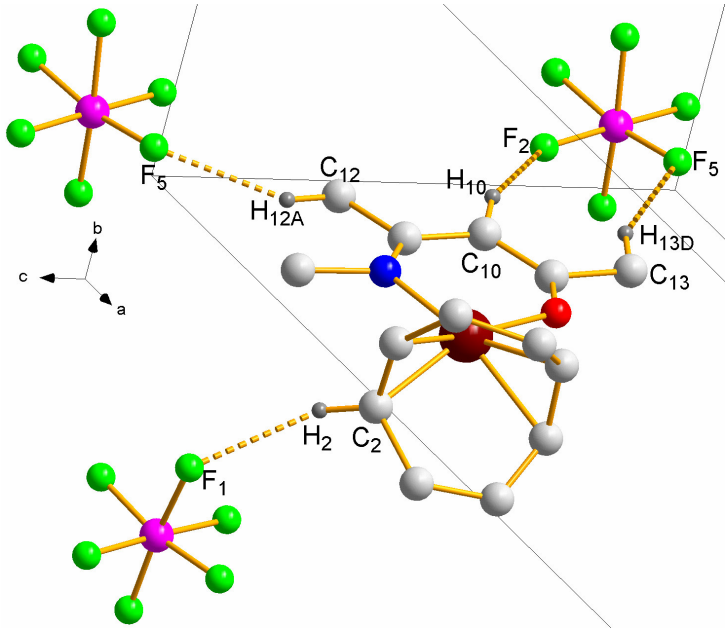

Figure 9.19 Partial unit cell of [Pt(cod)(NMe-acac)]PF_6 showing intermolecular hydrogen bonding interactions indicated by a dashed bond. Only selected hydrogen atoms are included. Platinum (dark red), carbon (grey), oxygen (red), nitrogen (blue), phosphorus (pink) and fluorine (green).

No intramolecular interactions of the type **22a**···**22a** were observed for [Pt(cod)(NMe-acac)]PF_6 (**22**). Several hydrogen interactions were observed (Figure 9.19) of the type **22a**···**22b** and are listed in Table 9.9. Only one hydrogen interaction was observed between the hydrogen of the alkene carbon (C_2) of the cyclo-octadiene ring and the fluorido ligand (F_1) of **22b**. The methyl hydrogens (H_{12A} and H_{13D}) of the 4-(methylamino)pent-3-en-2-onato moiety interacts with the fluorido ligand (F_5) of **22b**. Lastly, the methine hydrogen (H_{10}) interacts with the fluorido ligand (F_2).

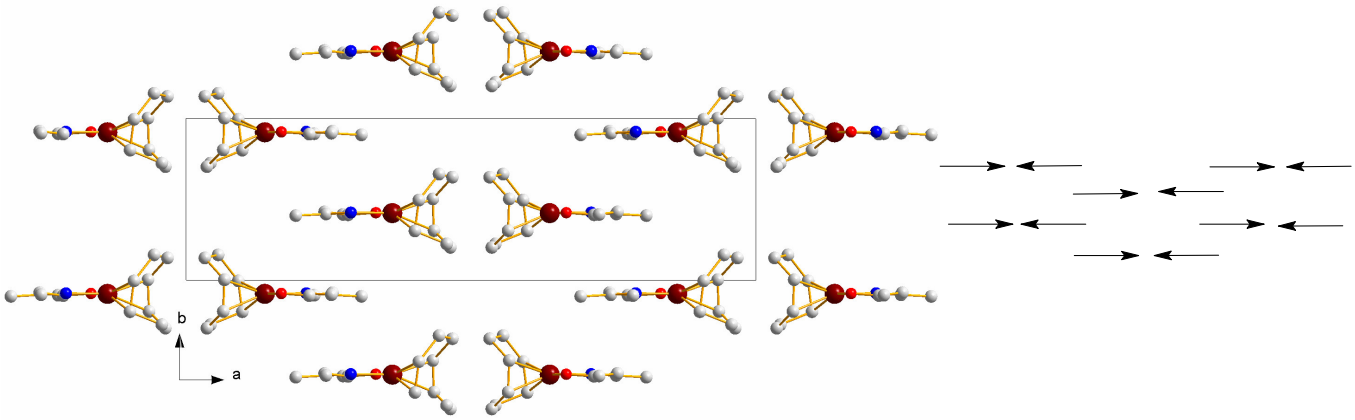

Figure 9.20 Packing of [Pt(cod)(NMe-acac)]PF_6 viewed along the *c*-axis with the packing motif incorporated to the right of the figure. Platinum (dark red), carbon (grey), oxygen (red) and nitrogen (blue). Hydrogens and PF_6^- have been omitted for clarity.

In the packing motif shown in Figure 9.20 the head of the arrow is defined as the cyclo-octadiene moiety whilst the tail of the arrow is the 4-(methylamino)pent-3-en-2-onato moiety. Head-to-tail packing is observed.

9.4.3 Crystal structures of [Pt(cod)(NPh-acac)]BF_4 and [Pt(cod)(NPh-acac)]PF_6

The compound [Pt(cod)(NPh-acac)]BF_4 (**23**) crystallizes in the monoclinic space group $P2_1/n$, with a cationic [Pt(cod)(NPh-acac)]$^+$ species (**23a**) and an anionic BF_4^- (**23b**) species in the asymmetric unit. The compound [Pt(cod)(NPh-acac)]PF_6 (**24**) crystallizes in the triclinic space group $P1$, with two cationic [Pt(cod)(NPh-acac)]$^+$ species (**24a1** and **24a2**) and two anionic PF_6^- species (**24b1** and **24b2**) in the asymmetric unit. The numbering scheme is presented in Figure 9.21, while atomic co-ordinates, bond angles and distances, anisotropic displacement parameters and hydrogen co-ordinates are reported in Appendix B.22 and B.23. General crystallographic data and refinement parameters are reported in Table 9.1, while significant bond angles and distances are reported in Table 9.13.

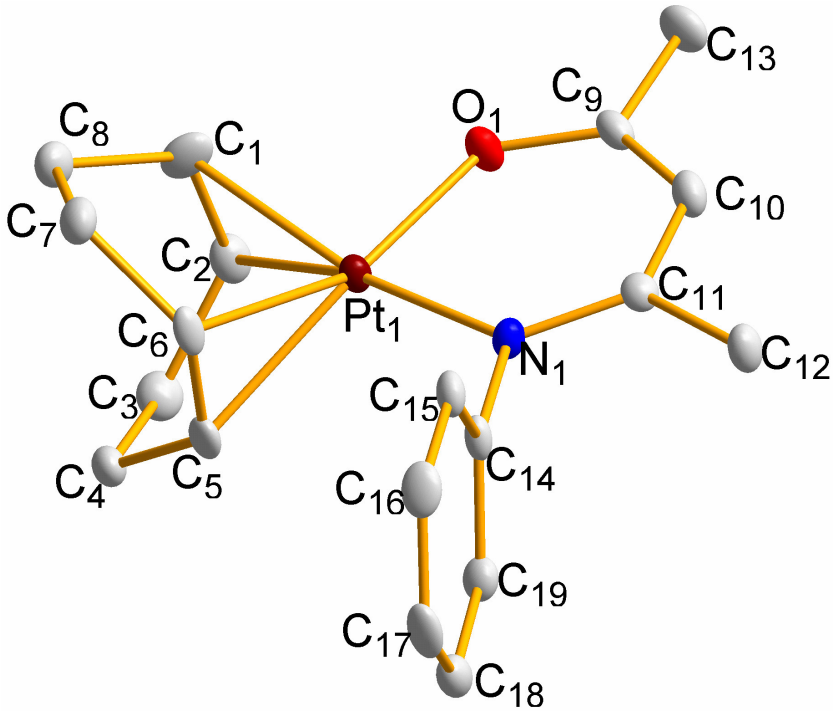

Figure 9.21 Diamond illustration of [Pt(cod)(NPh-acac)]BF_4 (23) at 100 K showing the numbering scheme and displacement ellipsoids (50 %) of the complex. Hydrogen atoms and anionic species omitted for clarity.

For [Pt(cod)(NPh-acac)]PF_6 (**24**) two molecules are present in the asymmetric unit. The numbering scheme is adjusted such that a prefix to the atom number as indicated in Figure 9.21 is appended depending on the molecule e.g. Pt_1-O_1 becomes Pt_1-O_{11} for the first molecule and Pt_2-O_{21} for the second.

Table 9.10 Selected bond distances and angles for [Pt(cod)(NPh-acac)]A

Bond Distance (Å)	Counter ion			Bond Angles (°)	Counter ion		
	PF_6 (**24**)		BF_4 (**23**)		PF_6 (**24**)		BF_4 (**23**)
	Mole[c] 1	Mole 2			Mole 1	Mole 2	
Pt-O_1	1.989(10)	1.994(11)	1.990(3)	O_1-Pt-N_1	94.4(4)	92.9(4)	91.8(1)
Pt-N_1	2.058(11)	2.058(11)	2.034(4)	C_1-Pt-C_2	38.5(9)	41.4(9)	37.7(2)
Pt-C_1	2.170(18)	2.238(18)	2.186(5)	C_5-Pt-C_6	36.2(6)	36.2(7)	37.6(2)
Pt-C_2	2.245(17)	2.164(17)	2.193(5)	C_1-Pt-C_6	81.1(6)	76.8(8)	80.9(2)
Pt-C_5	2.178(15)	2.161(15)	2.186(4)	C_2-Pt-C_5	78.9(7)	82.8(7)	80.7(2)
Pt-C_6	2.162(14)	2.181(17)	2.170(5)	χ^a	85.5(8)	85.8(8)	85.3(2)
C_1-C_2	1.46(4)	1.56(4)	1.415(7)	ψ^b – part A	71.3(10)	73.1(12)	79.7(2)
C_5-C_6	1.35(2)	1.35(2)	1.403(6)	ψ^b – part B	88.9(11)	80.4(12)	

a χ: $C_1MC_2 \cap C_5MC_6$ b ψ: $C_2C_3C_4C_5 \cap C_1C_8C_7C_6$ see Figure 1.2 c Mole ≡ molecule

The co-ordination geometry of complexes **23a** and **24a** are square planar with 1,5-cyclo-octadiene and 4-anilinopent-3-en-2-onato (NPh-acac) ligands bonded to the platinum, with the metal centre remaining in the +2 oxidation state. This cationic species is balanced by a tetrafluoroborate counter ion (**23b**) or a hexafluorophosphate counter ion (**24b1** and **24b2**). The Pt-O bonds for **23a**, **24a1** and **24a2** are 1.990(3) Å, 1.989(10) Å and 1.994(11) Å respectively. The mean average found for the Pt-O bonds for **24a1** and **24a2** is 1.992(11) Å which is similar to that of **23a**. The Pt-N bonds for **23a, 24a1** and **24a2** are 2.034(4) Å, 2.058(11) Å and 2.058(11) Å respectively. The Pt-N bonds for **24a1** and **24a2** were found to be equivalent and varying only slightly from **23a** by 0.024 Å. Oxygen and nitrogen have similar electron density only a marginal change in the bond distance was observed resulting in a difference of 0.044 Å for **23a** and 0.066 Å for **24a1** and **24a2** using the average values obtained above for the bonds with the nitrogen bond being longer in both complexes. The reason for the longer nitrogen bond is as a result of the electron donating ability of the phenyl group resulting in a weaker Pt-N bond. The electron donating ability of the phenyl group is less than the methyl counterpart as the proton affinity of the phenyl group is larger than that of the methyl group[12] resulting in a slightly shorter bond for **23a** than for **21a**. The C=C bond distances for **23a** were found to be similar with a mean distance of 1.409(6) Å. The average distance for

[12] Nam P., Nguyen M.T., *J. Phys. Chem. A.*, **110**, 4509, (2006)

Pt-C was found to be 2.184(5) Å with Pt-C_2 being the longest of the bonds as a result of the *trans* influence of the nitrogen. The intersection of the planes defined as the metal chelate ring and the phenyl ring was found to be 84.0(1)°.

In proceeding with [Pt(co)(NPh-acac)]PF_6 (24) a few points need to be addressed. Firstly the crystal was solved in the triclinic *P*1 space group, however when using PLATON it suggested the changing of the space group to monoclinic *C*2/*m*. When changing to this space group the best R value of 38 % is obtained. The other space group suggested was monoclinic *C*2/*c* and the best R value obtained is 12 %. The last option tried was that of monoclinic *Cc* in which case the best R value obtained was 6.3 %. The structure was solved as a racemic twin with a BASF of 0.47(3), however the thermal parameters were large and the maximum shift error was large, in an attempt to solve the maximum shift error additional refinements were done, but during these final refinements the whole structure became unstable. For the triclinic *P*1 refinement there is still some residual electron density in the unit cell that cannot be assigned, the values were low enough to be ignored. It was concluded that the structure be reported as triclinic *P*1 (R value of 4.2 %) with the future outlook to re-synthesize the compound and to grow a new crystal for an improved data collection. In Figure 9.22 the disorders of 1,5-cyclo-octadiene (cod) ring of **24a1** are depicted as dark grey bonds with tan carbon atoms with site occupancies of 50 %.

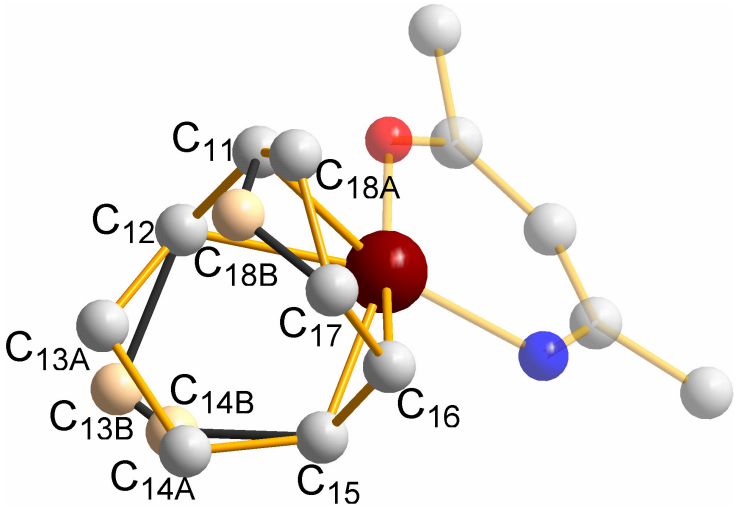

Figure 9.22 Diamond illustration of [Pt(cod)(NPh-acac)]$^+$ (24a1) depicting the disorder on the cyclo-octadiene ring, carbons of the second part of the disorder are colored tan with the bonds a dark grey. The 4-anilinopent-3-en-2-onato ligand shown is at 50% transparency, hydrogens and the 24b1 species have been omitted for clarity. Carbon (grey), oxygen (red), nitrogen (blue) and platinum (dark red).

The first disorder is that of C_{18A} and C_{18B} which is self expletory from Figure 9.22. The second disorder present is a little more complex. Firstly we need to define the side arms (or jaws) of the cod ring C_{12}, C_{13A}, C_{14A} and C_{15} for the lower jaw and C_{11}, C_{18A}, C_{17} and C_{16} as the upper jaw. The disorder simply put is the fluctuation (i.e. opening and closing) of the lower jaw resulting in an extremely short bond of 0.78(5) Å for C_{13B}-C_{14B} and an elongation of the C_{13A}-C_{14A} bond with a distance of 1.73(6) Å. The mean distance of the bond is 1.255(6) Å which is still very short for an alkane bond (1.378 Å – 1.72 Å)[13]. The longest experimentally determined C(sp^3)-C(sp^3) is 1.720 Å for 1,1,2,2-tetraphenyl-3,8-dichloronaphthocyclobutene[14,15]. In Figure 9.23 the disorders of 1,5-cyclo-octadiene (cod) ring of **24a2** are depicted as dark grey bonds with tan carbon atoms with site occupancies of 50 %.

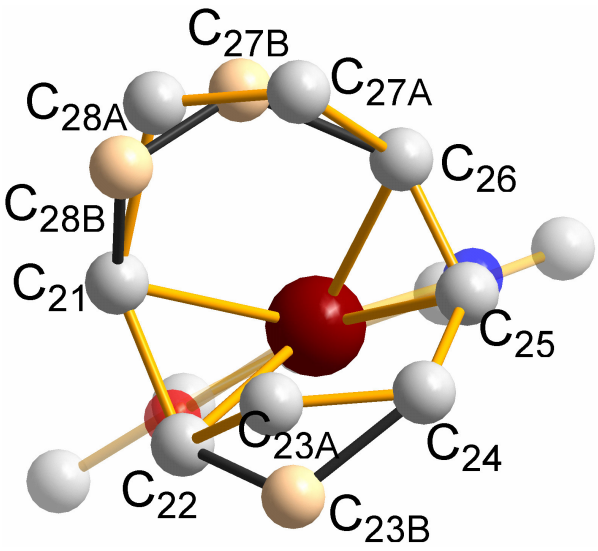

Figure 9.23 Diamond illustration of [Pt(cod)(NPh-acac)]$^+$ (24a2) depicting the disorder on the cyclo-octadiene ring, carbons of the second part of the disorder are colored tan with the bonds a dark grey. The 4-anilinopent-3-en-2-onato ligand shown is at 50% transparency, hydrogens and the 24b1 species have been omitted for clarity. Carbon (grey), oxygen (red), nitrogen (blue) and platinum (dark red).

A similar disorder exists for C_{23A} and C_{23B} as was found in **24a1** with the C_{18A} and C_{18B}. The major difference is found in the upper jaw of the cod ring (C_{21}, C_{28A}, C_{27A} and C_{26}) where the disorder is not a fluctuation (opening closing) but a twisting of the jaw. The other difference is that it is the upper jaw that is disordered for **24a2**

[13] Zavitsas A.A., *J. Phys. Chem. A.*, **107**, 897, (2003)
[14] Toda F., Tanaka K., Stein Z., Goldberg I., *Acta. Cryst.*, **C52**, 177, (1996)
[15] Baldridge K.K., Kasahara Y., Ogawa K., Siegel J.S., Tanaka K., Toda F., *J. Am. Chem. Soc.*, **120**, 6167, (1998)

whereas it is the lower jaw that is disordered for **24a1**. The disorder in **24a2** leads to more realistic bond lengths for C_{27A}-C_{28A} and C_{27B}-C_{28B} with distances of 1.37(6) Å and 1.33(5) Å respectively as opposed to those found in **24a1**, though still a little short for an alkene bond (1.378 Å – 1.72 Å)[13].

The C=C bond distances for **24a1** and **24a2** were found to be non-equivalent with a difference of 0.11 Å and 0.21 Å with a mean distance of 1.41(3) Å and 1.46(3) Å respectively. The C_5-C_6 bond for both **24a1** and **24a2** are equivalent and are adjacent to the nitrogen moiety. A possible reason for the elongation of C_1-C_2 could be the influence of the disorder that is present in the cyclo-octadiene ring. The mean C=C distance of **24a** is 1.44(3) Å. The average distance for Pt-C for **24a1** and **24a2** was found to be 2.189(16) Å and 2.186(17) Å, with a combined mean distance of 2.188(17) Å. Again the *trans* influence of the nitrogen affects the bond lengths with the longest bond being *trans* to the nitrogen. The intersection of the planes defined as the metal chelate ring and the phenyl ring were found to be 87.4(4)° for **24a1** and 87.4(4)° for **24a2**, pointing to the stability of the 4-anilinopent-3-en-2-onato ligand within this system.

The angle of distortion for the square planar co-ordination geometry (twist angle) as calculated by the planes defined by the mid-points of the alkene carbons of the cylo-octadiene ring and the oxygen and nitrogen of the 4-anilinopent-3-en-2-onato moieties and the platinum with the oxygen, nitrogen and the back-bone carbons of the 4-anilinopent-3-en-2-onato moiety was found to be 3.5(6)° for **23a**, 6.6(2)° for **24a1** and 6.8(2)° for **24a2** with a mean average for **24a** of 6.7(2)°.

In the following paragraphs a detailed discussion of the hydrogen interactions and the packing of [Pt(cod)(NPh-acac)]BF_4 (**23**) and [Pt(cod)(NPh-acac)]PF_6 (**24**) will be undertaken. The hydrogen bonding of complex **23** is graphically presented in Figure 9.24 with Table 9.11 listing the bond distances and angles.

Table 9.11 Hydrogen bond distances and angles for [Pt(cod)(NPh-acac)]BF_4 (23) [Å and °]

D-H...A	d(D-H)	d(H...A)	d(D...A)	<(DHA)
C_{12}-H_{12A}...F_2	0.98	2.43	3.272(6)	143.6
C_8-H_{8B}...$F_4^{\#1}$	0.99	2.35	3.258(5)	151.6
C_{12}-H_{12B}...$F_3^{\#2}$	0.98	2.54	3.374(5)	142.6

Symmetry transformations used to generate equivalent atoms:
#1 x+1,y,z #2 -x,-y,-z+1

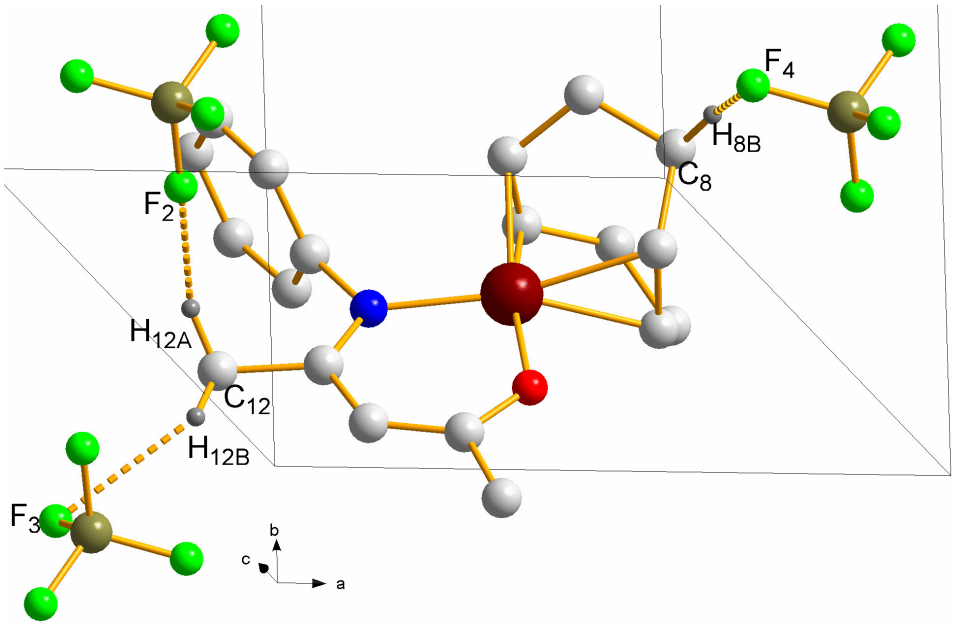

Figure 9.24 Partial unit cell of [Pt(cod)(NPh-acac)]BF_4 showing intermolecular hydrogen bonding interactions indicated by a dashed bond. Only selected hydrogen atoms are included. Platinum (dark red), carbon (grey), oxygen (red), nitrogen (blue), boron (olive) and fluorine (green).

No intramolecular interactions of the type **23a**···**23a** were observed for [Pt(cod)(NPh-acac)]BF_4 (**23**). A few hydrogen interactions were observed (Figure 9.24) of the type **23a**···**23b** and are listed in Table 9.11. Two hydrogen interactions were observed for the methyl hydrogens (H_{12A} and H_{12B}) of the 4-anilinopent-3-en-2-onato moiety with the fluorido ligands (F_2 and F_3) of **23b**. The last interaction observed is that of the hydrogen of the alkane carbon (C_8) of the 4-anilinopent-3-en-2-onato ligand with the fluorido ligand (F_4) of **23b**.

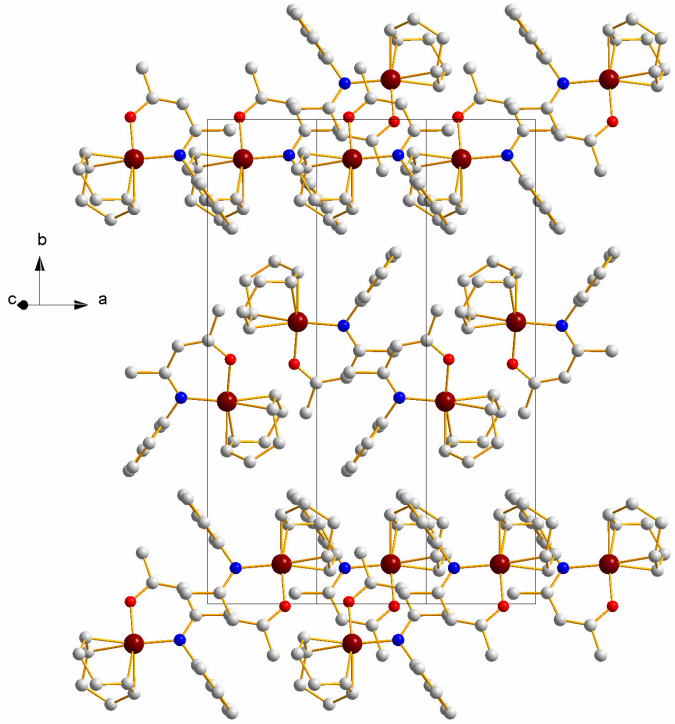

Figure 9.25 Packing of [Pt(cod)(NPh-acac)]BF_4. Platinum (dark red), carbon (grey), oxygen (red) and nitrogen (blue). Hydrogens and BF_4^- have been omitted for clarity.

In the packing motif shown in Figure 9.26 the head of the arrow is defined as the cyclo-octadiene moiety whilst the tail of the arrow is the 4-anilinopent-3-en-2-onato moiety. A zig-zag head-to-tail packing is observed, in Figure 9.25, no π-stacking was observed for the phenyl rings of the 4-anilinopent-3-en-2-onato ligand.

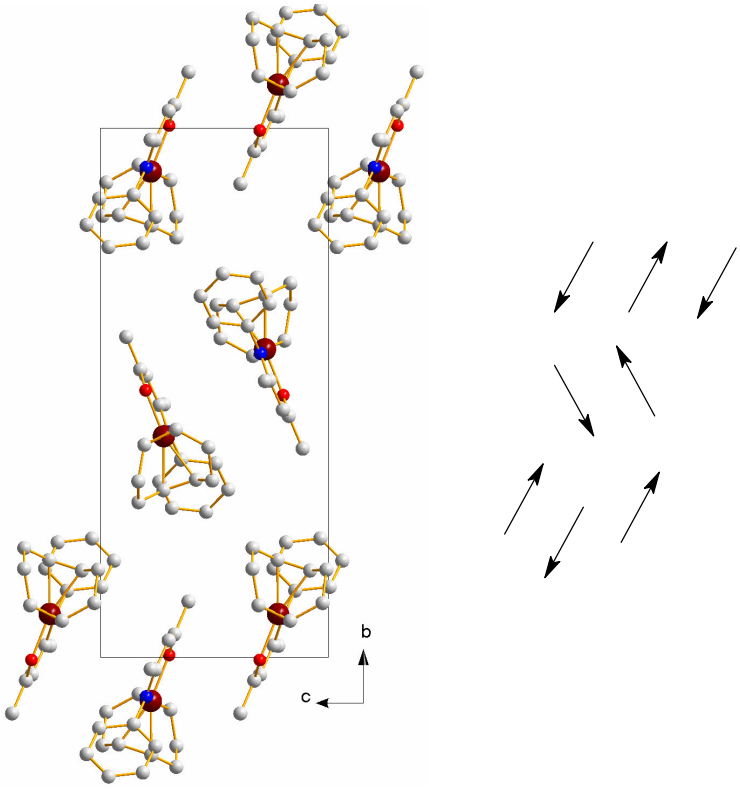

Figure 9.26 Packing of [Pt(cod)(NPh-acac)]BF_4 viewed along the *a*-axis with the packing motif incorporated to the right of the figure. Platinum (dark red), carbon (grey), oxygen (red) and nitrogen (blue). Hydrogens and BF_4^- have been omitted for clarity.

The hydrogen bonding of complex **24** is graphically presented in Figure 9.27 with Table 9.12 listing the bond distances and angles.

Table 9.12 Hydrogen bond distances and angles for [Pt(cod)(NPh-acac)]PF_6 (24) [Å and °].

D-H...A	d(D-H)	d(H...A)	d(D...A)	<(DHA)
C_{23B}-H_{23D}...F_{24}	0.99	2.47	3.44(5)	165.2
C_{213}-H_{21F}...$F_{22}^{\#1}$	0.98	2.48	3.15(2)	125.3
C_{113}-H_{11D}...$F_{15}^{\#1}$	0.98	2.47	3.14(2)	125.7
C_{24}-H_{24A}...F_{21}	0.99	2.55	3.33(2)	135.0
C_{119}-H_{119}...F_{15}	0.95	2.55	3.46(2)	162.7
C_{215}-H_{215}...F_{22}	0.95	2.55	3.47(2)	164.5

Symmetry transformations used to generate equivalent atoms:
#1 x-1,y,z

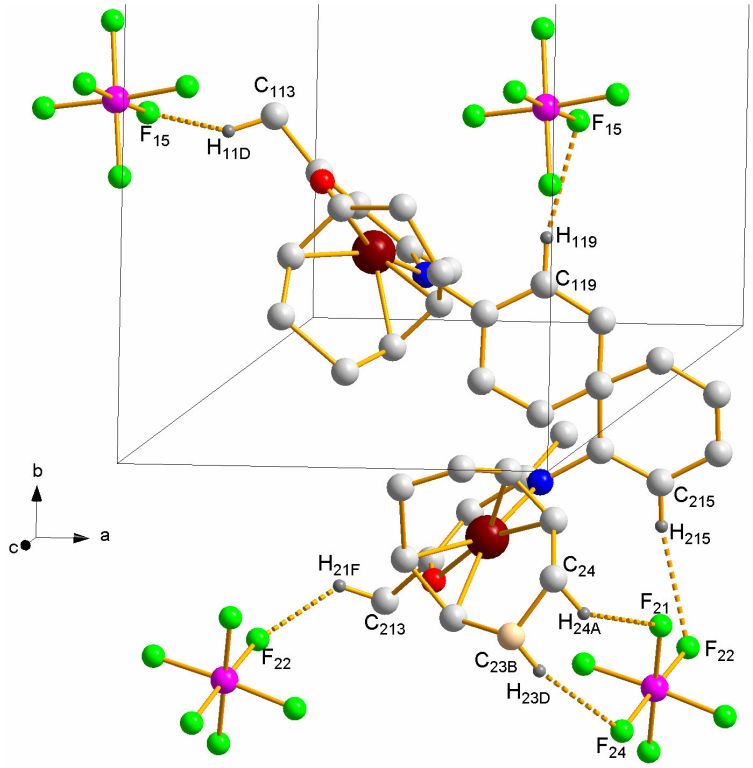

Figure 9.27 Partial unit cell of [Pt(cod)(NPh-acac)]PF_6 showing intermolecular hydrogen bonding interactions indicated by a dashed bond. Only selected hydrogen atoms are included. Platinum (dark red), carbon (grey), disordered carbon (tan), oxygen (red), nitrogen (blue), phosphorus (pink) and fluorine (green).

No intramolecular interactions of the type **24a**···**24a** were observed for [Pt(cod)(NPh-acac)]PF_6 (**24**). A few hydrogen interactions were observed (Figure 9.27) of the type **24a**···**24b** and are listed in Table 9.12. Two hydrogen interactions were observed for the methyl hydrogens (H_{11D} and H_{21F}) of the 4-anilinopent-3-en-2-onato moieties with the fluorido ligands (F_{15} and F_{22}) of the **24b1** and **24b2** complexes. For **24a2** three additional hydrogen interactions are observed, these are the hydrogens of the alkane carbons (C_{23B} and C_{24}) of the cyclo-octadine ring with the fluorido ligands (F_{24} and F_{21}) of **24b2** and the aromatic hydrogen (H_{215}) of the phenyl ring of the 4-anilinopent-3-en-2-onato moiety with the fluorido ligand (F_{22}) of **24b2**. The last interaction is with **24a1** where the aromatic hydrogen (H_{119}) of the 4-anilinopent-3-en-2-onato moiety interacts with the fluorido ligand (F_{15}) of the **24b1** complex.

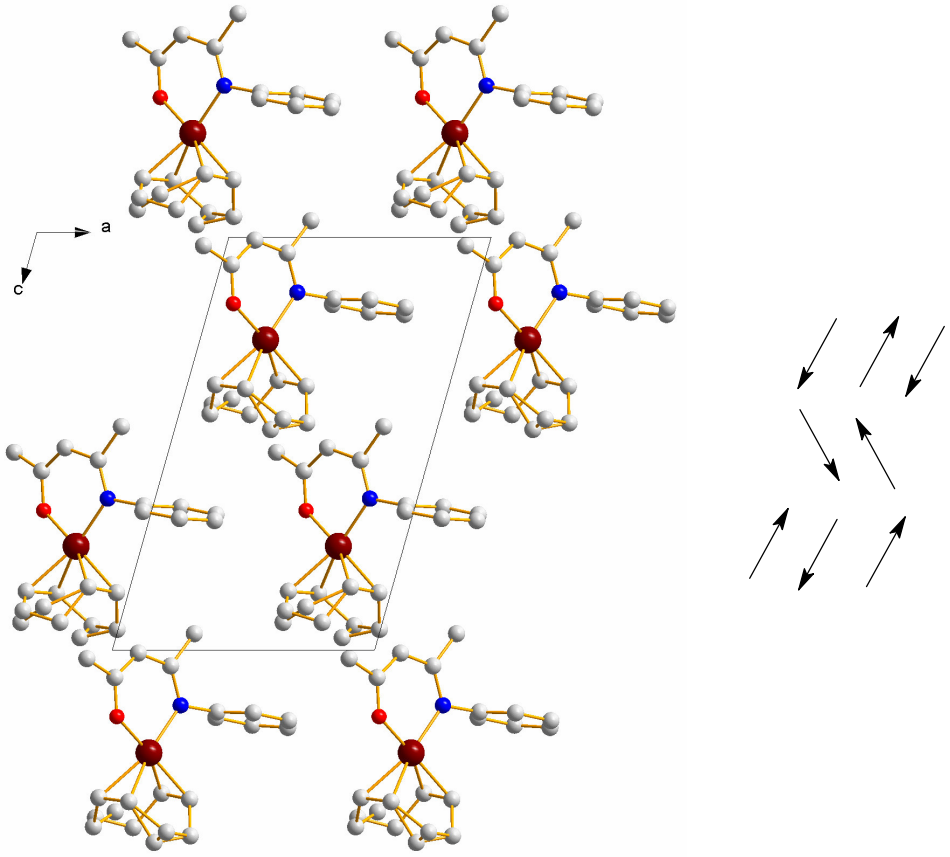

Figure 9.28 Packing of [Pt(cod)(NPh-acac)]PF_6 viewed along the *b*-axis with the packing motif incorporated to the right of the figure. Platinum (dark red), carbon (grey), oxygen (red) and nitrogen (blue). Hydrogens and PF_6^- have been omitted for clarity.

In the packing motif show in Figure 9.28 the head of the arrow is defined as the cyclo-octadiene moiety whilst the tail of the arrow is the 4-anilinopent-3-en-2-onato moiety. A zig-zag head-to-tail packing is observed this is the same packing as was found for [Pt(cod)(NPh-acac)]BF_4.

9.5 Discussion

The N,O-bidenate ligands that were chosen for this chapter were 4-aminopent-3-en-2-one (HNH-acac), 4-(methylamino)pent-3-en-2-one (HNMe-acac) and 4-anilinopent-3-en-2-one (HNPh-acac) which were synthesized in § 3.3. These ligands were chosen for their similarity to the acetylacetonato type ligands and the inclusion of the nitrogen donor creates a non-symmetrical system. Additionally the substituents on the nitrogen can be easily tailored to be electron-withdrawing or electron-donating.

The metal centers used in this study were platinum(II) and palladium(II) resulting in a cationic species, this was balanced with an anionic counter ion either tetrafluoroborate (BF_4^-) or hexafluorophosphate (PF_6^-).

Table 9.13 Cell dimension overview for Palladium(II) and Platinum(II) crystals obtained.

	[Pd(cod)(NH-acac)]A BF_4 (**18**)	[Pt(cod)(NH-acac)]A BF_4 (**19**)	PF_6 (**20**)	[Pt(cod)(NMe-acac)]A BF_4 (**21**)	PF_6 (**22**)	[Pt(cod)(NPh-acac)]A BF_4 (**23**)	PF_6 (**24**)
Crystal system	Monoclinic	Monoclinic	Monoclinic	Orthorhombic	Monoclinic	Monoclinic	Triclinic
Space group	$P2_1/c$	$P2_1/c$	$C2/m$	$P2_12_12_1$	$C2$	$P2_1/n$	$P1$
a	9.8665(3)	9.8588(2)	26.8871(12)	7.5277(2)	26.5792(6)	9.5952(7)	8.7064(2)
b	12.7836(3)	12.8652(2)	7.1009(3)	13.9653(4)	7.1903(1)	21.2609(16)	16.9618(3)
c	12.7126(3)	12.6969(3)	8.7130(4)	14.7872(4)	9.3146(2)	10.3335(8)	14.2377(3)
α	90	90	90	90	90	90	90
β	110.851(1)	111.040(2)	105.305(3)	90	106.250(1)	117.66	105.2377(3)
γ	90	90	90	90	90	90	90
Z	4	4	4	4	4	4	2

The cell dimensions of the crystal structures presented are summarized in Table 9.13 with selected bond distances and angles of the complexes listed in Table 9.14. All the complexes were found to have a slightly distorted square planar geometry, see Figure 4.2 for the definition of the co-ordination geometry. To determine a measure of this distortion the intersection of the planes defined by the mid-points of the alkene carbons of the cylo-octadiene ring and the oxygen and nitrogen of the N,O-bidentate moiety and the platinum with the oxygen, nitrogen and the back-bone carbons of the N,O-bidentate moiety were calculated. The series obtained is **20a < 22a < 18a < 23a < 19a < 24a** (**24a1** and **24a2**) **< 21a** the values are seen in Table 9.14. The difference found in the twist angle for **24a1** and **24a2** is as a result of the disorder in the cyclo-octadiene ring. The changing of the counter ion influences the distortion of the co-ordination geometry, but there is no discernable trend.

Compounds **18** and **19** were found to be isostructural and isomorphous, crystallizes in the monoclinic $P2_1/c$ space group. It is interesting to note that the general trend of the crystals is to the monoclinic space group, the exceptions to this are [Pt(cod)(NMe-acac)]BF_4 (**21**) complex being orthorhombic and [Pt(cod)(NPh-acac)]PF_6 (**24**) being triclinic. However as previously discussed (§ 9.4.3) the crystal structure can be solved in monoclinic *Cc*.

Table 9.14 Selected Geometric parameters (Å,º) for Palladium(II) and Platinum(II) metal complexes

	[Pd(cod)(NH-acac)]A	[Pt(cod)(NH-acac)]A		[Pt(cod)(NMe-acac)]A		[Pt(cod)(NPh-acac)]A	
	BF_4 (**18**)	BF_4 (**19**)	PF_6 (**20**)	BF_4 (**21**)	PF_6 (**22**)	BF_4 (**23**)	PF_6[c] (**24**)
M-O_1	1.999(2)	2.009(2)	2.006(9)	1.985(3)	1.975(5)	1.990(3)	1.992(11)
M-N_1	1.972(2)	1.978(3)	1.999(9)	2.036(4)	2.046(5)	2.034(4)	2.058(11)
M-C_1	2.185(3)	2.152(3)	2.195(8)	2.192(5)	2.20(2)	2.186(5)	2.204(18)
M-C_2	2.208(3)	2.168(3)	2.195(8)	2.182(5)	2.16(2)	2.193(5)	2.205(17)
M-C_5	2.222(3)	2.183(3)	2.151(8)	2.184(4)	2.26(2)	2.186(4)	2.170(15)
M-C_6	2.228(3)	2.187(3)	2.151(8)	2.168(4)	2.15(2)	2.170(5)	2.172(16)
C_1-C_2	1.384(4)	1.395(5)	1.38(2)	1.391(7)	1.38(1)	1.415(7)	1.51(4)
C_5-C_6	1.376(4)	1.396(5)	1.40(2)	1.397(7)	1.41(1)	1.403(6)	1.35(2)
O_1-M-N_1	92.03(9)	91.5(1)	92.0(4)	92.3(1)	92.7(2)	91.8(1)	92.7(4)
C_1-M-C_2	36.7(1)	37.7(1)	36.6(5)	37.1(2)	36.9(4)	37.7(2)	40.0(9)
C_5-M-C_6	36.0(1)	37.3(1)	37.9(6)	37.5(2)	37.2(3)	37.6(2)	36.2(7)
C_1-M-C_6	82.1(1)	82.7(1)	82.5(3)	81.5(2)	80.3(7)	80.9(2)	79.0(7)
C_2-M-C_5	81.8(1)	82.1(1)	82.5(3)	81.6(2)	81.3(8)	80.7(2)	80.9(7)
χ[a]	86.2(1)	87.2(2)	88.1(2)	86.3(1)	86.1(5)	85.3(2)	85.7(8)
ψ[b]	81.9(2)	78.6(2)	82.7(5)	79.1(2)	79.9(9)	79.7(2)	78.4(11)
twist	3.31(4)	3.77(5)	0	10.2(9)	2.3(6)	3.5(6)	6.7(2) [6.6(2) / 6.8(2)]

a χ: $C_1MC_2 \cap C_5MC_6$ b ψ: $C_2C_3C_4C_5 \cap C_1C_8C_7C_6$ see Figure 1.2 c averaged values of **24a1** and **24a2**

For the M-O, C=C and M-C bond distances the mean averages are 1.994(5) Å, 1.401(9) Å and 2.186(9) Å respectively, the values found for the different complexes do not vary greatly. For M-N there is a small increase (0.014 Å) in the bond distances as one progresses from complex **18** to complex **24**, the electron-donating ability of the substituents on the nitrogen are the result of this increase.

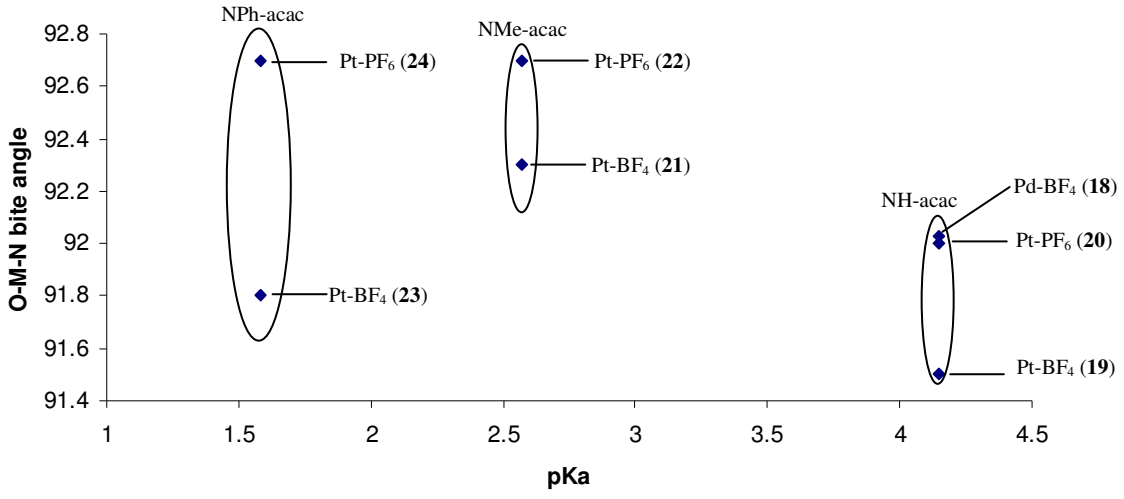

Figure 9.29 Graph of pK_a *vs.* O-M-N bite angle for the [M(cod)(LL')]A where M = Pt(II), Pd(II), LL' = NH-acac, NMe-acac, NPh-acac and A = PF_6^-, BF_4^- complexes.

The graph of the acid dissociation constant (pK_a) *vs.* O-M-N bite angle (Figure 9.29) shows an increase in the pK_a values as one progresses from NPh-acac → NMe-acac

→ NH-acac which is inversely proportional to the proton affinities for the nitrogen substituted group. The pK_a values of HPF_6 and HBF_4 are -20 and -5 respectively[16], it is interesting to note that the PF_6^- anion has a larger bite angle than that for the BF_4^- anion. In the graph the metal centre presented is mostly platinum the only palladium complex that was obtained shows that the bite angle is larger than platinum, which is expected as the atomic radii for platinum is smaller than palladium (see Table 2.4 for values).

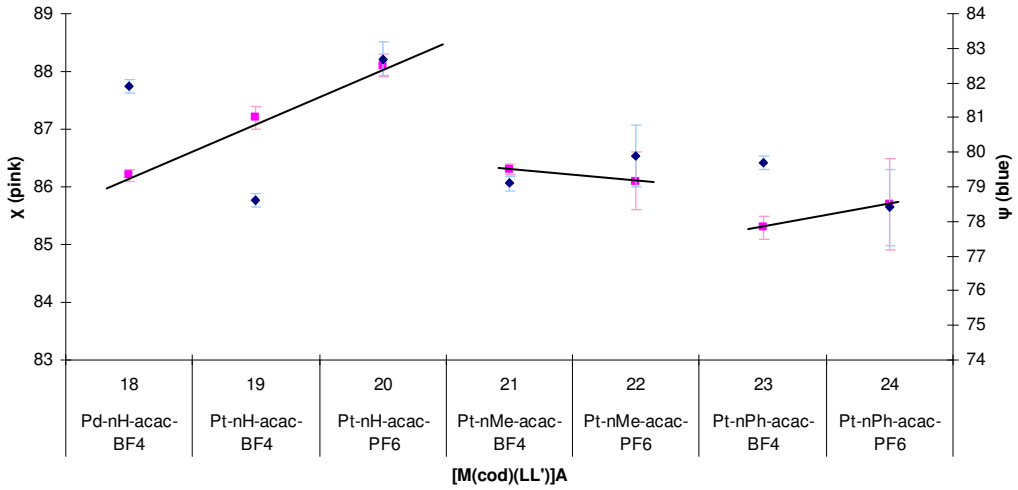

Figure 9.30 Graph of [M(cod)(LL')]A where LL' = NH-acac, NMe-acac, NPh-acac and A = PF_6^-, BF_4^- crystal complexes *vs.* χ (pink squares) and ψ (blue diamonds) angles (see Chapter 1 Figure 1.2 for definition of χ and ψ angles).

For the graph of [M(cod)(LL')]A where LL'= NH-acac, NMe-acac, NPh-acac and A = PF_6^-, BF_4^- *vs.* the χ and ψ angles. The maximum change in the ψ angle was found to be 4.3°. The error values on [Pt(cod)(NPh-acac)]PF_6 (**24**) are large as a result of the value plotted being a mean of four values for the ψ (71.3(10)° and 88.9(11)° for **24a1** and 73.1(12)° and 80.4(12)° for **24a2**) and two for χ (85.5(8)° for **24a1** and 85.8(8)° for **24a2**). The first trend that is observed is an increase in the χ value for the NH-acac ligand as the metal centre is changed from palladium to platinum the increase in the angle observed is inversely related to the atomic radii of the metal centers (platinum being the smaller of the two). The next change that occurs is that of the counter ion BF_4^- to PF_6^- with the pK_a of PF_6^- being smaller. This trend with the counter ions holds for both the NMe-acac and the NPh-acac complexes. The last

[16] Mori S., Ue M., Ida K., (Mistsubishi Petrochemical Co, Ltd), Electrolyte for aluminum electrolytic capacitor, US Patent 4774011, September 27, 1998

trend is again that of the χ angle for the NMe-acac complexes and [Pt(cod)(NPh-acac)]BF_4 where a decrease in the value is linked to the electron-donating ability of the substituent group on the nitrogen.

In Chapter 10 which follows, correlations between the crystal structures presented in this chapter and their respective calculated structures will be compared and discussed.

Chapter 10
Solid Sate *vs.* Optimized Structure Correlation of β-Enaminonato Complexes

10.1 Introduction

This chapter will present the comparison between the ketimine complexes of platinum(II) and palladium(II) with regards to their crystal structures and theoretical calculations. Table 10.1 presents a list of the crystal structures that will be discussed in the sections to follow.

Table 10.1 Ketimine complexes of platinum(II) and palladium(II)

Compound		Ref
[Pd(cod)(NH-acac)]BF_4	**18**	§ 9.3.1
[Pt(cod)(NH-acac)]BF_4	**19**	§ 9.4.1
[Pt(cod)(NH-acac)]PF_6	**20**	§ 9.4.1
[Pt(cod)(NMe-acac)]BF_4	**21**	§ 9.4.2
[Pt(cod)(NMe-acac)]PF_6	**22**	§ 9.4.2
[Pt(cod)(NPh-acac)]BF_4	**23**	§ 9.4.3
[Pt(cod)(NPh-acac)]PF_6	**24**	§ 9.4.3

For the theoretical calculations in this section of the study, the previously synthesized (§ 3.3) 4-aminopent-3-en-2-one (HNH-acac), 4-(methylamino)pent-3-en-2-one (HNMe-acac) and 4-anilinopent-3-en-2-one (HNPh-acac) ligands were selected for their increasing electron withdrawing capability. In addition to this, the substitution of an oxygen with a nitrogen includes a non-symmetrical aspect to the study. Furthermore the effect of these variations on the co-ordination geometry of the cyclo-octadiene ring was investigated. For the sake of completeness the entire group 10 metal triad was computed.

10.2 Experimental

The DFT molecular orbital calculations were carried out using the Gaussian 03[1] software suite. Becke's three parameter hybrid (B3LYP)[2,3] exchange correlation

[1] Frisch M.J., Trucks G.W., Schlegel H.B., Scuseria G.E., Robb M.A., Cheeseman J.R., Montgomery J.A. Jr., Vreven T., Kudin K.N., Burant J.C., Millam J.M., Iyengar S.S., Tomasi J., Barone V., Mennucci B., Cossi M., Scalmani G., Rega N., Petersson G.A., Nakatsuji H., Hada M., Ehara M.,

functional was used. The basis set employed in this study was 6-311++G(d,p)[4,5,6] for the main group elements and LanL2DZ[7] for the middle to late transition metals. Vibrational frequencies were calculated at the 6-311++G(d,p)[4,5,6] level for the main group elements and at the LanL2DZ[7] level for the middle to late transition metals with minimum energies confirmed to have zero imaginary frequencies. The frequencies are unscaled and were used to compute the zero-point vibrational energies. Molecular graphics were obtained using DIAMOND[8], while overlay graphics were obtained using HyperChem 7.5[9].

Toyota K., Fukuda R., Hasegawa J., Ishida M., Nakajima T., Honda Y., Kitao O., Nakai H., Klene M., Li X., Knox J.E., Hratchian H.P., Cross J.B., Bakken V., Adamo C., Jaramillo J., Gomperts R., Stratmann R.E., Yazyev O., Austin A.J., Cammi R., Pomelli C., Ochterski J.W., Ayala P.Y., Morokuma K., Voth G.A., Salvador P., Dannenberg J.J., Zakrzewski V.G., Dapprich S., Daniels A.D., Strain M.C., Farkas O., Malick D.K., Rabuck A.D., Raghavachari K., Foresman J.B., Ortiz J.V., Cui Q., Baboul A.G., Clifford S., Cioslowski J., Stefanov B.B., Liu G., Liashenko A., Piskorz P., Komaromi I., Martin R.L., Fox D.J., Keith T., Al-Laham M.A., Peng C.Y., Nanayakkara A., Challacombe M., Gill P.M.W., Johnson B., Chen W., Wong M.W., Gonzalez C., Pople J.A., Gaussian 03, Revision E.01, Gaussian Inc., Wallingford CT, (2004)

[2] Becke A.D., *J. Chem. Phys.*, **98**, 5648, (1993)

[3] Lee C., Yang W., Parr R.G., *Phys. Rev.*, **B37**, 785, (1988)

[4] Ditchfield R., Hehre W.J., Pople J.A., *J. Chem. Phys.*, **54**, 724, (1971)

[5] Gordon M.S., *Chem. Phys. Lett.*, **76**, 163, (1980)

[6] Rassolov V.A., Ratner M.A., Pople J.A., Redfern P.C., Curiss L.A., *J. Comp. Chem.*, **22**, 976, (2001)

[7] Hay P.J., Wadt W.R., *J. Chem. Phys.*, **82**, 299, (1985)

[8] Brandenburg K., Brendt M., DIAMOND, Release 2.1e. Crystal Impact GbR, Potfach 1251, D53002 Bonn, Germany., (2001)

[9] HyperChem™ Release 7.52, Windows Molecular Modeling System, HyperCube Inc., (2002)

10.3 Crystal Structure Correlation of Palladium(II) *vs.* Platinum(II) Complexes

In looking at the various radii (atomic, covalent and van der Waal) for palladium and platinum it is observed that there are only marginal differences between the two metal centers (Table 2.4). The values obtained in 2008 by Cordero[10] *et al.* show a value of 1.39 Å for palladium and 1.36 Å for platinum. Both metals are known for their square planar co-ordination geometry, with the +2 oxidation state being the most common.

Table 10.2 Cell dimension overview for Palladium(II) and Platinum(II) crystals obtained.

	[Pd(cod)(NH-acac)]A	[Pt(cod)(NH-acac)]A		[Pt(cod)(NMe-acac)]A		[Pt(cod)(NPh-acac)]A	
	BF_4 (**18**)	BF_4 (**19**)	PF_6 (**20**)	BF_4 (**21**)	PF_6 (**22**)	BF_4 (**23**)	PF_6 (**24**)
Crystal system	Monoclinic	Monoclinic	Monoclinic	Orthorhombic	Monoclinic	Monoclinic	Triclinic
Space group	$P2_1/c$	$P2_1/c$	$C2/m$	$P2_12_12_1$	$C2$	$P2_1/n$	$P1$
a	9.8665(3)	9.8588(2)	26.8871(12)	7.5277(2)	26.5792(6)	9.5952(7)	8.7064(2)
b	12.7836(3)	12.8652(2)	7.1009(3)	13.9653(4)	7.1903(1)	21.2609(16)	16.9618(3)
c	12.7126(3)	12.6969(3)	8.7130(4)	14.7872(4)	9.3146(2)	10.3335(8)	14.2377(3)
α	90	90	90	90	90	90	90
β	110.851(1)	111.040(2)	105.305(3)	90	106.250(1)	117.66	105.2377(3)
γ	90	90	90	90	90	90	90
Z	4	4	4	4	4	4	2

Reported in chapter 9, the compounds **18** and **19** were found to be isostructural with a general trend toward the monoclinic space group, the exceptions being those of compounds **21** and **24**. From a previous discussion (§ 9.4.3) compound **24** maybe solved in the monoclinic *Cc* space group.

[10] Cordero B., Gómez V., Platero-Prats A.E., Revés M., Echeverría J., Cremades E., Barragán F., Alvarez S., *Dalton Trans.*, (2008)

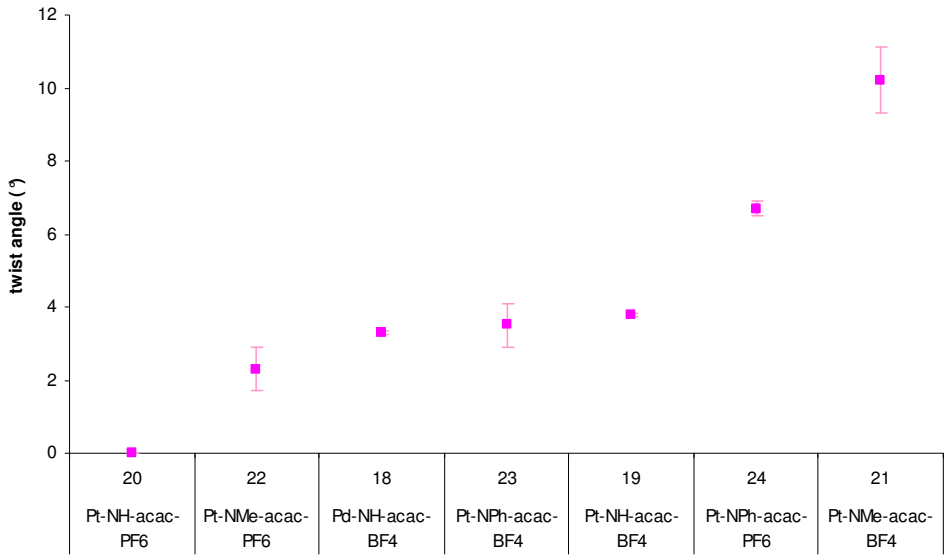

Figure 10.1 Graph of twist angle *vs.* [M(cod)(LL')]A where LL' = NH-acac, NMe-acac, NPh-acac and A = PF_6^-, BF_4^- arranged in ascending order of twist angle.

The distortion from the square planar geometry can be measured by the twist angle (*i.e.* the intersection of the planes defined by the mid-points of the alkene carbons of the cyclo-octadine ring with the oxygen and nitrogen of either the 4-amino, 4-methylamino and 4-anilinopent-3-en-onato ligand *vs.* the metal centre with the oxygen, nitrogen and the back-bone carbons of either the 4-amino, 4-methylamino and 4-anilinopent-3-en-onato ligand) and can be seen in Figure 10.1. A general increasing trend is observed for the compounds with compound **21** being the most distorted, even with the large error deviation as seen in Figure 10.1, possibly as a result of the orthorhombic $P2_12_12_1$. The changing of the counter ion does influence the twist angle but there is no discernable trend observed.

The overlay of the X-ray crystal structures is a graphical representation of the pair-wise differences of the related structures. This mathematical value is represented by the root mean square (RMS) value, which is a measure of how far the average is from zero, providing information on the variations of bond lengths and angles and to a certain degree the orientation of the structures in relation to each other. These comparisons are presented in Figure 10.2-10.5.

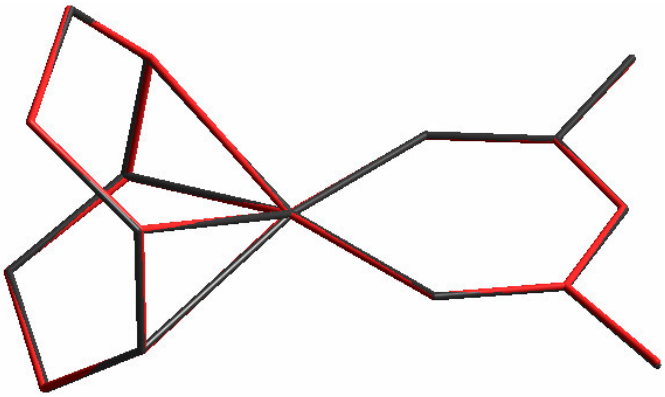

Figure 10.2 HyperChem superimposed image of [Pd(cod)(NH-acac)]BF_4 (18) (black) *vs.* [Pt(cod)(NH-acac)]BF_4 (19) (red) with an RMS error of 0.02 Å. Counter ions have been omitted for clarity.

The overlay of complexes **18** and **19** shown in Figure 10.2 has an RMS error of 0.023 Å based on all non-hydrogen atoms excluding the methyl carbons. These structures are isostructural and isomorphous to one another, with the twist angles (**18**: 3.31(4)° and **19**: 3.77(5)°) varying only slightly but not enough to affect either complex.

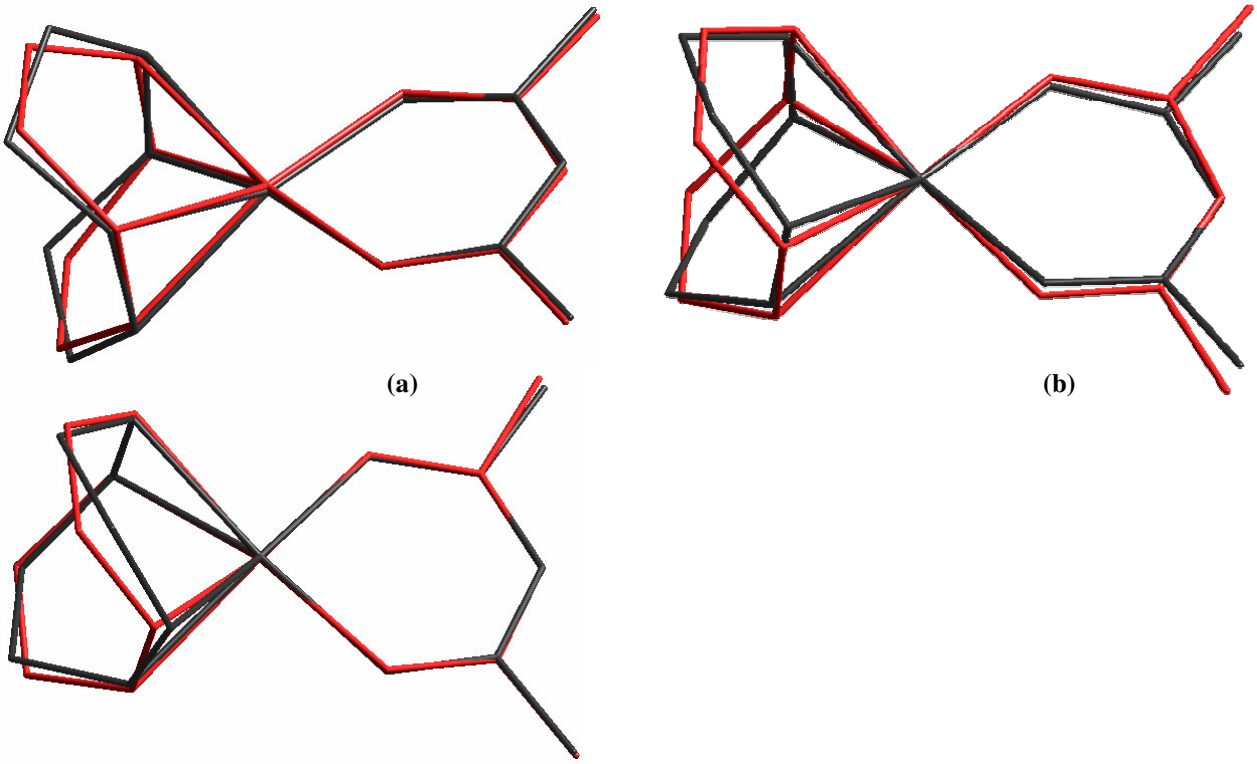

Figure 10.3 HyperChem superimposed image of (a) [Pt(cod)(NH-acac)]BF_4 (19) (black) *vs.* [Pt(cod)(NH-acac)]PF_6 (20) (red) with an RMS error of 0.16 Å (b) (a) [Pt(cod)(NH-acac)]BF_4 (19) inverted structure (black) *vs.* [Pt(cod)(NH-acac)]PF_6 (20) (red) with an RMS error of 1.7 Å (c) [Pt(cod)(NH-acac)]BF_4 (19) inverted structure (black) *vs.* [Pt(cod)(NH-acac)]PF_6 (20) (red) with an RMS error of 0.03 Å. Counter ions have been omitted for clarity.

The overlay of complexes **19** and **20** shown in Figure 10.3a has an RMS error of 0.16 Å based on all non-hydrogen atoms excluding the methyl carbons, while Figure 10.3b has an RMS error of 1.72 Å based on all non-hydrogen atoms excluding the methyl carbons, if however only the metal chelate ring of the 4-aminopent-3-en-2-onato ligand is used an RMS error of 0.03 Å is obtained, this overlay is seen in Figure 10.3c. The difference of these figures is in the fact that complex **19** has a centrosymmetric space group (Monoclinic $P2_1/c$) and thus both enantiomers have been overlayed with complex **20**. The difference observed is in the twisting of the alkane carbons of the cyclo-octadine ring to a second position, this does not in any way affect the twist angle (**19**: 3.77(5)° and **20**: 0°) for the complexes. The bond lengths and angles are not significantly affected by the alkane twisting into a secondary position.

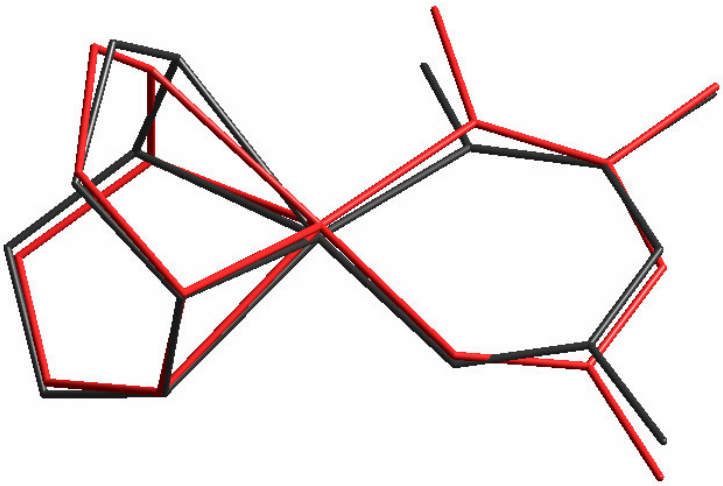

Figure 10.4 HyperChem superimposed image of [Pt(cod)(NMe-acac)]BF_4 (21) (black) *vs.* [Pt(cod)(NMe-acac)]PF_6 (22) (red) with an RMS error of 0.19 Å. Counter ions have been omitted for clarity.

The overlay of complexes **21** and **22** shown in Figure 10.4 has an RMS error of 0.195 Å based on all non-hydrogen atoms excluding the methyl carbons. The difference observed in the twist angle angle was found to be 7.9(8)°, where the twist values for complex **21** and **22** are 10.2(9)° and 2.3(6)° respectively. This large twist angle results in the larger RMS error value observed even though the general bond lengths and angles remain similar for both complexes.

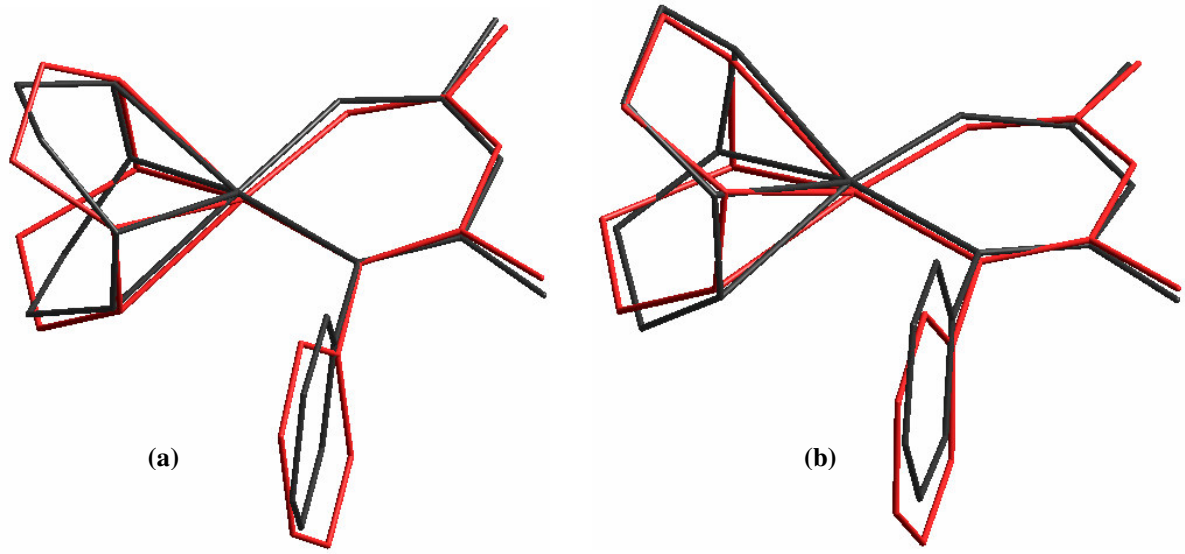

Figure 10.5 HyperChem superimposed image of (a) [Pt(cod)(NPh-acac)]BF_4 (23) (black) *vs.* [Pt(cod)(NPh-acac)]PF_6 (24) (red) with an RMS error of 0.35 Å (b) [Pt(cod)(NPh-acac)]BF_4 (23) inverted crystal structure (black) *vs.* [Pt(cod)(NPh-acac)]PF_6 (24) (red) with an RMS error of 0.22 Å. Counter ions have been omitted for clarity.

The overlay of complexes **23** and **24** shown in Figure 10.5a has an RMS error of 0.349 Å based on all non-hydrogen atoms excluding the methyl and phenyl ring carbons. The differences observed were in the twist angle angle with a difference of 3.2(4)°, with values of 3.5(6)° and 6.7(2)° for complexes **23** and **24** respectively. The intersection of the planes defined by the metal chelate ring and the phenyl ring with a difference of 3.4(3)° for the complexes **23** and **24** with values of 84.0(1)° and 87.4(4)° respectively. The last difference observed in the overlay of the complexes is the cross-over of the alkane carbons on the cyclo-octadiene ring. These differences contribute to the higher RMS error value observed for these complexes. Complex **23** is in the monoclinic $P2_1/n$ space group which is a known centrosymmetric space group the crystal structure has two enantiomers within the unit cell. Upon selection of the second enatiomer and overlaying this with complex **24** an RMS error of 0.222 Å is obtained.

For the overlay's of the complexes presented it was found that they were generally well behaved, with only minor differences in the twist angles and the cross-over positions of the alkane carbons of the cyclo-octadiene ring seen for complexes **19** and **20**. A similar cross-over was observed for **23** and **24** but on selection of the other

enantiomer this difference was resolved. The bond lengths and angles of the core atoms remained similar across the board.

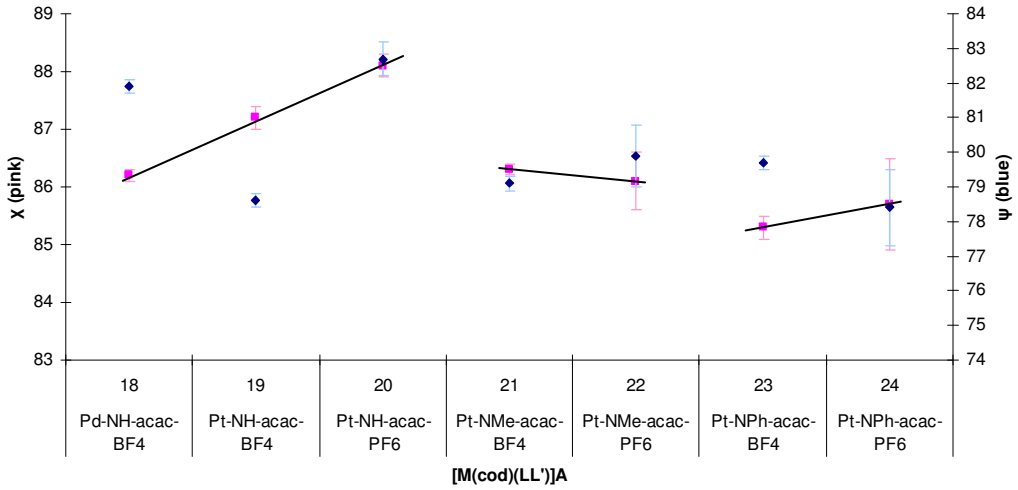

Figure 10.6 Graph of [M(cod)(LL')]A where M = Pd(II), Pt(II) and LL' = NH-acac, NMe-acac, NPh-acac and A = PF_6^-, BF_4^- complexes *vs.* χ (pink squares) and ψ (blue diamonds) angles (see Chapter 1 Figure 1.2 for definition of χ and ψ angles).

For the graph, seen in Figure 10.6, of [M(cod)(LL')]A where LL' = NH-acac, NMe-acac, NPh-acac and A = BF_4^-, PF_6^- *vs.* the χ and ψ angles. The trend observed is an increase in the χ angle as one changes the metal centre from platinum to palladium which is inversely proportional to the covalent atomic radii (see Table 2.4), the ψ angle however follows the covalent atomic radii. A further increase is observed as the counter ion is changed from BF_4^- to PF_6^- the reason for this is in the pK_a values of the counter ion with the PF_6^- counter ion having the smaller value thus creating stronger H···F interactions within the complexes. The exceptions to this trend are the complexes of the NMe-acac ligand where there are notably less hydrogen interactions on the cyclo-octadiene ring for complex **22** (see Figure 9.19) as opposed to that of complex **21** (see Figure 9.16).

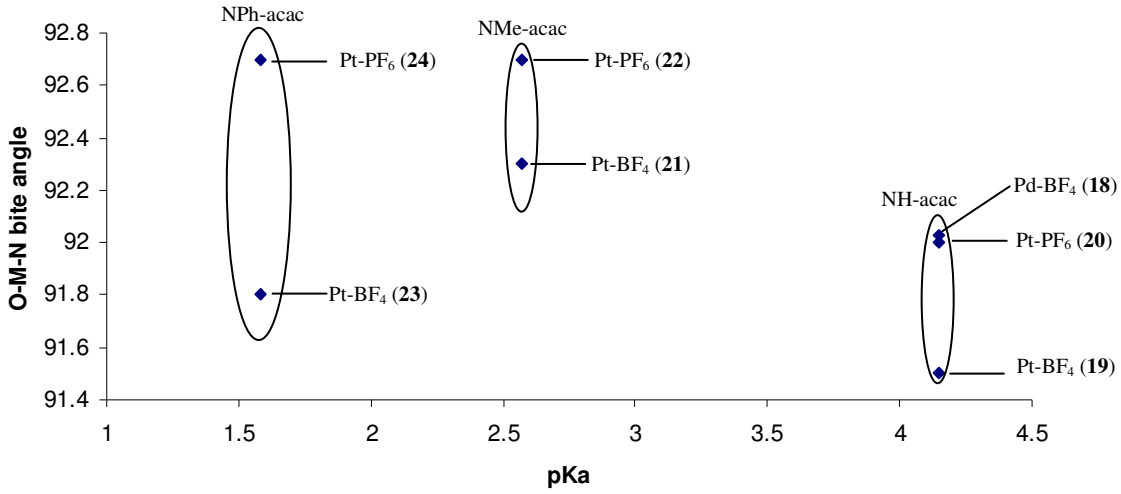

Figure 10.7 Graph of pK_a *vs.* O-M-N bite angle for the [M(cod)(LL')]A where M = Pd(II), Pt(II), LL' = NH-acac, NMe-acac, NPh-acac and A = BF_4^-, PF_6^- complexes.

The pKa values of HPF_6 and HBF_4 are -20 and -5 respectively[11]. Preliminary pKa studies done in ethanol with a 1M HCl solution were found to be 4.151, 2.569 and 1.579 for HNH-acac, HNMe-acac and HNPh-acac respectively. In Figure 10.7 a graph of the O-M-N bite angle *vs.* the pK_a of the respective ligands is presented. An influence was again observed for the changing of the counter ion, with the PF_6^- ion affecting the bite angle far more than the BF_4^- ion. Although a difference was observed for [Pd(cod)(NH-acac)]BF_4 (**18**) and [Pt(cod)(NH-acac)]BF_4 (**19**) complexes, with only one point of comparison the effect of the variation of the metal centre could not be completely evaluated.

Table 10.3 Overview of the division of the complexes into packing categories.

Complex		Packing Type	Ref
[Pd(cod)(NH-acac)]BF_4	(**18**)	clustered head-to-tail	Figure 9.5
[Pt(cod)(NH-acac)]BF_4	(**19**)	clustered head-to-tail	Figure 9.10
[Pt(cod)(NH-acac)]PF_6	(**20**)	head-to-tail	Figure 9.12
[Pt(cod)(NMe-acac)]BF_4	(**21**)	clustered head-to-tail	Figure 9.16
[Pt(cod)(NMe-acac)]PF_6	(**22**)	head-to-tail	Figure 9.18
[Pt(cod)(NPh-acac)]BF_4	(**23**)	zig-zag	Figure 9.24
[Pt(cod)(NPh-acac)]PF_6	(**24**)	zig-zag	Figure 9.26

Three different forms of packing for the β-enamino type complexes were observed, clustered head-to-tail (Figure 10.8), head-to-tail (Figure 10.9) and zig-zag (Figure 10.10). The packing motifs given in all the figures are defined as the head of the

[11] Mori S., Ue M., Ida K., (Mistsubishi Petrochemical Co, Ltd), Electrolyte for aluminum electrolytic capacitor, US Patent 4774011, September 27, 1998

arrow being the cylo-octadiene ring and the tail of the arrow representing the β-enaminonato type ligand.

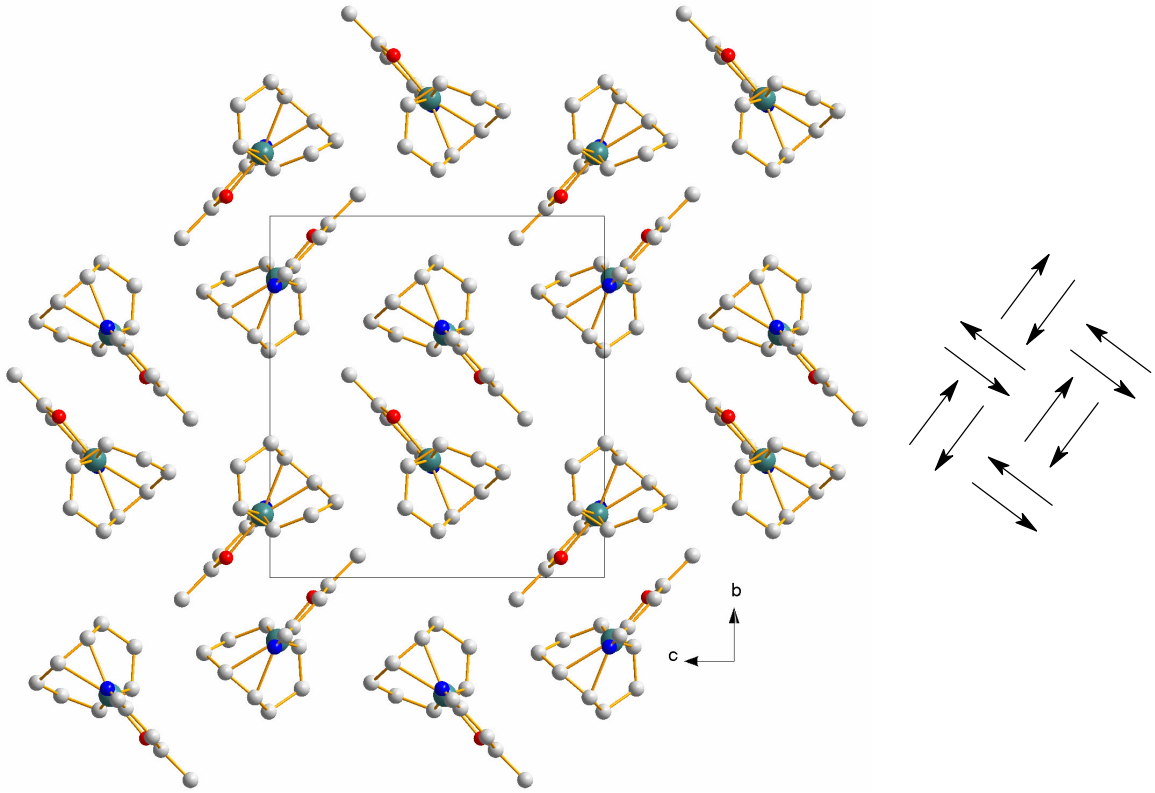

Figure 10.8 Packing of [Pd(cod)(NH-acac)]BF_4 viewed along the *a*-axis to the right the packing motif. Palladium (cyan), carbon (grey), oxygen (red) and nitrogen (blue). Hydrogens and BF_4^- have been omitted for clarity.

In Figure 10.8 an example of clustered head-to-tail packing is given, the figure represents the [Pd(cod)(NH-acac)]BF_4 (**18**) complex. The complexes found with a similar packing motif were [Pt(cod)(NH-acac)]BF_4 (**19**) and [Pt(cod)(NMe-acac)]BF_4 (**21**).

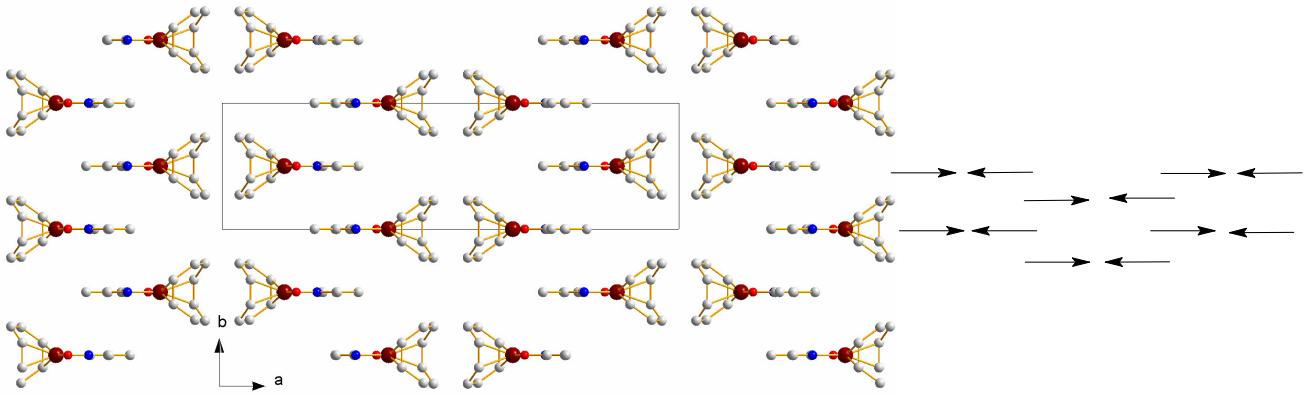

Figure 10.9 Packing of [Pt(cod)(NH-acac)]PF_6 viewed along the *c*-axis to the right the packing motif. Platinum (dark red), carbon (grey), oxygen (red) and nitrogen (blue). Hydrogens and PF_6^- have been omitted for clarity.

[Pt(cod)(NH-acac)]PF_6 (**20**) depicted in Figure 10.9 symbolizes an example of head-to-tail packing, the complex that shares this form of packing is [Pt(cod)(NMe-acac)]PF_6 (**22**).

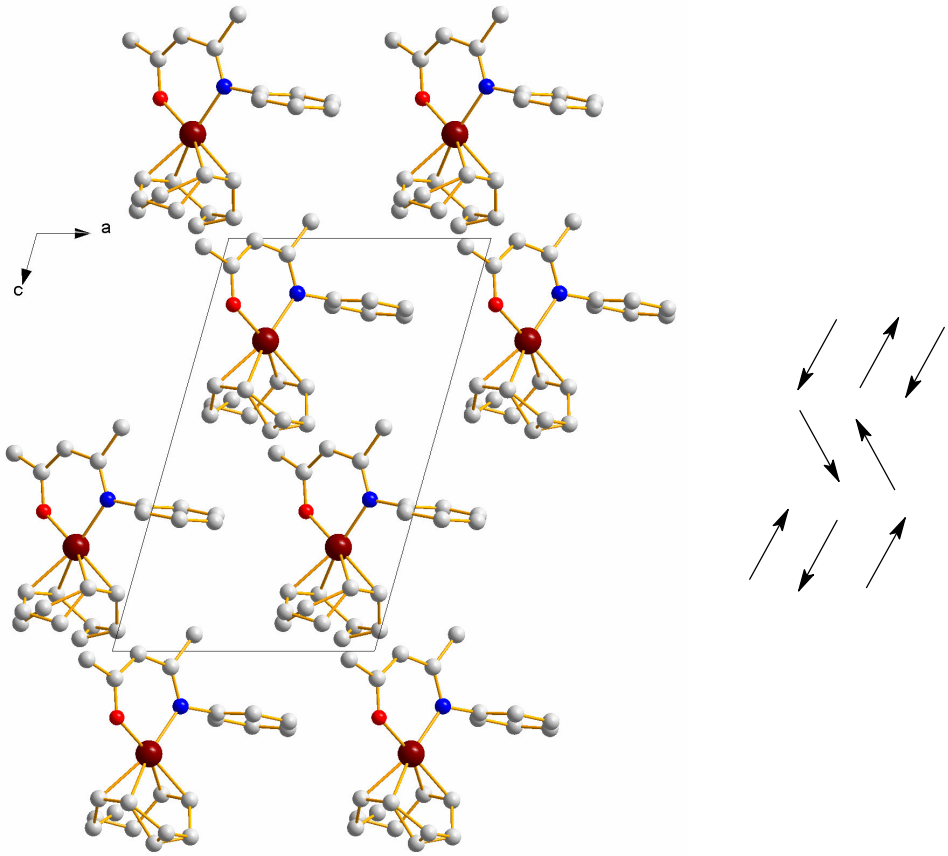

Figure 10.10 Packing of [Pt(cod)(NPh-acac)]PF_6 viewed along the *b*-axis to the right the packing motif. Platinum (dark red), carbon (grey), oxygen (red) and nitrogen (blue). Hydrogens and PF_6^- have been omitted for clarity.

[Pt(cod)(NPh-acac)]BF_4 (**23**) and [Pt(cod)(NPh-acac)]PF_6 (**24**) are instances of zig-zag head-to-tail packing and are depicted in Figure 10.10.

10.4 Theoretical Correlation of Palladium(II) *vs.* Platinum(II) Complexes

In the periodic table platinum and palladium fall into group 10, having similar reaction properties one finds that both the metals prefer the square planar co-ordination with a d^8 electron configuration resulting in an oxidation state of +2. The 2008 covalent radii of platinum and palladium are 1.36 Å and 1.39 Å respectively (see Table 2.4). Nickel being the last of the group 10 metals, also has a d^8 electron configuration though it does not have a preference for a specific co-ordination geometry with octahedral, trigonal bipyramidal, square pyramidal, tetrahedral and square planar all being observed. With this in mind the calculations for nickel were limited to only the square planar geometry with a +2 oxidation state, so as to match to the remaining metals of the group. The 2008 covalent radius of nickel was found to be 1.24 Å (see Table 2.4).

10.4.1 Visual Associations

Visual geometric comparisons of the computed structures *vs.* their X-ray crystal structures are presented. The overlay of the X-ray crystal structure and the calculated structure is a graphical representation of the pair-wise differences of the related structures. This mathematical value is represented by the root mean square (RMS) value, which is a measure of how far the average is from zero, providing information on the variations of bond lengths and angles and to a certain degree the orientation of the structures in relation to each other. These comparisons are presented in Figure 10.11-10.14.

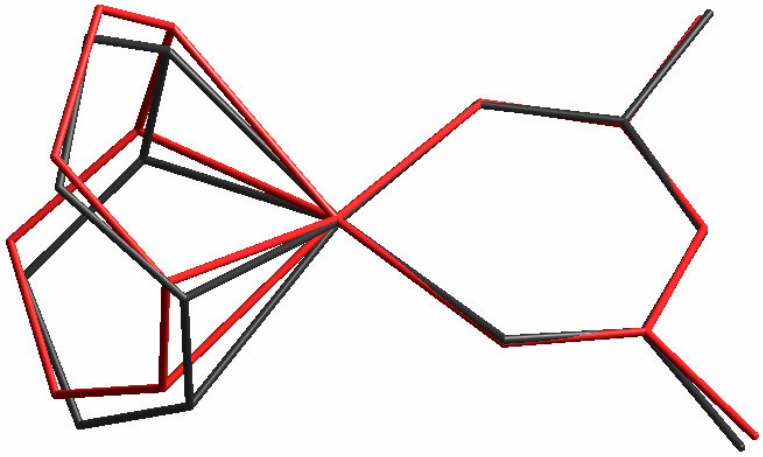

Figure 10.11 HyperChem superimposed image of [Pd(cod)(NH-acac)]BF_4 (18) (black) *vs.* [Pd(cod)(NH-acac)]$^+$ (computed) (red) with an RMS error of 0.03 Å. The counter ion of the X-ray crystal structure has been omitted for clarity.

The overlay of complexes **18** and [Pd(cod)(NH-acac)]$^+$ (calculated) shown in Figure 10.11 has an RMS error of 0.03 Å based on the metal centre and the oxygen, nitrogen and back-bone carbons of the 4-aminopent-3-en-2-onato ligand. The difference found in the twist angle (*i.e.* the intersection of the planes defined by the mid-points of the alkene carbons of the cyclo-octadine ring with the oxygen and nitrogen of the 4-aminopent-3-en-2-onato ligand *vs.* the metal centre with the oxygen, nitrogen and the back-bone carbons of the 4-aminopent-3-en-2-onato ligand) of 1.5° (**18** : 3.31(4)°; calc : 1.8°). The differences found in the χ and ψ angles (see Figure 1.2) are 1.9° (**18** : 86.2(1)°; calc : 84.267°) and 3.6° (**18** : 81.9(2)°; calc : 85.468°) respectively. If all the above differences are taken into account and a full RMS error based on all the atoms excluding the methyl carbons is computed a value of 1.8435 Å is obtained. The differences in the twist, χ and ψ angles can be ascribed to the effect of the counter ion on the complex, its H···F interactions (Figure 9.4 and 9.5) and the packing with its metal chelate ring interactions (Figure 9.6). The bond lengths and angles of the central section of the complex are still well defined (Table 10.5).

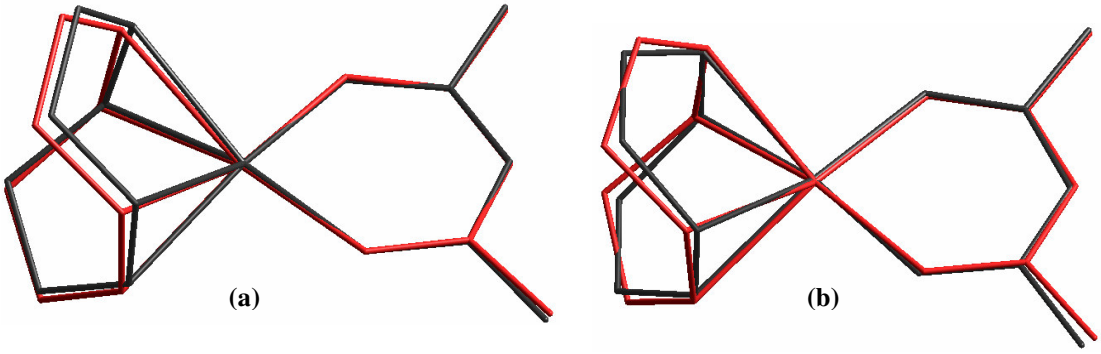

Figure 10.12 HyperChem superimposed image of (a) [Pt(cod)(NH-acac)]BF_4 (19) (black) *vs.* [Pt(cod)(NH-acac)]$^+$ (computed) (red) with an RMS error of 0.036 Å (b) [Pt(cod)(NH-acac)]PF_6 (20) (black) *vs.* [Pt(cod)(NH-acac)]$^+$ (computed) (red) with an RMS error of 0.16 Å. The counter ion of the X-ray crystal structure has been omitted for clarity.

The overlay of complexes **19** and **20** with [Pt(cod)(NH-acac)]$^+$ (calculated) are shown in Figure 10.12. The RMS error values are 0.04 Å for Figure 10.12a based on the metal centre and the oxygen, nitrogen and back-bone carbons of the 4-aminopent-3-en-2-onato ligand, and 0.16 Å for Figure 10.12b for the all atoms excluding the methyl carbons of the 4-aminopent-3-en-2-onato ligand. For complex **19** (Figure 10.12a) the differences found in the twist, χ and ψ angles are 2.2° (**19** : 3.77(5)°; calc : 1.544°), 1.9° (**19** : 87.2(2)°; calc : 85.271°) and 3.8° (**19** : 78.6(2)°; calc : 82.416°) respectively these differences can be ascribed to the effect of the counter ion on the complex, its H···F interactions (Figure 9.9 and 9.10) and the packing with its metal chelate ring interactions (Figure 9.11). If all the variations are taken into account and a full RMS error based on all the atoms excluding the methyl carbons is computed a value of 1.8433 Å is obtained.

For complex **20** (Figure 10.12b) the differences found in the twist and χ angles are 1.5° (**20** : 0°; calc : 1.544°) and 2.8° (**20** : 88.1(2)°; calc : 85.271°) these can be attributed to the counter ion and the H···F interactions (Figure 9.13). The last difference observed is that of the cross-over of the positions alkane carbons of the cyclo-octadine ring, however this does not affect the difference in the ψ angle with a value of 0.3° (**20** : 82.7(5)°; calc : 82.416°) indicating that the opening of the ring is similar but it has a large contributing factor in the calculation of an RMS error value. The bond lengths and angles of the central section of both complexes are still well defined (Table 10.5).

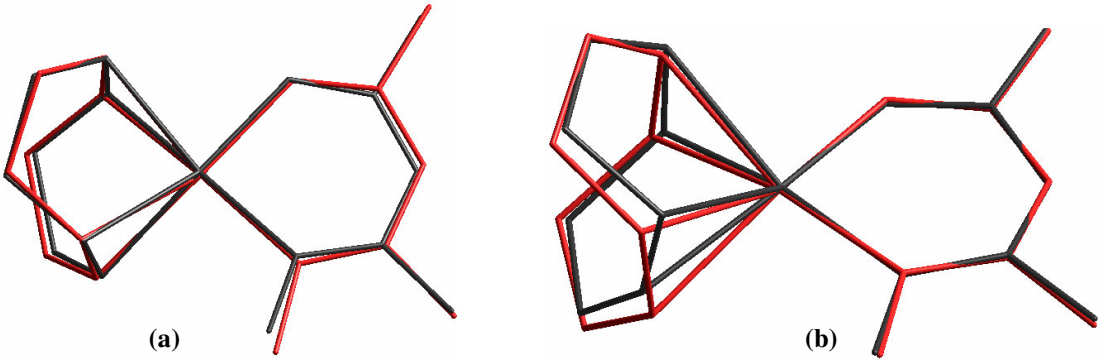

Figure 10.13 HyperChem superimposed image of (a) [Pt(cod)(NMe-acac)]BF_4 (21) (black) *vs.* [Pt(cod)(NMe-acac)]$^+$ (computed) (red) with an RMS error of 0.13 Å (b) [Pt(cod)(NMe-acac)]PF_6 (22) (black) *vs.* [Pt(cod)(NMe-acac)]$^+$ with an RMS error of 0.046 Å. The counter ion of the X-ray crystal structure has been omitted for clarity.

The overlay of complexes **21** and **22** with [Pt(cod)(NMe-acac)]$^+$ (calculated) are shown in Figure 10.13. The RMS error values are 0.13 Å for Figure 10.13a based on all atoms except the methyl carbons, and 0.05 Å for Figure 10.13b for the metal centre and the oxygen, nitrogen and back-bone carbons of the 4-(methylamino)pent-3-en-2-onato ligand. For complex **21** (Figure 10.13a) the differences found in the twist, χ and ψ angles are 7.4° (**21** : 10.2(9)°; calc : 2.774°), 2.0° (**21** : 86.3(1)°; calc : 84.259°) and 3.0° (**21** : 79.1(2)°; calc : 82.143°) respectively these differences can be ascribed to the effect of the counter ion on the complex, its H···F interactions (Figure 9.16) and the packing with its hydrogen metal chelate ring interactions (Figure 9.17).

The differences found for complex **22** (Figure 10.13b) in the twist, χ and ψ angles are 0.5° (**22** : 2.3(6)°; calc : 2.774°), 1.8° (**22** : 86.1(5)°; calc : 84.259°) and 2.2° (**22** : 79.9(9)°; calc : 82.143°) respectively these differences can be ascribed to the effect of the counter ion and the H···F interactions (Figure 9.19). Without the additional hydrogen metal chelate interaction the position of the cyclo-octadine ring is twisted toward the methyl carbon attached to the nitrogen of the 4-(methylamino)pent-3-en-2-onato ligand, leading to slightly longer bond lengths and angles (Table 10.5). When all the above are taken into account and a full RMS error based on all the atoms excluding the methyl carbons is computed a value of 1.8408 Å is acquired.

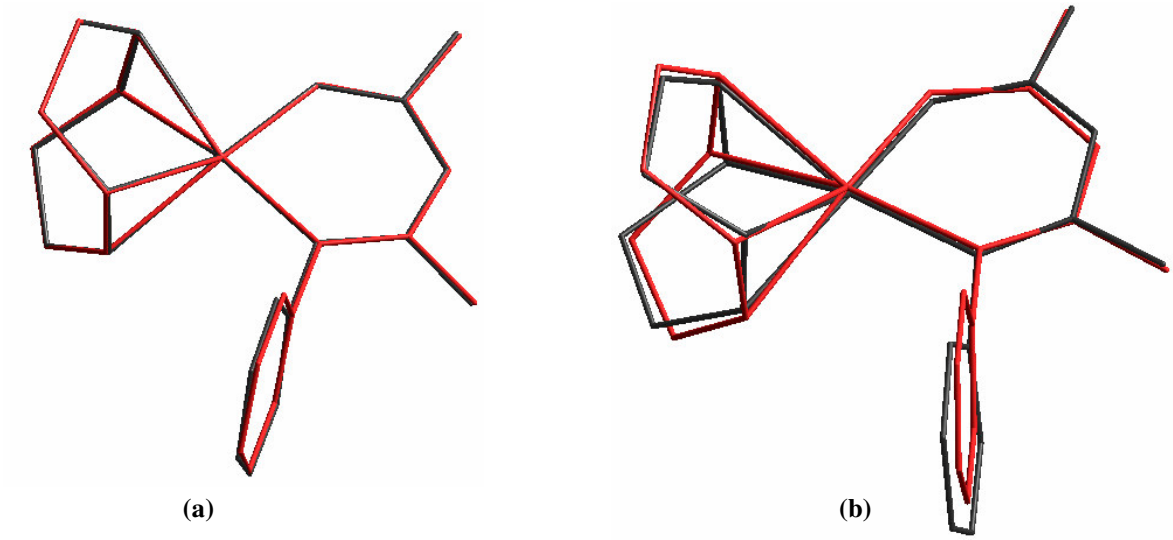

Figure 10.14 HyperChem superimposed image of (a) [Pt(cod)(NPh-acac)]BF_4 (23) (black) *vs.* [Pt(cod)(NPh-acac)]$^+$ (computed) (red) with an RMS error of 0.04 Å (b) [Pt(cod)(NPh-acac)]PF_6 (24) (black) *vs.* [Pt(cod)(NPh-acac)]$^+$ with an RMS error of 0.23 Å. The counter ion of the X-ray crystal structure has been omitted for clarity.

The overlay of complexes **23** and **24** with [Pt(cod)(NPh-acac)]$^+$ (calculated) are shown in Figure 10.14. The RMS error values are 0.04 Å for Figure 10.14a and 0.23 Å for Figure 10.14b based on all atoms except the methyl and phenyl carbons. For complex **23** (Figure 10.14a) the differences found in the twist, phenyl orientation (*i.e.* the intersection of the planes defined by the metal centre with the oxygen, nitrogen and the back-bone carbons of the 4-aminopent-3-en-2-onato ligand *vs.* the plane though the carbons of the phenyl ring of the 4-aminopent-3-en-2-onato ligand), χ and ψ angles are 1.1° (**23** : 3.5(6)°; calc : 2.413°), 2.2° (**23** : 84.0(1)°; calc : 86.214°), 1.0° (**23** : 85.3(2)°; calc : 84.287°) and 2.9° (**23** : 79.7(2)°; calc : 82.556°) respectively these differences can be ascribed to the effect of the counter ion on the complex and the H···F interactions (Figure 9.24).

In complex **24** the values for twist, phenyl orientation, χ and ψ angles were found to be 4.3° (**24** : 6.7(2)°; calc : 2.413°), 1.2° (**24** : 87.4(4)°; calc : 86.214°), 1.4° (**24** : 85.7(8)°; calc : 84.287°) and 4.2° (**24** : 78.4(1.1)°; calc : 82.556°). It should be noted here that the values given for the twist, phenyl orientation are based on a single isomer within the unit cell (**24a1**), however the values of χ and ψ were calculated based on the average of both complexes present in the unit cell. Another contributing factor was that for both complexes **24a1** (Figure 9.22) and **24a2** (Figure 9.23) disorder was observed in the cyclo-octadiene ring. Even though the RMS error value is lower

than expected it must be remembered that the disorder in the cyclo-octadiene ring was not taken into account when calculating the RMS error value and that only one of the complexes present in the unit cell is shown in Figure 10.14b. Even with all the problems encountered with complex **24**, the bond lengths and angles of the central section of both complexes are still well defined (Table 10.5).

10.4.2 Crystal Structure vs. Computed Structure Bond Relationships

In comparing the computed structures with their respective X-ray crystal structures only selected bond distances and angles were reported. The bond lengths and angles selected were those comprising of the "core" co-ordination geometry and the entire cyclo-octadiene ring so as to be able to compute the χ and ψ angles.

The *R*-values are given as a measure of the average accuracy of the computed (gas phase) bond lengths (Å) and angles (°) with the experimental crystal data (solid state) obtained. The following expression was used to calculate the *R*-values

$$R = n^{-1} \sum_{1 \to n}^{i} x_{e_i} - \left| x_{c_i} - x_{e_i} \right| \Big/ x_{e_i}$$

with n = number of data points, x_e = experimental data and x_c = calculated data.

The following graphs (Figure 10.15-10.18) and tables (Table 10.4 and 10.5) represent the general degree of accuracy between calculated structures and experimental values. Within the graphs the insert values are the actual calculated *R*-values for the complexes presented, the table that follows the graphs are the plotted values.

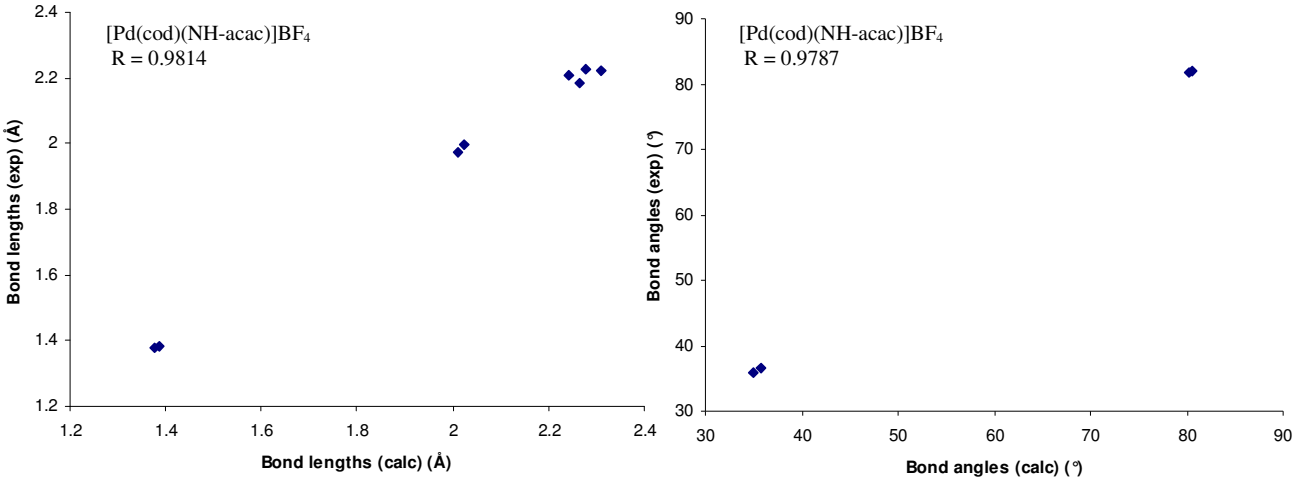

Figure 10.15 Graph of experimental *vs.* calculated bond lengths (Å) and angles (°) for [Pd(cod)(NH-acac)]BF_4 (18) with calculated *R*-values top left, plotted values are given in Table 10.4.

The graphs of [Pd(cod)(NH-acac)]BF_4 (18) *vs.* bond lengths (Å) and angles (°) (Figure 10.15) represent the general degree of accuracy between the calculated structures and the experimental values with an average *R*-value of ≥ 98 %. The values are listed in Table 10.4.

Table 10.4 Selected Geometric parameters (Å,°) for Palladium(II) metal complexes

	[Pd(cod)(NH-acac)] BF_4 (**18**)	calc
Pd-O_1	1.999(2)	2.024
Pd-N_1	1.972(2)	2.012
Pd-C_1	2.185(3)	2.266
Pd-C_2	2.208(3)	2.242
Pd-C_5	2.222(3)	2.309
Pd-C_6	2.228(3)	2.279
C_1-C_2	1.384(4)	1.385
C_5-C_6	1.376(4)	1.377
O_1-Pd-N_1	92.03(9)	90.846
C_1-Pd-C_2	36.7(1)	35.784
C_5-Pd-C_6	36.0(1)	34.926
C_1-Pd-C_6	82.1(1)	80.497
C_2-Pd-C_5	81.8(1)	80.238
χ^a	86.2(1)	84.267
ψ^b	81.9(2)	85.468

a χ: $C_1MC_2 \cap C_5MC_6$
b ψ: $C_2C_3C_4C_5 \cap C_1C_8C_7C_6$ see Figure 1.2

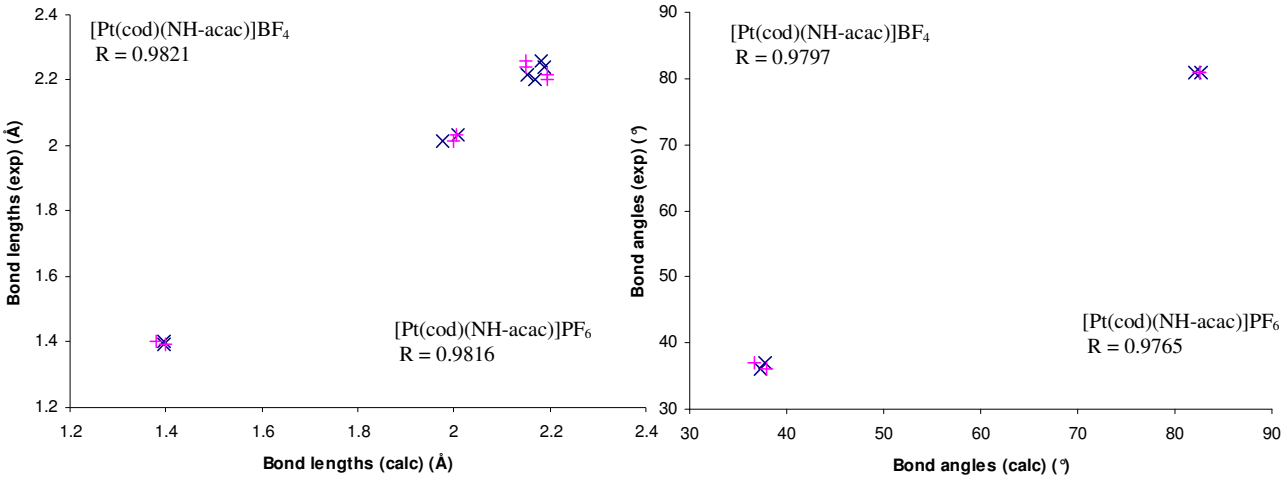

Figure 10.16 Graph of experimental *vs.* calculated bond lengths (Å) and angles (°) for [Pt(cod)(NH-acac)]BF_4 (19) (blue multiplication sign) and [Pt(cod)(NH-acac)]PF_6 (20) (pink plus sign) with calculated *R*-values shown, plotted values are given in Table 10.5 columns 1-3.

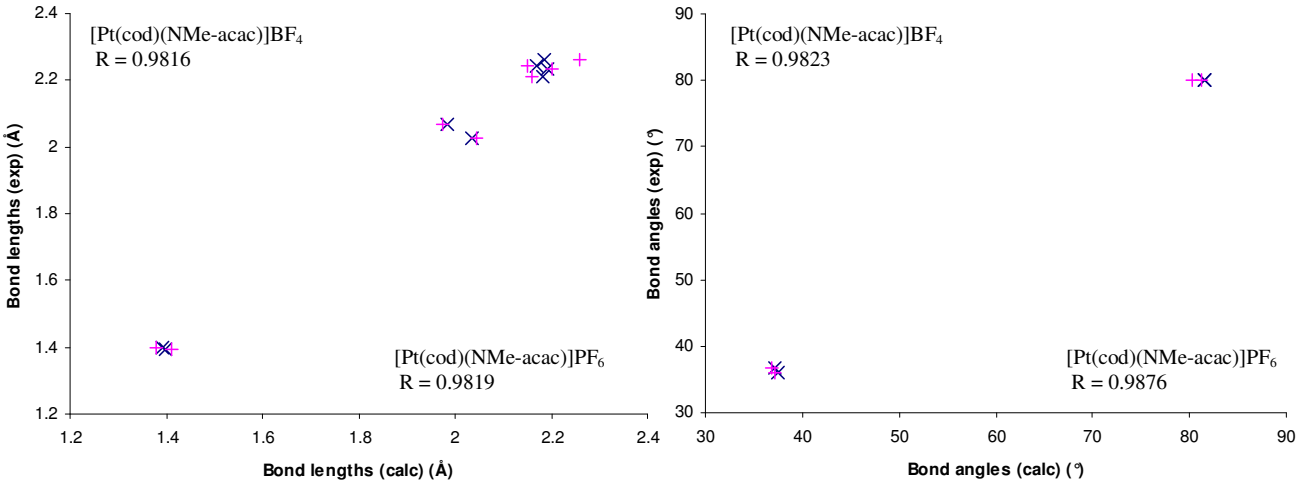

Figure 10.17 Graph of experimental *vs.* calculated bond lengths (Å) and angles (°) for [Pt(cod)(NMe-acac)]BF_4 (21) (blue multiplication sign) and [Pt(cod)(NMe-acac)]PF_6 (22) (pink plus sign) with calculated *R*-values shown, plotted values are given in Table 10.5 columns 4-6.

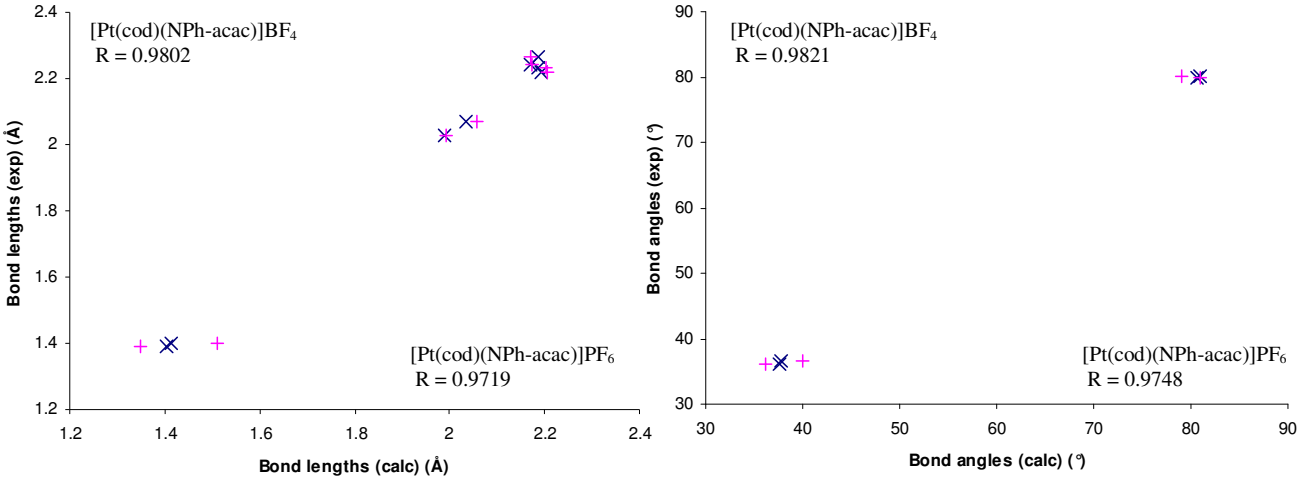

Figure 10.18 Graph of experimental *vs.* calculated bond lengths (Å) and angles (°) for [Pt(cod)(NPh-acac)]BF_4 (23) (blue multiplication sign) and [Pt(cod)(NPh-acac)]PF_6 (24) (pink plus sign) with calculated *R*-values shown, plotted values are given in Table 10.5 columns 7-9.

The graphs of [Pt(cod)(NH-acac)]BF_4 (**19**), [Pt(cod)(NH-acac)]PF_6 (**20**), [Pt(cod)(NMe-acac)]BF_4 (**21**), [Pt(cod)(NMe-acac)]PF_6 (**22**), [Pt(cod)(NPh-acac)]BF_4 (**23**) and [Pt(cod)(NPh-acac)]PF_6 (**24**) *vs.* bond lengths (Å) and angles (°) (Figure 10.16, 10.13 and 10.14) represent the general degree of accuracy between the calculated structures and the experimental values with an average *R*-value of ≥ 98 %. The values are listed in Table 10.5.

Table 10.5 Selected Geometric parameters (Å,°) for Platinum(II) metal complexes

	[Pt(NH-acac)]A			[Pt(cod)(NMe-acac)]A			[Pt(cod)(NPh-acac)]A		
	BF_4 (**19**)	PF_6 (**20**)	calc	BF_4 (**21**)	PF_6 (**22**)	calc	BF_4 (**23**)	PF_6[c] (**24**)	calc
$Pt\text{-}O_1$	2.009(2)	2.006(9)	2.0334	1.985(3)	1.975(5)	2.0244	1.990(3)	1.992(11)	2.0295
$Pt\text{-}N_1$	1.978(3)	1.999(9)	2.0133	2.036(4)	2.046(5)	2.0687	2.034(4)	2.058(11)	2.0702
$Pt\text{-}C_1$	2.152(3)	2.195(8)	2.2153	2.192(5)	2.20(2)	2.2327	2.186(5)	2.204(18)	2.2341
$Pt\text{-}C_2$	2.168(3)	2.195(8)	2.2005	2.182(5)	2.16(2)	2.2109	2.193(5)	2.205(17)	2.2175
$Pt\text{-}C_5$	2.183(3)	2.151(8)	2.2608	2.184(4)	2.26(2)	2.2602	2.186(4)	2.170(15)	2.2634
$Pt\text{-}C_6$	2.187(3)	2.151(8)	2.2409	2.168(4)	2.15(2)	2.2444	2.170(5)	2.172(16)	2.2425
$C_1\text{-}C_2$	1.395(5)	1.38(2)	1.4016	1.391(7)	1.38(1)	1.3998	1.415(7)	1.51(4)	1.3987
$C_5\text{-}C_6$	1.396(5)	1.40(2)	1.3912	1.397(7)	1.41(1)	1.3927	1.403(6)	1.35(2)	1.3929
$O_1\text{-}Pt\text{-}N_2$	91.5(1)	92.0(4)	90.413	92.3(1)	92.7(2)	92.075	91.8(1)	92.7(4)	91.783
$C_1\text{-}Pt\text{-}C_2$	37.7(1)	36.6(5)	37.01	37.1(2)	36.9(4)	36.72	37.7(2)	40.0(9)	36.624
$C_5\text{-}Pt\text{-}C_6$	37.3(1)	37.9(6)	35.999	37.5(2)	37.2(3)	36.015	37.6(2)	36.2(7)	36.01
$C_1\text{-}Pt\text{-}C_6$	82.7(1)	82.5(3)	81.002	81.5(2)	80.3(7)	79.954	80.9(2)	79.0(7)	80.154
$C_2\text{-}Pt\text{-}C_5$	82.1(1)	82.5(3)	80.797	81.6(2)	81.3(8)	80.142	80.7(2)	80.9(7)	79.942
χ[a]	87.2(2)	88.1(2)	85.271	86.3(1)	86.1(5)	84.259	85.3(2)	85.7(8)	84.287
ψ[b]	78.6(2)	82.7(5)	82.416	79.1(2)	79.9(9)	82.143	79.7(2)	78.4(11)	82.556

a χ: $C_1MC_2 \cap C_5MC_6$ b ψ: $C_2C_3C_4C_5 \cap C_1C_8C_7C_6$ see Figure 1.2 c averaged values of **24a1** and **24a2**

Generally the calculated structures are slightly longer as a result of the level of theory chosen, there are also no intramolecular interactions from the counter ions included in

the calculated values. Even with the factors mentioned the values obtained are in fair agreement.

10.4.3 Energies

In looking at the E_{corr} values of the computed complexes found in Figure 10.19 shows an increase as the ligand becomes more electron donating and conversely a decrease as one moves down the triad. This decrease is consistent with the 2008 covalent radii that have been obtained where there is a significant difference of 0.12 Å between nickel and platinum, with the radii of palladium and platinum being remarkably similar.

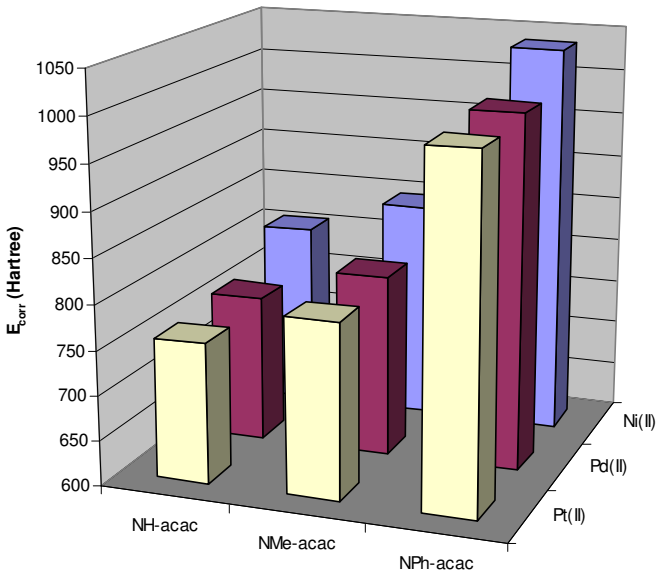

Figure 10.19 3D-graph of the total zero-point corrected energy (E_{corr}) for the computed complexes $[M(cod)(LL')]^+$ where M = group 10 transition metals and LL' = NH-acac, NMe-acac, NPh-acac. Counter ions have not been calculated.

The E_{rel} values corrected for the ligand effects (E_{rel}^{L}) is shown in Figure 10.20a indicating a clear increase as the metal centre is varied, with the nickel complexes having the lowest energies. The E_{rel} values corrected for the metal effects (E_{rel}^{M}) are depicted in Figure 10.20b show a decrease in energy as the ligand becomes more electron donating with the exception of the $[Ni(cod)(NH\text{-}acac)]^+$ complex.

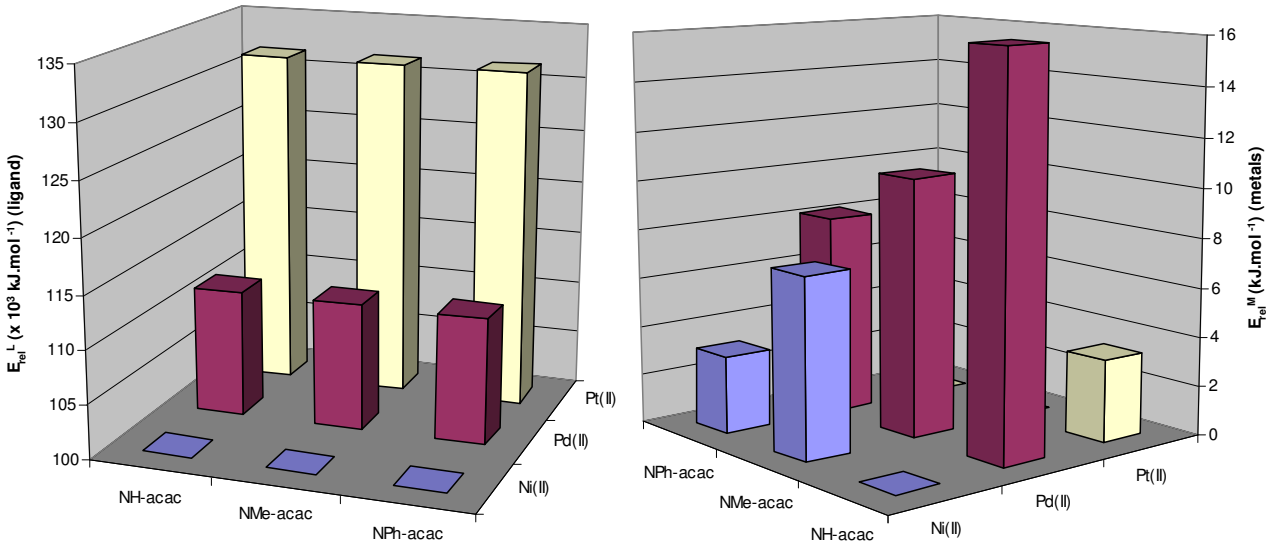

(**a**) (**b**)

Figure 10.20 3D-graphs of the total energy relative to the appropriate metal centre (E_{rel}) for the calculated complexes (a) is corrected for ligand (E_{rel}^{L}) and (b) is corrected for metal centre (E_{rel}^{M}).

The palladium complexes have the highest relative energy whereas platinum the lowest when moving from the NH-acac to NPh-acac ligands. These changes in the relative energy follow the stability pattern that was observed for the compounds that were synthesized, with $[Pd(cod)(NH\text{-}acac)]^+$ being the least stable at one day whilst the $[Pt(cod)(NPh\text{-}acac)]^+$ complex was found to be stable for several months.

10.4.4 Infra-red Spectroscopic Correlations

The infra-red spectra of the calculated complexes are presented to gain a further insight into the bonding character of the complexes studied. Although there are clearly defined bands on the calculated infra-red spectrum of the $[M(cod)(LL')]^+$ where M = Ni, Pt, Pd and LL' = NH-acac, NMe-acac, NPh-acac complexes most of the bands are not clearly assigned to a single isolated vibration. The reason behind this is that if a group includes relatively light atoms such as hydrogen (NH, CH, CH_2, CH_3 etc) or relatively heavy atoms such as halogens (CCl, CBr etc.) when compared to other atoms within the molecule, an isolated vibration may result since the amplitude (or velocity) of the harmonic oscillation of these atoms is relatively larger or smaller when compared with the other atoms in the same molecule. Additionally if atoms of similar masses are connected by bonds of similar strength the amplitude of

oscillation is comparable for each atom of the whole system, again not allowing the isolation of a single group vibration. A similar situation may occur in a system in which resonance effects average out the single and multiple bonds by conjugation (*e.g.* β-diketones). In the spectra that follow the band assignments will be denoted by the largest contributing vibration(s) to the band the reported calculated frequencies are unscaled.

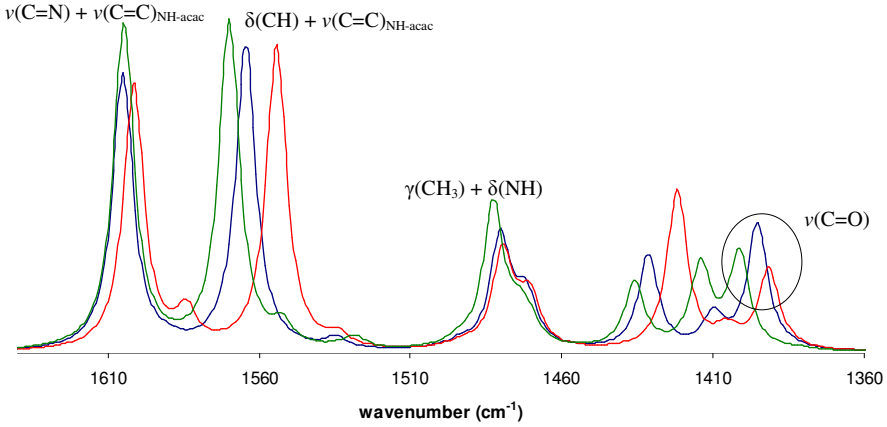

Figure 10.21 Calculated IR spectrum of [Ni(cod)(NH-acac)]$^+$ (blue), [Pd(cod)(NH-acac)]$^+$ (red) and [Pt(cod)(NH-acac)]$^+$(green). *ν* – stretching, δ – in-plane bending and γ – out-of-plane bending.

The band around 1610 cm^{-1} seen in Figure 10.21 contains the following vibrations ν(C=N), ν(C=C)$_{NH\text{-}acac}$, δ(CH), δ(NH) and γ(CH$_3$) with the largest contribution coming from the C=N stretching. It can be seen that there is not a large difference in the frequencies when changing the metal centre with values of 1605 cm^{-1}, 1601 cm^{-1} and 1605 cm^{-1} for nickel, palladium and platinum respectively. For the band centered at 1565 cm^{-1} the main vibrations observed are δ(CH), δ(NH), ν(C=O) and ν(C=C)$_{NH\text{-}acac}$ with the largest contribution coming from the C=C stretching of the 4-aminopent-3-end-2-onto ligand the contribution C=O stretching from the same ligand decreases as one proceeds from nickel to palladium and then to platinum. The next largest band is found at 1480 cm^{-1} comprises of γ(CH$_3$), δ(NH) and ν(C=N) with the out-of-plane bending of the methyl group the largest contributor and the stretching of the C=N being very little. The next group of bands encompasses the following vibrational contributions δ(CH$_2$)$_{cod}$, δ(CH$_3$), γ(CH)$_{cod}$, ν(C-C)$_{cod}$, ν(C=C), δ(NH),

$\delta(CH)_{cod + NH\text{-}acac}$, $\nu(C\text{-}CH_3)$. The bands circled include a largish contribution from the C=O stretching.

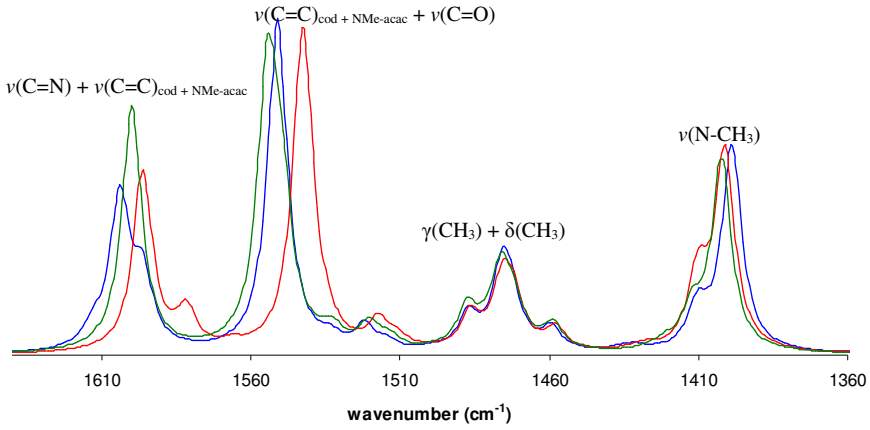

Figure 10.22 Calculated IR spectrum of $[Ni(cod)(NMe\text{-}acac)]^+$ (blue), $[Pd(cod)(NMe\text{-}acac)]^+$ (red) and $[Pt(cod)(NMe\text{-}acac)]^+$(green). *ν* – stretching, δ – in-plane bending and γ – out-of-plane bending.

The band around 1600 cm^{-1} seen in Figure 10.22 contains the following vibrations $\nu(C=N)$, $\nu(C=C)_{cod + NMe\text{-}acac}$, $\delta(CH)_{cod + NMe\text{-}acac}$ and $\gamma(CH_2)$ with the largest contribution coming from the C=N stretching. The shoulder observed for both nickel and palladium contains the asymmetrical vibrations of $\nu(C=C)$, this was not observed for the platinum complex. The next band at 1550 cm^{-1} comprises of $\nu(C=O)$, $\nu(C=C)_{cod + NMe\text{-}acac}$, $\delta(CH)_{NMe\text{-}acac}$ and $\delta(CH_3)$, however the contribution of the $\nu(C=O)$ frequency is small to non-existent for palladium and platinum leaving the $\nu(C=C)$ frequency is the largest contributing vibration. The triplet band that is seen at 1476 cm^{-1} is the in-plane and out-of-plane bend contribution of the methyl groups. The last of the bands found at 1400 cm^{-1} has a major contribution from the $\nu(N\text{-}CH_3)$ frequency as well as $\gamma(CH_3)$ the shoulder that is present for all three of the complexes major contribution is the $\nu(C\text{-}CH_3)$ frequency.

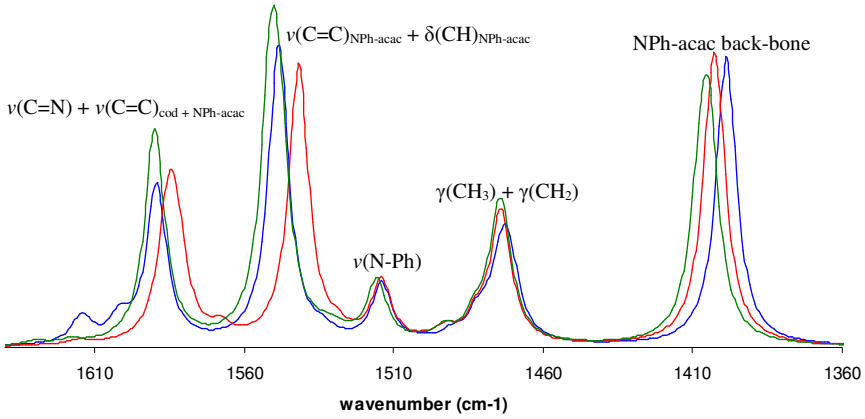

Figure 10.23 Calculated IR spectrum of $[Ni(cod)(NPh\text{-}acac)]^+$ (blue), $[Pd(cod)(NPh\text{-}acac)]^+$ (red) and $[Pt(cod)(NPh\text{-}acac)]^+$(green). *ν* – stretching, δ – in-plane bending and γ – out-of-plane bending.

In Figure 10.23 the band at 1590 cm^{-1} is comprised of $\nu(N{=}C)$, $\nu(C{=}C)_{NPh\text{-}acac\ +\ cod}$, $\delta(CH)$. For the nickel (blue) spectra the shoulder is the $\nu(C{=}C)_{cod}$ contribution and for the band above 1610 cm^{-1} the $\nu(C{=}C)_{phenyl}$ is observed. The band at around 1550 cm^{-1} major contributions are from $\nu(C{=}C)_{NPh\text{-}acac}$ and $\delta(CH)_{NPh\text{-}acac}$, however for platinum (green) we find an additional contribution from the in-plane wagging of the methine protons of the cyclo-octadiene ring. The band at 1515 cm^{-1} mainly comprises of ν(N-Ph) with minor contributions from $\delta(CH)_{phenyl}$ and $\nu(C{=}C)_{phenyl}$. The band at 1474 cm^{-1} can be attributed to the $\gamma(CH_3)$ and $\gamma(CH_2)$ vibrations. The last band at 1401 cm^{-1} is an interesting case of the vibration of the entire back-bone of the 4-anilinopent-3-en-2-onato ligand ($\nu(C{=}N)$, $\nu(C{=}O)$, $\nu(C{=}C)$ and $\delta(CH_3)$).

Table 10.6 Selected IR values (cm^{-1}) for the group 10 metal complexes.

	$[M(cod)(NH\text{-}acac)]^+$			$[M(cod)(NMe\text{-}acac)]^+$			$[M(cod)(NPh\text{-}acac)]^+$		
	Ni	Pd	Pt	Ni	Pd	Pt	Ni	Pd	Pt
$\nu(C{=}N)$	1605	1601	1605	1604	1596	1560	1589	1585	1590
ν(N-R)	1480	1480	1483	1399	1401	1402	1514	1514	1516

R = H, Me, Ph

Selected infra-red values are listed in Table 10.6. For the $\nu(C{=}N)$ frequency for the complexes presented there is a difference of *ca.* 10 cm^{-1} indicating that the changing of the R group attached to the nitrogen does not affect the vibration in the back-bone of the β-enaminonato ligands a contributing factor to this is the conjugation thus making the bonding character of the C-N, C-C and C-O very similar. It was

interesting to note that a clearly defined band was observed for $[M(cod)(NPh\text{-}acac)]^+$ at 1401 cm^{-1} for this conjugated vibration. The ν(N-R) frequency is related to the inverse order of the electronegativity[12] (Ph, H, CH_3) so as you decrease the electronegativity the vibrational band shifts up-field.

10.4.5 Molecular Orbital Comparisons

The molecular orbitals give valuable information as to the nature and location of probable electron density within the complexes. This graphical representation of the molecular orbitals is another method whereby interactions of the cyclo-octadiene with the various metal centers and the *trans* ligands may be observed. The second-highest (HOMO-1) and highest (HOMO) occupied molecular orbitals and the lowest (LUMO) and second-lowest (LUMO+1) unoccupied molecular orbitals for the calculated complexes of $[M(cod)(NH\text{-}acac)]^+$, $[M(cod)(NMe\text{-}acac)]^+$ and $[M(cod)(NPh\text{-}acac)]^+$ where M = Ni, Pd, Pt will be presented, along with the differences in the respective orbitals ($E_{g-1} \equiv \Delta|HOMO\text{-}1|\text{-}|HOMO|$; $E_g \equiv \Delta|HOMO|\text{-}|LUMO|$; $E_{g+1} \equiv \Delta|LUMO|\text{-}|LUMO+1|$). The contour plots shown with the molecular orbitals are viewed along the *z*-axis.

[12] Nam P-C, Nguyen M.T., Chandra A.K., *J. Phys. Chem. A.*, **110**, 4509, (2006)

Table 10.7 Molecular Orbitals of calculated structures $[M(cod)(NH\text{-}acac)]^+$.

	HOMO-1	HOMO	LUMO	LUMO+1
Ni(II)	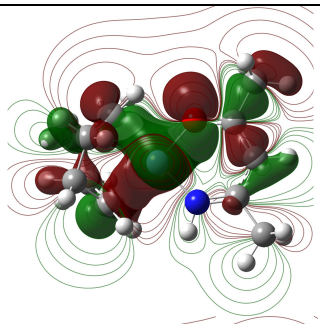	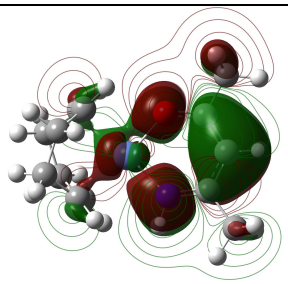	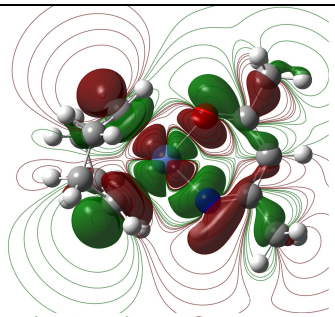	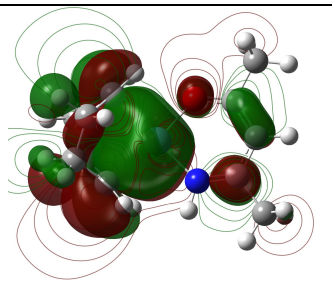
Pd(II)	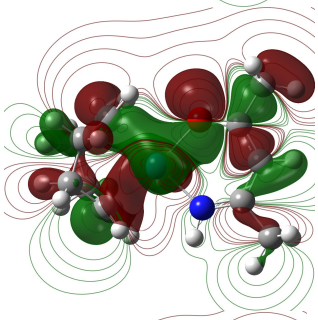	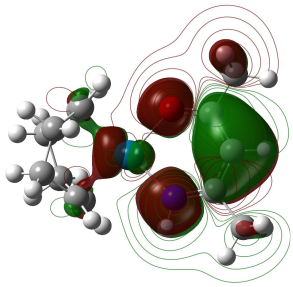	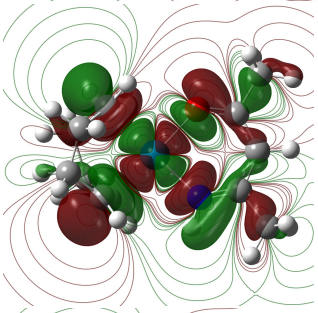	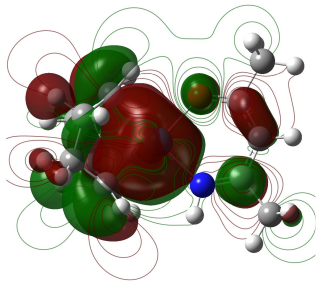
Pt(II)	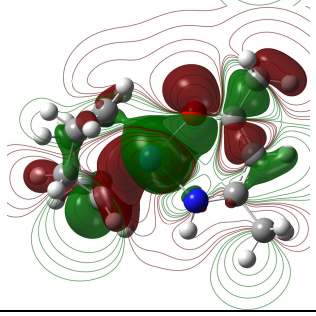	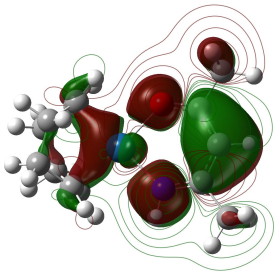	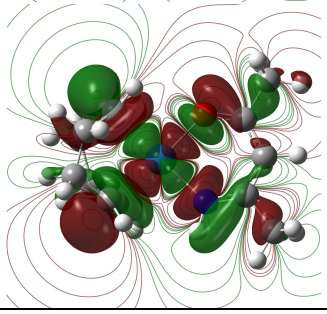	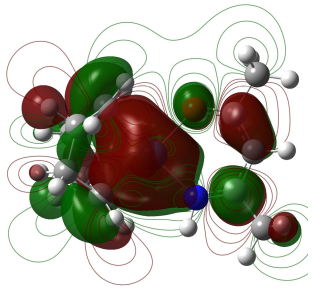

Table 10.8 Molecular Orbital Energies (Hartree) and energy gaps (eV) of the $[M(cod)(NH\text{-}acac)]^+$ calculated structures.

	HOMO-1	HOMO	LUMO	LUMO+1	E_{g-1}	E_g	E_{g+1}
Ni(II)	-0.40893	-0.35676	-0.23603	-0.18798	1.420	3.278	1.315
Pd(II)	-0.40619	-0.35328	-0.22951	-0.18299	1.440	3.368	1.266
Pt(II)	-0.40810	-0.35924	-0.19246	-0.18616	1.330	4.538	0.171

The molecular orbitals for $[M(cod)(NH\text{-}acac)]^+$ where the metal centers are nickel, palladium and platinum are given in Table 10.7 with their energies listed in Table 10.8. In the HOMO-1 molecular orbitals, the *p* orbitals seen on the carbon adjacent to the oxygen of the 4-aminopent-3-en-2-onato ligand, with an in-phase overlap of the metal orbitals with the alkene *p* orbitals of the cyclo-octadiene. For the HOMO molecular orbitals, π orbital delocalization on the 4-aminopent-3-en-2-onato ligand is observed for all computed structures. For the LUMO molecular orbitals, $d_{x^2-y^2}$

orbitals are observed around the metal centres, whereas for LUMO+1 molecular orbitals, a d_{z^2} orbital is seen.

Table 10.9 Molecular Orbitals of calculated structures [M(cod)(NMe-acac)]$^+$.

	HOMO-1	HOMO	LUMO	LUMO+1
Ni(II)	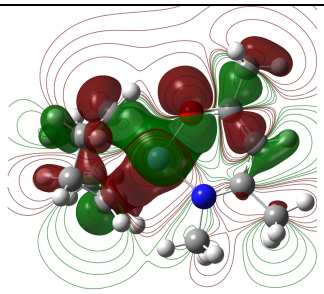	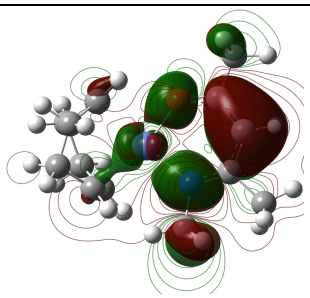	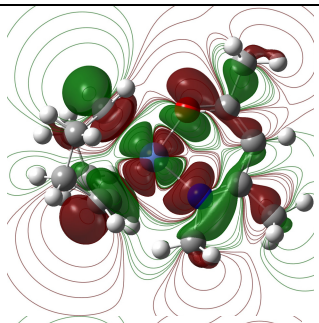	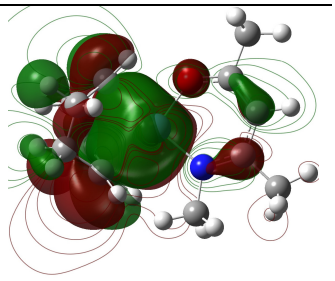
Pd(II)	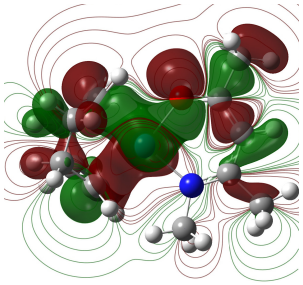	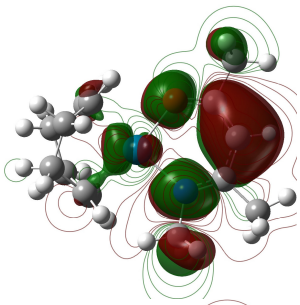	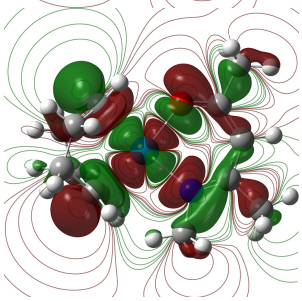	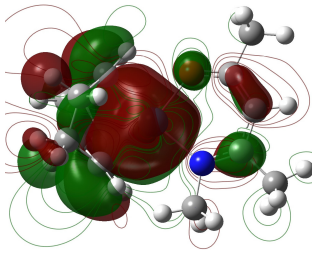
Pt(II)	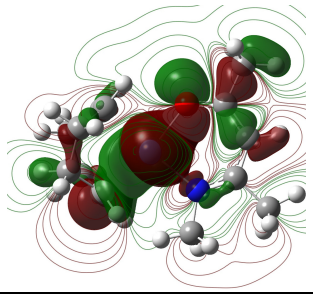	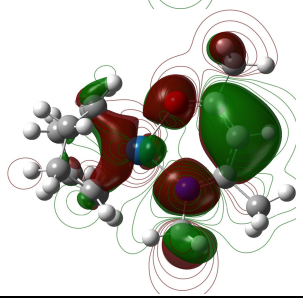	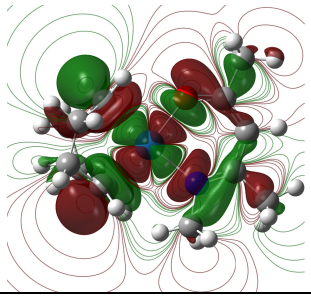	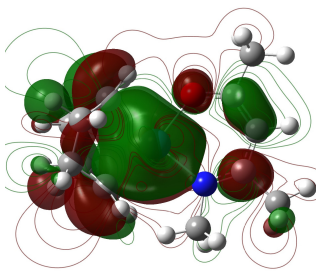

Table 10.10 Molecular Orbital Energies (Hartree) and energy gaps (eV) of the [M(cod)(NMe-acac)]$^+$ calculated structures.

	HOMO-1	HOMO	LUMO	LUMO+1	E_{g-1}	E_g	E_{g+1}
Ni(II)	-0.40565	-0.34794	-0.24074	-0.18502	1.570	2.917	1.516
Pd(II)	-0.40513	-0.34509	-0.23256	-0.18095	1.634	3.062	1.404
Pt(II)	-0.40713	-0.35095	-0.19542	-0.18401	1.529	4.232	0.310

The molecular orbitals for [M(cod)(NMe-acac)]$^+$ where the metal centers are nickel, palladium and platinum are given in Table 10.9 with their energies listed in Table 10.10. For the HOMO-1 molecular orbitals, an interesting feature is the *p* orbitals seen on the carbon adjacent to the oxygen of the NMe-acac ligand. With an in-phase overlap of the metal orbitals with the alkene *p* orbitals of the cyclo-octadiene. This is continued to a lesser extent in the HOMO molecular orbitals with the orbitals shifting to the NMe-acac ligand where the π delocalization on the back-bone is clearly visible.

The metal centers have d_{yz} orbitals, while the *p* orbital of the methyl carbon of the NMe-acac ligand is seen. In the LUMO molecular orbitals, a $d_{x^2-y^2}$ orbital is observed centered on the metals of the group. The LUMO+1 molecular orbitals, tend to a d_{z^2} orbital centered on the metal.

Table 10.11 Molecular Orbitals of calculated structures [M(cod)(NPh-acac)]$^+$.

	HOMO-1	HOMO	LUMO	LUMO+1
Ni(II)	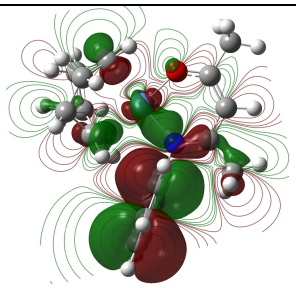	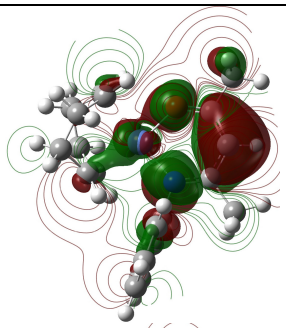	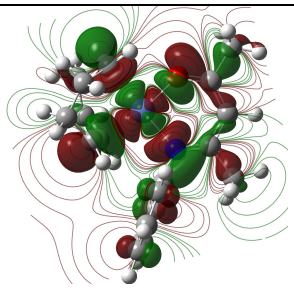	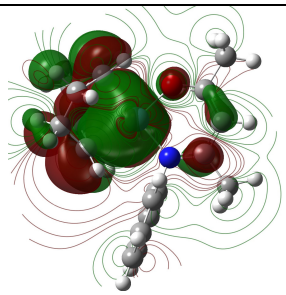
Pd(II)	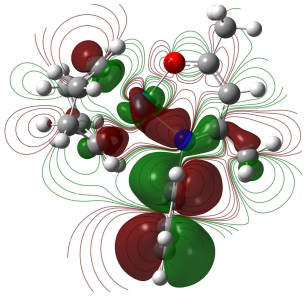	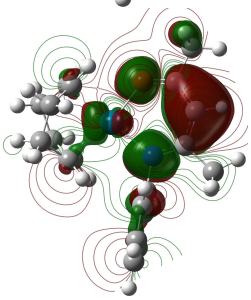	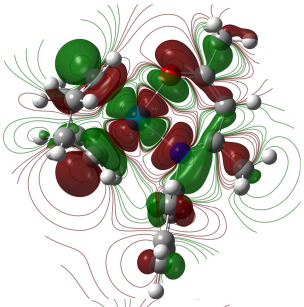	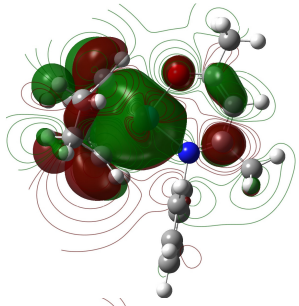
Pt(II)	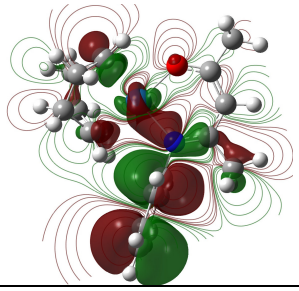	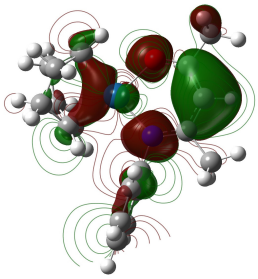	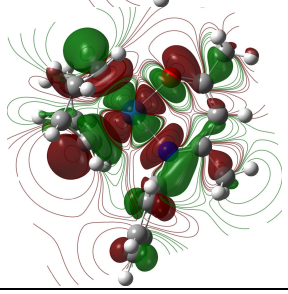	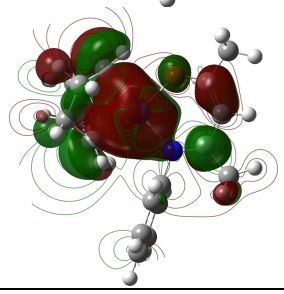

Table 10.12 Molecular Orbital Energies (Hartree) and energy gaps (eV) of the [M(cod)(NPh-acac)]$^+$ calculated structures.

	HOMO-1	HOMO	LUMO	LUMO+1	E_{g-1}	E_g	E_{g+1}
Ni(II)	-0.36571	-0.34707	-0.23568	-0.17787	0.507	3.031	1.573
Pd(II)	-0.36325	-0.34458	-0.22880	-0.17488	0.508	3.151	1.467
Pt(II)	-0.36565	-0.35001	-0.19263	-0.17921	0.426	4.283	0.365

The molecular orbitals for [M(cod)(NPh-acac)]$^+$ where the metal centers are nickel, palladium and platinum are given in Table 10.11 with their energies listed in Table 10.12. In the HOMO-1 molecular orbitals, the π orbitals on the phenyl ring system are clearly observed. For the HOMO molecular orbitals, π orbital delocalization on the 4-anilinopent-3-en-2-onato ligand is observed for all computed structures. For the

LUMO molecular orbitals, $d_{x^2-y^2}$ orbitals are observed around the metal centers, whereas for LUMO+1 molecular orbitals, a d_{z^2} orbital is seen.

The comparison of the HOMO, LUMO and LUMO+1 molecular orbitals with those of the NH-acac and NMe-acac group 10 metal complexes a marked similarity was found. It is therefore concluded that the varying of the R-group attached to the nitrogen of the β-enaminonato ligands does not play as significant role as originally postulated.

10.4.6 Venus fly-trap (χ and ψ) Angle Evaluation

Figure 10.24 shows the correlation of the different nickel(II) triad complexes comparison of the χ and ψ angles.

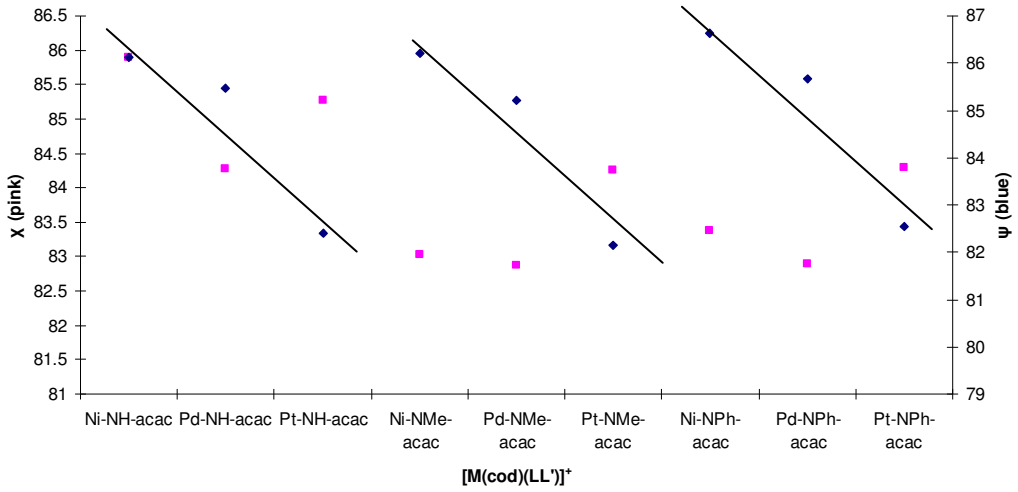

Figure 10.24 Graph of Nickel(II), Palladium(II) and Platinum(II) calculated complexes *vs.* χ (pink squares) and ψ (blue diamonds) angles (see Chapter 1 Figure 1.2 for definition of χ and ψ angles).

In Figure 10.24 there is a decreasing trend found in the ψ angle of the complexes which corresponds to that covalent atomic radii of the metal centers, thus as you move down the triad the radii become smaller and the ψ angle becomes smaller (*i.e.* the opening of the cyclo-octadiene ring closes). This pattern is similar to the pattern observed for the tropolonato complexes seen in Chapter 8 Figure 8.25. The maximum difference observed for the ψ angle was 4.5° between [Ni(cod)(NH-acac)] and [Pt(cod)(NMe-acac)].

In overview a good correlation was found between the X-ray crystal structures and that of the computed compounds. The molecular orbital diagrams show the influence of both the *p* and *d* orbitals of the ligands as well as the metal centers. The infra-red spectra showed that the change in the metal centre was not as great an influence on the *ν*(C=N) stretching frequency as was expected, however the electronegativity of the group attached to the nitrogen does have an influence on the *ν*(N-R) frequency.

This concludes the section on the β-enaminonato ligands for both platinum and palladium complexes and the comparison with their calculated structures, in continuing the study Chapter 11 focuses on an additional group of metals, group 9, which were characterized by X-ray crystal structures as well as computational work. With the experimental work limited only to the rhodium metal centre, in keeping with the idea of the study acetylacetonato and tropolonato type ligands were used.

Chapter 11
Crystallographic and Theoretical Study of Rhodium(I) Cyclo-octadiene Complexes

11.1 Introduction

So far this PhD investigation has concentrated on the platinum(II) and palladium(II) single crystal X-ray crystallography with a range of O,O- and N,O-bidentate ligands as well as the corresponding theoretical structures thereof. To continue building the experimental model of the co-ordination of cyclo-octadiene rhodium has been incorporated into the study. Rhodium brings to the table the fact that it has a +1 oxidation state resulting in a neutral complex being formed with the chosen range of O,O- and N,O-bidentate ligands, eliminating any possible interactions from counter ions which is the case found for both the platinum(II) and palladium(II) metal complexes.

This chapter describes the structural aspects of a range of rhodium(I) complexes containing the cyclo-octadiene ligand to allow comparison with the group 10 palladium(II) and platinum(II) complexes as described in Chapters 4,5 and 7. Since the [Rh(cod)(LL')] complexes described in this chapter are neutral, the packing effects induced by the anions are eliminated. The X-ray crystal structures of rhodium(I) β-diketonato metal complexes as synthesized previously (§ 3.6.2) will be presented Thereafter a comparison of the X-ray structures presented with their comparative calculated structures will follow.

Even though many rhodium cyclo-octadiene metal X-ray crystal structures are known only six are listed in the Cambridge Structural Database[1,2] (CSD) for rhodium(I) β-diketonato cyclo-octadiene metal complexes and one for rhodium β-enaminonato cyclo-octadiene metal complexes (Table 11.1).

[1] Allen F.H., *Acta Cryst.*, **B58**, 380, (2002)
[2] Bruno I.J., Cole J.C., Edginton P.R., Kessler M., Macrae C.F., McCabe P., Pearson J., Taylor R., *Acta Cryst.*, **B58**, 389, (2002)

Table 11.1 CSD Search results of Rh(cod)(L) systems.

Complex	Crystal System	Space Group	CSD Ref
[Rh(cod)(bta)][a]	Monoclinic	$P2_1/c$	BFACRH[3]
[Rh(cod)(acac)]	Monoclinic	Cc	COCACR[4]
[Rh(cod)(fca)][b]	Triclinic	$P\bar{1}$	LABLIJ[5]
[Rh(cod)(tfacac)]	Triclinic	$P\bar{1}$	LEVCEU[6]
[Rh(cod)(hfacac)]	Orthorhombic	$Pbca$	RAFNER[7]
[Rh(cod)(heptacac)][c]	Monoclinic	$P2_1$	ZIQXEC[8]
[Rh(cod)(N26iPrPh-acac)][d]	Triclinic	$P\bar{1}$	HIHRUM[9]

a bta – benzoyl-1,1,1-trifluoracetonato
complex name: (Benzoyl-1,1,1-trifluoroacetonato)-(cyclo-octa-1,5-diene)-rhodium(I)
b fca – 1-ferrocenyl-1,3-butanedionato
complex name: (η^4-1,5-Cyclo-octadiene)-(1-ferrocenyl-1,3-butanedionato)-rhodium(I)
c heptacac – 2,2-Dimethyl-7-(6,6-dimethylbicyclo(3.1.1)hept-2-en-2-yl)hept-6-ene-3,5-dionato
complex name: μ^2-η^4-2,2-Dimethyl-7-(6,6-dimethylbicyclo(3.1.1)hept-2-en-2-yl)hept-6-ene-3,5-dionato-O,O')-(η^4-1,5-cyclo-octadiene)-rhodium-tricarbonyl-iron
d N26iPrPh-acac – 4-(2,6-diisopropylphenylamino)pent-3-en-2-onato
complex name: (η^2,η^2-Cycloocta-1,5-diene)-(4-(2,6-diisopropylphenylamino)pent-3-en-2-onato-N,O)-rhodium

Previously the [Rh(cod)(acac)] X-ray structure was done at room temperature[4], a redetermination of this crystal structure will be presented.

The complexes that were prepared as described in § 3.6.2 were analyzed with X-ray single crystal diffraction and are summarized in Table 11.2. A molecular diagram indicating the numbering scheme of each compound is presented, along with selected bond lengths and angles, hydrogen bonding interactions and additional interactions if applicable. A discussion highlighting some of the important aspects of each particular structure is presented thereafter.

Additional correlations with other structures are presented in the second section of this chapter whilst complete lists of the crystals structures presented are given in the supplementary data.

[3] Leipoldt J.G., Basson S.S., Lamprecht G.J., Bok L.D.C., Schlebusch J.J.J., *Inorg. Chim. Acta.*, **40**, 43, (1980)
[4] Tucker P.A., Scutcher W., Russell D.R., *Acta. Cryst.*, **B31**, 592, (1975)
[5] Swarts J.C., Vosloo T.G., Leipoldt J.G., Lamprecht G.J., *Acta Cryst.*, **C49**, 760, (1993)
[6] Duan Z., Hamden-Smith M.J., Duesler E.N., Rheingold A.L., *Polyhedron*, **13**, 609, (1994)
[7] Angermund K., Baumann W., Dinius E., Fornika R., Gorls H., Kessler M., Kruger C., Leitner W., Lutz F., *Chem. Eur. J.*, **3**, 755, (1997)
[8] Englert U., Kaser M., Salzer A., *Inorg. Chem.*, **34**, 6231, (1995)
[9] Sasamori T., Matsumoto T., Takeda N., Tokitoh N., *Organometallics*, **26**, 3621, (2007)

11.2 Experimental

Data collections for $[Rh(cod)\mu\text{-}Cl]_2$ (293 K and 100 K), [Rh(cod)(acac)], [Rh(cod)(dbm)], [Rh(cod)(thtfac)], [Rh(cod)(trop)] and NMe-acac were obtained on a Bruker Apex II 4K CCD diffractometer, equipped with a graphite-monochromated Mo-Kα radiation, all the reflections were merged and integrated with SAINT-PLUS[10] and corrected for Lorentz, polarization and absorption effects with SADABS[11].

Structures were solved by direct and conventional Patterson methods using the SHELX-97[12] as part of the WinGX[13] package, and anisotropic refinement was performed on all non-hydrogen atoms by a full-matrix least-squares method. The positions of the hydrogen atoms were calculated using a riding model to the adjacent carbon, unless otherwise stipulated. Hydrogen interactions were calculated using the PLATON[14,15,16] and PARST[17] programs.

The DFT molecular orbital calculations were carried out using the Gaussian 03[18] software suite. Becke's three parameter hybrid (B3LYP)[19,20] exchange correlation functional was used. The basis set employed in this study was 6-311++G(d,p)[21,22,23]

[10] Bruker SAINT-PLUS (including XPREP), Version 7.12, Bruker AXS Inc., Madison, WI., (2004)
[11] Bruker SADABS (Version 2004/1), Bruker AXS Inc., Madison, WI., (1998)
[12] Sheldrick G.M., *Acta Cryst.*, **A64**, 112, (2008)
[13] Farrugia L.J., *Appl. Cryst.*, **32**, 837, (1999)
[14] Spek A.L., PLATON A multipurpose crystallographic tool, Utrecht University, Utrecht, Netherlands, (2005)
[15] Speck A.L., *J. Appl. Cryst.*, **36**, 7, (2003)
[16] Speck A.L., *Acta Cryst*, **D65**, 148, (2009)
[17] Nardelli M., *J. Appl. Cryst.*, **28**, 659, (1995)
[18] Frisch M.J., Trucks G.W., Schlegel H.B., Scuseria G.E., Robb M.A., Cheeseman J.R., Montgomery J.A. Jr., Vreven T., Kudin K.N., Burant J.C., Millam J.M., Iyengar S.S., Tomasi J., Barone V., Mennucci B., Cossi M., Scalmani G., Rega N., Petersson G.A., Nakatsuji H., Hada M., Ehara M., Toyota K., Fukuda R., Hasegawa J., Ishida M., Nakajima T., Honda Y., Kitao O., Nakai H., Klene M., Li X., Knox J.E., Hratchian H.P., Cross J.B., Bakken V., Adamo C., Jaramillo J., Gomperts R., Stratmann R.E., Yazyev O., Austin A.J., Cammi R., Pomelli C., Ochterski J.W., Ayala P.Y., Morokuma K., Voth G.A., Salvador P., Dannenberg J.J., Zakrzewski V.G., Dapprich S., Daniels A.D., Strain M.C., Farkas O., Malick D.K., Rabuck A.D., Raghavachari K., Foresman J.B., Ortiz J.V., Cui Q., Baboul A.G., Clifford S., Cioslowski J., Stefanov B.B., Liu G., Liashenko A., Piskorz P., Komaromi I., Martin R.L., Fox D.J., Keith T., Al-Laham M.A., Peng C.Y., Nanayakkara A., Challacombe M., Gill P.M.W., Johnson B., Chen W., Wong M.W., Gonzalez C., Pople J.A., Gaussian 03, Revision E.01, Gaussian Inc., Wallingford CT, (2004)
[19] Becke A.D., *J. Chem. Phys.*, **98**, 5648, (1993)
[20] Lee C., Yang W., Parr R.G., *Phys. Rev.*, **B37**, 785, (1988)
[21] Ditchfield R., Hehre W.J., Pople J.A., *J. Chem. Phys.*, **54**, 724, (1971)
[22] Gordon M.S., *Chem. Phys. Lett.*, **76**, 163, (1980)
[23] Rassolov V.A., Ratner M.A., Pople J.A., Redfern P.C., Curiss L.A., *J. Comp. Chem.*, **22**, 976, (2001)

for the main group elements and LanL2DZ[24] for the middle to late transition metals. Vibrational frequencies were calculated at the 6-311++G(d,p)[21,22,23] level for the main group elements and at the LanL2DZ[24] level for the middle to late transition metals with minimum energies confirmed to have zero imaginary frequencies. The frequencies were unscaled and used to compute the zero-point vibrational energies.

Molecular graphics were obtained using DIAMOND[25], while overlay graphics were obtained using HyperChem 7.5[26].

[24] Hay P.J., Wadt W.R., *J. Chem. Phys.*, **82**, 299, (1985)
[25] Brandenburg K., Brendt M., DIAMOND, Release 2.1e. Crystal Impact GbR, Potfach 1251, D53002 Bonn, Germany., (2001)
[26] HyperChem™ Release 7.52, Windows Molecular Modeling System, HyperCube Inc., (2002)

Table 11.2 Crystallographic data and refinement parameters

Crystal Data	[Rh(cod)(acac)] (**25**)	[Rh(cod)(dbm)] (**26**)	[Rh(cod)(thtfac)] (**27**)	[Rh(cod)(trop)] (**28**)	$[Rh(cod)Cl]_2$ (**29**)	$[Rh(cod)Cl]_2$ (**30**)	$[Rh(cod)Cl]_2$ published
Empirical formula	$C_{13}H_{19}O_2Rh$	$C_{23}H_{23}O_2Rh$	$C_{16}H_{16}F_3O_2RhS$	$C_{15}H_{17}O_2Rh$	$C_{16}H_{24}Cl_2Rh_2$	$C_{16}H_{24}Cl_2Rh_2$	$C_{16}H_{24}Cl_2Rh_2$
Formula weight	310.19	434.32	432.26	332.20	493.07	493.07	493.07
Temperature (K)	100(2)	100(2)	100(2)	100(2)	293(2)	100(2)	293
Wavelength (Å)	0.71073	0.71073	0.71073	0.71073	0.71073	0.71073	0.71069
Crystal system	Monoclinic	Monoclinic	Monoclinic	Orthorhombic	Monoclinic	Monoclinic	Monoclinic
Space group	*Cc*	*Cc*	$P2_1/n$	$P2_12_12_1$	$P2_1/n$	$P2_1/n$	$P2_1/n$
Unit cell dimensions							
a (Å)	6.7318(4)	17.1455(4)	11.140(2)	8.3210(2)	7.2856(3)	7.2913(5)	9.056 (1)
b (Å)	18.3864(10)	10.7094(4)	9.425(2)	11.2494(3)	25.4257(11)	25.1318(14)	25.475 (6)
c (Å)	9.8142(6)	13.0229(4)	15.277(3)	13.5631(4)	9.0497(4)	8.8599(6)	7.309 (1)
α (°)	90	90	90	90	90	90	90
β (°)	93.898(3)	130.526(2)	104.128(9)	90	92.006(2)	91.068(2)	91.79 (1)
γ (°)	90	90	90	90	90	90	90
Volume ($Å^3$)	1211.9(1)	1817.6(1)	1555.4(5)	1269.59(6)	1675.35(12)	1623.24(18)	1685.4 (5)
Z	4	4	4	4	4	4	4
Density (calculated) ($Mg.m^{-3}$)	1.700	1.587	1.846	1.738	1.955	2.018	1.943
Absorption coefficient (mm^{-1})	1.392	0.954	1.269	1.335	2.277	2.350	2.24
F(000)	632	888	864	672	976	976	
Crystal size (mm^3)	0.23 x 0.22 x 0.19	0.25 x 0.20 x 0.10	0.29 x 0.20 x 0.16	0.30 x 0.14 x 0.13	0.32 x 0.19 x 0.18	0.31 x 0.16 x 0.13	0.43 x 0.28 x 0.25
Theta range for data collection (°)	3.04 to 26.95	2.46 to 28.30	2.04 to 28.27	2.35 to 28.00	2.39 to 27.00	2.44 to 28.28	19.9 to 21.6
Index ranges	-8<=h<=8, -23<=k<=23, -11<=l<=12	-22<=h<=22, -13<=k<=14, -17<=l<=17	-14<=h<=12, -12<=k<=12, -17<=l<=20	-10<=h<=10, -14<=k<=14, -17<=l<=17	-9<=h<=9, -32<=k<=32, -11<=l<=11	-9<=h<=9, -33<=k<=21, -11<=l<=11	-14<=h<=14, 0<=k<=41, 0<=l<=11
Reflections collected	5364	22262	25905	16634	31149	18773	7601
Independent reflections	2404 [R(int) = 0.0280]	4367 [R(int) = 0.0377]	3730 [R(int) = 0.0833]	3059 [R(int) = 0.0275]	3658 [R(int) = 0.0376]	4026 [R(int) = 0.0436]	4820
Completeness to θ (°; %)	26.95, 98.3	28.30, 99.8	28.27, 96.7	28.00, 99.9	27.00 99.7	28.28 99.9	
Max. and min. transmission	0.7779 and 0.7402	0.9107 and 0.7965	0.8227 and 0.7098	0.8456 and 0.6901	0.6847 and 0.5295	0.7499 and 0.5295	
Refinement method	Full-matrix least-squares on F^2	Full-matrix least-squares on F^2	Full-matrix least-squares on F^2	Full-matrix least-squares on F^2	Full-matrix least-squares on F^2	Full-matrix least-squares on F^2	
Data / restraints / parameters	2404 / 2 / 147	4367 / 246 / 236	3730 / 0 / 208	3059 / 0 / 164	3658 / 0 / 181	4026 / 0 / 181	
Goodness-of-fit on F^2	1.070	1.203	1.048	1.105	1.210	1.036	
Final R indices [I>2σ(I)]	$R_1 = 0.0221$, $wR_2 = 0.0466$	$R_1 = 0.0280$, $wR_2 = 0.0768$	$R_1 = 0.0475$, $wR_2 = 0.1166$	$R_1 = 0.0139$, $wR_2 = 0.0350$	$R_1 = 0.0318$, $wR_2 = 0.0760$	$R_1 = 0.0308$, $wR_2 = 0.0574$	
R indices (all data)	$R_1 = 0.0231$, $wR_2 = 0.0471$	$R_1 = 0.0385$, $wR_2 = 0.1069$	$R_1 = 0.0604$, $wR_2 = 0.1312$	$R_1 = 0.0142$, $wR_2 = 0.0355$	$R_1 = 0.0362$, $wR_2 = 0.0796$	$R_1 = 0.0396$, $wR_2 = 0.0597$	$R_1 = 0.038$ $wR_2 = 0.063$
Largest diff. peak and hole ($e.Å^{-3}$)	0.287 and -0.506	0.686 and -0.803	1.809 and -1.283	0.282 and -0.381	0.620 and -1.031	0.693 and -0.672	

11.3 X-Ray Structures of Rhodium Complexes

11.3.1 Crystal structure of [Rh(cod)μ-Cl]$_2$[27,28]

The title compound was re-evaluated to obtain final clarification and accuracy of carbon and hydrogen bonding in the *cis,cis*-1,5-cyclo-octadiene ring system co-ordinated to the rhodium center.

The compound, [Rh(cod)μ-Cl]$_2$, crystallized in the monoclinic space group $P2_1/n$, with one molecule in the asymmetric unit. The numbering scheme is presented in Figure 11.1 for the 293 K and the 100 K collections, while atomic co-ordinates, bond angles and distances, anisotropic displacement parameters and hydrogen co-ordinates are reported in Appendix B.24 and B.25. General crystallographic data and refinement parameters are reported in Table 11.2, while significant bond angles and distances are reported in Table 11.3.

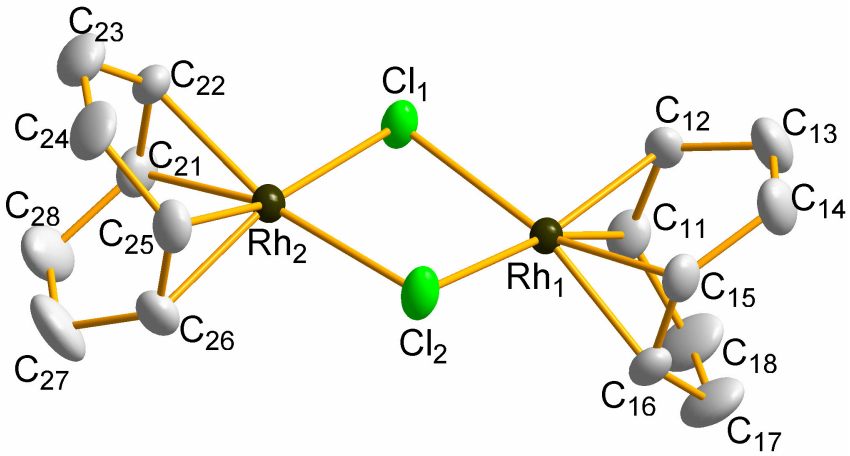

Figure 11.1 Diamond illustration of [Rh(cod)μ-Cl]$_2$ at 293 K showing the numbering scheme and displacement ellipsoids (30 %) of the complex. Hydrogen atoms omitted for clarity.

[27] Ibers J.A., Snyder R.G., *Acta. Cryst.*, **15**, 923, (1962)
[28] De Ridder D.J.A., *Acta. Cryst.*, **C50**, 1569, (1994)

Table 11.3 Selected bond distances and angles for $[Rh(cod)\mu\text{-}Cl]_2$

Bond Distance (Å)	Temperature		Bond Angles (°)	Temperature	
	293 K	100 K		293 K	100 K
Rh-C_{11}	2.089(5)	2.093(3)	C_{11}-Rh-C_{12}	38.4(2)	39.0(1)
Rh-C_{12}	2.108(4)	2.115(3)	C_{15}-Rh-C_{16}	38.5(2)	39.1(1)
Rh-C_{15}	2.088(4)	2.086(3)	χ^a	88.2(2)	88.6(2)
Rh-C_{16}	2.087(5)	2.098(3)	ψ^b	77.8(4)	77.0(2)
C_{11}-C_{12}	1.382(7)	1.404(5)			
C_{15}-C_{16}	1.376(8)	1.402(5)			

a χ: $C_1MC_2 \cap C_5MC_6$ b ψ: $C_2C_3C_4C_5 \cap C_1C_8C_7C_6$ see Figure 1.2

The co-ordination geometry around the chlorido bridged rhodium metal centers is square planar (Figure 4.2). The 1,5-cyclo-octadiene is bonded to the rhodium center via the alkene moieties of the ring giving rise to the boat conformation. The mean C=C bond distances for complexes **29** and **30** are 1.377(8) Å and 1.399(5) Å respectively, these values are in good agreement with free cyclo-octadiene 1.341 Å. The slight elongation of the alkene bonds can be ascribed to the co-ordination with the rhodium metal centre thus partially reducing the alkene bond character.

Table 11.4 Hydrogen bond distances and angles for $[Rh(cod)Cl]_2$ (29) (Å and °).

D-H...A	d(D-H)	d(H...A)	d(D...A)	<(DHA)
C_{11}-H_{11}...$Cl_2^{\#1}$	0.98	2.73	3.597(5)	148.1

Symmetry transformations used to generate equivalent atoms :
#1 x-1, y, z

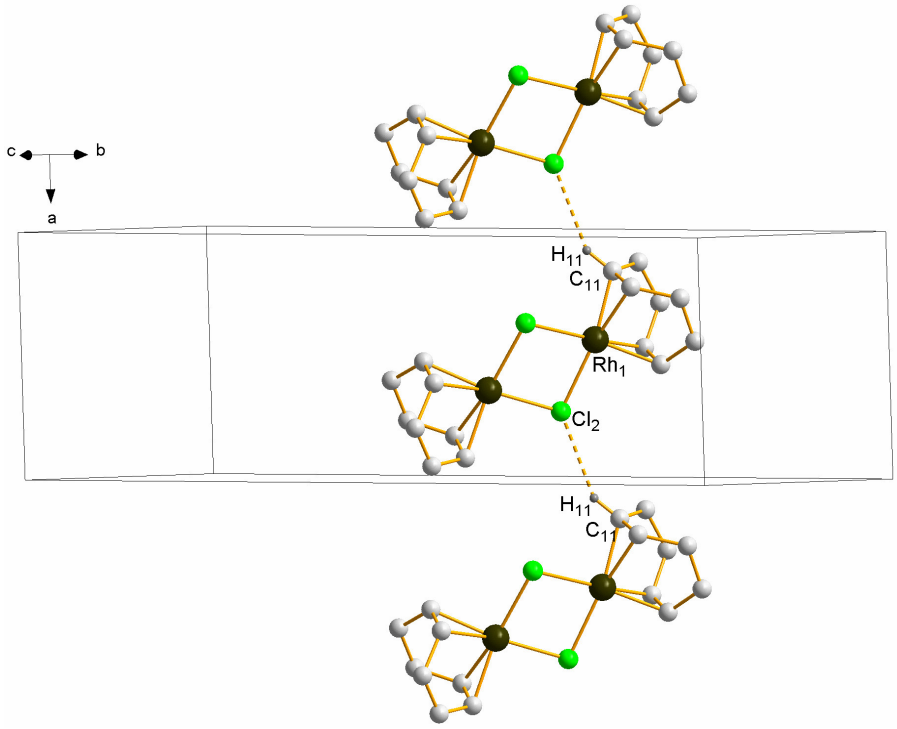

Figure 11.2 Partial unit cell of [Rh(cod)μ-Cl]$_2$ at 293 K showing intermolecular hydrogen bonding interactions indicated by a dashed bond. Only selected hydrogen atoms are included. Carbon (grey), rhodium (dark green) and chlorine (green).

The intramolecular distance between the rhodium metal centers is 3.5051(5) Å which is larger than the known value of 2.69 Å for bonded neutral metal radii. The shortest Rh-Rh intermolecular contact is 6.7275(5) Å confirming no rhodium interactions. The shortest intermolecular contact is between the bridging chlorine (Cl_2) and a hydrogen of the neighboring alkene carbon (C_{11}) (Figure 11.2). The intermolecular alkene carbon (C_{12}) – carbon (C_{15}) contact is 3.575 Å whereas the intermolecular alkane carbon (C_{24}) – carbon (C_{23}) contact is 4.097Å, this results in a staggered planar packing where the opening of the 1,5-cyclo-octadiene rings face toward each other. The high anisotropy of the alkane carbons on the 1,5-cyclo-octadiene ring lead to the low temperature study of this molecule so as to accurately determine the carbon-carbon bond distances of the 1,5-cyclo-octadiene moiety.

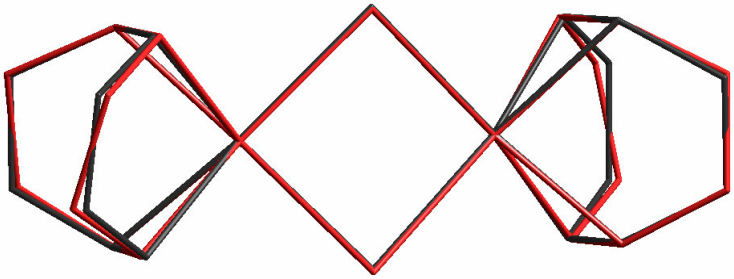

Figure 11.3 Hyperchem superimposed image of the low temperature determination (100 K, red) *vs.* the room temperature determination (295 K, black). RMS overlay error of 0.108 Å.

The overlay of the room temperature (293 K) crystal structure with the low temperature (100 K) crystal structure is illustrated in Figure 11.3, the RMS error is 0.108 Å.

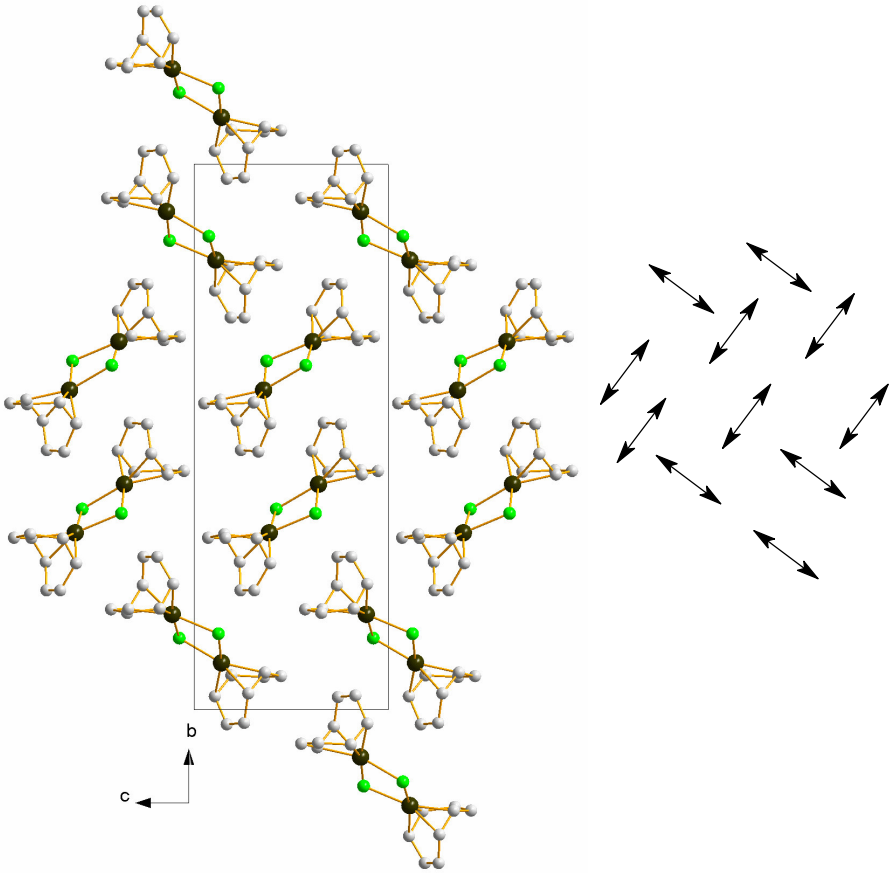

Figure 11.4 Packing of [Rh(cod)μ-Cl]$_2$ viewed along the *a*-axis with the packing motif incorporated to the right of the figure. Rhodium (dark green), carbon (grey) and chlorine (green). Hydrogens have been omitted for clarity.

The packing for [Rh(cod)μ-Cl]$_2$ viewed along the *a*-axis is presented in Figure 11.4, the packing motif as depicted to the right of the unit cell is defined as the head of the arrow being the 1,5-cyclo-octadiene moiety whilst the mid-point is the chloro

bridging. The packing observed is a clustered "head-to-tail", *i.e.* the tail being the mid-point of the arrow. This clustering is seen in the packing motif in that the arrows of the same direction form the cluster, this clustering is not tight and is slightly staggered.

11.3.2 Crystal structure of [Rh(cod)(acac)][4]

The structure of the title compound was re-determined at low temperature (100 K) to obtain a higher accuracy of the carbon and hydrogen positions within the *cis,cis*-1,5-cyclo-octadiene ring system co-ordinated to the rhodium(I) metal centre.

The compound, [Rh(cod)(acac)] (**25**), crystallized in the monoclinic space group *Cc*, with one molecule in the asymmetric unit. The numbering scheme is presented in Figure 11.5, while atomic co-ordinates, bond angles and distances, anisotropic displacement parameters and hydrogen co-ordinates are reported in Appendix B.26. General crystallographic data and refinement parameters are reported in Table 11.2, while significant bond angles and distances are reported in Table 11.5.

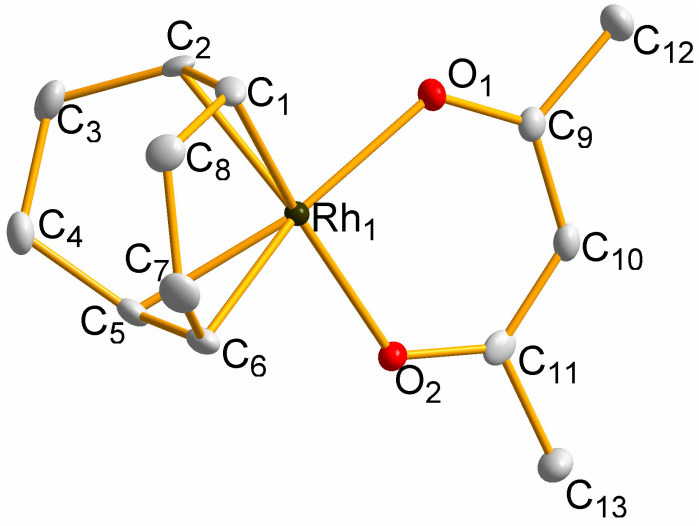

Figure 11.5 Diamond illustration of [Rh(cod)(acac)] (25) showing the numbering scheme and displacement ellipsoids (50 %) of the complex. Hydrogen atoms omitted for clarity.

Table 11.5 Selected bond distances and angles for [Rh(cod)(acac)] (25)

Bond Distance (Å)		Bond Angles (°)	
Rh-O_1	2.058(2)	O_1-Rh-O_2	90.9(1)
Rh-O_2	2.057(2)	C_1-Rh-C_2	38.5(1)
Rh-C_1	2.107(3)	C_5-Rh-C_6	38.8(1)
Rh-C_2	2.106(3)	C_1-Rh-C_6	83.0(1)
Rh-C_5	2.117(3)	C_2-Rh-C_5	82.1(1)
Rh-C_6	2.097(4)	χ^a	88.0(2)
C_1-C_2	1.388(4)	ψ^b	75.5(2)
C_5-C_6	1.399(4)		

a χ: $C_1MC_2 \cap C_5MC_6$ b ψ: $C_2C_3C_4C_5 \cap C_1C_8C_7C_6$ see Figure 1.2

The co-ordination geometry around the rhodium(I) metal centre is square planar as (Figure 4.2) formed by the co-ordination of the acetylacetonato and cyclo-octadiene moieties. Due to the twisted state of the co-ordinated cyclo-octadiene ring there is no 2-fold symmetry. The O_1-Rh-O_2 bite angle is 90.9(1)° which is close to the ideal value for a six membered bidentate ligand co-ordinated to a transition metal centre. The mean Rh-O and Rh-C bond lengths are 2.058(2) Å and 2.107(3) Å, which are comparable with the room temperature collection values of 2.06 Å and 2.103 Å respectively. The mean C=C bond distance was found to be 1.394(4) Å. The twist angle as defined by the intersection of the planes though the mid-point of the alkene carbons of the cyclo-octadiene ring and the oxygens of the acetylacetonato moiety and the rhodium with the back-bone of the acetylacetonato moiety was found to be 2.63(3)°.

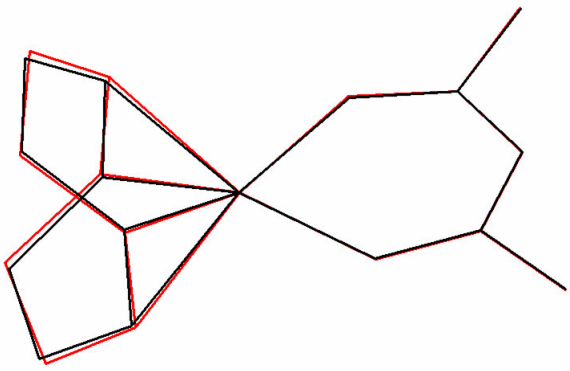

Figure 11.6 Hyperchem superimposed image of the low temperature determination (100 K, red) *vs.* the room temperature determination (295 K, black). RMS overlay error of 0.2 Å.

An illustration of the superimposed structures with an RMS overlay error of 0.2 Å can be seen in Figure 11.6. There were no major differences noted between the room

temperature collection and the low temperature recollection. The differences in the cell parameters and angles for the *a*-axis decreased from 6.854(5) Å to 6.7318(4) Å with a difference of Δa = 0.122(4) Å, the *b*-axis decreased from 18.645(10) Å to 18.3864(10) Å with a difference of Δb = 0.259(8) Å, the *c*-axis decreased from 9.864(7) Å to 9.8142(6) Å with a difference of Δc = 0.05(6) Å and the β angle increased from 93.1(2)° to 93.898(3)° with an absolute difference of Δβ = 0.8(2)°. There was an improvement in the *R*-value for the structure from 0.04 to 0.028.

The hydrogen bonding of complex **25** is graphically presented in Figure 11.7 with Table 11.6 listing the bond distances and angles.

Table 11.6 Hydrogen bond distances and angles for [Rh(cod)(acac)] (25) [Å and °].

D-H...A	d(D-H)	d(H...A)	d(D...A)	<(DHA)
C_{13}-H_{13C}...$O_1^{\#1}$	0.98	2.57	3.528(4)	164.2

Symmetry transformations used to generate equivalent atoms:
#1 x-1,y,z

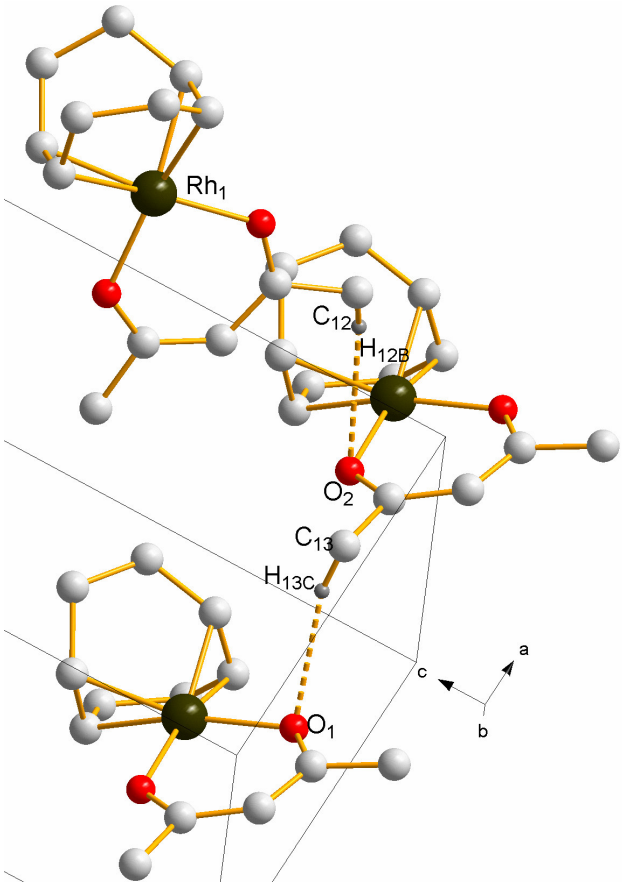

Figure 11.7 Partial unit cell of [Rh(cod)(acac)] showing intermolecular hydrogen bonding interactions indicated by a dashed bond. Only selected hydrogen atoms are included.

Figure 11.7 shows both the intermolecular hydrogen bonding as well as the weak hydrogen bonding interactions which are listed in Table 11.6. A weak hydrogen bonding interaction can be seen between oxygen (O_2) of the acetylacetonato moiety and the hydrogen of the methyl carbon (C_{12}) of the acetylacetonato moeity. A classical hydrogen bond can be found between O_1 and the hydrogen of the methyl carbon (C_{13}) of the acetylactonato moiety.

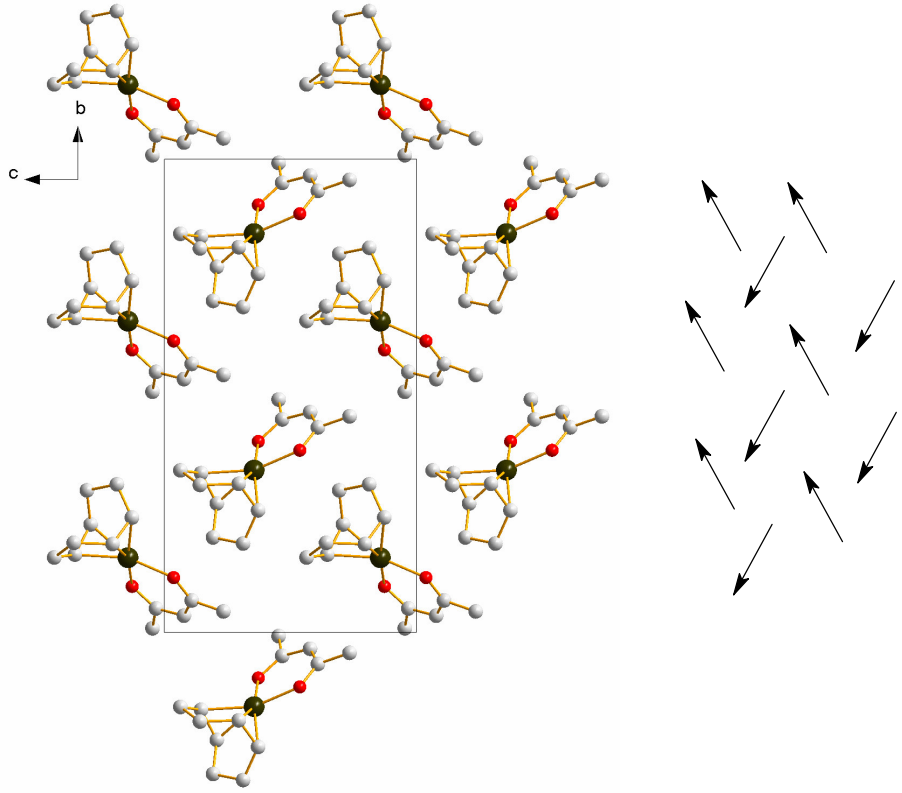

Figure 11.8 Packing of [Rh(cod)(acac)] viewed along the *a*-axis with the packing motif incorporated to the right of the figure. Rhodium (dark green), carbon (grey) and oxygen (red). Hydrogens omitted for clarity.

The packing motif to the right in Figure 11.9 is defined as the head of the arrow representing the cyclo-octadiene moiety whilst the tail of the arrow represents the acetylacetonato moiety. The molecular packing of [Rh(cod)(acac)] depicts a stepped head-to-tail across the diagonals. The closest rhodium-rhodium contact is 6.6892(5) Å it was therefore concluded that no metal interactions are present. No metal chelate ring interactions were observed for the conjugated rhodium acetylacetonato ring system.

11.3.3 Crystal structure of [Rh(cod)(dbm)]

The compound, [Rh(cod)(dbm)], was found to have a global pseudo-symmetry. Upon further inspection the value for $|E^2 - 1|$ (0.882) was too high for a non-centrosymmetric space group, as a result the centrosymmetric space group *C*2/*c* which had a lower CFOM (1.64) value than that for the *Cc* (3.19) a non-centrosymmetric space group was selected. Attempts to solve the structure in the monoclinic space group *C*2/*c*, the 2-fold crystallographic symmetry operator was *almost but not quite* related, resulting in a pseudo-centrosymmetric structure. The structure was then resolved with the 2-fold symmetry operator contributing to a racemic twin in the monoclinic space group *Cc* with one molecule in the asymmetric unit, improved *R*-values were the final selection.

The numbering scheme is presented in Figure 11.9, while atomic co-ordinates, bond angles and distances, anisotropic displacement parameters and hydrogen co-ordinates are reported in Appendix B.27. General crystallographic data and refinement parameters are reported in Table 11.2, while significant bond angles and distances are reported in Table 11.7.

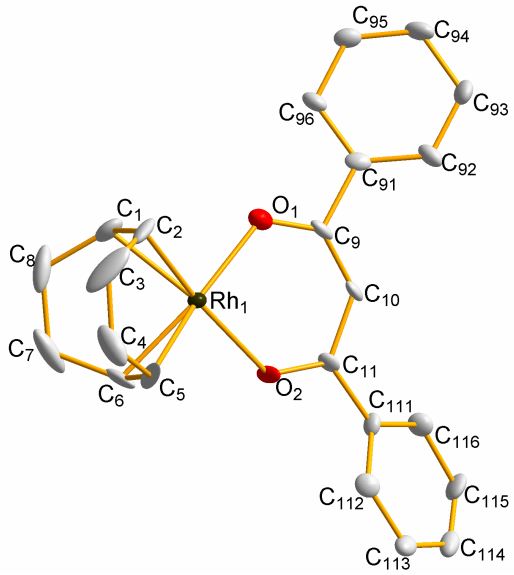

Figure 11.9 Diamond illustration of [Rh(cod)(dbm)] at 100 K showing the numbering scheme and displacement ellipsoids (50 %) of the complex. Hydrogen atoms omitted for clarity.

Table 11.7 Selected bond distances and angles for [Rh(cod)(dbm)]

Bond Distance (Å)		Bond Angles (°)	
Rh-O_1	2.051(10)	O_1-Rh-O_2	91.2(1)
Rh-O_2	2.052(9)	C_1-Rh-C_2	39.7(4)
Rh-C_1	2.128(13)	C_5-Rh-C_6	36.6(5)
Rh-C_2	2.116(12)	C_1-Rh-C_6	84.2(5)
Rh-C_5	2.079(12)	C_2-Rh-C_5	81.3(5)
Rh-C_6	2.067(11)	χ^a	88.8(2)
C_1-C_2	1.442(15)	ψ^b	74.8(7)
C_5-C_6	1.303(16)		

a χ: $C_1MC_2 \cap C_5MC_6$ b ψ: $C_2C_3C_4C_5 \cap C_1C_8C_7C_6$ see Figure 1.2

A square planar co-ordination geometry is present around the central metal atom formed by the cyclo-octadiene and dibenzoylmethane moieties. The mean Rh-O bond length was found to be 2.05(1) Å. The bond lengths to the alkene carbons were found to be non-symmetrical in that the mean distance for Rh-C_1 / Rh-C_2 and Rh-C_5 / Rh-C_6 were 2.12(1) Å and 2.07(1) Å respectively differing by 0.05 Å. The mean Rh-C bond distance observed was 2.098(12) Å. The average mean C=C bond distance was found to be 1.373(16) Å. This difference is as a result of the molecule being a merohedral racemic twin and the cyclo-octadiene ring system showing fairly large ellipsoids. No hydrogen bonds were observed in the complex. The two phenyl rings are twisted out of the plane defined by the rhodium and the acetylacetonato moiety by 30.0(4)° and 29.7(4)°. The shortest Rh-Rh contact is 6.585(7) Å, indicating no metal interactions. The measure of distortion from the square planar co-ordination geometry (*i.e.* twist angle) was obtained by the intersection of the planes defined as the mid-points of the alkene carbons of the cyclo-octadiene moiety and the oxygens of the dibenzoylmethane moiety, and the rhodium metal centre and the back-bone of the dibenzoylmethane moiety was found to be 1.4(3)°.

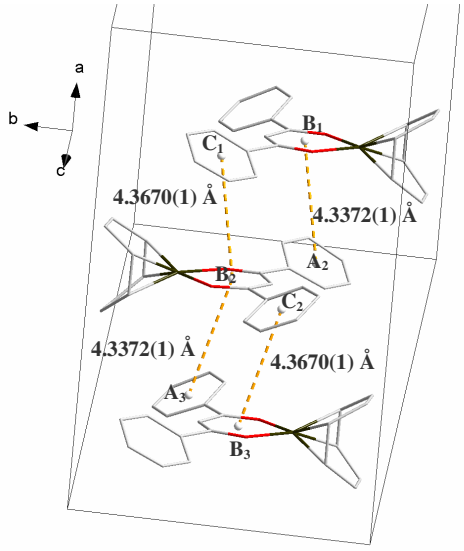

Figure 11.10 Diamond illustration indicating π···metal chelate ring interactions for [Rh(cod)(dbm)] are depicted by dashed bonds. Hydrogen atoms and counter ions have been omitted for clarity. Rhodium (dark green), carbon (grey) and oxygen (red).

The packing of the unit cell seen in Figure 11.10 for [Rh(cod)(dbm)] depicts the π···metal chelate ring interactions observed, the first type was that of a ladder between the B3 ring to C2 ring and the A2 ring to the B1 ring. The second type was that of a pipe structure formed by the A3 ring to the B2 ring to the C1 ring. The average distance was found to be 4.352 Å.

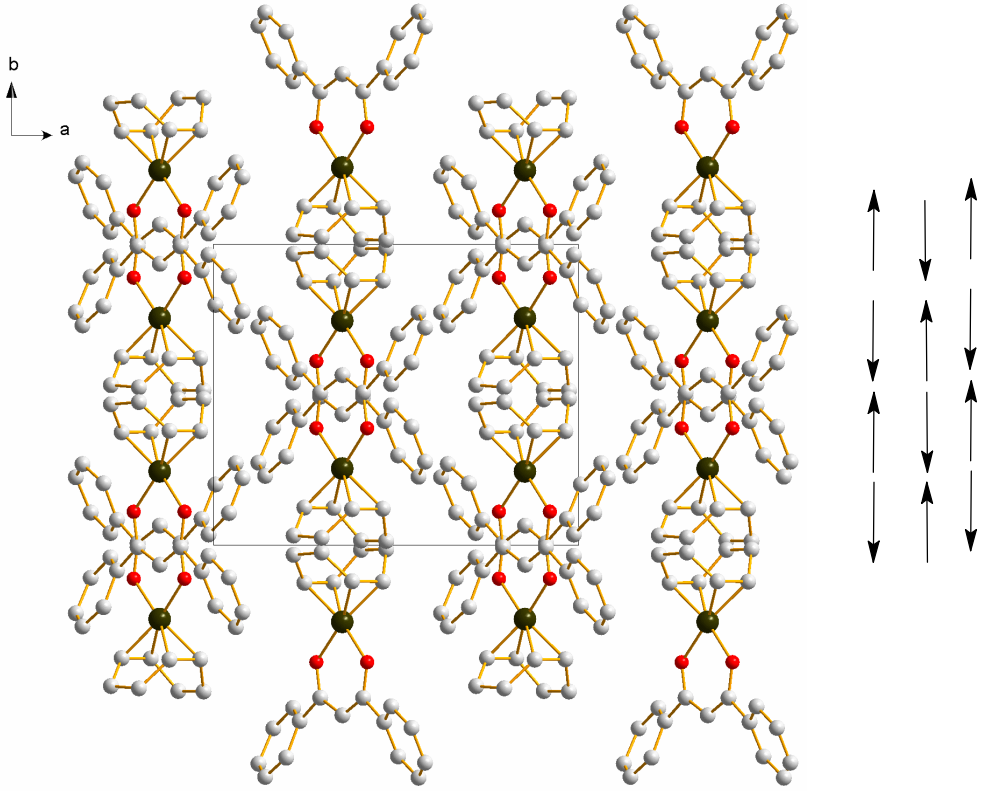

Figure 11.11 Packing of [Rh(cod)(dbm)] viewed along the *c*-axis, illustrating the packing of the phenyl rings with the packing motif incorporated to the right of the figure. Rhodium (dark green), carbon (grey) and oxygen (red).

The packing motif as found in Figure 11.11 is defined as the head of the arrow depicting the cyclo-octadiene ring whilst the tail of the arrow represents the dibenzoylmethane moiety. The packing was found to be tail-to-tail, as a result of this packing the phenyl rings form a diamond shaped structure enclosing the rest of the molecule as can be clearly seen in Figure 11.11.

11.3.4 Crystal structure of [Rh(cod)(thtfac)]

The compound [Rh(cod)(thtfac)] (**27**) crystallized in the monoclinic space group $P2_1/n$, with one molecule in the asymmetric unit. The numbering scheme is presented in Figure 11.12, while atomic co-ordinates, bond angles and distances, anisotropic displacement parameters and hydrogen co-ordinates are reported in Appendix B.28. General crystallographic data and refinement parameters are reported in Table 11.2, while significant bond angles and distances are reported in Table 11.8.

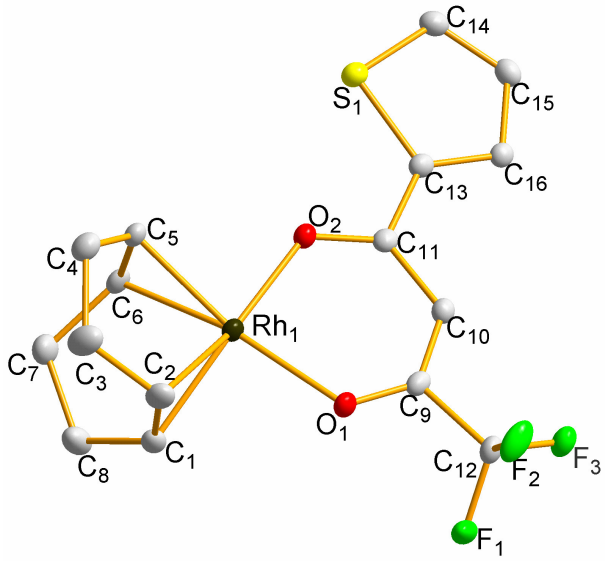

Figure 11.12 Diamond illustration of [Rh(cod)(thtfac)] at 100 K showing the numbering scheme and displacement ellipsoids (30 %) of the complex. Hydrogen atoms omitted for clarity.

Table 11.8 Selected bond distances and angles for [Rh(cod)(thtfac)]

Bond Distance (Å)		Bond Angles (°)	
Rh-O_1	2.074(3)	O_1-Rh-O_2	90.7(1)
Rh-O_2	2.051(3)	C_1-Rh-C_2	38.8(2)
Rh-C_1	2.095(4)	C_5-Rh-C_6	39.0(2)
Rh-C_2	2.114(4)	C_1-Rh-C_6	82.4(2)
Rh-C_5	2.095(4)	C_2-Rh-C_5	82.3(2)
Rh-C_6	2.112(4)	χ^a	88.3(2)
C_1-C_2	1.397(7)	ψ^b	76.4(3)
C_5-C_6	1.405(6)		

a χ: $C_1MC_2 \cap C_5MC_6$ b ψ: $C_2C_3C_4C_5 \cap C_1C_8C_7C_6$ see Figure 1.2

Square planar co-ordination geometry is found around the rhodium metal centre with the cyclo-octadiene and thenoyltrifluoacetonato moieties. The bidentate bite angle (O_1-Rh-O_2) is close to ideal 90.7(1)°. The Rh-O bond distances vary by 0.02 Å, which is due to the withdrawing effect of the CF_3 moiety with a mean distance of 2.063(3) Å. Interesting to note that the alkene bonds which are perpendicular to the rhodium acetylactonato plane are a slightly twisted, this can be seen in the Rh-C_1 and Rh-C_2 bond lengths 2.095(4) Å and 2.114(4) Å where C_1 is equal to C_5 and C_2 is equal to C_6. A mean Rh-C bond distance of 2.104(4) Å was observed. The C=C mean bond distance was found to be 1.401(7) Å. The intersection between the plane though the thenoyl ring and a plane defined by the rhodium, oxygen and carbon backbone of the acetylactonato-type moiety was found to be 11.0(7)°. No disorder was found for the fluorine atoms on the thenoyltrifluoroactonato moeity. The measure of distortion from the square planar co-ordination geometry (*i.e.* twist angle)

was obtained by the intersection of the planes defined as the mid-points of the alkene carbons of the cyclo-octadiene moiety, and the oxygens of the thenoyltrifluoroacetonato moiety with the rhodium metal centre and the back-bone of the thenoyltrifluoroacetonato moiety, was found to be 2.64(5)°.

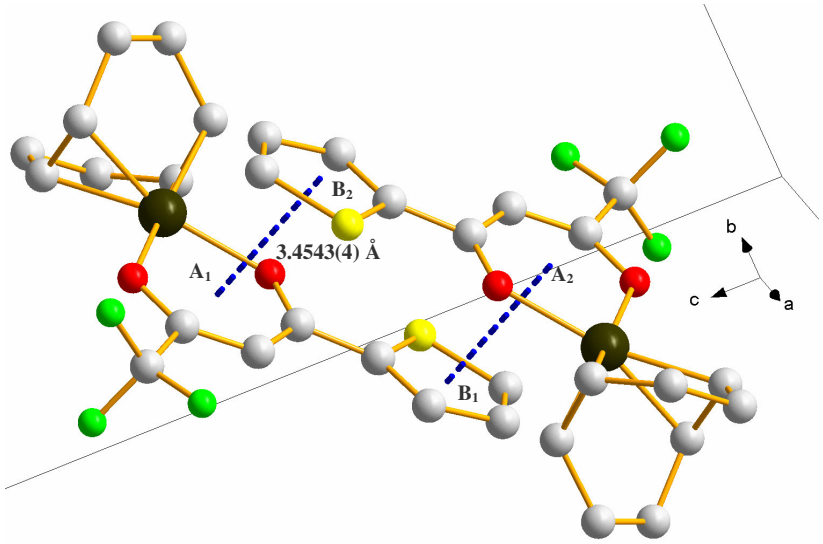

Figure 11.13 Diamond illustration indicating π···metal chelate ring interactions for [Rh(cod)(thtfac)]. Hydrogen atoms have been omitted for clarity. Rhodium (dark green), carbon (grey), fluorine (green), sulfur (yellow) and oxygen (red).

The π···metal chelate ring interactions were observed between the thenoyl ring (B_1) and the ring formed by the rhodium with the co-ordinated acetylactonato (A_2) moiety of an adjacent molecule, the distance was 3.4543(4) Å in all cases (Figure 11.13). A weak hydrogen interaction can be found between fluorine and an alkane carbon of the cyclo-octadiene ring ($F_3\cdots H_{8A}\text{-}C_8$, [0.5+x, 1.5-y, 0.5+z], d(H…A) 2.789(4) Å, <(DHA) 152.2(3)^o) this is depicted by the turquoise dashed bonds in Figure 11.14. The intra-cluster rhodium distance was found to be 7.043(1) Å, whereas the inter-cluster rhodium distance was found to be 5.491(1) Å, this is also the shortest Rh···Rh contact concluding that there are no interactions between the metal centers.

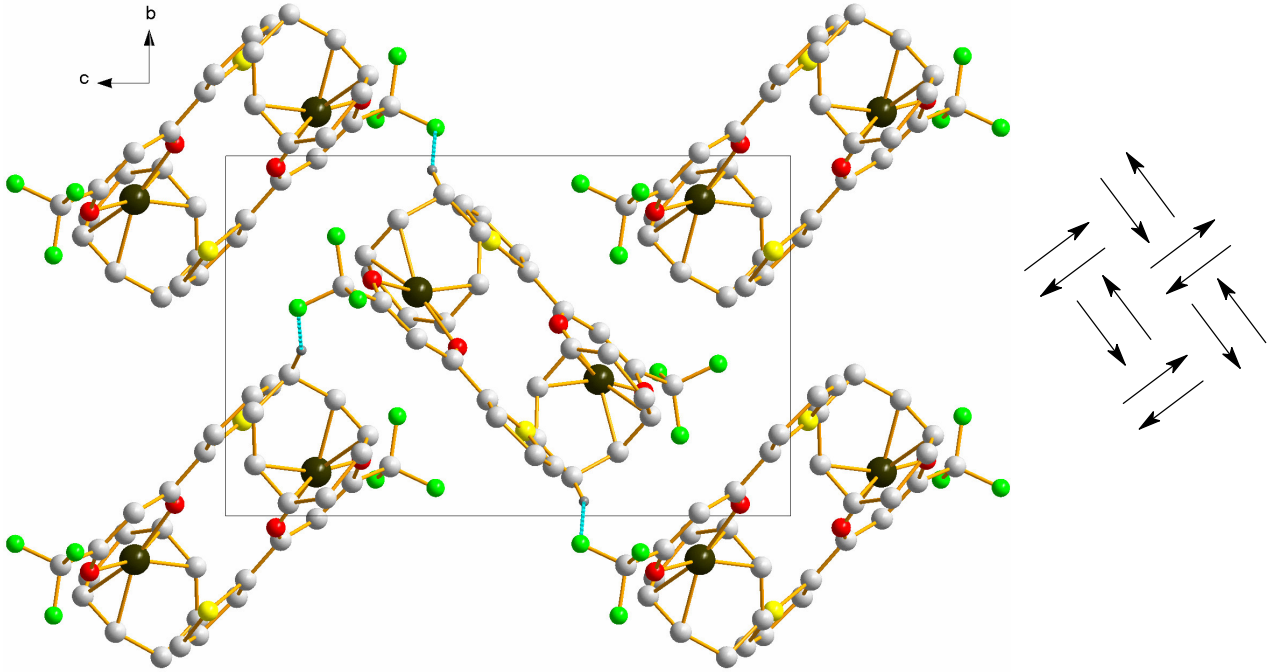

Figure 11.14 Unit cell of [Rh(cod)(thtfac)] viewed along the *a*-axis, illustrating the packing of the thenoyl and metal chelate rings as well as weak intermolecular hydrogen bonding interactions indicated by a dashed turquoise bond with the packing motif incorporated to the right of the figure. Only selected hydrogen atoms are included. Rhodium (dark green), carbon (grey), fluorine (green), sulfur (yellow) and oxygen (red).

The packing motif to the right of the unit cell as seen in Figure 11.14 is defined as the head of the arrow representing the cyclo-octadiene ring whilst the tail of the arrow represents the thenoyltrifluoroacetonato moiety. Clustered head-to-tail packing is seen where the CF_3 moieties are found on the opposite sides of the rectangular cluster of molecules, this can clearly be seen in Figure 11.14.

11.3.5 Crystal structure of [Rh(cod)(trop)]

The compound, [Rh(cod)(trop)], crystallized in the orthorhombic space group $P2_12_12_1$, with one molecule in the asymmetric unit and an absolute structure parameter of 0.52(2). The numbering scheme is presented in Figure 11.15, while atomic co-ordinates, bond angles and distances, anisotropic displacement parameters and hydrogen co-ordinates are reported in Appendix B.29. General crystallographic data and refinement parameters are reported in Table 11.2, while significant bond angles and distances are reported in Table 11.9.

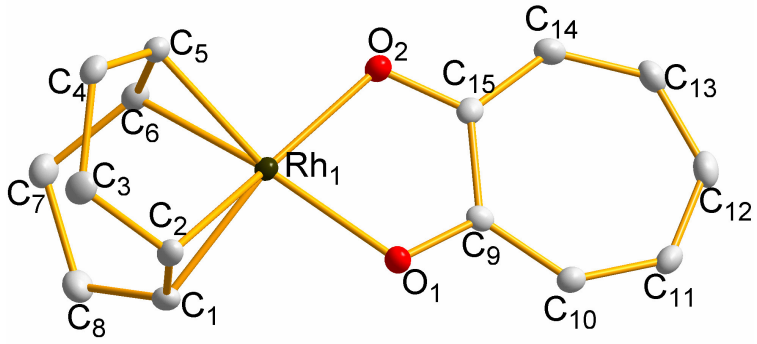

Figure 11.15 Diamond illustration of [Rh(cod)(trop)] at 100 K showing the numbering scheme and displacement ellipsoids (50 %) of the complex. Hydrogen atoms omitted for clarity.

Table 11.9 Selected bond distances and angles for [Rh(cod)(trop)]

Bond Distance (Å)		Bond Angles (°)	
Rh-O_1	2.057(1)	O_1-Rh-O_2	79.31(5)
Rh-O_2	2.060(1)	C_1-Rh-C_2	39.07(7)
Rh-C_1	2.097(2)	C_5-Rh-C_6	38.65(7)
Rh-C_2	2.107(2)	C_1-Rh-C_6	82.36(6)
Rh-C_5	2.102(2)	C_2-Rh-C_5	82.75(6)
Rh-C_6	2.112(2)	χ^a	88.02(7)
C_1-C_2	1.406(2)	ψ^b	73.7(1)
C_5-C_6	1.394(3)		

a χ: $C_1MC_2 \cap C_5MC_6$ b ψ: $C_2C_3C_4C_5 \cap C_1C_8C_7C_6$ see Figure 1.2

The co-ordination geometry around the metal centre is found to be square planar co-ordinating with a 1,5-cyclo-octadiene moiety and a tropolonato moiety. The shortest Rh-Rh contact was found to be 6.4045(2) Å, indicating no metal interactions. The compound was solved as a racemic twin with the percentage of twinning being 52.4%. The Rh-O, Rh-C and C=C average bond length were found to be 2.058(2) Å, 2.105(2) Å and 1.400(2) Å respectively. The measure of distortion from the square planar co-ordination geometry (twist angle) was obtained by the intersection of the planes defined as the mid-points of the alkene carbons of the cyclo-octadiene moiety and the oxygens of the tropolonato moiety and the rhodium metal centre and the back-bone of the troplonato moiety was found to be 2.35(2)°.

Table 11.10 Hydrogen bond distances and angles for [Rh(cod)(trop)] [Å and °].

D-H...A	d(D-H)	d(H...A)	d(D...A)	<(DHA)
C_{13}-H_{13}...$O_2^{\#1}$	0.95	2.45	3.387(2)	167.4

Symmetry transformations used to generate equivalent atoms:
#1 x-1/2,-y+1/2,-z+1

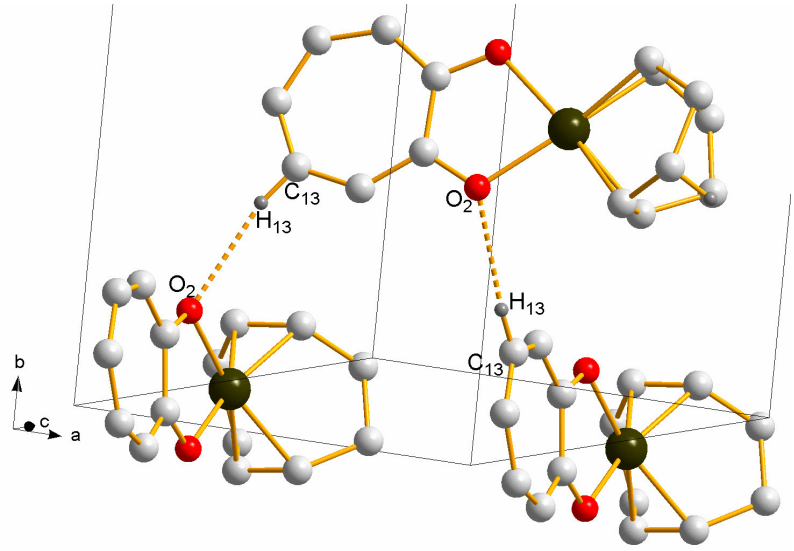

Figure 11.16 Partial unit cell of [Rh(cod)(top)] showing intermolecular hydrogen bonding interactions indicated by a dashed bond. Only selected hydrogen atoms are included. Rhodium (dark green), carbon (grey) and oxygen (red).

An intermolecular hydrogen interaction exists (Table 11.10) between the oxygen (O_2) of the tropolonato ring with a hydrogen of an adjacent tropolone (C_{13}) ring (Figure 11.16) this leads to an interesting zig-zag packing of the tropolone rings which is clearly observable in Figure 11.17.

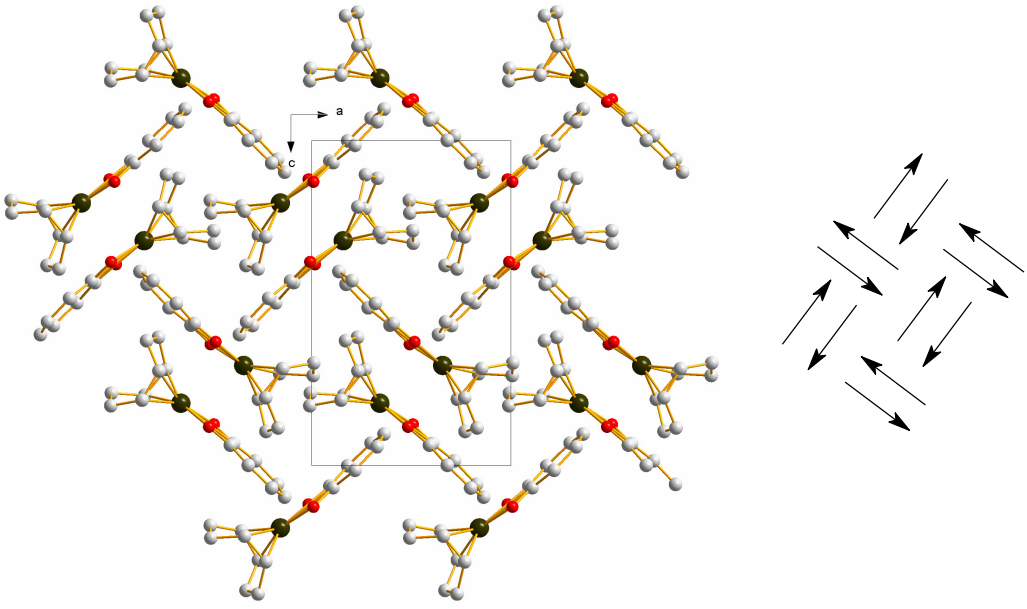

Figure 11.17 Packing of the unit cell of [Rh(cod)(trop)] viewed along the *b*-axis with the packing motif incorporated to the right of the figure. Rhodium (dark green), carbon (grey) and oxygen (red).

The packing motif as seen on the right in Figure 11.17 is defined as the head of the arrow being the cyclo-octadiene moiety whilst the tail of the arrow represents the

troplonato moiety. The packing found for [Rh(cod)(trop)] is a tight clustered head-to-tail.

11.4 Discussion

The rhodium single crystals that were obtained have been listed in Table 11.11 which includes the space group and cell dimensions. Selected bond distances and angles of the aforementioned complexes are listed in Table 11.12.

Table 11.11 Cell dimension overview of rhodium crystals obtained.

	$[Rh(cod)Cl]_2$ 293 K (**29**)	$[Rh(cod)Cl]_2$ 100 K (**30**)	[Rh(cod)(acac)] 100 K (**25**)	[Rh(cod)(dbm)] 100 K (**26**)	[Rh(cod)(thtfac)] 100 K (**27**)	[Rh(cod)(trop)] 100 K (**28**)
Crystal system	Monoclinic	Monoclinic	Monoclinic	Monoclinic	Monoclinic	Orthorhombic
Space group	$P2_1/n$	$P21/n$	Cc	Cc	$P2_1/n$	$P2_12_12_1$
a (Å)	7.2856(3)	7.2913(5)	6.7318(4)	17.1455(4)	11.140(2)	8.3210(2)
b (Å)	25.4257(11)	25.1318(14)	18.3864(10)	10.7094(4)	9.425(2)	11.2494(3)
c (Å)	9.0497(4)	8.8599(6)	9.8142(6)	13.0229(4)	15.277(3)	13.5631(4)
α (°)	90	90	90	90	90	90
β (°)	92.006(2)	91.068(2)	93.898(3)	130.526(2)	104.128(9)	90
γ (°)	90	90	90	90	90	90
Z	4	4	4	4	4	4

All the rhodium complexes reported in this chapter were found to have a slightly distorted square planar co-ordination geometry. The measure used for this distortion is known as the twist angle which is the intersection between the planes defined by the mid-points of the alkene carbons of the cyclo-octadiene and the oxygens of the O,O-bidentate type ligands and the metal centre with the back-bone of the O,O-bidentate type ligands. For the rhodium complexes it was found that the distortion is rather minor with the series being **26** > **28** > **25** ≈ **27** with values of 1.40(3)°, 2.35(2)°, 2.63(3)° and 2.64(5)°.

A similar clustered tail-to-head packing was found for $[Pt(cod)(dbm)]BF_4$ (**9**) (Figure 5.11), [Rh(cod)(thtfac)] (**27**) (Figure 11.14), [Rh(cod)(trop)] (**28**) (Figure 11.17), $[Pd(cod)(thtfac)]BF_4$ (**4**) (Figure 4.19) and $[Pd(cod)(thtfac)]PF_6$ (**3**) (Figure 4.20) complexes. The π···metal chelate ring interaction observed for complexes **9** and **26** are nearly identical in that both have a ladder and the pipe (Figure 11.11 and 5.10) type structures, the difference in the interaction distances was marginal at 0.5 Å. Both of these structures display twinning. In the case of the $[Pt(cod)(dbm)]BF_4$ crystal

structure a complete solution was not found due to the complexity of the twinning within the crystal, in the case of the [Rh(cod)(dbm)] (**26**) crystal structure the twinning was found to be a simple merohedral racemic twin. The average distance between the Pt-O is 2.014 Å and Rh-O is 2.051 Å. The O-M-O bite angles are 90.5(1)° for **9** and 91.2(1)° for **26**. This illustrates a well behaved O,O-bidentate system for both complexes. However the 1,5-cyclo-octadiene ring system is not so well behaved in complex **9** with bonding discrepancies from the standard 1,5-alkene bonding mode being observed. The reasons for this abnormality are at this point still unclear.

The other π···metal chelate ring interaction was found between [Pt(cod)(thtfac)]BF_4 (**10**) (Figure 5.17) and [Rh(cod)(thtfac)] (**27**) (Figure 11.13). Interestingly the [Pd(cod)(thtfac)]BF_4 and [Pd(cod)(thtfac)]PF_6 both have a F···metal chelate ring interaction and no π···metal chelate ring interaction. The distances for complex **10** were found at 4.1119(0) Å and 3.8751(0) Å and for complex **27** a value of 3.4543(4) Å was obtained. The difference in interaction distance was *c.a.* 0.66 Å and 0.42 Å with complex **10** found to be larger. With a similar difference in distance observed for complexes **9** and **26**. A possible reason for the differences in the distances of the π···metal chelate ring interactions are the inclusion of the counter ions in the packing of the crystal structures thus not allowing as tight a packing arrangement as is possible for a neutral complex such as **26** and **27**.

Table 11.12 Selected Geometric parameters (Å,°) where X = Cl, O or N respectively for rhodium metal complexes

	$[Rh(cod)Cl]_2$ 293 K (**29**)	$[Rh(cod)Cl]_2$ 100 K (**30**)	[Rh(cod)(acac)] 100 K (**25**)	[Rh(cod)(dbm)] 100 K (**26**)	[Rh(cod)(thtfac)] 100 K (**27**)	[Rh(cod)(trop)] 100K (**28**)
$Rh–X_1$			2.058(2)	2.051(10)	2.074(3)	2.057(1)
$Rh–X_2$			2.057(2)	2.052(9)	2.051(3)	2.060(1)
$Rh-C_1$	2.089(5)	2.093(3)	2.107(3)	2.128(13)	2.095(4)	2.097(2)
$Rh-C_2$	2.108(4)	2.115(3)	2.106(3)	2.116(12)	2.114(4)	2.107(2)
$Rh-C_5$	2.088(4)	2.086(3)	2.117(3)	2.079(12)	2.095(4)	2.102(2)
$Rh-C_6$	2.087(5)	2.098(3)	2.097(4)	2.067(11)	2.112(4)	2.112(2)
C_1-C_2	1.382(7)	1.404(5)	1.388(4)	1.442(15)	1.397(7)	1.406(2)
C_5-C_6	1.376(8)	1.402(5)	1.399(4)	1.303(16)	1.405(6)	1.394(3)
X_1-Rh-X_2			90.9(1)	91.2(1)	90.7(1)	79.31(5)
C_1-Rh-C_2	38.4(2)	39.0(1)	38.5(1)	39.7(4)	38.8(2)	39.07(7)
C_5-Rh-C_6	38.5(2)	39.1(1)	38.8(1)	36.6(5)	39.0(2)	38.65(7)
C_1-Rh-C_5			83.0(1)	84.2(5)	82.4(2)	82.36(6)
C_2-Rh-C_6			82.1(1)	81.3(5)	82.3(2)	82.75(6)
χ^a	88.2(2)	88.6(2)	88.0(2)	88.8(2)	88.3(2)	88.02(7)
ψ^b	77.8(4)	77.0(2)	75.5(2)	74.8(7)	76.4(3)	73.7(1)

a χ: $C_1MC_2 \cap C_5MC_6$ b ψ: $C_2C_3C_4C_5 \cap C_1C_8C_7C_6$ see Figure 1.2

There is however no systematic increase in the Rh-O and Rh-C bond lengths as the co-ordinating ligands were changed. The O-Rh-O bite angles observed for the six membered ring systems (those being acac, dbm and thtfac) are well within expected values for standard six membered O,O-bidentate systems (90°). An increase in the Rh-O bond distance is not observed between the five membered and six membered ring systems.

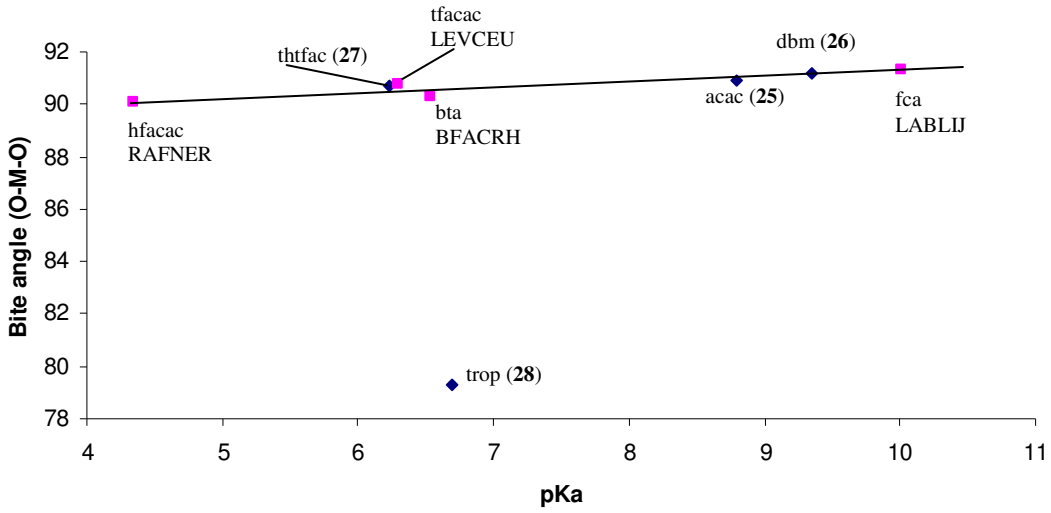

Figure 11.18 Graph of pK_a *vs*. O-M-O bite angle for the [Rh(cod)(LL')] where LL' = acac, thtfac, trop complexes (blue diamonds) and CSD complexes (pink squares).

The graph of the acid dissociation constant (pK_a) *vs*. the O-Rh-O bite angle as seen in Figure 11.18 shows a slight increasing tendency in the bite angle as the pK_a is increased. The points represented by the pink squares are previously published values the CSD reference code is listed with the ligand abbreviation (Table 11.1). The cluster that is seen in the centre of the graph represents ligands with only one CF_3 moiety. The electronegativity of the CH_3 moiety is 2.30 for phenyl 3.00 and for CF_3 a value of 3.35. As one proceeds from left to right the electronegativity of the ligands decreases and the bite angle increases. The reason for complex **28** to be an "outlier" is simply as a result of the metal chelate ring co-ordination number being five as opposed to six, resulting in a smaller bite angle.

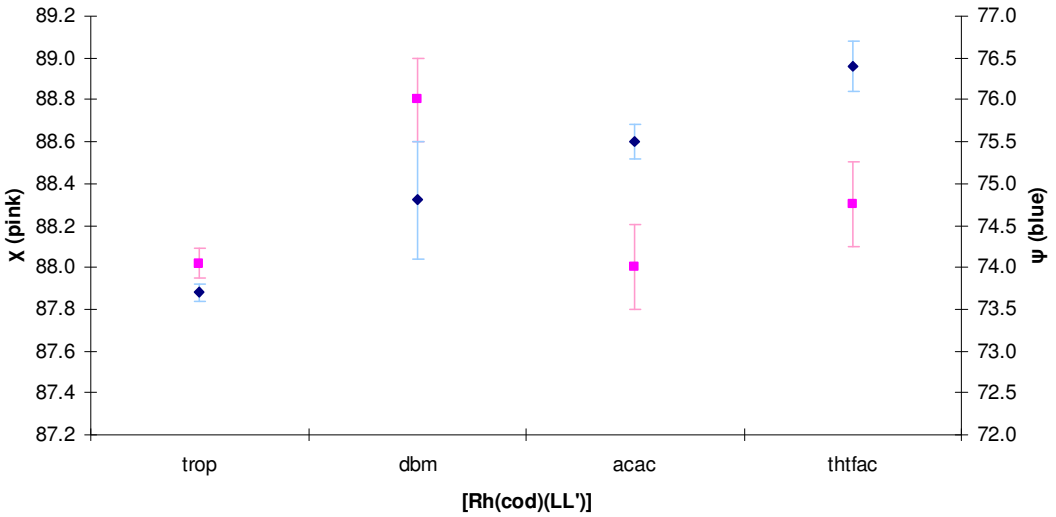

Figure 11.19 Graph of [Rh(cod)(L)] *vs.* χ angle (pink squares) *vs.* ψ angle (blue diamonds) (see Chapter 1 Figure 1.2 for definition of χ and ψ angles).

In the graph shown in Figure 11.19 it is observed that with an increase in the ψ angle we discover the χ angle remains virtually constant. The increase seems consistant with the decrease in pKa values as well as decreasing electronegativities. The ψ angle, on the other hand increases by 2.7° (*i.e.* an opening of the jaws of the venus-fly trap) as the electronegativity of the β-diketonato type counter ligand is decreased.

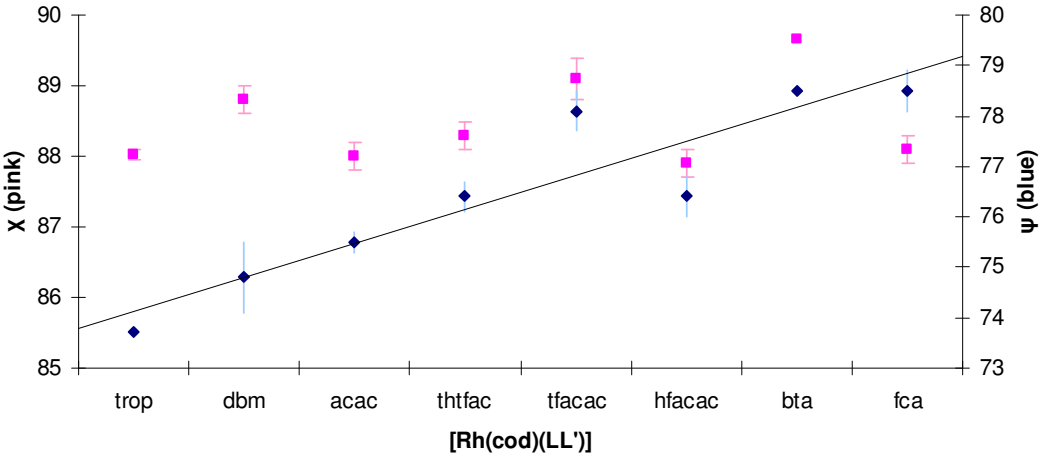

Figure 11.20 Graph of [Rh(cod)(L)] *vs.* χ angle (pink squares) *vs.* ψ angle (blue diamonds) (see Chapter 1 Figure 1.2 for definition of χ and ψ angles).

In Figure 11.20 the trend that was observed for the crystal structures presented in this chapter (Figure 11.19) was continued when the data from the structures (Table 11.1) obtained from the CSD were included. In total a 4.8° variation in the opening of the Venus fly-trap jaws (ψ angle) was observed.

The overlay of the X-ray crystal structures is a graphical representation of the pair-wise differences of the related structures. This mathematical value is represented by the root mean square (RMS) value, which is a measure of how far the average is from zero, providing information on the variations of bond lengths and angles and to a certain degree the orientation of the structures in relation to each other. These comparisons are presented in Figure 11.21 and 11.27.

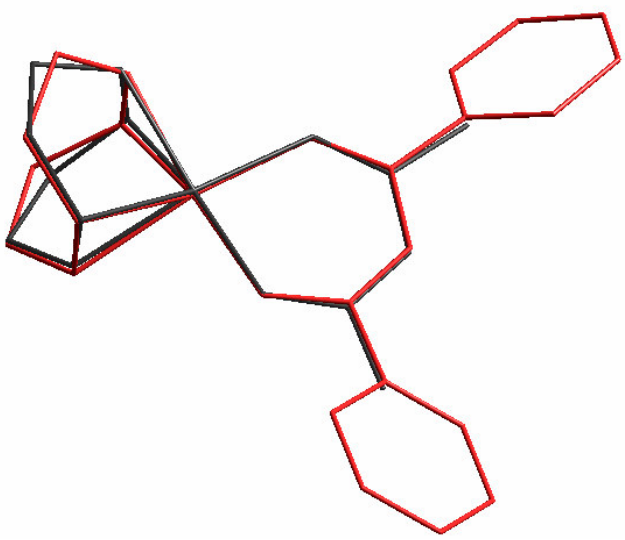

Figure 11.21 HyperChem superimposed image of [Rh(cod)(acac)] (25) (black) *vs*. [Rh(cod)(dbm)] (26) (red) with an RMS error of 0.18 Å.

In the overlay of complexes **25** and **26** (Figure 11.21) an RMS error of 0.18 Å was observed. The RMS error value was determined by the selection of the atoms that were in common with both structures, thus the phenyl rings of complex **26** were omitted from the determination. The differences found between the structures were that of the cyclo-octadiene ring where only two of the alkane carbons were found in different positions. This leads to the increase in ψ angle that was found in Figure 11.19 and explains why the χ angle is similar.

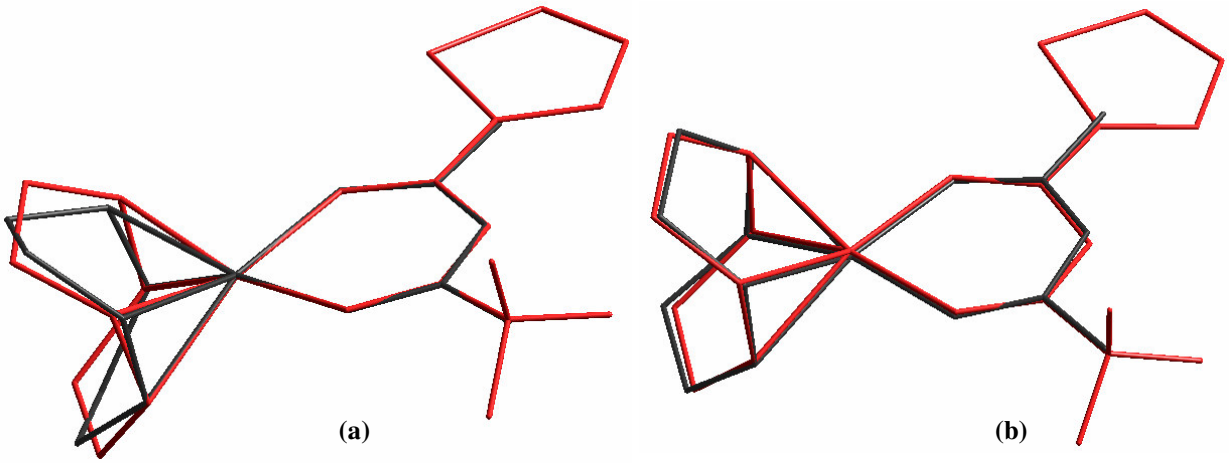

Figure 11.22 HyperChem superimposed image of (a) [Rh(cod)(acac)] (25) (black) *vs*. [Rh(cod)(thtfac)] (27) (red) with an RMS error 0.03 Å (b) [Rh(cod)(acac)] inverted crystal structure (25) (black) *vs*. [Rh(cod)(thtfac)] (27) (red) with an RMS error 0.125 Å.

In the overlay of complexes **25** and **27** an RMS error of 1.79 Å was determined by the selection of the atoms that were in common with both structures, thus the thenoyl and CF_3 moieties were omitted. The reason for this large RMS error value is due to the orientation of the alkane carbons thus creating a twist in the overlay of the structures. In Figure 11.22a the RMS error of 0.03 Å was obtained as the selection of atoms chosen for the overlay were the rhodium metal centre and the back-bond of the β-diketonato ligand, clearly showing the twist that was previously mentioned for the cyclo-octadiene ligand. Complex **25** is however in a centrosymmetric space group (monoclinic *Cc*) and as a result there is a second enantiomer in the unit cell, this enantiomer was overlaid with complex **27** (Figure 11.22b) and an RMS error of 0.125 Å was obtained for all atoms in common with both structures.

11.5 Theoretical Correlation of Rhodium(I) Complexes

In the periodic table rhodium falls into group 9 along with cobalt and iridium, the metals prefer a square planar co-ordination geometry with a d^8-electron configuration resulting in a +1 oxidation state. The covalent atomic radii, using the 2008 values determined by Cordero[29] *et. al.* of the metals are 1.26, 1.42 and 1.41 respectively for cobalt, rhodium and iridium (Table 2.4).

[29] Cordero B., Gómez V., Platero-Prats A.E., Revés M., Echeverría J., Cremades E., Barragán F., Alvarez S., *Dalton Trans.*, (2008)

11.5.1 Visual Associations

Visual geometric comparisons of the computed structures *vs.* their X-ray crystal structures are presented. The overlay of the X-ray crystal structure with the calculated structure is a graphical representation of the pair-wise differences of the related structures. This mathematical value is represented by the root mean square (RMS) value, which is a measure of how far the average is from zero, providing information on the variations of bond lengths and angles and to a certain degree the orientation of the structures in relation to each other. These comparisons are presented below in Figure 11.23 and 11.29.

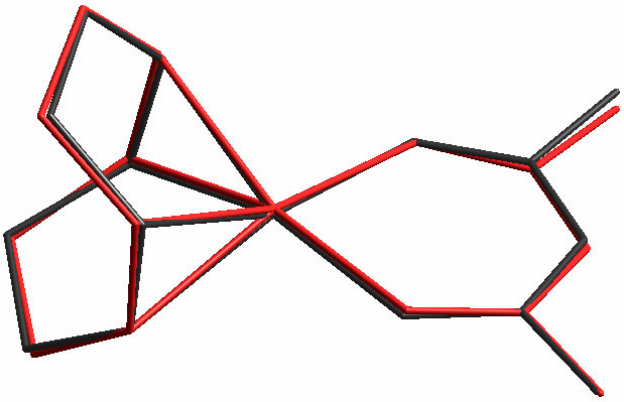

Figure 11.23 HyperChem superimposed image of [Rh(cod)(acac)] (25) (black) *vs*. [Rh(cod)(acac)] (calculated) (red) with an RMS error of 0.083 Å.

An overlay of the X-ray crystal structure of [Rh(cod)(acac)] (**25**) with the optimized computational structure is presented in Figure 11.23 with an RMS error value of 0.08 Å based on all the atoms excluding the methyl carbons of the acetylacetonato ligand. The only significant difference observed is with the cyclo-octadiene ring being slightly twisted.

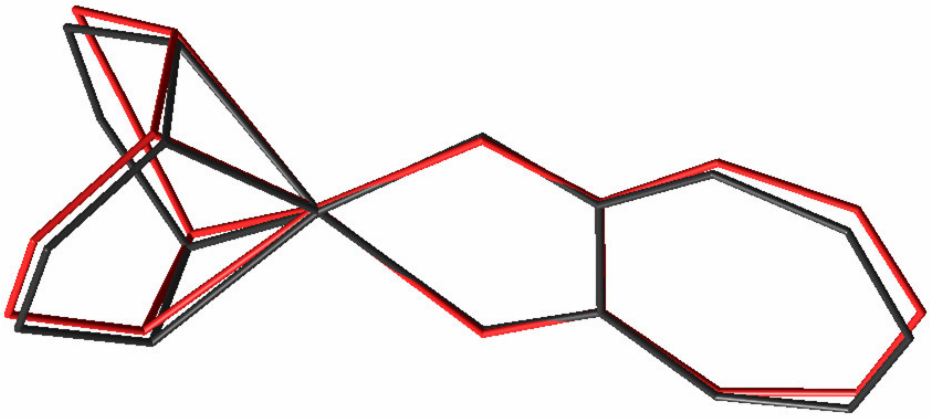

Figure 11.24 HyperChem superimposed image of [Rh(cod)(trop)] (28) (black) *vs*. [Rh(cod)(trop)] (calculated) (red) with an RMS error of 1.61 Å.

An overlay of the X-ray crystal structure of [Rh(cod)(trop)] (**28**) with the optimized computational structure is presented in Figure 11.24 with an RMS error value of 1.61 Å based on all atoms. The differences observed are that the complexes are not planar there is a slight concave bend across the plane of the complex, this results in a high RMS error value.

11.5.2 Crystal Structure vs. Computed Structure Bond Relationships

In comparing the computed structures with their respective X-ray crystal structures only selected bond distances and angles were selected. These being the "core" co-ordination geometry and the entire cyclo-octadiene ring so as to include and calculate the χ and ψ angles.

The *R*-values are given as a measure of the average accuracy of the computed (gas phase) bond lengths (Å) and angles (°) with the experimental crystal data (solid state) obtained. The following expression was used to calculate the *R*-values.

$$R = n^{-1} \sum_{1 \to n}^{i} x_{e_i} - \left| x_{c_i} - x_{e_i} \right| \Big/ x_{e_i}$$

with n = number of data points, x_e = experimental data and x_c = calculated data.

The following graphs (Figure 11.25 and 11.31) and tables (Table 11.13) represent the general degree of accuracy between calculated structures and experimental values.

Within the graphs the insert values are the actual calculated *R*-values for the complexes presented, the table that follows the graphs are the plotted values.

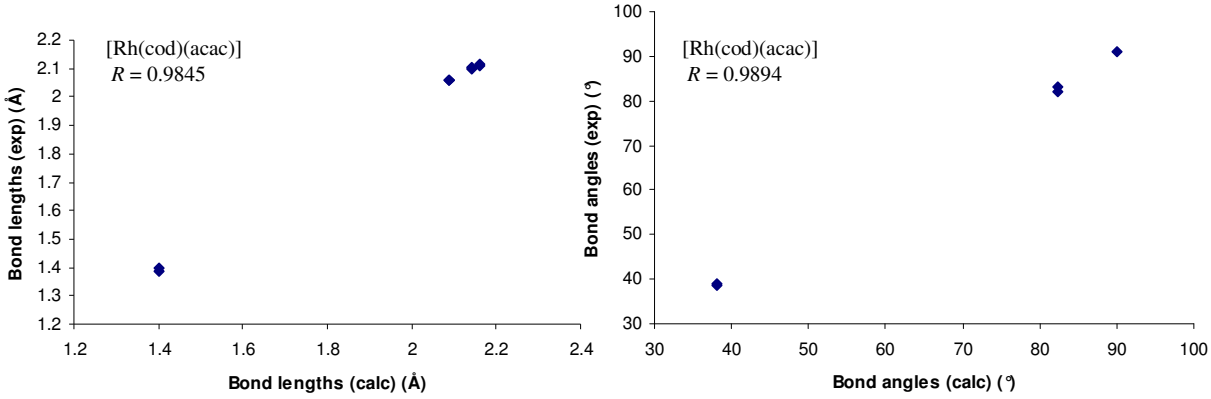

Figure 11.25 Graph of experimental *vs.* calculated bond lengths (Å) and angles (°) for [Rh(cod)(acac)] (25) with the calculated *R*-value top left, plotted values are given in Table 11.13 columns 1 and 2.

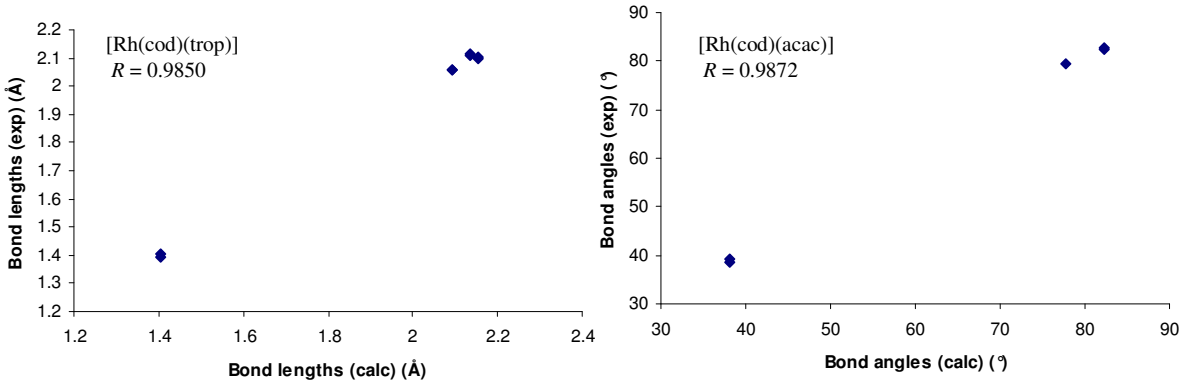

Figure 11.26 Graph of experimental *vs.* calculated bond lengths (Å) and angles (°) for [Rh(cod)(trop)] (28) with the calculated *R*-value top left, plotted values are given in Table 11.13 columns 3 and 4.

The graphs of [Rh(cod)(acac)] (**25**) and [Rh(cod)(trop)] (**28**) *vs.* bond lengths (Å) and angles (°) (Figure 11.25 and 11.31) represent the general degree of accuracy between the calculated structures and the experimental values with an average *R*-value of ≥ 98 %. The values are listed in Table 11.13.

Table 11.13 Selected Geometric parameters (Å,°) for rhodium metal complexes

	[Rh(cod)(acac)] (**25**)	calc	[Rh(cod)(trop)] (**28**)	calc
Rh–O_1	2.058(2)	2.0869	2.057(1)	2.0948
Rh–O_2	2.057(2)	2.087	2.060(1)	2.0948
Rh-C_1	2.107(3)	2.161	2.097(2)	2.1536
Rh-C_2	2.106(3)	2.1415	2.107(2)	2.1351
Rh-C_5	2.117(3)	2.161	2.102(2)	2.1537
Rh-C_6	2.097(4)	2.1414	2.112(2)	2.1351
C_1-C_2	1.388(4)	1.4012	1.406(2)	1.4031
C_5-C_6	1.399(4)	1.4012	1.394(3)	1.4031
O_1-Rh-O_2	90.9(1)	90.062	79.31(5)	77.717
C_1-Rh-C_2	38.5(1)	38.011	39.07(7)	38.19
C_5-Rh-C_6	38.8(1)	38.01	38.65(7)	38.189
C_1-Rh-C_5	83.0(1)	82.282	82.36(6)	82.184
C_2-Rh-C_6	82.1(1)	82.281	82.75(6)	82.181
χ^a	88.0(2)	87.336	88.02(7)	87.272
ψ^b	75.5(2)	79.463	73.7(1)	79.082

a χ: $C_1MC_2 \cap C_5MC_6$ b ψ: $C_2C_3C_4C_5 \cap C_1C_8C_7C_6$ see Figure 1.2

The experimental bond lengths and angles are in good agreement with the calculated bond lengths and angles with the calculated values being slightly larger overall.

11.5.3 Energies

The E_{corr} values of [Co(cod)(acac)], [Rh(cod)(acac)], [Ir(cod)(acac)], [Co(cod)(trop)], [Rh(cod)(trop)] and [Ir(cod)(trop)] are represented in Figure 11.27 showing a decrease in energy values as one proceeds down the metal triad, with only slight changes for rhodium and iridium.

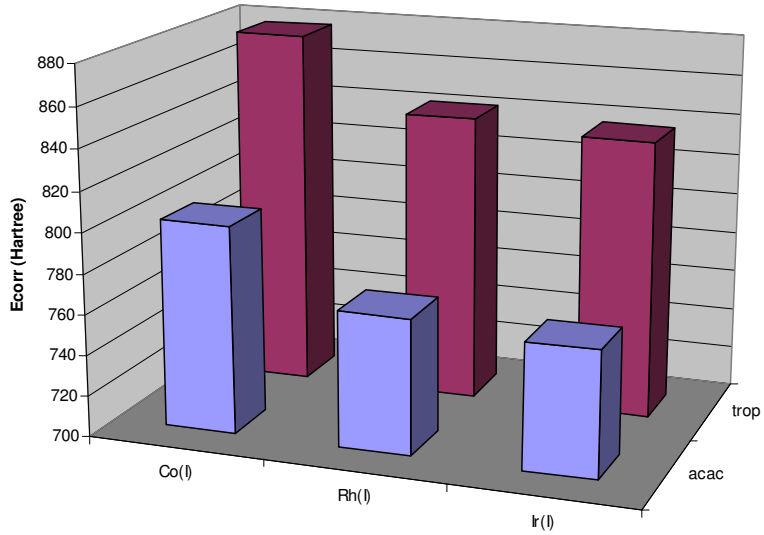

Figure 11.27 3D-graph of the total zero-point corrected energy (E_{corr}) for the computed complexes [M(cod)(LL')] where M = group 9 transition metals and LL' = acac, trop. Counter ions have not been calculated.

This trend follows the same pattern as for the 2008 covalent radii for the metal centers as previously mentioned those being 1.26, 1.42 and 1.41 for Co, Rh and Ir respectively. The total energy for the system increases as the ligand is changed from acetylacetonato to tropolonato. This is as a result of the increased strain on the metal due to the troplonato ligand forming a five memebered metal chelate ring system.

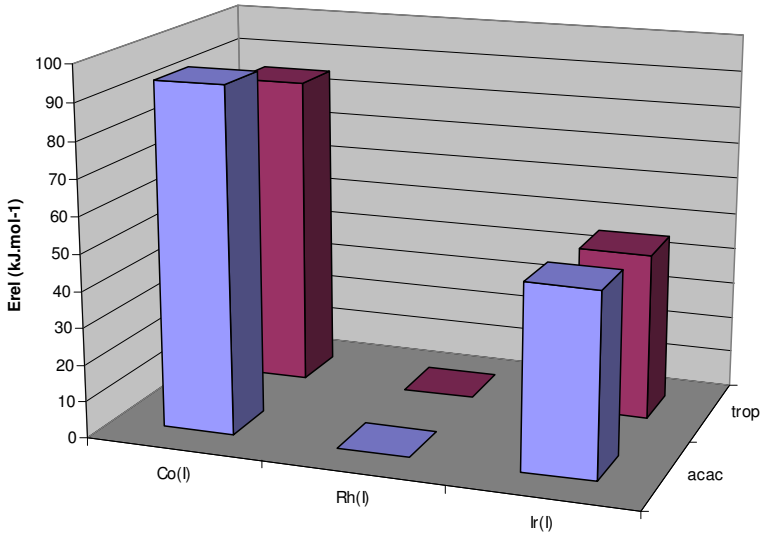

Figure 11.28 3D-graph of the total energy relative to the appropriate metal centre (E_{rel}) for the calculated complexes and are corrected by metal centre using standard methods.

The E_{rel} values represented in Figure 11.28 are corrected for metal effects for the calculated structures show only slight differences between the structures.

11.5.4 Infra-red Spectroscopic Correlations

The infra-red spectra of the calculated complexes are presented to gain a further insight into the bonding character of the complexes studied.

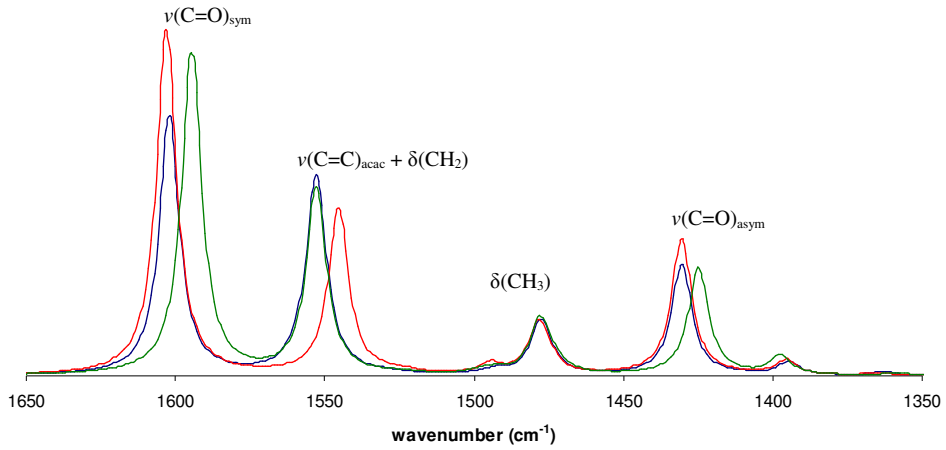

Figure 11.29 Calculated IR spectrum of [Co(cod)(acac)] (blue), [Rh(cod)(acac)] (red) and [Ir(cod)(acac)] (green). *ν* – stretching, δ – in plane bending (rocking, scissoring), sym – symmetrical and asym – asymmetrical.

In Figure 11.29 small changes to both the symmetrical and unsymmetrical stretching frequencies (ν(C=O)$_{sym}$, ν(C=O)$_{asym}$) of the acetylacetonato moiety were observed with [Ir(cod)(acac)] showing the greatest variance of 8 cm^{-1} in the wavenumber.

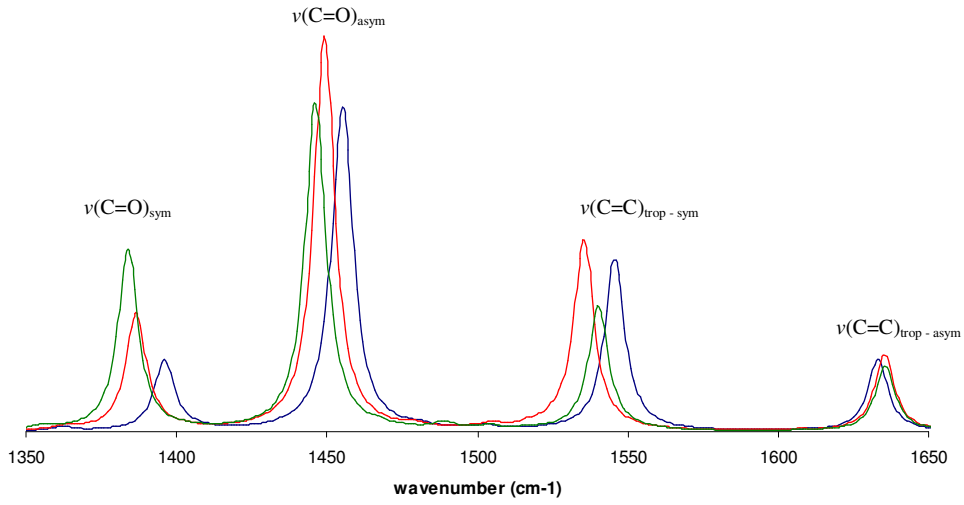

Figure 11.30 Calculated IR spectrum of [Co(cod)(trop)] (blue), [Rh(cod)(trop)] (red) and [Ir(cod)(trop)] (green). *ν* – stretching, δ – in plane bending (rocking, scissoring), sym – symmetrical and asym - asymmetrical.

In Figure 11.30 the calculated spectra of [Co(cod)(trop)] (blue), [Rh(cod)(trop)] (red) and [Ir(cod)(trop)] (green) show changes in both wavenumber and intensity for $\nu(C{=}O)_{sym}$ with the largest difference being between iridium and cobalt of 11 cm^{-1}, a decrease in intensity is observed as one moves from iridium to cobalt. For the asymmetrical stretching frequency of the C=O functionality of the tropolonato moeity this trend does not continue.

Table 11.14 Selected IR values (cm^{-1}) for the group 10 metal complexes.

	[M(cod)(acac)]			[M(cod)(trop)]		
	Co	Rh	Ir	Co	Rh	Ir
$\nu(C{=}O)_{sym}$	1602	1603	1595	1395	1387	1384
$\nu(C{=}C)_{A}$	1553	1545	1553	1546 / 1633[a]	1535 / 1635[a]	1540 / 1636
$\nu(C{=}C)_{cod}$	1549	1522	1495	1545	1526	1489
$\nu(C{=}O)_{asym}$	1430	1430	1425	1451	1449	1446

A = acac or trop a sym / asym

The values for $\nu(C{=}C)_{cod}$ are given in Table 11.14 are not found on the spectra given in Figure 11.29 and 11.35 as the calculated intensity of these peaks is too low to be detected. There is a decreasing trend for the frequency as the metal is systematically changed within the triad.

11.5.5 Molecular Orbital Comparisons

Even though molecular orbitals are a purely mathematical concept their presentation can yield valuable information as to the nature and type of chemical bonding present and possible within a co-ordination compound. The graphical representation of the molecular orbitals is another method whereby interactions of the cyclo-octadiene with the various metal centers and the *trans* ligands may be observed. The second-highest (HOMO-1) and highest (HOMO) occupied molecular orbitals and the lowest (LUMO) and second-lowest (LUMO+1) unoccupied molecular orbitals for the calculated complexes of [M(cod)(acac)] and [M(cod)(trop)] where M = Co, Rh, Ir will be presented, along with the differences in the respective orbitals ($E_{g-1} \equiv \Delta|$HOMO-1$|-|$HOMO$|$; $E_g \equiv \Delta|$HOMO$|-|$LUMO$|$; $E_{g+1} \equiv \Delta|$LUMO$|-|$LUMO+1$|$). The contour plots shown with the molecular orbitals are viewed along the *z*-axis.

Table 11.15 Molecular Orbitals of calculated structures [M(cod)(acac)].

	HOMO-1	HOMO	LUMO	LUMO+1
Co(I)	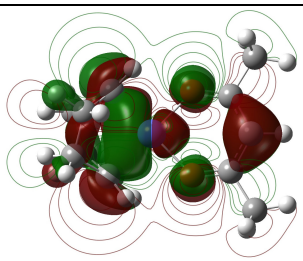	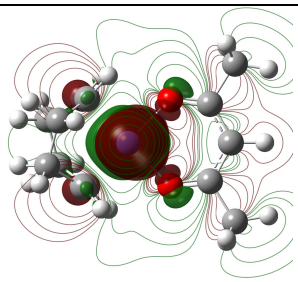	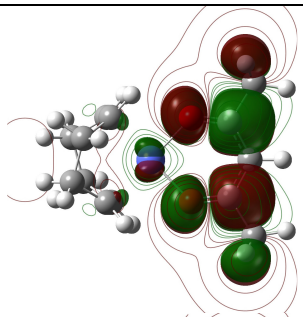	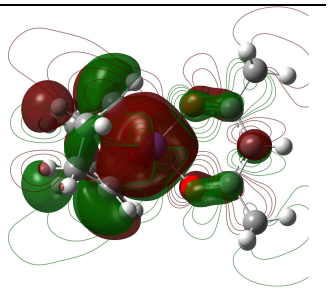
Rh(I)	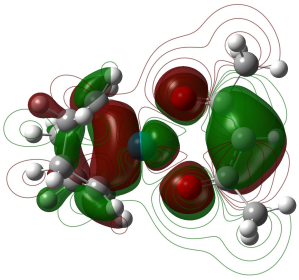	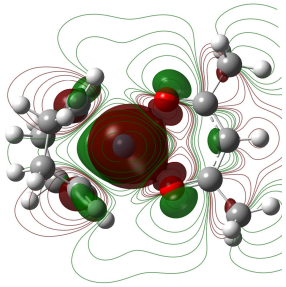	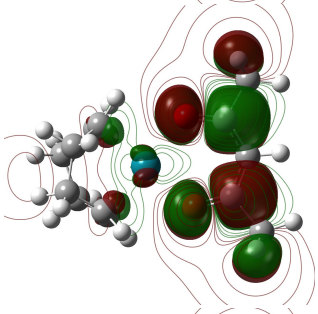	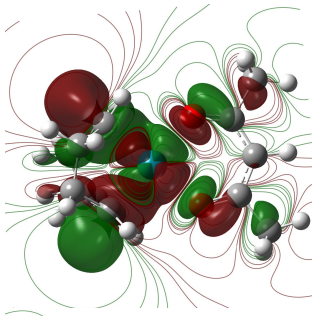
Ir(I)	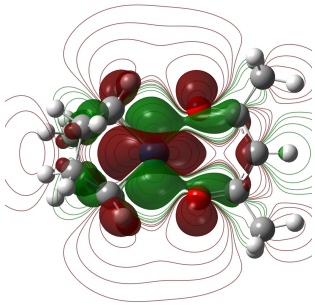	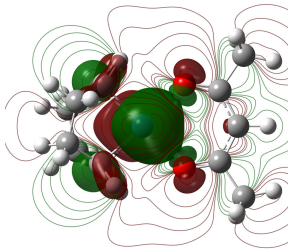	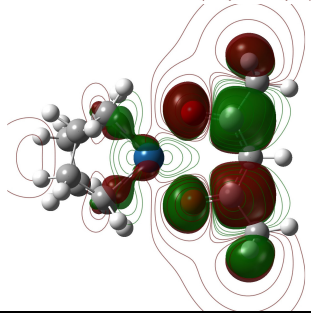	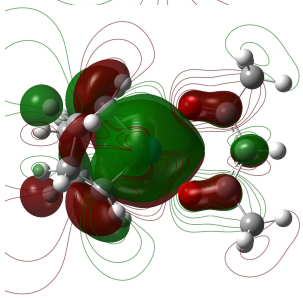

Table 11.16 Molecular Orbital Energies (Hartree) and energy gaps (eV) of the [M(cod)(acac)] calculated structures.

	HOMO-1	HOMO	LUMO	LUMO+1	E_{g-1}	E_g	E_{g+1}
Co(I)	-0.20259	-0.19064	-0.04069	-0.02711	0.325	4.080	0.370
Rh(I)	-0.22052	-0.2027	-0.04321	-0.02291	0.485	4.340	0.552
Ir(I)	-0.22107	-0.19721	-0.05459	-0.02341	0.649	3.881	0.848

The molecular orbitals for [M(cod)(acac)] where the metal centers are cobalt, rhodium and irridum are given in Table 11.15 with their energies listed in Table 11.16. For the HOMO-1 molecular orbitals, π delocalization was observed for acetylacetonato ligand in the cobalt and rhodium complexes. There is also a π orbital delocalization seen for the alkenes of the cylo-octadiene for all the group 9 metals with cobalt and rhodium being most pronounced. The HOMO was found to be the d_{z^2} orbital centered on the metal for all the complexes. In the LUMO molecular orbitals, *p* orbitals for the acetylacetonato ligand are clearly visible. While the d_{yz} orbital was seen for the

metals. For the LUMO+1 for the rhodium metal complex a $d_{x^2-y^2}$ orbital can be seen around the metal centre whereas for both the cobalt and iridium a d_{z^2} orbital is observed.

Table 11.17 Molecular Orbitals of calculated structures [M(cod)(trop)].

	HOMO-1	HOMO	LUMO	LUMO+1
Co(I)	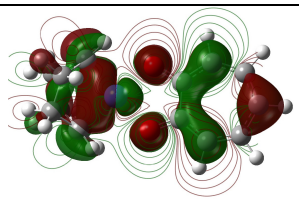	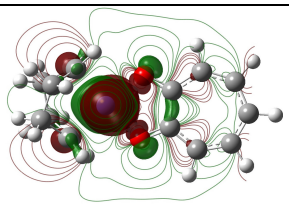	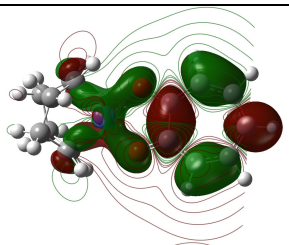	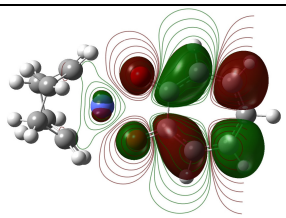
Rh(I)	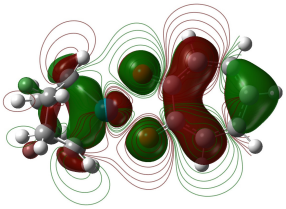	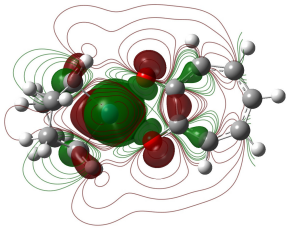	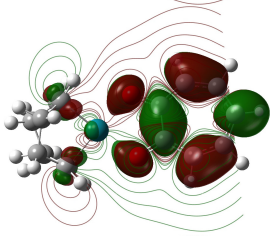	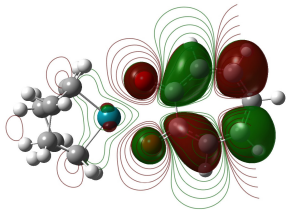
Ir(I)	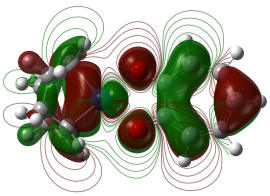	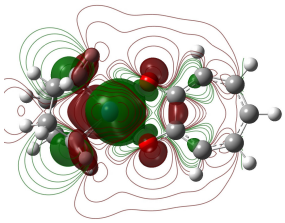	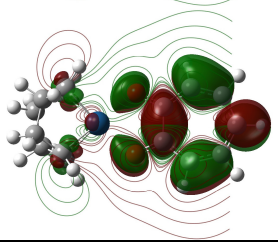	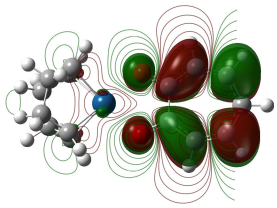

Table 11.18 Molecular Orbital Energies (Hartree) and energy gaps (eV) of the [M(cod)(trop)] calculated structures.

	HOMO-1	HOMO	LUMO	LUMO+1	E_{g-1}	E_g	E_{g+1}
Co(I)	-0.20083	-0.19239	-0.06876	-0.06778	0.230	3.364	0.027
Rh(I)	-0.21016	-0.20272	-0.06804	-0.06689	0.202	3.665	0.031
Ir(I)	-0.21856	-0.19527	-0.07929	-0.07775	0.634	3.156	0.042

The molecular orbitals for [M(cod)(trop)] where the metal centers are cobalt, rhodium and iridium are given in Table 11.17 with their energies listed in Table 11.18. In the HOMO-1 molecular orbitals, the π orbital delocalization of the alkenes of the cyclo-octadiene are seen there is also additional π orbital delocalization found for the tropolone ring. The metal centers were found to have a d_{yz} orbital. The HOMO was found to be the d_{z^2} orbital centered on the metal for all the complexes. The π orbital delocalization around the cobalt metal centre can be seen in the LUMO molecular orbitals. The *p* orbitals of the tropolonato moiety can be clearly seen in the LUMO+1 molecular orbitals for all the metal centers. For the HOMO-1 molecular orbitals, the

π orbital delocalization from the alkenes of the cyclo-octadiene to the metal centers are visible.

11.5.6 Venus fly-trap (χ and ψ) Angle Evaluation

Figure 11.31 shows the correlation of the different cobalt(I) triad complexes comparison of the χ and ψ angles.

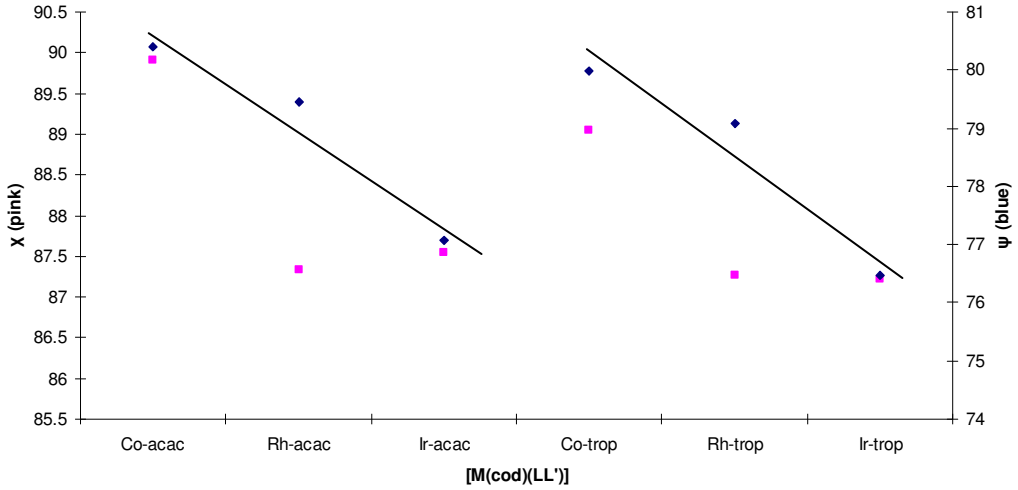

Figure 11.31 Graph of Cobalt(I), Rhodium(I) and Iridium(I) calculated complexes *vs.* χ (pink squares) and ψ (blue diamonds) angles (see Chapter 1 Figure 1.2 for definition of χ and ψ angles).

The same pattern that was observed for the nickel(II) triad in Chapters 8 and 10 is again found for the cobalt(I) triad complexes. A decrease in the ψ angle is observed as the metal is varied across the triad, with a maximum difference of 3.9° between [Co(cod)(acac)] and [Ir(cod)(trop)].

In overview a good correlation was found between the X-ray crystal structures and that of the computed compounds. The molecular orbital diagrams show the influence of both the *p* and *d* orbitals of the ligands as well as the metal centers. The infra-red spectra showed that the change in the metal centre was not as great an influence on the ν(C=O) stretching frequency as was expected. The $\nu(C=C)_{cod}$ stretching frequency showed a steady decrease in value but the calculated intensities were extremely low.

In continuing with the theme of this PhD investigation so far a fundamental computational study was undertaken with various transition metals (groups 7-11) and

a selection of β-diketonato, β-enaminonato and tropolonato type ligands was presented. The overarching correlations of energies, molecular orbitals, infra-red spectra and selected geometric statistics for all the complexes investigated will be presented in Chapter 12.

Chapter 12
Correlation of Computational Structures

12.1 Introduction

Chapters 6, 8, 10 and 11 presented the correlations between the solid state data of a range of complexes, correlated with their corresponding theoretically optimized analogues. A very good correlation was obtained. Thus, in this chapter the comparison between the calculated β-diketonato, β-enaminonato and the tropolonato complexes of the middle and late transition metals with regards to their energies (E_{corr}, E_{rel}), molecular orbitals (MOs), infra-red spectra (IRs), selected geometrical properties and the graphs of the χ and ψ angles will be presented and discussed.

The metals that were selected were the middle to late transition metals, groups 7-11, and were kept in a similar valence configuration resulting in d^6, d^8 and d^{10} metal complexes (see Table 2.4). The counter ions where applicable for the metal complexes were not computed. The ligands that were selected were cyclo-octadiene coupled with either β-diketonato (acetylacetone, trifluoroacetylacetone and hexafluoroacetylacetone), β-enaminonato (4-aminopent-3-en-2-one, 4-(methylamino)pent-3-en-2-one and 4-anilinopent-3-en-2-one) or tropolonato (tropolone and tribromotroplone) ligands. The principle aim of the correlations presented here, is to obtain the systematic variations in the bonding mode of 1,5-cyclo-octadiene, the model mimicking the Venus fly-trap.

Before proceeding a few points need to be highlighted. Firstly, that of the 2008 covalent radii (Table 12.1) which is used as a comparison for the metal complexes presented. Secondly, the definitions of a few angles and distances, used throughout this dissertation are once again presented (Figure 12.1 and 12.2).

Table 12.1 Excerpt from Table 2.4 showing the 2008 covalent radii for groups 7-11.

7		8		9		10		11	
Mn	1.39	Fe	1.32	Co	1.26	Ni	1.24	Cu	1.32
Tc	1.47	Ru	1.46	Rh	1.42	Pd	1.39	Ag	1.45
Re	1.51	Os	1.44	Ir	1.41	Pt	1.36	Au	1.36

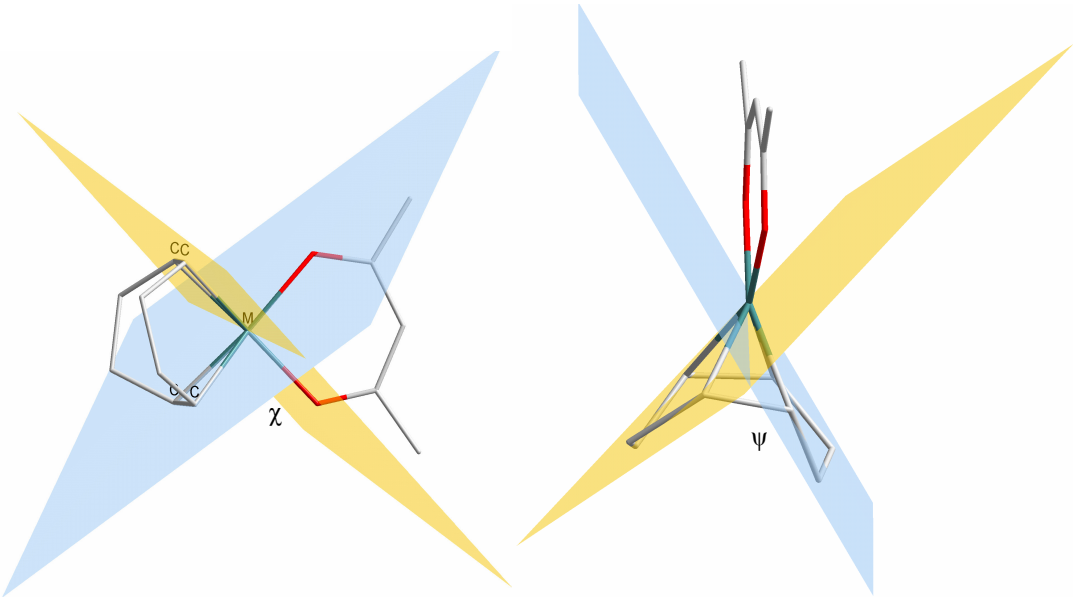

Figure 12.1 Left, the interplanar bond angle χ (bite angle) formed by the olefinic moieties through the metal centre. Right, the extent of the opening of the Venus fly-trap angle ψ (jaw angle) as defined by the planes through the alkane carbons of the cyclo-octadiene moiety.

The chi (χ) angle is defined by the intersection of the planes, defined by adjacent alkene carbons and the metal centre. The psi (ψ) angle is again an intersection between planes defined by the alkane carbons of the cyclo-ocatadiene moiety, as can be seen in Figure 12.1

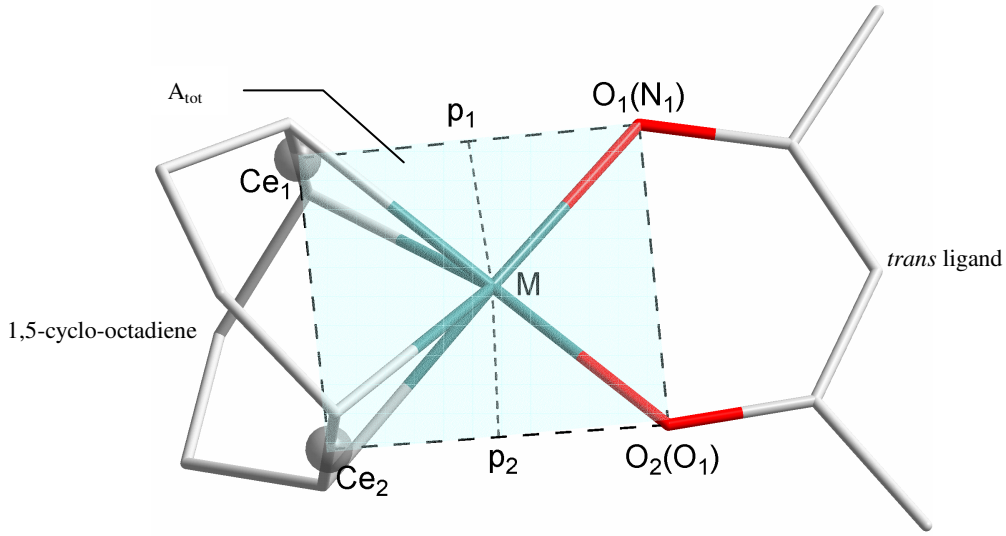

Figure 12.2 Diamond illustration of the geometry around the metal centre (M) with a rhombus defined by the mid-points of the alkene carbons (Ce_1 and Ce_2) of the cyclo-octadiene and the oxygen atoms of the *trans* ligand. The shaded area is represented by A_{tot}, while p_1 and p_2 are perpendiculars from the metal centre.

There are several points in Figure 12.2 which need to be defined. The dashed rhombus formed by $Ce_1Ce_2O_2O_1$, which refers to the square planar geometry which

has been reported in previous chapters. The area formed by the rhombus, the shaded area in Figure 12.2, will be referred to as the total area (A_{tot}). The perpendicular dashed lines formed from the metal centre (M) to the Ce_1O_1 (p_1) and Ce_2O_2 (p_2) lines are used to describe the position of the metal centre within the rhombus as a percentage of the total Ce_2O_2 or Ce_1O_1 distance. The values in the brackets in Figure 12.2 represent the atoms when using the β-enaminonato as opposed to the β-diketonato ligands for the *trans* ligand. The "core" bond lengths and angles are the angles and distances found contained within the dashed lines including the C_1-C_2 which has the centroid Ce_1 and C_5-C_6 with the centroid Ce_2 and the distances of the metals to these carbons and centroids.

12.2 Experimental

The DFT molecular orbital calculations were carried out using the Gaussian 03[1] software suite. Becke's three parameter hybrid (B3LYP)[2,3] exchange correlation functional was used. The basis set employed in this study was 6-311++G(d,p)[4,5,6] for the main group elements and LanL2DZ[7] for the middle to late transition metals. Vibrational frequencies were calculated at 6-311++G(d,p)[4,5,6] for the main group elements and LanL2DZ[7] for the middle to late transition metals with minimum energies confirmed to have zero imaginary frequencies. The frequencies are unscaled and were used to compute the zero-point vibrational energies. Molecular graphics

[1] Frisch M.J., Trucks G.W., Schlegel H.B., Scuseria G.E., Robb M.A., Cheeseman J.R., Montgomery J.A. Jr., Vreven T., Kudin K.N., Burant J.C., Millam J.M., Iyengar S.S., Tomasi J., Barone V., Mennucci B., Cossi M., Scalmani G., Rega N., Petersson G.A., Nakatsuji H., Hada M., Ehara M., Toyota K., Fukuda R., Hasegawa J., Ishida M., Nakajima T., Honda Y., Kitao O., Nakai H., Klene M., Li X., Knox J.E., Hratchian H.P., Cross J.B., Bakken V., Adamo C., Jaramillo J., Gomperts R., Stratmann R.E., Yazyev O., Austin A.J., Cammi R., Pomelli C., Ochterski J.W., Ayala P.Y., Morokuma K., Voth G.A., Salvador P., Dannenberg J.J., Zakrzewski V.G., Dapprich S., Daniels A.D., Strain M.C., Farkas O., Malick D.K., Rabuck A.D., Raghavachari K., Foresman J.B., Ortiz J.V., Cui Q., Baboul A.G., Clifford S., Cioslowski J., Stefanov B.B., Liu G., Liashenko A., Piskorz P., Komaromi I., Martin R.L., Fox D.J., Keith T., Al-Laham M.A., Peng C.Y., Nanayakkara A., Challacombe M., Gill P.M.W., Johnson B., Chen W., Wong M.W., Gonzalez C., Pople J.A., Gaussian 03, Revision E.01, Gaussian Inc., Wallingford CT, (2004)
[2] Becke A.D., *J. Chem. Phys.*, **98**, 5648, (1993)
[3] Lee C., Yang W., Parr R.G., *Phys. Rev.*, **B37**, 785, (1988)
[4] Ditchfield R., Hehre W.J., Pople J.A., *J. Chem. Phys.*, **54**, 724, (1971)
[5] Gordon M.S., *Chem. Phys. Lett.*, **76**, 163, (1980)
[6] Rassolov V.A., Ratner M.A., Pople J.A., Redfern P.C., Curiss L.A., *J. Comp. Chem.*, **22**, 976, (2001)
[7] Hay P.J., Wadt W.R., *J. Chem. Phys.*, **82**, 299, (1985)

were obtained using DIAMOND[8]. Overlay graphics were obtained using HyperChem 7.5[9].

12.3 Correlation of Group 7-11 Transition Metal Zero-Point Corrected Energies

The calculated zero-point corrected energy values (E_{corr}) of the group 7-11 transition metal β-diketonato, β-enaminonato and tropolonato complexes are presented separately in Figure 12.3 with the corresponding values found in Appendix C.5. The E_{corr} energy values were calculated by taking the total energy and correcting with the zero-point correction energy.

The E_{corr} values of the computed complexes found in Figure 12.3 show an increase as the ligand becomes more electron withdrawing (*i.e.* acac → tfacac → hfacac). A decrease was observed as one moves down the triads (*i.e.* 3*d* → 4*d* → 5*d* elements) with an overall increase in energy as one proceeds across the groups (*i.e.* group 7 → 11). These trends are also observed for both the β-enaminonato and tropolonato complexes. The relativistic effects (generally noted for the 5*d* elements) are seen in that the corrected energies for the first row transition metals are higher than for the second and third row of transition metals this pattern is consistent with the 2008 covalent radii (Table 12.1) and is observed for the β-diketonato, β-enaminonato and tropolonato complexes.

To allow for a more in-depth analysis of the different metal complexes, two variations of relative energy corrections were applied. Firstly, the correcting for the metal effect (§ 12.4 Figure 12.4), highlighting the changes of the various ligands. Secondly, corrections of the ligand effect (§ 12.5 Figure 12.5) thus highlighting the changes on the metal centers.

[8] Brandenburg K., Brendt M., DIAMOND, Release 2.1e. Crystal Impact GbR, Potfach 1251, D53002 Bonn, Germany., (2001)
[9] HyperChem™ Release 7.52, Windows Molecular Modeling System, HyperCube Inc., (2002)

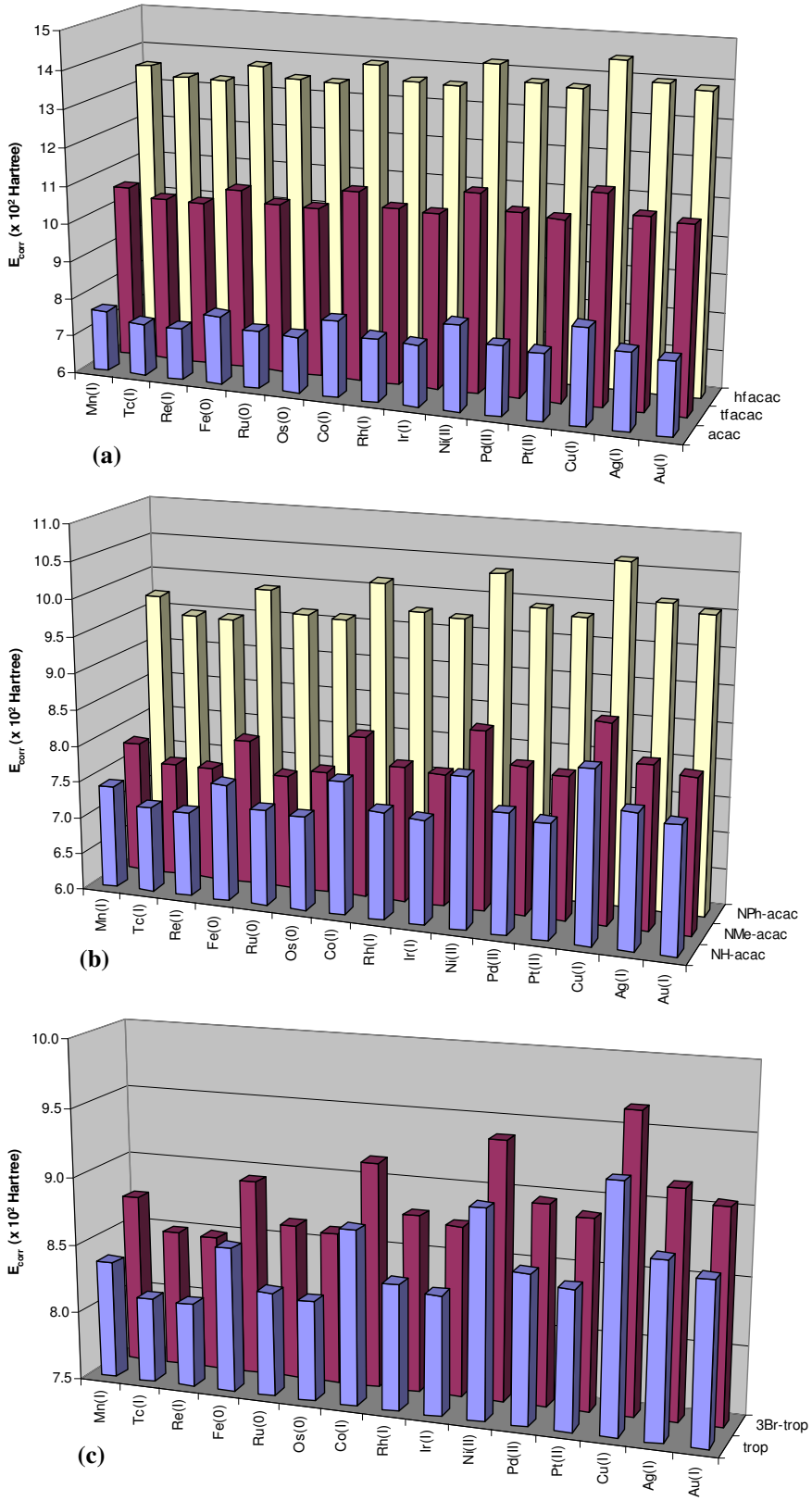

Figure 12.3 3D-graph of the total zero-point corrected energy (E_{corr}) for the computed complexes $[M(cod)(LL')]^n$ where M = group 7-11 metals, n = -1, 0, +1 (a) LL' = acac, tfacac, hfacac (b) LL' = NH-acac, NMe-acac, NPh-acac (c) LL' = trop, 3Br-trop. Counter ions where applicable have not been calculated or included.

12.4 Correlation of Group 7-11 Transition Metal Relative Energies (E_{rel}^{M})

The metal relative energy values (E_{rel}^{M}) of the group 7-11 transition metal β-diketonato, β-enaminonato and tropolonato complexes are presented separately in Figure 12.4 with the corresponding values found in Appendix C.6. The metal relative energy value (E_{rel}^{M}) was calculated by taking the corrected energy (E_{corr}) and correcting for metal effects, therefore the ligands can be directly compared.

In Figure 12.4a the acetylacetonato (acac) complexes, iron was found to have the lowest relative energy whereas for trifluoroacetylacetonato (tfacac) and hexafluoroacetylacetonato (hfacac) complexes cobalt was seen to have the lowest energy. With an average change of energy of *ca.* 906 kJ.mol^{-1} for the group 7 metals When looking at the group metal complexes it was found that there is an increase in the energy for groups 7 and 8 as the ligand is varied (acac → tfacac → hfacac) while groups 9 and 10 have a decrease in energy as the ligand is varied (hfacac → tfacac → acac). There is only a slight increase in the energy as the metal is varied (3*d* → 4*d* → 5*d*).

For the β-enaminonato complexes in Figure 12.4b, the rhenium complexes have been omitted from the discussion, due to errors that were encountered whilst correcting for the metal effects. A similar situation was experienced for the ruthenium 4-(methylamino)pent-3-en-2-onato (NMe-acac) complex, both have been included in the graph but the values have been zeroed. The lowest energies were found to be iron for all the β-enaminonato ligand complexes. Only a small change in energy *ca.* 8 kJ.mol^{-1} is observed when varying the ligands (NH-acac → NMe-acac → NPh-acac), which is considerably lower than the β-diketonato and tropolonato complexes. A small increase in energy was again observed for the metal triads (*i.e.* 3*d* → 4*d* → 5*d*).

In Figure 12.4c the tropolonato (trop) complexes, cobalt was found to have the lowest relative energy whereas for tribromotroplonato (3Br-trop) complexes iron was found to have the lowest relative energy. With an average change of energy of *ca.* 365 kJ.mol^{-1} for the group 7 metals. Whilst looking at the group metal complexes it was found that there is a decrease in the energy for groups 7 and 8 while group 9 and 10

was found to increase in energy as the ligand is varied (trop → 3Br-trop). This pattern is the reverse of what was observed for the β-diketonato complexes.

As the metals are varied within a group there is a steady increase in the energy which again links to the covalent radii, however the increases are not as prominent as they were for the E_{corr} (Figure 12.3c). As a result of the group 11 metals being mono co-ordinated their values have been omitted from the graph.

For the electron withdrawing ligands it was found that the lowest energy obtained was for the cobalt complexes, whilst the electron donating ligands the iron complexes were the lowest energy.

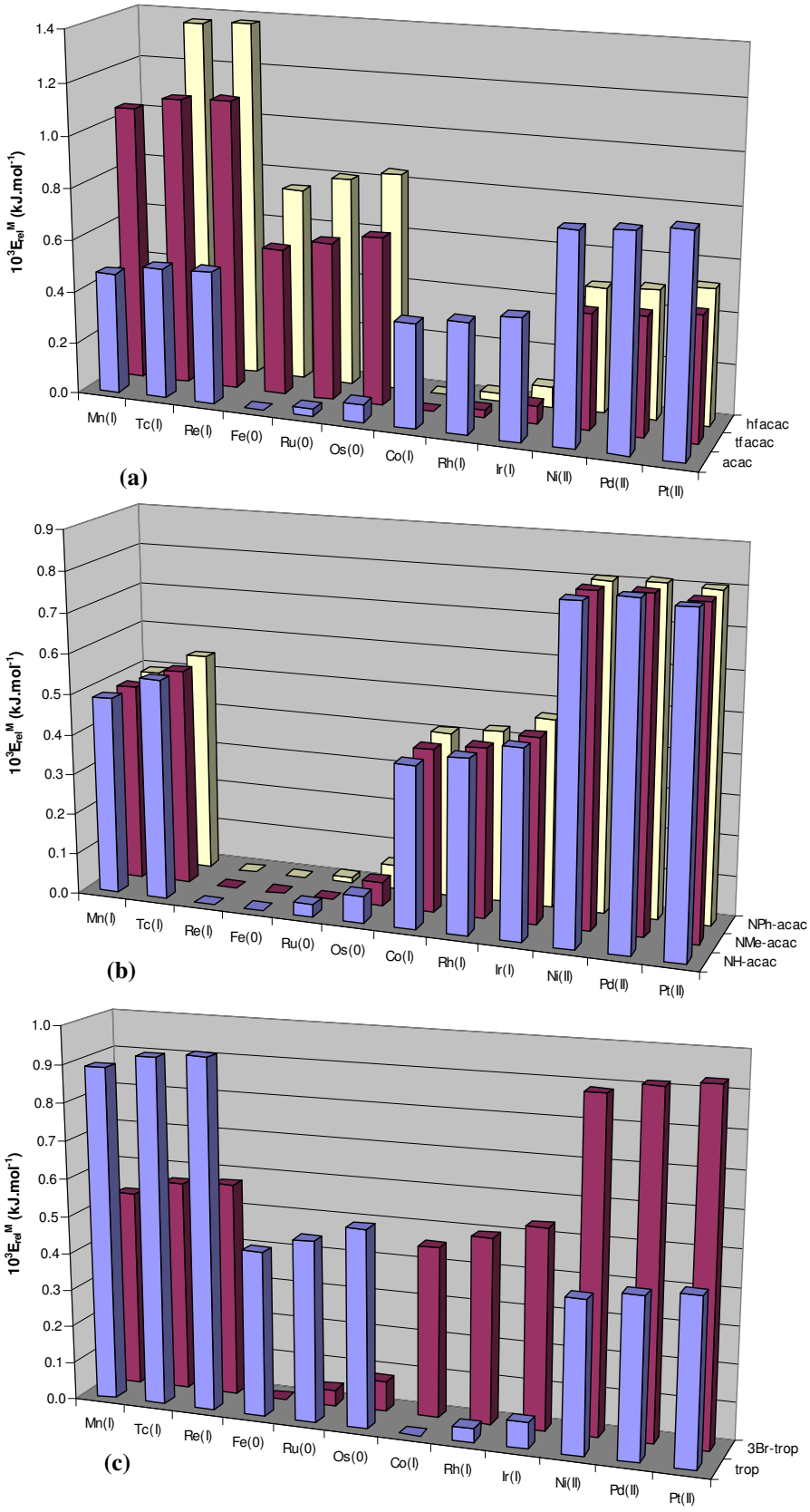

Figure 12.4 3D-graph of the total energy ($E_{rel}{}^M$) corrected for metal effects for the computed complexes [M(cod)(LL')]^n where M = group 7-10 metals, n = -1, 0, +1 (a) LL' = acac, tfacac, hfacac (b) LL' = NH-acac, NMe-acac, NPh-acac (c) LL' = trop, 3Br-trop. Counter ions where applicable have not been calculated or included.

12.5 Correlation of Groups 7-11 Transition Metal Ligand Relative Energies (E_{rel}^{L})

The ligand relative energy values (E_{rel}^{L}) of the group 7-11 transition metal β-diketonato, β-enaminonato and tropolonato complexes are presented separately in Figure 12.5 with the corresponding values found in Appendix C.7. The ligand relative energy value (E_{rel}^{L}) was calculated by taking the corrected energy (E_{corr}) and correcting for ligand effects. The correction applied for the ligand variation effect allows the direct comparison of the metal centers.

Only a marginal increase is observed as the electron withdrawing nature of the ligands is increased within a triad for all three the ligand sets (*i.e.* β-diketonato, β-enaminonato and tropolonato). A systematic decrease was found as one proceeds from group 7 to 11 which is in agreement with the 2008 covalent radii (Table 12.1). It should be mentioned that the ruthenium 4-(methylamino)pent-3-en-2-onato (NMe-acac) complex is an outlier to the general trend that was observed. The reason for this deviation is still unclear at this point.

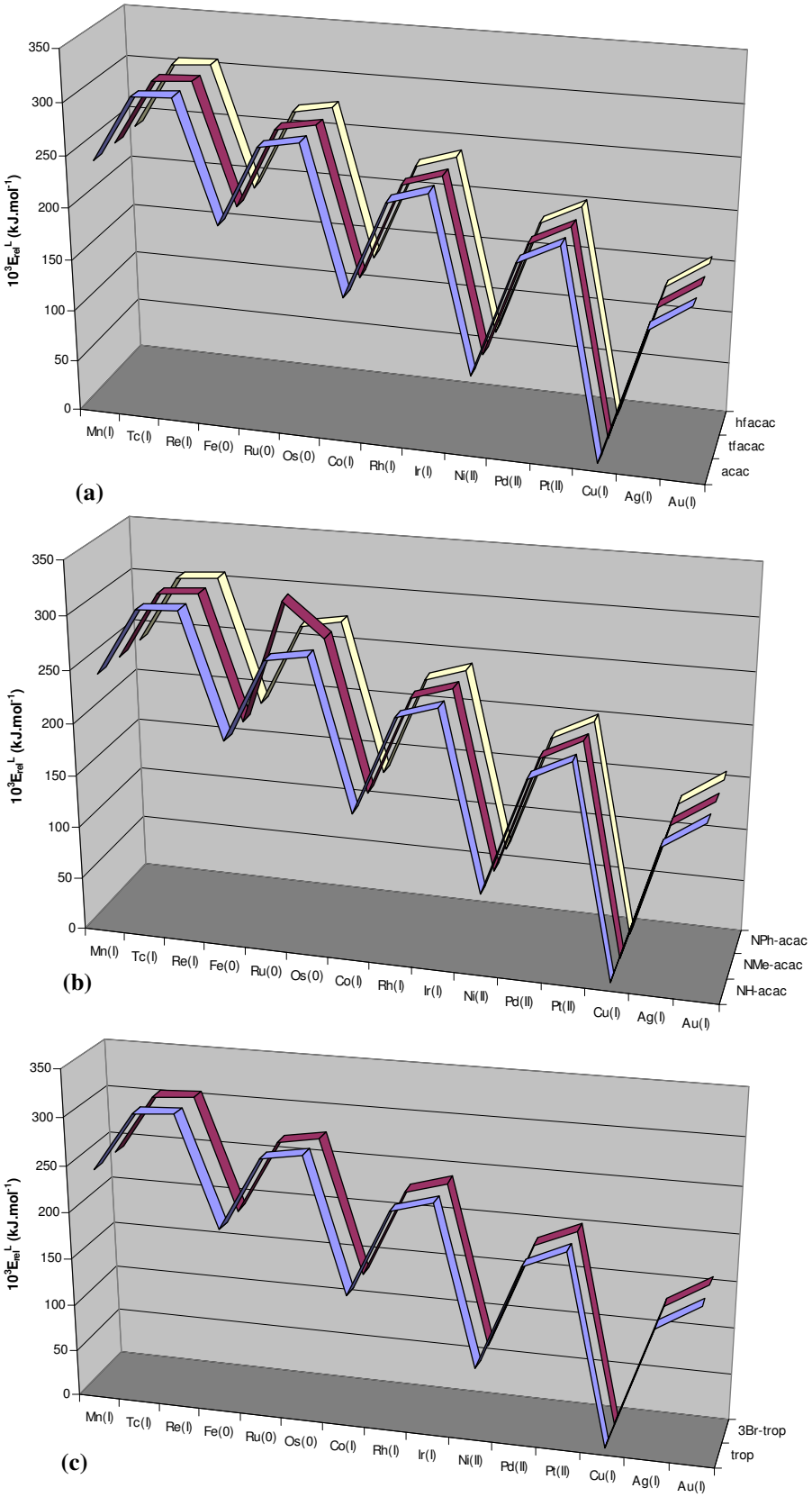

Figure 12.5 3D-graph of the total energy ($E_{rel}{}^{L}$) corrected for ligand effects for the computed complexes $[M(cod)(LL')]^n$ where M = group 7-10 metals, n = -1, 0, +1 (a) LL' = acac, tfacac, hfacac (b) LL' = NH-acac, NMe-acac, NPh-acac (c) LL' = trop, 3Br-trop. Counter ions where applicable have not been calculated or included.

12.6 Visual Correlation of Group 7-11 Transition Metal Molecular Orbitals

The molecular orbitals provide information as to the nature and location of possible electron density within the computed complexes. This graphical representation of the molecular orbitals is another method whereby interactions of the cyclo-octadiene with the various metal centers and the trans ligands may be observed Several tables and figures will be presented illustrating the second-highest (HOMO-1) and highest (HOMO) occupied molecular orbitals and the lowest (LUMO) and second-lowest (LUMO+1) unoccupied molecular orbitals for the calculated complexes of [M(cod)(LL')] (M = group 7-11 metal centers and LL' = β-diketonato, β-enaminonato, tropolonato) along with the differences in the respective orbitals ($E_{g-1} \equiv \Delta|\text{HOMO-1}|-|\text{HOMO}|$; $E_g \equiv \Delta|\text{HOMO}|-|\text{LUMO}|$; $E_{g+1} \equiv \Delta|\text{LUMO}|-|\text{LUMO+1}|$). The contour plots are shown with the molecular orbitals are viewed along the *z*-axis.

The complete molecular orbital (MO) tables for the different metal systems are given as follows:

- [M(cod)(acac)] in Appendix C.1.1 – C.1.5
- [M(cod)(tfacac)] in Appendix C.1.6 – C.1.10
- [M(cod)(hfacac)] in Appendix C.1.11 – C.1.15
- [M(cod)(NH-acac)] in Appendix C.1.16 – C.1.20
- [M(cod)(NMe-acac)] in Appendix C.1.21 – C.1.25
- [M(cod)(NPh-acac)] in Appendix C.1.26 – C.1.30
- [M(cod)(trop)] in Appendix C.1.31 – C.1.35
- [M(cod)(3Br-trop)] in Appendix C.1.36 – C.1.40

To assist in the evaluation of the ligand effects on the molecular orbitals, a systematic relative comparison is presented below. This simplified discussion is divided into two main components namely

- Symmetric O,O-bidentate ligands, both five and six membered chelate rings across the transition metals (*i.e.* the 4*d* elements)
- Unsymmetric β-enaminonato ligands across the transition metals (*i.e.* the 4*d* elements)

12.6.1 Symmetrical O,O-Bidentate Ligands

Table 12.2 represents a visual comparison of the molecular orbitals for the second row of group 7-11 transition metals of the acetylacetonato (acac) complexes. The molecular orbitals for the trifluoroacetylacetonato (tfacac) and hexafluoroacetylacetonato (hfacac) complexes are similar and thus only one illustration depicting the orbitals will be shown, even though the tropolonato complexes are five membered chelate rings they are similar to the symmetrical acac complexes. It is also of note that even though tfacac is theoretically an unsymmetrical ligand its molecular orbitals remain similar to the acac and hfacac as previously mentioned, and due to this reason the tfacac has been included in the group orbital discussions below.

It is clear that upon comparison of the second row for the group 7 to 11 (technetium(I), ruthenium(0), rhodium(I), palladium(II), silver(I)) metals that for the HOMO molecular orbitals a d_{z^2} orbital was observed for groups 7-9 while for group 10 a d_{xy} orbital was observed with an in-phase overlap of the p_y orbitals of the oxygen atoms of the acac ligand. While group 11 a d_{xy} orbital was again observed this time with an out of phase overlap of the *p* orbitals of the oxygen atoms of the acac ligand. Both group 10 and 11 show delocalization on the acac back-bone while groups 7-9 have additional orbitals on the cyclo-ocatadiene (cod) ligand centered mainly on the alkene carbons.

The tropolonato complexes molecular orbitals are mostly dominated by the *p* orbitals on the tropolonato ring, with similar metal orbitals that were found for the β-diketonato complexes.

An example of the molecular orbitals of the nickel acac triad (group 10) is presented in Table 12.3 to illustrate that there are no significant changes in the molecular orbitals as one proceeds down the triad. A discussion of the molecular orbitals per group follows.

For group 7 the HOMO-1 molecular orbitals for the acetylacetonato (acac) complexes (see Appendix C.1.1), a classic π orbital between the cyclo-octadiene ring's alkene carbons and the manganese metal centre can be clearly seen, the rest of the electron density is mostly situated on the cyclo-octadiene ring. For the

trifluoroacetylaceontato (tfacac) (see Appendix D.1.6) and hexafluoroacetylacetonato (hfacac) (see Appendix C.1.11) complexes, the manganese has a d_{xy} orbital with an in phase overlap of the π orbital of the alkene carbons of cyclo-octadiene, while technetium has similar orbitals to the acac complexes.

Table 12.2 Molecular Orbitals of the second row transition metals calculated structures of [M(cod)(acac)]. Metals (cyan), carbon (grey), oxygen (red) and hydrogen (light grey).

	HOMO-1	HOMO	LUMO	LUMO+1
Tc(I)	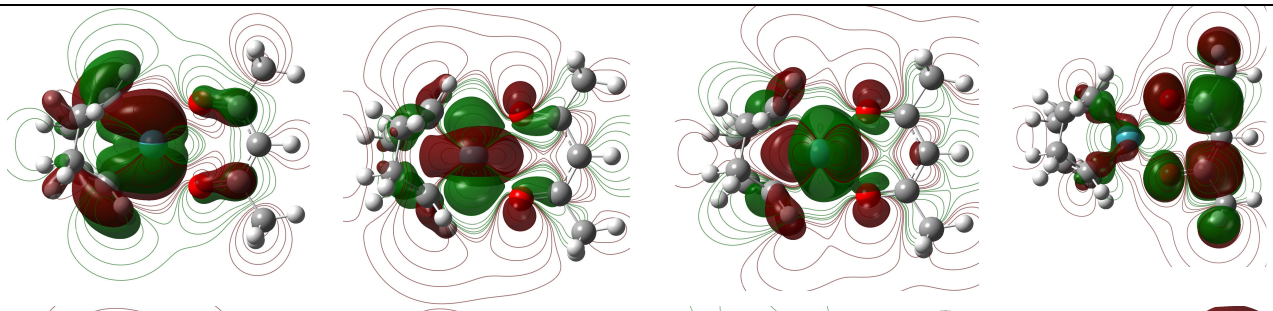			
Ru(0)	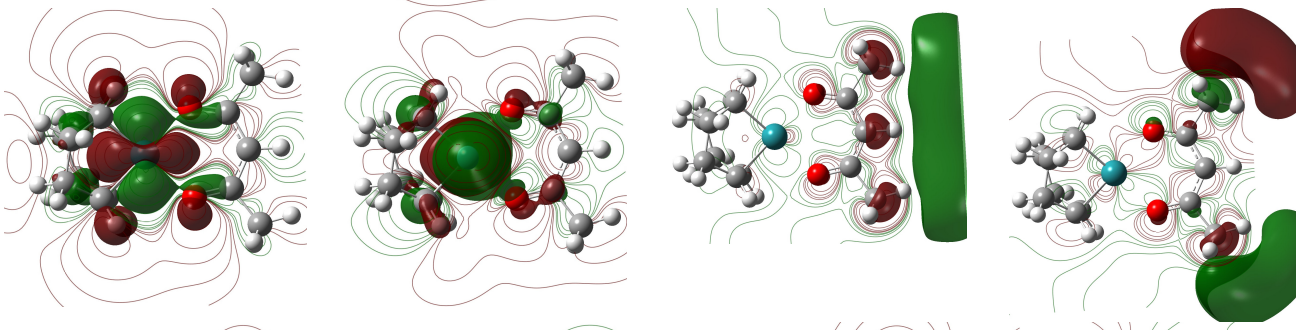			
Rh(I)	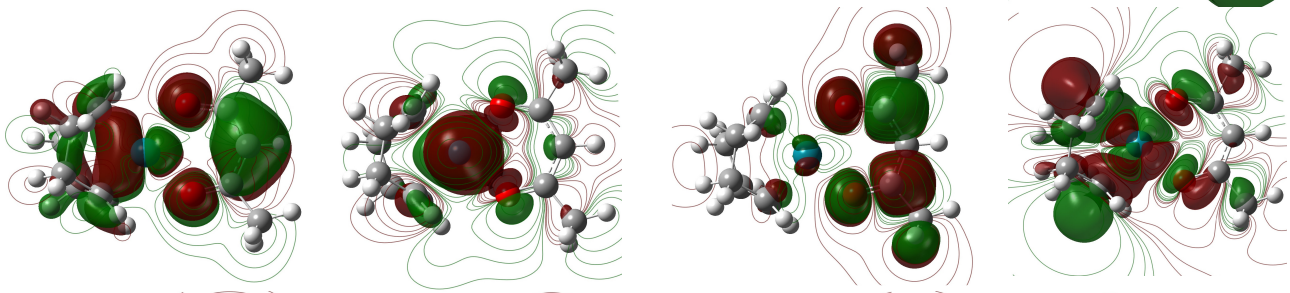			
Pd(II)	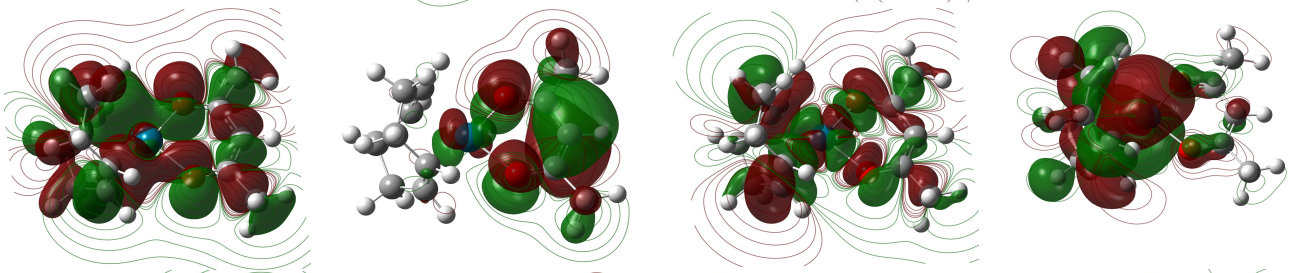			
Ag(I)	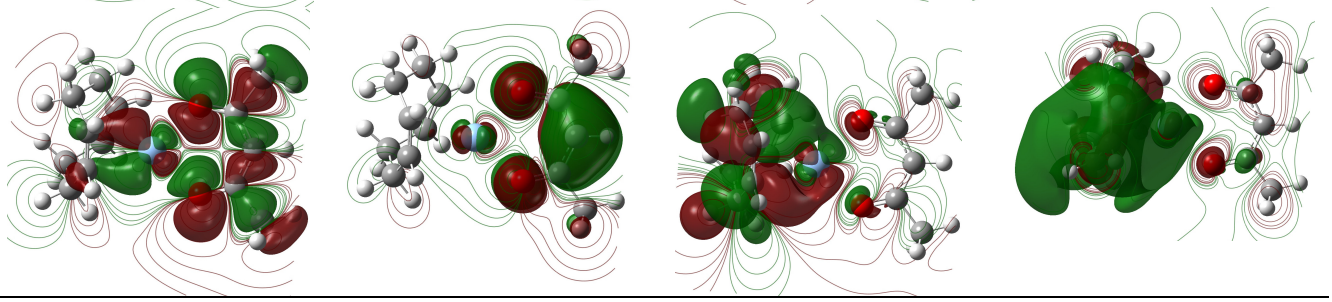			

The rhenium tfacac complex differs in the d_{yz} orbital overlaps with the *p* orbital of the alkene "trans" to the CF_3 group, while the hfacac complex is similar to the manganese acac complex. In the HOMO molecular orbitals, the acac, tfacac and hfacac complexes have a $d_{x^2-y^2}$ orbital centered on the manganese with very little density for either bonding ligands, whereas technetium and rhenium have a d_{z^2} orbital with similar density for the bonding ligands. For the LUMO molecular orbitals of the acac complexes, a d_{z^2} orbital was found for manganese with very little additional election density on the co-ordinating ligands, this density increases as one proceeds down the group. The acac, tfacac and hfacac complexes have comparable orbitals with only the manganese acac complex differing. In the LUMO+1 molecular orbitals for the acac complexes a *p* orbital indicating the delocalization of the acac ligand is seen, while the tfacac manganese complex has a d_{z^2} orbital overlapping the *p* orbitals of the oxygens of the tfacac ligand. The molecular orbitals of the hfacac complexes are similar to the tfacac complexes.

For group 8 the HOMO-1 molecular orbitals, for the acac (see Appendix C.1.2), tfacac (see Appendix C.1.7) and hfacac (see Appendix C.1.12) complexes, iron has a π orbital delocalization with the cyclo-octadiene ring, while ruthenium and osmium metal centers have a d_{z^2} orbital. In the HOMO molecular orbitals for the acac, tfacac and hfacac complexes all metals show a d_{z^2} orbital with similar orbitals seen on the co-ordinating ligands, with tfacac moieties showing increased overlap. For the LUMO molecular orbitals for the tfacac and hfacac complexes, delocalization of the *p* orbitals was observed, while the *p* and *s* orbitals of the fluorines and hydrogens (for the tfacac ligand only) was seen. In the LUMO+1 molecular orbitals for the tfacac and hfacac complexes a d_{xz} orbital was observed for all metals of the group.

For group 9 the HOMO-1 molecular orbitals for the acac (see Appendix C.1.3), tfacac (see Appendix C.1.8) and hfacac (see Appendix C.1.13) complexes, a π orbital is visible between cobalt, rhodium and the cyclo-octadiene ring. Delocalization is visible on the acac and tfacac ligands. A d_{z^2} orbital centered on iridium was observed, this has a similar configuration to the ruthenium, osmium acac complexes seen in Appendix C.1.2. In the HOMO molecular orbitals of the acac, tfacac and

hfacac complexes, a d_{z^2} is seen for all the group metals. For the LUMO molecular orbitals of the acac complexes the *p* orbitals of the acac ligand are clearly seen, while the *p* orbitals of the fluorines for the tfacac and hfacac moieties are visible. In the LUMO+1 molecular orbitals for the acac, tfacac and hfacac complexes, for rhodium a $d_{x^2-y^2}$ orbital is observed whereas a d_{z^2} orbital is seen for cobalt and iridium.

Table 12.3 Molecular Orbitals of calculated structures [M(cod)(acac)] where M = Ni(II), Pd(II), Pt(II). Metals (cyan), carbon (grey), oxygen (red) and hydrogen (light grey).

	HOMO-1	HOMO	LUMO	LUMO+1
Ni(II)	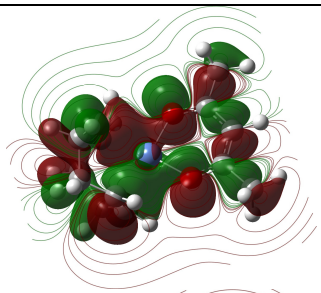	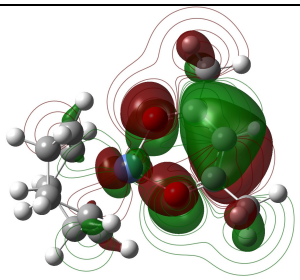	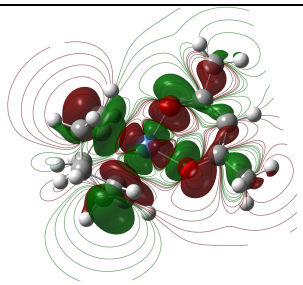	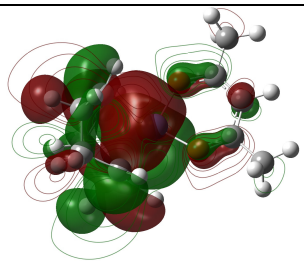
Pd(II)	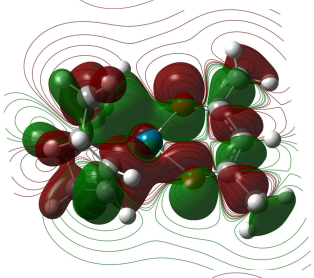	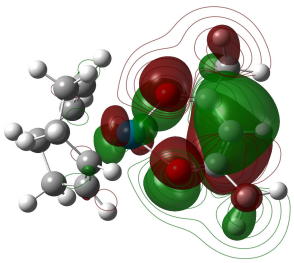	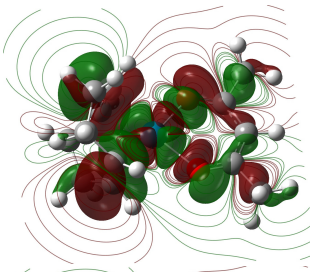	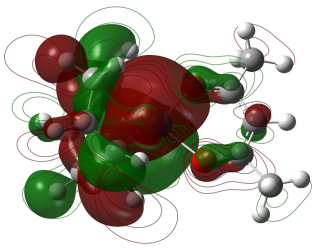
Pt(II)	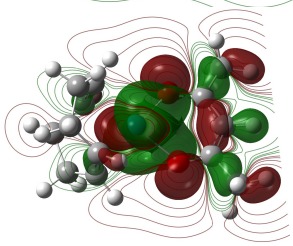	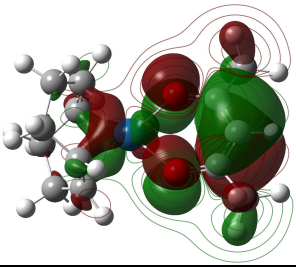	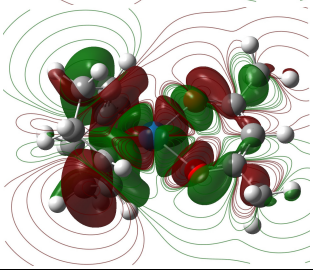	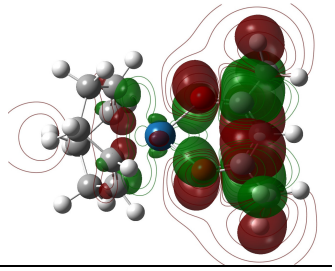

For group 10 the HOMO-1 molecular orbitals for the acac (see Table 12.3 and Appendix C.1.4) and hfacac (see Appendix C.1.14) complexes, π orbital delocalization between both nickel, palladium, cyclo-octadiene and acac and hfacac is observed. Platinum only shows the delocalization between itself and the acac moiety, with a d_{z^2} orbital seen in the hfacac platinum complex. In the HOMO molecular orbitals for the acac complexes, delocalization for the acac moiety is seen for all, with platinum having additional orbitals for the alkene carbons of the cyclo-octadiene moiety. For the hfacac complexes a d_{xy} metal orbital has an in-phase overlap of the p_y orbitals of the oxygens of the hfacac ligand. For the LUMO molecular orbitals of the

acac complexes a $d_{x^2-y^2}$ orbital was found for all metals of the group. The platinum hfacac complex however, has a d_{xy} orbital, with additional p_y orbitals seen for the hfacac moiety. The only difference found between the acac complexes and the tfacac (see Appendix C.1.9) complexes was in the LUMO+1 molecular orbitals of nickel and palladium having d_{xy} orbitals with π orbital delocalization on the tfacac back-bone. The hfacac platinum complex has a $d_{x^2-y^2}$ orbital centered on the metal.

For group 11 the HOMO-1 molecular orbitals of the acac complexes (see Appendix C.1.5), the metal d_{xz} orbitals overlap with the out of phase *p* orbitals of the alkene carbons of the cyclo-octadiene ring, while the hfacac copper complex (see Appendix C.1.15) has a similar orbital configuration. For the tfacac complexes (see Appendix C.1.10) a $d_{x^2-y^2}$ orbital was found for silver and gold, while a d_{z^2} orbital was observed for the hfacac gold complex. In the HOMO molecular orbitals of the acac complexes, the delocalization of the acac back-bone is evident, while for the tfacac complexes a d_{xy} orbital with an in-phase overlap of the *p* orbital of the alkene for silver tfacac complex with the copper complex being obscured. For the hfacac complexes a d_{yz} orbital was observed for all the group metals with delocalization seen on the hfacac back-bone. For the LUMO molecular orbitals for the acac complexes a d_{xy} orbitals was found. In the hfacac complexes a $d_{x^2-y^2}$ orbital was found on the copper whist d_{xy} orbitals were found for silver and gold. In the LUMO+1 molecular orbitals of the tfacac complexes a d_{xz} metal orbital is overshadowed by the *p* orbitals of the alkenes. For the hfacac complexes the molecular orbitals for copper an in-phase overlap with the p_y orbitals of the oxygens was observed, whilst silver and gold show π delocalization on the cyclo-octadiene. It is noted that the group 11 metals for all ligands are only mono-co-ordinated with the alkene "cis" to the CF_3 group being non co-ordinated.

12.6.2 Unsymmetrical β-Enaminonato Ligands

Table 12.4 represents the second row of transition metals of the 4-aminopent-3-en-2-onato (NH-acac) complexes, the molecular orbitals for the 4-(methylamino)pent-3-en-2-onato (NMe-acac) and 4-anilinopent-3-en-2-onato (NPh-acac) complexes are similar and thus only one table depicting the orbitals will be shown. The

unsymmetrical nature of the N,O-bidentate ligands is clearly reflected in the molecular orbitals (Table 12.4). In spite of this, the general similarity with that of the symmetrical acac complexes (Table 12.2) is clear. A discussion of the orbitals per group of the complexes will be presented.

For group 7 the HOMO-1 molecular orbitals for the 4-aminopent-3-en-2-onato (NH-acac) (see Appendix C.1.16), 4-(methylamino)pent-3-en-2-onato (NMe-acac) (see Appendix C.1.21) and the 4-anilinopent-3-en-2-onato (NPh-acac) (see Appendix C.1.26) complexes, the *trans* influence of the nitrogen is seen, with additional π orbital delocalization on the back-bone for both the NMe-acac and NPh-acac ligands. In the HOMO-1 molecular orbitals for the NH-acac and the NPh-acac complexes, a $d_{x^2-y^2}$ orbital is observed on the manganese metal centre while d_{z^2} orbitals are seen for technetium and rhenium. The NMe-acac complexes display a $d_{x^2-y^2}$ orbital for all the group metals, with the bonding orbitals of the methyl group to the nitrogen mirroring the oxygen leg of the ligand. It is interesting to note that the bonding orbitals for the nitrogen to both the phenyl ring and the back-bone carbons are nearly identical to those of the oxygen. For the LUMO molecular orbitals of the NH-acac, NMe-acac and NPh-acac complexes, d_{z^2} orbitals were found for all the metal centers. In the LUMO+1 molecular orbitals of NH-acac complexes , *p* orbitals for the NH-acac back-bone are clearly seen. With the NMe-acac complexes of technetium and rhenium showing a d_{xy} orbitals with the manganese metal centre being eclipsed. The *p* orbitals of the NMe-acac and NPh-acac ligand are clearly visible.

For group 8 the HOMO-1 molecular orbitals for the NH-acac (see Appendix C.1.17) and NMe-acac (see Appendix C.1.22) complexes, a $d_{x^2-y^2}$ orbital was observed for ruthenium and osmium, while the NPh-acac (see Appendix C.1.27) complexes have a d_{z^2} orbitals for these metals. In the HOMO molecular orbitals of the NH-acac, NMe-acac and NPh-acac complexes display a d_{z^2} metal orbital.

Table 12.4 Molecular Orbitals of the second row transition metal calculated structures of [M(cod)(NH-acac)]. Metals (cyan), carbon (grey), oxygen (red), nitrogen(blue) and hydrogen (light grey).

	HOMO-1	HOMO	LUMO	LUMO+1
Tc(I)	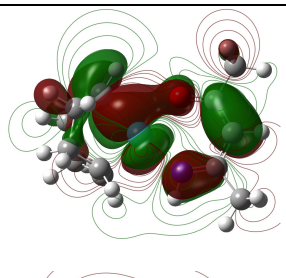	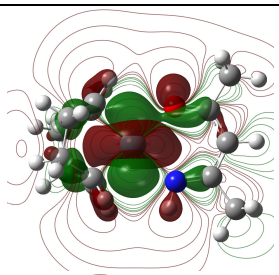	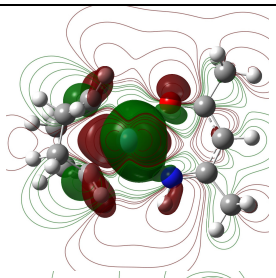	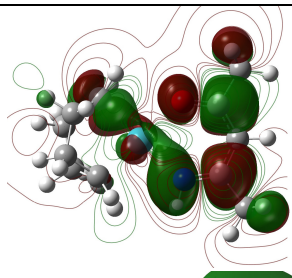
Ru(0)	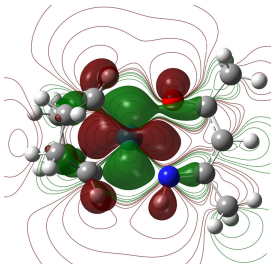	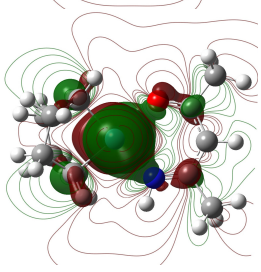	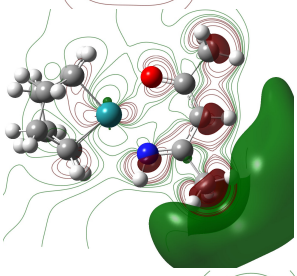	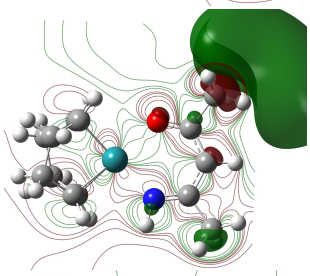
Rh(I)	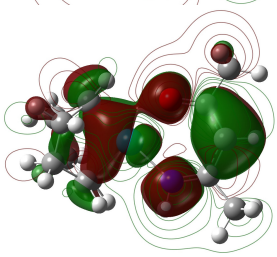	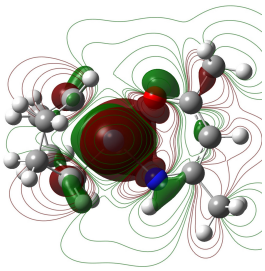	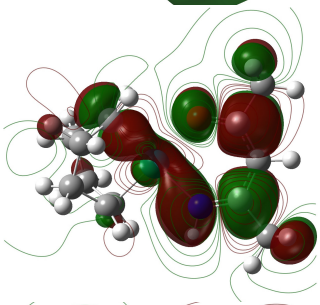	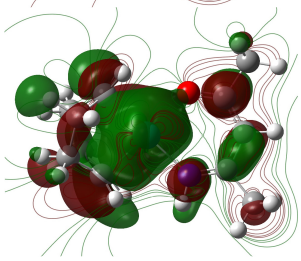
Pd(II)	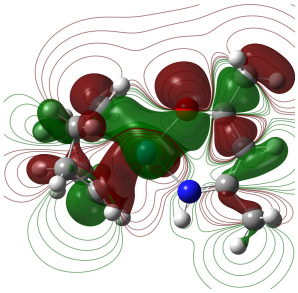	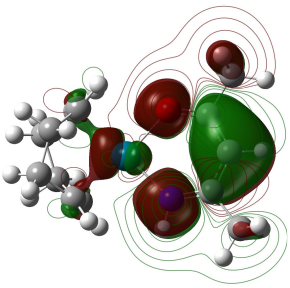	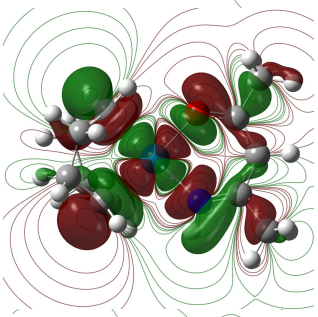	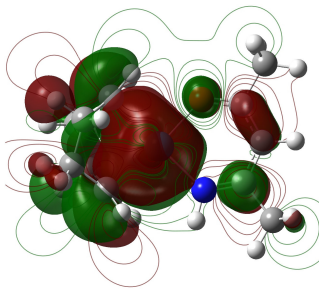
Ag(I)	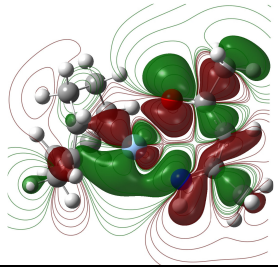	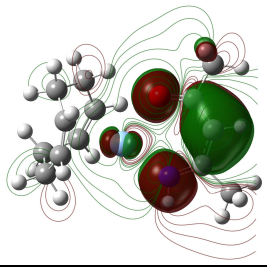	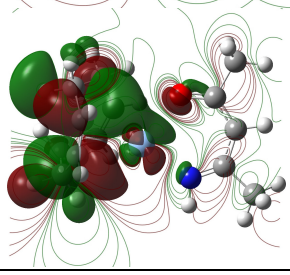	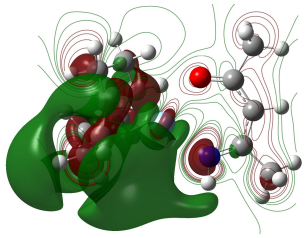

For group 9 the HOMO-1 molecular orbitals of the NH-acac complexes (see Appendix C.1.18), the *trans* influence on the π delocalization of the cyclo-octadiene was observed. While for the NMe-acac (see Appendix C.1.23) complexes a d_{xy} orbital with an in-phase overlap of the *p* orbitals of the alkene carbons of the cyclo-ocatdiene

was observed. For the NPh-acac (see Appendix C.1.28) complexes a d_{yz} orbital centered on the metals with an in-phase overlap of the *p* orbitals of the alkene carbons of the cyclo-octadiene was seen. Additionally the π orbital delocalizstion on the back-bone of the NPh-acac ligand was observed. In the HOMO molecular orbitals for the NH-acac, NMe-acac and NPh-acac complexes, a d_{z^2} orbital was found for all the metal centers. For the LUMO molecular orbitals of NH-acac, NMe-acac and NPh-acac complexes the *trans* influence can again be seen. In the LUMO+1 molecular orbitals of the NMe-acac complexes a d_{z^2} orbitals was seen for all group metals. For rhodium and iridium NPh-acac complexes the π orbital delocalization on the phenyl ring of the NPh-acac ligand is clearly visible, with the rhodium complex having a $d_{x^2-y^2}$ orbital.

For group 10 the HOMO-1 molecular orbitals of the NH-acac (see Appendix C.1.19) and the NMe-acac (see Appendix C.1.24) complexes, the *p* orbitals are seen on the carbon adjacent to the oxygen of the NH-acac ligand with an in-phase overlap of the metal orbitals with the alkene *p* orbitals of the cyclo-octadiene. For the NPh-acac (see Appendix C.1.29) molecular orbitals the π orbital delocalization on the phenyl ring is most prominent, whilst the pattern seen for the NH-acac and the NMe-acac complexes is not present in the NPh-acac complex molecular orbitals. In the HOMO molecular orbitals of the NH-acac and NPh-acac complexes, the π delocalization on the back-bone is clearly visible. In the NMe-acac complexes, the metals have a d_{yz} orbitals with the *p* orbitals of the methyl carbon of the NMe-acac ligand clearly seen. For the LUMO molecular orbitals of the NH-acac, NMe-acac and the NPh-acac complexes, a $d_{x^2-y^2}$ orbitals were observed for all metals of the group. In the LUMO+1 molecular orbitals for the NH-acac, NMe-acac and the NPh-acac complexes, a d_{z^2} orbital centered on the metals was seen.

For group 11 the HOMO-1 molecular orbitals of the NH-acac and the NMe-acac (see Appendix C.1.25) complexes, a similar pattern to the group 10 molecular orbitals was seen. For the NPh-acac (see Appendix C.1.30) complexes a d_{xz} orbital centered on the group metals is observed whilst the *p* orbital of the carbon adjacent to the oxygen is dominant. The *p* orbitals of the phenyl ring are also clearly visible. In the HOMO molecular orbitals of the NH-acac, NMe-acac and the NPh-acac complexes, the d_{yz}

orbitals for the metals is visible with π delocalization on the NH-acac ligand. For the LUMO molecular orbitals of the NH-acac complexes, the copper and gold complexes display a d_{xy} orbital with additional *p* orbitals centered on the NH-acac ligands whilst the silver complex has a d_{xz} orbital with additional orbitals seen on the cyclo-octadiene. While the NMe-acac complexes have a d_{xz} orbitals for the group metals, with silver displaying additional orbitals on the cyclo-octadiene. For the NPh-acac complexes a d_{xy} orbitals were observed for the group metals. In the LUMO+1 molecular orbitals of the NMe-acac and the NPh-acac complexes, the metals have a d_{xz} orbital configuration with sliver being obscured.

12.7 Correlation of Group 7-11 Transition Metal Molecular Orbital Energies

After visually comparing the orbitals it was deduced that there were indeed changes for the various molecular orbitals and as such a more concrete method of comparison would be needed. Two methods of achieving this goal were to firstly, look at the HOMO-1, HOMO, LUMO and LUMO+1 molecular orbital energies in conjunction with their respective groups and triads. Secondly, the energy gap (band gap, E_g) between the HOMO and LUMO molecular orbitals and compare these with their respective groups and triads.

12.7.1 Orbital Energies

The molecular orbital energies of the group 7-11 transition metal β-diketonato, β-enaminonato and tropolonato complexes are presented. In Figure 12.6a the combined molecular orbital energies of the acetylacetonato (acac), trifluoroacetylacetonato (tfacac) and hexafluoroacetylacetonato (hfacac) ligand complexes are displayed with the corresponding values given in Table 12.5. Upon inspection of the group 7 metals we see only small changes in energy for the HOMO orbitals. With the LUMO orbitals following the reverse trend to the covalent radii, with manganese having a larger energy value and the smaller radii, whilst technetium and rhenium having similar radii display a similar energy. The LUMO+1 orbitals follow a similar trend but are not as pronounced. This trend is not seen in either the HOMO-1 or the HOMO molecular orbitals.

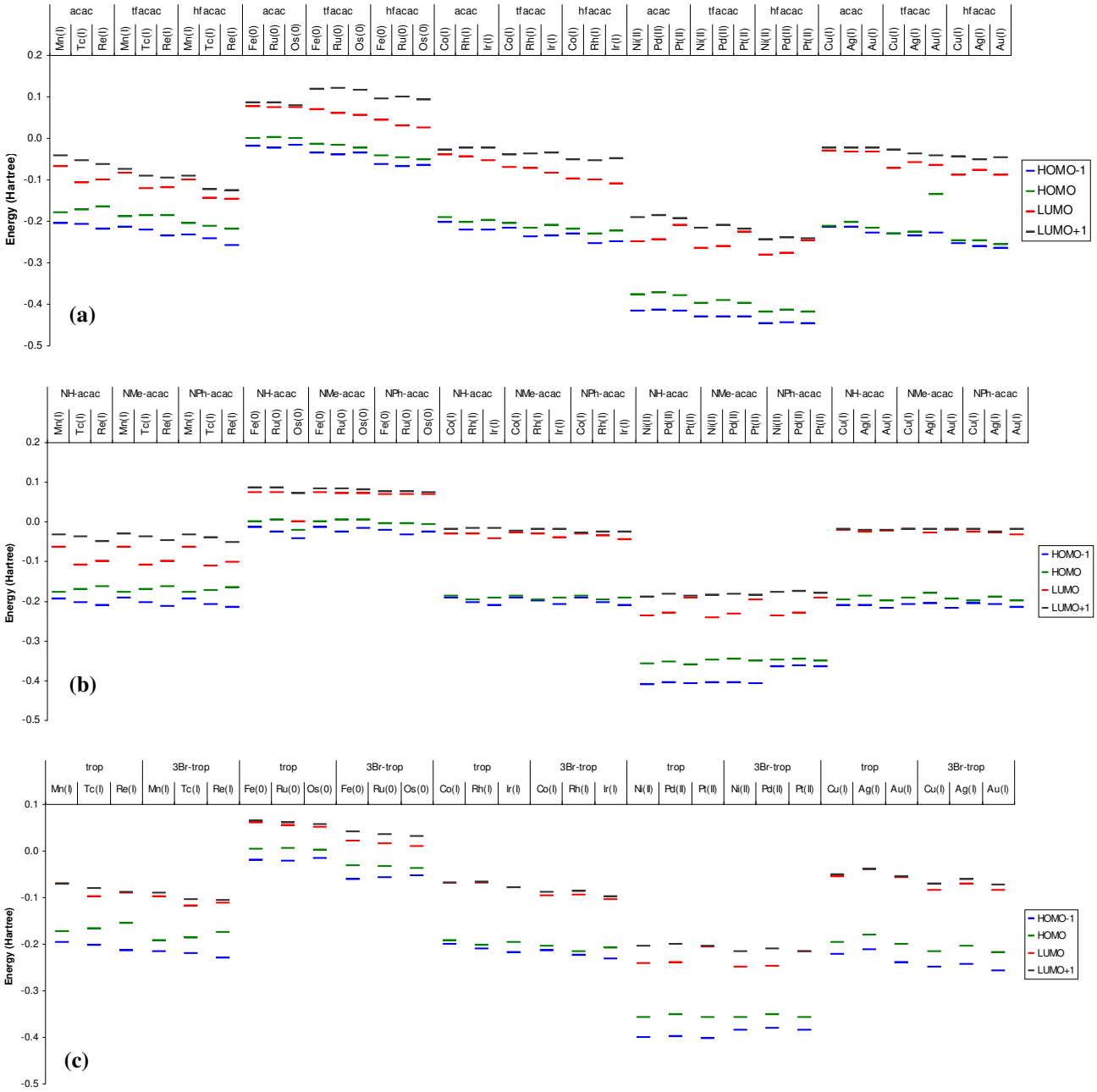

Figure 12.6 Combined graph of the Molecular Orbital Energies for the calculated structures of [M(cod)(LL')] where M = group 7-11 (a) LL' = acac, tfacac, hfacac (values in Table 12.5) (b) LL' = NH-acac, NMe-acac, NPh-acac (values in Table 12.6) (c) LL' = trop, 3Br-trop (values in Table 12.7).

For the group 8 metals the LUMO+1 grouping of the metals are similar, but when varying the ligand the higher energy was found to be the tfacac complexes with the hfacac complexes showing only slightly larger energy values than for the acac complexes. The major difference here is in the E_{g+1} energy gap which becomes significantly larger as a more electron withdrawing group is added. It is interesting to

note that the E_{g+1} of tfacac and hfacac are similar even though there is an additional CF_3 group. The HOMO-1 and HOMO orbitals display a similar decreasing pattern as the electron withdrawing groups are increased.

In the group 9 metals there is a small energy difference between the HOMO-1 and HOMO energies again following the trend of the covalent radii with the 3*d* elements generally being higher than the 4*d* and 5*d* elements with a small downward movement as the ligand is varied. A large E_g is observed which reduces as the ligand becomes more electron withdrawing.

The group 10 metals have an interesting pattern in their LUMO energies where the nickel and palladium have higher energies as opposed to that of the platinum. This pattern could result in the additional stability which was found for the platinum complexes of this study as opposed to the palladium complexes.

Even though the group 11 metals are mono co-ordinated they still have similar energies to their other counterparts. There is a consistently large E_g gap for the complexes, with no discernable trend.

In Figure 12.6b the combined molecular orbital energies of the group 7-11 metal 4-aminopent-3-en-2-onato (NH-acac), 4-(methylamino)pent-3-en-2-onato (NMe-acac) and 4-anilinopent-3-en-2-onato (NPh-acac) ligand complexes are displayed with the corresponding values in Table 12.6. By looking at the group 7 metals we see only small changes in energy for the HOMO orbitals following an increasing trend as the metal centers are varied. The HOMO-1 energies follow the reverse trend to the HOMO energies observed, creating an arrow head pattern.

For the group 8 metals the LUMO and LUMO+1 energies do not differ significantly the E_{g+1} is also similar for all the complexes. A similar pattern is seen for the HOMO and HOMO-1 energies with only slight differences as the metals are varied. Though the changing of the ligand does not significantly affect the energies. This pattern is observed for the group 9 and 11 metals.

The group 10 metals the E_{g-1} and E_{g+1} energies become smaller as the ligand is varied from the hydrogen, to the methyl and finally to the phenyl whilst the E_g value becomes larger. The LUMO energies show that nickel and palladium have lower

energies that was found for the platinum complexes, leading to the conclusion that the platinum complexes are more stable than the other metals of the triad. The LUMO+1 energies are however not influenced.

In Figure 12.6c the combined molecular orbital energies of the group 7-11 metal tropolonato (trop) and tribromotropolonato (3Br-trop) ligand complexes are displayed with the corresponding values in Table 12.7. By looking at the group 7 metals we see changes in energy for the HOMO orbitals following an increasing trend as the metal centers are varied. The HOMO-1 energies follow the reverse trend to the HOMO energies observed, creating an arrow head pattern. This pattern was clearly observed for the β-enaminonato metal complexes and to a lesser extent for the β-diketonato metal complexes.

In group 8 the HOMO and HOMO-1 energies are similar for the metals in the group, while the more electron withdrawing 3Br-trop ligand is found at a lower energy. For group 9 there is a large E_g energy gap, with the E_{g-1} and E_{g+1} energies being similar. When looking at the group 10 metals the LUMO orbitals show the same pattern as was found for the β-enaminonato metal complexes in that the nickel and palladium have a lower energy than that of platinum. For the group 11 metals it was observed that the energies follow the same pattern as the covalent radii in which silver is larger than gold with copper being the smallest.

In reviewing at the molecular orbital energies as well as the orbital diagrams it was observed that there is not much change between the different metals of a group when varying the ligand.

Table 12.5 Molecular Orbital Energies (Hartree) and energy gaps (eV) of the [M(cod)(LL')] where M = group 7-11 transition metals, LL' = acac, tfacac, hfacac calculated structures.

		HOMO-1	HOMO	LUMO	LUMO+1	E_{g-1}	E_g	E_{g+1}
acac	Mn(I)	-0.20518	-0.17857	-0.06776	-0.04222	0.724	3.015	0.695
	Tc(I)	-0.20782	-0.17265	-0.10786	-0.05271	0.957	1.763	1.501
	Re(I)	-0.21824	-0.16413	-0.09918	-0.06368	1.472	1.767	0.966
	Fe(0)	-0.01908	0.00031	0.07586	0.08644	0.528	2.056	0.288
	Ru(0)	-0.02429	0.00203	0.07467	0.08584	0.716	1.977	0.304
	Os(0)	-0.01664	0.00103	0.07373	0.08016	0.481	1.978	0.175
	Co(I)	-0.20259	-0.19064	-0.04069	-0.02711	0.325	4.080	0.370
	Rh(I)	-0.22052	-0.2027	-0.04321	-0.02291	0.485	4.340	0.552
	Ir(I)	-0.22107	-0.19721	-0.05459	-0.02341	0.649	3.881	0.848
	Ni(II)	-0.41512	-0.37704	-0.2485	-0.19038	1.036	3.498	1.582
	Pd(II)	-0.41333	-0.37277	-0.24407	-0.18711	1.104	3.502	1.550
	Pt(II)	-0.41536	-0.37796	-0.2089	-0.19198	1.018	4.600	0.460
	Cu(I)	-0.21446	-0.21275	-0.03095	-0.02222	0.047	4.947	0.238
	Ag(I)	-0.21381	-0.20262	-0.03302	-0.02321	0.304	4.615	0.267
	Au(I)	-0.22718	-0.21594	-0.03198	-0.02272	0.306	5.006	0.252
tfacac	Mn(I)	-0.21427	-0.18916	-0.08366	-0.07485	0.683	2.871	0.240
	Tc(I)	-0.21984	-0.18529	-0.12010	-0.09177	0.940	1.774	0.771
	Re(I)	-0.23494	-0.18704	-0.11941	-0.09599	1.303	1.840	0.637
	Fe(0)	-0.03413	-0.01331	0.06965	0.11841	0.567	2.257	1.327
	Ru(0)	-0.03893	-0.01728	0.06037	0.12038	0.589	2.113	1.633
	Os(0)	-0.03528	-0.02214	0.05647	0.11685	0.358	2.139	1.643
	Co(I)	-0.21678	-0.20386	-0.06975	-0.03921	0.352	3.649	0.831
	Rh(I)	-0.23809	-0.21609	-0.07161	-0.03822	0.599	3.932	0.909
	Ir(I)	-0.23516	-0.2101	-0.08299	-0.03560	0.682	3.459	1.290
	Ni(II)	-0.43120	-0.39845	-0.26550	-0.21647	0.891	3.618	1.334
	Pd(II)	-0.42921	-0.39186	-0.26038	-0.20955	1.016	3.578	1.383
	Pt(II)	-0.43061	-0.39882	-0.22539	-0.21889	0.865	4.719	0.177
	Cu(I)	-0.23134	-0.22934	-0.07155	-0.02734	0.054	4.294	1.203
	Ag(I)	-0.23476	-0.22546	-0.05830	-0.03648	0.253	4.549	0.594
	Au(I)	-0.22696	-0.13453	-0.06555	-0.04247	2.515	1.877	0.628
hfacac	Mn(I)	-0.23158	-0.20578	-0.09910	-0.09165	0.702	2.903	0.203
	Tc(I)	-0.24094	-0.21151	-0.14391	-0.12275	0.801	1.839	0.576
	Re(I)	-0.25700	-0.21761	-0.14712	-0.12550	1.072	1.918	0.588
	Fe(0)	-0.06342	-0.04070	0.04400	0.09620	0.618	2.305	1.420
	Ru(0)	-0.06670	-0.04710	0.03025	0.09915	0.533	2.105	1.875
	Os(0)	-0.06490	-0.05138	0.02674	0.09233	0.368	2.126	1.785
	Co(I)	-0.23116	-0.21777	-0.09765	-0.05155	0.364	3.269	1.254
	Rh(I)	-0.25425	-0.22933	-0.09930	-0.05364	0.678	3.538	1.242
	Ir(I)	-0.24932	-0.22313	-0.11044	-0.04807	0.713	3.066	1.697
	Ni(II)	-0.44688	-0.41904	-0.28213	-0.24358	0.758	3.726	1.049
	Pd(II)	-0.44519	-0.41317	-0.27726	-0.23849	0.871	3.698	1.055
	Pt(II)	-0.44604	-0.41874	-0.24547	-0.24215	0.743	4.715	0.090
	Cu(I)	-0.25267	-0.24765	-0.08765	-0.04372	0.137	4.354	1.195
	Ag(I)	-0.26026	-0.24607	-0.07579	-0.05214	0.386	4.634	0.644
	Au(I)	-0.26423	-0.25683	-0.08729	-0.04729	0.201	4.613	1.088

Table 12.6 Molecular Orbital Energies (Hartree) and energy gaps (eV) of the [M(cod)(LL')] where M = group 7-11 transition metals, LL' = NH-acac, NMe-acac, NPh-acac calculated structures.

		HOMO-1	HOMO	LUMO	LUMO+1	E_{g-1}	E_g	E_{g+1}
NH-acac	Mn(I)	-0.19394	-0.17725	-0.06413	-0.03232	0.454	3.078	0.866
	Tc(I)	-0.20340	-0.17122	-0.10739	-0.03797	0.876	1.737	1.889
	Re(I)	-0.21085	-0.16348	-0.09782	-0.04834	1.289	1.787	1.346
	Fe(0)	-0.01438	0.00113	0.07470	0.08602	0.422	2.002	0.308
	Ru(0)	-0.02485	0.00425	0.07363	0.08548	0.792	1.888	0.322
	Os(0)	-0.04307	-0.02008	0.00015	0.07297	0.626	0.550	1.982
	Co(I)	-0.19225	-0.18684	-0.02908	-0.01906	0.147	4.293	0.273
	Rh(I)	-0.20253	-0.19633	-0.03046	-0.01570	0.169	4.514	0.402
	Ir(I)	-0.21048	-0.19174	-0.04176	-0.01653	0.510	4.081	0.687
	Ni(II)	-0.40893	-0.35676	-0.23603	-0.18798	1.420	3.278	1.315
	Pd(II)	-0.40619	-0.35328	-0.22951	-0.18299	1.440	3.368	1.266
	Pt(II)	-0.40810	-0.35924	-0.19246	-0.18616	1.330	4.538	0.171
	Cu(I)	-0.21077	-0.19608	-0.02006	-0.01749	0.400	4.790	0.070
	Ag(I)	-0.21034	-0.18701	-0.02637	-0.02181	0.635	4.371	0.124
	Au(I)	-0.21852	-0.19768	-0.02264	-0.02064	0.567	4.763	0.054
NMe-acac	Mn(I)	-0.19218	-0.17730	-0.06388	-0.03029	0.405	3.086	0.914
	Tc(I)	-0.20321	-0.17133	-0.10931	-0.03658	0.867	1.688	1.979
	Re(I)	-0.21212	-0.16401	-0.10016	-0.04665	1.309	1.737	1.456
	Fe(0)	-0.01399	0.00161	0.07367	0.08405	0.424	1.961	0.282
	Ru(0)	-0.02464	0.00443	0.07287	0.08339	0.791	1.862	0.286
	Os(0)	-0.01659	0.00536	0.07178	0.08201	0.597	1.807	0.278
	Co(I)	-0.19055	-0.18605	-0.02729	-0.02219	0.122	4.320	0.139
	Rh(I)	-0.19859	-0.19683	-0.02942	-0.01771	0.048	4.555	0.319
	Ir(I)	-0.20732	-0.19196	-0.03996	-0.01784	0.418	4.136	0.602
	Ni(II)	-0.40565	-0.34794	-0.24074	-0.18502	1.570	2.917	1.516
	Pd(II)	-0.40513	-0.34509	-0.23256	-0.18095	1.634	3.062	1.404
	Pt(II)	-0.40713	-0.35095	-0.19542	-0.18401	1.529	4.232	0.310
	Cu(I)	-0.20778	-0.19058	-0.01881	-0.01819	0.468	4.674	0.017
	Ag(I)	-0.20564	-0.18069	-0.02798	-0.01944	0.679	4.155	0.232
	Au(I)	-0.21721	-0.19289	-0.02096	-0.01863	0.662	4.678	0.063
NPh-acac	Mn(I)	-0.19463	-0.17775	-0.06438	-0.03354	0.459	3.085	0.839
	Tc(I)	-0.20705	-0.17207	-0.11017	-0.04083	0.952	1.684	1.887
	Re(I)	-0.21489	-0.16457	-0.10081	-0.05040	1.369	1.735	1.372
	Fe(0)	-0.02131	-0.00494	0.06888	0.07660	0.445	2.009	0.210
	Ru(0)	-0.03231	-0.00390	0.06878	0.07586	0.773	1.978	0.193
	Os(0)	-0.02585	-0.00551	0.06873	0.07514	0.553	2.020	0.174
	Co(I)	-0.19230	-0.18596	-0.03121	-0.02695	0.173	4.211	0.116
	Rh(I)	-0.20356	-0.19744	-0.03407	-0.02644	0.167	4.446	0.208
	Ir(I)	-0.21104	-0.19225	-0.04389	-0.02515	0.511	4.037	0.510
	Ni(II)	-0.36571	-0.34707	-0.23568	-0.17787	0.507	3.031	1.573
	Pd(II)	-0.36325	-0.34458	-0.22880	-0.17488	0.508	3.151	1.467
	Pt(II)	-0.36565	-0.35001	-0.19263	-0.17921	0.426	4.283	0.365
	Cu(I)	-0.20650	-0.19812	-0.02643	-0.01913	0.228	4.672	0.199
	Ag(I)	-0.20704	-0.18903	-0.02799	-0.02428	0.483	4.389	0.101
	Au(I)	-0.21528	-0.19878	-0.03160	-0.01924	0.449	4.549	0.336

Table 12.7 Molecular Orbital Energies (Hartree) and energy gaps (eV) of the [M(cod)(LL')] where M = Group 7-11 transition metals, LL' = trop, 3Br-trop calculated structures.

		HOMO-1	HOMO	LUMO	LUMO+1	E_{g-1}	E_g	E_{g+1}
trop	Mn(I)	-0.19541	-0.17272	-0.07123	-0.07122	0.617	2.762	2.721 x 10^{-4}
	Tc(I)	-0.20189	-0.16578	-0.09806	-0.08014	0.983	1.843	0.488
	Re(I)	-0.21389	-0.15565	-0.08968	-0.08876	1.585	1.795	0.025
	Fe(0)	-0.01911	0.00485	0.05994	0.06529	0.652	1.499	0.146
	Ru(0)	-0.02104	0.00535	0.05546	0.06060	0.718	1.364	0.140
	Os(0)	-0.01541	0.0025	0.05114	0.05649	0.487	1.324	0.146
	Co(I)	-0.20083	-0.19239	-0.06876	-0.06778	0.230	3.364	0.027
	Rh(I)	-0.21016	-0.20272	-0.06804	-0.06689	0.202	3.665	0.031
	Ir(I)	-0.21856	-0.19527	-0.07929	-0.07775	0.634	3.156	0.042
	Ni(II)	-0.40097	-0.35675	-0.24139	-0.20315	1.203	3.139	1.041
	Pd(II)	-0.39855	-0.35141	-0.23860	-0.19929	1.283	3.070	1.070
	Pt(II)	-0.40108	-0.35754	-0.20510	-0.20299	1.185	4.148	0.057
	Cu(I)	-0.22140	-0.19629	-0.05473	-0.05123	0.683	3.852	0.095
	Ag(I)	-0.21234	-0.18093	-0.03922	-0.03844	0.855	3.856	0.021
	Au(I)	-0.23887	-0.19969	-0.05651	-0.05420	1.066	3.896	0.063
3Br-trop	Mn(I)	-0.21546	-0.19223	-0.09722	-0.08937	0.632	2.585	0.214
	Tc(I)	-0.21915	-0.18553	-0.11797	-0.10397	0.915	1.838	0.381
	Re(I)	-0.22916	-0.17434	-0.11228	-0.10621	1.492	1.689	0.165
	Fe(0)	-0.06070	-0.0304	0.02164	0.04145	0.825	1.416	0.539
	Ru(0)	-0.05753	-0.03276	0.01583	0.03611	0.674	1.322	0.552
	Os(0)	-0.05264	-0.03711	0.00973	0.03227	0.423	1.275	0.613
	Co(I)	-0.21387	-0.20447	-0.09621	-0.08815	0.256	2.946	0.219
	Rh(I)	-0.22399	-0.21566	-0.09491	-0.08681	0.227	3.286	0.220
	Ir(I)	-0.23047	-0.20694	-0.10412	-0.09714	0.640	2.798	0.190
	Ni(II)	-0.38410	-0.35685	-0.24880	-0.21481	0.742	2.940	0.925
	Pd(II)	-0.38007	-0.35190	-0.24708	-0.21047	0.767	2.852	0.996
	Pt(II)	-0.38347	-0.35707	-0.21540	-0.21536	0.718	3.855	0.001
	Cu(I)	-0.24891	-0.21643	-0.08435	-0.07125	0.884	3.594	0.356
	Ag(I)	-0.24257	-0.20410	-0.07104	-0.06046	1.047	3.621	0.288
	Au(I)	-0.25692	-0.21861	-0.08529	-0.07319	1.042	3.628	0.329

12.7.2 Relative Band Gap Energies

In this second half of the molecular orbital energy discussion, the HOMO-LUMO gap energy differences (E_g) are presented graphically in Figure 12.7 with their respective values given in Table 12.5-12.7. A brief discussion and the band energy differences per group are thus given.

For group 7, the β-diketonato complexes a maximum difference of 1.3 eV between manganese acetylacetonato (acac) and technetium acac, with nominal changes in E_g between the ligands but for the 3*d* to 4*d* elements a large drop is observed. This pattern is again similar to the 2008 covalent radii (Table 12.1). A similar arrangement was found for the β-enaminonato and tropolonato complexes. The maximum difference found for the β-enaminonato complexes was 1.4 eV between manganese 4-aminopent-3-en-2-onato (NH-acac) complex and the technetium NH-acac complex. While the maximum difference seen for the tropolonato complexes was 1.0 eV found

for manganese tropolonato (trop) complex and the rhenium tribromotropolonato (3Br-trop) complex.

In group 8, the β-diketonato complexes a difference of 0.9 eV was observed between iron hexafluoroacetylacetonato (hfacac) complex and either the ruthenium or osmium acac complexes. Very little change was observed for the β-enaminonato and tropolonato complexes with a difference of 0.2 eV for both sets. For the β-enaminonato complexes this was found to be between osmium 4-anilinopent-3-en-2-onato (NPh-acac) and osmium 4-(methylamino)pent-3-en-2-onato (NMe-acac) complexes, while the osmium NH-acac complex was excluded from the calculation for being an outlier. In the tropolonato complexes the difference was obtained between the iron trop and osmium 3Br-trop complexes.

Within group 9, the β-diketonato complexes a difference of 1.3 eV was observed between rhodium acac and iridium hfacac complexes, with a general downward trend as one varies the ligands. This trend is reflected in the β-enaminonato complexes where a difference of 0.5 eV was found between rhodium NMe-acac and iridium NPh-acac complexes, whilst a difference of 0.9 eV was seen for the tropolonato complexes between rhodium trop and iridium 3Br-trop complexes. With the 3*d* elements having an intermediate energy between the higher 4*d* and lower 5*d* elements, this pattern is seen for all the ligands.

For group 10, the β-diketonato complexes a maximum difference of 1.2 eV was found between either the platinum hfacac or the platinum tfacac and the nickel acac complexes. A difference of 1.6 eV between platinum NH-acac and nickel NMe-acac was observed for the β-enaminonato complexes while a difference of 1.3 eV was found between the platinum trop and palladium 3Br-trop complexes. A minor upward trend for the β-diketones was observed while a downward trend for the tropolones was found with the β-enaminones again remaining constant.

In group 11, a difference of 0.7 eV was observed for the β-diketonato complexes between gold acac and copper tfacac. While a difference of 0.6 eV and 0.3 eV was found for the β-enaminonato and tropolonato complexes respectively.

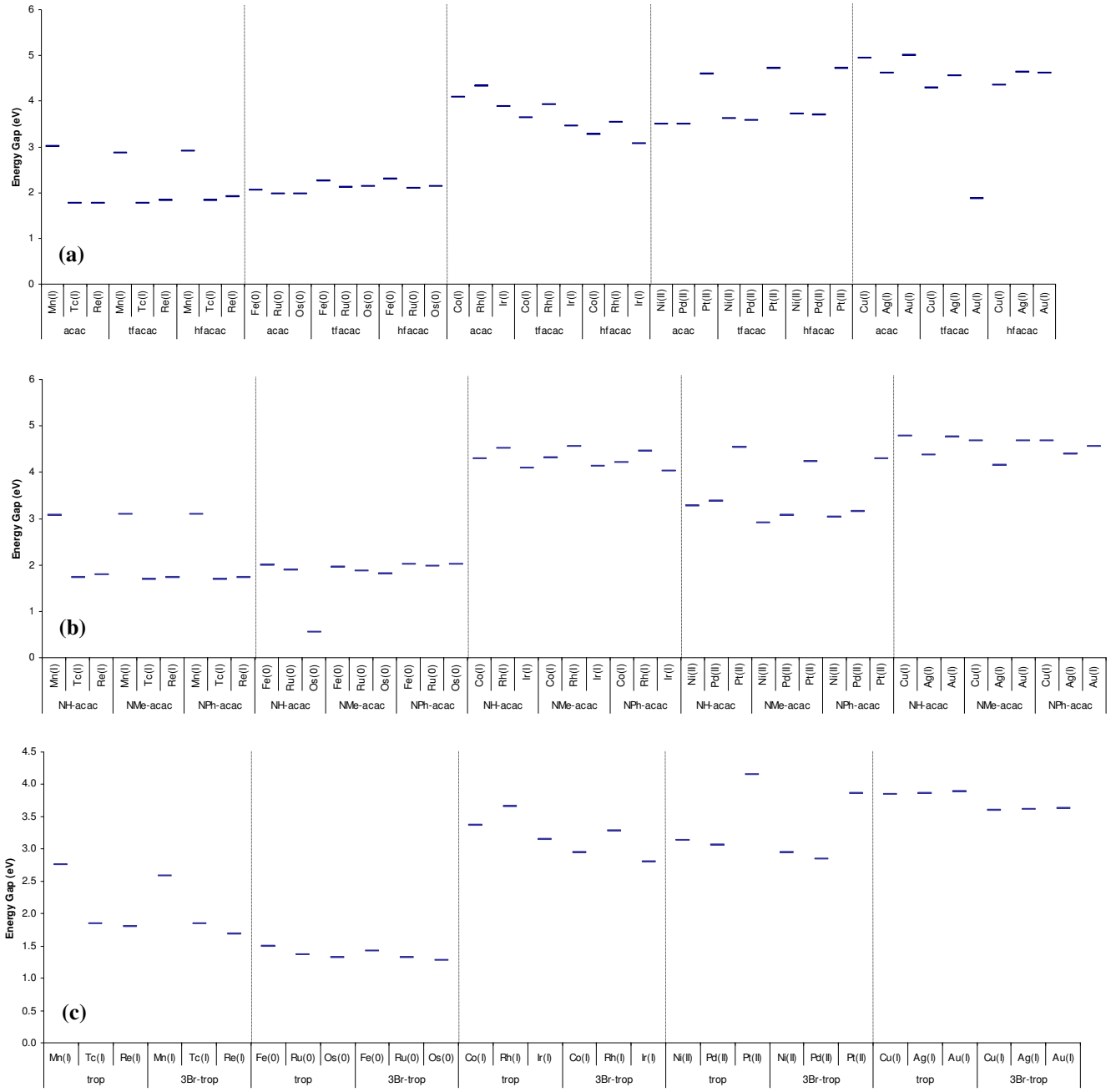

Figure 12.7 Combined graph of the Molecular Orbital Band Gap Energies (E_g) for the calculated structures of [M(cod)(LL')] where M = group 7-11 (a) LL' = acac, tfacac, hfacac (b) LL' = NH-acac, NMe-acac, NPh-acac (c) LL' = trop, 3Br-trop.

12.8 Correlation of Group 7-11 Transition Metal Infra-red Spectroscopic Data

In an attempt to further the understanding of the fundamental changes to the bonding of the cyclo-octadiene the infra-red (IRs) spectra of the complexes were calculated. Several problems were encountered as generally most of the frequency bands were

composed of many different vibrations making it difficult to assign a single vibration to a single peak. In the spectra presented only the major contributors to the peaks are listed. Another problem encountered with the peak assignments was the fact that the functional group ranges of the alkene's was found at 1680-1620 cm^{-1}, while C=O (ketone) was at 1690-1675 cm^{-1} / (1650-1590) cm^{-1} with the range in brackets being the conjugated ketone functionality. It is known that conjugation lowers the wavenumber of the functional group. The aromatic carbons also fall into this region with a range of 1615-1580 cm^{-1} / 1510-1450 cm^{-1}. The reported calculated frequencies are unscaled. The full infra-red spectra for all the metal complexes calculated per group is found in Appendix C.2.

A stacked graph (Figure 12.8) illustrating the symmetrical ν(C=O) and $\nu(C=C)_{cod}$ frequencies for the β-diktonato and tropolonato complexes is given. This is shown along with the combined ν(C=O) and ν(C=N) symmetrical frequency and the symmetrical stretching frequency for the alkene of the cyclo-octadine *cis* to the nitrogen group for the β-enaminonato complexes. Figure 12.8 represents an example of the calculated spectra for the β-diketonato, β-enaminonato and tropolonato complexes.

In Figure 12.8a the band at 1600 cm^{-1} is mainly comprised of $\nu(C=O)_{sym}$ stretching frequency, the iron (red) and palladium (cyan) are most shifted when looking at the HOMO molecular orbitals (see Appendix C.1.1) it is found that iron (red) has a very small contribution from the oxygen atoms of the acetylacetonato ligand which explains the small intensity of the peak seen in Figure 12.8a. Copper (purple), rhodium (green) and manganese (blue) have larger contributions. It is interesting to note that palladium (cyan) has an equally large molecular orbital contribution but is shifted down field as the contribution from the cyclo-octadiene is minimal. The largest shift was found between copper (purple) and iron (red) being 57 cm^{-1}. The band at around 1550 cm^{-1} mainly comprises of $\delta(CH)_{acac}$ (in-plane wag) of the methine proton of the acetylacetonato ligand, there is some shifting between the metal complexes but overall the frequency is in a very narrow range with the largest difference found between manganese (blue) and iron (red) of 22 cm^{-1}. The region from 1510 – 1400 cm^{-1} has the $\delta(CH_3)_{acac}$ with the larger of the peaks including the $\nu(C=O)_{asym}$ contribution, again palladium (cyan) is shifted.

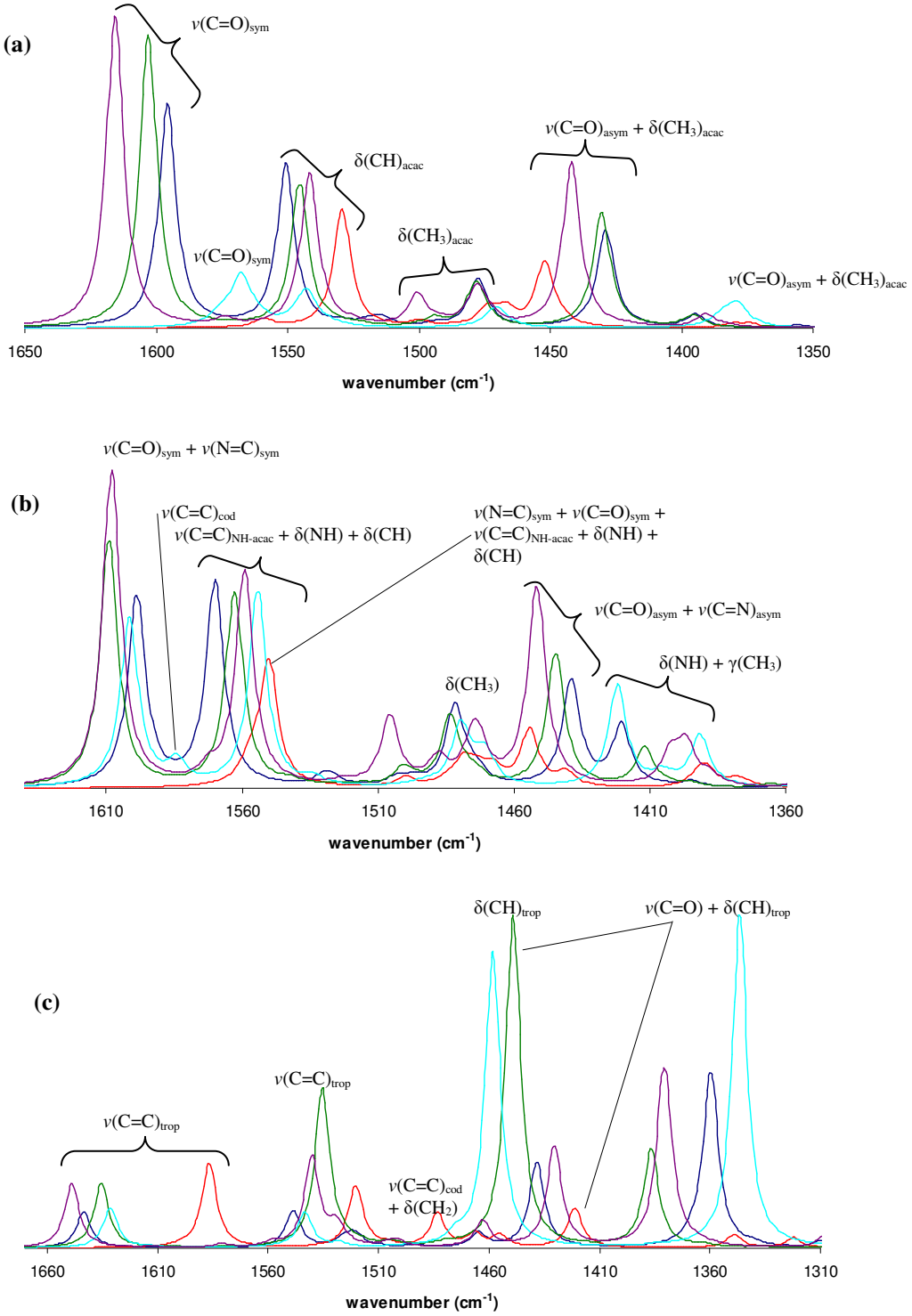

Figure 12.8 Calculated IR spectrum of (a) [Mn(cod)(acac)] (blue), $[Fe(cod)(acac)]^-$ (red), [Rh(cod)(acac)] (green), $[Pd(cod)(acac)]^+$ (cyan) and [Cu(cod)(acac)] (purple) (b) [Mn(cod)(NH-acac)] (blue), $[Fe(cod)(NH\text{-}acac)]^-$ (red), [Rh(cod)(NH-acac)] (green), $[Pd(cod)(NH\text{-}acac)]^+$ (cyan) and [Cu(cod)(NH-acac)] (purple) (c) [Mn(cod)(trop)] (blue), $[Fe(cod)(trop)]^-$ (red), [Rh(cod)(trop)] (green), $[Pd(cod)(trop)]^+$ (cyan) and [Cu(cod)(trop)] (purple). *ν* – stretching, δ – in-plane bending and γ – out-of-plane bending.

Within Figure 12.8b the band at 1610 cm^{-1} comprises of the symmetrical ν(C=O) and ν(C=N) frequencies, however iron (red) has these frequencies as the shoulder to the peak at around 1560 cm^{-1}. Additional peaks at 1584 cm^{-1} and 1573 cm^{-1} for palladium (cyan) and copper (purple) which are shoulders to the main peak are for the $\nu(C=C)_{cod}$ frequency. The band at 1560 cm^{-1} is comprised of $\nu(C=C)_{NH\text{-}acac}$, δ(NH) and $\delta(CH)_{NH\text{-}acac}$ frequencies for all the calculated metal complexes with the largest difference being manganese (blue) and iron (red) with a value of 20 cm^{-1}. For the band at 1440 cm^{-1} comprising of $\nu(C=N)_{asym}$ and $\nu(C=O)_{asym}$ frequencies it is interesting to note that palladium (cyan) did not have a comparable peak in this region, however the additional peaks that are grouped in the 1410 cm^{-1} band have additional vibrations of $\nu(C=C)_{NH\text{-}acac}$ and $\delta(CH)_{NH\text{-}acac}$.

In Figure 12.8c the region between 1510 cm^{-1} - 1660 cm^{-1} has the stretching frequencies of the aromatic carbons of the troplonato ligand, also included in this region is the in-plane wag of the hydrogens attached to the tropolone ring carbons. For iron (red) the $\nu(C=C)_{cod}$ frequency as well as $\delta(CH_2)$ vibrations are seen at 1483 cm^{-1} and 1467 cm^{-1}. It should be noted that for iron (red) the peak at 1421 cm^{-1} and the peak at 1449 cm^{-1} for rhodium (green) represent the ν(C=O) and $\delta(CH)_{trop}$ vibrations. While the lower peak at 1387 cm^{-1} for rhodium (green) is the pure $\delta(CH)_{trop}$. As was found for the molecular orbitals (see Appendix C.1.7) the spectra are dominated by the tropolone stretching frequencies. The region between 1410 cm^{-1} – 1310 cm^{-1} is assigned primarily to the ν(C=O) frequency.

In group 7, $\nu(C=C)_{cod}$ frequency was found that the $3d > 4d > 5d$ elements, while an increase is observed as one varies the ligands. This trend holds for the β-diketonato, β-enaminonato and tropolonato complexes.

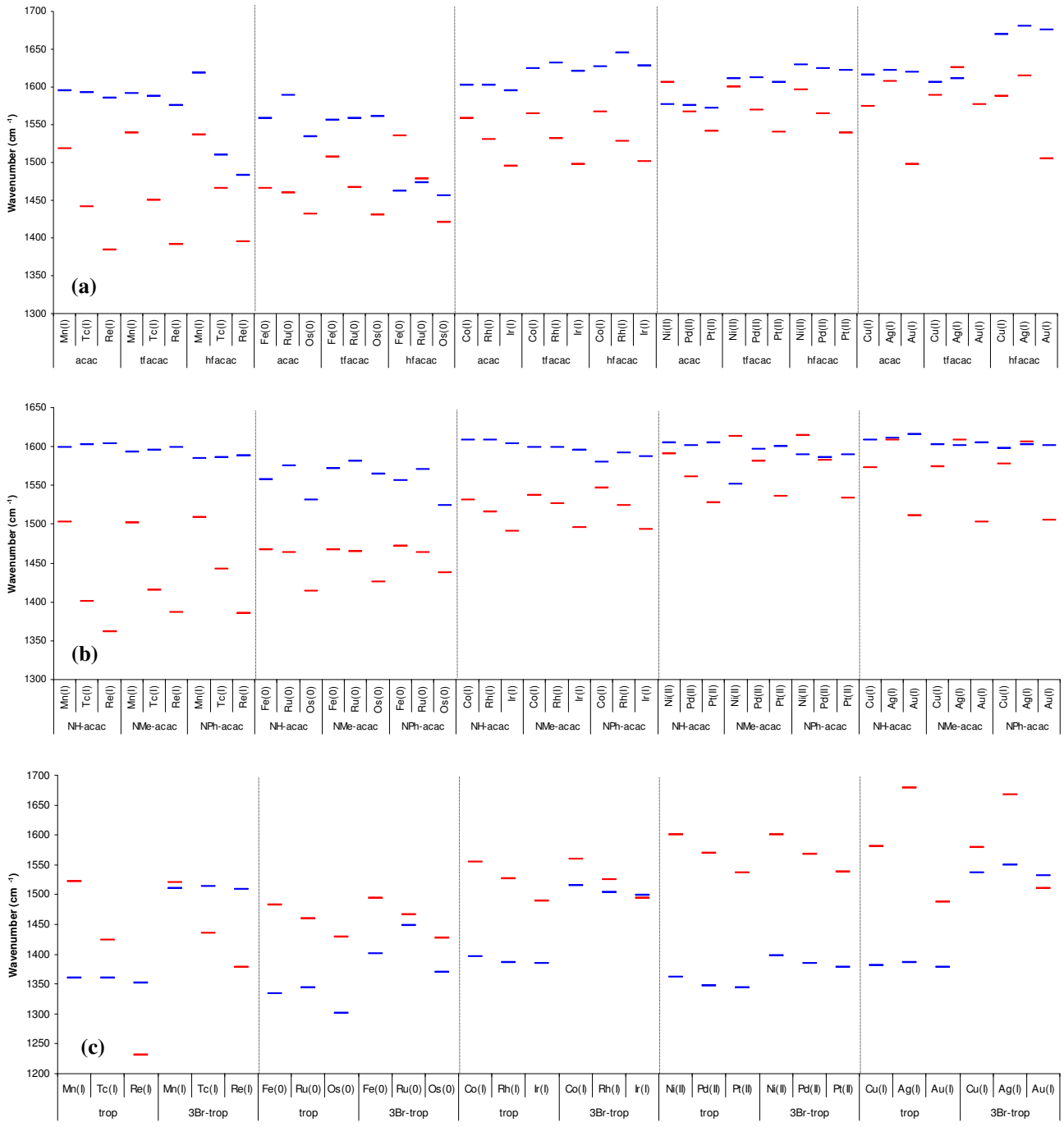

Figure 12.9 Plot of wavenumbers (cm^{-1}) of $[M(cod)(LL')]^n$ where M = group 7-11 transition metals, n = -1, 0, +1 (a) LL' = acac, tfacac, hfacac (b) LL' = NH-acac, NMe-acac, NPh-acac (c) LL' = trop, 3Br-trop. In (a) $\nu(C{=}O)_{sym}$ (blue) and $\nu(C{=}C)_{cod\text{-}sym}$ (red), (b) combined $\nu(C{=}O)$ and $\nu(C{=}N)$ symmetrical (blue) and $\nu(C{=}C)_{cod\text{-}transN}$ (red) and (c) $\nu(C{=}O)_{sym}$ (blue) and $\nu(C{=}C)_{cod\text{-}sym}$ (red) are plotted, with values found in Appendix C.2 Table C.2.1 and C.2.2.

For the ν(C=O) frequencies the β-diketonato complexes a decrease is observed, with the hexafluoroacetylacetonato (hfacac) complexes showing the greatest decrease down the triad. The β-enaminonato complexes show a small increase down the triad,

while a similar small decrease was seen as the ligand was varied. The tropolonato complexes are similar both down the triad and in the variation of the ligands.

For group 8, $\nu(C{=}C)_{coc}$ frequency was seen that $3d > 4d > 5d$ elements for the β-diketonato, β-enaminonato and tropolonato complexes. In varying the ligands, the β-diketonato complexes a large increase was seen for the iron, a small increase for ruthenium whilst a decrease for osmium was found. The β-enaminonato complexes for both iron and ruthenium remained invariant whilst osmium showed an increase. The tropolonato complexes remained invariant for all the metals. For the ν(C=O) frequencies the order $4d > 3d > 5d$ elements was seen for all the complexes with the exception of the trifluoroacetylacetonato (tfacac) complexes where $3d < 4d < 5d$ was found.

Within group 9, two prominent trends are observed for the $\nu(C{=}C)_{cod}$ frequencies for the complexes those being a downward trend for the triad with little to no increase as the ligands are varied. Upon inspection of the ν(C=O) frequencies a general upward trend was found for the tropolonato and β-diketonato complexes, whilst a downward trend was seen for the β-enaminonato complexes.

In group 10, the two trends that were seen in group 9 for the $\nu(C{=}C)_{cod}$ frequencies are repeated. A similar situation is found for the ν(C=O) frequencies.

The series $4d > 3d > 5d$ for the $\nu(C{=}C)_{cod}$ frequencies was observed for the group 11 complexes. For the combined ν(C=O) and ν(C=N) frequencies of the β-enaminonato complexes small changes between the complexes were observed both for the triad and the variation of ligands. For the tropolonato complexes, down the triad is generally unchanging with an increase as one changes ligands. In the β-diketonato complexes the triad again shows similar frequencies.

12.9 Correlation of Group 7-11 Transition Metal Geometrical Parameters – Total Core Area

After looking at both the molecular orbitals and the infra-red spectra the next logical progression in the study was to analyze the actual bond distances and angles of the computed structures. To this end the "core" bond angles and distances were

measured. The definition of the core can be seen in Figure 12.2, while the A_{tot} values are given in Appendix C.3 Table C.3.1.

The area total (A_{tot}) was calculated with the following formulae

$$x = d(O_1 - O_2) + d(Ce_2 - O_1) + d(Ce_2 - O_2) \Big/ 2$$

$$t_1 = \sqrt{x[x - d(Ce_2 - O_1)][x - d(O_1 - O_2)][x - d(Ce_2 - O_2)]}$$

$$y = d(Ce_2 - O_1) + d(Ce_1 - Ce_2) + d(Ce_1 - O_1) \Big/ 2$$

$$t_2 = \sqrt{y[y - d(Ce_2 - O_1)][y - d(Ce_1 - Ce_2)][y - d(Ce_1 - O_1)]}$$

$$A_{tot} = t_1 + t_2$$

where d is the distance between the points on the rhombus seen in Figure 12.2

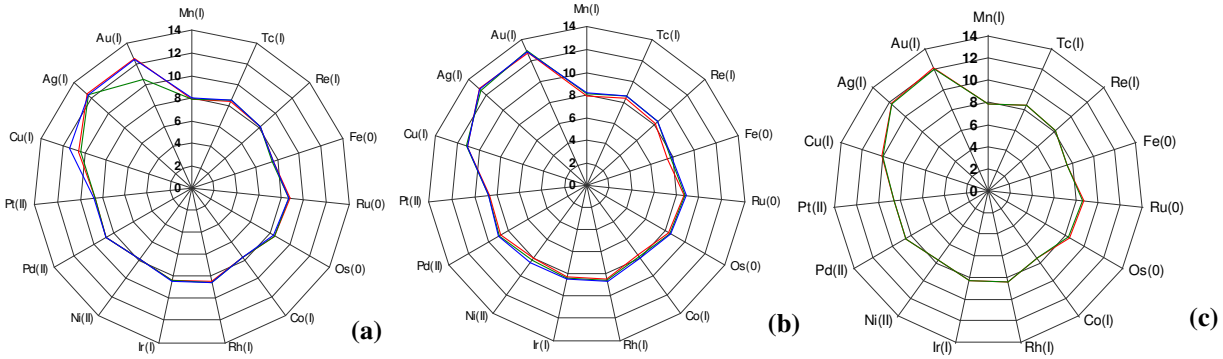

Figure 12.10 Spider plot of A_{tot} *vs.* [M(cod)(LL')] where M = group7-11 metals, (a) LL' = acac(red), tfacac (green), hfacac (blue) (b) LL' = NH-acac (red), NMe-acac (green), NPh-acac (blue) (c) LL' = trop (red), 3Br-trop (green). (see Figure 12.2 for the designation of the A_{tot} area)

In Figure 12.10 a spider plot of the total area of the "core" of the calculated β-dikentonato (Figure 12.10a), β-enaminonato (Figure 12.10b) and tropolonato (Figure 12.10c) metal complexes is presented, showing that the areas are well behaved for the group 7-10 metals, with the 3*d* elements showing a smaller area than that for the 4*d* and 5*d* elements, this is consistent with what has been found for the covalent radii of the metals (see Table 12.1). While the tropolonato complexes have a smaller total area than the β-enaminonato and β-diketonato complexes due to the difference in metal chelate ring size (*i.e.* five *vs.* six membered chelate rings).

For all the bidentate ligands the pattern was similar with only marginal differences being observed, leading to the conclusion that the area is not that significantly affected by the change of metal centre. This does not however hold for the group 11 metals. As has been repeatedly mentioned the cod at the metal centers are almost

mono co-ordinated, due to the reorientation of the cyclo-octadiene from a square planar configuration to a more trigonal pyramidal configuration. This reorientation drastically increases the calculated area, an example of the weaker co-ordination of the group 11 transition metals is seen in Figure 12.11

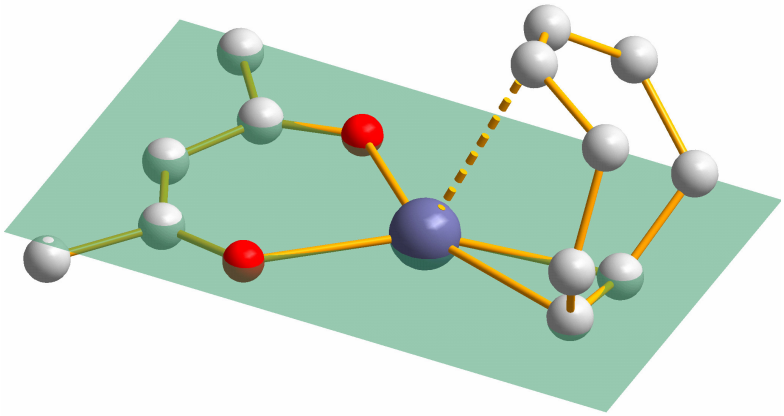

Figure 12.11 Diamond illustration of [Ag(cod)(acac)] illustrating the almost mono co-ordination of the group 11 complexes with 1,5-cyclo-octadiene, the equatorial plane passes though the oxygen atoms of the acetylaceonato ligand, the silver and one set of alkene carbons of the cyclo-octadiene. (Appendix C.8)

12.10 Correlation of Group 7-11 Lateral in-plane Metal Displacement

The area is not significantly affected by the change of metal (Figure 12.10) for the group 7-10 metals, a methodology was required to determine the "position" of the metal within the rhombus defined by the $Ce_1Ce_2O_2(N_1)O_1(N_1)$ atoms seen in Figure 12.2. A simple way of achieving this was the calculation of the percentage distance of the perpendicular from the metal (p_1) to the $Ce_1O_1(N_1)$ line (*i.e.* the $d(p_1\text{-}O_1)$ with the $Ce_1O_1(N_1)$ line). These are plotted in Figure 12.12 with the values in Appendix C.3.2, a line representing the middle point (*i.e.* 50 %) has been drawn on the graph, *i.e.* greater than 50 % the metal displacement is closer to the cyclo-octadiene ligand and less than 50 % it is closer to the bidentate ligand. As can be seen in Figure 12.12 most of the metals are hovering around the 50 % mark, with nickel and palladium β-diketonato, β-enaminonato and tropolonato complexes tending toward the cyclo-octadiene ligand. It is interesting to note that the 4-aminopent-3-en-2-onato (NH-acac) ligand has a higher affinity for the cyclo-octadiene ligand than that of the 4-(methylamino)pent-3-en-onato (NMe-acac) and 4-anilinopent-3-en-2-onato (NPh-acac) ligands (Figure 12.12b).

The general trend observed for the perpendicular distance is the 3*d* > 4*d* > 5*d* elements. For the β-diketonato group 8 complexes an average 2.4 % variance between the various ligands of the iron complexes was observed, with a reverse in the order for the comparable β-enaminonato complexes. It is of interest to note that the same ligands for the group 9 β-diketonato metals do not show the same ability that was observed for the group 8 metals. It is for this that the [Rh(cod)(acac)] complex was chosen as our model or "ideal" complex.

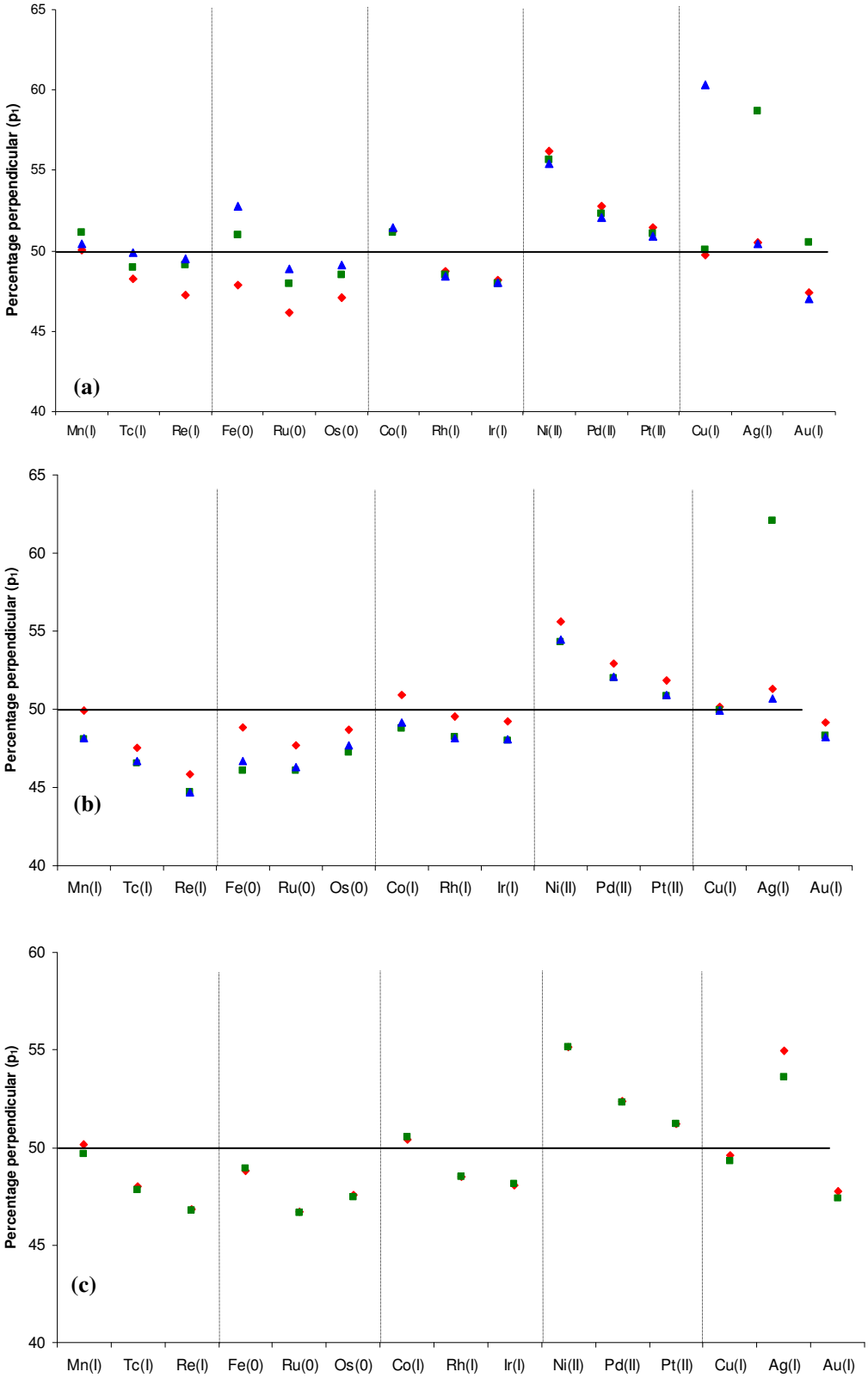

Figure 12.12 Graph of the percentage perpendicular p_1 [$d(Ce_1\text{-}O_1) - d(p_1\text{-}O_1) / d(Ce_1\text{-}O_1) * 100$] *vs.* [M(cod)(LL')] where M = group 7-11 metals, (a) LL' = acac (red), tfacac (green), hfacac (blue) (b) LL' = NH-acac (red), NMe-acac (green), NPh-acac (blue) (c) LL' = trop (red), 3Br-trop (green) with the mid-point marked as a solid line. (see Figure 12.2 for the definition of p_1).

12.11 Correlation of Group 7-11 Transition Metal Geometrical Parameters – "*trans* Ligand" Bite Angles

Next, the angles of the "core" need to be taken into account. The ideal angle for a square planar complex is 90°. The graph in Figure 12.13 represents the bite angles for the β-diketonato (O_1-M-O_2), β-enaminonato (O_1-M-N_1) and tropolonato (O_1-M-O_2) ligands as well as the cyclo-octadiene ligand with regards to the centroid angles of the alkenes (Ce_1-M-Ce_2) the values are given in Appendix C.3.3 and C.3.4. Most of the complexes are well behaved and are close to the ideal, it is interesting to note that as the one bite angle becomes smaller while the corresponding bite angle of the other ligand becomes bigger, this leads to a push-pull effect.

Generally the O_1-M-O_2, N_1-M-O_1 bite angles are larger than the Ce_1-M-Ce_2 bite angle with the exception of the group 7 metal complexes. The large variance for the group 11 metals for the Ce_1-M-Ce_2 bite angle is due to the mono co-ordination of the cyclo-octadiene (see Figure 12.11). The geometry of these metal complexes is also tending toward the trigonal pyriamidal as opposed to square planar. The variance pattern is very similar to the pattern observed for the percentage perpendicular as seen in Figure 12.12. The general trend for the triads was found to be $3d > 4d > 5d$ elements which is the same order that was observed for the lateral metal displacement (§ 12.10).

Due to the tropolonato complexes being a five membered chelating ligand the bite angle is much smaller, which is clearly seen in Figure 12.13c. It is of note that the O_1-M-O_2 bite angle follows a similar pattern to the covalent radii (see Table 12.1) in that as the radii increases the bite angle decreases. Again the group 11 metals are exceptions.

When looking across the groups one observes that the general trend of the Ce_1-M-Ce_2 bite angle is reasonably constant, while the bidentate bite angle increases (*i.e.* G7 < G8 < G9 < G10).

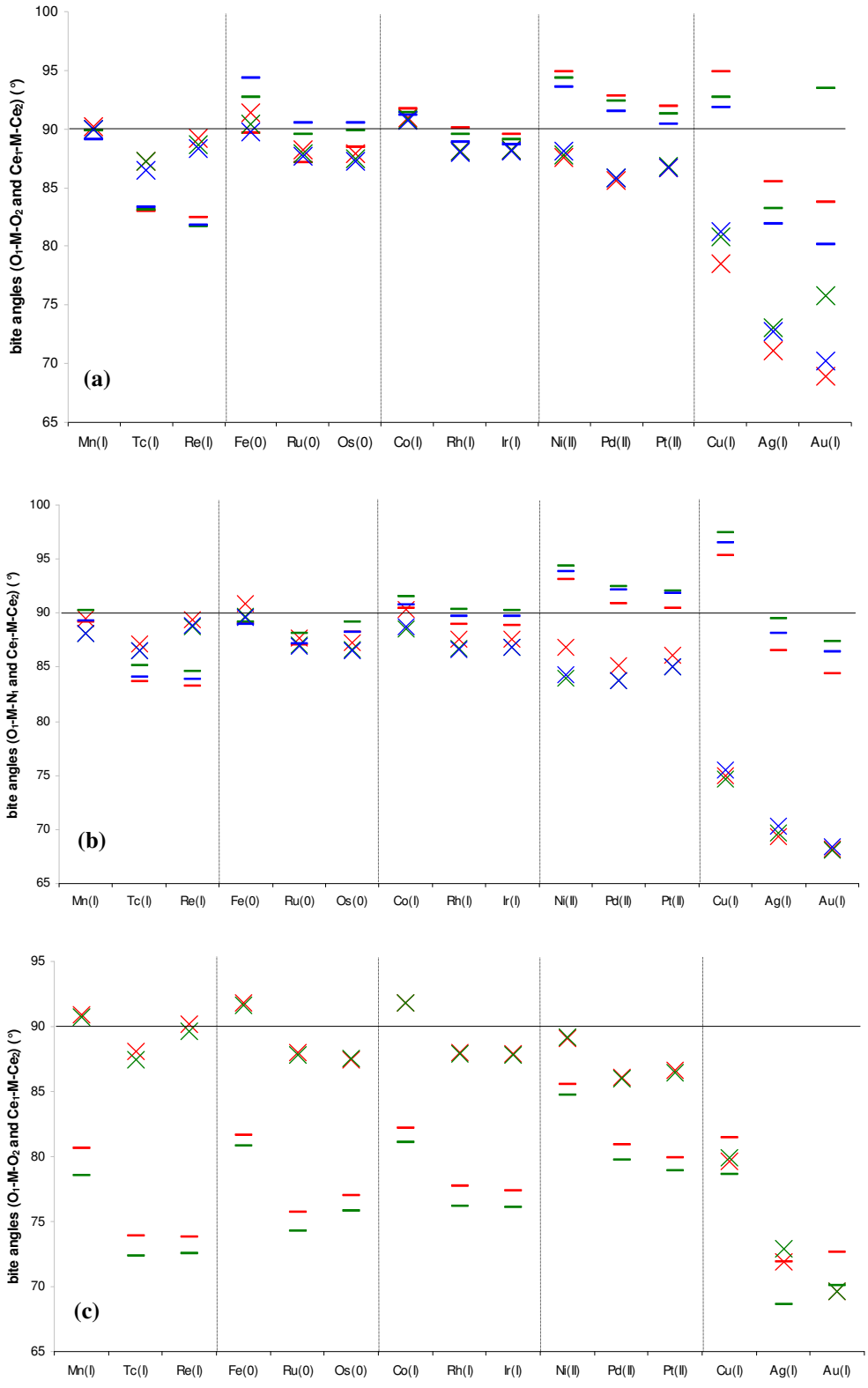

Figure 12.13 Graph of the *trans* ligand bite angle O_1-M-O_2 (line) and the cod ligand bite angle Ce_1-M-Ce_2 (multiplication sign)] *vs.* [M(cod)(LL')] where M = group 7-11 metals (a) LL' = acac (red), tfacac (green), hfacac (blue) (b) LL' = NH-acac (red), NMe-acac (green), NPh-acac (blue) (c) LL' = trop (red), 3Br-trop (green). (see Figure 12.2 for the definition).

12.12 Correlation of Group 7-11 Transition Metal Geometrical Parameters – Venus fly-trap Bite and Jaw (χ and ψ) Angles

After the discussion of the "core" geometry with regards to the area (A_{tot}), the percentage perpendicular distance (p_1) and the bite angles of the co-ordinating ligands a push-pull effect that was observed. Simply put as the metal moves within the "core" area, *i.e.* closer to one of the co-ordinating ligands, a decrease in the respective bite angle is observed.

With this observed push-pull effect within the "core" geometry, the influence of this on the Venus fly-trap angles needed to be investigated. The definition of the Venus fly-trap angles can be found in Figure 12.1. The χ and ψ angles for the $[M(cod)(LL')]^n$ where M = group 7-11 transition metals, LL' = acac, tfacac, hfacac (Figure 12.14a), NH-acac, NMe-acac, NPh-acac (Figure 12.14b), trop, 3Br-trop (Figure 12.14c) and n = -1, 0 , 1 metal complexes are presented.

For the ψ angle a downward increasing trend (*i.e.* $3d > 4d > 5d$) was observed for all the complexes. It was again found that iron had the greatest influence on the ψ angle with a difference of 13.8° between the acetylacetonato (acac) and hexafluoroacetylacetonato (hfacac) complexes, with the exception of the group 11 metals.

Upon inspection of the changes per group (Figure 12.14) of the ψ angle for the β-diketonato complexes the following was found

- Group 7: a difference of 5.5° between manganese hfacac and rhenium trifluoroacetylacetonato (tfacac) complexes
- Group 8: a difference of 6.2° between platinum hfacac and osmium tfacac complexes
- Group 9: a difference of 4.1° between cobalt hfacac and iridium acac complexes
- Group 10: a difference of 4.1° between nickel hfacac and platinum acac complexes

- Group 11: a difference of 9.4° between copper hfacac and gold acac complexes

A maximum change in the fly-trap angle (ψ) of the β-diketonato complexes was found to be 15.4°.

For the β-enaminonato complexes

- Group 7: a difference of 6.1° between manganese 4-anilinopent-3-en-2-onato (NPh-acac) and rhenium 4-(methylamino)pent-3-en-2-onato (NMe-acac) complexes
- Group 8: a difference of only 2.2° between iron NPh-acac and osmium 4-aminopent-3-en-2-onato (NH-acac) complexes
- Group 9: a difference of 4.0° between cobalt NPh-acac and iridium NMe-acac complexes
- Group 10: a difference of 4.5° between nickel NPh-acac and platinum NMe-acac complexes
- Group 11: a difference of 6.3° between copper NPh-acac and gold NH-acac complexes

The maximum change in the ψ angle for the β-enaminonato complexes was 14.2°.

For the tropolonato complexes

- Group 7: a difference of 5.5° between manganese tribromotropolonato (3Br-trop) and rhenium tropolonato (trop) complexes
- Group 8: a difference of 3.6° between iron 3Br-trop and osmium trop complexes
- Group 9: a difference of 3.9° between cobalt 3Br-trop and iridium trop complexes
- Group 10: a difference of 4.0° between nickel 3Br-trop and platinum 3Br-trop complexes
- Group 11: a difference of 10.2° between silver trop and gold 3Br-trop complexes

The maximum change in the ψ angle for the tropolonato complexes was 14.2°.

Upon comparing the χ (bite) angles of the cyclo-octadiene (cod) ligand, the variation across the ligand sets of 0.4°, 1.2° and 0.2° for the β-diketonato, β-enaminonato and

tropolonato ligands respectively, excluding the group 11 metals was observed. The largest variance was found for the nickel β-enaminonato complexes with a variance of 2.8°, the reason for the large deviation of the NH-acac complex is still unclear at this point.

The total variation in bite angle, excluding the copper triad for the β-diketonato, β-enaminonato and tropolonato are 5.2°, 6.9° and 4.9° respectively with an average of less than 6°.

The variation in bite angle within the coin metal triad is significant, *i.e.* 11.0°, 6.8°, 9.4° for the β-diketonato, β-enaminonato and tropolonato ligands respectively, assumed to be the result of the distortion from square planar geometry (Figure 12.11).

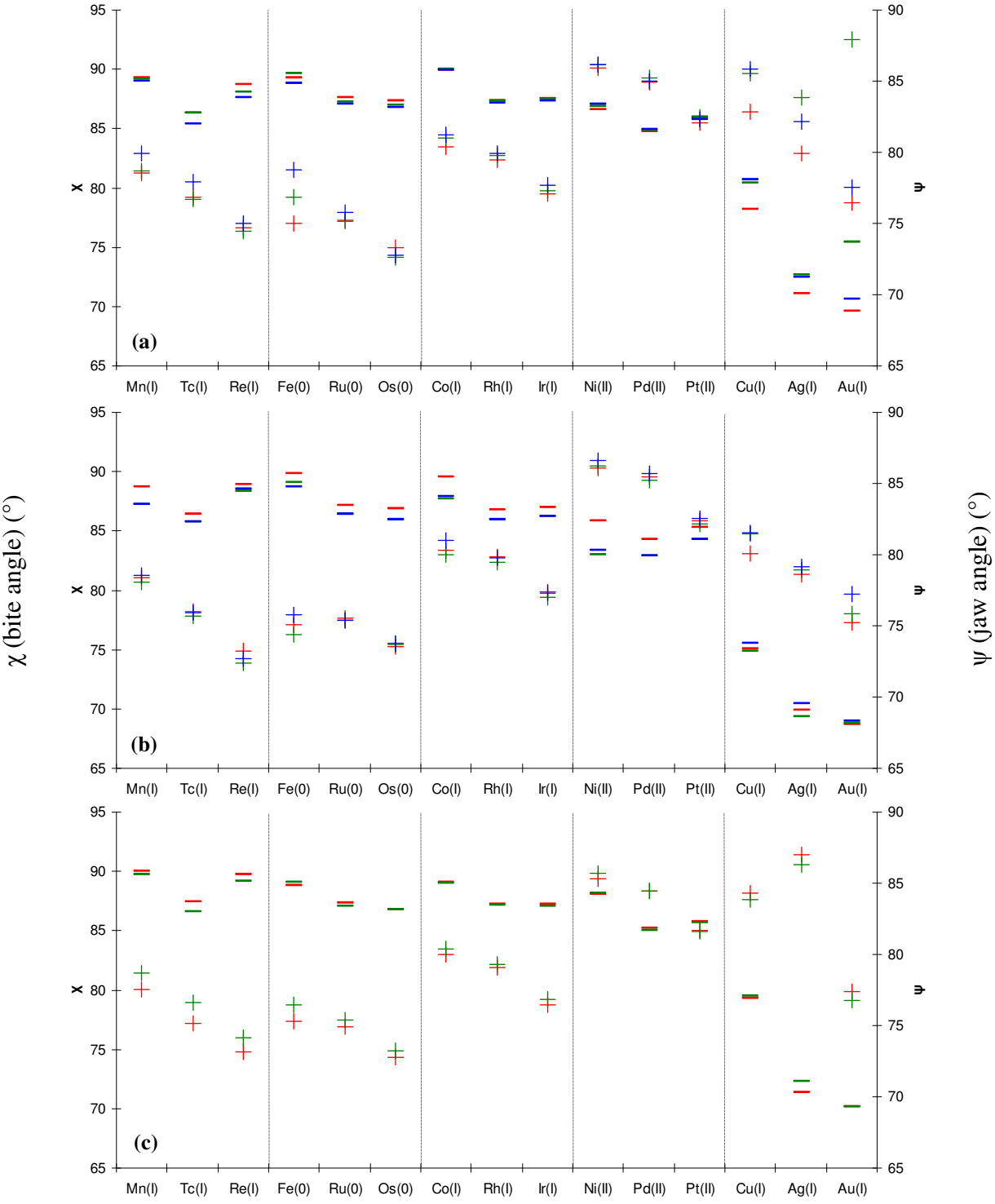

Figure 12.14 Graph of the [M(cod)(LL')]^n where M = group 7-11 transition metals, n = -1, 0, 1 (a) LL' = acac (red), tfacac (green), hfacac (blue) (b) LL' = NH-acac (red), NMe-acac (green), NPH-acac (blue) (c) LL' = trop (red), 3Br-trop (green) calculated complexes *vs*. χ (bite) (minus sign) and ψ (jaw) (plus sign) angles. The counter ions are omitted where applicable. (see Figure 12.1 for definition of χ (bite) and ψ (jaw) angles).

12.13 Discussion

For the X-ray crystal structures presented in this study (Chapters 4, 5, 7, 9 and 11) a large amount of hydrogen bonding interactions were observed. Even with these interactions the *R*-values obtained for the comparative computed structures (Chapters 6, 8, 10 and 11) were well above 97 %, with the overlays of the crystal structures with the computed structures showing an excellent agreement.

For the zero-point corrected energies (E_{corr}) it was found that an increase in energy as the ligand becomes more electron withdrawing, while the energy decreases as one moves down the triad.

For the energy corrected for metal effects (E_{rel}^{M}) for the electron withdrawing ligands the lowest energy found was for the cobalt complexes, whilst the donating ligands were seen to be the iron complexes. The energy across the triads was observed to increase (*i.e.* $3d < 4d < 5d$ elements)

In the energy corrected for ligand effects (E_{rel}^{L}) a trend matching the 2008 covalent radii (Table 12.1) was seen for all the triads. While a general decrease was seen across the groups.

For the molecular orbitals the metal centers for the HOMO and LUMO molecular orbitals were mostly either $d_{x^2-y^2}$ or d_{z^2}, with a few exceptions, while the *p* orbitals of both the cyclo-octadiene and the β-diketonato, β-enaminonato and the tropolonato ligands were observed. The π orbital delocalization of the bidentate ligands was also clearly seen. Of note was the fact that for the β-diketonato and β-enaminonato group ligands the orbital patterns found were remarkably similar for the comparable metal centers.

In the infra-red spectra of the computed complexes the $\nu(C{=}C)_{cod}$ frequencies were of a very low intensity mostly being overshadowed by other vibrations. For the d^6 and d^8 metals a similar pattern of $3d < 4d < 5d$ elements was observed for the frequencies for all the complexes. While the coin metals (d^{10}) a series of $4d > 3d > 5d$ was found. The peak assignments for the experimental spectra were assisted by the determination of the comparable computed structure. Interestingly enough in many cases in the

computed complexes the symmetrical and unsymmetrical stretching frequencies of the conjugated ketonoate and aminonate functionalities were observed.

The area graphs (A_{tot}) of the β-diketonato, β-enaminonato and tropolonato (see Figure 12.10) calculated metal complexes have a similar pattern that is linked to the covalent radii of the metals (see Table 12.1). For groups 7-10 the areas are well behaved whilst the mono co-ordinated group 11 metals fall outside of this behaviour. The areas are similar in values leading to the conclusion that the changing of the metal centre does not greatly influence the "core" distances (see Appendix D.3.1).

The percentage perpendicular graphs of β-diketonato, β-enaminonato and tropolonato (see Figure 12.12) calculated metal complexes have a similar pattern with most of the metal complexes tending toward the counter ligand than to the cyclo-octadiene with the most notable exceptions being the group 10 metals of nickel triad.

For the ligand bite angles (§ 12.11 Figure 12.13) the bidentate bite angles are mostly larger than the mid-point alkene bite angles. The general trend observed for the triads was $3d > 4d > 5d$, while across the groups the values remain constant for the mid-point alkene bite angle. While the bidentate bite angle increases as one proceeds from group 7-11.

With these effects combined the push-pull effect is seen where as one bite angle decreases the other increases. As previously mentioned the area remains similar and so the metal moves within the plane.

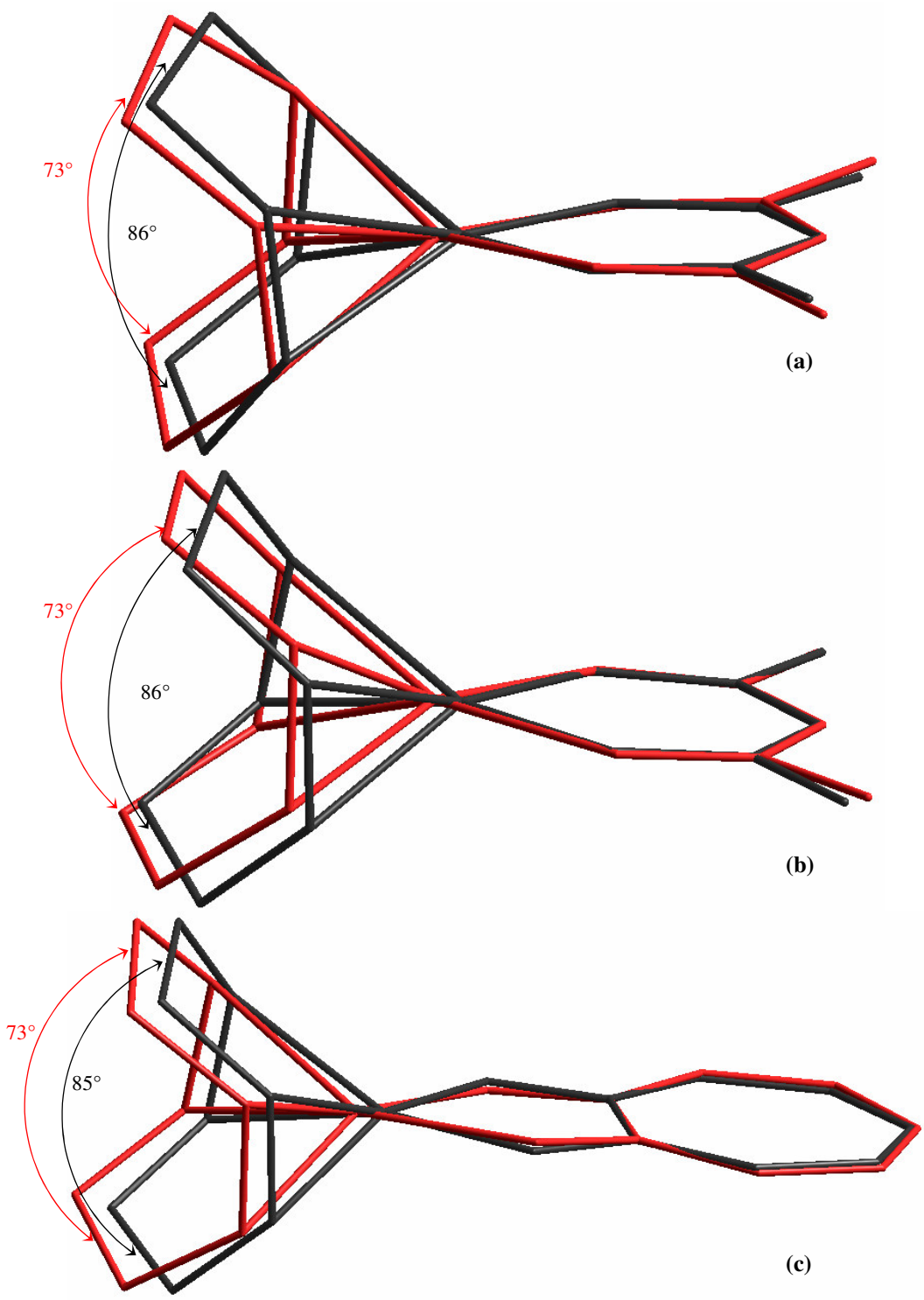

Figure 12.15 HyperChem superimposed image of (a) [Ni(cod)(acac)] (black) *vs.* [Os(cod)(acac)] (red) (b) [Ni(cod)(NH-acac)] (black) *vs.* [Re(cod)(NH-acac)] (red) (c) [Ni(cod)(trop)] (black) *vs.* [Os(cod)(trop)] (red) to show the opening of the ψ (jaw) angle of the cyclo-octadiene moiety.

Finally, the study of the various effects of the variations of the metal centers and the ligands to the bonding of the cyclo-octadiene moiety were investigated by the use of the χ and ψ angles (see Figure 12.1 for the definition). A maximum opening of the ψ angle of 15.4°, 14.2° and 14.2° for the β-diketonato, β-enaminonato and tropolonato

complexes were observed. While Figure 12.15 illustrates the opening of the ψ (jaw) angle for the various ligand sets (β-diketonato, β-enaminonato and tropolonato) utilizing the largest opening for a chosen ligand and metal centre. Similar downward trends are seen for the d^6 and d^8 metals, with the coin metals again being the exception due to the changing of the co-ordination geometry (Figure 12.11).

Chapter 13
Evaluation of Study

13.1 Introduction

One of the original motivations for this study was to gain further insight into the bonding modes of 1,5-cyclo-octadiene to various middle to late transition metal centers since these metals are known for its activities in a range of catalytic processes. The intension was the design of a theoretical model of the influences of the variations of the metal centers and ligands on the bonding mode and geometry of the 1,5-cyclo-octadiene ring, coined the "Venus fly-trap" system (see § 1.2 for the definition).

13.2 Evaluation

The first metal to be attempted was cobalt. The selection of the metal was due to its availability, cost and catalytic application. Several methods were attempted to synthesize the chosen model compound, [Co(cod)(acac)], but proved unsuccessful as cobalt(II) was a more stable oxidation state and had a tendency to form non-crystaline powders which were complex mixtures of different species.

Attention was then turned to copper which too has catalytic applications[1] as well as for chemical vapor deposition (CVD)[2] of thin films. A variation of the model complex [Cu(cod)(hfacac)][3] was previously prepared, however, upon a literature survey it was found that the model complex [Cu(cod)(acac)] could not be synthesized due to the lack of flourines in the ligand. Several synthetic methods were attempted to no success. Copper was thus left for future studies.

The search for an experimental metal center then proceeded to the second row of the transition metals. The first metal chosen was that of rhodium. The model complex [Rh(cod)(acac)] had both a simple synthetic route and was already characterized by X-ray single crystallography (§ 11.1).

---

[1] John A., Katiyar V., Pang K., Shaikh M.M, Nanavati H., Ghosh P., *Polyhedron*, **26**, 4033, (2007)
[2] Stabnikov P.A., Zharkova G.I., Baidina I.A., Tkachev S.V., Krisyuk V.V., Igumenov I.K., *Polyhedron*, **26**, 4445, (2007)
[3] Kunkely H., Vogler A., *Z. Naturforsch.*, **58b**, 704, (2003)

The study then proceeded to look at a range of ligands intended to systematically alter the binding mode of the 1,5-cyclo-octadiene to the metal centre.

The ligand sets were divided into three categories

- O,O-bidentate six membered metal chelate rings (β-diketonato type)
- O,N-bidentate six membered metal chelate rings (β-enaminonato type)
- O,O-bidentate five membered metal chelate rings (tropolonato type)

Within the first category, acetylacetone (Hacac), trifluoroacetylacetone (Htfacac), thenoyltrifluoroacetone (Hthtfac), hexafluoroacetylacetone (Hhfacac) and dibenzoylmethane (dbm) were chosen for their increasing electron withdrawing effect of the additional CF_3 moieties, whilst the phenyl for its electron donating capability.

The second category, the acetylacetone was functionalized with a primary amine. The amines selected were ammonium hydroxide, methylamine hydrochloride and aniline. The synthesis of these ligands were successful and are reported in § 3.3.

The ligands listed above were all mono anionic, thus, when co-ordinated, produced metal complexes which were molecular moieties.

Finally, the third category, tropolonato derivatives were chosen that of tropolone (Htrop) and tribromotropolone (H3Br-trop). Table 3.1 has a graphic representation of the ligands selected.

The synthesis of the rhodium complexes is reported in § 3.6.2. All compounds were successfully synthesized, with a few minor problems encountered for the β-enaminonato complexes. These were resolved by further purification however the [Rh(cod)(NMe-acac)] complex could not be synthesized. A possible reason for this may be that the final complex is partially water soluble. An initial precipitate was obtained, however on attempting to separate, the precipitate re-dissolves into the water. An alternative synthesis could not be found to date and the decision to leave the complex for a future study was taken.

Although the rhodium complexes were successfully synthesized, growing the crystals proved difficult. Several different techniques were attempted (vapor diffusion,

evaporation, layering, etc.) with several solvents and mixtures thereof. It was met with limited success. These crystal structures are presented in Chapter 11 and are listed below

- [Rh(cod)(acac)] (**25**)
- [Rh(cod)(dbm)] (**26**)
- [Rh(cod)(thtfac)] (**27**)
- [Rh(cod)(trop)] (**28**)

Hydrogen bonding interactions were observed for all the complexes, while π···metal chelate ring interactions were observed for complexes **26** and **27**.

The next metal selected palladium, with two different counter ions *i.e.* BF_4^- and PF_6^- to evaluate the effect of counter ion on the solid state properties. The synthesis of these most of the compounds were successful and are reported in § 3.4.2. The exceptions were [Pd(cod)(hfacac)]BF_4 and [Pd(cod)(NMe-acac)]BF_4, however, the PF_6^- version of the complexes low yields were obtained enough to partially characterize the complexes. The major problem encountered with the palladium compounds was that it was stable only for a limited period, generally 1 day up to a week depending on the complex prepared. The complexes also decomposed rapidly when in solution and as such crystal growing techniques proved difficult. Although a few palladium single crystals were obtained most decomposed before the crystals could be evaluated.

This lead the study to the last metal, platinum, which is known for its similarity in reactivity to palladium but without the side effect of rapid decomposition. Decomposition for the platinum complexes was found however, they were generally stable between 1-6 months depending on the complex. The complexes were successfully synthesized and are reported in § 3.5.2. Several single crystals were obtained and resolved.

The palladium β-diketonato single crystals that were obtained are presented in Chapter 4 and are listed below

- [Pd(cod)(acac)]PF_6 (**1**) and [Pd(cod)(acac)]BF_4 (**2**)
- [Pd(cod)(thtfac)]PF_6 (**3**) and [Pd(cod)(thtfac)]BF_4 (**4**)
- [Pd(cod)(tfacac)]PF_6 (**5**)

- [Pd(cod)(hfacac)]PF_6 (**6**)

A few interesting points were found for the palladium crystal structures. Extensive hydrogen bonding was observed for all the palladium crystal structures evaluated. While metal chelate ring interactions were seen for complex **2** and F···metal chelate ring interactions were found for complexes **3** and **4**. The complexes were not significantly distorted from the square planar co-ordination geometry (Figure 4.2), but some twisting was observed.

The platinum β-diketonato single crystals that were obtained are presented in Chapter 5 and are listed below

- [Pt(cod)(acac)]PF_6 (**8**) and [Pt(cod)(acac)]BF_4 (**7**)
- [Pt(cod)(dbm)]BF_4 (**9**)
- [Pt(cod)(thtfac)]BF_4 (**10**)

For the platinum complexes it was found that the complexes do not readily co-ordinate with electron withdrawing groups as a result the yields were low and fiber-like crystals were obtained. Modification of crystal growth techniques did not improve the situation. Hydrogen bonding interactions were seen for all platinum complexes. Metal chelate ring interactions were observed for complexes **8**, **9** and **10** leading to the clustered head-to-tail packing (an example is seen in Figure 5.8). The distortions seen in the square planar co-ordination geometry were of a similar order to those seen for the palladium crystal structures.

In continuing, the palladium and platinum tropolonato single crystal structures are presented in Chapter 7 and are listed below.

- [Pd(cod)(3Br-trop)]PF_6 (**11**) and [Pd(cod)(3Br-trop)]BF_4 (**12**)
- [Pd(cod)(trop)]PF_6 (**13**)
- [Pt(cod)(trop)]PF_6 (**14**) and [Pt(cod)(trop)]BF_4 (**15**)
- [Pt(cod)(3Br-trop)]PF_6 (**16**) and [Pt(cod)(3Br-trop)]BF_4 (**17**)

The palladium and platinum tropolonato complexes again show the hydrogen interactions which have become typical for this form of compound. It is interesting to note that π···π interactions were observed for selected tribromotropolonato complexes (**11** and **15**) while no such interactions were observed for the tropolonato complexes.

Br···Br and Br···F interactions were found for all the complexes. While Br···π interactions were only seen for complexes **11**, **12** and **14**. Additionally to the twist angle, this was still in the range of the previous crystals in the study. A bend angle (defined by the intersection of planes of the tropolone ring with the metal chelate ring) was included to describe the deviation of the tropolonato ligand from the plane of the complex.

For the second group of ligands that of the β-enaminonato type, the single crystal structures of palladium and platinum are presented in Chapter 9 and are listed below.

- [Pd(cod)(NH-acac)]BF_4 (**18**)
- [Pt(cod)(NH-acac)]BF_4 (**19**) and [Pt(cod)(NH-acac)]PF_6 (**20**)
- [Pt(cod)(NMe-acac)]BF_4 (**21**) and [Pt(cod)(NMe-acac)]PF_6 (**22**)
- [Pt(cod)(NPh-acac)]BF_4 (**23**) and [Pt(cod)(NPh-acac)]PF_6 (**24**)

Hydrogen bonding interactions are still prevalent for these complexes. Metal chelate ring interactions were observed for complexes **18**, **19** and **21** leading to the clustered head-to-tail packing. The twist angle still remains similar to the β-diketonato complexes.

For the transition metals chosen it was found that for selected complexes metal chelate ring interactions were observed as well as general hydrogen bonding. In furthering the understanding of the 1,5-cyclo-octadiene bonding mode to the various middle to late transition metals with a variety of counter ligands, a preliminary theoretical DFT study was undertaken.

The theoretical calculated structures of the group 7-11 transition metals with the following ligands were calculated.

- β-diketonato type
    - acetylacetone (Hacac)
    - trifluoroacetylacetone (Htfacac)
    - hexafluoroacetylacetone (Hhfacac)
- β-enaminonato type
    - 4-aminopent-3-en-2-one (HNH-acac)
    - 4-(methylamino)pent-3-en-2-one (HNMe-acac)
    - 4-anilinopent-3-en-2-one (HNPh-acac)

- tropolonato type
    - tropolone (Htrop)
    - tribromotropolone (H3Br-trop)

Initial DFT calculations were performed at the B3LYP/LanL2DZ level of theory, where the optimized structure (indicated by no imaginary frequencies) with the lowest energy was obtained. These structures were then re-calculated at a higher level of theory (B3LYP/6-311++G(d,p)) for the C, H, O, N, F, S atoms while the metals were kept at the same level of theory. Both infra-red spectra and molecular orbitals (HOMO-1, HOMO, LUMO, LUMO+1) were calculated and compared with the other calculated structures of the group. These are presented in Chapter 12.

A good correlation was observed between the crystal structures and the theoretical DFT calculations obtained with *R*-values (pair wise comparison of the bond lengths and angles) of with most > 99 %, these are presented in Chapters 6, 8, 10 and 11. It was interesting to note that the β-enaminonato ligands for the different metal triads were similar in their molecular orbitals, leading to the conclusion that the R-group attached to the nitrogen of the β-enaminonato ligand did not play as significant a role as was expected. The χ and ψ angles were calculated for all the structures and are presented in Chapter 12 shows a *c.a.* 15° variation induced by metal centre / ligand variation.

13.3 Future Studies

In this study only three β-enaminonato 1,5-cyclo-octadiene transition metal complexes were studied. A further study can be undertaken to fully understand the effect of the R-group of the β-enaminonato ligand on the 1,5-cyclo-octadiene transition metal complexes. This can be achieved both by experimental (synthetic and crystallographic) and theoretical work which would add to the data that has been collected and correlated within this study. Needless to say the inclusion of N,N-, N,S-, O,S-, P,P- and O,P- bidentate ligands would further the building of a complete theoretical model of the effect on the 1,5-cyclo-octadiene bonding mode.

By looking at the bonding mode of the 1,5-cyclo-octadiene, a complete kinetic study would assist in the adding of an additional parameter of the co-ordinated bond "strength" of the cyclo-octadine ligand, evaluating reactivity as a function of *trans* ligand.

To fully investigate the diolefin coin metal complexes co-ordination behaviour, both theoretically and experimentally *via* solid-state X-ray crystallography.

Finally, this study was investigating 1,5-cyclo-octadiene as a Venus fly-trap mimic, as previously mentioned in Chapter 2 there are several other diolefin ligands which have a similar mimicking capability. A fundamental study of with these diolefins in comparison with the 1,5-cyclo-octadiene investigation started here could provide valuable information with regards to alkene metal co-ordination. Which could in turn, assist in future catalytic processes to extend the theoretical model into more practical results driven process manipulation.

Appendix

A. Supplementary Infra-red Spectroscopic Data

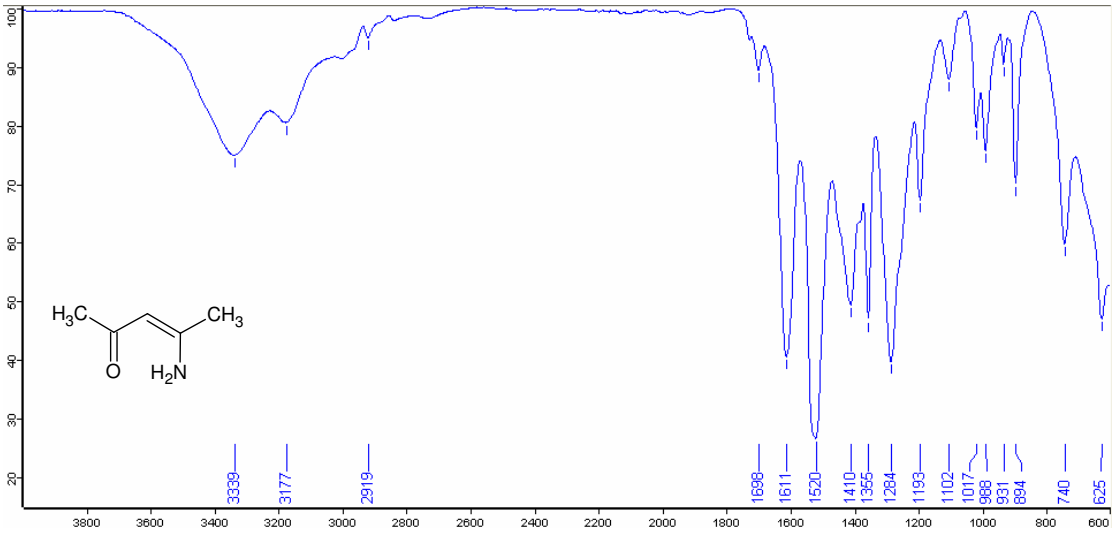

Figure A.1 Infra-red spectra of NH-acac

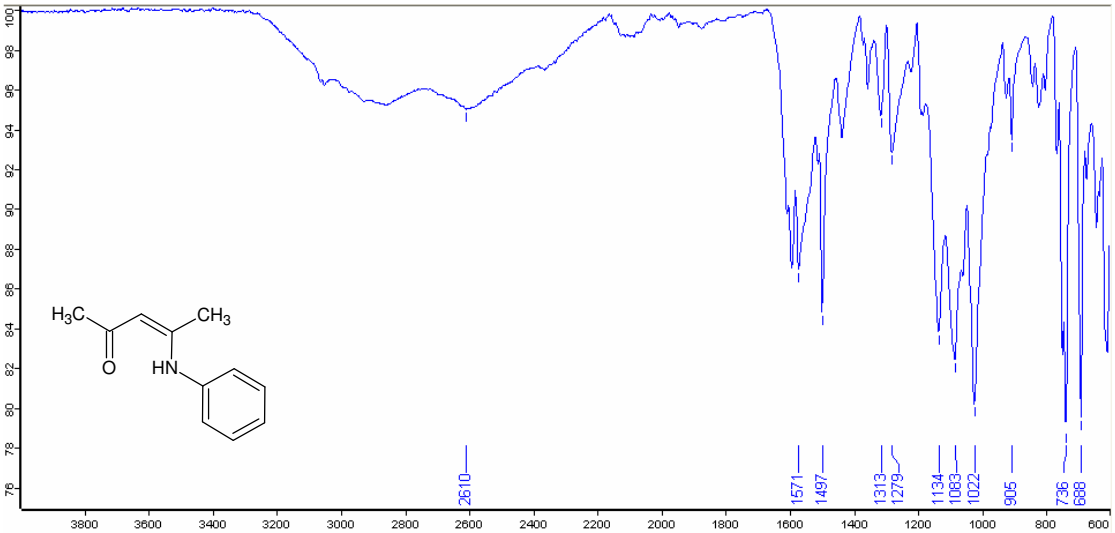

Figure A.2 Infra-red spectra of NPh-acac

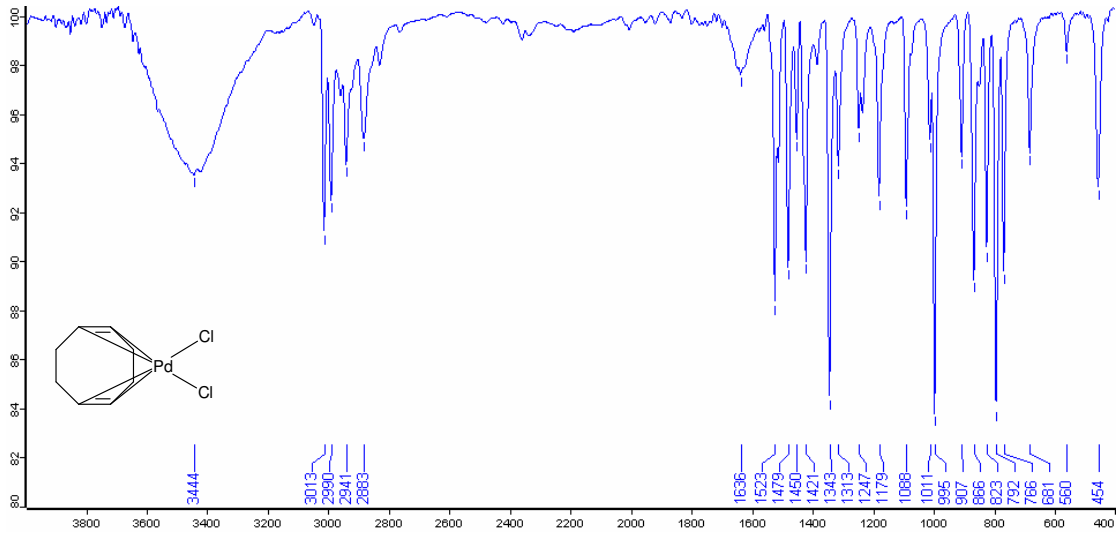

Figure A.3 Infra-red spectra of [Pd(cod)Cl_2]

Figure A.4 Infra-red spectra of [Pd(cod)(acac)]BF_4

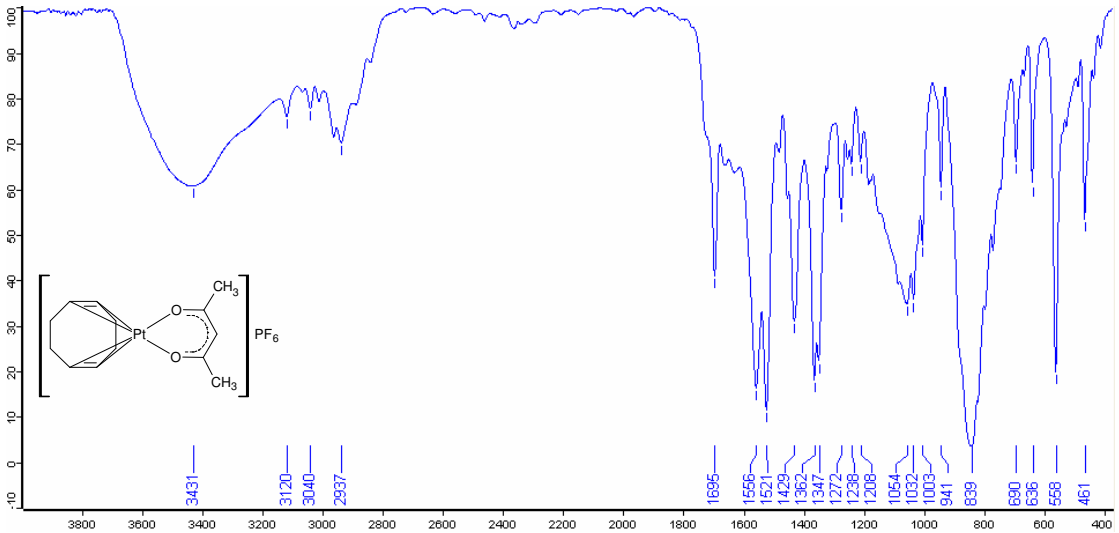

Figure A.5 Infra-red spectra of [Pd(cod)(acac)]PF_6

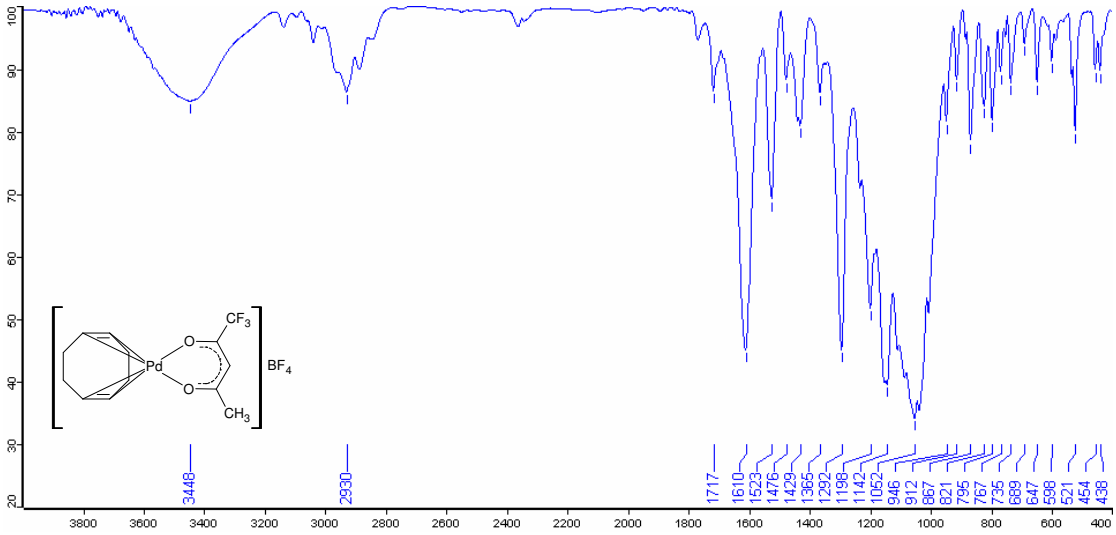

Figure A.6 Infra-red spectra of [Pd(cod)(tfacac)]BF_4

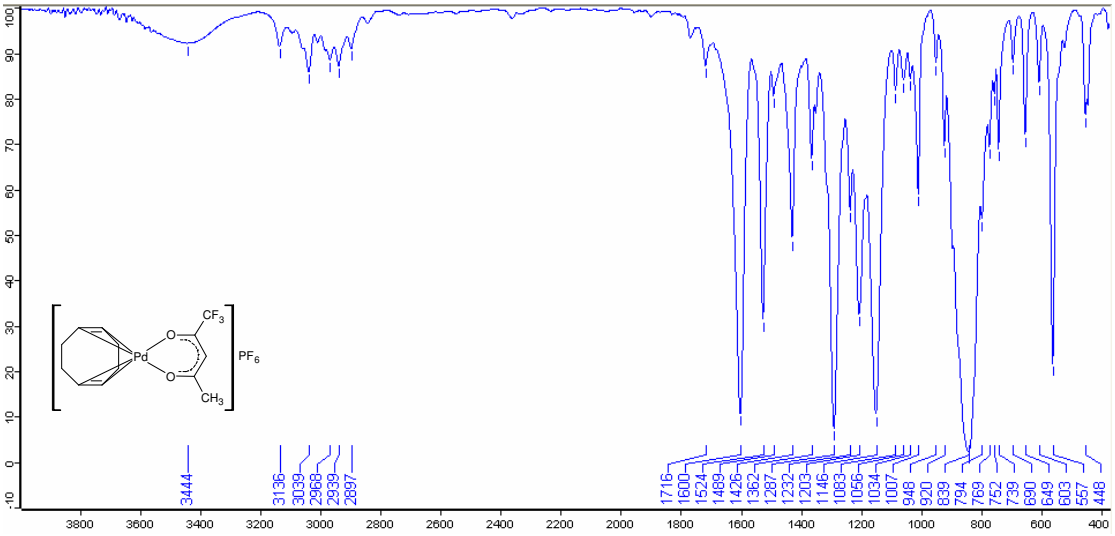

Figure A.7 Infra-red spectra of [Pd(cod)(tfacac)]PF_6

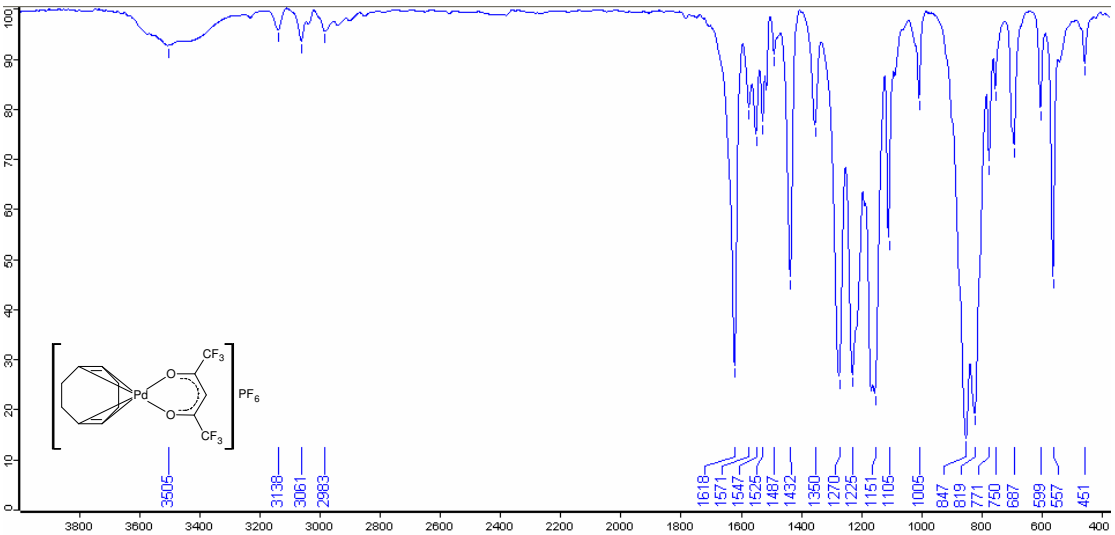

Figure A.8 Infra-red spectra of [Pd(cod)(hfacac)]PF_6

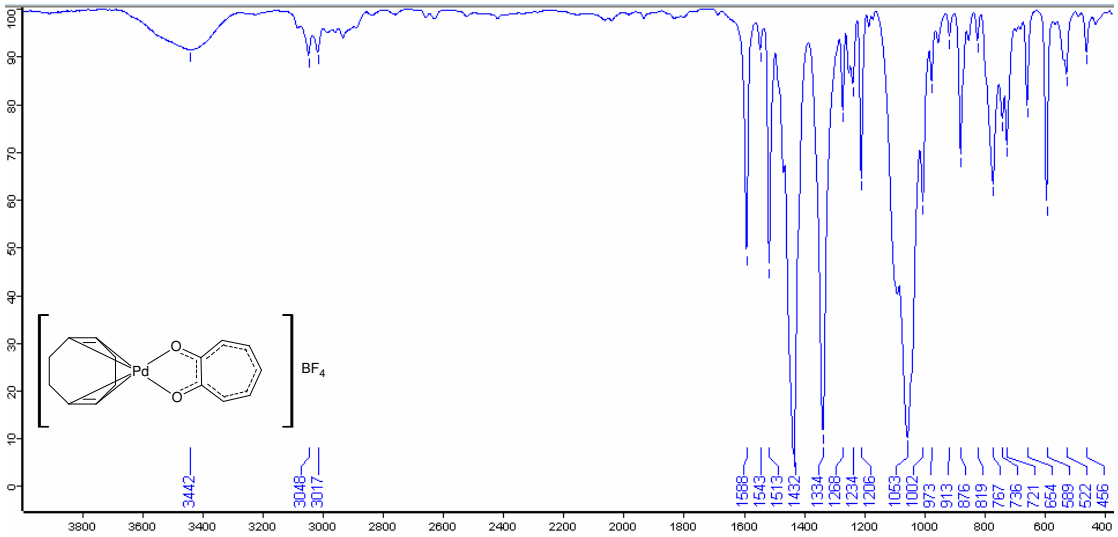

Figure A.9 Infra-red spectra of [Pd(cod)(trop)]BF_4

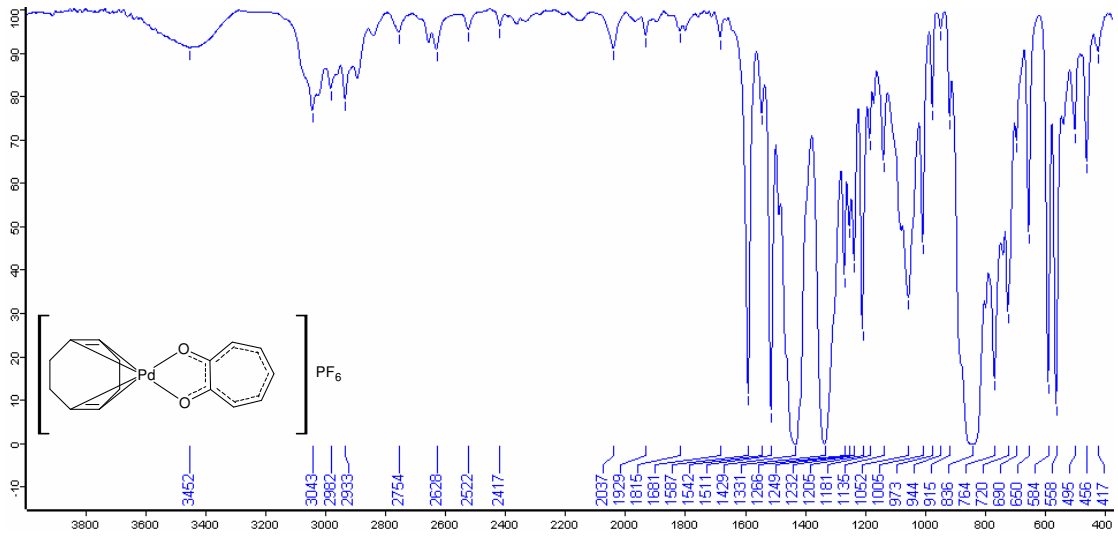

Figure A.10 Infra-red spectra of [Pd(cod)(trop)]PF_6

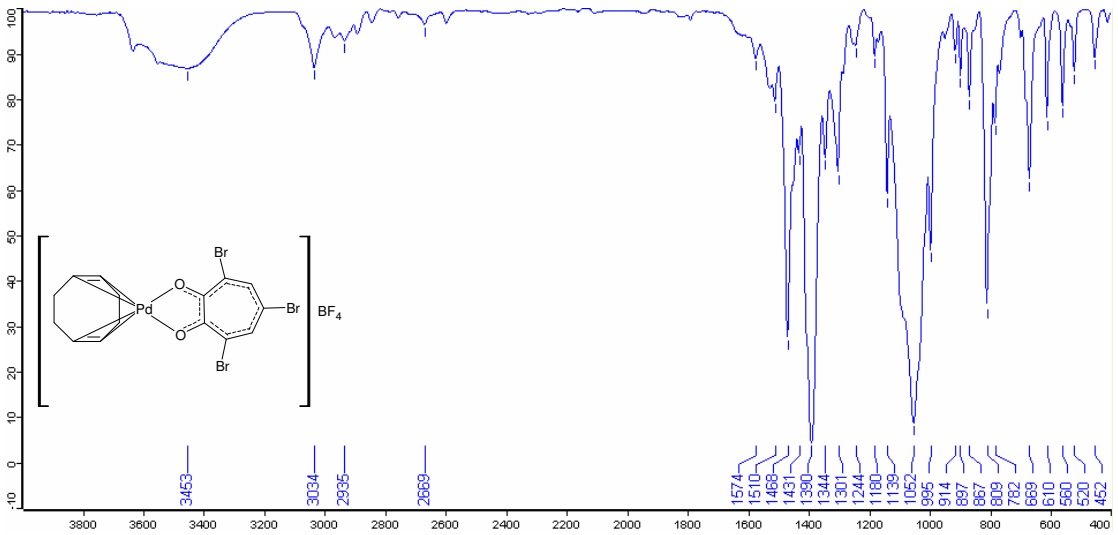

Figure A.11 Infra-red spectra of [Pd(cod)(3Br-trop)]BF_4

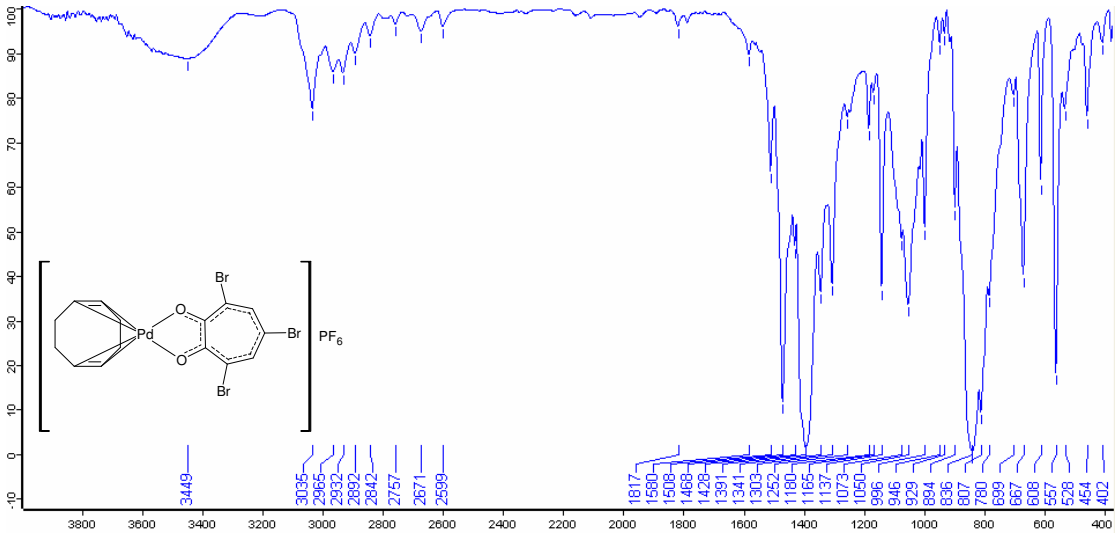

Figure A.12 Infra-red spectra of [Pd(cod)(3Br-trop)]PF_6

Figure A.13 Infra-red spectra of [Pd(cod)(NH-acac)]BF_4

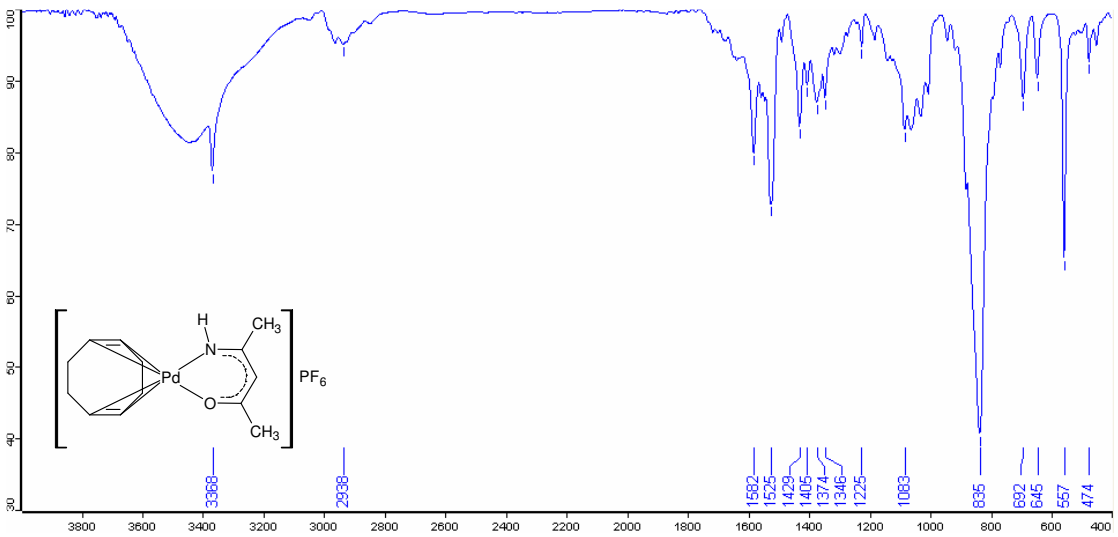

Figure A.14 Infra-red spectra of [Pd(cod)(NH-acac)]PF_6

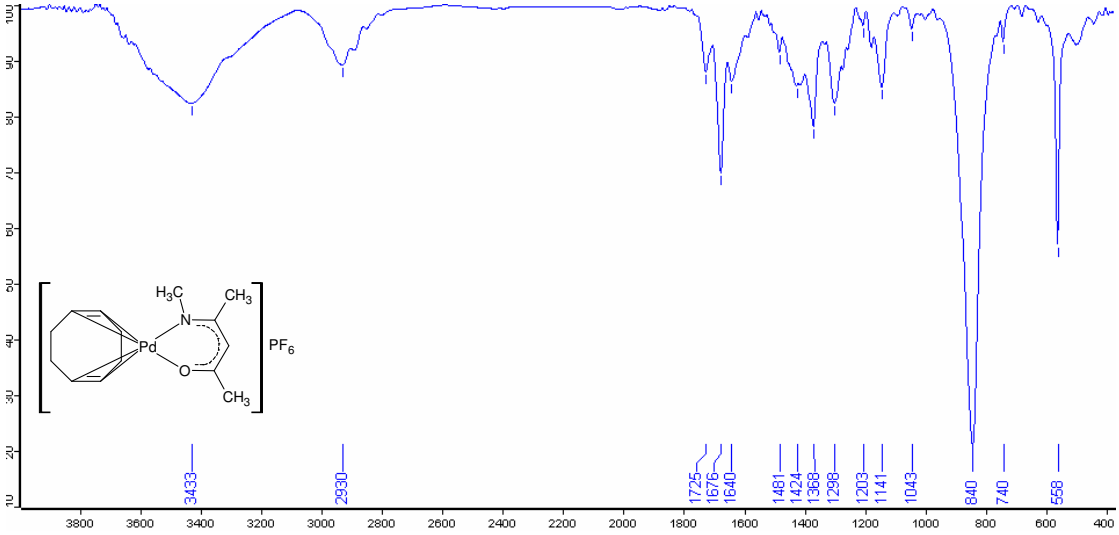

Figure A.15 Infra-red spectra of [Pd(cod)(NMe-acac)]PF_6

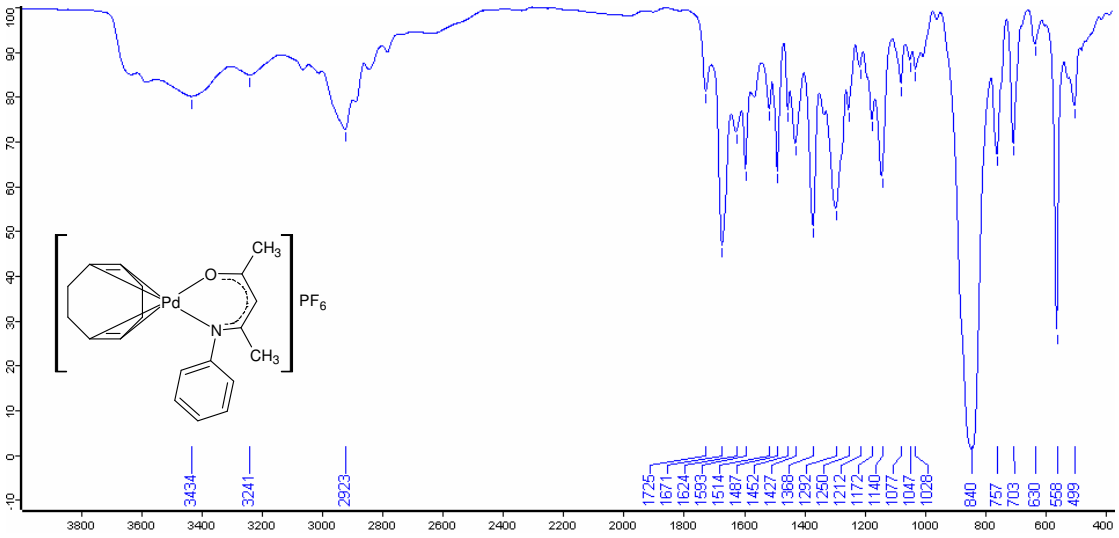

Figure A.16 Infra-red spectra of [Pd(cod)(NPh-acac)]PF_6

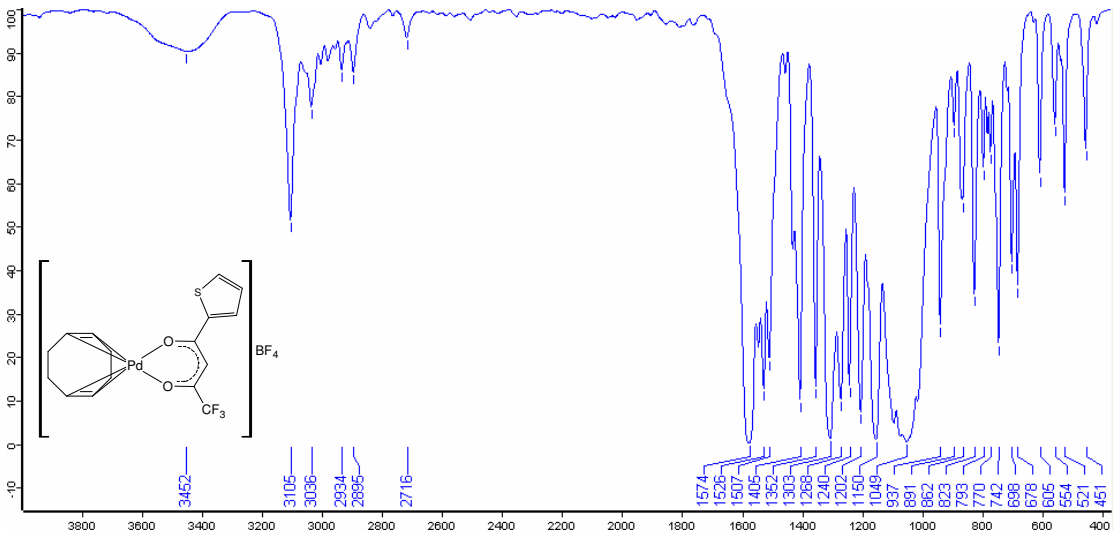

Figure A.17 Infra-red spectra of [Pd(cod)(thtfac)]BF_4

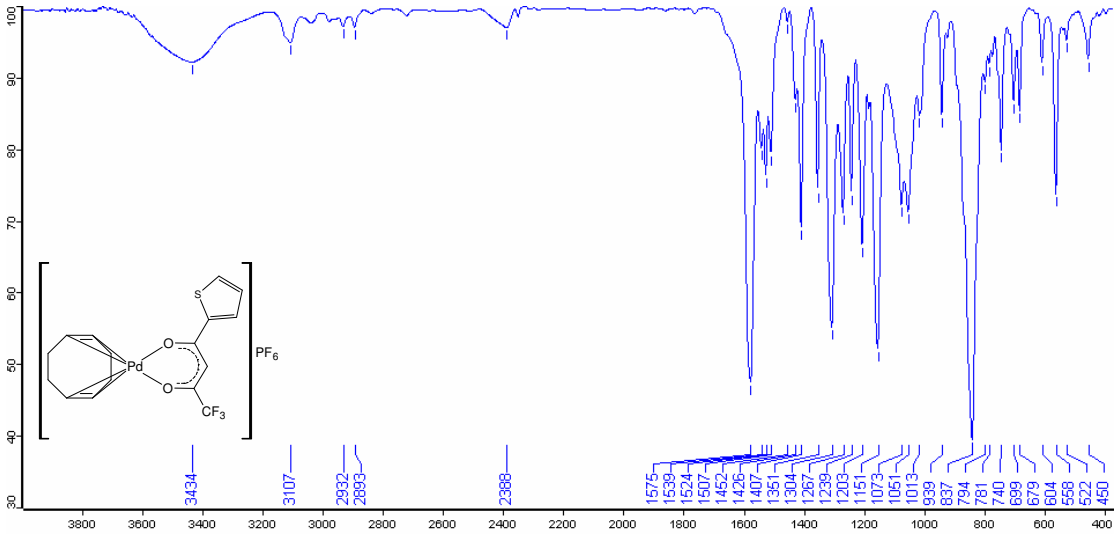

Figure A.18 Infra-red spectra of [Pd(cod)(thtfac)]PF_6

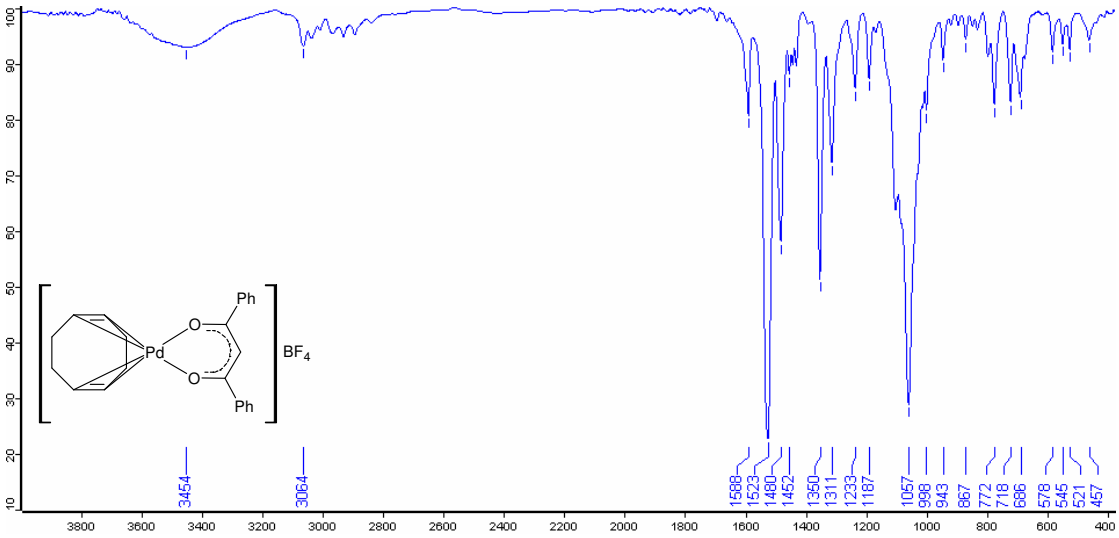

Figure A.19 Infra-red spectra of [Pd(cod)(dbm)]BF_4

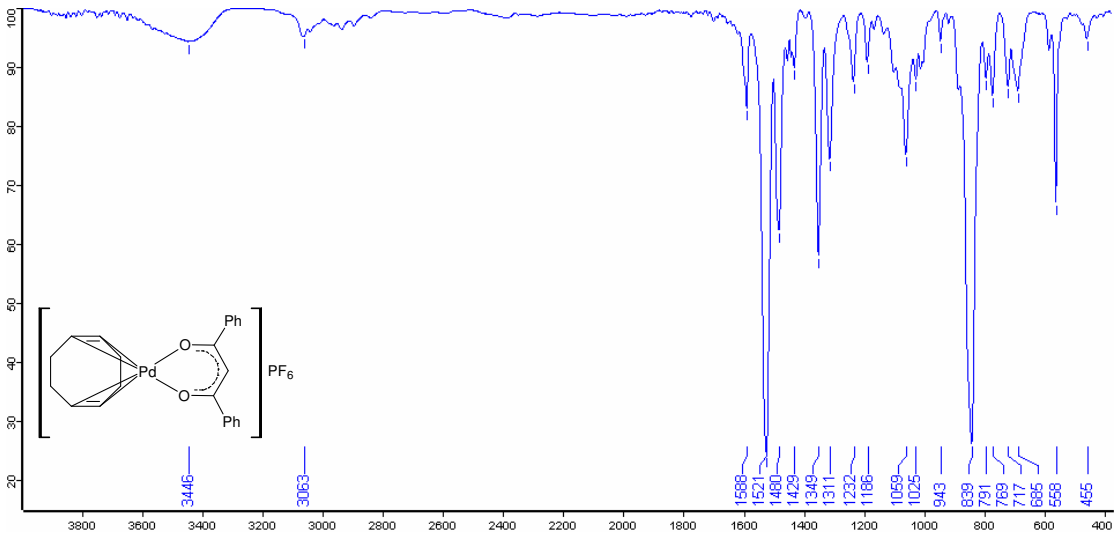

Figure A.20 Infra-red Spectra of [Pd(cod)(dbm)]PF_6

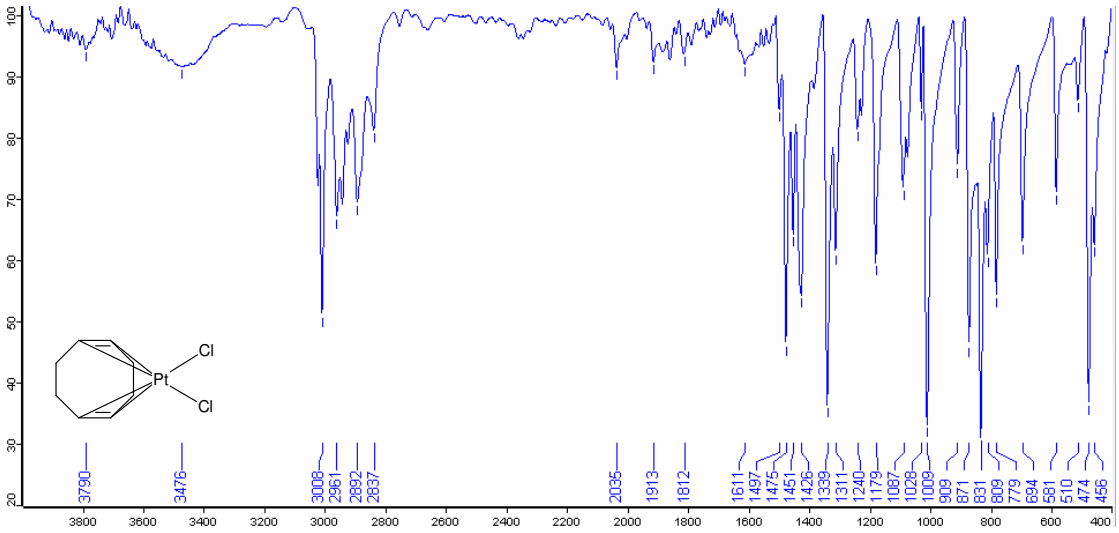

Figure A.21 Infra-red spectra of [Pt(cod)Cl_2]

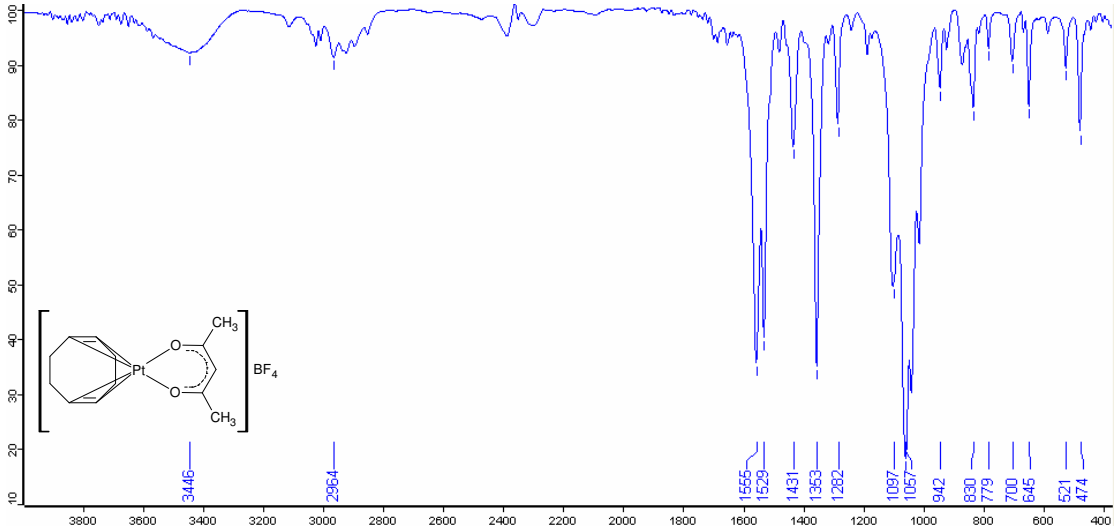

Figure A.22 Infra-red spectra of [Pt(cod)(acac)]BF_4

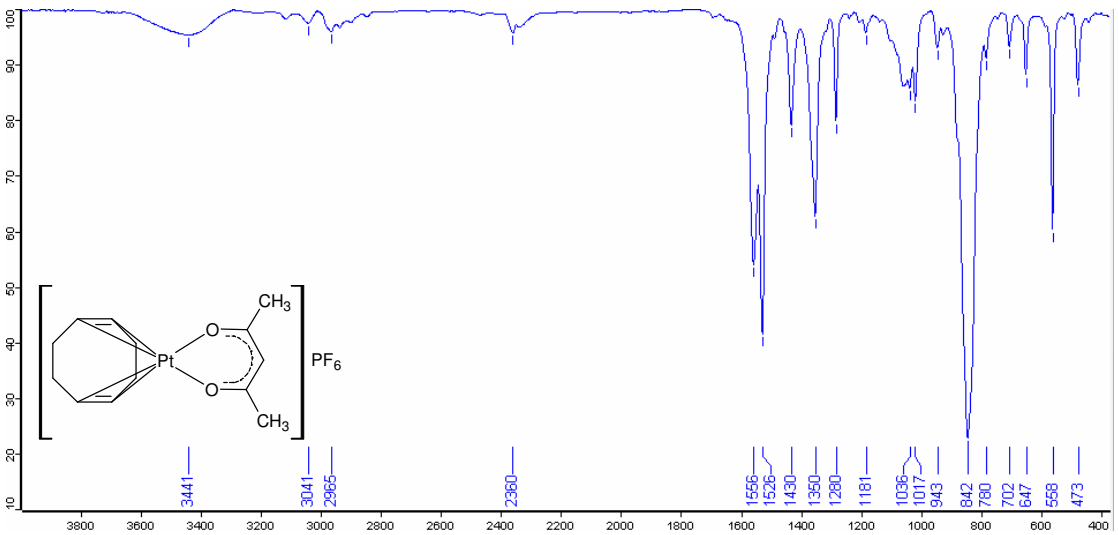

Figure A.23 Infra-red spectra of [Pt(cod)(acac)]PF_6

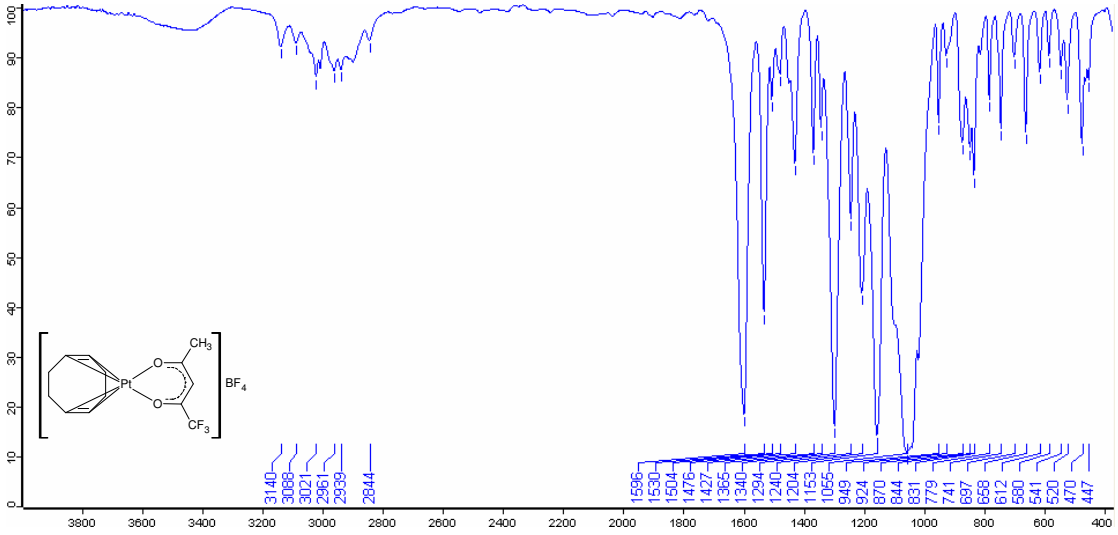

Figure A.24 Infra-red spectra of [Pt(cod)(tfacac)]BF_4

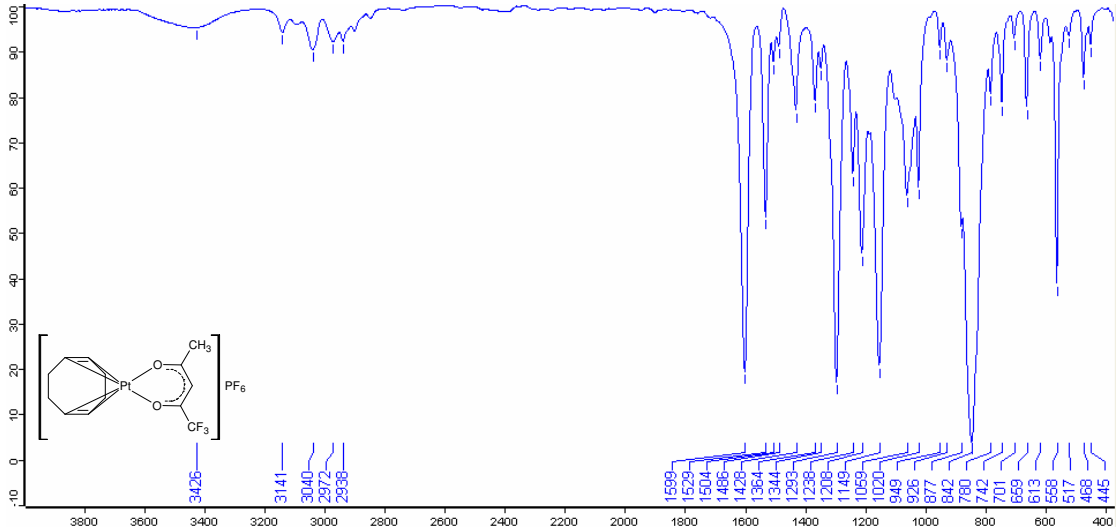

Figure A.25 Infra-red spectra of [Pt(cod)(tfacac)]PF_6

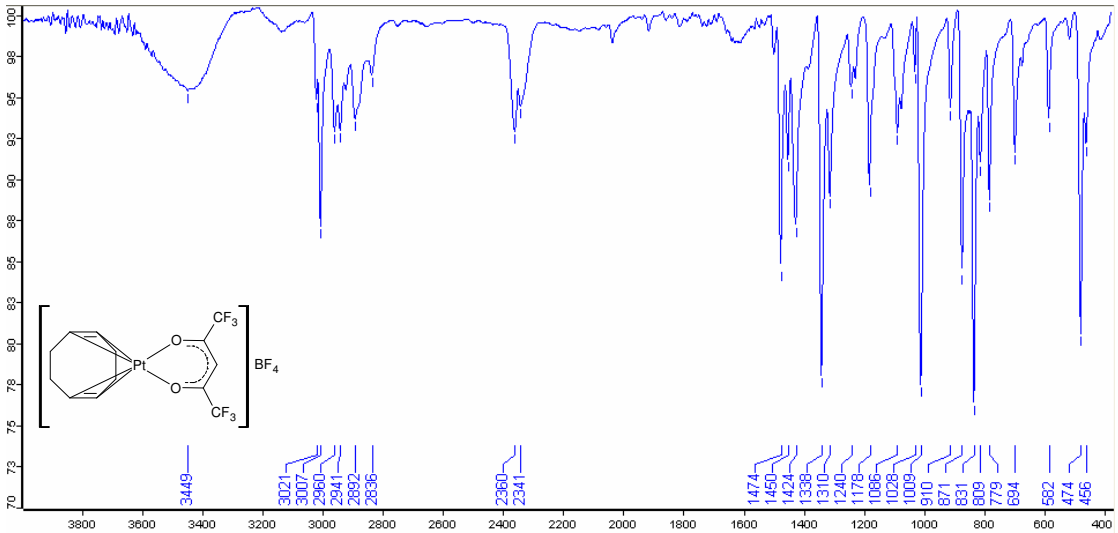

Figure A.26 Infra-red spectra of [Pt(cod)(hfacac)]BF_4

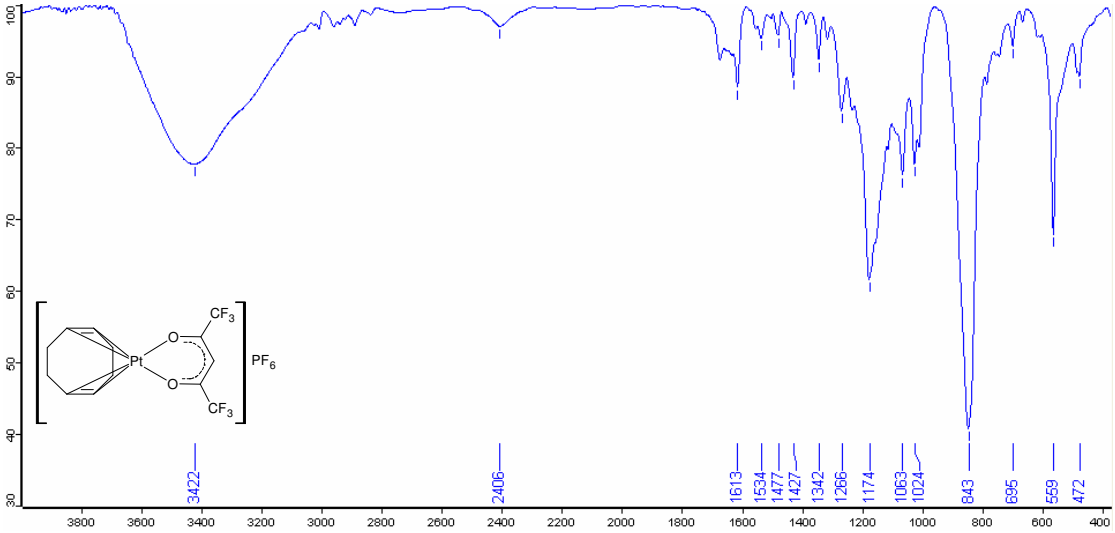

Figure A.27 Infra-red spectra of [Pt(cod)(hfacac)]PF_6

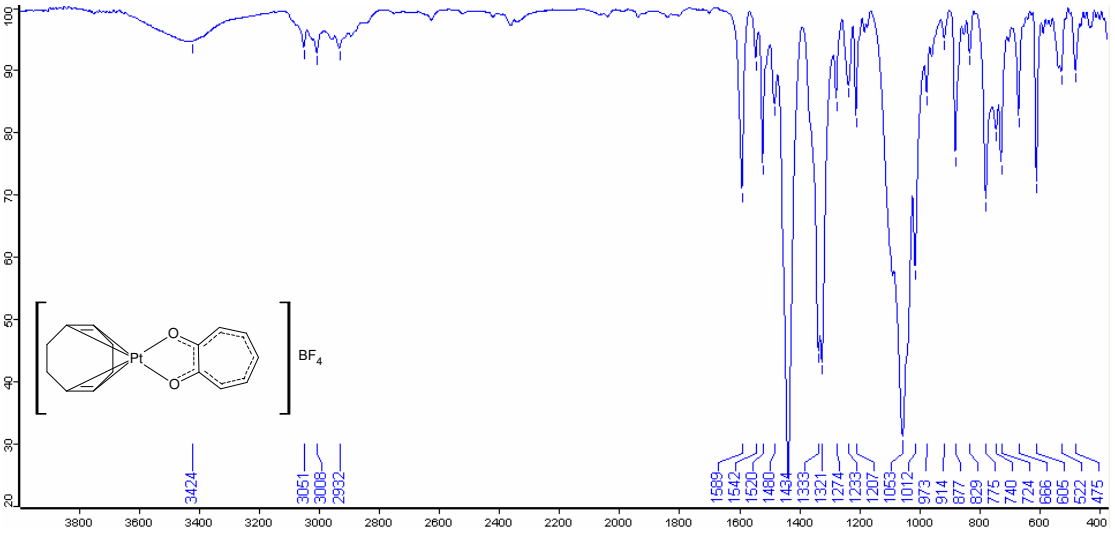

Figure A.28 Infra-red spectra of [Pt(cod)(trop)]BF_4

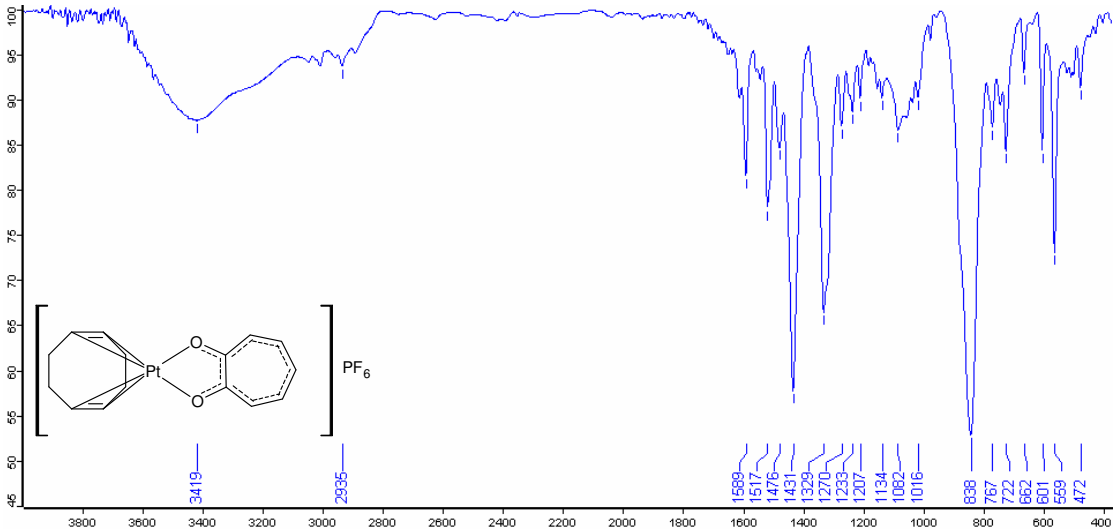

Figure A.29 Infra-red spectra of [Pt(cod)(trop)]PF_6

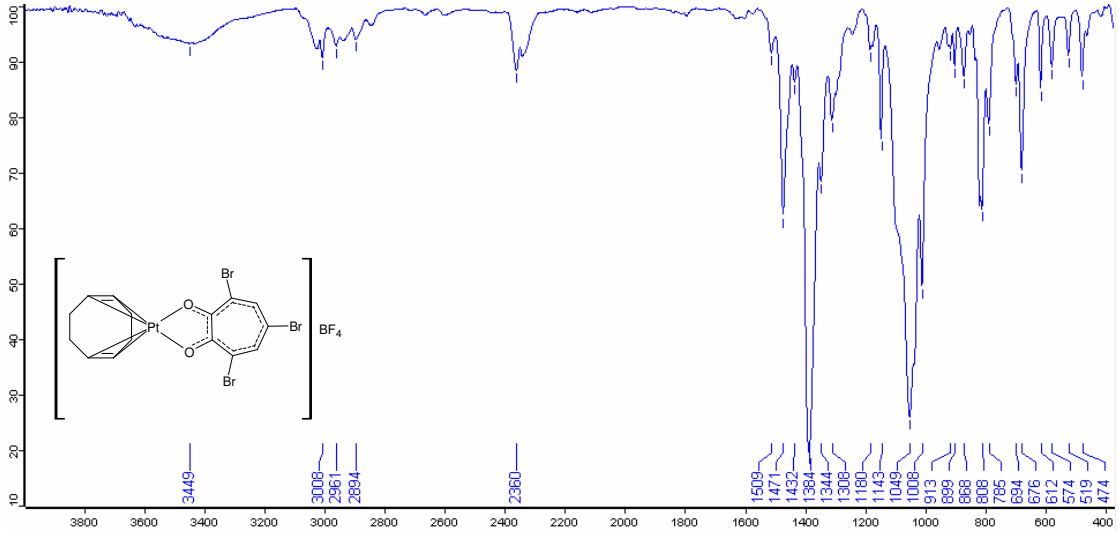

Figure A.30 Infra-red spectra of [Pt(cod)(3Br-trop)]BF_4

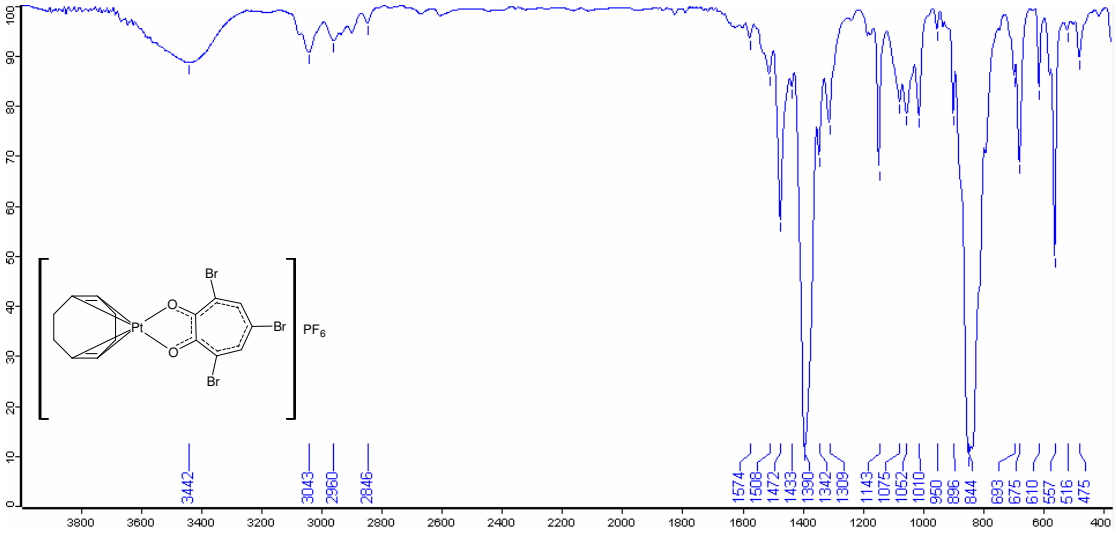

Figure A.31 Infra-red spectra of [Pt(cod)(3Br-trop)]PF_6

Figure A.32 Infra-red spectra of [Pt(cod)(NH-acac)]BF_4

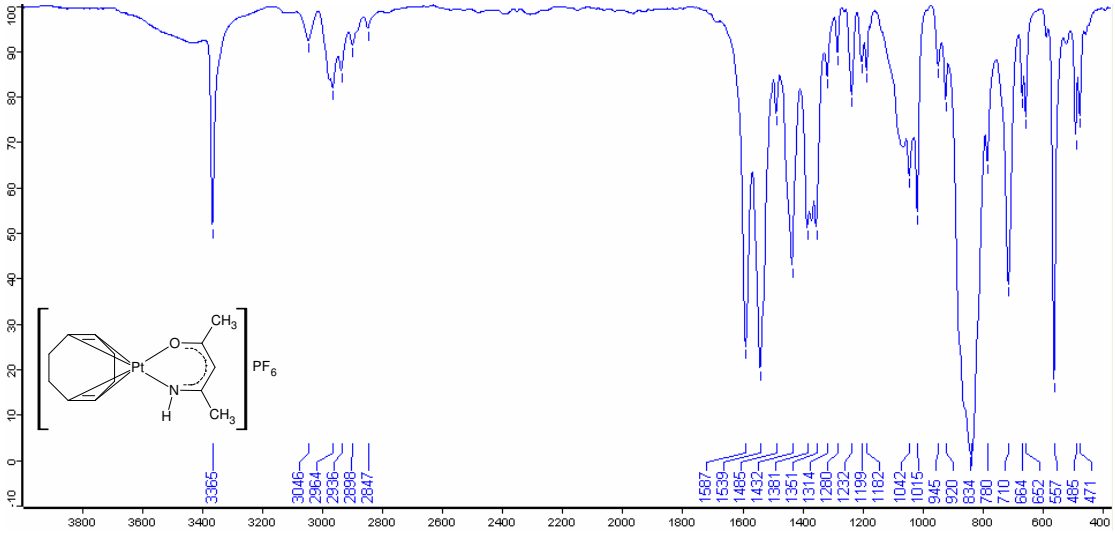

Figure A.33 Infra-red spectra of [Pt(cod)(NH-acac)]PF_6

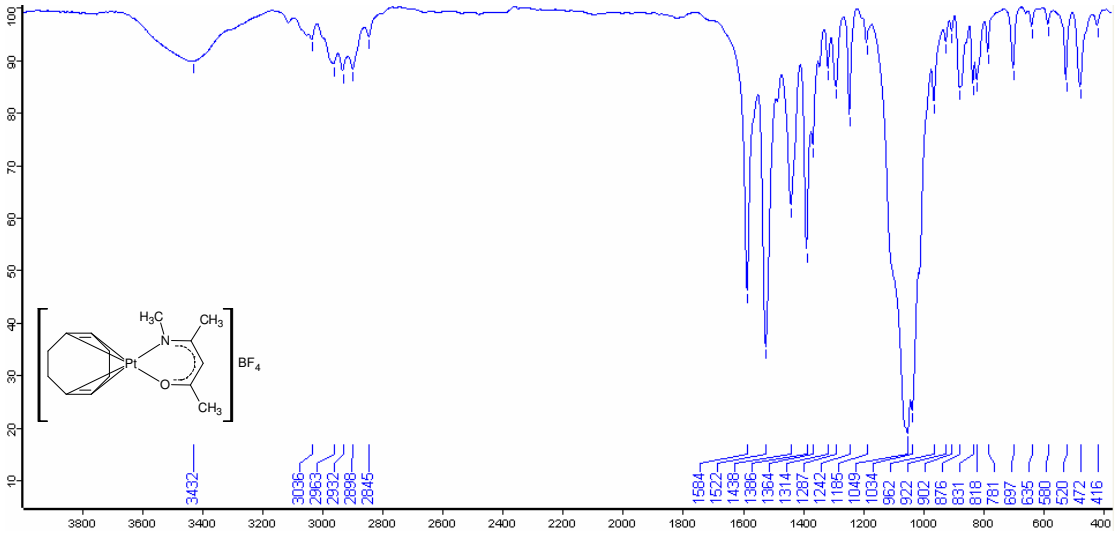

Figure A.34 Infra-red spectra of [Pt(cod)(NMe-acac)]BF_4

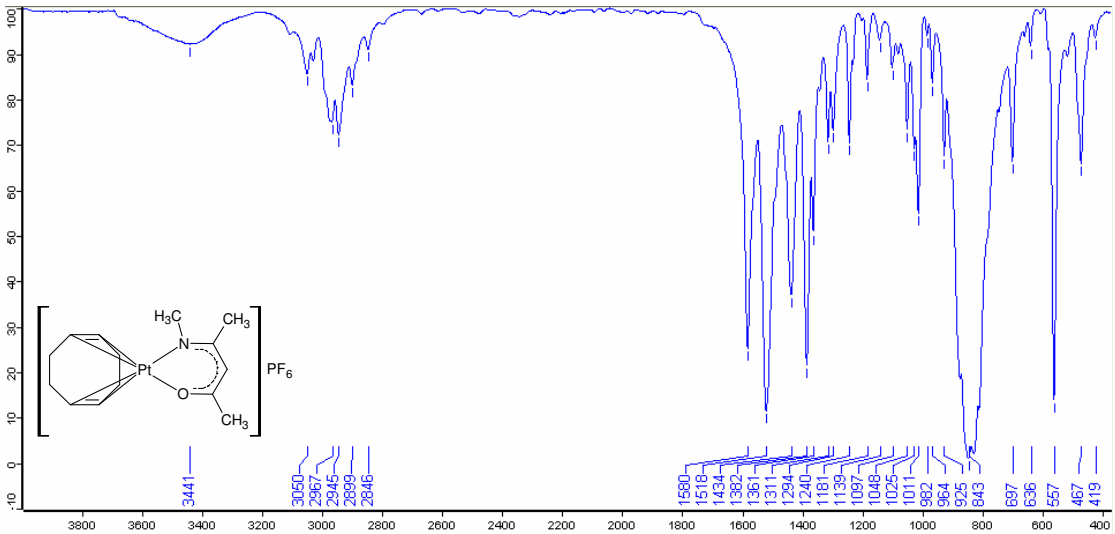

Figure A.35 Infra-red spectra of [Pt(cod)(NMe-acac)]PF_6

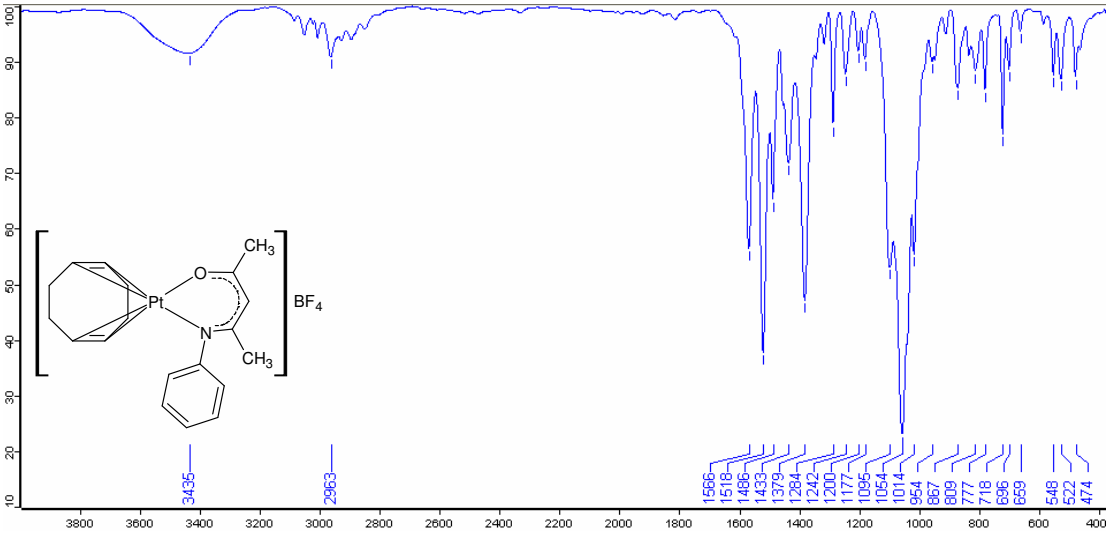

Figure A.36 Infra-red spectra of [Pt(cod)(NPh-acac)]BF_4

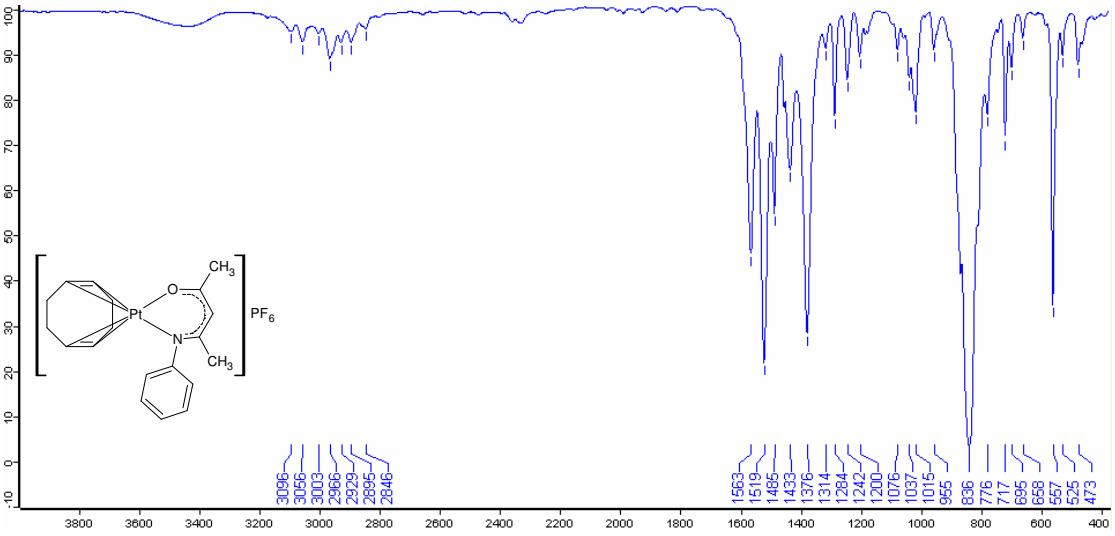

Figure A.37 Infra-red spectra of [Pt(cod)(NPh-acac)]PF_6

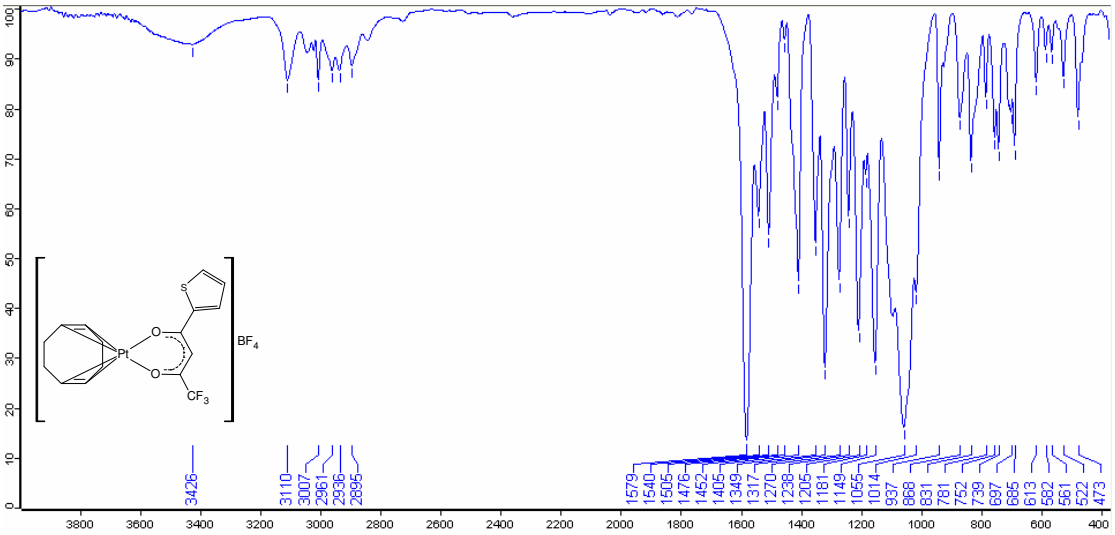

Figure A.38 Infra-red spectra of [Pt(cod)(thtfac)]BF_4

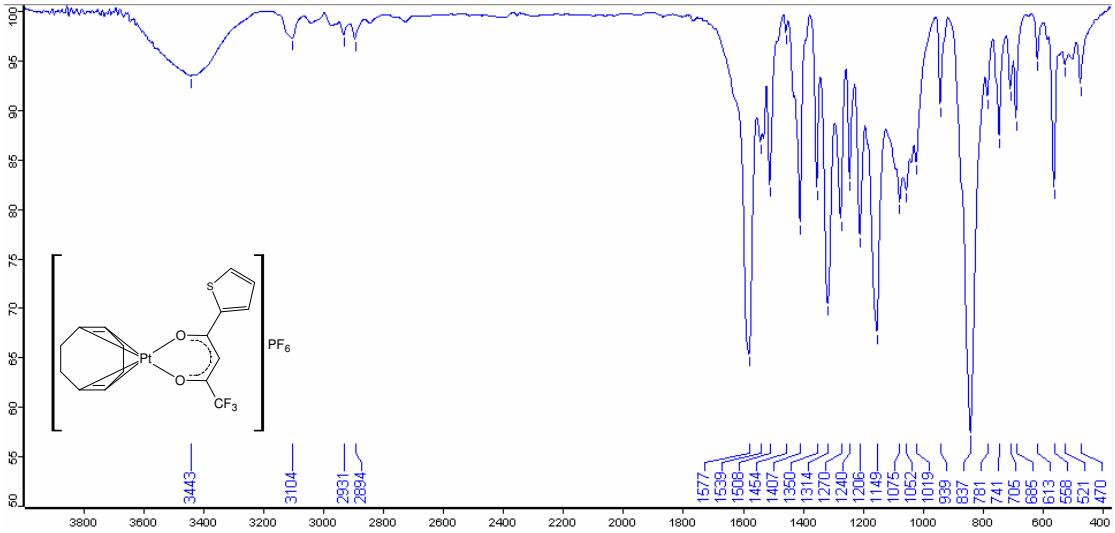

Figure A.39 Infra-red spectra of [Pt(cod)(thtfac)]PF_6

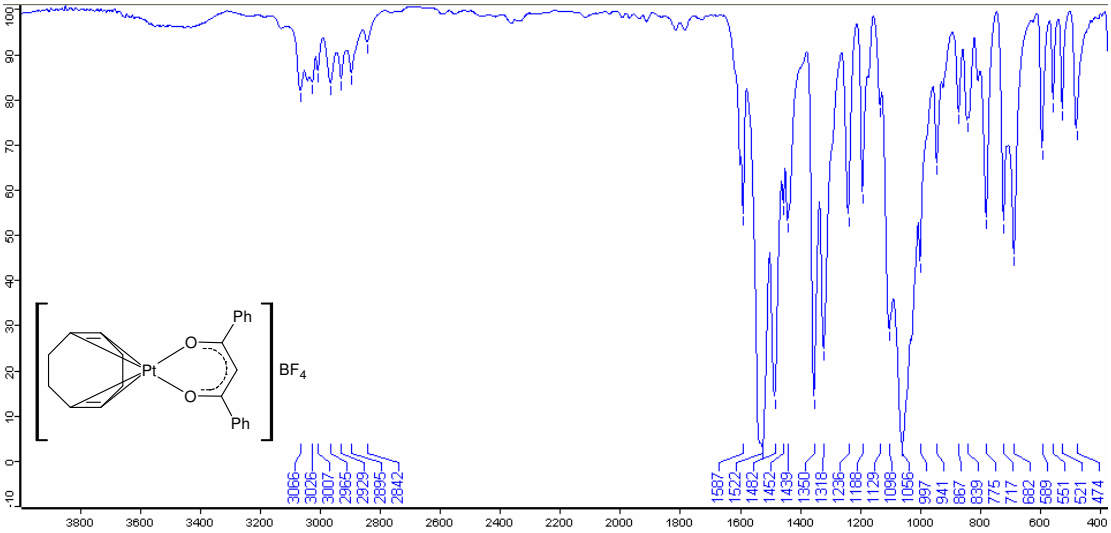

Figure A.40 Infra-red spectra of [Pt(cod)(dbm)]BF_4

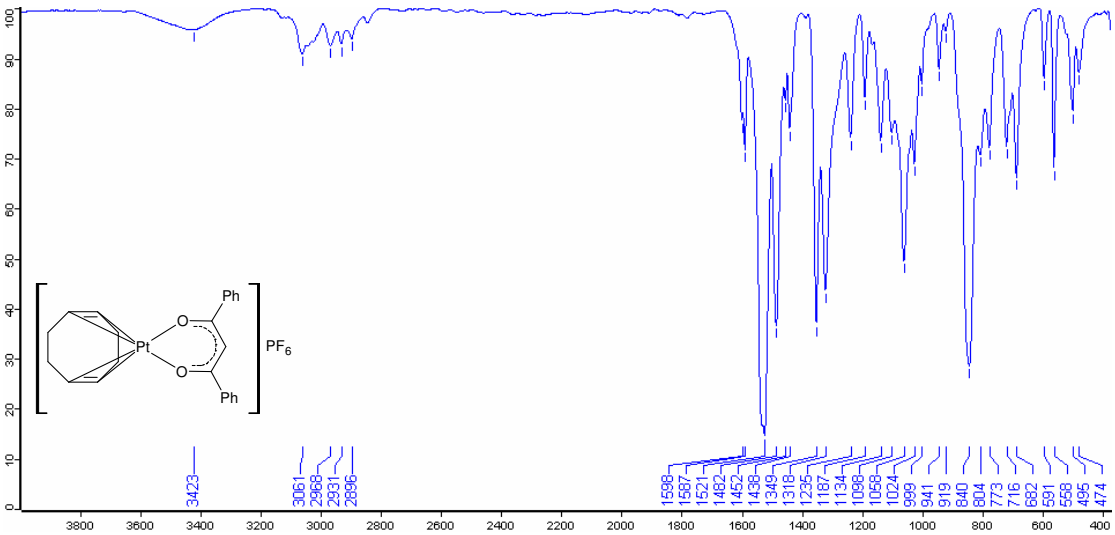

Figure A.41 Infra-red spectra of [Pt(cod)(dbm)]PF_6

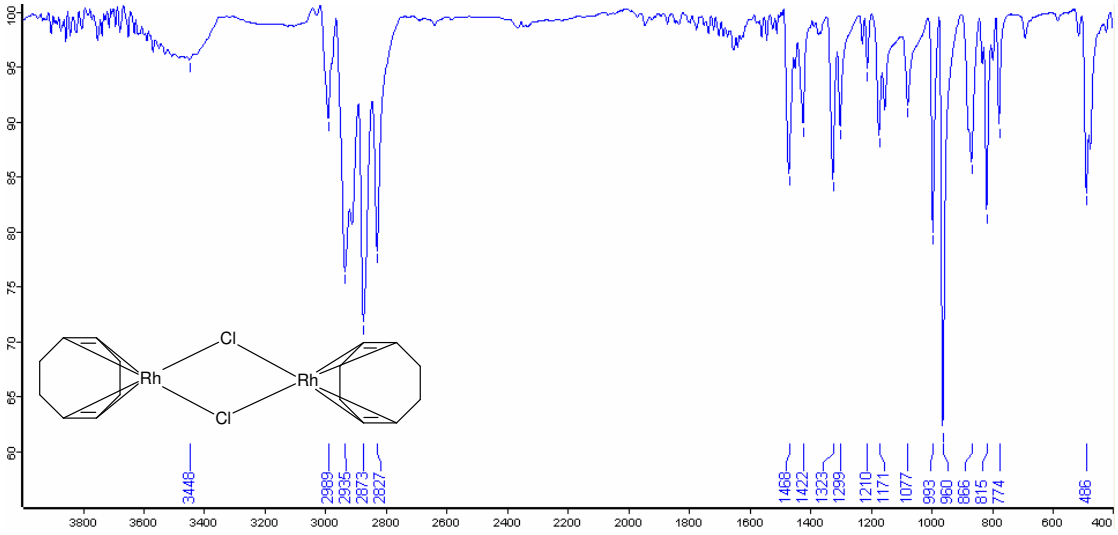

Figure A.42 Infra-red spectra of $[Rh(cod)Cl]_2$

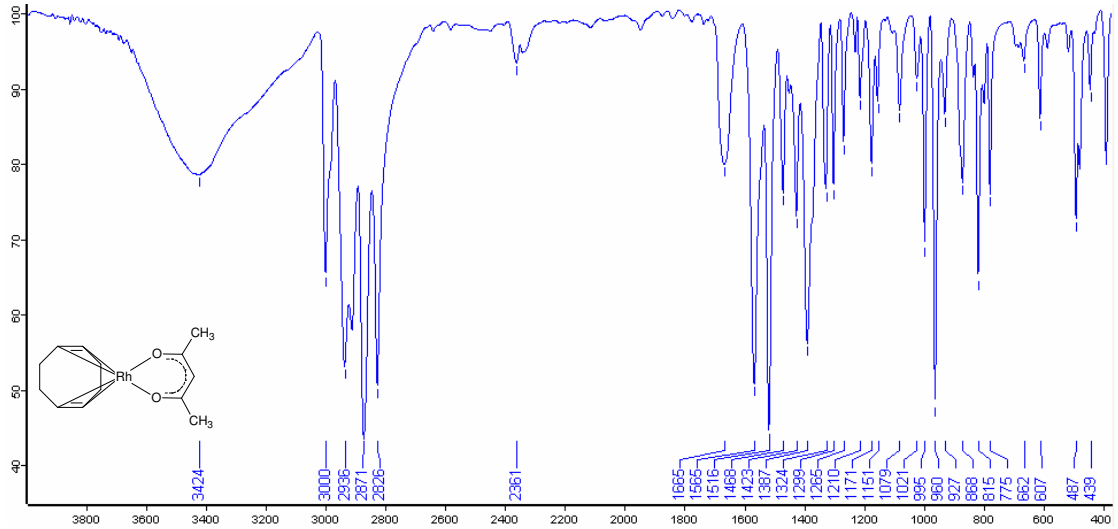

Figure A.43 Infra-red spectra of [Rh(cod)(acac)]

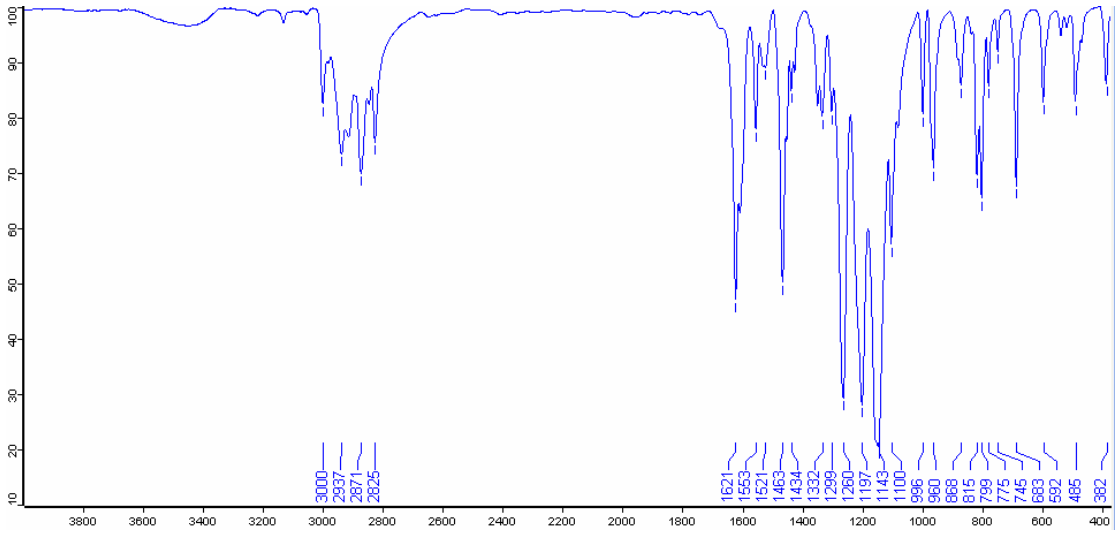

Figure A.44 Infra-red spectra of [Rh(cod)(hfacac)]

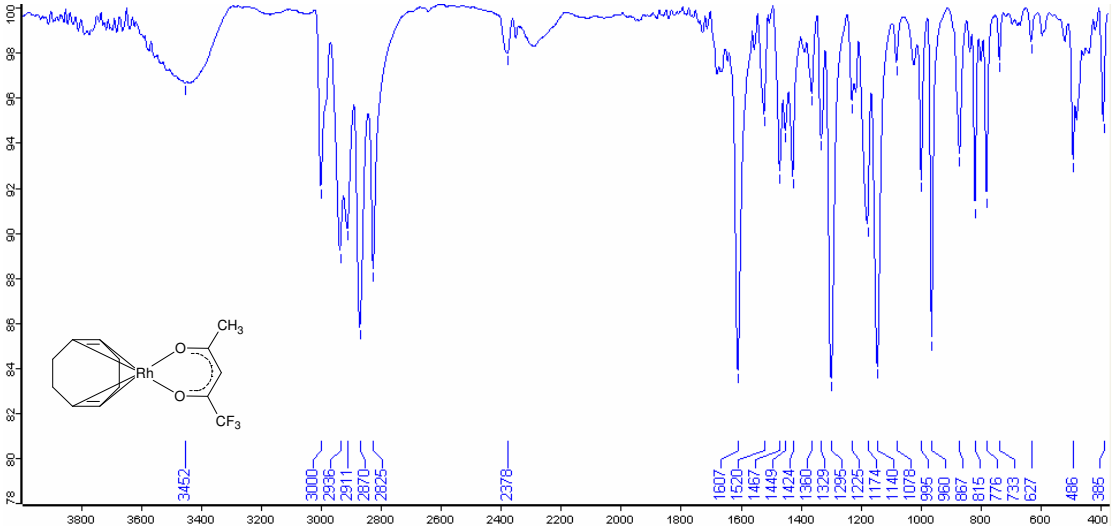

Figure A.45 Infra-red spectra of [Rh(cod)(tfacac)]

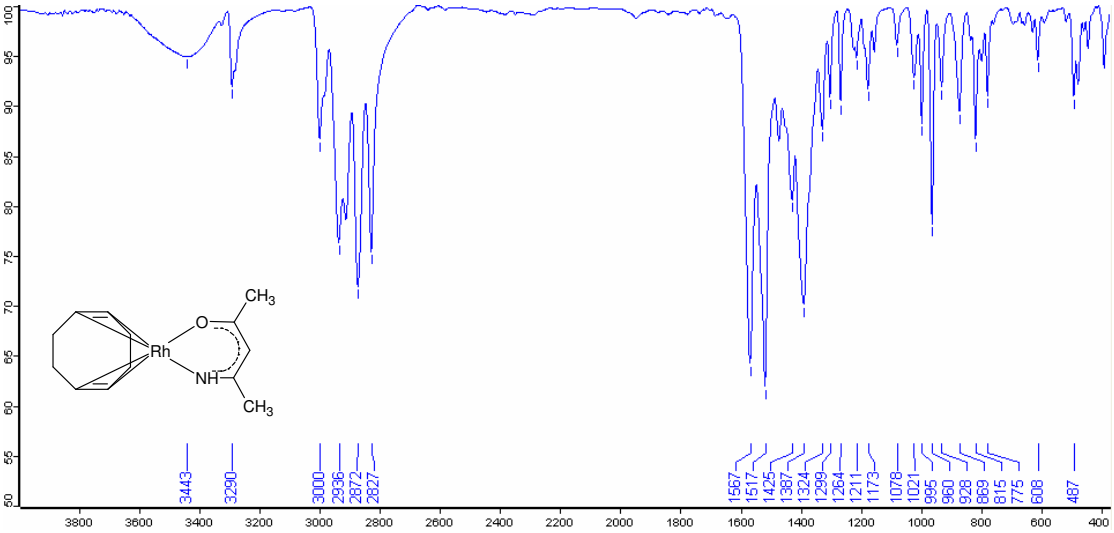

Figure A.46 Infra-red spectra of [Rh(cod)(NH-acac)]

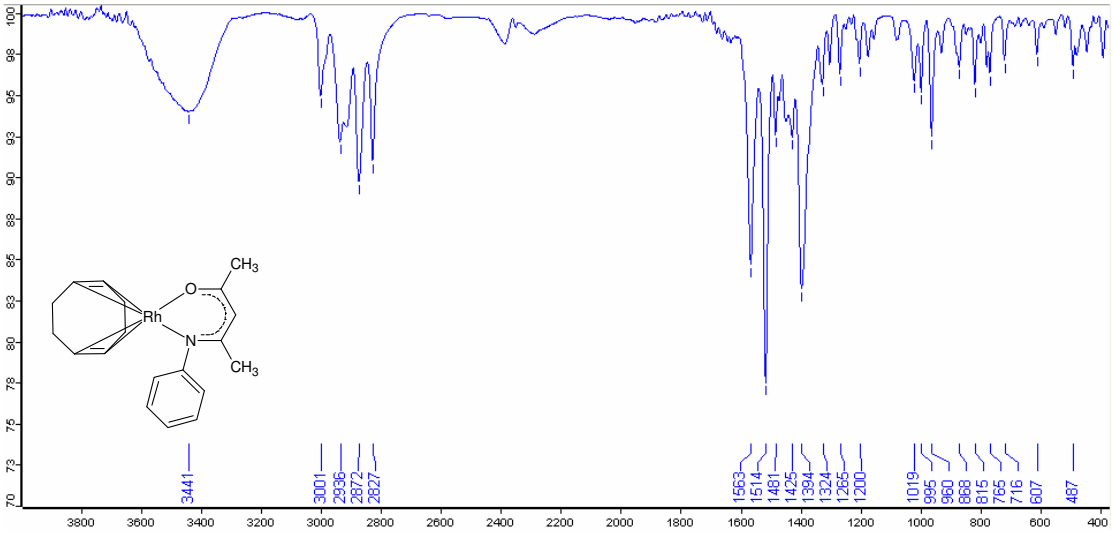

Figure A.47 Infra-red spectra of [Rh(cod)(NPh-acac)]

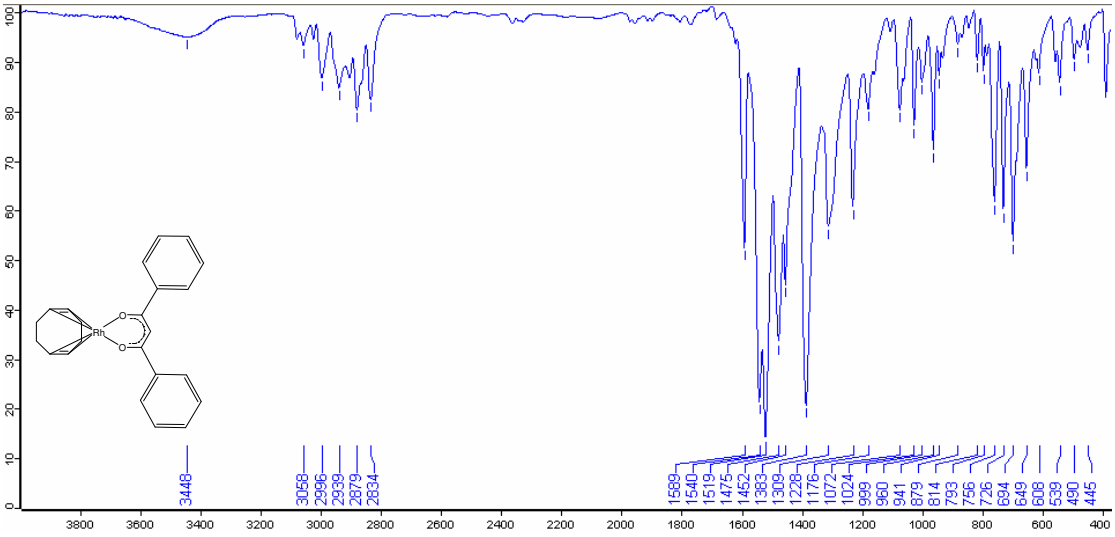

Figure A.48 Infra-red spectra of [Rh(cod)(dbm)]

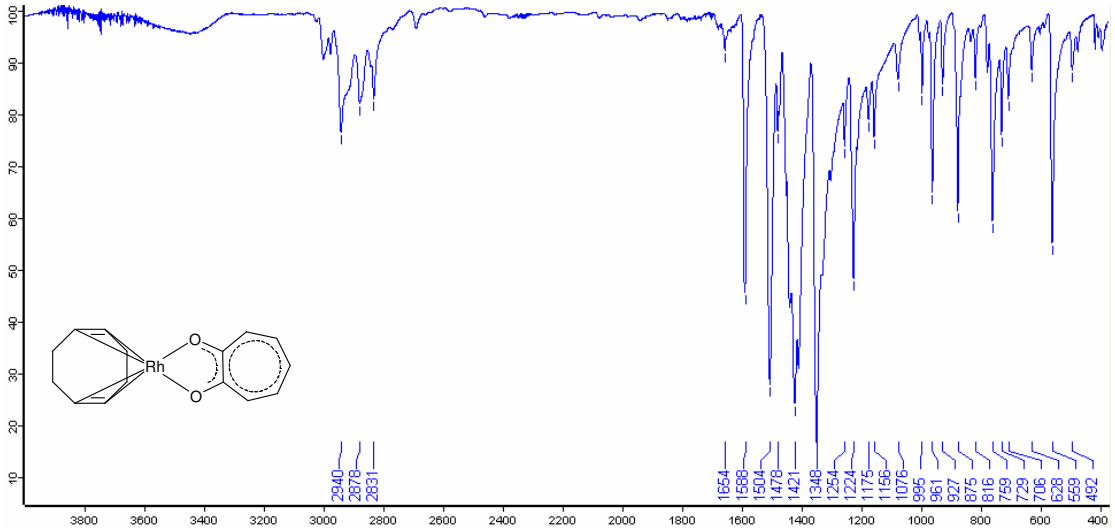

Figure A.49 Infra-red spectra of [Rh(cod)(trop)]

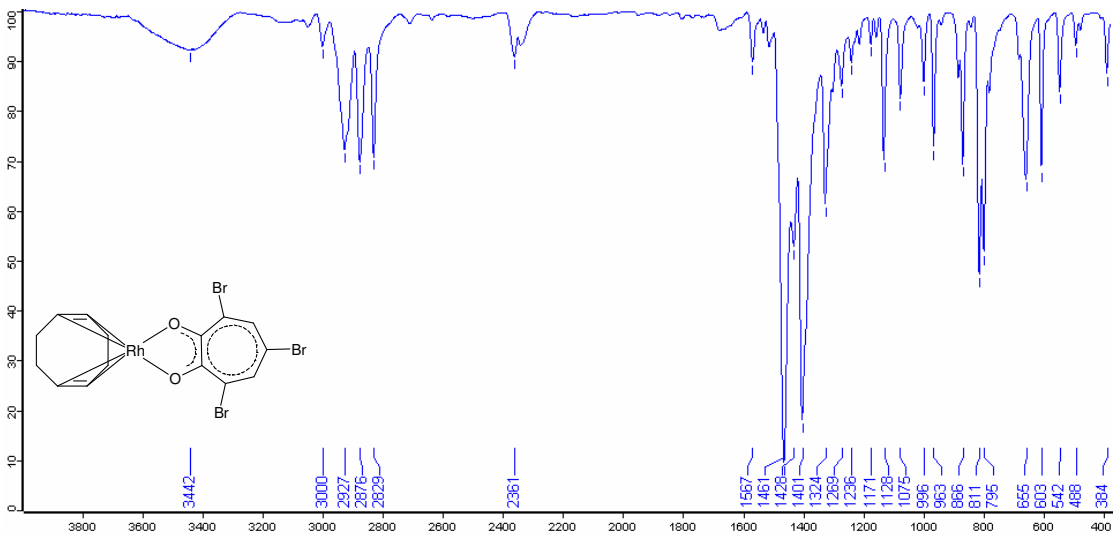

Figure A.50 Infra-red spectra of [Rh(cod)(3Br-trop)]

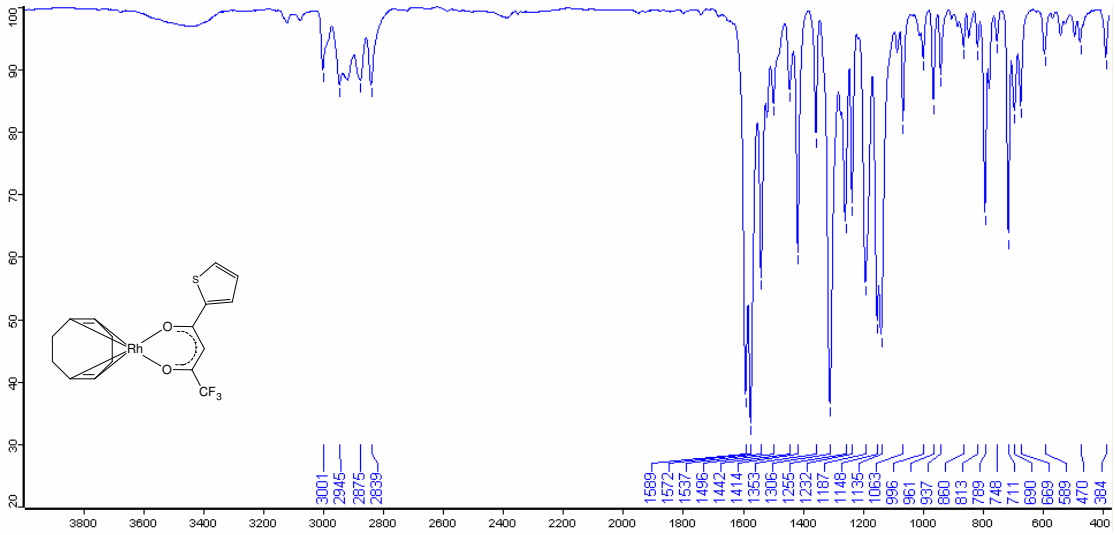

Figure A.51 Infra-red spectra of [Rh(cod)(thtfac)]

B. Supplementary Crystal Data

B.1 Crystal Data of [Pd(cod)(acac)]PF_6

Table B.1.1 Atomic co-ordinates (x 10^4) and equivalent isotropic displacement parameters ($Å^2$ x 10^3) for [Pd(cod)(acac)]PF_6. U(eq) is defined as one third of the trace of the orthogonalized U^{ij} tensor.

	x	y	z	U(eq)
C(1)	-43(5)	9172(3)	1354(4)	18(1)
C(2)	628(5)	8671(3)	658(4)	18(1)
C(3)	688(5)	7699(3)	623(4)	19(1)
C(4)	885(5)	7276(3)	1855(4)	18(1)
C(5)	1939(5)	7773(3)	2881(4)	14(1)
C(6)	1506(5)	8375(3)	3603(4)	15(1)
C(7)	-62(5)	8676(3)	3461(4)	19(1)
C(8)	-979(5)	8821(3)	2141(4)	20(1)
C(9)	4181(5)	10356(3)	1501(4)	16(1)
C(10)	5394(5)	10168(3)	2492(4)	16(1)
C(11)	5414(5)	9589(2)	3433(4)	12(1)
C(12)	4337(6)	11024(3)	584(5)	22(1)
C(13)	6823(5)	9484(3)	4449(4)	18(1)
O(1)	2865(3)	10017(2)	1264(3)	17(1)
O(2)	4321(4)	9127(2)	3546(3)	15(1)
F(1)	4419(4)	7143(2)	1012(3)	35(1)
F(2)	4380(4)	6417(2)	2713(3)	37(1)
F(3)	6857(4)	6218(2)	3162(3)	40(1)
F(4)	6929(4)	6943(2)	1461(3)	37(1)
F(5)	5401(4)	5807(2)	1333(3)	36(1)
F(6)	5892(4)	7566(2)	2826(3)	43(1)
P(1)	5646(1)	6689(1)	2084(1)	19(1)
Pd(1)	2355(1)	9073(1)	2275(1)	12(1)

Table B.1.2 Bond lengths (Å) and angles (°) for [Pd(cod)(acac)]PF_6

C(1)-C(2)	1.381(7)	C(8)-C(1)-H(1)	114.0	O(2)-C(11)-C(10)	126.5(4)
C(1)-C(8)	1.520(7)	Pd(1)-C(1)-H(1)	114.0	O(2)-C(11)-C(13)	114.1(4)
C(1)-Pd(1)	2.195(5)	C(1)-C(2)-C(3)	127.0(4)	C(10)-C(11)-C(13)	119.3(4)
C(1)-H(1)	1.0000	C(1)-C(2)-Pd(1)	72.2(3)	C(9)-C(12)-H(12A)	109.5
C(2)-C(3)	1.506(6)	C(3)-C(2)-Pd(1)	106.4(3)	C(9)-C(12)-H(12B)	109.5
C(2)-Pd(1)	2.181(4)	C(1)-C(2)-H(2)	114.0	H(12A)-C(12)-H(12B)	109.5
C(2)-H(2)	1.0000	C(3)-C(2)-H(2)	114.0	C(9)-C(12)-H(12C)	109.5
C(3)-C(4)	1.523(6)	Pd(1)-C(2)-H(2)	114.0	H(12A)-C(12)-H(12C)	109.5
C(3)-H(3A)	0.9900	C(2)-C(3)-C(4)	113.6(4)	H(12B)-C(12)-H(12C)	109.5
C(3)-H(3B)	0.9900	C(2)-C(3)-H(3A)	108.9	C(11)-C(13)-H(13A)	109.5
C(4)-C(5)	1.516(6)	C(4)-C(3)-H(3A)	108.9	C(11)-C(13)-H(13B)	109.5
C(4)-H(4A)	0.9900	C(2)-C(3)-H(3B)	108.9	H(13A)-C(13)-H(13B)	109.5
C(4)-H(4B)	0.9900	C(4)-C(3)-H(3B)	108.9	C(11)-C(13)-H(13C)	109.5
C(5)-C(6)	1.380(6)	H(3A)-C(3)-H(3B)	107.7	H(13A)-C(13)-H(13C)	109.5
C(5)-Pd(1)	2.197(4)	C(5)-C(4)-C(3)	112.9(3)	H(13B)-C(13)-H(13C)	109.5
C(5)-H(5)	1.0000	C(5)-C(4)-H(4A)	109.0	C(9)-O(1)-Pd(1)	122.6(3)
C(6)-C(7)	1.498(6)	C(3)-C(4)-H(4A)	109.0	C(11)-O(2)-Pd(1)	122.8(3)
C(6)-Pd(1)	2.189(4)	C(5)-C(4)-H(4B)	109.0	F(6)-P(1)-F(1)	90.22(18)
C(6)-H(6)	1.0000	C(3)-C(4)-H(4B)	109.0	F(6)-P(1)-F(5)	179.9(2)
C(7)-C(8)	1.536(6)	H(4A)-C(4)-H(4B)	107.8	F(1)-P(1)-F(5)	89.73(18)
C(7)-H(7A)	0.9900	C(6)-C(5)-C(4)	125.1(4)	F(6)-P(1)-F(3)	90.5(2)
C(7)-H(7B)	0.9900	C(6)-C(5)-Pd(1)	71.4(2)	F(1)-P(1)-F(3)	178.9(2)
C(8)-H(8A)	0.9900	C(4)-C(5)-Pd(1)	110.6(3)	F(5)-P(1)-F(3)	89.60(19)
C(8)-H(8B)	0.9900	C(6)-C(5)-H(5)	114.0	F(6)-P(1)-F(2)	89.78(19)
C(9)-O(1)	1.291(5)	C(4)-C(5)-H(5)	114.0	F(1)-P(1)-F(2)	90.27(18)
C(9)-C(10)	1.393(6)	Pd(1)-C(5)-H(5)	114.0	F(5)-P(1)-F(2)	90.32(19)
C(9)-C(12)	1.511(6)	C(5)-C(6)-C(7)	125.7(4)	F(3)-P(1)-F(2)	88.83(18)
C(10)-C(11)	1.399(6)	C(5)-C(6)-Pd(1)	72.0(2)	F(6)-P(1)-F(4)	90.98(19)
C(10)-H(10)	0.9500	C(7)-C(6)-Pd(1)	107.6(3)	F(1)-P(1)-F(4)	90.63(19)
C(11)-O(2)	1.280(5)	C(5)-C(6)-H(6)	114.3	F(5)-P(1)-F(4)	88.92(18)
C(11)-C(13)	1.502(6)	C(7)-C(6)-H(6)	114.3	F(3)-P(1)-F(4)	90.26(19)
C(12)-H(12A)	0.9800	Pd(1)-C(6)-H(6)	114.3	F(2)-P(1)-F(4)	178.82(19)
C(12)-H(12B)	0.9800	C(6)-C(7)-C(8)	114.2(4)	O(2)-Pd(1)-O(1)	94.35(12)
C(12)-H(12C)	0.9800	C(6)-C(7)-H(7A)	108.7	O(2)-Pd(1)-C(2)	160.29(15)
C(13)-H(13A)	0.9800	C(8)-C(7)-H(7A)	108.7	O(1)-Pd(1)-C(2)	87.26(15)
C(13)-H(13B)	0.9800	C(6)-C(7)-H(7B)	108.7	O(2)-Pd(1)-C(6)	86.96(14)
C(13)-H(13C)	0.9800	C(8)-C(7)-H(7B)	108.7	O(1)-Pd(1)-C(6)	162.46(14)
O(1)-Pd(1)	2.003(3)	H(7A)-C(7)-H(7B)	107.6	C(2)-Pd(1)-C(6)	97.38(17)
O(2)-Pd(1)	2.001(3)	C(1)-C(8)-C(7)	112.7(4)	O(2)-Pd(1)-C(1)	161.93(16)
F(1)-P(1)	1.591(3)	C(1)-C(8)-H(8A)	109.0	O(1)-Pd(1)-C(1)	92.50(15)
F(2)-P(1)	1.603(3)	C(7)-C(8)-H(8A)	109.0	C(2)-Pd(1)-C(1)	36.78(17)
F(3)-P(1)	1.600(3)	C(1)-C(8)-H(8B)	109.0	C(6)-Pd(1)-C(1)	81.57(17)
F(4)-P(1)	1.603(3)	C(7)-C(8)-H(8B)	109.0	O(2)-Pd(1)-C(5)	90.79(14)
F(5)-P(1)	1.596(3)	H(8A)-C(8)-H(8B)	107.8	O(1)-Pd(1)-C(5)	160.38(14)
F(6)-P(1)	1.584(3)	O(1)-C(9)-C(10)	126.4(4)	C(2)-Pd(1)-C(5)	81.69(16)
		O(1)-C(9)-C(12)	113.6(4)	C(6)-Pd(1)-C(5)	36.67(15)
C(2)-C(1)-C(8)	124.8(4)	C(10)-C(9)-C(12)	119.9(4)	C(1)-Pd(1)-C(5)	88.32(16)
C(2)-C(1)-Pd(1)	71.1(3)	C(9)-C(10)-C(11)	126.7(4)		
C(8)-C(1)-Pd(1)	111.3(3)	C(9)-C(10)-H(10)	116.6		
C(2)-C(1)-H(1)	114.0	C(11)-C(10)-H(10)	116.6		

Symmetry transformations used to generate equivalent atoms

Table B.1.3 Anisotropic displacement parameters ($Å^2$ x 10^3) for [Pd(cod)(acac)]PF_6. The anisotropic displacement factor exponent takes the form: $-2\pi^2 [h^2a^{*2}U^{11} + \ldots + 2 h k a^* b^* U^{12}]$

	U^{11}	U^{22}	U^{33}	U^{23}	U^{13}	U^{12}
C(1)	12(2)	18(2)	18(2)	4(2)	-3(2)	3(2)
C(2)	13(2)	22(2)	14(2)	1(2)	-4(2)	-1(2)
C(3)	20(2)	19(2)	14(2)	-2(2)	0(2)	-4(2)
C(4)	17(2)	12(2)	23(2)	2(2)	4(2)	-2(2)
C(5)	18(2)	11(2)	13(2)	4(2)	3(2)	-2(2)
C(6)	15(2)	15(2)	13(2)	5(2)	3(2)	0(2)
C(7)	17(2)	23(2)	19(2)	2(2)	10(2)	2(2)
C(8)	12(2)	21(2)	27(3)	5(2)	7(2)	2(2)
C(9)	21(2)	11(2)	21(2)	-2(2)	11(2)	2(2)
C(10)	13(2)	14(2)	22(2)	-4(2)	7(2)	-5(2)
C(11)	12(2)	10(2)	15(2)	-3(2)	5(2)	2(2)

C(12)	24(3)	19(2)	23(2)	4(2)	7(2)	0(2)
C(13)	13(2)	22(2)	21(2)	-1(2)	6(2)	0(2)
O(1)	15(2)	18(2)	18(2)	5(1)	6(1)	-2(1)
O(2)	12(2)	19(2)	14(2)	1(1)	5(1)	-1(1)
F(1)	38(2)	37(2)	25(2)	8(1)	1(1)	18(2)
F(2)	30(2)	42(2)	47(2)	15(2)	23(2)	12(1)
F(3)	29(2)	68(2)	22(2)	7(2)	6(1)	25(2)
F(4)	34(2)	44(2)	39(2)	-7(1)	21(2)	-9(2)
F(5)	47(2)	23(2)	38(2)	-10(1)	10(2)	2(1)
F(6)	57(2)	34(2)	40(2)	-23(1)	19(2)	-3(2)
P(1)	18(1)	21(1)	17(1)	-3(1)	6(1)	4(1)
Pd(1)	11(1)	12(1)	12(1)	1(1)	3(1)	0(1)

Table B.1.4 Hydrogen co-ordinates (x 10^4) and isotropic displacement parameters ($Å^2$ x 10^3) for [Pd(cod)(acac)]PF_6.

	x	y	z	U(eq)
H(1)	-363	9756	1003	21
H(2)	696	8958	-105	22
H(3A)	1528	7523	304	22
H(3B)	-246	7482	55	22
H(4A)	-103	7231	2015	21
H(4B)	1276	6683	1834	21
H(5)	2867	7449	3301	17
H(6)	2170	8404	4453	17
H(7A)	-28	9224	3913	23
H(7B)	-581	8242	3833	23
H(8A)	-1435	8266	1797	24
H(8B)	-1799	9232	2124	24
H(10)	6301	10463	2533	19
H(12A)	4242	10742	-198	33
H(12B)	5318	11302	864	33
H(12C)	3552	11461	492	33
H(13A)	6610	9591	5225	27
H(13B)	7574	9898	4345	27
H(13C)	7205	8895	4440	27

Table B.1.5 Hydrogen bonds for [Pd(cod)(acac)]PF_6 (Å and °).

D-H...A	d(D-H)	d(H...A)	d(D...A)	<(DHA)
C(3)-H(3A)...F(1)	0.99	2.65	3.487(6)	141.9
C(4)-H(4B)...F(2)	0.99	2.82	3.399(6)	118.3
C(5)-H(5)...F(2)	1.00	2.35	3.139(5)	135.2
C(13)-H(13C)...F(6)	0.98	2.81	3.483(5)	126.5
C(1)-H(1)...O(1)#1	1.00	2.99	3.623(5)	121.9
C(1)-H(1)...F(3)#2	1.00	2.95	3.702(6)	132.5
C(7)-H(7A)...F(5)#2	0.99	2.48	3.326(5)	143.4
C(1)-H(1)...F(2)#2	1.00	2.98	3.636(5)	124.4
C(3)-H(3A)...F(6)#3	0.99	2.74	3.295(6)	115.6
C(3)-H(3B)...O(2)#3	0.99	3.00	3.687(5)	127.9
C(2)-H(2)...F(2)#3	1.00	2.53	3.259(5)	129.4
C(2)-H(2)...F(3)#3	1.00	2.53	3.374(6)	141.9
C(8)-H(8A)...F(4)#4	0.99	2.52	3.463(6)	160.2
C(4)-H(4A)...F(4)#4	0.99	2.70	3.623(6)	155.9
C(7)-H(7B)...F(1)#5	0.99	2.57	3.347(5)	135.1
C(6)-H(6)...F(4)#5	1.00	2.44	3.232(5)	135.9
C(7)-H(7A)...F(5)#5	0.99	2.70	3.303(6)	120.0
C(10)-H(10)...F(4)#6	0.95	2.87	3.679(5)	143.8
C(12)-H(12B)...F(3)#6	0.98	2.56	3.449(6)	150.8

C(13)-H(13B)...F(5)#6	0.98	2.64	3.602(6)	167.9
C(10)-H(10)...F(3)#6	0.95	2.39	3.292(5)	158.4
C(13)-H(13A)...O(2)#7	0.98	2.71	3.523(5)	140.5
C(13)-H(13C)...F(1)#8	0.98	2.83	3.604(6)	136.3

Symmetry transformations used to generate equivalent atoms:

#1 -x,-y+2,-z	#2 -x+1/2,y+1/2,-z+1/2	#3 x-1/2,-y+3/2,z-1/2
#4 x-1,y,z	#5 x-1/2,-y+3/2,z+1/2	#6 -x+3/2,y+1/2,-z+1/2
#7 -x+1,-y+2,-z+1	#8 x+1/2,-y+3/2,z+1/2	

B.2 Crystal Data of [Pd(cod)(3Br-trop)]BF_4

Table B.2.1 Atomic coordinates (x 10^4) and equivalent isotropic displacement parameters (Å^{2}x 10^3) for [Pd(cod)(3Br-trop)]BF_4. U(eq) is defined as one third of the trace of the orthogonalized U^{ij} tensor.

	x	y	z	U(eq)
C(1)	1240(7)	2215(7)	1236(3)	20(1)
C(2)	610(7)	3933(7)	1185(3)	19(1)
C(3)	1565(7)	5321(7)	702(3)	18(1)
C(4)	2743(7)	6138(6)	1262(3)	18(1)
C(5)	3722(6)	4911(6)	1896(3)	16(1)
C(6)	4489(7)	3265(7)	1773(3)	21(1)
C(7)	4641(8)	2421(7)	941(3)	25(1)
C(8)	3069(8)	1403(7)	860(3)	25(1)
C(9)	-521(6)	2342(6)	3798(3)	12(1)
C(10)	1009(7)	2929(6)	4159(3)	13(1)
C(11)	1186(6)	3039(6)	5037(3)	12(1)
C(12)	97(7)	2617(6)	5745(3)	13(1)
C(13)	-1469(6)	1830(6)	5779(3)	12(1)
C(14)	-2338(6)	1309(6)	5125(3)	12(1)
C(15)	-1921(6)	1531(6)	4262(3)	13(1)
B(1)	-2482(8)	7899(8)	1666(4)	18(1)
O(1)	-557(5)	2509(4)	2991(2)	18(1)
O(2)	2275(4)	3430(4)	3622(2)	16(1)
F(1)	-1571(5)	6996(4)	2318(2)	34(1)
F(2)	-2889(4)	6757(4)	1099(2)	25(1)
F(3)	-4101(4)	8818(4)	1969(2)	27(1)
F(4)	-1355(5)	8984(4)	1238(2)	37(1)
Br(1)	-3437(1)	573(1)	3583(1)	16(1)
Br(2)	3317(1)	3940(1)	5279(1)	15(1)
Br(3)	-2606(1)	1356(1)	6863(1)	19(1)
Pd(1)	1724(1)	3273(1)	2409(1)	15(1)

Table B.2.2 Bond lengths (Å) and angles (^{o}) for [Pd(cod)(3Br-trop)]BF_4

C(1)-C(2)	1.387(7)	C(5)-Pd(1)	2.176(5)	C(10)-C(11)	1.424(6)
C(1)-C(8)	1.512(7)	C(5)-H(5)	1.0000	C(11)-C(12)	1.380(6)
C(1)-Pd(1)	2.180(5)	C(6)-C(7)	1.522(7)	C(11)-Br(2)	1.894(5)
C(1)-H(1)	1.0000	C(6)-Pd(1)	2.201(5)	C(12)-C(13)	1.385(6)
C(2)-C(3)	1.524(7)	C(6)-H(6)	1.0000	C(12)-H(14)	0.9500
C(2)-Pd(1)	2.177(5)	C(7)-C(8)	1.524(8)	C(13)-C(14)	1.384(6)
C(2)-H(2)	1.0000	C(7)-H(7A)	0.9900	C(13)-Br(3)	1.894(4)
C(3)-C(4)	1.531(7)	C(7)-H(7B)	0.9900	C(14)-C(15)	1.387(6)
C(3)-H(3A)	0.9900	C(8)-H(8A)	0.9900	C(14)-H(16)	0.9500
C(3)-H(3B)	0.9900	C(8)-H(8B)	0.9900	C(15)-Br(1)	1.887(5)
C(4)-C(5)	1.511(7)	C(9)-O(1)	1.284(5)	B(1)-F(3)	1.385(6)
C(4)-H(4A)	0.9900	C(9)-C(15)	1.423(6)	B(1)-F(1)	1.386(7)
C(4)-H(4B)	0.9900	C(9)-C(10)	1.455(6)	B(1)-F(4)	1.389(7)
C(5)-C(6)	1.381(7)	C(10)-O(2)	1.299(5)	B(1)-F(2)	1.408(6)

O(1)-Pd(1)	2.003(3)	Pd(1)-C(5)-H(5)	114.2	C(14)-C(13)-Br(3)	113.9(3)
O(2)-Pd(1)	2.023(3)	C(5)-C(6)-C(7)	125.4(5)	C(12)-C(13)-Br(3)	117.0(4)
		C(5)-C(6)-Pd(1)	70.6(3)	C(13)-C(14)-C(15)	128.7(4)
C(2)-C(1)-C(8)	125.5(5)	C(7)-C(6)-Pd(1)	111.2(4)	C(13)-C(14)-H(16)	115.6
C(2)-C(1)-Pd(1)	71.3(3)	C(5)-C(6)-H(6)	113.9	C(15)-C(14)-H(16)	115.6
C(8)-C(1)-Pd(1)	107.7(3)	C(7)-C(6)-H(6)	113.9	C(14)-C(15)-C(9)	131.0(4)
C(2)-C(1)-H(1)	114.5	Pd(1)-C(6)-H(6)	113.9	C(14)-C(15)-Br(1)	115.0(4)
C(8)-C(1)-H(1)	114.5	C(6)-C(7)-C(8)	112.7(4)	C(9)-C(15)-Br(1)	114.0(3)
Pd(1)-C(1)-H(1)	114.5	C(6)-C(7)-H(7A)	109.1	F(3)-B(1)-F(1)	111.0(4)
C(1)-C(2)-C(3)	126.7(5)	C(8)-C(7)-H(7A)	109.1	F(3)-B(1)-F(4)	109.7(5)
C(1)-C(2)-Pd(1)	71.6(3)	C(6)-C(7)-H(7B)	109.1	F(1)-B(1)-F(4)	109.5(5)
C(3)-C(2)-Pd(1)	110.9(3)	C(8)-C(7)-H(7B)	109.1	F(3)-B(1)-F(2)	109.0(4)
C(1)-C(2)-H(2)	113.3	H(7A)-C(7)-H(7B)	107.8	F(1)-B(1)-F(2)	108.9(5)
C(3)-C(2)-H(2)	113.3	C(1)-C(8)-C(7)	113.5(4)	F(4)-B(1)-F(2)	108.6(4)
Pd(1)-C(2)-H(2)	113.3	C(1)-C(8)-H(8A)	108.9	C(9)-O(1)-Pd(1)	113.4(3)
C(2)-C(3)-C(4)	112.2(4)	C(7)-C(8)-H(8A)	108.9	C(10)-O(2)-Pd(1)	112.8(3)
C(2)-C(3)-H(3A)	109.2	C(1)-C(8)-H(8B)	108.9	O(1)-Pd(1)-O(2)	80.64(13)
C(4)-C(3)-H(3A)	109.2	C(7)-C(8)-H(8B)	108.9	O(1)-Pd(1)-C(5)	160.86(18)
C(2)-C(3)-H(3B)	109.2	H(8A)-C(8)-H(8B)	107.7	O(2)-Pd(1)-C(5)	94.34(17)
C(4)-C(3)-H(3B)	109.2	O(1)-C(9)-C(15)	117.8(4)	O(1)-Pd(1)-C(2)	96.29(17)
H(3A)-C(3)-H(3B)	107.9	O(1)-C(9)-C(10)	116.9(4)	O(2)-Pd(1)-C(2)	160.61(17)
C(5)-C(4)-C(3)	114.0(4)	C(15)-C(9)-C(10)	125.2(4)	C(5)-Pd(1)-C(2)	82.30(19)
C(5)-C(4)-H(4A)	108.8	O(2)-C(10)-C(11)	118.7(4)	O(1)-Pd(1)-C(1)	91.78(17)
C(3)-C(4)-H(4A)	108.8	O(2)-C(10)-C(9)	115.9(4)	O(2)-Pd(1)-C(1)	160.89(17)
C(5)-C(4)-H(4B)	108.8	C(11)-C(10)-C(9)	125.4(4)	C(5)-Pd(1)-C(1)	98.2(2)
C(3)-C(4)-H(4B)	108.8	C(12)-C(11)-C(10)	132.2(5)	C(2)-Pd(1)-C(1)	37.14(19)
H(4A)-C(4)-H(4B)	107.7	C(12)-C(11)-Br(2)	113.8(4)	O(1)-Pd(1)-C(6)	162.26(18)
C(6)-C(5)-C(4)	126.7(5)	C(10)-C(11)-Br(2)	114.0(3)	O(2)-Pd(1)-C(6)	100.59(17)
C(6)-C(5)-Pd(1)	72.6(3)	C(11)-C(12)-C(13)	127.5(5)	C(5)-Pd(1)-C(6)	36.78(19)
C(4)-C(5)-Pd(1)	105.7(3)	C(11)-C(12)-H(14)	116.3	C(2)-Pd(1)-C(6)	88.17(19)
C(6)-C(5)-H(5)	114.2	C(13)-C(12)-H(14)	116.3	C(1)-Pd(1)-C(6)	81.4(2)
C(4)-C(5)-H(5)	114.2	C(14)-C(13)-C(12)	129.1(4)		

Symmetry transformations used to generate equivalent atoms:

Table B.2.3 Anisotropic displacement parameters ($Å^2 x\ 10^3$) for [Pd(cod)(3Br-trop)]BF_4. The anisotropic displacement factor exponent takes the form: $-2\pi^2[h^2 a^{*2} U^{11} + ... + 2\ h\ k\ a^*\ b^*\ U^{12}]$

	U^{11}	U^{22}	U^{33}	U^{23}	U^{13}	U^{12}
C(1)	26(3)	22(3)	13(3)	-4(2)	-6(2)	-7(2)
C(2)	20(3)	24(3)	13(2)	-1(2)	-7(2)	-5(2)
C(3)	19(3)	22(3)	12(2)	2(2)	-3(2)	1(2)
C(4)	18(3)	20(3)	16(3)	2(2)	-1(2)	-8(2)
C(5)	8(2)	23(3)	20(3)	3(2)	2(2)	-9(2)
C(6)	7(2)	32(3)	20(3)	5(2)	4(2)	1(2)
C(7)	26(3)	21(3)	22(3)	5(2)	3(2)	9(2)
C(8)	33(3)	22(3)	18(3)	-4(2)	-2(2)	3(3)
C(9)	13(2)	12(3)	10(2)	0(2)	-1(2)	1(2)
C(10)	15(3)	9(2)	13(2)	2(2)	2(2)	-1(2)
C(11)	8(2)	10(2)	19(3)	-2(2)	-3(2)	-2(2)
C(12)	17(3)	9(2)	12(2)	0(2)	1(2)	1(2)
C(13)	8(2)	15(3)	11(2)	-1(2)	1(2)	-2(2)
C(14)	6(2)	10(2)	20(3)	-1(2)	2(2)	-2(2)
C(15)	11(2)	9(2)	20(3)	-2(2)	-5(2)	1(2)
B(1)	13(3)	25(3)	17(3)	-6(2)	1(2)	-1(3)
O(1)	17(2)	23(2)	13(2)	2(2)	-1(2)	-8(2)
O(2)	13(2)	21(2)	15(2)	-1(2)	1(2)	-4(2)
F(1)	35(2)	40(2)	25(2)	-5(2)	-15(2)	6(2)
F(2)	24(2)	29(2)	23(2)	-8(1)	-4(1)	-1(1)
F(3)	19(2)	35(2)	26(2)	-7(1)	0(1)	2(1)
F(4)	30(2)	37(2)	46(2)	-4(2)	9(2)	-15(2)
Br(1)	16(1)	18(1)	17(1)	1(1)	-6(1)	-7(1)
Br(2)	11(1)	17(1)	19(1)	0(1)	-3(1)	-5(1)
Br(3)	20(1)	24(1)	13(1)	-2(1)	3(1)	-10(1)
Pd(1)	14(1)	19(1)	12(1)	1(1)	0(1)	-3(1)

Table B.2.4 Hydrogen coordinates (x 10^4) and isotropic displacement parameters ($Å^2$x 10^3) for [Pd(cod)(3Br-trop)]BF_4.

	x	y	z	U(eq)
H(1)	250	1469	1290	23
H(2)	-759	4187	1219	22
H(3A)	627	6200	468	22
H(3B)	2352	4835	223	22
H(4A)	3668	6691	897	21
H(4B)	1948	7029	1568	21
H(5)	4296	5460	2333	20
H(6)	5504	2836	2146	25
H(7A)	5819	1662	891	30
H(7B)	4653	3299	470	30
H(8A)	2963	1254	255	30
H(8B)	3366	266	1145	30
H(14)	464	2899	6269	16
H(16)	-3358	721	5288	14

Table B.2.5 Hydrogen bonds for [Pd(cod)(3Br-trop)]BF_4 [Å and °].

D-H...A	d(D-H)	d(H...A)	d(D...A)	<(DHA)
C(2)-H(2)...F(2)	1.00	2.42	3.192(6)	134.0
C(3)-H(3B)...F(2)#1	0.99	2.52	3.427(6)	152.8
C(6)-H(6)...Br(1)#2	1.00	2.90	3.765(5)	145.1
C(12)-H(14)...F(1)#3	0.95	2.46	3.401(6)	168.3
C(8)-H(8B)...F(3)#4	0.99	2.48	3.257(6)	135.6

Symmetry transformations used to generate equivalent atoms:
#1 -x,-y+1,-z #2 x+1,y,z #3 -x,-y+1,-z+1 #4 x+1,y-1,z

B.3 Crystal Data of [Pd(cod)(3Br-trop)]PF_6

Table B.3.1 Atomic coordinates (x 10^4) and equivalent isotropic displacement parameters ($Å^2$x 10^3) for [Pd(cod)(3Br-trop)]PF_6. U(eq) is defined as one third of the trace of the orthogonalized U^{ij} tensor.

	x	y	z	U(eq)
C(2)	1207(12)	-433(11)	3757(5)	23(2)
C(3)	2952(12)	-1237(11)	3988(6)	27(2)
C(4)	4408(12)	-9(11)	3799(6)	24(2)
C(5)	4098(11)	1443(10)	3055(5)	20(2)
C(1)	616(11)	1098(10)	3958(5)	19(2)
C(6)	3309(11)	3031(10)	3113(6)	23(2)
C(7)	2552(12)	3525(10)	3923(6)	25(2)
C(8)	1566(11)	2109(10)	4495(6)	22(2)
C(9)	-590(11)	1470(10)	1192(5)	18(2)
C(10)	862(10)	2459(10)	814(5)	19(2)
C(11)	1109(10)	3166(10)	-77(5)	18(2)
C(12)	103(12)	3143(10)	-810(6)	23(2)
C(13)	-1372(11)	2329(10)	-841(5)	17(2)
C(14)	-2315(11)	1346(10)	-166(5)	19(2)
C(15)	-1962(11)	954(10)	729(5)	20(2)
O(1)	-642(8)	938(7)	2017(3)	21(1)
O(2)	2011(9)	2622(8)	1359(4)	26(1)
F(1)	-1110(7)	4742(7)	2848(4)	36(1)
F(2)	-3164(7)	3427(6)	3735(4)	31(1)

F(3)	-1922(8)	7245(7)	3252(4)	39(1)
F(4)	-3996(8)	5925(7)	4121(4)	37(1)
F(5)	-3846(8)	5737(7)	2696(4)	41(2)
F(6)	-1278(7)	4945(7)	4284(3)	33(1)
P(1)	-2556(3)	5349(3)	3487(2)	24(1)
Br(1)	-3514(1)	-483(1)	1395(1)	24(1)
Br(2)	3156(1)	4345(1)	-330(1)	23(1)
Br(3)	-2382(1)	2597(1)	-1947(1)	26(1)
Pd(1)	1497(1)	1536(1)	2595(1)	19(1)

Table B.3.2 Bond lengths (Å) and angles (°) for [Pd(cod)(3Br-trop)]PF_6

C(2)-C(1)	1.382(12)	C(1)-C(2)-H(5)	114.8	C(11)-C(10)-C(9)	125.7(7)
C(2)-C(3)	1.514(13)	C(3)-C(2)-H(5)	114.6	C(10)-C(11)-C(12)	131.6(8)
C(2)-Pd(1)	2.182(8)	Pd(1)-C(2)-H(5)	114.8	C(10)-C(11)-Br(2)	113.9(6)
C(2)-H(5)	1.0000	C(2)-C(3)-C(4)	114.4(7)	C(12)-C(11)-Br(2)	114.5(6)
C(3)-C(4)	1.523(13)	C(2)-C(3)-H(6A)	108.6	C(13)-C(12)-C(11)	128.1(9)
C(3)-H(6A)	0.9900	C(4)-C(3)-H(6A)	108.6	C(13)-C(12)-H(13)	115.9
C(3)-H(6B)	0.9900	C(2)-C(3)-H(6B)	108.8	C(11)-C(12)-H(13)	116.0
C(4)-C(5)	1.498(12)	C(4)-C(3)-H(6B)	108.6	C(12)-C(13)-C(14)	129.6(8)
C(4)-H(7A)	0.9900	H(6A)-C(3)-H(6B)	107.6	C(12)-C(13)-Br(3)	116.4(6)
C(4)-H(7B)	0.9900	C(5)-C(4)-C(3)	114.1(7)	C(14)-C(13)-Br(3)	113.9(6)
C(5)-C(6)	1.410(11)	C(5)-C(4)-H(7A)	108.7	C(13)-C(14)-C(15)	128.4(8)
C(5)-Pd(1)	2.178(9)	C(3)-C(4)-H(7A)	108.7	C(13)-C(14)-H(11)	115.9
C(5)-H(8)	1.0000	C(5)-C(4)-H(7B)	108.7	C(15)-C(14)-H(11)	115.7
C(1)-C(8)	1.504(11)	C(3)-C(4)-H(7B)	108.7	C(14)-C(15)-C(9)	129.8(8)
C(1)-Pd(1)	2.193(8)	H(7A)-C(4)-H(7B)	107.6	C(14)-C(15)-Br(1)	114.2(6)
C(1)-H(4)	1.0000	C(6)-C(5)-C(4)	125.9(8)	C(9)-C(15)-Br(1)	116.0(6)
C(6)-C(7)	1.499(12)	C(6)-C(5)-Pd(1)	70.5(5)	C(9)-O(1)-Pd(1)	111.8(5)
C(6)-Pd(1)	2.165(8)	C(4)-C(5)-Pd(1)	112.1(6)	C(10)-O(2)-Pd(1)	115.0(6)
C(6)-H(1)	1.0000	C(6)-C(5)-H(8)	113.5	F(3)-P(1)-F(4)	90.1(3)
C(7)-C(8)	1.527(12)	C(4)-C(5)-H(8)	113.5	F(3)-P(1)-F(5)	90.4(3)
C(7)-H(2A)	0.9900	Pd(1)-C(5)-H(8)	113.5	F(4)-P(1)-F(5)	90.3(3)
C(7)-H(2B)	0.9900	C(2)-C(1)-C(8)	124.3(8)	F(3)-P(1)-F(6)	90.2(3)
C(8)-H(3A)	0.9900	C(2)-C(1)-Pd(1)	71.1(5)	F(4)-P(1)-F(6)	89.5(3)
C(8)-H(3B)	0.9900	C(8)-C(1)-Pd(1)	112.6(5)	F(5)-P(1)-F(6)	179.4(4)
C(9)-O(1)	1.281(9)	C(2)-C(1)-H(4)	113.9	F(3)-P(1)-F(2)	178.9(3)
C(9)-C(15)	1.432(11)	C(8)-C(1)-H(4)	113.7	F(4)-P(1)-F(2)	90.2(3)
C(9)-C(10)	1.460(12)	Pd(1)-C(1)-H(4)	113.8	F(5)-P(1)-F(2)	90.6(3)
C(10)-O(2)	1.287(10)	C(5)-C(6)-C(7)	125.8(8)	F(6)-P(1)-F(2)	88.8(3)
C(10)-C(11)	1.413(12)	C(5)-C(6)-Pd(1)	71.6(5)	F(3)-P(1)-F(1)	90.6(3)
C(11)-C(12)	1.415(11)	C(7)-C(6)-Pd(1)	108.7(6)	F(4)-P(1)-F(1)	179.2(3)
C(11)-Br(2)	1.890(8)	C(5)-C(6)-H(1)	114.1	F(5)-P(1)-F(1)	89.6(3)
C(12)-C(13)	1.358(12)	C(7)-C(6)-H(1)	114.1	F(6)-P(1)-F(1)	90.7(3)
C(12)-H(13)	0.9500	Pd(1)-C(6)-H(1)	114.1	F(2)-P(1)-F(1)	89.1(3)
C(13)-C(14)	1.403(11)	C(6)-C(7)-C(8)	113.5(6)	O(2)-Pd(1)-O(1)	80.1(2)
C(13)-Br(3)	1.897(7)	C(6)-C(7)-H(2A)	108.9	O(2)-Pd(1)-C(6)	93.5(3)
C(14)-C(15)	1.411(11)	C(8)-C(7)-H(2A)	108.8	O(1)-Pd(1)-C(6)	160.0(3)
C(14)-H(11)	0.9500	C(6)-C(7)-H(2B)	108.9	O(2)-Pd(1)-C(5)	96.9(3)
C(15)-Br(1)	1.865(8)	C(8)-C(7)-H(2B)	108.9	O(1)-Pd(1)-C(5)	161.2(3)
O(1)-Pd(1)	2.047(6)	H(2A)-C(7)-H(2B)	107.7	C(6)-Pd(1)-C(5)	37.9(3)
O(2)-Pd(1)	2.002(6)	C(1)-C(8)-C(7)	111.5(7)	O(2)-Pd(1)-C(2)	159.9(3)
F(1)-P(1)	1.615(6)	C(1)-C(8)-H(3A)	109.3	O(1)-Pd(1)-C(2)	94.8(3)
F(2)-P(1)	1.602(5)	C(7)-C(8)-H(3A)	109.2	C(6)-Pd(1)-C(2)	97.2(3)
F(3)-P(1)	1.588(6)	C(1)-C(8)-H(3B)	109.4	C(5)-Pd(1)-C(2)	81.6(3)
F(4)-P(1)	1.595(6)	C(7)-C(8)-H(3B)	109.3	O(2)-Pd(1)-C(1)	163.1(3)
F(5)-P(1)	1.600(6)	H(3A)-C(8)-H(3B)	107.9	O(1)-Pd(1)-C(1)	100.1(3)
F(6)-P(1)	1.600(5)	O(1)-C(9)-C(15)	115.1(7)	C(6)-Pd(1)-C(1)	80.5(3)
		O(1)-C(9)-C(10)	118.2(7)	C(5)-Pd(1)-C(1)	88.1(3)
C(1)-C(2)-C(3)	124.3(8)	C(15)-C(9)-C(10)	126.6(7)	C(2)-Pd(1)-C(1)	36.8(3)
C(1)-C(2)-Pd(1)	72.0(5)	O(2)-C(10)-C(11)	119.5(8)		
C(3)-C(2)-Pd(1)	108.0(6)	O(2)-C(10)-C(9)	114.8(7)		

Symmetry transformations used to generate equivalent atoms:

Table B.3.3 Anisotropic displacement parameters ($Å^2 x\ 10^3$) for [Pd(cod)(3Br-trop)]PF_6. The anisotropic displacement factor exponent takes the form: $-2\pi^2[h^2 a^{*2} U^{11} + ... + 2 h k a^* b^* U^{12}]$

	U^{11}	U^{22}	U^{33}	U^{23}	U^{13}	U^{12}
C(2)	31(5)	24(4)	14(4)	0(3)	-2(3)	-10(4)
C(3)	35(5)	30(5)	16(4)	-3(4)	-8(4)	-1(4)
C(4)	26(5)	25(4)	23(4)	-5(3)	-14(4)	0(4)
C(5)	22(4)	23(4)	17(4)	-7(3)	5(3)	-12(3)
C(1)	16(4)	24(4)	14(4)	2(3)	3(3)	-9(3)
C(6)	20(4)	18(4)	33(5)	-8(3)	-3(4)	-5(3)
C(7)	33(5)	18(4)	27(5)	-12(3)	-11(4)	-5(3)
C(8)	22(4)	22(4)	24(4)	-9(3)	-1(3)	-4(3)
C(9)	23(4)	17(4)	14(4)	-5(3)	-1(3)	-2(3)
C(10)	15(4)	20(4)	23(4)	-8(3)	0(3)	-6(3)
C(11)	13(4)	23(4)	18(4)	-6(3)	4(3)	-3(3)
C(12)	32(5)	19(4)	18(4)	-7(3)	-5(4)	-2(4)
C(13)	24(4)	17(4)	11(4)	-1(3)	-7(3)	-2(3)
C(14)	17(4)	19(4)	20(4)	-5(3)	3(3)	-1(3)
C(15)	24(4)	15(4)	20(4)	1(3)	1(3)	-5(3)
O(1)	28(3)	26(3)	8(3)	-1(2)	1(2)	-12(2)
O(2)	40(4)	26(3)	11(3)	1(2)	-8(3)	-1(3)
F(1)	30(3)	51(4)	27(3)	-9(3)	4(2)	-9(3)
F(2)	32(3)	21(3)	37(3)	2(2)	1(2)	-8(2)
F(3)	38(4)	30(3)	50(4)	-4(3)	-8(3)	-17(2)
F(4)	33(3)	39(3)	41(3)	-13(3)	5(3)	-2(3)
F(5)	43(4)	36(3)	42(4)	5(3)	-30(3)	-12(3)
F(6)	34(3)	46(3)	21(3)	-12(2)	-11(2)	2(3)
P(1)	24(1)	25(1)	22(1)	-1(1)	-4(1)	-6(1)
Br(1)	26(1)	27(1)	20(1)	-7(1)	3(1)	-11(1)
Br(2)	26(1)	25(1)	19(1)	-5(1)	1(1)	-10(1)
Br(3)	33(1)	29(1)	17(1)	-2(1)	-6(1)	-8(1)
Pd(1)	23(1)	21(1)	14(1)	-2(1)	-3(1)	-6(1)

Table B.3.4 Hydrogen coordinates ($x\ 10^4$) and isotropic displacement parameters ($Å^2 x\ 10^3$) for [Pd(cod)(3Br-trop)]PF_6.

	x	y	z	U(eq)
H(5)	301	-1260	3724	28
H(6A)	3172	-2168	3661	32
H(6B)	2943	-1750	4616	32
H(7A)	4609	457	4327	29
H(7B)	5458	-650	3670	29
H(8)	4983	1509	2579	24
H(4)	-651	1187	4034	22
H(1)	3753	4007	2679	28
H(2A)	1775	4532	3756	30
H(2B)	3479	3857	4265	30
H(3A)	2370	1340	4873	26
H(3B)	746	2614	4874	26
H(13)	511	3777	-1347	27
H(11)	-3322	885	-334	22

Table B.3.5 Hydrogen bonds for [Pd(cod)(3Br-trop)]PF_6 [Å and °].

D-H...A	d(D-H)	d(H...A)	d(D...A)	<(DHA)
C(7)-H(2A)...F(6)	0.99	2.54	3.245(11)	127.9
C(2)-H(5)...F(3)#1	1.00	2.37	3.340(10)	163.9
C(3)-H(6A)...Br(3)#2	0.99	2.86	3.615(8)	133.7
C(6)-H(1)...F(5)#3	1.00	2.39	3.142(10)	131.6
C(5)-H(8)...Br(1)#3	1.00	2.87	3.698(8)	140.9
C(12)-H(13)...F(1)#4	0.95	2.46	3.404(11)	169.9

Symmetry transformations used to generate equivalent atoms:
#1 x,y-1,z #2 -x,-y,-z #3 x+1,y,z #4 -x,-y+1,-z

B.4 Crystal Data of [Pd(cod)(thtfac)]PF_6

Table B.4.1 Atomic coordinates (x 10^4) and equivalent isotropic displacement parameters (Å^{2}x 10^3) for [Pd(cod)(thtfac)]PF_6. U(eq) is defined as one third of the trace of the orthogonalized U^{ij} tensor.

	x	y	z	U(eq)
C(1)	4492(2)	9033(1)	3193(2)	14(1)
C(2)	3889(2)	8538(1)	3896(2)	16(1)
C(3)	3918(3)	7655(1)	3887(2)	19(1)
C(4)	3728(2)	7293(1)	2632(2)	17(1)
C(5)	2753(2)	7764(1)	1710(2)	16(1)
C(6)	3135(2)	8342(1)	994(2)	14(1)
C(7)	4557(2)	8668(1)	1063(2)	16(1)
C(8)	5379(2)	8760(1)	2334(2)	16(1)
C(9)	-455(2)	9431(1)	1464(2)	14(1)
C(10)	-444(2)	9975(1)	2344(2)	15(1)
C(11)	691(2)	10128(1)	3282(2)	13(1)
C(12)	-1743(2)	9322(1)	530(2)	16(1)
C(13)	563(2)	10735(1)	4142(2)	14(1)
C(14)	-580(3)	11172(1)	4252(2)	16(1)
C(15)	-298(3)	11703(1)	5206(2)	19(1)
C(16)	1026(3)	11666(1)	5801(2)	20(1)
O(1)	494(2)	8958(1)	1283(1)	16(1)
O(2)	1834(2)	9777(1)	3438(1)	15(1)
F(01)	-3517(2)	11429(1)	1738(1)	27(1)
F(1)	-2686(1)	9872(1)	577(1)	26(1)
F(2)	-2320(1)	8627(1)	672(1)	22(1)
F(02)	-5769(2)	11121(1)	3331(1)	32(1)
F(03)	-5315(2)	10602(1)	1634(1)	29(1)
F(3)	-1479(1)	9332(1)	-568(1)	24(1)
F(04)	-3963(2)	11950(1)	3422(1)	34(1)
F(05)	-3668(1)	10635(1)	3293(1)	24(1)
F(06)	-5635(2)	11911(1)	1770(1)	31(1)
P(01)	-4652(1)	11274(1)	2526(1)	16(1)
S(1)	1962(1)	10985(1)	5217(1)	18(1)
Pd(1)	2314(1)	8911(1)	2400(1)	12(1)

Table B.4.2 Bond lengths (Å) and angles (°) for [Pd(cod)(thtfac)]PF_6.

C(1)-C(2)	1.383(3)	C(8)-C(1)-Pd(1)	110.87(15)	O(2)-C(11)-C(13)	115.8(2)
C(1)-C(8)	1.520(3)	C(2)-C(1)-H(1)	114.2	C(10)-C(11)-C(13)	118.8(2)
C(1)-Pd(1)	2.193(2)	C(8)-C(1)-H(1)	114.2	F(1)-C(12)-F(3)	107.46(19)
C(1)-H(1)	1.0000	Pd(1)-C(1)-H(1)	114.2	F(1)-C(12)-F(2)	106.93(18)
C(2)-C(3)	1.505(3)	C(1)-C(2)-C(3)	126.5(2)	F(3)-C(12)-F(2)	107.07(18)
C(2)-Pd(1)	2.181(2)	C(1)-C(2)-Pd(1)	72.05(14)	F(1)-C(12)-C(9)	113.08(19)
C(2)-H(2)	1.0000	C(3)-C(2)-Pd(1)	107.32(16)	F(3)-C(12)-C(9)	111.68(18)
C(3)-C(4)	1.542(3)	C(1)-C(2)-H(2)	114.1	F(2)-C(12)-C(9)	110.32(19)
C(3)-H(3A)	0.9900	C(3)-C(2)-H(2)	114.1	C(14)-C(13)-C(11)	128.8(2)
C(3)-H(3B)	0.9900	Pd(1)-C(2)-H(2)	114.1	C(14)-C(13)-S(1)	111.47(18)
C(4)-C(5)	1.518(3)	C(2)-C(3)-C(4)	113.96(19)	C(11)-C(13)-S(1)	119.70(17)
C(4)-H(4A)	0.9900	C(2)-C(3)-H(3A)	108.8	C(13)-C(14)-C(15)	111.9(2)
C(4)-H(4B)	0.9900	C(4)-C(3)-H(3A)	108.8	C(13)-C(14)-H(14)	124.0
C(5)-C(6)	1.383(3)	C(2)-C(3)-H(3B)	108.8	C(15)-C(14)-H(14)	124.0
C(5)-Pd(1)	2.184(2)	C(4)-C(3)-H(3B)	108.8	C(16)-C(15)-C(14)	112.7(2)
C(5)-H(5)	1.0000	H(3A)-C(3)-H(3B)	107.7	C(16)-C(15)-H(15)	123.6
C(6)-C(7)	1.510(3)	C(5)-C(4)-C(3)	112.63(19)	C(14)-C(15)-H(15)	123.6
C(6)-Pd(1)	2.174(2)	C(5)-C(4)-H(4A)	109.1	C(15)-C(16)-S(1)	112.68(18)
C(6)-H(6)	1.0000	C(3)-C(4)-H(4A)	109.1	C(15)-C(16)-H(16)	123.7
C(7)-C(8)	1.535(3)	C(5)-C(4)-H(4B)	109.1	S(1)-C(16)-H(16)	123.7
C(7)-H(7A)	0.9900	C(3)-C(4)-H(4B)	109.1	C(9)-O(1)-Pd(1)	121.47(15)
C(7)-H(7B)	0.9900	H(4A)-C(4)-H(4B)	107.8	C(11)-O(2)-Pd(1)	125.00(15)
C(8)-H(8A)	0.9900	C(6)-C(5)-C(4)	125.2(2)	F(03)-P(01)-F(06)	90.34(9)
C(8)-H(8B)	0.9900	C(6)-C(5)-Pd(1)	71.13(13)	F(03)-P(01)-F(02)	90.38(9)
C(9)-O(1)	1.290(3)	C(4)-C(5)-Pd(1)	111.44(15)	F(06)-P(01)-F(02)	90.08(8)
C(9)-C(10)	1.369(3)	C(6)-C(5)-H(5)	113.8	F(03)-P(01)-F(01)	90.32(8)
C(9)-C(12)	1.513(3)	C(4)-C(5)-H(5)	113.8	F(06)-P(01)-F(01)	90.38(8)
C(10)-C(11)	1.424(3)	Pd(1)-C(5)-H(5)	113.8	F(02)-P(01)-F(01)	179.16(10)
C(10)-H(10)	0.9500	C(5)-C(6)-C(7)	126.5(2)	F(03)-P(01)-F(05)	89.89(8)
C(11)-O(2)	1.268(3)	C(5)-C(6)-Pd(1)	71.88(12)	F(06)-P(01)-F(05)	179.62(9)
C(11)-C(13)	1.453(3)	C(7)-C(6)-Pd(1)	106.48(14)	F(02)-P(01)-F(05)	89.62(8)
C(12)-F(1)	1.335(3)	C(5)-C(6)-H(6)	114.3	F(01)-P(01)-F(05)	89.92(8)
C(12)-F(3)	1.337(3)	C(7)-C(6)-H(6)	114.3	F(03)-P(01)-F(04)	179.22(10)
C(12)-F(2)	1.340(3)	Pd(1)-C(6)-H(6)	114.3	F(06)-P(01)-F(04)	89.98(9)
C(13)-C(14)	1.387(3)	C(6)-C(7)-C(8)	114.08(19)	F(02)-P(01)-F(04)	90.33(9)
C(13)-S(1)	1.724(2)	C(6)-C(7)-H(7A)	108.7	F(01)-P(01)-F(04)	88.97(8)
C(14)-C(15)	1.406(3)	C(8)-C(7)-H(7A)	108.7	F(05)-P(01)-F(04)	89.80(9)
C(14)-H(14)	0.9500	C(6)-C(7)-H(7B)	108.7	C(16)-S(1)-C(13)	91.18(12)
C(15)-C(16)	1.363(3)	C(8)-C(7)-H(7B)	108.7	O(1)-Pd(1)-O(2)	93.34(6)
C(15)-H(15)	0.9500	H(7A)-C(7)-H(7B)	107.6	O(1)-Pd(1)-C(6)	88.21(8)
C(16)-S(1)	1.706(2)	C(1)-C(8)-C(7)	112.18(19)	O(2)-Pd(1)-C(6)	159.03(8)
C(16)-H(16)	0.9500	C(1)-C(8)-H(8A)	109.2	O(1)-Pd(1)-C(2)	159.22(8)
O(1)-Pd(1)	2.0071(16)	C(7)-C(8)-H(8A)	109.2	O(2)-Pd(1)-C(2)	88.04(8)
O(2)-Pd(1)	2.0120(15)	C(1)-C(8)-H(8B)	109.2	C(6)-Pd(1)-C(2)	97.86(9)
F(01)-P(01)	1.6036(15)	C(7)-C(8)-H(8B)	109.2	O(1)-Pd(1)-C(5)	91.40(8)
F(02)-P(01)	1.6012(15)	H(8A)-C(8)-H(8B)	107.9	O(2)-Pd(1)-C(5)	163.39(7)
F(03)-P(01)	1.5905(15)	O(1)-C(9)-C(10)	129.9(2)	C(6)-Pd(1)-C(5)	36.99(8)
F(04)-P(01)	1.6063(15)	O(1)-C(9)-C(12)	110.9(2)	C(2)-Pd(1)-C(5)	81.98(9)
F(05)-P(01)	1.6059(15)	C(10)-C(9)-C(12)	119.2(2)	O(1)-Pd(1)-C(1)	163.44(8)
F(06)-P(01)	1.5991(15)	C(9)-C(10)-C(11)	124.8(2)	O(2)-Pd(1)-C(1)	90.92(7)
		C(9)-C(10)-H(10)	117.6	C(6)-Pd(1)-C(1)	82.20(9)
C(2)-C(1)-C(8)	124.5(2)	C(11)-C(10)-H(10)	117.6	C(2)-Pd(1)-C(1)	36.88(9)
C(2)-C(1)-Pd(1)	71.07(14)	O(2)-C(11)-C(10)	125.4(2)	C(5)-Pd(1)-C(1)	89.03(9)

Symmetry transformations used to generate equivalent atoms

Table B.4.3 Anisotropic displacement parameters ($Å^2 x\ 10^3$)for [Pd(cod)(thtfac)]PF_6. The anisotropic displacement factor exponent takes the form: $-2\pi^2[\ h^2 a^{*2} U^{11} + ... + 2\ h\ k\ a^*\ b^*\ U^{12}\ ]$

	U^{11}	U^{22}	U^{33}	U^{23}	U^{13}	U^{12}
C(1)	13(1)	18(1)	11(1)	-3(1)	-2(1)	0(1)
C(2)	17(1)	19(1)	11(1)	-2(1)	1(1)	1(1)
C(3)	23(1)	17(1)	17(1)	4(1)	5(1)	3(1)
C(4)	18(1)	14(1)	21(1)	-2(1)	7(1)	-1(1)
C(5)	16(1)	14(1)	18(1)	-10(1)	4(1)	-2(1)
C(6)	18(1)	16(1)	11(1)	-5(1)	4(1)	0(1)
C(7)	17(1)	19(1)	12(1)	-1(1)	5(1)	-1(1)
C(8)	13(1)	19(1)	15(1)	-1(1)	4(1)	-2(1)

C(9)	15(1)	15(1)	14(1)	2(1)	5(1)	-2(1)
C(10)	14(1)	15(1)	18(1)	1(1)	5(1)	1(1)
C(11)	15(1)	11(1)	14(1)	3(1)	6(1)	-1(1)
C(12)	16(1)	16(1)	18(1)	-1(1)	5(1)	0(1)
C(13)	15(1)	13(1)	14(1)	2(1)	4(1)	1(1)
C(14)	14(1)	17(1)	19(1)	-1(1)	4(1)	-1(1)
C(15)	21(1)	14(1)	25(1)	-2(1)	11(1)	1(1)
C(16)	27(1)	15(1)	19(1)	-6(1)	8(1)	-2(1)
O(1)	13(1)	18(1)	16(1)	-4(1)	1(1)	1(1)
O(2)	15(1)	16(1)	13(1)	-3(1)	4(1)	2(1)
F(01)	26(1)	32(1)	24(1)	2(1)	11(1)	-1(1)
F(1)	20(1)	27(1)	26(1)	-7(1)	-4(1)	9(1)
F(2)	17(1)	23(1)	25(1)	-4(1)	3(1)	-7(1)
F(02)	31(1)	34(1)	35(1)	15(1)	20(1)	9(1)
F(03)	33(1)	26(1)	24(1)	-2(1)	-6(1)	-6(1)
F(3)	22(1)	37(1)	14(1)	0(1)	3(1)	-3(1)
F(04)	61(1)	20(1)	20(1)	-6(1)	6(1)	-10(1)
F(05)	20(1)	21(1)	28(1)	8(1)	-5(1)	2(1)
F(06)	31(1)	31(1)	32(1)	17(1)	7(1)	11(1)
P(01)	18(1)	17(1)	13(1)	2(1)	3(1)	2(1)
S(1)	18(1)	20(1)	16(1)	-5(1)	1(1)	2(1)
Pd(1)	12(1)	12(1)	12(1)	-2(1)	3(1)	0(1)

Table B.4.4 Hydrogen coordinates (x 10^4) and isotropic displacement parameters ($Å^2$x 10^3) for [Pd(cod)(thtfac)]PF_6.

	x	y	z	U(eq)
H(1)	4749	9560	3555	17
H(2)	3793	8771	4675	19
H(3A)	3185	7456	4279	22
H(3B)	4804	7475	4360	22
H(4A)	4629	7263	2394	21
H(4B)	3374	6752	2654	21
H(5)	1917	7466	1327	19
H(6)	2533	8381	189	17
H(7A)	4485	9187	668	19
H(7B)	5065	8315	617	19
H(8A)	5803	8250	2610	19
H(8B)	6124	9145	2335	19
H(10)	-1254	10273	2327	18
H(14)	-1450	11118	3743	20
H(15)	-958	12051	5413	23
H(16)	1387	11984	6469	24

Table B.4.5 Hydrogen bonds for [Pd(cod)(thtfac)]PF_6 [Å and °].

D-H...A	d(D-H)	d(H...A)	d(D...A)	<(DHA)
C(14)-H(14)...F(05)	0.95	2.32	3.193(3)	152.3
C(1)-H(1)...F(05)#1	1.00	2.47	3.277(3)	136.9
C(2)-H(2)...F(04)#2	1.00	2.48	3.175(3)	126.0
C(2)-H(2)...F(05)#2	1.00	2.57	3.566(3)	177.4
C(3)-H(3A)...F(2)#3	0.99	2.55	3.388(3)	141.7

Symmetry transformations used to generate equivalent atoms:
#1 x+1,y,z #2 -x,-y+2,-z+1 #3 x+1/2,-y+3/2,z+1/2

B.5 Crystal Data of [Pd(cod)(tfacac)]PF_6

Table B.5.1 Atomic coordinates (x 10^4) and equivalent isotropic displacement parameters ($Å^2$x 10^3) for [Pd(cod)(tfacac)]PF_6. U(eq) is defined as one third of the trace of the orthogonalized U^{ij} tensor.

	x	y	z	U(eq)
C(11)	5090(20)	2085(12)	4053(12)	14(2)
C(12)	4950(20)	2026(12)	4946(12)	14(2)
C(13)	5750(20)	1077(14)	5732(12)	21(4)
C(14)	7540(20)	1051(13)	6092(12)	22(4)
C(15)	8650(20)	1419(12)	5367(12)	16(3)
C(16)	8740(20)	1276(12)	4520(13)	20(4)
C(17)	7850(20)	654(13)	4157(13)	19(3)
C(18)	6080(20)	1272(12)	3642(10)	15(3)
C(19)	5660(20)	4924(12)	3797(11)	14(3)
C(21)	2001(18)	7970(11)	46(11)	13(2)
C(22)	2203(18)	7906(11)	954(11)	13(2)
C(23)	2370(20)	8731(12)	1361(11)	15(3)
C(24)	3510(20)	9350(13)	841(12)	18(3)
C(25)	4980(20)	8737(12)	472(13)	19(3)
C(26)	5060(20)	8591(12)	-360(13)	17(3)
C(27)	3590(20)	8948(13)	-1091(12)	22(4)
C(28)	1850(20)	8914(14)	-733(13)	23(4)
C(29)	5620(20)	5061(12)	1204(11)	14(3)
C(110)	7220(20)	5085(12)	3733(12)	17(3)
C(111)	8820(20)	4279(13)	4019(11)	14(3)
C(112)	4080(20)	5882(13)	3517(12)	20(3)
C(113)	10490(20)	4541(13)	3963(14)	23(4)
C(210)	7310(20)	4921(13)	1267(12)	18(3)
C(211)	8110(20)	5725(12)	987(11)	13(3)
C(212)	4970(20)	4119(13)	1475(12)	19(3)
C(213)	10020(20)	5475(15)	1034(15)	26(4)
O(11)	5193(14)	4132(8)	4030(8)	12(2)
O(12)	8953(15)	3352(9)	4336(8)	17(2)
O(21)	4331(13)	5863(8)	970(8)	10(2)
O(22)	7306(14)	6658(9)	664(8)	17(2)
F(11)	3146(17)	5848(10)	2820(8)	38(3)
F(12)	4494(18)	6740(9)	3306(14)	56(5)
F(13)	3028(14)	5916(9)	4179(8)	26(2)
F(21)	6238(18)	3274(9)	1716(14)	59(5)
F(22)	3947(15)	4080(9)	828(7)	26(2)
F(23)	3990(20)	4155(10)	2190(8)	41(3)
F(101)	8059(15)	8952(9)	3040(10)	36(3)
F(102)	10456(14)	7687(9)	2948(8)	29(3)
F(103)	8666(19)	6937(8)	2440(8)	35(3)
F(104)	6348(14)	8185(12)	2545(9)	37(3)
F(105)	8244(15)	7347(11)	3764(7)	30(3)
F(106)	8518(14)	8539(8)	1722(7)	24(2)
F(201)	587(18)	3081(9)	2548(8)	33(3)
F(202)	3147(14)	2318(10)	2042(8)	28(2)
F(203)	-479(14)	1805(11)	2456(8)	33(3)
F(204)	1993(16)	1054(9)	1947(10)	35(3)
F(205)	2051(12)	1472(8)	3277(7)	23(2)
F(206)	583(16)	2674(11)	1237(8)	34(3)
P(1)	8399(5)	7933(3)	2759(3)	16(1)
P(2)	1330(5)	2065(3)	2245(3)	16(1)
Pd(1)	6944(2)	2768(1)	4447(1)	13(1)
Pd(2)	4713(2)	7232(1)	553(1)	13(1)

Table B.5.2 Bond lengths [Å] and angles [°] for [Pd(cod)(tfacac)]PF_6.

C(11)-C(12)	1.37(2)	C(213)-H(21A)	0.9800	C(22)-C(21)-C(28)	126.0(14)
C(11)-C(18)	1.50(2)	C(213)-H(21B)	0.9800	C(22)-C(21)-Pd(2)	69.7(8)
C(11)-Pd(1)	2.171(14)	C(213)-H(21C)	0.9800	C(28)-C(21)-Pd(2)	110.2(10)
C(11)-H(11)	1.0000	O(11)-Pd(1)	2.007(11)	C(22)-C(21)-H(21)	114.1
C(12)-C(13)	1.55(2)	O(12)-Pd(1)	2.018(11)	C(28)-C(21)-H(21)	114.1
C(12)-Pd(1)	2.208(15)	O(21)-Pd(2)	2.011(10)	Pd(2)-C(21)-H(21)	114.1
C(12)-H(12)	1.0000	O(22)-Pd(2)	2.017(11)	C(21)-C(22)-C(23)	126.8(15)
C(13)-C(14)	1.54(3)	F(101)-P(1)	1.576(12)	C(21)-C(22)-Pd(2)	73.0(9)
C(13)-H(13A)	0.9900	F(102)-P(1)	1.614(11)	C(23)-C(22)-Pd(2)	106.9(10)
C(13)-H(13B)	0.9900	F(103)-P(1)	1.582(12)	C(21)-C(22)-H(22)	113.9
C(14)-C(15)	1.52(2)	F(104)-P(1)	1.613(11)	C(23)-C(22)-H(22)	113.9
C(14)-H(14A)	0.9900	F(105)-P(1)	1.590(12)	Pd(2)-C(22)-H(22)	113.9
C(14)-H(14B)	0.9900	F(106)-P(1)	1.634(11)	C(22)-C(23)-C(24)	113.0(14)
C(15)-C(16)	1.37(3)	F(201)-P(2)	1.594(11)	C(22)-C(23)-H(23A)	109.0
C(15)-Pd(1)	2.180(16)	F(202)-P(2)	1.624(10)	C(24)-C(23)-H(23A)	109.0
C(15)-H(15)	1.0000	F(203)-P(2)	1.625(11)	C(22)-C(23)-H(23B)	109.0
C(16)-C(17)	1.50(2)	F(204)-P(2)	1.579(12)	C(24)-C(23)-H(23B)	109.0
C(16)-Pd(1)	2.191(17)	F(205)-P(2)	1.623(11)	H(23A)-C(23)-H(23B)	107.8
C(16)-H(16)	1.0000	F(206)-P(2)	1.602(12)	C(25)-C(24)-C(23)	113.3(14)
C(17)-C(18)	1.55(2)			C(25)-C(24)-H(24A)	108.9
C(17)-H(17A)	0.9900	C(12)-C(11)-C(18)	127.3(15)	C(23)-C(24)-H(24A)	108.9
C(17)-H(17B)	0.9900	C(12)-C(11)-Pd(1)	73.3(9)	C(25)-C(24)-H(24B)	108.9
C(18)-H(18A)	0.9900	C(18)-C(11)-Pd(1)	106.6(10)	C(23)-C(24)-H(24B)	108.9
C(18)-H(18B)	0.9900	C(12)-C(11)-H(11)	113.7	H(24A)-C(24)-H(24B)	107.7
C(19)-O(11)	1.26(2)	C(18)-C(11)-H(11)	113.7	C(26)-C(25)-C(24)	127.7(16)
C(19)-C(110)	1.35(2)	Pd(1)-C(11)-H(11)	113.7	C(26)-C(25)-Pd(2)	71.4(10)
C(19)-C(112)	1.55(2)	C(11)-C(12)-C(13)	126.0(15)	C(24)-C(25)-Pd(2)	111.2(11)
C(21)-C(22)	1.39(2)	C(11)-C(12)-Pd(1)	70.4(9)	C(26)-C(25)-H(25)	112.9
C(21)-C(28)	1.54(3)	C(13)-C(12)-Pd(1)	109.9(11)	C(24)-C(25)-H(25)	112.9
C(21)-Pd(2)	2.197(14)	C(11)-C(12)-H(12)	114.0	Pd(2)-C(25)-H(25)	112.9
C(21)-H(21)	1.0000	C(13)-C(12)-H(12)	114.0	C(25)-C(26)-C(27)	127.2(16)
C(22)-C(23)	1.51(2)	Pd(1)-C(12)-H(12)	114.0	C(25)-C(26)-Pd(2)	72.6(10)
C(22)-Pd(2)	2.154(15)	C(14)-C(13)-C(12)	112.1(13)	C(27)-C(26)-Pd(2)	105.7(10)
C(22)-H(22)	1.0000	C(14)-C(13)-H(13A)	109.2	C(25)-C(26)-H(26)	114.1
C(23)-C(24)	1.54(2)	C(12)-C(13)-H(13A)	109.2	C(27)-C(26)-H(26)	114.1
C(23)-H(23A)	0.9900	C(14)-C(13)-H(13B)	109.2	Pd(2)-C(26)-H(26)	114.1
C(23)-H(23B)	0.9900	C(12)-C(13)-H(13B)	109.2	C(28)-C(27)-C(26)	113.6(15)
C(24)-C(25)	1.47(2)	H(13A)-C(13)-H(13B)	107.9	C(28)-C(27)-H(27A)	108.9
C(24)-H(24A)	0.9900	C(15)-C(14)-C(13)	114.0(15)	C(26)-C(27)-H(27A)	108.9
C(24)-H(24B)	0.9900	C(15)-C(14)-H(14A)	108.7	C(28)-C(27)-H(27B)	108.9
C(25)-C(26)	1.35(3)	C(13)-C(14)-H(14A)	108.7	C(26)-C(27)-H(27B)	108.9
C(25)-Pd(2)	2.197(16)	C(15)-C(14)-H(14B)	108.7	H(27A)-C(27)-H(27B)	107.7
C(25)-H(25)	1.0000	C(13)-C(14)-H(14B)	108.7	C(27)-C(28)-C(21)	112.4(14)
C(26)-C(27)	1.52(2)	H(14A)-C(14)-H(14B)	107.6	C(27)-C(28)-H(28A)	109.1
C(26)-Pd(2)	2.182(16)	C(16)-C(15)-C(14)	127.2(15)	C(21)-C(28)-H(28A)	109.1
C(26)-H(26)	1.0000	C(16)-C(15)-Pd(1)	72.1(10)	C(27)-C(28)-H(28B)	109.1
C(27)-C(28)	1.52(3)	C(14)-C(15)-Pd(1)	105.9(11)	C(21)-C(28)-H(28B)	109.1
C(27)-H(27A)	0.9900	C(16)-C(15)-H(15)	114.1	H(28A)-C(28)-H(28B)	107.8
C(27)-H(27B)	0.9900	C(14)-C(15)-H(15)	114.1	O(21)-C(29)-C(210)	132.1(15)
C(28)-H(28A)	0.9900	Pd(1)-C(15)-H(15)	114.1	O(21)-C(29)-C(212)	110.0(14)
C(28)-H(28B)	0.9900	C(15)-C(16)-C(17)	126.3(16)	C(210)-C(29)-C(212)	117.9(15)
C(29)-O(21)	1.28(2)	C(15)-C(16)-Pd(1)	71.3(10)	C(19)-C(110)-C(111)	122.7(15)
C(29)-C(210)	1.33(2)	C(17)-C(16)-Pd(1)	110.3(11)	C(19)-C(110)-H(110)	118.6
C(29)-C(212)	1.54(2)	C(15)-C(16)-H(16)	113.6	C(111)-C(110)-H(110)	118.6
C(110)-C(111)	1.45(2)	C(17)-C(16)-H(16)	113.6	O(12)-C(111)-C(110)	125.8(14)
C(110)-H(110)	0.9500	Pd(1)-C(16)-H(16)	113.6	O(12)-C(111)-C(113)	115.4(14)
C(111)-O(12)	1.26(2)	C(16)-C(17)-C(18)	113.6(13)	C(110)-C(111)-C(113)	118.7(15)
C(111)-C(113)	1.50(2)	C(16)-C(17)-H(17A)	108.9	F(12)-C(112)-F(13)	107.7(16)
C(112)-F(12)	1.33(2)	C(18)-C(17)-H(17A)	108.9	F(12)-C(112)-F(11)	108.5(17)
C(112)-F(13)	1.33(2)	C(16)-C(17)-H(17B)	108.9	F(13)-C(112)-F(11)	105.9(15)
C(112)-F(11)	1.34(2)	C(18)-C(17)-H(17B)	108.9	F(12)-C(112)-C(19)	113.7(15)
C(113)-H(11A)	0.9800	H(17A)-C(17)-H(17B)	107.7	F(13)-C(112)-C(19)	110.3(14)
C(113)-H(11B)	0.9800	C(11)-C(18)-C(17)	113.0(13)	F(11)-C(112)-C(19)	110.4(14)
C(113)-H(11C)	0.9800	C(11)-C(18)-H(18A)	109.0	C(111)-C(113)-H(11A)	109.5
C(210)-C(211)	1.45(2)	C(17)-C(18)-H(18A)	109.0	C(111)-C(113)-H(11B)	109.5
C(210)-H(210)	0.9500	C(11)-C(18)-H(18B)	109.0	H(11A)-C(113)-H(11B)	109.5
C(211)-O(22)	1.28(2)	C(17)-C(18)-H(18B)	109.0	C(111)-C(113)-H(11C)	109.5
C(211)-C(213)	1.48(2)	H(18A)-C(18)-H(18B)	107.8	H(11A)-C(113)-H(11C)	109.5
C(212)-F(21)	1.31(2)	O(11)-C(19)-C(110)	132.8(15)	H(11B)-C(113)-H(11C)	109.5
C(212)-F(22)	1.32(2)	O(11)-C(19)-C(112)	111.3(13)	C(29)-C(210)-C(211)	124.0(15)
C(212)-F(23)	1.36(2)	C(110)-C(19)-C(112)	115.9(15)	C(29)-C(210)-H(210)	118.0

C(211)-C(210)-H(210)	118.0	F(103)-P(1)-F(102)	90.8(7)	O(12)-Pd(1)-C(15)	87.2(6)
O(22)-C(211)-C(210)	125.3(14)	F(105)-P(1)-F(102)	91.0(6)	C(11)-Pd(1)-C(15)	98.2(6)
O(22)-C(211)-C(213)	115.2(15)	F(104)-P(1)-F(102)	178.6(7)	O(11)-Pd(1)-C(16)	164.3(6)
C(210)-C(211)-C(213)	119.5(15)	F(101)-P(1)-F(106)	89.7(7)	O(12)-Pd(1)-C(16)	89.5(6)
F(21)-C(212)-F(22)	109.8(15)	F(103)-P(1)-F(106)	88.6(6)	C(11)-Pd(1)-C(16)	82.3(6)
F(21)-C(212)-F(23)	106.7(17)	F(105)-P(1)-F(106)	178.9(6)	C(15)-Pd(1)-C(16)	36.6(7)
F(22)-C(212)-F(23)	105.5(14)	F(104)-P(1)-F(106)	88.6(6)	O(11)-Pd(1)-C(12)	92.4(5)
F(21)-C(212)-C(29)	112.5(14)	F(102)-P(1)-F(106)	90.1(6)	O(12)-Pd(1)-C(12)	165.0(6)
F(22)-C(212)-C(29)	111.6(14)	F(204)-P(2)-F(201)	177.7(7)	C(11)-Pd(1)-C(12)	36.4(6)
F(23)-C(212)-C(29)	110.4(14)	F(204)-P(2)-F(206)	90.4(8)	C(15)-Pd(1)-C(12)	82.6(6)
C(211)-C(213)-H(21A)	109.5	F(201)-P(2)-F(206)	89.3(7)	C(16)-Pd(1)-C(12)	88.8(6)
C(211)-C(213)-H(21B)	109.5	F(204)-P(2)-F(205)	91.1(7)	O(21)-Pd(2)-O(22)	93.5(5)
H(21A)-C(213)-H(21B)	109.5	F(201)-P(2)-F(205)	89.2(6)	O(21)-Pd(2)-C(22)	89.6(5)
C(211)-C(213)-H(21C)	109.5	F(206)-P(2)-F(205)	178.4(7)	O(22)-Pd(2)-C(22)	156.9(6)
H(21A)-C(213)-H(21C)	109.5	F(204)-P(2)-F(202)	91.4(6)	O(21)-Pd(2)-C(26)	159.3(6)
H(21B)-C(213)-H(21C)	109.5	F(201)-P(2)-F(202)	90.8(7)	O(22)-Pd(2)-C(26)	87.2(6)
C(19)-O(11)-Pd(1)	120.8(10)	F(206)-P(2)-F(202)	90.0(7)	C(22)-Pd(2)-C(26)	97.9(6)
C(111)-O(12)-Pd(1)	124.3(11)	F(205)-P(2)-F(202)	90.6(6)	O(21)-Pd(2)-C(25)	164.5(6)
C(29)-O(21)-Pd(2)	120.6(10)	F(204)-P(2)-F(203)	88.5(7)	O(22)-Pd(2)-C(25)	89.7(6)
C(211)-O(22)-Pd(2)	124.2(11)	F(201)-P(2)-F(203)	89.3(7)	C(22)-Pd(2)-C(25)	81.7(6)
F(101)-P(1)-F(103)	177.2(7)	F(206)-P(2)-F(203)	90.4(7)	C(26)-Pd(2)-C(25)	36.0(7)
F(101)-P(1)-F(105)	90.4(8)	F(205)-P(2)-F(203)	89.0(6)	O(21)-Pd(2)-C(21)	92.6(5)
F(103)-P(1)-F(105)	91.3(7)	F(202)-P(2)-F(203)	179.5(8)	O(22)-Pd(2)-C(21)	164.5(6)
F(101)-P(1)-F(104)	89.0(7)	O(11)-Pd(1)-O(12)	93.2(5)	C(22)-Pd(2)-C(21)	37.2(6)
F(103)-P(1)-F(104)	88.7(8)	O(11)-Pd(1)-C(11)	89.5(5)	C(26)-Pd(2)-C(21)	82.2(6)
F(105)-P(1)-F(104)	90.3(7)	O(12)-Pd(1)-C(11)	157.4(6)	C(25)-Pd(2)-C(21)	88.2(6)
F(101)-P(1)-F(102)	91.3(6)	O(11)-Pd(1)-C(15)	158.9(6)		

Symmetry transformations used to generate equivalent atoms:

Table B.5.3 Anisotropic displacement parameters ($Å^2 x\ 10^3$) for [Pd(cod)(tfacac)]PF_6. The anisotropic displacement factor exponent takes the form: $-2\pi^2[\ h^2 a^{*2} U^{11} + ... + 2\ h\ k\ a^*\ b^*\ U^{12}\ ]$

	U^{11}	U^{22}	U^{33}	U^{23}	U^{13}	U^{12}
C(11)	16(5)	9(5)	24(6)	-8(4)	3(4)	-9(4)
C(12)	16(5)	9(5)	24(6)	-8(4)	3(4)	-9(4)
C(13)	26(9)	21(8)	17(8)	-3(7)	16(7)	-8(7)
C(14)	30(9)	12(7)	16(8)	5(6)	8(7)	-2(7)
C(15)	13(7)	9(7)	23(9)	1(6)	-5(6)	-1(6)
C(16)	16(7)	6(7)	35(10)	1(7)	-3(7)	-3(6)
C(17)	10(7)	14(7)	33(10)	-8(7)	-5(7)	-2(6)
C(18)	27(8)	9(7)	8(7)	0(5)	-2(6)	-3(6)
C(19)	12(7)	15(7)	13(7)	-1(6)	-7(6)	-1(6)
C(21)	6(4)	9(5)	22(6)	-6(4)	-1(4)	4(4)
C(22)	6(4)	9(5)	22(6)	-6(4)	-1(4)	4(4)
C(23)	24(8)	15(7)	12(8)	-5(6)	7(6)	-11(6)
C(24)	17(7)	17(8)	22(9)	-1(6)	2(6)	-11(6)
C(25)	16(7)	10(7)	31(10)	1(7)	1(7)	-6(6)
C(26)	11(7)	11(7)	31(10)	-5(6)	7(6)	-5(6)
C(27)	33(10)	10(7)	17(8)	3(6)	-12(7)	-4(7)
C(28)	20(8)	19(8)	33(10)	-10(7)	-14(7)	-4(7)
C(29)	22(8)	11(7)	10(7)	0(6)	5(6)	-7(6)
C(110)	16(7)	12(7)	24(9)	-3(6)	6(6)	-5(6)
C(111)	11(7)	18(8)	15(8)	-8(6)	6(6)	-4(6)
C(112)	20(8)	16(8)	21(9)	-2(7)	8(7)	-3(7)
C(113)	22(8)	14(8)	38(11)	-10(7)	3(7)	-11(7)
C(210)	14(7)	13(7)	26(9)	-5(6)	-2(6)	-4(6)
C(211)	11(7)	10(7)	20(8)	-9(6)	-1(6)	0(6)
C(212)	23(8)	20(8)	19(9)	-8(7)	5(7)	-13(7)
C(213)	13(8)	27(10)	42(12)	-16(9)	5(7)	-5(7)
O(11)	12(5)	9(5)	14(5)	-1(4)	-1(4)	-3(4)
O(12)	16(5)	22(6)	19(6)	-9(5)	1(4)	-13(5)
O(21)	9(5)	4(5)	18(6)	-3(4)	8(4)	-3(4)
O(22)	7(5)	23(6)	20(6)	-9(5)	2(4)	-3(4)
F(11)	47(7)	34(7)	17(6)	-11(5)	-20(5)	20(6)
F(12)	36(7)	10(5)	108(14)	8(7)	9(8)	-7(5)

F(13)	22(5)	32(6)	21(6)	-10(5)	7(4)	2(4)
F(21)	32(7)	13(6)	111(15)	15(7)	-17(8)	-2(5)
F(22)	35(6)	32(6)	17(5)	-5(4)	3(4)	-22(5)
F(23)	85(11)	40(7)	18(6)	-16(5)	30(6)	-43(7)
F(101)	25(6)	26(6)	60(9)	-21(6)	-16(6)	-2(5)
F(102)	15(5)	35(6)	29(6)	-4(5)	-9(4)	-1(4)
F(103)	66(9)	15(5)	26(6)	-4(4)	-8(6)	-15(5)
F(104)	9(5)	75(10)	32(7)	-18(6)	5(4)	-18(6)
F(105)	28(6)	52(8)	14(5)	-12(5)	8(4)	-13(5)
F(106)	24(5)	21(5)	20(5)	9(4)	0(4)	-9(4)
F(201)	53(8)	18(5)	25(6)	-10(5)	5(5)	1(5)
F(202)	23(5)	42(7)	26(6)	-6(5)	6(4)	-26(5)
F(203)	15(5)	59(8)	31(6)	-11(6)	1(4)	-21(5)
F(204)	34(6)	23(6)	60(9)	-23(6)	27(6)	-17(5)
F(205)	12(4)	22(5)	26(6)	5(4)	-4(4)	-4(4)
F(206)	37(6)	49(8)	15(5)	-10(5)	-3(5)	-9(6)
P(1)	14(2)	16(2)	18(2)	-5(2)	-1(2)	-6(2)
P(2)	15(2)	17(2)	18(2)	-6(2)	2(2)	-5(2)
Pd(1)	12(1)	11(1)	15(1)	-3(1)	-1(1)	-4(1)
Pd(2)	12(1)	11(1)	15(1)	-3(1)	2(1)	-4(1)

Table B.5.4 Hydrogen coordinates (x 10^4) and isotropic displacement parameters (Å^{2}x 10^3) for [Pd(cod)(tfacac)]PF_6.

	x	y	z	U(eq)
H(11)	4079	2583	3659	17
H(12)	3870	2494	5080	17
H(13A)	4969	1069	6224	26
H(13B)	5861	463	5525	26
H(14A)	7378	1476	6519	26
H(14B)	8156	349	6428	26
H(15)	9716	1521	5603	20
H(16)	9854	1303	4254	25
H(17A)	7682	111	4660	23
H(17B)	8610	328	3748	23
H(18A)	6266	1584	3014	18
H(18B)	5383	808	3628	18
H(21)	1387	7501	-90	16
H(22)	1688	7409	1349	16
H(23A)	2877	8424	1987	19
H(23B)	1212	9193	1375	19
H(24A)	2794	9895	342	22
H(24B)	3961	9672	1248	22
H(25)	6127	8710	736	23
H(26)	6230	8496	-592	21
H(27A)	3495	9651	-1430	26
H(27B)	3864	8520	-1514	26
H(28A)	1063	8922	-1225	28
H(28B)	1343	9526	-523	28
H(110)	7275	5755	3490	21
H(11A)	11198	4201	4529	35
H(11B)	10249	5274	3851	35
H(11C)	11104	4320	3471	35
H(210)	8046	4253	1510	21
H(21A)	10362	5950	543	40
H(21B)	10512	4785	979	40
H(21C)	10438	5524	1610	40

Table B.5.5 Hydrogen bonds for [Pd(cod)(tfacac)]PF_6 [Å and °].

D-H...A	d(D-H)	d(H...A)	d(D...A)	<(DHA)
C(25)-H(25)...F(106)	1.00	2.38	3.36(2)	165.2
C(110)-H(110)...F(12)	0.95	2.27	2.68(2)	105.1
C(110)-H(110)...F(103)	0.95	2.54	3.38(2)	148.2
C(210)-H(210)...F(21)	0.95	2.27	2.67(2)	104.5
C(13)-H(13A)...F(104)#1	0.99	2.51	3.39(2)	148.9
C(12)-H(12)...F(105)#1	1.00	2.48	3.33(2)	142.2
C(210)-H(210)...F(201)#2	0.95	2.51	3.36(2)	148.7
C(16)-H(16)...F(205)#2	1.00	2.36	3.34(2)	165.2
C(21)-H(21)...F(206)#3	1.00	2.49	3.344(19)	142.9
C(28)-H(28A)...F(203)#3	0.99	2.49	3.38(2)	149.3

Symmetry transformations used to generate equivalent atoms:
#1 -x+1,-y+1,-z+1 #2 x+1,y,z #3 -x,-y+1,-z

B.6 Crystal Data of [Pd(cod)(hfacac)]PF_6

Table B.6.1 Atomic coordinates (x 10^4) and equivalent isotropic displacement parameters (Å^{2}x 10^3) for [Pd(cod)(hfacac)]PF_6. U(eq) is defined as one third of the trace of the orthogonalized U^{ij} tensor.

	x	y	z	U(eq)
C(1)	4161(3)	838(3)	2920(1)	19(1)
C(2)	2635(3)	1128(3)	2703(1)	20(1)
C(3)	1306(3)	219(3)	2578(1)	23(1)
C(4)	1312(3)	-855(3)	3103(1)	24(1)
C(5)	1809(3)	-419(3)	3828(1)	21(1)
C(6)	3312(3)	-486(2)	4125(1)	20(1)
C(7)	4754(3)	-903(3)	3780(2)	24(1)
C(8)	4804(3)	-474(3)	3028(2)	23(1)
C(9)	2922(3)	4150(3)	4013(1)	18(1)
C(10)	2409(3)	4069(3)	4672(1)	21(1)
C(11)	2161(3)	2926(3)	5000(1)	18(1)
C(12)	3198(4)	5460(3)	3714(2)	24(1)
C(13)	1588(3)	2996(3)	5730(2)	23(1)
O(1)	3194(2)	3290(2)	3583(1)	18(1)
O(2)	2347(2)	1817(2)	4788(1)	18(1)
F(01)	-1963(4)	3529(2)	4291(2)	77(1)
F(02)	-1071(3)	1624(4)	4602(1)	81(1)
F(03)	-313(2)	2535(2)	3624(1)	30(1)
F(04)	-2847(2)	2751(3)	3264(1)	52(1)
F(05)	-3612(2)	1872(2)	4247(1)	31(1)
F(06)	-1929(3)	862(2)	3588(2)	63(1)
P(01)	-1962(1)	2210(1)	3938(1)	19(1)
Pd(1)	2887(1)	1447(1)	3806(1)	15(1)
F(3)	3055(3)	6373(2)	4166(1)	42(1)
F(1)	4612(2)	5532(2)	3478(1)	41(1)
F(2)	2195(3)	5683(2)	3181(1)	50(1)
F(4)	2689(4)	3566(4)	6146(2)	33(1)
F(5)	311(4)	3605(6)	5755(2)	44(1)
F(6)	1461(6)	1849(3)	6002(2)	40(1)
F(4B)	2550(30)	3030(30)	6196(10)	33(1)
F(5B)	-24(17)	2820(30)	5729(9)	24(4)
F(6B)	1810(30)	4099(17)	6079(10)	40(1)
F(4C)	2230(20)	2330(20)	6188(7)	33(1)
F(5C)	420(50)	2190(20)	5808(13)	47(8)

F(6C)	670(40)	4122(18)	5820(13)	40(1)

Table B.6.2 Bond lengths (Å) and angles (°) for [Pd(cod)(hfacac)]PF_6.

C(1)-C(2)	1.387(4)	C(2)-C(3)-C(4)	113.5(2)	F(5C)-C(13)-F(4)	136.5(13)
C(1)-C(8)	1.511(4)	C(2)-C(3)-H(3A)	108.9	F(6)-C(13)-F(4)	104.1(3)
C(1)-Pd(1)	2.191(3)	C(4)-C(3)-H(3A)	108.9	F(4B)-C(13)-F(6B)	61.8(17)
C(1)-H(1)	1.0000	C(2)-C(3)-H(3B)	108.9	F(4C)-C(13)-F(6B)	95.3(14)
C(2)-C(3)	1.504(4)	C(4)-C(3)-H(3B)	108.9	F(5)-C(13)-F(6B)	68.8(12)
C(2)-Pd(1)	2.166(3)	H(3A)-C(3)-H(3B)	107.7	F(5C)-C(13)-F(6B)	125.3(12)
C(2)-H(2)	1.0000	C(5)-C(4)-C(3)	112.3(2)	F(6)-C(13)-F(6B)	127.0(8)
C(3)-C(4)	1.531(4)	C(5)-C(4)-H(4A)	109.2	F(4)-C(13)-F(6B)	41.0(12)
C(3)-H(3A)	0.9900	C(3)-C(4)-H(4A)	109.2	F(4B)-C(13)-F(5B)	130.5(13)
C(3)-H(3B)	0.9900	C(5)-C(4)-H(4B)	109.2	F(4C)-C(13)-F(5B)	108.6(13)
C(4)-C(5)	1.519(4)	C(3)-C(4)-H(4B)	109.2	F(5)-C(13)-F(5B)	38.4(13)
C(4)-H(4A)	0.9900	H(4A)-C(4)-H(4B)	107.9	F(5C)-C(13)-F(5B)	32.8(15)
C(4)-H(4B)	0.9900	C(6)-C(5)-C(4)	125.0(3)	F(6)-C(13)-F(5B)	76.8(13)
C(5)-C(6)	1.383(4)	C(6)-C(5)-Pd(1)	70.76(15)	F(4)-C(13)-F(5B)	136.2(9)
C(5)-Pd(1)	2.190(3)	C(4)-C(5)-Pd(1)	110.75(18)	F(6B)-C(13)-F(5B)	103.0(15)
C(5)-H(5)	1.0000	C(6)-C(5)-H(5)	114.1	F(4B)-C(13)-F(6C)	104.1(16)
C(6)-C(7)	1.510(4)	C(4)-C(5)-H(5)	114.1	F(4C)-C(13)-F(6C)	127.3(13)
C(6)-Pd(1)	2.171(3)	Pd(1)-C(5)-H(5)	114.1	F(5)-C(13)-F(6C)	26.1(10)
C(6)-H(6)	1.0000	C(5)-C(6)-C(7)	126.9(2)	F(5C)-C(13)-F(6C)	95.5(16)
C(7)-C(8)	1.531(4)	C(5)-C(6)-Pd(1)	72.26(16)	F(6)-C(13)-F(6C)	130.4(8)
C(7)-H(7A)	0.9900	C(7)-C(6)-Pd(1)	106.23(17)	F(4)-C(13)-F(6C)	85.7(12)
C(7)-H(7B)	0.9900	C(5)-C(6)-H(6)	114.1	F(6B)-C(13)-F(6C)	44.7(12)
C(8)-H(8A)	0.9900	C(7)-C(6)-H(6)	114.1	F(5B)-C(13)-F(6C)	64.3(14)
C(8)-H(8B)	0.9900	Pd(1)-C(6)-H(6)	114.1	F(4B)-C(13)-C(11)	117.2(11)
C(9)-O(1)	1.269(3)	C(6)-C(7)-C(8)	114.0(2)	F(4C)-C(13)-C(11)	119.0(8)
C(9)-C(10)	1.381(4)	C(6)-C(7)-H(7A)	108.8	F(5)-C(13)-C(11)	112.6(3)
C(9)-C(12)	1.532(4)	C(8)-C(7)-H(7A)	108.8	F(5C)-C(13)-C(11)	111.1(8)
C(10)-C(11)	1.394(4)	C(6)-C(7)-H(7B)	108.8	F(6)-C(13)-C(11)	111.1(3)
C(10)-H(10)	0.9500	C(8)-C(7)-H(7B)	108.8	F(4)-C(13)-C(11)	108.9(2)
C(11)-O(2)	1.262(3)	H(7A)-C(7)-H(7B)	107.7	F(6B)-C(13)-C(11)	117.5(7)
C(11)-C(13)	1.530(4)	C(1)-C(8)-C(7)	112.1(2)	F(5B)-C(13)-C(11)	111.4(7)
C(12)-F(3)	1.319(4)	C(1)-C(8)-H(8A)	109.2	F(6C)-C(13)-C(11)	111.1(9)
C(12)-F(1)	1.325(4)	C(7)-C(8)-H(8A)	109.2	C(9)-O(1)-Pd(1)	121.64(18)
C(12)-F(2)	1.328(4)	C(1)-C(8)-H(8B)	109.2	C(11)-O(2)-Pd(1)	121.90(17)
C(13)-F(4B)	1.19(2)	C(7)-C(8)-H(8B)	109.2	F(01)-P(01)-F(04)	91.28(19)
C(13)-F(4C)	1.237(17)	H(8A)-C(8)-H(8B)	107.9	F(01)-P(01)-F(02)	90.6(2)
C(13)-F(5)	1.276(4)	O(1)-C(9)-C(10)	130.2(3)	F(04)-P(01)-F(02)	178.11(19)
C(13)-F(5C)	1.33(2)	O(1)-C(9)-C(12)	111.6(2)	F(01)-P(01)-F(06)	178.91(19)
C(13)-F(6)	1.336(4)	C(10)-C(9)-C(12)	118.2(2)	F(04)-P(01)-F(06)	89.65(17)
C(13)-F(4)	1.350(4)	C(9)-C(10)-C(11)	122.9(3)	F(02)-P(01)-F(06)	88.47(19)
C(13)-F(6B)	1.361(18)	C(9)-C(10)-H(10)	118.5	F(01)-P(01)-F(05)	90.80(13)
C(13)-F(5B)	1.397(15)	C(11)-C(10)-H(10)	118.5	F(04)-P(01)-F(05)	89.91(10)
C(13)-F(6C)	1.45(3)	O(2)-C(11)-C(10)	129.8(3)	F(02)-P(01)-F(05)	90.19(12)
O(1)-Pd(1)	2.0272(19)	O(2)-C(11)-C(13)	113.7(2)	F(06)-P(01)-F(05)	89.79(12)
O(2)-Pd(1)	2.0261(18)	C(10)-C(11)-C(13)	116.6(2)	F(01)-P(01)-F(03)	89.83(13)
F(01)-P(01)	1.560(2)	F(3)-C(12)-F(1)	108.1(2)	F(04)-P(01)-F(03)	89.91(11)
F(02)-P(01)	1.585(2)	F(3)-C(12)-F(2)	107.7(3)	F(02)-P(01)-F(03)	89.97(12)
F(03)-P(01)	1.6128(18)	F(1)-C(12)-F(2)	106.6(3)	F(06)-P(01)-F(03)	89.58(12)
F(04)-P(01)	1.583(2)	F(3)-C(12)-C(9)	113.3(2)	F(05)-P(01)-F(03)	179.34(12)
F(05)-P(01)	1.6113(18)	F(1)-C(12)-C(9)	110.4(2)	O(2)-Pd(1)-O(1)	93.06(8)
F(06)-P(01)	1.587(2)	F(2)-C(12)-C(9)	110.4(2)	O(2)-Pd(1)-C(2)	160.91(9)
		F(4B)-C(13)-F(4C)	38.1(12)	O(1)-Pd(1)-C(2)	86.91(10)
C(2)-C(1)-C(8)	125.3(2)	F(4B)-C(13)-F(5)	121.2(12)	O(2)-Pd(1)-C(6)	87.70(9)
C(2)-C(1)-Pd(1)	70.43(15)	F(4C)-C(13)-F(5)	127.4(8)	O(1)-Pd(1)-C(6)	162.56(9)
C(8)-C(1)-Pd(1)	111.01(18)	F(4B)-C(13)-F(5C)	115.3(18)	C(2)-Pd(1)-C(6)	97.99(11)
C(2)-C(1)-H(1)	114.0	F(4C)-C(13)-F(5C)	81.8(19)	O(2)-Pd(1)-C(5)	92.10(9)
C(8)-C(1)-H(1)	114.0	F(5)-C(13)-F(5C)	70.5(16)	O(1)-Pd(1)-C(5)	160.04(9)
Pd(1)-C(1)-H(1)	114.0	F(4B)-C(13)-F(6)	78.2(14)	C(2)-Pd(1)-C(5)	81.99(10)
C(1)-C(2)-C(3)	126.9(3)	F(4C)-C(13)-F(6)	40.4(10)	C(6)-Pd(1)-C(5)	36.98(10)
C(1)-C(2)-Pd(1)	72.44(15)	F(5)-C(13)-F(6)	111.0(4)	O(2)-Pd(1)-C(1)	161.58(9)
C(3)-C(2)-Pd(1)	106.85(18)	F(5C)-C(13)-F(6)	44.8(18)	O(1)-Pd(1)-C(1)	92.27(9)
C(1)-C(2)-H(2)	114.0	F(4B)-C(13)-F(4)	26.0(14)	C(2)-Pd(1)-C(1)	37.13(10)
C(3)-C(2)-H(2)	114.0	F(4C)-C(13)-F(4)	64.0(10)	C(6)-Pd(1)-C(1)	82.02(10)
Pd(1)-C(2)-H(2)	114.0	F(5)-C(13)-F(4)	108.9(3)	C(5)-Pd(1)-C(1)	88.84(10)

Symmetry transformations used to generate equivalent atoms:

Table B.6.3 Anisotropic displacement parameters ($Å^2 x\ 10^3$)for [Pd(cod)(hfacac)]Pf_6. The anisotropic displacement factor exponent takes the form: $-2\pi^2[\ h^2a^{*2}U^{11} + ... + 2\ h\ k\ a^*\ b^*\ U^{12}\ ]$

	U^{11}	U^{22}	U^{33}	U^{23}	U^{13}	U^{12}
C(1)	24(1)	21(1)	12(1)	-3(1)	7(1)	-3(1)
C(2)	28(1)	25(1)	7(1)	-2(1)	2(1)	0(1)
C(3)	23(1)	33(2)	13(1)	-5(1)	-1(1)	-2(1)
C(4)	26(1)	31(2)	18(1)	-5(1)	4(1)	-10(1)
C(5)	25(1)	22(1)	16(1)	-1(1)	6(1)	-9(1)
C(6)	31(1)	14(1)	16(1)	2(1)	0(1)	-3(1)
C(7)	25(1)	17(1)	27(2)	1(1)	-2(1)	0(1)
C(8)	23(1)	23(1)	25(2)	-6(1)	4(1)	-1(1)
C(9)	16(1)	19(1)	17(1)	0(1)	0(1)	-1(1)
C(10)	23(1)	19(1)	19(1)	-4(1)	4(1)	-3(1)
C(11)	17(1)	24(1)	13(1)	-2(1)	1(1)	-3(1)
C(12)	30(1)	20(1)	23(1)	0(1)	7(1)	-4(1)
C(13)	28(1)	25(1)	16(1)	-4(1)	4(1)	-6(1)
O(1)	24(1)	17(1)	14(1)	1(1)	4(1)	0(1)
O(2)	25(1)	20(1)	11(1)	-1(1)	1(1)	-2(1)
F(01)	68(2)	58(2)	109(3)	-58(2)	46(2)	-28(1)
F(02)	30(1)	163(3)	49(2)	63(2)	-7(1)	-5(1)
F(03)	22(1)	38(1)	30(1)	4(1)	4(1)	-5(1)
F(04)	31(1)	82(2)	42(1)	40(1)	-10(1)	-13(1)
F(05)	22(1)	45(1)	26(1)	8(1)	3(1)	-3(1)
F(06)	62(2)	30(1)	101(2)	-20(1)	40(2)	-13(1)
P(01)	19(1)	23(1)	16(1)	1(1)	-1(1)	-2(1)
Pd(1)	21(1)	15(1)	9(1)	0(1)	1(1)	-1(1)
F(3)	68(2)	19(1)	43(1)	-6(1)	28(1)	-10(1)
F(1)	41(1)	32(1)	53(1)	5(1)	27(1)	-7(1)
F(2)	66(2)	33(1)	49(1)	20(1)	-19(1)	-2(1)
F(4)	38(2)	48(2)	13(1)	-6(1)	0(1)	-17(2)
F(5)	29(2)	78(4)	25(2)	-4(2)	7(1)	20(2)
F(6)	74(3)	24(1)	25(2)	0(1)	31(2)	-8(2)
F(4B)	38(2)	48(2)	13(1)	-6(1)	0(1)	-17(2)
F(5B)	4(6)	49(14)	18(7)	-10(10)	4(5)	-2(8)
F(6B)	74(3)	24(1)	25(2)	0(1)	31(2)	-8(2)
F(4C)	38(2)	48(2)	13(1)	-6(1)	0(1)	-17(2)
F(5C)	90(20)	14(10)	40(13)	-16(9)	56(15)	-22(11)
F(6C)	74(3)	24(1)	25(2)	0(1)	31(2)	-8(2)

Table B.6.4 Hydrogen coordinates ($x\ 10^4$) and isotropic displacement parameters ($Å^2 x\ 10^3$) for [Pd(cod)(hfacac)]PF_6.

	x	y	z	U(eq)
H(1)	4946	1463	2772	23
H(2)	2527	1917	2424	24
H(3A)	1356	-142	2110	28
H(3B)	310	685	2592	28
H(4A)	253	-1223	3104	29
H(4B)	2032	-1522	2963	29
H(5)	978	-498	4166	25
H(6)	3368	-614	4636	24
H(7A)	4814	-1832	3795	28
H(7B)	5684	-569	4045	28
H(8A)	5897	-496	2892	28
H(8B)	4191	-1067	2727	28
H(10)	2217	4826	4913	25

Table B.6.5 Hydrogen bonds for [Pd(cod)(hfacac)]PF_6 [Å and °].

D-H...A	d(D-H)	d(H...A)	d(D...A)	<(DHA)
C(7)-H(7B)...F(06)#1	0.99	2.74	3.449(4)	128.7
C(1)-H(1)...F(04)#1	1.00	2.48	3.313(3)	140.1
C(2)-H(2)...F(4B)#2	1.00	2.39	3.06(2)	123.8
C(2)-H(2)...F(4C)#2	1.00	2.53	3.366(17)	141.4
C(3)-H(3A)...F(6B)#2	0.99	2.34	3.053(16)	128.3
C(3)-H(3B)...F(2)#3	0.99	2.55	3.305(3)	133.1
C(8)-H(8B)...F(04)#3	0.99	2.52	3.489(3)	166.4
C(4)-H(4A)...F(6)#4	0.99	2.44	3.209(4)	134.6
C(5)-H(5)...F(5C)#4	1.00	2.17	2.806(18)	120.2
C(6)-H(6)...F(05)#4	1.00	2.55	3.482(3)	156.0
C(7)-H(7A)...F(3)#5	0.99	2.56	3.348(3)	136.2
C(10)-H(10)...F(01)#6	0.95	2.35	3.288(4)	168.1
C(10)-H(10)...F(3)	0.95	2.33	2.709(3)	102.8

Symmetry transformations used to generate equivalent atoms:
#1 x+1,y,z #2 x,-y+1/2,z-1/2 #3 -x,y-1/2,-z+1/2
#4 -x,-y,-z+1 #5 x,y-1,z #6 -x,-y+1,-z+1

B.7 Crystal Data of [Pd(cod)(acac)]BF_4

Table B.7.1 Atomic coordinates (x 10^4) and equivalent isotropic displacement parameters (Å^{2}x 10^3) for [Pd(cod)(acac)]BF_4. U(eq) is defined as one third of the trace of the orthogonalized U^{ij} tensor.

	x	y	z	U(eq)
C(1)	6079(1)	5372(4)	1034(8)	19(1)
C(2)	6087(1)	6156(5)	2663(5)	20(1)
C(3)	5648(2)	7085(7)	3559(6)	22(1)
C(4)	5318(2)	8295(5)	2371(6)	23(1)
C(5)	5628(1)	9321(5)	1044(7)	20(1)
C(6)	5719(1)	8682(6)	-620(5)	21(1)
C(7)	5570(2)	6829(6)	-1357(7)	26(1)
C(8)	5612(2)	5199(6)	-89(6)	26(1)
C(9)	7509(1)	8103(4)	1099(6)	13(1)
C(10)	7546(1)	9831(5)	293(5)	16(1)
C(11)	7141(1)	10964(5)	-217(5)	16(1)
C(12)	7990(1)	7096(5)	1600(5)	18(1)
C(13)	7253(2)	12846(5)	-1019(6)	20(1)
B(01)	3924(2)	7785(7)	49(7)	22(1)
O(1)	7098(1)	7203(3)	1446(3)	16(1)
O(2)	6667(1)	10607(3)	-62(3)	18(1)
F(01)	4381(1)	7571(5)	-799(5)	44(1)
F(02)	3844(2)	6312(4)	1115(6)	60(1)
F(03)	3547(1)	7841(6)	-1196(6)	63(1)
F(04)	3912(1)	9454(3)	946(6)	38(1)
Pd(1)	6407(1)	8195(1)	880(1)	13(1)

Table B.7.2 Bond lengths [Å] and angles [°] for [Pd(cod)(acac)]BF_4

C(1)-C(2)	1.386(7)	C(3)-C(4)	1.535(6)	C(5)-Pd(1)	2.205(3)
C(1)-C(8)	1.512(6)	C(3)-H(3A)	0.9900	C(5)-H(5)	1.0000
C(1)-Pd(1)	2.202(3)	C(3)-H(3B)	0.9900	C(6)-C(7)	1.498(6)
C(1)-H(1)	1.0000	C(4)-C(5)	1.506(6)	C(6)-Pd(1)	2.181(4)
C(2)-C(3)	1.504(6)	C(4)-H(4A)	0.9900	C(6)-H(6)	1.0000
C(2)-Pd(1)	2.183(4)	C(4)-H(4B)	0.9900	C(7)-C(8)	1.533(6)
C(2)-H(2)	1.0000	C(5)-C(6)	1.394(7)	C(7)-H(7A)	0.9900

C(7)-H(7B)	0.9900	C(4)-C(3)-H(3B)	108.8	O(2)-C(11)-C(13)	114.1(3)
C(8)-H(8A)	0.9900	H(3A)-C(3)-H(3B)	107.7	C(10)-C(11)-C(13)	119.0(3)
C(8)-H(8B)	0.9900	C(5)-C(4)-C(3)	112.5(3)	C(9)-C(12)-H(12A)	109.5
C(9)-O(1)	1.287(4)	C(5)-C(4)-H(4A)	109.1	C(9)-C(12)-H(12B)	109.5
C(9)-C(10)	1.391(5)	C(3)-C(4)-H(4A)	109.1	H(12A)-C(12)-H(12B)	109.5
C(9)-C(12)	1.507(5)	C(5)-C(4)-H(4B)	109.1	C(9)-C(12)-H(12C)	109.5
C(10)-C(11)	1.398(5)	C(3)-C(4)-H(4B)	109.1	H(12A)-C(12)-H(12C)	109.5
C(10)-H(10)	0.9500	H(4A)-C(4)-H(4B)	107.8	H(12B)-C(12)-H(12C)	109.5
C(11)-O(2)	1.278(4)	C(6)-C(5)-C(4)	124.6(4)	C(11)-C(13)-H(13A)	109.5
C(11)-C(13)	1.516(5)	C(6)-C(5)-Pd(1)	70.5(2)	C(11)-C(13)-H(13B)	109.5
C(12)-H(12A)	0.9800	C(4)-C(5)-Pd(1)	111.3(2)	H(13A)-C(13)-H(13B)	109.5
C(12)-H(12B)	0.9800	C(6)-C(5)-H(5)	114.1	C(11)-C(13)-H(13C)	109.5
C(12)-H(12C)	0.9800	C(4)-C(5)-H(5)	114.1	H(13A)-C(13)-H(13C)	109.5
C(13)-H(13A)	0.9800	Pd(1)-C(5)-H(5)	114.1	H(13B)-C(13)-H(13C)	109.5
C(13)-H(13B)	0.9800	C(5)-C(6)-C(7)	127.0(4)	F(02)-B(01)-F(01)	110.0(4)
C(13)-H(13C)	0.9800	C(5)-C(6)-Pd(1)	72.4(2)	F(02)-B(01)-F(04)	111.1(4)
B(01)-F(02)	1.359(6)	C(7)-C(6)-Pd(1)	106.2(3)	F(01)-B(01)-F(04)	110.9(4)
B(01)-F(01)	1.379(5)	C(5)-C(6)-H(6)	114.1	F(02)-B(01)-F(03)	109.7(4)
B(01)-F(04)	1.385(5)	C(7)-C(6)-H(6)	114.1	F(01)-B(01)-F(03)	107.0(4)
B(01)-F(03)	1.387(6)	Pd(1)-C(6)-H(6)	114.1	F(04)-B(01)-F(03)	108.1(4)
O(1)-Pd(1)	2.001(3)	C(6)-C(7)-C(8)	114.3(4)	C(9)-O(1)-Pd(1)	122.6(2)
O(2)-Pd(1)	1.998(2)	C(6)-C(7)-H(7A)	108.7	C(11)-O(2)-Pd(1)	122.8(2)
		C(8)-C(7)-H(7A)	108.7	O(2)-Pd(1)-O(1)	94.46(10)
C(2)-C(1)-C(8)	125.0(3)	C(6)-C(7)-H(7B)	108.7	O(2)-Pd(1)-C(6)	87.06(13)
C(2)-C(1)-Pd(1)	70.8(2)	C(8)-C(7)-H(7B)	108.7	O(1)-Pd(1)-C(6)	158.15(14)
C(8)-C(1)-Pd(1)	111.2(3)	H(7A)-C(7)-H(7B)	107.6	O(2)-Pd(1)-C(2)	160.70(14)
C(2)-C(1)-H(1)	114.0	C(1)-C(8)-C(7)	111.6(4)	O(1)-Pd(1)-C(2)	88.41(12)
C(8)-C(1)-H(1)	114.0	C(1)-C(8)-H(8A)	109.3	C(6)-Pd(1)-C(2)	97.33(15)
Pd(1)-C(1)-H(1)	114.0	C(7)-C(8)-H(8A)	109.3	O(2)-Pd(1)-C(1)	161.56(19)
C(1)-C(2)-C(3)	126.3(4)	C(1)-C(8)-H(8B)	109.3	O(1)-Pd(1)-C(1)	90.95(11)
C(1)-C(2)-Pd(1)	72.3(2)	C(7)-C(8)-H(8B)	109.3	C(6)-Pd(1)-C(1)	81.50(16)
C(3)-C(2)-Pd(1)	107.1(3)	H(8A)-C(8)-H(8B)	108.0	C(2)-Pd(1)-C(1)	36.8(2)
C(1)-C(2)-H(2)	114.1	O(1)-C(9)-C(10)	126.8(3)	O(2)-Pd(1)-C(5)	91.25(12)
C(3)-C(2)-H(2)	114.1	O(1)-C(9)-C(12)	114.2(3)	O(1)-Pd(1)-C(5)	163.97(16)
Pd(1)-C(2)-H(2)	114.1	C(10)-C(9)-C(12)	119.0(3)	C(6)-Pd(1)-C(5)	37.06(17)
C(2)-C(3)-C(4)	113.9(4)	C(9)-C(10)-C(11)	126.3(3)	C(2)-Pd(1)-C(5)	81.40(15)
C(2)-C(3)-H(3A)	108.8	C(9)-C(10)-H(10)	116.8	C(1)-Pd(1)-C(5)	88.29(12)
C(4)-C(3)-H(3A)	108.8	C(11)-C(10)-H(10)	116.8		
C(2)-C(3)-H(3B)	108.8	O(2)-C(11)-C(10)	126.9(3)		

Symmetry transformations used to generate equivalent atoms:

Table B.7.3 Anisotropic displacement parameters ($Å^2 x\ 10^3$) for [Pd(cod)(acac)]BF_4. The anisotropic displacement factor exponent takes the form: $-2\pi^2[\ h^2 a^{*2} U^{11} + ... + 2\ h\ k\ a^*\ b^*\ U^{12}\ ]$

	U^{11}	U^{22}	U^{33}	U^{23}	U^{13}	U^{12}
C(1)	16(1)	16(1)	26(2)	7(2)	-2(2)	-2(1)
C(2)	17(2)	21(2)	22(2)	9(2)	1(2)	-3(1)
C(3)	22(2)	28(2)	17(2)	3(2)	6(2)	-3(2)
C(4)	17(2)	30(2)	22(2)	4(2)	6(2)	3(1)
C(5)	12(1)	23(2)	24(2)	2(2)	-1(2)	6(1)
C(6)	11(2)	32(2)	21(2)	9(2)	-3(1)	4(2)
C(7)	19(2)	43(3)	17(2)	-1(2)	-1(2)	-4(2)
C(8)	21(2)	30(2)	27(2)	-4(2)	-3(2)	-7(2)
C(9)	14(1)	15(1)	10(2)	-1(1)	0(2)	0(1)
C(10)	14(2)	15(2)	17(2)	1(1)	1(1)	-3(1)
C(11)	20(2)	14(2)	13(2)	1(1)	0(1)	-3(1)
C(12)	12(2)	17(2)	25(2)	5(1)	1(1)	1(1)
C(13)	23(2)	12(2)	25(2)	5(2)	4(2)	-1(1)
B(01)	21(2)	20(2)	25(2)	-3(2)	-1(2)	0(2)
O(1)	12(1)	15(1)	22(1)	4(1)	-1(1)	0(1)
O(2)	17(1)	15(1)	21(1)	5(1)	0(1)	1(1)
F(01)	29(1)	44(2)	60(2)	-6(2)	14(1)	-2(1)
F(02)	98(3)	32(1)	49(2)	11(2)	34(2)	3(2)
F(03)	34(2)	87(3)	69(3)	-45(2)	-23(2)	31(2)
F(04)	53(1)	26(1)	34(1)	-12(2)	-2(2)	-3(1)
Pd(1)	10(1)	15(1)	14(1)	3(1)	0(1)	0(1)

Table B.7.4 Hydrogen coordinates (x 10^4) and isotropic displacement parameters (Å^{2}x 10^3) for [Pd(cod)(acac)]BF_4.

	x	y	z	U(eq)
H(1)	6333	4349	868	23
H(2)	6342	5585	3458	24
H(3A)	5782	7877	4498	27
H(3B)	5431	6112	4087	27
H(4A)	5067	7490	1780	28
H(4B)	5128	9211	3074	28
H(5)	5612	10711	1147	24
H(6)	5752	9698	-1495	26
H(7A)	5789	6565	-2363	32
H(7B)	5215	6907	-1771	32
H(8A)	5305	5166	646	31
H(8B)	5628	4012	-738	31
H(10)	7879	10284	68	19
H(12A)	7971	6729	2812	27
H(12B)	8283	7924	1431	27
H(12C)	8030	5981	884	27
H(13A)	7017	13070	-1972	30
H(13B)	7603	12859	-1452	30
H(13C)	7212	13826	-152	30

Table B.7.5 Hydrogen bonds for [Pd(cod)(acac)]BF_4 [Å and °]

D-H...A	d(D-H)	d(H...A)	d(D...A)	<(DHA)
C(7)-H(7B)...F(01)	0.99	2.37	3.200(6)	141.4
C(2)-H(2)...F(02)#1	1.00	2.52	3.221(6)	126.7
C(6)-H(6)...F(04)#2	1.00	2.26	3.140(6)	146.0
C(12)-H(12B)...F(04)#3	0.98	2.53	3.500(4)	169.1
C(10)-H(10)...F(03)#3	0.95	2.42	3.325(5)	159.0
C(13)-H(13B)...F(03)#3	0.98	2.54	3.440(5)	152.7

Symmetry transformations used to generate equivalent atoms:
#1 -x+1,-y+1,z+1/2 #2 -x+1,-y+2,z-1/2 #3 x+1/2,-y+2,z

B.8 Crystal Data of [Pd(cod)(thtfac)]BF_4

Table B.8.1 Atomic coordinates (x 10^4) and equivalent isotropic displacement parameters (Å^{2}x 10^3) for [Pd(cod)(thtfac)]BF_4. U(eq) is defined as one third of the trace of the orthogonalized U^{ij} tensor.

	x	y	z	U(eq)
C(1)	2991(3)	1730(2)	5993(3)	15(1)
C(2)	2410(3)	2252(2)	6710(3)	14(1)
C(3)	3148(3)	2734(2)	7806(3)	18(1)
C(4)	4309(3)	2276(2)	8682(3)	19(1)
C(5)	3974(3)	1395(2)	8807(3)	15(1)
C(6)	4327(3)	775(2)	8095(3)	15(1)
C(7)	4987(3)	855(2)	6992(3)	16(1)
C(8)	4504(3)	1582(2)	6156(3)	16(1)
C(9)	-587(3)	502(2)	6456(3)	14(1)
C(10)	-542(3)	-64(2)	7380(3)	15(1)
C(11)	623(3)	-216(2)	8336(3)	12(1)
C(12)	-1914(3)	621(2)	5472(3)	14(1)
C(13)	574(3)	-823(2)	9284(3)	13(1)

C(14)	-530(3)	-1274(2)	9489(3)	17(1)
C(15)	-124(3)	-1785(2)	10538(3)	21(1)
C(16)	1237(3)	-1727(2)	11075(3)	21(1)
B(01)	-4119(3)	-1363(2)	7594(3)	18(1)
O(1)	323(2)	998(1)	6254(2)	15(1)
O(2)	1777(2)	138(1)	8462(2)	15(1)
F(1)	-2856(2)	66(1)	5538(2)	21(1)
F(01)	-3062(2)	-1481(1)	6960(2)	24(1)
F(2)	-2448(2)	1338(1)	5621(2)	20(1)
F(02)	-3776(2)	-719(1)	8415(2)	22(1)
F(3)	-1677(2)	591(1)	4319(2)	19(1)
F(03)	-5319(2)	-1202(1)	6739(2)	31(1)
F(04)	-4268(2)	-2053(1)	8268(2)	29(1)
S(1)	2055(1)	-1046(1)	10350(1)	18(1)
Pd(1)	2180(1)	1040(1)	7382(1)	11(1)

Table B.8.2 Bond lengths [Å] and angles [°] for [Pd(cod)(thtfac)]BF_4.

C(1)-C(2)	1.382(4)	C(2)-C(1)-Pd(1)	70.74(17)	C(9)-C(10)-C(11)	123.8(3)
C(1)-C(8)	1.513(4)	C(8)-C(1)-Pd(1)	110.41(19)	C(9)-C(10)-H(10)	118.1
C(1)-Pd(1)	2.197(3)	C(2)-C(1)-H(1)	114.2	C(11)-C(10)-H(10)	118.1
C(1)-H(1)	1.0000	C(8)-C(1)-H(1)	114.2	O(2)-C(11)-C(10)	125.7(3)
C(2)-C(3)	1.500(4)	Pd(1)-C(1)-H(1)	114.2	O(2)-C(11)-C(13)	114.3(2)
C(2)-Pd(1)	2.176(3)	C(1)-C(2)-C(3)	126.4(3)	C(10)-C(11)-C(13)	120.1(2)
C(2)-H(2)	1.0000	C(1)-C(2)-Pd(1)	72.41(17)	F(2)-C(12)-F(3)	108.0(2)
C(3)-C(4)	1.542(4)	C(3)-C(2)-Pd(1)	107.18(19)	F(2)-C(12)-F(1)	107.6(2)
C(3)-H(3A)	0.9900	C(1)-C(2)-H(2)	114.1	F(3)-C(12)-F(1)	107.4(2)
C(3)-H(3B)	0.9900	C(3)-C(2)-H(2)	114.1	F(2)-C(12)-C(9)	109.9(2)
C(4)-C(5)	1.516(4)	Pd(1)-C(2)-H(2)	114.1	F(3)-C(12)-C(9)	110.6(2)
C(4)-H(4A)	0.9900	C(2)-C(3)-C(4)	114.2(3)	F(1)-C(12)-C(9)	113.0(2)
C(4)-H(4B)	0.9900	C(2)-C(3)-H(3A)	108.7	C(14)-C(13)-C(11)	129.6(3)
C(5)-C(6)	1.385(4)	C(4)-C(3)-H(3A)	108.7	C(14)-C(13)-S(1)	112.1(2)
C(5)-Pd(1)	2.195(3)	C(2)-C(3)-H(3B)	108.7	C(11)-C(13)-S(1)	118.3(2)
C(5)-H(5)	1.0000	C(4)-C(3)-H(3B)	108.7	C(13)-C(14)-C(15)	110.7(3)
C(6)-C(7)	1.504(4)	H(3A)-C(3)-H(3B)	107.6	C(13)-C(14)-H(14)	124.7
C(6)-Pd(1)	2.175(3)	C(5)-C(4)-C(3)	112.4(2)	C(15)-C(14)-H(14)	124.7
C(6)-H(6)	1.0000	C(5)-C(4)-H(4A)	109.1	C(16)-C(15)-C(14)	113.0(3)
C(7)-C(8)	1.532(4)	C(3)-C(4)-H(4A)	109.1	C(16)-C(15)-H(15)	123.5
C(7)-H(7A)	0.9900	C(5)-C(4)-H(4B)	109.1	C(14)-C(15)-H(15)	123.5
C(7)-H(7B)	0.9900	C(3)-C(4)-H(4B)	109.1	C(15)-C(16)-S(1)	112.7(2)
C(8)-H(8A)	0.9900	H(4A)-C(4)-H(4B)	107.8	C(15)-C(16)-H(16)	123.7
C(8)-H(8B)	0.9900	C(6)-C(5)-C(4)	125.4(3)	S(1)-C(16)-H(16)	123.7
C(9)-O(1)	1.285(3)	C(6)-C(5)-Pd(1)	70.75(16)	F(03)-B(01)-F(04)	109.9(3)
C(9)-C(10)	1.376(4)	C(4)-C(5)-Pd(1)	111.09(19)	F(03)-B(01)-F(02)	110.2(3)
C(9)-C(12)	1.535(4)	C(6)-C(5)-H(5)	113.9	F(04)-B(01)-F(02)	109.5(3)
C(10)-C(11)	1.414(4)	C(4)-C(5)-H(5)	113.9	F(03)-B(01)-F(01)	109.6(3)
C(10)-H(10)	0.9500	Pd(1)-C(5)-H(5)	113.9	F(04)-B(01)-F(01)	109.1(3)
C(11)-O(2)	1.281(3)	C(5)-C(6)-C(7)	126.8(3)	F(02)-B(01)-F(01)	108.6(2)
C(11)-C(13)	1.458(4)	C(5)-C(6)-Pd(1)	72.30(16)	C(9)-O(1)-Pd(1)	121.30(19)
C(12)-F(2)	1.333(3)	C(7)-C(6)-Pd(1)	105.68(18)	C(11)-O(2)-Pd(1)	125.00(18)
C(12)-F(3)	1.336(3)	C(5)-C(6)-H(6)	114.3	C(16)-S(1)-C(13)	91.48(16)
C(12)-F(1)	1.336(3)	C(7)-C(6)-H(6)	114.3	O(1)-Pd(1)-O(2)	93.27(8)
C(13)-C(14)	1.397(4)	Pd(1)-C(6)-H(6)	114.3	O(1)-Pd(1)-C(6)	159.00(11)
C(13)-S(1)	1.720(3)	C(6)-C(7)-C(8)	114.3(2)	O(2)-Pd(1)-C(6)	87.06(10)
C(14)-C(15)	1.416(4)	C(6)-C(7)-H(7A)	108.7	O(1)-Pd(1)-C(2)	88.69(9)
C(14)-H(14)	0.9500	C(8)-C(7)-H(7A)	108.7	O(2)-Pd(1)-C(2)	160.47(10)
C(15)-C(16)	1.370(5)	C(6)-C(7)-H(7B)	108.7	C(6)-Pd(1)-C(2)	97.98(11)
C(15)-H(15)	0.9500	C(8)-C(7)-H(7B)	108.7	O(1)-Pd(1)-C(5)	163.68(10)
C(16)-S(1)	1.695(3)	H(7A)-C(7)-H(7B)	107.6	O(2)-Pd(1)-C(5)	91.24(10)
C(16)-H(16)	0.9500	C(1)-C(8)-C(7)	112.2(2)	C(6)-Pd(1)-C(5)	36.95(12)
B(01)-F(03)	1.384(4)	C(1)-C(8)-H(8A)	109.2	C(2)-Pd(1)-C(5)	81.95(11)
B(01)-F(04)	1.390(4)	C(7)-C(8)-H(8A)	109.2	O(1)-Pd(1)-C(1)	91.60(10)
B(01)-F(02)	1.392(4)	C(1)-C(8)-H(8B)	109.2	O(2)-Pd(1)-C(1)	162.05(10)
B(01)-F(01)	1.403(4)	C(7)-C(8)-H(8B)	109.2	C(6)-Pd(1)-C(1)	82.28(11)
O(1)-Pd(1)	2.003(2)	H(8A)-C(8)-H(8B)	107.9	C(2)-Pd(1)-C(1)	36.85(11)
O(2)-Pd(1)	2.005(2)	O(1)-C(9)-C(10)	130.8(3)	C(5)-Pd(1)-C(1)	88.89(11)
		O(1)-C(9)-C(12)	109.9(2)		
C(2)-C(1)-C(8)	125.0(3)	C(10)-C(9)-C(12)	119.3(2)		

Symmetry transformations used to generate equivalent atoms:

Table B.8.3 Anisotropic displacement parameters ($Å^2 x\ 10^3$) for [Pd(cod)(thtfac)]BF_4. The anisotropic displacement factor exponent takes the form: $-2\pi^2[\ h^2 a^{*2} U^{11} + ... + 2\ h\ k\ a^*\ b^*\ U^{12}\ ]$

	U^{11}	U^{22}	U^{33}	U^{23}	U^{13}	U^{12}
C(1)	17(1)	16(2)	11(1)	4(1)	3(1)	-1(1)
C(2)	16(1)	11(1)	15(1)	5(1)	3(1)	0(1)
C(3)	22(1)	17(2)	17(2)	-1(1)	7(1)	-4(1)
C(4)	20(1)	21(2)	15(2)	-4(1)	1(1)	-5(1)
C(5)	13(1)	22(2)	9(1)	3(1)	0(1)	-1(1)
C(6)	9(1)	21(2)	13(1)	6(1)	-1(1)	2(1)
C(7)	12(1)	21(2)	16(2)	-1(1)	4(1)	2(1)
C(8)	15(1)	22(2)	13(1)	2(1)	5(1)	0(1)
C(9)	12(1)	13(1)	16(1)	-3(1)	3(1)	2(1)
C(10)	13(1)	15(1)	16(1)	1(1)	4(1)	-1(1)
C(11)	16(1)	10(1)	13(1)	0(1)	7(1)	0(1)
C(12)	13(1)	14(1)	16(1)	0(1)	2(1)	0(1)
C(13)	14(1)	13(1)	13(1)	1(1)	4(1)	2(1)
C(14)	21(1)	14(1)	17(2)	2(1)	9(1)	3(1)
C(15)	27(2)	14(2)	22(2)	0(1)	10(1)	-3(1)
C(16)	34(2)	14(2)	15(2)	1(1)	7(1)	2(1)
B(01)	21(2)	16(2)	15(2)	-1(1)	2(1)	-3(1)
O(1)	11(1)	16(1)	16(1)	4(1)	1(1)	-2(1)
O(2)	14(1)	16(1)	15(1)	2(1)	4(1)	-1(1)
F(1)	16(1)	23(1)	22(1)	2(1)	0(1)	-7(1)
F(01)	27(1)	26(1)	21(1)	-6(1)	11(1)	-8(1)
F(2)	17(1)	20(1)	22(1)	-1(1)	1(1)	5(1)
F(02)	28(1)	18(1)	18(1)	-3(1)	1(1)	1(1)
F(3)	19(1)	26(1)	12(1)	0(1)	4(1)	2(1)
F(03)	23(1)	38(1)	26(1)	-5(1)	-5(1)	0(1)
F(04)	43(1)	22(1)	25(1)	2(1)	15(1)	-5(1)
S(1)	21(1)	18(1)	16(1)	3(1)	2(1)	-1(1)
Pd(1)	10(1)	11(1)	11(1)	2(1)	3(1)	0(1)

Table B.8.4 Hydrogen coordinates ($x\ 10^4$) and isotropic displacement parameters ($Å^2 x\ 10^3$) for [Pd(cod)(thtfac)]BF_4.

	x	y	z	U(eq)
H(1)	2459	1666	5114	17
H(2)	1538	2501	6251	17
H(3A)	2483	2914	8296	22
H(3B)	3533	3220	7491	22
H(4A)	5149	2319	8353	23
H(4B)	4489	2529	9520	23
H(5)	3930	1232	9677	18
H(6)	4505	251	8546	18
H(7A)	4800	361	6479	19
H(7B)	5986	894	7303	19
H(8A)	5008	2066	6528	19
H(8B)	4717	1494	5325	19
H(10)	-1340	-371	7375	17
H(14)	-1429	-1243	8992	20
H(15)	-732	-2132	10838	25
H(16)	1675	-2036	11778	25

Table B.8.5 Hydrogen bonds for [Pd(cod)(thtfac)]BF_4 [Å and °].

D-H...A	d(D-H)	d(H...A)	d(D...A)	<(DHA)
C(10)-H(10)...F(01)	0.95	2.51	3.418(3)	161.2
C(14)-H(14)...F(01)	0.95	2.49	3.348(4)	149.6

C(14)-H(14)...F(02)	0.95	2.47	3.350(3)	154.8
C(8)-H(8B)...F(03)#1	0.99	2.51	3.500(4)	177.0
C(1)-H(1)...F(01)#1	1.00	2.49	3.277(4)	134.8
C(2)-H(2)...F(04)#2	1.00	2.56	3.368(3)	137.7
C(3)-H(3A)...F(03)#2	0.99	2.62	3.476(4)	144.9
C(4)-H(4B)...F(04)#3	0.99	2.60	3.370(4)	134.2
C(5)-H(5)...F(02)#3	1.00	2.29	3.289(4)	173.7
C(5)-H(5)...F(04)#3	1.00	2.59	3.337(4)	131.3
C(6)-H(6)...F(02)#4	1.00	2.39	3.105(4)	127.8
C(16)-H(16)...F(01)#5	0.95	2.48	3.165(4)	128.6
C(16)-H(16)...F(04)#5	0.95	2.56	3.266(4)	131.8

Symmetry transformations used to generate equivalent atoms:
#1 -x,-y,-z+1 #2 -x-1/2,y+1/2,-z+3/2 #3 -x,-y,-z+2
#4 x+1,y,z #5 x+1/2,-y-1/2,z+1/2

B.9 Crystal Data of [Pd(cod)(trop)PF$_6$

Table B.9.1 Atomic coordinates (x 10^4) and equivalent isotropic displacement parameters (Å^{2}x 10^3) for [Pd(cod)(trop)]PF$_6$. U(eq) is defined as one third of the trace of the orthogonalized U^{ij} tensor.

	x	y	z	U(eq)
C(1)	6826(7)	1028(8)	2248(12)	44(3)
C(2)	7377(8)	1670(7)	2134(12)	47(3)
C(3)	7296(8)	2414(7)	1369(10)	58(4)
C(4)	6877(7)	2256(6)	277(10)	46(3)
C(5)	7125(8)	1396(7)	-248(11)	43(4)
C(6)	6711(7)	696(7)	-68(11)	38(3)
C(7)	5969(6)	567(7)	657(10)	49(4)
C(8)	5971(7)	991(8)	1750(10)	50(3)
C(9)	8946(6)	-454(7)	1683(10)	16(1)
C(10)	8945(6)	-460(6)	474(10)	16(1)
C(11)	9430(7)	-972(7)	-243(12)	24(3)
C(12)	9996(7)	-1578(7)	71(11)	26(3)
C(13)	10245(4)	-1845(4)	1089(15)	27(2)
C(14)	9987(7)	-1560(7)	2143(11)	23(3)
C(15)	9419(7)	-953(8)	2354(11)	27(3)
O(1)	8497(5)	100(5)	2143(7)	29(2)
O(2)	8409(5)	17(5)	-54(6)	21(2)
F(1)	6289(6)	-2107(5)	3032(8)	88(3)
F(2)	6256(4)	-1556(6)	4739(8)	79(3)
F(3)	6754(5)	-891(5)	2339(7)	75(2)
F(4)	7421(4)	-1513(5)	3703(8)	67(2)
F(5)	5595(5)	-904(5)	3389(10)	97(4)
F(6)	6703(5)	-391(4)	4139(6)	68(2)
P(1)	6496(2)	-1244(2)	3529(4)	58(1)
Pd(1)	7751(1)	661(1)	1031(2)	22(1)

Table B.9.2 Bond lengths [Å] and angles [°] for [Pd(cod)(trop)]PF_6.

C(1)-C(2)	1.387(18)	C(2)-C(1)-H(1)	113.3	C(9)-C(10)-C(11)	126.8(12)
C(1)-C(8)	1.517(18)	C(8)-C(1)-H(1)	113.3	C(12)-C(11)-C(10)	127.9(13)
C(1)-Pd(1)	2.177(12)	Pd(1)-C(1)-H(1)	113.3	C(12)-C(11)-H(11)	116.1
C(1)-H(1)	1.0000	C(1)-C(2)-C(3)	127.2(13)	C(10)-C(11)-H(11)	116.0
C(2)-C(3)	1.524(17)	C(1)-C(2)-Pd(1)	70.8(7)	C(13)-C(12)-C(11)	131.6(12)
C(2)-Pd(1)	2.193(12)	C(3)-C(2)-Pd(1)	105.3(8)	C(13)-C(12)-H(12)	114.2
C(2)-H(2)	1.0000	C(1)-C(2)-H(2)	114.4	C(11)-C(12)-H(12)	114.2
C(3)-C(4)	1.493(16)	C(3)-C(2)-H(2)	114.4	C(12)-C(13)-C(14)	127.4(7)
C(3)-H(3A)	0.9900	Pd(1)-C(2)-H(2)	114.4	C(12)-C(13)-H(13)	116.3
C(3)-H(3B)	0.9900	C(4)-C(3)-C(2)	115.1(11)	C(14)-C(13)-H(13)	116.3
C(4)-C(5)	1.590(16)	C(4)-C(3)-H(3A)	108.5	C(15)-C(14)-C(13)	127.0(12)
C(4)-H(4A)	0.9900	C(2)-C(3)-H(3A)	108.5	C(15)-C(14)-H(14)	116.5
C(4)-H(4B)	0.9900	C(4)-C(3)-H(3B)	108.5	C(13)-C(14)-H(14)	116.5
C(5)-C(6)	1.343(16)	C(2)-C(3)-H(3B)	108.5	C(14)-C(15)-C(9)	134.0(13)
C(5)-Pd(1)	2.192(12)	H(3A)-C(3)-H(3B)	107.5	C(14)-C(15)-H(15)	113.0
C(5)-H(5)	1.0000	C(3)-C(4)-C(5)	112.3(10)	C(9)-C(15)-H(15)	113.0
C(6)-C(7)	1.501(17)	C(3)-C(4)-H(4A)	109.2	C(9)-O(1)-Pd(1)	112.4(8)
C(6)-Pd(1)	2.145(12)	C(5)-C(4)-H(4A)	109.1	C(10)-O(2)-Pd(1)	110.9(7)
C(6)-H(6)	1.0000	C(3)-C(4)-H(4B)	109.2	F(1)-P(1)-F(2)	90.1(5)
C(7)-C(8)	1.476(15)	C(5)-C(4)-H(4B)	109.2	F(1)-P(1)-F(5)	94.3(5)
C(7)-H(7A)	0.9900	H(4A)-C(4)-H(4B)	107.9	F(2)-P(1)-F(5)	88.8(5)
C(7)-H(7B)	0.9900	C(6)-C(5)-C(4)	124.0(11)	F(1)-P(1)-F(4)	90.3(5)
C(8)-H(8A)	0.9900	C(6)-C(5)-Pd(1)	70.1(7)	F(2)-P(1)-F(4)	91.6(5)
C(8)-H(8B)	0.9900	C(4)-C(5)-Pd(1)	109.1(9)	F(5)-P(1)-F(4)	175.3(5)
C(9)-O(1)	1.286(14)	C(6)-C(5)-H(5)	114.9	F(1)-P(1)-F(3)	92.6(5)
C(9)-C(15)	1.378(17)	C(4)-C(5)-H(5)	114.9	F(2)-P(1)-F(3)	177.2(5)
C(9)-C(10)	1.441(9)	Pd(1)-C(5)-H(5)	114.9	F(5)-P(1)-F(3)	91.4(5)
C(10)-O(2)	1.329(13)	C(5)-C(6)-C(7)	128.1(13)	F(4)-P(1)-F(3)	88.0(5)
C(10)-C(11)	1.435(16)	C(5)-C(6)-Pd(1)	73.9(8)	F(1)-P(1)-F(6)	175.3(6)
C(11)-C(12)	1.403(17)	C(7)-C(6)-Pd(1)	106.3(8)	F(2)-P(1)-F(6)	85.3(5)
C(11)-H(11)	0.9500	C(5)-C(6)-H(6)	113.4	F(5)-P(1)-F(6)	86.5(5)
C(12)-C(13)	1.35(2)	C(7)-C(6)-H(6)	113.4	F(4)-P(1)-F(6)	88.9(4)
C(12)-H(12)	0.9500	Pd(1)-C(6)-H(6)	113.4	F(3)-P(1)-F(6)	91.9(4)
C(13)-C(14)	1.40(2)	C(8)-C(7)-C(6)	116.2(11)	O(2)-Pd(1)-O(1)	82.09(18)
C(13)-H(13)	0.9500	C(8)-C(7)-H(7A)	108.2	O(2)-Pd(1)-C(6)	92.5(4)
C(14)-C(15)	1.379(16)	C(6)-C(7)-H(7A)	108.2	O(1)-Pd(1)-C(6)	152.9(3)
C(14)-H(14)	0.9500	C(8)-C(7)-H(7B)	108.2	O(2)-Pd(1)-C(1)	162.9(4)
C(15)-H(15)	0.9500	C(6)-C(7)-H(7B)	108.2	O(1)-Pd(1)-C(1)	96.0(5)
O(1)-Pd(1)	2.018(9)	H(7A)-C(7)-H(7B)	107.4	C(6)-Pd(1)-C(1)	81.5(4)
O(2)-Pd(1)	1.982(8)	C(7)-C(8)-C(1)	111.5(9)	O(2)-Pd(1)-C(5)	95.0(4)
F(1)-P(1)	1.563(8)	C(7)-C(8)-H(8A)	109.3	O(1)-Pd(1)-C(5)	170.2(4)
F(2)-P(1)	1.579(10)	C(1)-C(8)-H(8A)	109.3	C(6)-Pd(1)-C(5)	36.1(4)
F(3)-P(1)	1.588(9)	C(7)-C(8)-H(8B)	109.3	C(1)-Pd(1)-C(5)	89.5(4)
F(4)-P(1)	1.584(8)	C(1)-C(8)-H(8B)	109.3	O(2)-Pd(1)-C(2)	160.0(4)
F(5)-P(1)	1.579(7)	H(8A)-C(8)-H(8B)	108.0	O(1)-Pd(1)-C(2)	96.5(5)
F(6)-P(1)	1.606(8)	O(1)-C(9)-C(15)	119.1(12)	C(6)-Pd(1)-C(2)	97.3(5)
		O(1)-C(9)-C(10)	115.5(11)	C(1)-Pd(1)-C(2)	37.0(5)
C(2)-C(1)-C(8)	126.0(12)	C(15)-C(9)-C(10)	125.3(13)	C(5)-Pd(1)-C(2)	83.0(4)
C(2)-C(1)-Pd(1)	72.1(7)	O(2)-C(10)-C(9)	118.1(12)		
C(8)-C(1)-Pd(1)	111.4(8)	O(2)-C(10)-C(11)	114.9(11)		

Symmetry transformations used to generate equivalent atoms:

Table B.9.3 Anisotropic displacement parameters ($Å^2 x\ 10^3$) for [Pd(cod)(trop)]PF_6. The anisotropic displacement factor exponent takes the form: $-2\pi^2[\ h^2 a^{*2} U^{11} + ... + 2\ h\ k\ a^*\ b^*\ U^{12}\ ]$

	U^{11}	U^{22}	U^{33}	U^{23}	U^{13}	U^{12}
C(1)	50(9)	54(9)	27(7)	-19(7)	5(6)	30(6)
C(2)	59(8)	35(7)	46(8)	-14(6)	20(6)	6(6)
C(3)	58(8)	29(6)	86(13)	-12(6)	20(6)	17(5)
C(4)	45(7)	30(6)	64(9)	-1(5)	11(6)	8(5)
C(5)	48(8)	50(8)	32(7)	22(6)	22(6)	35(6)
C(6)	32(6)	44(7)	37(7)	23(6)	-9(5)	2(5)
C(7)	22(5)	38(6)	87(12)	14(6)	-6(5)	4(5)
C(8)	31(6)	64(8)	55(8)	15(7)	14(6)	17(6)
C(9)	14(2)	17(2)	19(3)	8(4)	-8(4)	-5(2)
C(10)	14(2)	17(2)	19(3)	8(4)	-8(4)	-5(2)

C(11)	29(6)	9(6)	34(8)	0(5)	23(6)	7(5)
C(12)	27(6)	23(6)	28(7)	-3(5)	14(5)	-11(6)
C(13)	22(4)	15(3)	43(5)	5(7)	-24(7)	-1(3)
C(14)	26(6)	20(6)	23(7)	0(5)	-8(5)	8(6)
C(15)	26(6)	38(8)	18(8)	-4(6)	11(5)	-12(6)
O(1)	15(4)	35(5)	36(5)	6(4)	1(4)	-3(3)
O(2)	26(4)	28(4)	9(4)	10(3)	2(3)	15(3)
F(1)	105(7)	66(5)	95(7)	-15(5)	-27(5)	-51(5)
F(2)	48(5)	93(6)	97(7)	18(5)	11(4)	19(4)
F(3)	96(6)	68(5)	62(5)	9(4)	13(4)	-17(4)
F(4)	38(4)	56(4)	108(7)	-25(4)	1(4)	-7(3)
F(5)	59(5)	112(8)	120(9)	63(8)	-30(5)	18(5)
F(6)	80(5)	56(4)	69(5)	-21(3)	-15(4)	30(4)
P(1)	38(2)	57(2)	79(2)	19(2)	-10(2)	-5(2)
Pd(1)	16(1)	21(1)	27(1)	0(1)	-1(1)	4(1)

Table B.9.4 Hydrogen coordinates (x 10^4) and isotropic displacement parameters ($Å^2$x 10^3) for [Pd(cod)(trop)]PF_6.

	x	y	z	U(eq)
H(1)	6875	734	2981	52
H(2)	7742	1756	2798	56
H(3A)	6989	2846	1775	69
H(3B)	7852	2631	1213	69
H(4A)	7020	2698	-258	56
H(4B)	6276	2271	393	56
H(5)	7414	1427	-986	52
H(6)	6749	299	-705	45
H(7A)	5480	748	232	59
H(7B)	5910	-29	794	59
H(8A)	5602	698	2275	60
H(8B)	5758	1555	1653	60
H(11)	9360	-892	-1027	29
H(12)	10250	-1850	-542	31
H(13)	10640	-2273	1092	32
H(14)	10230	-1813	2779	28
H(15)	9336	-858	3132	33

Table B.9.5 Hydrogen bonds for [Pd(cod)(trop)]PF_6 [Å and °].

D-H...A	d(D-H)	d(H...A)	d(D...A)	<(DHA)
C(1)-H(1)...F(6)	1.00	2.31	3.237(17)	153.1
C(2)-H(2)...F(1)#1	1.00	2.45	3.139(17)	125.4
C(5)-H(5)...F(4)#2	1.00	2.59	3.198(15)	118.8
C(7)-H(7B)...F(2)#3	0.99	2.59	3.310(14)	129.6
C(6)-H(6)...F(5)#3	1.00	2.28	3.091(17)	137.4
C(7)-H(7A)...F(6)#4	0.99	2.48	3.412(12)	156.7
C(8)-H(8A)...F(5)#5	0.99	2.39	3.220(13)	141.4
C(11)-H(11)...O(1)#6	0.95	2.56	3.324(17)	138.1
C(12)-H(12)...F(4)#6	0.95	2.54	3.384(15)	147.5
C(12)-H(12)...F(6)#6	0.95	2.40	3.084(15)	128.5
C(14)-H(14)...F(1)#7	0.95	2.49	3.219(14)	134.0

Symmetry transformations used to generate equivalent atoms:
#1 -x+3/2,y+1/2,z #2 y+1,-x+1,z-1/2 #3 -y+1/2,-x+1/2,z-1/2
#4 y+1/2,x-1/2,z-1/2 #5 -x+1,-y,z #6 -y+1,x-1,z-1/2
#7 x+1/2,-y-1/2,z

B.10 Crystal Data of [Pd(cod)(NH-acac)]BF_4

Table B.10.1 Atomic coordinates (x 10^4) and equivalent isotropic displacement parameters ($Å^2$x 10^3) for [Pd(cod)(NH-acac)]BF_4. U(eq) is defined as one third of the trace of the orthogonalized U^{ij} tensor.

	x	y	z	U(eq)
C(1)	1385(3)	2624(2)	-1330(2)	20(1)
C(2)	1954(3)	3319(2)	-447(3)	21(1)
C(3)	3513(4)	3713(2)	-33(3)	26(1)
C(4)	4529(4)	3076(2)	954(3)	27(1)
C(5)	4238(3)	1917(2)	871(3)	22(1)
C(6)	3845(3)	1326(2)	-96(2)	19(1)
C(7)	3753(3)	1727(2)	-1237(3)	19(1)
C(8)	2216(3)	2086(2)	-1968(2)	21(1)
C(9)	-844(3)	1378(2)	693(2)	16(1)
C(10)	-177(3)	589(2)	1484(2)	18(1)
C(11)	1222(3)	230(2)	1748(2)	17(1)
C(12)	-2423(3)	1614(2)	450(3)	23(1)
C(13)	1817(3)	-605(2)	2629(3)	25(1)
B(01)	2691(4)	-1026(2)	-3553(3)	21(1)
O(1)	2154(2)	547(1)	1304(2)	19(1)
N(01)	-183(3)	1924(2)	144(2)	18(1)
Pd(1)	1840(1)	1745(1)	232(1)	14(1)
F(01)	2711(3)	-199(2)	-2863(2)	44(1)
F(02)	4017(2)	-1143(2)	-3660(2)	36(1)
F(03)	2327(3)	-1939(2)	-3106(3)	33(1)
F(04)	1630(3)	-874(2)	-4615(2)	41(1)
F(01B)	1990(70)	-70(40)	-3720(90)	80(30)
F(02B)	4140(50)	-750(40)	-3160(50)	36(1)
F(03B)	2790(80)	-2030(60)	-3130(70)	33(1)
F(04B)	2430(70)	-1000(40)	-4620(40)	41(1)

Table B.10.2 Bond lengths [Å] and angles [°] for [Pd(cod)(NH-acac)]BF_4.

C(1)-C(2)	1.384(4)	C(11)-O(1)	1.302(3)	C(1)-C(2)-H(2)	114.4
C(1)-C(8)	1.509(4)	C(11)-C(13)	1.507(4)	C(3)-C(2)-H(2)	114.4
C(1)-Pd(1)	2.185(3)	C(12)-H(12A)	0.9800	Pd(1)-C(2)-H(2)	114.4
C(1)-H(1)	1.0000	C(12)-H(12B)	0.9800	C(2)-C(3)-C(4)	113.1(2)
C(2)-C(3)	1.524(4)	C(12)-H(12C)	0.9800	C(2)-C(3)-H(3A)	109.0
C(2)-Pd(1)	2.208(3)	C(13)-H(13A)	0.9800	C(4)-C(3)-H(3A)	109.0
C(2)-H(2)	1.0000	C(13)-H(13B)	0.9800	C(2)-C(3)-H(3B)	109.0
C(3)-C(4)	1.532(5)	C(13)-H(13C)	0.9800	C(4)-C(3)-H(3B)	109.0
C(3)-H(3A)	0.9900	B(01)-F(04B)	1.29(5)	H(3A)-C(3)-H(3B)	107.8
C(3)-H(3B)	0.9900	B(01)-F(01)	1.368(4)	C(5)-C(4)-C(3)	114.4(3)
C(4)-C(5)	1.506(4)	B(01)-F(02)	1.371(4)	C(5)-C(4)-H(4A)	108.7
C(4)-H(4A)	0.9900	B(01)-F(01B)	1.38(5)	C(3)-C(4)-H(4A)	108.7
C(4)-H(4B)	0.9900	B(01)-F(02B)	1.38(5)	C(5)-C(4)-H(4B)	108.7
C(5)-C(6)	1.376(4)	B(01)-F(03B)	1.38(8)	C(3)-C(4)-H(4B)	108.7
C(5)-Pd(1)	2.222(3)	B(01)-F(04)	1.396(4)	H(4A)-C(4)-H(4B)	107.6
C(5)-H(5)	1.0000	B(01)-F(03)	1.400(4)	C(6)-C(5)-C(4)	126.1(3)
C(6)-C(7)	1.510(4)	O(1)-Pd(1)	1.9991(19)	C(6)-C(5)-Pd(1)	72.22(16)
C(6)-Pd(1)	2.228(3)	N(01)-Pd(1)	1.972(2)	C(4)-C(5)-Pd(1)	105.9(2)
C(6)-H(6)	1.0000	N(01)-H(01)	0.90(4)	C(6)-C(5)-H(5)	114.5
C(7)-C(8)	1.540(4)			C(4)-C(5)-H(5)	114.5
C(7)-H(7A)	0.9900	C(2)-C(1)-C(8)	126.0(3)	Pd(1)-C(5)-H(5)	114.5
C(7)-H(7B)	0.9900	C(2)-C(1)-Pd(1)	72.54(16)	C(5)-C(6)-C(7)	125.0(3)
C(8)-H(8A)	0.9900	C(8)-C(1)-Pd(1)	106.21(17)	C(5)-C(6)-Pd(1)	71.76(16)
C(8)-H(8B)	0.9900	C(2)-C(1)-H(1)	114.4	C(7)-C(6)-Pd(1)	110.15(18)
C(9)-N(01)	1.313(4)	C(8)-C(1)-H(1)	114.4	C(5)-C(6)-H(6)	114.0
C(9)-C(10)	1.411(4)	Pd(1)-C(1)-H(1)	114.4	C(7)-C(6)-H(6)	114.0
C(9)-C(12)	1.507(4)	C(1)-C(2)-C(3)	124.1(3)	Pd(1)-C(6)-H(6)	114.0
C(10)-C(11)	1.378(4)	C(1)-C(2)-Pd(1)	70.74(15)	C(6)-C(7)-C(8)	113.0(2)
C(10)-H(10)	0.9500	C(3)-C(2)-Pd(1)	110.6(2)	C(6)-C(7)-H(7A)	109.0

C(8)-C(7)-H(7A)	109.0	C(11)-C(13)-H(13B)	109.5	F(04B)-B(01)-F(03)	118(2)
C(6)-C(7)-H(7B)	109.0	H(13A)-C(13)-H(13B)	109.5	F(01)-B(01)-F(03)	109.3(3)
C(8)-C(7)-H(7B)	109.0	C(11)-C(13)-H(13C)	109.5	F(02)-B(01)-F(03)	109.9(3)
H(7A)-C(7)-H(7B)	107.8	H(13A)-C(13)-H(13C)	109.5	F(01B)-B(01)-F(03)	127(3)
C(1)-C(8)-C(7)	114.7(2)	H(13B)-C(13)-H(13C)	109.5	F(02B)-B(01)-F(03)	117(2)
C(1)-C(8)-H(8A)	108.6	F(04B)-B(01)-F(01)	127(2)	F(03B)-B(01)-F(03)	20(3)
C(7)-C(8)-H(8A)	108.6	F(04B)-B(01)-F(02)	75(3)	F(04)-B(01)-F(03)	107.2(3)
C(1)-C(8)-H(8B)	108.6	F(01)-B(01)-F(02)	110.5(3)	C(11)-O(1)-Pd(1)	124.88(16)
C(7)-C(8)-H(8B)	108.6	F(04B)-B(01)-F(01B)	85(5)	C(9)-N(01)-Pd(1)	126.3(2)
H(8A)-C(8)-H(8B)	107.6	F(01)-B(01)-F(01B)	46(4)	C(9)-N(01)-H(01)	117(3)
N(01)-C(9)-C(10)	124.4(3)	F(02)-B(01)-F(01B)	122(3)	Pd(1)-N(01)-H(01)	117(3)
N(01)-C(9)-C(12)	117.2(2)	F(04B)-B(01)-F(02B)	100(3)	N(01)-Pd(1)-O(1)	92.03(9)
C(10)-C(9)-C(12)	118.4(2)	F(01)-B(01)-F(02B)	78(3)	N(01)-Pd(1)-C(1)	90.71(10)
C(11)-C(10)-C(9)	125.7(2)	F(02)-B(01)-F(02B)	33(3)	O(1)-Pd(1)-C(1)	160.96(10)
C(11)-C(10)-H(10)	117.1	F(01B)-B(01)-F(02B)	103(4)	N(01)-Pd(1)-C(2)	93.65(11)
C(9)-C(10)-H(10)	117.1	F(04B)-B(01)-F(03B)	113(4)	O(1)-Pd(1)-C(2)	161.34(11)
O(1)-C(11)-C(10)	126.2(2)	F(01)-B(01)-F(03B)	119(3)	C(1)-Pd(1)-C(2)	36.72(11)
O(1)-C(11)-C(13)	113.2(2)	F(02)-B(01)-F(03B)	90(3)	N(01)-Pd(1)-C(5)	159.06(12)
C(10)-C(11)-C(13)	120.5(2)	F(01B)-B(01)-F(03B)	147(4)	O(1)-Pd(1)-C(5)	86.57(10)
C(9)-C(12)-H(12A)	109.5	F(02B)-B(01)-F(03B)	100(4)	C(1)-Pd(1)-C(5)	97.40(11)
C(9)-C(12)-H(12B)	109.5	F(04B)-B(01)-F(04)	35(3)	C(2)-Pd(1)-C(5)	81.80(12)
H(12A)-C(12)-H(12B)	109.5	F(01)-B(01)-F(04)	110.3(3)	N(01)-Pd(1)-C(6)	164.88(11)
C(9)-C(12)-H(12C)	109.5	F(02)-B(01)-F(04)	109.5(3)	O(1)-Pd(1)-C(6)	90.63(9)
H(12A)-C(12)-H(12C)	109.5	F(01B)-B(01)-F(04)	64(4)	C(1)-Pd(1)-C(6)	82.08(10)
H(12B)-C(12)-H(12C)	109.5	F(02B)-B(01)-F(04)	130(2)	C(2)-Pd(1)-C(6)	88.50(10)
C(11)-C(13)-H(13A)	109.5	F(03B)-B(01)-F(04)	115(3)	C(5)-Pd(1)-C(6)	36.02(11)

Symmetry transformations used to generate equivalent atoms:

Table B.10.3 Anisotropic displacement parameters ($Å^2 x\ 10^3$) for [Pd(cod)(NH-acac)]BF_4. The anisotropic displacement factor exponent takes the form: $-2\pi^2[\ h^2 a^{*2} U^{11} + ... + 2\ h\ k\ a^*\ b^*\ U^{12}\ ]$

	U^{11}	U^{22}	U^{33}	U^{23}	U^{13}	U^{12}
C(1)	20(1)	21(1)	21(1)	9(1)	10(1)	5(1)
C(2)	25(2)	16(1)	28(2)	4(1)	17(1)	4(1)
C(3)	30(2)	20(1)	36(2)	-9(1)	22(1)	-5(1)
C(4)	20(2)	35(2)	29(2)	-13(1)	12(1)	-8(1)
C(5)	10(1)	34(2)	22(2)	-2(1)	5(1)	-1(1)
C(6)	13(1)	22(1)	24(1)	0(1)	9(1)	4(1)
C(7)	20(2)	20(1)	20(2)	-3(1)	9(1)	-1(1)
C(8)	25(1)	20(1)	20(1)	0(1)	11(1)	0(1)
C(9)	15(1)	18(1)	16(1)	-1(1)	6(1)	0(1)
C(10)	21(1)	18(1)	17(1)	2(1)	8(1)	-1(1)
C(11)	22(1)	14(1)	14(1)	0(1)	5(1)	0(1)
C(12)	16(1)	28(1)	26(2)	6(1)	10(1)	2(1)
C(13)	30(2)	19(1)	23(1)	6(1)	7(1)	4(1)
B(01)	25(2)	17(1)	24(2)	-1(1)	11(1)	-2(1)
O(1)	18(1)	20(1)	19(1)	5(1)	6(1)	5(1)
N(01)	13(1)	21(1)	19(1)	6(1)	7(1)	4(1)
Pd(1)	12(1)	16(1)	15(1)	2(1)	6(1)	2(1)
F(01)	60(2)	29(1)	60(2)	-24(1)	41(2)	-15(1)
F(02)	30(1)	36(1)	51(2)	5(1)	24(1)	6(1)
F(03)	47(2)	27(1)	29(1)	0(1)	18(1)	-14(1)
F(04)	34(2)	36(1)	38(1)	9(1)	-4(1)	-4(1)
F(01B)	50(40)	30(30)	160(80)	20(40)	50(50)	30(30)
F(02B)	30(1)	36(1)	51(2)	5(1)	24(1)	6(1)
F(03B)	47(2)	27(1)	29(1)	0(1)	18(1)	-14(1)
F(04B)	34(2)	36(1)	38(1)	9(1)	-4(1)	-4(1)

Table B.10.4 Hydrogen coordinates (x 10^4) and isotropic displacement parameters ($Å^2$x 10^3) for [Pd(cod)(NH-acac)]BF_4.

	x	y	z	U(eq)
H(1)	330	2725	-1771	24
H(2)	1236	3830	-356	25
H(3A)	3528	4452	204	31
H(3B)	3880	3689	-663	31
H(4A)	5541	3196	1002	32
H(4B)	4442	3337	1660	32
H(5)	4755	1518	1578	27
H(6)	4120	571	35	23
H(7A)	4066	1167	-1638	23
H(7B)	4431	2322	-1132	23
H(8A)	2290	2570	-2553	25
H(8B)	1655	1468	-2357	25
H(10)	-743	277	1868	22
H(12A)	-2595	2366	313	34
H(12B)	-2683	1408	1096	34
H(12C)	-3019	1224	-218	34
H(13A)	2029	-1235	2277	37
H(13B)	1099	-770	2974	37
H(13C)	2709	-352	3209	37
H(01)	-710(40)	2410(30)	-330(40)	43(12)

Table B.10.5 Hydrogen bonds for [Pd(cod)(NH-acac)]BF_4 [Å and °].

D-H...A	d(D-H)	d(H...A)	d(D...A)	<(DHA)
C(7)-H(7A)...F(01)	0.99	2.40	3.144(3)	131.0
C(12)-H(12A)...F(04B)#1	0.98	2.30	3.23(5)	158.2
N(01)-H(01)...F(03)#1	0.90(4)	2.22(5)	3.066(4)	157(4)
N(01)-H(01)...F(04)#1	0.90(4)	2.36(4)	3.120(3)	143(4)
N(01)-H(01)...F(03B)#1	0.90(4)	2.38(9)	3.20(8)	152(4)
C(3)-H(3B)...F(02)#2	0.99	2.52	3.409(4)	148.8
C(5)-H(5)...F(02B)#3	1.00	2.16	3.15(5)	176.2
C(5)-H(5)...F(02)#3	1.00	2.53	3.487(4)	159.4
C(12)-H(12B)...F(03)#4	0.98	2.55	3.370(4)	141.8
C(13)-H(13A)...F(03)#5	0.98	2.42	3.365(4)	160.9
C(13)-H(13A)...F(03B)#5	0.98	2.45	3.41(7)	166.0

Symmetry transformations used to generate equivalent atoms:
#1 -x,y+1/2,-z-1/2 #2 -x+1,y+1/2,-z-1/2 #3 -x+1,-y,-z
#4 -x,-y,-z #5 x,-y-1/2,z+1/2

B.11 Crystal Data of [Pt(cod)(acac)]BF_4

Table B.11.1 Atomic coordinates (x 10^4) and equivalent isotropic displacement parameters ($Å^2$x 10^3) for [Pt(cod)(acac)]BF_4. U(eq) is defined as one third of the trace of the orthogonalized U^{ij} tensor.

	x	y	z	U(eq)
C(1)	6075(1)	4555(5)	4201(10)	20(1)
C(2)	6077(2)	3747(6)	5834(6)	18(1)
C(3)	5628(2)	2842(8)	6710(7)	24(1)
C(4)	5307(2)	1630(6)	5501(6)	23(1)
C(5)	5631(1)	654(5)	4159(9)	17(1)

C(6)	5723(2)	1332(6)	2473(6)	20(1)
C(7)	5553(2)	3177(6)	1766(7)	23(1)
C(8)	5605(2)	4780(6)	3072(6)	23(1)
C(9)	7494(1)	1869(4)	4222(6)	14(1)
C(10)	7531(2)	136(5)	3429(5)	14(1)
C(11)	7127(2)	-992(5)	2922(5)	15(1)
C(12)	7971(2)	2884(5)	4708(6)	19(1)
C(13)	7236(2)	-2861(5)	2119(6)	18(1)
B(1)	6109(2)	7741(7)	8153(7)	20(1)
O(1)	7085(1)	2753(3)	4599(4)	14(1)
O(2)	6655(1)	-622(4)	3058(4)	16(1)
F(1)	6168(2)	6296(4)	9304(5)	52(1)
F(2)	5657(1)	7584(5)	7295(4)	39(1)
F(3)	6498(1)	7662(6)	6933(6)	54(1)
F(4)	6145(1)	9442(3)	9019(7)	33(1)
Pt(1)	6389(1)	1790(1)	4012(1)	12(1)

Table B.11.2 Bond lengths [Å] and angles [°] for [Pt(cod)(acac)]BF_4.

C(1)-C(2)	1.388(8)	Pt(1)-C(1)-H(1)	113.9	O(2)-C(11)-C(10)	126.9(3)
C(1)-C(8)	1.525(7)	C(1)-C(2)-C(3)	125.6(4)	O(2)-C(11)-C(13)	113.9(3)
C(1)-Pt(1)	2.160(3)	C(1)-C(2)-Pt(1)	71.5(2)	C(10)-C(11)-C(13)	119.2(4)
C(1)-H(1)	1.0000	C(3)-C(2)-Pt(1)	108.1(3)	C(9)-C(12)-H(12A)	109.5
C(2)-C(3)	1.513(8)	C(1)-C(2)-H(2)	114.3	C(9)-C(12)-H(12B)	109.5
C(2)-Pt(1)	2.153(4)	C(3)-C(2)-H(2)	114.3	H(12A)-C(12)-	109.5
C(2)-H(2)	1.0000	Pt(1)-C(2)-H(2)	114.3	H(12B)	
C(3)-C(4)	1.533(7)	C(2)-C(3)-C(4)	114.0(4)	C(9)-C(12)-H(12C)	109.5
C(3)-H(3A)	0.9900	C(2)-C(3)-H(3A)	108.8	H(12A)-C(12)-	109.5
C(3)-H(3B)	0.9900	C(4)-C(3)-H(3A)	108.8	H(12C)	
C(4)-C(5)	1.516(7)	C(2)-C(3)-H(3B)	108.8	H(12B)-C(12)-	109.5
C(4)-H(4A)	0.9900	C(4)-C(3)-H(3B)	108.8	H(12C)	
C(4)-H(4B)	0.9900	H(3A)-C(3)-H(3B)	107.7	C(11)-C(13)-	109.5
C(5)-C(6)	1.411(8)	C(5)-C(4)-C(3)	111.6(4)	H(13A)	
C(5)-Pt(1)	2.164(3)	C(5)-C(4)-H(4A)	109.3	C(11)-C(13)-	109.5
C(5)-H(5)	1.0000	C(3)-C(4)-H(4A)	109.3	H(13B)	
C(6)-C(7)	1.505(7)	C(5)-C(4)-H(4B)	109.3	H(13A)-C(13)-	109.5
C(6)-Pt(1)	2.147(4)	C(3)-C(4)-H(4B)	109.3	H(13B)	
C(6)-H(6)	1.0000	H(4A)-C(4)-H(4B)	108.0	C(11)-C(13)-	109.5
C(7)-C(8)	1.538(7)	C(6)-C(5)-C(4)	124.5(4)	H(13C)	
C(7)-H(7A)	0.9900	C(6)-C(5)-Pt(1)	70.2(2)	H(13A)-C(13)-	109.5
C(7)-H(7B)	0.9900	C(4)-C(5)-Pt(1)	112.5(3)	H(13C)	
C(8)-H(8A)	0.9900	C(6)-C(5)-H(5)	113.9	H(13B)-C(13)-	109.5
C(8)-H(8B)	0.9900	C(4)-C(5)-H(5)	113.9	H(13C)	
C(9)-O(1)	1.288(4)	Pt(1)-C(5)-H(5)	113.9	F(2)-B(1)-F(1)	110.4(4)
C(9)-C(10)	1.393(5)	C(5)-C(6)-C(7)	126.0(4)	F(2)-B(1)-F(3)	108.1(4)
C(9)-C(12)	1.504(6)	C(5)-C(6)-Pt(1)	71.5(2)	F(1)-B(1)-F(3)	108.7(4)
C(10)-C(11)	1.397(6)	C(7)-C(6)-Pt(1)	108.1(3)	F(2)-B(1)-F(4)	111.2(4)
C(10)-H(10)	0.9500	C(5)-C(6)-H(6)	114.2	F(1)-B(1)-F(4)	110.2(5)
C(11)-O(2)	1.278(5)	C(7)-C(6)-H(6)	114.2	F(3)-B(1)-F(4)	108.1(4)
C(11)-C(13)	1.508(5)	Pt(1)-C(6)-H(6)	114.2	C(9)-O(1)-Pt(1)	123.0(2)
C(12)-H(12A)	0.9800	C(6)-C(7)-C(8)	113.4(4)	C(11)-O(2)-Pt(1)	123.4(2)
C(12)-H(12B)	0.9800	C(6)-C(7)-H(7A)	108.9	O(2)-Pt(1)-O(1)	93.46(11)
C(12)-H(12C)	0.9800	C(8)-C(7)-H(7A)	108.9	O(2)-Pt(1)-C(6)	87.19(14)
C(13)-H(13A)	0.9800	C(6)-C(7)-H(7B)	108.9	O(1)-Pt(1)-C(6)	157.46(15)
C(13)-H(13B)	0.9800	C(8)-C(7)-H(7B)	108.9	O(2)-Pt(1)-C(2)	159.47(14)
C(13)-H(13C)	0.9800	H(7A)-C(7)-H(7B)	107.7	O(1)-Pt(1)-C(2)	88.64(14)
B(1)-F(2)	1.369(6)	C(1)-C(8)-C(7)	111.5(4)	C(6)-Pt(1)-C(2)	98.60(17)
B(1)-F(1)	1.377(6)	C(1)-C(8)-H(8A)	109.3	O(2)-Pt(1)-C(1)	162.4(2)
B(1)-F(3)	1.394(6)	C(7)-C(8)-H(8A)	109.3	O(1)-Pt(1)-C(1)	91.04(13)
B(1)-F(4)	1.398(6)	C(1)-C(8)-H(8B)	109.3	C(6)-Pt(1)-C(1)	82.22(19)
O(1)-Pt(1)	2.015(3)	C(7)-C(8)-H(8B)	109.3	C(2)-Pt(1)-C(1)	37.6(2)
O(2)-Pt(1)	2.013(3)	H(8A)-C(8)-H(8B)	108.0	O(2)-Pt(1)-C(5)	90.93(13)
		O(1)-C(9)-C(10)	126.9(4)	O(1)-Pt(1)-C(5)	163.92(19)
C(2)-C(1)-C(8)	124.6(4)	O(1)-C(9)-C(12)	114.0(3)	C(6)-Pt(1)-C(5)	38.2(2)
C(2)-C(1)-Pt(1)	70.9(2)	C(10)-C(9)-C(12)	119.1(3)	C(2)-Pt(1)-C(5)	81.95(17)
C(8)-C(1)-Pt(1)	111.8(3)	C(9)-C(10)-C(11)	126.2(4)	C(1)-Pt(1)-C(5)	89.41(13)
C(2)-C(1)-H(1)	113.9	C(9)-C(10)-H(10)	116.9		
C(8)-C(1)-H(1)	113.9	C(11)-C(10)-H(10)	116.9		

Symmetry operations used to generate symmetry equivalent atoms

Table B.11.3 Anisotropic displacement parameters ($Å^2 x\ 10^3$) for $[Pt(cod)(acac)]BF_4$. The anisotropic displacement factor exponent takes the form: $-2\pi^2[\ h^2 a^{*2} U^{11} + ... + 2\ h\ k\ a^*\ b^*\ U^{12}\ ]$

	U^{11}	U^{22}	U^{33}	U^{23}	U^{13}	U^{12}
C(1)	20(2)	11(1)	29(4)	-5(2)	3(2)	2(1)
C(2)	18(2)	17(2)	21(2)	-10(2)	-3(2)	5(2)
C(3)	25(3)	28(2)	20(3)	1(2)	7(2)	6(2)
C(4)	18(2)	26(2)	24(2)	1(2)	7(2)	-1(2)
C(5)	12(1)	15(2)	25(3)	0(2)	-1(2)	-4(1)
C(6)	14(2)	24(2)	23(2)	-10(2)	-4(2)	-2(2)
C(7)	17(2)	34(3)	17(3)	3(2)	-4(2)	5(2)
C(8)	22(2)	24(2)	23(2)	2(2)	-2(2)	8(2)
C(9)	14(1)	15(1)	13(2)	1(1)	1(1)	2(1)
C(10)	14(1)	15(1)	13(2)	1(1)	1(1)	2(1)
C(11)	23(2)	10(2)	12(2)	-1(1)	0(2)	3(2)
C(12)	16(2)	15(2)	26(2)	-2(2)	0(2)	2(2)
C(13)	20(2)	13(2)	22(2)	-6(2)	2(2)	-2(2)
B(1)	18(2)	18(2)	23(2)	1(2)	0(2)	3(2)
O(1)	11(1)	11(1)	21(1)	-4(1)	-2(1)	0(1)
O(2)	18(2)	13(1)	19(2)	-6(1)	2(1)	0(1)
F(1)	89(2)	28(1)	39(3)	10(2)	-22(2)	-4(2)
F(2)	28(2)	37(2)	52(2)	-4(2)	-13(1)	-1(1)
F(3)	31(2)	63(2)	68(3)	-42(2)	25(2)	-24(2)
F(4)	42(1)	22(1)	35(1)	-12(2)	7(3)	1(1)
Pt(1)	10(1)	13(1)	13(1)	-3(1)	0(1)	0(1)

Table B.11.4 Hydrogen coordinates ($x\ 10^4$) and isotropic displacement parameters ($Å^2 x\ 10^3$) for $[Pt(cod)(acac)]BF_4$.

	x	y	z	U(eq)
H(1)	6330	5569	4053	24
H(2)	6331	4291	6651	22
H(3A)	5410	3826	7207	29
H(3B)	5752	2065	7680	29
H(4A)	5122	692	6195	27
H(4B)	5053	2418	4907	27
H(5)	5621	-732	4238	21
H(6)	5762	339	1575	24
H(7A)	5194	3077	1406	27
H(7B)	5755	3473	722	27
H(8A)	5625	5973	2437	27
H(8B)	5300	4819	3819	27
H(10)	7863	-322	3211	17
H(12A)	8006	3998	3987	28
H(12B)	8264	2070	4522	28
H(12C)	7956	3246	5931	28
H(13A)	7207	-3830	3005	28
H(13B)	7579	-2864	1640	28
H(13C)	6991	-3102	1190	28

Table B.11.5 Hydrogen bonds for $[Pt(cod)(acac)]BF_4$ [Å and °].

D-H...A	d(D-H)	d(H...A)	d(D...A)	<(DHA)
C(2)-H(2)...F(1)	1.00	2.54	3.255(6)	128.1
C(2)-H(2)...F(3)	1.00	2.47	3.145(6)	123.9
C(3)-H(3B)...F(4)#1	0.99	2.39	3.320(7)	156.5
C(7)-H(7A)...F(2)#2	0.99	2.40	3.266(7)	146.2
C(6)-H(6)...F(4)#3	1.00	2.31	3.192(6)	146.7
C(13)-H(13C)...F(1)#3	0.98	2.65	3.609(6)	166.0

C(7)-H(7B)...F(1)#4	0.99	2.55	3.360(7)	138.7
C(12)-H(12B)...F(4)#5	0.98	2.48	3.445(5)	166.9
C(10)-H(10)...F(3)#5	0.95	2.44	3.328(5)	156.5
C(13)-H(13B)...F(3)#5	0.98	2.48	3.368(6)	151.2

Symmetry transformations used to generate equivalent atoms:
#1 x,y-1,z #2 -x+1,-y+1,z-1/2 #3 x,y-1,z-1
#4 x,y,z-1 #5 -x+3/2,y-1,z-1/2

B.12 Crystal Data of [Pt(cod)(acac)]PF_6

Table B.12.1 Atomic coordinates (x 10^4) and equivalent isotropic displacement parameters ($Å^2$x 10^3) for [Pt(cod)(acac)]PF_6. U(eq) is defined as one third of the trace of the orthogonalized U^{ij} tensor.

	x	y	z	U(eq)
C(1)	3475(8)	1607(5)	6413(6)	17(1)
C(2)	3033(8)	2210(5)	7134(6)	18(1)
C(3)	4114(9)	2716(5)	8144(7)	23(2)
C(4)	4364(9)	2301(5)	9386(6)	24(2)
C(5)	4317(8)	1334(5)	9336(6)	19(2)
C(6)	4988(8)	806(5)	8636(7)	22(2)
C(7)	5958(8)	1151(5)	7860(7)	24(2)
C(8)	5062(8)	1327(5)	6558(7)	23(2)
C(9)	-447(7)	391(4)	6572(6)	14(1)
C(10)	-418(8)	-184(5)	7509(7)	19(2)
C(11)	778(8)	-374(5)	8499(6)	18(2)
C(12)	-1823(8)	503(5)	5557(6)	19(2)
C(13)	651(10)	-1047(5)	9414(7)	24(2)
O(1)	658(5)	871(3)	6467(4)	16(1)
O(2)	2083(5)	-19(3)	8744(4)	18(1)
F(1)	603(6)	3576(4)	7299(5)	42(1)
F(2)	600(6)	2852(4)	9012(4)	41(1)
F(3)	-1914(6)	3024(4)	8572(5)	41(1)
F(4)	-1887(6)	3729(5)	6854(5)	52(2)
F(5)	-861(7)	2406(4)	7216(5)	50(2)
F(6)	-461(7)	4174(3)	8666(5)	42(1)
P(1)	-647(2)	3287(1)	7941(2)	23(1)
Pt(1)	2631(1)	931(1)	7740(1)	13(1)

Table B.12.2 Bond lengths [Å] and angles [°] for [Pt(cod)(acac)]PF_6.

C(1)-C(2)	1.382(10)	C(7)-C(8)	1.521(11)	O(2)-Pt(1)	2.016(5)
C(1)-C(8)	1.504(10)	C(7)-H(7A)	0.9900	F(1)-P(1)	1.602(5)
C(1)-Pt(1)	2.164(6)	C(7)-H(7B)	0.9900	F(2)-P(1)	1.589(5)
C(1)-H(1)	1.0000	C(8)-H(8A)	0.9900	F(3)-P(1)	1.597(5)
C(2)-C(3)	1.525(10)	C(8)-H(8B)	0.9900	F(4)-P(1)	1.600(6)
C(2)-Pt(1)	2.161(7)	C(9)-O(1)	1.300(8)	F(5)-P(1)	1.580(6)
C(2)-H(2)	1.0000	C(9)-C(10)	1.389(10)	F(6)-P(1)	1.588(5)
C(3)-C(4)	1.521(10)	C(9)-C(12)	1.486(10)		
C(3)-H(3A)	0.9900	C(10)-C(11)	1.386(11)	C(2)-C(1)-C(8)	124.9(7)
C(3)-H(3B)	0.9900	C(10)-H(10)	0.9500	C(2)-C(1)-Pt(1)	71.3(4)
C(4)-C(5)	1.495(10)	C(11)-O(2)	1.292(8)	C(8)-C(1)-Pt(1)	108.6(5)
C(4)-H(4A)	0.9900	C(11)-C(13)	1.505(10)	C(2)-C(1)-H(1)	114.5
C(4)-H(4B)	0.9900	C(12)-H(12A)	0.9800	C(8)-C(1)-H(1)	114.5
C(5)-C(6)	1.406(11)	C(12)-H(12B)	0.9800	Pt(1)-C(1)-H(1)	114.5
C(5)-Pt(1)	2.150(7)	C(12)-H(12C)	0.9800	C(1)-C(2)-C(3)	123.9(7)
C(5)-H(5)	1.0000	C(13)-H(13A)	0.9800	C(1)-C(2)-Pt(1)	71.5(4)
C(6)-C(7)	1.528(11)	C(13)-H(13B)	0.9800	C(3)-C(2)-Pt(1)	111.1(5)
C(6)-Pt(1)	2.161(7)	C(13)-H(13C)	0.9800	C(1)-C(2)-H(2)	114.2
C(6)-H(6)	1.0000	O(1)-Pt(1)	2.010(5)	C(3)-C(2)-H(2)	114.2

Pt(1)-C(2)-H(2)	114.2	H(7A)-C(7)-H(7B)	107.9	F(5)-P(1)-F(6)	179.1(4)
C(4)-C(3)-C(2)	113.3(6)	C(1)-C(8)-C(7)	114.7(6)	F(5)-P(1)-F(2)	90.1(3)
C(4)-C(3)-H(3A)	108.9	C(1)-C(8)-H(8A)	108.6	F(6)-P(1)-F(2)	90.5(3)
C(2)-C(3)-H(3A)	108.9	C(7)-C(8)-H(8A)	108.6	F(5)-P(1)-F(3)	91.0(3)
C(4)-C(3)-H(3B)	108.9	C(1)-C(8)-H(8B)	108.6	F(6)-P(1)-F(3)	88.3(3)
C(2)-C(3)-H(3B)	108.9	C(7)-C(8)-H(8B)	108.6	F(2)-P(1)-F(3)	90.9(3)
H(3A)-C(3)-H(3B)	107.7	H(8A)-C(8)-H(8B)	107.6	F(5)-P(1)-F(4)	89.9(4)
C(5)-C(4)-C(3)	112.9(6)	O(1)-C(9)-C(10)	126.1(7)	F(6)-P(1)-F(4)	89.5(3)
C(5)-C(4)-H(4A)	109.0	O(1)-C(9)-C(12)	113.2(6)	F(2)-P(1)-F(4)	179.3(4)
C(3)-C(4)-H(4A)	109.0	C(10)-C(9)-C(12)	120.7(6)	F(3)-P(1)-F(4)	89.9(3)
C(5)-C(4)-H(4B)	109.0	C(11)-C(10)-C(9)	127.6(7)	F(5)-P(1)-F(1)	90.0(3)
C(3)-C(4)-H(4B)	109.0	C(11)-C(10)-H(10)	116.2	F(6)-P(1)-F(1)	90.7(3)
H(4A)-C(4)-H(4B)	107.8	C(9)-C(10)-H(10)	116.2	F(2)-P(1)-F(1)	90.3(3)
C(6)-C(5)-C(4)	126.1(7)	O(2)-C(11)-C(10)	125.8(7)	F(3)-P(1)-F(1)	178.5(3)
C(6)-C(5)-Pt(1)	71.4(4)	O(2)-C(11)-C(13)	113.0(6)	F(4)-P(1)-F(1)	89.0(3)
C(4)-C(5)-Pt(1)	109.2(5)	C(10)-C(11)-C(13)	121.2(7)	O(1)-Pt(1)-O(2)	93.3(2)
C(6)-C(5)-H(5)	113.9	C(9)-C(12)-H(12A)	109.5	O(1)-Pt(1)-C(5)	160.0(3)
C(4)-C(5)-H(5)	113.9	C(9)-C(12)-H(12B)	109.5	O(2)-Pt(1)-C(5)	88.0(2)
Pt(1)-C(5)-H(5)	113.9	H(12A)-C(12)-H(12B)	109.5	O(1)-Pt(1)-C(6)	161.3(3)
C(5)-C(6)-C(7)	123.9(7)	C(9)-C(12)-H(12C)	109.5	O(2)-Pt(1)-C(6)	92.7(3)
C(5)-C(6)-Pt(1)	70.6(4)	H(12A)-C(12)-H(12C)	109.5	C(5)-Pt(1)-C(6)	38.1(3)
C(7)-C(6)-Pt(1)	112.2(5)	H(12B)-C(12)-H(12C)	109.5	O(1)-Pt(1)-C(2)	90.7(2)
C(5)-C(6)-H(6)	114.2	C(11)-C(13)-H(13A)	109.5	O(2)-Pt(1)-C(2)	160.6(2)
C(7)-C(6)-H(6)	114.2	C(11)-C(13)-H(13B)	109.5	C(5)-Pt(1)-C(2)	81.9(3)
Pt(1)-C(6)-H(6)	114.2	H(13A)-C(13)-H(13B)	109.5	C(6)-Pt(1)-C(2)	89.5(3)
C(8)-C(7)-C(6)	112.4(6)	C(11)-C(13)-H(13C)	109.5	O(1)-Pt(1)-C(1)	86.9(2)
C(8)-C(7)-H(7A)	109.1	H(13A)-C(13)-H(13C)	109.5	O(2)-Pt(1)-C(1)	162.0(2)
C(6)-C(7)-H(7A)	109.1	H(13B)-C(13)-H(13C)	109.5	C(5)-Pt(1)-C(1)	98.0(3)
C(8)-C(7)-H(7B)	109.1	C(9)-O(1)-Pt(1)	123.1(4)	C(6)-Pt(1)-C(1)	82.0(3)
C(6)-C(7)-H(7B)	109.1	C(11)-O(2)-Pt(1)	123.7(5)	C(2)-Pt(1)-C(1)	37.3(3)

Symmetry transformations used to generate equivalent atoms:

Table B.12.3 Anisotropic displacement parameters ($Å^2 x\ 10^3$) for [Pt(cod)(acac)]PF_6. The anisotropic displacement factor exponent takes the form: $-2\pi^2[\ h^2 a^{*2} U^{11} + ... + 2\ h\ k\ a^*\ b^*\ U^{12}\ ]$

	U^{11}	U^{22}	U^{33}	U^{23}	U^{13}	U^{12}
C(1)	16(3)	18(4)	16(3)	5(3)	5(3)	-4(3)
C(2)	21(4)	17(4)	13(3)	1(3)	-1(3)	-1(3)
C(3)	29(4)	13(4)	24(4)	-4(3)	4(3)	-4(3)
C(4)	35(4)	18(4)	16(3)	-3(3)	1(3)	-2(3)
C(5)	22(4)	23(4)	10(3)	2(3)	-1(3)	-5(3)
C(6)	15(4)	28(4)	19(4)	4(3)	-3(3)	2(3)
C(7)	15(4)	27(4)	28(4)	2(3)	3(3)	2(3)
C(8)	22(4)	25(4)	25(4)	4(3)	12(3)	2(3)
C(9)	13(3)	11(3)	21(3)	-5(3)	9(3)	2(3)
C(10)	18(3)	14(4)	27(4)	-1(3)	9(3)	-1(3)
C(11)	22(4)	15(4)	22(3)	-6(3)	12(3)	0(3)
C(12)	17(3)	22(4)	16(3)	-3(3)	3(3)	-1(3)
C(13)	32(4)	16(4)	23(4)	4(3)	8(3)	-3(3)
O(1)	15(2)	17(3)	15(2)	0(2)	2(2)	2(2)
O(2)	22(3)	17(3)	16(2)	3(2)	4(2)	-1(2)
F(1)	40(3)	39(3)	54(3)	15(3)	27(3)	14(3)
F(2)	46(3)	44(3)	30(3)	9(2)	7(2)	19(3)
F(3)	37(3)	49(4)	46(3)	-10(3)	26(2)	-11(3)
F(4)	39(3)	89(5)	26(3)	0(3)	7(2)	30(3)
F(5)	64(4)	40(3)	50(3)	-28(3)	20(3)	-4(3)
F(6)	57(4)	22(3)	47(3)	-8(2)	15(3)	4(2)
P(1)	24(1)	25(1)	21(1)	-4(1)	7(1)	6(1)
Pt(1)	14(1)	13(1)	12(1)	1(1)	2(1)	0(1)

Table B.12.4 Hydrogen coordinates (x 10^4) and isotropic displacement parameters (Å^{2}x 10^3) for [Pt(cod)(acac)]PF_6.

	x	y	z	U(eq)
H(1)	2815	1572	5564	20
H(2)	2106	2535	6715	22
H(3A)	5086	2765	7954	27
H(3B)	3719	3308	8170	27
H(4A)	5348	2486	9911	29
H(4B)	3588	2510	9760	29
H(5)	4230	1055	10100	23
H(6)	5289	221	8992	27
H(7A)	6448	1694	8223	29
H(7B)	6752	724	7861	29
H(8A)	5577	1783	6219	28
H(8B)	5053	794	6076	28
H(10)	-1324	-482	7466	23
H(12A)	-2277	1065	5633	28
H(12B)	-2532	40	5584	28
H(12C)	-1567	478	4784	28
H(13A)	1427	-1487	9477	35
H(13B)	-335	-1321	9155	35
H(13C)	779	-771	10205	35

Table B.12.5 Hydrogen bonds for [Pt(cod)(acac)]PF_6 [Å and °].

D-H...A	d(D-H)	d(H...A)	d(D...A)	<(DHA)
C(2)-H(2)...F(1)	1.00	2.35	3.138(9)	135.2
C(1)-H(1)...F(3)#1	1.00	2.45	3.230(8)	134.6
C(7)-H(7A)...F(3)#2	0.99	2.52	3.474(10)	160.8
C(5)-H(5)...F(4)#3	1.00	2.53	3.375(9)	142.2
C(8)-H(8B)...F(6)#4	0.99	2.54	3.364(10)	140.9
C(10)-H(10)...F(4)#5	0.95	2.36	3.263(9)	158.3
C(13)-H(13B)...F(4)#5	0.98	2.53	3.422(10)	151.8

Symmetry transformations used to generate equivalent atoms:
#1 x+1/2,-y+1/2,z-1/2 #2 x+1,y,z #3 x+1/2,-y+1/2,z+1/2
#4 -x+1/2,y-1/2,-z+3/2 #5 -x-1/2,y-1/2,-z+3/2

B.13 Crystal Data of [Pt(cod)(thtfac)]BF_4

Table B.13.1 Atomic coordinates (x 10^4) and equivalent isotropic displacement parameters (Å^{2}x 10^3) for [Pt(cod)(thtfac)]BF_4. U(eq) is defined as one third of the trace of the orthogonalized U^{ij} tensor.

	x	y	z	U(eq)
C(16)	534(3)	8428(3)	6849(2)	16(1)
C(17)	-327(3)	7934(3)	6346(3)	17(1)
C(18)	-1316(3)	8367(3)	6282(3)	18(1)
C(112)	2811(3)	8556(3)	9582(3)	22(1)
O(11)	1499(2)	8737(2)	8483(2)	18(1)
F(11)	3138(2)	7855(2)	9307(2)	38(1)
F(12)	3065(2)	8485(2)	10342(2)	28(1)
F(13)	3287(2)	9255(2)	9421(2)	36(1)
C(11)	-1314(3)	8817(3)	7037(3)	16(1)
C(12)	-1112(3)	9709(3)	7185(3)	19(1)

C(13)	-812(3)	10346(3)	6663(3)	22(1)
C(14)	-47(3)	9967(3)	6307(3)	20(1)
C(15)	650(3)	9343(3)	6854(3)	16(1)
C(26)	797(3)	5297(3)	12657(3)	17(1)
C(25)	963(3)	6206(3)	12653(3)	17(1)
C(24)	908(3)	6856(3)	13268(3)	21(1)
C(23)	64(3)	6696(3)	13607(3)	20(1)
C(22)	-831(3)	6352(3)	13008(3)	18(1)
C(21)	-1062(3)	5459(3)	12867(2)	16(1)
C(28)	-445(3)	4695(3)	13263(3)	20(1)
C(27)	635(3)	4815(3)	13343(3)	19(1)
C(109)	1714(3)	8674(3)	9219(3)	16(1)
C(110)	1135(3)	8703(3)	9688(3)	18(1)
C(111)	115(3)	8829(3)	9435(3)	16(1)
C(113)	-431(3)	8832(3)	9986(3)	18(1)
C(114)	-120(3)	8694(3)	10774(3)	24(1)
C(115)	-873(4)	8755(3)	11107(3)	29(1)
C(116)	-1745(4)	8930(3)	10578(3)	26(1)
C(209)	-2091(3)	6422(3)	10620(2)	16(1)
C(210)	-1527(3)	6454(3)	10135(3)	17(1)
C(211)	-519(3)	6237(3)	10351(3)	17(1)
C(212)	-3158(3)	6664(3)	10314(2)	18(1)
C(213)	8(3)	6294(3)	9794(3)	17(1)
C(214)	-315(3)	6556(3)	9024(3)	18(1)
C(215)	435(4)	6529(3)	8675(3)	25(1)
C(216)	1292(4)	6253(3)	9168(3)	29(1)
O(12)	-386(2)	8956(2)	8727(2)	19(1)
O(21)	-1873(2)	6222(2)	11345(2)	17(1)
O(22)	-21(2)	5988(2)	11031(2)	18(1)
F(21)	-3715(2)	5975(2)	10364(2)	26(1)
F(22)	-3386(2)	7316(2)	10723(2)	27(1)
F(23)	-3424(2)	6920(2)	9583(2)	27(1)
S(11)	-1665(1)	9023(1)	9669(1)	23(1)
S(21)	1220(1)	6020(1)	10062(1)	24(1)
Pt(1)	136(1)	8957(1)	7813(1)	13(1)
Pt(2)	-506(1)	5946(1)	11968(1)	13(1)
B(01)	2129(4)	1355(3)	7309(3)	21(1)
F(01)	2183(2)	807(2)	6703(2)	29(1)
F(02)	2752(2)	2063(2)	7353(2)	40(1)
F(03)	1182(2)	1654(2)	7172(2)	27(1)
F(04)	2397(2)	877(2)	7989(2)	33(1)
B(02)	2513(4)	3367(3)	2771(3)	21(1)
F(05)	2762(2)	4132(2)	3205(2)	26(1)
F(06)	2644(2)	3479(2)	2050(2)	36(1)
F(07)	1537(2)	3161(2)	2670(2)	23(1)
F(08)	3093(2)	2672(2)	3160(2)	35(1)

Table B.13.2 Bond lengths [Å] and angles [°] for [Pt(cod)(thtfac)]BF_4.

C(16)-C(15)	1.399(6)	O(11)-C(109)	1.284(5)	C(15)-Pt(1)	2.169(4)
C(16)-C(17)	1.507(6)	O(11)-Pt(1)	2.012(3)	C(15)-H(15)	1.0000
C(16)-Pt(1)	2.155(4)	C(11)-C(12)	1.395(6)	C(26)-C(25)	1.401(6)
C(16)-H(16)	1.0000	C(11)-Pt(1)	2.159(4)	C(26)-C(27)	1.522(6)
C(17)-C(18)	1.546(6)	C(11)-H(11)	1.0000	C(26)-Pt(2)	2.164(4)
C(17)-H(17A)	0.9900	C(12)-C(13)	1.505(6)	C(26)-H(21)	1.0000
C(17)-H(17B)	0.9900	C(12)-Pt(1)	2.153(4)	C(25)-C(24)	1.510(6)
C(18)-C(11)	1.532(6)	C(12)-H(12)	1.0000	C(25)-Pt(2)	2.155(4)
C(18)-H(18A)	0.9900	C(13)-C(14)	1.548(6)	C(25)-H(22)	1.0000
C(18)-H(18B)	0.9900	C(13)-H(13A)	0.9900	C(24)-C(23)	1.539(6)
C(112)-F(11)	1.322(5)	C(13)-H(13B)	0.9900	C(24)-H(23A)	0.9900
C(112)-F(12)	1.324(5)	C(14)-C(15)	1.518(6)	C(24)-H(23B)	0.9900
C(112)-F(13)	1.343(5)	C(14)-H(14A)	0.9900	C(23)-C(22)	1.514(6)
C(112)-C(109)	1.534(6)	C(14)-H(14B)	0.9900	C(23)-H(24A)	0.9900

C(23)-H(24B)	0.9900	F(12)-C(112)-F(13)	106.9(4)	C(27)-C(28)-H(27B)	108.9
C(22)-C(21)	1.401(6)	F(11)-C(112)-C(109)	111.8(4)	H(27A)-C(28)-H(27B)	107.7
C(22)-Pt(2)	2.168(4)	F(12)-C(112)-C(109)	112.9(4)	C(26)-C(27)-C(28)	112.2(4)
C(22)-H(25)	1.0000	F(13)-C(112)-C(109)	110.2(4)	C(26)-C(27)-H(28A)	109.2
C(21)-C(28)	1.508(6)	C(109)-O(11)-Pt(1)	122.2(3)	C(28)-C(27)-H(28A)	109.2
C(21)-Pt(2)	2.153(4)	C(12)-C(11)-C(18)	123.3(4)	C(26)-C(27)-H(28B)	109.2
C(21)-H(26)	1.0000	C(12)-C(11)-Pt(1)	70.9(2)	C(28)-C(27)-H(28B)	109.2
C(28)-C(27)	1.534(6)	C(18)-C(11)-Pt(1)	111.9(3)	H(28A)-C(27)-H(28B)	107.9
C(28)-H(27A)	0.9900	C(12)-C(11)-H(11)	114.4	O(11)-C(109)-C(110)	130.3(4)
C(28)-H(27B)	0.9900	C(18)-C(11)-H(11)	114.4	O(11)-C(109)-C(112)	110.8(4)
C(27)-H(28A)	0.9900	Pt(1)-C(11)-H(11)	114.4	C(110)-C(109)-C(112)	118.9(4)
C(27)-H(28B)	0.9900	C(11)-C(12)-C(13)	125.8(4)	C(109)-C(110)-C(111)	125.0(4)
C(109)-C(110)	1.360(6)	C(11)-C(12)-Pt(1)	71.4(2)	C(109)-C(110)-H(110)	117.5
C(110)-C(111)	1.420(6)	C(13)-C(12)-Pt(1)	108.8(3)	C(111)-C(110)-H(110)	117.5
C(110)-H(110)	0.9500	C(11)-C(12)-H(12)	114.1	O(12)-C(111)-C(110)	124.5(4)
C(111)-O(12)	1.288(5)	C(13)-C(12)-H(12)	114.1	O(12)-C(111)-C(113)	115.4(4)
C(111)-C(113)	1.447(6)	Pt(1)-C(12)-H(12)	114.1	C(110)-C(111)-C(113)	120.2(4)
C(113)-C(114)	1.384(6)	C(12)-C(13)-C(14)	113.5(3)	C(114)-C(113)-C(111)	129.7(4)
C(113)-S(11)	1.727(5)	C(12)-C(13)-H(13A)	108.9	C(114)-C(113)-S(11)	110.9(3)
C(114)-C(115)	1.396(7)	C(14)-C(13)-H(13A)	108.9	C(111)-C(113)-S(11)	119.4(3)
C(114)-H(114)	0.9500	C(12)-C(13)-H(13B)	108.9	C(113)-C(114)-C(115)	112.5(4)
C(115)-C(116)	1.365(7)	C(14)-C(13)-H(13B)	108.9	C(113)-C(114)-H(114)	123.7
C(115)-H(115)	0.9500	H(13A)-C(13)-H(13B)	107.7	C(115)-C(114)-H(114)	123.7
C(116)-S(11)	1.697(5)	C(15)-C(14)-C(13)	112.1(4)	C(116)-C(115)-C(114)	112.5(5)
C(116)-H(116)	0.9500	C(15)-C(14)-H(14A)	109.2	C(116)-C(115)-H(115)	123.7
C(209)-O(21)	1.296(5)	C(13)-C(14)-H(14A)	109.2	C(114)-C(115)-H(115)	123.7
C(209)-C(210)	1.368(6)	C(15)-C(14)-H(14B)	109.2	C(115)-C(116)-S(11)	112.7(4)
C(209)-C(212)	1.520(6)	C(13)-C(14)-H(14B)	109.2	C(115)-C(116)-H(116)	123.7
C(210)-C(211)	1.428(6)	H(14A)-C(14)-H(14B)	107.9	S(11)-C(116)-H(116)	123.7
C(210)-H(210)	0.9500	C(16)-C(15)-C(14)	124.1(4)	O(21)-C(209)-C(210)	130.7(4)
C(211)-O(22)	1.287(5)	C(16)-C(15)-Pt(1)	70.6(2)	O(21)-C(209)-C(212)	110.0(4)
C(211)-C(213)	1.440(6)	C(14)-C(15)-Pt(1)	112.0(3)	C(210)-C(209)-C(212)	119.3(4)
C(212)-F(23)	1.327(5)	C(16)-C(15)-H(15)	114.1	C(209)-C(210)-C(211)	124.6(4)
C(212)-F(22)	1.336(5)	C(14)-C(15)-H(15)	114.1	C(209)-C(210)-H(210)	117.7
C(212)-F(21)	1.338(5)	Pt(1)-C(15)-H(15)	114.1	C(211)-C(210)-H(210)	117.7
C(213)-C(214)	1.394(6)	C(25)-C(26)-C(27)	123.1(4)	O(22)-C(211)-C(210)	124.5(4)
C(213)-S(21)	1.723(5)	C(25)-C(26)-Pt(2)	70.7(2)	O(22)-C(211)-C(213)	115.4(4)
C(214)-C(215)	1.407(6)	C(27)-C(26)-Pt(2)	111.9(3)	C(210)-C(211)-C(213)	120.1(4)
C(214)-H(214)	0.9500	C(25)-C(26)-H(21)	114.4	F(23)-C(212)-F(22)	107.1(3)
C(215)-C(216)	1.361(7)	C(27)-C(26)-H(21)	114.4	F(23)-C(212)-F(21)	107.2(3)
C(215)-H(215)	0.9500	Pt(2)-C(26)-H(21)	114.4	F(22)-C(212)-F(21)	106.8(4)
C(216)-S(21)	1.697(5)	C(26)-C(25)-C(24)	126.4(4)	F(23)-C(212)-C(209)	113.4(4)
C(216)-H(216)	0.9500	C(26)-C(25)-Pt(2)	71.4(2)	F(22)-C(212)-C(209)	111.5(4)
O(12)-Pt(1)	2.017(3)	C(24)-C(25)-Pt(2)	106.7(3)	F(21)-C(212)-C(209)	110.5(3)
O(21)-Pt(2)	2.007(3)	C(26)-C(25)-H(22)	114.4	C(214)-C(213)-C(211)	129.3(4)
O(22)-Pt(2)	2.026(3)	C(24)-C(25)-H(22)	114.4	C(214)-C(213)-S(21)	111.2(3)
B(01)-F(04)	1.385(6)	Pt(2)-C(25)-H(22)	114.4	C(211)-C(213)-S(21)	119.5(3)
B(01)-F(02)	1.389(6)	C(25)-C(24)-C(23)	114.5(3)	C(213)-C(214)-C(215)	111.7(4)
B(01)-F(03)	1.392(6)	C(25)-C(24)-H(23A)	108.6	C(213)-C(214)-H(214)	124.1
B(01)-F(01)	1.401(6)	C(23)-C(24)-H(23A)	108.6	C(215)-C(214)-H(214)	124.1
B(02)-F(06)	1.389(6)	C(25)-C(24)-H(23B)	108.6	C(216)-C(215)-C(214)	112.6(4)
B(02)-F(05)	1.389(6)	C(23)-C(24)-H(23B)	108.6	C(216)-C(215)-H(215)	123.7
B(02)-F(08)	1.401(6)	H(23A)-C(24)-H(23B)	107.6	C(214)-C(215)-H(215)	123.7
B(02)-F(07)	1.402(6)	C(22)-C(23)-C(24)	112.1(4)	C(215)-C(216)-S(21)	113.0(4)
		C(22)-C(23)-H(24A)	109.2	C(215)-C(216)-H(216)	123.5
C(15)-C(16)-C(17)	125.0(4)	C(24)-C(23)-H(24A)	109.2	S(21)-C(216)-H(216)	123.5
C(15)-C(16)-Pt(1)	71.7(2)	C(22)-C(23)-H(24B)	109.2	C(111)-O(12)-Pt(1)	125.7(3)
C(17)-C(16)-Pt(1)	107.9(3)	C(24)-C(23)-H(24B)	109.2	C(209)-O(21)-Pt(2)	121.6(3)
C(15)-C(16)-H(16)	114.5	H(24A)-C(23)-H(24B)	107.9	C(211)-O(22)-Pt(2)	125.5(3)
C(17)-C(16)-H(16)	114.5	C(21)-C(22)-C(23)	124.9(4)	C(116)-S(11)-C(113)	91.3(2)
Pt(1)-C(16)-H(16)	114.5	C(21)-C(22)-Pt(2)	70.5(2)	C(216)-S(21)-C(213)	91.4(2)
C(16)-C(17)-C(18)	114.3(3)	C(23)-C(22)-Pt(2)	111.3(3)	O(11)-Pt(1)-O(12)	92.32(12)
C(16)-C(17)-H(17A)	108.7	C(21)-C(22)-H(25)	114.0	O(11)-Pt(1)-C(12)	157.54(14)
C(18)-C(17)-H(17A)	108.7	C(23)-C(22)-H(25)	114.0	O(12)-Pt(1)-C(12)	88.76(15)
C(16)-C(17)-H(17B)	108.7	Pt(2)-C(22)-H(25)	114.0	O(11)-Pt(1)-C(16)	88.80(14)
C(18)-C(17)-H(17B)	108.7	C(22)-C(21)-C(28)	125.6(4)	O(12)-Pt(1)-C(16)	157.53(13)
H(17A)-C(17)-H(17B)	107.6	C(22)-C(21)-Pt(2)	71.7(2)	C(12)-Pt(1)-C(16)	98.66(17)
C(11)-C(18)-C(17)	111.5(3)	C(28)-C(21)-Pt(2)	109.0(3)	O(11)-Pt(1)-C(11)	164.47(14)
C(11)-C(18)-H(18A)	109.3	C(22)-C(21)-H(26)	114.1	O(12)-Pt(1)-C(11)	90.59(15)
C(17)-C(18)-H(18A)	109.3	C(28)-C(21)-H(26)	114.1	C(12)-Pt(1)-C(11)	37.75(15)
C(11)-C(18)-H(18B)	109.3	Pt(2)-C(21)-H(26)	114.1	C(16)-Pt(1)-C(11)	82.77(16)
C(17)-C(18)-H(18B)	109.3	C(21)-C(28)-C(27)	113.3(3)	O(11)-Pt(1)-C(15)	91.31(14)
H(18A)-C(18)-H(18B)	108.0	C(21)-C(28)-H(27A)	108.9	O(12)-Pt(1)-C(15)	164.35(13)
F(11)-C(112)-F(12)	108.0(4)	C(27)-C(28)-H(27A)	108.9	C(12)-Pt(1)-C(15)	82.15(17)
F(11)-C(112)-F(13)	106.8(4)	C(21)-C(28)-H(27B)	108.9	C(16)-Pt(1)-C(15)	37.76(15)

C(11)-Pt(1)-C(15)	89.96(17)	C(25)-Pt(2)-C(26)	37.87(15)	F(02)-B(01)-F(01)	108.6(4)
O(21)-Pt(2)-O(22)	92.74(12)	O(21)-Pt(2)-C(22)	90.04(15)	F(03)-B(01)-F(01)	109.6(4)
O(21)-Pt(2)-C(21)	88.49(15)	O(22)-Pt(2)-C(22)	160.49(14)	F(06)-B(02)-F(05)	110.4(4)
O(22)-Pt(2)-C(21)	161.49(13)	C(21)-Pt(2)-C(22)	37.83(15)	F(06)-B(02)-F(08)	109.8(4)
O(21)-Pt(2)-C(25)	157.36(15)	C(25)-Pt(2)-C(22)	82.86(17)	F(05)-B(02)-F(08)	109.1(4)
O(22)-Pt(2)-C(25)	87.26(15)	C(26)-Pt(2)-C(22)	90.08(17)	F(06)-B(02)-F(07)	108.5(4)
C(21)-Pt(2)-C(25)	98.63(17)	F(04)-B(01)-F(02)	110.4(4)	F(05)-B(02)-F(07)	110.0(4)
O(21)-Pt(2)-C(26)	164.29(14)	F(04)-B(01)-F(03)	109.3(4)	F(08)-B(02)-F(07)	109.0(4)
O(22)-Pt(2)-C(26)	92.39(15)	F(02)-B(01)-F(03)	110.1(4)		
C(21)-Pt(2)-C(26)	82.01(16)	F(04)-B(01)-F(01)	108.9(4)		

Symmetry transformations used to generate equivalent atoms:

Table B.13.3 Anisotropic displacement parameters ($Å^2 x\ 10^3$) for [Pt(cod)(thtfac)]BF_4. The anisotropic displacement factor exponent takes the form: $-2\pi^2[\ h^2 a^{*2} U^{11} + ... + 2\ h\ k\ a^*\ b^*\ U^{12}\ ]$

	U^{11}	U^{22}	U^{33}	U^{23}	U^{13}	U^{12}
C(16)	16(2)	19(2)	15(2)	0(2)	8(2)	4(2)
C(17)	18(2)	16(2)	19(2)	-7(2)	6(2)	-3(2)
C(18)	16(2)	17(2)	22(2)	1(2)	5(2)	-1(2)
C(112)	19(2)	30(2)	17(2)	2(2)	4(2)	1(2)
O(11)	13(2)	24(1)	16(2)	4(1)	4(1)	7(1)
F(11)	25(2)	46(2)	38(2)	-14(1)	4(1)	14(1)
F(12)	22(2)	44(2)	15(1)	5(1)	1(1)	2(1)
F(13)	18(2)	51(2)	38(2)	14(2)	7(1)	-10(1)
C(11)	13(2)	21(2)	15(2)	0(2)	6(2)	1(2)
C(12)	15(2)	22(2)	18(2)	-2(2)	3(2)	5(2)
C(13)	24(3)	17(2)	25(3)	3(2)	10(2)	4(2)
C(14)	22(2)	19(2)	20(2)	3(2)	7(2)	-2(2)
C(15)	13(2)	20(2)	18(2)	0(2)	9(2)	2(2)
C(26)	13(2)	20(2)	20(2)	0(2)	7(2)	3(2)
C(25)	7(2)	26(2)	17(2)	-2(2)	3(2)	-1(2)
C(24)	16(2)	20(2)	24(3)	-4(2)	1(2)	-3(2)
C(23)	21(2)	20(2)	16(2)	-4(2)	3(2)	-1(2)
C(22)	23(2)	18(2)	16(2)	-3(2)	10(2)	1(2)
C(21)	16(2)	19(2)	17(2)	2(2)	10(2)	-1(2)
C(28)	25(3)	15(2)	24(3)	3(2)	13(2)	3(2)
C(27)	25(3)	16(2)	18(2)	2(2)	9(2)	7(2)
C(109)	13(2)	17(2)	18(2)	2(2)	4(2)	1(2)
C(110)	17(2)	24(2)	13(2)	1(2)	3(2)	-1(2)
C(111)	19(2)	15(2)	15(2)	-3(2)	7(2)	-1(2)
C(113)	15(2)	20(2)	19(2)	-3(2)	4(2)	-1(2)
C(114)	17(2)	41(3)	14(2)	-5(2)	6(2)	-4(2)
C(115)	30(3)	38(3)	19(3)	-5(2)	7(2)	-3(2)
C(116)	24(3)	28(2)	30(3)	-8(2)	15(2)	-7(2)
C(209)	18(2)	16(2)	14(2)	0(2)	4(2)	-2(2)
C(210)	20(2)	17(2)	14(2)	2(2)	5(2)	-1(2)
C(211)	17(2)	16(2)	19(2)	-2(2)	6(2)	-3(2)
C(212)	21(2)	20(2)	12(2)	0(2)	6(2)	1(2)
C(213)	19(2)	20(2)	16(2)	-2(2)	10(2)	-2(2)
C(214)	23(2)	17(2)	15(2)	-1(2)	7(2)	-2(2)
C(215)	36(3)	25(2)	20(3)	-1(2)	16(2)	-5(2)
C(216)	34(3)	32(2)	31(3)	-9(2)	25(3)	-9(2)
O(12)	20(2)	23(2)	16(2)	-2(1)	7(1)	0(1)
O(21)	13(2)	23(1)	16(2)	0(1)	3(1)	0(1)
O(22)	14(2)	27(2)	14(2)	1(1)	5(1)	1(1)
F(21)	18(1)	33(2)	26(2)	2(1)	4(1)	-6(1)
F(22)	24(2)	29(1)	29(2)	-4(1)	11(1)	6(1)
F(23)	22(2)	40(2)	16(1)	11(1)	3(1)	9(1)
S(11)	20(1)	30(1)	21(1)	-2(1)	9(1)	0(1)
S(21)	19(1)	32(1)	24(1)	-1(1)	11(1)	1(1)
Pt(1)	13(1)	15(1)	12(1)	-1(1)	5(1)	1(1)

Pt(2)	13(1)	15(1)	11(1)	1(1)	4(1)	0(1)
B(01)	19(3)	19(2)	26(3)	0(2)	8(2)	0(2)
F(01)	34(2)	29(1)	30(2)	-7(1)	19(1)	-7(1)
F(02)	37(2)	31(2)	50(2)	-5(1)	10(2)	-18(1)
F(03)	28(2)	20(1)	35(2)	0(1)	10(1)	4(1)
F(04)	40(2)	40(2)	27(2)	13(1)	21(2)	20(1)
B(02)	18(3)	20(2)	25(3)	0(2)	9(2)	-1(2)
F(05)	27(2)	21(1)	32(2)	-6(1)	11(1)	-4(1)
F(06)	33(2)	50(2)	32(2)	-4(1)	21(1)	-11(1)
F(07)	20(1)	20(1)	29(2)	0(1)	9(1)	-2(1)
F(08)	25(2)	22(1)	54(2)	2(1)	8(2)	6(1)

Table B.13.4 Hydrogen coordinates (x 10^4) and isotropic displacement parameters ($Å^2$x 10^3) for [Pt(cod)(thtfac)]BF_4.

	x	y	z	U(eq)
H(16)	1155	8087	6993	19
H(17A)	-325	7331	6554	21
H(17B)	-255	7881	5822	21
H(18A)	-1465	8809	5862	22
H(18B)	-1830	7912	6149	22
H(11)	-1793	8569	7281	19
H(12)	-1474	9987	7516	23
H(13A)	-546	10883	6960	26
H(13B)	-1394	10521	6241	26
H(14A)	-381	9649	5825	24
H(14B)	324	10459	6173	24
H(15)	1341	9542	7008	19
H(21)	1140	4942	12354	21
H(22)	1406	6388	12348	20
H(23A)	844	7457	13046	25
H(23B)	1524	6834	13692	25
H(24A)	270	6266	14034	23
H(24B)	-96	7255	13821	23
H(25)	-1409	6746	12914	21
H(26)	-1773	5333	12694	20
H(27A)	-679	4151	12967	24
H(27B)	-523	4621	13782	24
H(28A)	946	5150	13820	23
H(28B)	949	4229	13392	23
H(110)	1436	8633	10226	22
H(114)	534	8573	11057	28
H(115)	-787	8682	11643	35
H(116)	-2334	8993	10706	31
H(210)	-1825	6633	9617	21
H(214)	-961	6731	8766	22
H(215)	351	6687	8153	31
H(216)	1871	6197	9025	35

Table B.13.5 Hydrogen bonds for [Pt(cod)(thtfac)]BF_4 [Å and °].

D-H...A	d(D-H)	d(H...A)	d(D...A)	<(DHA)
C(110)-H(110)...F(12)	0.95	2.31	2.706(5)	104.3
C(210)-H(210)...F(23)	0.95	2.33	2.718(5)	103.6
C(114)-H(114)...F(08)#1	0.95	2.48	3.370(6)	156.2
C(16)-H(16)...F(02)#1	1.00	2.28	3.223(5)	156.4
C(25)-H(22)...F(08)#1	1.00	2.36	3.191(5)	139.8
C(216)-H(216)...F(01)#1	0.95	2.24	3.143(6)	157.5
C(214)-H(214)...F(06)#2	0.95	2.46	3.351(6)	155.5

C(214)-H(214)...F(07)#2	0.95	2.50	3.089(5)	120.4
C(12)-H(12)...F(05)#3	1.00	2.32	3.312(5)	169.7
C(15)-H(15)...F(01)#4	1.00	2.42	3.206(5)	134.6
C(27)-H(28B)...F(07)#5	0.99	2.39	3.231(5)	141.8
C(24)-H(23B)...F(23)#6	0.99	2.48	2.953(5)	109.1
C(115)-H(115)...F(03)#7	0.95	2.44	3.345(6)	159.2
C(22)-H(25)...F(03)#7	1.00	2.46	3.071(5)	118.8
C(116)-H(116)...F(04)#7	0.95	2.41	3.033(6)	123.2
C(21)-H(26)...F(04)#8	1.00	2.34	3.068(5)	128.9

Symmetry transformations used to generate equivalent atoms:
#1 -x+1/2,y+1/2,-z+3/2 #2 -x,-y+1,-z+1 #3 x-1/2,-y+3/2,z+1/2
#4 x,y+1,z #5 x,y,z+1 #6 x+1/2,-y+3/2,z+1/2
#7 -x,-y+1,-z+2 #8 x-1/2,-y+1/2,z+1/2

B.14 Crystal Data of [Pt(cod)(3Br-trop)]PF_6

Table B.14.1 Atomic coordinates (x 10^4) and equivalent isotropic displacement parameters ($Å^2$x 10^3) for [Pt(cod)(3Br-trop)]PF_6. U(eq) is defined as one third of the trace of the orthogonalized U^{ij} tensor.

	x	y	z	U(eq)
C(1)	6703(11)	263(11)	6628(5)	30(3)
C(2)	7056(11)	-927(11)	6544(4)	27(3)
C(3)	7522(12)	-1797(11)	6894(5)	32(3)
C(4)	8855(13)	-1736(13)	6976(5)	41(4)
C(5)	9420(12)	-511(12)	6847(5)	34(3)
C(6)	9020(12)	614(11)	6975(4)	27(3)
C(7)	8046(13)	813(13)	7279(4)	37(3)
C(8)	6828(12)	958(13)	7043(5)	36(3)
F(01)	7884(8)	3622(8)	7037(3)	52(2)
F(02)	8984(9)	4894(9)	6237(3)	57(3)
F(03)	7934(8)	3177(8)	6332(3)	46(2)
F(04)	8978(10)	5303(8)	6932(4)	64(3)
F(05)	9612(7)	3496(8)	6735(3)	54(3)
F(06)	7267(9)	4997(9)	6553(4)	70(3)
C(9)	8337(10)	852(9)	5431(4)	17(2)
C(10)	9540(10)	1134(10)	5604(4)	20(3)
C(11)	10456(10)	1586(9)	5373(4)	20(3)
C(12)	10497(10)	1931(10)	4940(4)	20(2)
C(13)	9595(9)	1833(9)	4618(4)	15(2)
C(14)	8434(9)	1397(9)	4645(4)	16(2)
C(15)	7909(9)	968(10)	4998(4)	18(2)
O(1)	7615(7)	455(7)	5713(3)	24(2)
O(2)	9776(7)	920(7)	6010(3)	23(2)
P(01)	8442(3)	4242(3)	6633(1)	28(1)
Br(1)	6339(1)	458(1)	4890(1)	21(1)
Br(2)	9996(1)	2427(1)	4076(1)	24(1)
Br(3)	11904(1)	1780(1)	5692(1)	25(1)
Pt(1)	8370(1)	268(1)	6317(1)	20(1)

Table B.14.2 Bond lengths [Å] and angles [°] for [Pt(cod)(3Br-trop)]PF_6.

C(1)-C(2)	1.400(17)	C(2)-H(2)	1.0000	C(4)-H(4B)	0.9900
C(1)-C(8)	1.50(2)	C(3)-C(4)	1.52(2)	C(5)-C(6)	1.387(19)
C(1)-Pt(1)	2.178(12)	C(3)-H(3A)	0.9900	C(5)-Pt(1)	2.153(13)
C(1)-H(1)	1.0000	C(3)-H(3B)	0.9900	C(5)-H(5)	1.0000
C(2)-C(3)	1.519(18)	C(4)-C(5)	1.557(19)	C(6)-C(7)	1.512(19)
C(2)-Pt(1)	2.141(12)	C(4)-H(4A)	0.9900	C(6)-Pt(1)	2.167(13)

C(6)-H(6)	1.0000	C(2)-C(3)-H(3B)	108.9	C(11)-C(12)-H(12)	116.5
C(7)-C(8)	1.54(2)	C(4)-C(3)-H(3B)	108.9	C(12)-C(13)-C(14)	129.4(11)
C(7)-H(7A)	0.9900	H(3A)-C(3)-H(3B)	107.8	C(12)-C(13)-Br(2)	114.0(8)
C(7)-H(7B)	0.9900	C(3)-C(4)-C(5)	114.6(11)	C(14)-C(13)-Br(2)	116.6(8)
C(8)-H(8A)	0.9900	C(3)-C(4)-H(4A)	108.6	C(15)-C(14)-C(13)	128.4(11)
C(8)-H(8B)	0.9900	C(5)-C(4)-H(4A)	108.6	C(15)-C(14)-H(14)	115.8
F(01)-P(01)	1.594(9)	C(3)-C(4)-H(4B)	108.6	C(13)-C(14)-H(14)	115.8
F(02)-P(01)	1.580(9)	C(5)-C(4)-H(4B)	108.6	C(14)-C(15)-C(9)	131.0(11)
F(03)-P(01)	1.586(9)	H(4A)-C(4)-H(4B)	107.6	C(14)-C(15)-Br(1)	114.7(9)
F(04)-P(01)	1.591(10)	C(6)-C(5)-C(4)	123.5(13)	C(9)-C(15)-Br(1)	114.3(8)
F(05)-P(01)	1.578(9)	C(6)-C(5)-Pt(1)	71.8(7)	C(9)-O(1)-Pt(1)	114.0(7)
F(06)-P(01)	1.580(10)	C(4)-C(5)-Pt(1)	108.9(9)	C(10)-O(2)-Pt(1)	113.4(7)
C(9)-O(1)	1.311(14)	C(6)-C(5)-H(5)	114.8	F(05)-P(01)-F(06)	177.4(7)
C(9)-C(15)	1.409(16)	C(4)-C(5)-H(5)	114.8	F(05)-P(01)-F(02)	91.7(6)
C(9)-C(10)	1.471(16)	Pt(1)-C(5)-H(5)	114.8	F(06)-P(01)-F(02)	90.2(6)
C(10)-O(2)	1.294(15)	C(5)-C(6)-C(7)	125.0(12)	F(05)-P(01)-F(03)	90.3(5)
C(10)-C(11)	1.391(16)	C(5)-C(6)-Pt(1)	70.7(8)	F(06)-P(01)-F(03)	91.3(6)
C(11)-C(12)	1.402(17)	C(7)-C(6)-Pt(1)	113.1(9)	F(02)-P(01)-F(03)	91.3(5)
C(11)-Br(3)	1.881(12)	C(5)-C(6)-H(6)	113.5	F(05)-P(01)-F(04)	88.7(6)
C(12)-C(13)	1.392(16)	C(7)-C(6)-H(6)	113.5	F(06)-P(01)-F(04)	89.7(6)
C(12)-H(12)	0.9500	Pt(1)-C(6)-H(6)	113.5	F(02)-P(01)-F(04)	88.2(6)
C(13)-C(14)	1.411(14)	C(6)-C(7)-C(8)	113.0(12)	F(03)-P(01)-F(04)	178.9(6)
C(13)-Br(2)	1.887(11)	C(6)-C(7)-H(7A)	109.0	F(05)-P(01)-F(01)	89.4(5)
C(14)-C(15)	1.363(16)	C(8)-C(7)-H(7A)	109.0	F(06)-P(01)-F(01)	88.6(6)
C(14)-H(14)	0.9500	C(6)-C(7)-H(7B)	109.0	F(02)-P(01)-F(01)	178.3(6)
C(15)-Br(1)	1.880(11)	C(8)-C(7)-H(7B)	109.0	F(03)-P(01)-F(01)	89.9(5)
O(1)-Pt(1)	2.024(9)	H(7A)-C(7)-H(7B)	107.8	F(04)-P(01)-F(01)	90.6(6)
O(2)-Pt(1)	2.040(8)	C(1)-C(8)-C(7)	113.2(11)	O(1)-Pt(1)-O(2)	80.3(3)
		C(1)-C(8)-H(8A)	108.9	O(1)-Pt(1)-C(2)	95.9(4)
C(2)-C(1)-C(8)	128.7(13)	C(7)-C(8)-H(8A)	108.9	O(2)-Pt(1)-C(2)	162.1(4)
C(2)-C(1)-Pt(1)	69.7(7)	C(1)-C(8)-H(8B)	108.9	O(1)-Pt(1)-C(5)	158.9(4)
C(8)-C(1)-Pt(1)	109.9(9)	C(7)-C(8)-H(8B)	108.9	O(2)-Pt(1)-C(5)	94.8(5)
C(2)-C(1)-H(1)	113.1	H(8A)-C(8)-H(8B)	107.8	C(2)-Pt(1)-C(5)	82.4(5)
C(8)-C(1)-H(1)	113.1	O(1)-C(9)-C(15)	118.4(10)	O(1)-Pt(1)-C(6)	163.3(4)
Pt(1)-C(1)-H(1)	113.1	O(1)-C(9)-C(10)	115.5(10)	O(2)-Pt(1)-C(6)	98.5(4)
C(1)-C(2)-C(3)	123.3(12)	C(15)-C(9)-C(10)	126.1(10)	C(2)-Pt(1)-C(6)	90.1(5)
C(1)-C(2)-Pt(1)	72.5(7)	O(2)-C(10)-C(11)	116.7(11)	C(5)-Pt(1)-C(6)	37.5(5)
C(3)-C(2)-Pt(1)	113.8(9)	O(2)-C(10)-C(9)	116.8(10)	O(1)-Pt(1)-C(1)	94.6(5)
C(1)-C(2)-H(2)	113.6	C(11)-C(10)-C(9)	126.5(11)	O(2)-Pt(1)-C(1)	159.3(4)
C(3)-C(2)-H(2)	113.6	C(10)-C(11)-C(12)	131.4(11)	C(2)-Pt(1)-C(1)	37.8(5)
Pt(1)-C(2)-H(2)	113.6	C(10)-C(11)-Br(3)	115.3(9)	C(5)-Pt(1)-C(1)	96.7(6)
C(2)-C(3)-C(4)	113.1(11)	C(12)-C(11)-Br(3)	113.3(8)	C(6)-Pt(1)-C(1)	80.7(5)
C(2)-C(3)-H(3A)	108.9	C(13)-C(12)-C(11)	127.0(11)		
C(4)-C(3)-H(3A)	108.9	C(13)-C(12)-H(12)	116.5		

Symmetry transformations used to generate equivalent atoms:

Table B.14.3 Anisotropic displacement parameters ($Å^2$x 10^3) for [Pt(cod)(3Br-trop)]PF_6. The anisotropic displacement factor exponent takes the form: $-2\pi^2[h^2a^{*2}U^{11} + ... + 2 h k a^* b^* U^{12}]$

	U^{11}	U^{22}	U^{33}	U^{23}	U^{13}	U^{12}
C(1)	17(6)	29(7)	45(9)	6(6)	15(6)	1(5)
C(2)	23(7)	22(6)	36(8)	0(5)	11(6)	-3(5)
C(3)	47(9)	18(6)	32(8)	1(5)	16(6)	-6(6)
C(4)	56(10)	38(8)	31(8)	17(6)	10(7)	9(7)
C(5)	26(7)	35(7)	40(9)	8(6)	-8(6)	4(6)
C(6)	37(8)	26(6)	19(7)	11(5)	-1(5)	-7(5)
C(7)	55(9)	32(8)	25(8)	2(6)	13(7)	14(7)
C(8)	35(8)	36(8)	40(9)	-5(6)	18(7)	-8(6)
F(01)	72(7)	45(5)	44(6)	-4(4)	28(5)	-14(5)
F(02)	59(6)	66(6)	47(6)	31(5)	6(5)	-25(5)
F(03)	51(5)	50(5)	36(5)	-8(4)	-1(4)	-5(4)
F(04)	87(8)	34(5)	69(7)	-7(5)	-2(6)	-20(5)
F(05)	36(5)	40(5)	83(8)	24(5)	-14(5)	-5(4)
F(06)	38(6)	53(6)	120(10)	22(6)	8(6)	12(4)
C(9)	18(6)	11(5)	24(7)	-1(4)	8(5)	-1(4)
C(10)	17(6)	10(5)	34(7)	0(5)	10(5)	0(4)
C(11)	16(6)	12(5)	33(7)	-5(5)	7(5)	0(4)
C(12)	20(6)	13(5)	28(7)	-4(5)	13(5)	6(4)

C(13)	13(5)	11(5)	21(6)	-3(4)	4(5)	2(4)
C(14)	11(5)	16(5)	22(6)	7(4)	1(4)	4(4)
C(15)	13(5)	15(5)	26(7)	5(5)	3(5)	4(4)
O(1)	21(4)	29(5)	22(5)	0(3)	7(4)	-6(3)
O(2)	17(4)	30(5)	21(5)	5(4)	2(3)	2(3)
P(01)	29(2)	24(2)	31(2)	4(1)	6(2)	-4(1)
Br(1)	14(1)	24(1)	27(1)	-4(1)	4(1)	-2(1)
Br(2)	20(1)	30(1)	23(1)	7(1)	6(1)	-1(1)
Br(3)	14(1)	35(1)	25(1)	-6(1)	2(1)	-2(1)
Pt(1)	21(1)	21(1)	20(1)	3(1)	6(1)	2(1)

Table B.14.4 Hydrogen coordinates (x 10^4) and isotropic displacement parameters (Å^{2}x 10^3) for [Pt(cod)(3Br-trop)]PF_6.

	x	y	z	U(eq)
H(1)	6021	539	6434	36
H(2)	6565	-1331	6307	32
H(3A)	7297	-2635	6809	38
H(3B)	7145	-1607	7165	38
H(4A)	9215	-2400	6814	49
H(4B)	9050	-1880	7287	49
H(5)	10285	-552	6804	41
H(6)	9652	1247	7001	33
H(7A)	8225	1550	7453	44
H(7B)	8025	115	7479	44
H(8A)	6217	678	7235	44
H(8B)	6685	1829	6982	44
H(12)	11219	2268	4857	24
H(14)	7956	1405	4383	19

Table B.14.5 Hydrogen bonds for [Pt(cod)(3Br-trop)]PF_6 [Å and °].

D-H...A	d(D-H)	d(H...A)	d(D...A)	<(DHA)
C(8)-H(8B)...F(01)	0.99	2.40	3.171(16)	134.3
C(1)-H(1)...F(02)#1	1.00	2.46	3.276(17)	138.0
C(2)-H(2)...Br(3)#1	1.00	2.87	3.654(13)	136.2
C(14)-H(14)...F(03)#2	0.95	2.43	3.359(14)	165.7
C(3)-H(3B)...F(01)#3	0.99	2.49	3.411(16)	154.1
C(5)-H(5)...F(06)#4	1.00	2.50	3.458(18)	160.2

Symmetry transformations used to generate equivalent atoms:
#1 x-1/2,y-1/2,z #2 -x+3/2,-y+1/2,-z+1 #3 -x+3/2,y-1/2,-z+3/2
#4 x+1/2,y-1/2,z

B.15 Crystal Data of [Pt(cod)(3Br-trop)]BF_4

Table B.15.1 Atomic coordinates (x 10^4) and equivalent isotropic displacement parameters ($Å^2$x 10^3) for [Pt(cod)(3Br-trop)]BF_4. U(eq) is defined as one third of the trace of the orthogonalized U^{ij} tensor.

	x	y	z	U(eq)
C(1)	4367(7)	1064(6)	3805(3)	17(1)
C(2)	3668(8)	2789(7)	3765(3)	23(1)
C(3)	1885(8)	3571(7)	4164(4)	27(1)
C(4)	311(9)	2563(7)	4061(4)	33(2)
C(5)	506(8)	1728(7)	3224(3)	26(1)
C(6)	1298(7)	74(7)	3085(3)	17(1)
C(7)	2238(7)	-1108(7)	3744(3)	22(1)
C(8)	3417(7)	-296(6)	4298(3)	17(1)
C(9)	5510(7)	2652(6)	1195(3)	15(1)
C(10)	3990(7)	2061(6)	843(3)	13(1)
C(11)	3804(6)	1960(6)	-23(3)	14(1)
C(12)	4903(6)	2386(6)	-739(3)	14(1)
C(13)	6448(7)	3156(6)	-771(3)	16(1)
C(14)	7323(7)	3679(6)	-113(3)	15(1)
C(15)	6915(6)	3459(6)	753(3)	12(1)
B(1)	7490(9)	-2886(8)	3296(4)	23(1)
O(1)	5518(5)	2516(4)	2012(2)	18(1)
O(2)	2726(5)	1569(4)	1385(2)	18(1)
F(1)	6633(5)	-1990(4)	2626(2)	37(1)
F(2)	7867(4)	-1743(4)	3858(2)	30(1)
F(3)	9133(4)	-3821(4)	3009(2)	30(1)
F(4)	6332(5)	-3944(4)	3691(2)	42(1)
Br(1)	8423(1)	4418(1)	1428(1)	19(1)
Br(2)	7590(1)	3640(1)	-1850(1)	21(1)
Br(3)	1673(1)	1066(1)	-274(1)	17(1)
Pt(1)	3249(1)	1727(1)	2603(1)	17(1)

Table B.15.2 Bond lengths [Å] and angles [°] for [Pt(cod)(3Br-trop)]BF_4.

C(1)-C(2)	1.402(7)	C(9)-C(15)	1.411(7)	Pt(1)-C(1)-H(01)	114.0
C(1)-C(8)	1.518(7)	C(9)-C(10)	1.445(7)	C(1)-C(2)-C(3)	126.2(5)
C(1)-Pt(1)	2.156(5)	C(10)-O(2)	1.301(6)	C(1)-C(2)-Pt(1)	71.1(3)
C(1)-H(01)	1.0000	C(10)-C(11)	1.408(7)	C(3)-C(2)-Pt(1)	110.1(4)
C(2)-C(3)	1.480(7)	C(11)-C(12)	1.395(7)	C(1)-C(2)-H(02)	113.7
C(2)-Pt(1)	2.154(5)	C(11)-Br(3)	1.898(5)	C(3)-C(2)-H(02)	113.7
C(2)-H(02)	1.0000	C(12)-C(13)	1.365(7)	Pt(1)-C(2)-H(02)	113.7
C(3)-C(4)	1.529(9)	C(12)-H(12)	0.9500	C(2)-C(3)-C(4)	112.6(5)
C(3)-H(03A)	0.9900	C(13)-C(14)	1.395(7)	C(2)-C(3)-H(03A)	109.1
C(3)-H(03B)	0.9900	C(13)-Br(2)	1.893(5)	C(4)-C(3)-H(03A)	109.1
C(4)-C(5)	1.521(8)	C(14)-C(15)	1.395(7)	C(2)-C(3)-H(03B)	109.1
C(4)-H(04A)	0.9900	C(14)-H(14)	0.9500	C(4)-C(3)-H(03B)	109.1
C(4)-H(04B)	0.9900	C(15)-Br(1)	1.881(5)	H(03A)-C(3)-H(03B)	107.8
C(5)-C(6)	1.392(7)	B(1)-F(4)	1.374(7)	C(5)-C(4)-C(3)	112.7(5)
C(5)-Pt(1)	2.171(5)	B(1)-F(3)	1.386(7)	C(5)-C(4)-H(04A)	109.0
C(5)-H(05)	1.0000	B(1)-F(1)	1.393(7)	C(3)-C(4)-H(04A)	109.0
C(6)-C(7)	1.511(7)	B(1)-F(2)	1.394(7)	C(5)-C(4)-H(04B)	109.0
C(6)-Pt(1)	2.151(5)	O(1)-Pt(1)	2.008(3)	C(3)-C(4)-H(04B)	109.0
C(6)-H(06)	1.0000	O(2)-Pt(1)	2.030(4)	H(04A)-C(4)-H(04B)	107.8
C(7)-C(8)	1.526(7)			C(6)-C(5)-C(4)	125.9(5)
C(7)-H(07A)	0.9900	C(2)-C(1)-C(8)	124.5(5)	C(6)-C(5)-Pt(1)	70.4(3)
C(7)-H(07B)	0.9900	C(2)-C(1)-Pt(1)	70.9(3)	C(4)-C(5)-Pt(1)	111.7(4)
C(8)-H(08A)	0.9900	C(8)-C(1)-Pt(1)	111.7(3)	C(6)-C(5)-H(05)	113.6
C(8)-H(08B)	0.9900	C(2)-C(1)-H(01)	114.0	C(4)-C(5)-H(05)	113.6
C(9)-O(1)	1.303(6)	C(8)-C(1)-H(01)	114.0	Pt(1)-C(5)-H(05)	113.6

C(5)-C(6)-C(7)	123.9(5)	O(2)-C(10)-C(11)	119.0(4)	F(4)-B(1)-F(2)	110.0(5)
C(5)-C(6)-Pt(1)	72.0(3)	O(2)-C(10)-C(9)	115.7(4)	F(3)-B(1)-F(2)	108.8(5)
C(7)-C(6)-Pt(1)	106.2(3)	C(11)-C(10)-C(9)	125.3(4)	F(1)-B(1)-F(2)	108.9(5)
C(5)-C(6)-H(06)	115.2	C(12)-C(11)-C(10)	132.1(5)	C(9)-O(1)-Pt(1)	114.1(3)
C(7)-C(6)-H(06)	115.2	C(12)-C(11)-Br(3)	113.1(4)	C(10)-O(2)-Pt(1)	113.8(3)
Pt(1)-C(6)-H(06)	115.2	C(10)-C(11)-Br(3)	114.7(3)	O(1)-Pt(1)-O(2)	79.75(14)
C(6)-C(7)-C(8)	115.2(4)	C(13)-C(12)-C(11)	127.2(5)	O(1)-Pt(1)-C(6)	160.29(17)
C(6)-C(7)-H(07A)	108.5	C(13)-C(12)-H(12)	116.4	O(2)-Pt(1)-C(6)	93.89(17)
C(8)-C(7)-H(07A)	108.5	C(11)-C(12)-H(12)	116.4	O(1)-Pt(1)-C(2)	92.67(18)
C(6)-C(7)-H(07B)	108.5	C(12)-C(13)-C(14)	129.2(5)	O(2)-Pt(1)-C(2)	160.55(17)
C(8)-C(7)-H(07B)	108.5	C(12)-C(13)-Br(2)	117.1(4)	C(6)-Pt(1)-C(2)	98.7(2)
H(07A)-C(7)-H(07B)	107.5	C(14)-C(13)-Br(2)	113.7(4)	O(1)-Pt(1)-C(1)	96.67(17)
C(1)-C(8)-C(7)	111.4(4)	C(15)-C(14)-C(13)	129.1(5)	O(2)-Pt(1)-C(1)	160.04(16)
C(1)-C(8)-H(08A)	109.4	C(15)-C(14)-H(14)	115.5	C(6)-Pt(1)-C(1)	82.9(2)
C(7)-C(8)-H(08A)	109.4	C(13)-C(14)-H(14)	115.5	C(2)-Pt(1)-C(1)	37.97(19)
C(1)-C(8)-H(08B)	109.4	C(14)-C(15)-C(9)	129.3(5)	O(1)-Pt(1)-C(5)	161.83(18)
C(7)-C(8)-H(08B)	109.4	C(14)-C(15)-Br(1)	115.3(4)	O(2)-Pt(1)-C(5)	100.68(18)
H(08A)-C(8)-H(08B)	108.0	C(9)-C(15)-Br(1)	115.4(4)	C(6)-Pt(1)-C(5)	37.6(2)
O(1)-C(9)-C(15)	116.6(5)	F(4)-B(1)-F(3)	109.9(5)	C(2)-Pt(1)-C(5)	81.0(2)
O(1)-C(9)-C(10)	116.3(4)	F(4)-B(1)-F(1)	109.0(5)	C(1)-Pt(1)-C(5)	88.8(2)
C(15)-C(9)-C(10)	126.9(5)	F(3)-B(1)-F(1)	110.4(5)		

Symmetry transformations used to generate equivalent atoms:

Table B.15.3 Anisotropic displacement parameters ($Å^2 x\ 10^3$) for [Pt(cod)(3Br-trop)]BF_4. The anisotropic displacement factor exponent takes the form: $-2\pi^2[\ h^2 a^{*2} U^{11} + ... + 2\ h\ k\ a^*\ b^*\ U^{12}\ ]$

	U^{11}	U^{22}	U^{33}	U^{23}	U^{13}	U^{12}
C(1)	24(3)	25(3)	7(2)	0(2)	-4(2)	-13(2)
C(2)	34(3)	23(3)	13(3)	0(2)	-3(2)	-5(2)
C(3)	42(4)	21(3)	16(3)	1(2)	-1(3)	2(2)
C(4)	39(4)	28(3)	26(3)	5(3)	10(3)	2(3)
C(5)	19(3)	38(3)	20(3)	4(3)	7(2)	-5(2)
C(6)	7(2)	30(3)	16(3)	-1(2)	2(2)	-9(2)
C(7)	22(3)	23(3)	22(3)	1(2)	0(2)	-11(2)
C(8)	18(3)	22(3)	12(3)	0(2)	-6(2)	-1(2)
C(9)	19(3)	10(2)	17(3)	1(2)	-5(2)	1(2)
C(10)	12(2)	13(2)	14(3)	3(2)	-1(2)	-3(2)
C(11)	14(2)	12(2)	16(3)	-3(2)	0(2)	-6(2)
C(12)	13(2)	12(2)	15(3)	1(2)	0(2)	0(2)
C(13)	16(3)	15(2)	15(3)	-2(2)	5(2)	-5(2)
C(14)	14(2)	9(2)	24(3)	-1(2)	-4(2)	-6(2)
C(15)	9(2)	12(2)	15(3)	1(2)	-9(2)	-2(2)
B(1)	22(3)	29(3)	18(3)	0(3)	0(3)	-7(3)
O(1)	21(2)	23(2)	13(2)	2(2)	-3(2)	-10(2)
O(2)	16(2)	20(2)	17(2)	7(2)	1(2)	-7(2)
F(1)	46(2)	41(2)	25(2)	-6(2)	-15(2)	2(2)
F(2)	25(2)	42(2)	23(2)	-10(2)	-4(1)	-2(1)
F(3)	24(2)	37(2)	28(2)	-7(2)	2(1)	-4(1)
F(4)	31(2)	44(2)	54(2)	-5(2)	11(2)	-20(2)
Br(1)	20(1)	21(1)	17(1)	2(1)	-7(1)	-10(1)
Br(2)	24(1)	28(1)	14(1)	-1(1)	3(1)	-14(1)
Br(3)	14(1)	19(1)	18(1)	1(1)	-2(1)	-9(1)
Pt(1)	20(1)	21(1)	12(1)	2(1)	1(1)	-7(1)

Table B.15.4 Hydrogen coordinates (x 10^4) and isotropic displacement parameters ($Å^2 x\ 10^3$) for [Pt(cod)(3Br-trop)]BF_4.

	x	y	z	U(eq)
H(01)	5743	829	3773	21
H(02)	4642	3550	3708	28
H(03A)	1578	4729	3911	33
H(03B)	2007	3660	4771	33
H(04A)	276	1681	4525	40

H(04B)	-871	3329	4106	40
H(05)	-503	2161	2851	32
H(06)	742	-489	2649	21
H(07A)	3028	-2040	3457	26
H(07B)	1282	-1612	4111	26
H(08A)	2629	209	4776	21
H(08B)	4356	-1175	4530	21
H(12)	4534	2110	-1263	17
H(14)	8340	4268	-278	18

Table B.15.5 Hydrogen bonds for [Pt(cod)(3Br-trop)]BF_4 [Å and °].

D-H...A	d(D-H)	d(H...A)	d(D...A)	<(DHA)
C(1)-H(01)...F(2)	1.00	2.40	3.167(6)	132.7
C(2)-H(02)...F(4)#1	1.00	2.51	3.477(7)	163.9
C(3)-H(03A)...F(3)#2	0.99	2.51	3.281(6)	135.1
C(12)-H(12)...F(1)#3	0.95	2.42	3.356(6)	168.8
C(5)-H(05)...Br(1)#4	1.00	2.90	3.767(6)	145.7

Symmetry transformations used to generate equivalent atoms:
#1 x,y+1,z #2 x-1,y+1,z #3 -x+1,-y,-z #4 x-1,y,z

B.16 Crystal Data of [Pt(cod)(trop)]PF_6

Table B.16.1 Atomic coordinates (x 10^4) and equivalent isotropic displacement parameters (Å^{2}x 10^3) for [Pt(cod)(trop)]PF_6. U(eq) is defined as one third of the trace of the orthogonalized U^{ij} tensor.

	x	y	z	U(eq)
C(1)	749(10)	3252(7)	1137(11)	122(4)
C(2)	1472(8)	2731(8)	1166(9)	111(3)
C(3)	2313(7)	2882(10)	537(11)	156(6)
C(8)	629(10)	4094(7)	520(12)	177(7)
C(9)	-495(4)	1033(4)	596(5)	40(1)
C(10)	-993(4)	562(4)	1283(5)	50(1)
C(11)	-1597(4)	4(4)	1024(6)	55(2)
C(12)	-1877(6)	-244(6)	0	58(2)
O(1)	32(3)	1529(3)	1075(3)	53(1)
F(1)	-1090(10)	3450(10)	1260(13)	255(6)
F(2)	-1301(7)	2760(5)	2711(12)	213(5)
F(3)	-1189(10)	4407(7)	2133(15)	277(8)
P(1)	-1417(2)	3583(2)	2500	122(2)
Pt(1)	630(1)	2241(1)	0	47(1)

Table B.16.2 Bond lengths [Å] and angles [°] for [Pt(cod)(trop)]PF_6.

C(1)-C(2)	1.460(19)	C(9)-C(10)	1.393(8)	P(1)-F(3)#2	1.468(11)
C(1)-C(8)	1.578(19)	C(9)-C(9)#1	1.434(11)	P(1)-F(1)#2	1.599(15)
C(1)-Pt(1)	2.155(10)	C(10)-C(11)	1.381(10)	Pt(1)-O(1)#1	1.999(4)
C(1)-H(1)	1.0000	C(10)-H(10)	0.9500	Pt(1)-C(2)#1	2.123(9)
C(2)-C(3)	1.591(18)	C(11)-C(12)	1.375(9)	Pt(1)-C(1)#1	2.155(10)
C(2)-Pt(1)	2.123(9)	C(11)-H(11)	0.9500		
C(2)-H(2)	1.0000	C(12)-C(11)#1	1.375(9)	C(2)-C(1)-C(8)	128.5(12)
C(3)-C(3)#1	1.29(3)	C(12)-H(12)	0.9500	C(2)-C(1)-Pt(1)	68.8(6)
C(3)-H(3A)	0.9900	O(1)-Pt(1)	1.999(4)	C(8)-C(1)-Pt(1)	111.2(9)
C(3)-H(3B)	0.9900	F(1)-P(1)	1.599(15)	C(2)-C(1)-H(1)	113.1
C(8)-C(8)#1	1.25(3)	F(2)-P(1)	1.384(9)	C(8)-C(1)-H(1)	113.1
C(8)-H(8A)	0.9900	F(3)-P(1)	1.468(11)	Pt(1)-C(1)-H(1)	113.1
C(8)-H(8B)	0.9900	F(3)-F(3)#2	1.64(3)	C(1)-C(2)-C(3)	126.9(12)
C(9)-O(1)	1.317(7)	P(1)-F(2)#2	1.384(9)	C(1)-C(2)-Pt(1)	71.3(6)

C(3)-C(2)-Pt(1)	107.9(7)	C(11)-C(10)-H(10)	114.7	F(2)-P(1)-F(1)#2	100.0(8)
C(1)-C(2)-H(2)	114.0	C(9)-C(10)-H(10)	114.7	F(2)#2-P(1)-F(1)#2	89.6(9)
C(3)-C(2)-H(2)	114.0	C(12)-C(11)-C(10)	129.4(7)	F(3)#2-P(1)-F(1)#2	76.1(9)
Pt(1)-C(2)-H(2)	114.0	C(12)-C(11)-H(11)	115.3	F(3)-P(1)-F(1)#2	90.4(10)
C(3)#1-C(3)-C(2)	118.4(6)	C(10)-C(11)-H(11)	115.3	F(1)-P(1)-F(1)#2	163.8(13)
C(3)#1-C(3)-H(3A)	107.7	C(11)#1-C(12)-C(11)	127.1(9)	O(1)-Pt(1)-O(1)#1	80.6(2)
C(2)-C(3)-H(3A)	107.7	C(11)#1-C(12)-H(12)	116.4	O(1)-Pt(1)-C(2)	96.4(3)
C(3)#1-C(3)-H(3B)	107.7	C(11)-C(12)-H(12)	116.4	O(1)#1-Pt(1)-C(2)	165.0(5)
C(2)-C(3)-H(3B)	107.7	C(9)-O(1)-Pt(1)	113.5(3)	O(1)-Pt(1)-C(2)#1	165.0(5)
H(3A)-C(3)-H(3B)	107.1	P(1)-F(3)-F(3)#2	56.1(7)	O(1)#1-Pt(1)-C(2)#1	96.4(3)
C(8)#1-C(8)-C(1)	118.0(7)	F(2)-P(1)-F(2)#2	107.5(10)	C(2)-Pt(1)-C(2)#1	82.6(6)
C(8)#1-C(8)-H(8A)	107.8	F(2)-P(1)-F(3)#2	93.8(7)	O(1)-Pt(1)-C(1)	94.7(4)
C(1)-C(8)-H(8A)	107.8	F(2)#2-P(1)-F(3)#2	156.2(10)	O(1)#1-Pt(1)-C(1)	154.5(5)
C(8)#1-C(8)-H(8B)	107.8	F(2)-P(1)-F(3)	156.2(10)	C(2)-Pt(1)-C(1)	39.9(5)
C(1)-C(8)-H(8B)	107.8	F(2)#2-P(1)-F(3)	93.8(7)	C(2)#1-Pt(1)-C(1)	94.0(4)
H(8A)-C(8)-H(8B)	107.1	F(3)#2-P(1)-F(3)	67.8(13)	O(1)-Pt(1)-C(1)#1	154.5(5)
O(1)-C(9)-C(10)	117.7(5)	F(2)-P(1)-F(1)	89.6(9)	O(1)#1-Pt(1)-C(1)#1	94.7(4)
O(1)-C(9)-C(9)#1	115.9(3)	F(2)#2-P(1)-F(1)	100.0(8)	C(2)-Pt(1)-C(1)#1	94.0(4)
C(10)-C(9)-C(9)#1	126.3(4)	F(3)#2-P(1)-F(1)	90.4(10)	C(2)#1-Pt(1)-C(1)#1	39.9(5)
C(11)-C(10)-C(9)	130.7(6)	F(3)-P(1)-F(1)	76.1(9)	C(1)-Pt(1)-C(1)#1	78.7(8)

Symmetry transformations used to generate equivalent atoms:
#1 x,y,-z #2 y-1/2,x+1/2,-z+1/2

Table B.16.3 Anisotropic displacement parameters ($Å^2 x\ 10^3$) for [Pt(cod)(trop)]PF_6. The anisotropic displacement factor exponent takes the form: $-2\pi^2[\ h^2 a^{*2} U^{11} + ... + 2\ h\ k\ a^*\ b^*\ U^{12}\ ]$

	U^{11}	U^{22}	U^{33}	U^{23}	U^{13}	U^{12}
C(1)	173(9)	92(6)	100(8)	-45(5)	32(8)	-66(6)
C(2)	136(8)	129(8)	69(5)	4(6)	-25(6)	-92(5)
C(3)	97(7)	229(15)	141(11)	48(10)	-42(6)	-86(8)
C(8)	270(17)	59(5)	203(18)	-23(7)	67(13)	-47(7)
C(9)	44(3)	41(3)	35(3)	2(2)	-2(2)	3(2)
C(10)	53(4)	56(4)	40(3)	9(3)	0(3)	-5(3)
C(11)	56(4)	50(4)	58(4)	13(3)	6(3)	-1(3)
C(12)	50(6)	42(5)	81(6)	0	0	-8(4)
O(1)	60(3)	64(3)	36(2)	2(2)	-6(2)	-19(2)
F(1)	256(14)	314(14)	195(9)	-49(9)	34(11)	-22(13)
F(2)	224(11)	123(6)	294(13)	28(7)	-68(10)	84(7)
F(3)	400(20)	140(7)	287(19)	43(8)	95(17)	-66(11)
P(1)	95(2)	95(2)	175(5)	24(2)	-24(2)	1(2)
Pt(1)	50(1)	41(1)	50(1)	0	0	-7(1)

Table B.16.4 Hydrogen coordinates ($x\ 10^4$) and isotropic displacement parameters ($Å^2 x\ 10^3$) for [Pt(cod)(trop)]PF_6.

	x	y	z	U(eq)
H(1)	398	3195	1813	146
H(2)	1525	2402	1862	134
H(3A)	2531	3415	788	187
H(3B)	2703	2458	788	187
H(8A)	104	4331	772	213
H(8B)	1068	4468	772	213
H(10)	-903	637	2056	60
H(11)	-1857	-245	1644	66
H(12)	-2311	-629	0	69

Table B.16.5 Hydrogen bonds for [Pt(cod)(trop)]PF_6 [Å and °].

D-H...A	d(D-H)	d(H...A)	d(D...A)	<(DHA)
C(8)-H(8A)...F(1)	0.99	2.50	3.13(2)	121.7
C(1)-H(1)...F(3)#2	1.00	2.29	3.16(2)	144.6
C(3)-H(3B)...F(1)#3	0.99	2.54	3.51(2)	168.8

C(8)-H(8B)...F(3)#4	0.99	2.47	3.258(17)	136.1
C(11)-H(11)...F(2)#5	0.95	2.40	3.241(11)	146.8

Symmetry transformations used to generate equivalent atoms:
#1 x,y,-z #2 y-1/2,x+1/2,-z+1/2 #3 x+1/2,-y+1/2,z
#4 -x,-y+1,z #5 -y,x,-z+1/2

B.17 Crystal Data of [Pt(cod)(trop)]BF_4

Table B.17.1 Atomic coordinates (x 10^4) and equivalent isotropic displacement parameters ($Å^2$x 10^3) for [Pt(cod)(trop)]BF_4. U(eq) is defined as one third of the trace of the orthogonalized U^{ij} tensor.

	x	y	z	U(eq)
C(1)	9241(14)	3169(8)	2751(18)	82(3)
C(2)	8498(9)	2627(10)	2830(17)	65(3)
C(3)	7753(16)	2990(20)	3490(20)	114(6)
C(4)	7748(18)	2830(20)	4680(30)	135(7)
C(5)	8751(13)	2844(12)	5169(19)	98(5)
C(6)	9306(16)	3384(12)	5070(19)	103(5)
C(7)	9144(12)	4059(11)	4760(16)	101(5)
C(8)	9426(11)	4056(8)	3600(12)	82(3)
C(9)	10559(11)	960(12)	3414(19)	36(3)
C(10)	10572(12)	999(12)	4620(17)	38(3)
C(11)	11092(12)	510(11)	5261(16)	41(3)
C(12)	11643(15)	-61(13)	5070(20)	55(4)
C(13)	11962(5)	-297(5)	4020(30)	55(3)
C(14)	11704(13)	-55(11)	3000(20)	47(4)
C(15)	11000(12)	491(13)	2690(20)	58(5)
B(01)	11340(20)	3558(18)	1580(60)	155(7)
O(1)	10025(8)	1516(9)	2846(12)	48(3)
O(2)	10049(10)	1458(10)	5009(12)	55(4)
F(1)	12167(12)	3772(11)	1124(18)	192(9)
F(2)	11079(15)	3710(11)	390(20)	289(13)
F(3)	11262(12)	2805(9)	1401(17)	167(7)
F(4)	11061(14)	4258(12)	1800(20)	243(13)
Pt(1)	9430(1)	2223(1)	3935(4)	46(1)

Table B.17.2 Bond lengths [Å] and angles [°] for [Pt(cod)(trop)]BF_4

C(1)-C(2)	1.48(2)	C(8)-H(8A)	0.9700		
C(1)-C(8)	1.78(2)	C(8)-H(8B)	0.9700	C(2)-C(1)-C(8)	124.8(17)
C(1)-Pt(1)	2.098(17)	C(9)-C(15)	1.35(3)	C(2)-C(1)-Pt(1)	69.4(9)
C(1)-H(1)	0.9800	C(9)-O(1)	1.41(2)	C(8)-C(1)-Pt(1)	100.0(11)
C(2)-C(3)	1.55(3)	C(9)-C(10)	1.440(11)	C(2)-C(1)-H(1)	116.5
C(2)-Pt(1)	2.100(16)	C(10)-O(2)	1.21(2)	C(8)-C(1)-H(1)	116.4
C(2)-H(2)	0.9800	C(10)-C(11)	1.38(3)	Pt(1)-C(1)-H(1)	116.3
C(3)-C(4)	1.44(2)	C(11)-C(12)	1.29(3)	C(1)-C(2)-C(3)	115.8(18)
C(3)-H(3A)	0.9700	C(11)-H(11)	0.9300	C(1)-C(2)-Pt(1)	69.3(10)
C(3)-H(3B)	0.9700	C(12)-C(13)	1.41(3)	C(3)-C(2)-Pt(1)	110.4(14)
C(4)-C(5)	1.71(4)	C(12)-H(12)	0.9300	C(1)-C(2)-H(2)	117.1
C(4)-H(4A)	0.9700	C(13)-C(14)	1.34(4)	C(3)-C(2)-H(2)	117.6
C(4)-H(4B)	0.9700	C(13)-H(13)	0.9300	Pt(1)-C(2)-H(2)	117.3
C(5)-C(6)	1.25(3)	C(14)-C(15)	1.48(3)	C(4)-C(3)-C(2)	116(3)
C(5)-Pt(1)	2.09(2)	C(14)-H(14)	0.9300	C(4)-C(3)-H(3A)	108.6
C(5)-H(5)	0.9800	C(15)-H(15)	0.9300	C(2)-C(3)-H(3A)	108.5
C(6)-C(7)	1.18(2)	B(01)-F(3)	1.23(4)	C(4)-C(3)-H(3B)	107.9
C(6)-Pt(1)	2.32(2)	B(01)-F(4)	1.24(3)	C(2)-C(3)-H(3B)	108.0
C(6)-H(6)	0.9800	B(01)-F(1)	1.48(4)	H(3A)-C(3)-H(3B)	107.4
C(7)-C(8)	1.457(19)	B(01)-F(2)	1.50(7)	C(3)-C(4)-C(5)	109(2)
C(7)-H(7A)	0.9700	O(1)-Pt(1)	1.974(15)	C(3)-C(4)-H(4A)	110.1
C(7)-H(7B)	0.9700	O(2)-Pt(1)	2.037(15)	C(5)-C(4)-H(4A)	109.8

C(3)-C(4)-H(4B)	109.7	C(7)-C(8)-H(8B)	107.6	F(3)-B(01)-F(4)	153(4)
C(5)-C(4)-H(4B)	109.9	C(1)-C(8)-H(8B)	107.3	F(3)-B(01)-F(1)	105(3)
H(4A)-C(4)-H(4B)	108.2	H(8A)-C(8)-H(8B)	106.9	F(4)-B(01)-F(1)	101(3)
C(6)-C(5)-C(4)	130(2)	C(15)-C(9)-O(1)	111(2)	F(3)-B(01)-F(2)	88(4)
C(6)-C(5)-Pt(1)	83.8(15)	C(15)-C(9)-C(10)	131(2)	F(4)-B(01)-F(2)	87(3)
C(4)-C(5)-Pt(1)	104.4(16)	O(1)-C(9)-C(10)	117(2)	F(1)-B(01)-F(2)	82(3)
C(6)-C(5)-H(5)	111.2	O(2)-C(10)-C(11)	124(2)	C(9)-O(1)-Pt(1)	110.1(14)
C(4)-C(5)-H(5)	111.0	O(2)-C(10)-C(9)	114(2)	C(10)-O(2)-Pt(1)	117.8(15)
Pt(1)-C(5)-H(5)	111.1	C(11)-C(10)-C(9)	123(2)	O(1)-Pt(1)-O(2)	80.2(2)
C(7)-C(6)-C(5)	121(3)	C(12)-C(11)-C(10)	136(2)	O(1)-Pt(1)-C(5)	173.4(7)
C(7)-C(6)-Pt(1)	125.5(18)	C(12)-C(11)-H(11)	111.5	O(2)-Pt(1)-C(5)	95.8(7)
C(5)-C(6)-Pt(1)	63.7(13)	C(10)-C(11)-H(11)	112.3	O(1)-Pt(1)-C(1)	92.5(7)
C(7)-C(6)-H(6)	112.7	C(11)-C(12)-C(13)	126(2)	O(2)-Pt(1)-C(1)	158.8(8)
C(5)-C(6)-H(6)	112.7	C(11)-C(12)-H(12)	117.1	C(5)-Pt(1)-C(1)	93.0(8)
Pt(1)-C(6)-H(6)	112.8	C(13)-C(12)-H(12)	116.4	O(1)-Pt(1)-C(2)	96.4(7)
C(6)-C(7)-C(8)	103.1(16)	C(14)-C(13)-C(12)	128.1(8)	O(2)-Pt(1)-C(2)	158.6(6)
C(6)-C(7)-H(7A)	111.2	C(14)-C(13)-H(13)	116.6	C(5)-Pt(1)-C(2)	85.5(5)
C(8)-C(7)-H(7A)	111.0	C(12)-C(13)-H(13)	115.2	C(1)-Pt(1)-C(2)	41.4(6)
C(6)-C(7)-H(7B)	111.4	C(13)-C(14)-C(15)	130(2)	O(1)-Pt(1)-C(6)	153.0(8)
C(8)-C(7)-H(7B)	110.9	C(13)-C(14)-H(14)	115.6	O(2)-Pt(1)-C(6)	99.3(8)
H(7A)-C(7)-H(7B)	109.1	C(15)-C(14)-H(14)	114.9	C(5)-Pt(1)-C(6)	32.5(7)
C(7)-C(8)-C(1)	119.5(15)	C(9)-C(15)-C(14)	125(2)	C(1)-Pt(1)-C(6)	78.3(6)
C(7)-C(8)-H(8A)	107.3	C(9)-C(15)-H(15)	117.2	C(2)-Pt(1)-C(6)	93.2(8)
C(1)-C(8)-H(8A)	107.5	C(14)-C(15)-H(15)	118.0		

Symmetry transformations used to generate equivalent atoms:

Table B.17.3 Anisotropic displacement parameters ($Å^2$x 10^3) for [Pt(cod)(trop)]BF_4. The anisotropic displacement factor exponent takes the form: $-2\pi^2[h^2a^{*2}U^{11} + ... + 2 h k a^* b^* U^{12}]$

	U^{11}	U^{22}	U^{33}	U^{23}	U^{13}	U^{12}
C(1)	119(7)	23(4)	103(6)	15(4)	6(6)	0(4)
C(2)	40(6)	65(8)	90(6)	13(6)	-16(5)	20(4)
C(3)	68(7)	149(15)	127(12)	-24(12)	2(7)	52(9)
C(4)	96(10)	160(20)	149(12)	51(16)	50(11)	44(11)
C(5)	140(15)	75(10)	78(6)	1(9)	15(8)	64(8)
C(6)	143(13)	86(8)	80(6)	-23(6)	4(9)	43(9)
C(7)	128(14)	58(7)	118(10)	-11(7)	16(10)	27(8)
C(8)	119(7)	23(4)	103(6)	15(4)	6(6)	0(4)
C(9)	30(8)	33(8)	45(5)	4(6)	-10(6)	-1(5)
C(10)	49(9)	28(8)	36(5)	0(6)	-5(7)	-6(5)
C(11)	44(8)	42(8)	36(6)	9(6)	-10(6)	-12(5)
C(12)	67(11)	47(10)	50(6)	12(8)	-13(9)	-1(7)
C(13)	52(5)	37(4)	77(8)	4(11)	-8(11)	8(3)
C(14)	39(8)	44(9)	58(7)	-13(7)	-5(7)	3(6)
C(15)	50(10)	65(11)	59(9)	-10(8)	-3(8)	18(7)
B(01)	100(16)	51(9)	310(20)	23(16)	-48(17)	-11(7)
O(1)	47(7)	53(7)	43(4)	6(5)	-10(5)	21(5)
O(2)	69(9)	57(7)	38(5)	7(6)	5(5)	11(5)
F(1)	155(11)	131(14)	290(20)	-100(15)	35(11)	-50(10)
F(2)	370(30)	128(11)	370(30)	-62(12)	-240(20)	76(14)
F(3)	183(14)	121(8)	196(13)	-80(8)	-6(10)	-69(9)
F(4)	270(30)	116(9)	340(30)	-14(12)	100(20)	42(15)
Pt(1)	44(1)	37(1)	56(1)	0(1)	0(1)	4(1)

Table B.17.4 Hydrogen coordinates (x 10^4) and isotropic displacement parameters ($Å^2$x 10^3) for [Pt(cod)(trop)]BF_4.

	x	y	z	U(eq)
H(1)	9565	3129	2057	98
H(2)	8371	2271	2186	78
H(3A)	7743	3587	3374	137
H(3B)	7245	2765	3176	137
H(4A)	7494	2299	4833	163

H(4B)	7425	3260	5060	163
H(5)	8793	2558	5892	117
H(6)	9700	3381	5695	123
H(7A)	9437	4475	5196	121
H(7B)	8551	4164	4807	121
H(8A)	10021	4154	3606	98
H(8B)	9171	4529	3230	98
H(11)	11032	617	6022	49
H(12)	11848	-343	5693	65
H(13)	12407	-666	4029	66
H(14)	12013	-260	2400	57
H(15)	10850	514	1934	69

Table B.17.5 Hydrogen bonds for [Pt(cod)(trop)]BF_4 [Å and °].

D-H...A	d(D-H)	d(H...A)	d(D...A)	<(DHA)
C(4)-H(4A)...F(3)#1	0.97	2.55	3.38(3)	143.1
C(4)-H(4A)...F(1)#1	0.97	2.56	3.18(3)	121.6
C(6)-H(6)...F(4)#2	0.98	2.31	3.22(4)	154.3
C(14)-H(14)...F(1)#3	0.93	2.55	3.44(3)	161.5
C(11)-H(11)...O(1)#4	0.93	2.53	3.28(2)	137.5
C(12)-H(12)...F(3)#4	0.93	2.29	3.12(3)	148.0

Symmetry transformations used to generate equivalent atoms:
#1 -y+1,x-1,z+1/2 #2 -y+3/2,-x+3/2,z+1/2 #3 -x+5/2,y-1/2,z
#4 y+1,-x+1,z+1/2

B.18 Crystal Data of [Pt(cod)(NH-acac)]BF_4

Table B.18.1 Atomic coordinates (x 10^4) and equivalent isotropic displacement parameters (Å^{2}x 10^3) for [Pt(cod)(NH-acac)]BF_4. U(eq) is defined as one third of the trace of the orthogonalized U^{ij} tensor.

	x	y	z	U(eq)
C(1)	6369(3)	2563(2)	3670(3)	20(1)
C(2)	6930(4)	3268(2)	4556(3)	20(1)
C(3)	8471(4)	3696(3)	4952(3)	28(1)
C(4)	9526(4)	3071(3)	5947(3)	28(1)
C(5)	9205(3)	1920(3)	5886(3)	23(1)
C(6)	8817(3)	1303(3)	4919(3)	18(1)
C(7)	8761(4)	1700(2)	3764(3)	20(1)
C(8)	7222(4)	2069(3)	3022(3)	22(1)
C(9)	4159(3)	1357(2)	5708(3)	17(1)
C(10)	4850(3)	586(2)	6506(2)	17(1)
C(11)	6245(3)	229(2)	6770(2)	18(1)
C(12)	6843(4)	-601(2)	7648(3)	25(1)
C(13)	2593(4)	1597(2)	5474(3)	23(1)
B(1)	12322(4)	1045(3)	8588(3)	22(1)
N(1)	4814(3)	1891(2)	5144(2)	18(1)
O(1)	7173(2)	542(2)	6321(2)	19(1)
F(1)	10991(2)	1147(2)	8688(2)	41(1)
F(2)	12656(3)	1962(2)	8137(2)	35(1)
F(3)	12312(3)	226(2)	7891(2)	47(1)
F(4)	13377(2)	901(2)	9645(2)	44(1)
Pt(1)	6847(1)	1730(1)	5231(1)	14(1)

Table B.18.2 Bond lengths [Å] and angles [°] for [Pt(cod)(NH-acac)]BF_4.

C(1)-C(2)	1.395(5)	C(8)-C(1)-Pt(1)	108.1(2)	N(1)-C(9)-C(13)	117.2(3)
C(1)-C(8)	1.511(4)	C(2)-C(1)-H(1)	114.4	C(10)-C(9)-C(13)	119.2(3)
C(1)-Pt(1)	2.152(3)	C(8)-C(1)-H(1)	114.4	C(11)-C(10)-C(9)	126.5(3)
C(1)-H(1)	1.0000	Pt(1)-C(1)-H(1)	114.4	C(11)-C(10)-H(10)	116.7
C(2)-C(3)	1.522(4)	C(1)-C(2)-C(3)	124.1(3)	C(9)-C(10)-H(10)	116.7
C(2)-Pt(1)	2.168(3)	C(1)-C(2)-Pt(1)	70.52(17)	O(1)-C(11)-C(10)	126.1(3)
C(2)-H(2)	1.0000	C(3)-C(2)-Pt(1)	112.0(2)	O(1)-C(11)-C(12)	113.2(3)
C(3)-C(4)	1.543(5)	C(1)-C(2)-H(2)	114.1	C(10)-C(11)-C(12)	120.7(3)
C(3)-H(3A)	0.9900	C(3)-C(2)-H(2)	114.1	C(11)-C(12)-H(12A)	109.5
C(3)-H(3B)	0.9900	Pt(1)-C(2)-H(2)	114.1	C(11)-C(12)-H(12B)	109.5
C(4)-C(5)	1.511(5)	C(2)-C(3)-C(4)	112.4(3)	H(12A)-C(12)-H(12B)	109.5
C(4)-H(4A)	0.9900	C(2)-C(3)-H(3A)	109.1	C(11)-C(12)-H(12C)	109.5
C(4)-H(4B)	0.9900	C(4)-C(3)-H(3A)	109.1	H(12A)-C(12)-H(12C)	109.5
C(5)-C(6)	1.396(5)	C(2)-C(3)-H(3B)	109.1	H(12B)-C(12)-H(12C)	109.5
C(5)-Pt(1)	2.183(3)	C(4)-C(3)-H(3B)	109.1	C(9)-C(13)-H(13A)	109.5
C(5)-H(5)	1.0000	H(3A)-C(3)-H(3B)	107.9	C(9)-C(13)-H(13B)	109.5
C(6)-C(7)	1.535(4)	C(5)-C(4)-C(3)	113.7(3)	H(13A)-C(13)-H(13B)	109.5
C(6)-Pt(1)	2.187(3)	C(5)-C(4)-H(4A)	108.8	C(9)-C(13)-H(13C)	109.5
C(6)-H(6)	1.0000	C(3)-C(4)-H(4A)	108.8	H(13A)-C(13)-H(13C)	109.5
C(7)-C(8)	1.546(5)	C(5)-C(4)-H(4B)	108.8	H(13B)-C(13)-H(13C)	109.5
C(7)-H(7A)	0.9900	C(3)-C(4)-H(4B)	108.8	F(1)-B(1)-F(3)	110.3(3)
C(7)-H(7B)	0.9900	H(4A)-C(4)-H(4B)	107.7	F(1)-B(1)-F(4)	109.5(3)
C(8)-H(8A)	0.9900	C(6)-C(5)-C(4)	126.0(3)	F(3)-B(1)-F(4)	110.6(3)
C(8)-H(8B)	0.9900	C(6)-C(5)-Pt(1)	71.56(18)	F(1)-B(1)-F(2)	109.3(3)
C(9)-N(1)	1.317(4)	C(4)-C(5)-Pt(1)	107.7(2)	F(3)-B(1)-F(2)	109.3(3)
C(9)-C(10)	1.407(4)	C(6)-C(5)-H(5)	114.2	F(4)-B(1)-F(2)	107.8(3)
C(9)-C(13)	1.496(4)	C(4)-C(5)-H(5)	114.2	C(9)-N(1)-Pt(1)	126.9(2)
C(10)-C(11)	1.372(4)	Pt(1)-C(5)-H(5)	114.2	C(9)-N(1)-H(01)	116(2)
C(10)-H(10)	0.9500	C(5)-C(6)-C(7)	123.8(3)	Pt(1)-N(1)-H(01)	117(2)
C(11)-O(1)	1.304(3)	C(5)-C(6)-Pt(1)	71.20(17)	C(11)-O(1)-Pt(1)	124.89(19)
C(11)-C(12)	1.503(4)	C(7)-C(6)-Pt(1)	111.1(2)	N(1)-Pt(1)-O(1)	91.51(10)
C(12)-H(12A)	0.9800	C(5)-C(6)-H(6)	114.3	N(1)-Pt(1)-C(1)	90.80(11)
C(12)-H(12B)	0.9800	C(7)-C(6)-H(6)	114.3	O(1)-Pt(1)-C(1)	160.30(11)
C(12)-H(12C)	0.9800	Pt(1)-C(6)-H(6)	114.3	N(1)-Pt(1)-C(2)	93.65(11)
C(13)-H(13A)	0.9800	C(6)-C(7)-C(8)	112.0(2)	O(1)-Pt(1)-C(2)	161.25(11)
C(13)-H(13B)	0.9800	C(6)-C(7)-H(7A)	109.2	C(1)-Pt(1)-C(2)	37.68(12)
C(13)-H(13C)	0.9800	C(8)-C(7)-H(7A)	109.2	N(1)-Pt(1)-C(5)	158.21(12)
B(1)-F(1)	1.370(4)	C(6)-C(7)-H(7B)	109.2	O(1)-Pt(1)-C(5)	86.42(11)
B(1)-F(3)	1.374(4)	C(8)-C(7)-H(7B)	109.2	C(1)-Pt(1)-C(5)	98.42(12)
B(1)-F(4)	1.384(4)	H(7A)-C(7)-H(7B)	107.9	C(2)-Pt(1)-C(5)	82.11(13)
B(1)-F(2)	1.401(4)	C(1)-C(8)-C(7)	114.5(3)	N(1)-Pt(1)-C(6)	164.54(12)
N(1)-Pt(1)	1.978(3)	C(1)-C(8)-H(8A)	108.6	O(1)-Pt(1)-C(6)	90.05(10)
N(1)-H(01)	0.93(4)	C(7)-C(8)-H(8A)	108.6	C(1)-Pt(1)-C(6)	82.70(11)
O(1)-Pt(1)	2.009(2)	C(1)-C(8)-H(8B)	108.6	C(2)-Pt(1)-C(6)	89.74(12)
		C(7)-C(8)-H(8B)	108.6	C(5)-Pt(1)-C(6)	37.25(12)
C(2)-C(1)-C(8)	125.1(3)	H(8A)-C(8)-H(8B)	107.6		
C(2)-C(1)-Pt(1)	71.81(18)	N(1)-C(9)-C(10)	123.7(3)		

Symmetry transformations used to generate equivalent atoms:

Table B.18.3 Anisotropic displacement parameters ($Å^2 x\ 10^3$) for [Pt(cod)(NH-acac)]BF_4. The anisotropic displacement factor exponent takes the form: $-2\pi^2[\ h^2 a^{*2} U^{11} + ... + 2\ h\ k\ a^*\ b^*\ U^{12}\ ]$

	U^{11}	U^{22}	U^{33}	U^{23}	U^{13}	U^{12}
C(1)	20(2)	19(2)	22(2)	8(1)	8(1)	3(1)
C(2)	23(2)	15(1)	28(2)	6(1)	16(1)	3(1)
C(3)	34(2)	19(2)	39(2)	-7(2)	23(2)	-5(1)
C(4)	22(2)	33(2)	30(2)	-14(2)	13(2)	-10(1)
C(5)	12(1)	37(2)	22(2)	-3(1)	7(1)	0(1)
C(6)	12(1)	20(2)	24(2)	0(1)	8(1)	3(1)
C(7)	27(2)	18(2)	21(2)	-3(1)	15(1)	0(1)
C(8)	26(2)	22(2)	20(2)	2(1)	10(1)	0(1)
C(9)	17(1)	17(1)	19(2)	-4(1)	7(1)	-1(1)
C(10)	20(2)	17(1)	16(1)	2(1)	8(1)	-1(1)
C(11)	23(2)	14(1)	14(1)	-2(1)	4(1)	1(1)
C(12)	30(2)	20(2)	23(2)	4(1)	7(1)	2(1)
C(13)	17(2)	26(2)	27(2)	4(1)	9(1)	-1(1)
B(1)	26(2)	19(2)	24(2)	0(1)	12(2)	-2(1)

N(1)	14(1)	20(1)	19(1)	6(1)	6(1)	5(1)
O(1)	19(1)	19(1)	17(1)	4(1)	4(1)	5(1)
F(1)	31(1)	42(1)	57(2)	7(1)	26(1)	6(1)
F(2)	52(2)	26(1)	27(1)	2(1)	15(1)	-15(1)
F(3)	67(2)	30(1)	58(2)	-24(1)	40(1)	-17(1)
F(4)	39(1)	40(1)	37(1)	11(1)	-6(1)	-5(1)
Pt(1)	12(1)	15(1)	14(1)	1(1)	5(1)	2(1)

Table B.18.4 Hydrogen coordinates (x 10^4) and isotropic displacement parameters (Å^{2}x 10^3) for [Pt(cod)(NH-acac)]BF_4.

	x	y	z	U(eq)
H(1)	5309	2650	3226	24
H(2)	6196	3764	4641	24
H(3A)	8461	4429	5185	33
H(3B)	8826	3682	4315	33
H(4A)	10529	3175	5965	33
H(4B)	9480	3349	6661	33
H(5)	9715	1535	6604	28
H(6)	9098	555	5066	22
H(7A)	9069	1137	3368	24
H(7B)	9452	2285	3875	24
H(8A)	7309	2578	2465	27
H(8B)	6667	1466	2598	27
H(10)	4295	281	6902	21
H(12A)	6971	-1246	7282	37
H(12B)	6164	-723	8041	37
H(12C)	7783	-377	8192	37
H(13A)	2434	2348	5364	34
H(13B)	2332	1371	6113	34
H(13C)	1987	1231	4790	34
H(01)	4260(40)	2390(30)	4650(30)	30(10)

Table B.18.5 Hydrogen bonds for [Pt(cod)(NH-acac)]BF_4 [Å and °].

D-H...A	d(D-H)	d(H...A)	d(D...A)	<(DHA)
C(5)-H(5)...F(1)	1.00	2.54	3.499(4)	161.2
N(1)-H(01)...F(2)#1	0.93(4)	2.17(4)	3.051(3)	158(3)
N(1)-H(01)...F(4)#1	0.93(4)	2.36(4)	3.136(3)	141(3)
C(3)-H(3B)...F(1)#2	0.99	2.54	3.413(4)	146.8
C(7)-H(7A)...F(3)#3	0.99	2.43	3.175(4)	131.3
C(12)-H(12A)...F(2)#4	0.98	2.42	3.379(4)	164.6

Symmetry transformations used to generate equivalent atoms:
#1 x-1,-y+1/2,z-1/2 #2 x,-y+1/2,z-1/2 #3 -x+2,-y,-z+1
#4 -x+2,y-1/2,-z+3/2

B.19 Crystal Data of [Pt(cod)(NH-acac)]PF_6

Table B.19.1 Atomic coordinates (x 10^4) and equivalent isotropic displacement parameters (Å^{2}x 10^3) for [Pt(cod)(NH-acac)]PF_6. U(eq) is defined as one third of the trace of the orthogonalized U^{ij} tensor.

	x	y	z	U(eq)
C(1)	3931(3)	971(14)	7880(9)	19(2)
C(6)	4380(3)	985(15)	5242(9)	20(2)
C(7)	4623(5)	2270(30)	6647(13)	68(6)

C(8)	4403(5)	2210(20)	7981(12)	43(3)
C(12)	2797(6)	0	440(15)	31(3)
C(13)	2020(5)	0	5119(19)	26(3)
F(2)	471(3)	0	-1153(8)	24(2)
F(3)	1287(3)	0	420(9)	33(2)
F(4)	1578(4)	0	-1774(12)	67(5)
F(5)	758(3)	0	-3331(9)	29(2)
C(9)	2501(5)	0	4521(17)	20(3)
C(10)	2476(5)	0	2905(16)	24(3)
C(11)	2892(5)	0	2222(15)	21(3)
N(1)	2924(3)	0	5679(11)	8(2)
O(1)	3379(4)	0	3034(11)	26(2)
F(1)	1019(3)	2253(11)	-1452(7)	40(2)
P(1)	1027(1)	0	-1456(4)	23(1)
Pt(1)	3640(1)	0	5414(1)	13(1)

Table B.19.2 Bond lengths [Å] and angles [°] for [Pt(cod)(NH-acac)]PF_6.

C(1)-C(1)#1	1.38(2)	C(8)-C(1)-H(1)	114.4	C(9)-C(10)-H(10)	116.6
C(1)-C(8)	1.530(14)	Pt(1)-C(1)-H(1)	114.4	C(11)-C(10)-H(10)	116.6
C(1)-Pt(1)	2.195(8)	C(6)#1-C(6)-C(7)	126.6(9)	O(1)-C(11)-C(10)	124.5(12)
C(1)-H(1)	1.0000	C(6)#1-C(6)-Pt(1)	71.0(3)	O(1)-C(11)-C(12)	115.4(12)
C(6)-C(6)#1	1.40(2)	C(7)-C(6)-Pt(1)	110.3(6)	C(10)-C(11)-C(12)	120.2(12)
C(6)-C(7)	1.527(14)	C(6)#1-C(6)-H(6)	113.6	C(9)-N(1)-Pt(1)	125.4(8)
C(6)-Pt(1)	2.151(8)	C(7)-C(6)-H(6)	113.6	C(9)-N(1)-H(1A)	117.3
C(6)-H(6)	1.0000	Pt(1)-C(6)-H(6)	113.6	Pt(1)-N(1)-H(1A)	117.3
C(7)-C(8)	1.437(13)	C(8)-C(7)-C(6)	116.9(10)	C(11)-O(1)-Pt(1)	125.7(9)
C(7)-H(7A)	0.9900	C(8)-C(7)-H(7A)	108.1	F(4)-P(1)-F(2)	179.5(5)
C(7)-H(7B)	0.9900	C(6)-C(7)-H(7A)	108.1	F(4)-P(1)-F(3)	90.1(5)
C(8)-H(8A)	0.9900	C(8)-C(7)-H(7B)	108.1	F(2)-P(1)-F(3)	90.4(4)
C(8)-H(8B)	0.9900	C(6)-C(7)-H(7B)	108.1	F(4)-P(1)-F(1)	90.7(3)
C(12)-C(11)	1.506(18)	H(7A)-C(7)-H(7B)	107.3	F(2)-P(1)-F(1)	89.3(3)
C(12)-H(12A)	0.9800	C(7)-C(8)-C(1)	118.8(9)	F(3)-P(1)-F(1)	90.0(2)
C(12)-H(12B)	0.9800	C(7)-C(8)-H(8A)	107.6	F(4)-P(1)-F(1)#1	90.7(3)
C(12)-H(12C)	0.9800	C(1)-C(8)-H(8A)	107.6	F(2)-P(1)-F(1)#1	89.3(3)
C(13)-C(9)	1.518(17)	C(7)-C(8)-H(8B)	107.6	F(3)-P(1)-F(1)#1	90.0(2)
C(13)-H(13A)	0.9800	C(1)-C(8)-H(8B)	107.6	F(1)-P(1)-F(1)#1	178.5(6)
C(13)-H(13B)	0.9800	H(8A)-C(8)-H(8B)	107.1	F(4)-P(1)-F(5)	90.7(5)
C(13)-H(13C)	0.9800	C(11)-C(12)-H(12A)	109.5	F(2)-P(1)-F(5)	88.8(4)
F(2)-P(1)	1.585(8)	C(11)-C(12)-H(12B)	109.5	F(3)-P(1)-F(5)	179.2(5)
F(3)-P(1)	1.600(8)	H(12A)-C(12)-	109.5	F(1)-P(1)-F(5)	90.0(2)
F(4)-P(1)	1.579(9)	H(12B)		F(1)#1-P(1)-F(5)	90.0(2)
F(5)-P(1)	1.602(8)	C(11)-C(12)-H(12C)	109.5	N(1)-Pt(1)-O(1)	92.0(4)
C(9)-N(1)	1.306(15)	H(12A)-C(12)-	109.5	N(1)-Pt(1)-C(6)	160.9(3)
C(9)-C(10)	1.391(19)	H(12C)		O(1)-Pt(1)-C(6)	90.3(3)
C(10)-C(11)	1.398(18)	H(12B)-C(12)-	109.5	N(1)-Pt(1)-C(6)#1	160.9(3)
C(10)-H(10)	0.9500	H(12C)		O(1)-Pt(1)-C(6)#1	90.3(3)
C(11)-O(1)	1.314(16)	C(9)-C(13)-H(13A)	109.5	C(6)-Pt(1)-C(6)#1	37.9(6)
N(1)-Pt(1)	1.999(9)	C(9)-C(13)-H(13B)	109.5	N(1)-Pt(1)-C(1)	89.5(3)
N(1)-H(1A)	0.8800	H(13A)-C(13)-	109.5	O(1)-Pt(1)-C(1)	161.6(3)
O(1)-Pt(1)	2.006(9)	H(13B)		C(6)-Pt(1)-C(1)	82.5(3)
F(1)-P(1)	1.600(8)	C(9)-C(13)-H(13C)	109.5	C(6)#1-Pt(1)-C(1)	94.2(3)
P(1)-F(1)#1	1.600(8)	H(13A)-C(13)-	109.5	N(1)-Pt(1)-C(1)#1	89.5(3)
Pt(1)-C(6)#1	2.151(8)	H(13C)		O(1)-Pt(1)-C(1)#1	161.6(3)
Pt(1)-C(1)#1	2.195(8)	H(13B)-C(13)-	109.5	C(6)-Pt(1)-C(1)#1	94.2(3)
		H(13C)		C(6)#1-Pt(1)-C(1)#1	82.5(3)
C(1)#1-C(1)-C(8)	125.2(7)	N(1)-C(9)-C(10)	125.6(11)	C(1)-Pt(1)-C(1)#1	36.6(5)
C(1)#1-C(1)-Pt(1)	71.7(3)	N(1)-C(9)-C(13)	112.4(12)		
C(8)-C(1)-Pt(1)	108.2(5)	C(10)-C(9)-C(13)	122.0(12)		
C(1)#1-C(1)-H(1)	114.4	C(9)-C(10)-C(11)	126.9(11)		

Symmetry transformations used to generate equivalent atoms:
#1 x,-y,z

Table B.19.3 Anisotropic displacement parameters ($Å^2 x\ 10^3$) for [Pt(cod)(NH-acac)]PF_6. The anisotropic displacement factor exponent takes the form: $-2\pi^2[\ h^2 a^{*2} U^{11} + ... + 2\ h\ k\ a^*\ b^*\ U^{12}\ ]$

	U^{11}	U^{22}	U^{33}	U^{23}	U^{13}	U^{12}
C(1)	24(4)	24(5)	9(3)	-4(3)	6(3)	-2(4)
C(6)	12(3)	29(6)	19(3)	-3(4)	9(3)	-9(4)
C(7)	62(8)	118(16)	36(6)	-43(8)	33(6)	-71(10)
C(8)	58(7)	50(9)	30(5)	-21(6)	26(5)	-31(7)
C(12)	26(7)	41(10)	18(6)	0	-6(5)	0
C(13)	16(6)	12(7)	55(9)	0	16(6)	0
F(2)	17(3)	33(5)	20(3)	0	2(3)	0
F(3)	21(4)	58(7)	14(3)	0	-5(3)	0
F(4)	23(5)	145(15)	36(5)	0	16(4)	0
F(5)	41(5)	33(5)	13(3)	0	6(3)	0
C(9)	11(5)	10(6)	40(7)	0	8(5)	0
C(10)	12(5)	24(8)	31(6)	0	-1(5)	0
C(11)	21(6)	18(7)	20(5)	0	0(4)	0
N(1)	9(4)	2(4)	15(4)	0	4(3)	0
O(1)	27(5)	26(6)	22(4)	0	2(4)	0
F(1)	58(4)	38(4)	21(3)	0(3)	5(3)	-25(4)
P(1)	17(1)	39(2)	13(1)	0	3(1)	0
Pt(1)	11(1)	15(1)	13(1)	0	4(1)	0

Table B.19.4 Hydrogen coordinates ($x\ 10^4$) and isotropic displacement parameters ($Å^2 x\ 10^3$) for [Pt(cod)(NH-acac)]PF_6.

	x	y	z	U(eq)
H(1)	3663	1553	8339	23
H(6)	4372	1548	4185	23
H(7A)	4993	1937	7033	82
H(7B)	4604	3579	6252	82
H(8A)	4309	3520	8188	52
H(8B)	4677	1806	8922	52
H(12A)	3128	0	167	46
H(12B)	2601	1127	-3	46
H(12C)	2601	-1127	-3	46
H(13A)	2119	0	6285	39
H(13B)	1815	-1127	4730	39
H(13C)	1815	1127	4730	39
H(10)	2141	0	2191	28
H(1A)	2891	0	6658	10

Table B.19.5 Hydrogen bonds for [Pt(cod)(NH-acac)]PF_6 [Å and °]

D-H...A	d(D-H)	d(H...A)	d(D...A)	<(DHA)
C(10)-H(10)...F(3)	0.95	2.40	3.354(14)	179.0
C(8)-H(8A)...F(3)#2	0.99	2.48	3.265(15)	135.6
C(8)-H(8A)...F(3)#3	0.99	2.48	3.265(15)	135.6
C(6)-H(6)...F(1)#4	1.00	2.49	3.428(10)	157.0
C(13)-H(13A)...F(4)#5	0.98	2.50	3.230(17)	130.8
C(13)-H(13A)...F(4)#6	0.98	2.50	3.230(17)	130.8

Symmetry transformations used to generate equivalent atoms:
#1 x,-y,z #2 -x+1/2,-y+1/2,-z+1 #3 -x+1/2,y+1/2,-z+1
#4 -x+1/2,-y+1/2,-z #5 x,y,z+1 #6 x,-y,z+1

B.20 Crystal Data of [Pt(cod)(NMe-acac)]BF_4

Table B.20.1 Atomic coordinates (x 10^4) and equivalent isotropic displacement parameters (Å^{2}x 10^3) for [Pt(cod)(NMe-acac)]BF_4. U(eq) is defined as one third of the trace of the orthogonalized U^{ij} tensor.

	x	y	z	U(eq)
C(1)	3042(7)	-565(4)	8584(3)	19(1)
C(2)	1246(7)	-646(3)	8794(3)	17(1)
C(3)	451(6)	-1379(3)	9420(3)	18(1)
C(4)	1520(6)	-1517(3)	10300(3)	18(1)
C(5)	2397(7)	-597(3)	10632(3)	17(1)
C(6)	4140(6)	-342(3)	10414(3)	19(1)
C(7)	5348(7)	-876(4)	9787(4)	24(1)
C(8)	4439(7)	-1247(4)	8925(3)	25(1)
C(9)	2393(7)	2562(3)	10135(3)	17(1)
C(10)	2337(7)	2820(3)	9208(3)	18(1)
C(11)	1969(6)	2241(3)	8491(3)	18(1)
C(12)	2435(8)	3399(4)	10791(3)	27(1)
C(13)	1742(8)	2620(4)	7548(3)	26(1)
C(14)	2262(7)	1503(4)	11430(3)	24(1)
B(1)	8029(8)	-678(4)	11922(4)	23(1)
N(1)	2376(6)	1675(3)	10438(2)	16(1)
O(1)	1760(5)	1319(2)	8531(2)	18(1)
F(1)	7008(7)	-131(3)	12489(3)	63(1)
F(2)	9646(5)	-880(3)	12331(2)	42(1)
F(3)	7191(5)	-1535(2)	11740(2)	42(1)
F(4)	8343(4)	-181(2)	11117(2)	28(1)
Pt(1)	2359(1)	519(1)	9598(1)	11(1)

Table B.20.2 Bond lengths [Å] and angles [°] for [Pt(cod)(NMe-acac)]BF_4.

C(1)-C(2)	1.391(7)	C(12)-H(12C)	0.9800	C(5)-C(4)-C(3)	113.1(4)
C(1)-C(8)	1.506(7)	C(13)-H(13A)	0.9800	C(5)-C(4)-H(4A)	109.0
C(1)-Pt(1)	2.192(5)	C(13)-H(13B)	0.9800	C(3)-C(4)-H(4A)	109.0
C(1)-H(1)	1.0000	C(13)-H(13C)	0.9800	C(5)-C(4)-H(4B)	109.0
C(2)-C(3)	1.504(6)	C(14)-N(1)	1.489(5)	C(3)-C(4)-H(4B)	109.0
C(2)-Pt(1)	2.182(5)	C(14)-H(14A)	0.9800	H(4A)-C(4)-H(4B)	107.8
C(2)-H(2)	1.0000	C(14)-H(14B)	0.9800	C(6)-C(5)-C(4)	123.1(5)
C(3)-C(4)	1.542(6)	C(14)-H(14C)	0.9800	C(6)-C(5)-Pt(1)	70.6(3)
C(3)-H(3A)	0.9900	B(1)-F(1)	1.370(7)	C(4)-C(5)-Pt(1)	111.7(3)
C(3)-H(3B)	0.9900	B(1)-F(3)	1.380(6)	C(6)-C(5)-H(5)	114.5
C(4)-C(5)	1.525(7)	B(1)-F(2)	1.388(7)	C(4)-C(5)-H(5)	114.5
C(4)-H(4A)	0.9900	B(1)-F(4)	1.397(6)	Pt(1)-C(5)-H(5)	114.5
C(4)-H(4B)	0.9900	N(1)-Pt(1)	2.036(4)	C(5)-C(6)-C(7)	125.9(5)
C(5)-C(6)	1.397(7)	O(1)-Pt(1)	1.985(3)	C(5)-C(6)-Pt(1)	71.9(3)
C(5)-Pt(1)	2.184(4)			C(7)-C(6)-Pt(1)	107.9(3)
C(5)-H(5)	1.0000	C(2)-C(1)-C(8)	123.5(5)	C(5)-C(6)-H(6)	114.2
C(6)-C(7)	1.497(7)	C(2)-C(1)-Pt(1)	71.1(3)	C(7)-C(6)-H(6)	114.2
C(6)-Pt(1)	2.168(4)	C(8)-C(1)-Pt(1)	111.8(3)	Pt(1)-C(6)-H(6)	114.2
C(6)-H(6)	1.0000	C(2)-C(1)-H(1)	114.3	C(6)-C(7)-C(8)	114.3(4)
C(7)-C(8)	1.536(7)	C(8)-C(1)-H(1)	114.3	C(6)-C(7)-H(7A)	108.7
C(7)-H(7A)	0.9900	Pt(1)-C(1)-H(1)	114.3	C(8)-C(7)-H(7A)	108.7
C(7)-H(7B)	0.9900	C(1)-C(2)-C(3)	125.4(5)	C(6)-C(7)-H(7B)	108.7
C(8)-H(8A)	0.9900	C(1)-C(2)-Pt(1)	71.8(3)	C(8)-C(7)-H(7B)	108.7
C(8)-H(8B)	0.9900	C(3)-C(2)-Pt(1)	109.0(3)	H(7A)-C(7)-H(7B)	107.6
C(9)-N(1)	1.318(6)	C(1)-C(2)-H(2)	114.1	C(1)-C(8)-C(7)	112.0(4)
C(9)-C(10)	1.417(6)	C(3)-C(2)-H(2)	114.1	C(1)-C(8)-H(8A)	109.2
C(9)-C(12)	1.519(6)	Pt(1)-C(2)-H(2)	114.1	C(7)-C(8)-H(8A)	109.2
C(10)-C(11)	1.362(7)	C(2)-C(3)-C(4)	113.3(4)	C(1)-C(8)-H(8B)	109.2
C(10)-H(10)	0.9500	C(2)-C(3)-H(3A)	108.9	C(7)-C(8)-H(8B)	109.2
C(11)-O(1)	1.298(6)	C(4)-C(3)-H(3A)	108.9	H(8A)-C(8)-H(8B)	107.9
C(11)-C(13)	1.502(6)	C(2)-C(3)-H(3B)	108.9	N(1)-C(9)-C(10)	124.6(4)
C(12)-H(12A)	0.9800	C(4)-C(3)-H(3B)	108.9	N(1)-C(9)-C(12)	120.4(4)
C(12)-H(12B)	0.9800	H(3A)-C(3)-H(3B)	107.7	C(10)-C(9)-C(12)	115.0(4)

C(11)-C(10)-C(9)	127.4(4)	H(13B)-C(13)-H(13C)	109.5	O(1)-Pt(1)-N(1)	92.26(14)
C(11)-C(10)-H(10)	116.3	N(1)-C(14)-H(14A)	109.5	O(1)-Pt(1)-C(6)	153.53(18)
C(9)-C(10)-H(10)	116.3	N(1)-C(14)-H(14B)	109.5	N(1)-Pt(1)-C(6)	95.55(17)
O(1)-C(11)-C(10)	125.3(4)	H(14A)-C(14)-H(14B)	109.5	O(1)-Pt(1)-C(2)	84.25(16)
O(1)-C(11)-C(13)	112.2(4)	N(1)-C(14)-H(14C)	109.5	N(1)-Pt(1)-C(2)	157.75(17)
C(10)-C(11)-C(13)	122.5(4)	H(14A)-C(14)-H(14C)	109.5	C(6)-Pt(1)-C(2)	97.29(18)
C(9)-C(12)-H(12A)	109.5	H(14B)-C(14)-H(14C)	109.5	O(1)-Pt(1)-C(5)	164.00(17)
C(9)-C(12)-H(12B)	109.5	F(1)-B(1)-F(3)	110.3(5)	N(1)-Pt(1)-C(5)	97.97(17)
H(12A)-C(12)-H(12B)	109.5	F(1)-B(1)-F(2)	109.7(5)	C(6)-Pt(1)-C(5)	37.46(19)
C(9)-C(12)-H(12C)	109.5	F(3)-B(1)-F(2)	108.0(5)	C(2)-Pt(1)-C(5)	81.62(18)
H(12A)-C(12)-H(12C)	109.5	F(1)-B(1)-F(4)	109.9(5)	O(1)-Pt(1)-C(1)	84.17(17)
H(12B)-C(12)-H(12C)	109.5	F(3)-B(1)-F(4)	110.0(4)	N(1)-Pt(1)-C(1)	164.37(16)
C(11)-C(13)-H(13A)	109.5	F(2)-B(1)-F(4)	108.9(4)	C(6)-Pt(1)-C(1)	81.52(19)
C(11)-C(13)-H(13B)	109.5	C(9)-N(1)-C(14)	119.1(4)	C(2)-Pt(1)-C(1)	37.10(18)
H(13A)-C(13)-H(13B)	109.5	C(9)-N(1)-Pt(1)	122.6(3)	C(5)-Pt(1)-C(1)	89.0(2)
C(11)-C(13)-H(13C)	109.5	C(14)-N(1)-Pt(1)	118.2(3)		
H(13A)-C(13)-H(13C)	109.5	C(11)-O(1)-Pt(1)	124.5(3)		

Symmetry transformations used to generate equivalent atoms:

Table B.20.3 Anisotropic displacement parameters ($Å^2$x 10^3) for [Pt(cod)(NMe-acac)]BF_4. The anisotropic displacement factor exponent takes the form: $-2\pi^2[h^2a^{*2}U^{11} + ... + 2 h k a^* b^* U^{12}]$

	U^{11}	U^{22}	U^{33}	U^{23}	U^{13}	U^{12}
C(1)	28(3)	14(2)	14(2)	-5(2)	6(2)	0(2)
C(2)	24(3)	13(2)	13(2)	-5(2)	-3(2)	-1(2)
C(3)	17(2)	15(2)	20(2)	-1(2)	-2(2)	-3(2)
C(4)	19(2)	15(2)	19(2)	5(2)	1(2)	-1(2)
C(5)	23(2)	13(2)	15(2)	4(2)	-6(2)	2(3)
C(6)	18(2)	17(2)	23(2)	4(2)	-10(2)	1(2)
C(7)	13(2)	17(2)	43(3)	1(2)	-4(2)	2(2)
C(8)	23(3)	20(3)	31(3)	-1(2)	8(2)	5(2)
C(9)	11(2)	15(2)	24(2)	-3(2)	-1(2)	0(2)
C(10)	15(2)	10(2)	28(2)	5(2)	0(2)	1(2)
C(11)	14(2)	17(2)	22(2)	6(2)	2(2)	3(2)
C(12)	35(3)	16(2)	32(2)	-6(2)	-8(2)	2(3)
C(13)	32(3)	22(3)	23(2)	10(2)	4(2)	1(2)
C(14)	36(3)	22(2)	14(2)	-3(2)	-1(2)	0(3)
B(1)	23(3)	19(3)	29(3)	0(2)	5(2)	-1(2)
N(1)	18(2)	14(2)	15(2)	-2(1)	-3(2)	-1(2)
O(1)	27(2)	14(2)	13(1)	2(1)	-4(1)	-1(2)
F(1)	80(4)	33(2)	76(3)	8(2)	58(3)	18(2)
F(2)	25(2)	76(3)	26(2)	9(2)	-7(1)	-11(2)
F(3)	49(2)	28(2)	50(2)	7(2)	-19(2)	-20(2)
F(4)	24(2)	24(2)	34(2)	6(1)	2(1)	2(1)
Pt(1)	12(1)	10(1)	11(1)	1(1)	0(1)	0(1)

Table B.20.4 Hydrogen coordinates (x 10^4) and isotropic displacement parameters ($Å^2$x 10^3) for [Pt(cod)(NMe-acac)]BF_4.

	x	y	z	U(eq)
H(1)	3284	-300	7968	22
H(2)	430	-431	8301	20
H(3A)	377	-2000	9100	21
H(3B)	-774	-1181	9576	21
H(4A)	715	-1760	10777	21
H(4B)	2450	-2006	10196	21
H(5)	1997	-382	11244	20
H(6)	4770	23	10899	23
H(7A)	5863	-1427	10116	29
H(7B)	6338	-449	9611	29
H(8A)	5346	-1343	8449	30
H(8B)	3883	-1875	9053	30

H(10)	2585	3471	9071	21
H(12A)	1300	3435	11114	41
H(12B)	2629	3995	10455	41
H(12C)	3402	3307	11226	41
H(13A)	2703	2378	7164	38
H(13B)	1779	3321	7559	38
H(13C)	596	2407	7305	38
H(14A)	2363	2114	11751	36
H(14B)	3230	1077	11617	36
H(14C)	1119	1204	11573	36

Table B.20.5 Hydrogen bonds for [Pt(cod)(NMe-acac)]BF_4 [Åand °].

D-H...A	d(D-H)	d(H...A)	d(D...A)	<(DHA)
C(1)-H(1)...F(2)#1	1.00	2.46	3.246(6)	135.5
C(2)-H(2)...F(1)#2	1.00	2.33	3.302(6)	164.0
C(5)-H(5)...F(2)#3	1.00	2.49	3.279(6)	135.5
C(13)-H(13B)...F(1)#4	0.98	2.54	3.514(7)	176.5
C(10)-H(10)...F(4)#4	0.95	2.47	3.418(5)	173.9

Symmetry transformations used to generate equivalent atoms:
#1 -x+3/2,-y,z-1/2 #2 -x+1/2,-y,z-1/2 #3 x-1,y,z
#4 x-1/2,-y+1/2,-z+2

B.21 Crystal Data of [Pt(cod)(NMe-acac)]PF_6

Table B.21.1 Atomic coordinates (x 10^4) and equivalent isotropic displacement parameters (Å^{2}x 10^3) for [Pt(cod)(NMe-acac)]PF_6. U(eq) is defined as one third of the trace of the orthogonalized U^{ij} tensor.

	x	y	z	U(eq)
C(1)	4085(8)	4950(30)	13070(18)	41(2)
C(2)	4015(8)	3040(30)	12987(19)	41(2)
C(3)	4572(6)	2240(30)	12990(20)	74(4)
C(4)	4636(10)	2020(40)	11520(30)	74(4)
C(5)	4349(8)	3060(30)	10300(30)	50(6)
C(6)	4329(7)	5020(30)	10326(17)	30(4)
C(7)	4673(10)	6370(40)	11580(30)	72(4)
C(8)	4438(6)	6560(30)	12820(20)	72(4)
C(9)	2453(2)	4090(50)	10021(8)	34(2)
C(10)	2430(3)	4220(50)	8484(8)	40(2)
C(11)	2839(3)	4040(50)	7849(8)	34(3)
C(12)	1924(3)	3990(40)	10376(11)	50(3)
C(13)	2753(3)	4060(60)	6205(8)	52(3)
C(14)	2843(3)	4040(50)	12701(8)	46(3)
N(1)	2891(2)	4180(40)	11145(6)	32(2)
O(1)	3329(2)	4170(30)	8610(5)	40(1)
F(1)	947(9)	6316(19)	3710(20)	120(7)
F(2)	1317(2)	4080(40)	5455(6)	83(3)
F(3)	1109(9)	2017(17)	3620(20)	125(7)
F(4)	813(2)	4150(40)	1924(6)	77(2)
F(5)	1614(3)	4470(60)	3477(9)	165(10)
F(6)	511(2)	4300(30)	3932(8)	101(3)
P(1)	1070(1)	4164(15)	3687(2)	44(1)
Pt(1)	3619(1)	4145(5)	10808(1)	26(1)

Table B.21.2 Bond lengths [Å] and angles [°] for [Pt(cod)(NMe-acac)]PF_6.

C(1)-C(2)	1.382(14)	C(1)-C(2)-C(3)	104.4(18)	H(13A)-C(13)-H(13B)	109.5
C(1)-C(8)	1.55(3)	C(1)-C(2)-Pt(1)	73.2(16)	C(11)-C(13)-H(13C)	109.5
C(1)-Pt(1)	2.20(2)	C(3)-C(2)-Pt(1)	110.1(10)	H(13A)-C(13)-H(13C)	109.5
C(1)-H(1)	1.0000	C(1)-C(2)-H(2)	119.9	H(13B)-C(13)-H(13C)	109.5
C(2)-C(3)	1.59(3)	C(3)-C(2)-H(2)	119.9	C(11)-C(13)-H(13D)	109.5
C(2)-Pt(1)	2.16(2)	Pt(1)-C(2)-H(2)	119.9	H(13A)-C(13)-H(13D)	141.1
C(2)-H(2)	1.0000	C(4)-C(3)-C(2)	113.4(16)	H(13B)-C(13)-H(13D)	56.3
C(3)-C(4)	1.43(3)	C(4)-C(3)-H(3A)	108.9	H(13C)-C(13)-H(13D)	56.3
C(3)-H(3A)	0.9900	C(2)-C(3)-H(3A)	108.9	C(11)-C(13)-H(13E)	109.5
C(3)-H(3B)	0.9900	C(4)-C(3)-H(3B)	108.9	H(13A)-C(13)-H(13E)	56.3
C(4)-C(5)	1.39(3)	C(2)-C(3)-H(3B)	108.9	H(13B)-C(13)-H(13E)	141.1
C(4)-H(4A)	0.9900	H(3A)-C(3)-H(3B)	107.7	H(13C)-C(13)-H(13E)	56.3
C(4)-H(4B)	0.9900	C(5)-C(4)-C(3)	122.4(19)	H(13D)-C(13)-H(13E)	109.5
C(5)-C(6)	1.409(14)	C(5)-C(4)-H(4A)	106.7	C(11)-C(13)-H(13F)	109.5
C(5)-Pt(1)	2.26(2)	C(3)-C(4)-H(4A)	106.7	H(13A)-C(13)-H(13F)	56.3
C(5)-H(5)	1.0000	C(5)-C(4)-H(4B)	106.7	H(13B)-C(13)-H(13F)	56.3
C(6)-C(7)	1.60(3)	C(3)-C(4)-H(4B)	106.7	H(13C)-C(13)-H(13F)	141.1
C(6)-Pt(1)	2.152(19)	H(4A)-C(4)-H(4B)	106.6	H(13D)-C(13)-H(13F)	109.5
C(6)-H(6)	1.0000	C(4)-C(5)-C(6)	123(3)	H(13E)-C(13)-H(13F)	109.5
C(7)-C(8)	1.47(3)	C(4)-C(5)-Pt(1)	108.7(15)	N(1)-C(14)-H(14A)	109.5
C(7)-H(7A)	0.9900	C(6)-C(5)-Pt(1)	67.3(15)	N(1)-C(14)-H(14B)	109.5
C(7)-H(7B)	0.9900	C(4)-C(5)-H(5)	116.0	H(14A)-C(14)-H(14B)	109.5
C(8)-H(8A)	0.9900	C(6)-C(5)-H(5)	116.0	N(1)-C(14)-H(14C)	109.5
C(8)-H(8B)	0.9900	Pt(1)-C(5)-H(5)	116.0	H(14A)-C(14)-H(14C)	109.5
C(9)-N(1)	1.331(9)	C(5)-C(6)-C(7)	127(2)	H(14B)-C(14)-H(14C)	109.5
C(9)-C(10)	1.418(10)	C(5)-C(6)-Pt(1)	75.6(15)	C(9)-N(1)-C(14)	117.8(6)
C(9)-C(12)	1.533(9)	C(7)-C(6)-Pt(1)	112.4(12)	C(9)-N(1)-Pt(1)	122.3(5)
C(10)-C(11)	1.384(12)	C(5)-C(6)-H(6)	112.0	C(14)-N(1)-Pt(1)	119.3(5)
C(10)-H(10)	0.9500	C(7)-C(6)-H(6)	112.0	C(11)-O(1)-Pt(1)	127.2(5)
C(11)-O(1)	1.301(8)	Pt(1)-C(6)-H(6)	112.0	F(5)-P(1)-F(3)	93.5(18)
C(11)-C(13)	1.484(10)	C(8)-C(7)-C(6)	110.5(18)	F(5)-P(1)-F(6)	168.2(19)
C(12)-H(12A)	0.9800	C(8)-C(7)-H(7A)	109.5	F(3)-P(1)-F(6)	98.4(13)
C(12)-H(12B)	0.9800	C(6)-C(7)-H(7A)	109.5	F(5)-P(1)-F(1)	93.9(18)
C(12)-H(12C)	0.9800	C(8)-C(7)-H(7B)	109.5	F(3)-P(1)-F(1)	172.3(8)
C(13)-H(13A)	0.9800	C(6)-C(7)-H(7B)	109.5	F(6)-P(1)-F(1)	74.3(12)
C(13)-H(13B)	0.9800	H(7A)-C(7)-H(7B)	108.1	F(5)-P(1)-F(4)	91.0(4)
C(13)-H(13C)	0.9800	C(7)-C(8)-C(1)	117.2(16)	F(3)-P(1)-F(4)	88.0(12)
C(13)-H(13D)	0.9800	C(7)-C(8)-H(8A)	108.0	F(6)-P(1)-F(4)	90.0(3)
C(13)-H(13E)	0.9800	C(1)-C(8)-H(8A)	108.0	F(1)-P(1)-F(4)	89.5(12)
C(13)-H(13F)	0.9800	C(7)-C(8)-H(8B)	108.0	F(5)-P(1)-F(2)	90.4(4)
C(14)-N(1)	1.494(9)	C(1)-C(8)-H(8B)	108.0	F(3)-P(1)-F(2)	89.5(12)
C(14)-H(14A)	0.9800	H(8A)-C(8)-H(8B)	107.3	F(6)-P(1)-F(2)	89.2(4)
C(14)-H(14B)	0.9800	N(1)-C(9)-C(10)	124.9(6)	F(1)-P(1)-F(2)	92.8(12)
C(14)-H(14C)	0.9800	N(1)-C(9)-C(12)	119.0(6)	F(4)-P(1)-F(2)	177.2(14)
N(1)-Pt(1)	2.046(5)	C(10)-C(9)-C(12)	115.9(6)	O(1)-Pt(1)-N(1)	92.7(2)
O(1)-Pt(1)	1.975(5)	C(11)-C(10)-C(9)	127.3(9)	O(1)-Pt(1)-C(6)	83.7(5)
F(1)-P(1)	1.583(18)	C(11)-C(10)-H(10)	116.3	N(1)-Pt(1)-C(6)	161.9(9)
F(2)-P(1)	1.594(6)	C(9)-C(10)-H(10)	116.3	O(1)-Pt(1)-C(2)	157.6(7)
F(3)-P(1)	1.550(17)	O(1)-C(11)-C(10)	123.3(9)	N(1)-Pt(1)-C(2)	95.4(6)
F(4)-P(1)	1.592(5)	O(1)-C(11)-C(13)	113.8(6)	C(6)-Pt(1)-C(2)	94.5(6)
F(5)-P(1)	1.530(8)	C(10)-C(11)-C(13)	121.8(8)	O(1)-Pt(1)-C(1)	160.2(7)
F(6)-P(1)	1.567(6)	C(9)-C(12)-H(12A)	109.5	N(1)-Pt(1)-C(1)	98.8(6)
		C(9)-C(12)-H(12B)	109.5	C(6)-Pt(1)-C(1)	80.3(7)
C(2)-C(1)-C(8)	144.4(19)	H(12A)-C(12)-H(12B)	109.5	C(2)-Pt(1)-C(1)	36.9(4)
C(2)-C(1)-Pt(1)	69.8(17)	C(9)-C(12)-H(12C)	109.5	O(1)-Pt(1)-C(5)	84.1(7)
C(8)-C(1)-Pt(1)	104.9(10)	H(12A)-C(12)-H(12C)	109.5	N(1)-Pt(1)-C(5)	160.3(9)
C(2)-C(1)-H(1)	107.5	H(12B)-C(12)-H(12C)	109.5	C(6)-Pt(1)-C(5)	37.2(3)
C(8)-C(1)-H(1)	107.5	C(11)-C(13)-H(13A)	109.5	C(2)-Pt(1)-C(5)	81.3(8)
Pt(1)-C(1)-H(1)	107.5	C(11)-C(13)-H(13B)	109.5	C(1)-Pt(1)-C(5)	90.2(8)

Symmetry transformations used to generate equivalent atoms:

Table B.21.3 Anisotropic displacement parameters ($Å^2$x 10^3) for [Pt(cod)(NMe-acac)]PF_6. The anisotropic displacement factor exponent takes the form: $-2\pi^2[h^2a^{*2}U^{11} + ... + 2 h k a^* b^* U^{12}]$

	U^{11}	U^{22}	U^{33}	U^{23}	U^{13}	U^{12}
C(1)	42(5)	58(6)	20(2)	-8(4)	4(3)	3(4)
C(2)	42(5)	58(6)	20(2)	-8(4)	4(3)	3(4)
C(3)	67(6)	89(8)	63(8)	23(6)	16(6)	59(6)
C(4)	67(6)	89(8)	63(8)	23(6)	16(6)	59(6)
C(5)	40(9)	52(10)	72(13)	-6(8)	41(9)	1(7)

C(6)	27(7)	43(7)	19(6)	-2(5)	4(5)	-15(5)
C(7)	64(7)	99(10)	57(8)	-36(7)	25(6)	-31(6)
C(8)	64(7)	99(10)	57(8)	-36(7)	25(6)	-31(6)
C(9)	33(3)	29(4)	42(3)	7(12)	12(2)	-2(10)
C(10)	33(3)	42(6)	40(3)	-7(11)	4(3)	-12(11)
C(11)	33(3)	28(7)	35(3)	12(8)	-3(2)	0(7)
C(12)	37(3)	48(8)	68(5)	-27(9)	23(3)	4(7)
C(13)	53(4)	73(8)	26(3)	-3(13)	5(3)	-19(14)
C(14)	51(4)	64(8)	32(3)	-24(10)	25(3)	-20(10)
N(1)	32(2)	36(4)	31(3)	12(10)	13(2)	-2(10)
O(1)	37(2)	59(4)	24(2)	-20(8)	7(2)	-4(10)
F(1)	206(17)	80(9)	71(8)	2(7)	35(9)	48(10)
F(2)	70(4)	134(7)	36(3)	-1(11)	1(3)	-37(11)
F(3)	211(16)	65(8)	96(10)	11(7)	36(11)	88(10)
F(4)	85(4)	99(5)	42(3)	-9(12)	8(3)	29(11)
F(5)	49(4)	380(30)	68(4)	1(15)	27(3)	-62(14)
F(6)	55(3)	167(10)	85(4)	3(11)	26(3)	54(9)
P(1)	37(1)	59(1)	35(1)	2(5)	9(1)	11(4)
Pt(1)	29(1)	31(1)	20(1)	0(1)	7(1)	0(1)

Table B.21.4 Hydrogen coordinates (x 10^4) and isotropic displacement parameters (Å^{2}x 10^3) for [Pt(cod)(NMe-acac)]PF_6.

	x	y	z	U(eq)
H(1)	3838	5471	13603	49
H(2)	3808	2425	13598	49
H(3A)	4848	3089	13573	88
H(3B)	4622	1019	13499	88
H(4A)	5011	2250	11612	88
H(4B)	4568	699	11251	88
H(5)	4298	2479	9299	60
H(6)	4259	5566	9302	36
H(7A)	5032	5867	11959	86
H(7B)	4697	7612	11141	86
H(8A)	4228	7718	12668	86
H(8B)	4726	6724	13757	86
H(10)	2094	4470	7815	47
H(12A)	1983	3982	11463	75
H(12B)	1739	2857	9944	75
H(12C)	1713	5081	9949	75
H(13A)	3090	3916	5980	78
H(13B)	2593	5248	5799	78
H(13C)	2519	3038	5751	78
H(13D)	2379	4218	5707	78
H(13E)	2875	2887	5888	78
H(13F)	2949	5097	5935	78
H(14A)	3193	3971	13409	70
H(14B)	2643	2925	12790	70
H(14C)	2660	5144	12924	70

Table B.21.5 Hydrogen bonds for [Pt(cod)(NMe-acac)]PF_6 [Å and °].

D-H...A	d(D-H)	d(H...A)	d(D...A)	<(DHA)
C(10)-H(10)...F(2)	0.95	2.58	3.470(9)	156.9
C(13)-H(13D)...F(5)	0.98	2.47	3.377(13)	153.3
C(2)-H(2)...F(1)#1	1.00	2.53	3.29(2)	132.3
C(12)-H(12A)...F(5)#2	0.98	2.37	3.236(12)	146.5

Symmetry transformations used to generate equivalent atoms:
#1 -x+1/2,y-1/2,-z+2 #2 x,y,z+1

B.22 Crystal Data of [Pt(cod)(NPh-acac)]BF_4

Table B.22.1 Atomic coordinates (x 10^4) and equivalent isotropic displacement parameters ($Å^2$x 10^3) for [Pt(cod)(NPh-acac)]BF_4. U(eq) is defined as one third of the trace of the orthogonalized U^{ij} tensor.

	x	y	z	U(eq)
C(1)	7013(5)	985(2)	3070(5)	21(1)
C(2)	6435(5)	695(2)	1683(5)	19(1)
C(3)	6029(6)	1029(2)	264(5)	21(1)
C(4)	5166(5)	1658(2)	96(5)	18(1)
C(5)	4091(5)	1642(2)	811(5)	17(1)
C(6)	4491(4)	1842(2)	2235(4)	14(1)
C(7)	6099(5)	2067(2)	3328(5)	20(1)
C(8)	7437(5)	1674(2)	3335(5)	19(1)
C(9)	4156(5)	-438(2)	3254(4)	15(1)
C(10)	2639(5)	-323(2)	2997(5)	18(1)
C(11)	1755(5)	231(2)	2411(4)	14(1)
C(12)	100(5)	221(2)	2207(5)	18(1)
C(13)	4931(6)	-1057(2)	3863(5)	22(1)
C(14)	1206(5)	1263(2)	1459(4)	13(1)
C(15)	1026(5)	1681(2)	2412(5)	15(1)
C(16)	0(5)	2174(2)	1861(5)	19(1)
C(17)	-919(5)	2248(2)	361(5)	21(1)
C(18)	-763(5)	1827(2)	-600(5)	20(1)
C(19)	308(5)	1334(2)	-47(5)	16(1)
N(1)	2287(4)	742(2)	2018(4)	13(1)
O(1)	5046(4)	-47(1)	3012(3)	18(1)
Pt(1)	4490(1)	821(1)	2214(1)	12(1)
B(1)	1328(6)	1262(2)	6560(5)	19(1)
F(1)	2075(3)	1817(1)	6487(3)	31(1)
F(2)	907(4)	914(1)	5303(3)	35(1)
F(3)	2352(3)	914(1)	7784(3)	26(1)
F(4)	-2(3)	1413(1)	6724(3)	26(1)

Table B.22.2 Bond lengths [Å] and angles [°] for [Pt(cod)(NPh-acac)]BF_4.

C(1)-C(2)	1.415(7)	C(8)-H(8A)	0.9900	C(17)-C(18)	1.394(7)
C(1)-C(8)	1.511(6)	C(8)-H(8B)	0.9900	C(17)-H(17)	0.9500
C(1)-Pt(1)	2.186(5)	C(9)-O(1)	1.297(5)	C(18)-C(19)	1.392(6)
C(1)-H(1)	1.0000	C(9)-C(10)	1.374(6)	C(18)-H(18)	0.9500
C(2)-C(3)	1.508(7)	C(9)-C(13)	1.500(6)	C(19)-H(19)	0.9500
C(2)-Pt(1)	2.193(5)	C(10)-C(11)	1.412(6)	N(1)-Pt(1)	2.034(4)
C(2)-H(2)	1.0000	C(10)-H(10)	0.9500	O(1)-Pt(1)	1.990(3)
C(3)-C(4)	1.540(6)	C(11)-N(1)	1.342(5)	B(1)-F(2)	1.383(6)
C(3)-H(3A)	0.9900	C(11)-C(12)	1.502(6)	B(1)-F(3)	1.399(5)
C(3)-H(3B)	0.9900	C(12)-H(12A)	0.9800	B(1)-F(1)	1.400(6)
C(4)-C(5)	1.523(6)	C(12)-H(12B)	0.9800	B(1)-F(4)	1.401(6)
C(4)-H(4A)	0.9900	C(12)-H(12C)	0.9800		
C(4)-H(4B)	0.9900	C(13)-H(13A)	0.9800	C(2)-C(1)-C(8)	123.5(5)
C(5)-C(6)	1.403(6)	C(13)-H(13B)	0.9800	C(2)-C(1)-Pt(1)	71.4(3)
C(5)-Pt(1)	2.186(4)	C(13)-H(13C)	0.9800	C(8)-C(1)-Pt(1)	112.4(3)
C(5)-H(5)	1.0000	C(14)-C(19)	1.393(6)	C(2)-C(1)-H(1)	114.1
C(6)-C(7)	1.506(6)	C(14)-C(15)	1.396(6)	C(8)-C(1)-H(1)	114.1
C(6)-Pt(1)	2.170(5)	C(14)-N(1)	1.443(5)	Pt(1)-C(1)-H(1)	114.1
C(6)-H(6)	1.0000	C(15)-C(16)	1.368(6)	C(1)-C(2)-C(3)	125.7(4)
C(7)-C(8)	1.530(7)	C(15)-H(15)	0.9500	C(1)-C(2)-Pt(1)	70.9(3)
C(7)-H(7A)	0.9900	C(16)-C(17)	1.391(6)	C(3)-C(2)-Pt(1)	108.7(3)
C(7)-H(7B)	0.9900	C(16)-H(16)	0.9500	C(1)-C(2)-H(2)	114.3

C(3)-C(2)-H(2)	114.3	C(7)-C(8)-H(8A)	109.2	C(16)-C(17)-C(18)	120.0(4)
Pt(1)-C(2)-H(2)	114.3	C(1)-C(8)-H(8B)	109.2	C(16)-C(17)-H(17)	120.0
C(2)-C(3)-C(4)	113.7(4)	C(7)-C(8)-H(8B)	109.2	C(18)-C(17)-H(17)	120.0
C(2)-C(3)-H(3A)	108.8	H(8A)-C(8)-H(8B)	107.9	C(19)-C(18)-C(17)	119.6(4)
C(4)-C(3)-H(3A)	108.8	O(1)-C(9)-C(10)	125.6(4)	C(19)-C(18)-H(18)	120.2
C(2)-C(3)-H(3B)	108.8	O(1)-C(9)-C(13)	113.6(4)	C(17)-C(18)-H(18)	120.2
C(4)-C(3)-H(3B)	108.8	C(10)-C(9)-C(13)	120.8(4)	C(18)-C(19)-C(14)	119.7(4)
H(3A)-C(3)-H(3B)	107.7	C(9)-C(10)-C(11)	127.0(4)	C(18)-C(19)-H(19)	120.1
C(5)-C(4)-C(3)	112.0(4)	C(9)-C(10)-H(10)	116.5	C(14)-C(19)-H(19)	120.1
C(5)-C(4)-H(4A)	109.2	C(11)-C(10)-H(10)	116.5	C(11)-N(1)-C(14)	116.1(4)
C(3)-C(4)-H(4A)	109.2	N(1)-C(11)-C(10)	124.6(4)	C(11)-N(1)-Pt(1)	124.1(3)
C(5)-C(4)-H(4B)	109.2	N(1)-C(11)-C(12)	119.6(4)	C(14)-N(1)-Pt(1)	119.8(3)
C(3)-C(4)-H(4B)	109.2	C(10)-C(11)-C(12)	115.8(4)	C(9)-O(1)-Pt(1)	126.9(3)
H(4A)-C(4)-H(4B)	107.9	C(11)-C(12)-H(12A)	109.5	O(1)-Pt(1)-N(1)	91.77(13)
C(6)-C(5)-C(4)	125.8(4)	C(11)-C(12)-H(12B)	109.5	O(1)-Pt(1)-C(6)	157.53(13)
C(6)-C(5)-Pt(1)	70.6(2)	H(12A)-C(12)-H(12B)	109.5	N(1)-Pt(1)-C(6)	94.59(14)
C(4)-C(5)-Pt(1)	113.0(3)	C(11)-C(12)-H(12C)	109.5	O(1)-Pt(1)-C(5)	161.00(16)
C(6)-C(5)-H(5)	113.3	H(12A)-C(12)-H(12C)	109.5	N(1)-Pt(1)-C(5)	98.43(15)
C(4)-C(5)-H(5)	113.3	H(12B)-C(12)-H(12C)	109.5	C(6)-Pt(1)-C(5)	37.58(15)
Pt(1)-C(5)-H(5)	113.3	C(9)-C(13)-H(13A)	109.5	O(1)-Pt(1)-C(1)	86.90(16)
C(5)-C(6)-C(7)	124.7(4)	C(9)-C(13)-H(13B)	109.5	N(1)-Pt(1)-C(1)	163.31(18)
C(5)-C(6)-Pt(1)	71.8(2)	H(13A)-C(13)-H(13B)	109.5	C(6)-Pt(1)-C(1)	80.86(16)
C(7)-C(6)-Pt(1)	108.8(3)	C(9)-C(13)-H(13C)	109.5	C(5)-Pt(1)-C(1)	87.77(18)
C(5)-C(6)-H(6)	114.4	H(13A)-C(13)-H(13C)	109.5	O(1)-Pt(1)-C(2)	83.95(15)
C(7)-C(6)-H(6)	114.4	H(13B)-C(13)-H(13C)	109.5	N(1)-Pt(1)-C(2)	158.55(17)
Pt(1)-C(6)-H(6)	114.4	C(19)-C(14)-C(15)	120.3(4)	C(6)-Pt(1)-C(2)	97.33(16)
C(6)-C(7)-C(8)	113.2(4)	C(19)-C(14)-N(1)	119.2(4)	C(5)-Pt(1)-C(2)	80.70(17)
C(6)-C(7)-H(7A)	108.9	C(15)-C(14)-N(1)	120.5(4)	C(1)-Pt(1)-C(2)	37.71(18)
C(8)-C(7)-H(7A)	108.9	C(16)-C(15)-C(14)	119.7(4)	F(2)-B(1)-F(3)	110.0(4)
C(6)-C(7)-H(7B)	108.9	C(16)-C(15)-H(15)	120.2	F(2)-B(1)-F(1)	109.5(4)
C(8)-C(7)-H(7B)	108.9	C(14)-C(15)-H(15)	120.2	F(3)-B(1)-F(1)	109.4(4)
H(7A)-C(7)-H(7B)	107.7	C(15)-C(16)-C(17)	120.7(4)	F(2)-B(1)-F(4)	110.5(4)
C(1)-C(8)-C(7)	112.0(4)	C(15)-C(16)-H(16)	119.6	F(3)-B(1)-F(4)	108.0(4)
C(1)-C(8)-H(8A)	109.2	C(17)-C(16)-H(16)	119.6	F(1)-B(1)-F(4)	109.4(4)

Symmetry transformations used to generate equivalent atoms:

Table B.22.3 Anisotropic displacement parameters ($Å^2 x\ 10^3$) for [Pt(cod)(NPh-acac)]BF_4. The anisotropic displacement factor exponent takes the form: $-2\pi^2[\ h^2 a^{*2} U^{11} + ... + 2\ h\ k\ a^*\ b^*\ U^{12}\ ]$

	U^{11}	U^{22}	U^{33}	U^{23}	U^{13}	U^{12}
C(1)	13(2)	20(2)	26(2)	-3(2)	5(2)	7(2)
C(2)	18(2)	18(2)	26(2)	2(2)	15(2)	3(2)
C(3)	23(2)	24(2)	22(2)	-2(2)	15(2)	0(2)
C(4)	19(2)	16(2)	18(2)	3(2)	8(2)	-4(2)
C(5)	16(2)	10(2)	25(2)	7(2)	8(2)	1(2)
C(6)	14(2)	10(2)	26(2)	3(2)	16(2)	3(2)
C(7)	22(2)	18(2)	21(2)	-3(2)	10(2)	-7(2)
C(8)	15(2)	21(2)	23(2)	2(2)	10(2)	-1(2)
C(9)	22(2)	11(2)	14(2)	1(2)	11(2)	0(2)
C(10)	22(2)	14(2)	21(2)	0(2)	13(2)	-4(2)
C(11)	16(2)	14(2)	14(2)	-1(2)	9(2)	0(2)
C(12)	17(2)	15(2)	25(2)	2(2)	14(2)	-1(2)
C(13)	28(3)	13(2)	25(2)	5(2)	13(2)	5(2)
C(14)	13(2)	9(2)	22(2)	1(2)	12(2)	-1(2)
C(15)	17(2)	11(2)	21(2)	-1(2)	12(2)	-4(2)
C(16)	23(2)	12(2)	29(2)	-7(2)	18(2)	-1(2)
C(17)	19(2)	9(2)	37(3)	7(2)	16(2)	4(2)
C(18)	16(2)	20(2)	22(2)	5(2)	9(2)	-2(2)
C(19)	17(2)	12(2)	20(2)	-2(2)	10(2)	-2(2)
N(1)	11(2)	12(2)	18(2)	-1(1)	8(2)	0(1)
O(1)	17(2)	13(2)	25(2)	6(1)	12(1)	4(1)
Pt(1)	12(1)	11(1)	16(1)	1(1)	8(1)	1(1)
B(1)	20(3)	18(3)	19(2)	1(2)	8(2)	0(2)
F(1)	34(2)	18(1)	48(2)	7(1)	25(2)	0(1)
F(2)	40(2)	37(2)	26(2)	-8(1)	14(1)	3(1)
F(3)	24(2)	21(1)	26(1)	6(1)	7(1)	-2(1)

F(4)	22(1)	34(2)	28(1)	4(1)	15(1)	2(1)

Table B.22.4 Hydrogen coordinates (x 10^4) and isotropic displacement parameters ($Å^2$x 10^3) for [Pt(cod)(NPh-acac)]BF_4.

	x	y	z	U(eq)
H(1)	7690	705	3905	26
H(2)	6776	249	1714	23
H(3A)	5359	750	-557	25
H(3B)	7011	1109	198	25
H(4A)	5951	1998	544	22
H(4B)	4533	1755	-956	22
H(5)	2958	1710	105	21
H(6)	3603	2034	2348	17
H(7A)	6173	2057	4316	25
H(7B)	6230	2510	3106	25
H(8A)	7691	1831	2568	23
H(8B)	8387	1723	4290	23
H(10)	2131	-652	3240	22
H(12A)	-25	552	2806	26
H(12B)	-117	-189	2507	26
H(12C)	-637	295	1176	26
H(13A)	5438	-1214	3293	33
H(13B)	4138	-1360	3812	33
H(13C)	5725	-1002	4884	33
H(15)	1612	1623	3439	18
H(16)	-86	2470	2510	23
H(17)	-1652	2584	-9	25
H(18)	-1385	1877	-1625	23
H(19)	427	1047	-694	19

Table B.22.5 Hydrogen bonds for [Pt(cod)(NPh-acac)]BF_4 [Å and °]

D-H...A	d(D-H)	d(H...A)	d(D...A)	<(DHA)
C(12)-H(12A)...F(2)	0.98	2.43	3.272(6)	143.6
C(8)-H(8B)...F(4)#1	0.99	2.35	3.258(5)	151.6
C(12)-H(12B)...F(3)#2	0.98	2.54	3.374(5)	142.6

Symmetry transformations used to generate equivalent atoms:
#1 x+1,y,z #2 -x,-y,-z+1

B.23 Crystal Data of [Pt(cod)(NPh-acac)]PF_6

Table B.23.1 Atomic coordinates (x 10^4) and equivalent isotropic displacement parameters ($Å^2$x 10^3) for [Pt(cod)(NPh-acac)]PF_6. U(eq) is defined as one third of the trace of the orthogonalized U^{ij} tensor.

	x	y	z	U(eq)
C(11)	2260(20)	2018(16)	3673(12)	65(5)
C(12)	1070(20)	1397(16)	3576(12)	65(5)
C(13A)	1180(50)	790(30)	4280(30)	65(5)
C(14A)	2700(50)	130(18)	4300(30)	36(9)
C(18A)	4020(50)	2170(20)	4410(20)	40(4)
C(23A)	8630(50)	-1700(20)	9700(20)	37(3)
C(27A)	7700(60)	-110(20)	9330(30)	42(4)
C(28A)	6170(50)	-400(30)	9050(30)	64(4)

C(13B)	1160(50)	380(30)	4060(30)	65(5)
C(14B)	1850(60)	170(20)	3920(30)	36(4)
C(18B)	3660(50)	1750(20)	4660(20)	40(4)
C(23B)	8960(50)	-2130(20)	9410(20)	37(3)
C(27B)	6910(60)	-200(20)	8960(30)	42(4)
C(28B)	6210(50)	-770(30)	9330(30)	64(4)
C(15)	3420(20)	290(9)	3471(10)	36(4)
C(16)	4550(20)	858(9)	3615(9)	34(4)
C(17)	4970(20)	1393(10)	4501(11)	40(4)
C(19)	391(18)	1894(10)	666(11)	32(3)
C(21)	6080(20)	-1361(15)	8576(13)	64(4)
C(22)	7260(20)	-2060(16)	8633(13)	64(4)
C(24)	9960(20)	-1400(10)	9500(10)	37(3)
C(25)	9540(20)	-853(10)	8609(10)	37(3)
C(26)	8400(30)	-293(9)	8473(11)	42(4)
C(29)	5375(19)	-1905(9)	5662(10)	28(3)
C(110)	1021(18)	1396(9)	73(10)	26(3)
C(111)	2393(16)	926(7)	384(9)	20(3)
C(112)	2948(19)	530(9)	-397(9)	29(3)
C(113)	-880(20)	2492(13)	208(12)	54(5)
C(114)	4659(16)	360(8)	1498(9)	20(3)
C(115)	4670(20)	-439(9)	1632(9)	30(3)
C(116)	6140(20)	-792(10)	1819(10)	38(4)
C(117)	7520(20)	-415(13)	1874(12)	51(6)
C(118)	7480(19)	339(13)	1709(13)	44(5)
C(119)	6048(17)	733(10)	1522(11)	30(3)
C(210)	6018(19)	-1410(9)	5100(10)	25(3)
C(211)	7418(17)	-934(7)	5399(9)	20(3)
C(212)	7940(20)	-535(9)	4589(11)	32(3)
C(213)	4130(20)	-2492(13)	5212(12)	55(6)
C(214)	9648(15)	-365(7)	6503(9)	18(3)
C(215)	11075(19)	-740(10)	6539(10)	32(4)
C(216)	12495(19)	-336(12)	6721(12)	40(4)
C(217)	12500(20)	407(14)	6864(12)	49(6)
C(218)	11140(20)	796(10)	6815(10)	38(4)
C(219)	9671(18)	445(8)	6643(9)	24(3)
N(1)	3199(14)	793(6)	1338(8)	22(2)
N(2)	8193(13)	-801(6)	6333(7)	19(2)
O(1)	886(13)	1959(8)	1611(7)	40(3)
O(2)	5881(13)	-1974(8)	6620(7)	41(3)
F(11)	6785(14)	2219(6)	2970(7)	53(3)
F(12)	8292(11)	3327(7)	2919(8)	54(3)
F(13)	6116(11)	3944(5)	1986(7)	38(2)
F(14)	4606(13)	2884(7)	2103(9)	63(3)
F(15)	6758(18)	2742(7)	1506(7)	75(5)
F(16)	6144(15)	3433(7)	3450(7)	54(3)
F(21)	11788(13)	-2227(5)	7979(6)	48(3)
F(22)	11776(17)	-2754(7)	6515(7)	68(4)
F(23)	11116(11)	-3947(5)	6984(7)	34(2)
F(24)	11142(14)	-3437(7)	8447(7)	51(3)
F(25)	13295(11)	-3333(7)	7922(8)	54(3)
F(26)	9605(13)	-2880(7)	7065(9)	65(4)
P(1)	6447(5)	3072(2)	2485(3)	26(1)
P(2)	11452(5)	-3080(2)	7481(3)	26(1)
Pt(1)	2502(1)	1268(1)	2488(1)	19(1)
Pt(2)	7501(1)	-1274(1)	7486(1)	19(1)

Table B.23.2 Bond lengths [Å] and angles [°] for [Pt(cod)(NPh-acac)]PF_6.

C(11)-C(12)	1.46(4)	C(26)-Pt(2)	2.181(17)	C(18B)-C(11)-Pt(1)	107.0(15)
C(11)-C(18A)	1.62(4)	C(26)-H(26)	1.0000	C(12)-C(11)-H(11)	110.8
C(11)-C(18B)	1.65(4)	C(29)-O(2)	1.319(16)	C(18A)-C(11)-H(11)	110.8
C(11)-Pt(1)	2.170(18)	C(29)-C(210)	1.379(19)	C(18B)-C(11)-H(11)	134.9
C(11)-H(11)	1.0000	C(29)-C(213)	1.48(2)	Pt(1)-C(11)-H(11)	110.8
C(12)-C(13A)	1.43(5)	C(110)-C(111)	1.403(19)	C(13A)-C(12)-C(11)	123(2)
C(12)-C(13B)	1.85(6)	C(110)-H(110)	0.9500	C(13A)-C(12)-C(13B)	22.1(17)
C(12)-Pt(1)	2.245(17)	C(111)-N(1)	1.367(16)	C(11)-C(12)-C(13B)	133(2)
C(12)-H(12)	1.0000	C(111)-C(112)	1.488(18)	C(13A)-C(12)-Pt(1)	118.2(19)
C(13A)-C(14A)	1.73(6)	C(112)-H(11A)	0.9800	C(11)-C(12)-Pt(1)	68.0(10)
C(13A)-H(13A)	0.9900	C(112)-H(11B)	0.9800	C(13B)-C(12)-Pt(1)	101.3(16)
C(13A)-H(13B)	0.9900	C(112)-H(11C)	0.9800	C(13A)-C(12)-H(12)	113.3
C(14A)-C(15)	1.51(3)	C(113)-H(11D)	0.9800	C(11)-C(12)-H(12)	113.3
C(14A)-H(14A)	0.9900	C(113)-H(11E)	0.9800	C(13B)-C(12)-H(12)	112.7
C(14A)-H(14B)	0.9900	C(113)-H(11F)	0.9800	Pt(1)-C(12)-H(12)	113.3
C(18A)-C(17)	1.54(4)	C(114)-C(119)	1.36(2)	C(12)-C(13A)-C(14A)	112(3)
C(18A)-H(18A)	0.9900	C(114)-C(115)	1.37(2)	C(12)-C(13A)-H(13A)	109.1
C(18A)-H(18B)	0.9900	C(114)-N(1)	1.432(16)	C(14A)-C(13A)-H(13A)	109.1
C(23A)-C(24)	1.36(4)	C(115)-C(116)	1.37(2)	C(12)-C(13A)-H(13B)	109.1
C(23A)-C(22)	1.77(4)	C(115)-H(115)	0.9500	C(14A)-C(13A)-H(13B)	109.1
C(23A)-H(23A)	0.9900	C(116)-C(117)	1.35(3)	H(13A)-C(13A)-H(13B)	107.9
C(23A)-H(23B)	0.9900	C(116)-H(116)	0.9500	C(15)-C(14A)-C(13A)	111(3)
C(27A)-C(28A)	1.37(6)	C(117)-C(118)	1.30(3)	C(15)-C(14A)-H(14A)	109.5
C(27A)-C(26)	1.54(3)	C(117)-H(117)	0.9500	C(13A)-C(14A)-H(14A)	109.5
C(27A)-H(27A)	0.9900	C(118)-C(119)	1.38(2)	C(15)-C(14A)-H(14B)	109.5
C(27A)-H(27B)	0.9900	C(118)-H(118)	0.9500	C(13A)-C(14A)-H(14B)	109.5
C(28A)-C(21)	1.75(6)	C(119)-H(119)	0.9500	H(14A)-C(14A)-H(14B)	108.1
C(28A)-H(28A)	0.9900	C(210)-C(211)	1.43(2)	C(17)-C(18A)-C(11)	108(2)
C(28A)-H(28B)	0.9900	C(210)-H(210)	0.9500	C(17)-C(18A)-H(18A)	110.0
C(13B)-C(14B)	0.78(5)	C(211)-N(2)	1.336(16)	C(11)-C(18A)-H(18A)	110.0
C(13B)-H(13C)	0.9900	C(211)-C(212)	1.513(18)	C(17)-C(18A)-H(18B)	110.0
C(13B)-H(13D)	0.9900	C(212)-H(21A)	0.9800	C(11)-C(18A)-H(18B)	110.0
C(14B)-C(15)	1.68(5)	C(212)-H(21B)	0.9800	H(18A)-C(18A)-H(18B)	108.4
C(14B)-H(14C)	0.9900	C(212)-H(21C)	0.9800	C(24)-C(23A)-C(22)	112(2)
C(14B)-H(14D)	0.9900	C(213)-H(21D)	0.9800	C(24)-C(23A)-H(23A)	109.3
C(18B)-C(17)	1.36(4)	C(213)-H(21E)	0.9800	C(22)-C(23A)-H(23A)	109.3
C(18B)-H(18C)	0.9900	C(213)-H(21F)	0.9800	C(24)-C(23A)-H(23B)	109.3
C(18B)-H(18D)	0.9900	C(214)-C(215)	1.38(2)	C(22)-C(23A)-H(23B)	109.3
C(23B)-C(24)	1.50(4)	C(214)-C(219)	1.388(19)	H(23A)-C(23A)-H(23B)	108.0
C(23B)-C(22)	1.60(4)	C(214)-N(2)	1.430(17)	C(28A)-C(27A)-C(26)	105(3)
C(23B)-H(23C)	0.9900	C(215)-C(216)	1.37(2)	C(28A)-C(27A)-H(27A)	110.8
C(23B)-H(23D)	0.9900	C(215)-H(215)	0.9500	C(26)-C(27A)-H(27A)	110.8
C(27B)-C(28B)	1.33(5)	C(216)-C(217)	1.28(3)	C(28A)-C(27A)-H(27B)	110.8
C(27B)-C(26)	1.64(5)	C(216)-H(216)	0.9500	C(26)-C(27A)-H(27B)	110.8
C(27B)-H(27C)	0.9900	C(217)-C(218)	1.34(3)	H(27A)-C(27A)-H(27B)	108.9
C(27B)-H(27D)	0.9900	C(217)-H(217)	0.9500	C(27A)-C(28A)-C(21)	113(4)
C(28B)-C(21)	1.44(5)	C(218)-C(219)	1.37(2)	C(27A)-C(28A)-H(28A)	109.0
C(28B)-H(28C)	0.9900	C(218)-H(218)	0.9500	C(21)-C(28A)-H(28A)	109.0
C(28B)-H(28D)	0.9900	C(219)-H(219)	0.9500	C(27A)-C(28A)-H(28B)	109.0
C(15)-C(16)	1.35(2)	N(1)-Pt(1)	2.058(11)	C(21)-C(28A)-H(28B)	109.0
C(15)-Pt(1)	2.178(15)	N(2)-Pt(2)	2.058(11)	H(28A)-C(28A)-H(28B)	107.8
C(15)-H(15)	1.0000	O(1)-Pt(1)	1.989(10)	C(14B)-C(13B)-C(12)	107(6)
C(16)-C(17)	1.52(2)	O(2)-Pt(2)	1.994(11)	C(14B)-C(13B)-H(13C)	110.2
C(16)-Pt(1)	2.162(14)	F(11)-P(1)	1.596(9)	C(12)-C(13B)-H(13C)	110.2
C(16)-H(16)	1.0000	F(12)-P(1)	1.615(11)	C(14B)-C(13B)-H(13D)	110.2
C(17)-H(17A)	0.9900	F(13)-P(1)	1.632(9)	C(12)-C(13B)-H(13D)	110.2
C(17)-H(17B)	0.9900	F(14)-P(1)	1.579(11)	H(13C)-C(13B)-H(13D)	108.5
C(19)-O(1)	1.302(18)	F(15)-P(1)	1.592(10)	C(13B)-C(14B)-C(15)	144(6)
C(19)-C(110)	1.41(2)	F(16)-P(1)	1.590(11)	C(13B)-C(14B)-H(14C)	100.8
C(19)-C(113)	1.51(2)	F(21)-P(2)	1.604(10)	C(15)-C(14B)-H(14C)	100.8
C(21)-C(22)	1.56(4)	F(22)-P(2)	1.577(10)	C(13B)-C(14B)-H(14D)	100.8
C(21)-Pt(2)	2.238(18)	F(23)-P(2)	1.623(9)	C(15)-C(14B)-H(14D)	100.8
C(21)-H(21)	1.0000	F(24)-P(2)	1.591(10)	H(14C)-C(14B)-H(14D)	104.4
C(22)-Pt(2)	2.164(17)	F(25)-P(2)	1.614(10)	C(17)-C(18B)-C(11)	116(2)
C(22)-H(22)	1.0000	F(26)-P(2)	1.592(10)	C(17)-C(18B)-H(18C)	108.2
C(24)-C(25)	1.534(18)			C(11)-C(18B)-H(18C)	108.2
C(24)-H(24A)	0.9900	C(12)-C(11)-C(18A)	134(2)	C(17)-C(18B)-H(18D)	108.3
C(24)-H(24B)	0.9900	C(12)-C(11)-C(18B)	103(2)	C(11)-C(18B)-H(18D)	108.2
C(25)-C(26)	1.35(2)	C(18A)-C(11)-C(18B)	31.4(17)	H(18C)-C(18B)-H(18D)	107.4
C(25)-Pt(2)	2.161(15)	C(12)-C(11)-Pt(1)	73.5(11)	C(24)-C(23B)-C(22)	114(2)
C(25)-H(25)	1.0000	C(18A)-C(11)-Pt(1)	108.6(15)	C(24)-C(23B)-H(23C)	108.8

C(22)-C(23B)-H(23C)	108.8	C(26)-C(25)-C(24)	123.0(16)	C(219)-C(214)-N(2)	120.9(12)
C(24)-C(23B)-H(23D)	108.8	C(26)-C(25)-Pt(2)	72.7(11)	C(216)-C(215)-C(214)	122.1(16)
C(22)-C(23B)-H(23D)	108.8	C(24)-C(25)-Pt(2)	112.0(10)	C(216)-C(215)-H(215)	119.0
H(23C)-C(23B)-H(23D)	107.7	C(26)-C(25)-H(25)	114.1	C(214)-C(215)-H(215)	119.0
C(28B)-C(27B)-C(26)	126(3)	C(24)-C(25)-H(25)	114.1	C(217)-C(216)-C(215)	119.2(17)
C(28B)-C(27B)-H(27C)	105.8	Pt(2)-C(25)-H(25)	114.1	C(217)-C(216)-H(216)	120.4
C(26)-C(27B)-H(27C)	105.8	C(25)-C(26)-C(27A)	117.4(18)	C(215)-C(216)-H(216)	120.4
C(28B)-C(27B)-H(27D)	105.8	C(25)-C(26)-C(27B)	130.3(18)	C(216)-C(217)-C(218)	120.7(16)
C(26)-C(27B)-H(27D)	105.8	C(27A)-C(26)-C(27B)	27.8(18)	C(216)-C(217)-H(217)	119.7
H(27C)-C(27B)-H(27D)	106.2	C(25)-C(26)-Pt(2)	71.1(9)	C(218)-C(217)-H(217)	119.7
C(27B)-C(28B)-C(21)	99(3)	C(27A)-C(26)-Pt(2)	121.1(19)	C(217)-C(218)-C(219)	124.3(17)
C(27B)-C(28B)-H(28C)	111.9	C(27B)-C(26)-Pt(2)	99.3(19)	C(217)-C(218)-H(218)	117.8
C(21)-C(28B)-H(28C)	111.9	C(25)-C(26)-H(26)	113.6	C(219)-C(218)-H(218)	117.8
C(27B)-C(28B)-H(28D)	111.9	C(27A)-C(26)-H(26)	113.6	C(218)-C(219)-C(214)	115.6(15)
C(21)-C(28B)-H(28D)	111.9	C(27B)-C(26)-H(26)	114.7	C(218)-C(219)-H(219)	122.2
H(28C)-C(28B)-H(28D)	109.6	Pt(2)-C(26)-H(26)	113.6	C(214)-C(219)-H(219)	122.2
C(16)-C(15)-C(14A)	116.7(19)	O(2)-C(29)-C(210)	125.4(14)	C(111)-N(1)-C(114)	115.9(11)
C(16)-C(15)-C(14B)	131.6(18)	O(2)-C(29)-C(213)	112.7(13)	C(111)-N(1)-Pt(1)	122.9(9)
C(14A)-C(15)-C(14B)	28.2(16)	C(210)-C(29)-C(213)	121.5(13)	C(114)-N(1)-Pt(1)	121.0(8)
C(16)-C(15)-Pt(1)	71.3(8)	C(111)-C(110)-C(19)	126.1(13)	C(211)-N(2)-C(214)	116.1(11)
C(14A)-C(15)-Pt(1)	118.8(18)	C(111)-C(110)-H(110)	117.0	C(211)-N(2)-Pt(2)	123.3(9)
C(14B)-C(15)-Pt(1)	98.3(16)	C(19)-C(110)-H(110)	117.0	C(214)-N(2)-Pt(2)	120.3(8)
C(16)-C(15)-H(15)	114.4	N(1)-C(111)-C(110)	124.8(12)	C(19)-O(1)-Pt(1)	125.3(9)
C(14A)-C(15)-H(15)	114.4	N(1)-C(111)-C(112)	118.9(12)	C(29)-O(2)-Pt(2)	124.6(9)
C(14B)-C(15)-H(15)	112.8	C(110)-C(111)-C(112)	116.3(11)	F(14)-P(1)-F(16)	89.1(7)
Pt(1)-C(15)-H(15)	114.4	C(111)-C(112)-H(11A)	109.5	F(14)-P(1)-F(15)	91.4(8)
C(15)-C(16)-C(17)	123.7(15)	C(111)-C(112)-H(11B)	109.5	F(16)-P(1)-F(15)	178.0(7)
C(15)-C(16)-Pt(1)	72.6(10)	H(11A)-C(112)-H(11B)	109.5	F(14)-P(1)-F(11)	90.9(6)
C(17)-C(16)-Pt(1)	112.9(10)	C(111)-C(112)-H(11C)	109.5	F(16)-P(1)-F(11)	91.7(6)
C(15)-C(16)-H(16)	113.6	H(11A)-C(112)-H(11C)	109.5	F(15)-P(1)-F(11)	90.2(6)
C(17)-C(16)-H(16)	113.6	H(11B)-C(112)-H(11C)	109.5	F(14)-P(1)-F(12)	175.4(8)
Pt(1)-C(16)-H(16)	113.6	C(19)-C(113)-H(11D)	109.5	F(16)-P(1)-F(12)	87.0(7)
C(18B)-C(17)-C(16)	112.3(19)	C(19)-C(113)-H(11E)	109.5	F(15)-P(1)-F(12)	92.4(8)
C(18B)-C(17)-C(18A)	35(2)	H(11D)-C(113)-H(11E)	109.5	F(11)-P(1)-F(12)	91.7(6)
C(16)-C(17)-C(18A)	115.9(16)	C(19)-C(113)-H(11F)	109.5	F(14)-P(1)-F(13)	89.4(5)
C(18B)-C(17)-H(17A)	134.9	H(11D)-C(113)-H(11F)	109.5	F(16)-P(1)-F(13)	88.7(6)
C(16)-C(17)-H(17A)	108.3	H(11E)-C(113)-H(11F)	109.5	F(15)-P(1)-F(13)	89.4(6)
C(18A)-C(17)-H(17A)	108.3	C(119)-C(114)-C(115)	119.2(14)	F(11)-P(1)-F(13)	179.5(7)
C(18B)-C(17)-H(17B)	77.5	C(119)-C(114)-N(1)	120.7(13)	F(12)-P(1)-F(13)	88.0(5)
C(16)-C(17)-H(17B)	108.3	C(115)-C(114)-N(1)	120.1(13)	F(22)-P(2)-F(24)	178.2(7)
C(18A)-C(17)-H(17B)	108.3	C(114)-C(115)-C(116)	115.4(16)	F(22)-P(2)-F(26)	90.1(8)
H(17A)-C(17)-H(17B)	107.4	C(114)-C(115)-H(115)	122.3	F(24)-P(2)-F(26)	90.7(7)
O(1)-C(19)-C(110)	126.7(13)	C(116)-C(115)-H(115)	122.3	F(22)-P(2)-F(21)	90.8(6)
O(1)-C(19)-C(113)	112.8(13)	C(117)-C(116)-C(115)	125.1(17)	F(24)-P(2)-F(21)	90.8(6)
C(110)-C(19)-C(113)	120.2(13)	C(117)-C(116)-H(116)	117.4	F(26)-P(2)-F(21)	90.9(6)
C(28B)-C(21)-C(22)	125(2)	C(115)-C(116)-H(116)	117.4	F(22)-P(2)-F(25)	92.2(7)
C(28B)-C(21)-C(28A)	24.6(16)	C(118)-C(117)-C(116)	118.6(15)	F(24)-P(2)-F(25)	87.0(6)
C(22)-C(21)-C(28A)	137(2)	C(118)-C(117)-H(117)	120.7	F(26)-P(2)-F(25)	176.7(8)
C(28B)-C(21)-Pt(2)	121(2)	C(116)-C(117)-H(117)	120.7	F(21)-P(2)-F(25)	91.4(6)
C(22)-C(21)-Pt(2)	66.8(9)	C(117)-C(118)-C(119)	119.4(17)	F(22)-P(2)-F(23)	89.5(6)
C(28A)-C(21)-Pt(2)	103.2(17)	C(117)-C(118)-H(118)	120.3	F(24)-P(2)-F(23)	88.9(6)
C(28B)-C(21)-H(21)	113.3	C(119)-C(118)-H(118)	120.3	F(26)-P(2)-F(23)	89.2(6)
C(22)-C(21)-H(21)	111.5	C(114)-C(119)-C(118)	122.2(16)	F(21)-P(2)-F(23)	179.7(6)
C(28A)-C(21)-H(21)	111.5	C(114)-C(119)-H(119)	118.9	F(25)-P(2)-F(23)	88.4(5)
Pt(2)-C(21)-H(21)	111.5	C(118)-C(119)-H(119)	118.9	O(1)-Pt(1)-N(1)	92.4(4)
C(21)-C(22)-C(23B)	125(2)	C(29)-C(210)-C(211)	128.3(12)	O(1)-Pt(1)-C(16)	162.6(5)
C(21)-C(22)-C(23A)	94(2)	C(29)-C(210)-H(210)	115.9	N(1)-Pt(1)-C(16)	95.9(5)
C(23B)-C(22)-C(23A)	31.5(17)	C(211)-C(210)-H(210)	115.9	O(1)-Pt(1)-C(11)	86.6(6)
C(21)-C(22)-Pt(2)	71.9(10)	N(2)-C(211)-C(210)	123.5(11)	N(1)-Pt(1)-C(11)	163.7(8)
C(23B)-C(22)-Pt(2)	108.0(15)	N(2)-C(211)-C(212)	120.5(12)	C(16)-Pt(1)-C(11)	81.1(6)
C(23A)-C(22)-Pt(2)	104.4(14)	C(210)-C(211)-C(212)	115.9(11)	O(1)-Pt(1)-C(15)	157.9(6)
C(21)-C(22)-H(22)	124.2	C(211)-C(212)-H(21A)	109.5	N(1)-Pt(1)-C(15)	94.4(5)
C(23B)-C(22)-H(22)	101.8	C(211)-C(212)-H(21B)	109.5	C(16)-Pt(1)-C(15)	36.2(6)
C(23A)-C(22)-H(22)	124.2	H(21A)-C(212)-H(21B)	109.5	C(11)-Pt(1)-C(15)	92.5(7)
Pt(2)-C(22)-H(22)	124.2	C(211)-C(212)-H(21C)	109.5	O(1)-Pt(1)-C(12)	86.9(6)
C(23A)-C(24)-C(23B)	37(2)	H(21A)-C(212)-H(21C)	109.5	N(1)-Pt(1)-C(12)	157.7(7)
C(23A)-C(24)-C(25)	111.8(19)	H(21B)-C(212)-H(21C)	109.5	C(16)-Pt(1)-C(12)	91.0(6)
C(23B)-C(24)-C(25)	115.4(15)	C(29)-C(213)-H(21D)	109.5	C(11)-Pt(1)-C(12)	38.5(9)
C(23A)-C(24)-H(24A)	109.3	C(29)-C(213)-H(21E)	109.5	C(15)-Pt(1)-C(12)	78.9(7)
C(23B)-C(24)-H(24A)	73.5	H(21D)-C(213)-H(21E)	109.5	O(2)-Pt(2)-N(2)	92.9(4)
C(25)-C(24)-H(24A)	109.2	C(29)-C(213)-H(21F)	109.5	O(2)-Pt(2)-C(25)	162.7(5)
C(23A)-C(24)-H(24B)	109.2	H(21D)-C(213)-H(21F)	109.5	N(2)-Pt(2)-C(25)	95.9(5)
C(23B)-C(24)-H(24B)	132.0	H(21E)-C(213)-H(21F)	109.5	O(2)-Pt(2)-C(22)	84.4(7)
C(25)-C(24)-H(24B)	109.2	C(215)-C(214)-C(219)	118.1(13)	N(2)-Pt(2)-C(22)	162.2(7)
H(24A)-C(24)-H(24B)	107.9	C(215)-C(214)-N(2)	121.0(12)	C(25)-Pt(2)-C(22)	82.8(7)

O(2)-Pt(2)-C(26)	157.3(7)	C(22)-Pt(2)-C(26)	94.3(8)	C(25)-Pt(2)-C(21)	90.3(7)
N(2)-Pt(2)-C(26)	94.9(5)	O(2)-Pt(2)-C(21)	87.6(7)	C(22)-Pt(2)-C(21)	41.4(9)
C(25)-Pt(2)-C(26)	36.2(7)	N(2)-Pt(2)-C(21)	156.3(7)	C(26)-Pt(2)-C(21)	76.8(8)

Symmetry transformations used to generate equivalent atoms:

Table B.23.3 Anisotropic displacement parameters ($Å^2 x\ 10^3$) for [Pt(cod)(NPh-acac)]PF_6. The anisotropic displacement factor exponent takes the form: $-2\pi^2[\ h^2 a^{*2} U^{11} + ... + 2\ h\ k\ a^*\ b^*\ U^{12}\ ]$

	U^{11}	U^{22}	U^{33}	U^{23}	U^{13}	U^{12}
C(11)	39(6)	141(16)	15(5)	-23(7)	8(5)	35(8)
C(12)	39(6)	141(16)	15(5)	-23(7)	8(5)	35(8)
C(13A)	39(6)	141(16)	15(5)	-23(7)	8(5)	35(8)
C(14A)	70(30)	22(16)	25(17)	-3(13)	30(17)	-15(17)
C(18A)	50(9)	42(9)	17(6)	-21(6)	-10(6)	6(7)
C(23A)	56(7)	37(6)	10(4)	4(4)	-5(4)	-19(5)
C(27A)	90(14)	20(6)	27(7)	-4(6)	35(8)	9(7)
C(28A)	44(7)	125(14)	24(6)	26(7)	14(5)	-22(7)
C(13B)	39(6)	141(16)	15(5)	-23(7)	8(5)	35(8)
C(14B)	81(12)	17(7)	18(7)	1(5)	26(7)	-10(7)
C(18B)	50(9)	42(9)	17(6)	-21(6)	-10(6)	6(7)
C(23B)	56(7)	37(6)	10(4)	4(4)	-5(4)	-19(5)
C(27B)	90(14)	20(6)	27(7)	-4(6)	35(8)	9(7)
C(28B)	44(7)	125(14)	24(6)	26(7)	14(5)	-22(7)
C(15)	81(12)	17(7)	18(7)	1(5)	26(7)	-10(7)
C(16)	59(11)	32(8)	5(6)	-6(5)	-1(6)	18(8)
C(17)	50(9)	42(9)	17(6)	-21(6)	-10(6)	6(7)
C(19)	21(7)	52(10)	23(7)	-3(7)	4(6)	4(7)
C(21)	44(7)	125(14)	24(6)	26(7)	14(5)	-22(7)
C(22)	44(7)	125(14)	24(6)	26(7)	14(5)	-22(7)
C(24)	56(7)	37(6)	10(4)	4(4)	-5(4)	-19(5)
C(25)	56(7)	37(6)	10(4)	4(4)	-5(4)	-19(5)
C(26)	90(14)	20(6)	27(7)	-4(6)	35(8)	9(7)
C(29)	33(8)	37(9)	14(6)	2(6)	3(6)	-6(7)
C(110)	22(7)	30(8)	18(7)	-6(6)	-6(6)	-5(6)
C(111)	29(7)	19(7)	11(6)	-2(5)	6(5)	-12(5)
C(112)	40(8)	41(9)	9(6)	-1(6)	10(6)	11(7)
C(113)	42(9)	78(14)	28(9)	-30(9)	-14(8)	27(9)
C(114)	20(6)	27(7)	14(6)	-9(5)	5(5)	-1(5)
C(115)	51(9)	26(8)	14(6)	0(5)	9(6)	14(7)
C(116)	58(12)	38(9)	14(7)	-10(6)	0(7)	17(8)
C(117)	27(9)	89(16)	27(8)	-26(9)	-9(7)	29(9)
C(118)	17(7)	71(14)	41(10)	-24(9)	1(7)	-2(8)
C(119)	21(7)	41(9)	26(7)	-12(6)	4(6)	-5(6)
C(210)	36(8)	22(7)	14(6)	5(5)	2(6)	2(6)
C(211)	36(8)	12(6)	12(6)	-3(5)	7(5)	1(5)
C(212)	38(9)	35(9)	24(7)	-5(6)	12(7)	-18(7)
C(213)	37(9)	86(15)	33(9)	21(10)	-4(8)	-33(10)
C(214)	22(7)	20(7)	15(6)	2(5)	8(5)	-2(5)
C(215)	33(8)	45(10)	18(7)	13(6)	7(6)	7(7)
C(216)	22(8)	67(13)	28(8)	14(8)	2(6)	4(8)
C(217)	26(9)	93(17)	21(8)	16(9)	-4(6)	-32(10)
C(218)	67(12)	33(9)	12(7)	5(6)	4(7)	-27(8)
C(219)	30(7)	29(8)	14(6)	-3(5)	6(6)	-11(6)
N(1)	31(6)	19(6)	19(5)	6(4)	13(5)	2(5)
N(2)	20(5)	20(6)	16(5)	-6(4)	3(4)	0(4)
O(1)	26(5)	67(8)	21(5)	-24(5)	-2(4)	24(5)
O(2)	25(6)	74(9)	19(5)	21(5)	-4(4)	-21(5)
F(11)	85(8)	35(6)	27(5)	8(4)	-9(5)	-11(5)
F(12)	28(5)	76(8)	55(7)	40(6)	4(5)	8(5)
F(13)	29(5)	34(5)	47(6)	13(4)	5(4)	3(4)

F(14)	39(6)	67(8)	67(8)	27(6)	-13(5)	-25(5)
F(15)	132(12)	74(8)	19(5)	4(5)	20(6)	61(8)
F(16)	82(8)	54(7)	34(5)	1(5)	30(5)	1(6)
F(21)	74(7)	32(5)	26(5)	-10(4)	-6(5)	9(5)
F(22)	111(11)	69(8)	27(5)	-11(5)	22(6)	-52(8)
F(23)	29(4)	27(5)	42(5)	-8(4)	3(4)	-2(4)
F(24)	70(7)	59(7)	27(5)	0(5)	19(5)	2(6)
F(25)	28(5)	74(8)	51(7)	-32(6)	-5(5)	1(5)
F(26)	42(6)	76(8)	60(7)	-25(6)	-16(5)	32(6)
P(1)	32(2)	29(2)	16(2)	2(2)	3(2)	-2(2)
P(2)	30(2)	26(2)	20(2)	-6(2)	2(2)	2(2)
Pt(1)	18(1)	27(1)	13(1)	-5(1)	6(1)	-4(1)
Pt(2)	18(1)	28(1)	12(1)	5(1)	6(1)	4(1)

Table B.23.4 Hydrogen coordinates (x 10^4) and isotropic displacement parameters (Å^{2}x 10^3) for [Pt(cod)(NPh-acac)]PF_6.

	x	y	z	U(eq)
H(11)	1743	2530	3417	78
H(12)	-43	1583	3278	78
H(13A)	154	496	4132	78
H(13B)	1355	1026	4936	78
H(14A)	3539	179	4930	43
H(14B)	2285	-415	4251	43
H(18A)	4575	2587	4147	48
H(18B)	3925	2334	5055	48
H(23A)	8114	-1279	9989	44
H(23B)	8942	-2129	10179	44
H(27A)	8331	-376	9937	50
H(27B)	7701	464	9455	50
H(28A)	5510	-48	8547	76
H(28B)	5724	-401	9617	76
H(13C)	1348	396	4779	78
H(13D)	135	108	3774	78
H(14C)	1260	-251	3488	43
H(14D)	2359	-109	4543	43
H(18C)	4023	2223	5064	48
H(18D)	3181	1385	5041	48
H(23C)	8796	-2259	10057	44
H(23D)	9546	-2579	9222	44
H(27C)	7257	197	9486	50
H(27D)	6039	57	8450	50
H(28C)	5157	-616	9401	76
H(28D)	6896	-958	9968	76
H(15)	3680	-194	3141	43
H(16)	5482	716	3368	41
H(17A)	6116	1524	4649	48
H(17B)	4806	1095	5064	48
H(21)	4952	-1522	8260	76
H(22)	6923	-2625	8529	76
H(24A)	10624	-1840	9379	44
H(24B)	10586	-1103	10075	44
H(25)	10472	-704	8365	44
H(26)	8645	189	8136	50
H(110)	466	1375	-600	31
H(11A)	3958	766	-433	44
H(11B)	2145	596	-1024	44
H(11C)	3108	-33	-247	44
H(11D)	-1920	2307	265	81
H(11E)	-929	2557	-483	81

H(11F)	-626	2999	544	81
H(115)	3720	-729	1596	36
H(116)	6182	-1346	1918	46
H(117)	8500	-694	2030	61
H(118)	8433	615	1717	53
H(119)	6030	1285	1405	36
H(210)	5458	-1383	4428	30
H(21A)	8017	35	4704	48
H(21B)	7166	-642	3962	48
H(21C)	8991	-739	4575	48
H(21D)	4390	-2999	5549	83
H(21E)	4088	-2558	4521	83
H(21F)	3092	-2309	5268	83
H(215)	11074	-1293	6435	38
H(216)	13458	-607	6740	48
H(217)	13486	687	7007	58
H(218)	11202	1351	6906	46
H(219)	8731	737	6622	29

Table B.23.5 Hydrogen bonds for [Pt(cod)(NPh-acac)]PF_6 [Å and °].

D-H...A	d(D-H)	d(H...A)	d(D...A)	<(DHA)
C(23B)-H(23D)...F(24)	0.99	2.47	3.44(5)	165.2
C(213)-H(21F)...F(22)#1	0.98	2.48	3.15(2)	125.3
C(113)-H(11D)...F(15)#1	0.98	2.47	3.14(2)	125.7
C(24)-H(24A)...F(21)	0.99	2.55	3.33(2)	135.0
C(119)-H(119)...F(15)	0.95	2.55	3.46(2)	162.7
C(215)-H(215)...F(22)	0.95	2.55	3.47(2)	164.5

Symmetry transformations used to generate equivalent atoms:
#1 x-1,y,z

B.24 Crystal Data of [Rh(cod)(Cl)]$_2$ (293 K)

Table B.24.1 Atomic co-ordinates (x 10^4) and equivalent isotropic displacement parameters (Å^2 x 10^3) for [Rh(cod)Cl]$_2$. U(eq) is defined as one third of the trace of the orthogonalized U^{ij} tensor.

	x	y	z	U(eq)
C(11)	1586(6)	6857(2)	3231(6)	53(1)
C(12)	2205(7)	7311(2)	3922(5)	48(1)
C(13)	2667(10)	7807(2)	3108(8)	78(2)
C(14)	4424(10)	7807(2)	2394(8)	74(2)
C(15)	5376(7)	7285(2)	2357(5)	50(1)
C(16)	4718(8)	6847(2)	1617(5)	54(1)
C(17)	2920(10)	6844(4)	724(7)	92(2)
C(18)	1268(9)	6778(4)	1558(7)	94(3)
C(21)	5167(8)	5303(2)	7793(6)	57(1)
C(22)	6000(8)	5685(2)	8648(5)	51(1)
C(23)	7794(10)	5620(3)	9478(7)	82(2)
C(24)	9352(9)	5605(3)	8604(7)	78(2)
C(25)	9065(7)	5635(2)	6923(6)	54(1)
C(26)	8204(8)	5251(2)	6072(7)	58(1)
C(27)	7565(12)	4736(2)	6685(11)	103(3)
C(28)	5936(13)	4763(2)	7584(9)	96(3)
Cl(3)	3622(2)	6397(1)	6260(1)	49(1)
Cl(4)	7239(2)	6317(1)	4237(1)	53(1)
Rh(1)	4343(1)	6753(1)	3877(1)	32(1)
Rh(2)	6347(1)	5863(1)	6414(1)	35(1)

Table B.24.2 Bond lengths (Å) and angles (°) for [Rh(cod)Cl]$_2$.

C(11)-C(12)	1.382(7)	C(12)-C(11)-C(18)	126.2(6)	C(28)-C(21)-H(21)	113.9	C(16)-Rh(1)-Cl(4)	92.37(15)
C(11)-C(18)	1.536(8)	C(12)-C(11)-Rh(1)	71.5(3)	Rh(2)-C(21)-H(21)	113.9	C(15)-Rh(1)-Cl(4)	93.03(14)
C(11)-Rh(1)	2.089(5)	C(18)-C(11)-Rh(1)	111.7(4)	C(21)-C(22)-C(23)	124.7(5)	C(11)-Rh(1)-Cl(4)	158.49(16)
C(11)-H(11)	0.9800	C(12)-C(11)-H(11)	113.3	C(21)-C(22)-Rh(2)	71.0(3)	C(12)-Rh(1)-Cl(4)	163.02(16)
C(12)-C(13)	1.504(7)	C(18)-C(11)-H(11)	113.3	C(23)-C(22)-Rh(2)	112.1(4)	C(16)-Rh(1)-Cl(3)	163.50(17)
C(12)-Rh(1)	2.108(4)	Rh(1)-C(11)-H(11)	113.3	C(21)-C(22)-H(22)	113.8	C(15)-Rh(1)-Cl(3)	157.88(16)
C(12)-H(12)	0.9800	C(11)-C(12)-C(13)	123.7(5)	C(23)-C(22)-H(22)	113.8	C(11)-Rh(1)-Cl(3)	93.46(15)
C(13)-C(14)	1.454(8)	C(11)-C(12)-Rh(1)	70.0(3)	Rh(2)-C(22)-H(22)	113.8	C(12)-Rh(1)-Cl(3)	92.94(13)
C(13)-H(13A)	0.9700	C(13)-C(12)-Rh(1)	112.1(3)	C(24)-C(23)-C(22)	115.4(5)	Cl(4)-Rh(1)-Cl(3)	85.61(4)
C(13)-H(13B)	0.9700	C(11)-C(12)-H(12)	114.3	C(24)-C(23)-H(23A)	108.4	C(26)-Rh(2)-C(22)	94.7(2)
C(14)-C(15)	1.499(7)	C(13)-C(12)-H(12)	114.3	C(22)-C(23)-H(23A)	108.4	C(26)-Rh(2)-C(21)	82.2(2)
C(14)-H(14A)	0.9700	Rh(1)-C(12)-H(12)	114.3	C(24)-C(23)-H(23B)	108.4	C(22)-Rh(2)-C(21)	38.1(2)
C(14)-H(14B)	0.9700	C(14)-C(13)-C(12)	115.7(5)	C(22)-C(23)-H(23B)	108.4	C(26)-Rh(2)-C(25)	38.4(2)
C(15)-C(16)	1.376(8)	C(14)-C(13)-H(13A)	108.4	H(23A)-C(23)-H(23B)	107.5	C(22)-Rh(2)-C(25)	82.7(2)
C(15)-Rh(1)	2.088(4)	C(12)-C(13)-H(13A)	108.4	C(23)-C(24)-C(25)	118.2(5)	C(21)-Rh(2)-C(25)	94.9(2)
C(15)-H(15)	0.9800	C(14)-C(13)-H(13B)	108.4	C(23)-C(24)-H(24A)	107.8	C(26)-Rh(2)-Cl(4)	92.38(16)
C(16)-C(17)	1.515(8)	C(12)-C(13)-H(13B)	108.4	C(25)-C(24)-H(24A)	107.8	C(22)-Rh(2)-Cl(4)	160.72(16)
C(16)-Rh(1)	2.087(5)	H(13A)-C(13)-H(13B)	107.4	C(23)-C(24)-H(24B)	107.8	C(21)-Rh(2)-Cl(4)	161.11(16)
C(16)-H(16)	0.9800	C(13)-C(14)-C(15)	115.1(5)	C(25)-C(24)-H(24B)	107.8	C(25)-Rh(2)-Cl(4)	91.88(15)
C(17)-C(18)	1.453(10)	C(13)-C(14)-H(14A)	108.5	H(24A)-C(24)-H(24B)	107.1	C(26)-Rh(2)-Cl(3)	161.40(17)
C(17)-H(17A)	0.9700	C(15)-C(14)-H(14A)	108.5	C(26)-C(25)-C(24)	124.3(5)	C(22)-Rh(2)-Cl(3)	92.91(15)
C(17)-H(17B)	0.9700	C(13)-C(14)-H(14B)	108.5	C(26)-C(25)-Rh(2)	70.5(3)	C(21)-Rh(2)-Cl(3)	93.58(17)
C(18)-H(18A)	0.9700	C(15)-C(14)-H(14B)	108.5	C(24)-C(25)-Rh(2)	109.1(4)	C(25)-Rh(2)-Cl(3)	159.99(17)
C(18)-H(18B)	0.9700	H(14A)-C(14)-H(14B)	107.5	C(26)-C(25)-H(25)	114.7	Cl(4)-Rh(2)-Cl(3)	85.84(4)
C(21)-C(22)	1.370(8)	C(16)-C(15)-C(14)	125.0(5)	C(24)-C(25)-H(25)	114.7		
C(21)-C(28)	1.498(9)	C(16)-C(15)-Rh(1)	70.7(3)	Rh(2)-C(25)-H(25)	114.7		
C(21)-Rh(2)	2.097(5)	C(14)-C(15)-Rh(1)	112.4(3)	C(25)-C(26)-C(27)	123.4(6)		
C(21)-H(21)	0.9800	C(16)-C(15)-H(15)	113.7	C(25)-C(26)-Rh(2)	71.0(3)		
C(22)-C(23)	1.493(8)	C(14)-C(15)-H(15)	113.7	C(27)-C(26)-Rh(2)	112.6(4)		
C(22)-Rh(2)	2.096(5)	Rh(1)-C(15)-H(15)	113.7	C(25)-C(26)-H(26)	114.1		
C(22)-H(22)	0.9800	C(15)-C(16)-C(17)	122.9(6)	C(27)-C(26)-H(26)	114.1		
C(23)-C(24)	1.407(10)	C(15)-C(16)-Rh(1)	70.8(3)	Rh(2)-C(26)-H(26)	114.1		
C(23)-H(23A)	0.9700	C(17)-C(16)-Rh(1)	112.4(4)	C(28)-C(27)-C(26)	115.6(5)		
C(23)-H(23B)	0.9700	C(15)-C(16)-H(16)	114.4	C(28)-C(27)-H(27A)	108.4		
C(24)-C(25)	1.530(8)	C(17)-C(16)-H(16)	114.4	C(26)-C(27)-H(27A)	108.4		
C(24)-H(24A)	0.9700	Rh(1)-C(16)-H(16)	114.4	C(28)-C(27)-H(27B)	108.4		
C(24)-H(24B)	0.9700	C(18)-C(17)-C(16)	116.1(5)	C(26)-C(27)-H(27B)	108.4		
C(25)-C(26)	1.380(8)	C(18)-C(17)-H(17A)	108.3	H(27A)-C(27)-H(27B)	107.5		
C(25)-Rh(2)	2.099(5)	C(16)-C(17)-H(17A)	108.3	C(27)-C(28)-C(21)	115.3(5)		
C(25)-H(25)	0.9800	C(18)-C(17)-H(17B)	108.3	C(27)-C(28)-H(28A)	108.4		
C(26)-C(27)	1.503(9)	C(16)-C(17)-H(17B)	108.3	C(21)-C(28)-H(28A)	108.4		
C(26)-Rh(2)	2.092(5)	H(17A)-C(17)-H(17B)	107.4	C(27)-C(28)-H(28B)	108.4		
C(26)-H(26)	0.9800	C(17)-C(18)-C(11)	113.4(5)	C(21)-C(28)-H(28B)	108.4		
C(27)-C(28)	1.464(10)	C(17)-C(18)-H(18A)	108.9	H(28A)-C(28)-H(28B)	107.5		
C(27)-H(27A)	0.9700	C(11)-C(18)-H(18A)	108.9	Rh(2)-Cl(3)-Rh(1)	93.34(4)		
C(27)-H(27B)	0.9700	C(17)-C(18)-H(18B)	108.9	Rh(2)-Cl(4)-Rh(1)	94.11(4)		
C(28)-H(28A)	0.9700	C(11)-C(18)-H(18B)	108.9	C(16)-Rh(1)-C(15)	38.5(2)		
C(28)-H(28B)	0.9700	H(18A)-C(18)-H(18B)	107.7	C(16)-Rh(1)-C(11)	82.5(2)		
Cl(3)-Rh(2)	2.4048(11)	C(22)-C(21)-C(28)	124.1(6)	C(15)-Rh(1)-C(11)	95.7(2)		
Cl(3)-Rh(1)	2.4137(11)	C(22)-C(21)-Rh(2)	70.9(3)	C(16)-Rh(1)-C(12)	93.6(2)		
Cl(4)-Rh(2)	2.3934(12)	C(28)-C(21)-Rh(2)	112.6(4)	C(15)-Rh(1)-C(12)	81.96(19)		
Cl(4)-Rh(1)	2.3950(12)	C(22)-C(21)-H(21)	113.9	C(11)-Rh(1)-C(12)	38.4(2)		

Symmetry transformations used to generate equivalent atoms

Table B.24.3 Anisotropic displacement parameters (Å^2 x 10^3) for [Rh(cod)Cl]$_2$. The anisotropic displacement factor exponent takes the form: $-2\pi^2$ [h^{2}a^{*2}U^{11} +… + 2 h k a* b* U^{12}]

	U^{11}	U^{22}	U^{33}	U^{23}	U^{13}	U^{12}
C(11)	31(2)	71(3)	57(3)	9(3)	-6(2)	0(2)
C(12)	48(3)	52(3)	46(3)	6(2)	16(2)	17(2)
C(13)	92(5)	48(3)	95(5)	15(3)	23(4)	26(3)
C(14)	91(5)	51(3)	83(4)	26(3)	27(4)	9(3)
C(15)	49(3)	55(3)	48(3)	19(2)	15(2)	2(2)
C(16)	60(3)	70(4)	32(2)	3(2)	9(2)	17(3)
C(17)	82(5)	146(7)	45(3)	-14(4)	-21(3)	15(5)
C(18)	60(4)	160(8)	61(4)	-8(4)	-28(3)	3(4)
C(21)	58(3)	57(3)	56(3)	16(3)	6(2)	-11(2)

C(22)	63(3)	59(3)	32(2)	5(2)	0(2)	15(3)
C(23)	96(5)	94(5)	53(4)	6(3)	-24(4)	11(4)
C(24)	71(4)	98(5)	62(4)	11(3)	-43(3)	7(4)
C(25)	36(2)	58(3)	67(3)	16(3)	-2(2)	9(2)
C(26)	59(3)	47(3)	68(4)	-1(3)	12(3)	16(2)
C(27)	105(6)	36(3)	167(9)	0(4)	19(6)	13(3)
C(28)	143(8)	42(3)	105(6)	7(4)	34(5)	-18(4)
Cl(3)	39(1)	62(1)	47(1)	19(1)	10(1)	12(1)
Cl(4)	33(1)	68(1)	57(1)	24(1)	9(1)	8(1)
Rh(1)	30(1)	34(1)	33(1)	3(1)	1(1)	1(1)
Rh(2)	34(1)	33(1)	38(1)	4(1)	0(1)	0(1)

Table B.24.4 Hydrogen co-ordinates (x 10^4) and isotropic displacement parameters (Å^2 x 10^3) for [Rh(cod)Cl]$_2$.

	x	y	z	U(eq)
H(11)	741	6652	3825	64
H(12)	1714	7369	4903	58
H(13A)	1707	7872	2362	93
H(13B)	2657	8097	3802	93
H(14A)	5231	8057	2902	89
H(14B)	4230	7930	1385	89
H(15)	6719	7310	2396	60
H(16)	5673	6622	1218	65
H(17A)	2820	7173	184	110
H(17B)	2966	6563	1	110
H(18A)	785	6427	1382	113
H(18B)	349	7027	1199	113
H(21)	3822	5315	7785	68
H(22)	5138	5918	9136	62
H(23A)	7936	5908	10176	98
H(23B)	7751	5297	10044	98
H(24A)	10013	5283	8835	94
H(24B)	10146	5895	8908	94
H(25)	10000	5836	6415	64
H(26)	8631	5229	5059	69
H(27A)	7308	4498	5865	123
H(27B)	8563	4585	7282	123
H(28A)	6243	4615	8549	115
H(28B)	4986	4544	7127	115

Table B.24.5 Hydrogen bonds for [Rh(cod)Cl]$_2$ (Å and ^{o}).

D-H...A	d(D-H)	d(H...A)	d(D...A)	<(DHA)
C(11)-H(11)...Cl(4)#1	0.98	2.73	3.597(5)	148.1

Symmetry transformations used to generate equivalent atoms :
#1 x-1, y, z

B.25 Crystal Data of [Rh(cod)(Cl)]$_2$ (100 K)

Table B.25.1 Atomic coordinates (x 10^4) and equivalent isotropic displacement parameters (Å^{2}x 10^3) for [Rh(cod)Cl]$_2$. U(eq) is defined as one third of the trace of the orthogonalized U^{ij} tensor.

	x	y	z	U(eq)
C(1)	1534(5)	6819(1)	3199(4)	17(1)
C(2)	2073(5)	7304(1)	3856(4)	17(1)

C(3)	2434(5)	7802(1)	2934(4)	23(1)
C(4)	4442(5)	7852(1)	2506(4)	20(1)
C(5)	5386(5)	7319(1)	2394(4)	16(1)
C(6)	4707(5)	6885(1)	1563(4)	16(1)
C(7)	2938(5)	6915(2)	631(4)	23(1)
C(8)	1300(5)	6717(2)	1524(4)	25(1)
C(11)	9028(5)	5625(1)	6911(4)	18(1)
C(12)	8165(5)	5248(1)	5980(4)	20(1)
C(13)	7465(7)	4715(2)	6480(6)	44(1)
C(14)	6073(7)	4741(2)	7687(5)	43(1)
C(15)	5179(5)	5282(1)	7857(4)	19(1)
C(16)	5961(5)	5688(1)	8722(4)	16(1)
C(17)	7792(6)	5659(2)	9548(4)	34(1)
C(18)	9350(5)	5548(2)	8586(4)	33(1)
Rh(1)	4293(1)	6762(1)	3874(1)	11(1)
Rh(2)	6305(1)	5861(1)	6428(1)	11(1)
Cl(1)	3545(1)	6392(1)	6307(1)	17(1)
Cl(2)	7199(1)	6335(1)	4219(1)	20(1)

Table B.25.2 Bond lengths (Å) and angles (°) for $[Rh(cod)Cl]_2$.

C(1)-C(2)	1.404(5)	Rh(1)-Cl(1)	2.4188(8)	C(1)-C(8)-H(8B)	109.2
C(1)-C(8)	1.513(5)	Rh(2)-Cl(2)	2.3918(9)	C(7)-C(8)-H(8B)	109.2
C(1)-Rh(1)	2.093(3)	Rh(2)-Cl(1)	2.4153(9)	H(8A)-C(8)-H(8B)	107.9
C(1)-H(1)	1.0000			C(12)-C(11)-C(18)	123.5(3)
C(2)-C(3)	1.521(5)	C(2)-C(1)-C(8)	125.4(3)	C(12)-C(11)-Rh(2)	70.09(19)
C(2)-Rh(1)	2.115(3)	C(2)-C(1)-Rh(1)	71.4(2)	C(18)-C(11)-Rh(2)	111.3(2)
C(2)-H(2)	1.0000	C(8)-C(1)-Rh(1)	111.0(2)	C(12)-C(11)-H(11)	114.6
C(3)-C(4)	1.525(5)	C(2)-C(1)-H(1)	113.8	C(18)-C(11)-H(11)	114.6
C(3)-H(3A)	0.9900	C(8)-C(1)-H(1)	113.8	Rh(2)-C(11)-H(11)	114.6
C(3)-H(3B)	0.9900	Rh(1)-C(1)-H(1)	113.8	C(11)-C(12)-C(13)	125.6(4)
C(4)-C(5)	1.511(5)	C(1)-C(2)-C(3)	122.8(3)	C(11)-C(12)-Rh(2)	71.07(19)
C(4)-H(4A)	0.9900	C(1)-C(2)-Rh(1)	69.66(19)	C(13)-C(12)-Rh(2)	112.0(3)
C(4)-H(4B)	0.9900	C(3)-C(2)-Rh(1)	113.2(2)	C(11)-C(12)-H(12)	113.5
C(5)-C(6)	1.402(5)	C(1)-C(2)-H(2)	114.4	C(13)-C(12)-H(12)	113.5
C(5)-Rh(1)	2.086(3)	C(3)-C(2)-H(2)	114.4	Rh(2)-C(12)-H(12)	113.5
C(5)-H(5)	1.0000	Rh(1)-C(2)-H(2)	114.4	C(14)-C(13)-C(12)	114.4(3)
C(6)-C(7)	1.520(5)	C(2)-C(3)-C(4)	112.2(3)	C(14)-C(13)-H(13A)	108.7
C(6)-Rh(1)	2.098(3)	C(2)-C(3)-H(3A)	109.2	C(12)-C(13)-H(13A)	108.7
C(6)-H(6)	1.0000	C(4)-C(3)-H(3A)	109.2	C(14)-C(13)-H(13B)	108.7
C(7)-C(8)	1.528(5)	C(2)-C(3)-H(3B)	109.2	C(12)-C(13)-H(13B)	108.7
C(7)-H(7A)	0.9900	C(4)-C(3)-H(3B)	109.2	H(13A)-C(13)-H(13B)	107.6
C(7)-H(7B)	0.9900	H(3A)-C(3)-H(3B)	107.9	C(13)-C(14)-C(15)	114.2(3)
C(8)-H(8A)	0.9900	C(5)-C(4)-C(3)	112.5(3)	C(13)-C(14)-H(14A)	108.7
C(8)-H(8B)	0.9900	C(5)-C(4)-H(4A)	109.1	C(15)-C(14)-H(14A)	108.7
C(11)-C(12)	1.398(5)	C(3)-C(4)-H(4A)	109.1	C(13)-C(14)-H(14B)	108.7
C(11)-C(18)	1.511(5)	C(5)-C(4)-H(4B)	109.1	C(15)-C(14)-H(14B)	108.7
C(11)-Rh(2)	2.108(3)	C(3)-C(4)-H(4B)	109.1	H(14A)-C(14)-H(14B)	107.6
C(11)-H(11)	1.0000	H(4A)-C(4)-H(4B)	107.8	C(16)-C(15)-C(14)	122.7(4)
C(12)-C(13)	1.503(5)	C(6)-C(5)-C(4)	124.7(3)	C(16)-C(15)-Rh(2)	70.37(19)
C(12)-Rh(2)	2.096(3)	C(6)-C(5)-Rh(1)	70.88(19)	C(14)-C(15)-Rh(2)	112.8(3)
C(12)-H(12)	1.0000	C(4)-C(5)-Rh(1)	112.0(2)	C(16)-C(15)-H(15)	114.5
C(13)-C(14)	1.489(6)	C(6)-C(5)-H(5)	113.9	C(14)-C(15)-H(15)	114.5
C(13)-H(13A)	0.9900	C(4)-C(5)-H(5)	113.9	Rh(2)-C(15)-H(15)	114.5
C(13)-H(13B)	0.9900	Rh(1)-C(5)-H(5)	113.9	C(15)-C(16)-C(17)	125.5(3)
C(14)-C(15)	1.516(5)	C(5)-C(6)-C(7)	122.3(3)	C(15)-C(16)-Rh(2)	70.99(19)
C(14)-H(14A)	0.9900	C(5)-C(6)-Rh(1)	69.98(19)	C(17)-C(16)-Rh(2)	111.0(2)
C(14)-H(14B)	0.9900	C(7)-C(6)-Rh(1)	113.7(2)	C(15)-C(16)-H(16)	113.8
C(15)-C(16)	1.392(5)	C(5)-C(6)-H(6)	114.4	C(17)-C(16)-H(16)	113.8
C(15)-Rh(2)	2.107(3)	C(7)-C(6)-H(6)	114.4	Rh(2)-C(16)-H(16)	113.8
C(15)-H(15)	1.0000	Rh(1)-C(6)-H(6)	114.4	C(18)-C(17)-C(16)	114.6(3)
C(16)-C(17)	1.512(5)	C(6)-C(7)-C(8)	111.5(3)	C(18)-C(17)-H(17A)	108.6
C(16)-Rh(2)	2.099(3)	C(6)-C(7)-H(7A)	109.3	C(16)-C(17)-H(17A)	108.6
C(16)-H(16)	1.0000	C(8)-C(7)-H(7A)	109.3	C(18)-C(17)-H(17B)	108.6
C(17)-C(18)	1.460(6)	C(6)-C(7)-H(7B)	109.3	C(16)-C(17)-H(17B)	108.6
C(17)-H(17A)	0.9900	C(8)-C(7)-H(7B)	109.3	H(17A)-C(17)-H(17B)	107.6
C(17)-H(17B)	0.9900	H(7A)-C(7)-H(7B)	108.0	C(17)-C(18)-C(11)	116.1(3)
C(18)-H(18A)	0.9900	C(1)-C(8)-C(7)	112.2(3)	C(17)-C(18)-H(18A)	108.3
C(18)-H(18B)	0.9900	C(1)-C(8)-H(8A)	109.2	C(11)-C(18)-H(18A)	108.3
Rh(1)-Cl(2)	2.3894(9)	C(7)-C(8)-H(8A)	109.2	C(17)-C(18)-H(18B)	108.3

C(11)-C(18)-H(18B)	108.3	C(5)-Rh(1)-Cl(1)	155.89(10)	C(16)-Rh(2)-Cl(2)	159.30(10)
H(18A)-C(18)-H(18B)	107.4	C(1)-Rh(1)-Cl(1)	92.82(10)	C(15)-Rh(2)-Cl(2)	162.04(10)
C(5)-Rh(1)-C(1)	98.68(14)	C(6)-Rh(1)-Cl(1)	164.84(10)	C(11)-Rh(2)-Cl(2)	92.07(10)
C(5)-Rh(1)-C(6)	39.14(13)	C(2)-Rh(1)-Cl(1)	93.93(9)	C(12)-Rh(2)-Cl(1)	159.97(11)
C(1)-Rh(1)-C(6)	82.31(14)	Cl(2)-Rh(1)-Cl(1)	85.85(3)	C(16)-Rh(2)-Cl(1)	92.49(10)
C(5)-Rh(1)-C(2)	82.20(13)	C(12)-Rh(2)-C(16)	96.89(14)	C(15)-Rh(2)-Cl(1)	94.31(11)
C(1)-Rh(1)-C(2)	38.97(13)	C(12)-Rh(2)-C(15)	82.31(14)	C(11)-Rh(2)-Cl(1)	160.92(10)
C(6)-Rh(1)-C(2)	91.26(13)	C(16)-Rh(2)-C(15)	38.65(13)	Cl(2)-Rh(2)-Cl(1)	85.88(3)
C(5)-Rh(1)-Cl(2)	91.93(10)	C(12)-Rh(2)-C(11)	38.85(14)	Rh(2)-Cl(1)-Rh(1)	92.88(3)
C(1)-Rh(1)-Cl(2)	155.85(10)	C(16)-Rh(2)-C(11)	82.76(14)	Rh(1)-Cl(2)-Rh(2)	94.22(3)
C(6)-Rh(1)-Cl(2)	92.74(10)	C(15)-Rh(2)-C(11)	93.41(14)		
C(2)-Rh(1)-Cl(2)	165.17(10)	C(12)-Rh(2)-Cl(2)	91.36(10)		

Symmetry transformations used to generate equivalent atoms:

Table B.25.3 Anisotropic displacement parameters ($Å^2$x 10^3)for $[Rh(cod)Cl]_2$. The anisotropic displacement factor exponent takes the form: $-2\pi^2[h^2a^{*2}U^{11} + ... + 2 h k a^* b^* U^{12}]$

	U^{11}	U^{22}	U^{33}	U^{23}	U^{13}	U^{12}
C(1)	7(2)	22(2)	20(2)	2(1)	-1(1)	0(1)
C(2)	18(2)	16(2)	16(2)	3(1)	9(1)	6(1)
C(3)	31(2)	14(2)	24(2)	4(2)	3(2)	7(2)
C(4)	27(2)	15(2)	19(2)	4(1)	2(2)	0(2)
C(5)	17(2)	20(2)	13(2)	8(1)	5(1)	0(1)
C(6)	19(2)	20(2)	9(2)	1(1)	2(1)	3(1)
C(7)	27(2)	31(2)	12(2)	-4(2)	-5(2)	3(2)
C(8)	17(2)	32(2)	27(2)	-1(2)	-10(2)	-3(2)
C(11)	8(2)	24(2)	21(2)	6(2)	-1(1)	4(1)
C(12)	19(2)	14(2)	27(2)	2(2)	6(2)	8(1)
C(13)	43(3)	12(2)	77(4)	4(2)	17(3)	3(2)
C(14)	73(4)	13(2)	45(3)	0(2)	29(3)	-6(2)
C(15)	26(2)	17(2)	16(2)	3(1)	7(2)	-6(2)
C(16)	20(2)	21(2)	8(2)	3(1)	3(1)	5(1)
C(17)	32(2)	54(3)	16(2)	2(2)	-5(2)	9(2)
C(18)	20(2)	60(3)	18(2)	7(2)	-8(2)	1(2)
Rh(1)	11(1)	11(1)	10(1)	1(1)	0(1)	1(1)
Rh(2)	11(1)	11(1)	11(1)	1(1)	-1(1)	0(1)
Cl(1)	13(1)	21(1)	16(1)	6(1)	2(1)	3(1)
Cl(2)	12(1)	27(1)	20(1)	10(1)	4(1)	4(1)

Table B.25.4 Hydrogen coordinates (x 10^4) and isotropic displacement parameters ($Å^2$x 10^3) for $[Rh(cod)Cl]_2$.

	x	y	z	U(eq)
H(1)	687	6605	3835	20
H(2)	1543	7373	4870	20
H(3A)	2077	8119	3525	27
H(3B)	1663	7794	2003	27
H(4A)	4518	8038	1523	24
H(4B)	5095	8072	3272	24
H(5)	6755	7341	2437	20
H(6)	5675	6654	1119	19
H(7A)	3063	6696	-292	28
H(7B)	2720	7288	315	28
H(8A)	174	6898	1150	30
H(8B)	1144	6330	1351	30
H(11)	9984	5843	6403	21
H(12)	8615	5250	4920	24
H(13A)	6918	4530	5594	52
H(13B)	8517	4500	6849	52
H(14A)	6669	4642	8660	52
H(14B)	5106	4474	7465	52

H(15)	3808	5274	7857	23
H(16)	5043	5920	9226	19
H(17A)	8012	6002	10070	41
H(17B)	7727	5379	10331	41
H(18A)	9735	5174	8760	39
H(18B)	10383	5779	8911	39

B.26 Crystal Data of [Rh(cod)(acac)]

Table B.26.1 Atomic coordinates (x 10^4) and equivalent isotropic displacement parameters ($Å^2$x 10^3) for [Rh(cod)(acac)]. U(eq) is defined as one third of the trace of the orthogonalized U^{ij} tensor.

	x	y	z	U(eq)
O(1)	1993(3)	1155(1)	-384(2)	13(1)
O(2)	-1449(3)	968(1)	1261(2)	13(1)
C(1)	4081(5)	1863(2)	2038(4)	15(1)
C(2)	3195(5)	2424(2)	1271(3)	14(1)
C(3)	2434(6)	3125(2)	1864(4)	20(1)
C(4)	1135(6)	2998(2)	3056(4)	19(1)
C(5)	19(5)	2278(2)	2906(3)	14(1)
C(6)	758(5)	1639(2)	3528(4)	15(1)
C(7)	2743(6)	1580(2)	4351(4)	20(1)
C(8)	4492(5)	1889(2)	3577(3)	17(1)
C(9)	1053(5)	671(2)	-1099(3)	12(1)
C(10)	-753(5)	349(2)	-789(3)	14(1)
C(11)	-1865(5)	502(2)	317(3)	13(1)
C(12)	1999(6)	438(2)	-2354(4)	20(1)
C(13)	-3755(5)	82(2)	457(4)	19(1)
Rh(1)	1124(1)	1575(1)	1427(1)	9(1)

Table B.26.2 Bond lengths (Å) and angles (°) for [Rh(cod)(acac)].

O(1)-C(9)	1.275(4)	C(9)-C(12)	1.487(5)	C(4)-C(3)-H(3B)	109.0
O(1)-Rh(1)	2.058(2)	C(10)-C(11)	1.389(5)	H(3A)-C(3)-H(3B)	107.8
O(2)-C(11)	1.279(4)	C(10)-H(10)	0.9500	C(5)-C(4)-C(3)	111.4(3)
O(2)-Rh(1)	2.057(2)	C(11)-C(13)	1.502(5)	C(5)-C(4)-H(4A)	109.4
C(1)-C(2)	1.388(4)	C(12)-H(12A)	0.9800	C(3)-C(4)-H(4A)	109.4
C(1)-C(8)	1.518(5)	C(12)-H(12B)	0.9800	C(5)-C(4)-H(4B)	109.4
C(1)-Rh(1)	2.107(3)	C(12)-H(12C)	0.9800	C(3)-C(4)-H(4B)	109.4
C(1)-H(1)	1.0000	C(13)-H(13A)	0.9800	H(4A)-C(4)-H(4B)	108.0
C(2)-C(3)	1.518(4)	C(13)-H(13B)	0.9800	C(6)-C(5)-C(4)	121.9(3)
C(2)-Rh(1)	2.106(3)	C(13)-H(13C)	0.9800	C(6)-C(5)-Rh(1)	69.85(19)
C(2)-H(2)	1.0000			C(4)-C(5)-Rh(1)	113.8(2)
C(3)-C(4)	1.526(5)	C(9)-O(1)-Rh(1)	125.3(2)	C(6)-C(5)-H(5)	114.6
C(3)-H(3A)	0.9900	C(11)-O(2)-Rh(1)	124.2(2)	C(4)-C(5)-H(5)	114.6
C(3)-H(3B)	0.9900	C(2)-C(1)-C(8)	124.0(3)	Rh(1)-C(5)-H(5)	114.6
C(4)-C(5)	1.524(4)	C(2)-C(1)-Rh(1)	70.72(18)	C(5)-C(6)-C(7)	124.5(3)
C(4)-H(4A)	0.9900	C(8)-C(1)-Rh(1)	113.3(2)	C(5)-C(6)-Rh(1)	71.4(2)
C(4)-H(4B)	0.9900	C(2)-C(1)-H(1)	113.8	C(7)-C(6)-Rh(1)	111.2(2)
C(5)-C(6)	1.399(4)	C(8)-C(1)-H(1)	113.8	C(5)-C(6)-H(6)	114.0
C(5)-Rh(1)	2.117(3)	Rh(1)-C(1)-H(1)	113.8	C(7)-C(6)-H(6)	114.0
C(5)-H(5)	1.0000	C(1)-C(2)-C(3)	124.5(3)	Rh(1)-C(6)-H(6)	114.0
C(6)-C(7)	1.517(5)	C(1)-C(2)-Rh(1)	70.83(18)	C(6)-C(7)-C(8)	112.6(3)
C(6)-Rh(1)	2.097(4)	C(3)-C(2)-Rh(1)	111.1(2)	C(6)-C(7)-H(7A)	109.1
C(6)-H(6)	1.0000	C(1)-C(2)-H(2)	114.1	C(8)-C(7)-H(7A)	109.1
C(7)-C(8)	1.551(5)	C(3)-C(2)-H(2)	114.1	C(6)-C(7)-H(7B)	109.1
C(7)-H(7A)	0.9900	Rh(1)-C(2)-H(2)	114.1	C(8)-C(7)-H(7B)	109.1
C(7)-H(7B)	0.9900	C(2)-C(3)-C(4)	112.9(3)	H(7A)-C(7)-H(7B)	107.8
C(8)-H(8A)	0.9900	C(2)-C(3)-H(3A)	109.0	C(1)-C(8)-C(7)	112.5(3)
C(8)-H(8B)	0.9900	C(4)-C(3)-H(3A)	109.0	C(1)-C(8)-H(8A)	109.1
C(9)-C(10)	1.404(5)	C(2)-C(3)-H(3B)	109.0	C(7)-C(8)-H(8A)	109.1

C(1)-C(8)-H(8B)	109.1	C(9)-C(12)-H(12B)	109.5	O(2)-Rh(1)-C(6)	87.37(11)
C(7)-C(8)-H(8B)	109.1	H(12A)-C(12)-H(12B)	109.5	O(1)-Rh(1)-C(2)	89.23(11)
H(8A)-C(8)-H(8B)	107.8	C(9)-C(12)-H(12C)	109.5	O(2)-Rh(1)-C(2)	162.61(11)
O(1)-C(9)-C(10)	125.4(3)	H(12A)-C(12)-H(12C)	109.5	C(6)-Rh(1)-C(2)	98.73(13)
O(1)-C(9)-C(12)	115.6(3)	H(12B)-C(12)-H(12C)	109.5	O(1)-Rh(1)-C(1)	91.24(11)
C(10)-C(9)-C(12)	118.9(3)	C(11)-C(13)-H(13A)	109.5	O(2)-Rh(1)-C(1)	158.87(11)
C(11)-C(10)-C(9)	127.2(3)	C(11)-C(13)-H(13B)	109.5	C(6)-Rh(1)-C(1)	82.95(14)
C(11)-C(10)-H(10)	116.4	H(13A)-C(13)-H(13B)	109.5	C(2)-Rh(1)-C(1)	38.46(12)
C(9)-C(10)-H(10)	116.4	C(11)-C(13)-H(13C)	109.5	O(1)-Rh(1)-C(5)	162.72(10)
O(2)-C(11)-C(10)	126.8(3)	H(13A)-C(13)-H(13C)	109.5	O(2)-Rh(1)-C(5)	93.00(11)
O(2)-C(11)-C(13)	115.0(3)	H(13B)-C(13)-H(13C)	109.5	C(6)-Rh(1)-C(5)	38.78(12)
C(10)-C(11)-C(13)	118.2(3)	O(1)-Rh(1)-O(2)	90.92(8)	C(2)-Rh(1)-C(5)	82.06(13)
C(9)-C(12)-H(12A)	109.5	O(1)-Rh(1)-C(6)	158.39(11)	C(1)-Rh(1)-C(5)	91.14(13)

Symmetry transformations used to generate equivalent atoms

Table B.26.3 Anisotropic displacement parameters ($Å^2$x 10^3)for [Rh(cod)(acac)]. The anisotropic displacement factor exponent takes the form: $-2\pi^2[h^2a^{*2}U^{11} + ... + 2 h k a^* b^* U^{12}]$

	U^{11}	U^{22}	U^{33}	U^{23}	U^{13}	U^{12}
O(1)	14(1)	14(1)	12(1)	-4(1)	1(1)	-2(1)
O(2)	12(1)	12(1)	14(1)	-1(1)	2(1)	-1(1)
C(1)	8(2)	19(2)	20(2)	-7(1)	3(1)	-4(1)
C(2)	13(2)	18(2)	12(2)	-1(1)	4(1)	-10(1)
C(3)	27(2)	13(2)	19(2)	-2(1)	-1(2)	-7(1)
C(4)	23(2)	14(2)	19(2)	-6(1)	0(2)	1(1)
C(5)	13(2)	18(2)	11(2)	-3(1)	5(1)	1(1)
C(6)	14(2)	20(2)	12(2)	-4(1)	5(2)	-2(1)
C(7)	27(2)	24(2)	9(2)	2(1)	1(2)	1(1)
C(8)	16(2)	21(2)	14(2)	2(1)	-4(2)	-2(1)
C(9)	14(2)	10(1)	13(2)	0(1)	-2(1)	1(1)
C(10)	18(2)	10(1)	13(2)	-2(1)	-1(1)	0(1)
C(11)	11(2)	9(1)	17(2)	5(1)	-4(1)	3(1)
C(12)	26(2)	20(2)	14(2)	-5(1)	6(2)	-2(2)
C(13)	16(2)	18(2)	23(2)	-3(1)	3(2)	-5(1)
Rh(1)	9(1)	10(1)	9(1)	-1(1)	1(1)	-1(1)

Table B.26.4 Hydrogen coordinates (x 10^4) and isotropic displacement parameters ($Å^2$x 10^3) for [Rh(cod)(acac)].

	x	y	z	U(eq)
H(1)	5102	1587	1554	18
H(2)	3701	2479	342	17
H(3A)	1654	3395	1137	23
H(3B)	3585	3431	2178	23
H(4A)	1981	2996	3921	22
H(4B)	165	3400	3099	22
H(5)	-1464	2324	2858	17
H(6)	-295	1309	3848	18
H(7A)	3010	1063	4574	24
H(7B)	2665	1848	5221	24
H(8A)	4741	2399	3863	21
H(8B)	5711	1605	3832	21
H(10)	-1273	-13	-1405	17
H(12A)	1672	788	-3089	30
H(12B)	1501	-44	-2632	30
H(12C)	3446	417	-2168	30
H(13A)	-3683	-171	1338	29
H(13B)	-3927	-274	-284	29
H(13C)	-4888	418	409	29

Table B.26.5 Hydrogen bonds for [Rh(cod)(acac)] [Å and °].

D-H...A	d(D-H)	d(H...A)	d(D...A)	<(DHA)
C(13)-H(13C)...O(1)#1	0.98	2.57	3.528(4)	164.2

Symmetry transformations used to generate equivalent atoms:
#1 x-1,y,z

B.27 Crystal Data of [Rh(cod)(dbm)]

Table B.27.1 Atomic coordinates (x 10^4) and equivalent isotropic displacement parameters (Å^{2}x 10^3) for [Rh(cod)(dbm)]. U(eq) is defined as one third of the trace of the orthogonalized U^{ij} tensor.

	x	y	z	U(eq)
C(1)	3789(11)	1198(12)	3724(13)	28(2)
C(2)	4631(9)	1210(11)	3725(13)	29(2)
C(3)	4726(11)	140(14)	3051(14)	57(3)
C(4)	4035(10)	156(11)	1602(15)	41(3)
C(5)	3281(11)	1238(10)	964(13)	24(2)
C(6)	2484(9)	1250(11)	888(12)	30(2)
C(7)	2189(10)	321(13)	1445(14)	49(2)
C(8)	2957(10)	245(11)	3017(16)	43(2)
C(9)	4095(8)	5070(10)	3548(10)	17(2)
C(10)	3527(11)	5650(3)	2353(15)	18(1)
C(11)	2919(7)	5066(9)	1020(10)	15(2)
C(91)	4670(8)	5871(10)	4813(11)	17(2)
C(92)	5051(9)	7017(12)	4876(11)	21(2)
C(93)	5610(12)	7724(12)	6051(14)	26(3)
C(94)	5789(13)	7226(13)	7235(15)	25(3)
C(95)	5420(9)	6069(11)	7150(11)	21(2)
C(96)	4861(8)	5355(11)	5966(10)	19(2)
C(111)	2356(8)	5842(9)	-200(11)	15(2)
C(112)	2176(8)	5406(11)	-1333(11)	19(2)
C(113)	1636(9)	6085(11)	-2518(12)	22(2)
C(114)	1228(13)	7259(14)	-2553(17)	25(3)
C(115)	1412(12)	7697(12)	-1492(14)	28(3)
C(116)	1988(10)	7057(12)	-273(12)	22(2)
O(1)	4204(7)	3886(9)	3805(8)	21(2)
O(2)	2813(7)	3887(7)	847(8)	18(2)
Rh(1)	3523(4)	2546(1)	2327(5)	14(1)

Table B.27.2 Bond lengths [Å] and angles [°] for [Rh(cod)(dbm)].

C(1)-C(2)	1.442(15)	C(6)-Rh(1)	2.067(11)	C(92)-H(92)	0.9500
C(1)-C(8)	1.489(18)	C(6)-H(6)	1.0000	C(93)-C(94)	1.46(2)
C(1)-Rh(1)	2.128(13)	C(7)-C(8)	1.558(18)	C(93)-H(93)	0.9500
C(1)-H(1)	1.0000	C(7)-H(7A)	0.9900	C(94)-C(95)	1.361(19)
C(2)-C(3)	1.516(19)	C(7)-H(7B)	0.9900	C(94)-H(94)	0.9500
C(2)-Rh(1)	2.116(12)	C(8)-H(8A)	0.9900	C(95)-C(96)	1.400(15)
C(2)-H(2)	1.0000	C(8)-H(8B)	0.9900	C(95)-H(95)	0.9500
C(3)-C(4)	1.435(17)	C(9)-O(1)	1.294(13)	C(96)-H(96)	0.9500
C(3)-H(3A)	0.9900	C(9)-C(10)	1.336(16)	C(111)-C(112)	1.378(16)
C(3)-H(3B)	0.9900	C(9)-C(91)	1.521(14)	C(111)-C(116)	1.423(16)
C(4)-C(5)	1.520(16)	C(10)-C(11)	1.463(15)	C(112)-C(113)	1.382(15)
C(4)-H(4A)	0.9900	C(10)-H(10)	0.9500	C(112)-H(112)	0.9500
C(4)-H(4B)	0.9900	C(11)-O(2)	1.275(11)	C(113)-C(114)	1.43(2)
C(5)-C(6)	1.303(16)	C(11)-C(111)	1.467(14)	C(113)-H(113)	0.9500
C(5)-Rh(1)	2.079(12)	C(91)-C(92)	1.367(16)	C(114)-C(115)	1.29(2)
C(5)-H(5)	1.0000	C(91)-C(96)	1.423(16)	C(114)-H(114)	0.9500
C(6)-C(7)	1.499(18)	C(92)-C(93)	1.389(19)	C(115)-C(116)	1.389(19)

C(115)-H(115)	0.9500	C(7)-C(6)-H(6)	112.1	C(95)-C(96)-H(96)	121.0
C(116)-H(116)	0.9500	Rh(1)-C(6)-H(6)	112.2	C(91)-C(96)-H(96)	120.8
O(1)-Rh(1)	2.051(10)	C(6)-C(7)-C(8)	114.0(10)	C(112)-C(111)-C(116)	117.3(11)
O(2)-Rh(1)	2.052(9)	C(6)-C(7)-H(7A)	108.6	C(112)-C(111)-C(11)	120.0(9)
		C(8)-C(7)-H(7A)	108.8	C(116)-C(111)-C(11)	122.8(10)
C(2)-C(1)-C(8)	124.2(12)	C(6)-C(7)-H(7B)	108.9	C(111)-C(112)-C(113)	122.6(11)
C(2)-C(1)-Rh(1)	69.7(7)	C(8)-C(7)-H(7B)	108.7	C(111)-C(112)-H(112)	118.7
C(8)-C(1)-Rh(1)	110.4(9)	H(7A)-C(7)-H(7B)	107.6	C(113)-C(112)-H(112)	118.7
C(2)-C(1)-H(1)	114.5	C(1)-C(8)-C(7)	115.4(10)	C(112)-C(113)-C(114)	117.3(13)
C(8)-C(1)-H(1)	114.7	C(1)-C(8)-H(8A)	108.2	C(112)-C(113)-H(113)	121.4
Rh(1)-C(1)-H(1)	114.6	C(7)-C(8)-H(8A)	108.6	C(114)-C(113)-H(113)	121.3
C(1)-C(2)-C(3)	118.5(11)	C(1)-C(8)-H(8B)	108.4	C(115)-C(114)-C(113)	120.9(14)
C(1)-C(2)-Rh(1)	70.6(7)	C(7)-C(8)-H(8B)	108.4	C(115)-C(114)-H(114)	119.5
C(3)-C(2)-Rh(1)	112.8(8)	H(8A)-C(8)-H(8B)	107.5	C(113)-C(114)-H(114)	119.6
C(1)-C(2)-H(2)	115.4	O(1)-C(9)-C(10)	129.1(9)	C(114)-C(115)-C(116)	122.9(14)
C(3)-C(2)-H(2)	115.9	O(1)-C(9)-C(91)	112.9(9)	C(114)-C(115)-H(115)	118.5
Rh(1)-C(2)-H(2)	115.9	C(10)-C(9)-C(91)	117.9(9)	C(116)-C(115)-H(115)	118.6
C(4)-C(3)-C(2)	116.4(11)	C(9)-C(10)-C(11)	127.0(3)	C(115)-C(116)-C(111)	118.8(11)
C(4)-C(3)-H(3A)	108.3	C(9)-C(10)-H(10)	116.5	C(115)-C(116)-H(116)	120.5
C(2)-C(3)-H(3A)	108.1	C(11)-C(10)-H(10)	116.5	C(111)-C(116)-H(116)	120.7
C(4)-C(3)-H(3B)	108.1	O(2)-C(11)-C(10)	122.9(9)	C(9)-O(1)-Rh(1)	123.0(8)
C(2)-C(3)-H(3B)	108.3	O(2)-C(11)-C(111)	116.8(9)	C(11)-O(2)-Rh(1)	126.7(8)
H(3A)-C(3)-H(3B)	107.4	C(10)-C(11)-C(111)	120.2(8)	O(1)-Rh(1)-O(2)	91.19(10)
C(3)-C(4)-C(5)	114.2(11)	C(92)-C(91)-C(96)	120.8(11)	O(1)-Rh(1)-C(6)	161.8(4)
C(3)-C(4)-H(4A)	108.7	C(92)-C(91)-C(9)	121.3(10)	O(2)-Rh(1)-C(6)	89.0(4)
C(5)-C(4)-H(4A)	108.7	C(96)-C(91)-C(9)	117.8(9)	O(1)-Rh(1)-C(5)	161.5(5)
C(3)-C(4)-H(4B)	108.5	C(91)-C(92)-C(93)	121.1(11)	O(2)-Rh(1)-C(5)	90.1(4)
C(5)-C(4)-H(4B)	109.0	C(91)-C(92)-H(92)	119.4	C(6)-Rh(1)-C(5)	36.6(5)
H(4A)-C(4)-H(4B)	107.5	C(93)-C(92)-H(92)	119.6	O(1)-Rh(1)-C(2)	91.1(5)
C(6)-C(5)-C(4)	121.8(12)	C(92)-C(93)-C(94)	119.0(12)	O(2)-Rh(1)-C(2)	159.2(4)
C(6)-C(5)-Rh(1)	71.2(7)	C(92)-C(93)-H(93)	120.5	C(6)-Rh(1)-C(2)	95.08(16)
C(4)-C(5)-Rh(1)	114.9(9)	C(94)-C(93)-H(93)	120.6	C(5)-Rh(1)-C(2)	81.3(5)
C(6)-C(5)-H(5)	114.1	C(95)-C(94)-C(93)	118.5(13)	O(1)-Rh(1)-C(1)	89.8(5)
C(4)-C(5)-H(5)	113.9	C(95)-C(94)-H(94)	120.7	O(2)-Rh(1)-C(1)	161.0(5)
Rh(1)-C(5)-H(5)	114.1	C(93)-C(94)-H(94)	120.8	C(6)-Rh(1)-C(1)	84.2(5)
C(5)-C(6)-C(7)	128.6(12)	C(94)-C(95)-C(96)	122.4(12)	C(5)-Rh(1)-C(1)	94.90(15)
C(5)-C(6)-Rh(1)	72.2(8)	C(94)-C(95)-H(95)	118.8	C(2)-Rh(1)-C(1)	39.7(4)
C(7)-C(6)-Rh(1)	111.7(8)	C(96)-C(95)-H(95)	118.8		
C(5)-C(6)-H(6)	112.7	C(95)-C(96)-C(91)	118.2(11)		

Symmetry transformations used to generate equivalent atoms:

Table B.27.3 Anisotropic displacement parameters ($Å^2$x 10^3)for [Rh(cod)(dbm)]. The anisotropic displacement factor exponent takes the form: $-2\pi^2[h^2a^{*2}U^{11} + ... + 2 h k a^* b^* U^{12}]$

	U^{11}	U^{22}	U^{33}	U^{23}	U^{13}	U^{12}
C(1)	47(6)	26(5)	21(4)	7(4)	26(5)	6(4)
C(2)	14(3)	36(5)	23(4)	22(3)	6(3)	1(3)
C(3)	75(7)	60(6)	75(6)	55(5)	65(6)	56(5)
C(4)	27(5)	21(5)	66(5)	-17(4)	25(5)	-3(4)
C(5)	55(6)	2(3)	27(4)	1(3)	32(5)	6(4)
C(6)	24(4)	19(4)	16(3)	-11(3)	-1(3)	-1(3)
C(7)	50(5)	46(5)	78(6)	-46(4)	53(4)	-35(4)
C(8)	39(5)	19(4)	86(6)	20(5)	48(5)	8(4)
C(9)	14(4)	21(4)	16(3)	-12(3)	10(3)	-9(4)
C(10)	19(2)	18(2)	17(2)	-10(4)	12(1)	-13(4)
C(11)	17(4)	16(3)	15(3)	-8(3)	12(3)	-3(3)
C(91)	10(5)	25(5)	13(4)	-1(3)	6(4)	4(4)
C(92)	17(5)	16(4)	20(5)	-7(4)	7(4)	-1(4)
C(93)	29(7)	16(4)	23(6)	7(3)	13(5)	-1(4)
C(94)	28(7)	22(4)	14(5)	-5(4)	9(6)	4(5)
C(95)	22(5)	27(5)	15(5)	-1(4)	12(5)	3(4)
C(96)	16(5)	18(5)	15(4)	-6(4)	6(4)	-1(4)
C(111)	16(5)	10(4)	21(4)	4(3)	12(4)	3(3)
C(112)	14(4)	21(5)	23(4)	-2(4)	13(4)	3(4)
C(113)	14(5)	26(5)	17(5)	2(4)	6(4)	-5(4)
C(114)	14(7)	22(5)	26(6)	11(5)	7(6)	0(5)
C(115)	27(7)	19(5)	26(6)	14(4)	12(6)	4(4)

C(116)	25(6)	19(4)	22(5)	-4(4)	16(5)	2(4)
O(1)	22(4)	24(3)	18(3)	-5(3)	13(3)	-4(3)
O(2)	24(4)	8(3)	12(3)	-2(2)	8(3)	7(3)
Rh(1)	15(1)	14(1)	10(1)	0(1)	7(1)	0(1)

Table B.27.4 Hydrogen coordinates (x 10^4) and isotropic displacement parameters (Å^{2}x 10^3) for [Rh(cod)(dbm)].

	x	y	z	U(eq)
H(1)	3954	1558	4554	33
H(2)	5293	1555	4557	35
H(3A)	5437	132	3391	69
H(3B)	4622	-652	3340	69
H(4A)	3644	-636	1259	50
H(4B)	4442	195	1309	50
H(5)	3152	1612	162	29
H(6)	1873	1651	39	36
H(7A)	2134	-514	1078	59
H(7B)	1503	545	1128	59
H(8A)	2566	329	3331	51
H(8B)	3277	-593	3288	51
H(10)	3516	6536	2371	21
H(92)	4932	7333	4104	25
H(93)	5871	8519	6086	31
H(94)	6154	7698	8045	30
H(95)	5547	5735	7922	25
H(96)	4617	4547	5933	23
H(112)	2432	4607	-1299	22
H(113)	1541	5782	-3278	27
H(114)	815	7726	-3369	30
H(115)	1142	8493	-1547	33
H(116)	2133	7425	500	26

B.28 Crystal Data of [Rh(cod)(thtfac)]

Table B.28.1 Atomic coordinates (x 10^4) and equivalent isotropic displacement parameters (Å^{2}x 10^3) for [Rh(cod)(thtfac)]. U(eq) is defined as one third of the trace of the orthogonalized U^{ij} tensor.

	x	y	z	U(eq)
Rh(1)	7629(1)	8784(1)	1605(1)	23(1)
O(1)	9400(3)	8449(3)	2403(2)	27(1)
O(2)	8278(2)	10328(3)	894(2)	26(1)
F(1)	11611(2)	7234(3)	3041(2)	51(1)
F(2)	12570(2)	8990(3)	2657(2)	36(1)
F(3)	11639(3)	9223(4)	3718(2)	50(1)
S(1)	8365(1)	12643(1)	-306(1)	30(1)
C(1)	7077(4)	6774(4)	1943(3)	32(1)
C(2)	6758(4)	7775(5)	2521(3)	35(1)
C(3)	5435(5)	8266(6)	2411(4)	48(1)
C(4)	5075(4)	9504(5)	1777(3)	35(1)
C(5)	5860(3)	9648(4)	1117(2)	26(1)
C(6)	6045(4)	8575(4)	524(3)	27(1)
C(7)	5432(4)	7126(5)	493(3)	37(1)
C(8)	6223(5)	6079(5)	1132(4)	48(1)
C(9)	10335(4)	9065(4)	2242(2)	26(1)

C(10)	10430(4)	10080(4)	1617(2)	25(1)
C(11)	9396(4)	10671(4)	980(2)	24(1)
C(12)	11544(4)	8628(4)	2913(3)	28(1)
C(13)	9629(4)	11777(4)	362(2)	25(1)
C(14)	9304(4)	13623(4)	-802(3)	31(1)
C(15)	10521(4)	13317(4)	-479(3)	30(1)
C(16)	10725(4)	12256(4)	202(2)	24(1)

Table B.28.2 Bond lengths [Å] and angles [°] for [Rh(cod)(thtfac)].

Rh(1)-O(2)	2.051(3)	O(2)-Rh(1)-C(1)	159.23(15)	Rh(1)-C(5)-H(5)	113.7
Rh(1)-O(1)	2.074(3)	O(1)-Rh(1)-C(1)	90.70(14)	C(5)-C(6)-C(7)	122.1(4)
Rh(1)-C(1)	2.095(4)	O(2)-Rh(1)-C(5)	87.59(13)	C(5)-C(6)-Rh(1)	69.9(2)
Rh(1)-C(5)	2.095(4)	O(1)-Rh(1)-C(5)	161.06(14)	C(7)-C(6)-Rh(1)	113.0(3)
Rh(1)-C(6)	2.112(4)	C(1)-Rh(1)-C(5)	97.57(16)	C(5)-C(6)-H(6)	114.7
Rh(1)-C(2)	2.114(4)	O(2)-Rh(1)-C(6)	89.27(13)	C(7)-C(6)-H(6)	114.7
O(1)-C(9)	1.268(5)	O(1)-Rh(1)-C(6)	159.86(15)	Rh(1)-C(6)-H(6)	114.7
O(2)-C(11)	1.262(5)	C(1)-Rh(1)-C(6)	82.44(15)	C(8)-C(7)-C(6)	112.3(3)
F(1)-C(12)	1.328(5)	C(5)-Rh(1)-C(6)	39.03(16)	C(8)-C(7)-H(7A)	109.1
F(2)-C(12)	1.339(5)	O(2)-Rh(1)-C(2)	161.50(15)	C(6)-C(7)-H(7A)	109.1
F(3)-C(12)	1.332(5)	O(1)-Rh(1)-C(2)	93.86(14)	C(8)-C(7)-H(7B)	109.1
S(1)-C(14)	1.705(5)	C(1)-Rh(1)-C(2)	38.77(18)	C(6)-C(7)-H(7B)	109.1
S(1)-C(13)	1.729(4)	C(5)-Rh(1)-C(2)	82.32(16)	H(7A)-C(7)-H(7B)	107.9
C(1)-C(2)	1.397(7)	C(6)-Rh(1)-C(2)	92.54(17)	C(1)-C(8)-C(7)	113.4(4)
C(1)-C(8)	1.514(6)	C(9)-O(1)-Rh(1)	121.6(2)	C(1)-C(8)-H(8A)	108.9
C(1)-H(1)	1.0000	C(11)-O(2)-Rh(1)	126.3(2)	C(7)-C(8)-H(8A)	108.9
C(2)-C(3)	1.515(7)	C(14)-S(1)-C(13)	91.1(2)	C(1)-C(8)-H(8B)	108.9
C(2)-H(2)	1.0000	C(2)-C(1)-C(8)	127.1(4)	C(7)-C(8)-H(8B)	108.9
C(3)-C(4)	1.507(7)	C(2)-C(1)-Rh(1)	71.3(2)	H(8A)-C(8)-H(8B)	107.7
C(3)-H(3A)	0.9900	C(8)-C(1)-Rh(1)	110.7(3)	O(1)-C(9)-C(10)	131.3(4)
C(3)-H(3B)	0.9900	C(2)-C(1)-H(1)	113.3	O(1)-C(9)-C(12)	112.0(3)
C(4)-C(5)	1.493(6)	C(8)-C(1)-H(1)	113.3	C(10)-C(9)-C(12)	116.6(4)
C(4)-H(4A)	0.9900	Rh(1)-C(1)-H(1)	113.3	C(9)-C(10)-C(11)	124.0(4)
C(4)-H(4B)	0.9900	C(1)-C(2)-C(3)	121.8(4)	C(9)-C(10)-H(10)	118.0
C(5)-C(6)	1.405(6)	C(1)-C(2)-Rh(1)	69.9(2)	C(11)-C(10)-H(10)	118.0
C(5)-H(5)	1.0000	C(3)-C(2)-Rh(1)	112.4(3)	O(2)-C(11)-C(10)	125.7(4)
C(6)-C(7)	1.522(6)	C(1)-C(2)-H(2)	114.9	O(2)-C(11)-C(13)	116.0(3)
C(6)-H(6)	1.0000	C(3)-C(2)-H(2)	114.9	C(10)-C(11)-C(13)	118.3(4)
C(7)-C(8)	1.511(6)	Rh(1)-C(2)-H(2)	114.9	F(1)-C(12)-F(3)	107.0(4)
C(7)-H(7A)	0.9900	C(4)-C(3)-C(2)	114.0(4)	F(1)-C(12)-F(2)	105.9(3)
C(7)-H(7B)	0.9900	C(4)-C(3)-H(3A)	108.7	F(3)-C(12)-F(2)	106.3(3)
C(8)-H(8A)	0.9900	C(2)-C(3)-H(3A)	108.7	F(1)-C(12)-C(9)	111.9(3)
C(8)-H(8B)	0.9900	C(4)-C(3)-H(3B)	108.7	F(3)-C(12)-C(9)	111.2(3)
C(9)-C(10)	1.373(6)	C(2)-C(3)-H(3B)	108.7	F(2)-C(12)-C(9)	114.1(3)
C(9)-C(12)	1.537(5)	H(3A)-C(3)-H(3B)	107.6	C(16)-C(13)-C(11)	130.4(4)
C(10)-C(11)	1.427(5)	C(5)-C(4)-C(3)	113.4(4)	C(16)-C(13)-S(1)	111.7(3)
C(10)-H(10)	0.9500	C(5)-C(4)-H(4A)	108.9	C(11)-C(13)-S(1)	117.9(3)
C(11)-C(13)	1.471(6)	C(3)-C(4)-H(4A)	108.9	C(15)-C(14)-S(1)	113.0(3)
C(13)-C(16)	1.378(6)	C(5)-C(4)-H(4B)	108.9	C(15)-C(14)-H(14)	123.5
C(14)-C(15)	1.356(6)	C(3)-C(4)-H(4B)	108.9	S(1)-C(14)-H(14)	123.5
C(14)-H(14)	0.9500	H(4A)-C(4)-H(4B)	107.7	C(14)-C(15)-C(16)	112.5(4)
C(15)-C(16)	1.421(5)	C(6)-C(5)-C(4)	124.9(4)	C(14)-C(15)-H(15)	123.8
C(15)-H(15)	0.9500	C(6)-C(5)-Rh(1)	71.1(2)	C(16)-C(15)-H(15)	123.8
C(16)-H(16)	0.9500	C(4)-C(5)-Rh(1)	112.3(3)	C(13)-C(16)-C(15)	111.8(4)
		C(6)-C(5)-H(5)	113.7	C(13)-C(16)-H(16)	124.1
O(2)-Rh(1)-O(1)	90.67(11)	C(4)-C(5)-H(5)	113.7	C(15)-C(16)-H(16)	124.1

Symmetry transformations used to generate equivalent atoms:

Table B.28.3 Anisotropic displacement parameters ($Å^2 x\ 10^3$)for [Rh(cod)(thtfac)]. The anisotropic displacement factor exponent takes the form: $-2\pi^2[\ h^2 a^{*2} U^{11} + ... + 2\ h\ k\ a^*\ b^*\ U^{12}\ ]$

	U^{11}	U^{22}	U^{33}	U^{23}	U^{13}	U^{12}
Rh(1)	20(1)	25(1)	22(1)	3(1)	1(1)	0(1)
O(1)	22(1)	30(1)	25(1)	3(1)	-2(1)	-1(1)
O(2)	21(1)	29(1)	27(1)	1(1)	2(1)	0(1)
F(1)	33(2)	33(1)	74(2)	17(1)	-16(1)	-2(1)
F(2)	23(1)	48(2)	36(1)	6(1)	2(1)	2(1)
F(3)	35(2)	84(2)	26(1)	-9(1)	-5(1)	10(1)

S(1)	28(1)	30(1)	29(1)	4(1)	4(1)	3(1)
C(1)	30(2)	29(2)	32(2)	11(2)	-3(2)	-3(2)
C(2)	35(2)	36(2)	35(2)	14(2)	8(2)	1(2)
C(3)	42(3)	54(3)	53(3)	19(3)	19(2)	10(2)
C(4)	30(2)	40(2)	34(2)	1(2)	5(2)	6(2)
C(5)	19(2)	29(2)	27(2)	5(2)	0(2)	1(2)
C(6)	22(2)	34(2)	22(2)	5(2)	-3(2)	2(2)
C(7)	33(2)	39(2)	34(2)	-2(2)	-3(2)	-5(2)
C(8)	49(3)	35(2)	49(3)	10(2)	-9(2)	-10(2)
C(9)	24(2)	26(2)	23(2)	-6(1)	-1(2)	4(2)
C(10)	23(2)	26(2)	25(2)	-3(1)	3(2)	-1(2)
C(11)	27(2)	22(2)	23(2)	-4(1)	5(2)	2(2)
C(12)	21(2)	34(2)	27(2)	-2(2)	0(2)	-1(2)
C(13)	27(2)	24(2)	22(2)	-2(1)	1(2)	1(2)
C(14)	39(3)	26(2)	27(2)	0(2)	7(2)	0(2)
C(15)	33(2)	27(2)	33(2)	-3(2)	11(2)	-5(2)
C(16)	25(2)	25(2)	20(2)	-4(1)	2(1)	0(2)

Table B.28.4 Hydrogen coordinates (x 10^4) and isotropic displacement parameters (Å^{2}x 10^3) for [Rh(cod)(thtfac)].

	x	y	z	U(eq)
H(1)	7786	6155	2246	39
H(2)	7264	7735	3159	42
H(3A)	4872	7462	2184	58
H(3B)	5316	8535	3010	58
H(4A)	4200	9391	1441	42
H(4B)	5137	10387	2136	42
H(5)	5865	10627	866	31
H(6)	6151	8924	-70	33
H(7A)	4627	7231	651	45
H(7B)	5270	6749	-130	45
H(8A)	5676	5403	1344	58
H(8B)	6728	5531	799	58
H(10)	11233	10408	1608	30
H(14)	9005	14311	-1257	37
H(15)	11166	13762	-686	37
H(16)	11519	11918	509	28

B.29 Crystal Data of [Rh(cod)(trop)]

Table B.29.1 Atomic coordinates (x 10^4) and equivalent isotropic displacement parameters (Å^{2}x 10^3) for [Rh(cod)(trop)]. U(eq) is defined as one third of the trace of the orthogonalized U^{ij} tensor.

	x	y	z	U(eq)
C(3)	3304(2)	-397(2)	1158(1)	17(1)
C(4)	2700(2)	893(2)	1050(1)	15(1)
C(5)	2317(2)	1460(2)	2038(1)	14(1)
C(6)	3386(2)	1473(2)	2830(1)	15(1)
C(7)	5071(2)	949(2)	2772(1)	18(1)
C(8)	5099(2)	-343(2)	3158(2)	20(1)
C(1)	3531(2)	-981(2)	2985(1)	15(1)
C(2)	2681(2)	-997(2)	2089(1)	14(1)
C(9)	-908(2)	-549(2)	4370(1)	11(1)
C(10)	-1807(2)	-1300(2)	4992(1)	13(1)

C(11)	-2981(2)	-1061(2)	5691(1)	15(1)
C(12)	-3635(2)	28(2)	5971(1)	17(1)
C(13)	-3277(2)	1134(2)	5578(1)	16(1)
C(14)	-2169(2)	1438(2)	4855(1)	15(1)
C(15)	-1068(2)	752(2)	4321(1)	12(1)
O(1)	164(2)	-1027(1)	3807(1)	13(1)
O(2)	-82(2)	1300(1)	3732(1)	14(1)
Rh(1)	1578(1)	191(1)	3081(1)	10(1)

Table B.29.2 Bond lengths [Å] and angles [°] for [Rh(cod)(trop)]

C(3)-C(2)	1.522(2)	C(4)-C(3)-H(3A)	109.1	C(1)-C(2)-H(2)	114.3
C(3)-C(4)	1.543(2)	C(2)-C(3)-H(3B)	109.1	C(3)-C(2)-H(2)	114.3
C(3)-H(3A)	0.9900	C(4)-C(3)-H(3B)	109.1	Rh(1)-C(2)-H(2)	114.3
C(3)-H(3B)	0.9900	H(3A)-C(3)-H(3B)	107.8	O(1)-C(9)-C(10)	118.08(16)
C(4)-C(5)	1.518(3)	C(5)-C(4)-C(3)	112.34(14)	O(1)-C(9)-C(15)	116.70(16)
C(4)-H(4A)	0.9900	C(5)-C(4)-H(4A)	109.1	C(10)-C(9)-C(15)	125.20(16)
C(4)-H(4B)	0.9900	C(3)-C(4)-H(4A)	109.1	C(11)-C(10)-C(9)	131.78(17)
C(5)-C(6)	1.394(3)	C(5)-C(4)-H(4B)	109.1	C(11)-C(10)-H(10)	114.1
C(5)-Rh(1)	2.1015(18)	C(3)-C(4)-H(4B)	109.1	C(9)-C(10)-H(10)	114.1
C(5)-H(5)	1.0000	H(4A)-C(4)-H(4B)	107.9	C(10)-C(11)-C(12)	129.18(17)
C(6)-C(7)	1.522(3)	C(6)-C(5)-C(4)	123.38(15)	C(10)-C(11)-H(11)	115.4
C(6)-Rh(1)	2.1116(19)	C(6)-C(5)-Rh(1)	71.07(10)	C(12)-C(11)-H(11)	115.4
C(6)-H(6)	1.0000	C(4)-C(5)-Rh(1)	111.69(11)	C(13)-C(12)-C(11)	126.93(16)
C(7)-C(8)	1.545(3)	C(6)-C(5)-H(5)	114.3	C(13)-C(12)-H(12)	116.5
C(7)-H(7A)	0.9900	C(4)-C(5)-H(5)	114.3	C(11)-C(12)-H(12)	116.5
C(7)-H(7B)	0.9900	Rh(1)-C(5)-H(5)	114.3	C(12)-C(13)-C(14)	129.43(17)
C(8)-C(1)	1.508(3)	C(5)-C(6)-C(7)	122.93(15)	C(12)-C(13)-H(13)	115.3
C(8)-H(8A)	0.9900	C(5)-C(6)-Rh(1)	70.28(11)	C(14)-C(13)-H(13)	115.3
C(8)-H(8B)	0.9900	C(7)-C(6)-Rh(1)	113.59(12)	C(13)-C(14)-C(15)	131.64(18)
C(1)-C(2)	1.406(2)	C(5)-C(6)-H(6)	114.2	C(13)-C(14)-H(14)	114.2
C(1)-Rh(1)	2.0971(18)	C(7)-C(6)-H(6)	114.2	C(15)-C(14)-H(14)	114.2
C(1)-H(1)	1.0000	Rh(1)-C(6)-H(6)	114.2	O(2)-C(15)-C(14)	118.03(17)
C(2)-Rh(1)	2.1065(17)	C(6)-C(7)-C(8)	111.14(15)	O(2)-C(15)-C(9)	116.29(16)
C(2)-H(2)	1.0000	C(6)-C(7)-H(7A)	109.4	C(14)-C(15)-C(9)	125.68(17)
C(9)-O(1)	1.292(2)	C(8)-C(7)-H(7A)	109.4	C(9)-O(1)-Rh(1)	113.62(11)
C(9)-C(10)	1.409(2)	C(6)-C(7)-H(7B)	109.4	C(15)-O(2)-Rh(1)	113.55(11)
C(9)-C(15)	1.471(2)	C(8)-C(7)-H(7B)	109.4	O(1)-Rh(1)-O(2)	79.31(5)
C(10)-C(11)	1.388(2)	H(7A)-C(7)-H(7B)	108.0	O(1)-Rh(1)-C(1)	93.10(6)
C(10)-H(10)	0.9500	C(1)-C(8)-C(7)	112.44(15)	O(2)-Rh(1)-C(1)	157.99(6)
C(11)-C(12)	1.393(3)	C(1)-C(8)-H(8A)	109.1	O(1)-Rh(1)-C(5)	160.41(6)
C(11)-H(11)	0.9500	C(7)-C(8)-H(8A)	109.1	O(2)-Rh(1)-C(5)	94.22(6)
C(12)-C(13)	1.385(3)	C(1)-C(8)-H(8B)	109.1	C(1)-Rh(1)-C(5)	99.11(7)
C(12)-H(12)	0.9500	C(7)-C(8)-H(8B)	109.1	O(1)-Rh(1)-C(2)	97.60(6)
C(13)-C(14)	1.389(3)	H(8A)-C(8)-H(8B)	107.8	O(2)-Rh(1)-C(2)	161.79(6)
C(13)-H(13)	0.9500	C(2)-C(1)-C(8)	125.19(17)	C(1)-Rh(1)-C(2)	39.07(7)
C(14)-C(15)	1.401(2)	C(2)-C(1)-Rh(1)	70.83(10)	C(5)-Rh(1)-C(2)	82.75(6)
C(14)-H(14)	0.9500	C(8)-C(1)-Rh(1)	111.21(11)	O(1)-Rh(1)-C(6)	159.98(6)
C(15)-O(2)	1.300(2)	C(2)-C(1)-H(1)	113.9	O(2)-Rh(1)-C(6)	97.69(6)
O(1)-Rh(1)	2.0573(13)	C(8)-C(1)-H(1)	113.9	C(1)-Rh(1)-C(6)	82.36(6)
O(2)-Rh(1)	2.0599(13)	Rh(1)-C(1)-H(1)	113.9	C(5)-Rh(1)-C(6)	38.65(7)
		C(1)-C(2)-C(3)	122.66(16)	C(2)-Rh(1)-C(6)	91.13(7)
C(2)-C(3)-C(4)	112.61(14)	C(1)-C(2)-Rh(1)	70.10(10)		
C(2)-C(3)-H(3A)	109.1	C(3)-C(2)-Rh(1)	113.39(12)		

Symmetry transformations used to generate equivalent atoms:

Table B.29.3 Anisotropic displacement parameters ($Å^2 x\ 10^3$) for [Rh(cod)(trop)]. The anisotropic displacement factor exponent takes the form: $-2\pi^2[\ h^2 a^{*2} U^{11} + ... + 2\ h\ k\ a^*\ b^*\ U^{12}\ ]$

	U^{11}	U^{22}	U^{33}	U^{23}	U^{13}	U^{12}
C(3)	23(1)	17(1)	12(1)	-3(1)	3(1)	-1(1)
C(4)	16(1)	16(1)	12(1)	3(1)	1(1)	-2(1)
C(5)	15(1)	11(1)	17(1)	2(1)	3(1)	0(1)
C(6)	17(1)	12(1)	16(1)	-1(1)	2(1)	-2(1)
C(7)	16(1)	20(1)	19(1)	1(1)	-1(1)	-4(1)
C(8)	15(1)	24(1)	21(1)	3(1)	-1(1)	2(1)
C(1)	17(1)	12(1)	18(1)	2(1)	3(1)	3(1)
C(2)	17(1)	11(1)	15(1)	-1(1)	5(1)	0(1)

C(9)	11(1)	11(1)	11(1)	-2(1)	-3(1)	0(1)
C(10)	14(1)	11(1)	14(1)	0(1)	-2(1)	-1(1)
C(11)	14(1)	15(1)	15(1)	3(1)	-1(1)	-4(1)
C(12)	12(1)	25(1)	14(1)	-1(1)	1(1)	-1(1)
C(13)	13(1)	18(1)	17(1)	-5(1)	1(1)	3(1)
C(14)	16(1)	11(1)	18(1)	-2(1)	-2(1)	1(1)
C(15)	12(1)	14(1)	10(1)	1(1)	-2(1)	-1(1)
O(1)	14(1)	12(1)	14(1)	-1(1)	2(1)	1(1)
O(2)	16(1)	11(1)	16(1)	0(1)	3(1)	-1(1)
Rh(1)	12(1)	9(1)	10(1)	0(1)	1(1)	0(1)

Table B.29.4 Hydrogen coordinates (x 10^4) and isotropic displacement parameters (Å^{2}x 10^3) for [Rh(cod)(trop)].

	x	y	z	U(eq)
H(3A)	2956	-863	577	21
H(3B)	4494	-396	1171	21
H(4A)	3532	1371	711	17
H(4B)	1722	898	635	17
H(5)	1608	2176	1997	17
H(6)	3301	2194	3258	18
H(7A)	5816	1441	3169	22
H(7B)	5445	964	2079	22
H(8A)	5975	-783	2825	24
H(8B)	5334	-336	3874	24
H(1)	3401	-1720	3386	18
H(2)	2060	-1743	1968	17
H(10)	-1565	-2121	4919	16
H(11)	-3397	-1735	6026	18
H(12)	-4408	10	6486	20
H(13)	-3878	1777	5842	19
H(14)	-2156	2260	4695	18

Table B.29.5 Hydrogen bonds for [Rh(cod)(trop)] [Å and º].

D-H...A	d(D-H)	d(H...A)	d(D...A)	<(DHA)
C(13)-H(13)...O(2)#1	0.95	2.45	3.387(2)	167.4

Symmetry transformations used to generate equivalent atoms:
#1 x-1/2,-y+1/2,-z+1

C. Supplementary Theoretical / Computational Data

C.1 Theoretical / Calculation Data of the Molecular Energy Orbitals

C.1.1 Group 7-11 Transition Metal Acetylaceonato Complexes Molecular Orbitals

Table C.1.1 Molecular Orbitals of calculated structures [M(cod)(acac)].

	HOMO-1	HOMO	LUMO	LUMO+1
Mn(I)	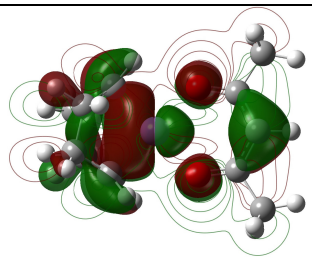	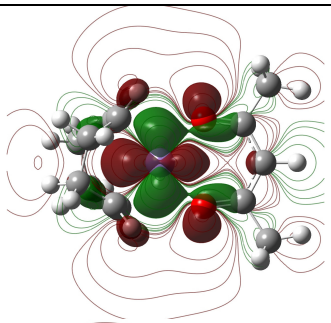	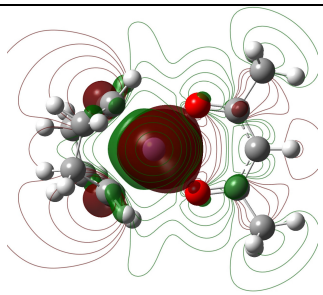	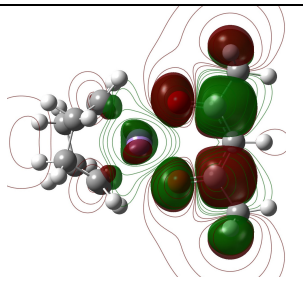
Tc(I)	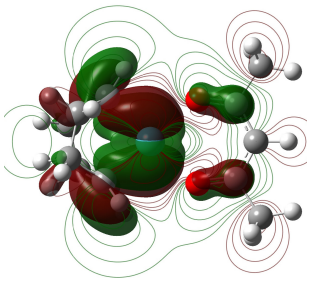	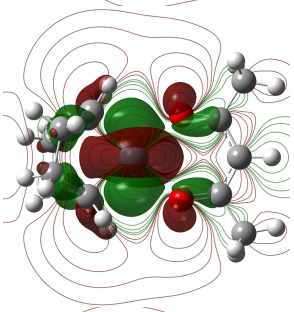	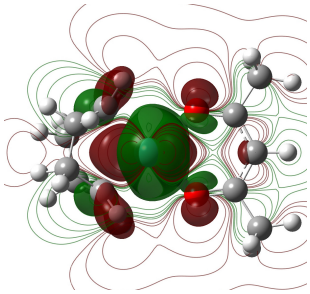	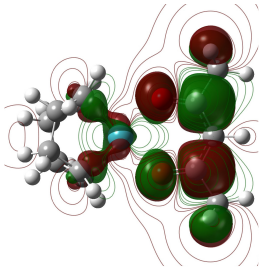
Re(I)	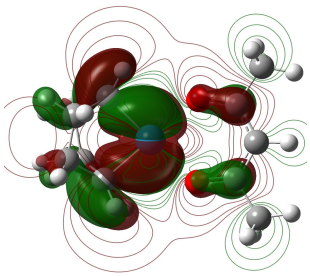	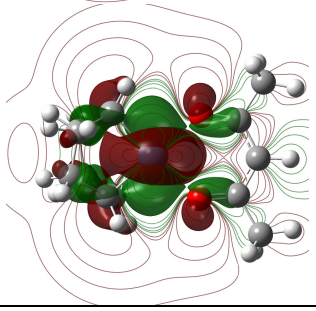	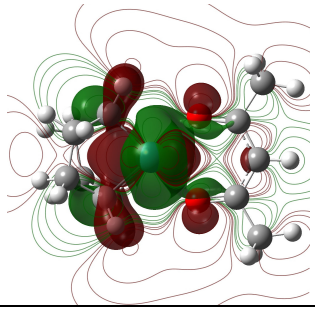	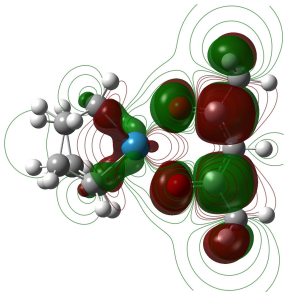

Group 7 contains manganese, technetium and rhenium (Table C.1.1) a classic π-orbital between the cyclo-octadiene ring's alkene carbons and the manganese metal centre can be clearly seen in the HOMO-1 orbital with the rest of the electron density mostly situated on the cyclo-octadiene ring. For the HOMO orbitals, a $d_{x^2-y^2}$ orbital is observed around the manganese metal centre with very little density observed for either bonding ligands whereas technetium and rhenium display a d_{z^2} orbital around the metal centers and similar density for the bonding ligands. For the LUMO orbitals,

a d_{z^2} orbital is found around the manganese metal centre again very little addition electron density is seen on the co-ordinating ligands this density progressively increases as one proceeds down the group. For all the metals of the group the LUMO+1 orbitals show the *p* orbitals depicting the delocalization of the acetylacetonato ligand.

Table C.1.2 Molecular Orbitals of calculated structures [M(cod)(acac)].

	HOMO-1	HOMO	LUMO	LUMO+1
Fe(0)	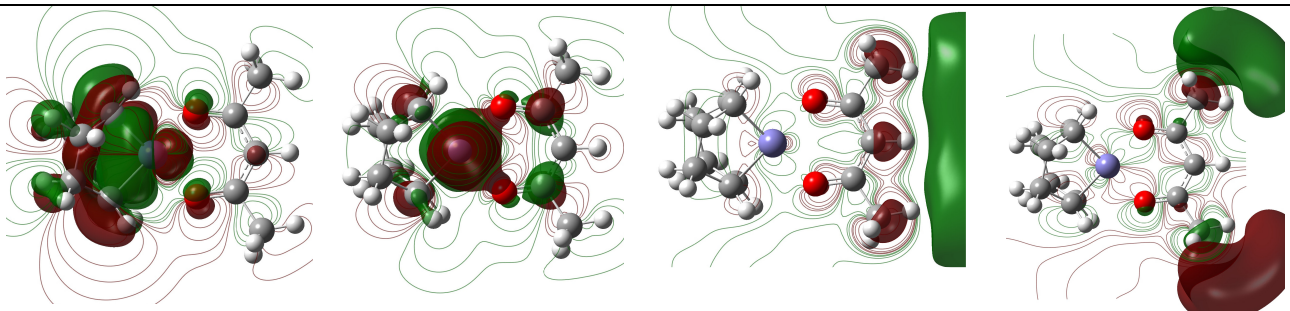			
Ru(0)	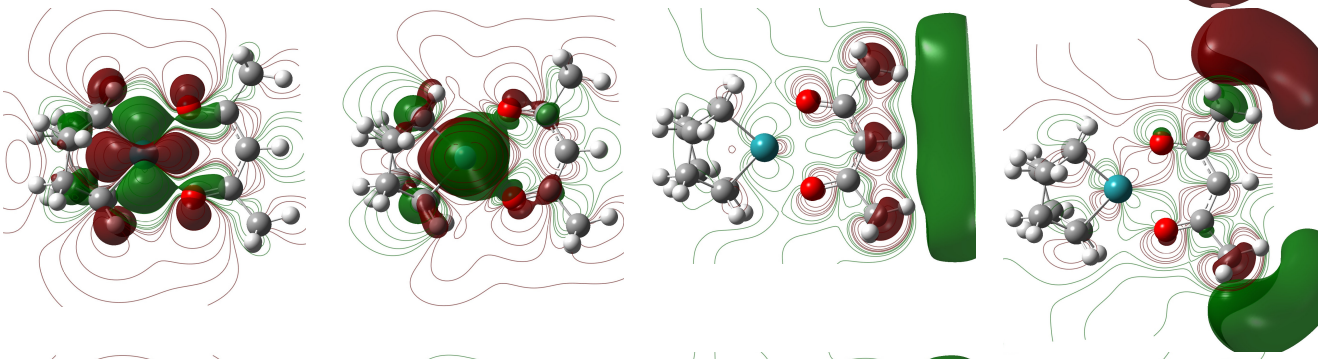			
Os(0)	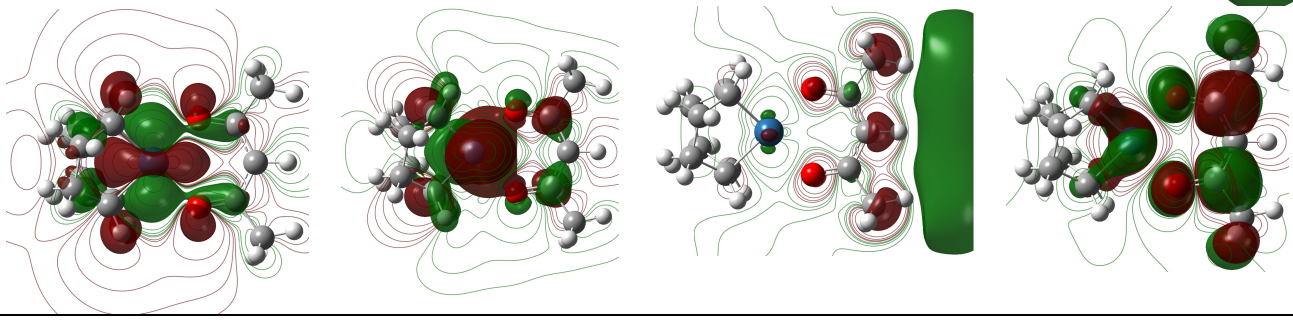			

In Table C.1.2 the iron triad molecular orbitals are shown. In the HOMO-1 orbitals of iron we see a π-orbital delocalization between iron and the cyclo-octadiene ring, for ruthenium and osmium a d_{z^2} orbital is observed around the metal centre. The HOMO orbitals show d_{z^2} orbitals for all the metal centers of the group with similar orbitals on the co-ordinating ligands.

Table C.1.3 Molecular Orbitals of calculated structures [M(cod)(acac)].

	HOMO-1	HOMO	LUMO	LUMO+1
Co(I)	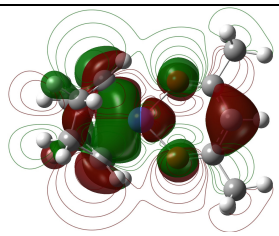	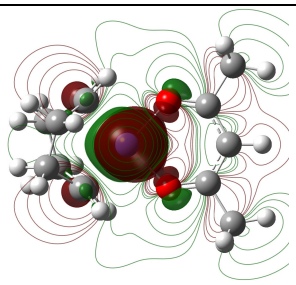	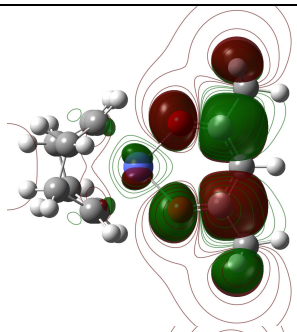	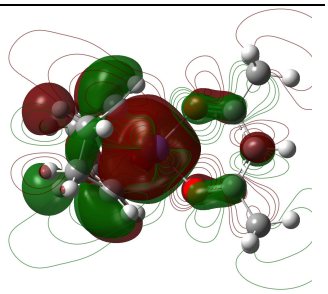
Rh(I)	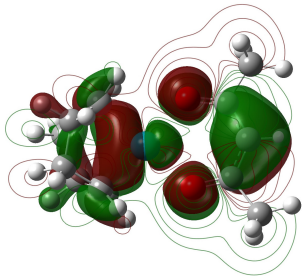	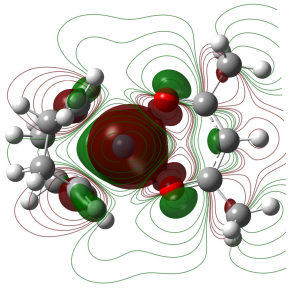	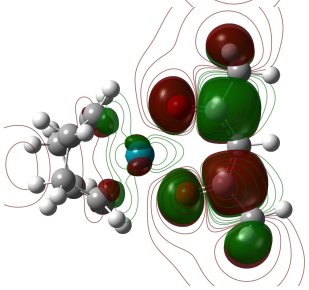	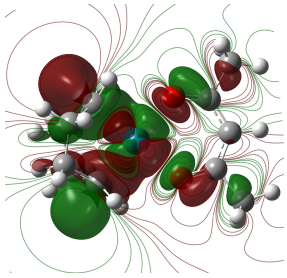
Ir(I)	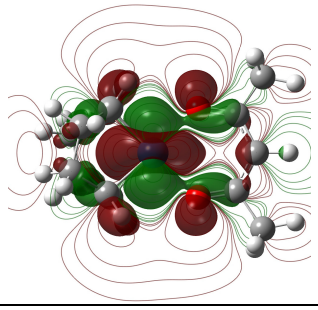	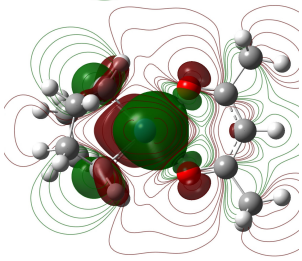	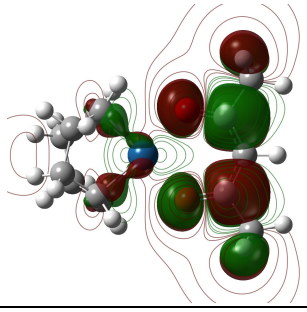	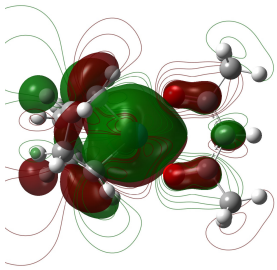

In the HOMO-1 molecular orbitals for cobalt and rhodium (Table C.1.3), a π orbital is observed between the metal centre and the cyclo-octadiene ring. The delocalization of the acetylaceonato ligand is also represented. The iridium has a d_{z^2} orbital which is a similar configuration to ruthenium and osmium seen in Appendix D.1.2. For the HOMO molecular orbital all metals of group 9 display a d_{z^2} orbital centered on the metal centre with little additional orbitals found on the co-ordinating ligands. The LUMO molecular orbital depicts the *p* orbitals on the acetylacetonato ligand which gives rise to the conjugation.

Table C.1.4 Molecular Orbitals of calculated structures [M(cod)(acac)].

	HOMO-1	HOMO	LUMO	LUMO+1
Ni(II)	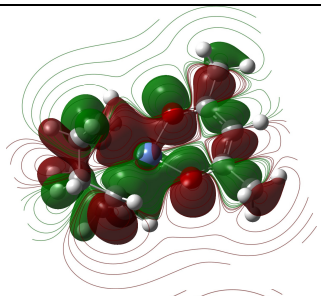	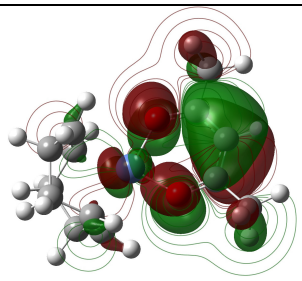	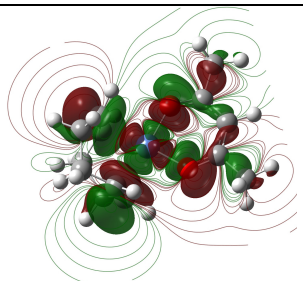	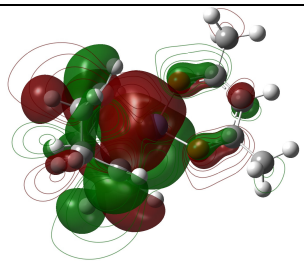
Pd(II)	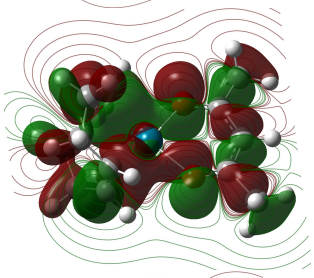	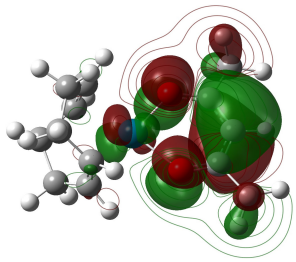	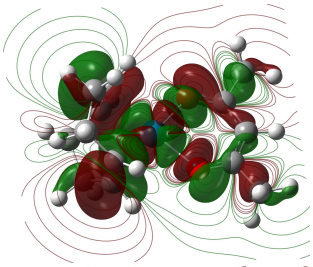	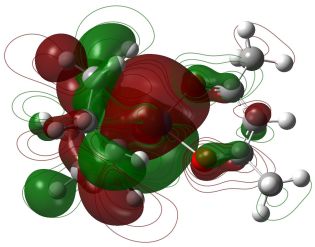
Pt(II)	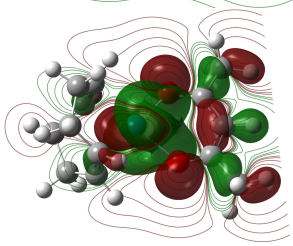	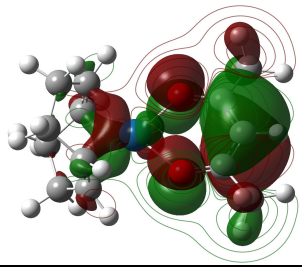	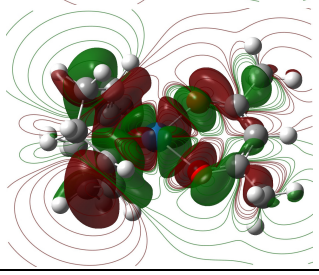	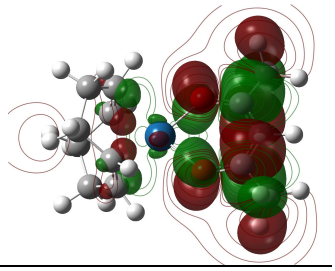

A table showing the group 10 molecular orbitals is found in Table C.1.4. The HOMO-1 molecular orbitals of nickel and palladium are comparable with π orbital delocalization occurring between both the cyclo-octadiene moiety and the acetylacetonato moiety. Platinum however only shows delocalization between the metal and the acetylacetonato moiety. For the HOMO molecular orbitals delocalization on the back-bone of the acetylacetonato moiety is seen for all three complexes, with the platinum complex showing some electron density around the cyclo-octadiene alkene carbons. A $d_{x^2-y^2}$ orbital is observed on the metal centers for the LUMO molecular orbitals.

Table C.1.5 Molecular Orbitals of calculated structures [M(cod)(acac)].

	HOMO-1	HOMO	LUMO	LUMO+1
Cu(I)	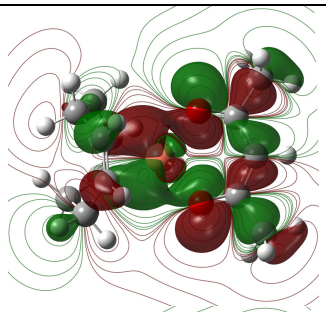	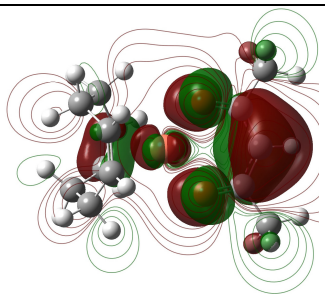	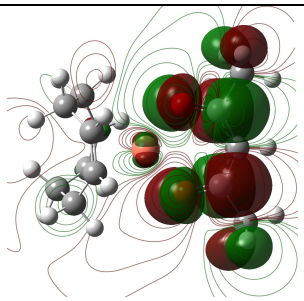	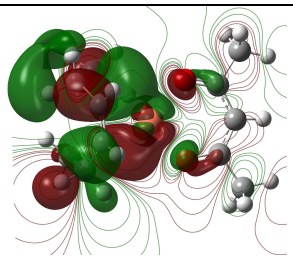
Ag(I)	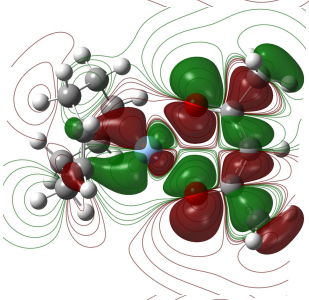	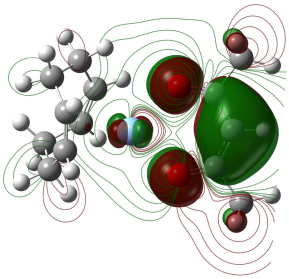	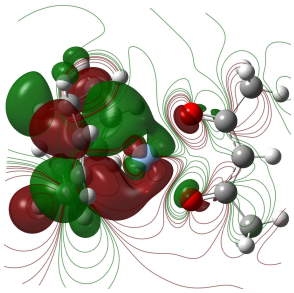	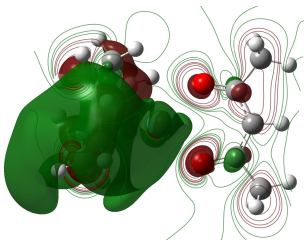
Au(I)	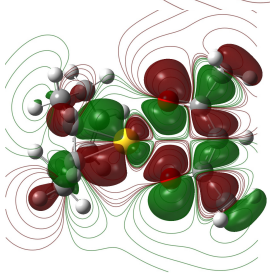	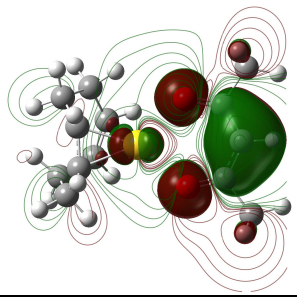	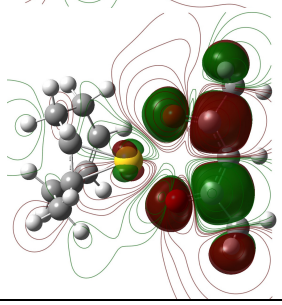	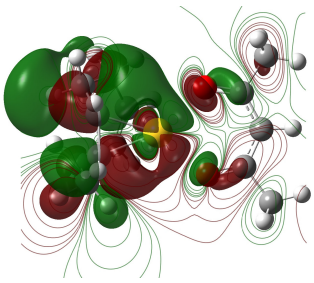

A table showing the group 11 molecular orbitals and contour plots is found in Table C.1.5. It is of interest to note here that for the group 11 metals the cyclo-octadiene ring is mono co-ordinated to the metal centers. In the HOMO molecular orbitals of copper the *p* orbital around the alkene carbons of the cyclo-octadiene ring can be seen. The delocalization on the acetylacetonato back-bone is also evident. For the HOMO-1 orbital the d_{xz} orbital around the metal centers are clearly overlapping with the *p* orbitals of the alkene carbons of the cyclo-octadiene ring. The *p* orbitals of the oxygens are out of phase with those of the metal centers. For the LUMO molecular orbitals the d_{xy} orbital is seen around the metal centers.

C.1.2 Group 7-11 Transition Metal Trifluoroacetylaceonato Complexes Molecular Orbitals

Table C.1.6 Molecular Orbitals of calculated structures [M(cod)(tfacac)].

	HOMO-1	HOMO	LUMO	LUMO+1
Mn(I)	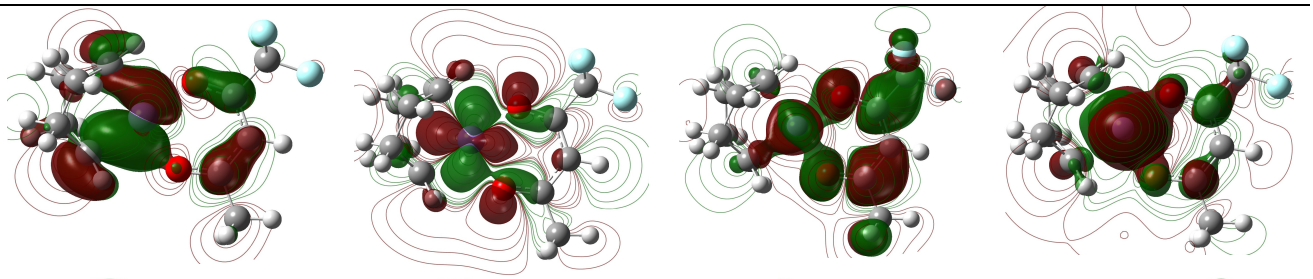			
Tc(I)	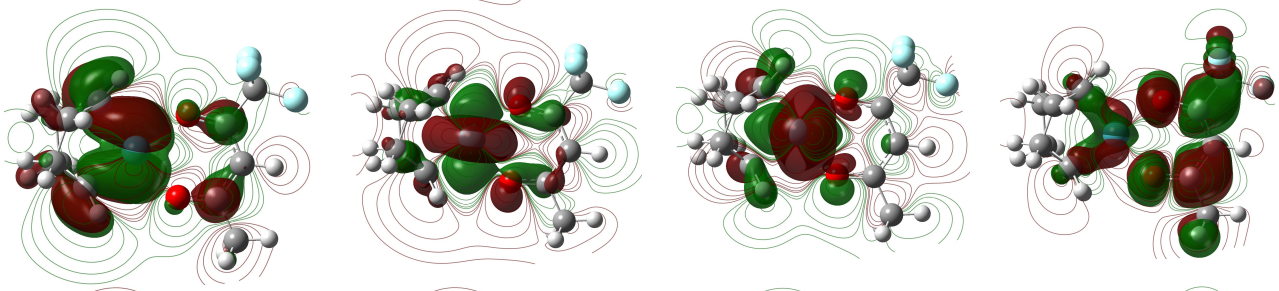			
Re(I)	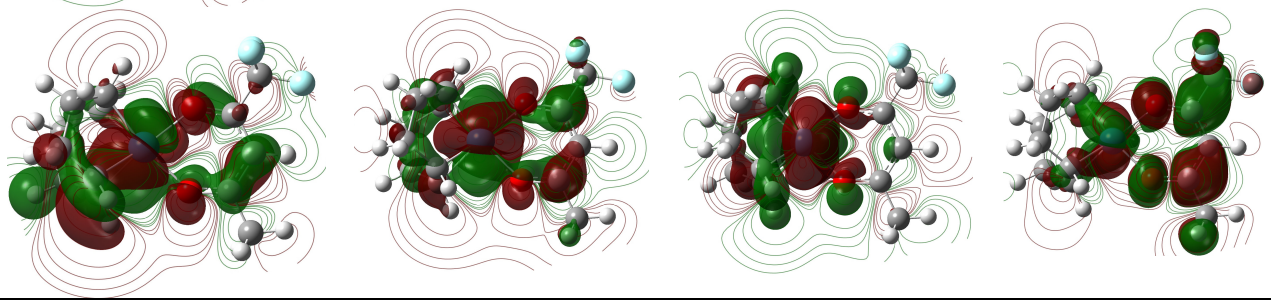			

The complete molecular orbitals for the group 7 metal trifluoroacetylactonato complexes are presented in Table C.1.6. In the HOMO-1 molecular orbitals the π orbital overlap seen in the [Mn(cod)(acac)] (see Table 12.2 or Table 2.2) has changed to a d_{xy} metal orbital with an in phase overlap of the π-orbital of the alkene carbons of the cyclo-octadiene ring. The [Tc(cod)(acac)] (see Table C.1.1) and [Tc(cod)(tfacac)] complexes have similar molecular orbitals, whist the rhenium complex differs in that the d_{yz} metal orbital overlaps with the p orbital form the alkene "trans" to the CF_3 group, with more conjuation present in the trifluoroacetylacetonato back-bone. For the HOMO molecular orbitals the [Mn(cod)(acac)] and [Mn(cod)(tfacac)] complexes are akin with a $d_{x^2-y^2}$ orbital centered on the manganese. For the technetium and rhenium complexes for both the acetylacetonato and trifluoroacetylacetono complexes a d_{z^2} orbital is observed. The LUMO+1 molecular orbitals for the

trifluoroacetylacetonato complexes show *p* orbitals on the ligand for technetium and rhenium whilst the manganese complex has d_{z^2} orbital overlapping with the *p* orbitals of the oxygens of the trifluoroacetylacetonato ligand.

Table C.1.7 Molecular Orbitals of calculated structures [M(cod)(tfacac)].

	HOMO-1	HOMO	LUMO	LUMO+1
Fe(0)	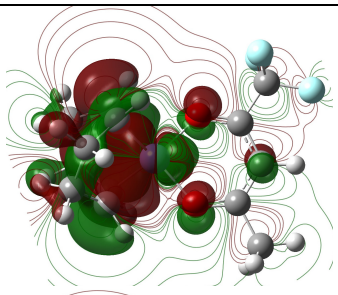	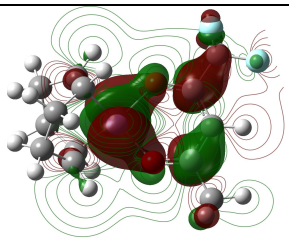	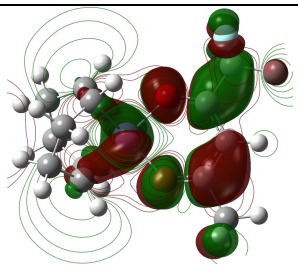	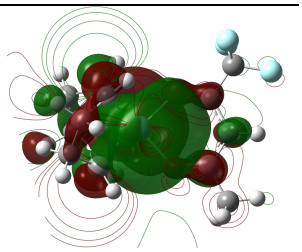
Ru(0)	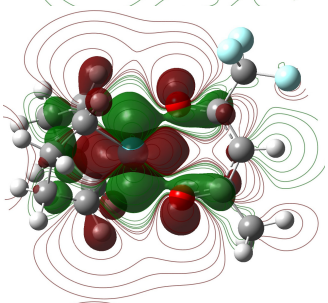	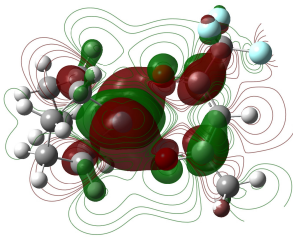	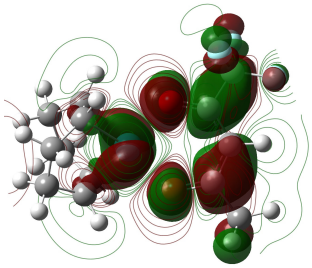	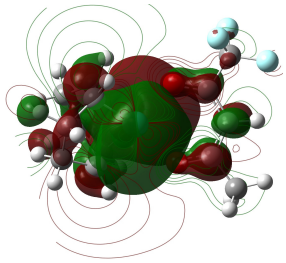
Os(0)	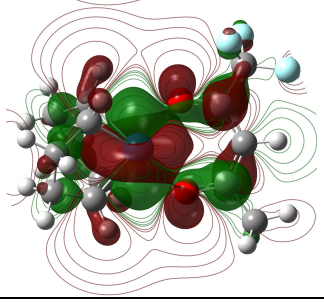	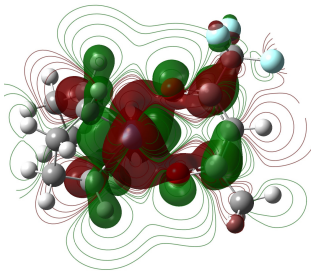	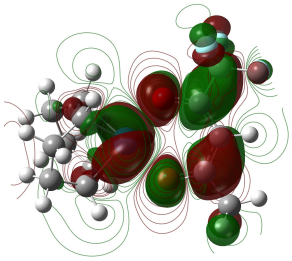	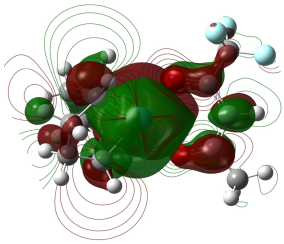

The group 8 metal complexes the complete molecular orbitals table is given in Table C.1.7. The iron HOMO-1 molecular orbital displays the same π orbital delocalization as was found for the iron acetylacetonato complex (see Table 12.2 or Table 2.2) with both the ruthenium and osmium complexes demonstrating the same d_{z^2} orbital for the metal complexes as was found for the acetylacetonato complexes (see Table C.1.2). The HOMO molecular orbitals for both the acetylacetonato and the trifluoroacetylacetonato complexes are similar in that the orbital found centered on the metal centre is a d_{z^2}, the main difference observed is that of increased overlap of orbitals of the trifluoroacetylacetonato ligand. For the LUMO molecular orbitals the delocalization of the *p* orbitals on the back-bone of the trifluoroacetylactonato ligand are visible. Additionally both the *p* orbitals and *s* orbitals of the fluorines and

hydrogens are also observed. The second highest unoccupied molecular orbital displays a d_{xz} orbital for all the group 8 metal centers.

Table C.1.8 Molecular Orbitals of calculated structures [M(cod)(tfacac)].

	HOMO-1	HOMO	LUMO	LUMO+1
Co(I)	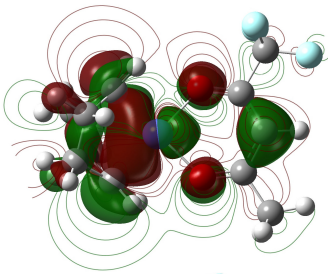	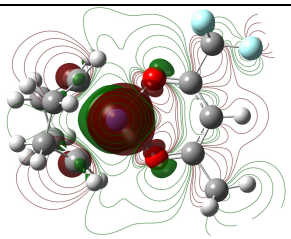	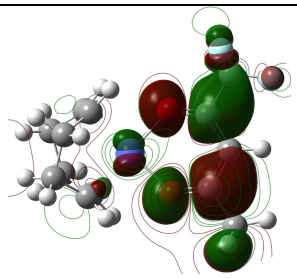	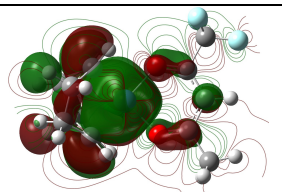
Rh(I)	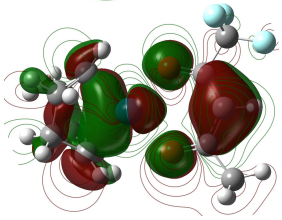	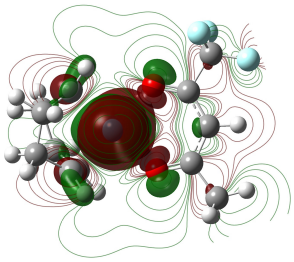	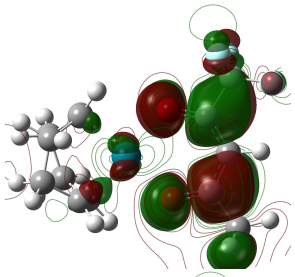	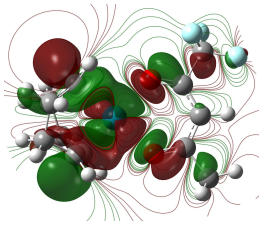
Ir(I)	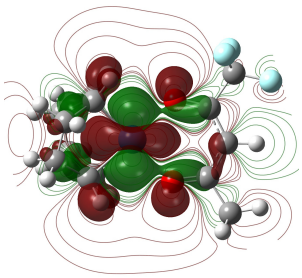	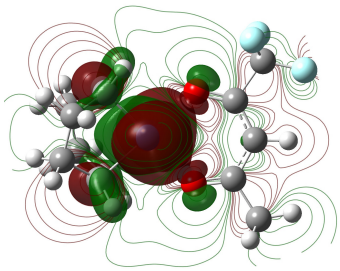	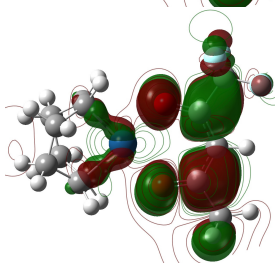	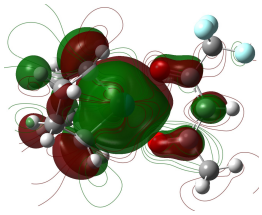

The complete molecular orbital table for group 9 metal complexes of trifluoroactylactonato and cylo-octadiene are given in Table C.1.8. On comparison with the group 9 acetylacetonato complexes (see Table C.1.3) the orbitals show a marked similarity. For the HOMO-1 molecular orbitals one finds the π orbital delocalization for the cobalt and rhodium complexes whilst the iridium displays a d_{z^2} orbital. The HOMO molecular orbitals have a d_{z^2} orbital centered on the metal centers. The only difference observed between the acetylacetonato complexes and that of the trifluoroacetylacetonato complexes are the *p* orbitals which are present on the flourines of the ligand seen in the LUMO molecular orbitals. These orbitals however do not play any significant role in the bonding.

Table C.1.9 Molecular Orbitals of calculated structures [M(cod)(tfacac)].

	HOMO-1	HOMO	LUMO	LUMO+1
Ni(II)	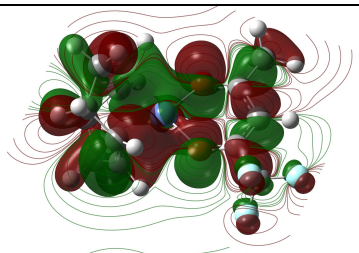	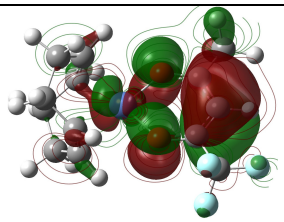	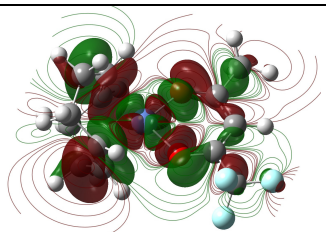	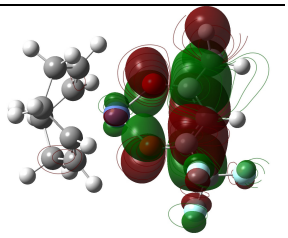
Pd(II)	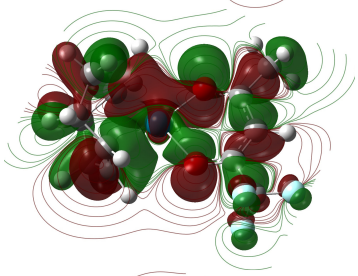	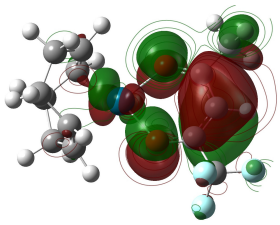	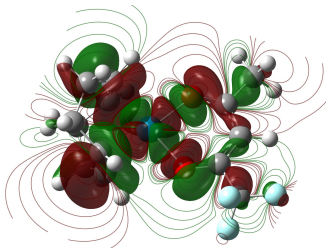	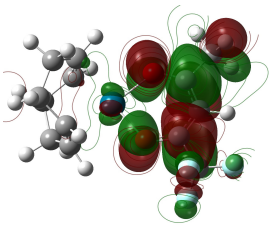
Pt(II)	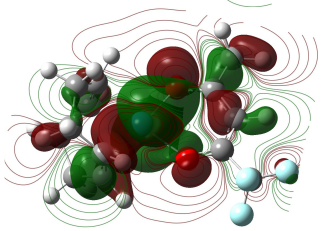	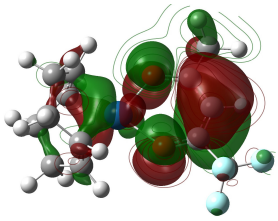	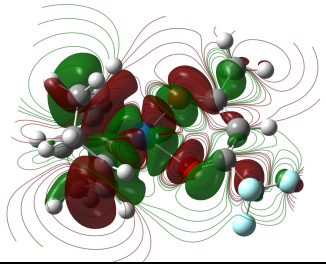	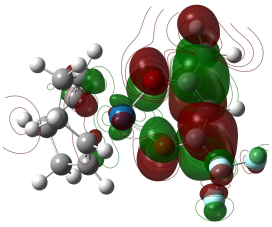

The complete molecular orbital table for group 10 metal trifluoracetylacetonato complexes is given in Table C.1.9. A similar situation is found to that of the group 9 metals where the molecular orbitals only differ with regards to the LUMO+1 molecular orbitals of nickel and palladium with both metals having d_{xy} orbital and delocalization on the trifluoroacetylacetonato back-bone.

Table C.1.10 Molecular Orbitals of calculated structures [M(cod)(tfacac)].

	HOMO-1	HOMO	LUMO	LUMO+1
Cu(I)	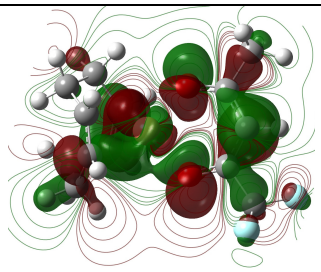	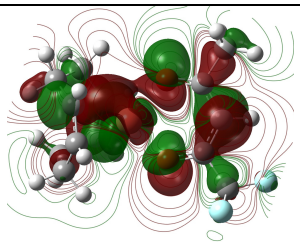	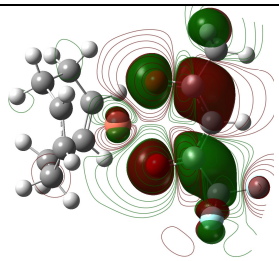	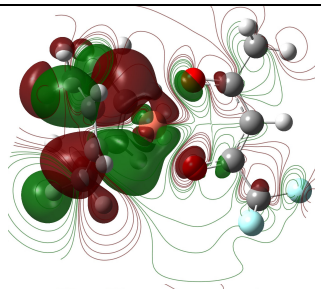
Ag(I)	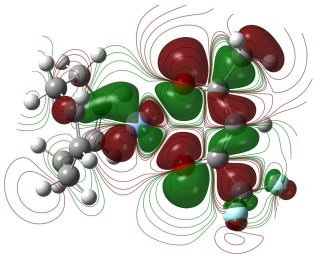	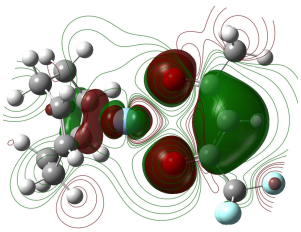	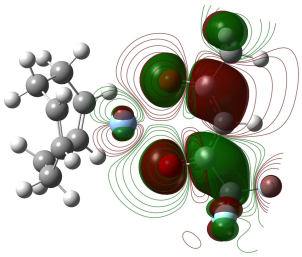	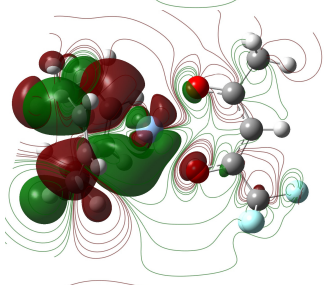
Au(I)	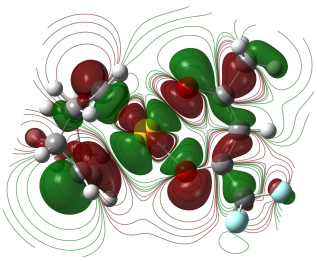	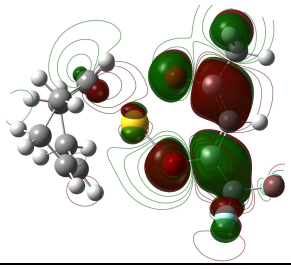	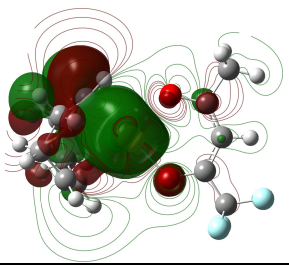	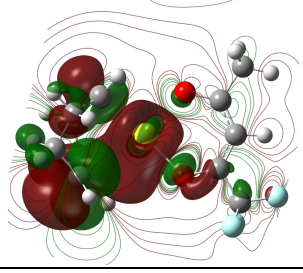

The complete molecular orbital table for group 11 metal trifluoracetylacetonato complexes is given in Table C.1.10. For the HOMO-1 molecular orbital $d_{x^2-y^2}$ orbitals were found for silver and gold. It must be mentioned that the group 11 complexes are mono co-ordinated cyclo-octadine complexes with the alkene "cis" to the CF_3 group being non-co-ordinated. In the HOMO molecular orbitals a d_{xy} orbital is seen around the metal centre, with an in phase overlap of the *p* orbital of the alkene for silver whilst the orbitals for copper are obscured. For the LUMO+1 molecular obitals there is a d_{xz} orbital on the metal centre this is however overshadowed by the *p* orbitals of the alkenes.

C.1.3 Group 7-11 Transition Metal Hexafluoroacetylaceonato Complexes Molecular Orbitals

Table C.1.11 Molecular Orbitals of calculated structures [M(cod)(hfacac)].

	HOMO-1	HOMO	LUMO	LUMO+1
Mn(I)	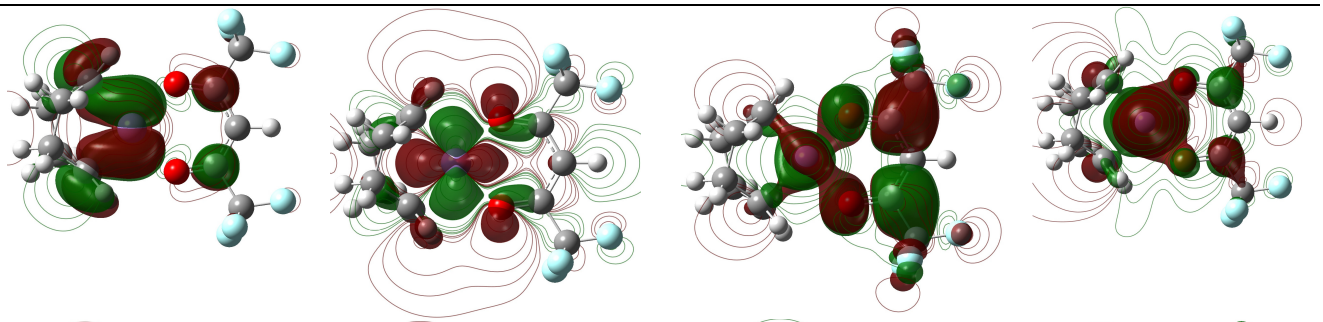			
Tc(I)	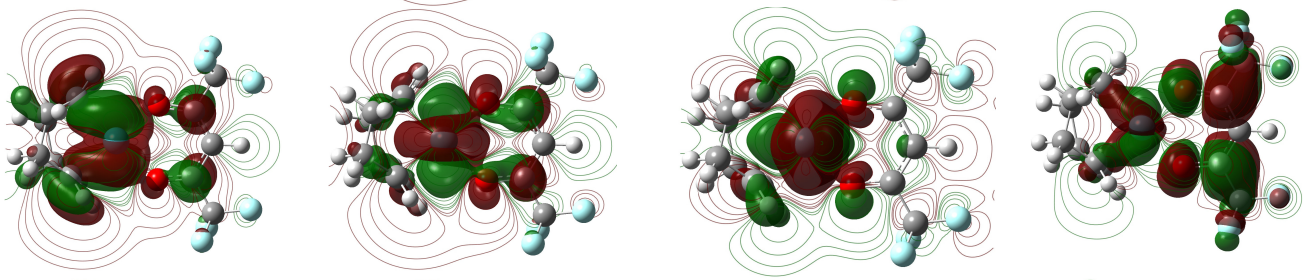			
Re(I)	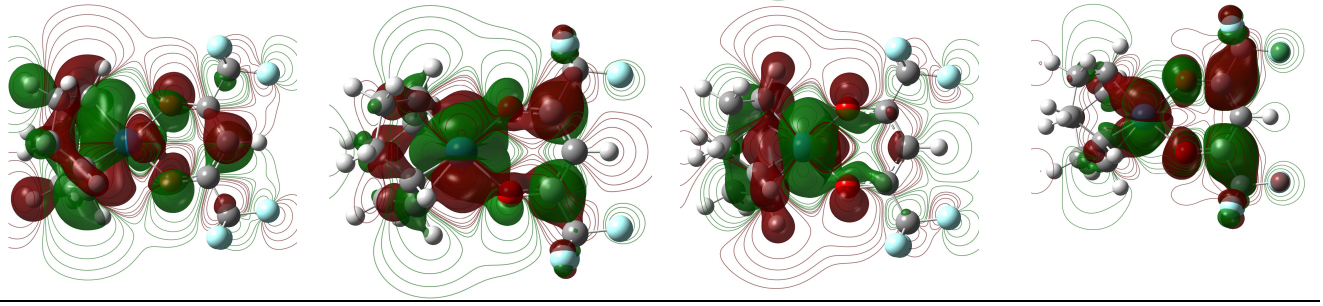			

The complete molecular orbital table for group 7 metal hexafluoracetylacetonato (hfacac) complexes is given in Table C.1.11. In the comparison of the HOMO-1 molecular orbitals it was found that for manganese and technetium the orbitals were the same for trifluoroacetylacetonato (tfacac) complexes, with the rhenium complex being similar to the [Mn(cod)(acac)] with an in phase overlap of the π orbitals. For the HOMO molecular orbitals the acetylacetonato (acac), tfacac and the hfacac complexes are analogous, with the manganese having a $d_{x^2-y^2}$ orbital on the metal centre and both technetium and rhenium with a d_{z^2} orbital. In the LUMO molecular orbitals technetium and rhenium both have d_{z^2} orbitals with the tfacac complexes displaying a comparable pattern with *p* orbitals seen on the flourines. For the acac

complexes only the manganese complex does not follow the pattern. Lastly the LUMO+1 molecular orbitals are again comparable with the tfacac complexes.

Table C.1.12 Molecular Orbitals of calculated structures [M(cod)(hfacac)].

	HOMO-1	HOMO	LUMO	LUMO+1
Fe(0)	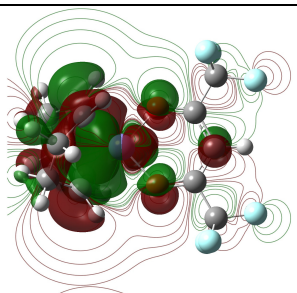	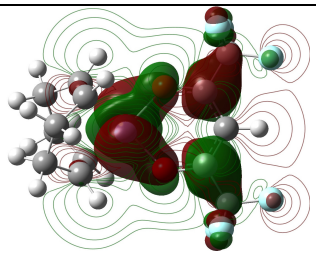	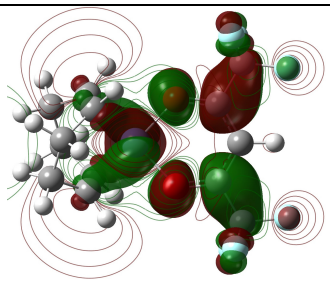	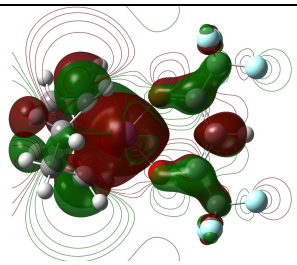
Ru(0)	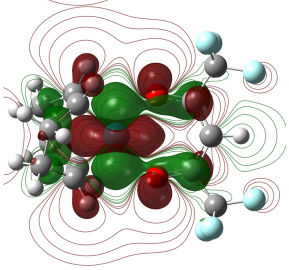	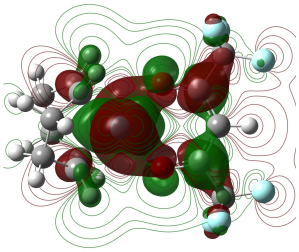	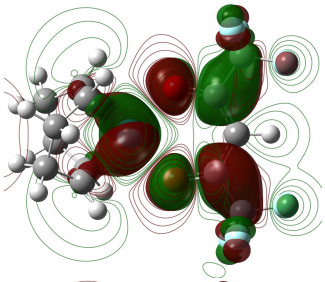	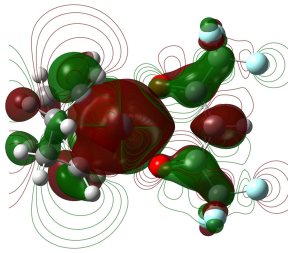
Os(0)	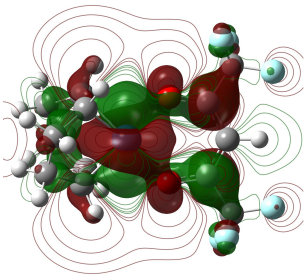	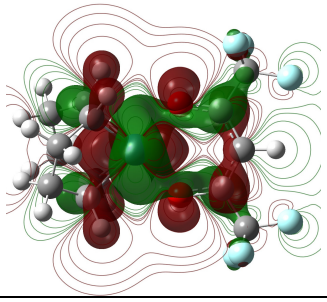	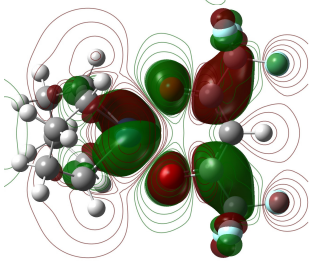	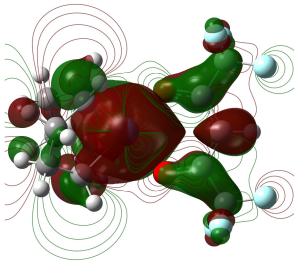

The complete molecular orbital table for group 8 metal hexafluoracetylacetonato (hfacac) complexes are given in Table C.1.12. In the comparison between the molecular orbitals of the trifluoroacetylacetonato (tfacac) complexes with the hfacac complexes it was observed that they match. For the HOMO-1 molecular orbitals d_{z^2} orbitals were observed centered on the metals centers, this was also the case for the acetylacetonato (acac) HOMO-1 molecular orbitals. In the HOMO molecular orbitals the d_{z^2} orbital is still present for all metal centers again the molecular orbitals observed for acac complexes were similar. In the LUMO molecular orbitals the delocalization of the hfacac ligand is clearly observed with *p* orbitals for the fluorine atoms also seen. Lastly for the LUMO+1 molecular orbitals the d_{xz} orbitals are seen on the metals.

Table C.1.13 Molecular Orbitals of calculated structures [M(cod)(hfacac)].

	HOMO-1	HOMO	LUMO	LUMO+1
Co(I)	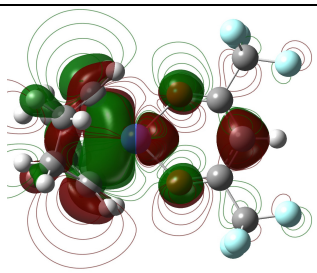	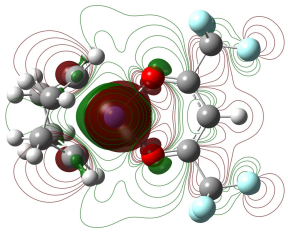	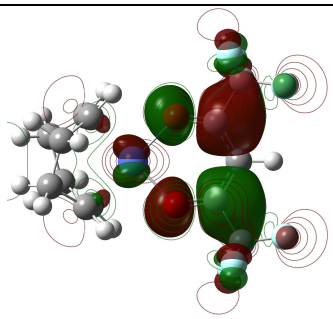	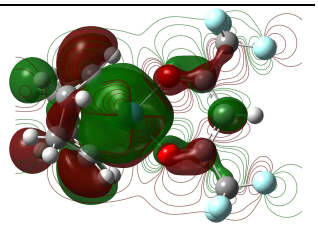
Rh(I)	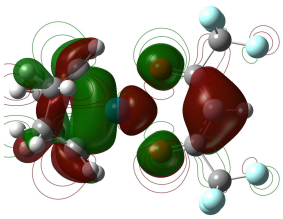	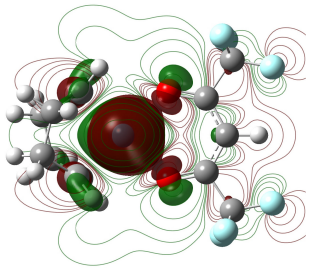	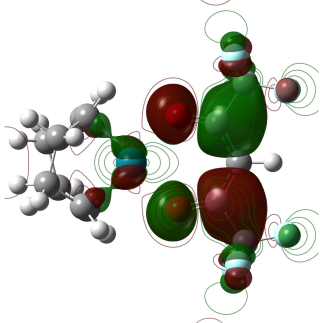	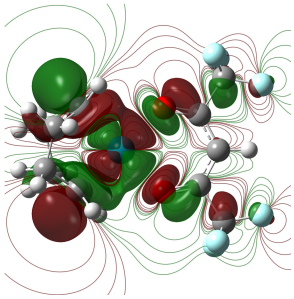
Ir(I)	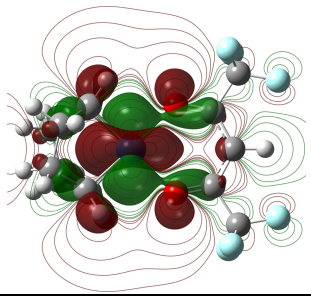	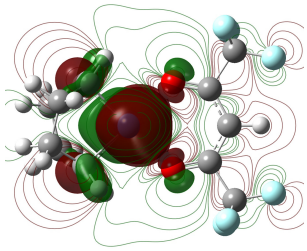	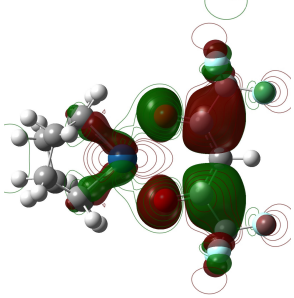	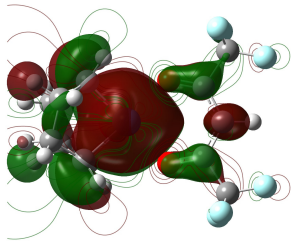

The complete molecular orbital table for group 9 metal hexafluoracetylacetonato (hfacac) complexes are given in Table C.1.13. For the HOMO-1 molecular orbitals, for the cobalt and rhodium complexes the π orbitals are clearly visible between the metal centre and the cyclo-octadiene. The iridium complex however, has a d_{z^2} orbital found on the metal this is the same as found for the acetylacetonato (acac) and trifluoroacetylacetonato (tfacac) complexes. In the HOMO molecular orbitals the d_{z^2} orbital is present for all the metal centers, the orbitals observed for acac and tfacac complexes are similar. In the LUMO molecular orbitals the d_{xy} orbitals are found on the metal centers with the *p* orbitals clearly seen on the fluorine atoms. Again both the acac and tfacac complexes display similar characteristics. Lastly for the LUMO+1 molecular orbitals a $d_{x^2-y^2}$ orbital is seen for the rhodium metal centre whereas both cobalt and iridium have a d_{z^2} orbital. The orbitals are again similar to the ones found for both the acac and tfacac complexes.

Table C.1.14 Molecular Orbitals of calculated structures [M(cod)(hfacac)].

	HOMO-1	HOMO	LUMO	LUMO+1
Ni(II)	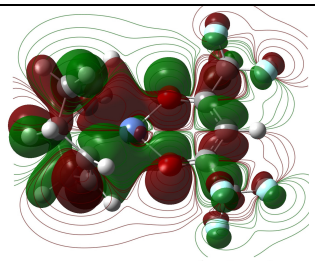	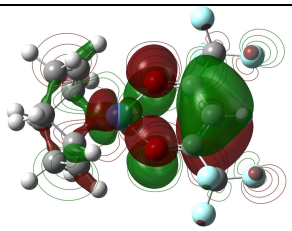	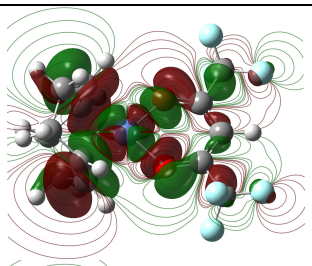	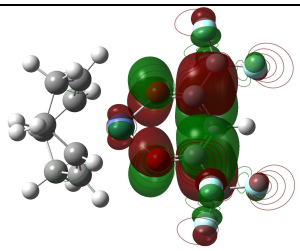
Pd(II)	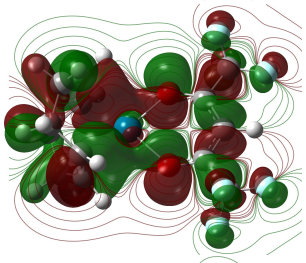	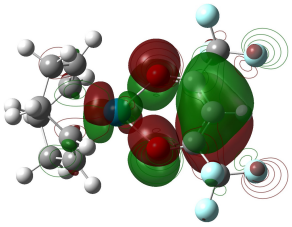	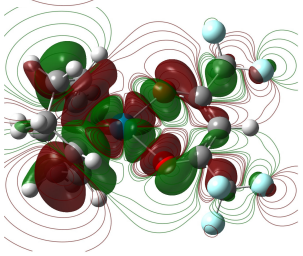	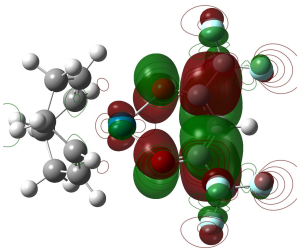
Pt(II)	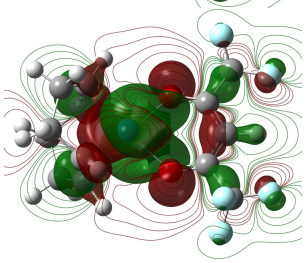	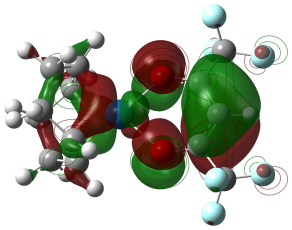	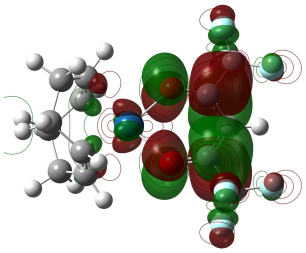	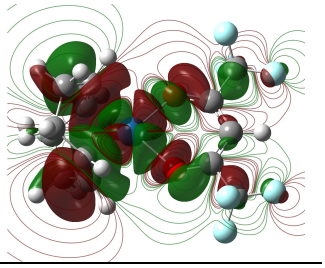

The complete molecular orbital table for group 10 metal hexafluoracetylacetonato (hfacac) complexes are given in Table C.1.14. For the HOMO-1 molecular orbitals, π orbital delocalization is seen for the nickel and palladium complexes with a d_{z^2} orbital for platinum. In the HOMO molecular orbitals, the d_{xy} orbital is centered on the metals whilst an in-phase overlap of the p_y obitals of the oxygen atoms of the hfacac ligand is observed. This orbital pattern is also found for the acetylacetonato (acac) and trifluoroacetylaceonato (tfacac) complexes. In the LUMO molecular orbitals, a $d_{x^2-y^2}$ orbital is seen on the nickel and palladium metals, with an in-phase overlap of the d_{xy} orbitals of the platinum metal and p_y orbitals of the hfacac ligand. For the LUMO+1 molecular orbitals, the p orbitals for the fluorine atoms of the hfacac ligand are seen whilst π orbital delocalization is seen in the carbon back-bone of the ligand and the p_y orbitals of the oxygens overlap with the d_{xy} orbitals of the nickel and palladium metal. With platinum having a $d_{x^2-y^2}$ orbital.

Table C.1.15 Molecular Orbitals of calculated structures [M(cod)(hfacac)].

	HOMO-1	HOMO	LUMO	LUMO+1
Cu(I)	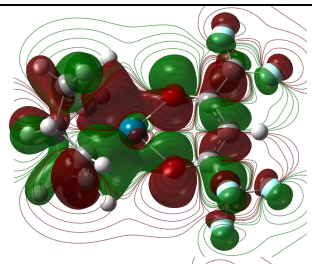	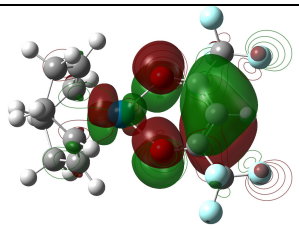	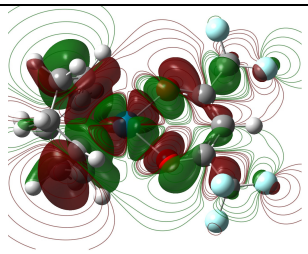	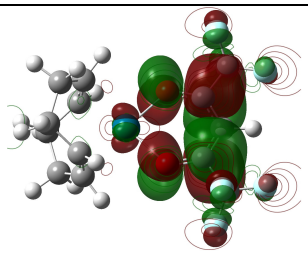
Ag(I)	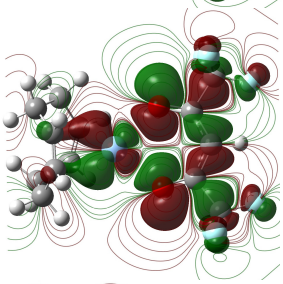	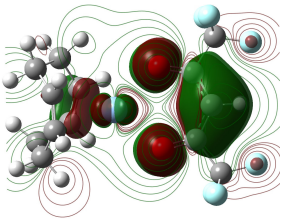	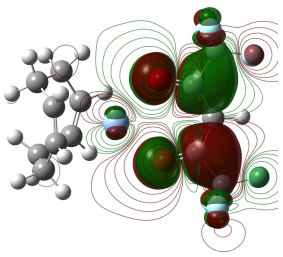	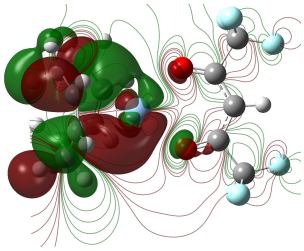
Au(I)	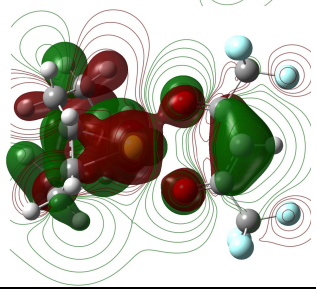	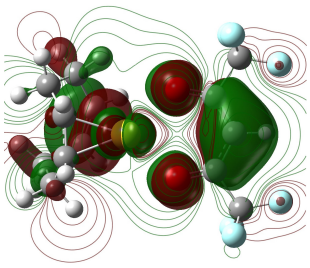	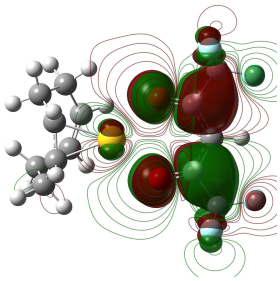	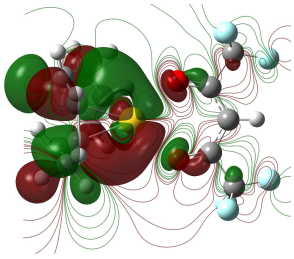

The complete molecular orbital table for group 11 metal hexafluoracetylacetonato (hfacac) complexes are given in Table C.1.15. For the HOMO-1 molecular orbitals, a d_{xz} orbital is found on the copper metal with π orbital delocalization clearly visible. For the silver metal centre a $d_{x^2-y^2}$ orbital is visible with out-of phase *p* orbitals on the hfacac ligand. For gold a d_{z^2} orbital was observed. In the HOMO molecular orbitals, d_{yz} orbitals were observed for all metals with delocalization on the hfacac back-bone. In the LUMO molecular orbitals, a $d_{x^2-y^2}$ orbital was found on the copper metal centre whilst d_{xy} orbitals were seen for silver and gold, *p* orbitals were seen on the fluorine atoms. Lastly for the LUMO+1 molecular orbitals, a d_{xy} orbital was observed for copper with an in-phase overlap with the p_y orbitals of the oxygen atoms of the hfacac ligand while d_{xz} orbitals were observed for silver and gold with π delocalization seen on the cyclo-octadiene.

C.1.4 Group 7-11 Transition Metal 4-Aminopent-3-en-2-onato Complexes Molecular Orbitals

Table C.1.16 Molecular Orbitals of calculated structures [M(cod)(NH-acac)].

	HOMO-1	HOMO	LUMO	LUMO+1
Mn(I)	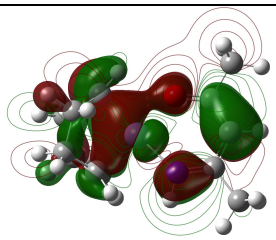	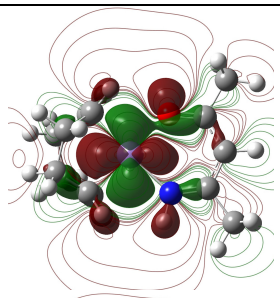	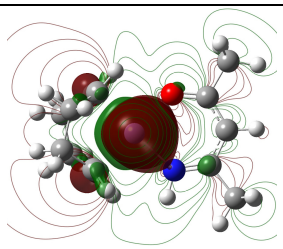	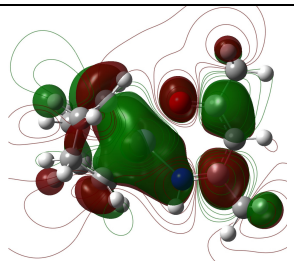
Tc(I)	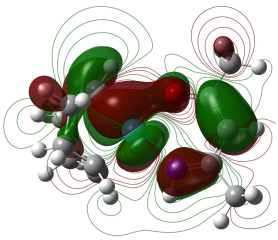	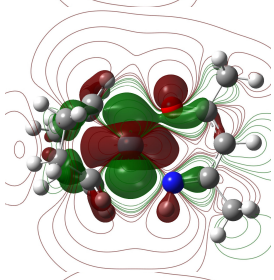	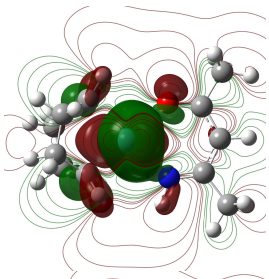	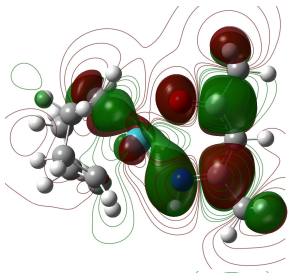
Re(I)	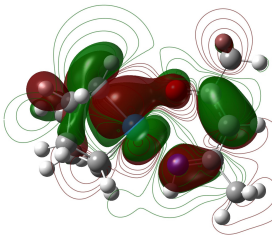	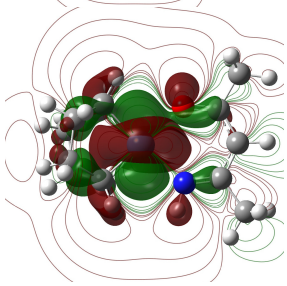	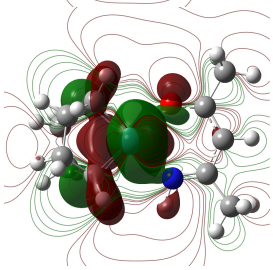	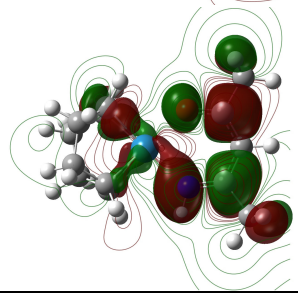

The complete molecular orbital table for group 7 metal 4-aminopent-3-en-2-onato (NH-acac) complexes is given in Table C.1.16. For the HOMO-1 molcular orbitals the *trans* influence of the nitrogen is seen. In the HOMO molecular orbitals, a $d_{x^2-y^2}$ orbital is observed on the manganese metal centre while d_{z^2} orbitals are seen for technetium and rhenium. For the LUMO molecular orbitals, d_{z^2} orbitals were found for all the metal centers. Lastly in the LUMO+1 molecular orbitals, *p* orbitals for the NH-acac back-bone are clearly seen.

Table C.1.17 Molecular Orbitals of calculated structures [M(cod)(NH-acac)].

	HOMO-1	HOMO	LUMO	LUMO+1
Fe(0)	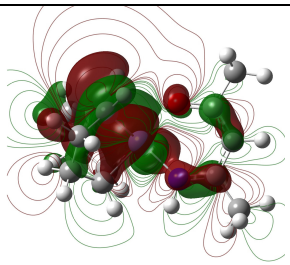	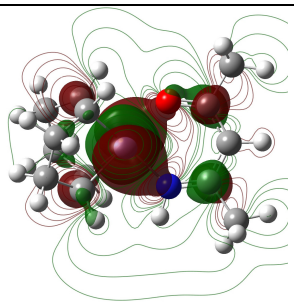	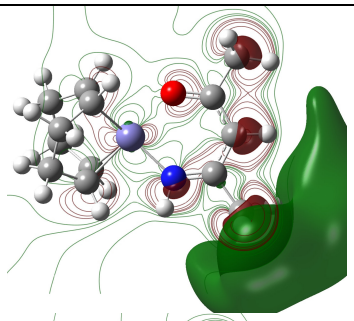	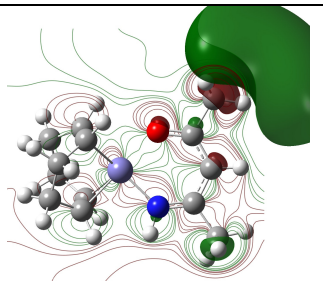
Ru(0)	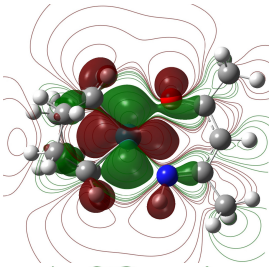	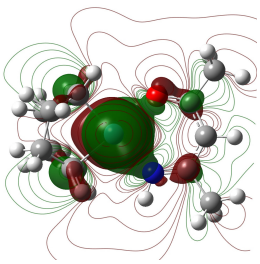	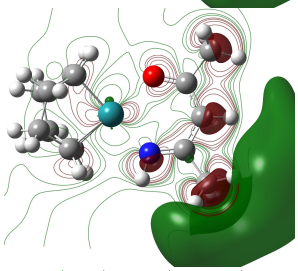	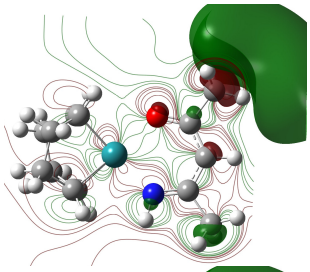
Os(0)	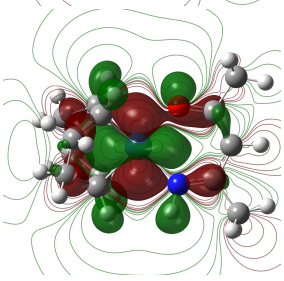	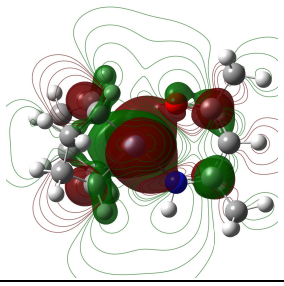	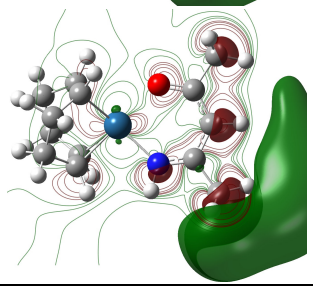	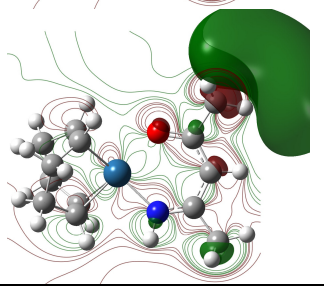

The complete molecular orbital table for group 8 metal 4-aminopent-3-en-2-onato (NH-acac) complexes are given in Table C.1.17. For the HOMO-1 molecular orbitals, a $d_{x^2-y^2}$ orbital is observed for ruthenium and osmium. In the HOMO molecular orbitals, a d_{z^2} orbital was found for all the metals.

Table C.1.18 Molecular Orbitals of calculated structures [M(cod)(NH-acac)].

	HOMO-1	HOMO	LUMO	LUMO+1
Co(I)	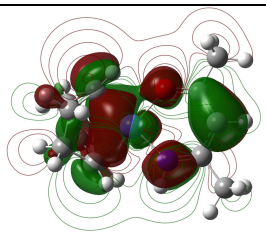	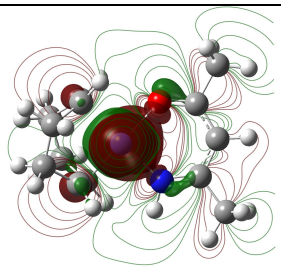	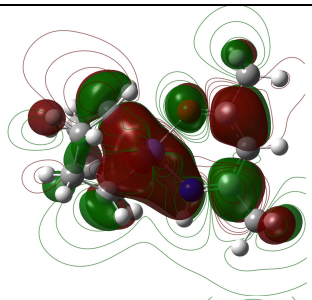	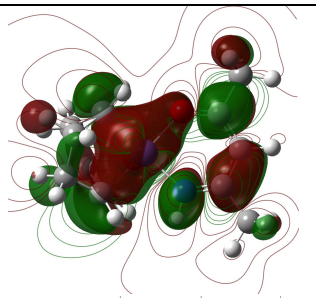
Rh(I)	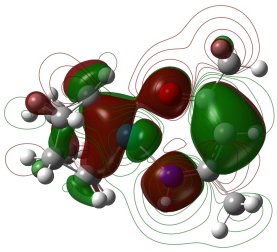	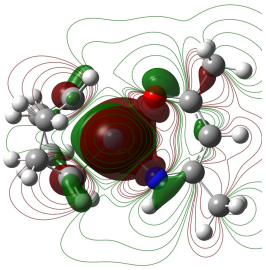	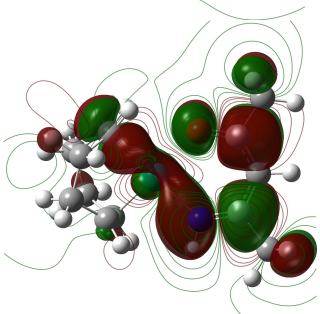	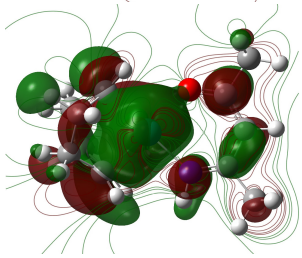
Ir(I)	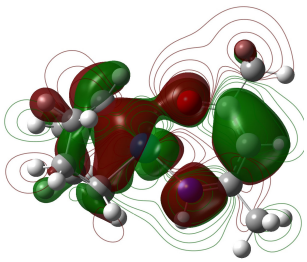	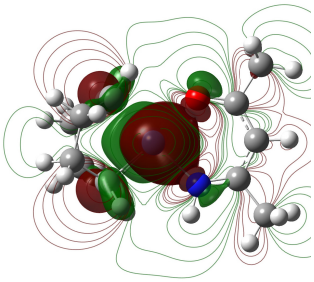	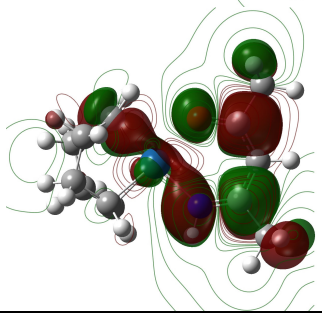	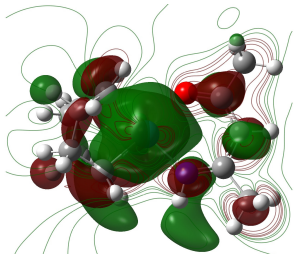

The complete molecular orbital table for group 9 metal 4-aminopent-3-en-2-onato (NH-acac) complexes are given in Table C.1.18. For the HOMO-1 molecular orbitals, the *trans* influence on the π delocalization of the cyclo-octadiene is seen. In the HOMO molecular orbitals, a d_{z^2} orbital was found for all the metal centers. Lastly in the LUMO molecular orbitals, the *trans* influence can again be seen.

Table C.1.19 Molecular Orbitals of calculated structures [M(cod)(NH-acac)].

	HOMO-1	HOMO	LUMO	LUMO+1
Ni(II)	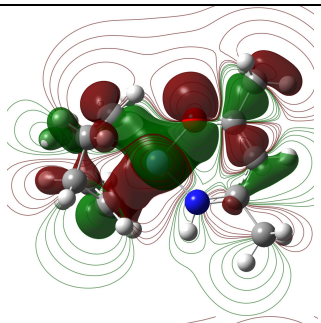	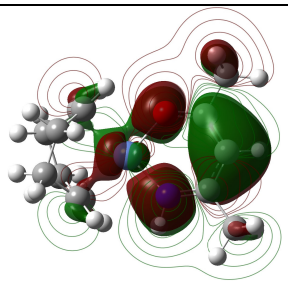	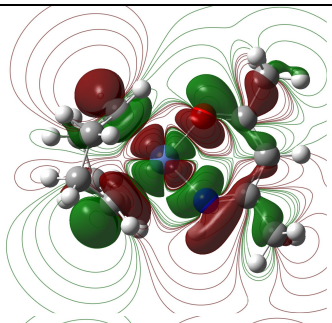	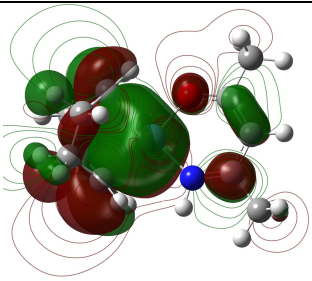
Pd(II)	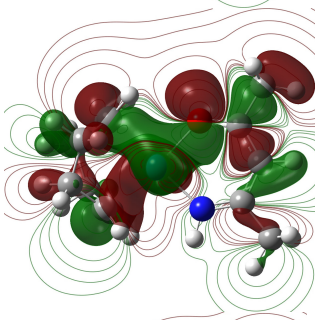	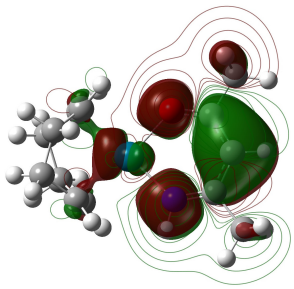	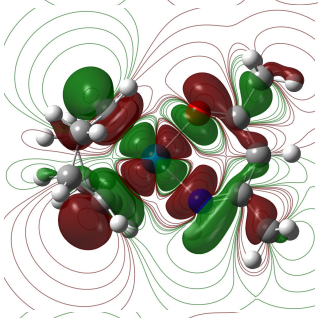	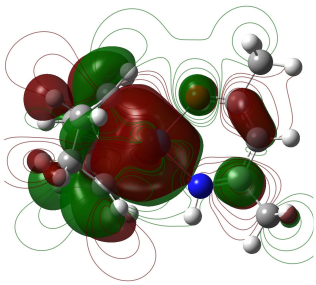
Pt(II)	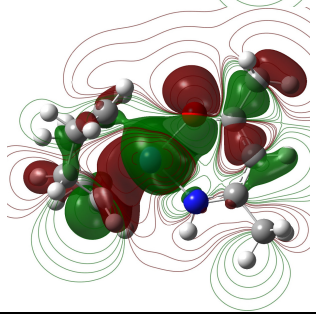	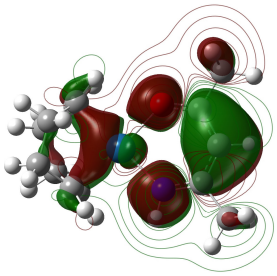	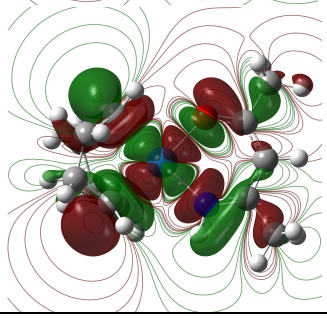	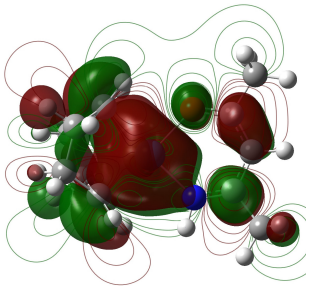

The complete molecular orbital table for group 10 metal 4-aminopent-3-en-2-onato (NH-acac) complexes are given in Table C.1.19. For the HOMO-1 molecular orbitals, the most interesting feature is the *p* orbitals seen on the carbon adjacent to the oxygen of the 4-aminopent-3-en-2-onato ligand. With in-phase overlap of the metal orbitals with the alkene *p* orbitals of the cyclo-octadiene. This is continued to a lesser extent in the HOMO molecular orbitals with the orbitals shifting to the NH-acac ligand where the π delocalization on the back-bone is clearly visible. In the LUMO molecular orbitals, a $d_{x^2-y^2}$ orbital is observed centered on the metals of the group. Lastly, in the LUMO+1 molecular orbitals, a d_{z^2} orbital was found for the metal centers.

Table C.1.20 Molecular Orbitals of calculated structures [M(cod)(NH-acac)].

	HOMO-1	HOMO	LUMO	LUMO+1
Cu(I)	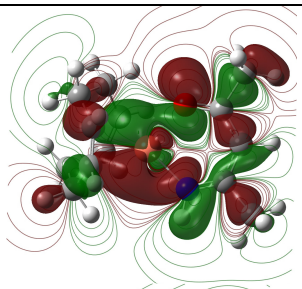	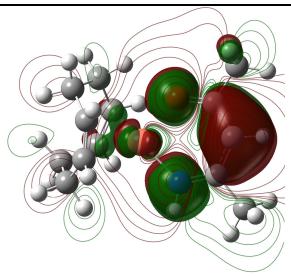	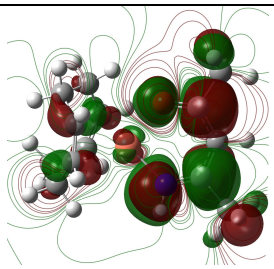	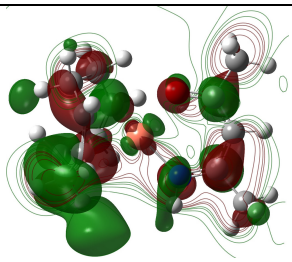
Ag(I)	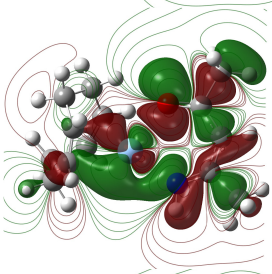	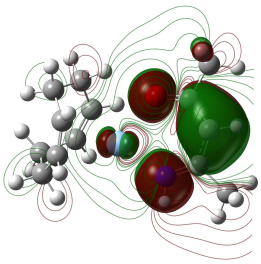	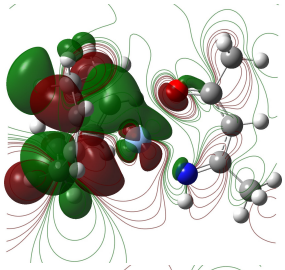	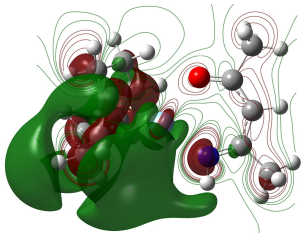
Au(I)	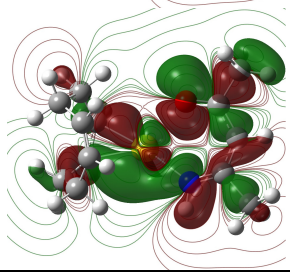	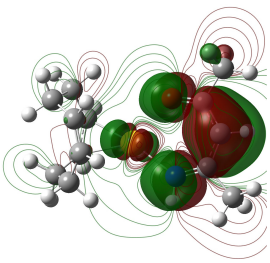	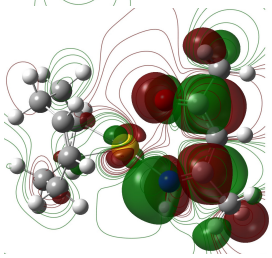	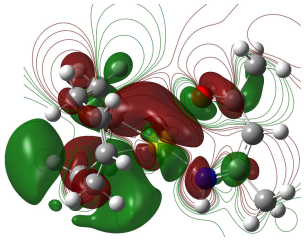

The complete molecular orbital table for group 11 metal 4-aminopent-3-en-2-onato (NH-acac) complexes are given in Table C.1.20. For the HOMO-1 molecular orbitals, as was found for the group 10 metals the *p* orbital of the carbon adjacent to the oxygens is clearly visible, in addition the delocalization around the metal centre is observed with a d_{xz} orbital centered on the metal. In the HOMO molecular orbitals the d_{yz} orbital is clearly seen with π delocalization seen on the NH-acac ligand. In the case of the LUMO molecular orbitals it was found that both the copper and gold have a d_{xy} orbital with the additional *p* orbitals centered on the NH-acac ligand whilst the silver has a d_{xz} orbital with most of the additional orbitals found on the cyclo-octadiene ring.

C.1.5 Group 7-11 Transition Metal 4-(Methylamino)pent-3-en-2-onato Complexes Molecular Orbitals

Table C.1.21 Molecular Orbitals of calculated structures [M(cod)(NMe-acac)].

	HOMO-1	HOMO	LUMO	LUMO+1
Mn(I)	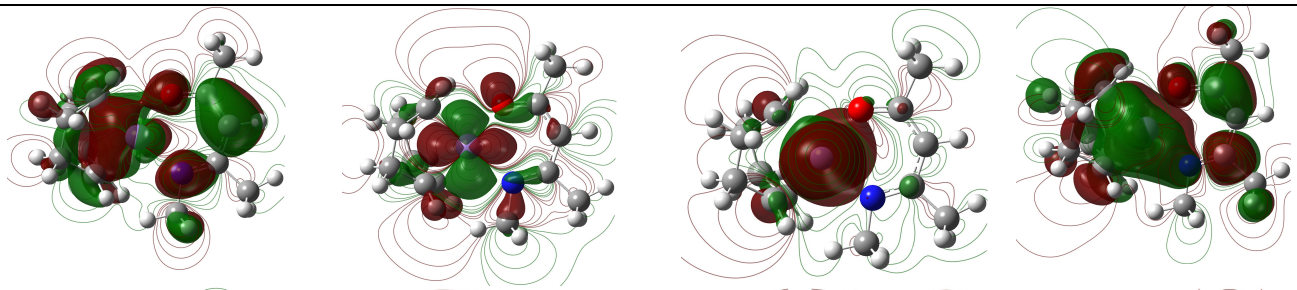			
Tc(I)	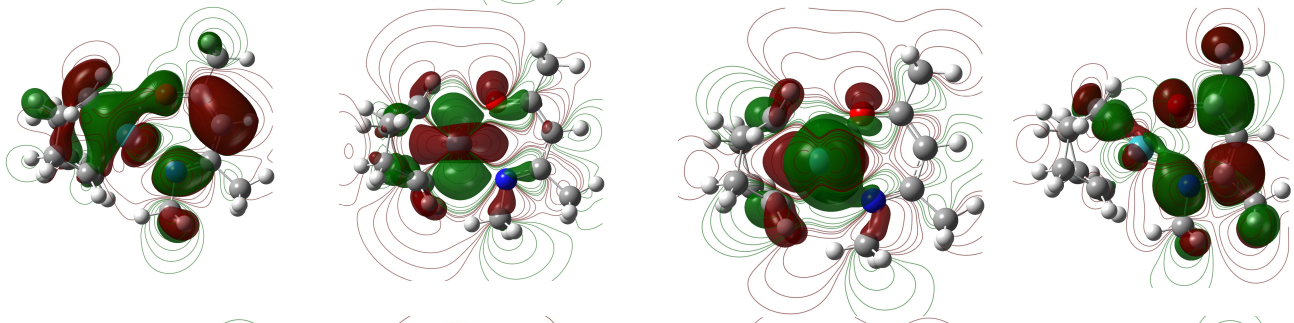			
Re(I)	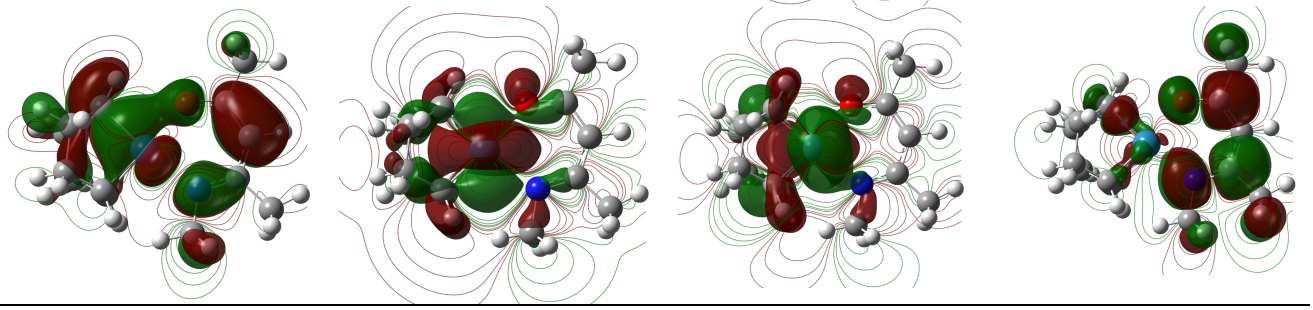			

The complete molecular orbital table for group 7 metal 4-(methylamino)pent-3-en-2-onato (NMe-acac) complexes is given in Table C.1.21. For the HOMO-1 molecular orbitals, the *trans* effect of the nitrogen of the NMe-acac ligand is clearly seen for both technetium and rhenium but to a lesser extent for the manganese complex. There is also π delocalization on the back-bone of the NMe-acac ligand. In the HOMO molecular orbitals, a $d_{x^2-y^2}$ orbital is observed for all the metals. It is of interest to note the bonding orbitals seen for the methyl group to the nitrogen of the NMe-acac are almost mirrored in the oxygen leg of the ligand. For the LUMO molecular orbitals a d_{z^2} orbital was found. Lastly, for the LUMO+1 molecular orbitals a d_{xy} orbital was observed for technetium and rhenium with the metal being eclipsed for the manganese. With *p* orbitals clearly visible on the NMe-acac ligand.

Table C.1.22 Molecular Orbitals of calculated structures [M(cod)(NMe -acac)].

	HOMO-1	HOMO	LUMO	LUMO+1
Fe(0)	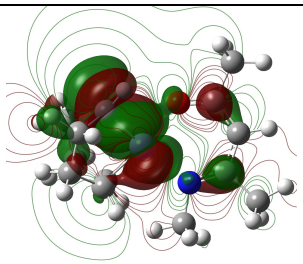	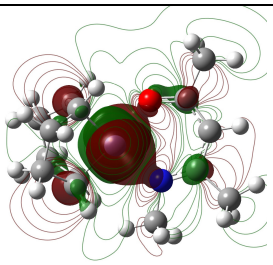	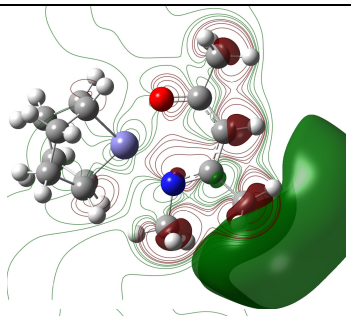	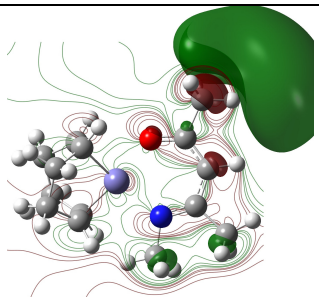
Ru(0)	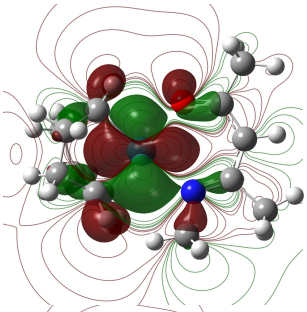	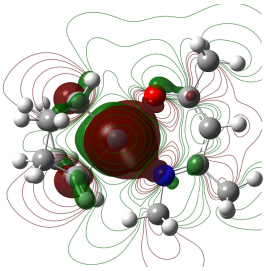	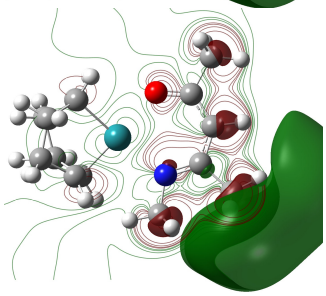	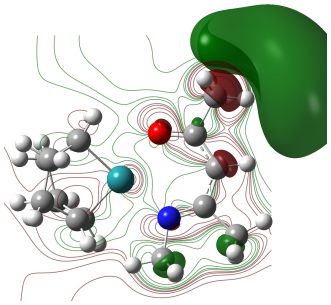
Os(0)	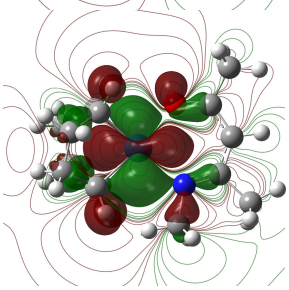	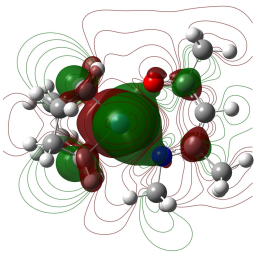	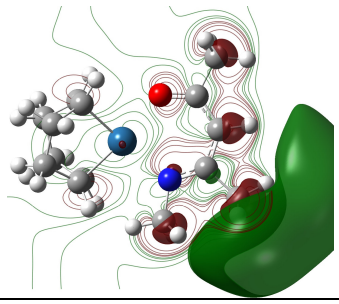	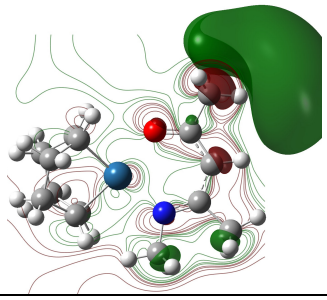

The complete molecular orbital table for group 8 metal 4-(methylamino)pent-3-en-2-onato (NMe-acac) complexes are given in Table C.1.22. For the HOMO-1 molecular orbitals, a $d_{x^2-y^2}$ orbital was observed for ruthenium and osmium. In the HOMO molecular orbitals, a d_{z^2} orbital is clearly seen for all the group metals.

Table C.1.23 Molecular Orbitals of calculated structures [M(cod)(NMe-acac)].

	HOMO-1	HOMO	LUMO	LUMO+1
Co(I)	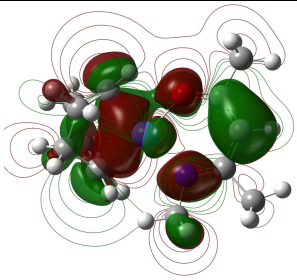	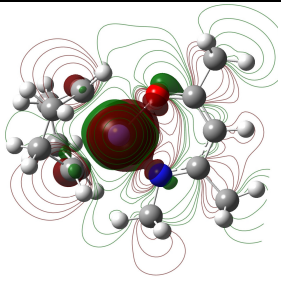	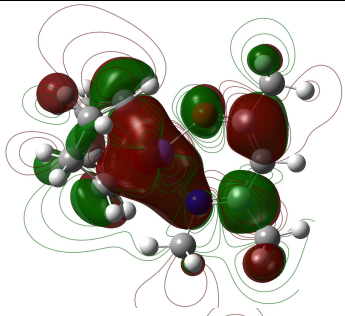	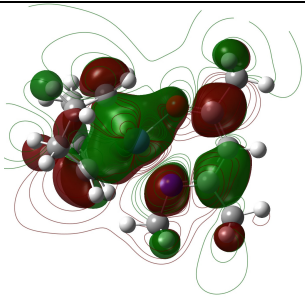
Rh(I)	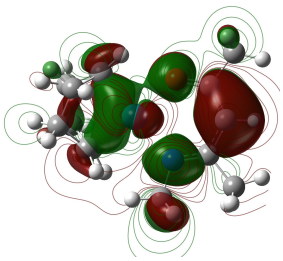	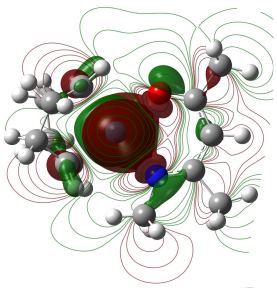	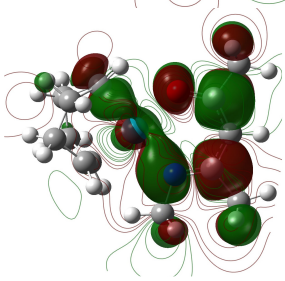	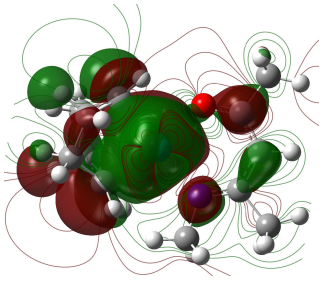
Ir(I)	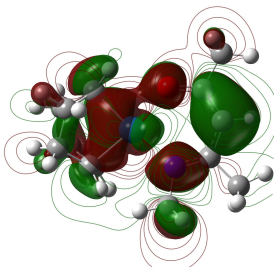	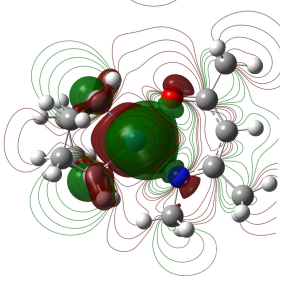	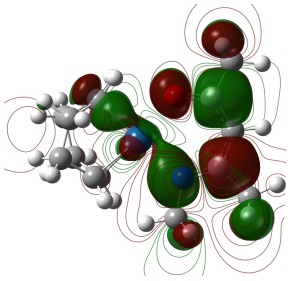	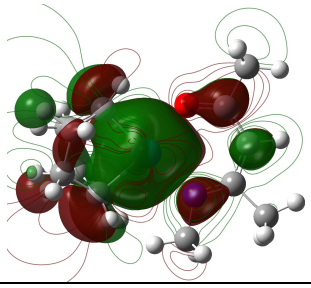

The complete molecular orbital table for group 9 metal 4-(methylamino)pent-3-en-2-onato (NMe-acac) complexes are given in Table C.1.23. For the HOMO-1 molecular orbitals, π delocalization is seen for both the cyclo-octadiene and the back-bone of the NMe-acac ligands while the metals centers display a d_{xy} orbital with the in-phase overlap of the *p* orbitals of the alkene carbons of the cyclo-octadiene. In the HOMO molecular orbitals, a d_{z^2} orbital was observed for all the metal centers. In the LUMO molecular orbitals, the *trans* influence is seen though the delocalization of the orbitals of the nitrogen of the NMe-acac, the metal centre and the alkene carbons of the cyclo-octadiene. While in the LUMO+1 molecular orbitals, a d_{z^2} orbital was found for all the group metals.

Table C.1.24 Molecular Orbitals of calculated structures [M(cod)(NMe-acac)].

	HOMO-1	HOMO	LUMO	LUMO+1
Ni(II)	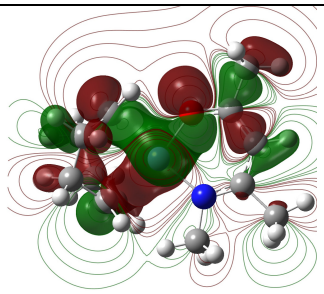	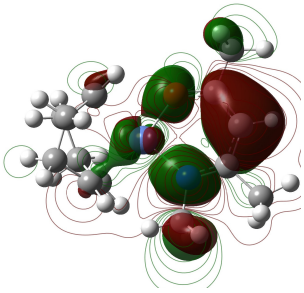	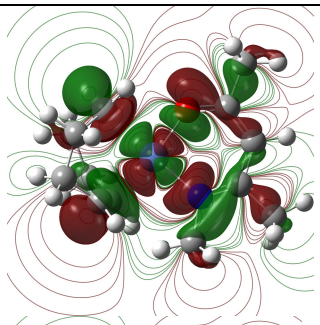	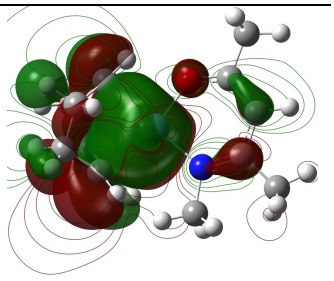
Pd(II)	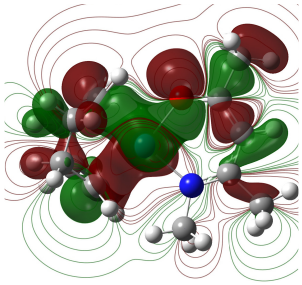	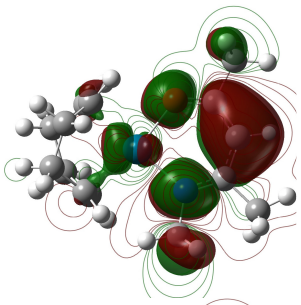	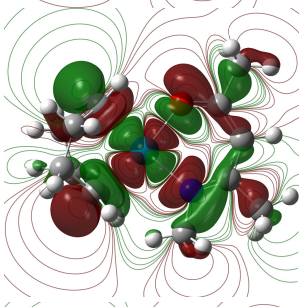	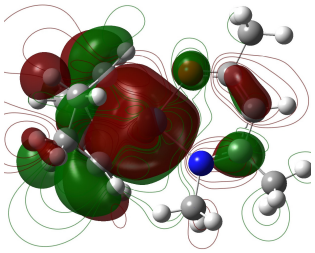
Pt(II)	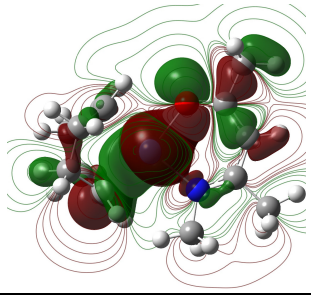	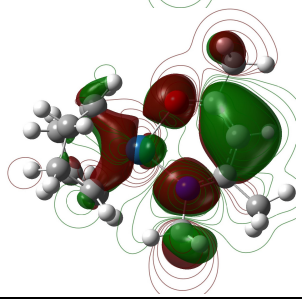	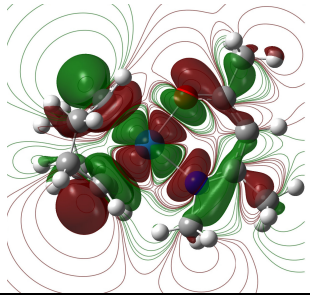	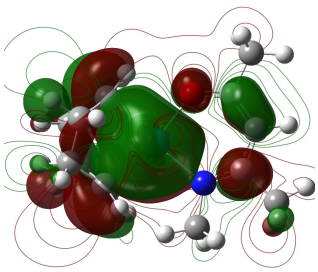

The complete molecular orbital table for group 10 metal 4-(methylamino)pent-3-en-2-onato (NMe-acac) complexes are given in Table C.1.24. For the HOMO-1 molecular orbitals, the most interesting feature is the *p* orbitals seen on the carbon adjacent to the oxygen of the NMe-acac ligand. With an in-phase overlap of the metal orbitals with the alkene *p* orbitals of the cyclo-octadiene. This is continued to a lesser extent in the HOMO molecular orbitals with the orbitals shifting to the NMe-acac ligand where the π delocalization on the back-bone is clearly visible. The metal centers have d_{yz} orbitals, while the *p* orbital of the methyl carbon of the NMe-acac ligand is seen. In the LUMO molecular orbitals, a $d_{x^2-y^2}$ orbital is observed centered on the metals of the group. Lastly, in the LUMO+1 molecular orbitals, a d_{z^2} orbital was found for the metal centers. Even with the additional methyl group for the NMe-acac ligand it was observed that the molecular orbitals for the NH-acac group 10 metals (see Table C.1.19) are nearly identical leading to the conclusion that the addition of the methyl group to the ligand does not play a significant role in the molecular orbitals.

Table C.1.25 Molecular Orbitals of calculated structures [M(cod)(NMe-acac)].

	HOMO-1	HOMO	LUMO	LUMO+1
Cu(I)	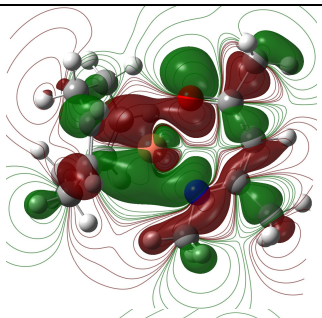	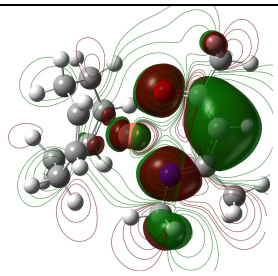	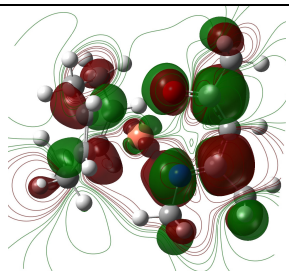	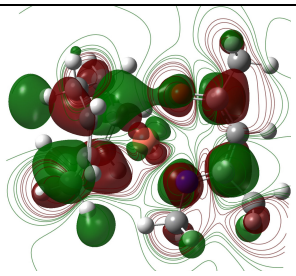
Ag(I)	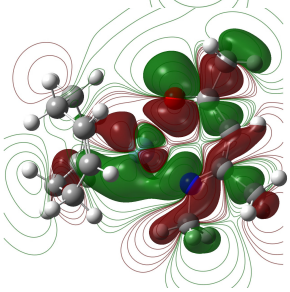	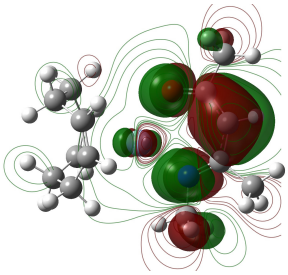	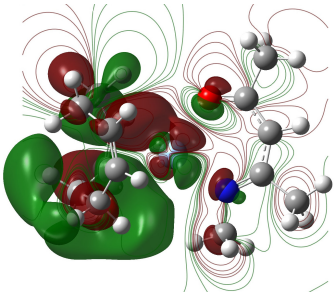	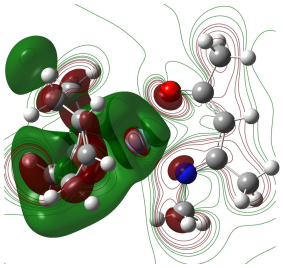
Au(I)	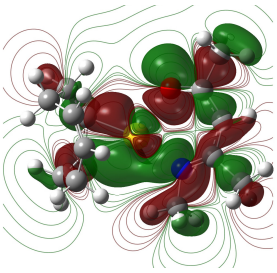	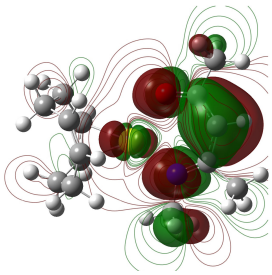	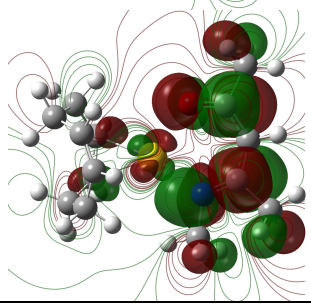	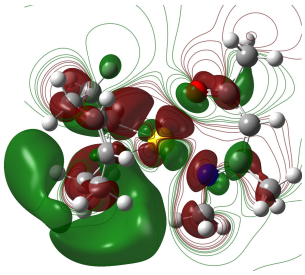

The complete molecular orbital table for group 11 metal 4-(methylamino)pent-3-en-2-onato (NMe-acac) complexes are given in Table C.1.25. For the HOMO-1 molecular orbitals, a d_{xz} orbital was observed for the group metals with the p orbital on the carbon adjacent to the oxygen of the NMe-acac ligand visible. This is the same pattern that was observed for the group 10 metals, the difference is that there is an additional orbital delocalization seen on the methyl, nitrogen and methine carbon of the NMe-acac ligand. In the HOMO molecular orbitals, the group metals have a d_{yz} orbital whilst the π delocalization on the back-bone of the NMe-acac is clearly seen. For the LUMO molecular orbitals, a d_{xz} orbitals was observed for the metals, whilst silver displayed additional orbitals on the cyclo-octadiene which were not present for the copper and gold complexes. Lastly, the LUMO+1 molecular orbitals have a d_{xz} orbital, however this orbital is unclear on the silver. In comparing these orbitals with those of the group 11 metal NH-acac complexes it was again found that the orbital patterns were similar.

C.1.6 Group 7-11 Transition Metal 4-Anilinopent-3-en-2-onato Complexes Molecular Orbitals

Table C.1.26 Molecular Orbitals of calculated structures [M(cod)(NPh-acac)].

	HOMO-1	HOMO	LUMO	LUMO+1
Mn(I)	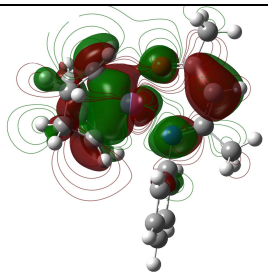	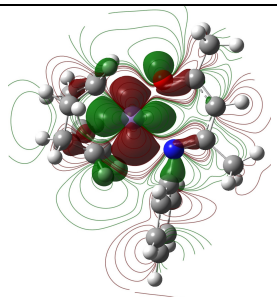	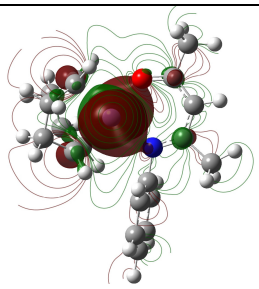	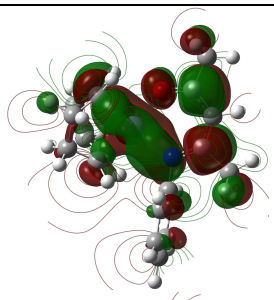
Tc(I)	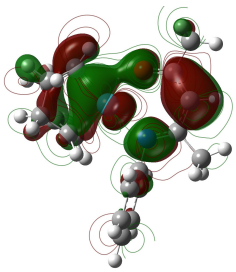	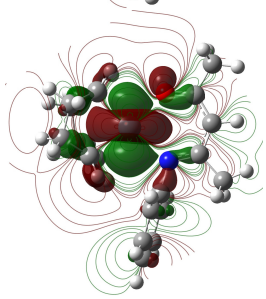	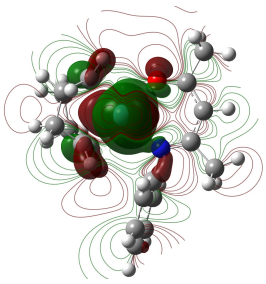	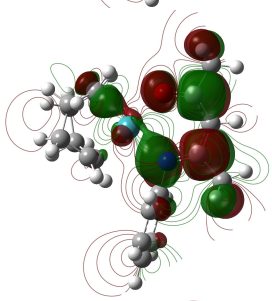
Re(I)	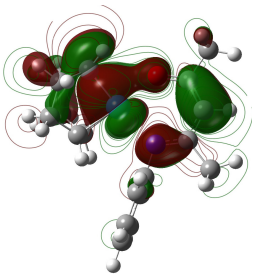	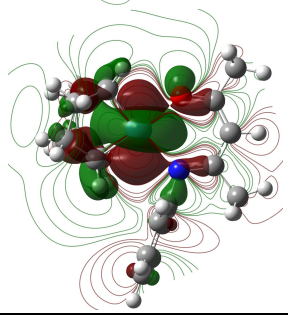	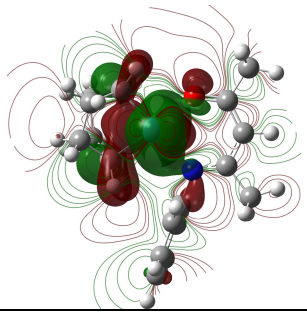	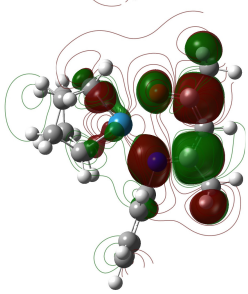

The complete molecular orbital table for group 7 metal 4-anilinopent-3-en-2-onato (NPh-acac) complexes is given in Table C.1.26. For the HOMO-1 molecular orbitals, the *trans* effect on the molecular orbitals of technetium and rhenium can be clearly seen and to a lesser extent in the manganese complex. The π delocalization on the back-bone of the NPh-acac ligand is seen for all the complexes. In the HOMO molecular orbitals a $d_{x^2-y^2}$ orbital was observed for the manganese complex, whilst a d_{z^2} orbital was found for both technetium and rhenium. It is interesting to note that the bonding orbitals for the nitrogen to both the phenyl ring and the back-bone carbons are nearly identical to those of the oxygen. This pattern is repeated from the NH-acac to the NMe-acac complexes. In the LUMO molecular orbitals, a d_{z^2} orbital

was observed for the group metals. Lastly, for the LUMO+1 molecular orbitals the *p* orbitals on the NPh-acac ligand are clearly visible. In the comparison of the molecular orbitals found for the NPh-acac group 7 metals with the orbitals of the NH-acac and the NMe-acac we observe a similar orbital pattern.

Table C.1.27 Molecular Orbitals of calculated structures [M(cod)(NPh-acac)].

	HOMO-1	HOMO	LUMO	LUMO+1
Fe(0)	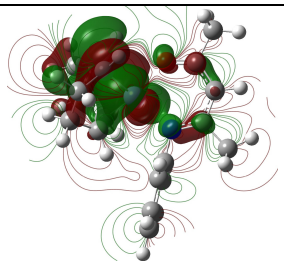	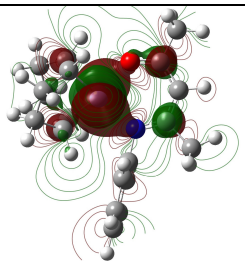	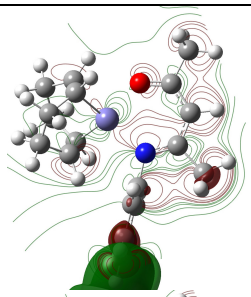	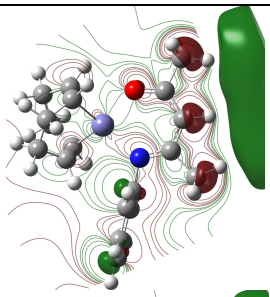
Ru(0)	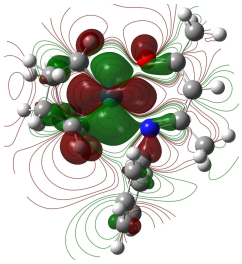	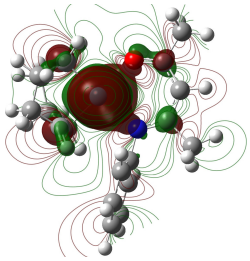	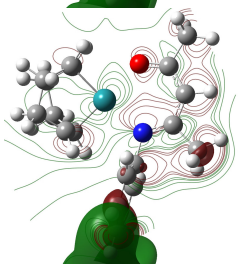	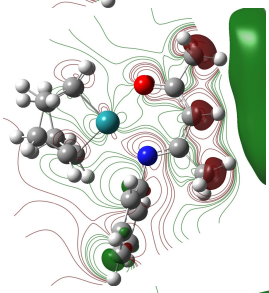
Os(0)	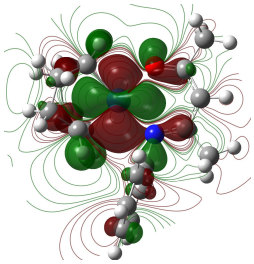	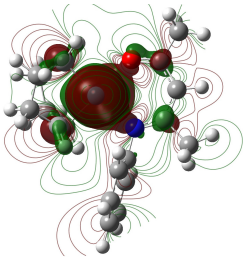	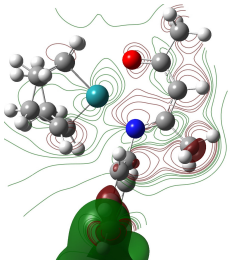	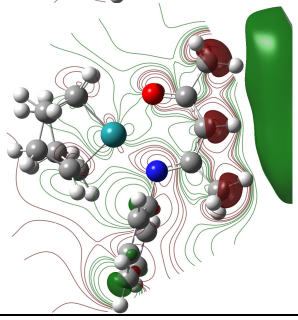

The complete molecular orbital table for group 8 metal 4-anilinopent-3-en-2-onato (NPh-acac) complexes are given in Table C.1.27. For the HOMO-1 molecular orbitals, a d_{z^2} orbital was observed for ruthenium and osmium. In the HOMO molecular orbitals, the d_{z^2} orbital was clearly seen for all the group metals. In comparison with both the NH-acac and the NMe-acac group 8 metal complexes we find a similar orbital pattern for the HOMO-1 and HOMO molecular orbitals.

Table C.1.28 Molecular Orbitals of calculated structures [M(cod)(NPh-acac)].

	HOMO-1	HOMO	LUMO	LUMO+1
Co(I)	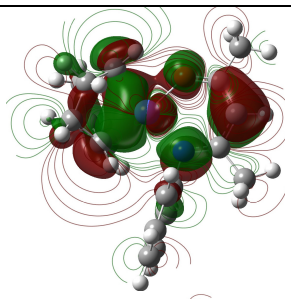	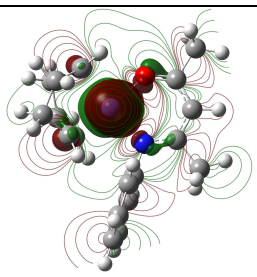	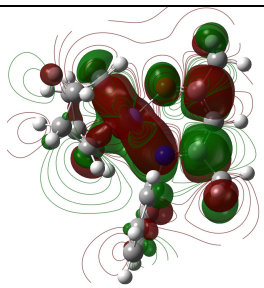	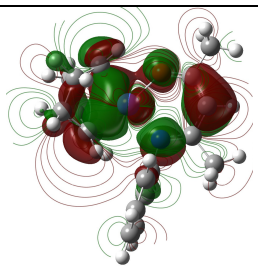
Rh(I)	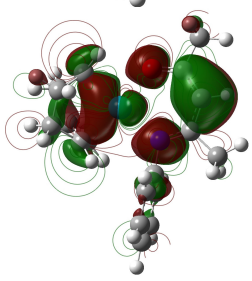	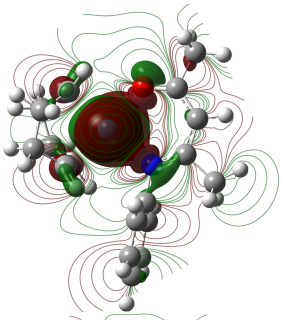	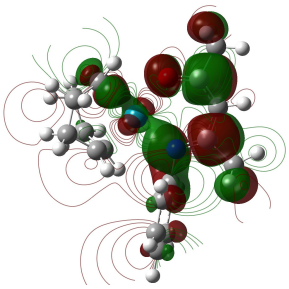	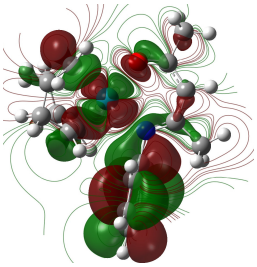
Ir(I)	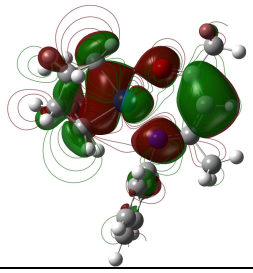	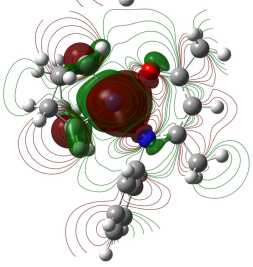	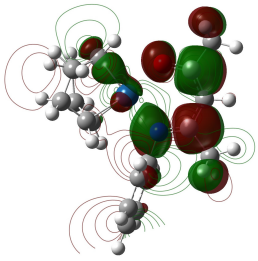	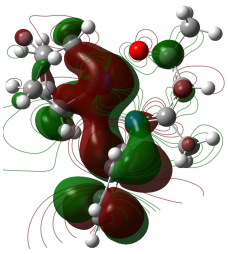

The complete molecular orbital table for group 9 metal 4-anilinopent-3-en-2-onato (NPh-acac) complexes are given in Table C.1.28. For the HOMO-1 molecular orbitals, a d_{yz} orbital is centered on the metals with an in-phase overlap of the *p* orbitals of the alkene carbons of the cyclo-octadiene. Additionally the π delocalization can be seen on the back-bone of the NPh-acac ligand. In the HOMO molecular orbitals, a d_{z^2} orbital was found for the group 9 metals. For the LUMO molecular orbitals, the *trans* effect is seen with the delocalization of the orbitals from the phenyl ring, through the nitrogen and the metal as well as the alkene carbons of the cyclo-octadiene ring. Lastly, the LUMO+1 molecular orbitals, for rhodium and iridium the π delocalization on the phenyl ring of the NPh-acac is clearly visible this is not the case for the cobalt complex. For the rhodium a $d_{x^2-y^2}$ orbital is observed, whilst cobalt has more π delocalization on the back-bone of the NPh-acac. Taking into account that the NH-acac and NMe-acac complexes do not have the additional phenyl ring it is interesting to note that the orbital patterns are again similar.

Table C.1.29 Molecular Orbitals of calculated structures [M(cod)(NPh-acac)].

	HOMO-1	HOMO	LUMO	LUMO+1
Ni(II)	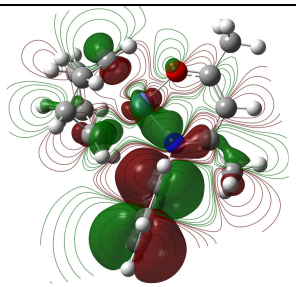	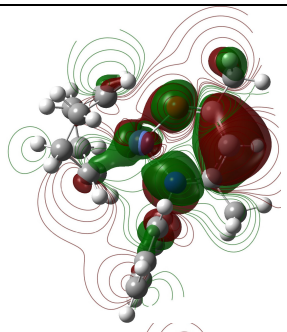	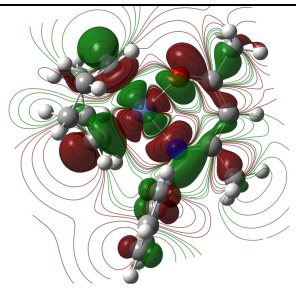	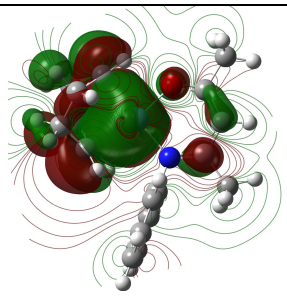
Pd(II)	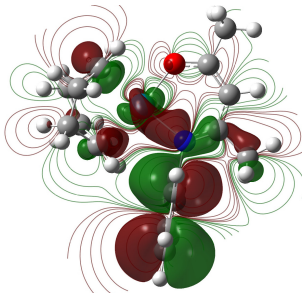	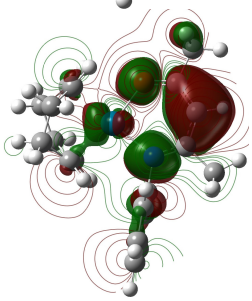	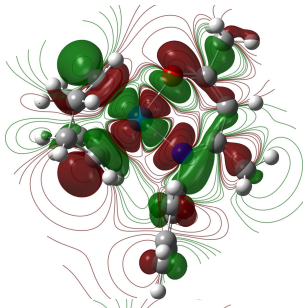	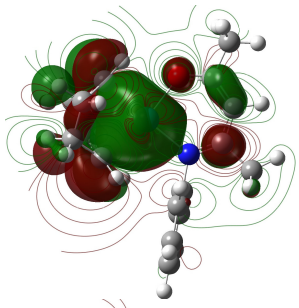
Pt(II)	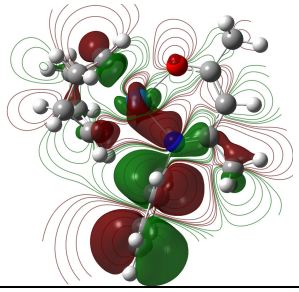	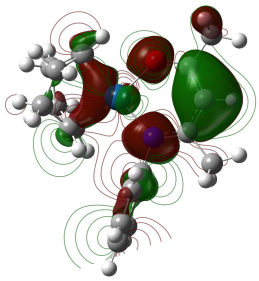	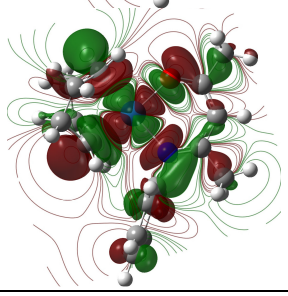	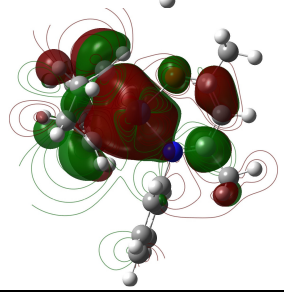

The complete molecular orbital table for group 10 metal 4-anilinopent-3-en-2-onato (NPh-acac) complexes are given in Table C.1.29. For the HOMO-1 molecular orbitals, the π orbital delocalization on the phenyl ring is most prominent. The interesting pattern observed in the carbon of the back-bone of the NH-acac and NMe-acac is not found in the NPh-acac complexes. In the HOMO molecular orbitals, the π orbital delocalization of the back-bone of the NPh-acac ligand is clearly visible. For the LUMO molecular orbitals, a clear $d_{x^2-y^2}$ orbital was found for all the group metals, with the *p* orbitals on the carbons of the phenyl ring also seen. Lastly, in the LUMO+1 molecular orbitals a d_{z^2} orbital was found for the group metals. The comparison of the HOMO, LUMO and LUMO+1 molecular orbitals with those of the NH-acac and NMe-acac group 10 metal complexes find a marked similarity.

Table C.1.30 Molecular Orbitals of calculated structures [M(cod)(NPh-acac)].

	HOMO-1	HOMO	LUMO	LUMO+1
Cu(I)	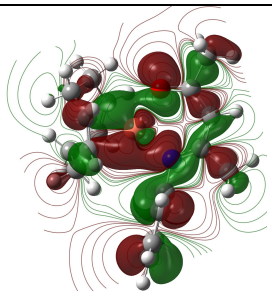	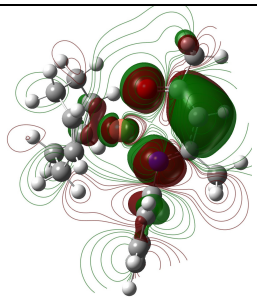	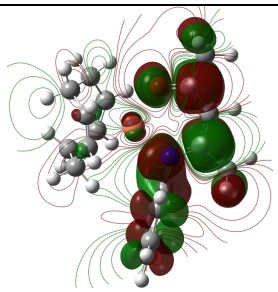	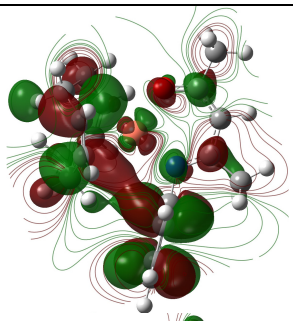
Ag(I)	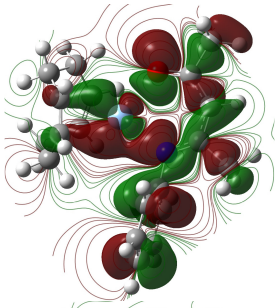	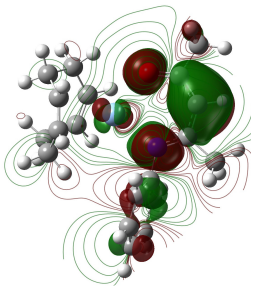	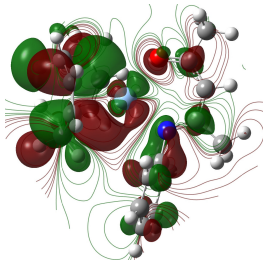	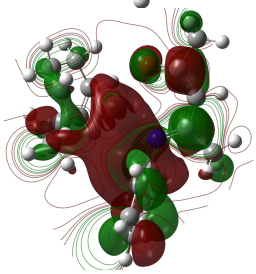
Au(I)	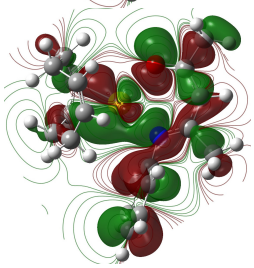	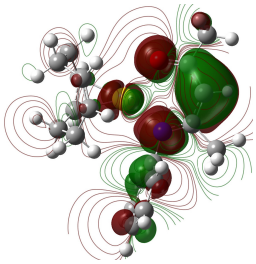	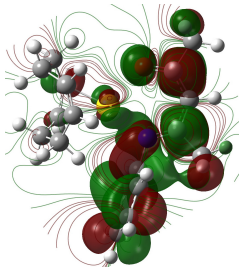	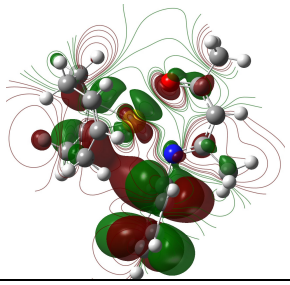

The complete molecular orbital table for group 11 metal 4-anilinopent-3-en-2-onato (NPh-acac) complexes are given in Table C.1.30. For the HOMO-1 molecular orbitals, there is a d_{xz} orbital centered on the group metals whilst the *p* orbital of the carbon adjacent to the oxygen is again dominant. The *p* orbitals are also clearly seen for the phenyl ring of the NPh-acac ligand. The delocalization of the orbitals between the phenyl, nitrogen and back-bone of the NPh-acac ligand are also visible. The other delocalization which is seen is the surrounding of the metal centers. In the HOMO molecular orbitals, the π delocalization of the back-bone of the NPh-acac ligand is seen whilst minor d_{yz} orbitals were found on the metals. For the LUMO molecular orbitals, again minor d_{xy} orbitals were seen for the metal centers whilst *p* orbitals were observed for both the phenyl ring and the back-bone of the NPh-acac ligand. Lastly the LUMO+1 orbitals, with d_{xz} orbitals found for the metal centers and π delocalization for the phenyl ring was present, the majority of the orbitals were found on the cyclo-octadiene ring.

C.1.7 Group 7-11 Transition Metal Tropolonato Complexes Molecular Orbitals

Table C.1.31 Molecular Orbitals of calculated structures [M(cod)(trop)].

	HOMO-1	HOMO	LUMO	LUMO+1
Mn(I)	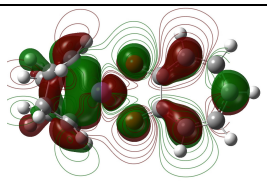	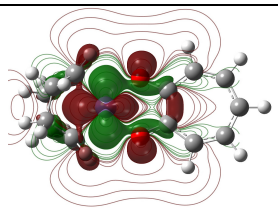	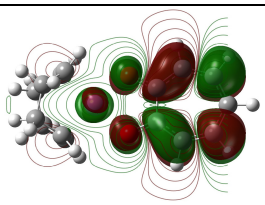	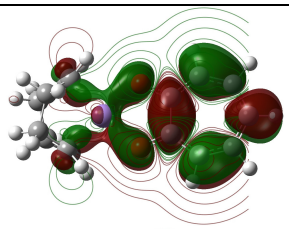
Tc(I)	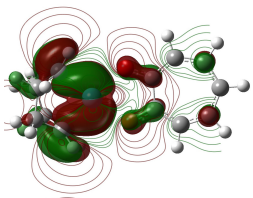	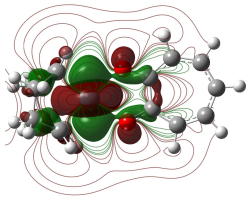	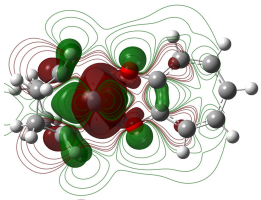	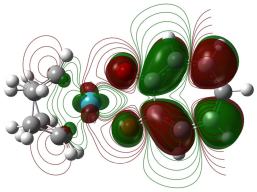
Re(I)	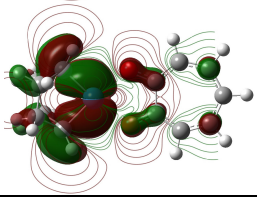	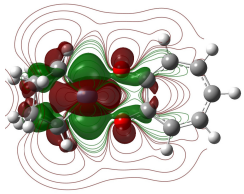	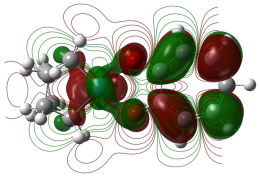	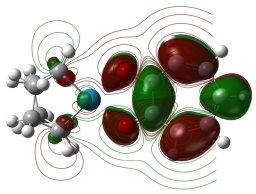

The complete molecular orbital table for group 7 metal tropolonato complexes is given in Table C.1.31. For the HOMO-1 molecular orbitals, for manganese *p* orbitals are observed for the tropolonato (trop) ligand while there is an in-phase overlap of the metal orbitals with the π orbital of the alkene carbons of the cyclo-octadiene. In the HOMO molecular orbitals, a d_{z^2} orbital was found centered on the metals. For the LUMO molecular orbitals, the manganese and rhenium metal complexes display *p* orbitals on the trop ligand, whilst technetium has a d_{z^2} orbital centered on it. Lastly, the LUMO+1 molecular orbitals, again show the π-orbital delocalization of the tropolone ring.

Table C.1.32 Molecular Orbitals of calculated structures [M(cod)(trop)].

	HOMO-1	HOMO	LUMO	LUMO+1
Fe(0)	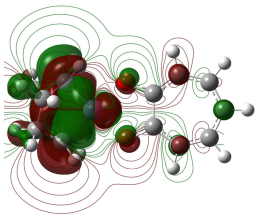	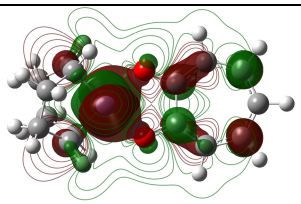	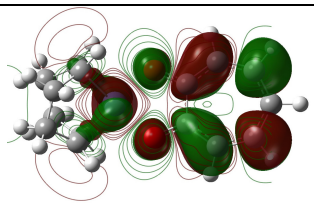	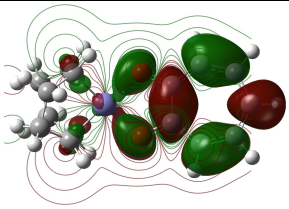
Ru(0)	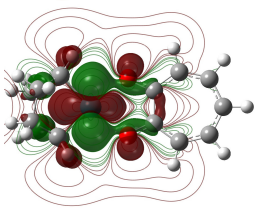	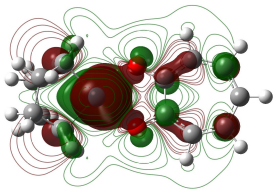	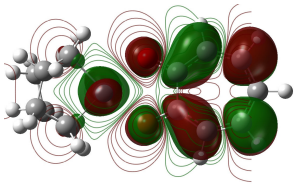	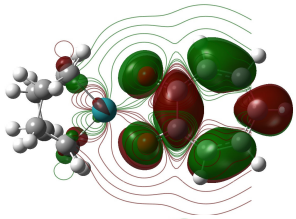
Os(0)	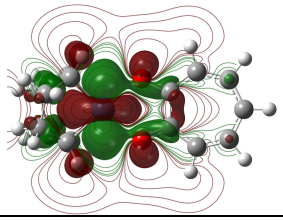	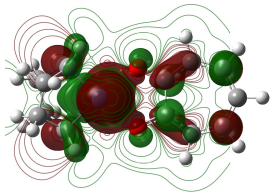	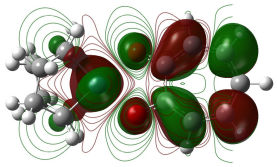	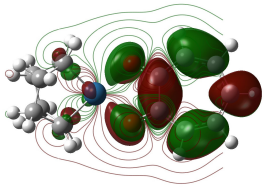

The complete molecular orbital table for group 8 metal tropolonato (trop) complexes are given in Table C.1.32. For the HOMO-1 molecular orbitals, a d_{z^2} orbital was observed for the group metals. In the HOMO molecular orbitals, the d_{z^2} orbital is still seen for the group metals whilst there is some minor *p* orbitals visible for the carbons of the tropolone ring. For the LUMO molecular orbitals, the *p* orbitals of the tropolone dominate, this is continued into to the LUMO+1 molecular orbitals.

Table C.1.33 Molecular Orbitals of calculated structures [M(cod)(trop)].

	HOMO-1	HOMO	LUMO	LUMO+1
Co(I)	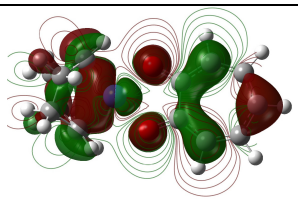	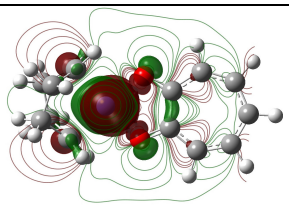	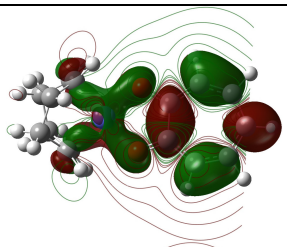	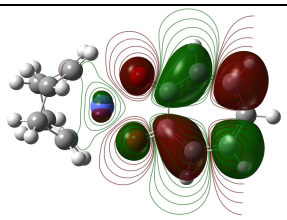
Rh(I)	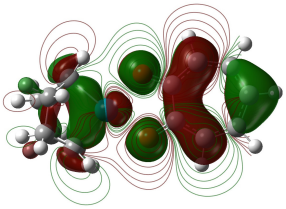	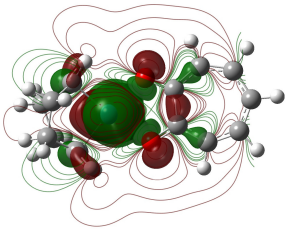	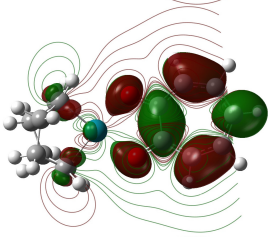	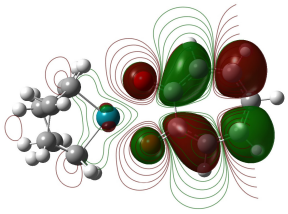
Ir(I)	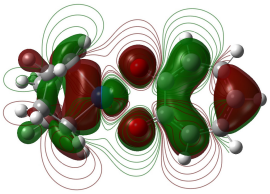	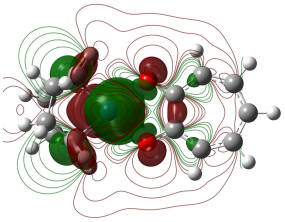	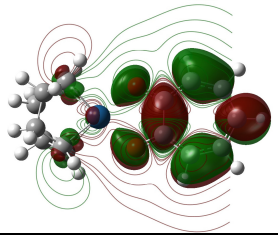	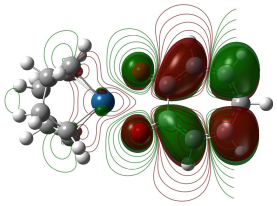

The complete molecular orbital table for group 9 metal tropolonato (trop) complexes are given in Table C.1.33. For the HOMO-1 molecular orbitals the π orbital delocalization on the tropolone ring is clearly visible, while there is in-phase overlap of the metal orbitals with the π-orbitals of the alkene carbons of the cyclo-octadiene ligand. In the HOMO molecular orbitals, a d_{z^2} orbital was found for the group metals. For the LUMO and LUMO+1 molecular orbitals the *p* orbitals of the trop ligand dominate.

Table C.1.34 Molecular Orbitals of calculated structures [M(cod)(trop)].

	HOMO-1	HOMO	LUMO	LUMO+1
Ni(II)	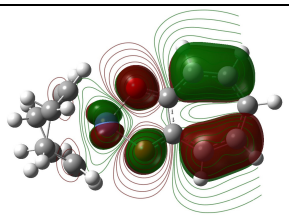	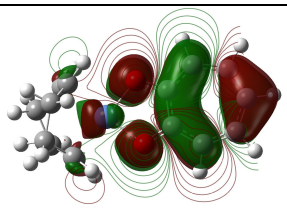	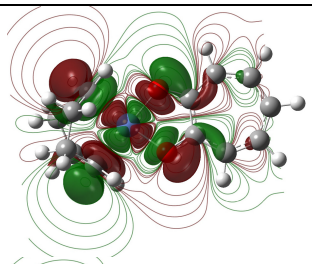	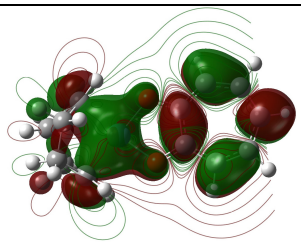
Pd(II)	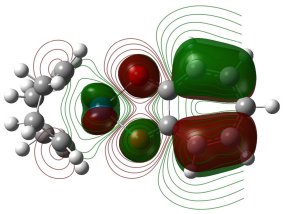	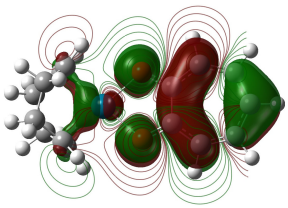	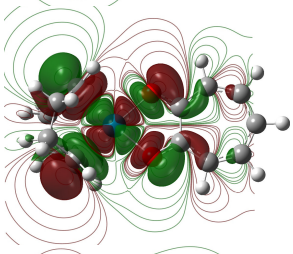	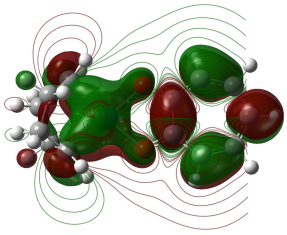
Pt(II)	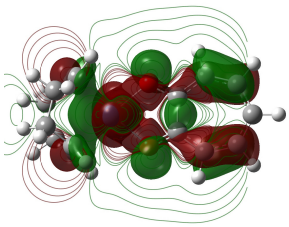	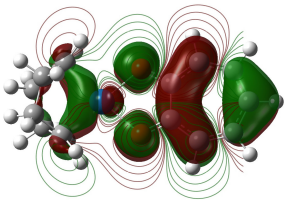	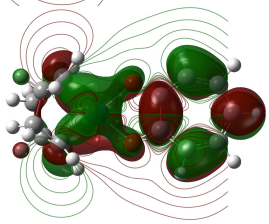	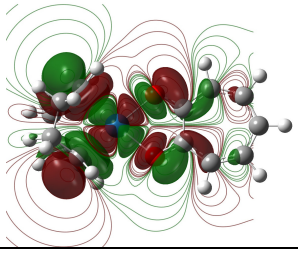

The complete molecular orbital table for group 10 metal tropolonato (trop) complexes are given in Table C.1.34. For the HOMO-1 molecular orbitals, π orbital delocalization is seen in the tropolone ring, whilst platinum has additional orbitals seen for the overlap of the metal with the alkene π-bond. This π orbital delocalization is continued into the HOMO molecular orbitals with minor overlap for the metal and the alkene of the cyclo-octadiene being visible for palladium and platinum. In the LUMO molecular orbitals, both nickel and palladium have a $d_{x^2-y^2}$ orbital, whilst platinum has delocalization around the metal. This pattern found for the platinum is seen in the LUMO+1 molecular orbitals of nickel and palladium whilst platinum here has the $d_{x^2-y^2}$ orbital reminiscent of the LUMO molecular orbitals of nickel and palladium.

Table C.1.35 Molecular Orbitals of calculated structures [M(cod)(trop)].

	HOMO-1	HOMO	LUMO	LUMO+1
Cu(I)	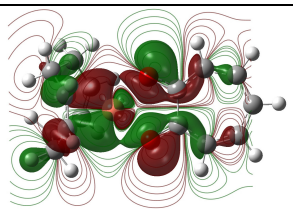	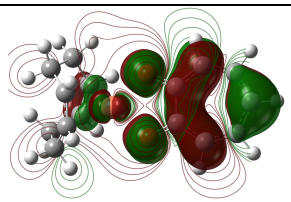	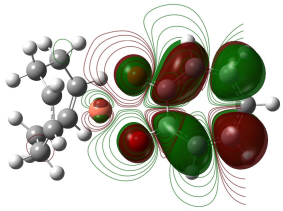	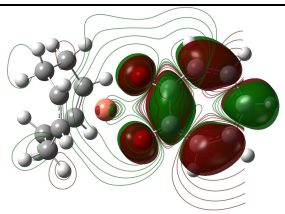
Ag(I)	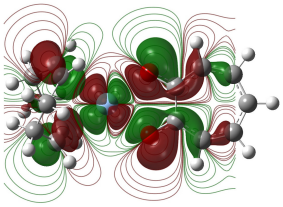	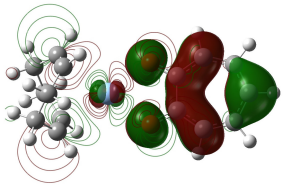	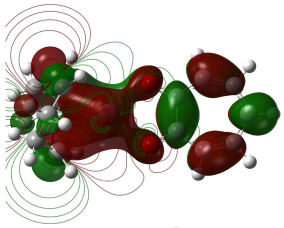	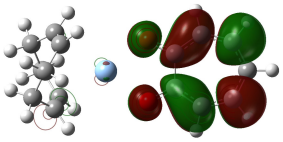
Au(I)	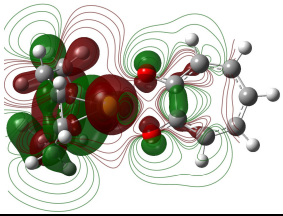	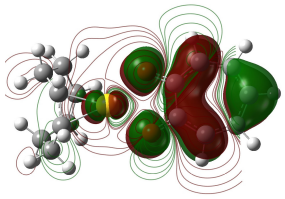	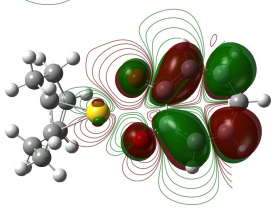	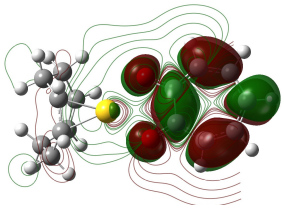

The complete molecular orbital table for group 11 metal tropolonato (trop) complexes are given in Table C.1.35. For the HOMO-1 molecular orbitals, copper is seen to have a d_{xz} orbital whilst there is delocalization surround the metal center from both the cyclo-octadiene ring and the tropolonato ligand. The HOMO molecular orbitals are dominated by the π orbital delocalization on the tropolone ring. This is carried through to the LUMO molecular orbitals where silver is the only complex demonstrating additional molecular orbitals on the metal centre. Again the LUMO+1 molecular orbitals are dominated by the *p* orbitals of the troplonato ligand.

C.1.8 Group 7-11 Transition Metal Tribromotropolonato Complexes Molecular Orbitals

Table C.1.36 Molecular Orbitals of calculated structures [M(cod)(3Br-trop)].

	HOMO-1	HOMO	LUMO	LUMO+1
Mn(I)	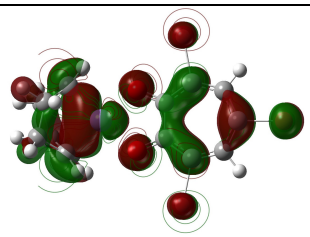	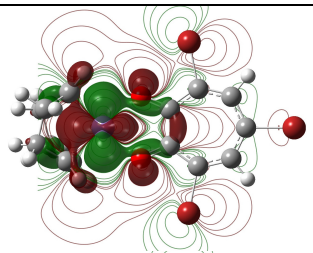	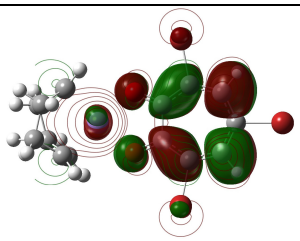	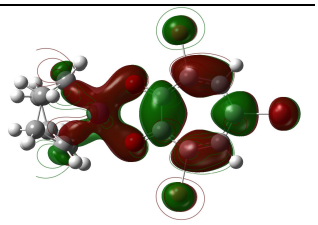
Tc(I)	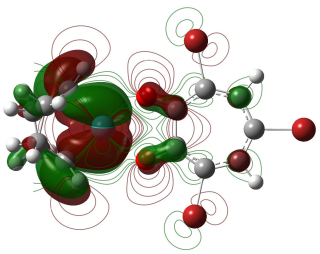	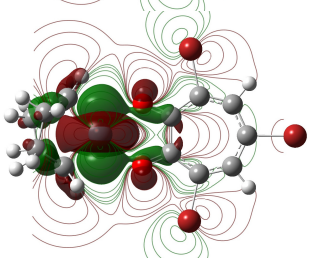	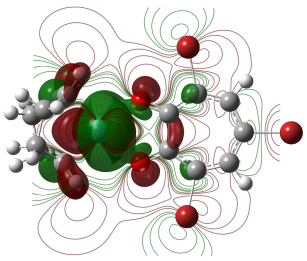	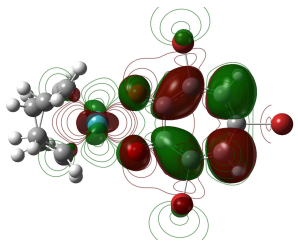
Re(I)	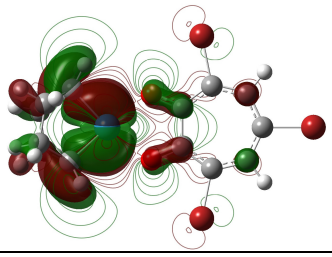	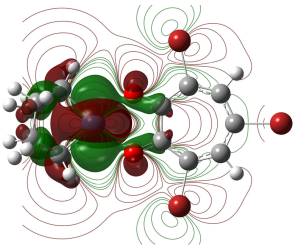	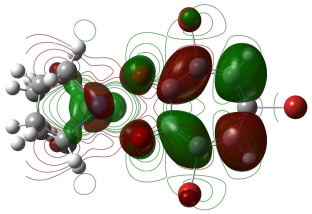	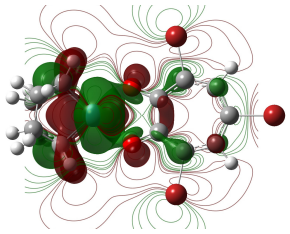

The complete molecular orbital table for group 7 metal tribromotropolonato complexes is given in Table C.1.36. For the HOMO-1 molecular orbitals, π orbital delocalization is seen on the tropolone ring for the manganese complex while the *p* orbitals are found for the bromines on the 3Br-trop ligand. The in-phase overlap of the metal orbitals with those of the alkene of the cyclo-octadiene are seen for all complexes of the group. In the HOMO molecular orbitals, a d_{z^2} orbital was observed centered on the group metals. In the LUMO molecular orbitals manganese and rhenium display a similar orbital pattern with the *p* orbitals of the tropolone ring dominating. The technetium metal displays a d_{z^2} orbital with minor orbitals on the cyclo-octadiene. In the LUMO+1 molecular orbitals, the *p* orbitals of the tropolone ring again dominate for manganese and technetium, while rhenium has a d_{z^2} centered on it with the additional orbitals found on the cyclo-octadiene.

Table C.1.37 Molecular Orbitals of calculated structures [M(cod)(3Br-trop)].

	HOMO-1	HOMO	LUMO	LUMO+1
Fe(0)	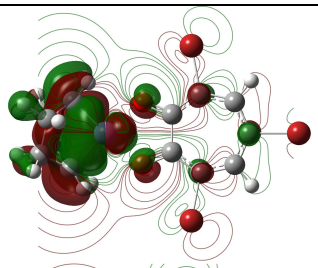	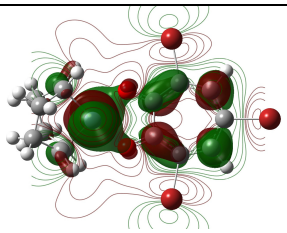	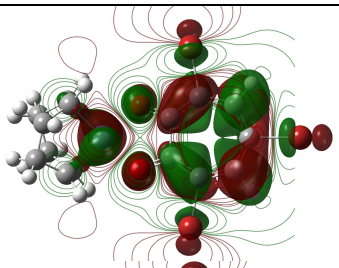	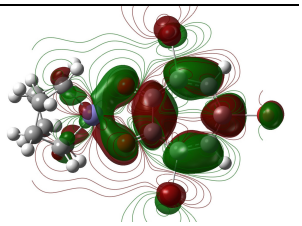
Ru(0)	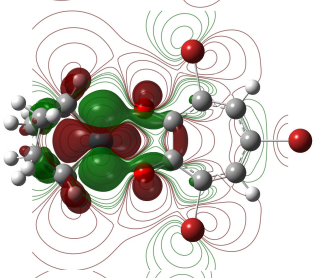	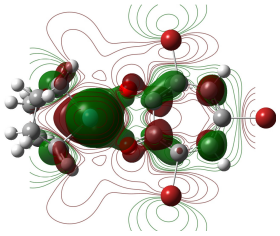	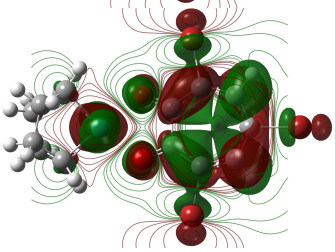	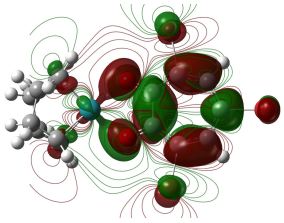
Os(0)	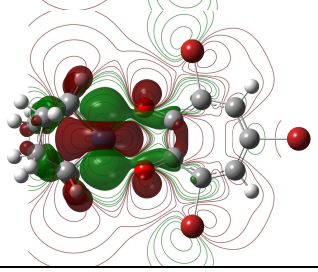	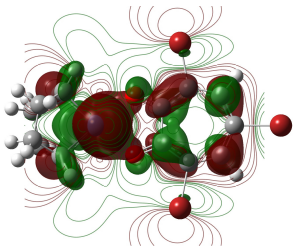	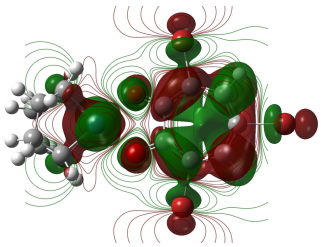	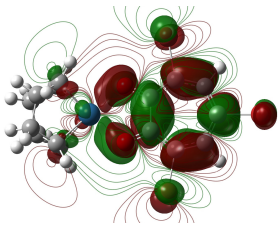

The complete molecular orbital table for group 8 tribromotropolonato (3Br-trop) complexes are given in Table C.1.37. For the HOMO-1 molecular orbitals, iron displays an in-phase overlap of the metal with the π orbital of the alkene of the cyclo-octadiene. Whist ruthenium and osmium have d_{z^2} orbitals. In the HOMO molecular orbitals, the d_{z^2} orbitals for the group metal is clearly seen, with delocalization on the tropolone ring. This delocalization become prominent in the LUMO molecular orbitals where the *p* orbitals of the bromines of the ring are also observed. This delocalization pattern is similar for an aromatic system, showing clearly tropolones aromatic nature. The *p* orbitals of the tropolone ring continue into the LUMO+1 molecular orbitals where the in-phase overlap of the metal orbitals with the oxygens of the 3Br-trop ligand are seen.

Table C.1.38 Molecular Orbitals of calculated structures [M(cod)(3Br-trop)].

	HOMO-1	HOMO	LUMO	LUMO+1
Co(I)	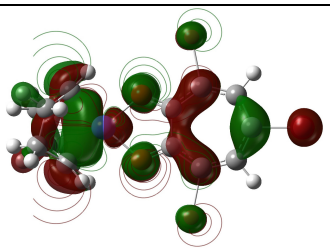	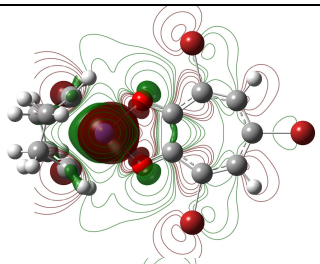	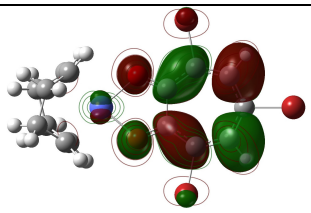	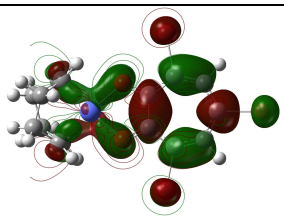
Rh(I)	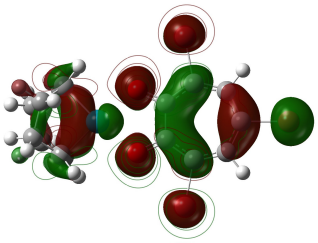	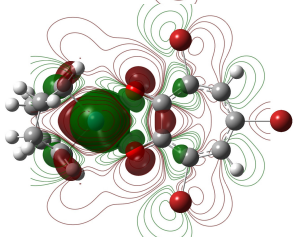	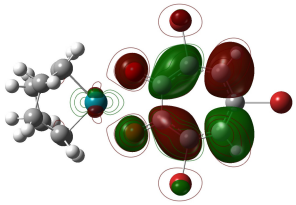	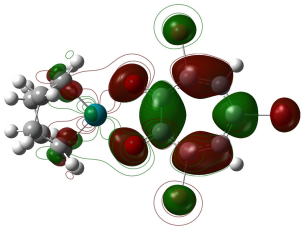
Ir(I)	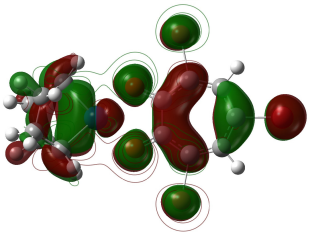	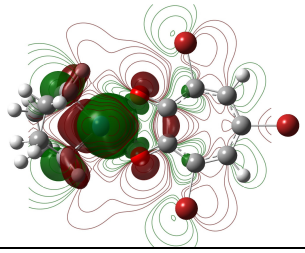	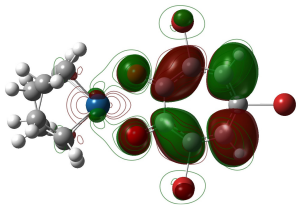	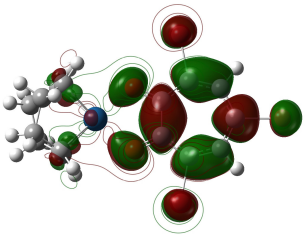

The complete molecular orbital table for group 9 metal tribromotropolonato (3Br-trop) complexes are given in Table C.1.38. For the HOMO-1 molecular orbitals the delocalization of the tropolone ring is clearly seen with the in-phase overlap of the group metals with the π orbital of the alkenes of the cyclo-octadiene. Lastly, the *p* orbitals of the bromines of the 3Br-trop ligand are also observed. In the HOMO molecular orbitals, a d_{z^2} orbital focused on the group metals is observed. In the LUMO molecular orbitals the *p* orbitals of the 3Br-trop ligand dominate this is carried into the LUMO+1 molecular orbitals.

Table C.1.39 Molecular Orbitals of calculated structures [M(cod)(3Br-trop)].

	HOMO-1	HOMO	LUMO	LUMO+1
Ni(II)	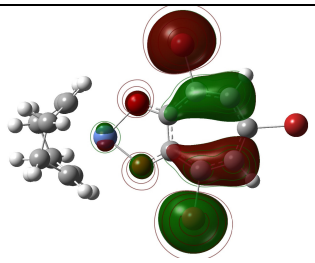	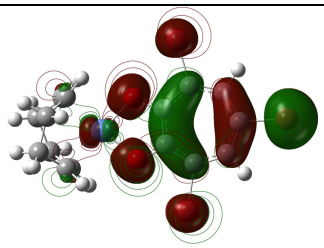	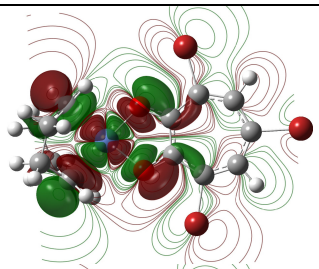	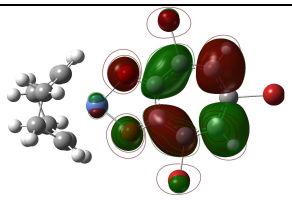
Pd(II)	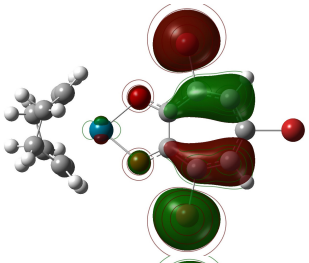	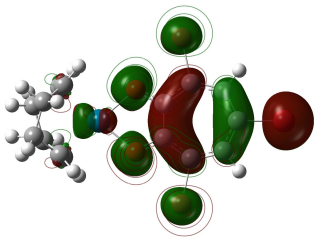	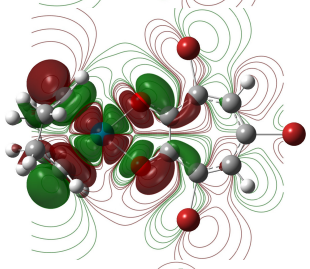	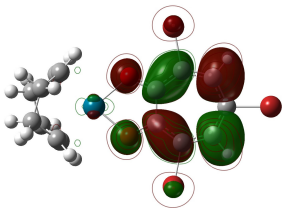
Pt(II)	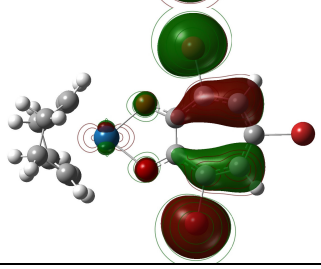	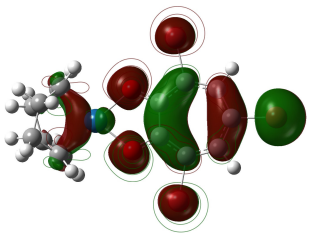	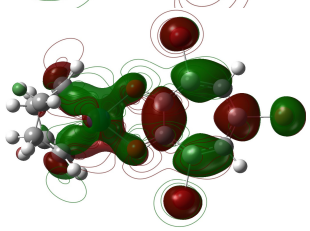	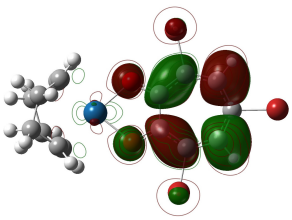

The complete molecular orbital table for group 10 metal tribromotropolonato (3Br-trop) complexes are given in Table C.1.39. The HOMO-1 and HOMO molecular orbitals are dominated by the π orbital delocalization on the tropolone ring as well as the *p* orbitals of the bromines on the 3Br-trop ligand. For the LUMO molecular orbitals, a $d_{x^2-y^2}$ orbital is observed for nickel and palladium while platinum has delocalization between the alkenes of the cyclo-octadiene and the oxygen atoms of the 3Br-trop ligands. The LUMO+1 molecular orbitals are again dominated by the *p* orbitals seen on the tropolone ring.

Table C.1.40 Molecular Orbitals of calculated structures [M(cod)(3Br-trop)].

	HOMO-1	HOMO	LUMO	LUMO+1
Cu(I)	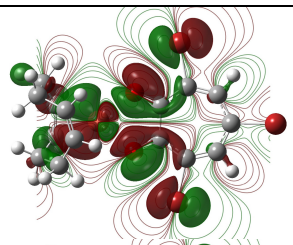	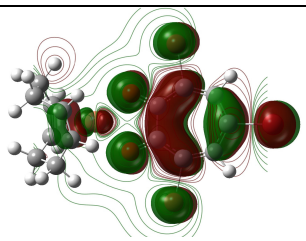	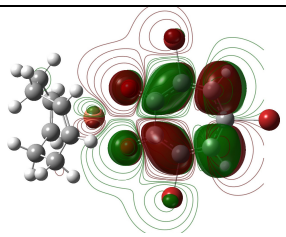	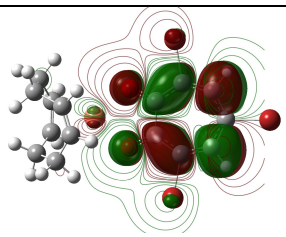
Ag(I)	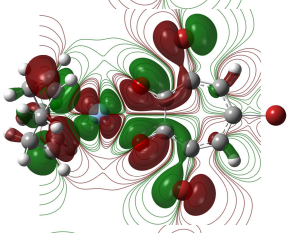	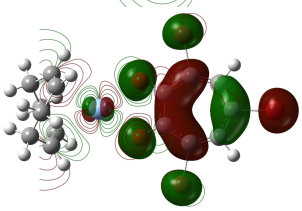	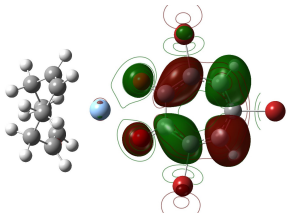	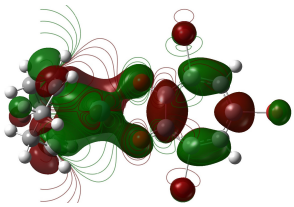
Au(I)	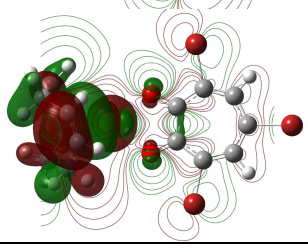	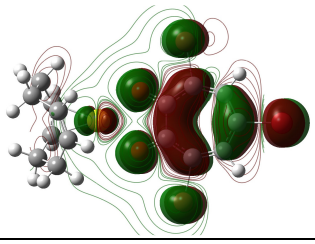	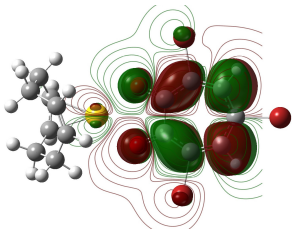	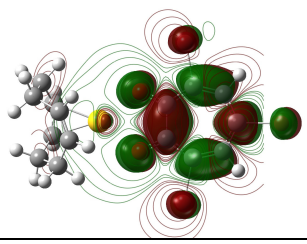

The complete molecular orbital table for group 11 metal tribromotroplonato (3Br-trop) complexes are given in Table C.1.40. For the HOMO-1 molecular orbitals a d_{xz} orbital was observed for copper and silver with extensive delocalization between the oxygens, the ring and the *p* orbitals of the bromines of the 3Br-trop ligand. This pattern was not found for the gold complex, the delocalization was seen primarily on the cyclo-octadine. The HOMO, LUMO and LUMO+1 molecular orbitals are dominated again by the *p* orbitals of the ring of the 3Br-trop ligand.

C.2 Theoretical / Calculation Data of the Calculated Infra-red Spectra

Table C.2.1 The ν(C=O) and ν(C=N) frequencies of the 7-11 calculated metal complexes of the [M(cod)(LL')]A where M = group 7-11 metals, LL' = acac, tfacac, hfacac, NH-acac, NMe-acac, trop, 3Br-trop.

	$\nu(C=O)_{sym}$			ν(C=O) / ν(C=N)			$\nu(C=O)_{sym}$	
	acac	tfacac	hfacac	NH-acac	NMe-acac	NPh-acac	trop	3Br-trop
Mn(I)	1595.69	1591.72	1617.79	1598.77	1592.90	1585.20	1359.51	1509.69
Tc(I)	1592.12	1587.63	1509.84	1602.93	1594.86	1585.34	1359.96	1513.66
Re(I)	1585.19	1575.95	1482.85	1603.83	1598.70	1588.44	1352.11	1509.42
Fe(0)	1558.93	1555.82	1461.68	1557.40	1572.28	1556.45	1334.69	1400.88
Ru(0)	1588.88	1558.91	1473.20	1574.90	1580.61	1570.16	1343.98	1448.59
Os(0)	1533.72	1560.65	1456.54	1531.50	1564.60	1524.69	1301.61	1370.03
Co(I)	1602.00	1624.93	1626.95	1608.31	1598.54	1580.48	1395.98	1515.54
Rh(I)	1602.99	1631.35	1645.61	1609.04	1598.54	1591.43	1386.50	1503.30
Ir(I)	1594.57	1621.13	1628.52	1603.22	1595.85	1587.06	1383.84	1498.78
Ni(II)	1577.24	1611.31	1628.91	1605.04	1551.03	1589.23	1362.20	1397.26
Pd(II)	1575.62	1611.87	1624.78	1601.45	1596.21	1585.44	1346.55	1385.28
Pt(II)	1571.64	1606.50	1622.27	1604.75	1599.85	1589.80	1343.85	1378.02
Cu(I)	1615.67	1606.28	1669.01	1607.98	1602.15	1597.35	1381.04	1536.15
Ag(I)	1622.31	1611.38	1680.73	1610.87	1601.16	1602.01	1386.02	1548.94
Au(I)	1620.02		1675.23	1616.11	1605.20	1601.83	1378.81	1530.95

Table C.2.2 The symmetrical ν(C=C) frequencies of the 7-11 calculated metal complexes of the [M(cod)(LL')]A where M = group 7-11 metals, LL' = acac, tfacac, hfacac, NH-acac, NMe-acac, trop, 3Br-trop.

	$\nu(C=C)_{cod}$							
	acac	tfacac	hfacac	NH-acac	NMe-acac	NPh-acac	trop	3Br-trop
Mn(I)	1518.77	1538.97	1536.02	1503.09	1501.89	1508.89	1521.36	1519.47
Tc(I)	1441.10	1449.40	1465.29	1401.01	1414.79	1442.26	1424.56	1434.48
Re(I)	1384.44	1391.12	1395.43	1362.03	1386.95	1384.92	1231.14	1378.04
Fe(0)	1466.43	1506.98	1535.11	1467.43	1467.69	1472.33	1483.22	1494.17
Ru(0)	1459.50	1467.62	1477.60	1463.52	1464.60	1464.12	1460.15	1465.61
Os(0)	1432.14	1430.59	1421.27	1414.14	1425.66	1437.17	1428.96	1426.37
Co(I)	1558.71	1564.09	1567.31	1531.56	1536.88	1546.90	1554.46	1558.87
Rh(I)	1530.97	1531.53	1528.38	1515.88	1526.02	1524.07	1526.25	1525.40
Ir(I)	1495.37	1496.96	1500.82	1490.61	1495.27	1493.32	1489.39	1494.61
Ni(II)	1605.88	1599.79	1595.79	1590.66	1612.91	1614.05	1600.31	1600.19
Pd(II)	1567.55	1569.46	1564.73	1560.75	1581.63	1582.27	1568.67	1567.99
Pt(II)	1541.23	1539.72	1538.81	1528.02	1535.96	1533.83	1537.10	1538.69
Cu(I)	1573.99	1589.58	1587.53	1572.59	1574.19	1577.40	1580.82	1579.49
Ag(I)	1607.24	1625.42	1614.23	1609.01	1608.00	1606.58	1678.84	1668.08
Au(I)	1497.92	1577.10	1505.14	1511.44	1502.66	1505.63	1488.09	1510.77

C.2.1 Group 7-11 Transition Metal Acetylacetonato Complexes Infra-red Spectra

Below are the individual figures of the metal triads.

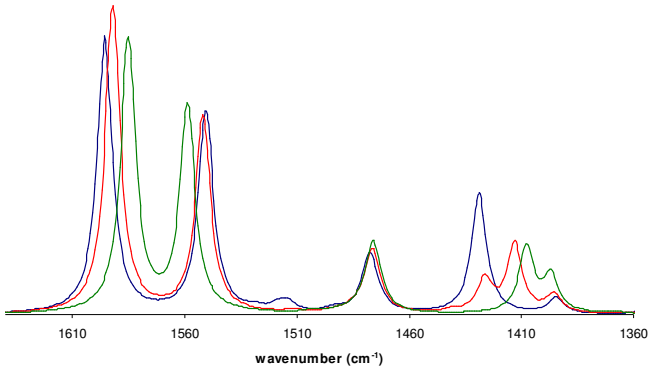

Figure C.1 Calculated IR spectra of [Mn(cod)(acac)] (blue), [Tc(cod)(acac)] (red), [Re(cod)(acac)] (green).

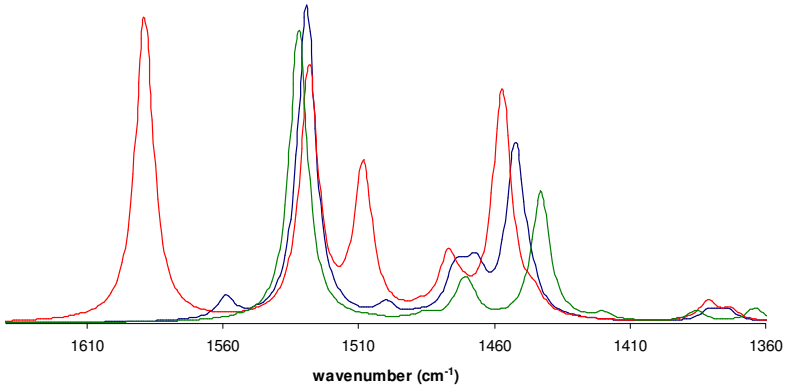

Figure C.2 Calculated IR spectra of $[Fe(cod)(acac)]^-$ (blue), $[Ru(cod)(acac)]^-$ (red), $[Os(cod)(acac)]^-$ (green).

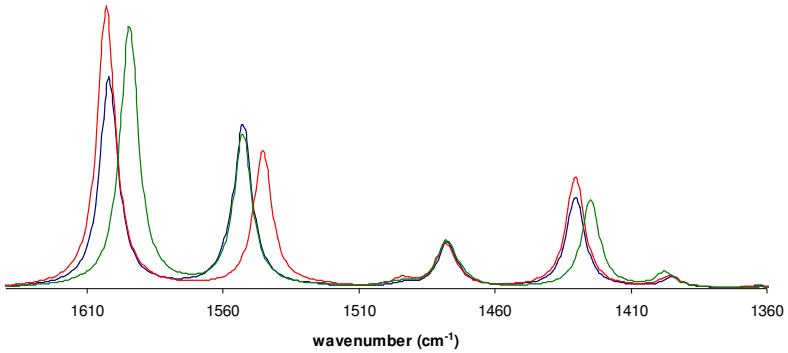

Figure C.3 Calculated IR spectra of [Co(cod)(acac)] (blue), [Rh(cod)(acac)] (red), [Ir(cod)(acac)] (green).

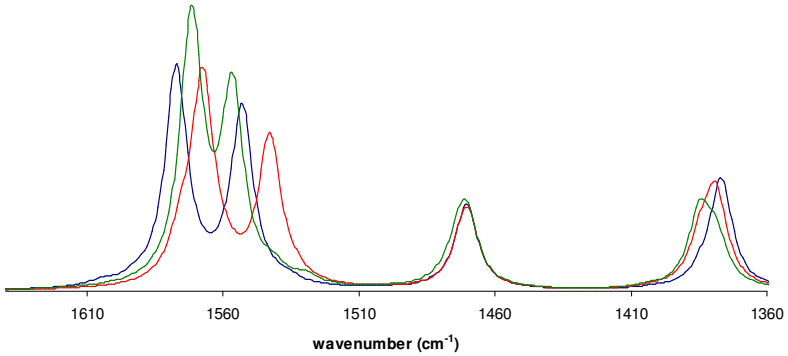

Figure C.4 Calculated IR spectra of $[Ni(cod)(acac)]^+$ (blue), $[Pd(cod)(acac)]^+$ (red), $[Pt(cod)(acac)]^+$ (green).

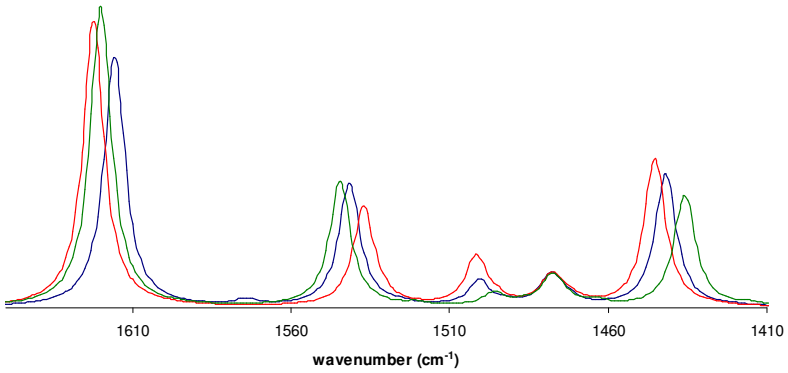

Figure C.5 Calculated IR spectra of [Cu(cod)(acac)] (blue), [Ag(cod)(acac)] (red), [Ag(cod)(acac)] (green).

C.2.2 Group 7-11 Transition Metal Trifluoroacetylacetonato Complexes Infra-red Spectra

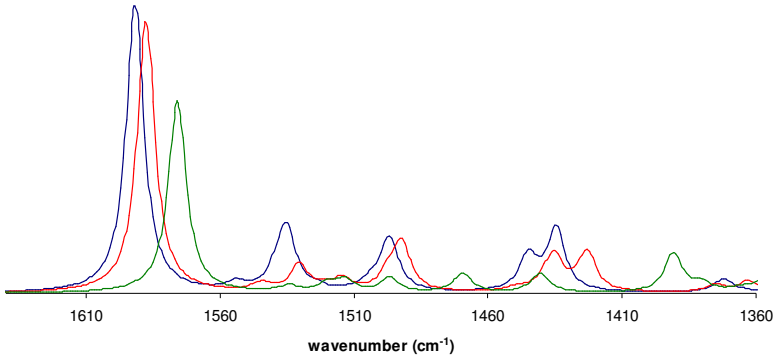

Figure C.6 Calculated IR spectra of [Mn(cod)(tfacac)] (blue), [Tc(cod)(tfacac)] (red), [Re(cod)(tfacac)] (green).

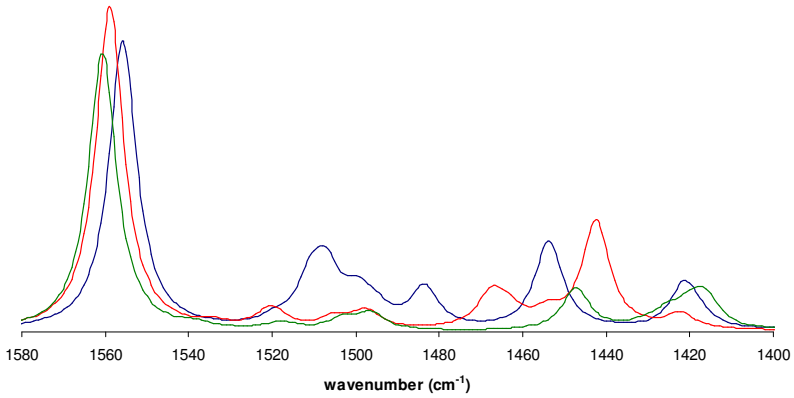

Figure C.7 Calculated IR spectra of $[Fe(cod)(tfacac)]^-$ (blue), $[Ru(cod)(tfacac)]^-$ (red), $[Os(cod)(tfacac)]^-$ (green).

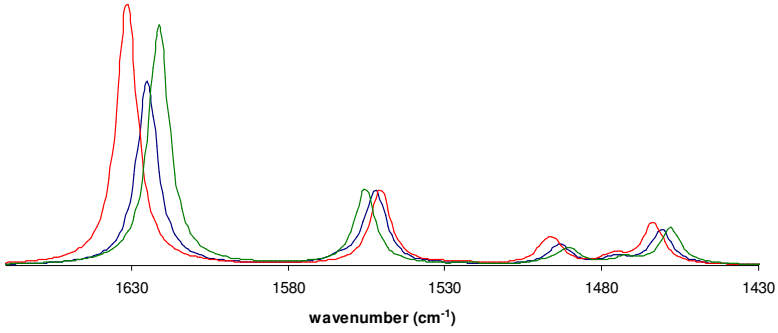

Figure C.8 Calculated IR spectra of [Co(cod)(tfacac)] (blue), [Rh(cod)(tfacac)] (red), [Ir(cod)(tfacac)] (green).

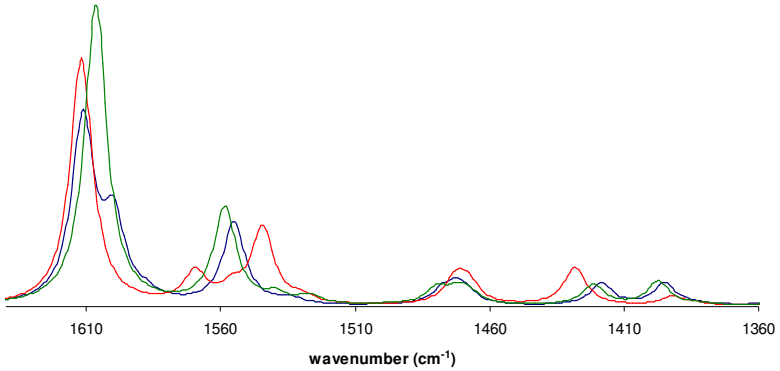

Figure C.9 Calculated IR spectra of [Ni(cod)(tfacac)]$^+$ (blue), [Pd(cod)(tfacac)]$^+$ (red), [Pt(cod)(tfacac)]$^+$ (green).

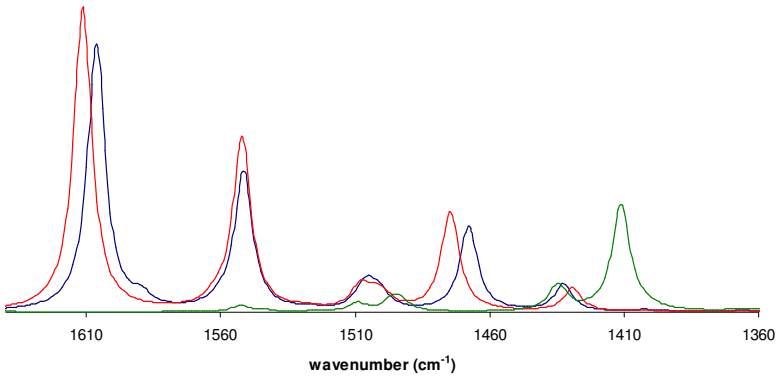

Figure C.10 Calculated IR spectra of [Cu(cod)(tfacac)] (blue), [Ag(cod)(tfacac)] (red), [Au(cod)(tfacac)] (green).

C.2.3 Group 7-11 Transition Metal Hexafluoroacetylacetonato Complexes Infra-red Spectra

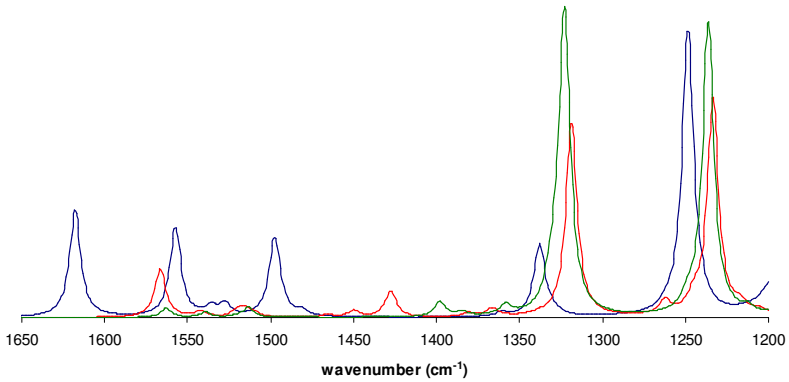

Figure C.11 Calculated IR spectra of [Mn(cod)(hfacac)] (blue), [Tc(cod)(hfacac)] (red), [Re(cod)(hfacac)] (green).

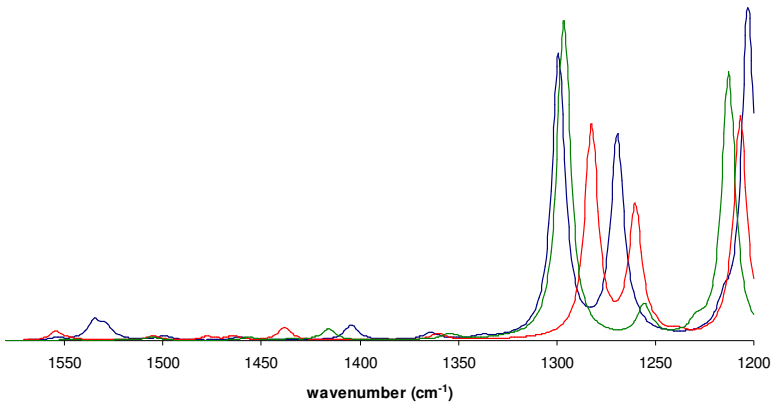

Figure C.12 Calculated IR spectra of [Fe(cod)(hfacac)]$^-$ (blue), [Ru(cod)(hfacac)]$^-$ (red), [Os(cod)(hfacac)]$^-$ (green).

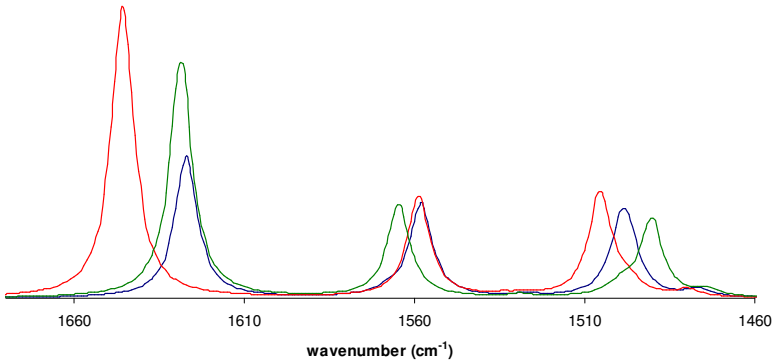

Figure C.13 Calculated IR spectra of [Co(cod)(hfacac)] (blue), [Rh(cod)(hfacac)] (red), [Ir(cod)(hfacac)] (green).

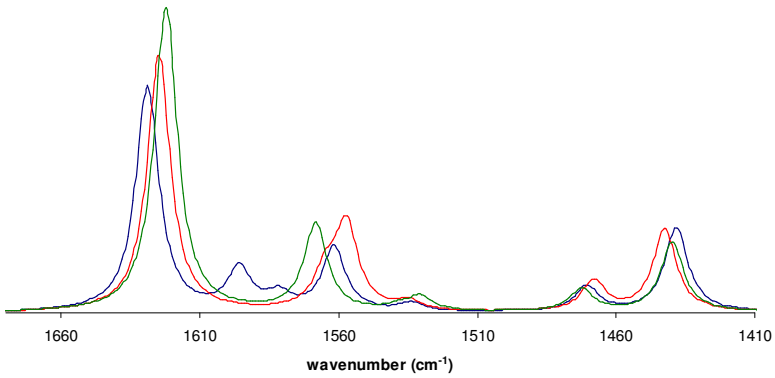

Figure C.14 Calculated IR spectra of [Ni(cod)(hfacac)]$^+$ (blue), [Pd(cod)(hfacac)]$^+$ (red), [Pt(cod)(hfacac)]$^+$ (green).

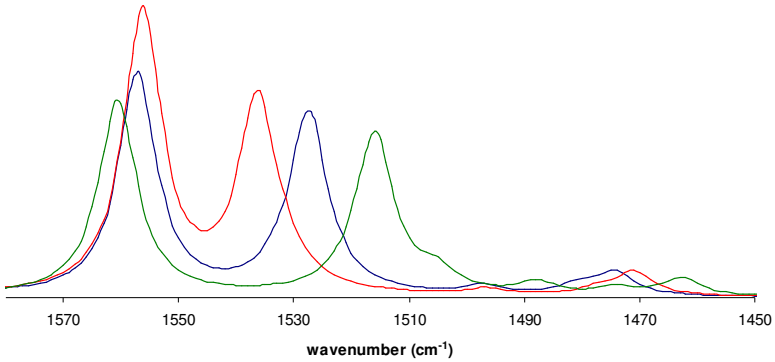

Figure C.15 Calculated IR spectra of [Cu(cod)(hfacac)] (blue), [Ag(cod)(hfacac)] (red), [Au(cod)(hfacac)] (green).

C.2.4 Group 7-11 Transition Metal 4-Aminopent-3-en-2-onato Complexes Infra-red Spectra

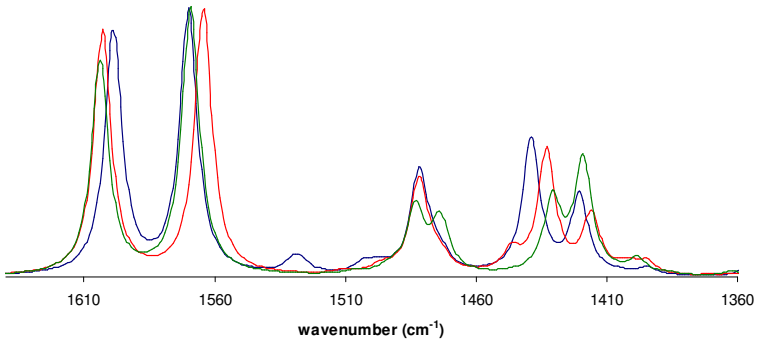

Figure C.16 Calculated IR spectra of [Mn(cod)(NH-acac)] (blue), [Tc(cod)(NH-acac)] (red), [Re(cod)(NH-acac)] (green).

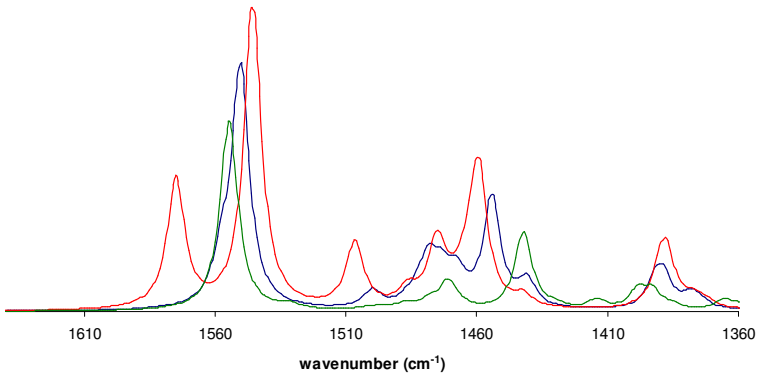

Figure C.17 Calculated IR spectra of $[Fe(cod)(NH\text{-}acac)]^-$ (blue), $[Ru(cod)(NH\text{-}acac)]^-$ (red), $[Os(cod)(NH\text{-}acac)]^-$ (green).

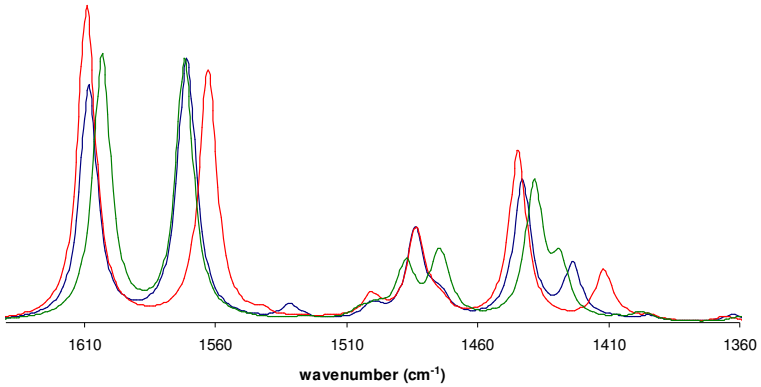

Figure C.18 Calculated IR spectra of [Co(cod)(NH-acac)] (blue), [Rh(cod)(NH-acac)] (red), [Ir(cod)(NH-acac)] (green).

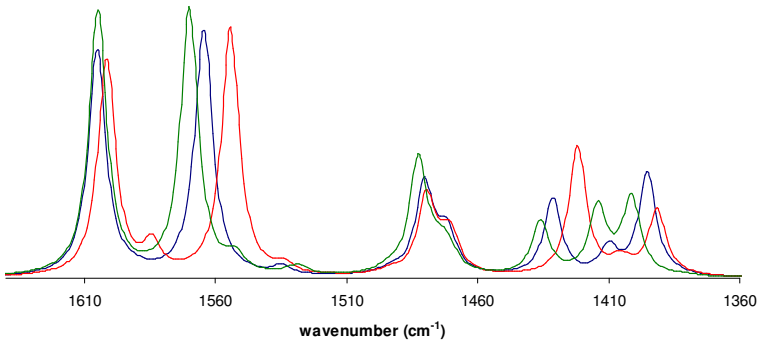

Figure C.19 Calculated IR spectra of $[Ni(cod)(NH\text{-}acac)]^+$ (blue), $[Pd(cod)(NH\text{-}acac)]^+$ (red), $[Pt(cod)(NH\text{-}acac)]^+$ (green).

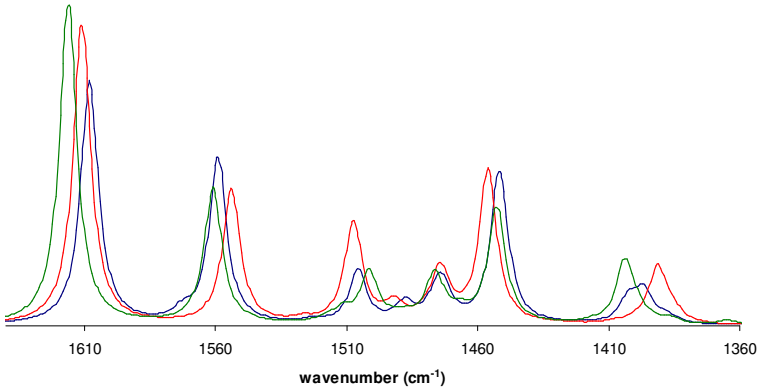

Figure C.20 Calculated IR spectra of [Cu(cod)(NH-acac)] (blue), [Ag(cod)(NH-acac)] (red), [Au(cod)(NH-acac)] (green).

C.2.5 Group 7-11 Transition Metal 4-(Methylamino)pent-3-en-2-onato Complexes Infra-red Spectra

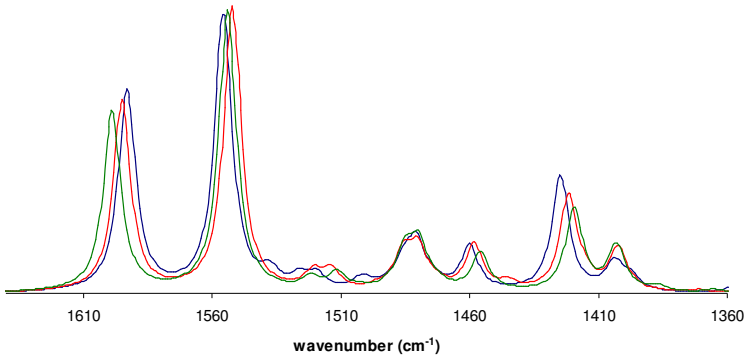

Figure C.21 Calculated IR spectra of [Mn(cod)(NMe-acac)] (blue), [Tc(cod)(NMe-acac)] (red), [Re(cod)(NMe-acac)] (green).

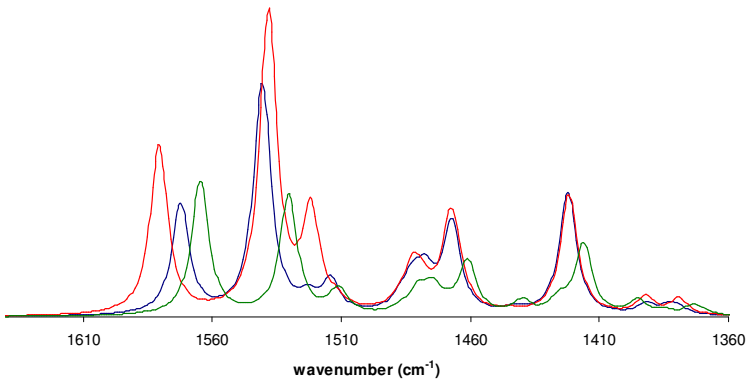

Figure C.22 Calculated IR spectra of [Fe(cod)(NMe-acac)]$^-$ (blue), [Ru(cod)(NMe-acac)]$^-$ (red), [Os(cod)(NMe-acac)]$^-$ (green).

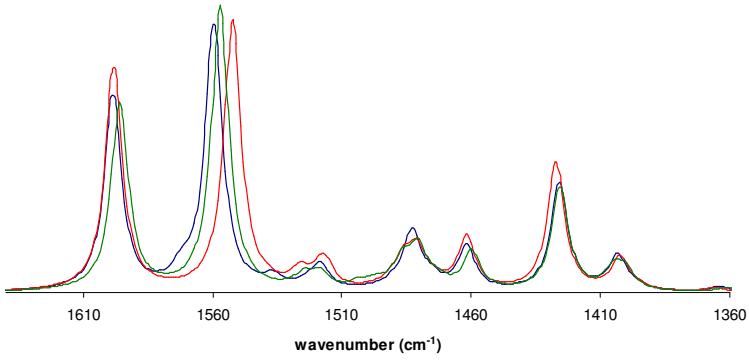

Figure C.23 Calculated IR spectra of [Co(cod)(NMe-acac)] (blue), [Rh(cod)(NMe-acac)] (red), [Ir(cod)(NMe-acac)] (green).

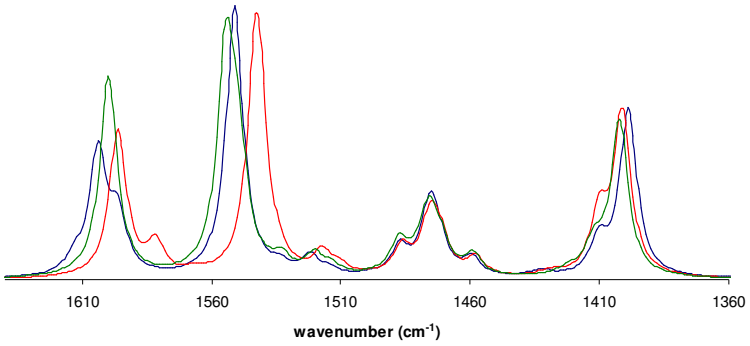

Figure C.24 Calculated IR spectra of [Ni(cod)(NMe-acac)]$^+$ (blue), [Pd(cod)(NMe-acac)]$^+$ (red), [Pt(cod)(NMe-acac)]$^+$ (green).

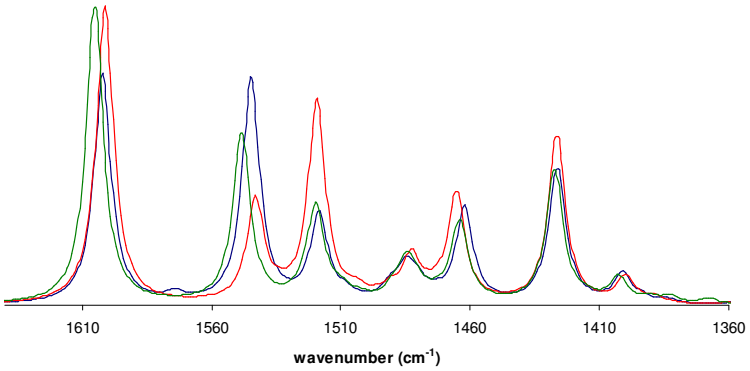

Figure C.25 Calculated IR spectra of [Cu(cod)(NMe-acac)] (blue), [Ag(cod)(NMe-acac)] (red), [Au(cod)(NMe-acac)] (green).

C.2.6 Group 7-11 Transition Metal 4-Anilinopent-3-en-2-onato Complexes Infra-red Spectra

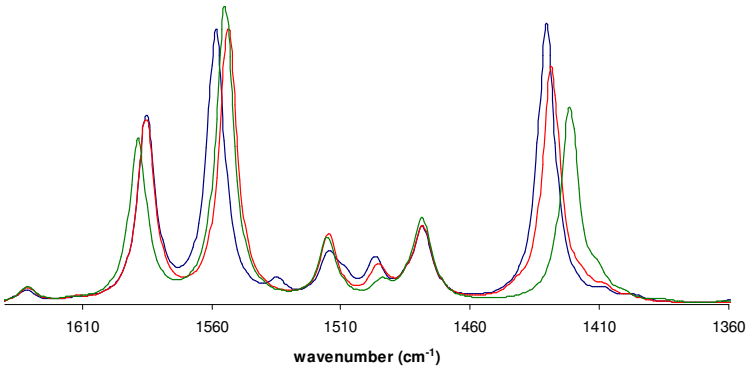

Figure C.26 Calculated IR spectra of [Mn(cod)(NPh-acac)] (blue), [Tc(cod)(NPh-acac)] (red), [Re(cod)(NPh-acac)] (green).

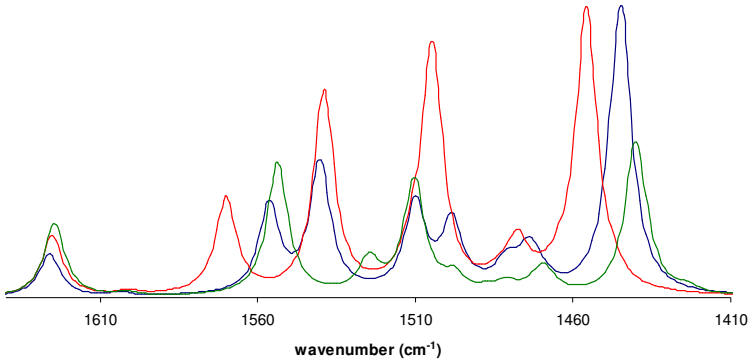

Figure C.27 Calculated IR spectra of [Fe(cod)(NPh-acac)]$^-$ (blue), [Ru(cod)(NPh-acac)]$^-$ (red), [Os(cod)(NPh-acac)]$^-$ (green).

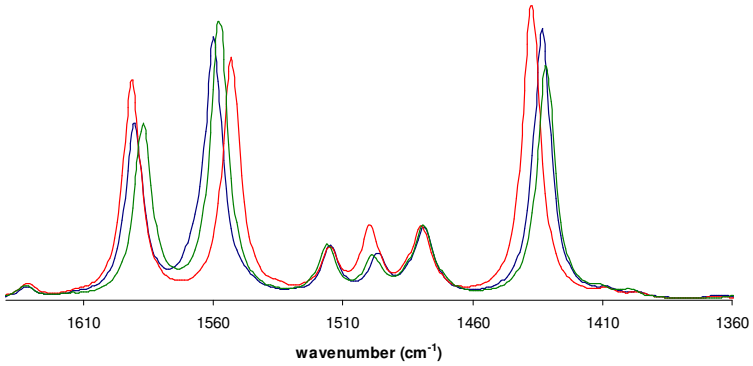

Figure C.28 Calculated IR spectra of [Co(cod)(NPh-acac)] (blue), [Rh(cod)(NPh-acac)] (red), [Ir(cod)(NPh-acac)] (green).

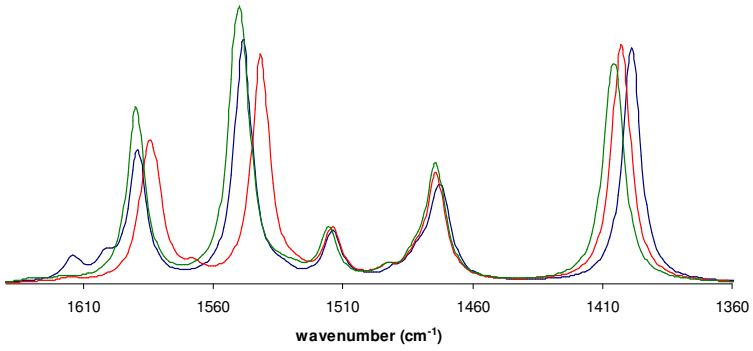

Figure C.29 Calculated IR spectra of [Ni(cod)(NPh-acac)]$^+$ (blue), [Pd(cod)(NPh-acac)]$^+$ (red), [Pt(cod)(NPh-acac)]$^+$ (green).

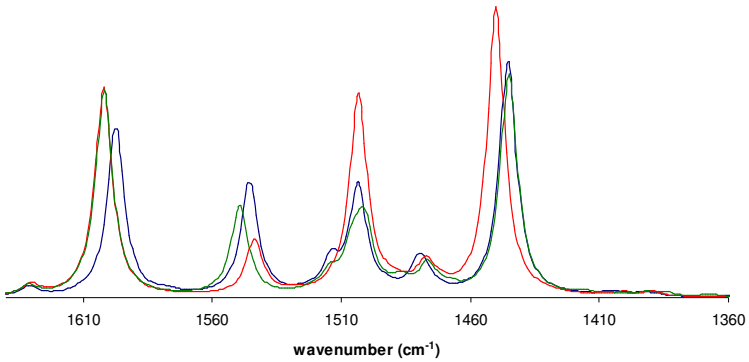

Figure C.30 Calculated IR spectra of [Cu(cod)(NPh-acac)] (blue), [Ag(cod)(NPh-acac)] (red), [Au(cod)(NPh-acac)] (green).

C.2.7 Group 7-11 Transition Metal Tropolonato Complexes Infra-red Spectra

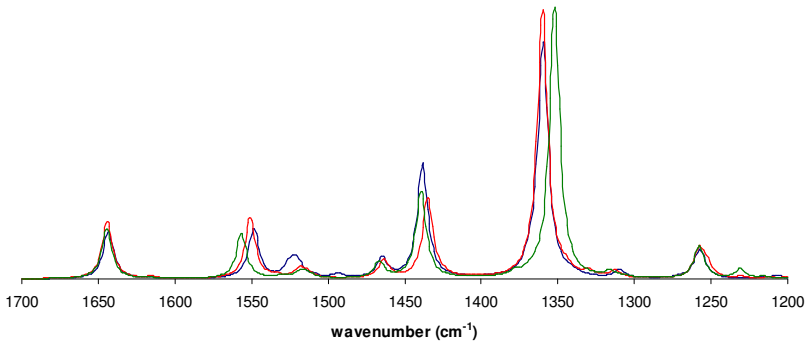

Figure C.31 Calculated IR spectra of [Mn(cod)(trop)] (blue), [Tc(cod)(trop)] (red), [Re(cod)(trop)] (green).

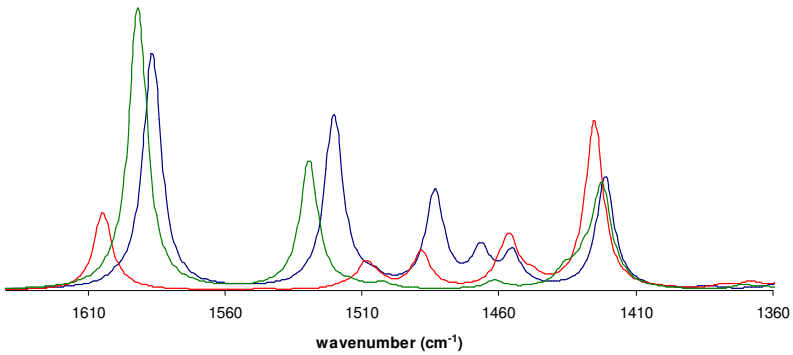

Figure C.32 Calculated IR spectra of $[Fe(cod)(trop)]^-$ (blue), $[Ru(cod)(trop)]^-$ (red), $[Os(cod)(trop)]^-$ (green).

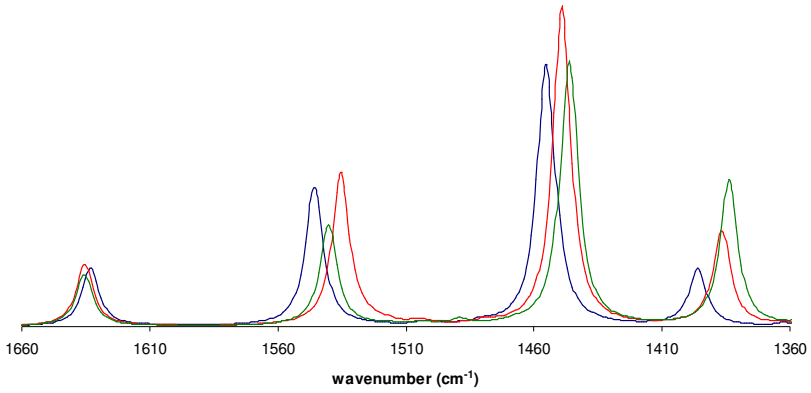

Figure C.33 Calculated IR spectra of [Co(cod)(trop)] (blue), [Rh(cod)(trop)] (red), [Ir(cod)(trop)] (green).

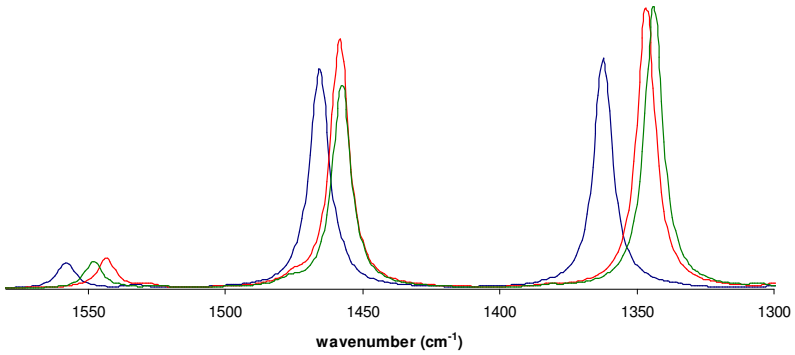

Figure C.34 Calculated IR spectra of $[Ni(cod)(trop)]^+$ (blue), $[Pd(cod)(trop)]^+$ (red), $[Pt(cod)(trop)]^+$ (green).

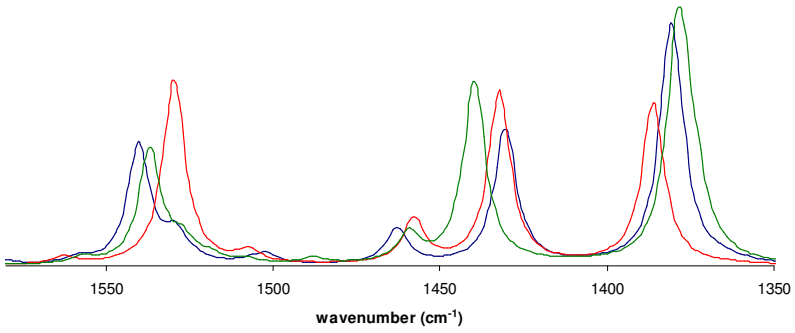

Figure C.35 Calculated IR spectra of [Cu(cod)(trop)] (blue), [Ag(cod)(trop)] (red), [Au(cod)(trop)] (green).

C.2.8 Group 7-11 Transition Metal Tribromotropolonato Complexes Infra-red Spectra

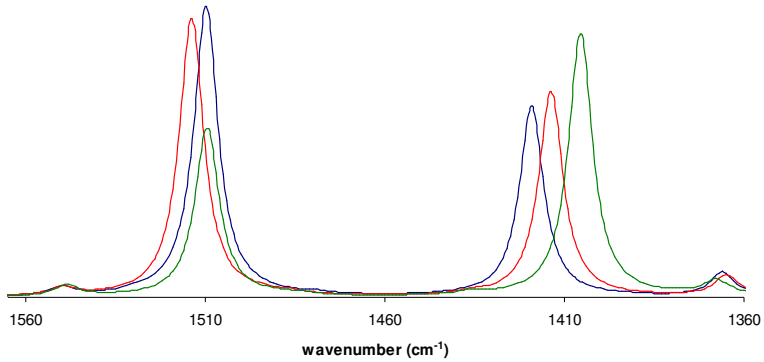

Figure C.36 Calculated IR spectra of [Mn(cod)(3Br-trop)] (blue), [Tc(cod)(3Br-trop)] (red), [Re(cod)(3Br-trop)] (green).

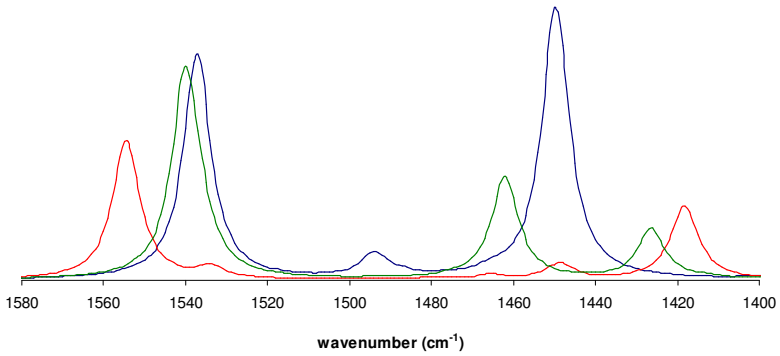

Figure C.37 Calculated IR spectra of $[Fe(cod)(3Br\text{-}trop)]^-$ (blue), $[Ru(cod)(3Br\text{-}trop)]^-$ (red), $[Os(cod)(3Br\text{-}trop)]^-$ (green).

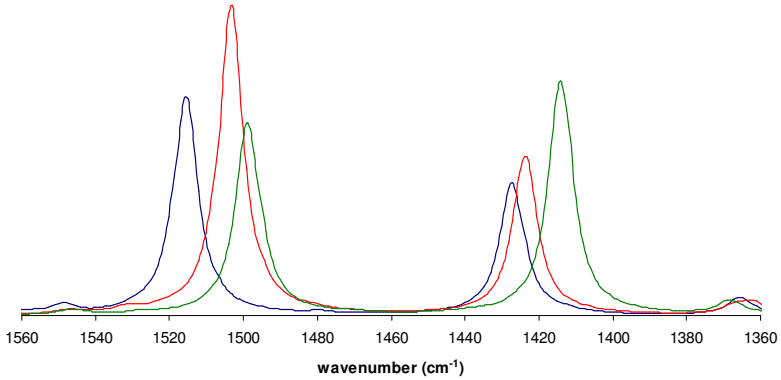

Figure C.38 Calculated IR spectra of [Co(cod)(3Br-trop)] (blue), [Rh(cod)(3Br-trop)] (red), [Ir(cod)(3Br-trop)] (green).

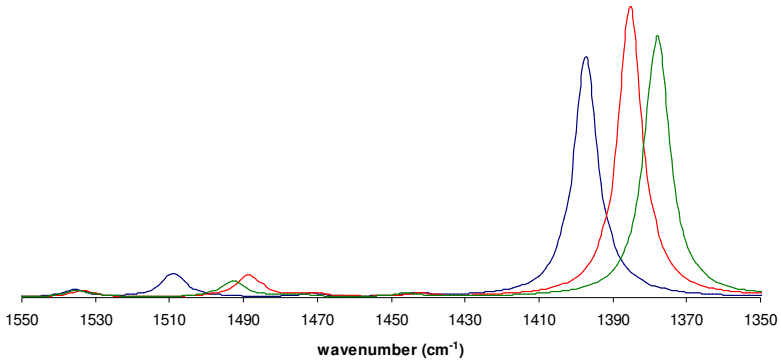

Figure C.39 Calculated IR spectra of [Ni(cod)(3Br-trop)]$^+$ (blue), [Pd(cod)(3Br-trop)]$^+$ (red), [Pt(cod)(3Br-trop)]$^+$ (green).

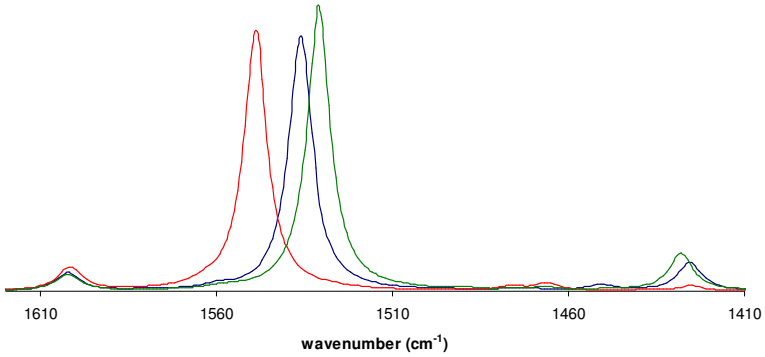

Figure C.40 Calculated IR spectra of [Cu(cod)(3Br-trop)] (blue), [Ag(cod)(3Br-trop)] (red), [Au(cod)(3Br-trop)] (green).

C.3 Theoretical / Calculation Data of the Calculated Bond Distances and Angles

Table C.3.1 Total area (A_{tot}) of the group 7-11 calculated metal complexes of the [M(cod)(LL')]A where M = group 7-11 metals, LL' = acac, tfacac, hfacac, NH-acac, NMe-acac, trop, 3Br-trop.

	A_{tot} acac	tfacac	hfacac	NH-acac	NMe-acac	NPh-acac	trop	3Br-trop
Mn(I)	7.873612	7.923441	7.981625	7.852276	8.080673	8.127793	7.813776	7.826840
Tc(I)	8.481345	8.511891	8.535081	8.506753	8.663815	8.693070	8.365735	8.383783
Re(I)	8.186785	8.130576	8.117023	8.169130	8.312688	8.327230	8.078024	8.084613
Fe(0)	7.558202	7.52812	7.562752	7.523999	7.737979	7.830439	7.498360	7.474182
Ru(0)	8.651470	8.574055	8.564971	8.556740	8.699209	8.731159	8.576108	8.522920
Os(0)	8.447817	8.420276	8.405528	8.386338	8.491222	8.513112	8.388043	8.285525
Co(I)	7.547571	7.590421	7.619248	7.544154	7.777486	7.828549	7.487695	7.499498
Rh(I)	8.493255	8.535237	8.578636	8.464073	8.592759	8.625214	8.407880	8.418998
Ir(I)	8.350336	8.389188	8.429480	8.301636	8.408383	8.437222	8.277523	8.282500
Ni(II)	7.792511	7.805212	7.809516	7.870714	8.121731	8.327854	7.652869	7.641839
Pd(II)	8.719676	8.745915	8.770510	8.743171	8.886286	8.926216	8.567568	8.559091

Pt(II)	8.568156	8.600026	8.637560	8.562123	8.664226	8.696551	8.450574	8.439608
Cu(I)	10.48101	10.2923	11.34247	11.03665	11.16490	11.05279	10.08110	9.981164
Ag(I)	12.49069	12.32926	12.32991	12.70398	12.53954	12.67462	11.73069	11.62291
Au(I)	12.57032	10.54675	12.47341	12.77793	12.90234	12.86724	12.14670	11.96915

Table C.3.2 Percentage perpendicular ($\%p_1$) of the group 7-11 calculated metal complexes of the [M(cod)(LL')]A where M = group 7-11 metals, LL' = acac, tfacac, hfacac, NH-acac, NMe-acac, trop, 3Br-trop.

	$\%p_1$							
	acac	tfacac	hfacac	NH-acac	NMe-acac	NPh-acac	trop	3Br-trop
Mn(I)	50.06797	51.16487	50.47154	49.94940228	48.04045	48.1821	50.14788	49.65704
Tc(I)	48.23949	48.98106	49.91422	47.54710571	46.5198	46.69475	47.98759	47.80236
Re(I)	47.25902	49.07875	49.51461	45.82881467	44.67347	44.67532	46.85912	46.79314
Fe(0)	47.88673	50.96543	52.78577	48.86563538	46.07486	46.70632	48.81018	48.94653
Ru(0)	46.12241	47.90698	48.8668	47.71161783	46.10897	46.32946	46.73834	46.66649
Os(0)	47.10365	48.45934	49.10918	48.69523635	47.24881	47.7081	47.55535	47.47654
Co(I)	51.19822	51.1412	51.48088	50.95800439	48.79271	49.1536	50.38191	50.50891
Rh(I)	48.73812	48.47478	48.42657	49.51878616	48.1955	48.19085	48.51535	48.49034
Ir(I)	48.16181	47.96827	48.04207	49.21412974	48.02607	48.06293	48.08547	48.15139
Ni(II)	56.23557	55.66508	55.42861	55.62950894	54.32892	54.49717	55.12453	55.12353
Pd(II)	52.78743	52.30813	52.06577	52.94266424	52.01236	52.11154	52.34682	52.33432
Pt(II)	51.41321	51.05376	50.92162	51.81833433	50.84838	50.90334	51.19891	51.22896
Cu(I)	49.70599	50.08048	60.35263	50.19212054	49.94949	49.95783	49.60814	49.27327
Ag(I)	50.48635	58.72759	50.40044	51.32394751	62.07624	50.65814	54.94901	53.59204
Au(I)	47.37354	50.51926	47.01811	49.13744487	48.31368	48.21816	47.75606	47.35506

Table C.3.3 O_1-M-O_2 / N_1-M-O_1 bite angles of the group 7-11 calculated metal complexes of the [M(cod)(LL')]A where M = group 7-11 metals, LL' = acac, tfacac, hfacac, NH-acac, NMe-acac, trop, 3Br-trop.

	O_1-M-O_2			N_1-M-O_1			O_1-M-O_2	
	acac	tfacac	hfacac	NH-acac	NMe-acac	NPh-acac	trop	3Br-trop
Mn(I)	89.828	89.898	89.111	89.155	90.202	89.316	80.6	78.519
Tc(I)	82.983	83.135	83.291	83.62	85.1	84.119	73.9	72.363
Re(I)	82.461	81.713	81.799	83.218	84.657	83.831	73.836	72.522
Fe(0)	89.667	92.729	94.363	89.04	89.177	88.979	81.631	80.841
Ru(0)	87.102	89.538	90.566	87.102	88.085	87.173	75.759	74.245
Os(0)	88.473	89.909	90.498	88.274	89.179	88.225	76.978	75.784
Co(I)	91.755	91.433	91.129	90.446	91.53	90.811	82.184	81.093
Rh(I)	90.062	89.501	88.89	88.968	90.369	89.758	77.717	76.159
Ir(I)	89.558	89.132	88.691	88.841	90.22	89.691	77.378	76.054
Ni(II)	94.923	94.308	93.537	93.067	94.34	93.848	85.573	84.759
Pd(II)	92.851	92.349	91.442	90.846	92.507	92.187	80.906	79.739
Pt(II)	91.95	91.284	90.396	90.413	92.075	91.783	79.93	78.879
Cu(I)	94.902	92.743	91.812	95.385	97.5	96.473	81.472	78.638
Ag(I)	85.483	83.21	81.881	86.523	89.453	88.118	71.873	68.651
Au(I)	83.79	93.468	80.104	84.427	87.353	86.45	72.654	70.13

Table C.3.4 Ce_1-M-Ce_2 bite angles of the group 7-11 calculated metal complexes of the [M(cod)(LL')]A where M = group 7-11 metals, LL' = acac, tfacac, hfacac, NH-acac, NMe-acac, trop, 3Br-trop.

	Ce_1-M-Ce_2							
	acac	tfacac	hfacac	NH-acac	NMe-acac	NPh-acac	trop	3Br-trop
Mn(I)	90.18	89.96	89.93	89.53	88.09	88.11	90.87	90.7
Tc(I)	87.22	87.2	86.43	87.19	86.54	86.5	88.12	87.45
Re(I)	89.22	88.7	88.33	89.35	88.8	88.89	90.17	89.66
Fe(0)	91.36	90.44	89.74	90.85	89.76	89.57	91.84	91.67

Ru(0)	88.18	87.86	87.68	87.67	87.01	87	87.97	87.81
Os(0)	87.88	87.43	87.29	87.32	86.6	86.54	87.41	87.51
Co(I)	90.91	90.84	90.76	90.34	88.59	88.74	91.78	91.8
Rh(I)	88.08	88.07	87.96	87.55	86.7	86.67	88.03	87.93
Ir(I)	88.24	88.24	88.09	87.63	86.9	86.87	87.92	87.78
Ni(II)	87.55	87.84	88.08	86.85	84.02	84.33	89.07	89.18
Pd(II)	85.66	85.78	85.81	85.13	83.77	83.75	86.09	85.97
Pt(II)	86.74	86.77	86.72	86.07	85.09	85.08	86.6	86.49
Cu(I)	78.52	80.86	81.29	74.93	74.67	75.49	79.6	79.91
Ag(I)	71.14	73.05	72.74	69.4	69.62	70.33	71.94	72.93
Au(I)	68.96	75.78	70.21	68.14	68.03	68.43	69.65	69.68

C.4 Theoretical / Calculation Data of the Molecular Orbital Energies

C.4.1 Group7-11 Transition Metal Acetylacetonato Complexes Molecular Orbital Energies

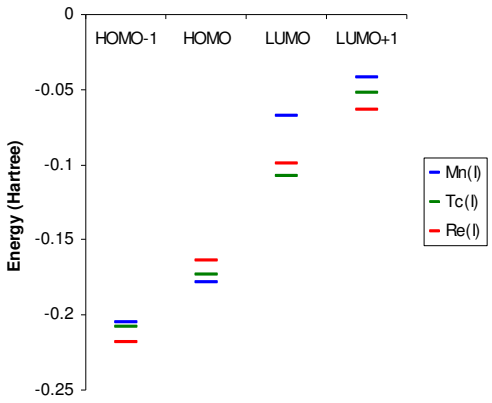

Figure C.41 Graph of the Molecular Orbital Energies of the [M(cod)(acac)] M = Mn(I), Tc(I), Re(I).

Table C.4.1 Molecular Orbital Energies (Hartree) and energy gaps (eV) of the [M(cod)(acac)] calculated structures.

	HOMO-1	HOMO	LUMO	LUMO+1	E_{g-1}	E_g	E_{g+1}
Mn(I)	-0.20518	-0.17857	-0.06776	-0.04222	0.724	3.015	0.695
Tc(I)	-0.20782	-0.17265	-0.10786	-0.05271	0.957	1.763	1.501
Re(I)	-0.21824	-0.16413	-0.09918	-0.06368	1.472	1.767	0.966

In Figure C.41 the graph of the molecular orbital energies of the group 7 metals for acetylactonato ligands are displayed with the corresponding values in Table C.4.1, also included in the table are the energy gap values. The HOMO-1 molecular energies differ by *ca.* 0.012 Hartree using manganese and rhenium energies, an average value for E_{g-1} of 1.051 eV was obtained. The HOMO molecular energies differ by *ca.* 0.014 Hartree again using manganese and rhenium with an average value for E_g of 2.182 eV. The decrease in E_g from manganese to technetium and rhenium is

1.2 eV. The 2008 covalent radii for the group 7 metals, (see Table 2.2) manganese is found to be smaller than both technetium and rhenium leading to an increased energy requirement for the excitation from the ground state and resulting in a more stable complex. The LUMO molecular energies differ by *ca.* 0.04 Hartree between manganese and techneticum with the E_{g+1} energy average found to be 1.054 eV. Lastly the LUMO+1 molecular energies vary by *ca.* 0.02 Hartree between manganese and rhenium.

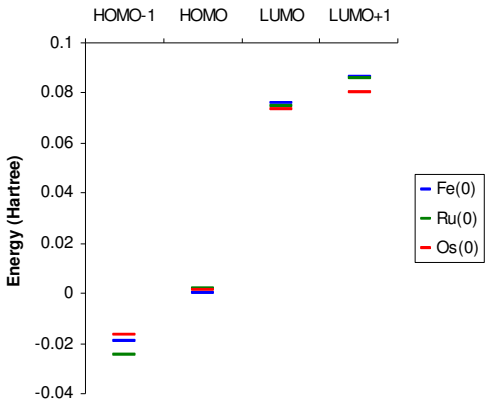

Figure C.42 Graph of the Molecular Orbital Energies of the [M(cod)(acac)] M = Fe(0), Ru(0), Os(0).

Table C.4.2 Molecular Orbital Energies (Hartree) and energy gaps (eV) of the [M(cod)(acac)] calculated structures.

	HOMO-1	HOMO	LUMO	LUMO+1	E_{g-1}	E_g	E_{g+1}
Fe(0)	-0.01908	0.00031	0.07586	0.08644	0.528	2.056	0.288
Ru(0)	-0.02429	0.00203	0.07467	0.08584	0.716	1.977	0.304
Os(0)	-0.01664	0.00103	0.07373	0.08016	0.481	1.978	0.175

In Figure C.42 the graph of the molecular orbital energies of the group 8 metals for acetylactonato ligands are displayed with the corresponding values in Table C.4.2, also included in the table are the energy gap values. The HOMO-1 molecular energies differ by *ca.* 7.6 x 10^{-3} Hartree using ruthenium and osmium energies, an average value for E_{g-1} of 0.575 eV was obtained. The HOMO molecular energies differ by *ca.* 1.7 x 10^{-3} Hartree using iron and osmium with an average value for E_g of 2.004 eV. The LUMO molecular energies differ by *ca.* 2.1 x 10^{-3} Hartree between iron and osmium with the E_{g+1} energy average found to be 0.256 eV. Lastly the LUMO+1 molecular energies vary by *ca.* 6.3 x 10^{-3} Hartree between iron and osmium.

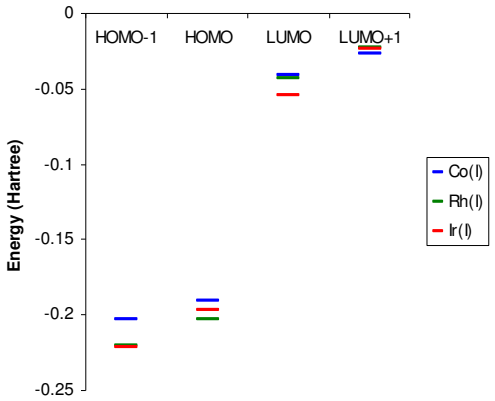

Figure C.43 Graph of the Molecular Orbital Energies of the [M(cod)(acac)] M = Co(I), Rh(I), Ir(I).

Table C.4.3 Molecular Orbital Energies (Hartree) and energy gaps (eV) of the [M(cod)(acac)] calculated structures.

	HOMO-1	HOMO	LUMO	LUMO+1	E_{g-1}	E_g	E_{g+1}
Co(I)	-0.20259	-0.19064	-0.04069	-0.02711	0.325	4.080	0.370
Rh(I)	-0.22052	-0.2027	-0.04321	-0.02291	0.485	4.340	0.552
Ir(I)	-0.22107	-0.19721	-0.05459	-0.02341	0.649	3.881	0.848

In Figure C.43 the graph of the molecular orbital energies of the group 9 metals for acetylactonato ligands are displayed with the corresponding values in Table C.4.3, also included in the table are the energy gap values. The HOMO-1 molecular energies differ by *ca.* 1.8 x 10^{-2} Hartree using cobalt and iridium energies whilst the rhodium and iridium energies only differ by 5.5 x 10^{-4} Hartree, an average value for E_{g-1} of 0.486 eV was obtained. The HOMO molecular energies vary by *ca.* 1.2 x 10^{-2} Hartree using cobalt and rhodium with an average value for E_g of 4.1 eV. The LUMO molecular energies differ by *ca.* 1.4 x 10^{-2} Hartree between cobalt and iridium with the E_{g+1} energy average found to be 0.59 eV. Lastly the LUMO+1 molecular energies vary by *ca.* 4.2 x 10^{-3} Hartree between cobalt and rhodium. The similar energy values observed for rhodium and iridium can be attributed to their nearly identical covalent radii (see Table 12.1 or Table 2.2).

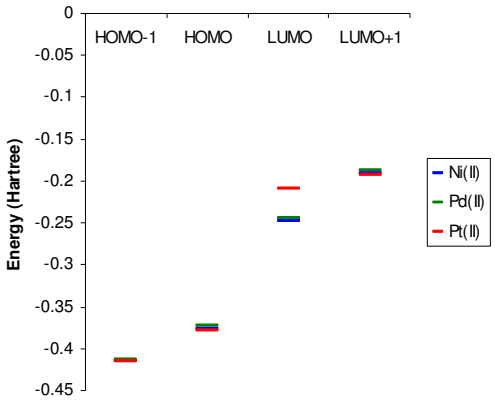

Figure C.44 Graph of the Molecular Orbital Energies of the [M(cod)(acac)] M = Ni(II), Pd(II), Pt(II).

Table C.4.4 Molecular Orbital Energies (Hartree) and energy gaps (eV) of the [M(cod)(acac)] calculated structures.

	HOMO-1	HOMO	LUMO	LUMO+1	E_{g-1}	E_g	E_{g+1}
Ni(II)	-0.41512	-0.37704	-0.2485	-0.19038	1.036	3.498	1.582
Pd(II)	-0.41333	-0.37277	-0.24407	-0.18711	1.104	3.502	1.550
Pt(II)	-0.41536	-0.37796	-0.2089	-0.19198	1.018	4.600	0.460

In Figure C.44 the graph of the molecular orbital energies of the group 10 metals for acetylactonato ligands are displayed with the corresponding values in Table C.4.4, also included in the table are the energy gap values. The HOMO-1 molecular energies differ by *ca.* 2.03 x 10^{-3} Hartree using palladium and platinum energies, an average value for E_{g-1} of 1.053 eV was obtained. The HOMO molecular energies differ by *ca.* 5.2 x 10^{-3} Hartree again using palladium and platinum with an average value for E_g of 3.867 eV. The LUMO molecular energies differ by *ca.* 3.96 x 10^{-2} Hartree between palladium and platinum with the E_{g+1} energy average found to be 1.197 eV. Lastly the LUMO+1 molecular energies vary by *ca.* 4.87 x 10^{-3} Hartree between palladium and platinum. For the E_{g+1} energy gap a large difference is found for platinum as opposed to the comparable values of nickel and palladium this difference observed accounts for the variance found in the LUMO and LUMO+1 molecular orbitals of the group 10 (see § C.1.4) complexes.

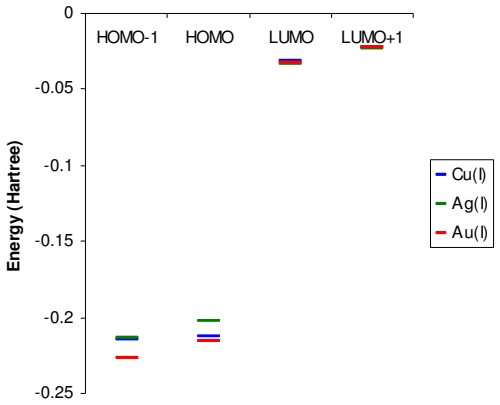

Figure C.45 Graph of the Molecular Orbital Energies of the [M(cod)(acac)] M = Cu(I), Ag(I), Au(I).

Table C.4.5 Molecular Orbital Energies (Hartree) and energy gaps (eV) of the [M(cod)(acac)] calculated structures.

	HOMO-1	HOMO	LUMO	LUMO+1	E_{g-1}	E_g	E_{g+1}
Cu(I)	-0.21446	-0.21275	-0.03095	-0.02222	0.047	4.947	0.238
Ag(I)	-0.21381	-0.20262	-0.03302	-0.02321	0.304	4.615	0.267
Au(I)	-0.22718	-0.21594	-0.03198	-0.02272	0.306	5.006	0.252

In Figure C.45 the graph of the molecular orbital energies of the group 11 metals for acetylactonato ligands are displayed with the corresponding values in Table C.4.5, also included in the table are the energy gap values. The HOMO-1 molecular energies differ by *ca.* 1.34 x 10^{-2} Hartree using silver and gold energies, an average value for E_{g-1} of 0.219 eV was obtained. The HOMO molecular energies differ by *ca.* 1.33 x 10^{-2} Hartree again using silver and gold with an average value for E_g of 4.856 eV. The LUMO molecular energies differ by *ca.* 2.07 x 10^{-3} Hartree between copper and silver with the E_{g+1} energy average found to be 0.252 eV. Lastly the LUMO+1 molecular energies vary by *ca.* 9.9 x 10^{-4} Hartree between copper and silver. The molecular orbital energies presented in Figure C.45 show small energy changes for E_{g-1} and E_{g+1}. With the E_g energy difference being larger than for the previous groups. This increased energy barrier could be as a result of the group 11 metal complexes being stable whilst mono co-ordinated to the cyclo-octadiene ring.

C.4.2 Group 7-11 Transition Metal Trifluoroacetylacetonato Complexes Molecular Orbital Energies

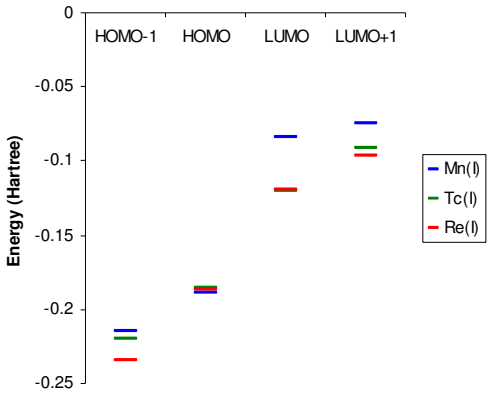

Figure C.46 Graph of the Molecular Orbital Energies of the [M(cod)(tfacac)] M = Mn(I), Tc(I), Re(I).

Table C.4.6 Molecular Orbital Energies (Hartree) and energy gaps (eV) of the [M(cod)(tfacac)] calculated structures.

	HOMO-1	HOMO	LUMO	LUMO+1	E_{g-1}	E_g	E_{g+1}
Mn(I)	-0.21427	-0.18916	-0.08366	-0.07485	0.683	2.871	0.240
Tc(I)	-0.21984	-0.18529	-0.12010	-0.09177	0.940	1.774	0.771
Re(I)	-0.23494	-0.18704	-0.11941	-0.09599	1.303	1.840	0.637

In Figure C.46 the graph of the molecular orbital energies of the group 7 metals for trifluoroacetylactonato ligands are displayed with the corresponding values in Table C.4.6, also included in the table are the energy gap values. The HOMO-1 molecular energies differ by *ca.* 2.07 x 10^{-2} Hartree using manganese and rhenium energies, an average value for E_{g-1} of 0.976 eV was obtained. The HOMO molecular energies differ by *ca.* 3.87 x 10^{-3} Hartree using manganese and technetium with an average value for E_g of 2.162 eV. The LUMO molecular energies differ by *ca.* 3.64 x 10^{-2} Hartree between manganese and technetium with the E_{g+1} energy average found to be 0.549 eV. Lastly the LUMO+1 molecular energies vary by *ca.* 2.11 x 10^{-2} Hartree between iron and osmium. The molecular orbital energies display a similar pattern to the acetylacetonato complexes with the average energy gaps E_{g-1}, E_g being comparable whilst E_{g+1} was observed as being 0.5 eV lower than for the acetylacetonato complexes. The larger E_g value for manganese as opposed to those of both technetium and rhenium result in a higher stability for the manganese complexes. This pattern of manganese having a larger E_g value is linked to the pattern seen for the

covalent radii of the group 7 metals (see Table 12.1 or Table 2.2) in which manganese has the smallest value whilst technetium and rhenium differ only marginally.

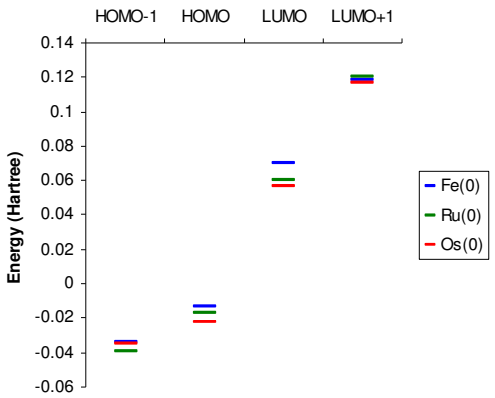

Figure C.47 Graph of the Molecular Orbital Energies of the [M(cod)(tfacac)] M = Fe(0), Ru(0), Os(0).

Table C.4.7 Molecular Orbital Energies (Hartree) and energy gaps (eV) of the [M(cod)(tfacac)] calculated structures.

	HOMO-1	HOMO	LUMO	LUMO+1	E_{g-1}	E_g	E_{g+1}
Fe(0)	-0.03413	-0.01331	0.06965	0.11841	0.567	2.257	1.327
Ru(0)	-0.03893	-0.01728	0.06037	0.12038	0.589	2.113	1.633
Os(0)	-0.03528	-0.02214	0.05647	0.11685	0.358	2.139	1.643

In Figure C.47 the graph of the molecular orbital energies of the group 8 metals for trifluoroacetylactonato ligands are displayed with the corresponding values in Table C.4.7, also included in the table are the energy gap values. The HOMO-1 molecular energies differ by *ca.* 4.8 x 10^{-3} Hartree using ruthenium and iron energies, an average value for E_{g-1} of 0.504 eV was obtained. The HOMO molecular energies differ by *ca.* 8.83 x 10^{-3} Hartree using iron and osmium with an average value for E_g of 2.17 eV. The LUMO molecular energies differ by *ca.* 1.32 x 10^{-2} Hartree between iron and osmium with the E_{g+1} energy average found to be 1.534 eV. Lastly the LUMO+1 molecular energies vary by *ca.* 3.53 x 10^{-3} Hartree between ruthenium and osmium. The E_g for the trifluoroacetylactonato group 8 metals is smaller than that found for the corresponding acetylacetonato complexes. In the LUMO+1 molecular orbitals a d_{xz} orbital is observed for all group metals leading to two vacant sites on the metal centre, which are known for forming five co-ordinate or octahedral complexes.

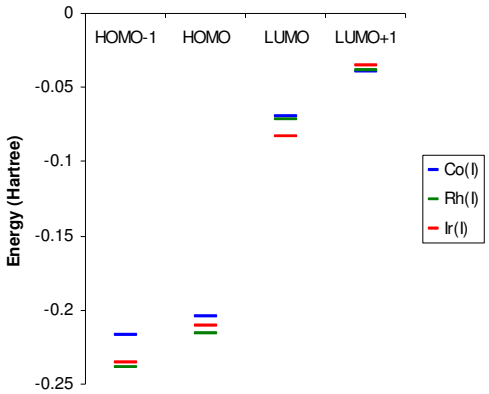

Figure C.48 Graph of the Molecular Orbital Energies of the [M(cod)(tfacac)] M = Co(I), Rh(I), Ir(I).

Table C.4.8 Molecular Orbital Energies (Hartree) and energy gaps (eV) of the [M(cod)(tfacac)] calculated structures.

	HOMO-1	HOMO	LUMO	LUMO+1	E_{g-1}	E_g	E_{g+1}
Co(I)	-0.21678	-0.20386	-0.06975	-0.03921	0.352	3.649	0.831
Rh(I)	-0.23809	-0.21609	-0.07161	-0.03822	0.599	3.932	0.909
Ir(I)	-0.23516	-0.2101	-0.08299	-0.03560	0.682	3.459	1.290

In Figure C.48 the graph of the molecular orbital energies of the group 9 metals for trifluoroacetylactonato ligands are displayed with the corresponding values in Table C.4.8, also included in the table are the energy gap values. The HOMO-1 molecular energies differ by *ca.* 2.13 x 10^{-2} Hartree using cobalt and rhodium energies, an average value for E_{g-1} of 0.544 eV was obtained. The HOMO molecular energies differ by *ca.* 1.22 x 10^{-2} Hartree again using cobalt and rhodium with an average value for E_g of 3.68 eV. The LUMO molecular energies differ by *ca.* 1.32 x 10^{-2} Hartree between cobalt and iridium with the E_{g+1} energy average found to be 1.01 eV. Lastly the LUMO+1 molecular energies vary by *ca.* 3.61 x 10^{-3} Hartree between cobalt and iridium. The molecular orbital energies seen in Figure C.48 display a similar pattern to the acetylacetonato complexes with the energy gaps E_{g-1}, E_g and E_{g+1} being comparable.

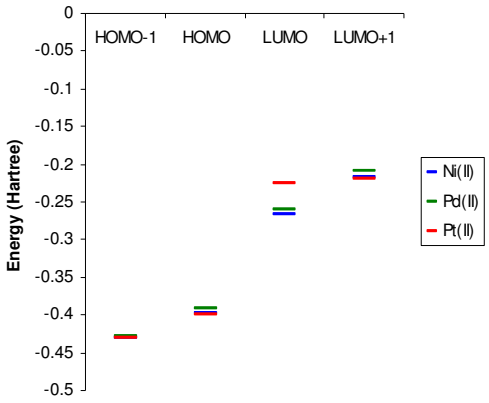

Figure C.49 Graph of the Molecular Orbital Energies of the [M(cod)(tfacac)] M = Ni(II), Pd(II), Pt(II).

Table C.4.9 Molecular Orbital Energies (Hartree) and energy gaps (eV) of the [M(cod)(tfacac)] calculated structures.

	HOMO-1	HOMO	LUMO	LUMO+1	E_{g-1}	E_g	E_{g+1}
Ni(II)	-0.43120	-0.39845	-0.26550	-0.21647	0.891	3.618	1.334
Pd(II)	-0.42921	-0.39186	-0.26038	-0.20955	1.016	3.578	1.383
Pt(II)	-0.43061	-0.39882	-0.22539	-0.21889	0.865	4.719	0.177

In Figure C.49 the graph of the molecular orbital energies of the group 10 metals for trifluoroacetylactonato ligands are displayed with the corresponding values in Table C.4.9, also included in the table are the energy gap values. The HOMO-1 molecular energies differ by *ca.* 1.99 x 10^{-3} Hartree using palladium and nickel energies, an average value for E_{g-1} of 0.924 eV was obtained. The HOMO molecular energies differ by *ca.* 6.96 x 10^{-3} Hartree using palladium and platinum with an average value for E_g of 3.972 eV. The LUMO molecular energies differ by *ca.* 4.01 x 10^{-2} Hartree between platinum and nickel with the E_{g+1} energy average found to be 0.965 eV. Lastly the LUMO+1 molecular energies vary by *ca.* 9.34 x 10^{-3} Hartree between palladium and platinum. The pattern generated here is the same as that for the acetylacetonato complexes seen previously, with the a difference in the average E_g of 0.1 eV.

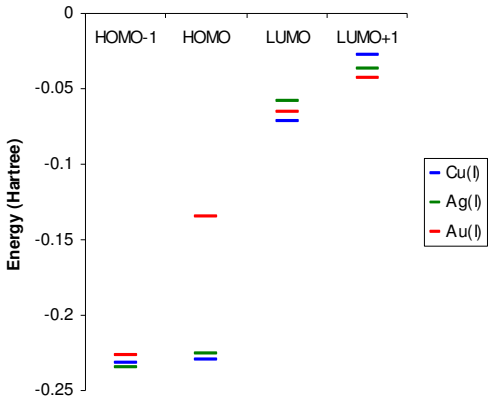

Figure C.50 Graph of the Molecular Orbital Energies of the [M(cod)(tfacac)] M = Cu(I), Ag(I), Au(I).

Table C.4.10 Molecular Orbital Energies (Hartree) and energy gaps (eV) of the [M(cod)(tfacac)] calculated structures.

	HOMO-1	HOMO	LUMO	LUMO+1	E_{g-1}	E_g	E_{g+1}
Cu(I)	-0.23134	-0.22934	-0.07155	-0.02734	0.054	4.294	1.203
Ag(I)	-0.23476	-0.22546	-0.05830	-0.03648	0.253	4.549	0.594
Au(I)	-0.22696	-0.13453	-0.06555	-0.04247	2.515	1.877	0.628

In Figure C.50 the graph of the molecular orbital energies of the group 11 metals for trifluoroacetylactonato ligands are displayed with the corresponding values in Table C.4.10, also included in the table are the energy gap values. The HOMO-1 molecular energies differ by *ca.* 7.8 x 10^{-3} Hartree using gold and silver energies, an average value for E_{g-1} of 0.941 eV was obtained. The HOMO molecular energies differ by *ca.* 9.48 x 10^{-2} Hartree using gold and copper with an average value for E_g of 3.573 eV. The LUMO molecular energies differ by *ca.* 1.33 x 10^{-2} Hartree between silver and copper with the E_{g+1} energy average found to be 0.808 eV. Lastly the LUMO+1 molecular energies vary by *ca.* 1.51 x 10^{-2} Hartree between copper and gold. In comparing the E_g energies for the acetylacetonato complexes we find a drop in energy for the trifluoroacetylacetonato complexes with a difference of 1.3 eV, leading to less stable trifluoroacetylacetonato complexes. It is also interesting to note that the HOMO energy of gold is significantly larger than for the other metals of the group the reason for this deviation is still unknown at this point in the study.

C.4.3 Group 7-11 Transition Metal Hexafluoroacetylacetonato Complexes Molecular Orbital Energies

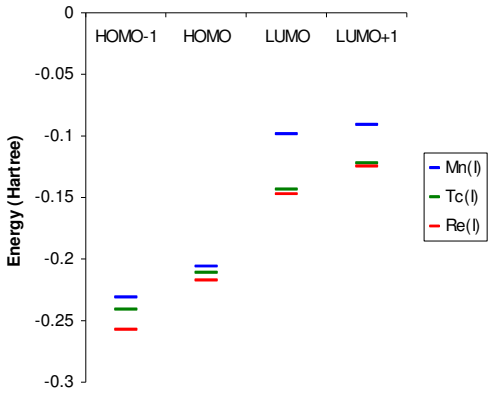

Figure C.51 Graph of the Molecular Orbital Energies of the [M(cod)(hfacac)] M = Mn(I), Tc(I), Re(I).

Table C.4.11 Molecular Orbital Energies (Hartree) and energy gaps (eV) of the [M(cod)(hfacac)] calculated structures.

	HOMO-1	HOMO	LUMO	LUMO+1	E_{g-1}	E_g	E_{g+1}
Mn(I)	-0.23158	-0.20578	-0.09910	-0.09165	0.702	2.903	0.203
Tc(I)	-0.24094	-0.21151	-0.14391	-0.12275	0.801	1.839	0.576
Re(I)	-0.25700	-0.21761	-0.14712	-0.12550	1.072	1.918	0.588

The molecular orbital energies of the group 7 metal complexes are presented in Figure C.51. The energy gaps for the hfacac molecular energies compare favorably with those of the tfacac molecular energies. The molecular orbital energy diagrams also have a similar pattern. For the LUMO and LUMO+1 molecular energies it was found that the pattern observed is comparable with the pattern observed for the tfacac molecular energies. The HOMO-1 molecular energies differ by *ca.* 0.03 Hartree using manganese and rhenium energies, an average value for E_{g-1} of 0.86 eV was obtained. The HOMO molecular energies differ by *ca.* 0.01 Hartree again using manganese and rhenium. An average value for E_g of 2.2 eV was obtained which is identical to the value obtained for the tfacac complexes leading to the conclusion that the additional electron withdrawing CF_3 group do not feature as greatly as originally anticipated. The LUMO molecular energies differ by *ca.* 0.05 Hartree between manganese and rhenium with the E_{g+1} energy average found to be 0.46 eV with manganese being far lower than either technetium or rhenium. This difference is the result of the lack of a d_{z^2} orbital on the manganese metal centre making a

neucleophilic attack on the metal more unlikely. But with the lower E_{g+1} gap the manganese is easily excited to the LUMO+1 where the d_{z^2} orbital is infact observed. Lastly the low LUMO+1 molecular energy difference of *ca.* 0.03 Hartree between the manganese and rhenium supports this hypothesis. The 2008 covalent radii for the group 7 metals (see Table 12.1 or Table 2.2) follows a similar trend with the molecular energies in that manganese is found to have the smallest radii whilst rhenium the largest.

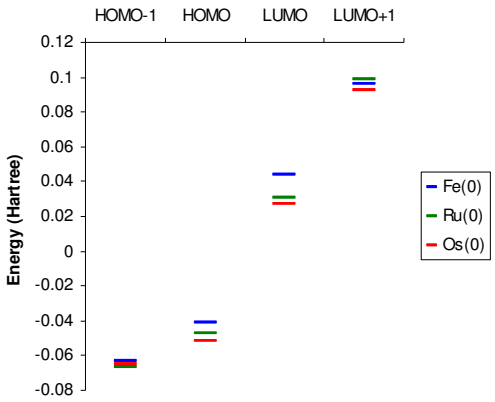

Figure C.52 Graph of the Molecular Orbital Energies of the [M(cod)(hfacac)] M = Fe(0), Ru(0), Os(0).

Table C.4.12 Molecular Orbital Energies (Hartree) and energy gaps (eV) of the [M(cod)(hfacac)] calculated structures.

	HOMO-1	HOMO	LUMO	LUMO+1	E_{g-1}	E_g	E_{g+1}
Fe(0)	-0.06342	-0.04070	0.04400	0.09620	0.618	2.305	1.420
Ru(0)	-0.06670	-0.04710	0.03025	0.09915	0.533	2.105	1.875
Os(0)	-0.06490	-0.05138	0.02674	0.09233	0.368	2.126	1.785

In Figure C.52 the graph of the molecular orbital energies of the group 8 metals for hexafluoroacetylactonato (hfacac) ligands are displayed with the corresponding values in Table C.4.12, also included in the table are the energy gap values. The HOMO-1 molecular energies differ by *ca.* 3.28 x 10^{-3} Hartree using ruthenium and iron energies, an average value for E_{g-1} of 0.506 eV was obtained. The HOMO molecular energies differ by *ca.* 1.07 x 10^{-2} Hartree using iron and osmium with an average value for E_g of 2.178 eV. The LUMO molecular energies differ by *ca.* 1.73 x 10^{-2} Hartree between iron and osmium with the E_{g+1} energy average found to be 1.693 eV. Lastly the LUMO+1 molecular energies vary by *ca.* 6.82 x 10^{-3} Hartree between ruthenium and osmium. The energy gaps for the hfacac molecular energies nearly identical to those of the tfacac molecular energies with a similar pattern being

observed for the molecular orbital energy graphs. This similarity in the energies leads to the conclusion that the additional CF_3 group again does not play a significant role in the molecular orbital energies.

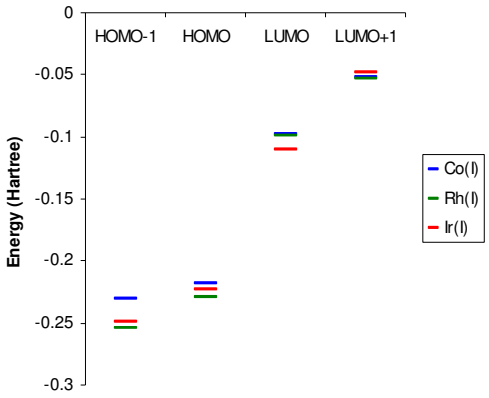

Figure C.53 Graph of the Molecular Orbital Energies of the [M(cod)(hfacac)] M = Co(I), Rh(I), Ir(I).

Table C.4.13 Molecular Orbital Energies (Hartree) and energy gaps (eV) of the [M(cod)(hfacac)] calculated structures.

	HOMO-1	HOMO	LUMO	LUMO+1	E_{g-1}	E_g	E_{g+1}
Co(I)	-0.23116	-0.21777	-0.09765	-0.05155	0.364	3.269	1.254
Rh(I)	-0.25425	-0.22933	-0.09930	-0.05364	0.678	3.538	1.242
Ir(I)	-0.24932	-0.22313	-0.11044	-0.04807	0.713	3.066	1.697

In Figure C.53 the graph of the molecular orbital energies of the group 9 metals for hexafluoroacetylactonato ligands are displayed with the corresponding values in Table C.4.13, also included in the table are the energy gap values. The HOMO-1 molecular energies differ by *ca.* 2.31 x 10^{-2} Hartree using cobalt and rhodium energies, an average value for E_{g-1} of 0.585 eV was obtained. The HOMO molecular energies differ by *ca.* 1.16 x 10^{-2} Hartree again using cobalt and rhodium with an average value for E_g of 3.291 eV. The LUMO molecular energies differ by *ca.* 1.28 x 10^{-2} Hartree between cobalt and iridium with the E_{g+1} energy average found to be 1.398 eV. Lastly the LUMO+1 molecular energies vary by *ca.* 5.57 x 10^{-3} Hartree between iridium and rhodium.

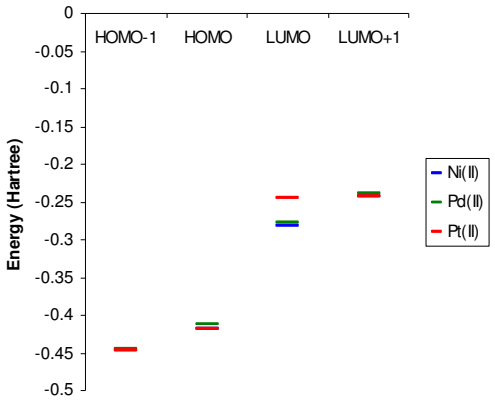

Figure C.54 Graph of the Molecular Orbital Energies of the [M(cod)(hfacac)] M = Ni(II), Pd(II), Pt(II).

Table C.4.14 Molecular Orbital Energies (Hartree) and energy gaps (eV) of the [M(cod)(hfacac)] calculated structures.

	HOMO-1	HOMO	LUMO	LUMO+1	E_{g-1}	E_g	E_{g+1}
Ni(II)	-0.44688	-0.41904	-0.28213	-0.24358	0.758	3.726	1.049
Pd(II)	-0.44519	-0.41317	-0.27726	-0.23849	0.871	3.698	1.055
Pt(II)	-0.44604	-0.41874	-0.24547	-0.24215	0.743	4.715	0.090

In Figure C.54 the graph of the molecular orbital energies of the group 10 metals for hexafluoroacetylactonato ligands are displayed with the corresponding values in Table C.4.14, also included in the table are the energy gap values. The HOMO-1 molecular energies differ by *ca.* 1.69 x 10^{-3} Hartree using palladium and nickel energies, an average value for E_{g-1} of 0.791 eV was obtained. The HOMO molecular energies differ by *ca.* 5.87 x 10^{-3} Hartree again using palladium and nickel with an average value for E_g of 4.046 eV. The LUMO molecular energies differ by *ca.* 3.67 x 10^{-2} Hartree between platinum and nickel with the E_{g+1} energy average found to be 0.731 eV. Lastly the LUMO+1 molecular energies vary by *ca.* 5.09 x 10^{-3} Hartree between palladium and platinum.

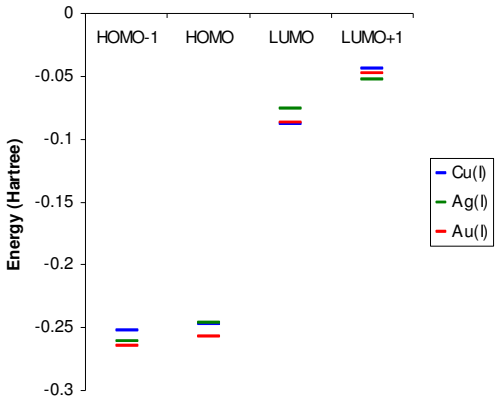

Figure C.55 Graph of the Molecular Orbital Energies of the [M(cod)(hfacac)] M = Cu(I), Ag(I), Au(I).

Table C.4.15 Molecular Orbital Energies (Hartree) and energy gaps (eV) of the [M(cod)(hfacac)] calculated structures.

	HOMO-1	HOMO	LUMO	LUMO+1	E_{g-1}	E_g	E_{g+1}
Cu(I)	-0.25267	-0.24765	-0.08765	-0.04372	0.137	4.354	1.195
Ag(I)	-0.26026	-0.24607	-0.07579	-0.05214	0.386	4.634	0.644
Au(I)	-0.26423	-0.25683	-0.08729	-0.04729	0.201	4.613	1.088

In Figure C.55 the graph of the molecular orbital energies of the group 11 metals for hexafluoroacetylactonato (hfacac) ligands are displayed with the corresponding values in Table C.4.15, also included in the table are the energy gap values. The HOMO-1 molecular energies differ by *ca.* 1.16 x 10^{-2} Hartree using copper and silver energies, an average value for E_{g-1} of 0.241 eV was obtained. The HOMO molecular energies differ by *ca.* 1.08 x 10^{-2} Hartree using gold and copper with an average value for E_g of 4.534 eV. The LUMO molecular energies differ by *ca.* 1.19 x 10^{-2} Hartree between silver and copper with the E_{g+1} energy average found to be 0.976 eV. Lastly the LUMO+1 molecular energies vary by *ca.* 8.42 x 10^{-3} Hartree between copper and silver.

C.4.4 Group 7-11 Transition Metal 4-Aminopent-3-en-2-onato Complexes Molecular Orbital Energies

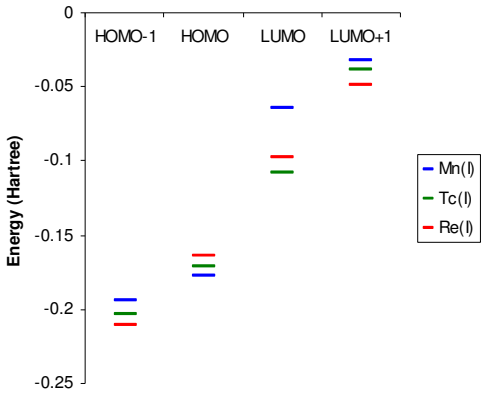

Figure C.56 Graph of the Molecular Orbital Energies of the [M(cod)(NH-acac)] M = Mn(I), Tc(I), Re(I).

Table C.4.16 Molecular Orbital Energies (Hartree) and energy gaps (eV) of the [M(cod)(NH-acac)] calculated structures.

	HOMO-1	HOMO	LUMO	LUMO+1	E_{g-1}	E_g	E_{g+1}
Mn(I)	-0.19394	-0.17725	-0.06413	-0.03232	0.454	3.078	0.866
Tc(I)	-0.20340	-0.17122	-0.10739	-0.03797	0.876	1.737	1.889
Re(I)	-0.21085	-0.16348	-0.09782	-0.04834	1.289	1.787	1.346

In Figure C.56 the graph of the molecular orbital energies of the group 7 metals for 4-aminopent-3-en-2-onato (NH-acac) ligands are displayed with the corresponding values in Table C.4.16, also included in the table are the energy gap values. The HOMO-1 molecular energies differ by *ca.* 1.69 x 10^{-2} Hartree using manganese and rhenium energies, an average value for E_{g-1} of 0.873 eV was obtained. The HOMO molecular energies differ by *ca.* 1.38 x 10^{-2} Hartree again using rhenium and manganese with an average value for E_g of 2.201 eV. The LUMO molecular energies differ by *ca.* 4.33 x 10^{-2} Hartree between manganese and technetium with the E_{g+1} energy average found to be 1.367 eV. Lastly the LUMO+1 molecular energies vary by *ca.* 1.6 x 10^{-2} Hartree between manganese and rhenium.

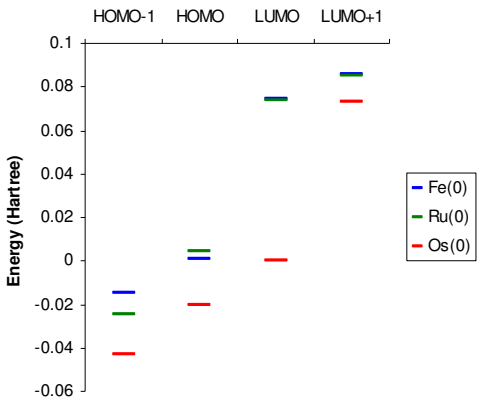

Figure C.57 Graph of the Molecular Orbital Energies of the [M(cod)(NH-acac)] M = Fe(0), Ru(0), Os(0).

Table C.4.17 Molecular Orbital Energies (Hartree) and energy gaps (eV) of the [M(cod)(NH-acac)] calculated structures.

	HOMO-1	HOMO	LUMO	LUMO+1	E_{g-1}	E_g	E_{g+1}
Fe(0)	-0.01438	0.00113	0.07470	0.08602	0.422	2.002	0.308
Ru(0)	-0.02485	0.00425	0.07363	0.08548	0.792	1.888	0.322
Os(0)	-0.04307	-0.02008	0.00015	0.07297	0.626	0.550	1.982

In Figure C.57 the graph of the molecular orbital energies of the group 8 metals for 4-aminopent-3-en-2-onato (NH-acac) ligands are displayed with the corresponding values in Table C.4.17, also included in the table are the energy gap values. The HOMO-1 molecular energies differ by *ca.* 2.87 x 10^{-2} Hartree using iron and osmium energies, an average value for E_{g-1} of 0.613 eV was obtained. The HOMO molecular energies differ by *ca.* 2.43 x 10^{-2} Hartree using ruthenium and osmium with an average value for E_g of 1.48 eV. The LUMO molecular energies differ by *ca.* 7.46 x 10^{-2} Hartree between iron and osmium with the E_{g+1} energy average found to be 0.871 eV. Lastly the LUMO+1 molecular energies vary by *ca.* 1.31 x 10^{-2} Hartree between iron and osmium.

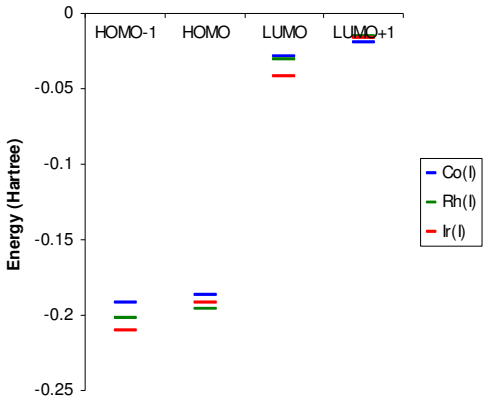

Figure C.58 Graph of the Molecular Orbital Energies of the [M(cod)(NH-acac)] M = Co(I), Rh(I), Ir(I).

Table C.4.18 Molecular Orbital Energies (Hartree) and energy gaps (eV) of the [M(cod)(NH-acac)] calculated structures.

	HOMO-1	HOMO	LUMO	LUMO+1	E_{g-1}	E_g	E_{g+1}
Co(I)	-0.19225	-0.18684	-0.02908	-0.01906	0.147	4.293	0.273
Rh(I)	-0.20253	-0.19633	-0.03046	-0.01570	0.169	4.514	0.402
Ir(I)	-0.21048	-0.19174	-0.04176	-0.01653	0.510	4.081	0.687

In Figure C.58 the graph of the molecular orbital energies of the group 9 metals for 4-aminopent-3-en-2-onato (NH-acac) ligands are displayed with the corresponding values in Table C.4.18, also included in the table are the energy gap values. The HOMO-1 molecular energies differ by *ca.* 1.82 x 10^{-2} Hartree using cobalt and iridium energies, an average value for E_{g-1} of 0.275 eV was obtained. The HOMO molecular energies differ by *ca.* 9.49 x 10^{-3} Hartree using cobalt and rhodium with an average value for E_g of 4.296 eV. The LUMO molecular energies differ by *ca.* 1.27 x 10^{-2} Hartree between cobalt and iridium with the E_{g+1} energy average found to be 0.454 eV. Lastly the LUMO+1 molecular energies vary by *ca.* 3.36 x 10^{-3} Hartree between rhodium and cobalt.

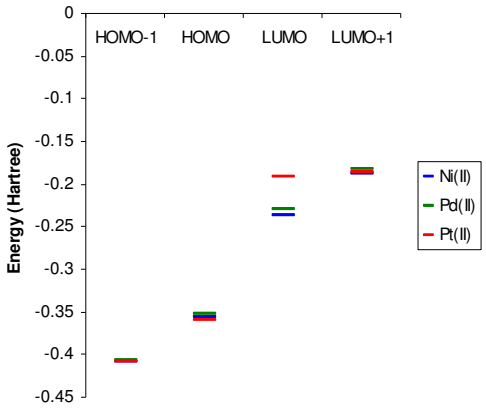

Figure C.59 Graph of the Molecular Orbital Energies of the [M(cod)(NH-acac)] M = Ni(II), Pd(II), Pt(II).

Table C.4.19 Molecular Orbital Energies (Hartree) and energy gaps (eV) of the [M(cod)(NH-acac)] calculated structures.

	HOMO-1	HOMO	LUMO	LUMO+1	E_{g-1}	E_g	E_{g+1}
Ni(II)	-0.40893	-0.35676	-0.23603	-0.18798	1.420	3.278	1.315
Pd(II)	-0.40619	-0.35328	-0.22951	-0.18299	1.440	3.368	1.266
Pt(II)	-0.40810	-0.35924	-0.19246	-0.18616	1.330	4.538	0.171

In Figure C.42 the graph of the molecular orbital energies of the group 10 metals for 4-aminopent-3-en-2-onato (NH-acac) ligands are displayed with the corresponding values in Table C.4.19, also included in the table are the energy gap values. The HOMO-1 molecular energies differ by *ca.* 2.74 x 10^{-3} Hartree using palladium and nickel energies, an average value for E_{g-1} of 1.396 eV was obtained. The HOMO molecular energies differ by *ca.* 5.96 x 10^{-3} Hartree using palladium and platinum with an average value for E_g of 3.728 eV. The LUMO molecular energies differ by *ca.* 4.38 x 10^{-2} Hartree between platinum and nickel with the E_{g+1} energy average found to be 0.917 eV. Lastly the LUMO+1 molecular energies vary by *ca.* 4.99 x 10^{-3} Hartree between palladium and platinum.

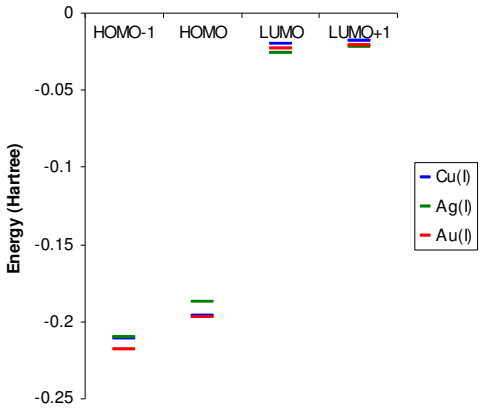

Figure C.60 Graph of the Molecular Orbital Energies of the [M(cod)(NH-acac)] M = Cu(I), Ag(I), Au(I).

Table C.4.20 Molecular Orbital Energies (Hartree) and energy gaps (eV) of the [M(cod)(NH-acac)] calculated structures.

	HOMO-1	HOMO	LUMO	LUMO+1	E_{g-1}	E_g	E_{g+1}
Cu(I)	-0.21077	-0.19608	-0.02006	-0.01749	0.400	4.790	0.070
Ag(I)	-0.21034	-0.18701	-0.02637	-0.02181	0.635	4.371	0.124
Au(I)	-0.21852	-0.19768	-0.02264	-0.02064	0.567	4.763	0.054

In Figure C.60 the graph of the molecular orbital energies of the group 8 metals for 4-aminopent-3-en-2-onato (NH-acac) ligands are displayed with the corresponding values in Table C.4.20, also included in the table are the energy gap values. The HOMO-1 molecular energies differ by *ca.* 8.18 x 10^{-3} Hartree using silver and gold energies, an average value for E_{g-1} of 0.534 eV was obtained. The HOMO molecular energies differ by *ca.* 1.07 x 10^{-2} Hartree again using silver and gold with an average value for E_g of 4.641 eV. The LUMO molecular energies differ by *ca.* 6.31 x 10^{-3} Hartree between copper and silver with the E_{g+1} energy average found to be 0.083 eV. Lastly the LUMO+1 molecular energies vary by *ca.* 4.32 x 10^{-3} Hartree between copper and silver.

C.4.5 Group 7-11 Transition Metal 4-(Methylamino)pent-3-en-2-onato Complexes Molecular Orbital Energies

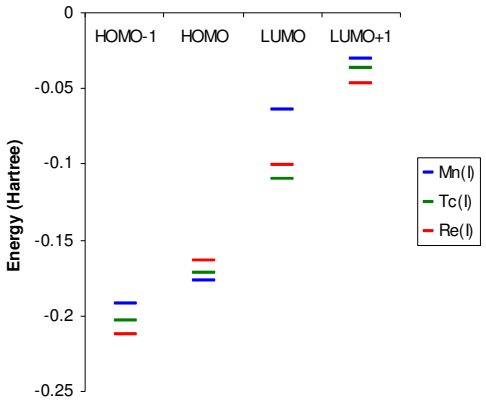

Figure C.61 Graph of the Molecular Orbital Energies of the [M(cod)(NMe-acac)] M = Mn(I), Tc(I), Re(I).

Table C.4.21 Molecular Orbital Energies (Hartree) and energy gaps (eV) of the [M(cod)(NMe-acac)] calculated structures.

	HOMO-1	HOMO	LUMO	LUMO+1	E_{g-1}	E_g	E_{g+1}
Mn(I)	-0.19218	-0.17730	-0.06388	-0.03029	0.405	3.086	0.914
Tc(I)	-0.20321	-0.17133	-0.10931	-0.03658	0.867	1.688	1.979
Re(I)	-0.21212	-0.16401	-0.10016	-0.04665	1.309	1.737	1.456

In Figure C.61 the graph of the molecular orbital energies of the group 7 metals for 4-(methylamino)pent-3-en-2-onato (NMe-acac) ligands are displayed with the corresponding values in Table C.4.21, also included in the table are the energy gap values. The HOMO-1 molecular energies differ by *ca.* 1.99 x 10^{-2} Hartree using manganese and rhenium energies, an average value for E_{g-1} of 0.861 eV was obtained. The HOMO molecular energies differ by *ca.* 1.33 x 10^{-2} Hartree again using manganese and rhenium with an average value for E_g of 2.17 eV. The LUMO molecular energies differ by *ca.* 4.54 x 10^{-2} Hartree between manganese and technetium with the E_{g+1} energy average found to be 1.45 eV. Lastly the LUMO+1 molecular energies vary by *ca.* 1.64 x 10^{-2} Hartree between manganese and rhenium.

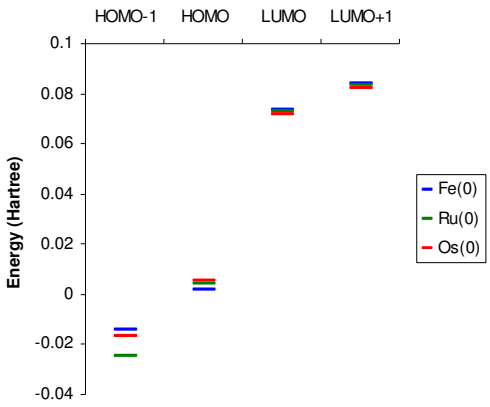

Figure C.62 Graph of the Molecular Orbital Energies of the [M(cod)(NMe-acac)] M = Fe(0), Ru(0), Os(0).

Table C.4.22 Molecular Orbital Energies (Hartree) and energy gaps (eV) of the [M(cod)(NMe-acac)] calculated structures.

	HOMO-1	HOMO	LUMO	LUMO+1	E_{g-1}	E_g	E_{g+1}
Fe(0)	-0.01399	0.00161	0.07367	0.08405	0.424	1.961	0.282
Ru(0)	-0.02464	0.00443	0.07287	0.08339	0.791	1.862	0.286
Os(0)	-0.01659	0.00536	0.07178	0.08201	0.597	1.807	0.278

In Figure C.62 the graph of the molecular orbital energies of the group 8 metals for 4-(methylamino)pent-3-en-2-onato (NMe-acac) ligands are displayed with the corresponding values in Table C.4.22, also included in the table are the energy gap values. The HOMO-1 molecular energies differ by *ca.* 1.07 x 10^{-2} Hartree using iron and ruthenium energies, an average value for E_{g-1} of 0.604 eV was obtained. The HOMO molecular energies differ by *ca.* 3.75 x 10^{-3} Hartree using iron and osmium with an average value for E_g of 1.877 eV. The LUMO molecular energies differ by *ca.* 1.89 x 10^{-3} Hartree between iron and osmium with the E_{g+1} energy average found to be 0.282 eV. Lastly the LUMO+1 molecular energies vary by *ca.* 2.04 x 10^{-3} Hartree between iron and osmium.

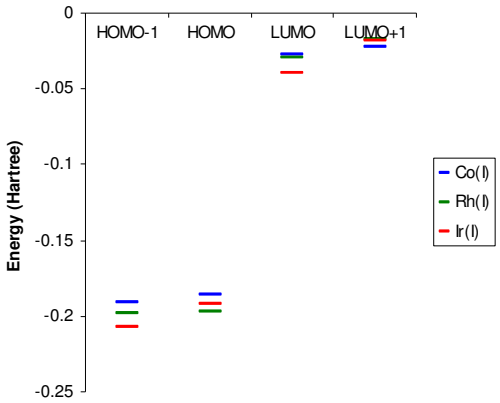

Figure C.63 Graph of the Molecular Orbital Energies of the [M(cod)(NMe-acac)] M = Co(I), Rh(I), Ir(I).

Table C.4.23 Molecular Orbital Energies (Hartree) and energy gaps (eV) of the [M(cod)(NMe-acac)] calculated structures.

	HOMO-1	HOMO	LUMO	LUMO+1	E_{g-1}	E_g	E_{g+1}
Co(I)	-0.19055	-0.18605	-0.02729	-0.02219	0.122	4.320	0.139
Rh(I)	-0.19859	-0.19683	-0.02942	-0.01771	0.048	4.555	0.319
Ir(I)	-0.20732	-0.19196	-0.03996	-0.01784	0.418	4.136	0.602

In Figure C.63 the graph of the molecular orbital energies of the group 9 metals for 4-(methylamino)pent-3-en-2-onato (NMe-acac) ligands are displayed with the corresponding values in Table C.4.23, also included in the table are the energy gap values. The HOMO-1 molecular energies differ by *ca.* 1.68 x 10^{-2} Hartree using cobalt and iridium energies, an average value for E_{g-1} of 0.196 eV was obtained. The HOMO molecular energies differ by *ca.* 1.08 x 10^{-2} Hartree using cobalt and rhodium with an average value for E_g of 4.337 eV. The LUMO molecular energies differ by *ca.* 1.27 x 10^{-2} Hartree between cobalt and iridium with the E_{g+1} energy average found to be 0.353 eV. Lastly the LUMO+1 molecular energies vary by *ca.* 4.48 x 10^{-3} Hartree between rhodium and cobalt.

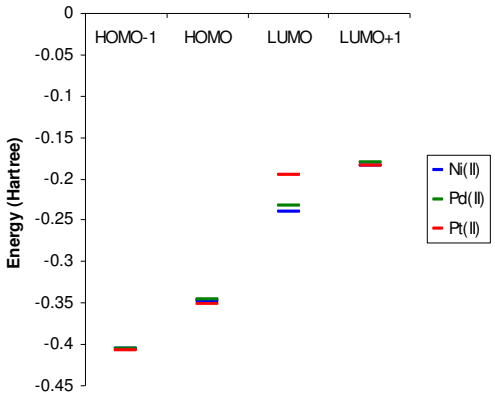

Figure C.64 Graph of the Molecular Orbital Energies of the [M(cod)(NMe-acac)] M = Ni(II), Pd(II), Pt(II).

Table C.4.24 Molecular Orbital Energies (Hartree) and energy gaps (eV) of the [M(cod)(NMe-acac)] calculated structures.

	HOMO-1	HOMO	LUMO	LUMO+1	E_{g-1}	E_g	E_{g+1}
Ni(II)	-0.40565	-0.34794	-0.24074	-0.18502	1.570	2.917	1.516
Pd(II)	-0.40513	-0.34509	-0.23256	-0.18095	1.634	3.062	1.404
Pt(II)	-0.40713	-0.35095	-0.19542	-0.18401	1.529	4.232	0.310

In Figure C.64 the graph of the molecular orbital energies of the group 10 metals for 4-(methylamino)pent-3-en-2-onato (NMe-acac) ligands are displayed with the corresponding values in Table C.4.24, also included in the table are the energy gap values. The HOMO-1 molecular energies differ by *ca.* 2.0 x 10^{-3} Hartree using palladium and platinum energies, an average value for E_{g-1} of 1.578 eV was obtained. The HOMO molecular energies differ by *ca.* 5.86 x 10^{-3} Hartree using palladium and nickel with an average value for E_g of 3.404 eV. The LUMO molecular energies differ by *ca.* 4.53 x 10^{-2} Hartree between platinum and nickel with the E_{g+1} energy average found to be 1.077 eV. Lastly the LUMO+1 molecular energies vary by *ca.* 4.07 x 10^{-3} Hartree between palladium and nickel.

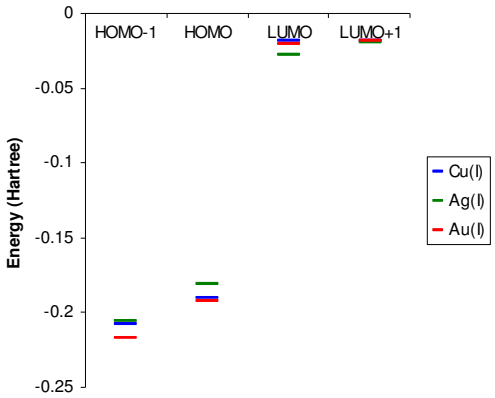

Figure C.65 Graph of the Molecular Orbital Energies of the [M(cod)(NMe-acac)] M = Cu(I), Ag(I), Au(I).

Table C.4.25 Molecular Orbital Energies (Hartree) and energy gaps (eV) of the [M(cod)(NMe-acac)] calculated structures.

	HOMO-1	HOMO	LUMO	LUMO+1	E_{g-1}	E_g	E_{g+1}
Cu(I)	-0.20778	-0.19058	-0.01881	-0.01819	0.468	4.674	0.017
Ag(I)	-0.20564	-0.18069	-0.02798	-0.01944	0.679	4.155	0.232
Au(I)	-0.21721	-0.19289	-0.02096	-0.01863	0.662	4.678	0.063

In Figure C.65 the graph of the molecular orbital energies of the group 11 metals for 4-(methylamino)pent-3-en-2-onato (NMe-acac) ligands are displayed with the corresponding values in Table C.4.25, also included in the table are the energy gap values. The HOMO-1 molecular energies differ by *ca.* 1.16 x 10^{-2} Hartree using silver and gold energies, an average value for E_{g-1} of 0.603 eV was obtained. The HOMO molecular energies differ by *ca.* 1.22 x 10^{-2} Hartree again using silver and gold with an average value for E_g of 4.503 eV. The LUMO molecular energies differ by *ca.* 9.17 x 10^{-3} Hartree between copper and silver with the E_{g+1} energy average found to be 0.104 eV. Lastly the LUMO+1 molecular energies vary by *ca.* 1.25 x 10^{-3} Hartree between silver and copper.

C.4.6 Group 7-11 Transition Metal 4-Anilinopent-3-en-2-onato Complexes Molecular Orbital Energies

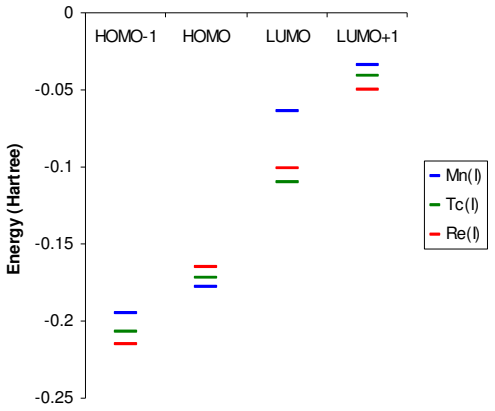

Figure C.66 Graph of the Molecular Orbital Energies of the [M(cod)(NPh-acac)] M = Mn(I), Tc(I), Re(I).

Table C.4.26 Molecular Orbital Energies (Hartree) and energy gaps (eV) of the [M(cod)(NPh-acac)] calculated structures.

	HOMO-1	HOMO	LUMO	LUMO+1	E_{g-1}	E_g	E_{g+1}
Mn(I)	-0.19463	-0.17775	-0.06438	-0.03354	0.459	3.085	0.839
Tc(I)	-0.20705	-0.17207	-0.11017	-0.04083	0.952	1.684	1.887
Re(I)	-0.21489	-0.16457	-0.10081	-0.05040	1.369	1.735	1.372

In Figure C.66 the graph of the molecular orbital energies of the group 7 metals for 4-anilinopent-3-en-2-onato (NPh-acac) ligands are displayed with the corresponding values in Table C.4.26, also included in the table are the energy gap values. The HOMO-1 molecular energies differ by *ca.* 2.03 x 10^{-2} Hartree using manganese and rhenium energies, an average value for E_{g-1} of 0.927 eV was obtained. The HOMO molecular energies differ by *ca.* 1.32 x 10^{-2} Hartree again using rhenium and manganese with an average value for E_g of 2.168 eV. The LUMO molecular energies differ by *ca.* 4.58 x 10^{-2} Hartree between manganese and technetium with the E_{g+1} energy average found to be 1.366 eV. Lastly the LUMO+1 molecular energies vary by *ca.* 1.69 x 10^{-2} Hartree between manganese and rhenium.

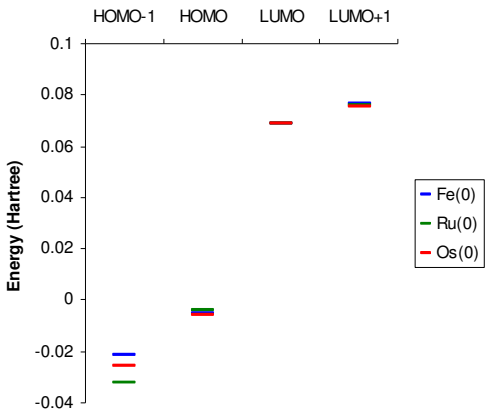

Figure C.67 Graph of the Molecular Orbital Energies of the [M(cod)(NPh-acac)] M = Fe(0), Ru(0), Os(0).

Table C.4.27 Molecular Orbital Energies (Hartree) and energy gaps (eV) of the [M(cod)(NPh-acac)] calculated structures.

	HOMO-1	HOMO	LUMO	LUMO+1	E_{g-1}	E_g	E_{g+1}
Fe(0)	-0.02131	-0.00494	0.06888	0.07660	0.445	2.009	0.210
Ru(0)	-0.03231	-0.00390	0.06878	0.07586	0.773	1.978	0.193
Os(0)	-0.02585	-0.00551	0.06873	0.07514	0.553	2.020	0.174

In Figure C.67 the graph of the molecular orbital energies of the group 8 metals for 4-anilinopent-3-en-2-onato (NPh-acac)ligands are displayed with the corresponding values in Table C.4.27, also included in the table are the energy gap values. The HOMO-1 molecular energies differ by *ca.* 1.1 x 10^{-2} Hartree using ruthenium and iron energies, an average value for E_{g-1} of 0.591 eV was obtained. The HOMO molecular energies differ by *ca.* 1.61 x 10^{-3} Hartree using ruthenium and osmium with an average value for E_g of 2.002 eV. The LUMO molecular energies differ by *ca.* 1.5 x 10^{-4} Hartree between iron and osmium with the E_{g+1} energy average found to be 0.192 eV. Lastly the LUMO+1 molecular energies vary by *ca.* 1.46 x 10^{-3} Hartree between iron and osmium.

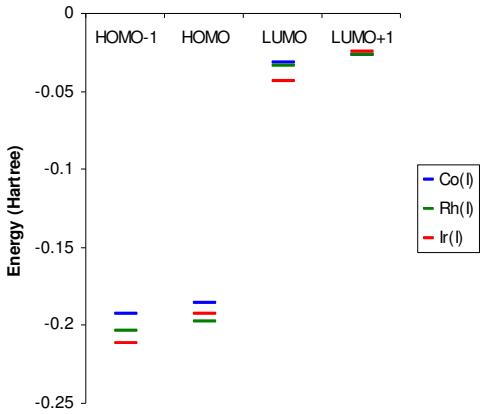

Figure C.68 Graph of the Molecular Orbital Energies of the [M(cod)(NPh-acac)] M = Co(I), Rh(I), Ir(I).

Table C.4.28 Molecular Orbital Energies (Hartree) and energy gaps (eV) of the [M(cod)(NPh-acac)] calculated structures.

	HOMO-1	HOMO	LUMO	LUMO+1	E_{g-1}	E_g	E_{g+1}
Co(I)	-0.19230	-0.18596	-0.03121	-0.02695	0.173	4.211	0.116
Rh(I)	-0.20356	-0.19744	-0.03407	-0.02644	0.167	4.446	0.208
Ir(I)	-0.21104	-0.19225	-0.04389	-0.02515	0.511	4.037	0.510

In Figure C.68 the graph of the molecular orbital energies of the group 9 metals for 4-anilinopent-3-en-2-onato (NPh-acac) ligands are displayed with the corresponding values in Table C.4.28, also included in the table are the energy gap values. The HOMO-1 molecular energies differ by *ca.* 1.87 x 10^{-2} Hartree using cobalt and iridium energies, an average value for E_{g-1} of 0.283 eV was obtained. The HOMO molecular energies differ by *ca.* 1.15 x 10^{-2} Hartree using cobalt and rhodium with an average value for E_g of 4.231 eV. The LUMO molecular energies differ by *ca.* 1.27 x 10^{-2} Hartree between cobalt and iridium with the E_{g+1} energy average found to be 0.278 eV. Lastly the LUMO+1 molecular energies vary by *ca.* 1.8 x 10^{-3} Hartree between iridium and cobalt.

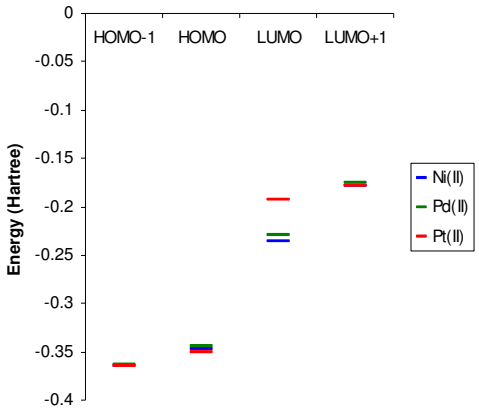

Figure C.69 Graph of the Molecular Orbital Energies of the [M(cod)(NPh-acac)] M = Ni(II), Pd(II), Pt(II).

Table C.4.29 Molecular Orbital Energies (Hartree) and energy gaps (eV) of the [M(cod)(NPh-acac)] calculated structures.

	HOMO-1	HOMO	LUMO	LUMO+1	E_{g-1}	E_g	E_{g+1}
Ni(II)	-0.36571	-0.34707	-0.23568	-0.17787	0.507	3.031	1.573
Pd(II)	-0.36325	-0.34458	-0.22880	-0.17488	0.508	3.151	1.467
Pt(II)	-0.36565	-0.35001	-0.19263	-0.17921	0.426	4.283	0.365

In Figure C.69 the graph of the molecular orbital energies of the group 10 metals for 4-anilinopent-3-en-2-onato (NPh-acac) ligands are displayed with the corresponding values in Table C.4.29, also included in the table are the energy gap values. The HOMO-1 molecular energies differ by *ca.* 2.46 x 10^{-3} Hartree using palladium and nickel energies, an average value for E_{g-1} of 0.480 eV was obtained. The HOMO molecular energies differ by *ca.* 5.43 x 10^{-3} Hartree using palladium and platinum with an average value for E_g of 3.488 eV. The LUMO molecular energies differ by *ca.* 4.31 x 10^{-2} Hartree between platinum and nickel with the E_{g+1} energy average found to be 1.135 eV. Lastly the LUMO+1 molecular energies vary by *ca.* 4.33 x 10^{-3} Hartree between palladium and platinum.

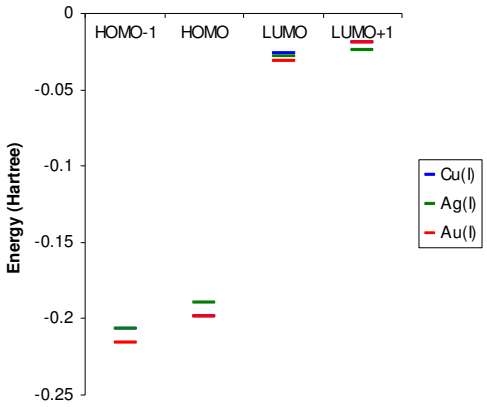

Figure C.70 Graph of the Molecular Orbital Energies of the [M(cod)(NPh-acac)] M = Cu(I), Ag(I), Au(I).

Table C.4.30 Molecular Orbital Energies (Hartree) and energy gaps (eV) of the [M(cod)(NPh-acac)] calculated structures.

	HOMO-1	HOMO	LUMO	LUMO+1	E_{g-1}	E_g	E_{g+1}
Cu(I)	-0.20650	-0.19812	-0.02643	-0.01913	0.228	4.672	0.199
Ag(I)	-0.20704	-0.18903	-0.02799	-0.02428	0.483	4.389	0.101
Au(I)	-0.21528	-0.19878	-0.03160	-0.01924	0.449	4.549	0.336

In Figure C.70 the graph of the molecular orbital energies of the group 11 metals for 4-anilinopent-3-en-2-onato (NPh-acac) ligands are displayed with the corresponding values in Table C.4.30, also included in the table are the energy gap values. The HOMO-1 molecular energies differ by *ca.* 8.78 x 10^{-3} Hartree using gold and silver energies, an average value for E_{g-1} of 0.387 eV was obtained. The HOMO molecular energies differ by *ca.* 9.48 x 10^{-3} Hartree again using silver and gold with an average value for E_g of 4.537 eV. The LUMO molecular energies differ by *ca.* 5.17 x 10^{-3} Hartree between copper and gold with the E_{g+1} energy average found to be 0.212 eV. Lastly the LUMO+1 molecular energies vary by *ca.* 5.15 x 10^{-3} Hartree between copper and silver.

C.4.7 Group 7-11 Transition Metal Tropolonato Complexes Molecular Orbital Energies

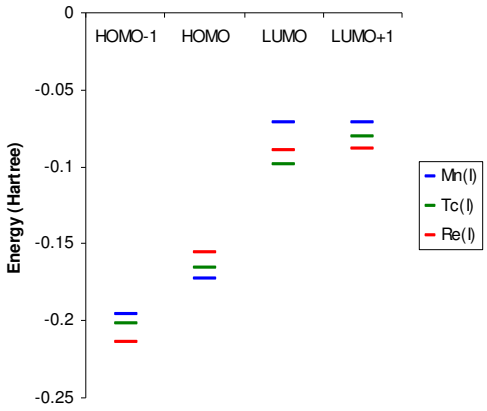

Figure C.71 Graph of the Molecular Orbital Energies of the [M(cod)(trop)] M = Mn(I), Tc(I), Re(I).

Table C.4.31 Molecular Orbital Energies (Hartree) and energy gaps (eV) of the [M(cod)(trop)] calculated structures.

	HOMO-1	HOMO	LUMO	LUMO+1	E_{g-1}	E_g	E_{g+1}
Mn(I)	-0.19541	-0.17272	-0.07123	-0.07122	0.617	2.762	2.721×10^{-4}
Tc(I)	-0.20189	-0.16578	-0.09806	-0.08014	0.983	1.843	0.488
Re(I)	-0.21389	-0.15565	-0.08968	-0.08876	1.585	1.795	0.025

In Figure C.71 the graph of the molecular orbital energies of the group 7 metals for tropolonato ligands are displayed with the corresponding values in Table C.4.31, also included in the table are the energy gap values. The HOMO-1 molecular energies differ by *ca.* 1.85×10^{-2} Hartree using manganese and rhenium energies, an average value for E_{g-1} of 1.062 eV was obtained. The HOMO molecular energies differ by *ca.* 1.71×10^{-2} Hartree again using rhenium and manganese with an average value for E_g of 2.133 eV. The LUMO molecular energies differ by *ca.* 2.68×10^{-2} Hartree between manganese and technetium with the E_{g+1} energy average found to be 0.171 eV. Lastly the LUMO+1 molecular energies vary by *ca.* 1.75×10^{-2} Hartree between manganese and rhenium.

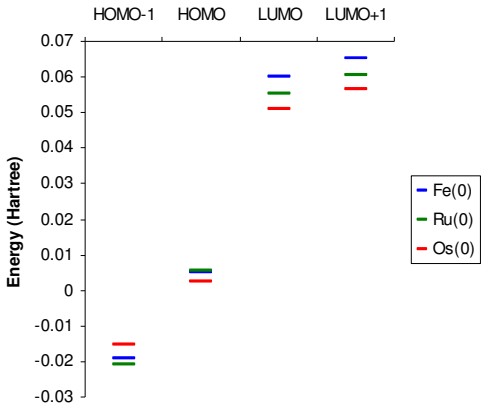

Figure C.72 Graph of the Molecular Orbital Energies of the [M(cod)(trop)] M = Fe(0), Ru(0), Os(0).

Table C.4.32 Molecular Orbital Energies (Hartree) and energy gaps (eV) of the [M(cod)(trop)] calculated structures.

	HOMO-1	HOMO	LUMO	LUMO+1	E_{g-1}	E_g	E_{g+1}
Fe(0)	-0.01911	0.00485	0.05994	0.06529	0.652	1.499	0.146
Ru(0)	-0.02104	0.00535	0.05546	0.06060	0.718	1.364	0.140
Os(0)	-0.01541	0.0025	0.05114	0.05649	0.487	1.324	0.146

In Figure C.72 the graph of the molecular orbital energies of the group 8 metals for tropolonato ligands are displayed with the corresponding values in Table C.4.32, also included in the table are the energy gap values. The HOMO-1 molecular energies differ by *ca.* 5.63 x 10^{-3} Hartree using ruthenium and osmium energies, an average value for E_{g-1} of 0.619 eV was obtained. The HOMO molecular energies differ by *ca.* 2.85 x 10^{-3} Hartree using ruthenium and osmium with an average value for E_g of 1.395 eV. The LUMO molecular energies differ by *ca.* 8.8 x 10^{-3} Hartree between iron and osmium with the E_{g+1} energy average found to be 0.144 eV. Lastly the LUMO+1 molecular energies vary by *ca.* 8.8 x 10^{-3} Hartree between iron and osmium.

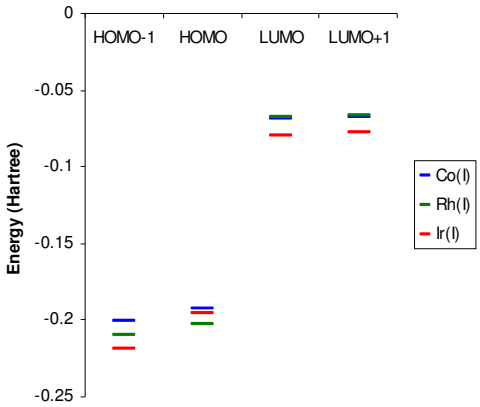

Figure C.73 Graph of the Molecular Orbital Energies of the [M(cod)(trop)] M = Co(I), Rh(I), Ir(I).

Table C.4.33 Molecular Orbital Energies (Hartree) and energy gaps (eV) of the [M(cod)(trop)] calculated structures.

	HOMO-1	HOMO	LUMO	LUMO+1	E_{g-1}	E_g	E_{g+1}
Co(I)	-0.20083	-0.19239	-0.06876	-0.06778	0.230	3.364	0.027
Rh(I)	-0.21016	-0.20272	-0.06804	-0.06689	0.202	3.665	0.031
Ir(I)	-0.21856	-0.19527	-0.07929	-0.07775	0.634	3.156	0.042

In Figure C.73 the graph of the molecular orbital energies of the group 9 metals for tropolonato ligands are displayed with the corresponding values in Table C.4.33, also included in the table are the energy gap values. The HOMO-1 molecular energies differ by *ca.* 1.77 x 10^{-2} Hartree using cobalt and iridium energies, an average value for E_{g-1} of 0.355 eV was obtained. The HOMO molecular energies differ by *ca.* 1.03 x 10^{-2} Hartree using cobalt and rhodium with an average value for E_g of 3.395 eV. The LUMO molecular energies differ by *ca.* 1.13 x 10^{-2} Hartree between rhodium and iridium with the E_{g+1} energy average found to be 0.033 eV. Lastly the LUMO+1 molecular energies vary by *ca.* 1.09 x 10^{-2} Hartree between cobalt and iridium.

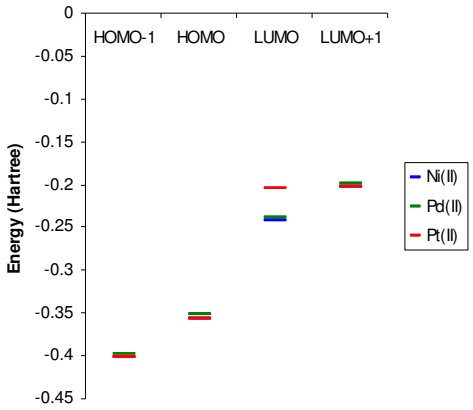

Figure C.74 Graph of the Molecular Orbital Energies of the [M(cod)(trop)] M = Ni(II), Pd(II), Pt(II).

Table C.4.34 Molecular Orbital Energies (Hartree) and energy gaps (eV) of the [M(cod)(trop)] calculated structures.

	HOMO-1	HOMO	LUMO	LUMO+1	E_{g-1}	E_g	E_{g+1}
Ni(II)	-0.40097	-0.35675	-0.24139	-0.20315	1.203	3.139	1.041
Pd(II)	-0.39855	-0.35141	-0.23860	-0.19929	1.283	3.070	1.070
Pt(II)	-0.40108	-0.35754	-0.20510	-0.20299	1.185	4.148	0.057

In Figure C.74 the graph of the molecular orbital energies of the group 10 metals for tropolonato ligands are displayed with the corresponding values in Table C.4.34, also included in the table are the energy gap values. The HOMO-1 molecular energies differ by *ca.* 2.53 x 10^{-3} Hartree using palladium and platinum energies, an average value for E_{g-1} of 1.224 eV was obtained. The HOMO molecular energies differ by *ca.* 6.13 x 10^{-3} Hartree again using palladium and platinum with an average value for E_g of 3.452 eV. The LUMO molecular energies differ by *ca.* 3.62 x 10^{-2} Hartree between platinum and nickel with the E_{g+1} energy average found to be 0.723 eV. Lastly the LUMO+1 molecular energies vary by *ca.* 3.86 x 10^{-3} Hartree between palladium and nickel.

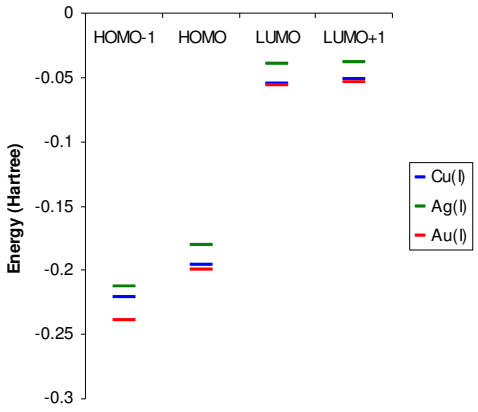

Figure C.75 Graph of the Molecular Orbital Energies of the [M(cod)(trop)] M = Cu(I), Ag(I), Au(I).

Table C.4.35 Molecular Orbital Energies (Hartree) and energy gaps (eV) of the [M(cod)(trop)] calculated structures.

	HOMO-1	HOMO	LUMO	LUMO+1	E_{g-1}	E_g	E_{g+1}
Cu(I)	-0.22140	-0.19629	-0.05473	-0.05123	0.683	3.852	0.095
Ag(I)	-0.21234	-0.18093	-0.03922	-0.03844	0.855	3.856	0.021
Au(I)	-0.23887	-0.19969	-0.05651	-0.05420	1.066	3.896	0.063

In Figure C.74 the graph of the molecular orbital energies of the group 11 metals for tropolonato ligands are displayed with the corresponding values in Table C.4.34, also included in the table are the energy gap values. The HOMO-1 molecular energies differ by *ca.* 2.65 x 10^{-2} Hartree using silver and gold energies, an average value for E_{g-1} of 0.868 eV was obtained. The HOMO molecular energies differ by *ca.* 1.88 x 10^{-2} Hartree again using silver and gold with an average value for E_g of 3.868 eV. The LUMO molecular energies differ by *ca.* 1.73 x 10^{-2} Hartree between silver and gold with the E_{g+1} energy average found to be 0.06 eV. Lastly the LUMO+1 molecular energies vary by *ca.* 1.58 x 10^{-2} Hartree between silver and gold.

C.4.8 Group 7-11 Transition Metal Tribromotropolonato Complexes Molecular Orbital Energies

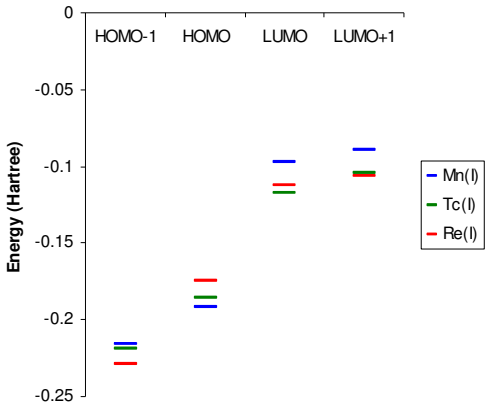

Figure C.76 Graph of the Molecular Orbital Energies of the [M(cod)(3Br-trop)] M = Mn(I), Tc(I), Re(I).

Table C.4.36 Molecular Orbital Energies (Hartree) and energy gaps (eV) of the [M(cod)(3Br-trop)] calculated structures.

	HOMO-1	HOMO	LUMO	LUMO+1	E_{g-1}	E_g	E_{g+1}
Mn(I)	-0.21546	-0.19223	-0.09722	-0.08937	0.632	2.585	0.214
Tc(I)	-0.21915	-0.18553	-0.11797	-0.10397	0.915	1.838	0.381
Re(I)	-0.22916	-0.17434	-0.11228	-0.10621	1.492	1.689	0.165

In Figure C.76 the graph of the molecular orbital energies of the group 7 metals for tribromotroplonato ligands are displayed with the corresponding values in Table C.4.36, also included in the table are the energy gap values. The HOMO-1 molecular energies differ by *ca.* 1.37 x 10^{-2} Hartree using manganese and rhenium energies, an average value for E_{g-1} of 1.013 eV was obtained. The HOMO molecular energies differ by *ca.* 1.79 x 10^{-2} Hartree again using rhenium and manganese with an average value for E_g of 2.037 eV. The LUMO molecular energies differ by *ca.* 2.08 x 10^{-2} Hartree between manganese and technetium with the E_{g+1} energy average found to be 0.253 eV. Lastly the LUMO+1 molecular energies vary by *ca.* 1.68 x 10^{-2} Hartree between manganese and rhenium.

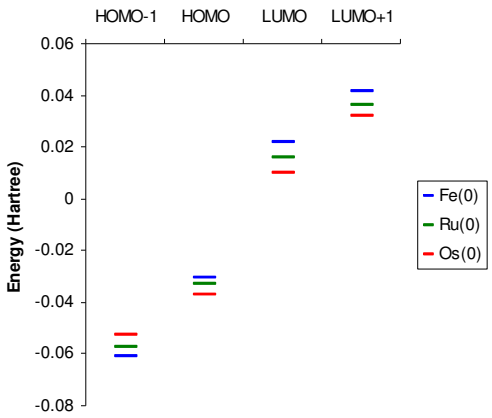

Figure C.77 Graph of the Molecular Orbital Energies of the [M(cod)(3Br-trop)] M = Fe(0), Ru(0), Os(0).

Table C.4.37 Molecular Orbital Energies (Hartree) and energy gaps (eV) of the [M(cod)(3Br-trop)] calculated structures.

	HOMO-1	HOMO	LUMO	LUMO+1	E_{g-1}	E_g	E_{g+1}
Fe(0)	-0.06070	-0.0304	0.02164	0.04145	0.825	1.416	0.539
Ru(0)	-0.05753	-0.03276	0.01583	0.03611	0.674	1.322	0.552
Os(0)	-0.05264	-0.03711	0.00973	0.03227	0.423	1.275	0.613

In Figure C.77 the graph of the molecular orbital energies of the group 8 metals for tribromotroplonato ligands are displayed with the corresponding values in Table C.4.37, also included in the table are the energy gap values. The HOMO-1 molecular energies differ by *ca.* 8.06 x 10^{-3} Hartree using osmium and iron energies, an average value for E_{g-1} of 0.64 eV was obtained. The HOMO molecular energies differ by *ca.* 6.71 x 10^{-3} Hartree again using iron and osmium with an average value for E_g of 1.338 eV. The LUMO molecular energies differ by *ca.* 1.19 x 10^{-2} Hartree between iron and osmium with the E_{g+1} energy average found to be 0.568 eV. Lastly the LUMO+1 molecular energies vary by *ca.* 9.18 x 10^{-3} Hartree between iron and osmium.

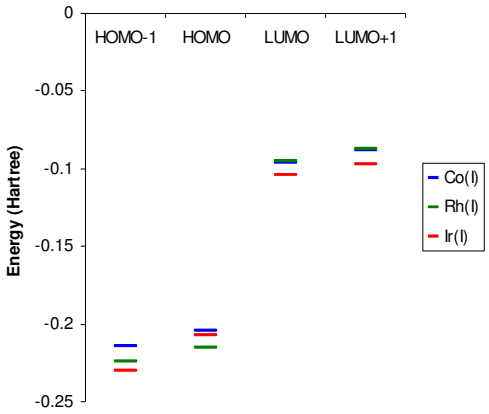

Figure C.78 Graph of the Molecular Orbital Energies of the [M(cod)(3Br-trop)] M = Co(I), Rh(I), Ir(I).

Table C.4.38 Molecular Orbital Energies (Hartree) and energy gaps (eV) of the [M(cod)(3Br-trop)] calculated structures.

	HOMO-1	HOMO	LUMO	LUMO+1	E_{g-1}	E_g	E_{g+1}
Co(I)	-0.21387	-0.20447	-0.09621	-0.08815	0.256	2.946	0.219
Rh(I)	-0.22399	-0.21566	-0.09491	-0.08681	0.227	3.286	0.220
Ir(I)	-0.23047	-0.20694	-0.10412	-0.09714	0.640	2.798	0.190

In Figure C.78 the graph of the molecular orbital energies of the group 9 metals for tribromotroplonato ligands are displayed with the corresponding values in Table C.4.38, also included in the table are the energy gap values. The HOMO-1 molecular energies differ by *ca.* 1.66 x 10^{-2} Hartree using cobalt and iridium energies, an average value for E_{g-1} of 0.374 eV was obtained. The HOMO molecular energies differ by *ca.* 1.12 x 10^{-2} Hartree using cobalt and rhodium with an average value for E_g of 3.01 eV. The LUMO molecular energies differ by *ca.* 9.21 x 10^{-3} Hartree between rhodium and iridium with the E_{g+1} energy average found to be 0.21 eV. Lastly the LUMO+1 molecular energies vary by *ca.* 1.03 x 10^{-2} Hartree between rhodium and iridium.

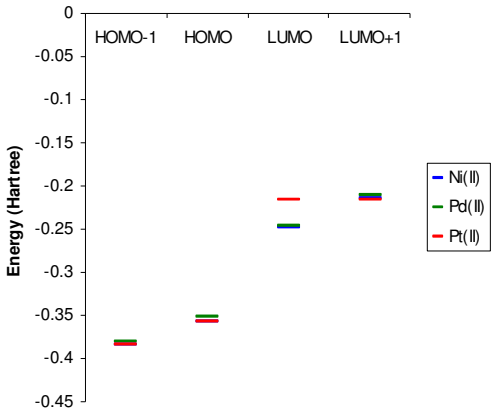

Figure C.79 Graph of the Molecular Orbital Energies of the [M(cod)(3Br-trop)] M = Ni(II), Pd(II), Pt(II).

Table C.4.39 Molecular Orbital Energies (Hartree) and energy gaps (eV) of the [M(cod)(3Br-trop)] calculated structures.

	HOMO-1	HOMO	LUMO	LUMO+1	E_{g-1}	E_g	E_{g+1}
Ni(II)	-0.38410	-0.35685	-0.24880	-0.21481	0.742	2.940	0.925
Pd(II)	-0.38007	-0.35190	-0.24708	-0.21047	0.767	2.852	0.996
Pt(II)	-0.38347	-0.35707	-0.21540	-0.21536	0.718	3.855	0.001

In Figure C.79 the graph of the molecular orbital energies of the group 10 metals for tribromotropolonato ligands are displayed with the corresponding values in Table C.4.39, also included in the table are the energy gap values. The HOMO-1 molecular energies differ by *ca.* 4.03 x 10^{-3} Hartree using palladium and platinum energies, an average value for E_{g-1} of 0.742 eV was obtained. The HOMO molecular energies differ by *ca.* 5.17 x 10^{-3} Hartree using palladium and platinum with an average value for E_g of 3.216 eV. The LUMO molecular energies differ by *ca.* 3.34 x 10^{-2} Hartree between platinum and nickel with the E_{g+1} energy average found to be 0.641 eV. Lastly the LUMO+1 molecular energies vary by *ca.* 4.89 x 10^{-3} Hartree between palladium and platinum.

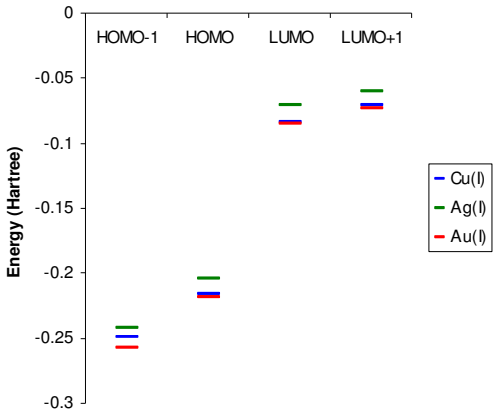

Figure C.80 Graph of the Molecular Orbital Energies of the [M(cod)(3Br-trop)] M = Cu(I), Ag(I), Au(I).

Table C.4.40 Molecular Orbital Energies (Hartree) and energy gaps (eV) of the [M(cod)(3Br-trop)] calculated structures.

	HOMO-1	HOMO	LUMO	LUMO+1	E_{g-1}	E_g	E_{g+1}
Cu(I)	-0.24891	-0.21643	-0.08435	-0.07125	0.884	3.594	0.356
Ag(I)	-0.24257	-0.20410	-0.07104	-0.06046	1.047	3.621	0.288
Au(I)	-0.25692	-0.21861	-0.08529	-0.07319	1.042	3.628	0.329

In Figure C.80 the graph of the molecular orbital energies of the group 11 metals for tribromotropolonato ligands are displayed with the corresponding values in Table C.4.40, also included in the table are the energy gap values. The HOMO-1 molecular energies differ by *ca.* 1.44 x 10^{-2} Hartree using silver and gold energies, an average value for E_{g-1} of 0.991 eV was obtained. The HOMO molecular energies differ by *ca.* 1.45 x 10^{-2} Hartree using silver and gold with an average value for E_g of 3.614 eV. The LUMO molecular energies differ by *ca.* 1.43 x 10^{-2} Hartree between silver and gold with the E_{g+1} energy average found to be 0.325 eV. Lastly the LUMO+1 molecular energies vary by *ca.* 1.27 x 10^{-2} Hartree between silver and gold.

C.5 Theoretical / Calculation Data of the Calculated Zero-point Corrected Energies

Table C.5.1 The zero-point corrected energies (E_{corr}) of the group 7-11 calculated metal complexes of the [M(cod)(LL')]A where M = group 7-11 metals, LL' = acac, tfacac, hfacac, NH-acac, NMe-acac, trop, 3Br-trop.

	E_{corr} acac	tfacac	hfacac	NH-acac	NMe-acac	NPh-acac	trop	3Br-trop
Mn(I)	761.0657	1058.537	1356.763	741.171	780.4441184	972.1819	835.7544	873.7691
Tc(I)	737.2248	1034.693	1332.441	717.3314	756.6069173	948.3444	811.915	849.9279
Re(I)	736.2476	1033.714	1331.463	716.3576	755.6318555	947.3683	810.9367	848.9502

Fe(0)	780.6439	1078.126	1375.903	760.747	800.0192409	991.7599	855.3261	893.3689
Ru(0)	751.1319	1048.608	1346.38	731.237	755.6318555	962.2556	825.8091	863.852
Os(0)	748.2892	1045.766	1343.539	728.4022	767.6773138	959.4181	822.9652	861.0099
Co(I)	802.2743	1100.125	1397.971	782.3797	821.6507599	1013.389	877.2774	914.9777
Rh(I)	766.7315	1064.581	1362.427	746.8405	786.1166462	977.8547	841.7313	879.4308
Ir(I)	761.9268	1059.775	1357.619	742.0424	781.3178185	973.0548	836.9283	874.6255
Ni(II)	826.2911	1124.127	1421.958	806.4025	845.6755252	1037.417	901.2943	938.9852
Pd(II)	783.7124	1081.548	1379.381	763.8277	803.1055925	994.8465	858.7122	896.4023
Pt(II)	776.1456	1073.981	1371.812	756.2669	795.543943	987.284	851.1489	888.8381
Cu(I)	853.3608	1150.83	1449.061	833.4636	872.7457885	1064.485	928.0461	966.0662
Ag(I)	802.9463	1100.419	1398.651	783.0478	822.3288833	1014.07	877.6296	915.6514
Au(I)	792.6254	1090	1388.325	772.7332	812.0135126	1003.752	867.3119	905.3346

C.6 Theoretical / Calculation Data of the Calculated Metal Relative Energies (E_{rel}^{M})

Table C.6.1 The metal corrected relative energies (E_{rel}^{M}) of the group 7-11 calculated metal complexes of the [M(cod)(LL')]A where M = group 7-11 metals, LL' = acac, tfacac, hfacac, NH-acac, NMe-acac, trop, 3Br-trop.

	E_{rel}^{M} acac	tfacac	hfacac	NH-acac	NMe-acac	NPh-acac	trop	3Br-trop
Mn(I)	468.23609	1063.588	66.49026	966322.6	966325.4	966321.7	893.0632	525.1409
Tc(I)	507.76535	1110.677	1368.62	966379	966375.7	966373	928.6175	565.2436
Re(I)	514.40891	1122.137	1376.495	0	0	0	938.0451	573.4044
Fe(0)	0	565.3785	748.0469	965834.3	965839.5	965828.4	441.7808	0
Ru(0)	28.960312	610.2948	806.3695	965864.2	0	965843.3	483.7777	41.93737
Os(0)	71.161283	650.0204	842.9246	965901.3	965898.9	965887.5	529.1023	82.50265
Co(I)	400.72688	0	0	966233.3	966241.4	966236.9	0	457.4182
Rh(I)	428.24028	28.65996	29.96509	966261.8	966256.7	966252.5	36.16206	495.8285
Ir(I)	466.6046	71.8573	78.20812	966298.6	966295.5	966294	70.23396	535.7083
Ni(II)	806.94105	444.8702	483.7916	966644.8	966648	966634.4	406.0207	888.2533
Pd(II)	822.38949	459.2445	496.5571	966660.7	966651.2	966639.4	430.2338	914.5359
Pt(II)	844.39485	482.9903	522.8202	966648.1	966640.7	966631.3	443.0024	929.7105

C.7 Theoretical / Calculation Data of the Calculated Ligand Relative Energies (E_{rel}^{L})

Table C.7.1 The ligand corrected relative energies (E_{rel}^{L}) of the group 7-11 calculated metal complexes of the [M(cod)(LL')]A where M = group 7-11 metals, LL' = acac, tfacac, hfacac, NH-acac, NMe-acac, trop, 3Br-trop.

	E_{rel}^{L} acac	tfacac	hfacac	NH-acac	NMe-acac	NPh-acac	trop	3Br-trop
Mn(I)	242320.6	242317.2	242329.6	242314.3	242338.0116	242342.4	242311.8	242326
Tc(I)	304915	304919.2	306186.6	304905	304922.5771	304927.9	304902.3	304921
Re(I)	307480.6	307489.6	308753.4	307461.7	307482.6016	307490.6	307470.6	307488.1
Fe(0)	190918.1	190884.8	192076.9	190917.4	190943.5324	190940.4	190926.3	190866.6
Ru(0)	268401.9	268384.5	269590.1	268395.9	307482.6016	268403.9	268423.1	268363.4
Os(0)	275865.5	275845.6	277048	275838.8	275857.2538	275853.8	275889.8	275825.3
Co(I)	134127.5	133128.1	134137.6	134120.9	134149.9847	134153.4	133293.2	134132.7
Rh(I)	227445.2	226446.8	227457.6	227429	227444.7913	227448.6	226619.5	227461.2
Ir(I)	240059.9	239066.4	240082.2	240026.3	240044.1122	240050.6	239229.9	240077.5
Ni(II)	71071.42	70110.61	71159.01	71048.86	71072.96947	71067.37	70236.89	71101.23
Pd(II)	182861.8	181900	182946.8	182829	182840.317	182836.6	182036.1	182902.5
Pt(II)	202728.5	201768.4	202817.7	202679.9	202693.4259	202692	201893.5	202762.4
Cu(I)	0	0	0	0	0	0	0	0
Ag(I)	132363.1	132355.1	132351.9	132366.6	132369.5719	132365.7	132368.5	132364
Au(I)	159460.6	159709.7	159463.3	159447.8	159452.5751	159455.6	159457.6	159450.7

C.8 Theoretical / Calculation Data of the Co-ordination Geometry

Table C.8.1 Diamond illustrations of the co-ordination geometry of selected computed complexes for group 7-11 transition metals. Carbons (grey), oxygens (red), metals (various). Hydrogens omitted for clarity.

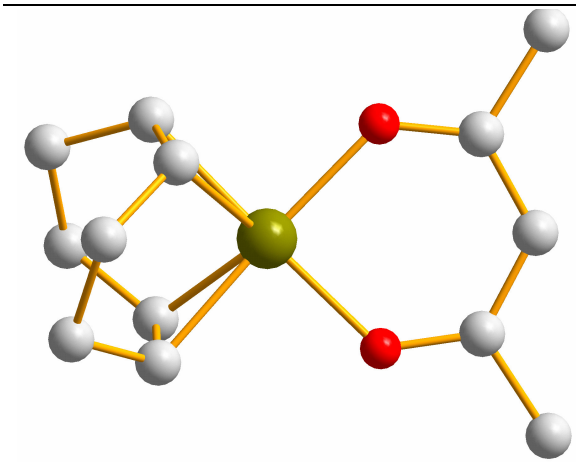

[Fe(cod)(acac)]

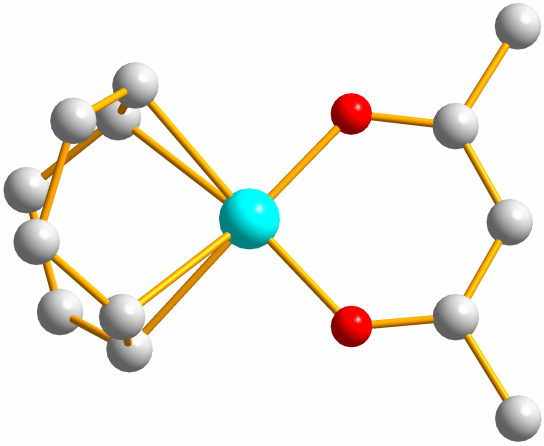

[Ni(cod)(acac)]

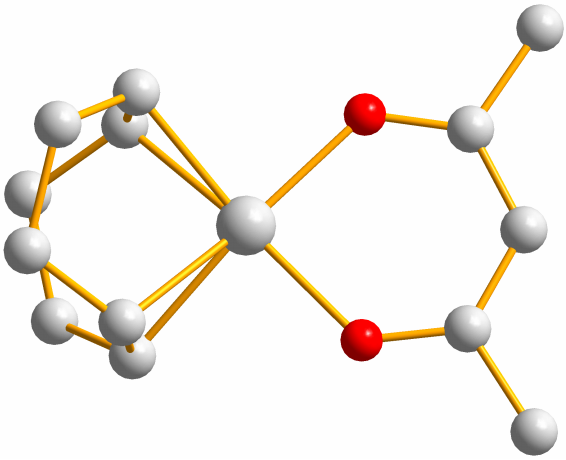

[Mn(cod)(acac)]

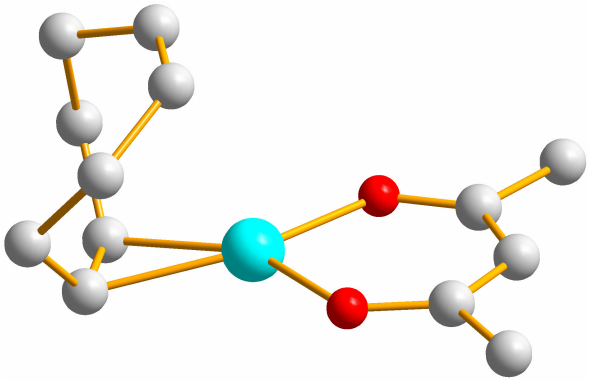

[Cu(cod)(acac)]

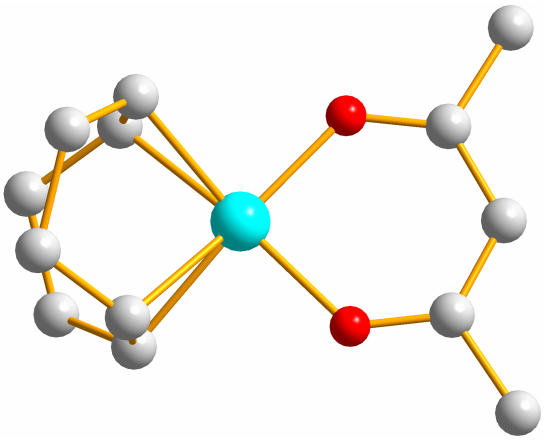

[Co(cod)(acac)]

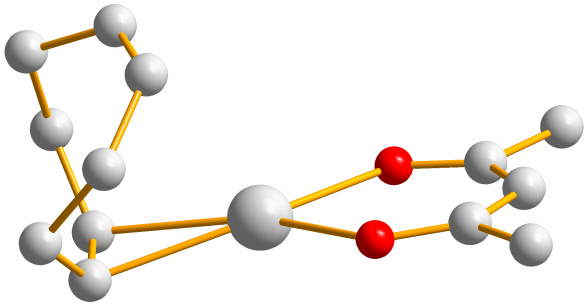

[Ag(cod)(acac)]

C.9 Theoretical / Calculation Output Data

The *.log and *.out files for the computed structures are included on a CD.

Summary

The aim of this study was to gain a further insight into the bonding modes of 1,5-cyclo-octadiene to various middle to late transition metal centres. The intension was to design a theoretical model of the influences of the variations of the metal centres and ligands on the "Venus fly-trap" system. Two principle geometric features were classified in the 1,5-cyclo-octadine when co-ordinated, *i.e.* the χ (bite) angle of the olefinic moieties to the metal centre, and the ψ (jaw) angle, *i.e.* the dihedral angle between the two planes formed between the alkane ethylene groups. The latter mimicking the "jaws" of the Venus fly-trap.

A range of 1,5-cyclo-octadiene metal complexes were successfully synthesized and characterized *via* NMR and IR spectroscopy, the metal centers chosen were that of rhodium(I), platinum(II) and palladium(II). The ligands selected were divided into three categories namely

- β-diketonato
- β-enaminonato
- tropolonato

From each of these categories ligands were selected to vary the electron withdrawing or donating ability. Both symmetrical and non-symmetrical ligands were made use of, to see the influence of the nitrogen *trans* effect on the 1,5-cyclo-octadiene moiety. Finally, the tropolonato category added the influence of the smaller five membered metal chelate ring.

A single crystal X-ray crystallographic study of the complexes was undertaken. The reported X-ray crystallographic structure determinations include the following complexes: [Pd(cod)(acac)]PF_6 (**1**, Monoclinic $P2_1/n$, R = 3.59 %), [Pd(cod)(acac)]BF_4 (**2**, Orthorhombic $Pca2_1$, R = 2.24 %), [Pd(cod)(thtfac)]PF_6 (**3**, Monoclinic $P2_1/n$, R = 2.43 %), [Pd(cod)(thtfac)]BF_4 (**4**, Monoclinic $P2_1/n$, R = 2.83 %), [Pd(cod)(tfacac)]PF_6 (**5**, Triclinic $P\bar{1}$, R = 13.41 %), [Pd(cod)(hfacac)]PF_6 (**6**, Monoclinic $P2_1/c$, R = 2.60 %),

[Pt(cod)(acac)] (**7**, Orthorhombic $Pca2_1$, R = 1.75 %), [Pt(cod)(acac)]PF_6 (**8**, Monoclinic $P2_1/n$, R = 3.02 %), [Pt(cod)(dbm)]BF_4 (**9**, Triclinic $P1$), [Pt(cod)(thtfac)]BF_4 (**10**, Monoclinic $P2_1/n$, R =2.80 %), [Pd(cod)(3Br-trop)]PF_6 (**11**, Triclinic $P\bar{1}$, R = 5.90 %), [Pd(cod)(3Br-trop)]BF_4 (**12**, Triclinic $P\bar{1}$, R = 3.40 %), [Pd(cod)(trop)]PF_6 (**13**, Tetragonal $P4_2bc$, R = 4.08 %), [Pt(cod)(trop)]PF_6 (**14**, Tetragonal $P4_2/mbc$, R = 3.45 %), [Pt(cod)(trop)]BF_4 (**14**, Tetragonal $P4_2bc$, R = 2.91 %), [Pt(cod)(3Br-trop)]PF_6 (**16**, Monoclinic $C2/c$, R = 4.38 %), [Pt(cod)(3Br-trop)]BF_4 (**17**, Triclinic $P\bar{1}$, R = 2.66 %), [Pd(cod)(NH-acac)]BF_4 (**18**, Monoclinic $P2_1/c$, R = 2.24 %), [Pt(cod)(NH-acac)]BF_4 (**19**, Monoclinic $P2_1/c$, R = 2.09 %), [Pt(cod)(NH-acac)]PF_6 (**20**, Monoclinic $C2/m$, R = 3.88 %), [Pt(cod)(NMe-acac)]BF_4 (**21**, Orthorhombic $P2_12_12_1$, R = 1.50 %), [Pt(cod)(NMe-acac)]PF_6 (**22**, Monoclinic $C2$, R = 2.44 %), [Pt(cod)(NPh-acac)]BF_4 (**23**, Monoclinic $P2_1/n$, R = 3.25 %), [Pt(cod)(NPh-acac)]PF_6 (**24**, Triclinic $P1$, R = 3.29 %), [Rh(cod)(acac)] (**25**, Monoclinic Cc, R = 2.21 %), [Rh(cod)(dbm)] (**26**, Monoclinic Cc, R = 2.80 %), [Rh(cod)(thtfac)] (**27**, Monoclinic $P2_1/n$, R = 4.75 %) and [Rh(cod)(trop)] (**28**, Orthorhombic $P2_12_12_1$, R = 1.39 %).

The co-ordination geometry of the crystal structures was square planar, for palladium(II) and platinum(II) crystal structures resulting in a cationic charged species which was balanced with either BF_4^- or PF_6^- counter ions. Extensive hydrogen bonding was observed for the solid state structures with some interesting metal ring chelate interactions. The twist angle, the distortion from the square planar co-ordination geometry, for the crystal structures was found to be of a similar order.

A theoretical DFT study was carried out on the group 7-11 transition metals with acetylacetone (Hacac), trifluoroacetylacetone (Htfacac), hexafluoroacetylacetone (Hhfacac), 4-aminopent-3-en-2-one (HNH-acac), 4-(methylamino)pent-3-en-2-one (HNMe-acac), 4-anilinopent-3-en-2-one (HNPh-acac), tropolone (Htrop) and tribromotropolone (H3Br-trop). The comparison of the calculated structures with the X-ray crystal structures was found to be in good agreement with *R*-values of greater than 98 %. The molecular orbitals showed the influences of the π orbital delocalization and the bonding orbitals of the cyclo-octadiene with the various transition metal centres and provided an easy graphical method to compare both the variations of ligands and metal

centres. Both the molecular orbital energies and band gap energies were presented and reflected the changes in the cyclo-octadiene complexes. A push-pull effect was observed though the use of the "core" co-ordination geometry, where the metal displays a lateral movement within the co-ordination area (A_{tot}). The χ and ψ angles (bite and jaw angles) were determined for all the theoretical structures as well as the solid state crystal structures obtained. A maximum opening of *c.a.* 15° for the β-diketonato complexes while both the β-enaminonato and tropolonato complexes have a *c.a.* 14° variation in the jaw angle affected by both the metal and *trans* ligand manipulations.

Keywords: Synthesis, Crystallography, Theoretical Calculations, β-diketone, β-enaminone, tropolone, rhodium , platinum and palladium complexes, transition metals, hydrogen bonding interactions, metal chelate ring interactions

Opsomming

Die doelwit van hierdie studie was om 'n meer breedvoerige insig te verkry oor die verbindings van 1,5-siklo-oktadieen met verskeie middel- tot laat oorgangs metal kerne, met die doel om 'n teoretiese model te skep. Hierdie model sal die invloed van die wisseling van die metal kerne en die ligande op die "Venus fly-trap" sisteem illustreer. Twee hoof geometriese karakter eienskappe was geklassifiseer wanneer die siklo-oktadieen gekoordineer is, (a) die χ (bite) hoek van die olefeniese gedeeltes na die metal kern, en (b) die ψ (jaw) hoek wat die dihidriese hoek tussen die twee oppervlakkes is wat gevorm het tussen die alkaan eteen groepe. Laasgenoemde naboots die "jaws" van die "Venus fly-trap".

'n Reeks van 1,5-siklo-oktadieen metal komplekse was suksesvol gesintetiseer en geklassifiseer met behulp van KMR en IR spektroskopie. The metal kerne wat gekies was, is rhodium(I), platinum(II) en palladium(II). Die ligande wat gekies was kan gegroepeer word in drie afdelings, naamlik:

- β-diketonato
- β-enaminonato
- tropolonato

Ligande uit hierdie kategorieë is gekies om elektron ontrekking of skenking vermoeë te varieer. Beide simmetries en nie-simmetriese ligande is gebruik om die invloed van die stikstof *trans* effek op die 1,5-siklo-oktadieen gedeelte. Laastens het die tropolonato kategorie die invloed van die kleiner vyf-lid metal chelaat ring bygedra.

'n Enkel kristal x-straal kristallografiese studie van die komplekse was ook onderneem. Die x-straal kristallografiese struktuur bepalings wat verkryg was het die volgende komplekse ingesluit: [Pd(cod)(acac)]PF_6 (**1**, Monoklien $P2_1/n$, R = 3.59 %), [Pd(cod)(acac)]BF_4 (**2**, Orthorombies $Pca2_1$, R = 2.24 %), [Pd(cod)(thtfac)]PF_6 (**3**, Monoklien $P2_1/n$, R = 2.43 %), [Pd(cod)(thtfac)]BF_4 (**4**, Monoklien $P2_1/n$, R = 2.83 %), [Pd(cod)(tfacac)]PF_6 (**5**, Triklien $P\bar{1}$, R = 13.41 %), [Pd(cod)(hfacac)]PF_6 (**6**, Monoklien

$P2_1/c$, R = 2.60 %), [Pt(cod)(acac)] (**7**, Orthorombies $Pca2_1$, R = 1.75 %), [Pt(cod)(acac)]PF_6 (**8**, Monoklien $P2_1/n$, R = 3.02 %), [Pt(cod)(dbm)]BF_4 (**9**, Triklien $P\bar{1}$), [Pt(cod)(thtfac)]BF_4 (**10**, Monoklien $P2_1/n$, R =2.80 %), [Pd(cod)(3Br-trop)]PF_6 (**11**, Triklien $P\bar{1}$, R = 5.90 %), [Pd(cod)(3Br-trop)]BF_4 (**12**, Triklien $P\bar{1}$, R = 3.40 %), [Pd(cod)(trop)]PF_6 (**13**, Tetragonal $P4_2bc$, R = 4.08 %), [Pt(cod)(trop)]PF_6 (**14**, Tetragonal $P4_2/mbc$, R = 3.45 %), [Pt(cod)(trop)]BF_4 (**14**, Tetragonal $P4_2bc$, R = 2.91 %), [Pt(cod)(3Br-trop)]PF_6 (**16**, Monoklien $C2/c$, R = 4.38 %), [Pt(cod)(3Br-trop)]BF_4 (**17**, Triklien $P\bar{1}$, R = 2.66 %), [Pd(cod)(NH-acac)]BF_4 (**18**, Monoklien $P2_1/c$, R = 2.24 %), [Pt(cod)(NH-acac)]BF_4 (**19**, Monoklien $P2_1/c$, R = 2.09 %), [Pt(cod)(NH-acac)]PF_6 (**20**, Monoklien $C2/m$, R = 3.88 %), [Pt(cod)(NMe-acac)]BF_4 (**21**, Orthorombies $P2_12_12_1$, R = 1.50 %), [Pt(cod)(NMe-acac)]PF_6 (**22**, Monoklien $C2$, R = 2.44 %), [Pt(cod)(NPh-acac)]BF_4 (**23**, Monoklien $P2_1/n$, R = 3.25 %), [Pt(cod)(NPh-acac)]PF_6 (**24**, Triklien $P1$, R = 3.29 %), [Rh(cod)(acac)] (**25**, Monoklien Cc, R = 2.21 %), [Rh(cod)(dbm)] (**26**, Monoklien Cc, R = 2.80 %), [Rh(cod)(thtfac)] (**27**, Monoklien $P2_1/n$, R = 4.75 %) and [Rh(cod)(trop)] (**28**, Orthorombies $P2_12_12_1$, R = 1.39 %).

Die gekoördineerde geometrie van die kristal strukture was vierkantige planêr vir beide die palladium (II) en platinum (II) kristal strukture. Hierdie koördinasie lei tot ‘n kationiese gelaaide spesie wat gebalanseerd is met BF of BF teenstellende ione. ‘n Oorgroote merderheid waterstof bindings was waargeneem vir die soliede toestand strukture, asook noemswaardige metal ring chelaat interaksies. Die “twist” hoek, wat die vervorming van die vierkantig planêre koördinasie geometrie vir die kristal strukture is, is bevind om van dieselfde orde te wees.

‘n Teoretiese DFT studie is uitgevoer op die groep 7-11 oorgangs metale met asetielasetoon (Hacac), trifluoroasetielasetoon (Htfacac), hexafluoroasetielasetoon (Hhfacac), 4-aminopent-3-en-2-one (HNH-acac), 4-(methylamino)pent-3-en-2-one (HNMe-acac), 4-anilinopent-3-en-2-one (HNPh-acac), tropolone (Htrop) and tribromotropolone (H3Br-trop). Die R-waarde wat verkry is wanneer die x-straal kristal strukture met die berekende teoretiese strukture vergelyk was, was > 98 %. Die molekulêre orbitale dui die invloed van die gedelokaliseerde π orbital en die verbindings orbital van die siklo-oktadieen met die verskillende oorgangs metal kerne aan. Die

molekulêre orbitale voorsien ‘n maklike grafiese metode vir die vergelyking van beide die ligande en die metaal kerne. Beide die molekulêre orbitale energieë en die “band gap” energieë is teenwoordig en reflekteer die veranderinge in die siklo-oktadieten komplekse. ‘n Aftoot-aantrek effek was waargeneem deur die gebruik van die “core” gekoordineerde geometrie, waar die metal ‘n sywaartse beweging binne die koordinasie area getoon het. Die χ en ψ hoeke (bite en jaw hoeke) was bereken vir al die teoretiese strukture, asook vir die vaste toestand kristal strukture. ‘n Maksimum opening van *c.a.* 15° vir die β-diketonato kompleks is waargeneem, terwyl vir beide die β-enaminonato en tropolonato komplekse ‘n 14° variasie in die jaw hoek waargeneem is wat geaffekteerd is deur metaal en *trans* ligand manipulasies.